Agenzia nazionale per le nuove tecnologie,
l'energia e lo sviluppo economico sostenibile

MINISTERO DELLO SVILUPPO ECONOMICO

Ricerca di Sistema elettrico

Workshop Tematico Accordo di Programma MiSE – ENEA PAR2017 – Progetto B.3 LP2 GENERATION IV Lead Cooled Fast Reactor Stato attuale della tecnologia e prospettive di sviluppo

D. Martelli

Report RdS/PAR2017/120

Workrkshop Tematico Accordo di Programma MiSE – ENEA PAR2017 –
Progetto B.3 LP2
GENERATION IV
Lead Cooled Fast Reactor
Stato attuale della tecnologia e
prospettive di sviluppo

D. Martelli (UniPi)

Settembre 2018

Report Ricerca di Sistema Elettrico

Accordo di Programma Ministero dello Sviluppo Economico - ENEA
Piano Annuale di Realizzazione 2017
Area: Generazione di Energia Elettrica con Basse Emissioni di Carbonio
Progetto: Sviluppo competenze scientifiche nel campo della sicurezza nucleare e collaborazione ai programmi internazionali per il nucleare di IV Generazione.
Linea: Collaborazione ai programmi internazionali per il nucleare di IV Generazione
Obiettivo: Progettazione di sistema e analisi di sicurezza
Responsabile del Progetto: Mariano Tarantino, ENEA

Titolo

Workshop Tematico Accordo di Programma MiSE – ENEA PAR2017 – Progetto B.3 LP2
GENERATION IV
Lead Cooled Fast Reactor

Stato attuale della tecnologia e prospettive di sviluppo

Descrittori

Tipologia del documento: **Rapporto Tecnico**
Collocazione contrattuale: Accordo di programma ENEA-MSE su sicurezza nucleare e reattori di IV generazione
Argomenti trattati: Generation IV reactors

Sommario

Presso il Dipartimento di Ingegneria Astronautica, Elettrica ed Energetica dell'Università di Roma "La Sapienza" si è tenuto dal 14 al 15 giugno 2018, un Workshop tematico dal titolo "GENERATION-IV LEAD COOLED FAST REACTOR STATO ATTUALE DELLA TECNOLOGIA E PROSPETTIVE DI SVILUPPO", organizzato da ENEA in collaborazione con le principali università italiane che svolgono attività di ricerca in campo nucleare. Il Workshop, promosso nell'ambito delle attività inerenti la Linea Progettuale 2 "Collaborazione internazionale per il nucleare di IV generazione" dell'AdP MiSE-ENEA, è finalizzato a analizzare lo stato dell'arte dei sistemi LFR, supportare la programmazione delle attività future, definendo le priorità di intervento in ambito italiano ed europeo, in sinergia con l'industria del settore e infine armonizzare le strategie di sviluppo mediante l'incontro di tutti gli stakeholder italiani.

Note

Autori: D. Martelli[1]
(1) UniPi

Copia n. **In carico a:**

2			**NOME**			
			FIRMA			
1			**NOME**			
			FIRMA			
0	**EMISSIONE**	**3/12/2018**	**NOME**	D. Martelli	M. Tarantino	M. Tarantino
			FIRMA			
REV.	**DESCRIZIONE**	**DATA**		**REDAZIONE**	**CONVALIDA**	**APPROVAZIONE**

Sommario

1. LFR-GEN IV Stato attuale della tecnologia e prospettive di sviluppo

Dal 14 al 15 giugno 2018, presso il dipartimento di Ingegneria Astronautica, Elettrica ed Energetica dell'Università di Roma "La Sapienza", si è tenuto il Workshop tematico dal titolo "GENERATION-IV LEAD COOLED FAST REACTOR STATO ATTUALE DELLA TECNOLOGIA E PROSPETTIVE DI SVILUPPO", organizzato da ENEA in collaborazione con le principali università italiane che svolgono attività di ricerca in campo nucleare.

Il Workshop, promosso nell'ambito delle attività inerenti la Linea Progettuale 2 "Collaborazione internazionale per il nucleare di IV generazione" dell'AdP MSE-ENEA, è stato finalizzato ad:

- Analizzare lo stato progettuale della tecnologia dei sistemi LFR partendo dal lavoro svolto in ambito ADP;
- *la programmazione delle attività future, definendo le priorità di intervento in ambito italiano in maniera che siano sinergiche al contesto europeo ed internazionale;*
- armonizzazione le strategie di sviluppo mediante l'incontro di tutti gli stakeholder italiani.

Fig. 1: Ingresso Università La Sapienza in Roma

L'Italia, grazie all'ENEA, ANSALDO NUCLEARE e con il contributo fondamentale del CIRTEN, continua a conservare la leadership internazionale sulla progettazione e sullo sviluppo tecnologico dei sistemi LFR, nonostante il sempre più ampio interesse (accompagnato da ingenti investimenti economici) di altri Paesi quali ad esempio la Cina. Ciò è stato possibile grazie ai continui sforzi fatti da ENEA (che ha sfruttato efficacemente i fondi dell'ADP), sia per accrescere e migliorare le proprie infrastrutture di ricerca (Brasimone e Casaccia), sia per rafforzare le proprie capacità e competenze sulla progettazione dei sistemi nucleari innovativi. (es. gruppo core design di Bologna).

Tutto ciò è stato fatto sinergicamente con ANSALDO NUCLEARE - capofila del progetto – e progettista del Dimostratore ALFRED.
Il sistema Italia deve continuare ad investire nel settore, a focalizzare gli sforzi, evitando di disperdere risorse (il progetto di riferimento è ALFRED), cercando di sensibilizzare le istituzioni e coinvolgendo il maggior numero possibile di istituti di ricerca e industrie del settore.
I lavori sono iniziati con i saluti e la presentazione del workshop da parte del Prof. Gianfranco Caruso. A seguire sono state delineate nel dettaglio le strategie di intervento e sviluppo dal Dr. Mariano Tarantino, Responsabile Divisione Ingegneria Sperimentale Dipartimento Fusione e Tecnologie per la sicurezza Nucleare del Brasimone, attualmente uno dei più vasti ed attrezzati parco impianti a livello internazionale sulla tecnologia dei metalli liquidi pesanti.
La sessione di Apertura si è conclusa con l'intervento dell'Ing. M. Frignani di Ansaldo Nucleare relativao a " DEMO-LFR ALFRED Technical Overview".
Referente scientifico è il Dr. M. Tarantino mentre il comitato Organizzatore è costituito dal Dr. A. Del Nevo, il Dr. I. Di Piazza ricercatori FSN-ING ENEA Brasimone ed infine il Prof. Gianfranco Caruso, il Dr. Fabio Giannetti afferenti al dipartimento ospitante e la Sig.ra Annamaria Masinara (ENEA.
Gli oltre 60 partecipanti (Allegato 1) di cui 38 rappresentanti delle più prestigiose università italiane (Bologna, Milano, Pisa Roma, Torino e Treviso) e del Consorzio Interuniversitario Nazionale per la Scienza e Tecnologia dei Materiali (INSTM) e del Consorzio Interuniversitario per la Ricerca Tecnologica Nucleare (CIRTEN), 1 rappresentante della Bangor University (UK), 16 rappresentanti dell'Agenzia Nazionale per le Nuove Tecnologie, l'Energia e lo Sviluppo Economico Sostenibile (ENEA), 6 rappresentanti delle eccellenze industriali presenti sul territorio nazionale come Ansaldo Nucleare, CSM S.p.a, Istituto Italiano di Tecnologia (IIT) ed SRS SERVIZI DI RICERCHE E SVILUPPO S.R.L. ed 1 rappresentante di una delle eccellenze internazionali quale Westighouse sono stati accolti presso l'università La Sapienza (Fig. 1).
L'agenda del Workshop (Allegato 2) è stata suddivisa in 6 sessioni. All'interno della sessione di apertura sono state presentate le strategie e prospettive nazionali ed internazionali sui reattori di quarta generazione refrigerati a piombo liquido. Inoltre, è stata fornita un'ampia panoramica sullo stato attuale e sulle problematiche ancora aperte relative alla progettazione del reattore dimostratore ALFRED (Advanced Lead Fast Reactor Demonstrator).
All'interno delle 5 sessioni tecniche, sono stati presentati ben 29 lavori di ricerca sulle tematiche della progettazione di sistema, l'analisi di sicurezza, sviluppo materiali e chimica del refrigerante, termofluidodinamica dei sistemi LFR e lo sviluppo e validazione di codici e modelli multi-fisici per analisi di sicurezza di reattori veloci di iv generazione. Nell'Allegato 3 vengono infine riportati i contributi presentati all'interno delle varie sessioni.

2 ALLEGATI

1. LISTA DEI PARTECIPANTI AL CONGRESSO
2. AGENDA
3. CONTRIBUTI PRESENTATI NELLE VARIE SESSIONI

	NOME	COGNOME	ISTITUTO
1	Mariano	Tarantino	ENEA
2	Massimo	Angiolini	ENEA
3	Marianna	Rinaldi	INSTM
4	Lorenzo	Melchiorri	UNIROMA1
5	Alessandro	Tassone	UNIROMA1
6	Matteo	D'Onofrio	UNIROMA1
7	Giovanni	Padula	UNIROMA1
8	Sante	Spina	UNIROMA1
9	Pierdomenico	Lorusso	UNIROMA1
10	Vincenzo	Narcisi	UNIROMA1
11	Ivan	Di Piazza	ENEA
12	Valentina	Fabrizio	ENEA
13	Mario	Carta	ENEA
14	Serena	Bassini	ENEA
15	Edoardo	Cotroneo	UNIROMA1
16	Alessandro	Del Nevo	ENEA
17	Antonio	Naviglio	SRS
18	Sandra	Dulla	POLITO
19	Cristiano	Ciurluini	UNIROMA1
20	Luca	Cretara	UNIROMA1
21	Gianluca	Palumbo	POLIMI
22	Federico	Di Rocco	Bangor University
23	Gianfranco	Caruso	UNIROMA1
24	Fabio	Giannetti	UNIROMA1
25	Annamaria	Masinara	ENEA
26	Sandro	Manservisi	UNIBO
27	Carlo	Cristalli	ENEA
28	Stefano	Lorenzi	POLIMI
29	Lelio	Luzzi	POLIMI
30	Ilaria	Naclerio	UNIROMA1
31	Giancarlo	Bianchini	ENEA
32	Elena	Macerata	POLIMI
33	Nunzio	Burgio	ENEA
34	Vincenzo	Peluso	ENEA
35	Ranieri	Marinari	UNIPI
36	Marica	Eboli	UNIPI
37	Simone	Siriano	UNIROMA1
38	Massimo	Sarotto	ENEA
39	Ulisse	Pasquali	SRS
40	Giacomo	Grasso	ENEA
41	Michele	Frignani	ANSALDO
42	Fausto	Franceschini	Westinghouse
43	Marco	Beghi	POLIMI
44	Fabio	Di Fonzo	IIT

45	Letizia	Chiasso	UNIROMA1
46	Gufi	Rebecca	UNIROMA1
47	Alessio	Pesetti	UNIPI
48	Alfonso	Santagata	ENEA
49	Alessandra	Santoro	UNIROMA1
50	Paolo	Scassera	UNIROMA1
51	Egidio	Zanin	RINA
52	Lorenza	Moretti	UNIROMA1
53	Domenico	Lorusso	UNIROMA1
54	Augusto	Gandini	CIRTEN
55	Luisa	Ferroni	UNIROMA1
56	Elena	Macerata	POLIMI
57	Mario	Mariani	POLIMI
58	Matteo	Vanazzi	IIT
59	Laura	Savoldi	POLITO
60	Nicola	Forgione	UNIPI
61	Mario	Bragaglia	UNITV
62	Alessandro	Poggianti	ENEA
63	Roberto	Zanino	POLITO
64	Marco	Sumini	UNIBO

Agenzia nazionale per le nuove tecnologie, l'energia e lo sviluppo economico sostenibile

Ministero dello Sviluppo Economico

WORKSHOP TEMATICO

ACCORDO DI PROGRAMMA MISE – ENEA
PAR2017 – PROGETTO B.3 - LP2

GENERATION IV

LEAD COOLED FAST REACTOR

STATO ATTUALE DELLA TECNOLOGIA E PROSPETTIVE DI SVILUPPO

ADP MiSE-ENEA (PAR2017-LP2)

Dipartimento di Ingegneria Astronautica, Elettrica ed Energetica
Università di Roma "La Sapienza"
San Pietro in Vincoli, Via Eudossiana 18
14-15 Giugno 2018

Il Workshop, promosso nell'ambito delle attività inerenti la Linea Progettuale 2 "**Collaborazione internazionale per il nucleare di IV generazione**" dell'AdP MiSE-ENEA, è finalizzato a:

- *analizzare lo stato attuale della tecnologia dei sistemi LFR*
- *supportare la programmazione delle attività future, definendo le priorità di intervento in ambito italiano ed europeo, in sinergia con l'industria del settore*
- *armonizzazione le strategie di sviluppo mediante l'incontro di tutti gli stakeholder italiani.*

Il Workshop assume quindi il duplice obiettivo di condividere lo stato dell'arte dei sistemi LFR tra gli stakeholder italiani definendo al contempo, in maniera condivisa e sinergica con il contesto Europeo, le linee di intervento future in ambito LFR.

Referente Scientifico

Ing. Mariano Tarantino (ENEA) — mariano.tarantino@enea.it

Comitato Organizzatore

Prof. Gianfranco Caruso (UNROMA1) — gianfranco.caruso@uniroma1.it
Ing. Fabio Giannetti (UNIROMA1) — fabio.giannetti@uniroma1.it
Ing. Alessandro Del Nevo (ENEA) — alessandro.delnevo@enea.it
Ing. Ivan di Piazza (ENEA) — ivan.dipiazza@enea.it
Sig.ra Annamaria Masinara (ENEA) — annamaria.masinara@enea.it

GIOVEDÌ 14 GIUGNO, 2018

	Ora	TITOLO	SPEAKER
A	**9,00**	**SESSIONE DI APERTURA**	**Chair: G. Caruso**
A-1	**10'**	Saluti e Presentazione del Workshop	G. Caruso
A-2	**20'**	Gen-IV LFR Development. Status & Perspectives	M. Tarantino
A-3	**30'**	DEMO-LFR ALFRED: Technical Overview	M. Frignani
1	**10,00**	**SVILUPPO E VALIDAZIONE DI CODICI E MODELLI MULTI-FISICI PER ANALISI DI SICUREZZA DI REATTORI VELOCI DI IV GENERAZIONE**	**Chair: A. Del Nevo**
1-1	**20'**	Development of best estimate numerical tools for LFR design and safety analysis	A. Del Nevo
1-2	**20'**	Development/Assessment of models describing the inert gas behaviour in the fuel for application to the TRANSURANUS fuel pin thermo-mechanical code	L. Luzzi
1-3	**20'**	Fuel-coolant interactions studies	E. Macerata
	20'	**Coffe Break**	
1-4	**20'**	LFR Multiphysics Model Development. OpenFoam – Serpent codes coupling.	S. Lorenzi
1-5	**20'**	ALFRED Design Analysis by FRENETIC code	S. Dulla/ L. Savoldi
1-6	**20'**	HLM - Water Interaction. SIMMER – RELAP5 code coupling development.	N. Forgione
1-7	**20'**	Phenix Asymmetrical Test Simulation by 3D STH code.	F. Giannetti
1-8	**20'**	CIRCE-HERO Transient Simulation by 3D STH code	V. Narcisi
1-9	**20'**	OpenFoam-SALOME-FEMLCORE-CATHARE coupling development and validation against TALL-3D experimental data.	S. Manservisi
	13,30	**Pausa Pranzo**	
2	**15,00**	**TERMOFLUIDODINAMICA DEI SISTEMI LFR**	**Chair: F. Giannetti**
2-1	**20'**	CLEAR-S Experimental Facility Overview	U. Pasquali
2-2	**20'**	CIRCE-HERO Experiment Overview.	A. Pesetti
2-3	**20'**	HERO numerical characterization by STH code	P. Lorusso
	20'	**Coffe Break**	
2-4	**20'**	Small Leakage Detection in LFR SG	M. Eboli
2-5	**20'**	Natural Circulation Experiments in NACIE-UP Loop	I. Di Piazza
2-6	**20'**	Flow Blockage Experiments in NACIE-UP Loop	R. Marinari
	17,30	**Fine dei Lavori**	

Cena (ore 20,30)

VENERDÌ 15 GIUGNO, 2018

3	**9,00**	**SVILUPPO MATERIALI E CHIMICA DEL REFRIGERANTE**	**Chair: M. Angiolini**
3-1	**20'**	Structural Material for LFR Application. Research Program Overview.	M. Angiolini
3-2	**20'**	PLD coating for LFR application. Status and future developments	F. Di Fonzo
3-3	**20'**	Coating characterization under irradiation. Heavy ions irradiation against neutron irradiation.	M. Beghi
3-4	**20'**	Corrosion qualification of materials and coatings in liquid lead for LFR.	S. Bassini
3-5	**20'**	Coating mechanical characterization.	M. Bragaglia
	20'	**Coffee Break**	
3-6	**20'**	Coolant chemistry control study for HLM systems.	S. Bassini
3-7	**20'**	Double stabilized stainless steels. Status and future developments.	C. Cristalli
3-8	**20'**	Criticality of manufacturing and advanced processes	E. Zanin
4	**12,00**	**PROGETTAZIONE DI SISTEMA**	**Chair: M. Frignani**
4-1	**20'**	ALFRED Core Design. Thermo-mechanical analysis of the fuel element	A. Poggianti
4-2	**20'**	ALFRED Fuel Assembly Design	G. Grasso
4-3	**20'**	Feasibility studies of an experimental campaign in TAPIRO devoted to the analysis of nuclear database for minor actinides	M. Carta / S. Dulla
	13,00	**Pausa Pranzo**	
	14,30	**PROGETTAZIONE DI SISTEMA**	**Chair: M. Frignani**
4-4	**20'**	Advances in Generalized Perturbation Methods.	A. Gandini
4-5	**20'**	Neutronic code validation for LFR application. Status & Perspectives	M. Sarotto
4-6	**20'**	ALFRED Core Design. Status and future work.	G. Grasso
5	**15,30**	**CONCLUSIONI E SVILUPPI FUTURI**	**M. Frignani / M. Tarantino**
	16,30	**Fine Lavori**	

Italian National Agency for New Technologies,
Energy and Sustainable Economic Development

GENERATION IV LEAD COOLED FAST REACTOR
STATO ATTUALE DELLA TECNOLOGIA E PROSPETTIVE DI SVILUPPO

WORKSHOP TEMATICO ACCORDO DI PROGRAMMA MISE – ENEA
PAR2017 – PROGETTO B.3. LP2

DIAEE Università di Roma "La Sapienza", 14-15 giugno, 2018

Mariano Tarantino, Responsabile Divisione Ingegneria Sperimentale
Dipartimento Fusione e Tecnologie per la Sicurezza Nucleare

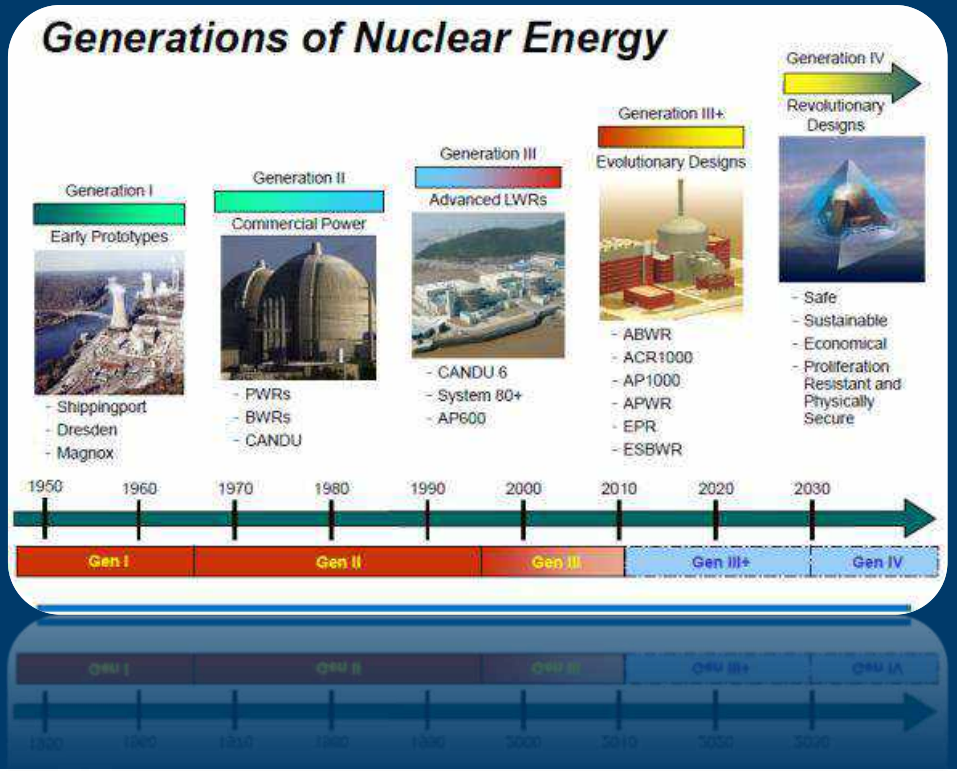

GEN-IV LFR Development

Strategies & Perspectives

Outline

- Why Nuclear?!
- Why Fast Reactor?!
- Why Lead-cooled Fast Reactor?
- Italian Contribution
- International Context
- Final Remarks

Energy Demand

- Oil remains the world's primary energy source through 2040, meeting about one-third of demand
- Natural gas grows the most of any energy type, reaching a quarter of all demand
- Coal remains important in parts of the world, but loses significant share as the world transitions toward energy sources with lower emissions
- Nuclear and renewables see strong growth, contributing close to 40 percent of incremental energy supplies to meet demand growth

Source: **Exxon Mobil Energy Outlook 2017**

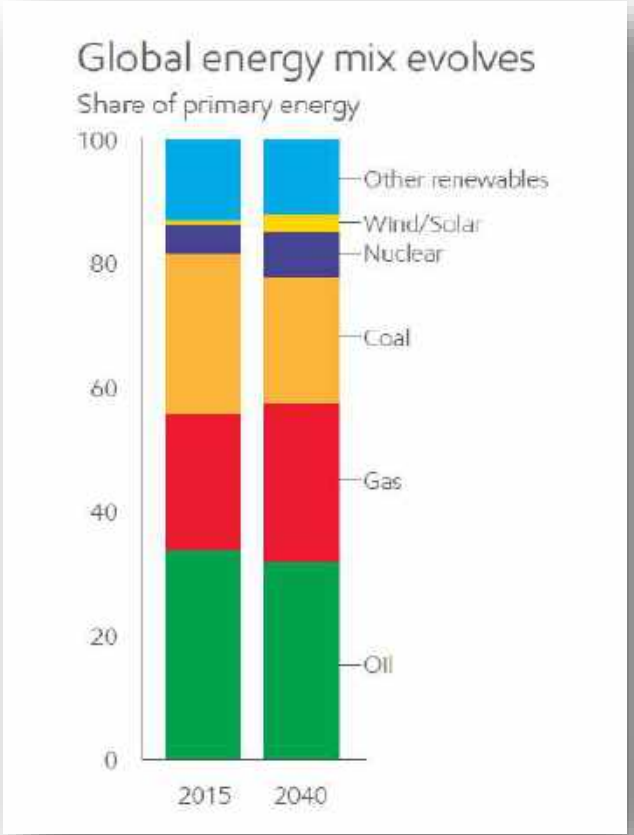

Electricity Demand

- World shifts to less carbon-intensive energy for electricity generation, led by gas, renewables (wind, solar) and **nuclear**
- Coal provides less than 30 percent of world's electricity in 2040, versus about 40 percent in 2015
- Wind and solar electricity supplies grow about 360 percent, approaching 15 percent of global electricity by 2040
- Renewables growth supported by policies to reduce CO2 emissions

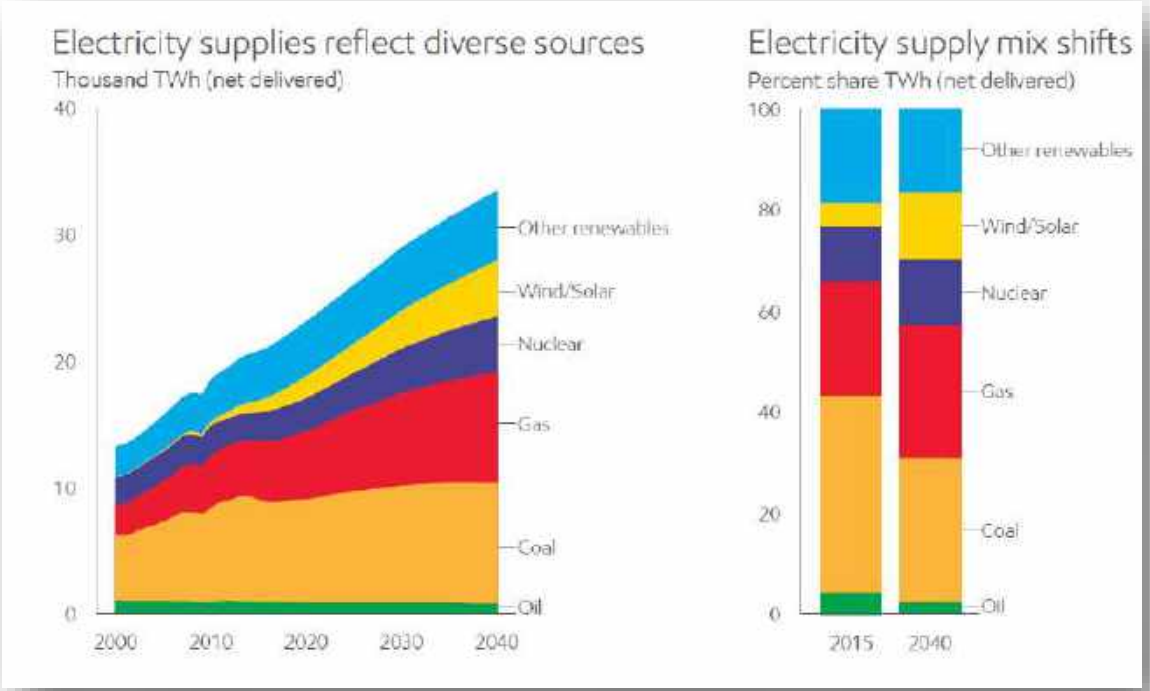

Source: Exxon Mobil Energy Outlook 2017

Electricity Generation & Nuclear Role

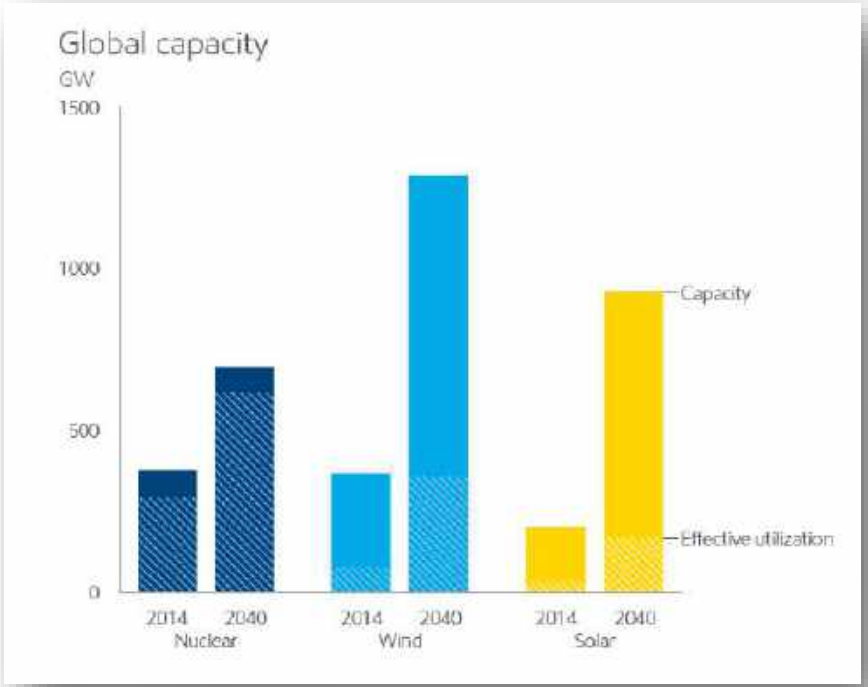

- Global nuclear, wind, solar all see big capacity additions
- **Nuclear capacity to grow 85% 2014-2020, led by China**
- **Intermittency limits the utilization of wind, solar capacity**
- Globally, less than 30% of wind capacity is utilized; solar less than 20%
- **Wind, solar provide less electricity in 2040 than nuclear despite 3 times the capacity**

Source: **Exxon Mobil Energy Outlook 2017**

Electricity Generation & Nuclear Role

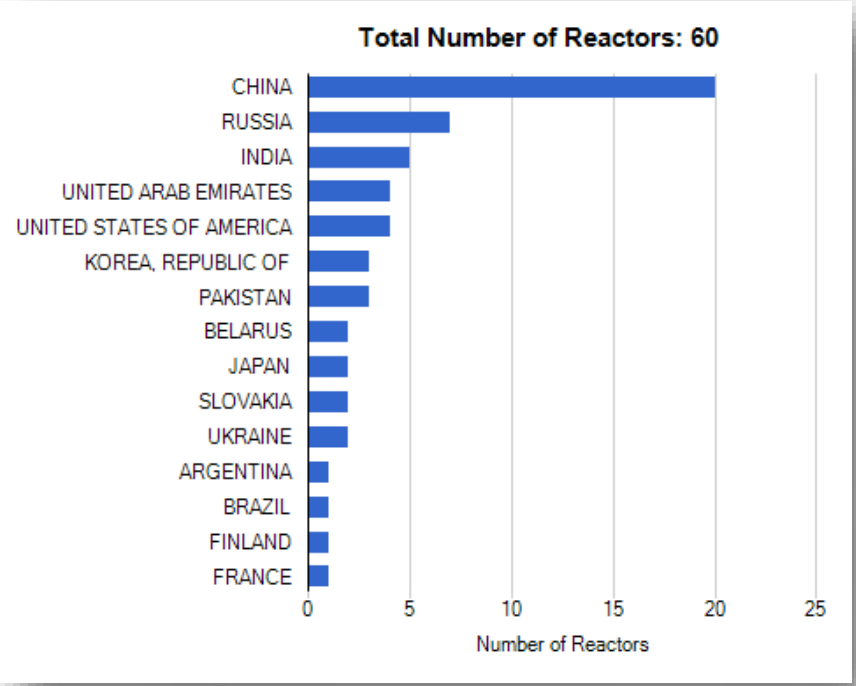

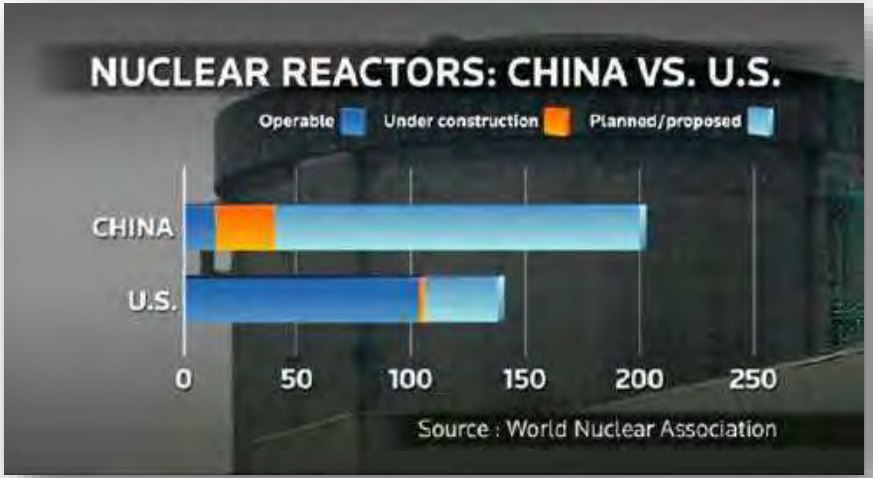

Source: **IAEA – Power Reactor Information System**

Electricity Generation & Nuclear Role

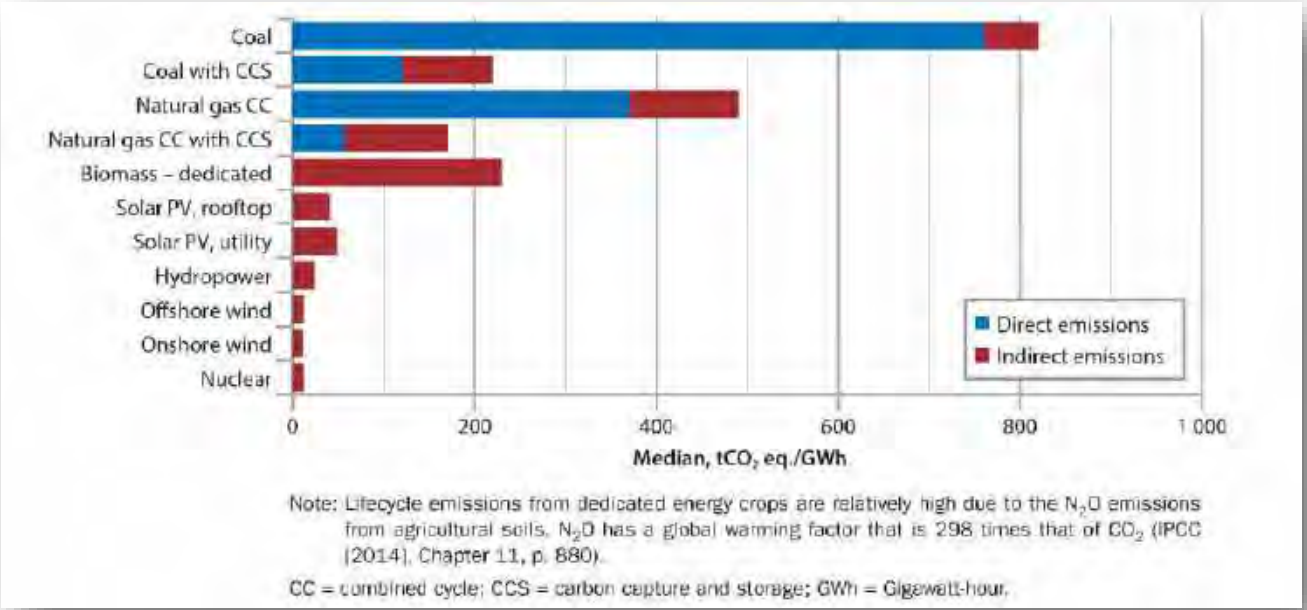

- Nuclear energy produced **11% of global electricity supply in 2013**.
- This corresponds to 18% of electricity supply in OECD countries and slightly more than 4% in non-OECD countries.
- **Nuclear is the largest low-carbon source of electricity in OECD countries**. Its share in non-OECD countries is still low but is expected to rise substantially in coming years.

Source: **IPCC (Intergovernmental Panel on Climate Change), 2014**

Nuclear Open Issues

- Nuclear Energy
  good but not good enough
- Improvement Safety
- Waste
  - Too much of it
  - Too long lived
- Economy
  Once through strata
  uses less than 0,5% of the fuel

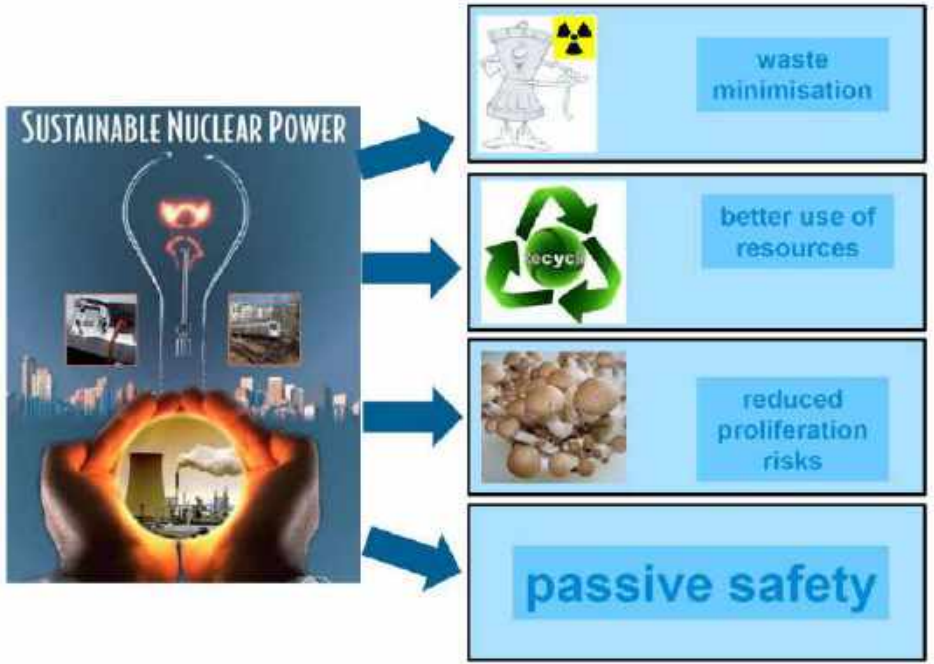

Waste Minimization & Economy

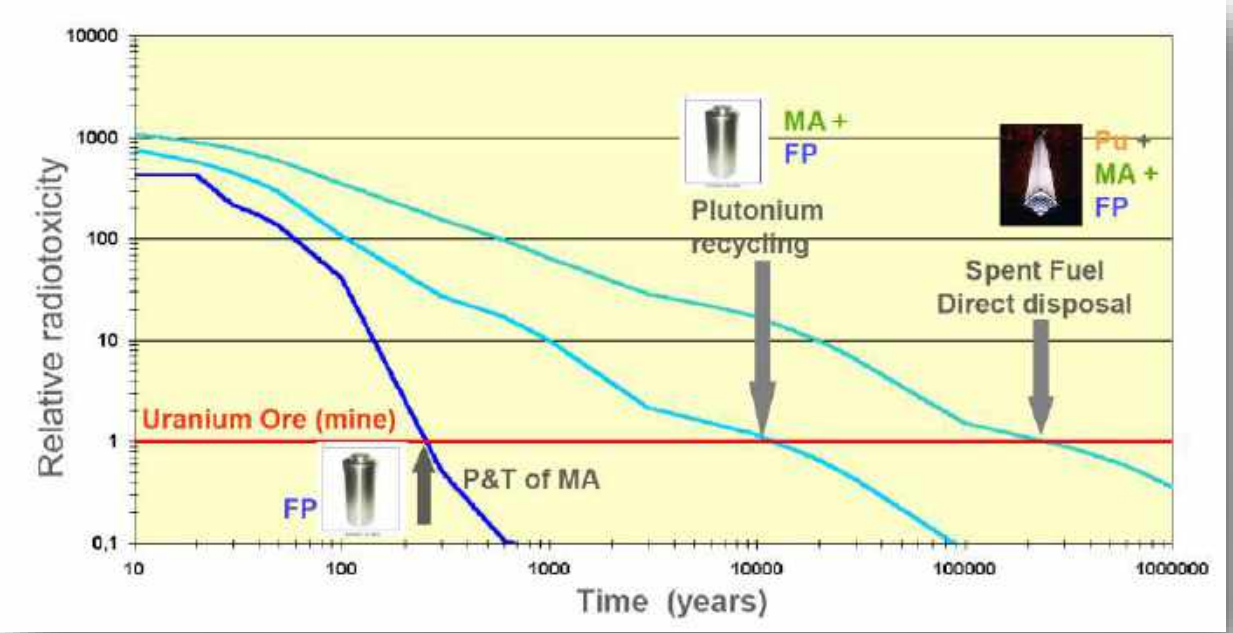

Recycle of all actinides in spent LWR fuel in fast reactors provides a significant reduction in the time required for radiotoxicity to decrease to that of the original natural uranium ore used for the LWR fuel (i.e., man-made impact is eliminated). From 250,000 years down to about 400 years with 0.1% actinide loss to wastes

Safety Improvement

Severe Nuclear Accidents. During the historically short period several low probability NPP accidents occurred with significant radioactivity release into environment and considerable economical losses

Three Mile Island-2
(PWR)
1979

Chernobyl-4
(RBMK)
1986

Fukushima-1
(BWR)
2011

The initial events for these accidents are of extremely low probability

technical failure **human error** **extreme external impact**

Generation IV

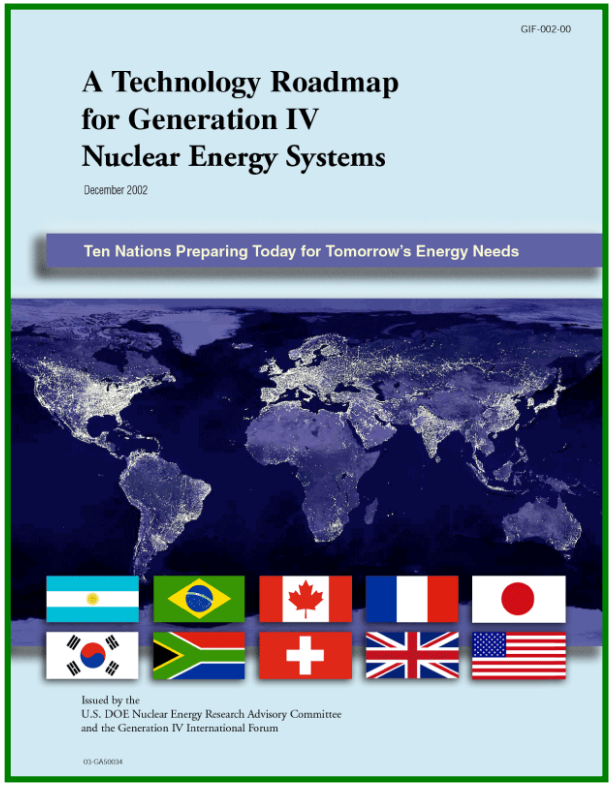

The path from current nuclear systems to Generation IV systems is described in a 2002 Roadmap Report entitled "***A technology Roadmap for Generation IV Nuclear Energy Systems"*** which:

defines challenging technology goals for Generation IV nuclear energy systems in four areas:

- ✓ **sustainability,**
- ✓ **economics,**
- ✓ **safety and reliability, and**
- ✓ **proliferation resistance and physical protection.**

identifies six systems known as Generation IV to enhance the future role of nuclear energy**;**

defines and plans the necessary R&D

Generation IV

Generation IV Systems	*Acronym*
Gas-Cooled **F**ast **R**eactor	**GFR**
Lead-Cooled **F**ast **R**eactor	**LFR**
Molten **S**alt **R**eactor	**MSR**
Sodium-Cooled **F**ast **R**eactor	**SFR**
Super**c**ritical **W**ater-Cooled **R**eactor	**SCWR**
Very-**H**igh-**T**emperature **R**eactor	**VHTR**

Because the capability of fast reactors to meet the sustainability goal and hence to re-position nuclear energy from the present transition-energy role into an inexhaustible source of clean energy

- three out of the six systems selected by GIF (GFR, LFR and SFR) are fast reactors and
- for two systems (MSR and SCWR) studies have been carried out recently to explore the possibility of them to become fast reactors.

Lead cooled Fast Reactor

- For heavy liquid metal coolants (lead-bismuth alloy, lead) the stored thermal potential energy cannot be converted into kinetic energy.
- There is no significant release of energy and hydrogen in an events of coolant contacting with air, water, structural materials.
- There is no loss of core cooling in an event of tightness failure in the gas system of the primary circuit.
- The way to improve the NPP safety and economic performance is to implement reactor facilities with **the lowest stored potential energy**, where the inherent self-protection and passive safety properties are used to the maximal extent.

Lead cooled Fast Reactor

Main advantages and main drawbacks of Lead

Atomic mass	Absorption cross-section	Boiling Point (°C)	Chemical Reactivity (w/Air and Water)	Risk of Hydrogen formation	Heat transfer properties	Retention of fission products	Density (Kg/m^3) @400°C	Melting Point (°C)	Opacity	Compatibility with structural materials
207	Low	1737	Inert	No	Good	High	10580 10580	327	Yes	Corrosive

Lead cooled Fast Reactor

A comprehensive R&D program is necessary because of:

- **The use of a new coolant and associated technology, properties, neutronic characteristics, and compatibility with structural materials of the primary system and of the core.**
- **Innovations which require validation programs of new components and systems (the SG and its integration inside the reactor vessel, the extended stem fuel element, the dip coolers of the safety-related DHR system, pump, OCS, …)**
- **The use of advanced fuels (*at least in a further stage*).**

Italian Position

- The **industrial interest on LFR technology increased worldwide**, thanks to the enhanced safety and sustainability performances, the potential for economic competitiveness and the unique flexibility in terms of plant size and potential applications.

- In the European context, the attractive features of the LFR technology are being considered for the industrial deployment of a **lead-cooled Small Modular Reactors (SMR), able to achieve commercial maturity in a short-term.** It will offer a more advanced **alternative to current generation reactors facing retirement between 2035-2040**, while progressively achieving top-scoring performances in economics, safety, sustainability and proliferation resistance in line with the Generation-IV objectives.

- The **ALFRED Project** is framed as a priority to address the challenges of the European Union energy policy. **Italian industries, research centers and academia** have invested in developing and promoting the Project. The ALFRED implementation in Romania will represent an opportunity for the Italian system and is worth support towards the decision makers and European level.

Italian Contribution: ALFRED

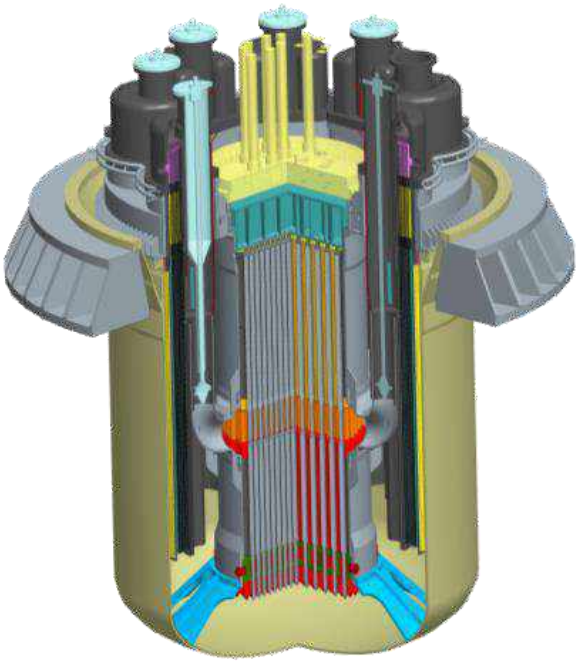

Advanced, since integrating innovation-intensive solutions in nuclear technology

Lead, because of its intrinsic properties as primary coolant to achieve superior safety

Fast, for the full exploitation of fuel energy and the reduction of long-term radiotoxicity

Reactor, as a representative training system for industry, utilities and safety authorities

European, because conceived and developed by a pan-European collaboration of experts

Demonstrator, to prove the viability LFR for a safe, clean, economic, and sustainable nuclear energy source

Italian Contribution

Framework Agreement (AdP)
between the Italian Ministry for Economic Development (MiSE) and ENEA.

- **Project B.3.→ Nuclear Fission**
  - **LP2 "International Collaboration on Gen-IV Nuclear Systems"**

- **Design and Safety Analysis**
- **Structural Materials and Coolant Chemistry**
- **Thermalfluidynamic & Innovative Components**

Towards Lead-cooled Fast Reactors

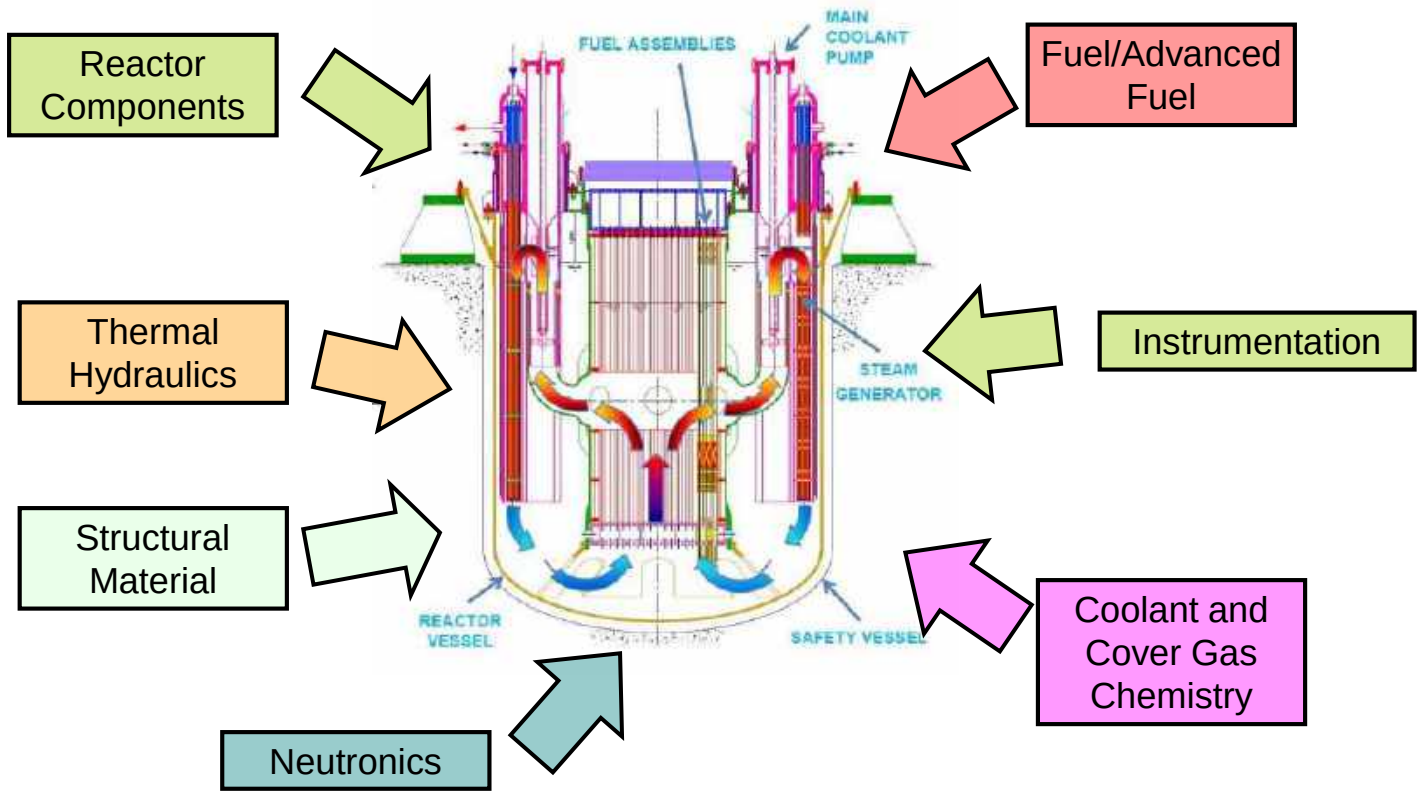

Towards Lead-cooled Fast Reactors

	TRL	TRL Function	Generic Definition	Phase
achieved	1	Technology Down-Selection	•Basic principles definition	Screening
achieved	2		•Technology concepts and applications definition	
Ongoing	3		•Demonstration of critical function •Proof of concept	Pre-qualification
Ongoing	4	Final Process Selections & integration	•Lab-scale component validation	
Ongoing	5		•Component validation in a relevant environment	Qualification
Further Development	6	Full-scale integrated testing	•System/subsystem model or prototype demonstration in relevant environment	
Further Development	7		•System prototype demonstration in prototypic environment	Demo
Further Development	8	Full-scale demo	•Actual system completed and qualified through test and demonstration	
Further Development	9		•Actual system proven through successful operations	

DEMO is needed!

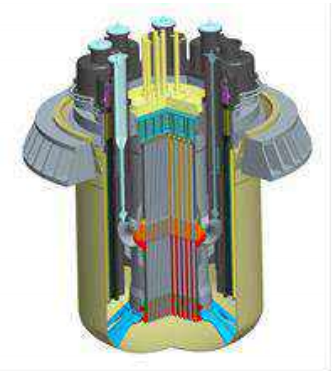

ALFRED

European Scenario

SNETP → Sustainable Nuclear Energy Technological Platform

To ensure the long-term sustainability of nuclear energy, **Gen IV Fast Neutron Reactors should be available for deployment by 2040** or even earlier. Therefore an ambitious yet realistic R&D and demonstration programme is to be put in place.

ESNII → European Sustainable Nuclear Industrial Initiative

ESNII addresses the need for **demonstration of Generation IV Fast Neutron Reactor technologies**, together with supporting research infrastructures, fuel facilities and R&D work.

SRIA → Strategic Research and Innovative Agenda (2013)

The **main objective of Europe** is to maintain the leadership in fast spectrum reactor technologies that will **excel in safety** and will be able to achieve a more **sustainable development of nuclear energy**.

"……Lead Fast Reactor technology has significantly extended its technological base and can be considered as the shorter-term alternative technology (to SFR), whereas the Gas Fast reactor technology has to be considered as a longer-term alternative option.

FALCON Consortium

- **FALCON** Consortium Agreement established in **2013** to bring LFR technology to **industrial maturity**.
- **Infrastructures** in Mioveni platform:
  - European "**Lead School**" for E&T and dissemination services,
  - **CoE on HLM** equipped with unique facilities,
  - **ALFRED** playing the role of ETDR of the LFR technology
- New members sharing the **objective** of a rapid deployment of an LFR demonstrator, interested in the R&D supporting **infrastructure** and in the **ALFRED** industrial outcomes are welcome to join.

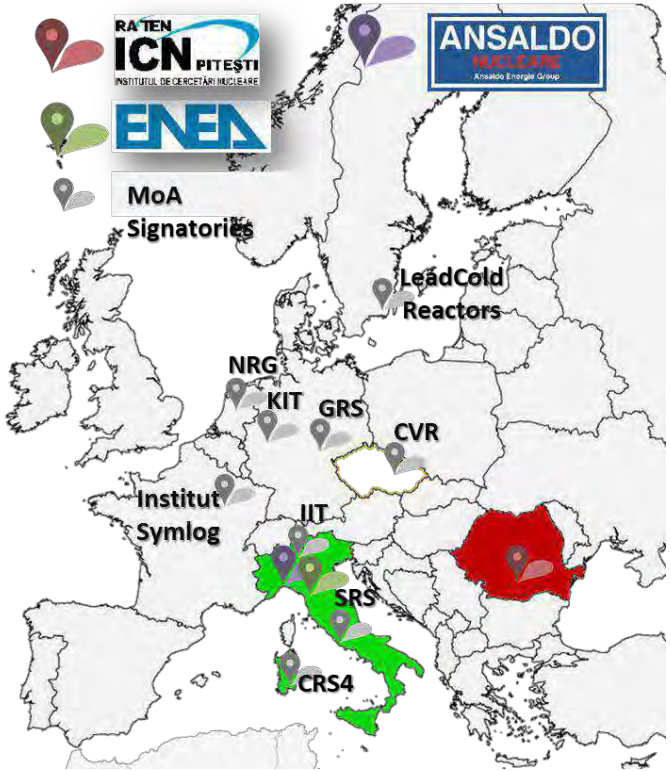

Final Remarks

- Nuclear will play still an important roles in the next years.
- Nuclear energy technology **is among the most reliable and safer technologies**. Nevertheless a in improvement is required about:
  - **Safety**
  - **Waste**
  - **Economy**
- Gen-IV reactors have been conceived to match these goals. Among the others, **Lead cooled Fast Reactors** seems to be the most promising! (but R&D needs are not negligible…)
- In this context the **Italian contribution is significant worldwide**. ENEA and its industrial partners led the technology development.
- International Context is positive (everyday more!!)

Mariano Tarantino
mariano.tarantino@enea.it

DEMO-LFR ALFRED: Technical Overview

Michele Frignani

Project Engineer – Nuclear Technologies and Safety
Member of Expert Board, FALCON Consortium

ALFRED: Design di riferimento Europeo ed Italiano

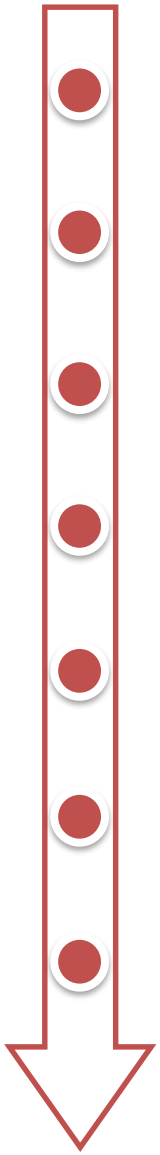

2010 — Fine del progetto **ELSY**: serve un Dimostratore…

2 mesi dopo — KOM di **LEADER**: nasce l'**idea di ALFRED**

2011 — La **Romania** si candida per ospitare ALFRED

2013 — Fine del progetto LEADER: **ALFRED concept**

2 mesi dopo — Firma del Consorzio **FALCON**: inizia la **Technical Review** di ALFRED

2016 — FALCON punta sulle potenzialità di ALFRED come **SMFR**

2017 — ALFRED viene inserito nella **Strategia nazionale** in Romania

Colmare il divario tra aspettative, necessità e risultato

Cosa vorremmo fare…	Cosa promettiamo …	Cosa rischiamo di fare…	Cosa abbiamo…	Cosa dovremmo fare…
		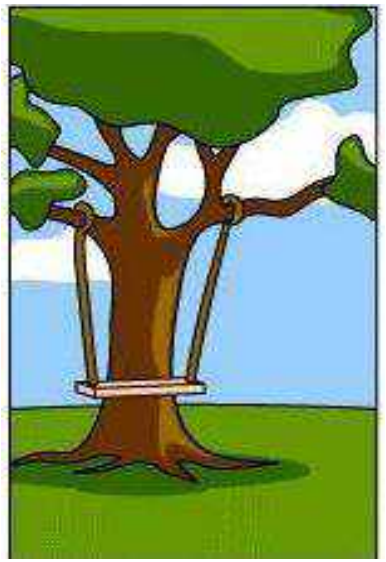	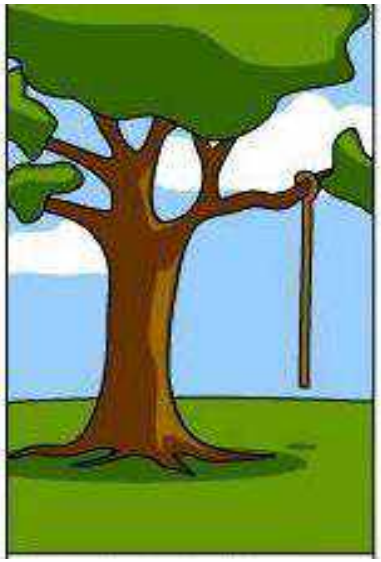	

Dalla dimostrazione alla commercializzazione

Cosa
vorremmo fare…

Cosa
promettiamo…

Cosa
dovremmo fare…

Principali caratteristiche prototipiche

	FOAK	ALFRED (n^{th} stage)	ALFRED (1^{st} stage)
POWER (MWth)	600	300	100
POWER (MWe)	250	125	40
DELTA – T (°C)	120 (400-520)	120 (400-520)	40 (390-430)
Dia. INNER VESSEL (m)	4	3	
Dia. MAIN VESSEL (m)	9 (investigation to decrease)	8	
Height VESSEL (m)	10 (investigation to decrease)	10 (investigation to decrease)	
Volume/Power (m^3/MWe)	2,5	4	12
FUEL	MOX (or UO2 - 19.75% enrichment)	MOX	MOX
CLADDING	15-15 Ti + PLD coating	15-15 Ti + PLD coating	15-15 Ti
FUEL ASSEMBLIES	Hex, wrap, grid, orifice, diagrid, stem		
PRIMARY PUMP	Mechanical, hot leg		
STEAM GENERATOR	Once through		

Dimostratore, Prototipo o entrambi

ALFRED
Advanced Lead-cooled Fast Reactor
European Demonstrator

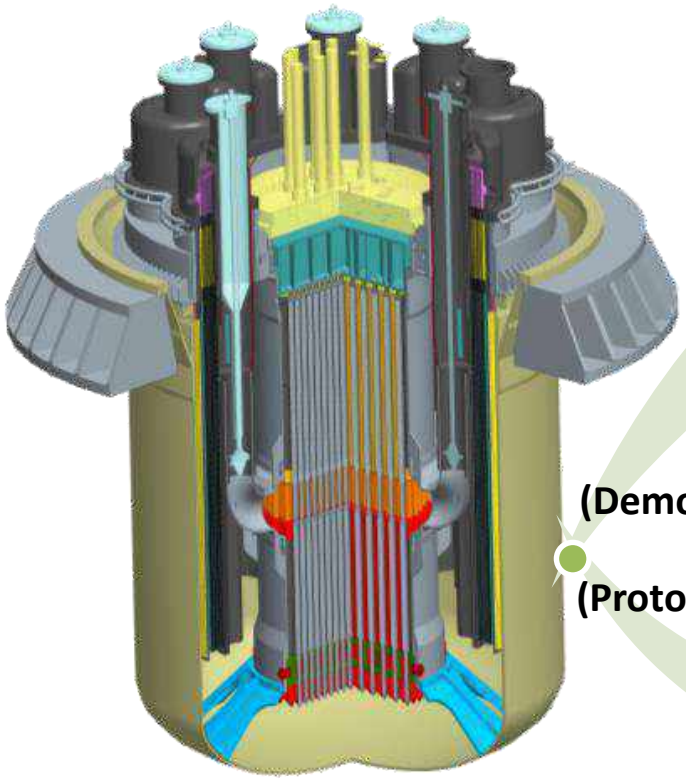

(Demonstrator)

(Prototype)

Pro-LFR
(Prototype)

ELFR
(FOAK)

Commercial Deployment Gen-IV
(European LFR Roadmap)

Anticipated SMFR commercial deployment
(FALCON revised strategy)

ALFRED per risolvere le problematiche

Area	Approccio per affrontare la problematica con il dimostratore
Design	Focalizzato sugli obiettivi di breve termine R&D in parallelo per traguardare il lungo termine
Safety	Potenza ragionevole per dare evidenza della sicurezza della tecnologia e risolvere le incertezze facendo leva sui margini
Licensing	Mezzo per migliorare il regulatory framework da utilizzare per il licensing di reattori commerciali
Operation	Maturare esperienza operazionale Commissioning e operazione a stadi
Financing	Ridurre il tempo necessario per la commercializzazione Rinforzare le sinergie e le opportunità tra pubblico e privato

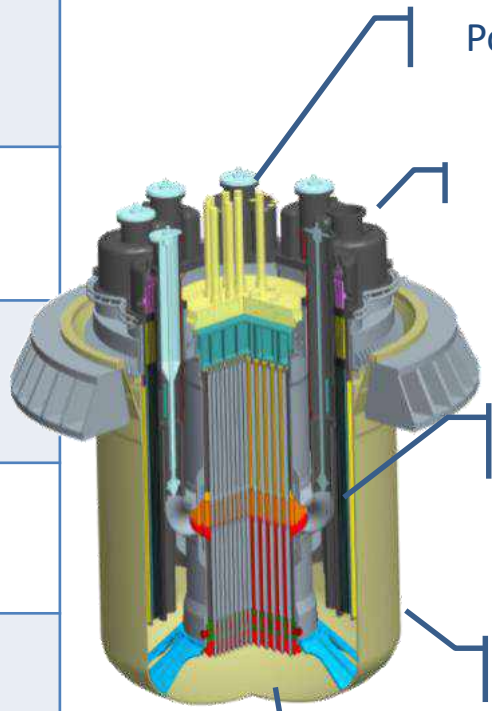

Potenza intermedia

Design compatto
Componenti rimovibili
Tecnologia provata

Semplificazione
Sicurezza passiva

Refrigerato a Pb
Proprietà intrinseche

Configurazione a pool

A volte occorre fermarsi e reindirizzare

Cosa
rischiamo di fare…

Cosa
abbiamo…

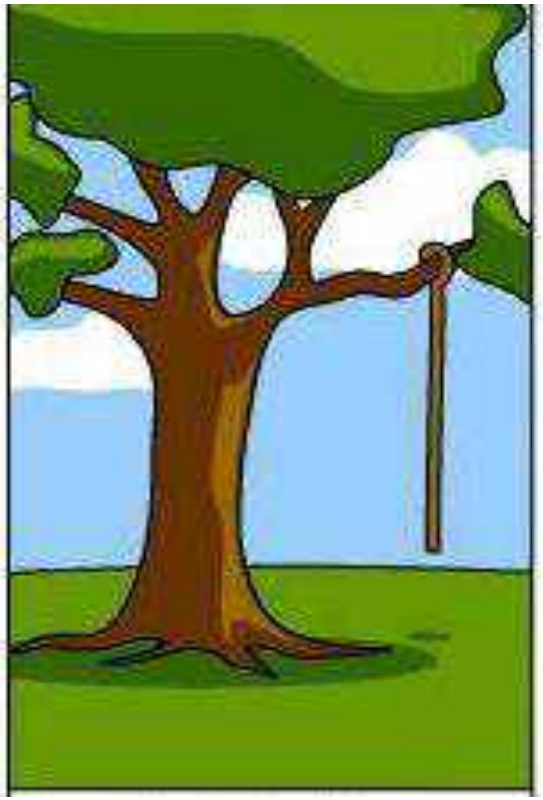

ALFRED Conceptual Design

Configurazione ampiamente analizzata mediante analisi di sicurezza mirate a mostrarne la robustezza

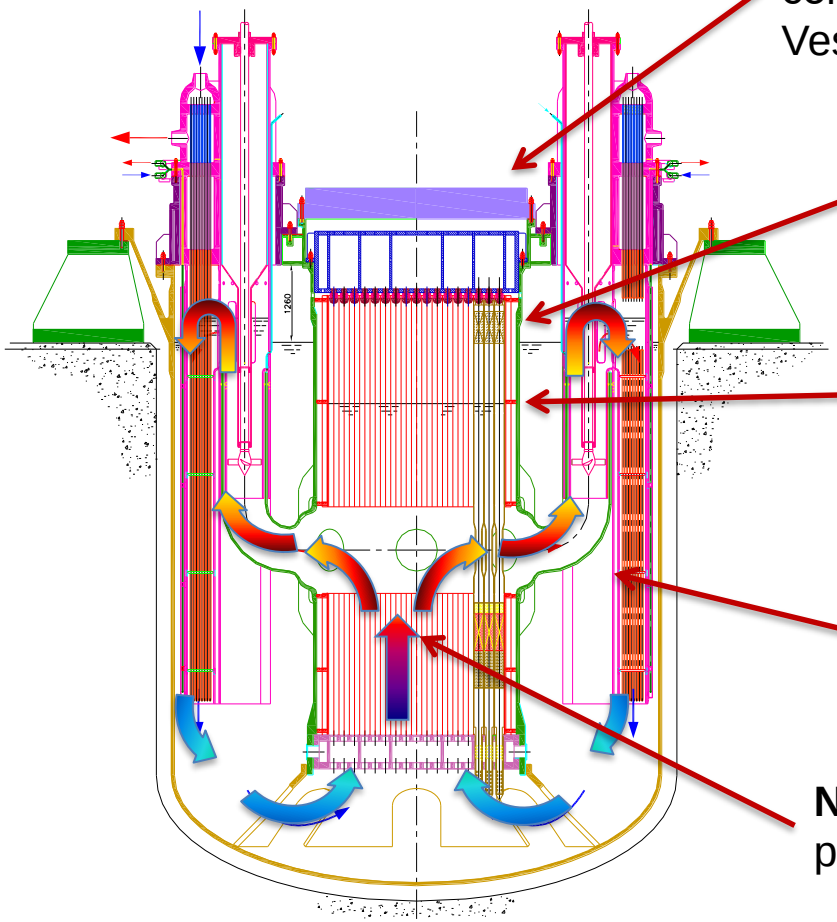

Reattore a pool: design compatto, principali componenti integrati all'interno del Reactor Vessel

Configurazione del Reactor Coolant System: flow-path semplificato ed ottimizzato per la circolazione naturale

Temperatura del refrigerante: temperatura media uscita nocciolo compatibile con i materiali strutturali

Componenti principali: pompe primarie e generatori di vapore integrati con funzione di DHR

Nocciolo: basato sulla esperienza pregressa per quanto possibile

Tipici stadi di progettazione in applicazioni nucleari

Conceptual design

- Assessment of the feasibility of the conceptual solutions (through a minimum set of scoping calculations)
- Development of enveloping safety analysis

L'impianto è descritto chiaramente in tutte le sue parti (sistemi e sotto-sistemi), inclusi i requisiti di design e sicurezza, funzioni, soluzioni di riferimento.

Preliminary (or Basic) design

- Procurement specifications for main Systems, Structures and Components (SSCs).
- Preliminary licensing documents for certification (Preliminary Safety Design Report).
- Itemized cost estimate and master schedule

Il design concettuale viene ulteriormente sviluppato aumentando il livello di dettaglio di tutte le sue parti.

Final (or Detailed) design

- Largely completed design.
- Construction schedule.
- Manufacturing, procurement specifications.
- Inspections, testing and commissioning specifications.
- Finalization of Safety Design Report

Il licensing è uno dei principali rischi da valutare e gestire!

Quando passare da design concettuale a preliminare

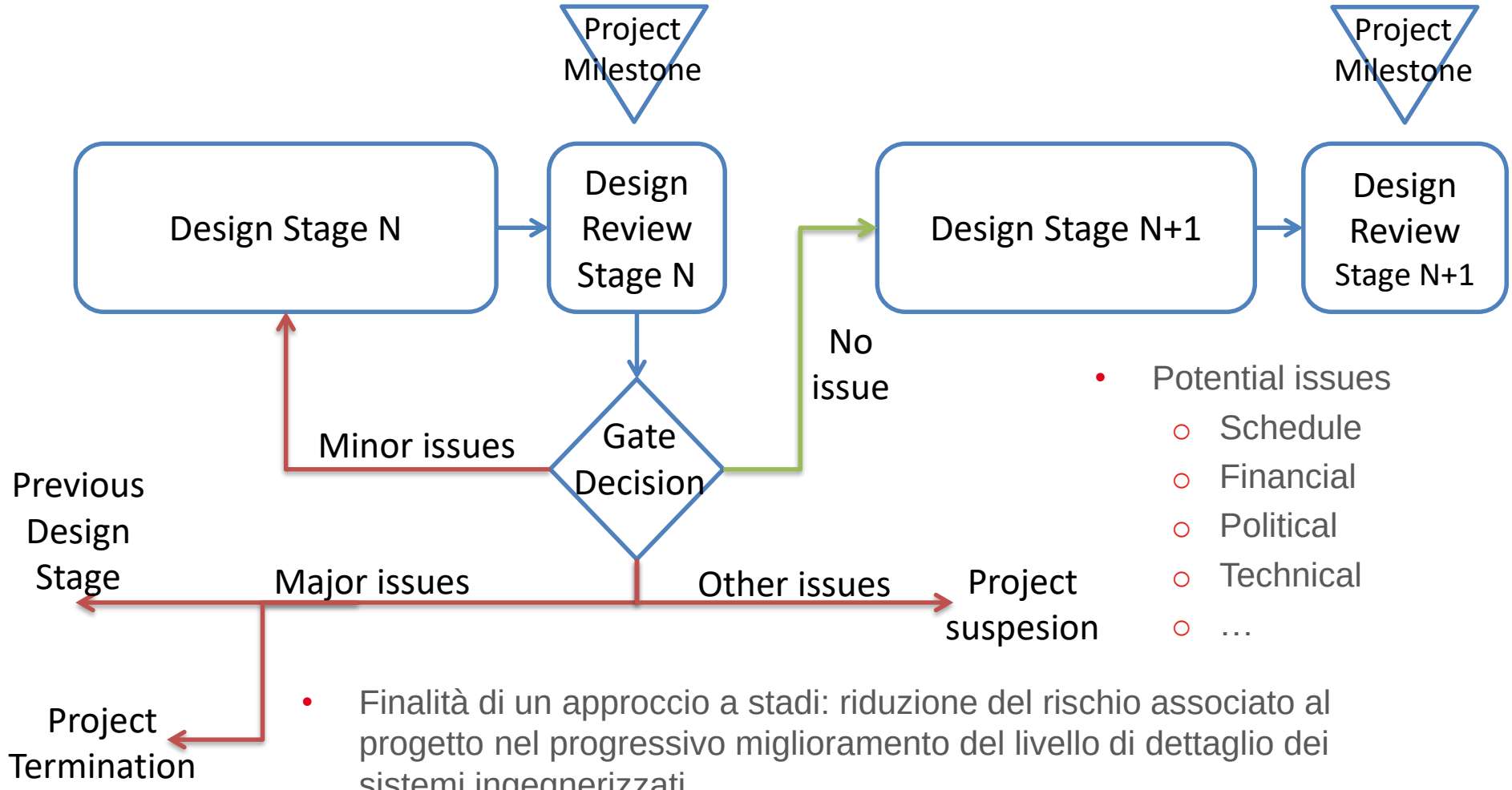

- Potential issues
  - Schedule
  - Financial
  - Political
  - Technical
  - …

- Finalità di un approccio a stadi: riduzione del rischio associato al progetto nel progressivo miglioramento del livello di dettaglio dei sistemi ingegnerizzati.
- Principale ragione: i costi per l'eliminazione di inconsistenze o errori nel design aumentato drammaticamente con il livello di dettaglio raggiunto nella progettazione dei sistemi.

Revisione del design di ALFRED

Sistema a pool fortemente integrato per definizione: sono necessari compromessi non esistendo una buona soluzione di per sé

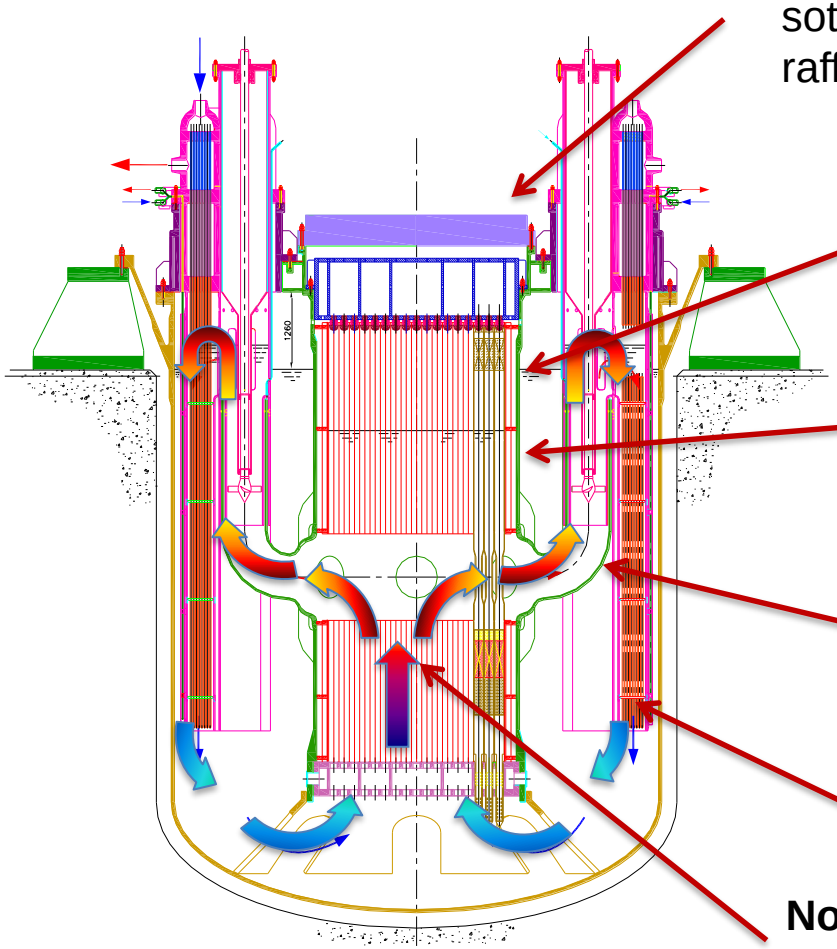

Refueling: fuel assembly da movimentare sotto il pelo libero del piombo per assicurare il raffreddamento passivo in caso di incidente

Configurazione del Reactor Coolant System: afflitta da rischi termo-idraulici tipici del reattori veloci

Temperatura del refrigerante: incompatibile con il cladding hot-spot comprese le incertezze

Componenti principali: affetti da vulnus di fabbricabilità, ispezionabilità, performance

DHR: sistema non sufficientemente diversificato

Nocciolo: da ottimizzare ed equipaggiare con un canale caldo per la qualifica di stadi futuri

Valorizzare il pregresso pensando al futuro

Cosa
abbiamo…

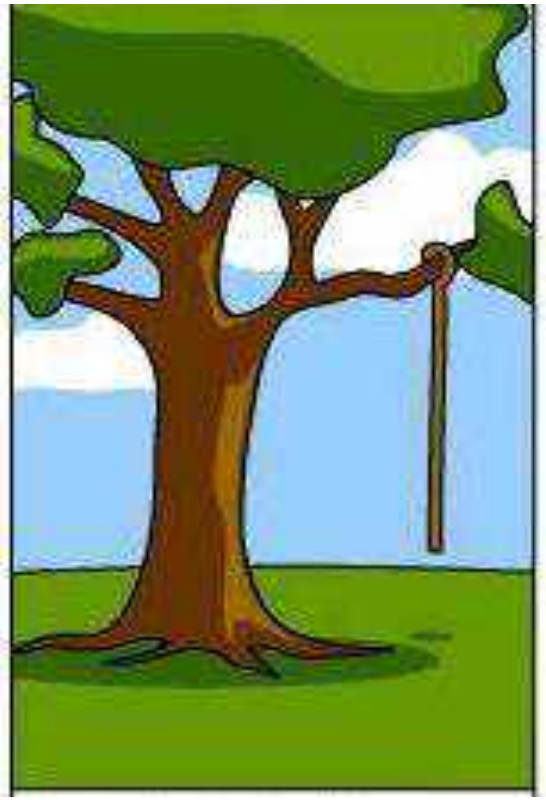

Cosa
dovremmo fare…

Derivazione sistematica di criteri e requisiti

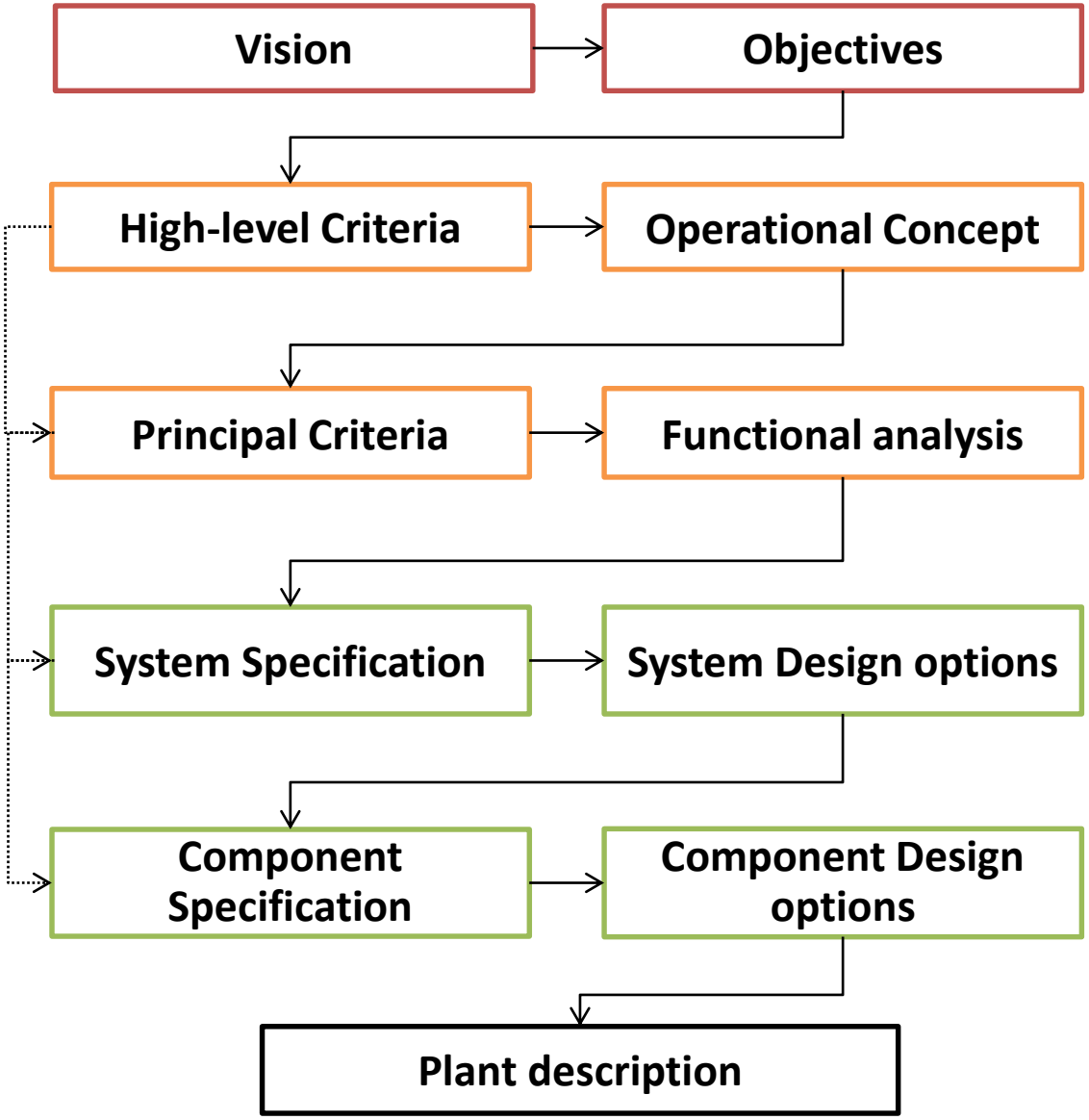

ALFRED: i nuovi Obiettivi

- Deve fornire una **dimostrazione** robusta della operazione in **sicurezza** di un LFR in ogni condizione
- Deve consentire un **licensing** in accordo con **standard internazionali**, facendo leva sulle caratteristiche di dimostratore (**elevati margini**, sistemi di sicurezza)
- Deve permettere la **verifica** dei principali parametri progettuali, consentendo di **acquisire esperienza** per **ridurre le incertezze** per futuri LFR
- Deve garantire l'**estrapolabilità** del concetto (principali componenti) su **scala industriale**
- Deve fornire la possibilità di **testare** nuovi combustibili, materiali e componenti
- Deve consentire di supportare la **dimostrazione di sicurezza e sostenibilità** per futuri LFR commerciali
- Deve permettere il **training** di personale di organizzazioni interessate

Contributo dal basso grazie alle soluzioni esaminate

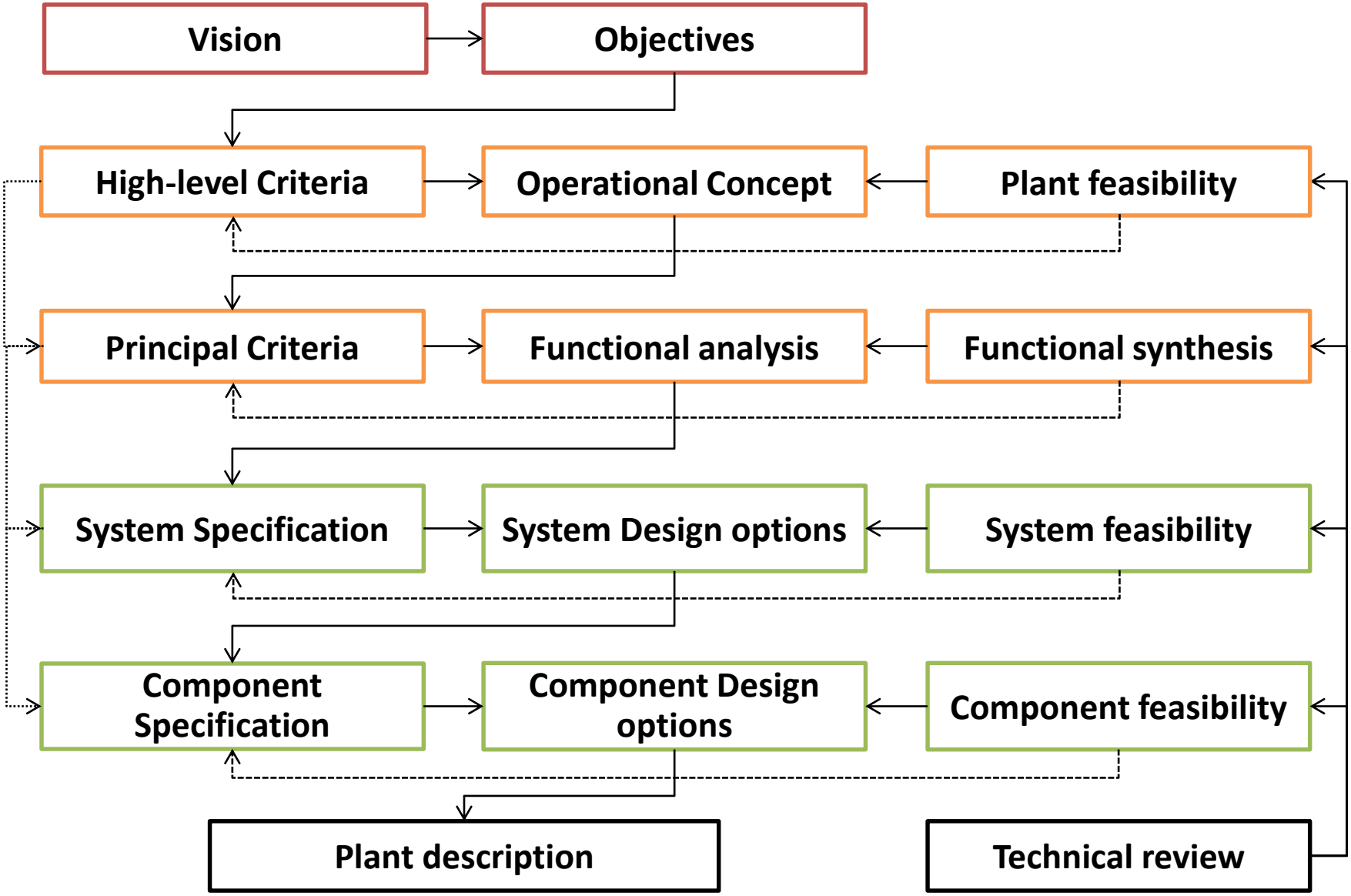

Aree migliorate

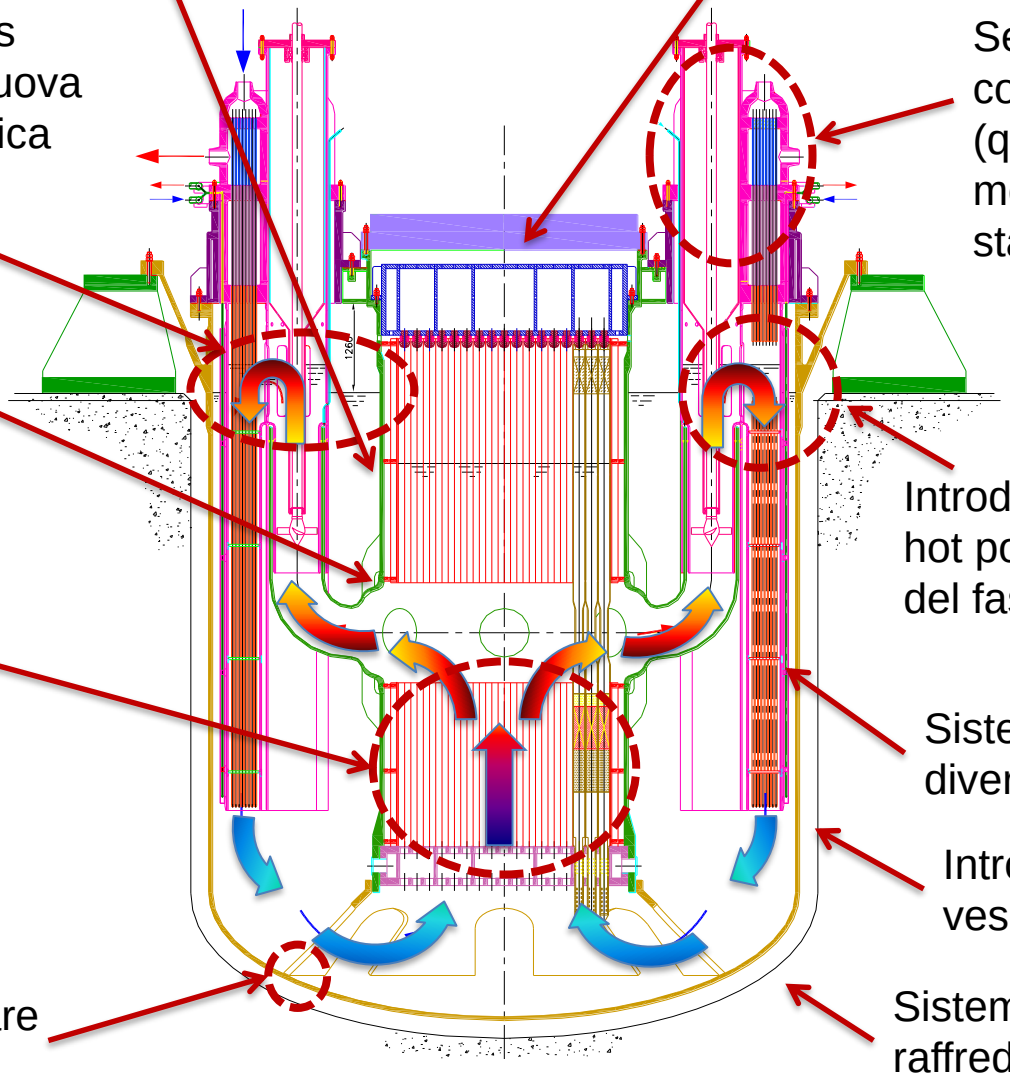

Inner Vessel reso estraibile

Refueling strategy

Stratificazione termica e gas entrainment eliminati con nuova configurazione termo-idraulica

Separazione dei componenti (qualifica meccanica, standardizzazione)

Funzioni di sicurezza delle strutture interne separate

Introduzione di una hot pool (bagnabilità del fascio tubiero)

Ottimizzazione ed ingegnerizzazione del core

Sistemi DHR diversificati

Introdotto un safety vessel

Radial restraint ripensato per evitare ispezioni

Sistema passivo di raffreddamento della cavity

Aree da migliorare

Analisi termoidrauliche di sistema (circolazione naturale)
Analisi CFD (thermal striping, gas entrainment, free level fluctuation,…)

Fuel handling system

Ottimizzazione del Reactor cover (layout, mechanical design)

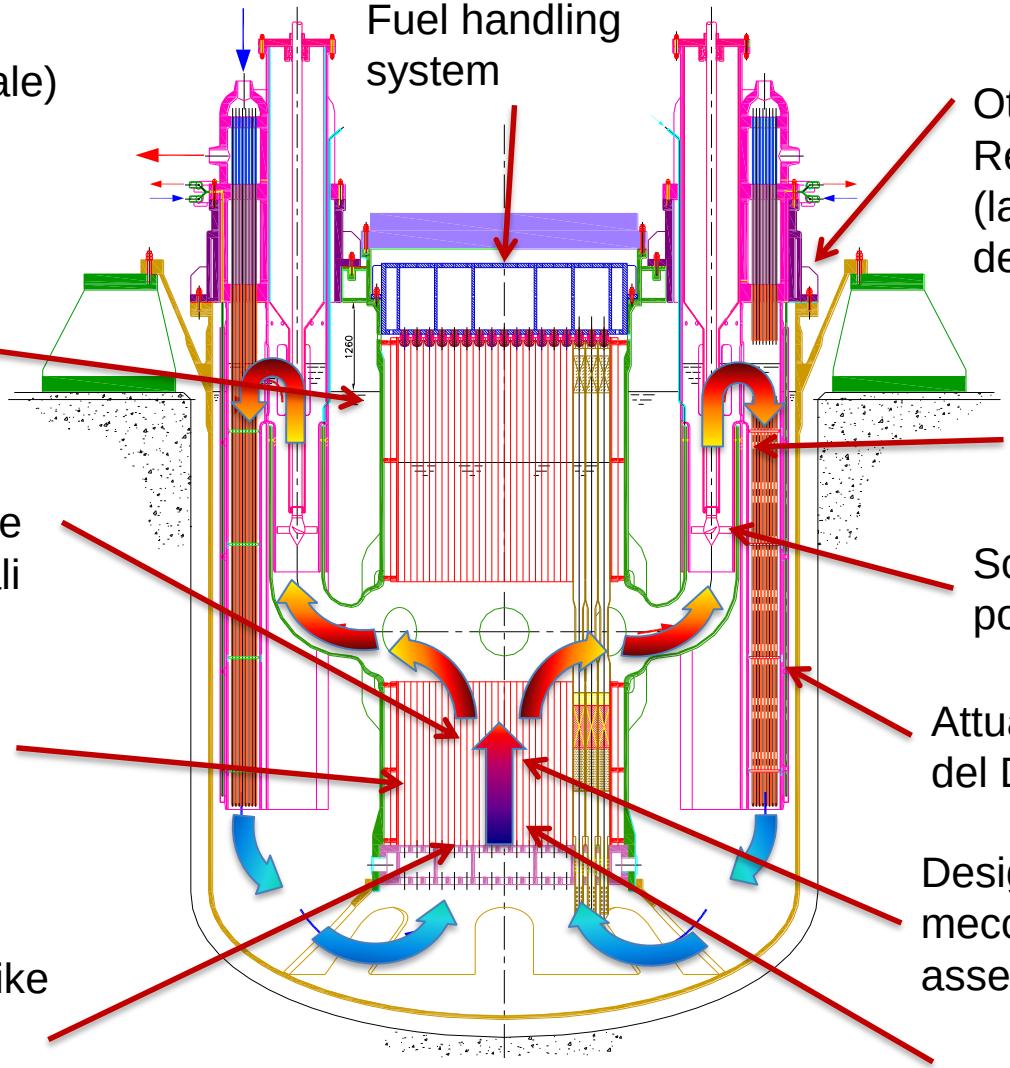

Ottimizzazione o ridefinizione dello SG

Condizioni operative (massima temperatura) e compatibilità coi materiali

Scalatura della pompa primaria

Introduzione di un sistema di spegnimento passivo

Attuazione passiva del DHR2

Design termo-meccanico del fuel assembly

Ottimizzazione dello spike del fuel assembly

Qualifica del fuel assembly (grid spaced)

Staged operation

Stages of operation:

- 1st – Qualification of PLD coating
- 2nd – Operation with PLD coated FAs
- Final – Operation at reference temperature for commercial reactor

	Thermal power (MW)	Core inlet temperature (°C)	Core outlet temperature (°C)	Temperature variation (°C)	Mass flow rate @avg. Temp. (kg/s)	Volum. flow rate (m^3/s)
ALFRED - LEADER	300	400	480	80	25177,2	2,4
ALFRED - 1st stage	101	390	430	40	16845,7	1,6
ALFRED - 2nd stage	201	400	480	80	16845,7	1,6
ALFRED - Final	300	400	520	120	16845,7	1,6

Lead density: ~10500 kg/m3
Lead specific heat capacity: ~150 J/kgK

Impact of temperature (1st stage)

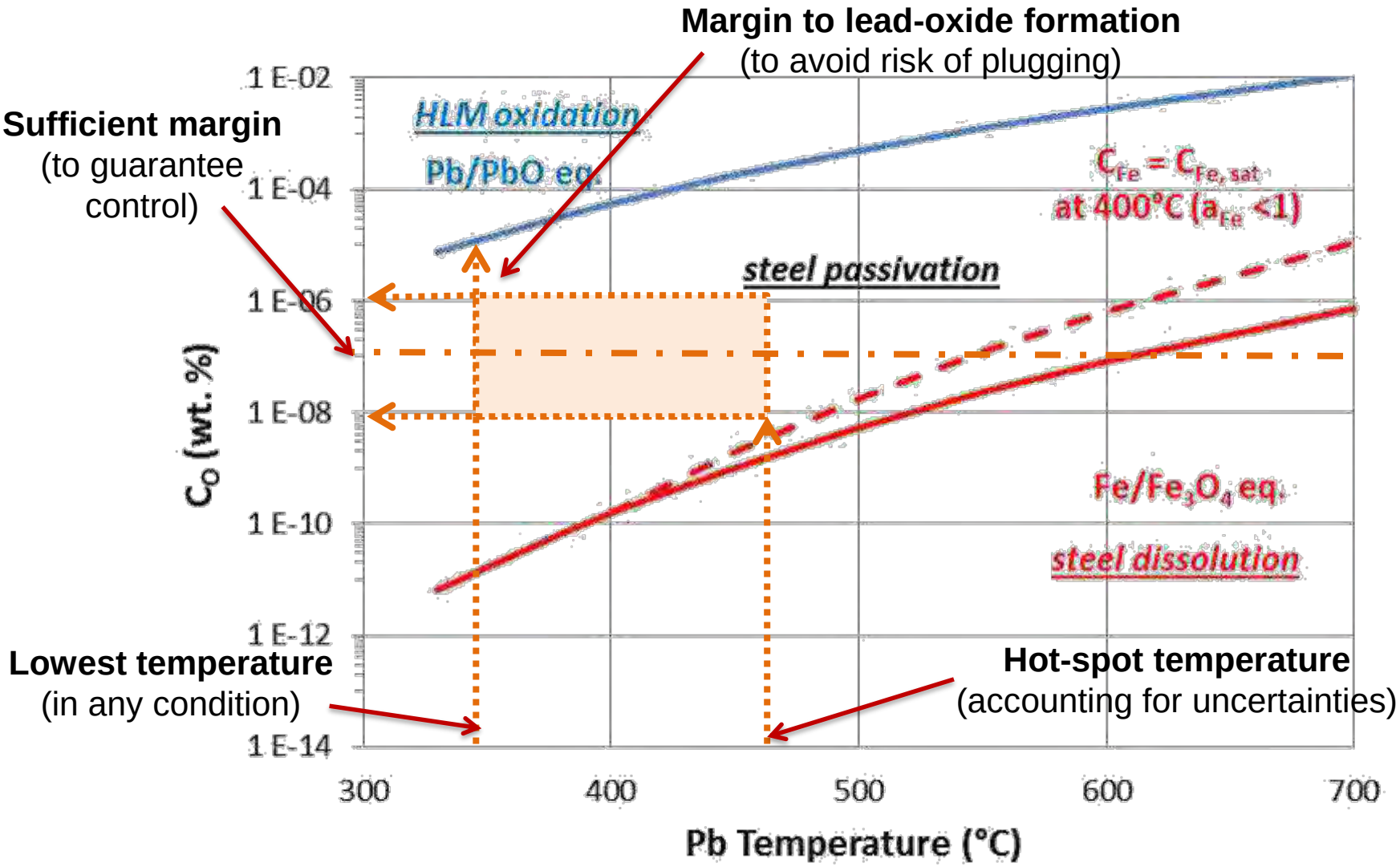

Impact of temperature (final stage)

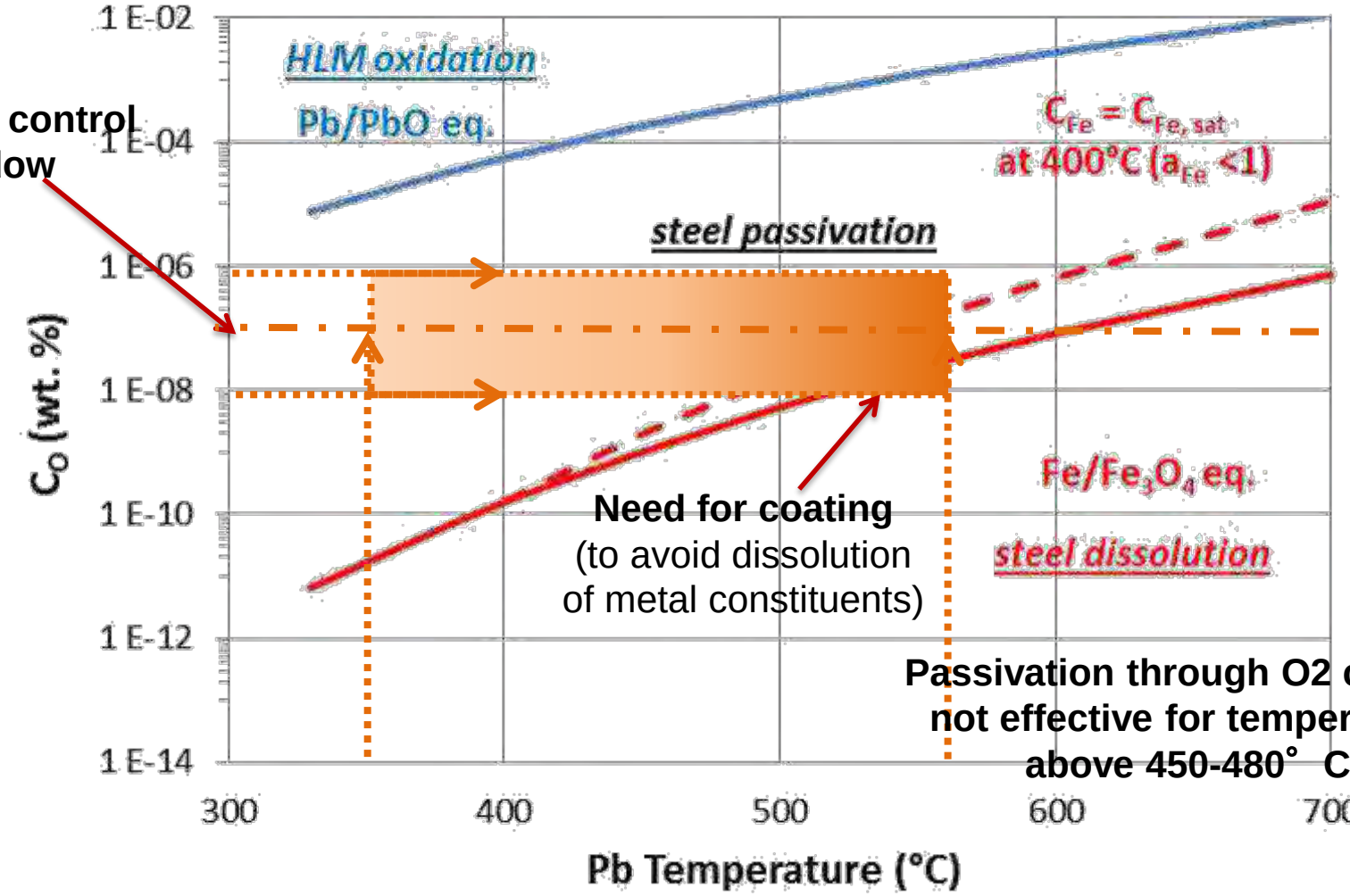

Conciliare breve termine con lungo termine

- Strategia per lo **short-term**
  - Definire un design consistente ed un piano sistematico di R&D
  - Adeguare la potenza del reattore per mantenere ridotte dimensioni
  - Concentrarsi su materiali esistenti e colmare i gap
  - Esercire il dimostratore a bassa temperatura
  - Utilizzare il dimostratore stesso per qualificare nuovi materiali

- Strategia di **lungo termine**
  - Perseverare sulla qualifica di materiali innovativi e coating
  - Migliorare le prestazioni nel lungo termine
  - Integrare soluzioni ottimizzate grazie alla flessibilità del dimostratore

Scambio continuo tra R&D program e Dimostratore

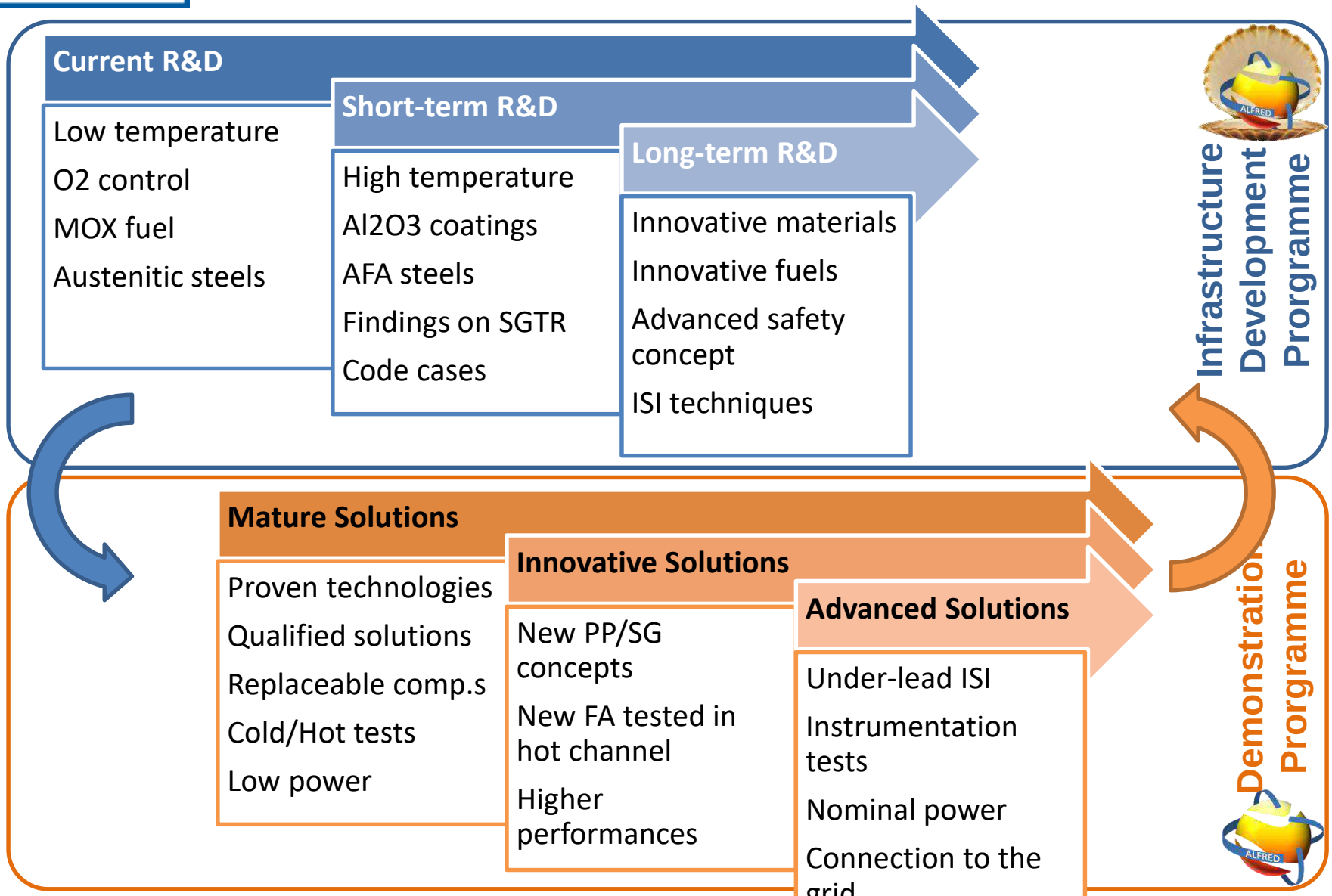

Risultati recenti

Feb 2017	**Strategia Nazionale** per **RDI** e Piano **Nazionale per RDI** (2015-2020)
Mag 2017	Impegno del Primo Ministro per coprire il **20% del costo totale**
Set 2017	Inclusione in **Roadmap Nazionale** per **Infrastrutture di Ricerca** (CRIC)
Gen 2018	**Finanziamenti dedicati** al supporto delle attività **preparatorie**
Feb 2018	**Position Paper** della **Rumenia**

- ESNII Executive Board – 21 Marzo, 2018:
  - Riconosce gli avanzamenti del progetto
  - Riconosce la maggiore maturità raggiunta
  - Sostiene la richiesta FALCON di un maggiore supporto

Il progetto ALFRED è ora incluso nella "fast track" dei dimostratori Europei

Il Consorzio FALCON

- **FALCON** è stato rinnovato nel Novembre 2017
- **Obiettivi principali**:
  - Impegno della Romania a investire in ALFRED come Major Project per il Paese
  - **Finalizzazione** del feasibility study di ALFRED come dimostratore LFR,
  - Inizio della **construzione** di infrastrutture di ricerca e di un Centro di Eccellenza.
- **Full-members:**
  - Ansaldo Nucleare,
  - ENEA,
  - RATEN-ICN
- **Supporting organizations:** in fase di definizione

Principali risultati raggiunti

Governance, Management and Financing

- Nuovo Consortium Agreement (nuovi obiettivi e regole)
- Identificazione di potenziali supporting organizations
- Azioni informative a livello Nazionale ed Europeo

Research, Development and Qualification

- Identificazione di infrastrutture di ricerca chiave e priorità
- Studi di fattibilità e stima dei costi
- Costruzione di facility attingendo a fondi infrastrutturali

Safety, Siting and Licensing

- Dialogo con CNCAN iniziato nel 2017
- Draft del Licensing Basis Documents
- Nuove investigazioni per il sito e consultazioni pubbliche

Engineering, Procurement and Construction

- Review tecnica di ALFRED e selezione delle opzioni di design
- Nuovo approccio per l'aumento progressivo di temperatura
- Identificazione di soluzioni tecniche più robuste

Human resources, Education and Training

- Education program che copra moduli su GenIV and LFR
- CESINA partnership tra istituti del mondo E&T e R&D
- Mobilità e training di ricercatori ICN

Multi-annual Funding Scheme (under discussion)

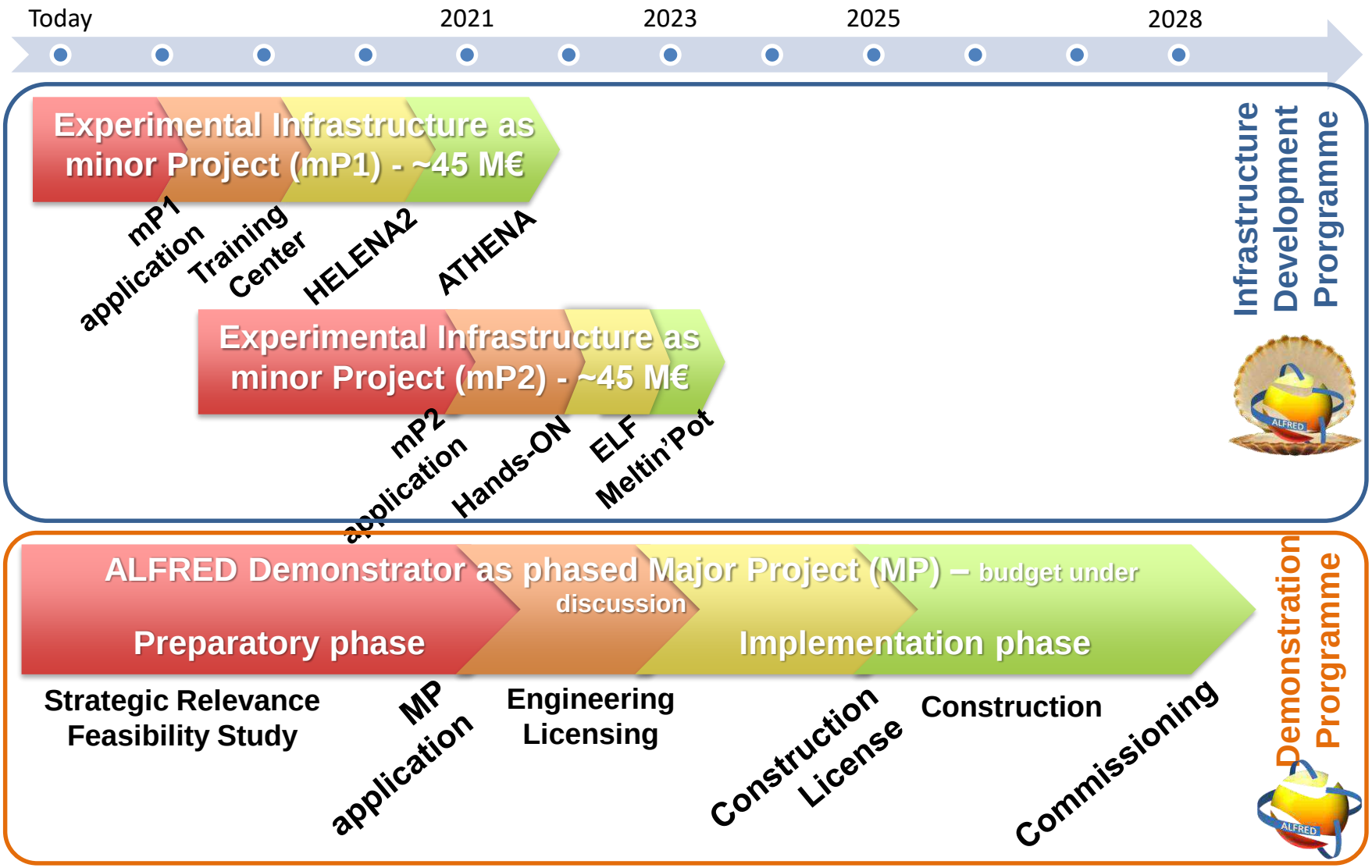

ALFRED come parte di una Infrastruttura di Ricerca

CIRCE – large pool, assisted/force circ., int. test
LIFUS5 – small pool, stagnant, lead-water int. (high p)
HELENA1 – loop, forced circ., bundle exp.
LECOR – loop, forced circ., corrosion exp.
NACIE-UP – loop, nat. circ., bundle exp.
PLACE – large plant, controlled env., comp. cleaning
RACHEL – 10 capsules, stagnant, chemistry exp.
TAPIRO – 0-pwr reactor, propagation and calibration
SOLIDX – small vessel, stagnant, freez/melt exp.
BID1 – small pool, stagnant/mixed, O2 control exp.

HELENA2 – loop, forced circ., full-scale FA qual.
ATHENA – large pool, forced circ., comp. qual., SGTR
ChemLab – capsules/loop, stagant/flowing, chem ctrl
ELF – large pool, forced circ., integral and endurance
Hands-ON – vessel with core mock-up, handling sys
Meltin'Pot – vessels and loop, fuel/coolant int.
Lead School – E&T facilities, supercomp., conf. center

Viability | Preparation | Construction | Commissioning | Operation

9 Obiettivi scientifici

- **Material** science for qualified solutions
- **HLMs** physical-chemical properties
- HLMs as coolants in **practical applications**
- **Solutions and provisions** to exploit HLMs
- **Characterization** of concepts
- **Qualification** of prototypical SSCs
- **Integral tests** for NESs
- **Viability** of LFR concept
- **Safe and sustainable** operation of future LFRs

Come superare la valle della morte

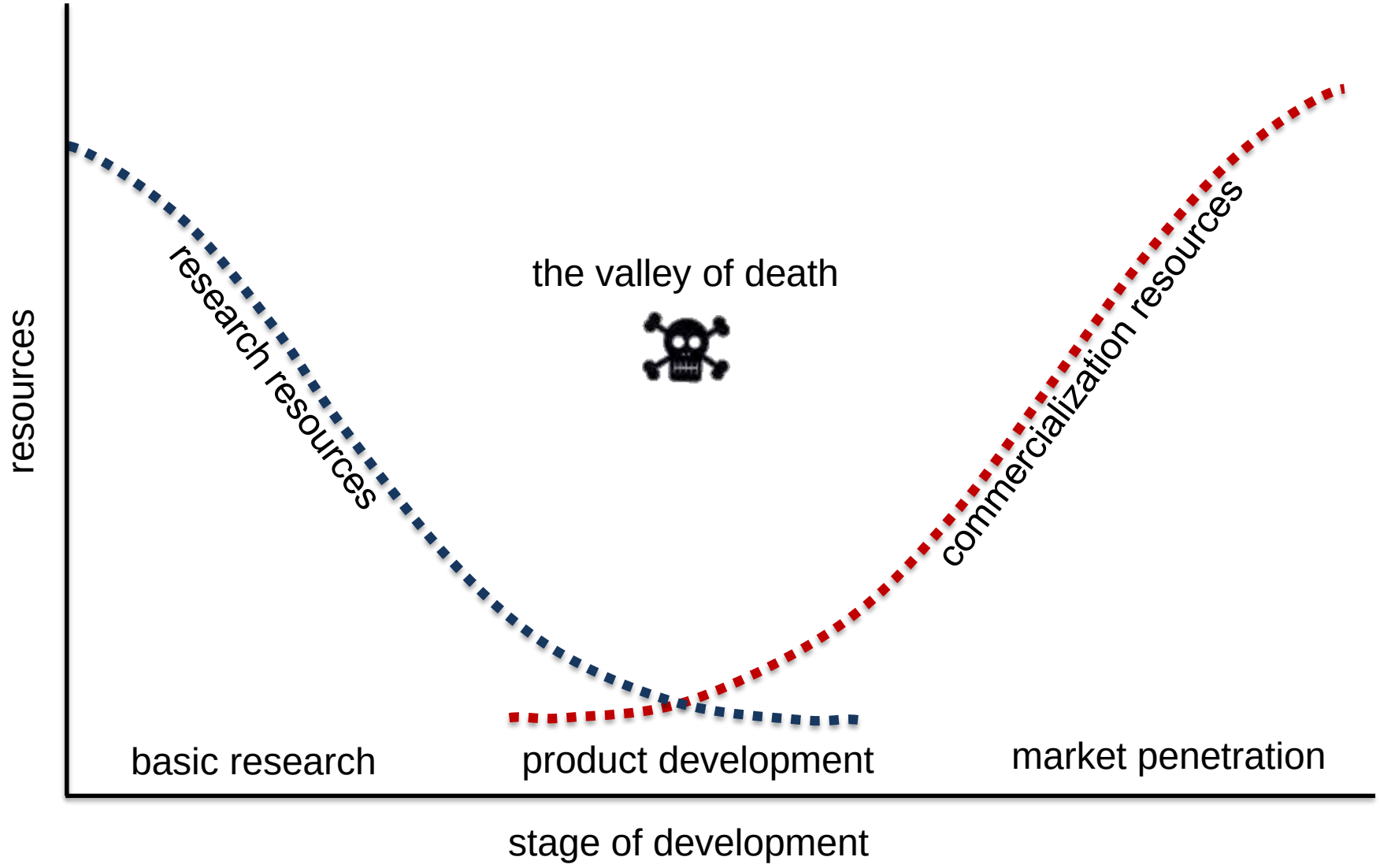

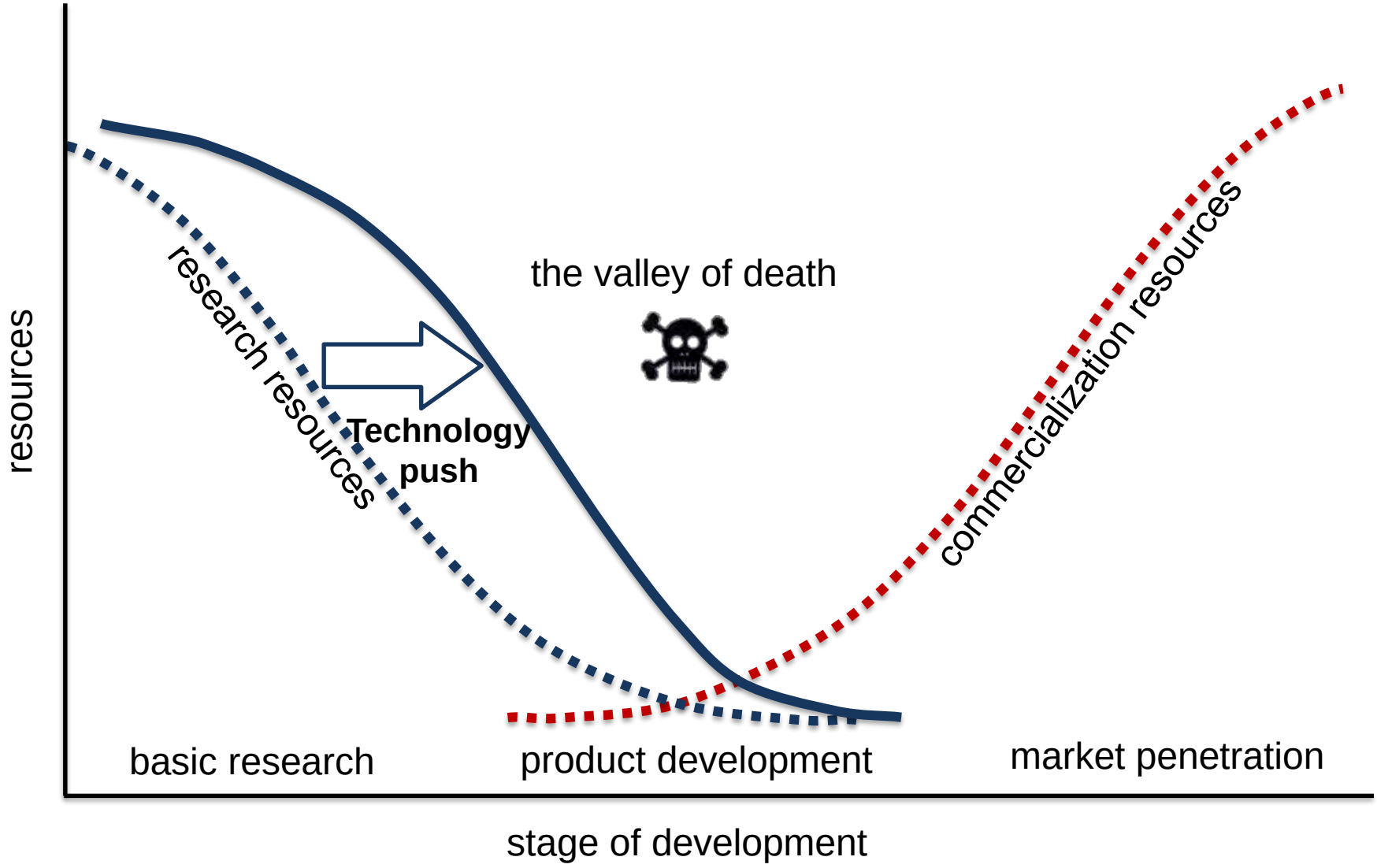
resources
research resources
the valley of death
Technology push
commercialization resources
basic research
product development
market penetration
stage of development

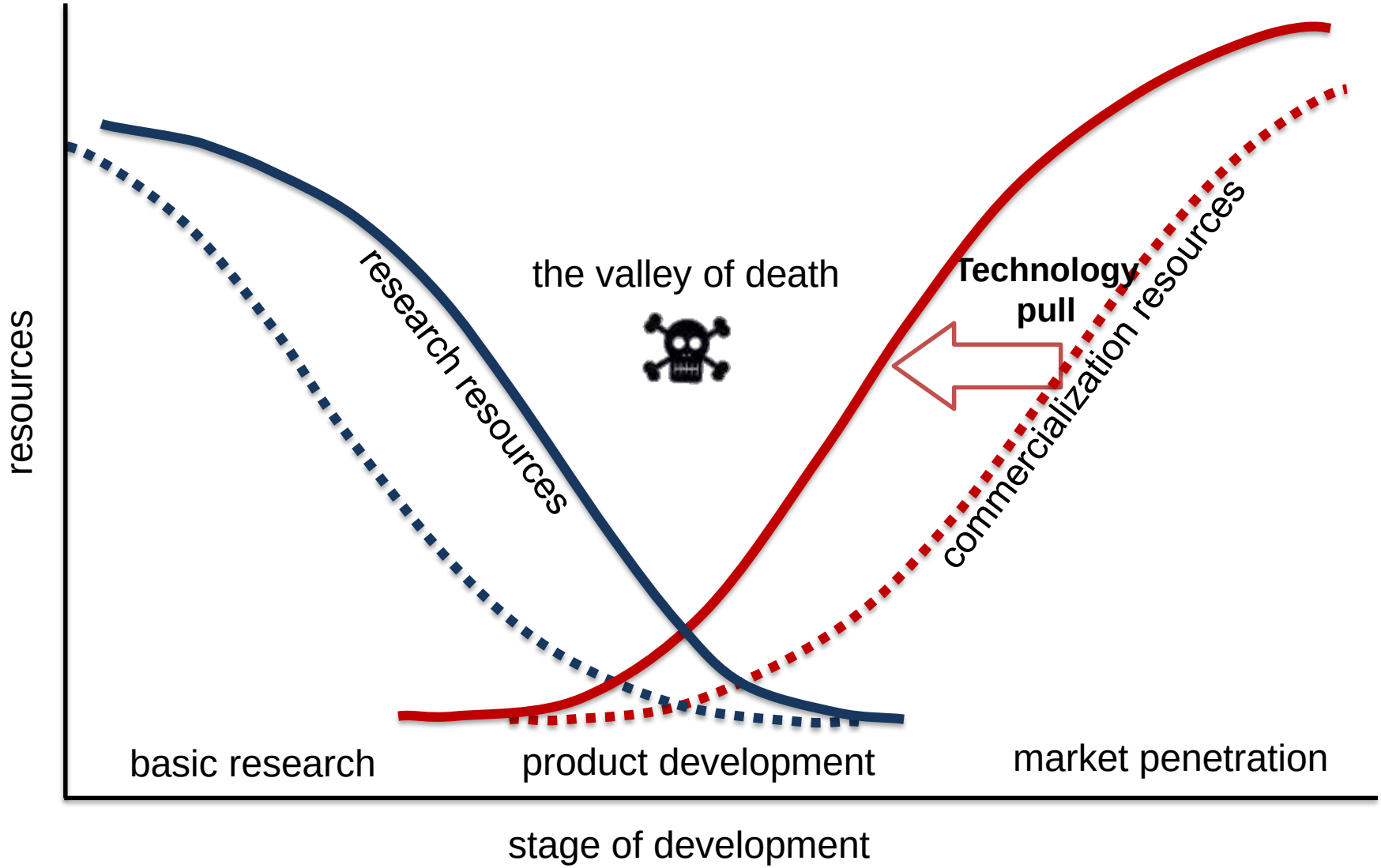
resources
research resources
the valley of death
Technology pull
commercialization resources
basic research
product development
market penetration
stage of development

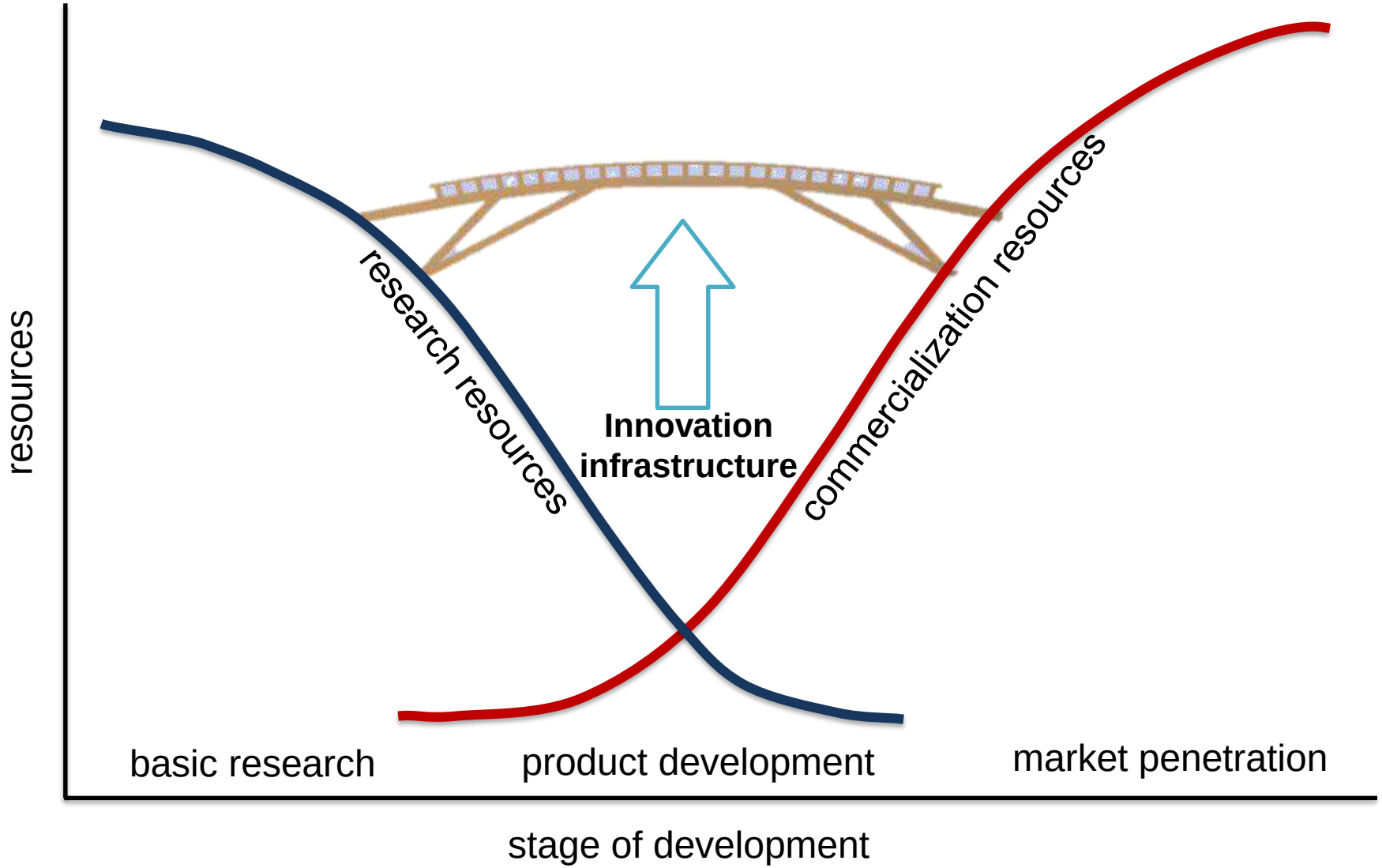
resources
research resources
Innovation infrastructure
commercialization resources
basic research
product development
market penetration
stage of development

Temi di collaborazione tra ricerca e industria

- Temi di interesse trasversale
  - Strumentazione e logica di controllo
  - Strategia di confinamento
  - Gestione degli incidenti severi (difficili da escludere per un dimostratore)
  - Strategie di ispezione, manutenzione, refueling
  - Analisi termo-idrauliche di performance e di sicurezza
  - Analisi CFD delle fenomenologie termo-idrauliche

- Piano sistematico di R&D
  - Test per colmare i gap dei codes & standards applicabili
  - Perseverare sulla qualifica di materiali innovativi e coating
  - Qualifica di componenti prototipici
  - Sviluppo di nuovi codici per assistere la progettazione
  - Verifica e validazione di codici di calcolo

Grazie per l'attenzione

www.alfred-reactor.eu

Italian National Agency for New Technologies,
Energy and Sustainable Economic Development

[1-1] Development of best estimate numerical tools for LFR design and safety analysis

WORKSHOP TEMATICO – AdP MISE – ENEA, PAR2017 –B.3 - LP2
DIAEE- Università di Roma "La Sapienza" - San Pietro in Vincoli, Via Eudossiana 18, Roma
14 Giugno 2018

Alessandro Del Nevo – ENEA FSN-ING-PAN

Introductory remarks

AdP PAR LP2 (>2012)

Collaborative activity between ENEA-CIRTEN carried out (also) in synergy with EC H2020 Project and Research International Activity (e.g. NEA, IAEA)

- A.2 Progettazione nocciolo
- A.3 Analisi di sicurezza
- C. Termoidraulica (parzialmente)

Development and validation of codes and multi-physics models for the design and the safety analysis of Gen. IV fast reactors

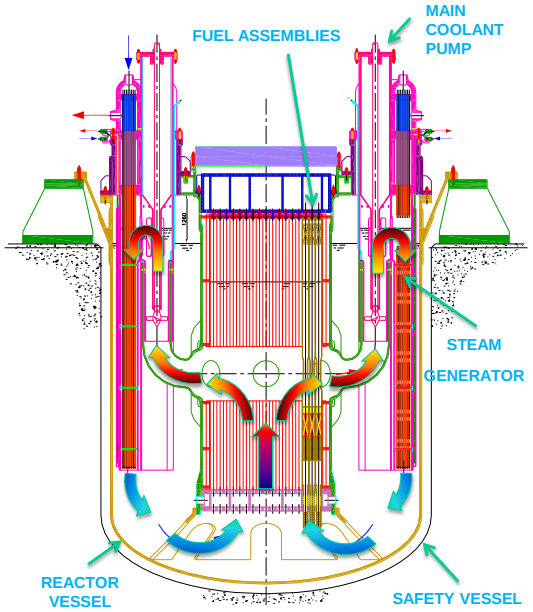

- *Power: 300 MWth (125 MWe)*
- *Prim. cycle:Molten Lead 400-480* °C
- *Sec. cycle: Water/superheated steam:335-450* °C

Strategic objectives of the Task

The Task "***sviluppo e convalida di codici e modelli multi-fisica per progetto e analisi di sicurezza di reattori veloci di IV generazione***" has the following objectives

1. **Collaborazione** tra ENEA-CIRTEN. Attività condotte (anche) in **sinergia con progetti EC e attività di ricerca internazionali (e.g. NEA, IAEA)**

2. **Continuità**. Le attività tecniche dovrebbero essere condotte in continuità con quanto svolto fino ad oggi
   → rendere gradualmente **l'attività coordinata e finalizzata**
   → **no brusche discontinuità** che possano penalizzare know-how acquisiti ed investimenti delle istituzioni coinvolte

3. **Coinvolgimento**. ENEA/Università CIRTEN coinvolte su un **unico progetto dove ognuno contribuisce per l'obiettivo comune**

Progetto di riferimento

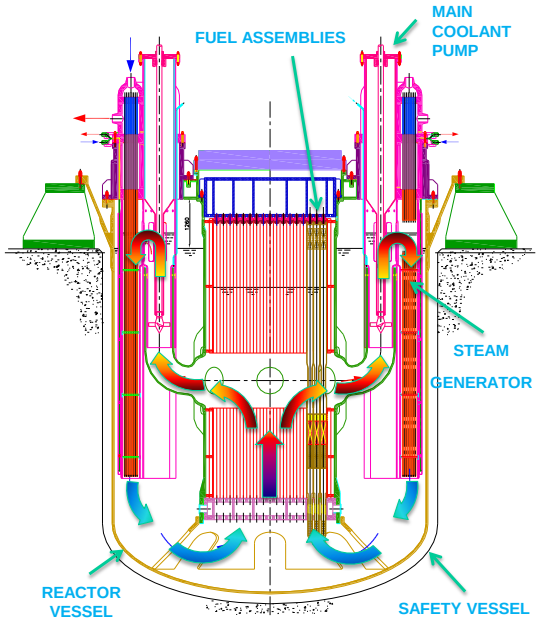

Strategic objectives of the Task and involved Institutions

4. **R&D e qualità**. Attività **orientata allo sviluppo di strumenti di calcolo, integrazione degli stessi, identificazione delle aree di utilizzo e documentazione, validazione ed applicazione**. **Risultati tangibili**.

5. **ENEA** stakeholder delle attività a supporto delle attività di R&D in corso e della progettazione ed implementazione delle campagne sperimentali al CR Brasimone

CIRTEN - CONSORZIO INTERUNIVERSITARIO PER LA RICERCA TECNOLOGICA NUCLEARE

POLITECNICO MILANO 1863

POLITECNICO DI TORINO

UNIVERSITÀ DI PISA

SAPIENZA UNIVERSITÀ DI ROMA

Design and safety analysis framework

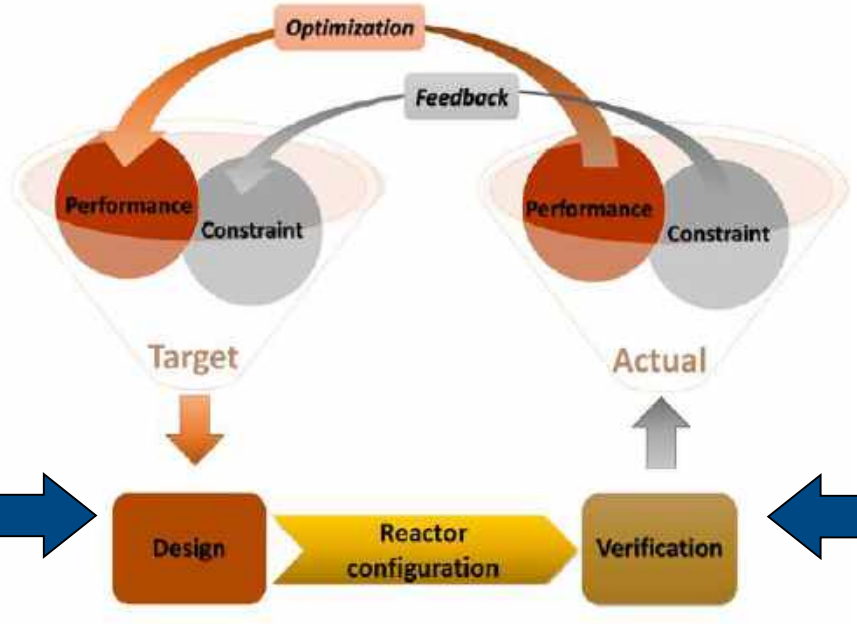

Design rules

Codes and standards

National regulation

Acceptance criteria for each plant conditions

Regulatory framework

Iterative process of reactor configuration development

Specific Objectives of the Task

The objective is to make available numerical tools for supporting the design and the DSA of the LFR

- ❑ Developing and validating new tools
- ❑ Extending the capability and the area of application of existing codes and their validation
- ❑ Setting-up chain of codes and interfaces
- ❑ Developing code coupling techniques

Reactor		Encompassed aspect				
		N	TH	TM	C	E
Sub-system	Core system	×	×	×		
	Primary system		×	×		
	Auxiliary and Ancillary systems		×	×	×	
	Instrumentation and control systems					×
	Reactor (integration)	×	×	×	×	×

Aspects encompassed in the design and verification of main reactor sub-systems

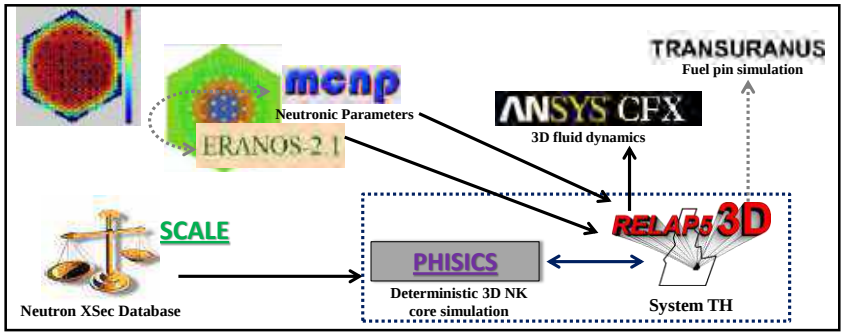

Sample chain of codes set up in the framework of IAEA EBR-II benchmark

Computer codes: the relevance of the qualification

- Employed computer codes
  - range from specialized reactor physics codes to coupled codes
  - provide “Best Estimate” predictions
  - Require demonstration of qualification
- The level of qualification
  - depends by the availability of experimental data or NPP data, and the extent of independent assessment → *Experimental data are fundamental for supporting the development and demonstrating the reliability of computer codes in simulating the behavior of an NPP during a postulated accident scenario: in general, this is a regulatory requirement*
  - is strictly related to the user → *The user always has the responsibility of the appropriate use of such codes.*

Computer codes: the relevance of the qualification

Identified categories of codes

- ❑ Core physics codes
- ❑ Component specific or phenomenon specific codes
  - Fuel behaviour codes
  - Sub-channel codes
  - Porous media codes
  - Containment analysis codes, with features for the transport of radioactive materials
  - Atmospheric dispersion and dose codes
- ❑ Structural analysis codes
- ❑ System thermo-hydraulic codes
- ❑ CFD
- ❑ Coupled codes

Validation and verification are essential steps in qualifying any computational method and are the primary means of assessing the accuracy of computational simulations

Overview of the R&D efforts in AdP2015-2017

	Core Physics						Component specific or phenomenon specific								System			
	X-sec generation	Reactor Physics	Burn-up Calculation	3D NK	3D NK	Shielding	FPC	TH lumped parameters	CFD			Fission product dispersion & dose	TM	Material molecular dynamics	SYS-TH	SYS-TH	SYS-TH	SA
pellet	SERPENT	SERPENT	SERPENT				Transuranus								RELAP5-3D	RELAP5/Mod3.3	CATHARE2	SIMMER
gap																		
cladding									COMSOL	FEM-LCORE	FLUENT							
subchannel							1-2											
fuel assembly																		
core				FRENETIC	SIMMER			FRENETIC										
coolant												SIMMER		CALPHAD				
primary system																		
secondary system																		
containemnt																		
I&C																		
site																		

Design and Licensing

Design (including safety analysis)

Code Coupling ⟷

Chain of Code ⋯→

Uncertainty

Fuel Performance Code [1-2]

Development/assessment of models describing the inert gas behavior in the fuel for application to the TRANSURANUS fuel pin thermo-mechanical code

Main Results

1. Development of new **correlations for Helium diffusivity**
2. Development of a new **model for High Burn-up Structure porosity evolution**

Future developments

- Development of new **correlations for Helium solubility**
- Development of **dedicated numerical algorithms**
- Fuel rod integral analysis in support of design of FRs using the improved version of TRANSURANUS fuel pin thermo-mechanical code

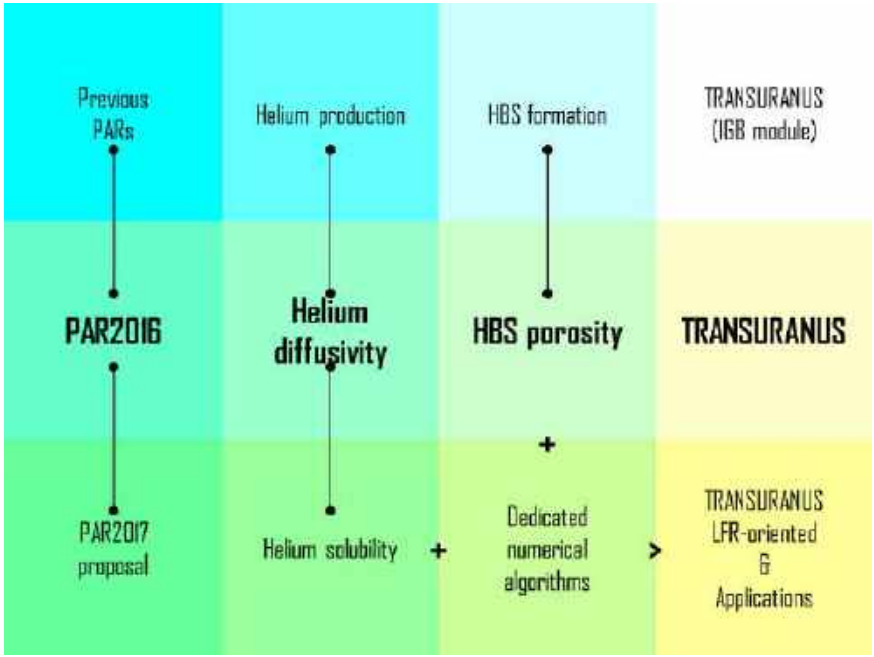

Improvements of TRANSURANUS code models in AdP PAR-2016

Overview of the R&D efforts in AdP2015-2017

	Core Physics						Component specific or phenomenon specific								System			
	X-sec generation	Reactor Physics	Burn-up Calculation	3D NK	3D NK	Shielding	FPC	TH lumped parameters	CFD			Fission product dispersion & dose	TM	Material molecular dynamics	SYS-TH	SYS-TH	SYS-TH	SA
pellet	SERPENT	SERPENT	SERPENT				Transuranus								RELAP5-3D	RELAP5/Mod3.3	CATHARE2	SIMMER
gap																		
cladding																		
subchannel																		
fuel assembly														1-3				
core				FRENETIC	SIMMER			FRENETIC	COMSOL	FEM-LCORE	FLUENT							
coolant												SIMMER		CALPHAD				
primary system																		
secondary system																		
containemnt																		
I&C																		
site																		

Design and Licensing

Design (including safety analysis)

Code Coupling ⟷

Chain of Code ⇢

Uncertainty

Fuel-coolant chemical interactions [1-3]

Fuel-coolant chemical interactions

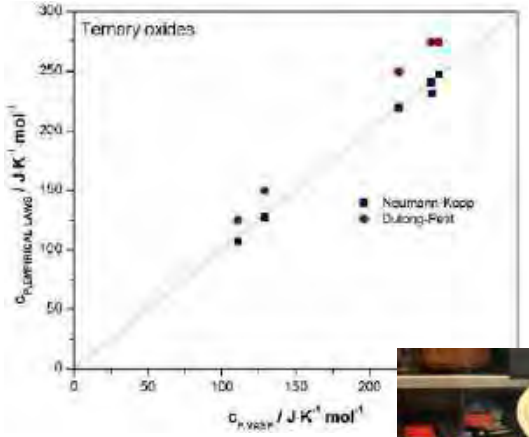

Computational activities:

- Evaluation of thermodynamic properties for ternary oxides (An/FPs – O – Pb) by DFT approach
- Investigations on computational thermodynamics by CALPHAD method

Experimental activities

- Interaction studies on different oxide-Pb systems:
  - Preliminary characterization of reagents by XRD, DSC and EDX
  - Preparation of pellets of SrO, ZrO_2, La_2O_3 and CeO_2
  - Thermal treatment at 500-550°C under argon atmosphere
  - Reaction time of 3-7 hours
- Post-treatment characterization:
  - Identification of new phases by XRD on powder or pellet
  - Thermal analyses on powder by DSC
  - ICP-MS measurements of Pb
  - Investigations on pellet cross section by SEM-EDS
    - Sample preparation under evaluation

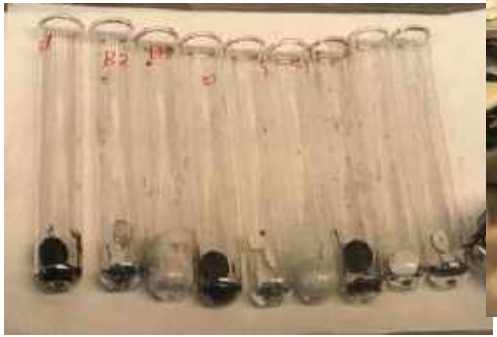

Overview of the R&D efforts in AdP2015-2017

	Core Physics						Component specific or phenomenon specific							System			
	X-sec generation	Reactor Physics	Burn-up Calculation	3D NK	3D NK	Shielding	FPC	TH lumped parameters	CFD			Fission product dispersion & dose	TM	Material molecular dynamics	SYS-TH	SYS-TH	SYS-TH	SA
pellet	SERPENT	SERPENT	SERPENT				Transuranus								RELAP5-3D	RELAP5/Mod3.3	CATHARE2	SIMMER
gap																		
cladding																		
subchannel																		
fuel assembly		1-4							COMSOL	FEM-LCORE	FLUENT							
core				FRENETIC	SIMMER			FRENETIC										
coolant									1-4			SIMMER		CALPHAD				
primary system																		
secondary system																		
containemnt																		
I&C																		
site																		

Design and Licensing

Design (including safety analysis)

Code Coupling ⟷

Chain of Code ⋯→

Uncertainty

Multi-physics code for LFR [1-4]

Implicit multi-physics approach for studying the LFR single-channel (average conditions)

Multiphysics for:
. **Deeper** physics insight
. **Better** reactor paramter **evaluation**
. **Verification** of operational constraint
. **Combined analysis** with system codes

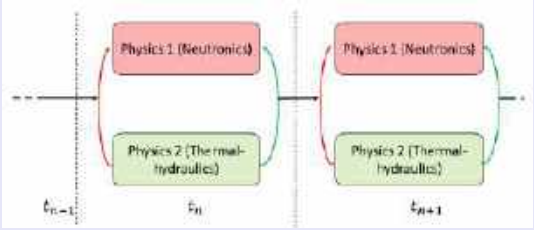

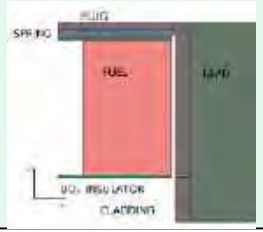

LFR single-channel test – COMSOL tool

Physics	Modelling approach
Neutornics	Multi-group neutron diffusion
Thermal-hydraulics	CFD
Mechanics	Linear elasticity

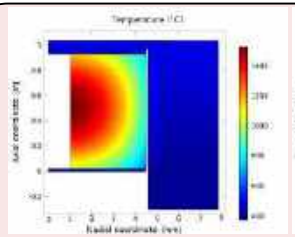

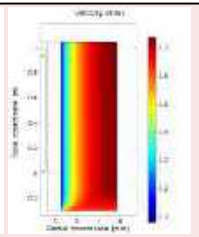

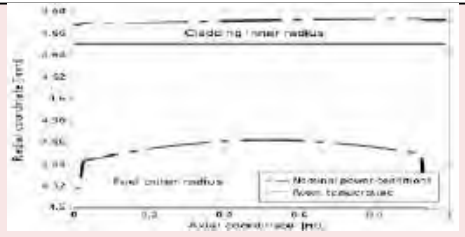

Results and conclusion
. **Good representation** of physical phenomena occurring in the reactor
. **Evaluation** of coupling approaches
. Near-term efforts on **OpenFOAM**

Overview of the R&D efforts in AdP2015-2017

	Core Physics						Component specific or phenomenon specific							System			
	X-sec generation	Reactor Physics	Burn-up Calculation	3D NK	3D NK	Shielding	FPC	TH lumped parameters	CFD			Fission product dispersion & dose	TM	Material molecular dynamics	SYS-TH	SYS-TH	SYS-TH	SA
pellet	SERPENT	SERPENT	SERPENT	1-5			Transuranus	1-5	COMSOL	FEM-LCORE	FLUENT				RELAP5-3D	RELAP5/Mod3.3	CATHARE2	SIMMER
gap																		
cladding																		
subchannel																		
fuel assembly																		
core				FRENETIC	SIMMER			FRENETIC										
coolant												SIMMER		CALPHAD				
primary system																		
secondary system																		
containemnt																		
I&C																		
site																		

Design and Licensing

Design (including safety analysis)

Code Coupling ⟷

Chain of Code ⋯→

Uncertainty

Core TH / NK coupled code FRENETIC [1-5]

R&D on FRENETIC quasi-static time step adaptiveness

- Approach: to monitor and to control the variation of the local error of the shape during the integration algorithm.
- Step size relation $\frac{\Delta t_{\psi,n}}{\Delta t_{\psi,n-1}} = \left(\frac{1}{\hat{r}_n}\right)^{1/(q+1)}$
- Excess local error estimated according to an appropriate definition

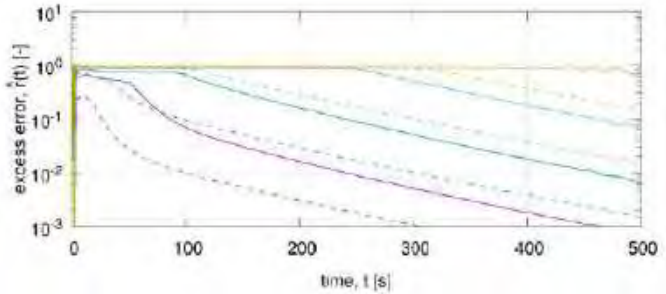

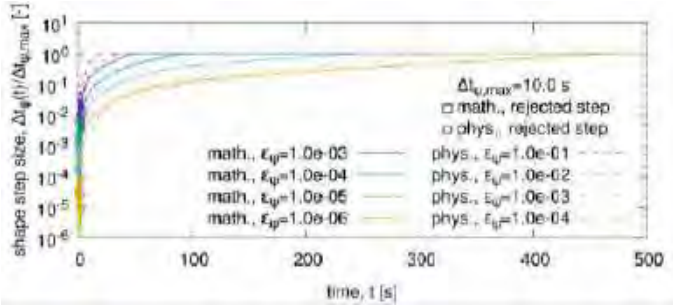

- Excess error: in absence of artificial limitations, maintained close to unity
- Time step: expansion or contraction as appropriate for the current conditions of the transient

Overview of the R&D efforts in AdP2015-2017

	Core Physics						Component specific or phenomenon specific							System			
	X-sec generation	Reactor Physics	Burn-up Calculation	3D NK	3D NK	Shielding	FPC	TH lumped parameters	CFD			Fission product dispersion & dose	TM	Material molecular dynamics	SYS-TH	SYS-TH	SYS-TH	SA
pellet	SERPENT	SERPENT	SERPENT				Transuranus		COMSOL	FEM-LCORE	FLUENT	1-6			RELAP5-3D	RELAP5/Mod3.3	CATHARE2	SIMMER
gap																		
cladding																		
subchannel																		
fuel assembly																		
core				FRENETIC	SIMMER			FRENETIC										
coolant												SIMMER		CALPHAD				
primary system																		
secondary system																		
containemnt																		
I&C																		
site																		

Design and Licensing

Design (including safety analysis)

Code Coupling ⟷

Chain of Code ⋯→

Uncertainty

SYS/TH – CFD code coupling [1-6]

RELAP5/Mod3.3 – Fluent coupling codes to CIRCE-HERO

RELAP5 domain: 2 pipes for water side + inner tube solid structure

- one representative of central tube
- one representative of 6 external tubes

CFD domain: LBE side + annulus solid structures (1/6 of the transversal section)

- In **blue** the LBE domain
- In **red** the AISI304 tube in contact with LBE
- In **green** the AISI304 tube in contact with H_2O
- In **orange** the AISI316 powder in between the tubes

Data are exchanged at the interface of water tubes

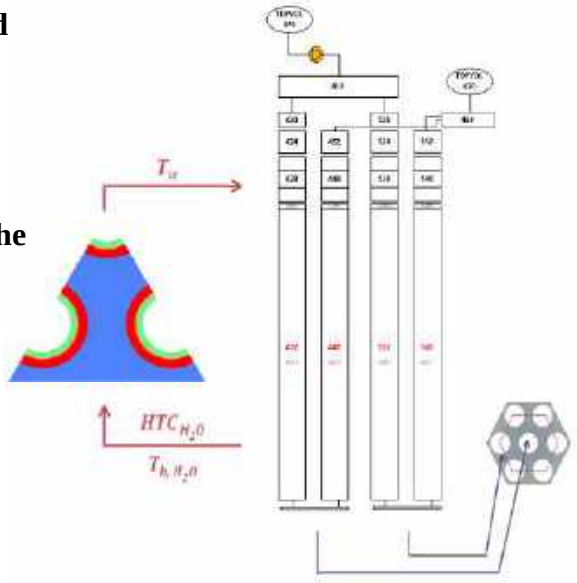

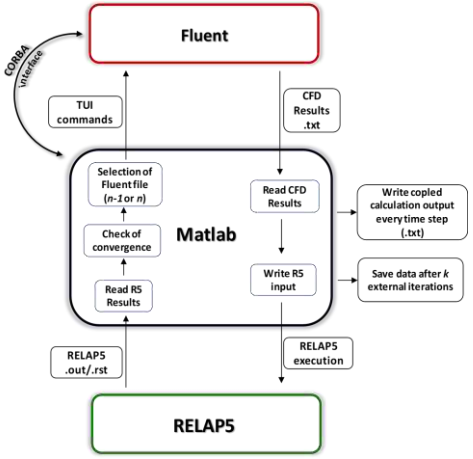

Coupling logic managed by Matlab software

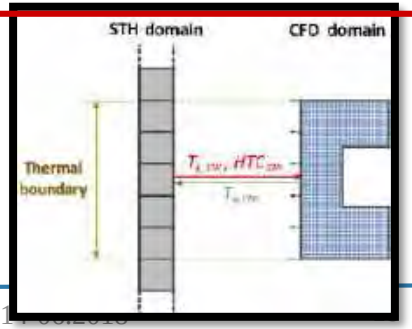

The wall temperature (calculated by the CFD code) is given to the STH code as BC, the STH code gives to the CFD code the bulk temperature and the heat transfer coefficient (calculated in the STH side)

SIMMER-III code validation [1-6]

SIMMER-III validation on LIFUS5/Mod2 data

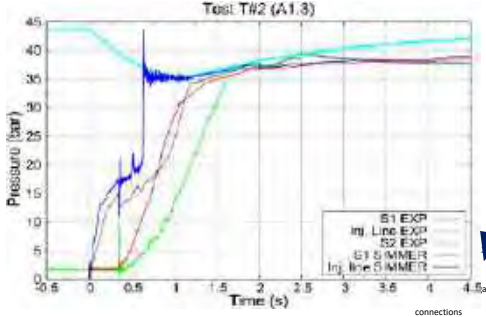

SIMMER-III results: pressure trends

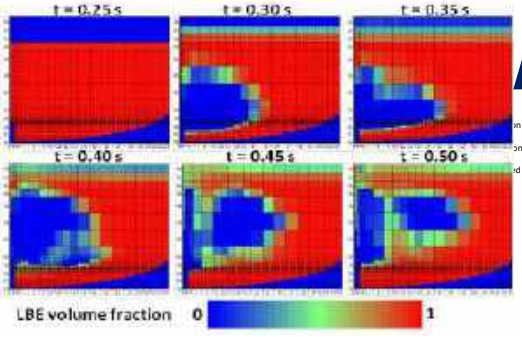

SIMMER-III results: Steam bubble formation

SIMMER-III model

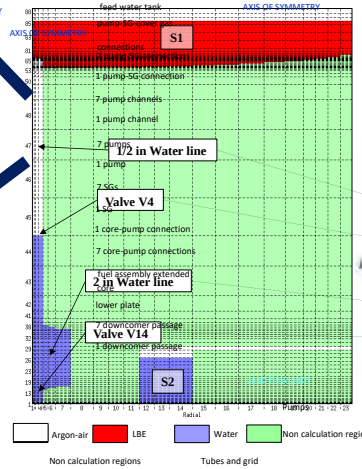

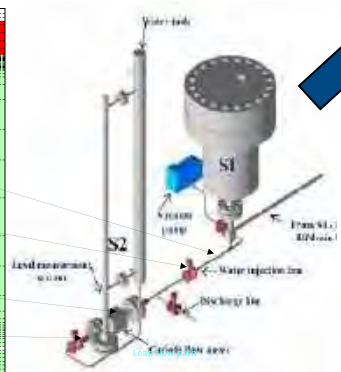

LIFUS5/Mod2 facility

LIFUS5/Mod2 S1 interaction vessel

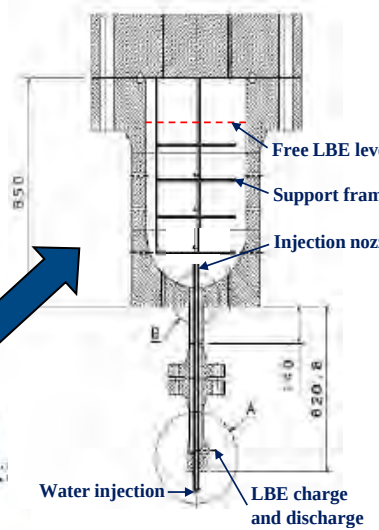

LIFUS5/Mod2 injector cap

Overview of the R&D efforts in AdP2015-2017

	Core Physics						Component specific or phenomenon specific							System			
	X-sec generation	Reactor Physics	Burn-up Calculation	3D NK	3D NK	Shielding	FPC	TH lumped parameters	CFD			Fission product dispersion & dose	TM	Material molecular dynamics	SYS-TH	SYS-TH	SYS-TH	SA
pellet	SERPENT	SERPENT	SERPENT				Transuranus		COMSOL	FEM-LCORE	FLUENT				RELAP5-3D	RELAP5/Mod3.3	CATHARE2	SIMMER
gap																		
cladding																		
subchannel																		
fuel assembly																		
core				FRENETIC	SIMMER			FRENETIC										
coolant												SIMMER		CALPHAD				
primary system																		
secondary system															1-7			
containemnt																		
I&C																		
site																		

Design and Licensing

Design (including safety analysis)

Code Coupling ⟷

Chain of Code ⋯→

Uncertainty

REALP5-3D independent assessment [1-7]

APPLICATION OF RELAP3D ON PHENIX EXPERIMENTAL TEST

- Framework. *Application of SYS-TH to Gen. IV reactors. Synergy with H2020 SESAME Project*
- Objectives. *1) Assessment of RELAP5, 2) Application of RELAP5 to nuclear reactor scale test, 3) Enhancing the experience of using SYS-TH to LM FR, 4) Mastering the code limitations and developing modelling approaches, 5) Availability of numerical tool for supporting design and safety analysis, 6) Developing reliable approaches for SYS analysis of new gen. FR systems, including coupling*

PHENIX reactor

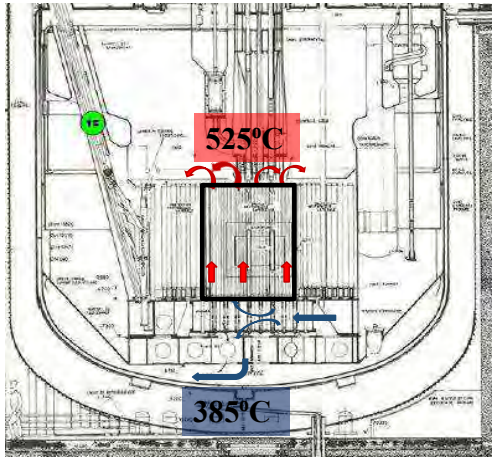

3D model of PHENIX reactor by RELAP5-3D

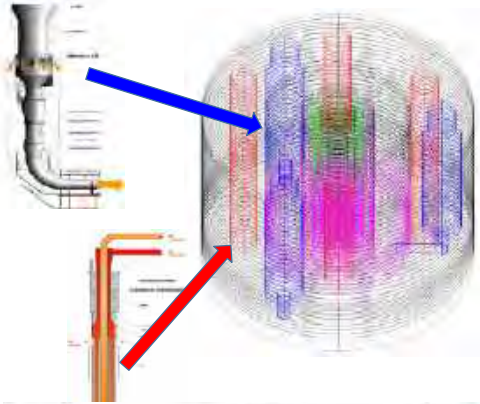

#	QUANTITY	Value
1	# of HYDR volumes	7492
2	# of HYDR junctions	12419
3	# of HEAT structures	8100
4	# of HEAT structures mesh points	45054

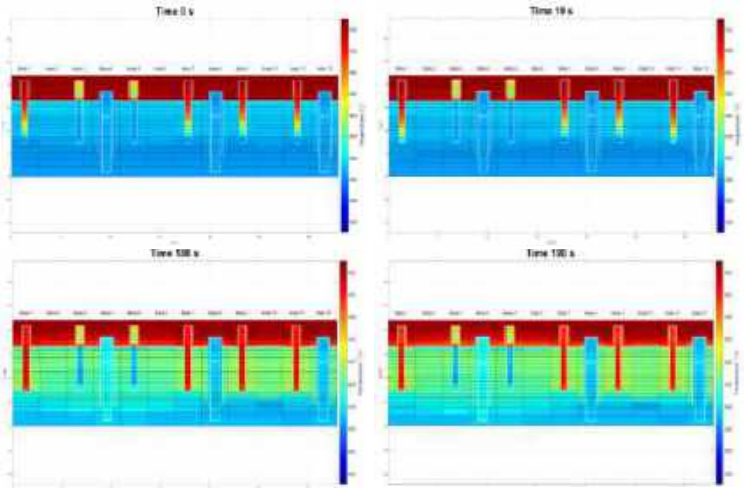

RELAP5-3D results: pool temperature distribution

Overview of the R&D efforts in AdP2015-2017

	Core Physics						Component specific or phenomenon specific							System			
	X-sec generation	Reactor Physics	Burn-up Calculation	3D NK	3D NK	Shielding	FPC	TH lumped parameters	CFD			Fission product dispersion & dose	TM	Material molecular dynamics	SYS-TH	SYS-TH	SYS-TH	SA
pellet	SERPENT	SERPENT	SERPENT				Transuranus		COMSOL	FEM-LCORE	FLUENT				RELAP5-3D	RELAP5/Mod3.3	CATHARE2	SIMMER
gap																		
cladding																		
subchannel																		
fuel assembly																		
core				FRENETIC	SIMMER			FRENETIC										
coolant												SIMMER		CALPHAD				
primary system																		
secondary system															1-8			
containemnt																		
I&C																		
site																		

Design and Licensing

Design (including safety analysis)

Code Coupling ⟷

Chain of Code ⋯→

Uncertainty

REALP5-3D independent assessment [1-8]

APPLICATION OF RELAP3D ON CIRCE-ICE EXPERIMENTAL TEST

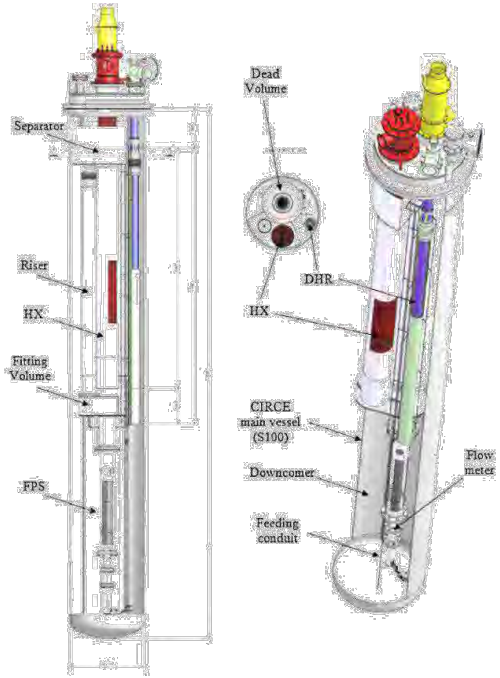

CIRCE-ICE facility

RELAP5/Mod3.3 nodalization of CIRCE -ICE

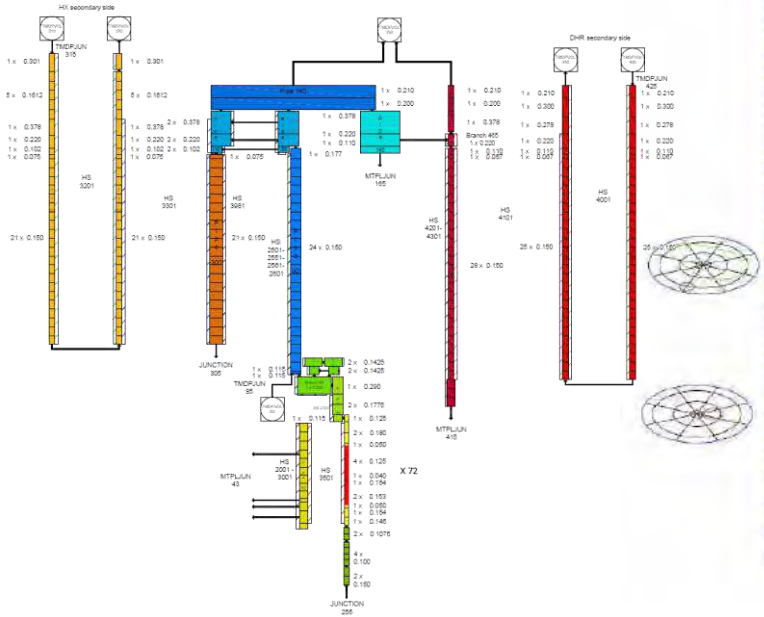

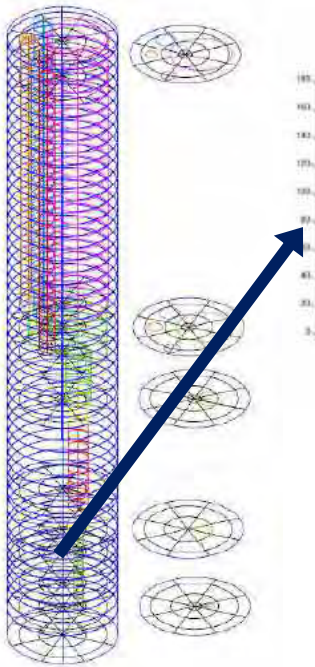

RELAP5-3D nodalization of CIRCE -ICE

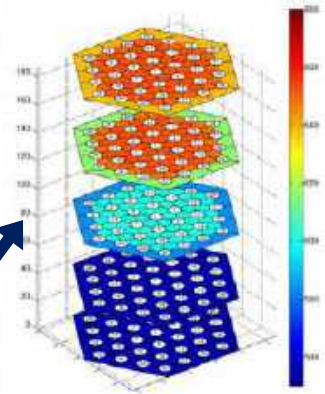

Sample FRSB temperature distribution @ end of steady state

Overview of the R&D efforts in AdP2015-2017

	Core Physics						Component specific or phenomenon specific							System			
	X-sec generation	Reactor Physics	Burn-up Calculation	3D NK	3D NK	Shielding	FPC	TH lumped parameters	CFD			Fission product dispersion & dose	TM	Material molecular dynamics	SYS-TH	SYS-TH	SYS-TH	SA
pellet	SERPENT	SERPENT	SERPENT				Transuranus		COMSOL	FEM-LCORE	FLUENT				RELAP5-3D	RELAP5/Mod3.3	CATHARE2	SIMMER
gap																		
cladding																		
subchannel																		
fuel assembly																		
core				FRENETIC	SIMMER			FRENETIC										
coolant												SIMMER		CALPHAD				
primary system										1-9								
secondary system																		
containemnt																	1-9	
I&C																		
site																		

Design and Licensing

Design (including safety analysis)

Code Coupling ⟷

Chain of Code ⋯→

Uncertainty

SYS/TH – CFD code coupling [1-9]

Validation of FEM-LCORE/CATHARE coupled code by TALL-3D experimental tests

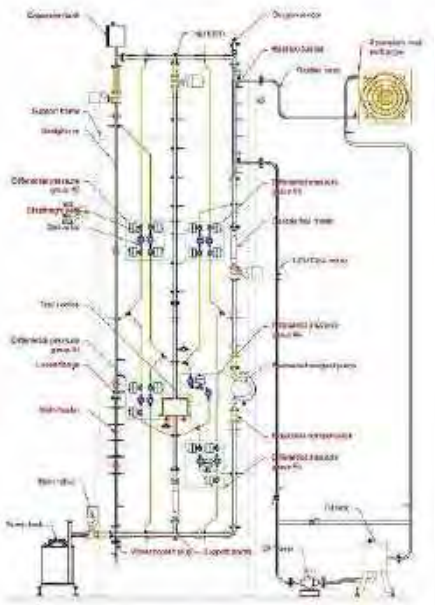

Tall-3D facility

Model of Tall-3D by CATHARE2 / FEM-LCORE coupled code

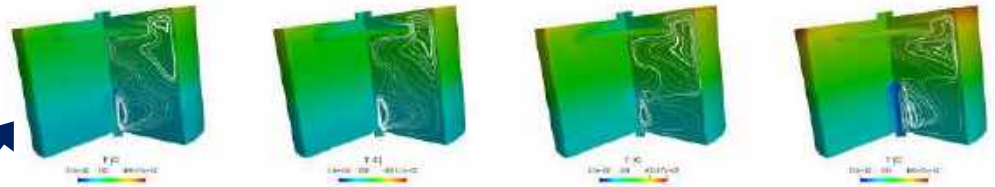

Sample CFD T prediction in 3D test section

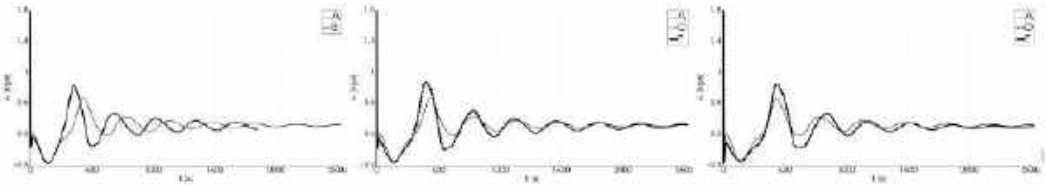

Sample mass flow rate predictions

Alessandro Del Nevo
Alessandro.delnevo@enea.it

Workshop Tematico, Accordo di Programma MiSE-ENEA, PAR2017, Progetto B.3 - LP2 **(Roma, 14-15 giugno 2018)**

Development / Assessment of models describing the inert gas behaviour in the fuel for application to the TRANSURANUS fuel pin thermo-mechanical code

Lelio Luzzi, Tommaso Barani, Luana Cognini, Davide Pizzocri

Politecnico di Milano, Energy Department
CeSNEF-Nuclear Engineering Division

Nuclear Reactors Group

Fuel pin for LMFR

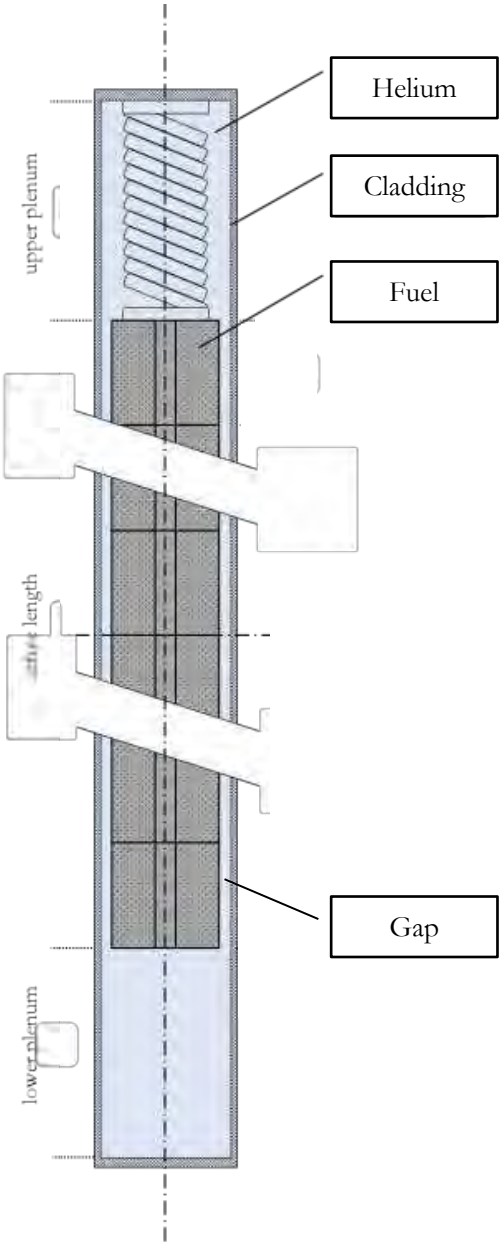

- Nuclear fuel pin (LMFR) is made of a stack of MOX fuel pellets wrapped in steel cladding (BOTH IMPORTANT!)
- Its performance is fundamental for **safe operation** of the reactor (and for **design** & **licensing** as well)

- Need of **fuel performance codes (FPCs)** and Integral Irradiation Experiments to asses the fuel pin thermo-mechanical behaviour ($\bar{\bar{\sigma}}$, $\bar{\bar{\epsilon}}$, $\bar{u}$, and T)

- Focus on fuel (**gaseous swelling & fission gas release**), and cladding materials as well

LMFR fuel pin behaviour

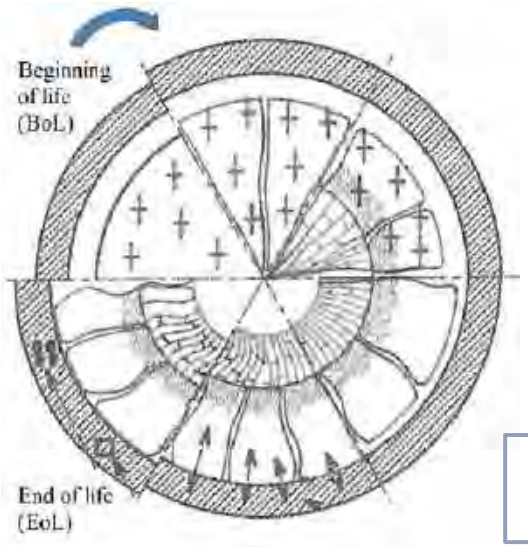

Interrelationship of multiple physical phenomena featured by *different time* and *space scales* concerning both fuel and cladding as a "coupled system"

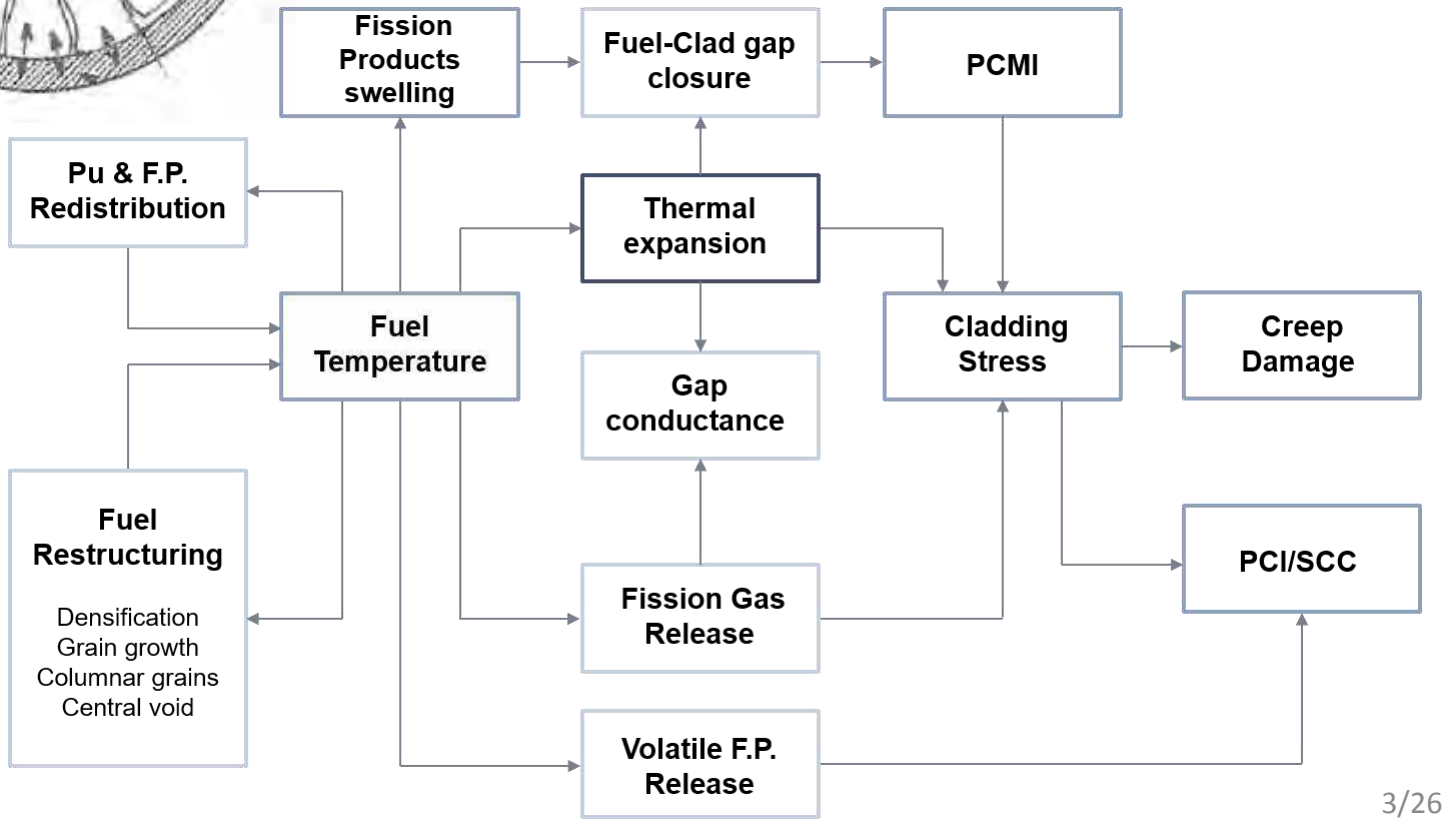

TRANSURANUS code

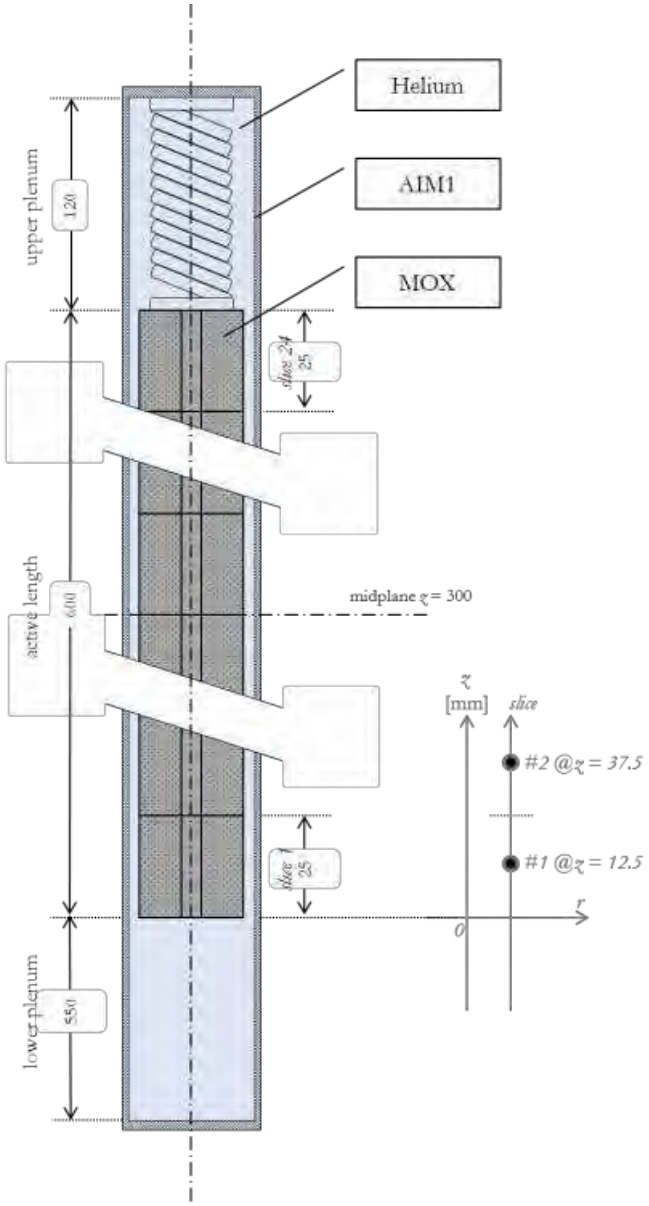

- Thermo-mechanical code for analysing integral fuel pin behaviour under irradiation
- Developed at JRC-Karlsruhe, and extensively validated for LWRs (design & licensing)
- Fuel pin axial and radial discretization with 1½-D solution of thermo-mechanics ($\bar{\bar{\sigma}}$, $\bar{\bar{\epsilon}}$, $\bar{u}$, and T)
- Mathematical/numerical frame into which models for the fuel pin performance of other types of reactors (Na, LBE, Pb) can be easily incorporated

v1m3j12

LFR-oriented

Strategy (Fuel + Cladding models → FPC → IFPE)

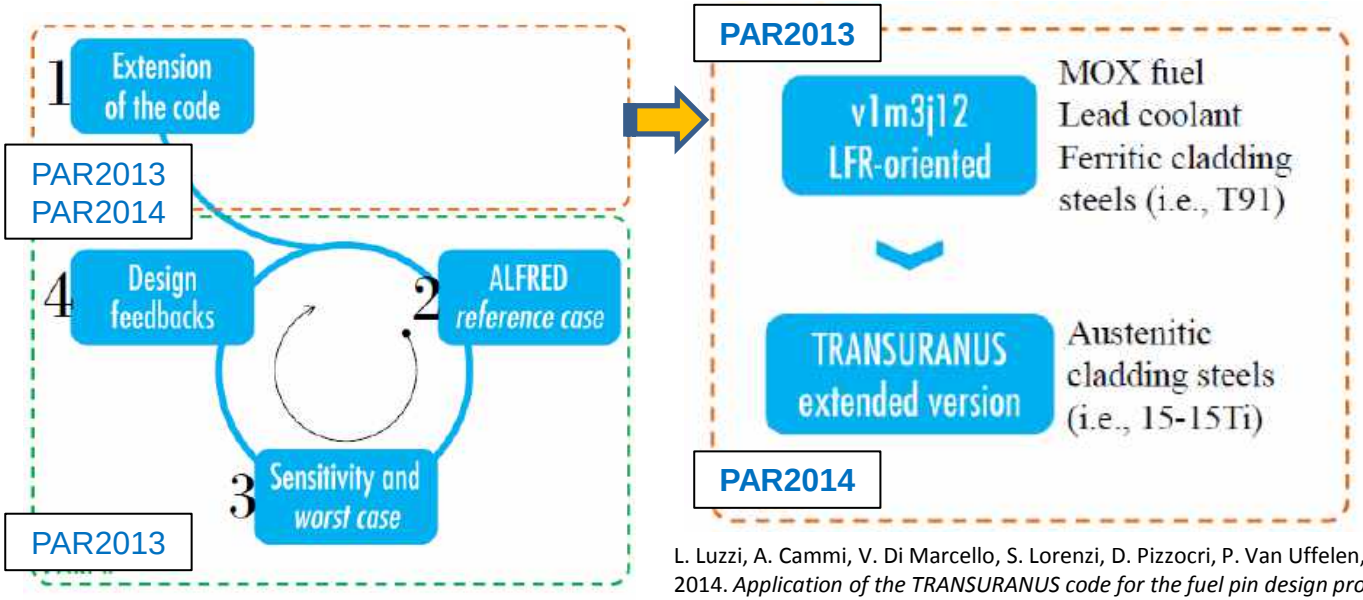

L. Luzzi, A. Cammi, V. Di Marcello, S. Lorenzi, D. Pizzocri, P. Van Uffelen, 2014. *Application of the TRANSURANUS code for the fuel pin design process of the ALFRED reactor.* Nuclear Engineering and Design, 277, 173–187.

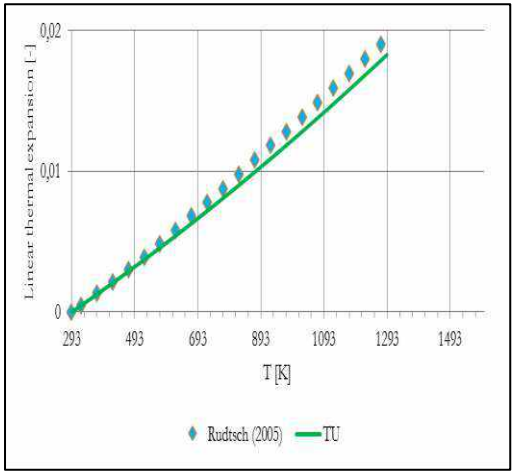

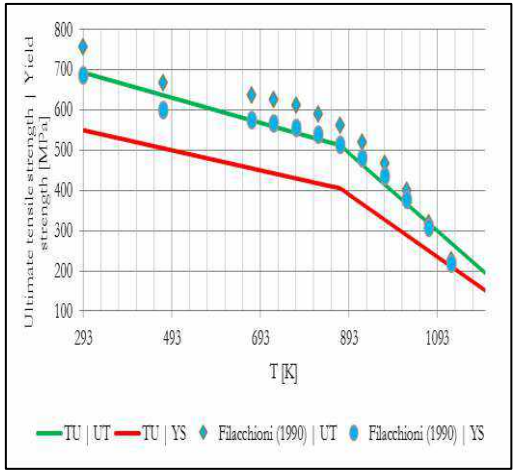

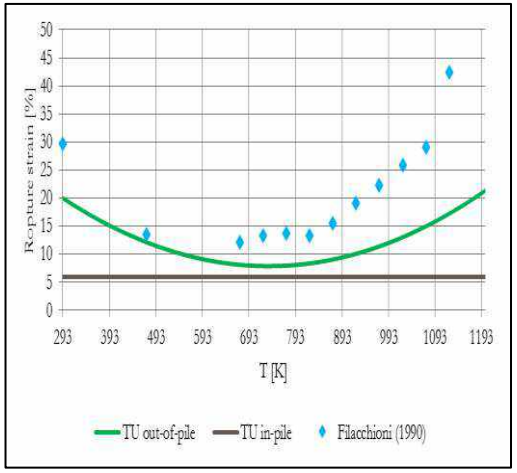

Previous activities (PAR-2013&2014)

PAR-2014

1 Extension of the code

PAR-2013

4 Design feedbacks

2 ALFRED *reference case*

3 Sensitivity and *worst case*

. Critical overview of 15-15Ti physical and mechanical properties
. Cladding swelling
. Cladding creep (*ad hoc* P & LMP – CDF)

Cladding swelling

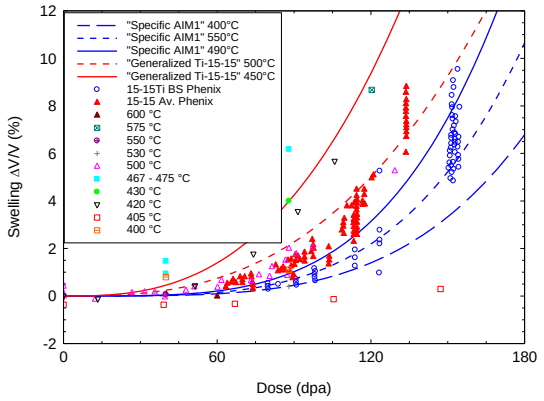

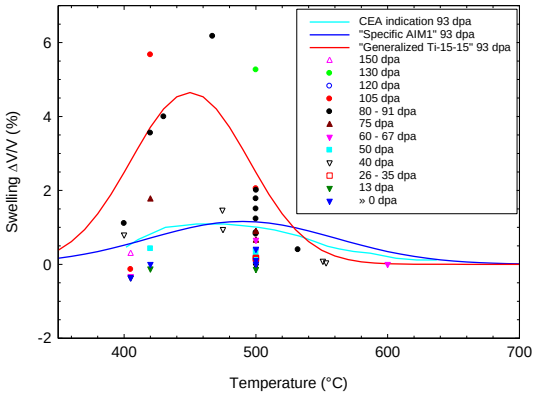

TRANSURANUS application to the ALFRED reactor

Fuel pin performance integrated in the conceptual design phase

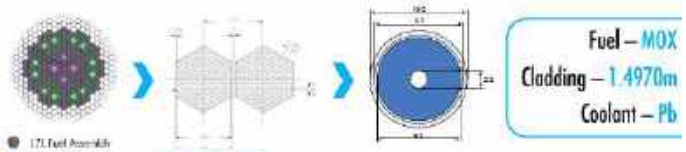

ALFRED

Only operative conditions have been considered: safety analysis to be performed

To reduce FCMI, neutronic design should be changed, optimizing core radial peak factor and/or core refueling scheme

Previous activities (PAR-2013&2014)

PAR-2014

1 Extension of the code

PAR-2013

2 ALFRED *reference case*

3 Sensitivity and *worst case*

4 Design feedbacks

. Critical overview of 15-15Ti physical and mechanical properties
. Cladding swelling
. Cladding creep (*ad hoc* P & LMP – CDF)

Cladding creep

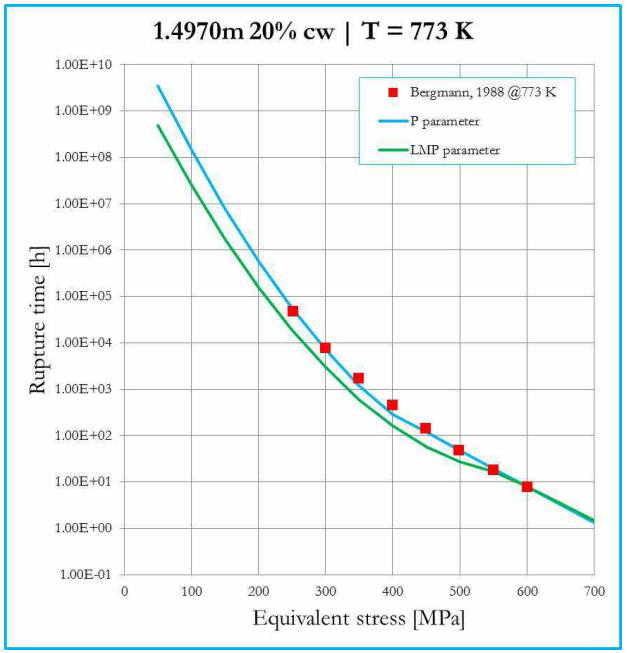

$$LMP = T(C + \mathrm{Log}\, t_R)$$

$$P \equiv T\left(C + \mathrm{Log}\frac{t_R}{T}\right)$$

TRANSURANUS application to the ALFRED reactor

Fuel pin performance integrated in the conceptual design phase

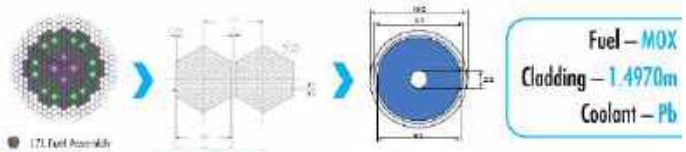

ALFRED

Only operative conditions have been considered: safety analysis to be performed

To reduce FCMI, neutronic design should be changed, optimizing core radial peak factor and/or core refueling scheme

Previous activities (PAR-2013&2014)

PAR-2014

1 Extension of the code

PAR-2013

2 ALFRED *reference case*

3 Sensitivity and *worst case*

4 Design feedbacks

. Critical overview of 15-15Ti physical and mechanical properties
. Cladding swelling
. Cladding creep (*ad hoc* P & LMP – CDF)

Cladding creep

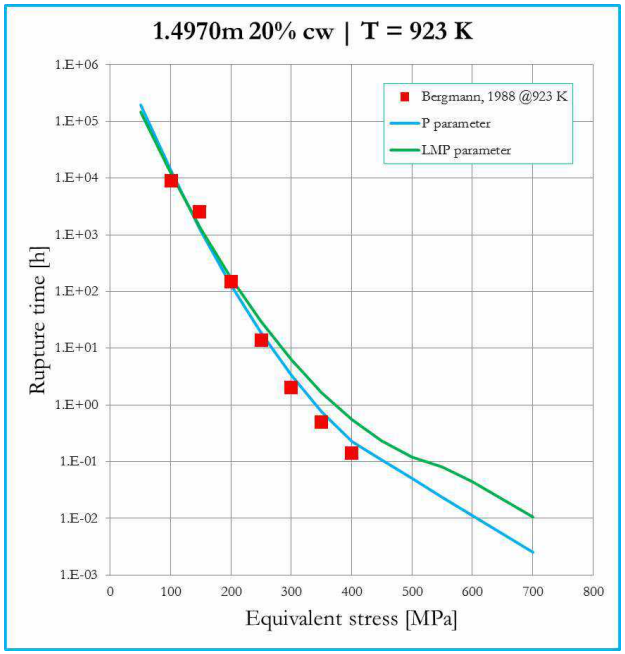

$$LMP = T(C + \mathrm{Log}\, t_R)$$

$$P \equiv T\left(C + \mathrm{Log}\frac{t_R}{T}\right)$$

TRANSURANUS application to the ALFRED reactor

Fuel pin performance integrated in the conceptual design phase

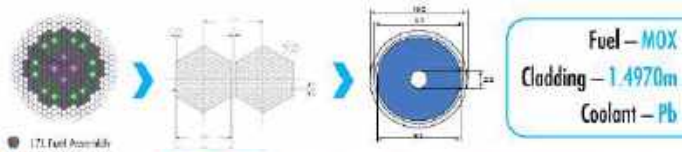

ALFRED

Only operative conditions have been considered: safety analysis to be performed

To reduce FCMI, neutronic design should be changed, optimizing core radial peak factor and/or core refueling scheme

Previous activities (PAR-2013&2014) + future …

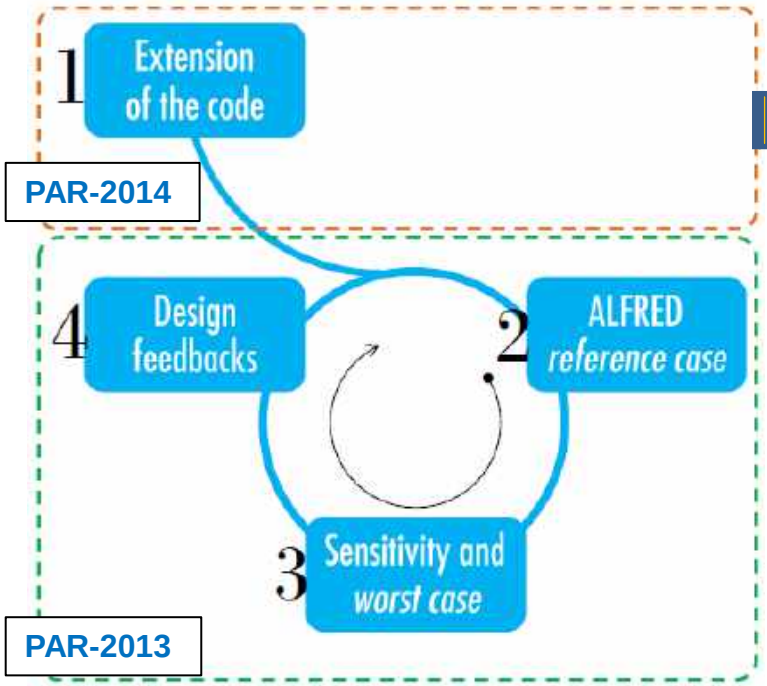

. Critical overview of 15-15Ti physical and mechanical properties
. Cladding swelling
. Cladding creep (*ad hoc* P & LMP – CDF)

Open issues and further developments

. Coating selection and in-reactor qualification is still an open technological issue
. More detailed cladding swelling modelling (e.g., stress dependence and coupling with creep)
. PCMI
. Chemical interaction
. JOG formation
. Cesium migration
. Availability of in-pile data for various properties/phenomena of the cladding will be welcome

TRANSURANUS application to the ALFRED reactor

Fuel pin performance integrated in the conceptual design phase

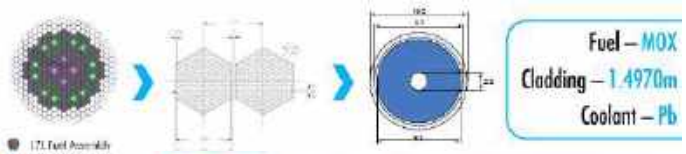

ALFRED

Only operative conditions have been considered: safety analysis to be performed

To reduce FCMI, neutronic design should be changed, optimizing core radial peak factor and/or core refueling scheme

L. Luzzi, A. Cammi, V. Di Marcello, S. Lorenzi, D. Pizzocri, P. Van Uffelen, 2014. *Application of the TRANSURANUS code for the fuel pin design process of the ALFRED reactor.* Nuclear Engineering and Design, 277, 173–187.

Extension of the code, Fuel

Problem. Need to improve the modelling of inert gas behaviour (IGB) in transient conditions, within fuel pin performance codes (TRANSURANUS)

- IGB modelling is fundamental for **performance** & **safety** (post-Fukushima) analysis of fuel pins
- IGB can represent a limiting life factor for their permanence in reactor, thus limiting the **economic** gain related to the safe operation of the fuel at extended burn-up

- EERA-JPNM Project
- COMBATFUEL & **INSPYRE** (EC)
- ENEN+ Project (EC)
- Several **previous PARs**

State of the art

Modelling of inert gas behaviour is currently available in fuel performance codes (FPCs), but has **several critical limitations in transients** (and in DBAs)

- Majority of current models are **correlation-based**
- Modelling of several phenomena is neglected
- Generally assumed that FGR is 100% (extreme approximation for LFRs, *may be* reasonable for high temperature SFRs)

1. Intra-granular trapping and resolution are assumed in equilibrium and lumped in an *effective diffusion coefficient* (D_{eff})
2. Currently used algorithms for intra-granular gas diffusion can handle only simplified equations
3. The description of helium behaviour is oversimplified
4. Present models for IGB in the high burn-up structure (HBS) are oversimplified, usually assuming quasi-stationary conditions

Inert gas behaviour: A multi-scale problem

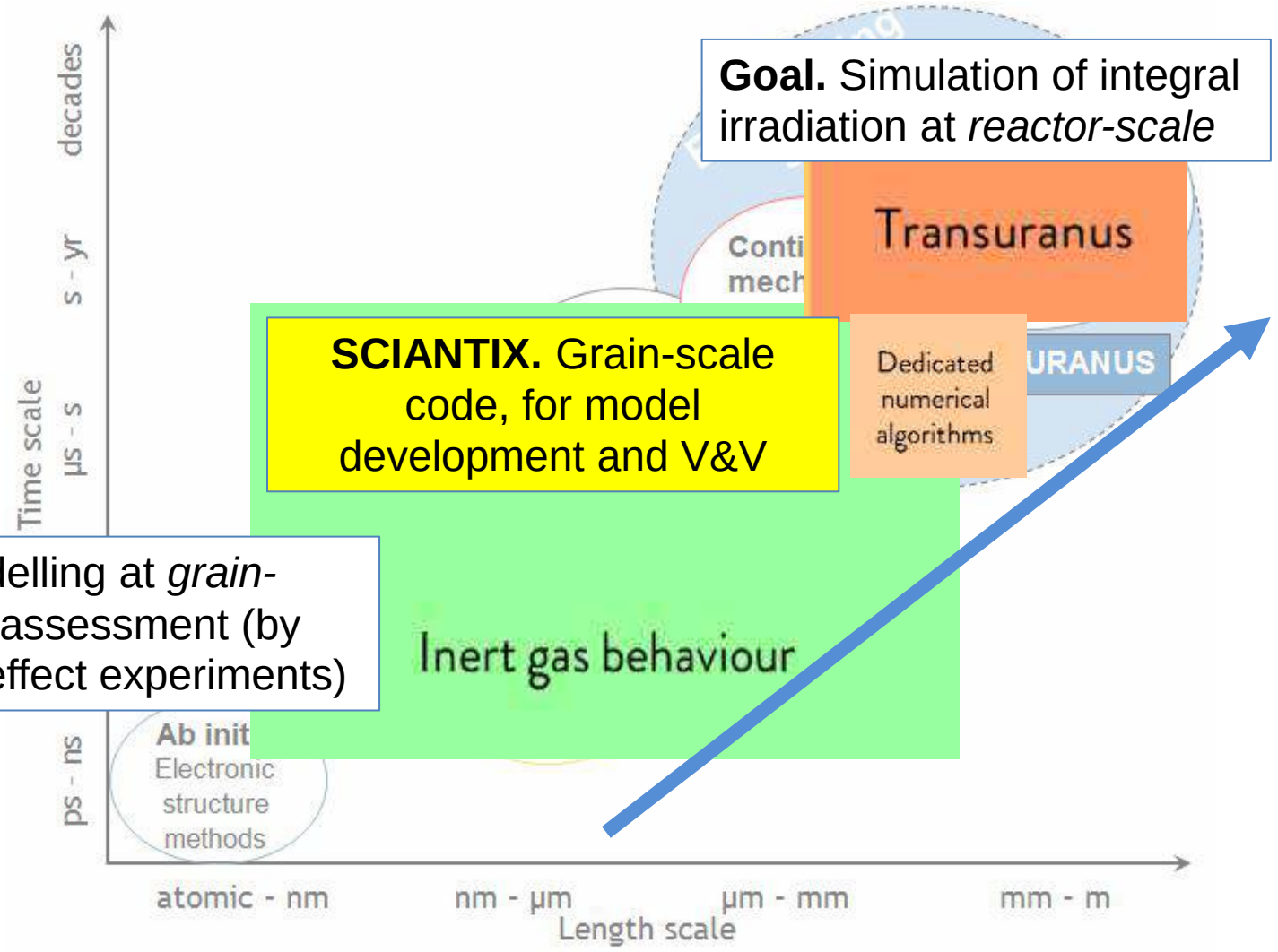

Goal. Simulation of integral irradiation at *reactor-scale*

SCIANTIX. Grain-scale code, for model development and V&V

Goal. Modelling at *grain-scale* and assessment (by separate effect experiments)

Physically-based modelling is required to act as a bridge from lower-length scale to engineering scale

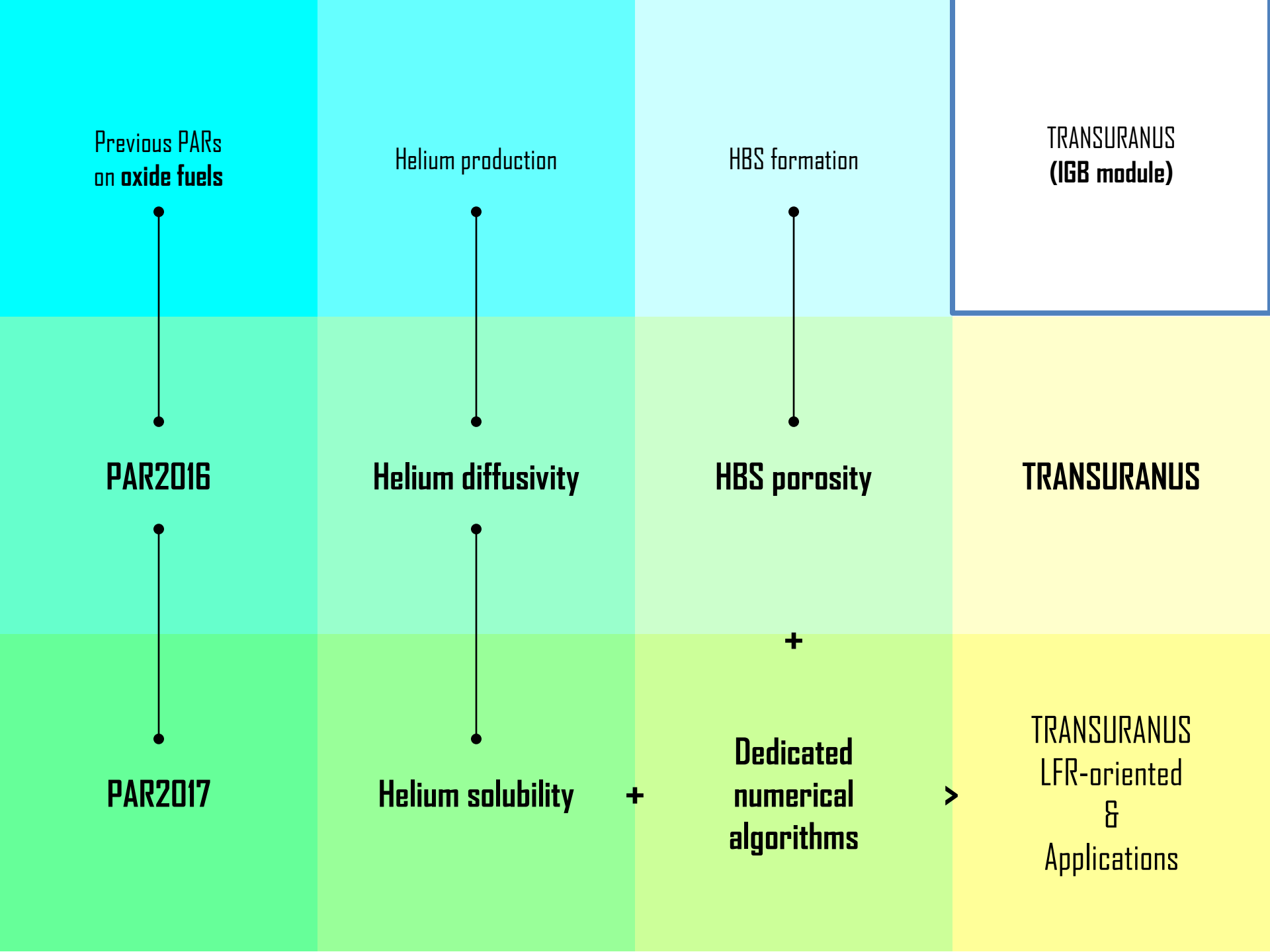
Previous PARs on **oxide fuels**
Helium production
HBS formation
TRANSURANUS **(IGB module)**
PAR2016
Helium diffusivity
HBS porosity
TRANSURANUS
PAR2017
Helium solubility
+
Dedicated numerical algorithms
+
>
TRANSURANUS LFR-oriented & Applications

Physics- based IGB module

- **Giovanni Pastore**
  Modelling of Fission Gas Swelling and Release in Oxide Nuclear Fuel and Application to the TRANSURANUS Code
  PhD thesis, Politecnico di Milano, 2012.

- **Davide Pizzocri**
  Modelling and assessment of inert gas behaviour in UO_2 nuclear fuel for transient analysis
  PhD thesis, Politecnico di Milano, 2018.

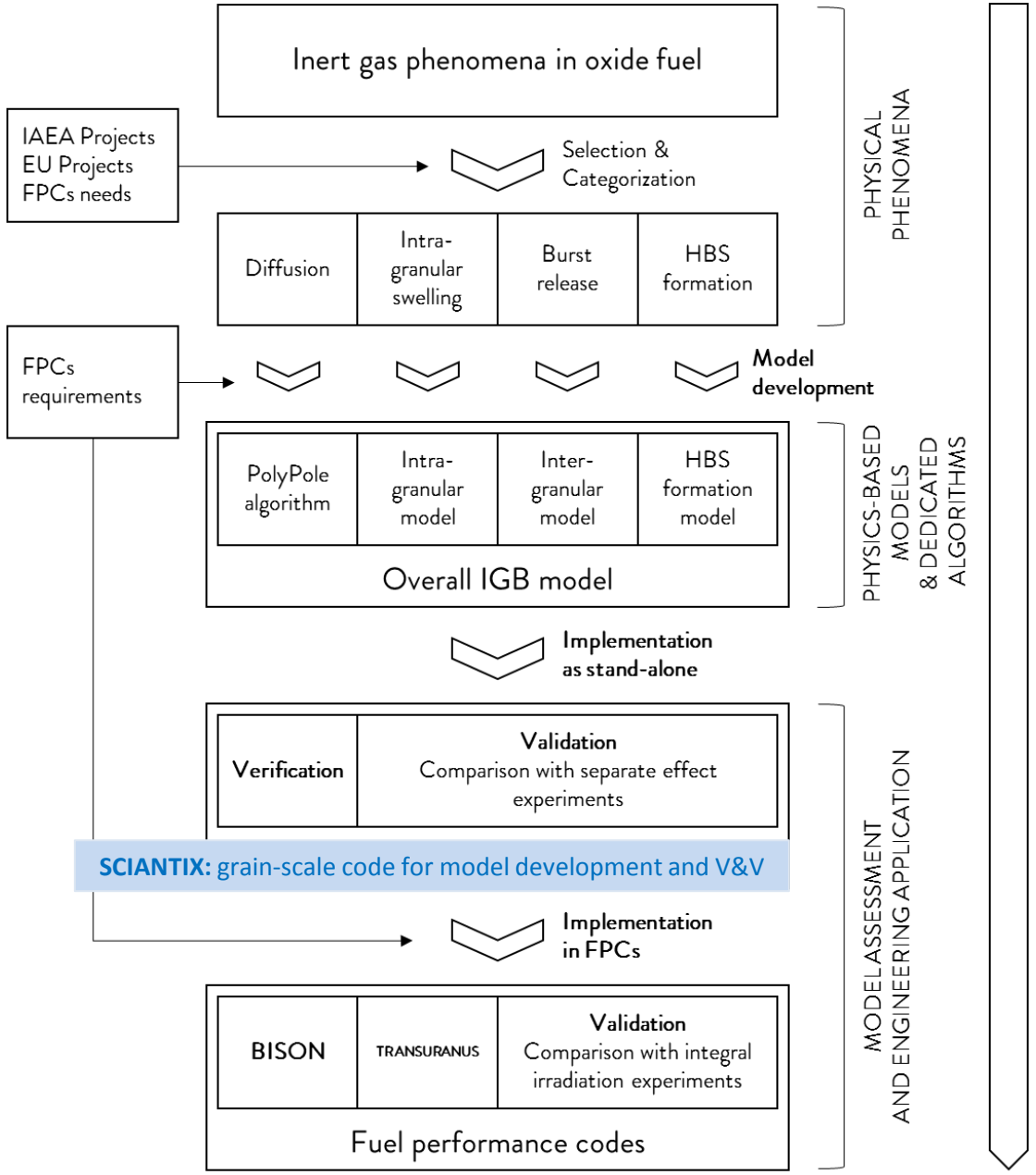

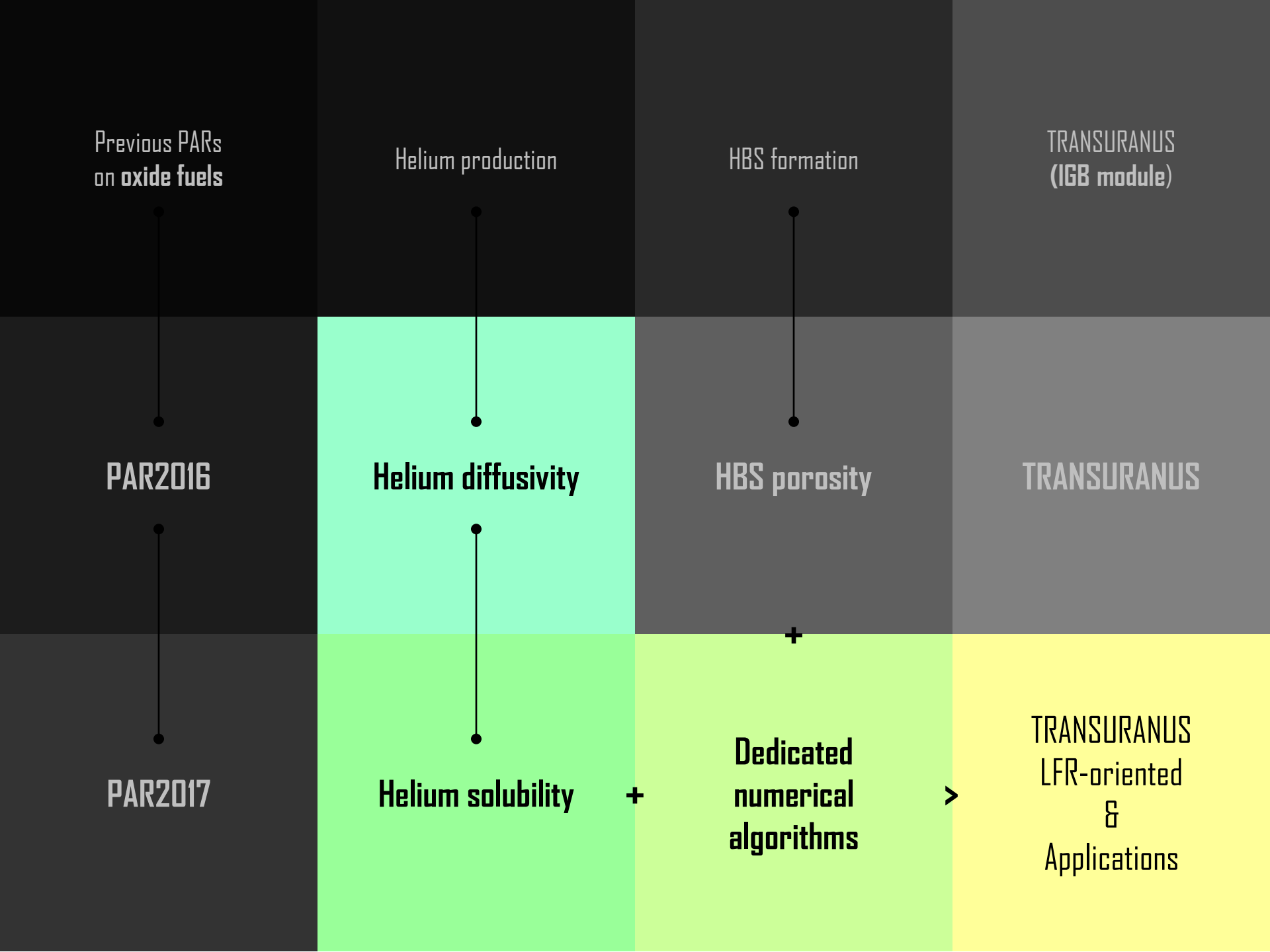
Previous PARs on **oxide fuels**
Helium production
HBS formation
TRANSURANUS **(IGB module)**
PAR2016
Helium diffusivity
HBS porosity
TRANSURANUS
PAR2017
Helium solubility
+
Dedicated numerical algorithms
+
>
TRANSURANUS LFR-oriented & Applications

The importance of being Helium

Helium behaviour
is fundamental to assess the fuel performance

- **In-pile conditions**, especially
  - at high burnup
  - employing **MOX** fuel
  - employing **MA-bearing** fuel

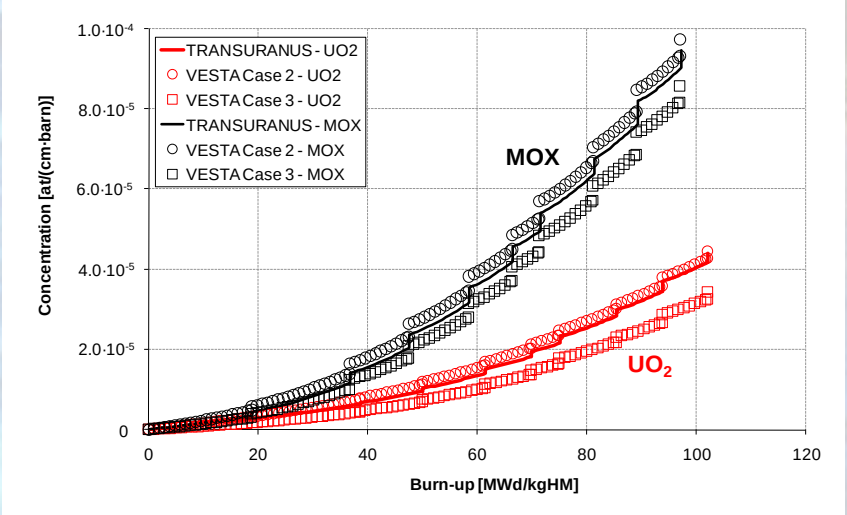

P. Botazzoli, L. Luzzi, S. Brémier, A. Schubert, P. Van Uffelen, C.T. Walker, W. Haeck, W. Goll, 2011. *Extension and Validation of the TRANSURANUS Burn-up Model for Helium Production in High Burn-up LWR Fuels* . Journal of Nuclear Materials, 419(1-3), 329–338.

- **In storage conditions,** due the continuous production from α-emitters

Helium behaviour (intra- and inter-granular)

Previous PAR

Ternary fissions, (n,α)-reactions, α-decay

Production of Helium

DIFFUSIVITY & SOLUBILITY

Intra-granular gas (single atoms)

Trapping

Re-solution

Intra-granular gas (bubbles, with Xe and Kr)

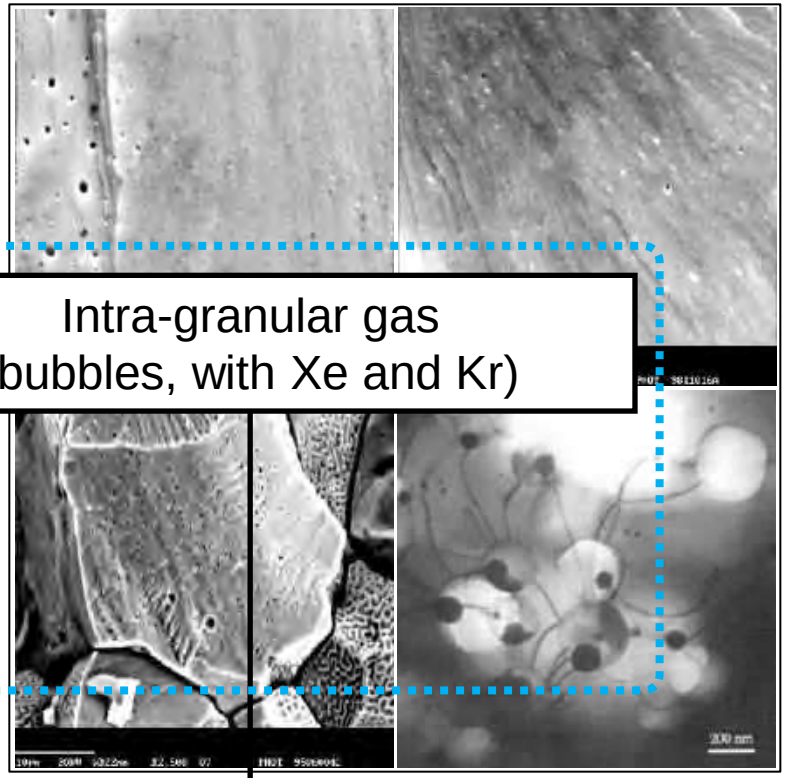

Diffusion

Inter-granular gas

Inter-granular bubble swelling

Intra-granular bubble swelling

FGR / Absorption

Modelling Helium behaviour in FPCs

$$\begin{cases} \dfrac{\partial c_{He}}{\partial t} = D_{He}\nabla^2 c_{He} - \beta_{He}(c_{He} - C_{s,p_{ig}}) + \alpha_{He} m_{He} + S_{He} \\ \dfrac{\partial m_{He}}{\partial t} = \beta_{He}(c_{He} - C_{s,p_{ig}}) - \alpha_{He} m_{He} \end{cases}$$

C_{He} - He dissolved in matrix
m_{He} - He present in bubbles
α_{He} - thermal re-solution rate
β_{He} - trapping rate

Helium diffusivity

Helium solubility

Helium production

- Model including the **mechanistic** description of helium behaviour in oxide fuels
- Definition of the model parameters is the first fundamental step
- Dedicated algorithms required in FPCs (PDEs to be solved in each mesh point…)

Helium diffusivity (part of PAR2016)

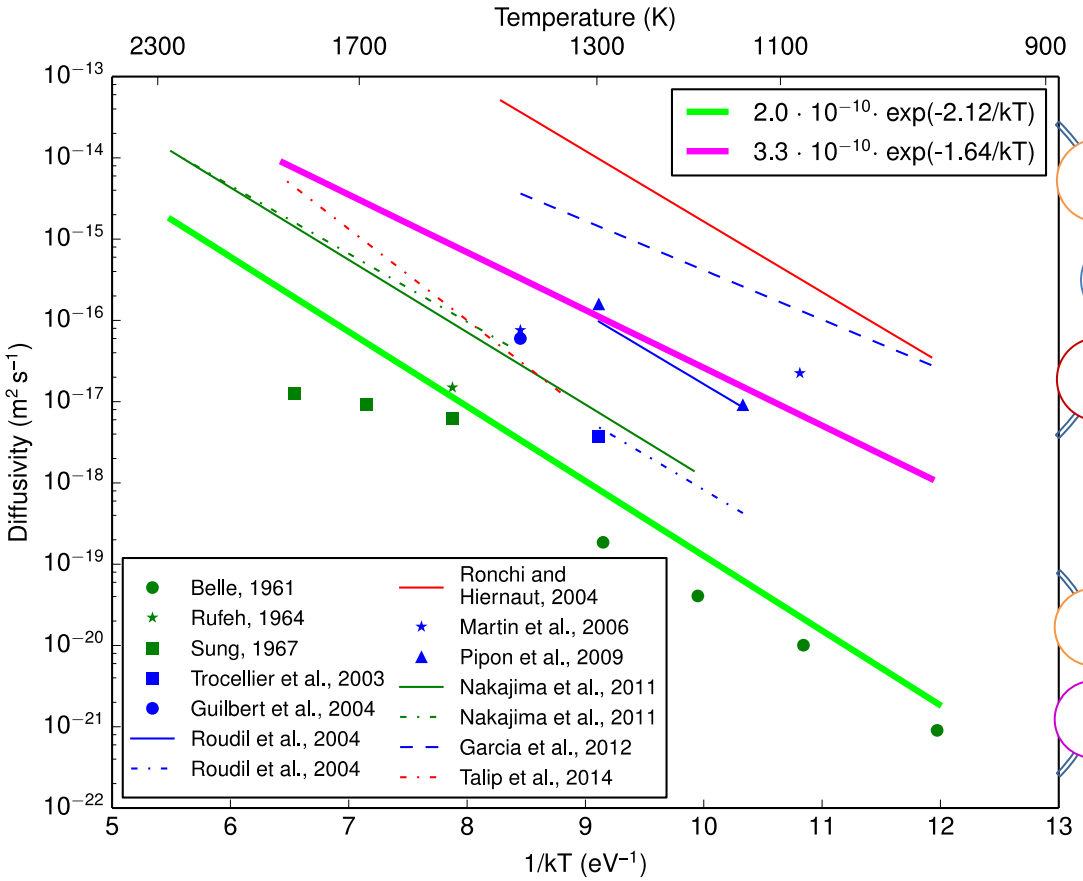

Experimental data

- Infusion
- Ion implantation
- Doping

Derived correlations

- Infusion
- Implantation + doping

specific application frame!

Data	Log D_0 (m^2 s^{-1})	Q (eV)	Range (K)	R^2
Infusion	-9.7 (-11, -8.4)	2.12 (1.77, 2.56)	968–2110	0.93
Ion implantation and doping	-9.5 (-13, -5.8)	1.64 (0.74, 2.56)	973–1800	0.52[b]

[b] This value of R^2 does not seem fully satisfactory. Nevertheless, we still choose to report this fit since it includes all the data available in the literature. Further refinement of this correlation is of major interest, once more data will become available.

L. Luzzi, L. Cognini, D. Pizzocri, T. Barani, G. Pastore, A. Schubert, T. Wiss, P. Van Uffelen, 2018. *Helium diffusivity in oxide nuclear fuel: Critical data analysis and new correlations.* Nuclear Engineering and Design, 330, 265-271.

Helium solubility (part of PAR2017)

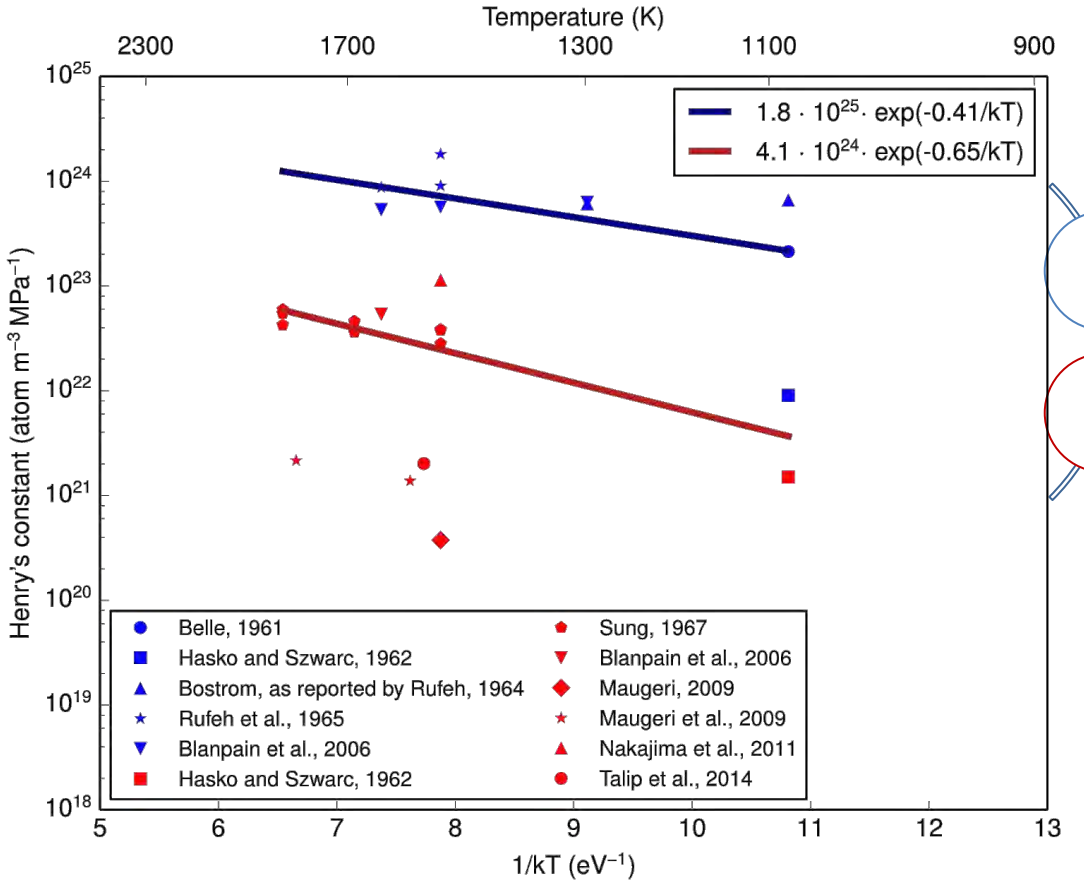

Experimental data & derived correlations

- Powder
- Single crystal

Data	Log *A* (at m^{-3} MPa^{-1})	*B* (eV)	Range (K)	R^2
Powder	25.25 (23.91,26.6)	0.41 (0.75, 0.06)	1073–1773	0.83
Single crystal	24.61 (23.41, 25.82)	0.65 (1.01, 0.28)	1073–1773	0.83

L. Cognini, D. Pizzocri, T. Barani, P. Van Uffelen, A. Schubert, T. Wiss, L. Luzzi. *Helium solubility in oxide nuclear fuel: Critical review and derivation of new correlations for Henry's constant.* Submitted to Nuclear Engineering and Design.

Numerical algorithms (part of PAR2015)

PolyPole-1

MULTI-SCALE !

SotA. *Effective diffusion*
SotA. URGAS and FORMAS

$$\frac{\partial c_t}{\partial t} = \beta + \mathbf{D_{eff}} \nabla^2 c_t$$

In FPC time-steps, D_{eff} can vary order of magnitudes !

Based on **modal expansion** in space and including corrective polynomial factors to **account for the time dependency of the parameters**

Assessed against reference algorithm

Released OpenSource

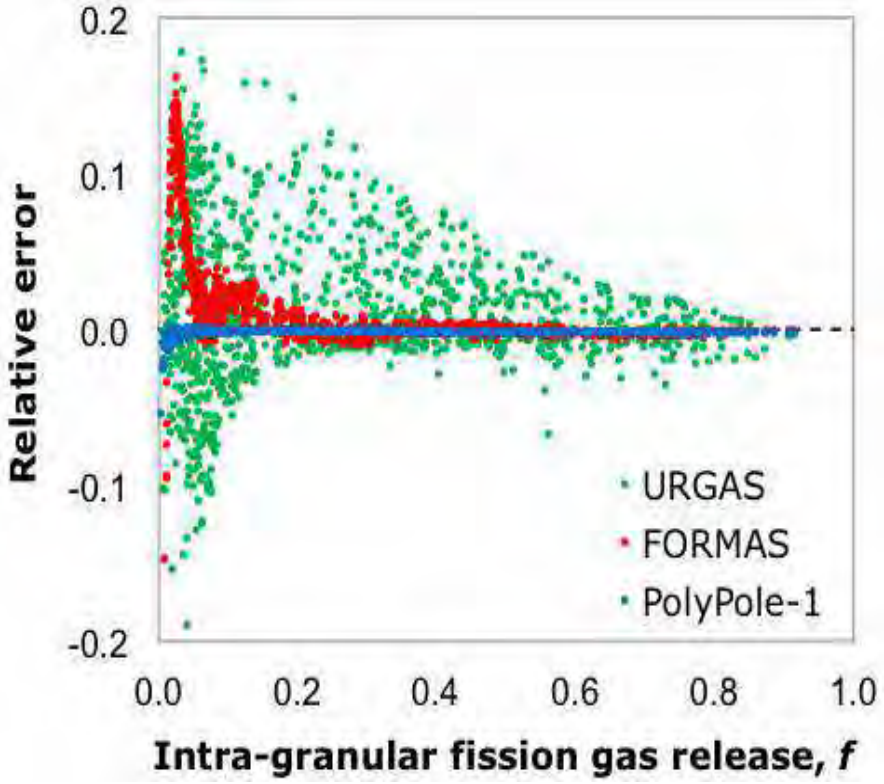

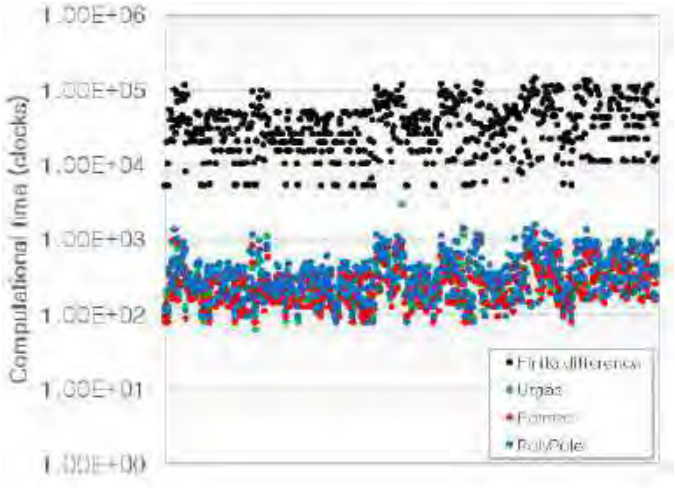

D. Pizzocri, C. Rabiti, L. Luzzi, T. Barani, P. Van Uffelen, G. Pastore, 2016. *PolyPole-1: An accurate numerical algorithm for intra-granular fission gas release*. Journal of Nuclear Materials, 478, 333–342.

Numerical algorithms (part of PAR2017)

PolyPole-2

$$\frac{\partial}{\partial t}\bar{c} = \bar{\beta} + \bar{\bar{D}}\bar{c} + \bar{\bar{S}}\bar{c}$$

SotA. Not available

Allows considering all the physical time-scales of the system, overcoming the *effective diffusion* hypothesis
→ **Fundamental in fast transients !**

Identical numerical scheme of PolyPole-1

Numerical experiment with randomly generated transients

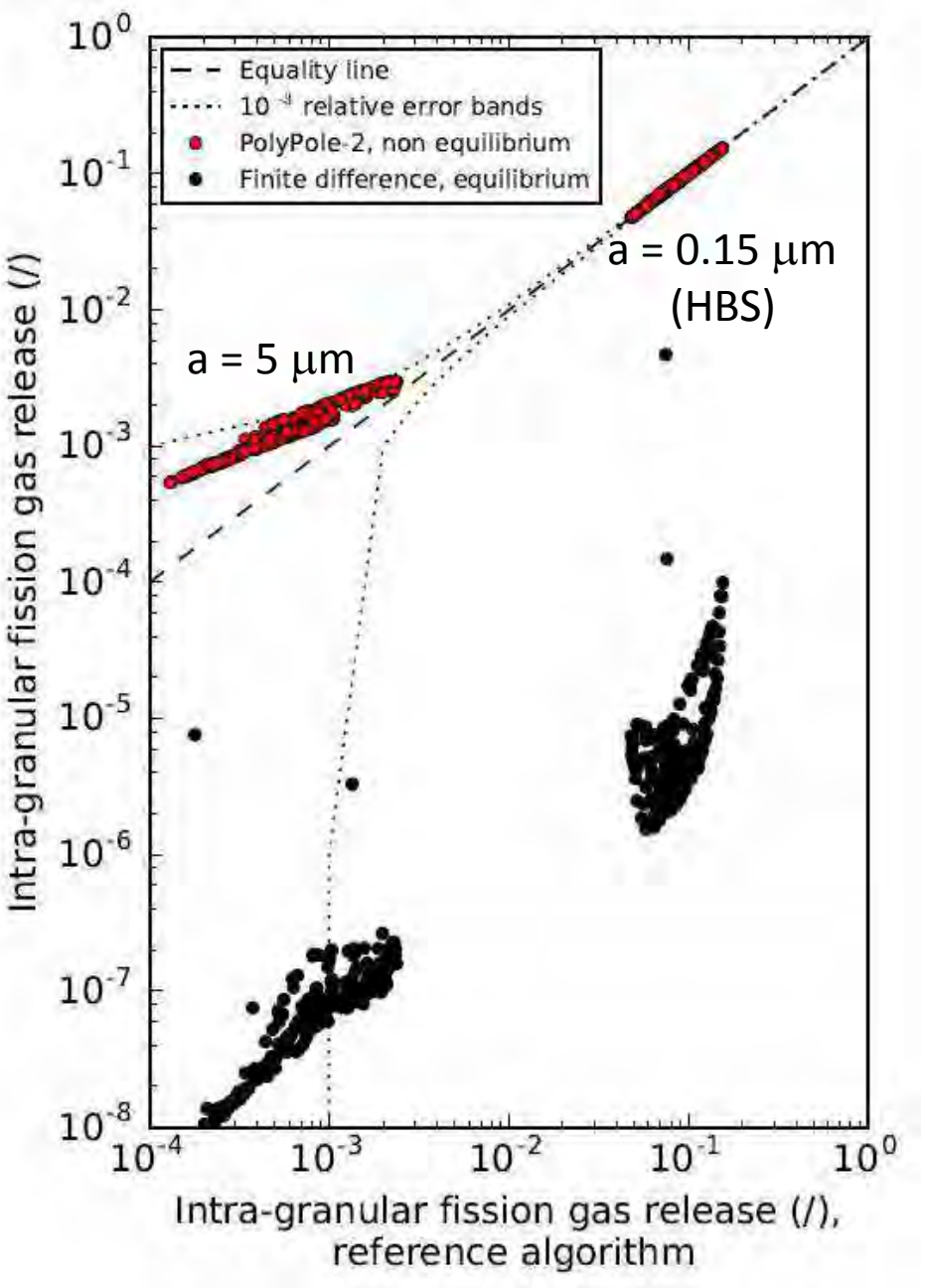

Assessed against reference algorithm

G. Pastore, D. Pizzocri, C. Rabiti, T. Barani, P. Van Uffelen, L. Luzzi, 2017. *An effective numerical algorithm for intra-granular fission gas release during non-equilibrium trapping and resolution.* Submitted to Journal of Nuclear Materials.

Conclusions (PAR2017) and future steps

1. Development of new **correlations for Helium diffusivity and solubility**
   - Accounting for all available data
   - Greatly reducing calculation uncertainties
   - Clarified scope of application

   NEXT: Assessment of Helium model in TRANSURANUS

2. Development of new **dedicated numerical algorithms** (PolyPole-1, PolyPole-2)
   - Superior accuracy with respect to SotA
   - Similar computational effort
   - Allowing for the treatment of multiple PDEs (fundamental for **Helium**)

   NEXT: Implementation in TRANSURANUS (coupled with **SCIANTIX** *mesoscale* module)

   NEXT: Keep going the activity of extending TRANSURANUS (both fuel and cladding) towards LFR-oriented version, as more data/knowledge (e.g., HBS, restructuring and Pu redistribution, FP chemistry, intra-granular bubble coarsening) **become available…**

   NEXT: Fuel rod integral analysis in support of design of LFRs using the improved version of TRANSURANUS (assessed against Integral Irradiation Experiments, e.g., SUPERFACT, RAPSODIE-1, NESTOR-3 **--->** Task Force of INSPYRE H2020 Project)

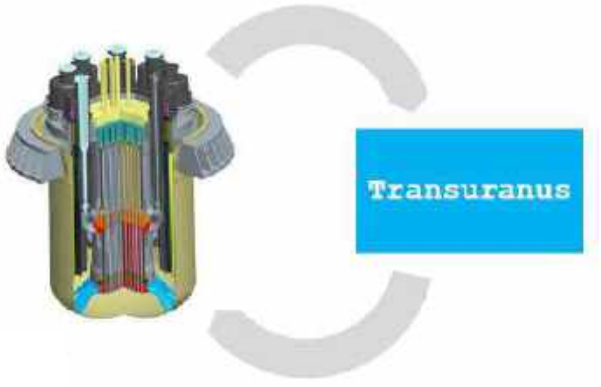

MORE IN PERSPECTIVE …

Starting multi-physics coupling of FPCs (TRANSURANUS, Bison) with neutronics & thermal-hydraulics for LFR conditions

Development of a **well-structured module** able to provide TRANSURANUS with accurate information from the reactor scale, typically the initial and boundary conditions for the fuel rod thermo-mechanical analysis:

- Modelling of the neutronics and thermal-hydraulics reactor conditions typical of Gen-IV LFRs, in normal, transient and annealing/storage conditions.
- Creation of initial and boundary conditions needed by TRANSURANUS, starting from the multi-physics and high-fidelity simulations, for normal, transient and annealing/storage conditions.
- Evaluation of reactor dynamics and feedback effects during transient conditions with a specific focus on the safety-related key parameters and their influence on the TRANSURANUS modelling and simulation capabilities.
- Assessment of the burn-up model of TRANSURANUS with MOX (and more in perspective with MA-bearing fuels) against Monte Carlo simulations.
- Development of ad-hoc coupling scheme among **SERPENT**, **OpenFOAM / RELAP** and **TRANSURANUS** to provide an accurate multi-physics modelling approach that can serve as reference solution for the evaluation of TRANSURANUS outcomes.

Publications (---> PAR2013÷2017)

1. P. Van Uffelen, P. Botazzoli, L. Luzzi, S. Bremier, A. Schubert, P. Raison, R. Eloirdi, M.A. Barker - *An experimental study of grain growth in mixed oxide samples with various microstructures and plutonium concentrations* - **Journal of Nuclear Materials**, 434, 287-290, **2013**.
2. G. Pastore, L. Luzzi, V. Di Marcello, P. Van Uffelen - *Physics-based modelling of fission gas swelling and release in UO_2 applied to integral fuel rod analysis* - **Nuclear Engineering and Design**, 256, 75-86, **2013**.
3. V. Di Marcello, S. Lorenzi, L. Luzzi, D. Pizzocri - *Improvements of the Transuranus Code for Lead-Cooled Fast Reactor Analysis: ALFRED Reactor Fuel Rod* - Proceedings of the International Workshop "Towards Nuclear Fuel Modelling in the Various Reactor Types across Europe", Karlsruhe, Germany, June 10-11, 2013.
4. L. Luzzi, A. Cammi, V. Di Marcello, S. Lorenzi, D. Pizzocri, P. Van Uffelen - *Application of the TRANSURANUS code for the fuel pin design process of the ALFRED reactor* - **Nuclear Engineering and Design**, 277, 173-187, **2014**.
5. G. Pastore, D. Pizzocri, J.D. Hales, S.R. Novascone, D.M. Perez, B.W. Spencer, R.L. Williamson, P. Van Uffelen, L. Luzzi - *Modelling of Transient Fission Gas Behaviour in Oxide Fuel and Application to the BISON Code* - Proceedings of the Enlarged Halden Programme Group (EHPG) Meeting, Session F7, Paper 4, Røros, Norway, September 7-12, 2014.
6. D. Pizzocri, S. Lorenzi, L. Luzzi - *Extension of the TRANSURANUS code to the 15-15Ti austenitic steels for the fuel pin performance analysis of Gen-IV Liquid Metal-cooled Fast Reactors* - CESNEF-IN-03-2015 Technical Report, pp. 1-68, Department of Energy, Nuclear Engineering Division, Politecnico di Milano, March 2015.
7. D. Pizzocri, T. Barani, E. Bruschi, L. Luzzi, P. Van Uffelen - *Development and validation of a transient fission gas release model for TRANSURANUS* - Proceedings of the International Workshop "Towards Nuclear Fuel Modelling in the Various Reactor Types across Europe", Karlsruhe, Germany, June 8-9, 2015.
8. D. Pizzocri, G. Pastore, T. Barani, E. Bruschi, L. Luzzi, P. Van Uffelen - *Modelling of Burst Release in Oxide Fuel and Application to the Transuranus Code* - Proceedings of the 11th International Conference on WWER Fuel Performance, Modelling and Experimental Support, Vol. I, pp. 311-320, Golden Sands Resort, Bulgaria, September 26 - October 3, 2015.
9. D. Pizzocri, G. Pastore, T. Barani, S. Lorenzi, L. Luzzi - *An efficient energy remainder criterion for intra-granular diffusion calculations: Improving the PolyPole-1 algorithm* - The Nuclear Materials Conference (NuMat 2016), Montpellier, France, November 7-10, 2016.
10. D. Pizzocri, F. Cappia, V.V. Rondinella, P. Van Uffelen - *Preliminary model for the fission gas behaviour in the high burnup structure (HBS)* - JRC Technical Report, JRC-Karlsruhe, 2016.
11. D. Pizzocri, C. Rabiti, L. Luzzi, T. Barani, P. Van Uffelen, G. Pastore - *PolyPole-1: An accurate numerical algorithm for intra-granular fission gas release* - **Journal of Nuclear Materials**, 478, 333-342, **2016**.

12. F. Cappia, D. Pizzocri, A. Schubert, P. Van Uffelen, G. Paperini, D. Pellottiero, R. Maciàn-Juan, V.V. Rondinella - *Critical assessment of the pore size distribution in the rim region of high burnup UO_2 fuel* - **Journal of Nuclear Materials**, 480, 138-149, **2016**.

13. D. Pizzocri, F. Cappia, L. Luzzi, G. Pastore, V.V. Rondinella, P. Van Uffelen - *A semi-empirical model for the formation and depletion of the high burnup structure in UO_2* - **Journal of Nuclear Materials**, 487, 23-29, **2017**.

14. T. Barani, E. Bruschi, D. Pizzocri, G. Pastore, P. Van Uffelen, R.L. Williamson, L. Luzzi - *Analysis of transient fission gas behaviour in oxide fuel using BISON and TRANSURANUS* - **Journal of Nuclear Materials**, 486, 96-110, **2017**.

15. P. Van Uffelen, A. Schubert, J. van de Laar, W. Li, C. Gyori, R. Dubourg, T. Pavlov, F. Cappia, L. Cognini, T. Barani, D. Pizzocri, G. Pastore, L. Luzzi - *Current meso-scale modelling developments for TRANSURANUS* - NEA Workshop: Advanced Fuel Modelling for Safety and Performance Enhancement, Paris, France, March 7-9, 2017.

16. D. Pizzocri, F. Cappia, L. Luzzi, V.V. Rondinella, P. Van Uffelen - *Modelling of high burnup structure in fuel performance codes: formation and porosity evolution* - Proceedings of the International Workshop "Towards Nuclear Fuel Modelling in the Various Reactor Types Across Europe", Lappeenranta, Finland, June 15-16, 2017.

17. T. Barani, L. Cognini, D. Pizzocri, A. Schubert, L. Luzzi, P. Van Uffelen - *Modelling and assessment of helium intra-granular behaviour in oxide fuels* - Proceedings of the International Workshop "Towards Nuclear Fuel Modelling in the Various Reactor Types Across Europe", Lappeenranta, Finland, June 15-16, 2017.

18. L. Luzzi, D. Pizzocri, T. Barani - *Physically-based inert gas behaviour modelling for fuel performance codes* - Proceedings of the Second Workshop on Research into Nuclear Fuel and Cladding in Europe (NuFuel), Lecco, Italy, September 4-6, 2017.

19. L. Luzzi, L. Cognini, D. Pizzocri, T. Barani, G., Pastore, A. Schubert, T. Wiss, P. Van Uffelen - *Helium diffusivity in oxide nuclear fuel: Critical data analysis and new correlations* - **Nuclear Engineering and Design**, 330, 265-271, **2018**.

20. G. Pastore, T. Barani, D. Pizzocri, A. Magni, L. Luzzi - *Modeling Fission Gas Release and Bubble Evolution in UO_2 for Engineering Fuel Rod Analysis* - Proceedings of the International Conference on Reactor Fuel Performance (Top Fuel 2018), Paper A0240, Prague, Czech Republic, September 30 - October 4, 2018.

21. L. Cognini, D. Pizzocri, T. Barani, P. Van Uffelen, A. Schubert, T. Wiss, L. Luzzi - *Helium solubility in oxide nuclear fuel: Critical review and derivation of new correlations for Henry's constant* - **Nuclear Engineering and Design**, **2018** (*submitted*).

22. G. Pastore, D. Pizzocri, C. Rabiti, T. Barani, P. Van Uffelen, L. Luzzi - *An effective numerical algorithm for intra-granular fission gas release during non-equilibrium trapping and resolution* - **Journal of Nuclear Materials**, **2018** (*accepted*).

Thank you for your kind attention

WORKSHOP TEMATICO

LFR-GEN IV: STATO ATTUALE DELLA TECNOLOGIA E PROSPETTIVE DI SVILUPPO

ADP ENEA-MSE (PAR2017-LP2)

POLIMI contribution

Chemical issues within the development of Lead-cooled Fast Reactors

E. Macerata, M. Mariani, M. Giola

POLITECNICO MILANO 1863

14-15 June, 2018, Roma

ENEA
Agenzia nazionale per le nuove tecnologie, l'energia e lo sviluppo economico sostenibile

Summary

- Chemical issue in LFRs
  - Fuel-coolant chemical interaction
  - System features
  - Approach
- Computational studies
- Experimental activities

Chemical issue....

Fuel-coolant chemical interaction

Cladding failure event

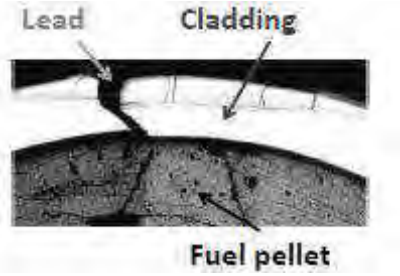

under nominal operation

in accidental conditions

What influences do chemical effects have?

- Fuel material properties and behaviour
  - Thermal conductivity
  - Melting point
  - Swelling
- Cladding material properties and behaviour
  - Chemical composition of the gas: corrosion and oxidation of cladding
- Release of radionuclides from fuel
  - Different volatility and solubilities of the species

The system under study: irradiated fuel-cladding-lead

1 H																	2 He
3 Li	4 Be											5 B	6 C	7 N	8 O	9 F	10 Ne
11 Na	12 Mg											13 Al	14 Si	15 P	16 S	17 Cl	18 Ar
19 K	20 Ca	21 Sc	22 Ti	23 V	24 Cr	25 Mn	26 Fe	27 Co	28 Ni	29 Cu	30 Zn	31 Ga	32 Ge	33 As	34 Se	35 Br	36 Kr
37 Rb	38 Sr	39 Y	40 Zr	41 Nb	42 Mo	43 Tc	44 Ru	45 Rh	46 Pd	47 Ag	48 Cd	49 In	50 Sn	51 Sb	52 Te	53 I	54 Xe
55 Cs	56 Ba	57 La	72 Hf	73 Ta	74 W	75 Re	76 Os	77 Ir	78 Pt	79 Au	80 Hg	81 Tl	82 Pb	83 Bi	84 Po	85 At	86 Rn
87 Fr	88 Ra	89 Ac	104 Rf	105 Db	106 Sg	107 Bh	108 Hs	109 Mt	110 Ds	111 Rg	112 Cn	113 Nh	114 Fl	115 Mc	116 Lv	117 Ts	118 Og
119 Uue																	

58 Ce	59 Pr	60 Nd	61 Pm	62 Sm	63 Eu	64 Gd	65 Tb	66 Dy	67 Ho	68 Er	69 Tm	70 Yb	71 Lu
90 Th	91 Pa	92 U	93 Np	94 Pu	95 Am	96 Cm	97 Bk	98 Cf	99 Es	100 Fm	101 Md	102 No	103 Lr

VOLATILE FISSION PRODUCTS

METALLIC PRECIPITATES AS ALLOYS

OXIDES DISSOLVED IN THE FUEL MATRIX

CERAMIC PRECIPITATES AS OXIDES

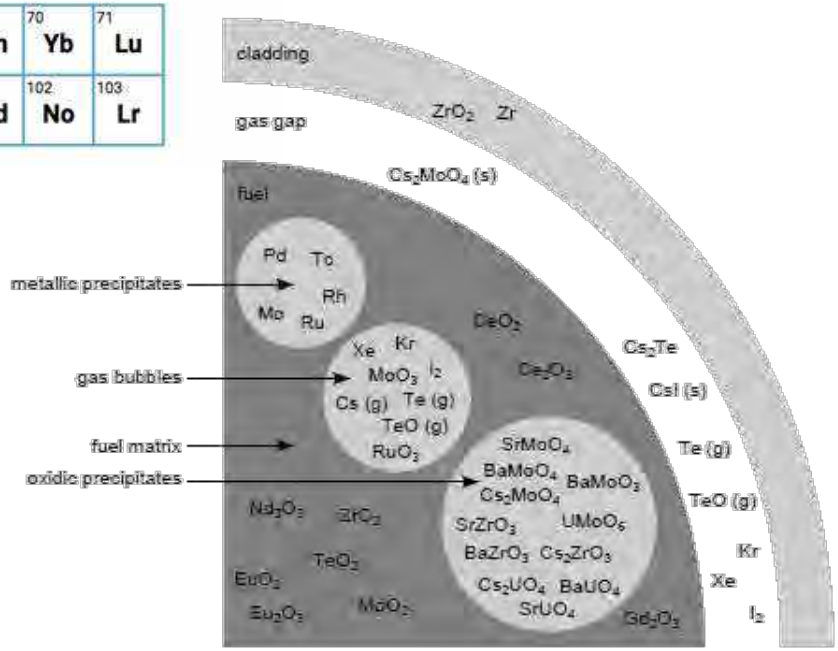

The system under study: irradiated fuel-cladding-lead

IRRADIATED FUEL

COMPOSITION

MIGRATION PHENOMENA/ RELEASE MECHANISMS

TEMPERATURE GRADIENT

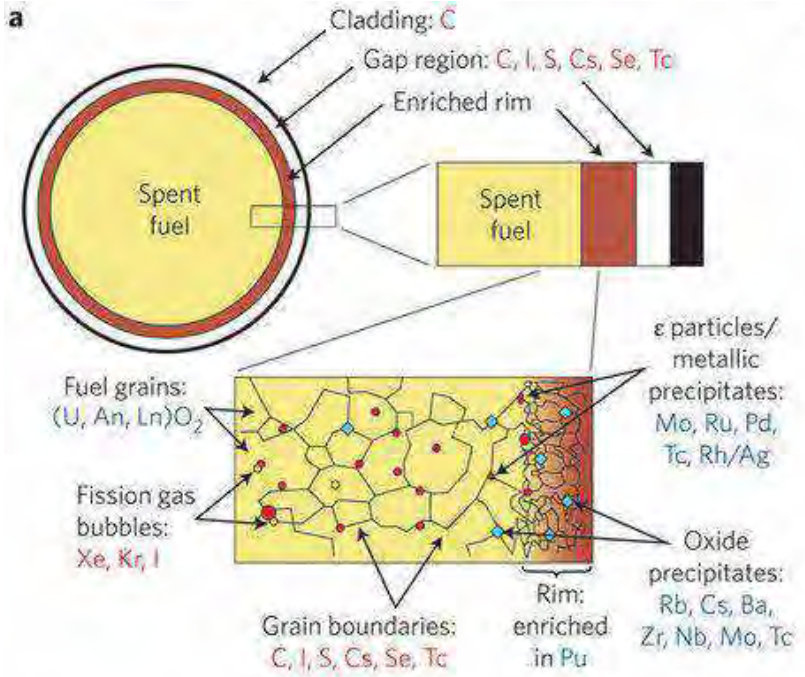

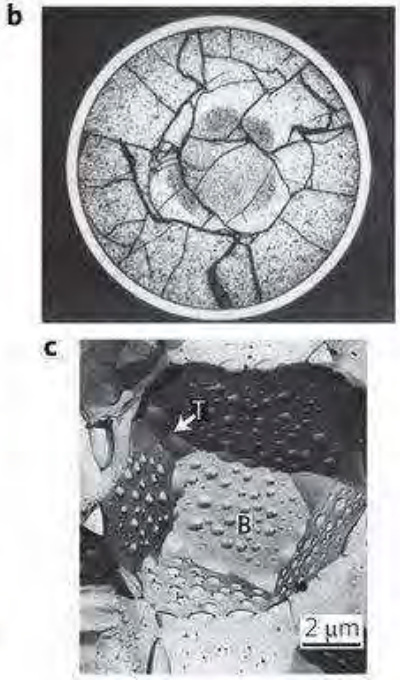

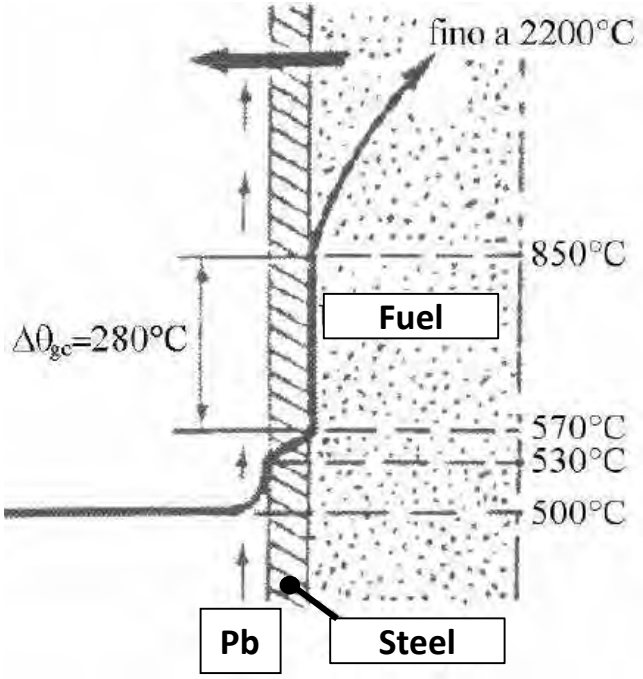

Chemical issue....

Fuel-coolant = multi-component and multi-phase system

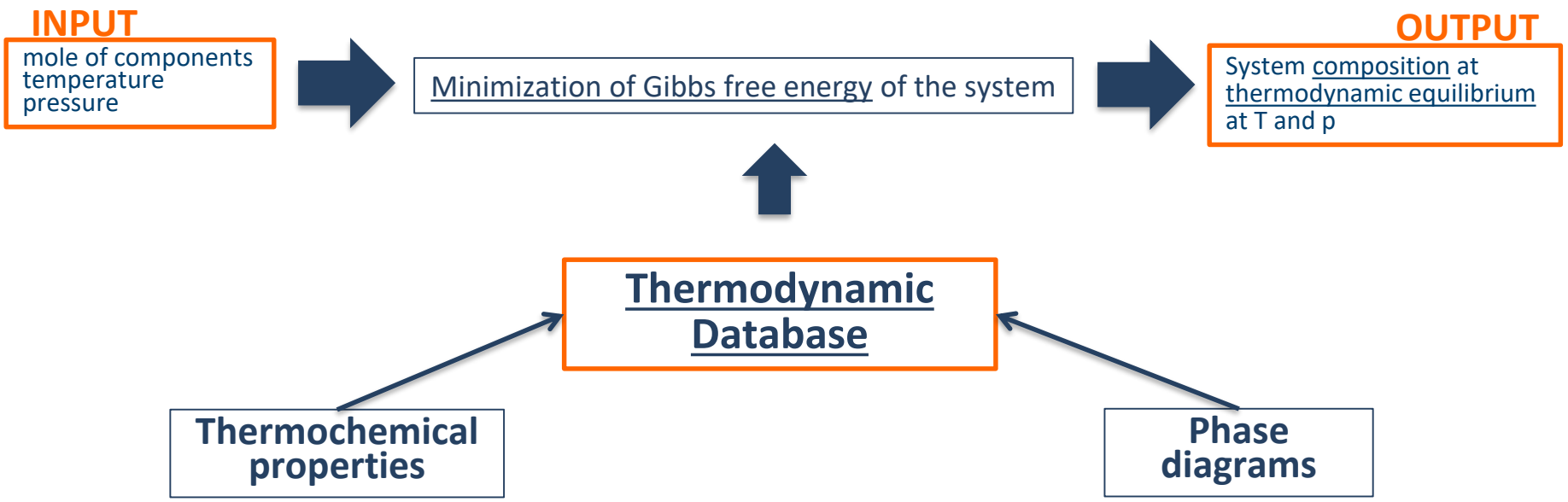

Experimental phase diagrams
Semi-empirical methods
DFT-GGA simulations

→ Implementation of **Thermochemical Database** of interest for LFR

Thermodynamic simulation by **CALPHAD method**

- based on minimization of the Gibbs free energy of the system under specific assumptions
- enable the modeling of thermochemical properties and phase diagrams
- by using experimental or calculated data
- enable to study multi-phase and multi-component systems by extrapolation of the description of the lower component subsystems
- Software: old free source codes, a number of commercial software packages (FactSage, Thermo-Calc), recent development of free CALPHAD software (OpenCalphad)
- Database: specific commercial databases in continuous development in order to improve accuracy and reliability

Hickel et al., *Phys. Status Solidi B* **251**, 1, 9-13 (2014)
Kattern et al., Tecnol. Metal. Mater. Miner., 13, 3-15 (2016)
Kattern et al., *Calphad*, 24, 55-94 (2000)

Computational activities – PAR2017

Thermodynamic simulation by CALPHAD

Methodology

Application to:

La-Pb-O and U-Pb-O systems

by using:

- the data estimated by DFT-GGA approach
- experimental binary phase diagrams

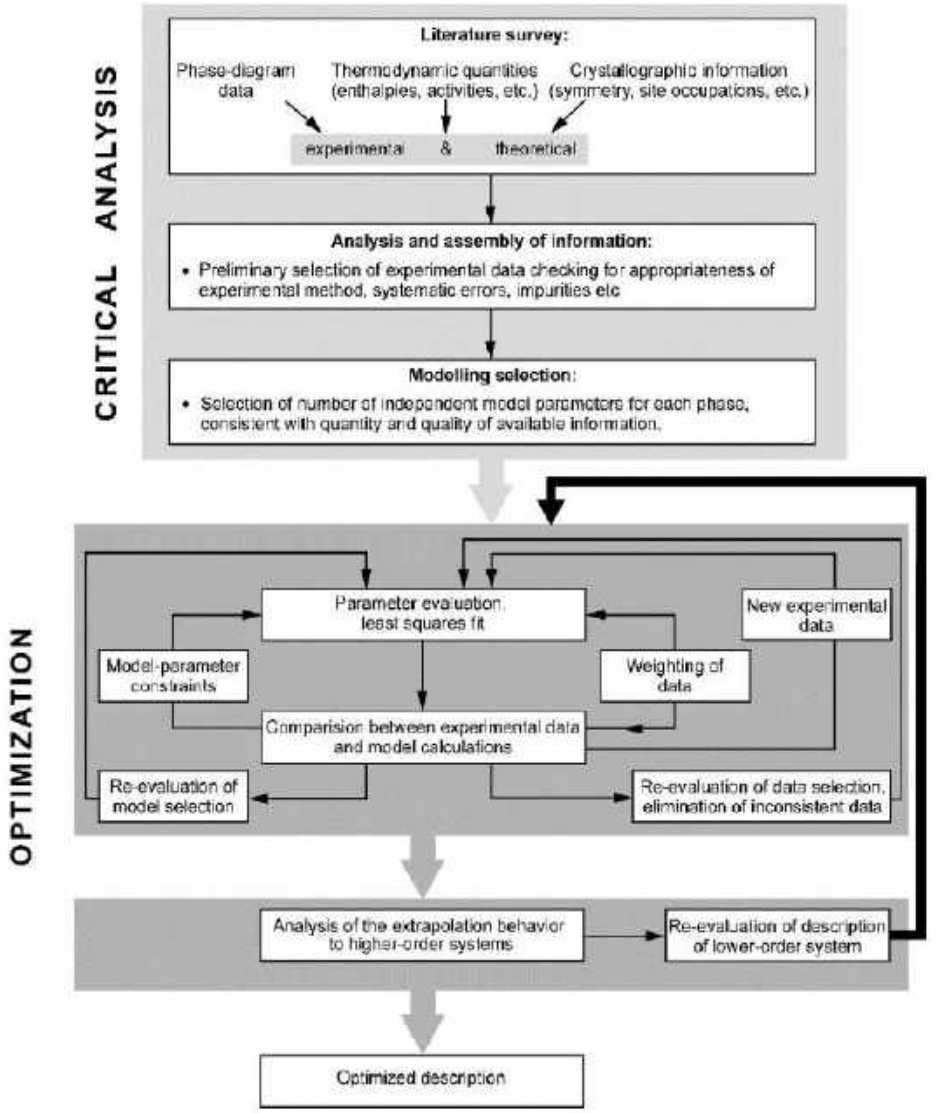

Modeling chemical processes in nuclear fuel

Integrating thermodynamic calculations in multi-physics codes for nuclear applications

Thermodynamic calculations provide, directly or indirectly, material properties, boundary conditions and source terms

Multi-physics simulations predict nuclear fuel behavior to support performance and safety analysis

Some examples…

Report NEA/NSC/R/(2015)5
Loukusa et al., JNM 481 (2016) 101-110
Piro et al., JNM 441 (2013) 240-251
Baurens et al., JNM 452 (2014) 578-594

Modeling chemical processes in nuclear fuel

In 1995

SOLGASMIX program + Royal Military College of Canada Nuclear Fuel Thermochemical Treatment (RNFTT)

PGE algorithm + Thermochemistry library Thermochimica

In 2013, *Piro et al.* simulated the temporal and spatial evolution of coupled thermochemical and nuclear reactions of irradiated fuel

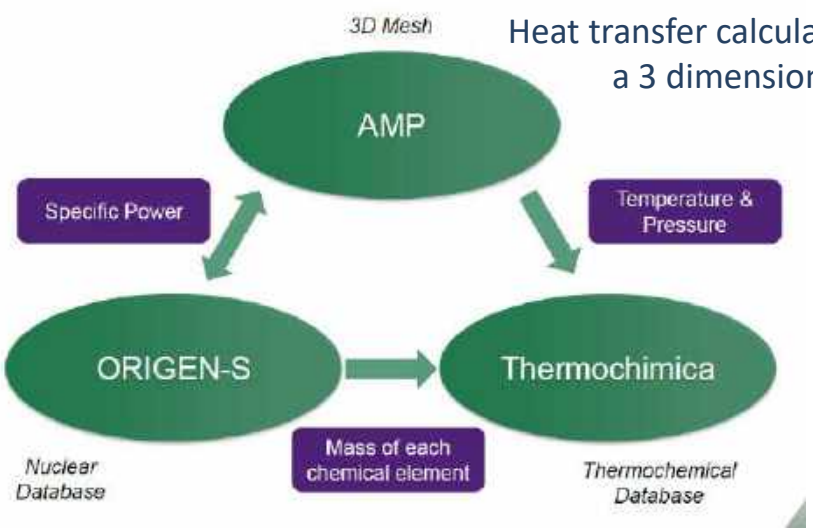

Heat transfer calculations on a 3 dimensional mesh

Isotopic calculations

Thermochemical calculations

- Able to predict oxygen chemical potential including fission products and minor phases formed;
- Able to predict chemical potentials of all the system components;
- Able to predict the formation of new phases in the fuel;
- Incorporation of chemical effects on the fuel surface with cladding.

Modeling chemical processes in nuclear fuel

In 2014, *Baurens et al.* studied the phenomena behind iodine stress corrosion cracking

Thermomechanical fuel behavior code

AdvaNced Gibbs Energy

SOLGASMIX

Fission gas release module

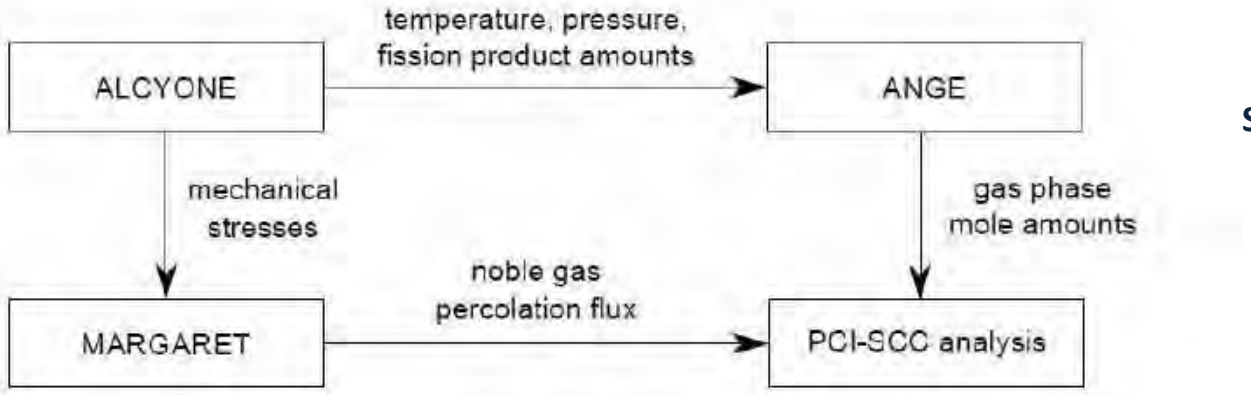

Figure 11. *The usage of the ANGE thermochemical solver coupled to the ALCYONE fuel performance code in stress corrosion cracking studies [11]. Note that there is no feedback from ANGE to ALCYONE.*

Modeling chemical processes in nuclear fuel

Next activity…

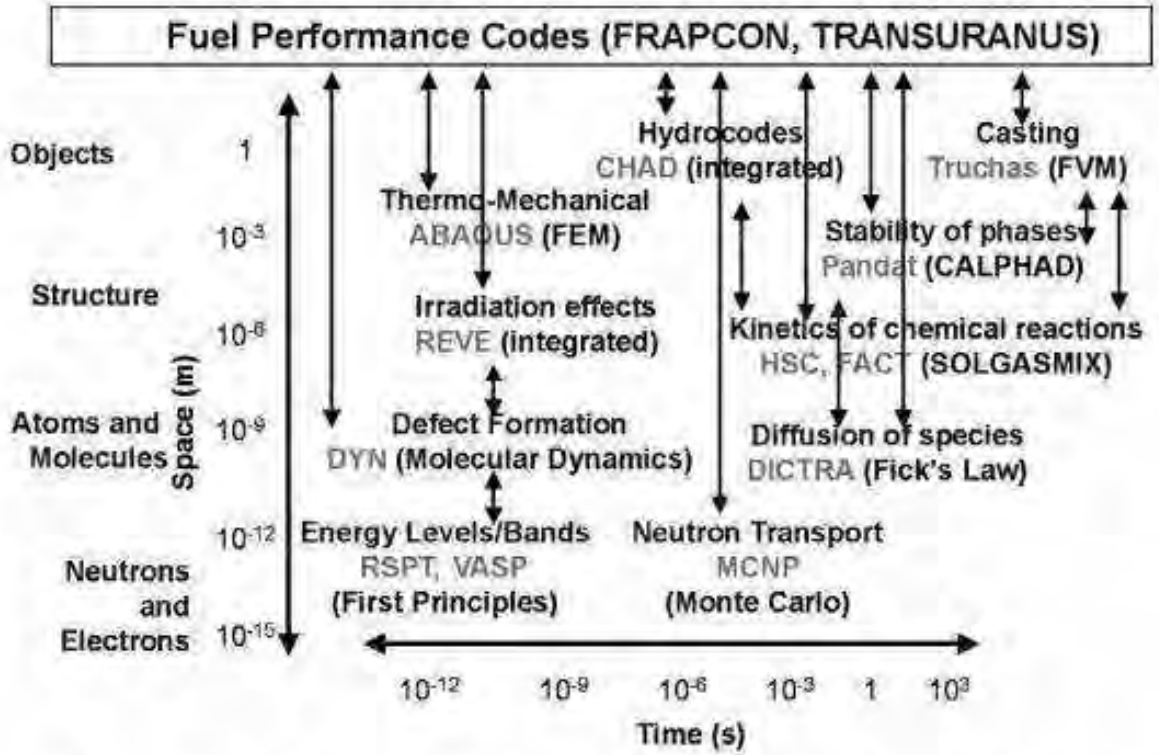

Figure 2. Space and time scales involved in simulating phenomena relevant for nuclear materials (black). The methods are shown in parenthesis. Several software packages (gray) are used to illustrate the type of simulation. [M. Stan, T. Amer. Nucl. Soc, 91 (2004) 131]

Experimental Activities – PAR2017

AIMS:

- To observe a possible reactivity between Pb and an element/compound simulating the irradiated fuel
- To identify the new products formed
- To evaluate possible solubilities in Pb

SELECTED SYSTEMS:

- Metallic elements
- SrO, CeO_2, La_2O_3
- Fe_2O_3
- Pb as powder or wire

EXPERIMENTS

- Preliminary investigations
- Reactivity experiments

High reactivity of Pb and metals in presence of air

Glove box with inert atmosphere (Ar with a O content < 0.1 ppm)

PRELIMINARY EXPERIMENTS BY DIFFERENTIAL SCANNING CALORIMETRY

- Check of pure reagents
- First check of a possible reactivity between lead and oxide powder
  - Pieces of Pb and oxide powders are placed in the DSC crucible
  - The T profile is set through the software
  - Melting and enthalpy values are compared with the reference ones

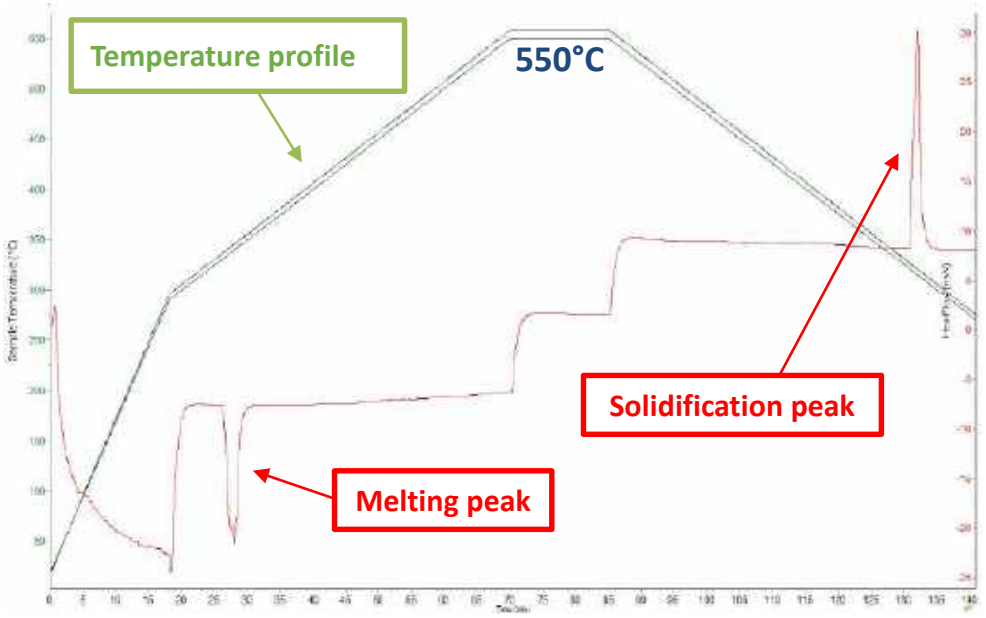

RESULTS

	Lead Melting Temperature [°C]	Lead Melting Enthalpy [J/g]
Reference Pb	327.4 ± 0.1	23.0 ± 2.6
Pb	327.3 ± 0.1	21.6 ± 1.9
Pb - La_2O_3	327.9 ± 0.1	21.5 ± 2.1
Pb - Fe_2O_3	327.0 ± 0.1	21.5 ± 1.8
Pb - CeO_2	327.2 ± 0.1	21.5 ± 1.9
Pb - SrO	327.9 ± 0.1	21.7 ± 2.1

No interaction between oxide powders and Pb

Reactivity Experiments

Materials:

CeO_2, Fe_2O_3, La_2O_3, SrO in powder or pellet
Pb (99.9%) in wire

Pellet Preparation:

Pressure = 100 bar
Inert atmosphere (Ar)

Thermal treatment:

Temperature range: 500-550-750°C
Reaction time: 2-6 hours
Inert atmosphere (Ar)
In glass or Pyrex test tubes

Experimental Activities – PAR2017

Thermal Treatment in furnace

	Pellet (1 g)	Pb [g]	T [°C]	t [min]	pellet setup
A1	-	2.5	500	310	air
A2	La_2O_3	2.3	500	310	air
A3	Fe_2O_3	2.5	500	310	air
B1	Fe_2O_3	4	500	210	air
B2	La_2O_3	4.3	500	210	air
B3	SrO	4.2	500	210	air
C1	Fe_2O_3	4.5	550	290	argon
C2	CeO_2	4.7	550	290	argon
C3	SrO	4.3	550	290	argon
D1	Fe_2O_3	4.6	550	345	argon
D2	La_2O_3	4.5	550	345	argon
D3	La_2O_3	4.2	550	345	argon
E1	Fe_2O_3	4.4	750	300	argon
E2	La_2O_3	4.3	750	300	argon
E3	CeO_2	4.5	750	300	argon
F1	La_2O_3	4.9	550	290	argon
F2	SrO	4.8	550	290	argon
G1	CeO_2	4.9	750	290	argon
G2	Fe_2O_3	4.8	750	290	argon

Optimization of sample preparation has been needed.

First macroscopic observations

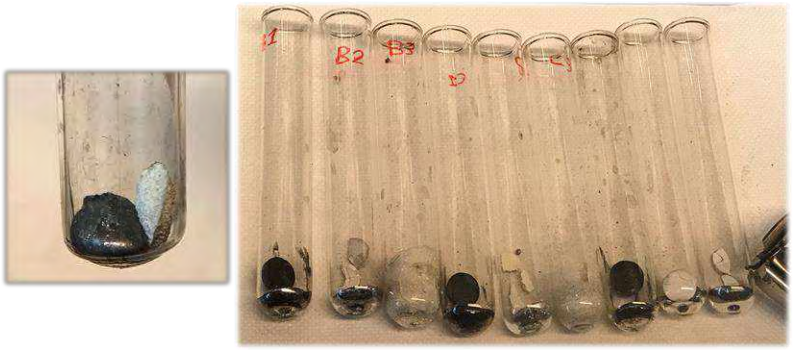

Temperature = 500-550 °C

Pellet	Floats over Pb	Change in shape	Change in colour
CeO_2	✓	✗	✗
Fe_2O_3	✓	✗	✓
La_2O_3	✓	✗	✗
SrO	✗	✓	✗

Temperature = 750 °C

Same behaviour at higher temperature.

Lead vapours are not detected.

Characterization by X-ray Diffraction

- Check of pure reagents

- The contact surface between lead and oxide pellet is scratched
- The powder is placed in the sample holder with the dome
- The measured pattern is compared with a reference pattern

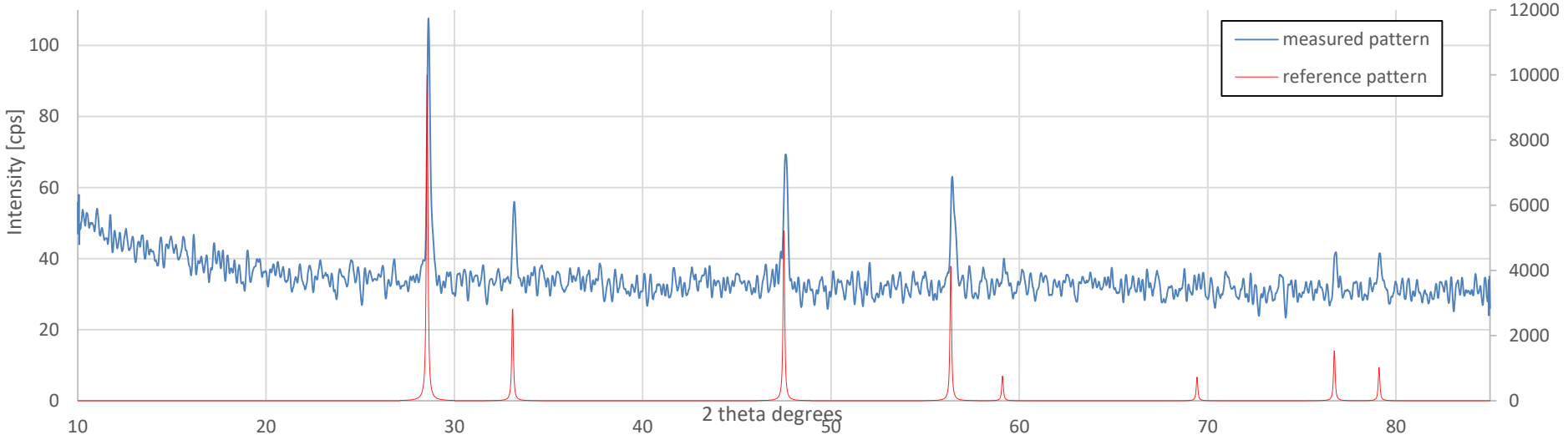

CHARACTERIZATION BY SEM-EDX

- The contact surface between lead and oxide pellet is scratched
- The powder is placed in the sample holder (in vacuum) and opened inside the SEM
- The image is sent to EDX for the elemental analysis

Spectrum processing :
Peak possibly omitted : 0.257 keV

Processing option : All elements analyzed (Normalised)
Number of iterations = 3

Standard :
O SiO2 1-Jun-1999 12:00 AM
Sr SrF2 1-Jun-1999 12:00 AM

Element	App Conc.	Intensity Corrn.	Weight %	Weight % Sigma	Atomic %
O K	31.24	0.5107	25.66	0.37	65.41
Sr L	173.67	0.9802	74.34	0.37	34.59
Totals			100.00		

Sample: SrO tq
Type: Default
ID:

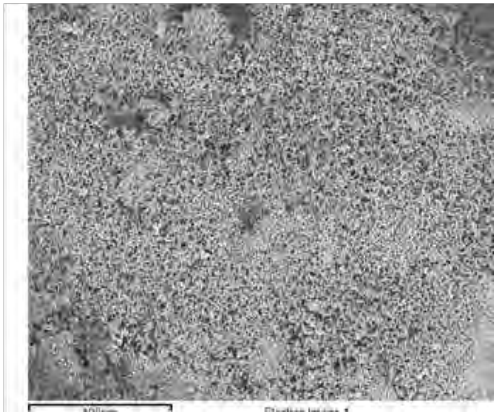

CHARACTERIZATION RESULTS

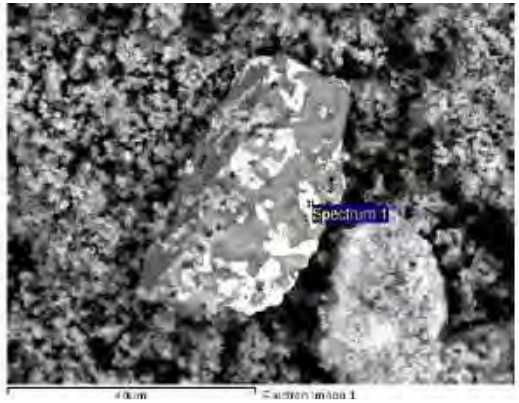

XRD ANALYSES

Sample	Check on pristine powders	After the experiment
CeO_2	Cerianite	Cerianite
Fe_2O_3	Hematite	Maghemite
La_2O_3	Lanthanum (III) oxide	Lanthanum (III) oxide
SrO	Strontium (II) oxide	Strontium (II) oxide

SEM-EDX ANALYSES

Compound	Pristine powders	After the experiment
CeO_2	Ce, O	Ce, O Impurities (< 1%)
Fe_2O_3	Fe, O Impurities (Ca, Ba, S, Si > 1%)	Fe, O Impurities (Ca, Ba, S, Si > 1%) Pb adherent on Ba and S
La_2O_3	La, O	La, O
SrO	Sr, O	Sr, O

- No interaction compounds at the pellet surface are found
- The only change is in the iron oxide structure from **α**-Fe_2O_3 to **γ**-Fe_2O_3

Future Experimental Activities

INTERACTION STUDIES:

- Evaluation of solubility in liquid Pb by ICP-MS measurements
- Longer reaction time and T > 750°C
- Study a different setup for liquid-liquid interaction

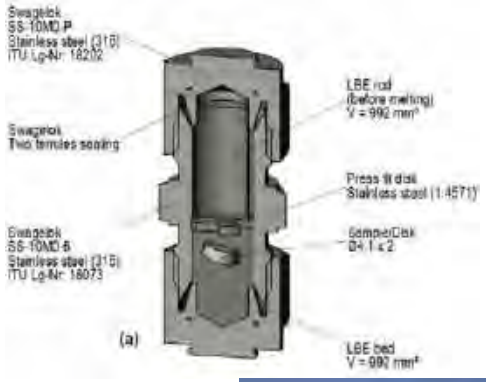

a) Sample container

Vigier et al., *Journal of Nu clear Materials,* 467 (2015), 840-847.

b) Inert atmosphere

Gas purifier to reach lower O content (< 1 ppb) in a small volume

- Metallic fission products
- Preparation of Pb intermetallics to obtain missing thermodynamic data by experiments
- Further investigations on pellet cross section
  - Sample preparation under evaluation

Conclusions

Computational studies

- Investigations of U-Pb-O and La-Pb-O systems by CALPHAD approach by exploiting data previously estimated by DFT-GGA approach;
- Go deepen in the integration of the thermochemical simulations with multi-physics codes;

E. Macerata, *Studies on fuel-coolant chemical interaction in Lead-cooled Fast Reactors at Politecnico di Milano*, oral talk, CHERNE 2018 – 14° Workshop on European Collaboration on Radiological and Nuclear Engineering and Radiation Protection, 29/5-01/06/2018, Macugnaga (VB), Italy

Experimental studies

- Reactivity experiments at higher temperatures;
- Development of a new experimental set up.

M. Cerini, O. Benes, K.Popa, E. Macerata, J.-C. Griveau, E. Colineau, M. Mariani, R.J.M. Konings, *Thermodynamic properties of* $Pb_3U_{11}O_{36}$, submitted to J. Nucl. Mater.

Contacts:

elena.macerata@polimi.it
mario.mariani@polimi.it

Workshop Tematico AdP MiSE – ENEA, PAR2017 – Progetto B.3 - LP2

Roma, 14th June, 2018

LFR Multiphysics Model Development: OpenFoam – Serpent codes coupling

Antonio Cammi, Stefano Lorenzi

Nuclear Reactors Group

Activity overview

LP2: Development and benchmark of codes and multiphysics model for Generation-IV Fast Reactor design and safety analysis

PoliMi activity Development of a LFR multiphysics model for

i) design support

ii) code verification (e.g., FRENETIC – collaboration with PoliTo)

PAR 2016

Single channel LFR. Main physical pheomena – and their couplings – considered. Evaluation of the modelling approach and how to couple them.

PAR 2017

Monte Carlo – CFD coupling for a better accuracy in neutronics modelling (relevant for design support).

…

Activity overview

PAR 2017

. **Monte Carlo – CFD coupling** for a better accuracy in neutronics modelling (relevant for design support)

. Starting **collaboration with PoliTo** (S. Dulla, P. Ravetto, L. Savoldi, R. Zanino) for interaction/comparison with FRENETIC

. SERPENT code for Monte Carlo calculation and OpenFOAM for CFD analysis

- **SERPENT** continuous energy Monte Carlo code with constant group capabilities
- **OpenFOAM open source library** for numerical simulation with FV method. Flexible (obj-or prgramming), users can customize, extend and implement complex physical model
- Multiphysics interface already present

. **Neutronics** code provided with **realistic temperature profile** (improvement in reactivity and power outcomes)

. **CFD** code provided with **realistic volumetric fission power distribution** (improvement in temperature profile)

Motivation and background

Multiphysics: the study of the mutual interaction of different physical phenomena

. Fluid dynamics
. Neutronics
. Mechanics
. Heat Transfer
. Chemistry
. BoP

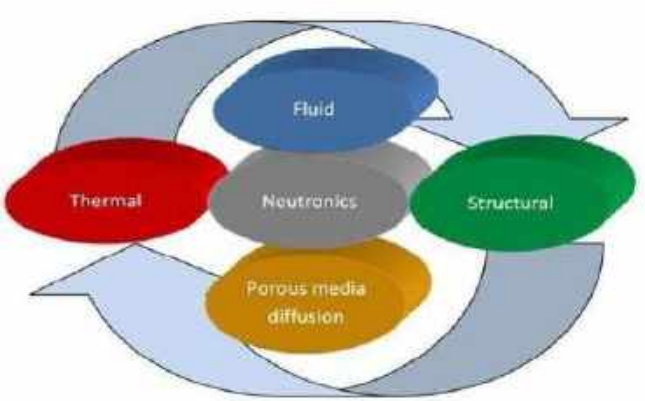

Purpose of multi-physics code:

. **deeper insight** about the complex physical phenomena occurring in the reactor system (and their mutual interactions)

. allows **evaluating** a wide set of core parameters (e.g., temperature field, velocity field, and neutron fluxes) with a unique simulation tool

. valuable for core designing, when **verifying** the satisfaction of the operational constraints

. **combined analysis** with system codes (not replacing)

Multiphysics modelling

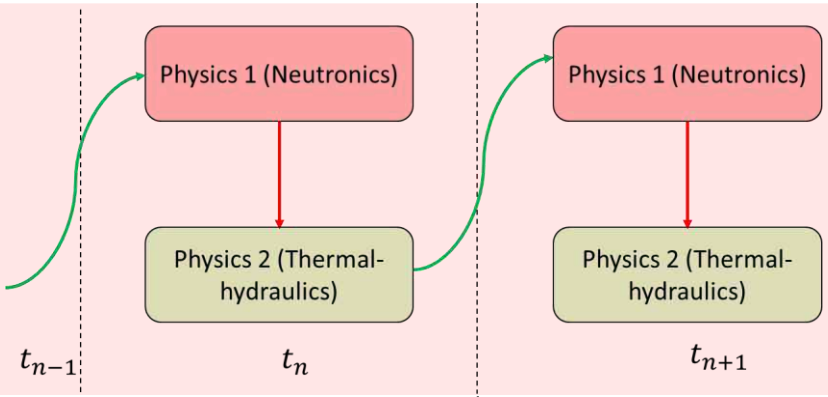

Explicit coupling:

. Operator splitting approach

. OK if coupling among physics is weak otherwise low accuracy in resolving multiphysics nonlinearities

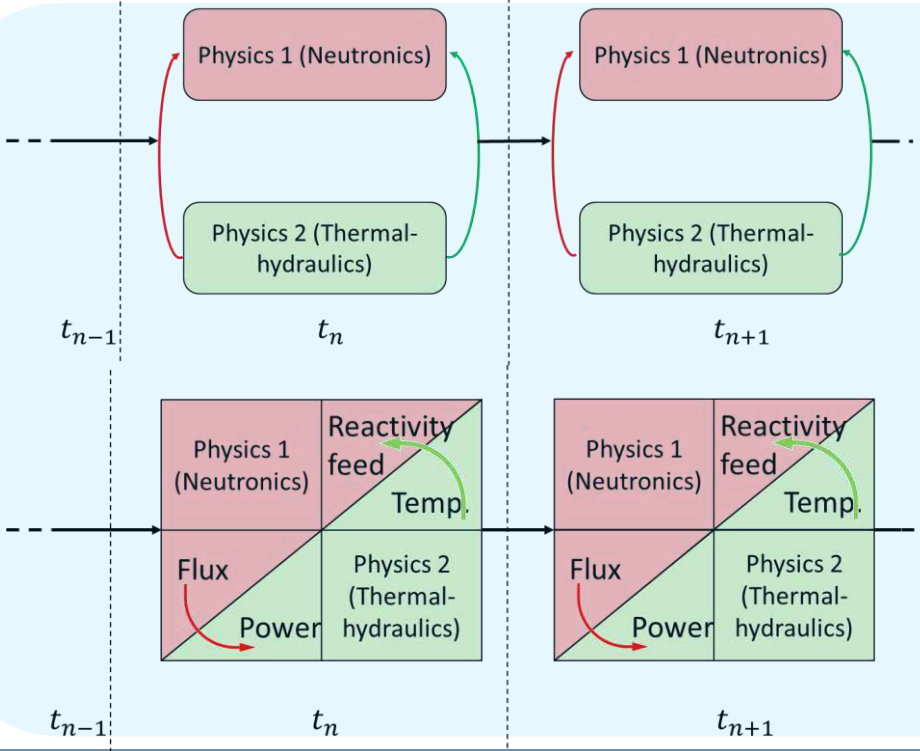

Implicit coupling:

. Iterative (Picard iteration) or monolithic approach (Jacobian-Free Newton Krylov)

. Highest level of accuracy but also strong computational burden

Neutronics – Thermal hydraulics coupling

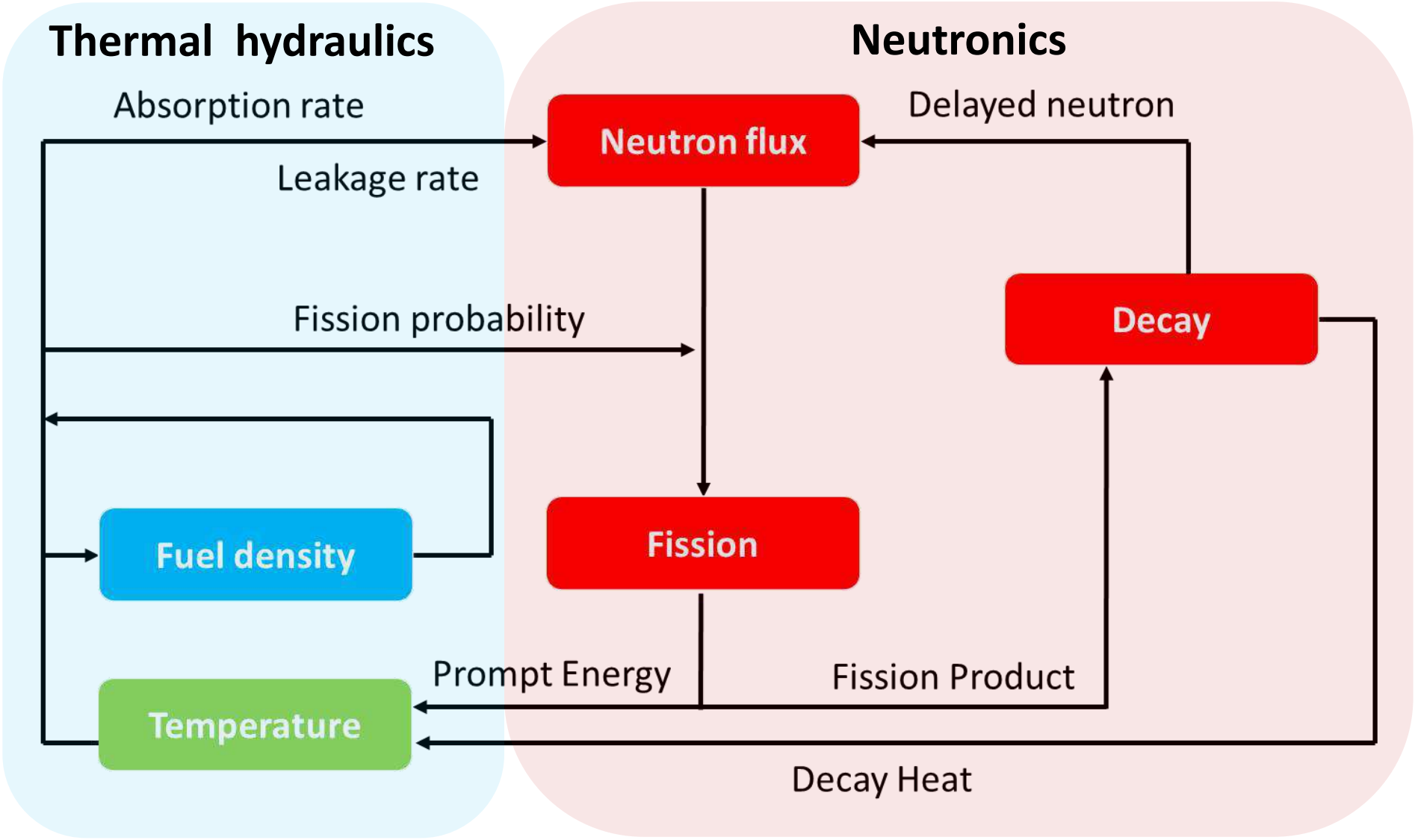

Neutronics – Thermal hydraulics coupling

Thermal hydraulics (CFD)

$$\frac{\partial T}{\partial t} =$$

$$= -\nabla(\boldsymbol{u}T) +$$

$$+\nabla \cdot \frac{k}{\rho C_p} \nabla T + \frac{E_f}{\rho C_p} \Sigma_f \phi$$

Neutronics (Monte Carlo)

$$(\boldsymbol{L} - \boldsymbol{S})\, \phi = \frac{1}{k_{eff}} \boldsymbol{F} \phi$$

Neutronics – Thermal hydraulics coupling

Thermal hydraulics (CFD)

$$\frac{\partial T}{\partial t} =$$

$$= -\nabla(\boldsymbol{u}T) +$$

$$+\nabla \cdot \frac{k}{\rho C_p}\nabla T + \frac{E_f}{\rho C_p}\Sigma_f \phi$$

Neutronics (Monte Carlo)

$$\left(\boldsymbol{L}(T) - \boldsymbol{S}(T)\right)\phi = \frac{1}{k_{eff}}\boldsymbol{F}(T)\phi$$

Neutronics – Thermal hydraulics coupling

Thermal hydraulics

$$T = \mathcal{T}(q)$$

Neutronics

$$q = \mathcal{N}(T)$$

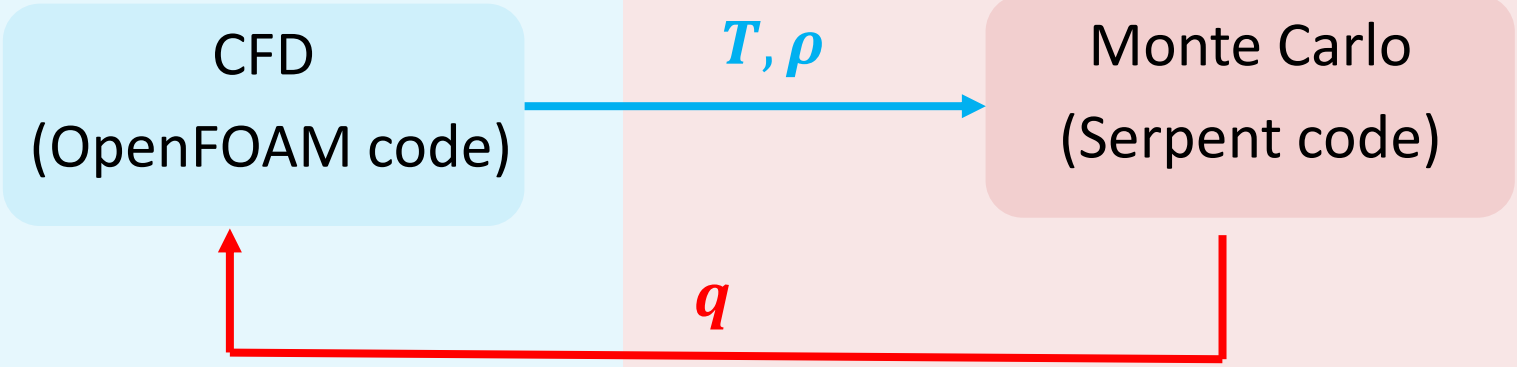

$$q = \mathcal{N}(\mathcal{T}(q) = G(q)$$

The steady-state power distribution q is the fixed point of the coupled problem

$$q_{n+1} = G(q_n)$$

Neutronics – Thermal hydraulics coupling

Easy (and wrong) way: use the brute force

Can the numerical (not the physical) coupling be unstable?

$$J_{i,j} = \frac{\partial G_i}{\partial q_j} \qquad \rho(J) < 1$$

Stability condition

Is numerical stability a problem for typical nuclear reactor problem?

Neutronics – Thermal hydraulics coupling

EPR case – Iteration 0

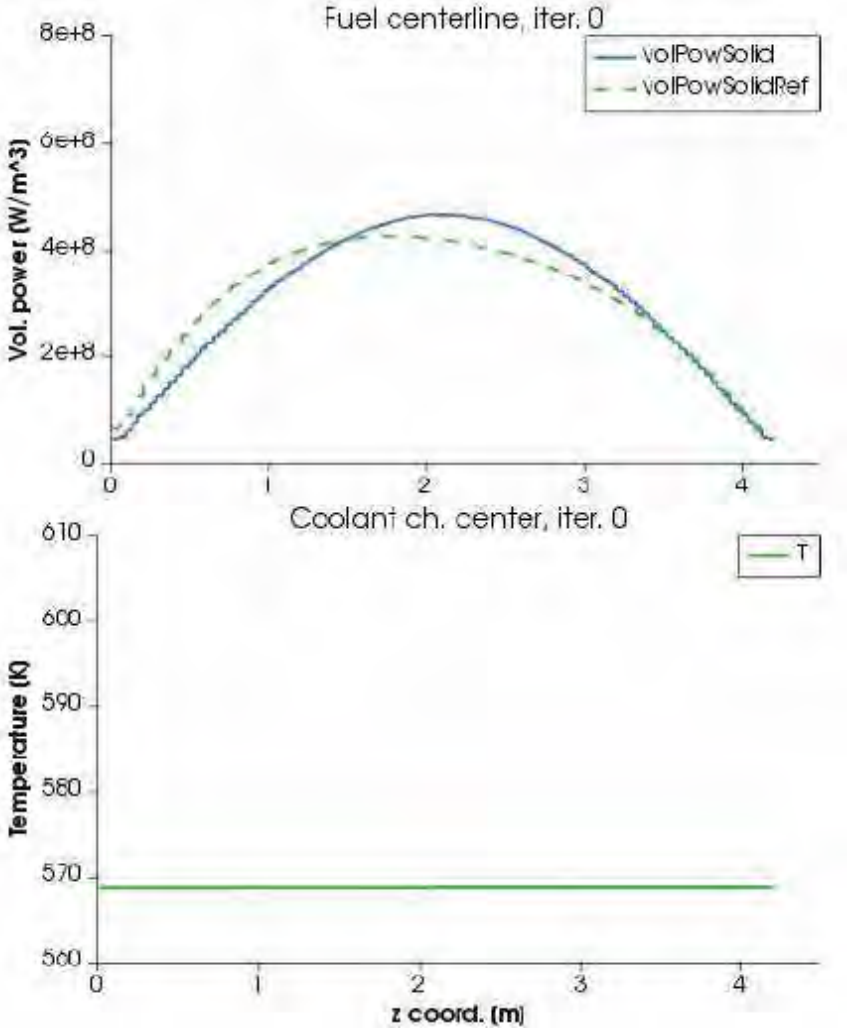

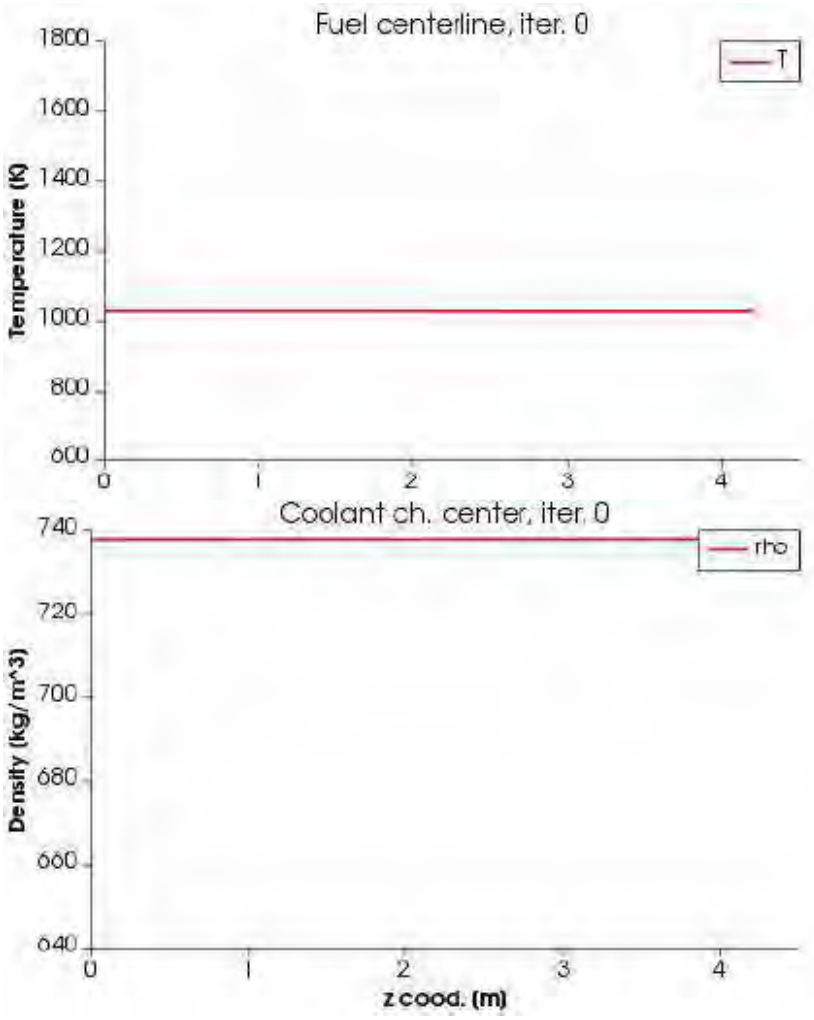

Neutronics – Thermal hydraulics coupling

EPR case – Iteration 1

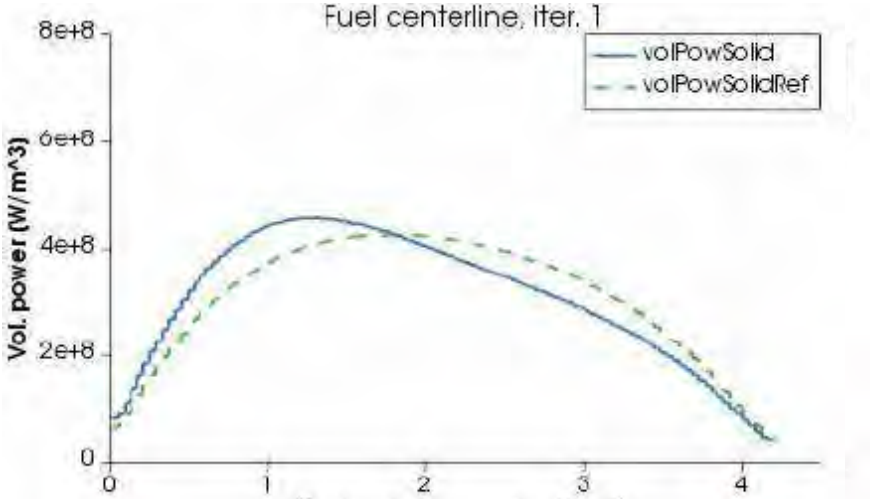

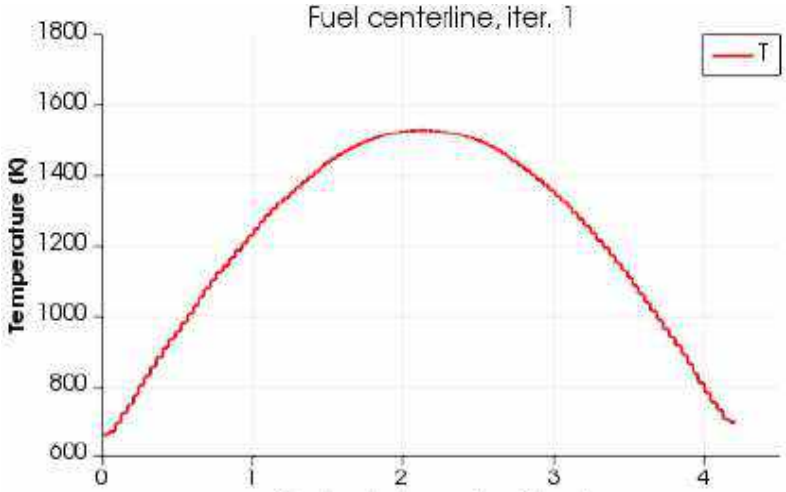

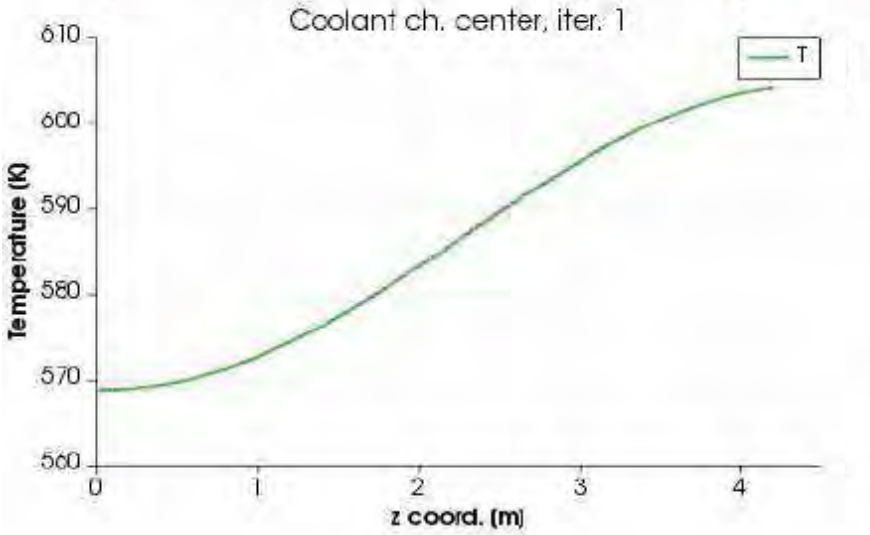

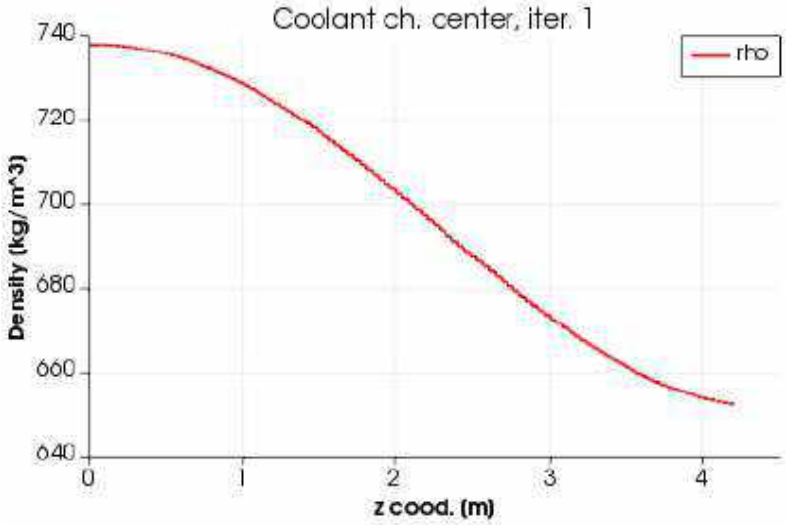

Neutronics – Thermal hydraulics coupling

EPR case – Iteration 2

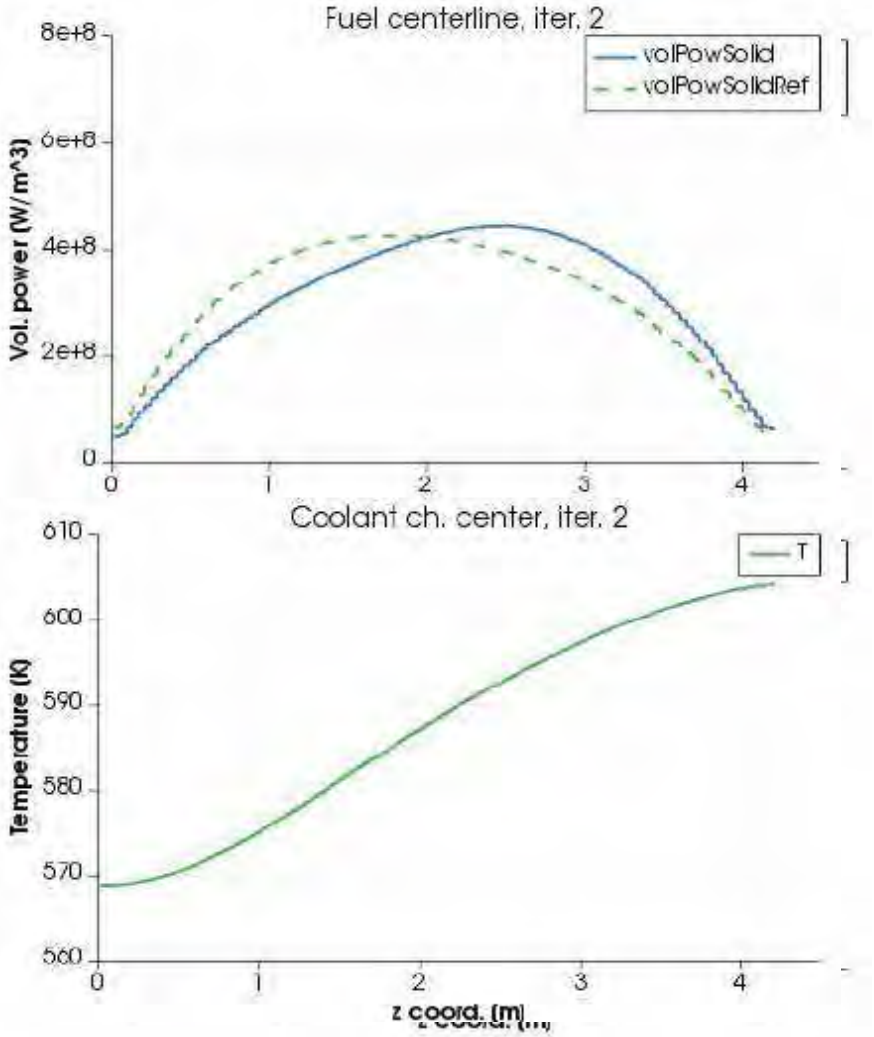

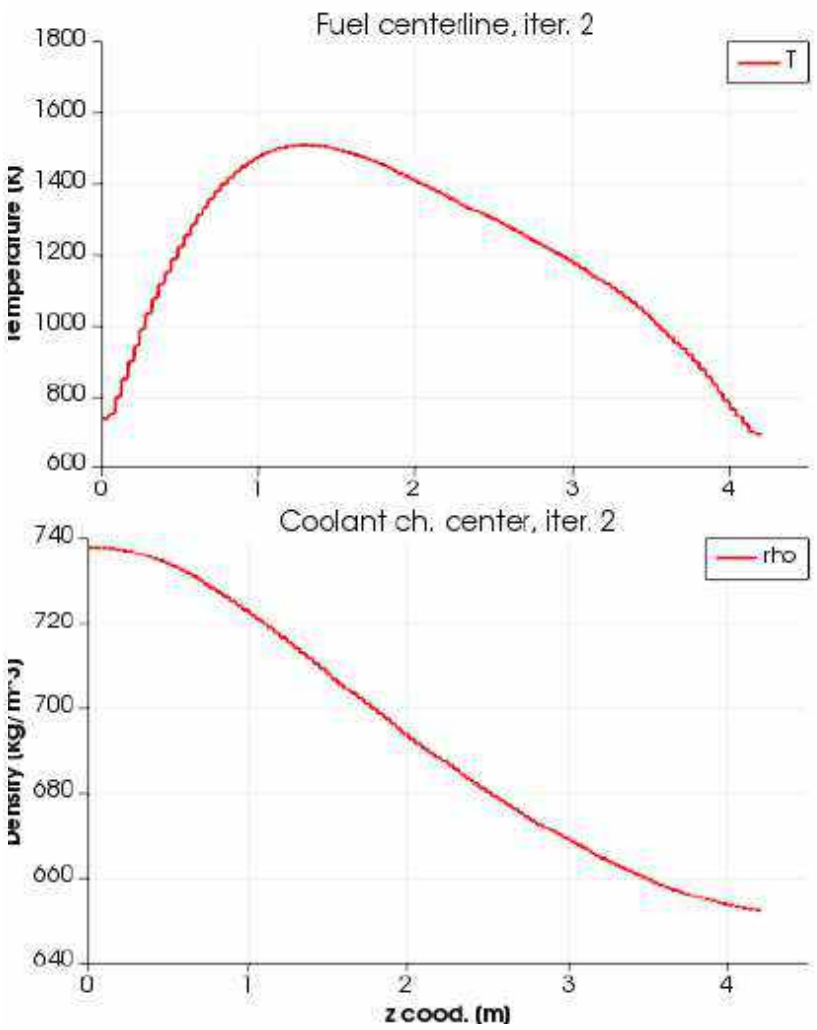

Neutronics – Thermal hydraulics coupling

EPR case – Iteration 3

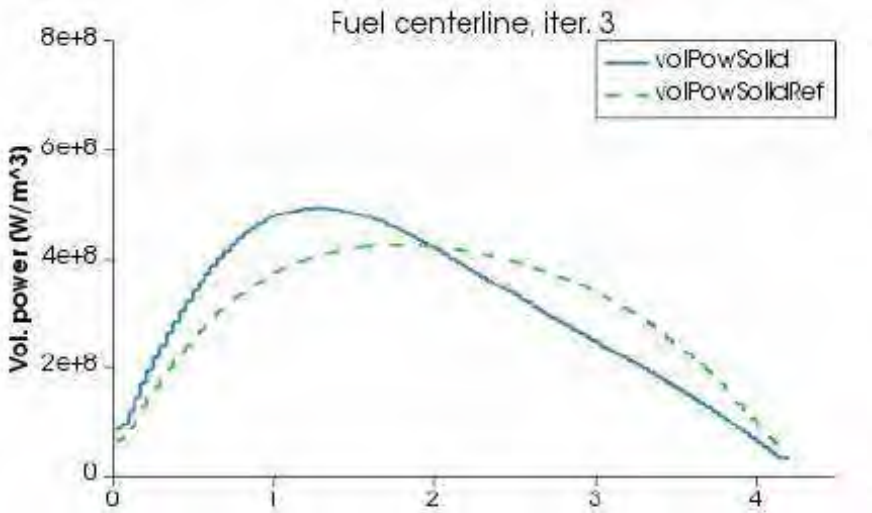

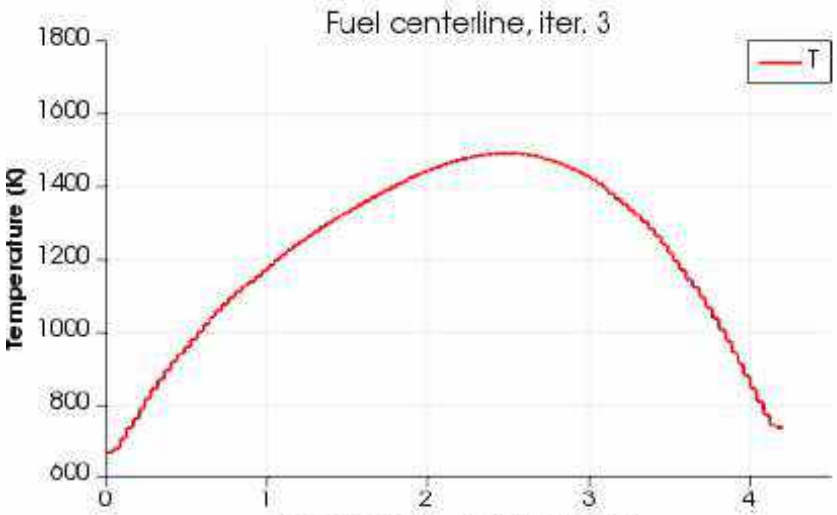

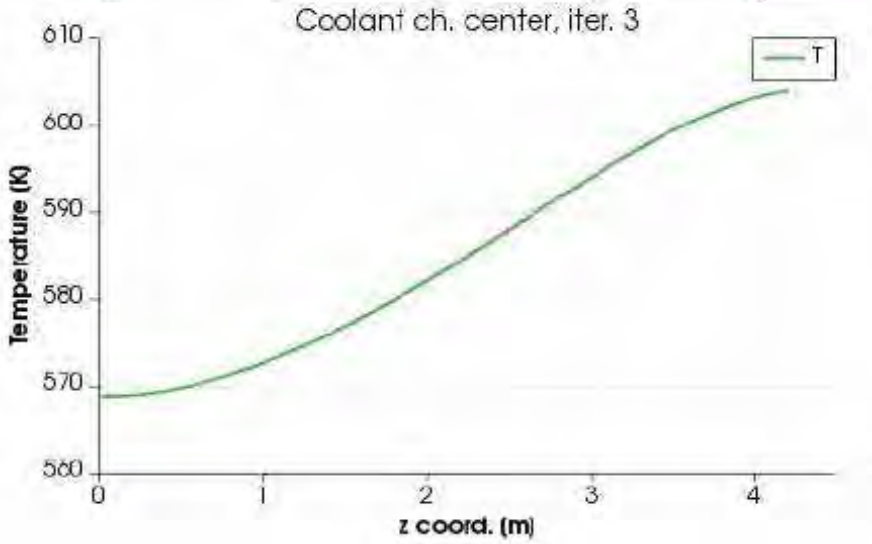

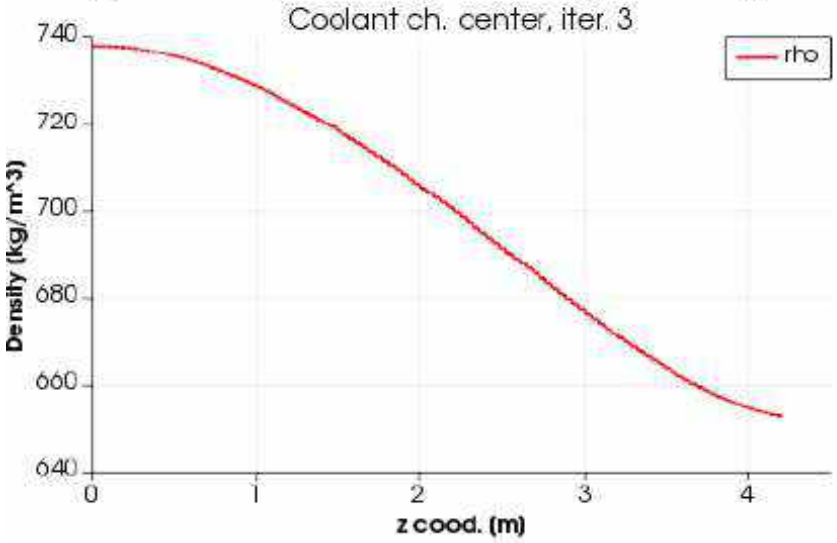

Neutronics – Thermal hydraulics coupling

EPR case – Iteration 4

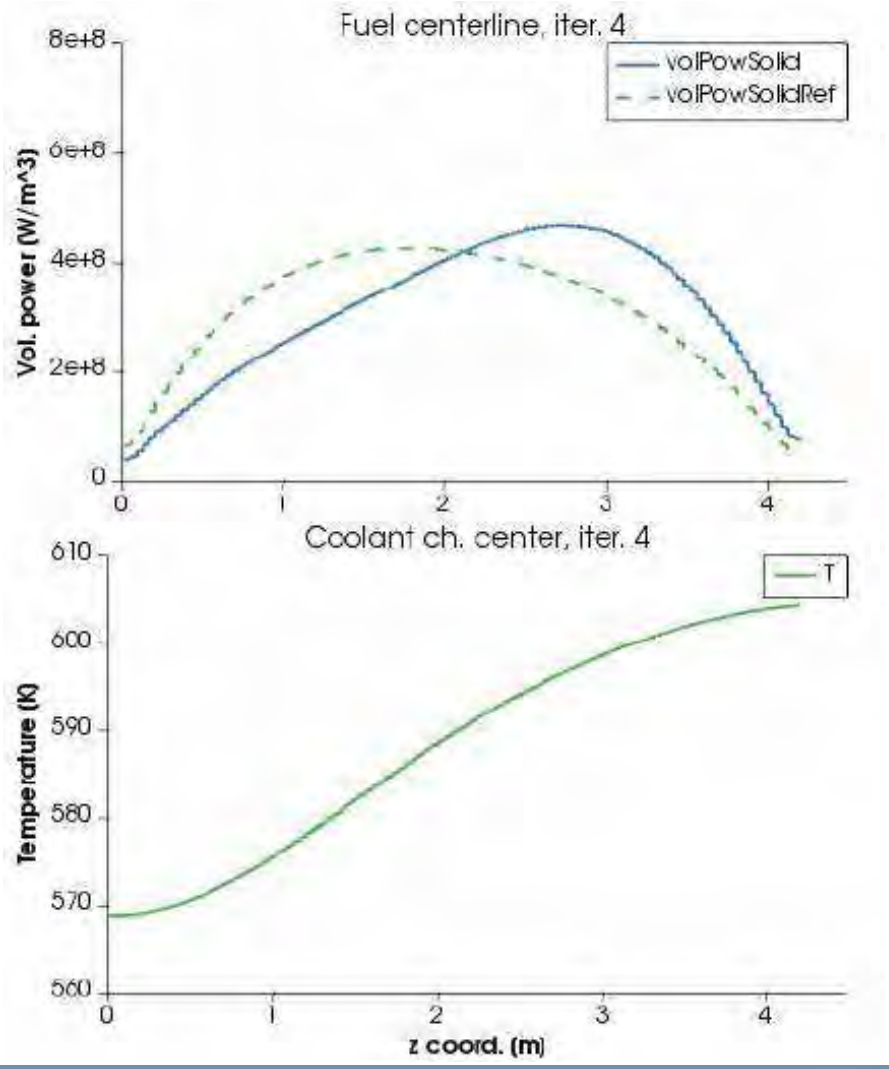

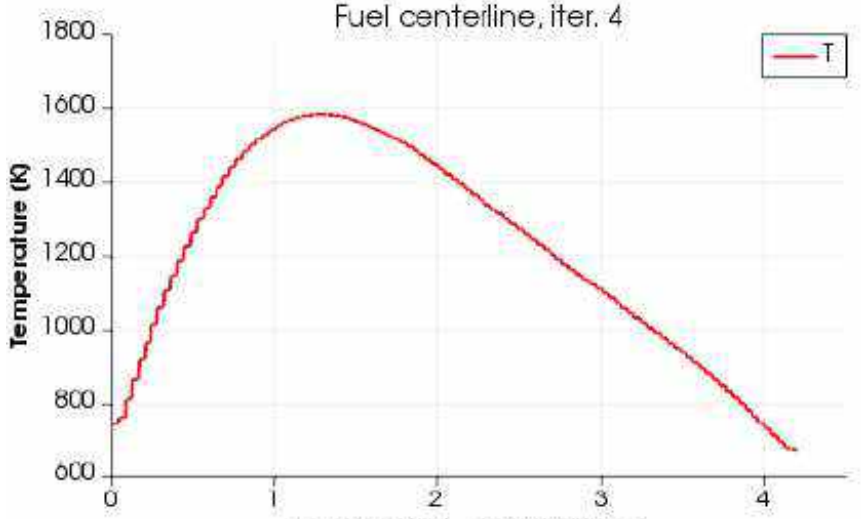

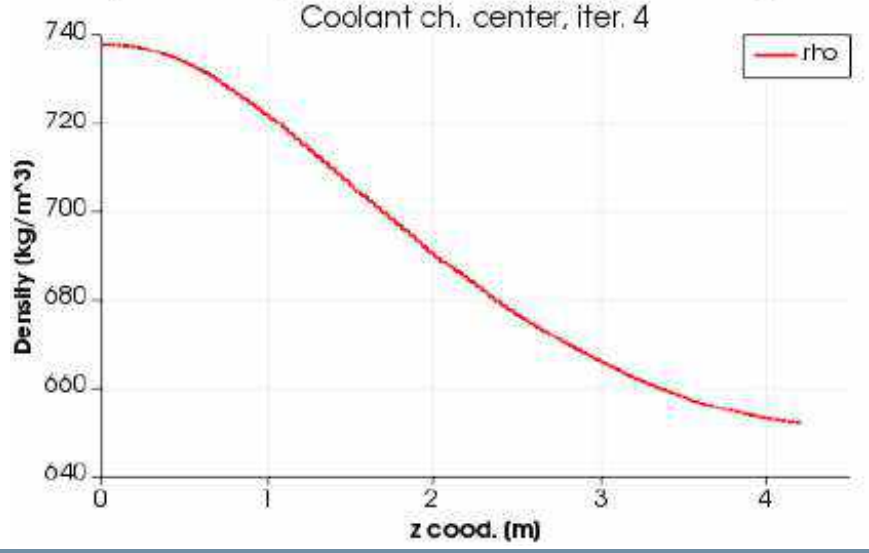

Neutronics – Thermal hydraulics coupling

EPR case – Iteration 5

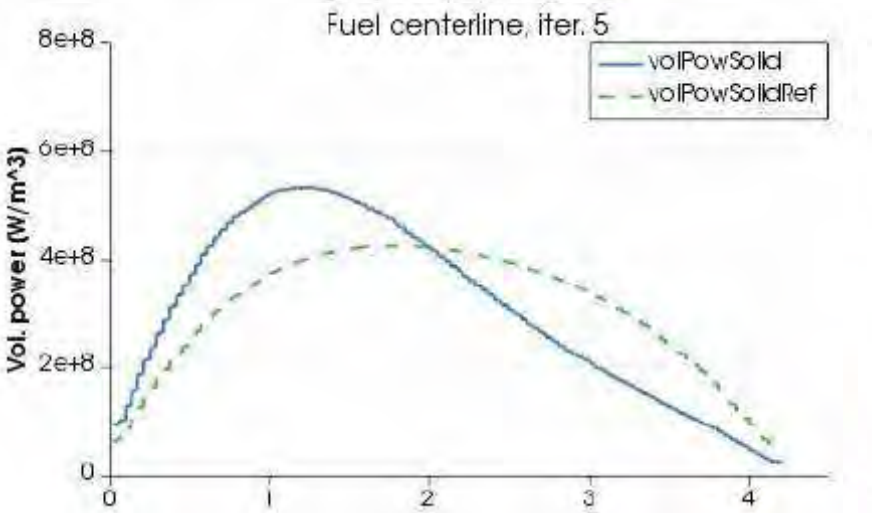

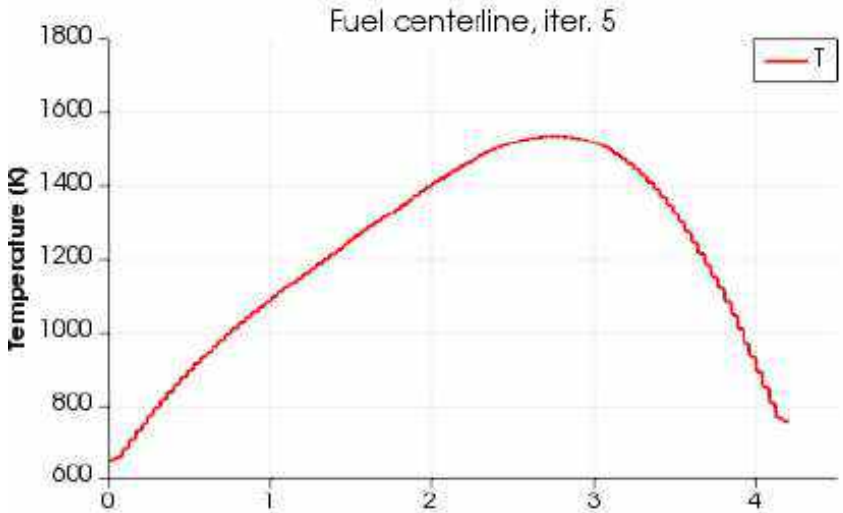

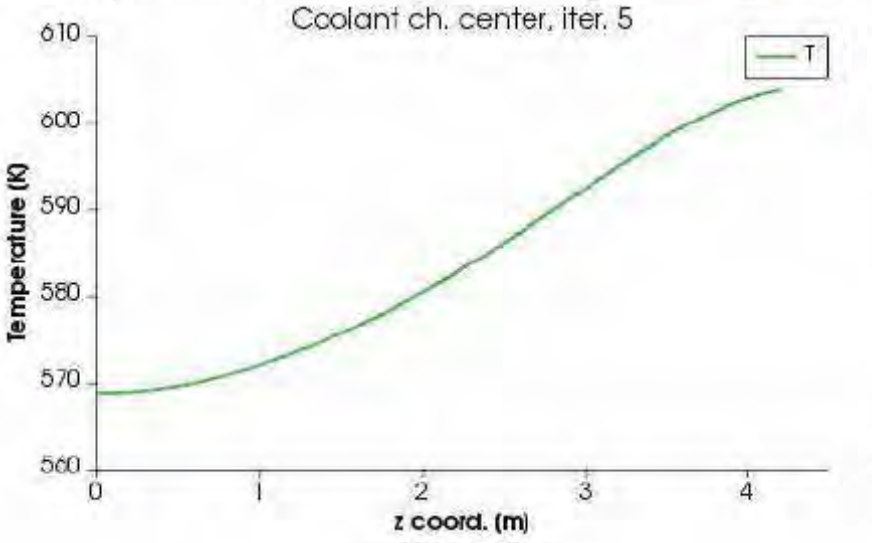

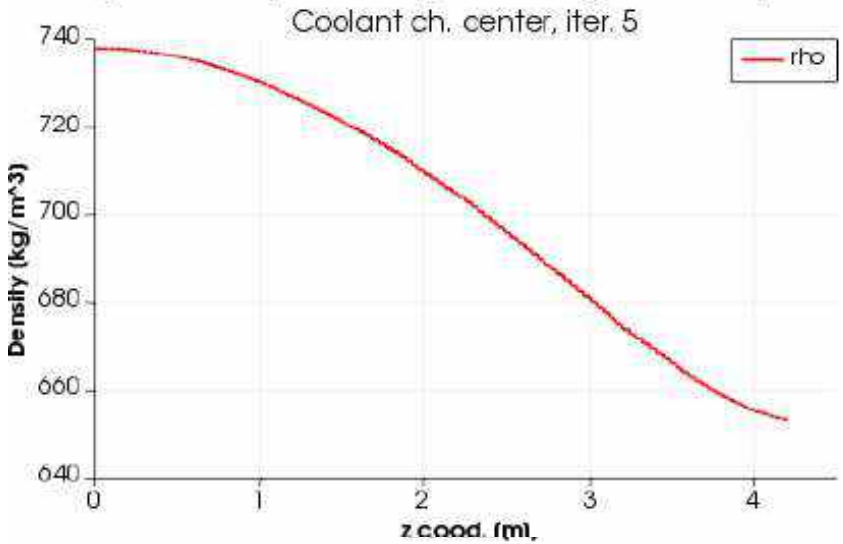

Under relaxation techniques

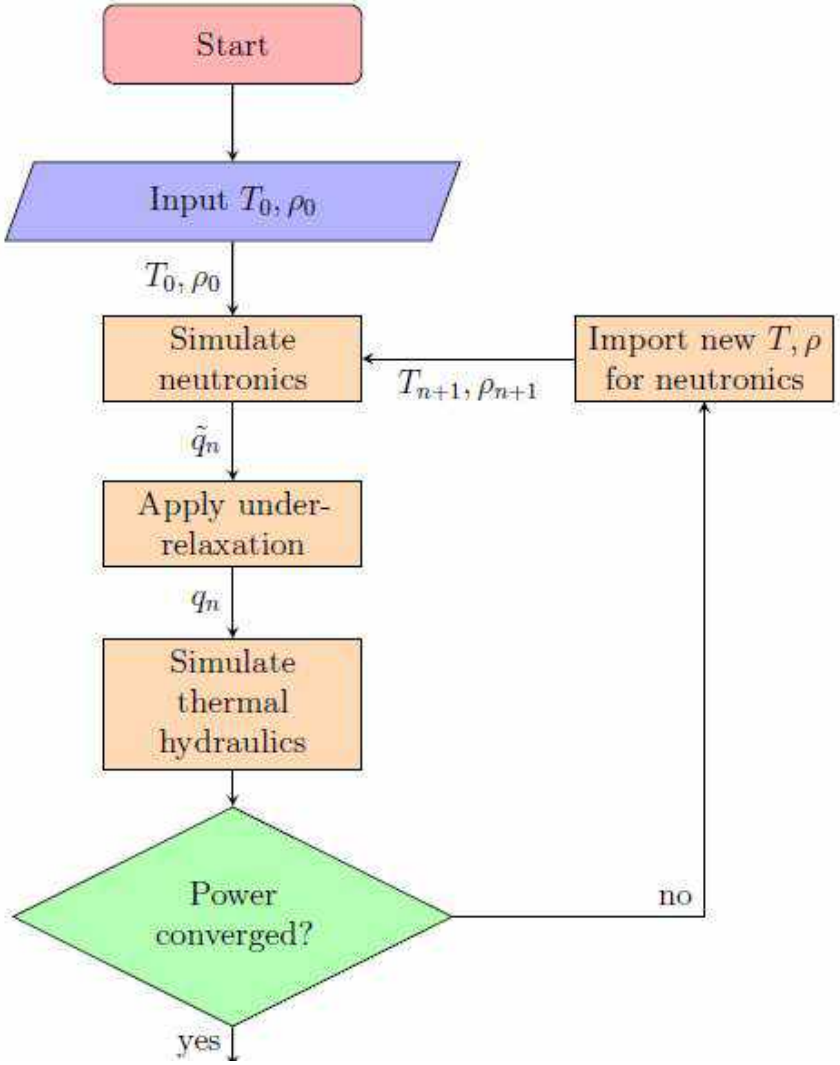

Constant under relaxation factor

$$q^{(n+1)} = \alpha G(q^{(n)}) + (1-\alpha)q^{(n)}, \quad 0 \leq \alpha \leq 1$$

Convergence criterion

$$\beta = \frac{\int_V |q_{n+1} - q_n| dV}{\int_V |q_n| dV} = \frac{\|q_{n+1} - q_n\|_{L^1}}{\|q_n\|_{L^1}}$$

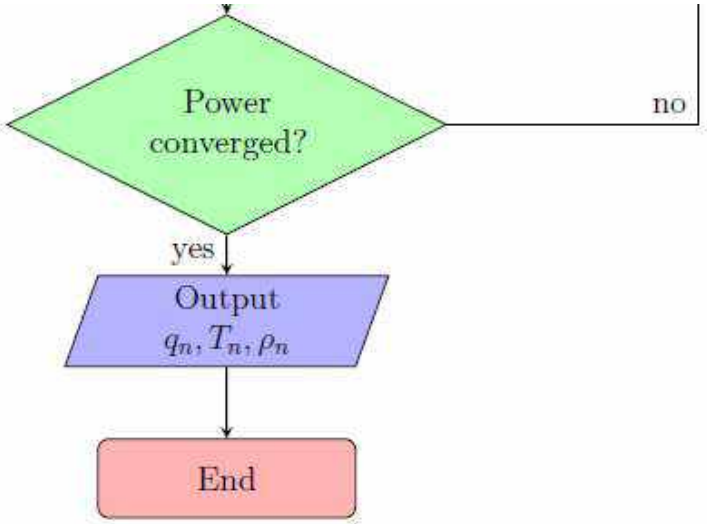

Underrelaxation techniques

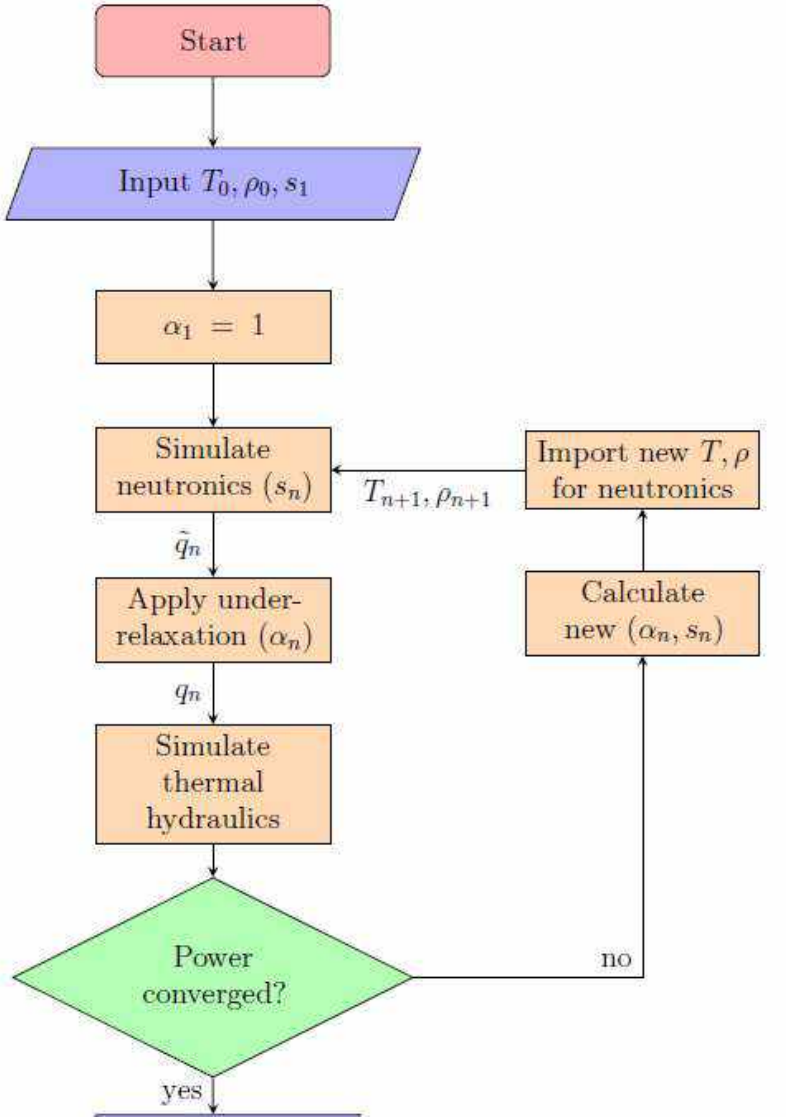

Stochastic approximation algorithm (Dufek, Gudowski)

$$q^{(n+1)} = \alpha G(q^{(n)}) + (1-\alpha)q^{(n)}\,, \quad 0 \le \alpha \le 1$$

$$\begin{cases} \alpha_n = \dfrac{s_n}{\sum_{i=1}^{n} s_i} \\ s_n = \dfrac{s_1 + \sqrt{s_1^2 + 4 s_1 \sum_{i=1}^{n-1} s_i}}{2} \end{cases}$$

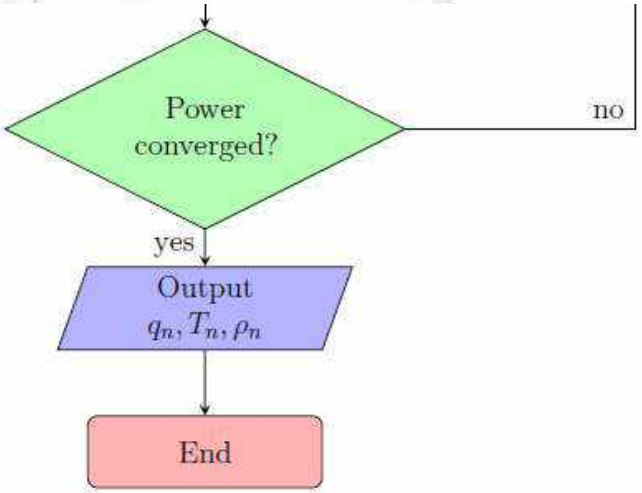

Application to ALFRED reactor

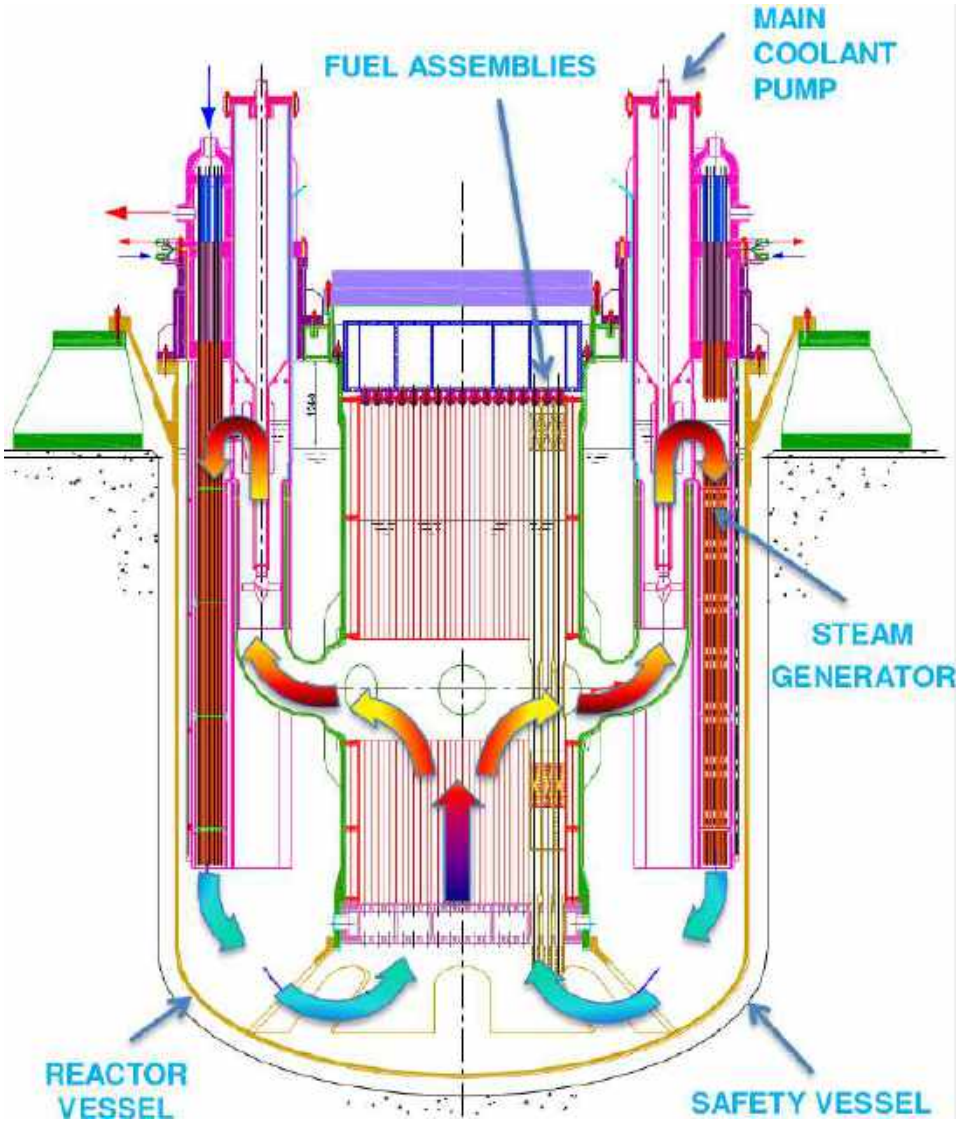

. Advanced Lead Fast Reactor European Demonstrator

. 300 MW_{th}

. Pool reactor – 8 loops

. Hexagonal FA

. MOX fuel

Application to ALFRED reactor

PAR 2017 Monte Carlo – CFD coupling for ALFRED reactor

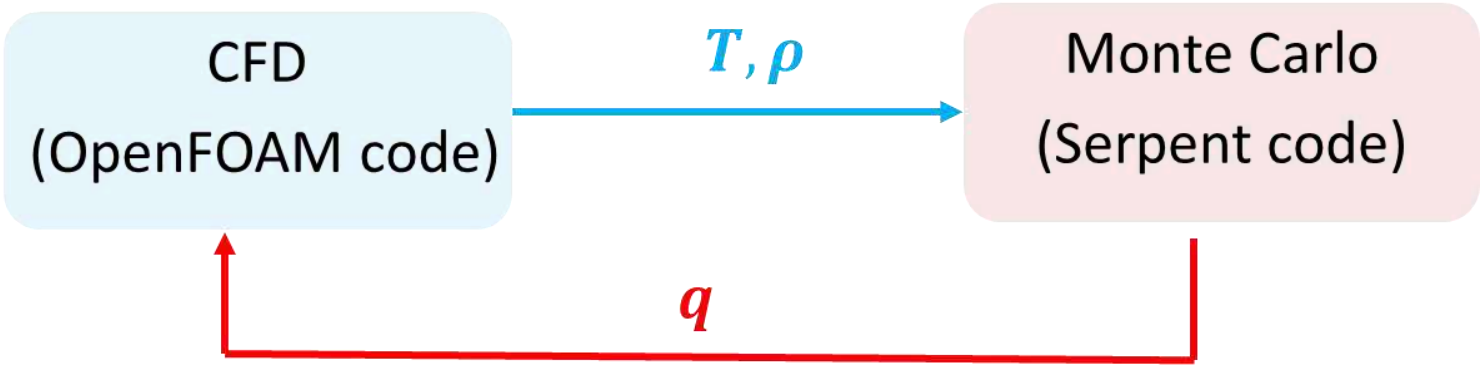

Development step:

1) Creation of a full core Serpent model of ALFRED
2) Creation of a CFD model for the FA of ALFRED
   a) 1/12 of FA (done)
   b) Entire FA (ongoing collaboration with PoliTo)
3) Coupling between the two models
   a) 1/12 of FA (done)
   b) Entire FA (ongoing collaboration with PoliTo)

Full core Serpent model

Monte Carlo model of the ALFRED reactor

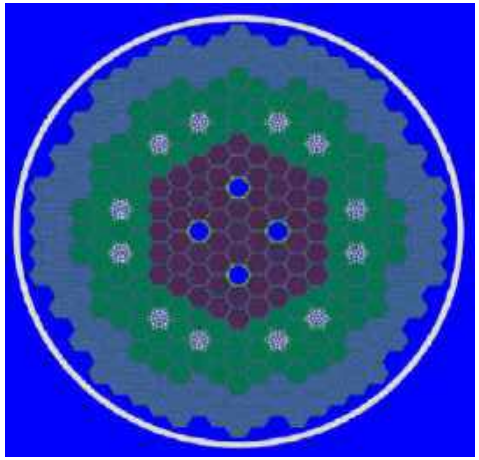

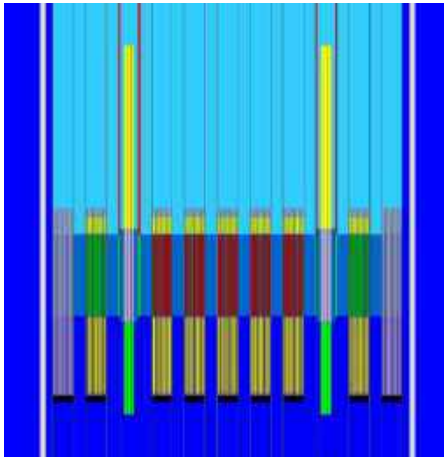

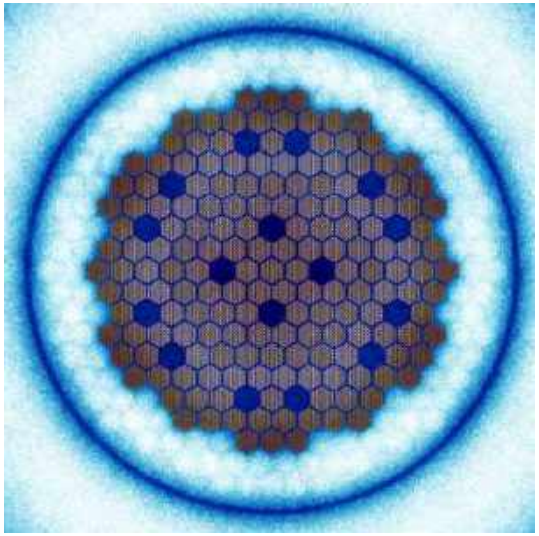

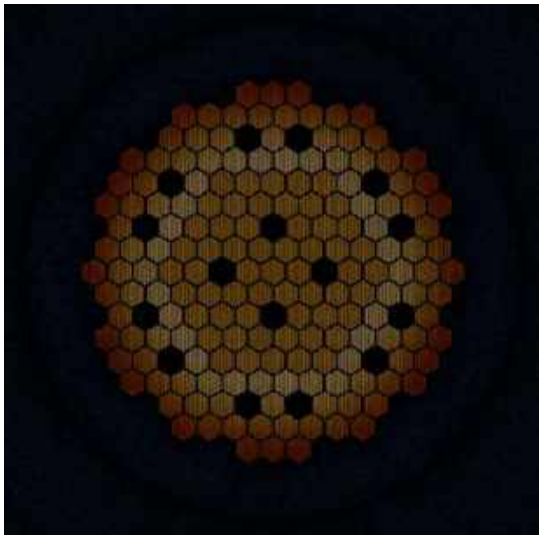

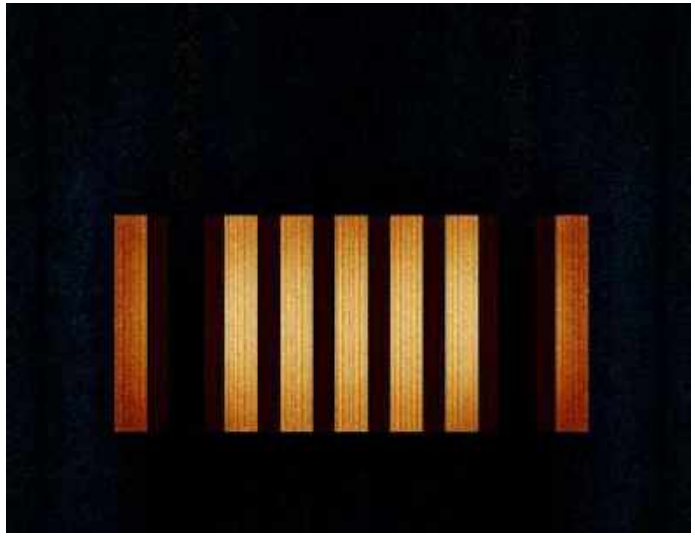

Full core Serpent model

Parameter	SERPENT	ERANOS[1]	MCNPX[1]
Max power in FA (MW)	2.25	2.42	2.21
Total worth of 12 CRs (pcm)	-8511	-9100	-8500
Total worth of 4 SRs (pcm)	-2957	-3700	-3300
Effective delayed neutron fraction (pcm)	336	336	-

Parameter	SERPENT	Uncertainty (σ)	ERANOS[1]
Doppler constant (pcm)	-580	18.219	-555
Lead expansion coefficient (pcm/K) 1st method	-0.282	0.113	-0.271
Lead expansion coefficient (pcm/K) 2nd method	-0.302	0.019	-0.271
Axial fuel expansion (pcm/K)	-0.153	0.006	-0.148
Axial cladding expansion (pcm/K)	0.044	0.006	0.037
Grid expansion (pcm/K)	-0.766	0.007	-0.762
Axial wrapper expansion (pcm/K)	0.036	0.006	0.022

1 Grasso, G., Petrovich, C., Mattioli, D., Artioli, C., Sciora, P., Gugiu, D., Bandini, G., Bubelis, E., Mikityuk, K., 2014. The core design of ALFRED, a demonstrator for the European lead-cooled reactors. Nuclear Engineering and Design 278, 287-301.

Full core Serpent model

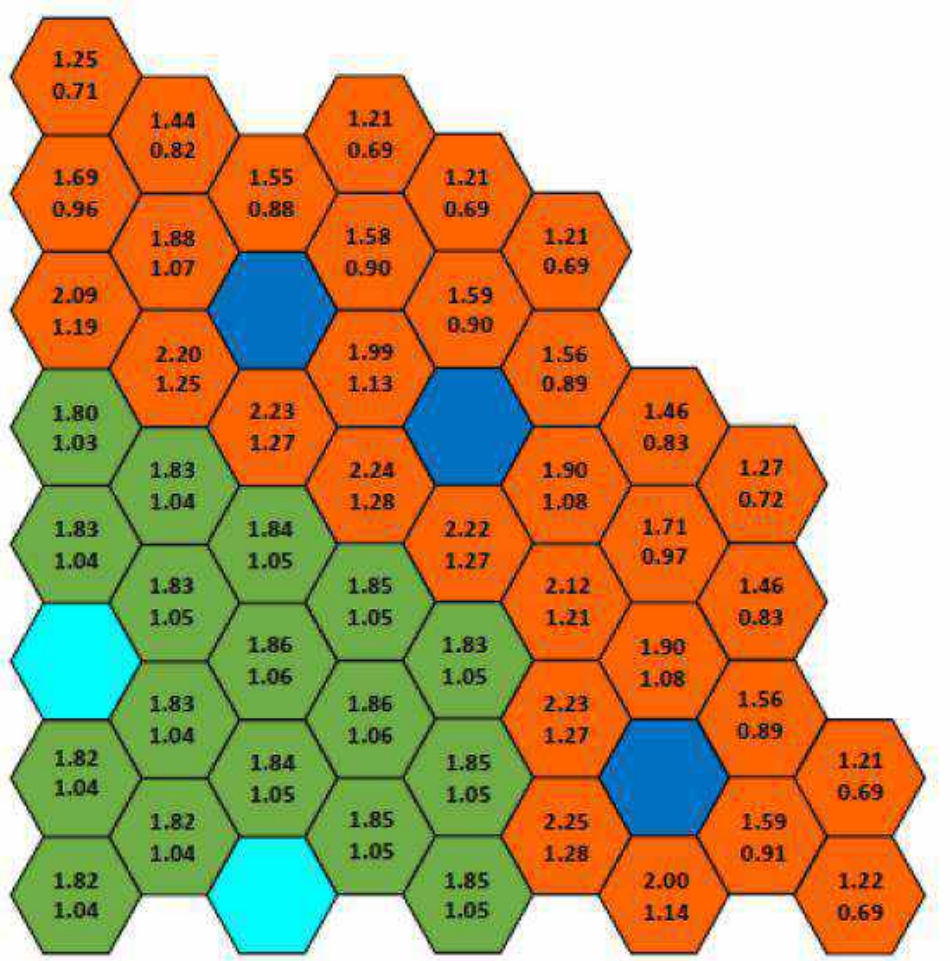

Power peaking factor of one-fourth of ALFRED reactor core for BOC

CFD OpenFoam model for ALFRED

Conjugate Heat Transfer multi region model

Fluid (Lead) | k – ε model

$$\begin{cases} \boldsymbol{u}_t + (\boldsymbol{u}\cdot\nabla)u = \nabla\cdot\left[-p\boldsymbol{I} + (\nu+\nu_t)(\nabla\boldsymbol{u} + (\nabla\boldsymbol{u})^T) - \frac{2}{3}k\boldsymbol{I}\right] \\ \nabla\cdot u = 0 \\ \frac{\partial k}{\partial t} + (\boldsymbol{u}\cdot\nabla)k = \nabla\cdot\left[\left(\nu + \frac{\nu_T}{\sigma_k}\right)\nabla k\right] - \varepsilon + P \\ \frac{\partial \varepsilon}{\partial t} + (\boldsymbol{u}\cdot\nabla)\varepsilon = \nabla\cdot\left[\left(\nu + \frac{\nu_T}{\sigma_\varepsilon}\right)\nabla\varepsilon\right] - C_{2\varepsilon}\frac{\varepsilon^2}{k}\nu_T + 2C_{1\varepsilon}\frac{\varepsilon}{k}\nu_T P \end{cases}$$

Solid (Fuel) | Heat conduction

$$\rho_F C_{p,F}\frac{\partial T_f}{\partial t} = \nabla\cdot(K_F\nabla T) + Q_f + Q_{decay}$$

CFD OpenFoam model for ALFRED

ALFRED FA – CFD analysis (collaboration with PoliTo, E. Guadagni MSc thesis and G. F Nallo PhD activity)

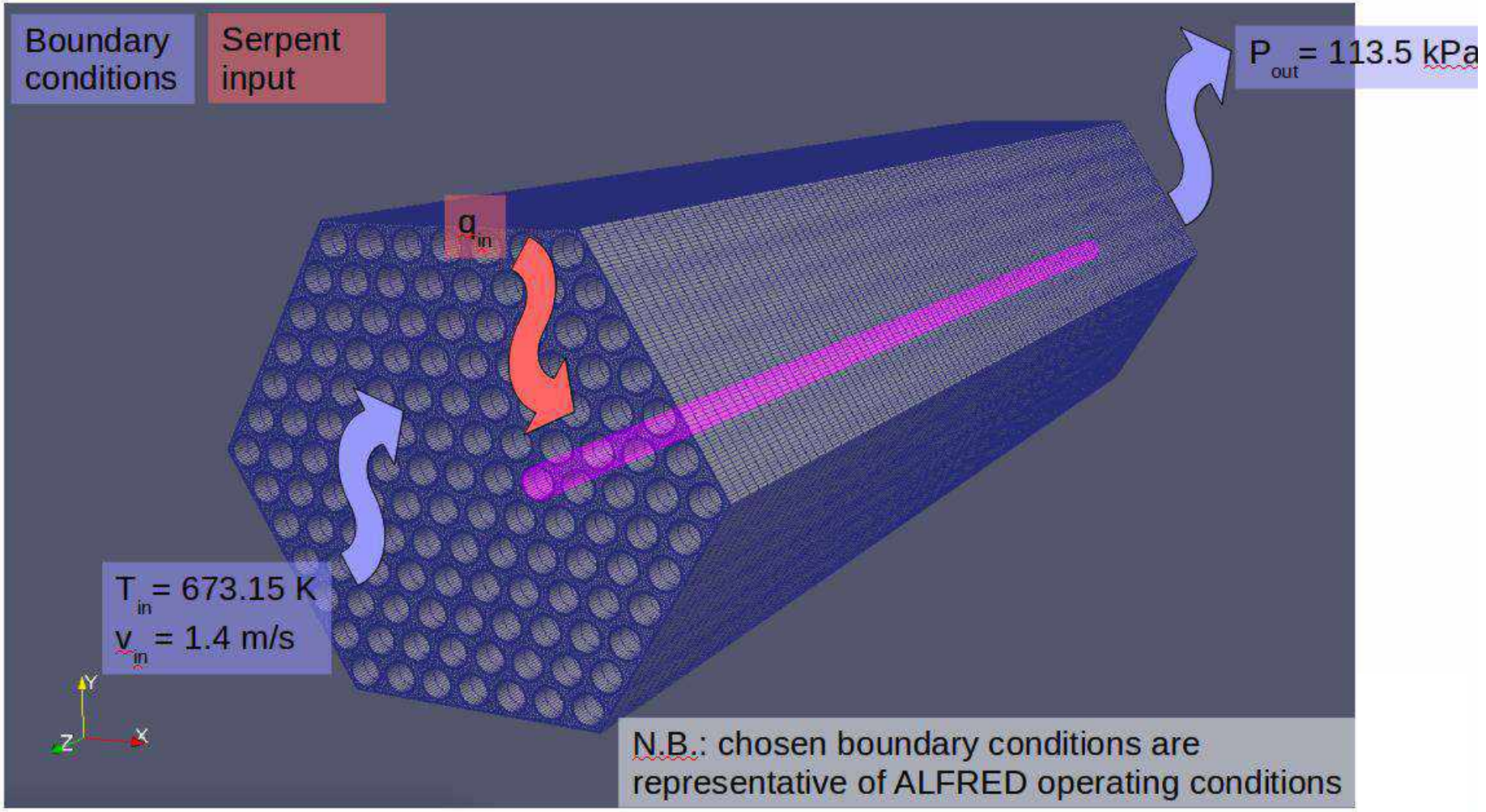

CFD OpenFoam model for ALFRED

ALFRED FA – CFD analysis (collaboration with PoliTo, E. Guadagni MSc thesis and G. F Nallo PhD activity)

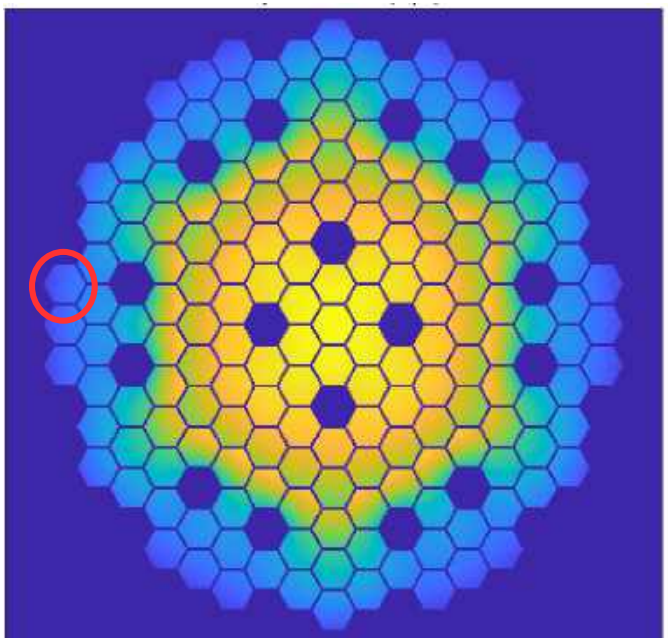

One specific FA, placed near the border of the reactor, was chosen for the CFD calculations due to its strongly asymmetric power distribution, evaluated with a preliminary Serpent neutronic simulation (one way coupling)

CFD OpenFoam model for ALFRED

ALFRED FA – CFD analysis (collaboration with PoliTo, E. Guadagni MSc thesis and G. F Nallo PhD activity)

Mesh #1 (coarsest)

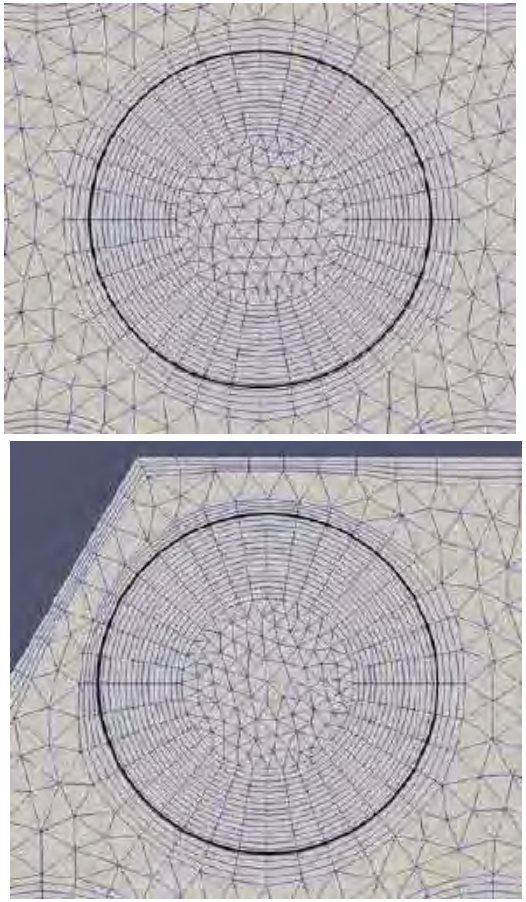

Mesh #2 (medium)

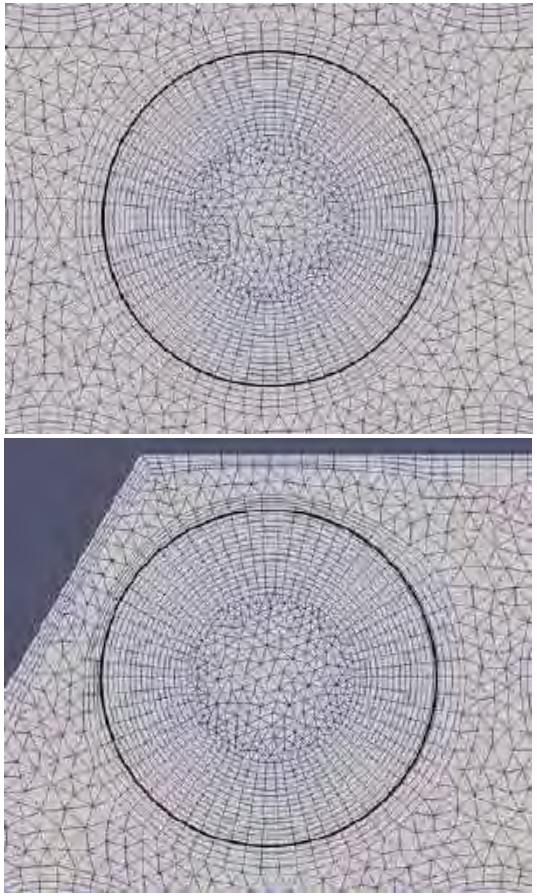

Mesh #3 (finest)

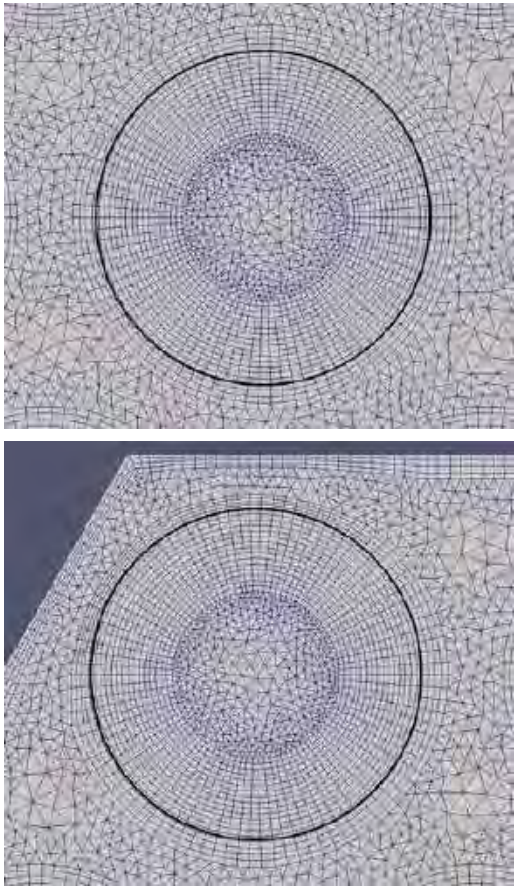

CFD OpenFoam model for ALFRED

ALFRED FA – CFD analysis (collaboration with PoliTo, E. Guadagni MSc thesis and G. F Nallo PhD activity)

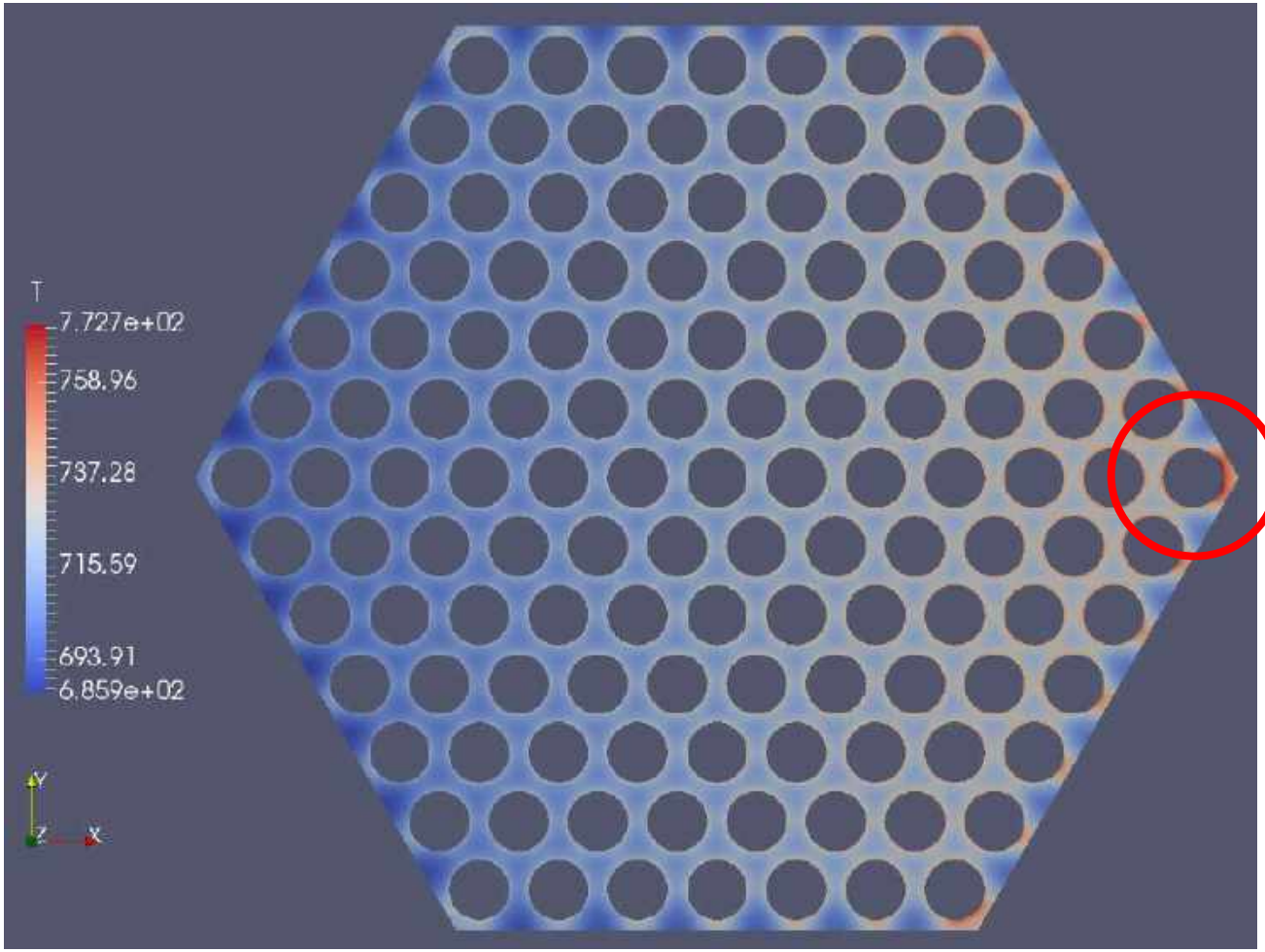

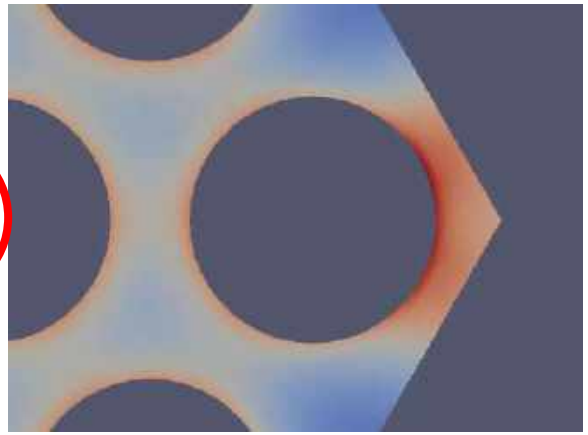

CFD OpenFoam model for ALFRED

ALFRED FA – CFD analysis (collaboration with PoliTo, E. Guadagni MSc thesis and G. F Nallo PhD activity)

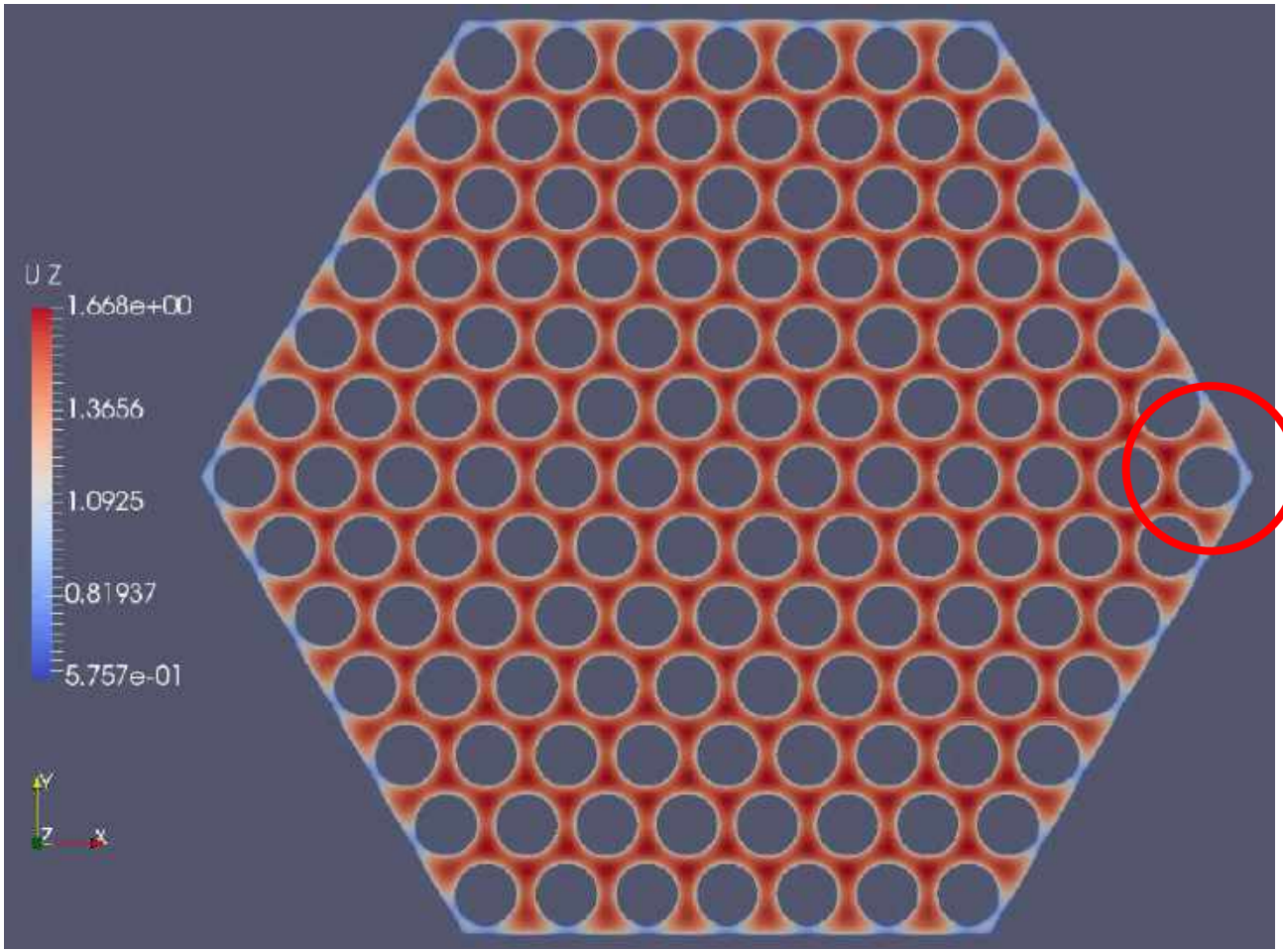

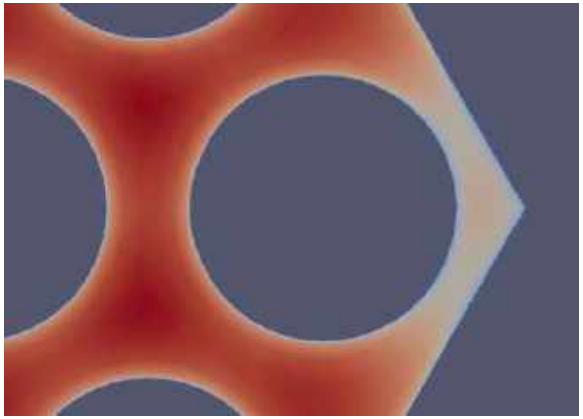

Monte Carlo – CFD coupling

ALFRED 1/12 central FA – Monte Carlo - CFD coupling

. Serpent/OF coupling managed by an **external proxy file**

. The simulation starts with a Serpent run to obtain the volumetric power distribution, which is then **translated into the OpenFOAM input file**

. Temperature and density for fuel and coolant are calculated by OpenFOAM and they are passed to the next Serpent run using the **multi-physics interface**

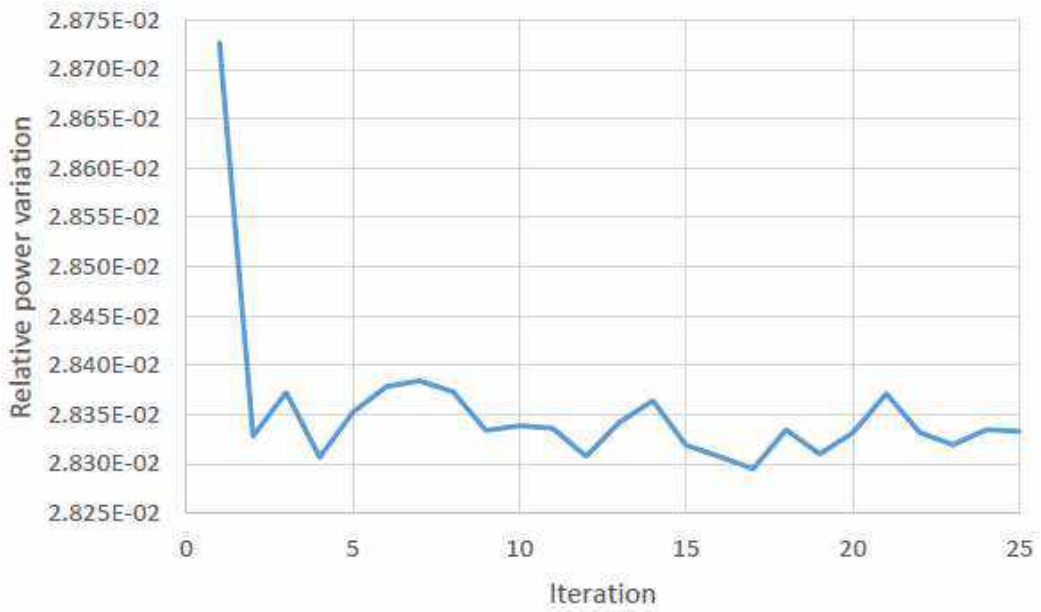

. The procedure iterates **until convergence is reached** (constant under relaxation factor and stochastic approximation algorithm available)

Monte Carlo – CFD coupling

ALFRED 1/12 central FA – Monte Carlo - CFD coupling

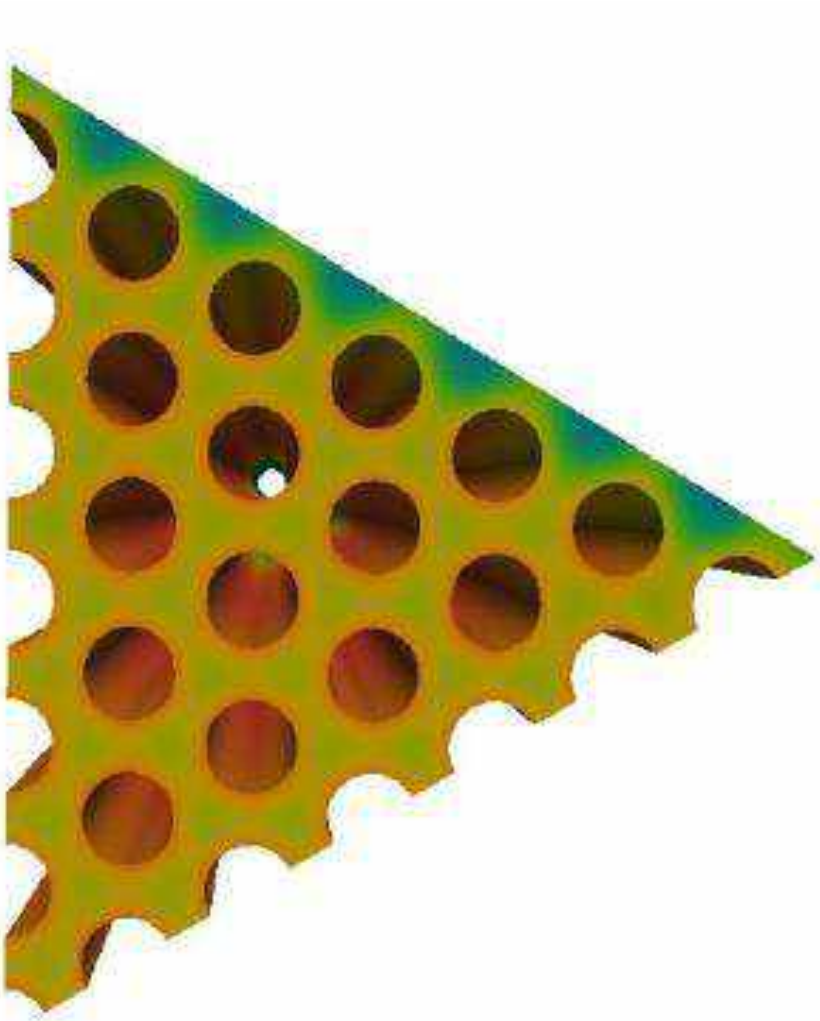

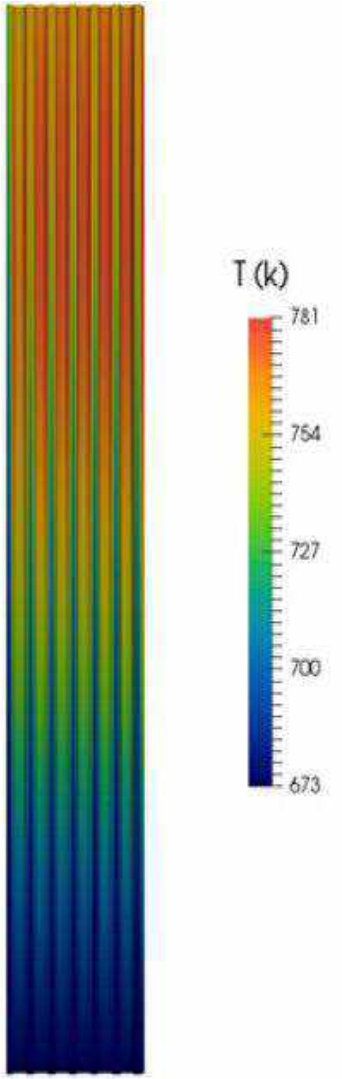

Monte Carlo – CFD coupling

ALFRED 1/12 central FA – Monte Carlo - CFD coupling

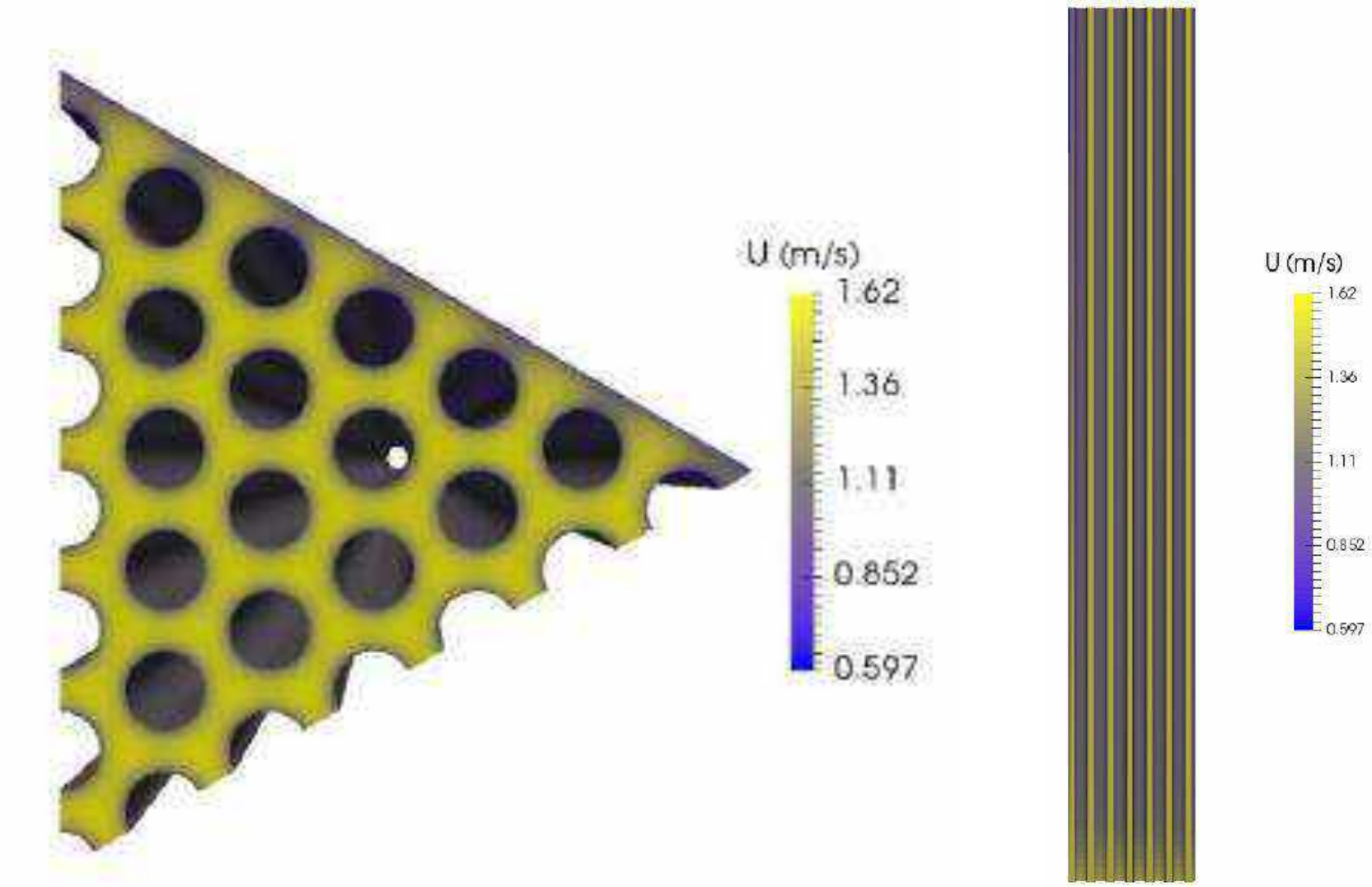

Conclusions and future developments

Ongong activities

. Finalization of coupling with entire FA

. Analysis of the impact of the neutronics - thermal hydraulics coupling (difference between one way and two ways coupling)

Conclusions and future developments

. The activity is the step forward for the development of a multi-physics code for lead-cooled fast reactor aimed at supporting both the design choice and the verification of other numerical tools

. Monte Carlo – CFD coupling for a better accuracy in neutronics modelling (relevant for design support) for ALFRED reactor

. Near-term efforts focus on efficient use of the available computational resources (i.e., parallelization, optimization) and easy modification of the modelling description with OpenFOAM to develop a multi-physics platform

ISReCTHA – Lecco, August 29 – 21, 2018

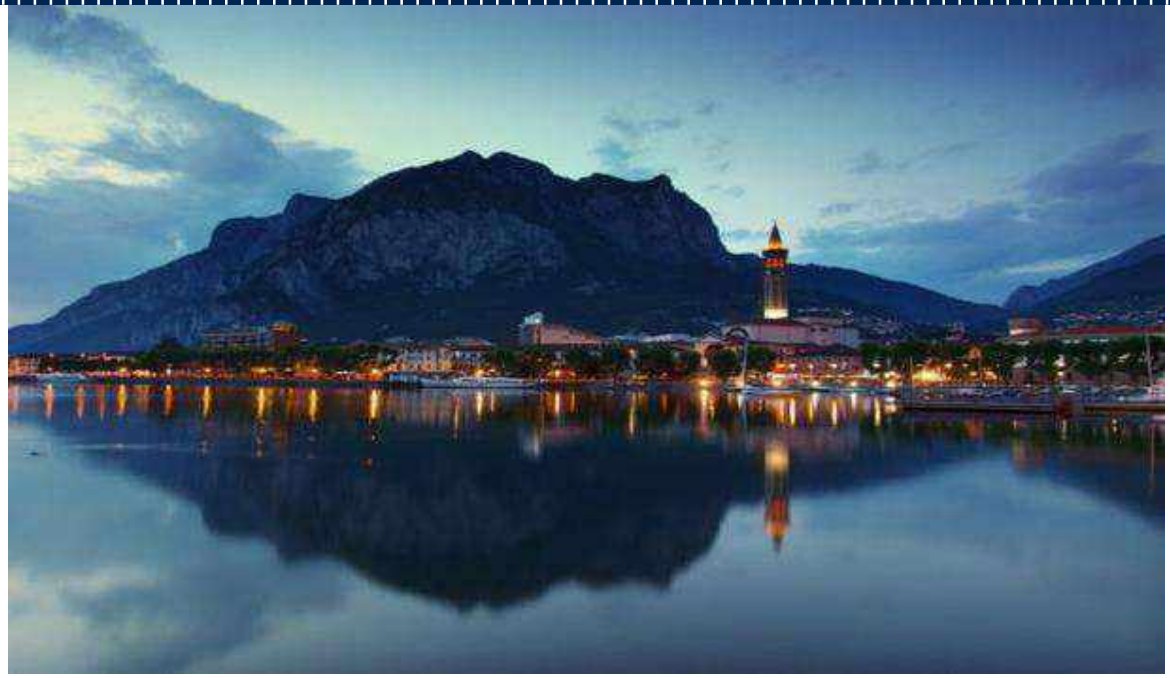

PoliMi is glad to announce the **International Seminar on Nuclear Reactor Core Thermal Hydraulics Analysis**
Lecco, August 29 - 31

Forum on the nuclear reactor core and fuel assembly thermal hydraulics analysis, by professionals for young professionals and students

Organizer: Prof. H. Ninokata
TPC: E. Baglietto, N. Toderas, E. Merzari, BW. Yang, F. Roelofs, Y. Hassan, H-M Prasser

https://www.eko.polimi.it/index.php/rectha/rectha

Opener – Milano, September 3 – 7, 2018

PoliMi and Milano Multiphysics are glad to announce the first summer school on **OpenFOAM for multiphysics modeling of Nuclear Reactors**
Milano, September 3 - 7

The students will be guided through a full multi-physics modeling (front lectures and tutorial) of a nuclear reactor, how to tailor the available OpenFOAM CFD solvers to the needs of nuclear reactor analysis, how to create new solvers for neutronics, and how to couple OpenFOAM to a Monte Carlo code like Serpent.

https://www.eventbrite.it/e/opener-openfoam-for-multiphysics-modeling-of-nuclear-reactors-registration-42198523921

Thank you for attention

ALFRED Design Analysis by FRENETIC code

FRENETIC benchmark activity based on comparison to coupled Serpent/OpenFoam simulations for the ALFRED design

G.F. Nallo[1], E. Guadagni[1,2], S. Dulla[1], N. Abrate[1], P. Ravetto[1], L. Savoldi[1], R. Zanino[1], S. Lorenzi[2], A. Cammi[2]

[1]*Politecnico di Torino, Italy*

[2]*Politecnico di Milano, Italy*

Outline

- The ALFRED design
- The FRENETIC code
  - Neutronic module
  - Thermal-hydraulic module
  - Coupling strategy and feedback
- FRENETIC - Serpent/OpenFoam interaction
  - Use of FRENETIC to upgrade the Serpent code calculation
  - Use of FRENETIC to provide BC to OpenFoam
  - Comparison of FRENETIC and Serpent/OpenFoam results
- Conclusions and perspectives

The ALFRED design

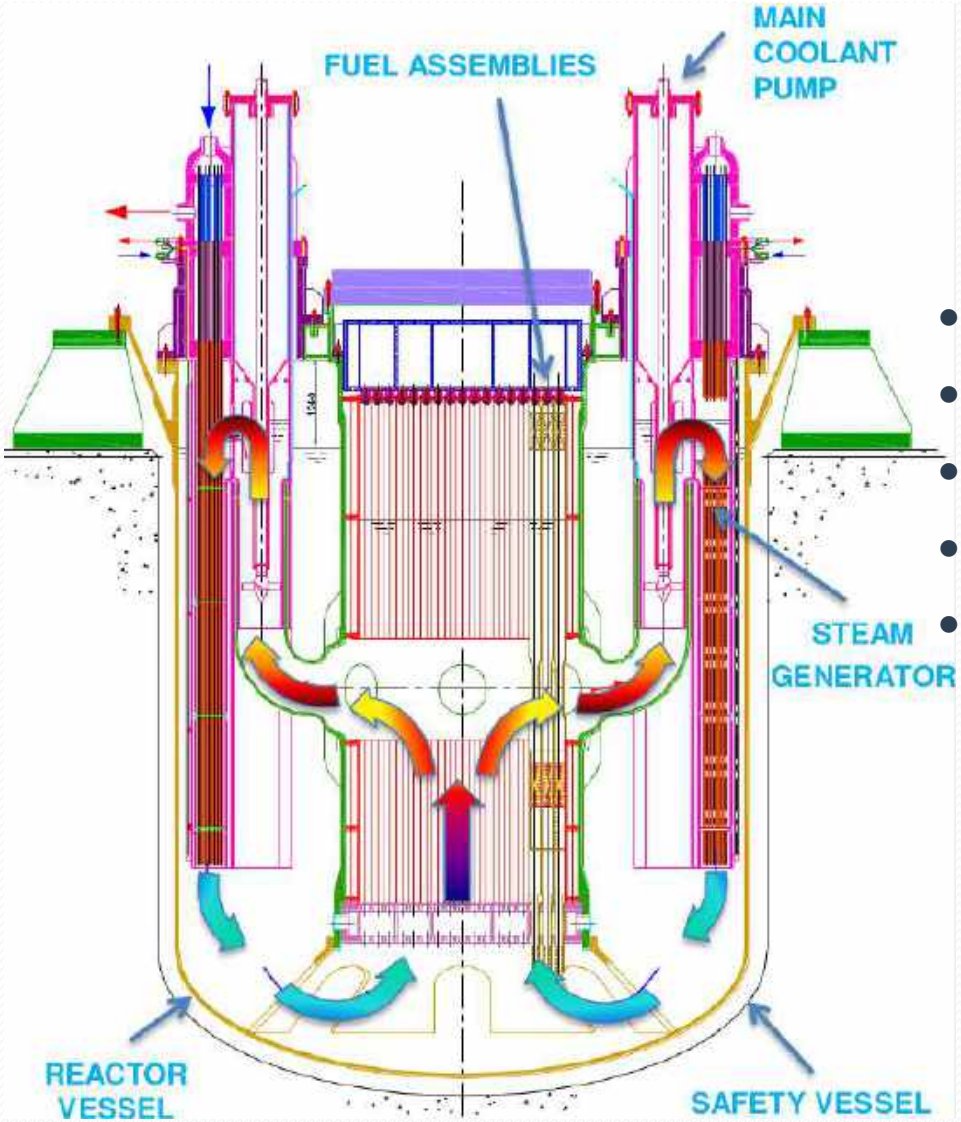

- 300 MWth LFR
- Forced/natural circulation
- MOX fuel
- Hexagonal Fuel Assemblies (FA)
- Two different enrichment zones

A. Alemberti, ALFRED presentation, *Education Training Seminar on Fast Reactors Science and Technology at ITESM Campus Santa Fe*, Mexico City, 2015

FRENETIC

- Fast **RE**actor **NE**utronics/Thermal-hydraul**IC**s code for full-core coupled analyses of fast reactors with liquid-metal coolant [R. Bonifetto et al., Nucl. Eng. Des., 2013]

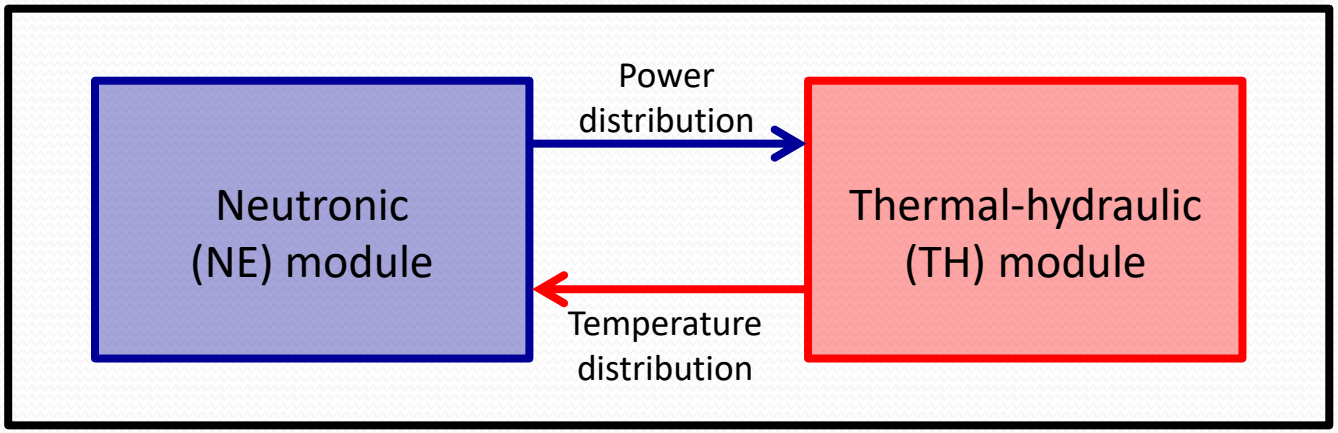

- **Principal objective**: computationally efficient, multiphysics analyses suitable for design and safety studies
- **Preliminary validation** of coupled code on EBR-II experimental data [D. Caron et al., Int. J. Energy Res., 2016]

FRENETIC-NE module

- Physical model
  - Multigroup neutron diffusion theory with delayed neutron precursors

$$\begin{cases} \dfrac{1}{v_g}\dfrac{\partial}{\partial t}\phi_g(\mathbf{r},t) = \nabla\cdot D_g(\mathbf{r},t)\nabla\phi_g(\mathbf{r},t) - \Sigma_g(\mathbf{r},t)\phi_g(\mathbf{r},t) + \displaystyle\sum_{g'=1}^{G}\Sigma_{gg'}(\mathbf{r},t)\phi_{g'}(\mathbf{r},t) \\ \quad + (1-\beta)\chi_g(\mathbf{r})\displaystyle\sum_{g'=1}^{G}\nu\Sigma_{fg'}(\mathbf{r},t)\phi_{g'}(\mathbf{r},t) + \sum_{i=1}^{R}\chi_{gi}(\mathbf{r})\lambda_i c_i(\mathbf{r},t) + S_g(\mathbf{r},t), \qquad g=1,\ldots,G, \\ \dfrac{\partial}{\partial t}c_i(\mathbf{r},t) = \beta_i\displaystyle\sum_{g'=1}^{G}\nu\Sigma_{fg'}(\mathbf{r},t)\phi_{g'}(\mathbf{r},t) - \lambda_i c_i(\mathbf{r},t), \qquad i=1,\ldots,R, \end{cases}$$

Temperature-dependent cross sections

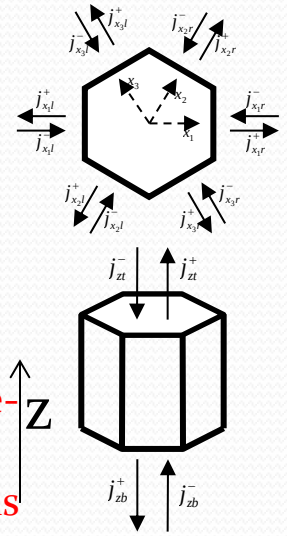

  - Decay and photon heat (with photon transport) [D. Caron et al., PHYSOR, 2016]
  - Space discretization: polynomial nodal method [D. Caron et al., ICENES, 2013]
  - Time discretization: point-kinetic, direct and quasi-static methods [D. Caron et al., Ann. Nuc. Energy, 2015]

FRENETIC-TH module (1)

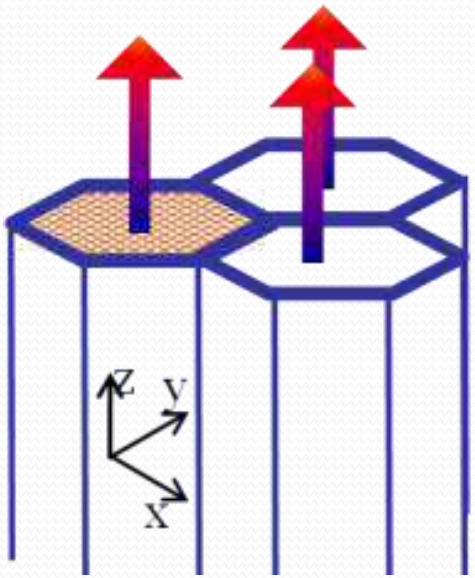

IN EACH fuel assembly:
Coolant: 1D axial model (mass, momentum, and energy eqs.) along each closed assembly (**z**), for 1+ regions in each hexagonal fuel assembly (FA)

- **Single FA** (1D) **validation** against experimental data from CIRCE facility @ ENEA Brasimone (**Pb-Bi eutectic**) [R. Zanino et al., Trans. Am. Nucl. Soc., 2012]

Pins: **1D** radial model, locally coupled to coolant

Coupling through thermal resistance

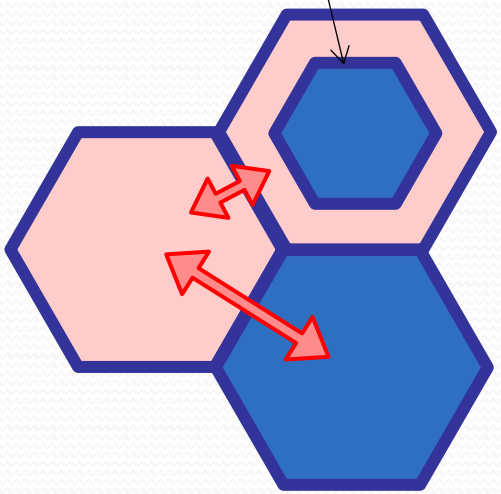

BETWEEN HAs: (weak) **2D** inter-assembly thermal coupling (**xy**)

- Steady-state **benchmark** against RELAP5-3D© in a simplified EBR-II geometry (**Na**) [R. Zanino et al., Trans. Am. Nucl. Soc., 2013]
- Preliminary **validation** against EBR-II data (**Na**) [R. Zanino et al., Proc. ATH, 2014]

FRENETIC-TH module (2)

Coolant: compressible flow with buoyancy (1D, axial)

$$\begin{cases} \dfrac{\partial v}{\partial t} + v\dfrac{\partial v}{\partial z} + \dfrac{1}{\rho}\dfrac{\partial p}{\partial z} = -Fv - g\cos\beta \\ \dfrac{\partial p}{\partial t} + \rho c_s^2 \dfrac{\partial v}{\partial z} + v\dfrac{\partial p}{\partial z} - \Phi\dfrac{\partial}{\partial z}\left(k\dfrac{\partial T}{\partial z}\right) = \Phi\left[\dfrac{\Pi_{fuel}H}{A}\left(T_{fuel,s} - T\right) + v\rho F\right] \\ \rho c_v \dfrac{\partial T}{\partial t} + \rho c_v v\dfrac{\partial T}{\partial z} + \rho c_v \Phi T\dfrac{\partial v}{\partial z} - \dfrac{\partial}{\partial z}\left(k\dfrac{\partial T}{\partial z}\right) = \\ = \dfrac{\Pi_{fuel}H}{A}\left(T_{fuel,s} - T\right) + v\rho F + \sum_{i=1}^{6}\dfrac{\Pi_{hex}h_i}{A}\left(T_i - T\right) \end{cases}$$

Used to compute coolant-pin heat transfer

Inter-channel coupling

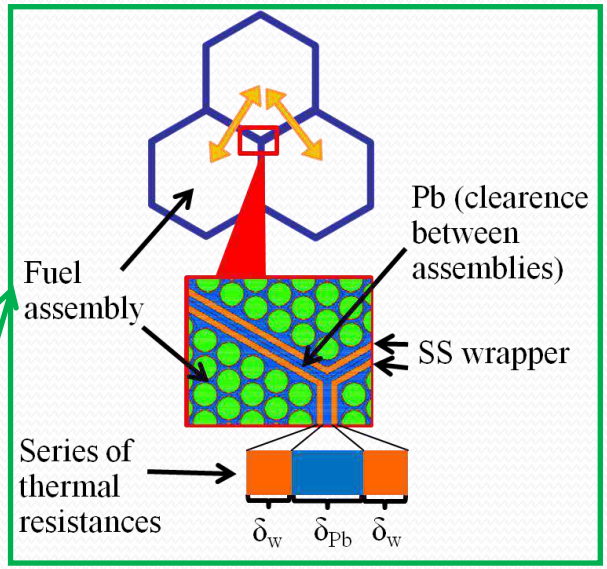

Pin: thermal conduction (1D, axial or radial to be chosen)

$$\rho_{fuel}c_{fuel}\frac{\partial T_{fuel}}{\partial t} - \frac{\partial}{\partial z}\left(k_{fuel}\frac{\partial T_{fuel}}{\partial z}\right) = \frac{\Pi_{fuel}H}{A_{fuel}}\left(T - T_{fuel,s}\right) + \frac{q^{lin}_{fuel}}{A_{fuel}}$$

Neutronics-dependent heat source term

Friction term $F = 2f\dfrac{|v_x|}{D_h}$

Gruneisen parameter $\Phi = \left(\dfrac{\rho}{T}\dfrac{\partial T}{\partial \rho}\right)_s$

2D+1D heat exchange model

- ***1D:*** *advection + diffusion in each FA*
- ***2D:*** *simplified «slab» inter-FA heat exchange*

Coupling strategy

- Spatial coupling procedure:
  - TH→NE: fuel and coolant average temperatures attributed to entire node

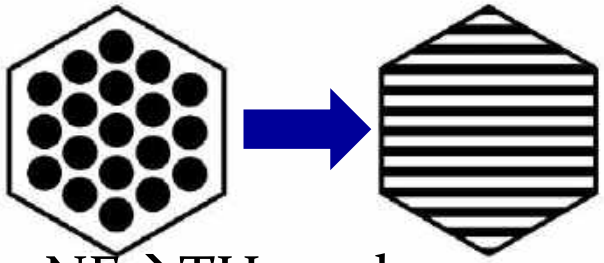

  - NE→TH: node-averaged power localised in appropriate region

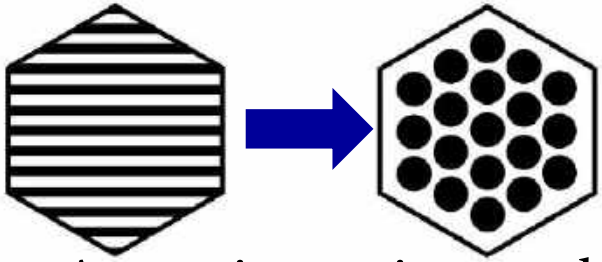

  - Averaging or interpolation on mesh as necessary

- Temporal coupling algorithm accounts for different time scales

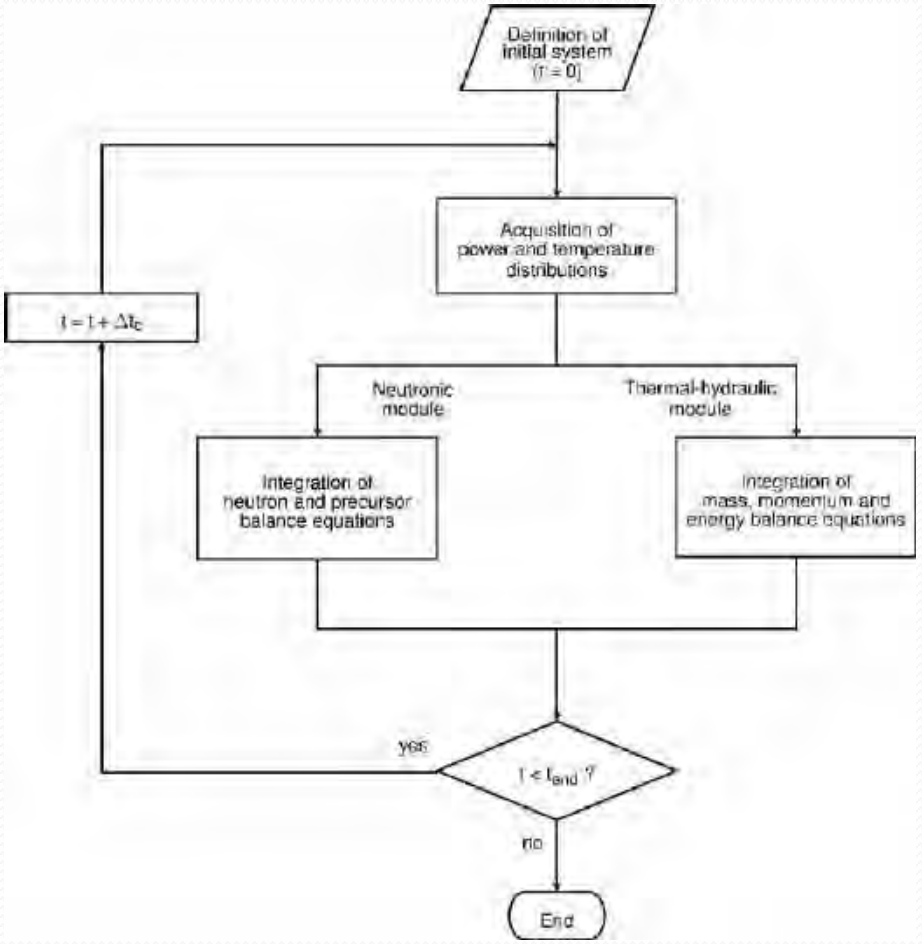

Coupling feedback

- TH module
  - neutronic effects accounted for directly by time- and position-dependent heat source term
- NE module
  - thermal effects accounted for indirectly by dependence of macroscopic cross sections on fuel and coolant temperatures
  - linear feedback model:

$$\Sigma(T_f, T_c) = \Sigma(T_{f0}, T_{c0}) + \left(\frac{\partial \Sigma}{\partial T_f}\right)_{T_c} (T_f - T_{f0}) + \left(\frac{\partial \Sigma}{\partial T_c}\right)_{T_f} (T_c - T_{c0})$$

  - tabular lookup model: bivariate linear interpolation

FRENETIC vs Serpent/OpenFoam

- It is not a competition !
  - Different physical modelling for both NE and TH
  - Different domain of application → with FRENETIC, we are looking at the full-core
- Interest in
  - Exploiting the more detailed information provided by Monte Carlo and CFD to improve FRENETIC modelization
  - Use the full-core results available with FRENETIC to «improve» the CFD simulation of the single FA

Serpent simulation

- Full-core k_{eff} calculation
- Material and geometrical data from G. Grasso, et al., The core design of ALFRED, a demonstrator for the European lead-cooled reactors, Nuclear Engineering and Design 278, 2014
- Nuclear data depend on temperature

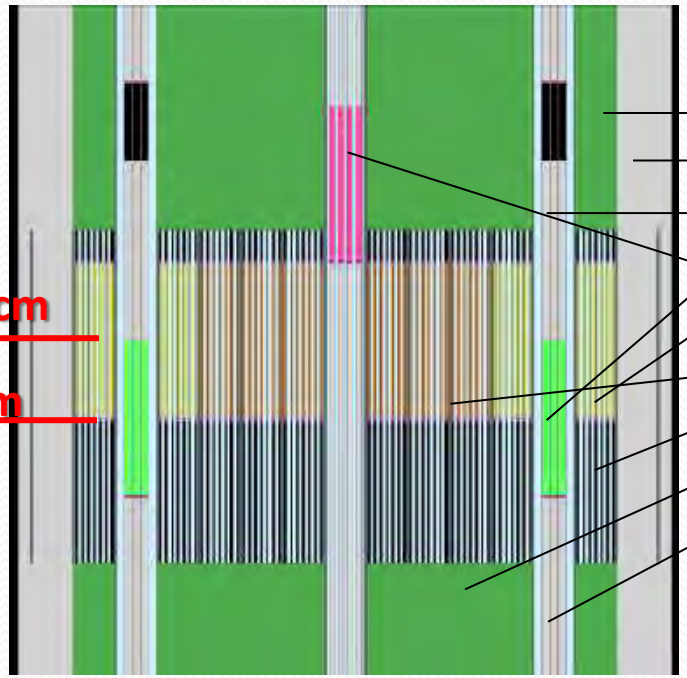

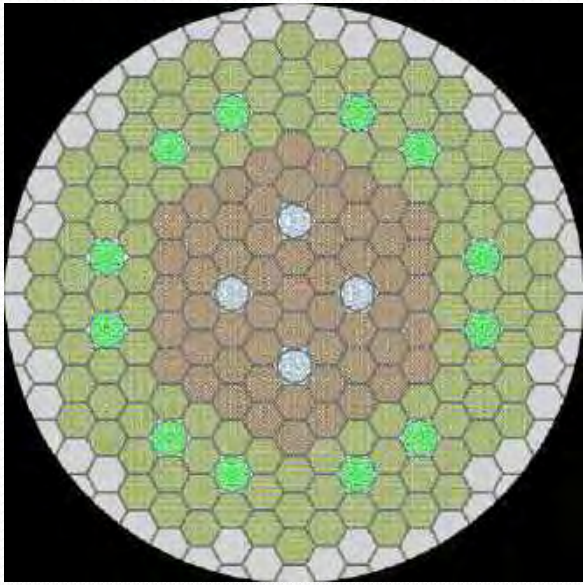

OpenFoam simulation

- On a single FA
- Info on power source from Serpent (thus depending on the location in the core)
- BC ?

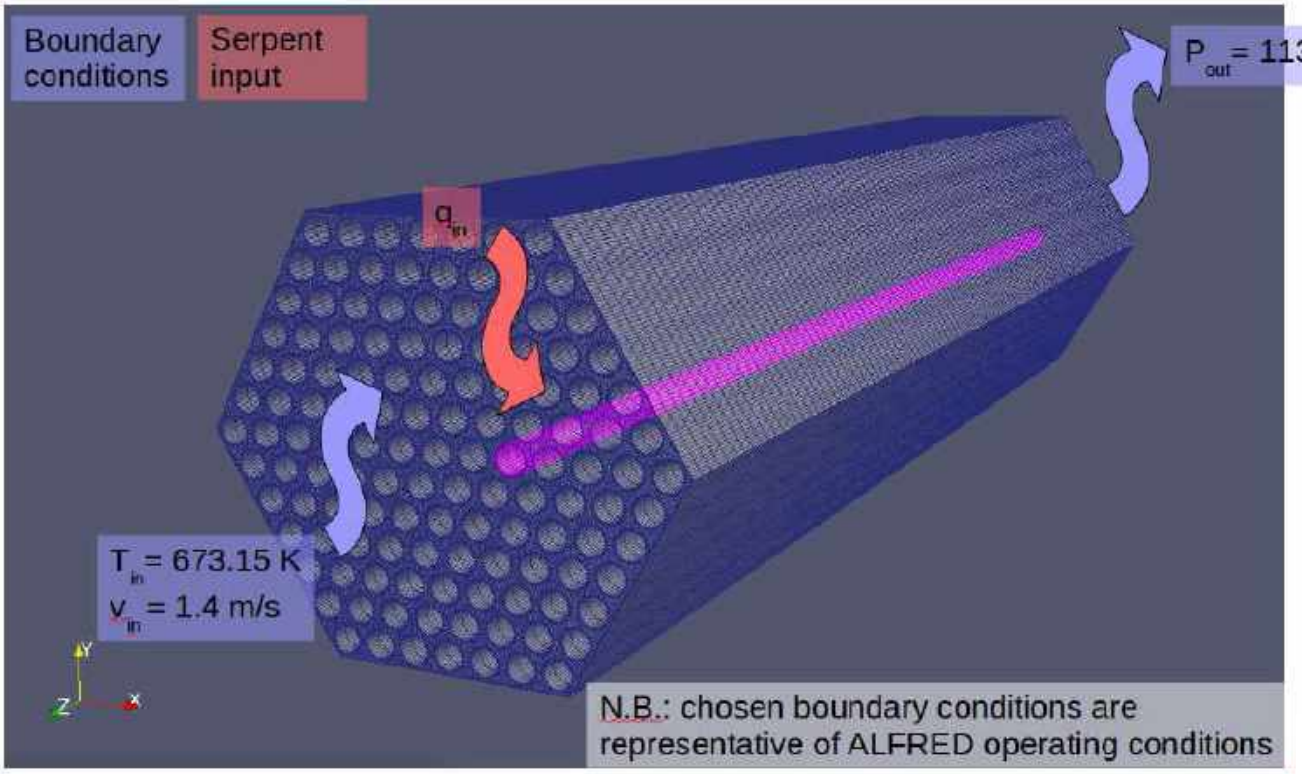

General calculation scheme

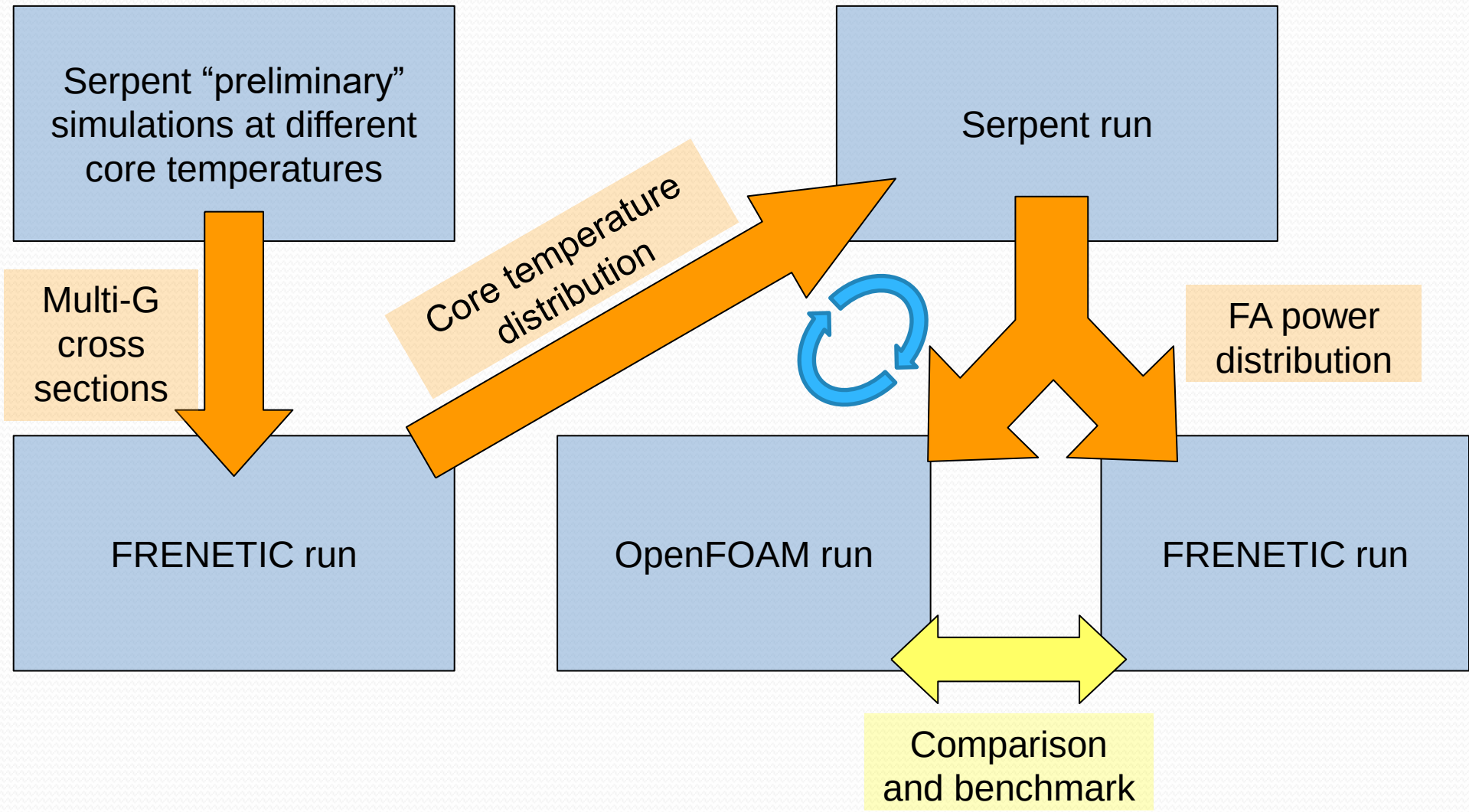

FRENETIC
cross section generation

- FRENETIC requires homogenized, few-groups cross sections, which are generated by Serpent runs (four, in our case) at different temperatures

	$T_{fuel}\ (K)$	$T_{coolant}\ (K)$
$T_{fuel}\ (K)$	673	1073
$T_{coolant}\ (K)$	673	1073

$$\Sigma(T_f, T_c) = \Sigma(T_{f,0}, T_{c,0}) + \left(\frac{\partial \Sigma}{\partial T_f}\right)_{Tc} (T_f - T_{f,0}) + \left(\frac{\partial \Sigma}{\partial T_c}\right)_{Tf} (T_c - T_{c,0})$$

Group	$Upper\ energy\ (MeV)$
1	19.64
2	1.3534
3	0.18316
4	0.067379
5	0.00091188

- The output of FRENETIC, i.e. the full core temperature distribution, is then fed to Serpent to perform the NE simulation with “improved” temperature information

Serpent results (1)

- Comparison of Serpent core keff calculations at
  - 673 K («cold») → k_{eff}=1.01027±3e-5
  - 1073 K («hot») → k_{eff}=1.00772 ±3e-5
- Power distribution, affected by temperature feedbacks

cold

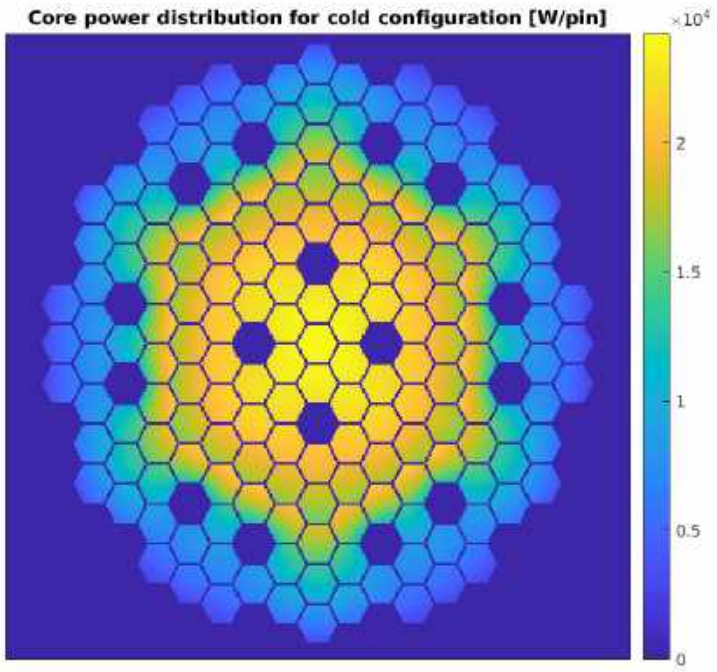

hot

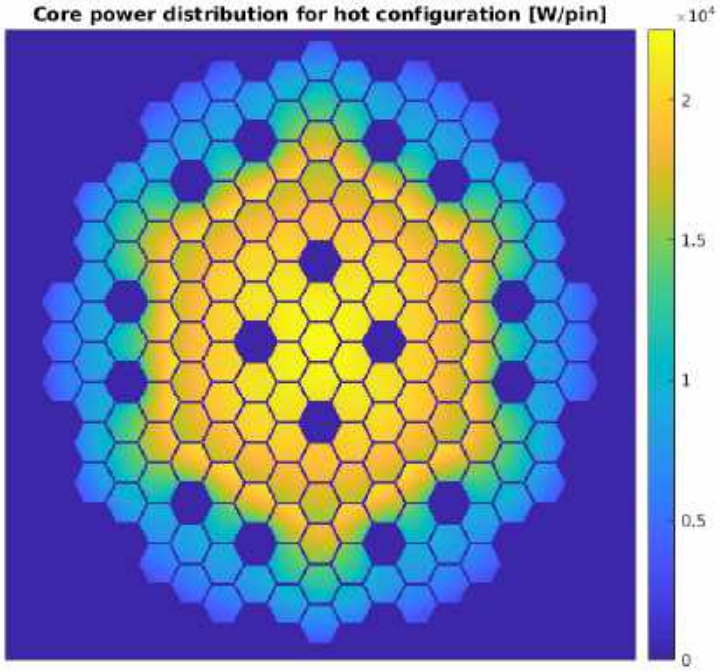

Serpent results (2)

- Radial and axial profiles (power distribution flattening)

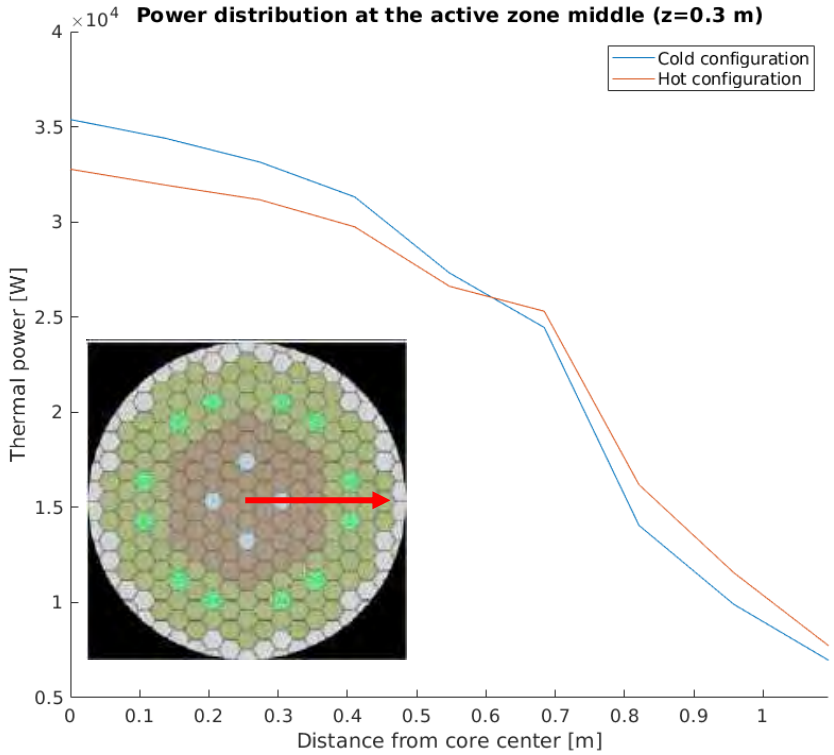

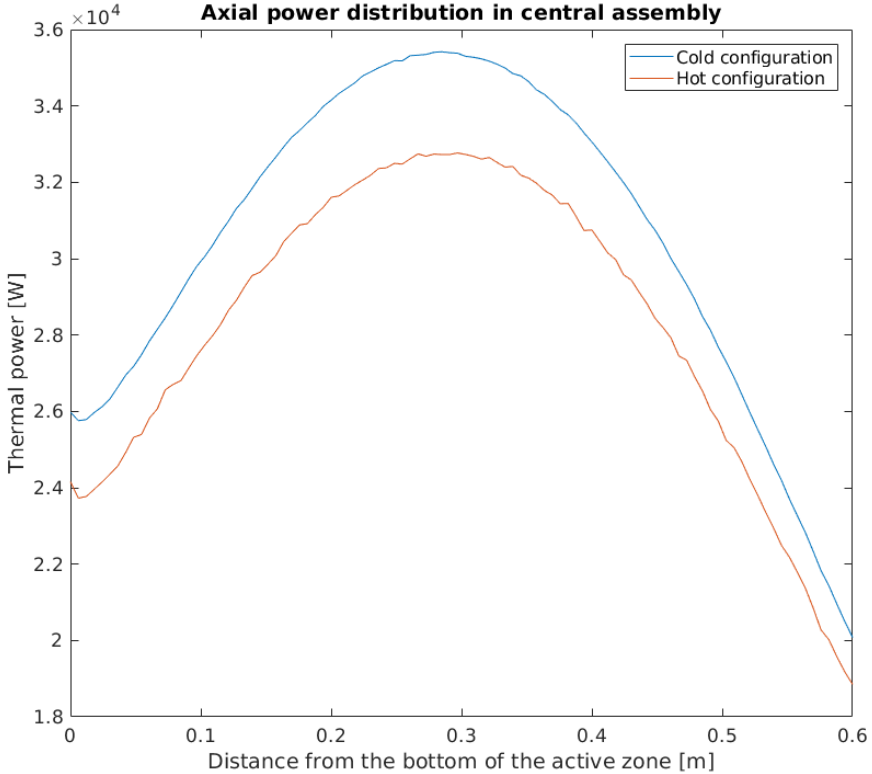

- ***Next step***: Serpent run with representative temperature of the core at full power → FRENETIC run

FRENETIC run (1)

- Coupled NE-TH run on full-core level to reach equilibrium (free evolution transient)
- Cross section homogenized at the fuel assembly level
- Focus on the core domain (consistently with the FRENETIC modelling capabilites)

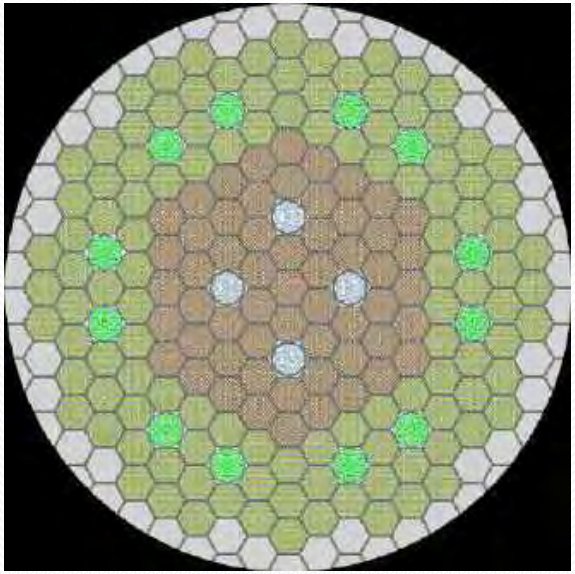

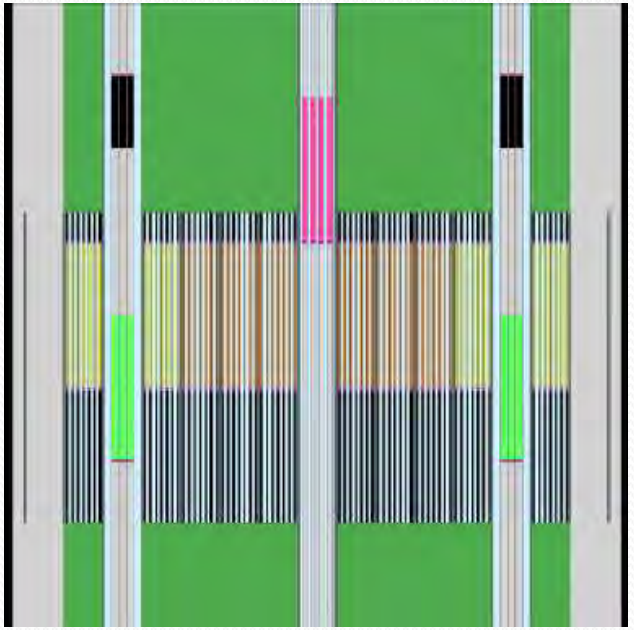

FRENETIC run (2)

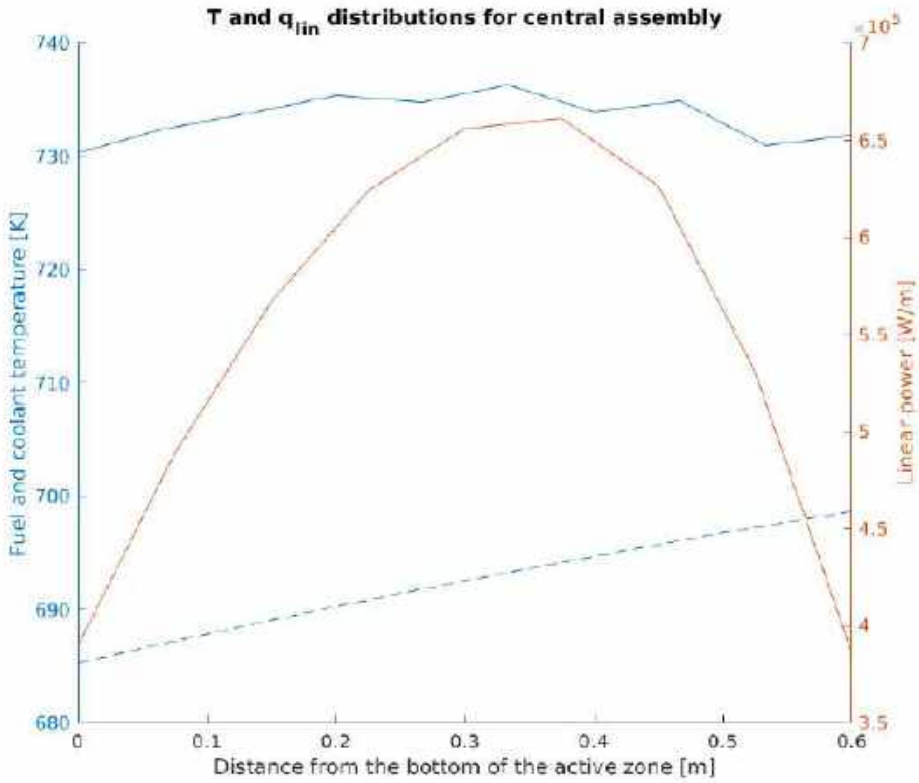

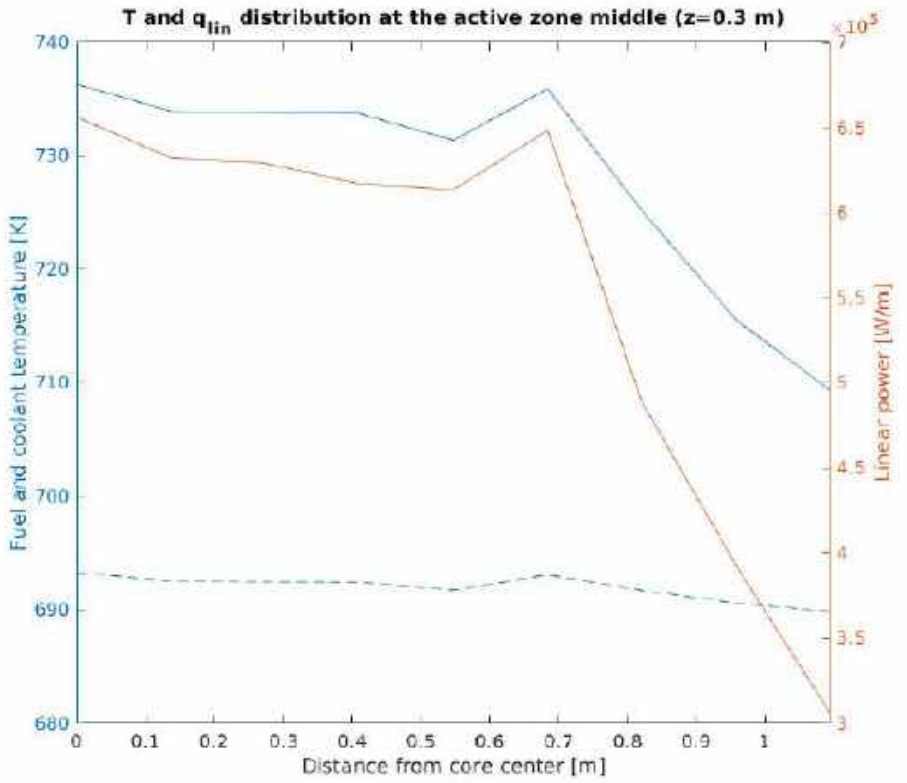

«Upgraded» Serpent run

- Temperature distribution from FRENETIC
  - T for both fuel and coolant
  - Value at the FA level for different axial positions
  - If transferred directly into Serpent, memory issus arise …
- Solution:
  - Definition of concentric regions
  - T associated to each region
  - Axial distribution preserved
- Serpent run … in progress

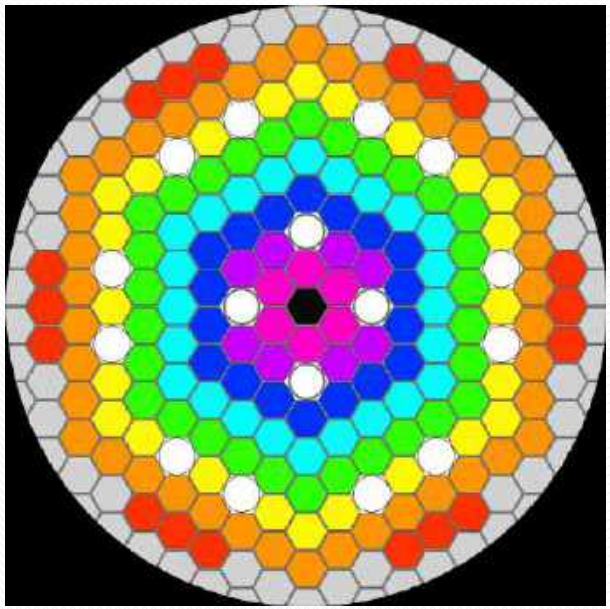

Work in progress

- Comparison of «upgraded» Serpent run with FRENETIC in terms of power distribution
  - Assessment of the quality of FRENETIC modelling w.r.t. reference Monte Carlo in the same thermal conditions
- OpenFoam calculation of the single FA with
  - «improved» boundary condition provided by FRENETIC (heat flux)
  - Power distribution representative of different regions in the core (from «upgraded» Serpent)

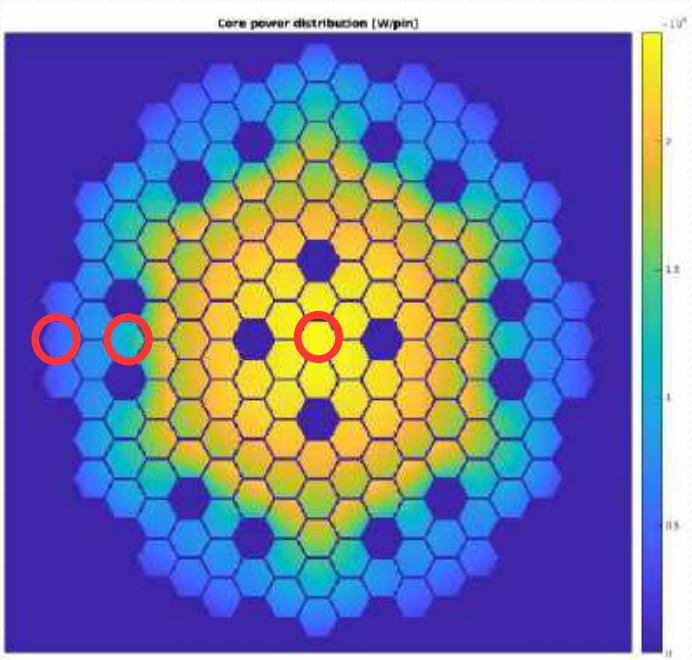

Work in progress

- Comparison of OpenFoam results with FRENETIC on the single FA
  - Evaluation of the relevance of specific TH effects that FRENETIC may not be able to reproduce
  - Improvement of the current correlations and averaging processes currently existing in FRENETIC, based on CFD results

Conclusions and perspectives

- The activity is part of a fruitful collaboration between PoliTO and PoliMI in the frame of the POLY²NUC program
- The work is still in progress and results are progressively produced and analyzed (both steps take time …)
- The resulting upgraded models will be applied to the analysis of the forthcoming upgraded ALFRED design

UNIVERSITY OF PISA

Dipartimento di Ingegneria Civile e Industriale (DICI)

HLM-Water Interaction & SIMMER-RELAP5 code coupling development

N. Forgione

Introduction

- The interaction between two fluids, of which one is less volatile and at higher temperature than the other one, results in the production of high pressure vapour.

  Thus, this is one of the most important concerns for safety issues of:

  - Lead and Sodium cooled reactors belonging to "Generation IV" systems
  - ADS where both core and target are cooled by LBE

- In HLM reactors, the heavy liquid metal might come into contact with the water flowing in the steam generator because of an accidental Steam Generator Tube Rupture (SGTR).

  → CCI

- In sodium cooled reactors a loss of coolant accident can increase the core temperature up to the fuel and steel melting, leading this mixture to interact with the surrounding coolant.

  → FCI

- One of the crucial issue is represented by the evaluation of the energy released in such interactions, in order to have indications of the potential loads and the resulting damage on reactor structures.

SIMMER III Features

SIMMER III, jointly developed by JAEA (Japan), KIT (Germany), IRSN & CEA (France), is a 2D axysimmetric, three velocity-field, multi-component, multiphase, Eulerian fluid-dynamics code coupled with neutron kinetics model. It can deals with safety analysis problems in advanced fast reactors.

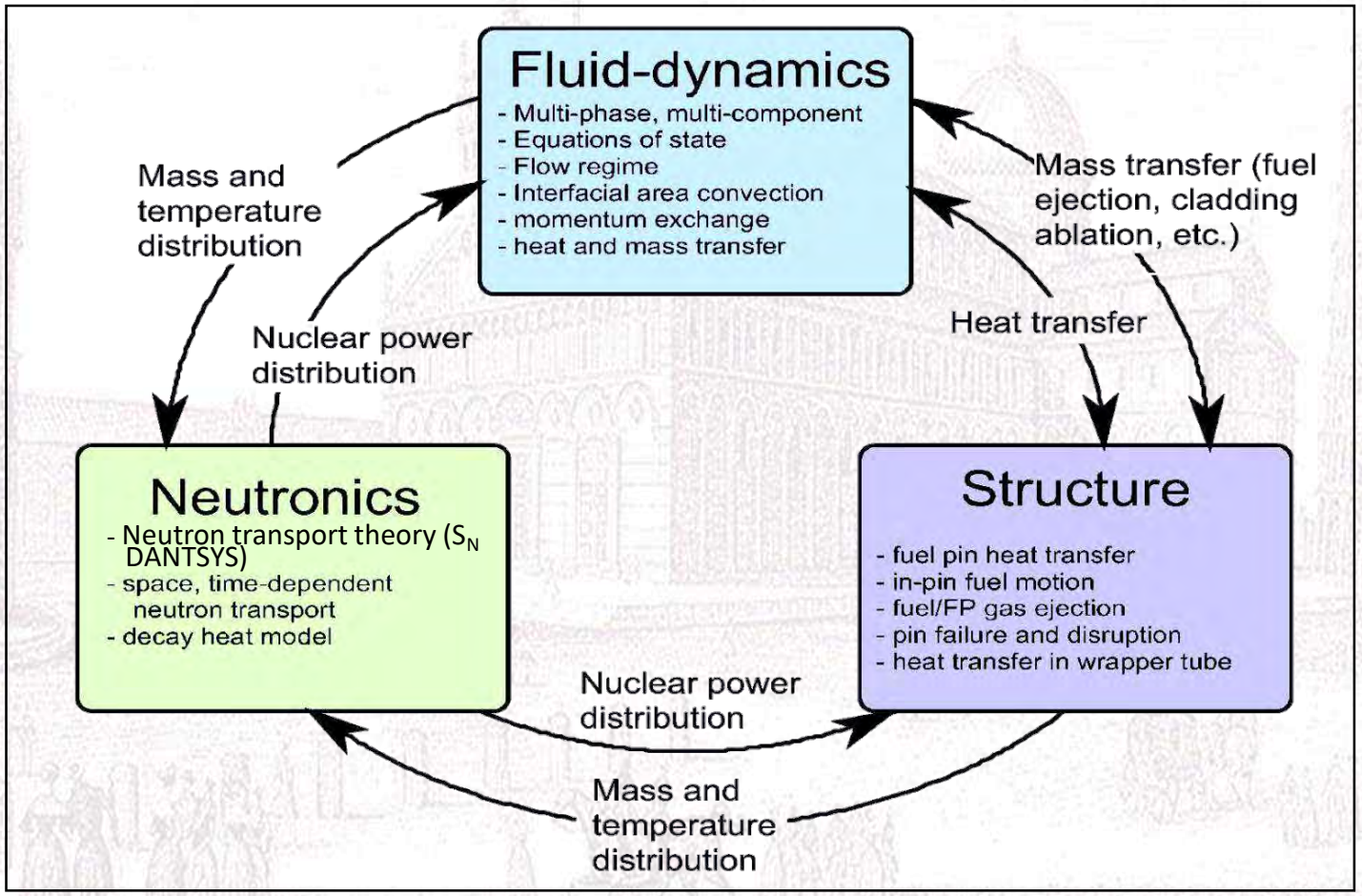

THINS experimental campaign and SIMMER III validation
LIFUS5/Mod2 injection line analysis

Test A1.2_2

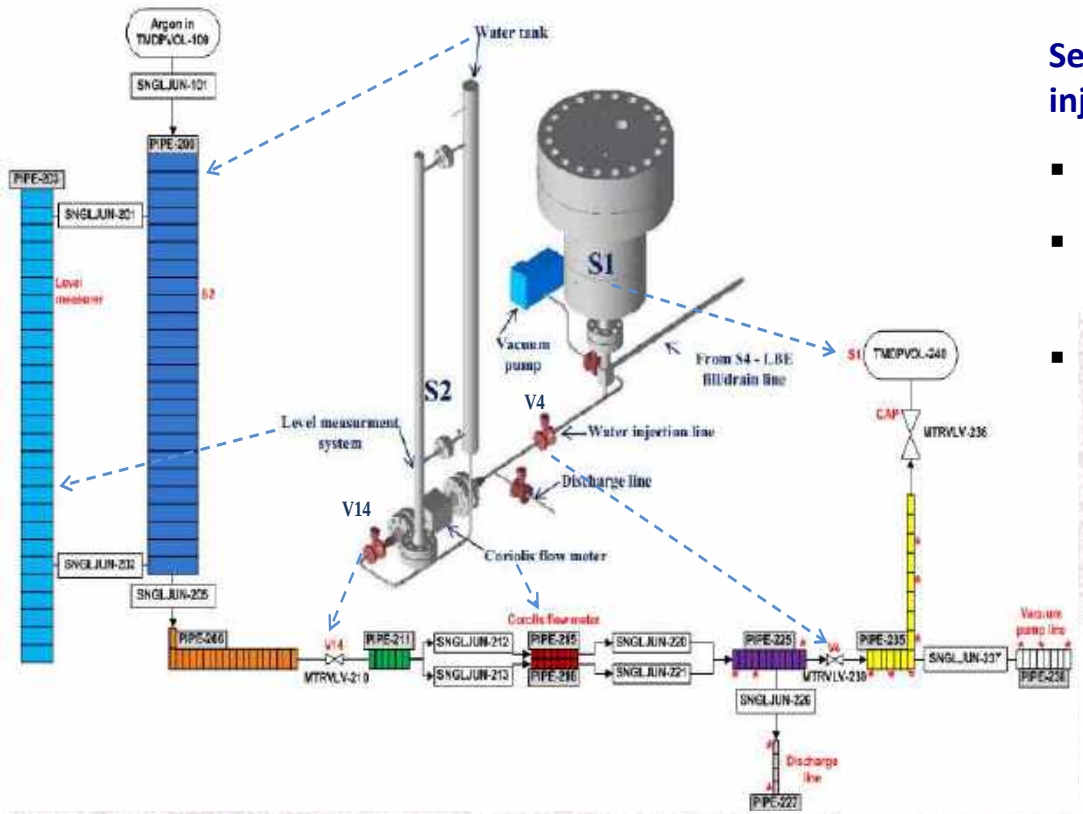

Sensitivity analysis by RELAP5/MOD3.3 of the water injection line for characterizing:

- **Valves (V4, V14) opening/closing time → 0.25 s**
- **Valves (V4, V14) and Coriolis energy loss coefficient K → 7**
- **Coriolis tubes area → 4.53e-5 m²**

T_{H2O} = 240°C

P_{H2O} = 40 bar

T_{LBE} = 400°C

V_{Ar}/ V_{LBE}= 30%

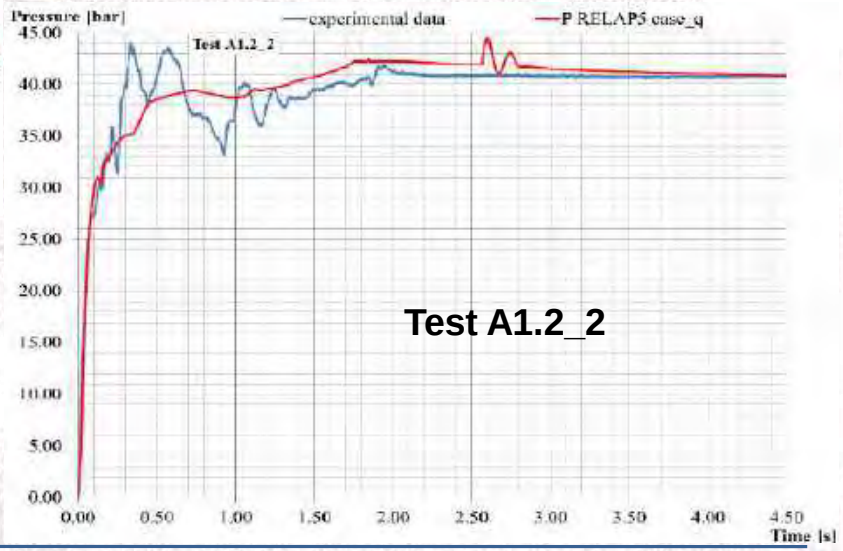

- ❑ **RELAP5/Mod3.3 was able to predict pressure time trend in the injection line**
- ❑ **Pressure evolution in the injection line is a key parameter for evaluating water/LBE interaction → S1 pressurization**
- ❑ **Post-test analysis of THINS tests (done by SIMMER III) could be significantly improved by SIMMER-RELAP5 coupling**

THINS experimental campaign and SIMMER III validation
LIFUS5/Mod2 injection line analysis

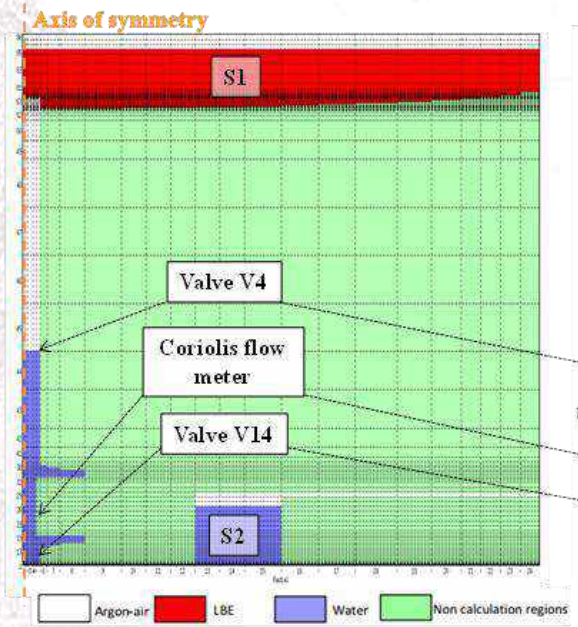

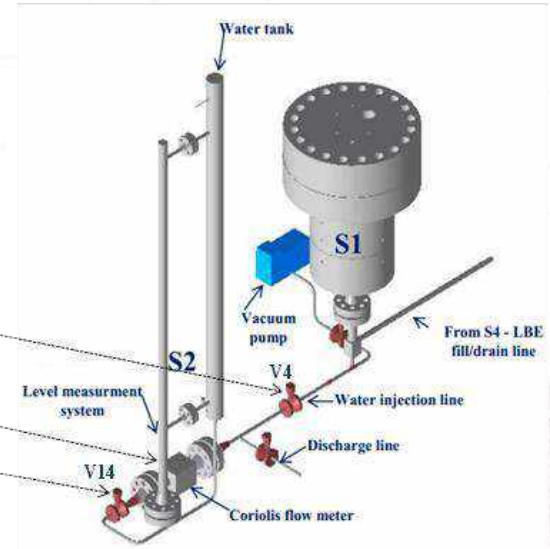

SIMMER III calculation with injection line parameters based on RELAP5/Mod3.3 sensitivity

- **SIMMER III has improved the prediction of injection line pressurization**
- **Mass flow rate computed by SIMMER III is qualitatively analogous to that on compute by RELAP5/Mod3.3**

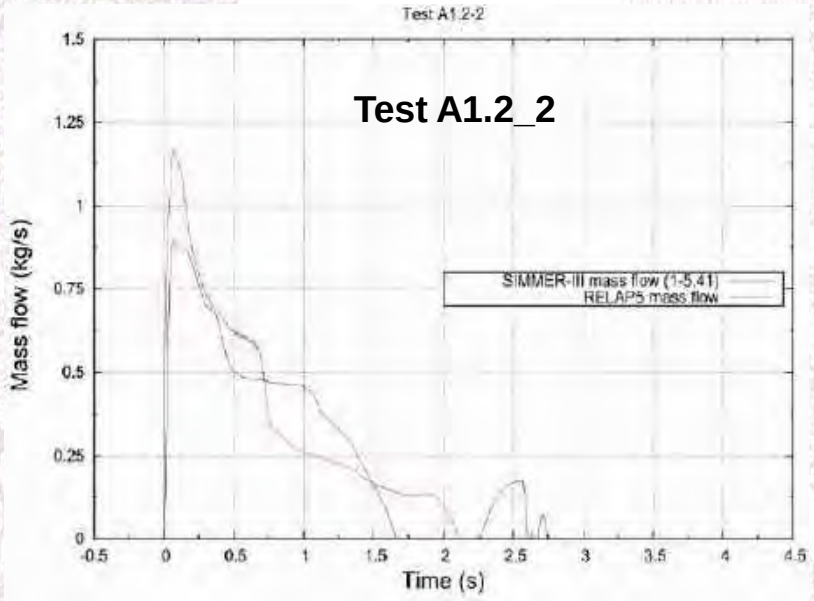

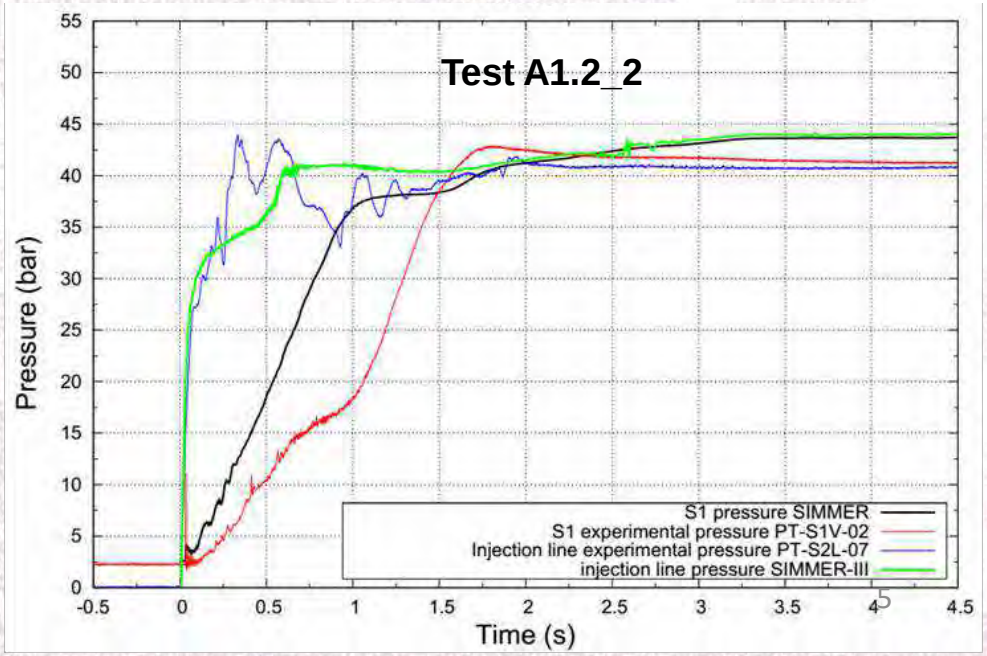

Goals & Tasks for the AdP 2017 Activity

Main aim

- Set up a coupling tool capable to reproduce part of a TH system, in which 2D/3D phenomena occur, with SIMMER code and the remaining part of the system with RELAP5 code.

UNIPI activities foreseen inside AdP2017

- Set up of SIMMER-RELAP5 coupled tool and application to a simple configuration quite similar to the LIFUS5 test section.
- Development of SIMMER III model of LIFUS5/Mod3 facility.
- Development of RELAP5 nodalization of the LIFUS5/Mod3 facility.
- Preliminary application of the coupled tool to LIFUS5/Mod3 facility.

Manometer flow oscillation problem

The geometry of the problem, used as preliminary verification of the coupling technique, consists of two tanks partially filled with water at different pressure ($p_2 > p_1$).

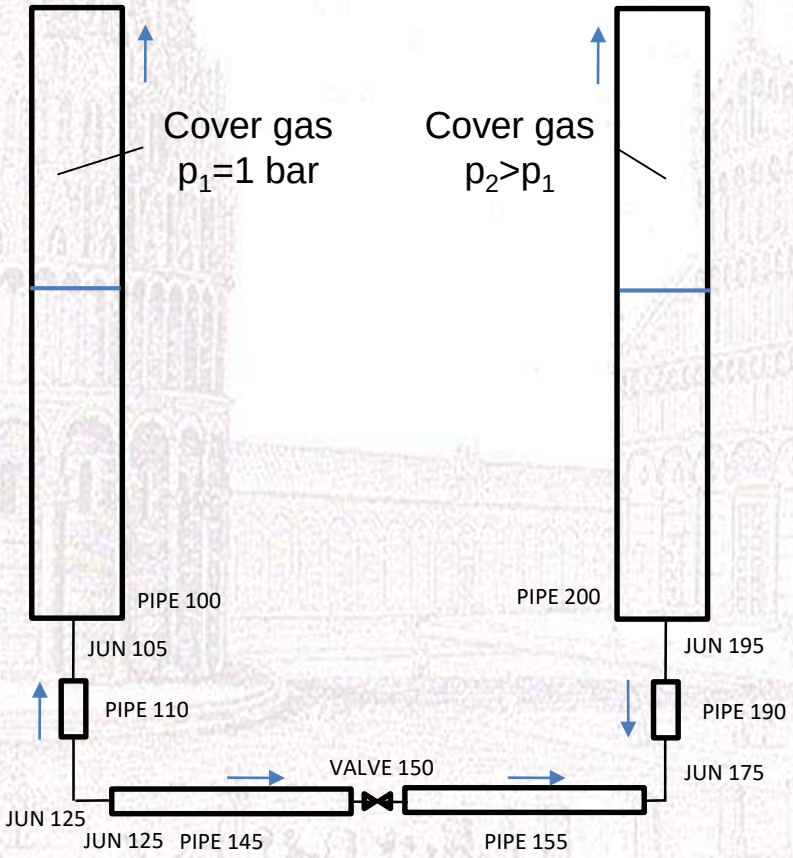

- **Pipe 200 is the "High pressure tank", and Pipe 100 is the "Low pressure tank".**
- **Pipes 190, 155, 145, and 110 are the "Injection line".**
- **Valve 150 isolates the two zones at different pressure. It opens in 0.01 s, 2.1 s after the beginning of each calculation.**
- **Pressure drop coefficients across junctions 105, 150, 175 and 195 set to 1.**

Pipe	Dimensions
100, 200	H = 1 m, D = 0.5 m, 20 cells
110, 190	H = 0.1 m, D = 0.05 m, 10 cells
145, 155	H = 2.5 m, D = 0.05 m, 10 cells

Manometer flow oscillation problem

When possible, for the different test cases of the validation matrix, a comparison between the standalone (RELAP5) and the coupled calculation has been performed.

RELAP5 STANDALONE

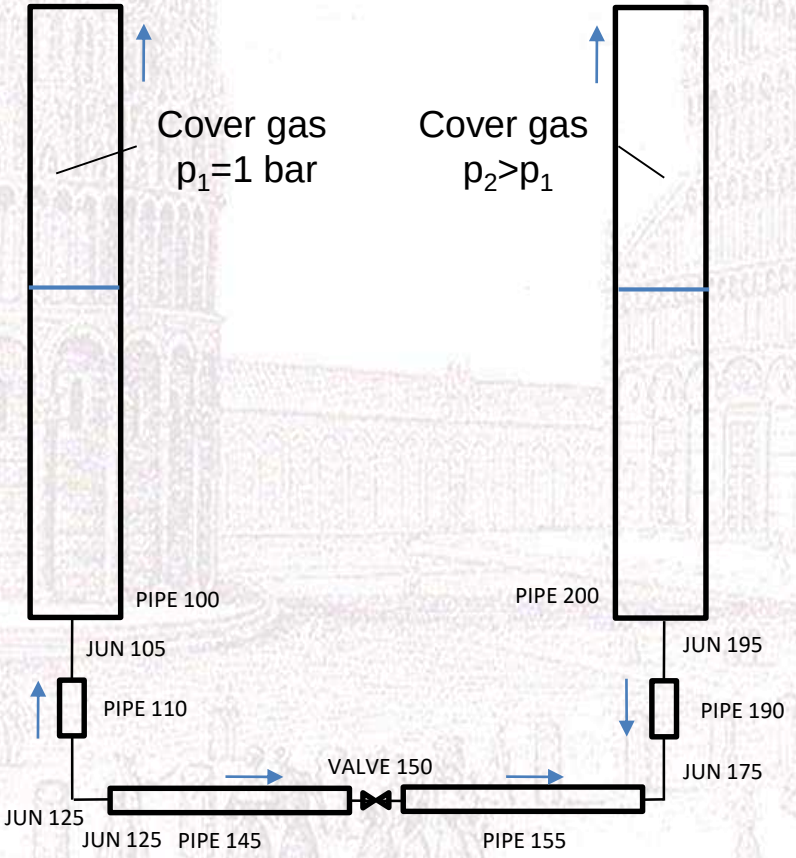

SIMMER-RELAP5 COUPLED

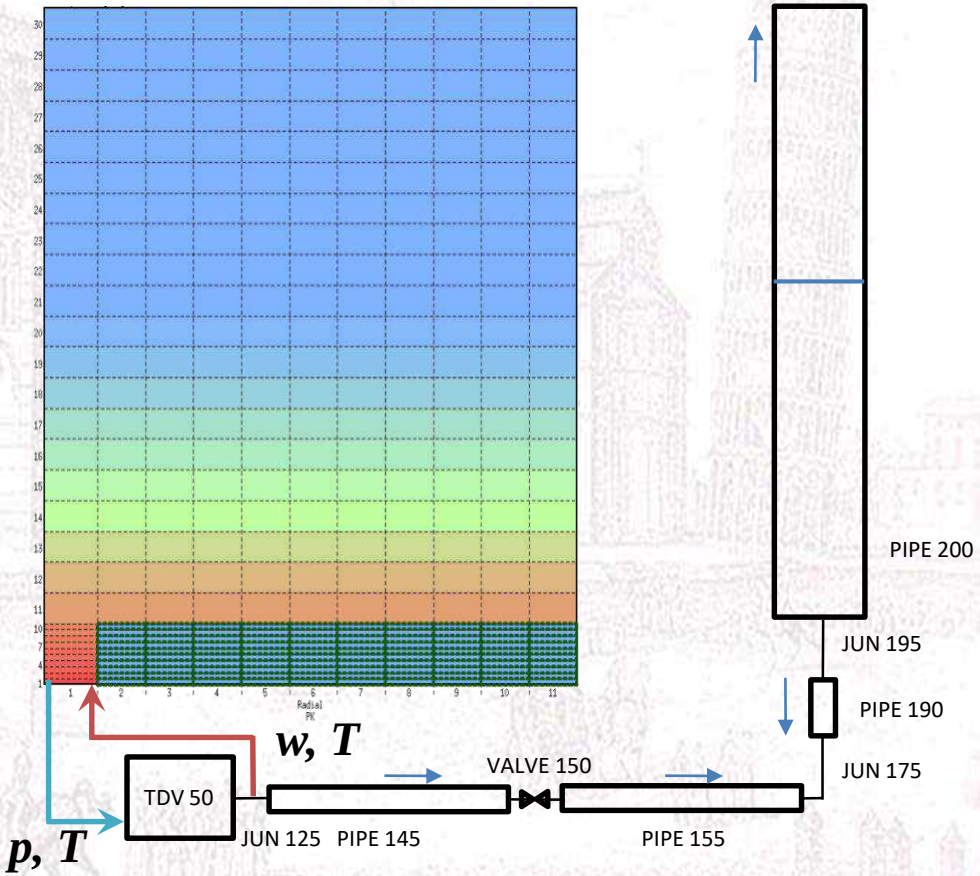

Manometer flow oscillation problem

Low pressure tank (Pipe 100) and the Pipe 110 were replaced by a SIMMER III axial-symmetric domain discretized by 20 vertical cells and 11 radial cells.

Concentrated pressure drop coefficients (K = 0.05) are set-up on the cells reproducing the Pipe 110 to account for the distributed pressure drops which are not automatically evaluated by SIMMER III code.

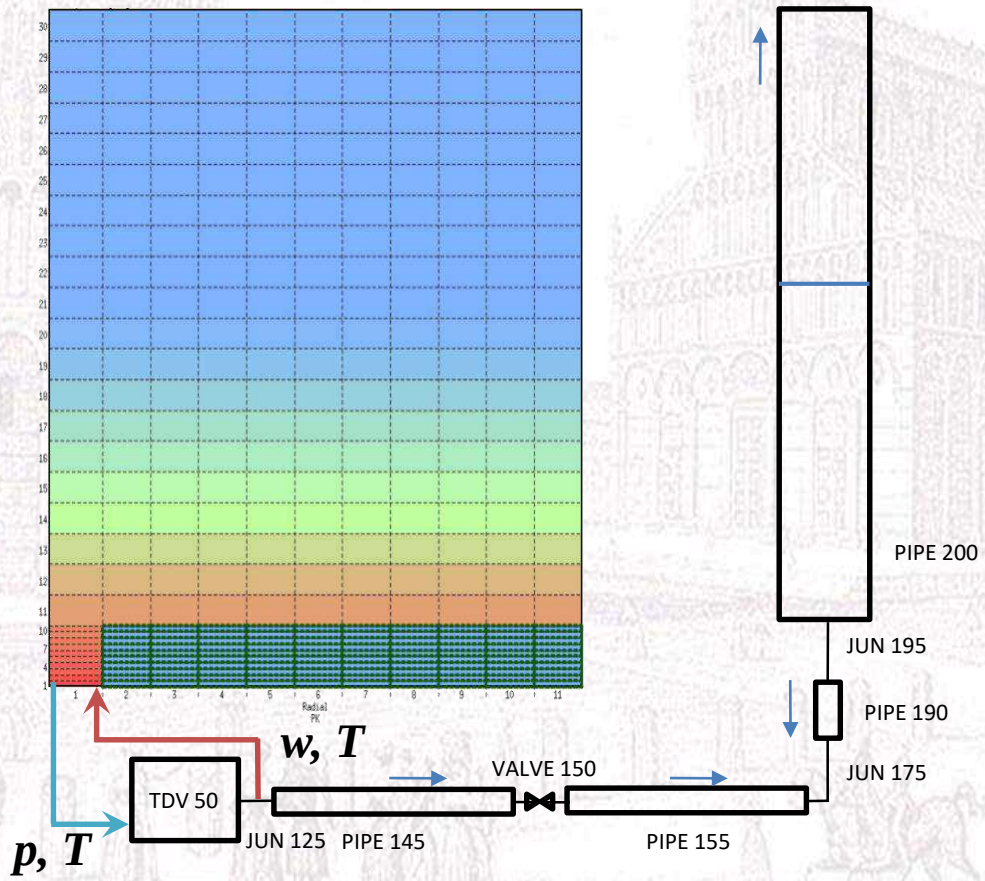

Management of macro time-step:

1) A SIMMER III run is performed imposing as b.c. the fluid velocity and temperature through junction 125 (RELAP5).
2) The pressure and the temperature of inlet section (cell (1,1)) obtained a the end of the SIMMER III run are then given back to RELAP5 as b.c..
3) According to this new b.c., the RELAP5 code calculates a new fluid velocity and temperature across junction 125.
4) The macro time-step is over, and the coupling moves to the evaluation of the next macro time-step.

Manometer flow oscillation problem

Coupling Numerical Scheme

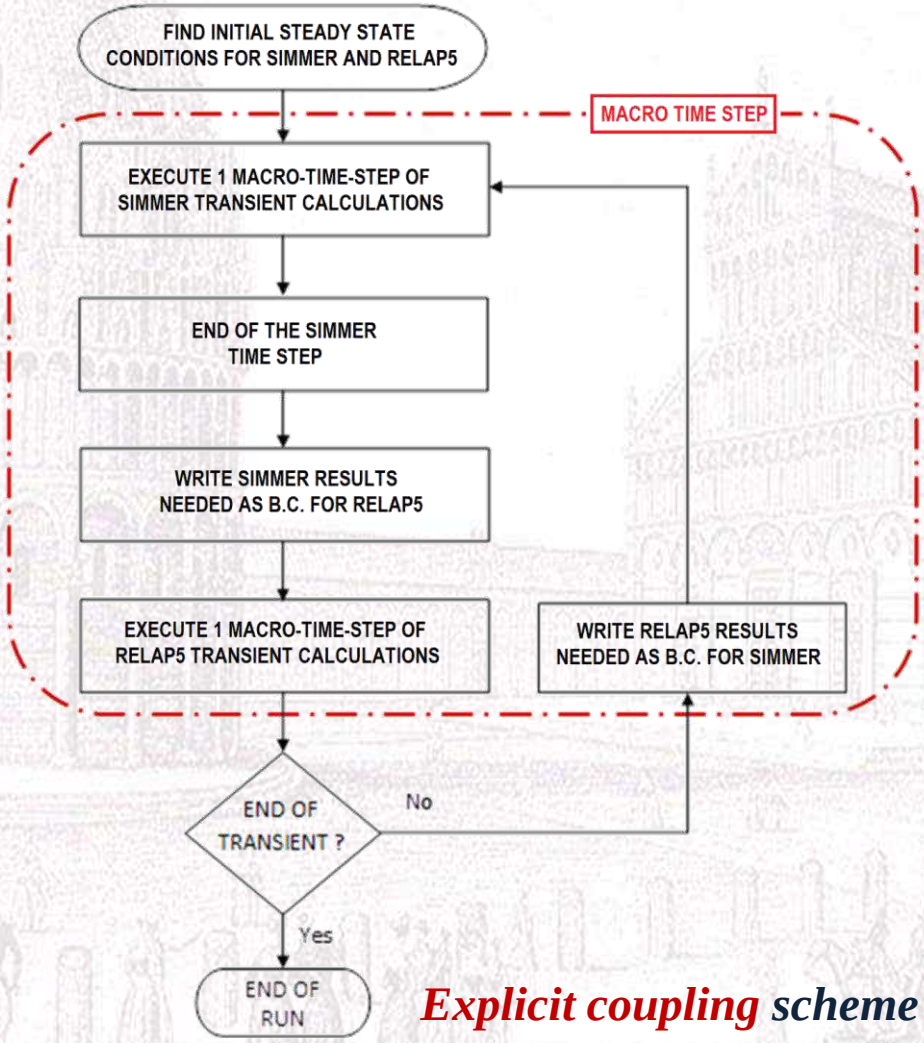

Explicit coupling scheme

- Execution of the SIMMER III and of the RELAP5/Mod3.3 code is operated by an appropriate MATLAB script.
- MATLAB algorithm implemented to receive b.c. data from SIMMER, and to send b.c. data to RELAP5, and vice versa.
- Domain decomposition (non overlapping) coupling approach.
- "Two way" coupling calculation.
- SIMMER III code is the master code.
- RELAP5 code is the slave code.
- Both the codes work on the Linux operating system.
- The RELAP5 version is that modified at UNIPI to take into account for the properties of the liquid metals.

Manometer flow oscillation problem

A matrix of test cases was initially set-up to check the stability and the capabilities of the coupling tools.

Test case	Init. Cond. (RELAP5)	Init. Cond. (SIMMER III)
1. Tanks at different initial pressure	10 bar / 20°C	1 bar / 20°C
2. High pressure tank kept at 10 bar during the transient	10 bar / 20°C	1 bar / 20°C
3. High pressure tank kept at 10 bar with different water temperature in the two tanks	10 bar / 80°C / 0.5 m	1 bar / 20°C / 0.5 m
4. High pressure tank kept at 50 bar	50 bar / 20°C / 0.95 m	1 bar / 20°C / 0.25 m
5. High pressure tank kept at 100 bar	100 bar / 20°C / 0.95 m	1 bar / 20°C / 0.25 m

The matrix is still under development. New test cases can be added.

Case 1: “Tanks at different pressure”

The tanks are initially at different pressure. The valve isolating the two sides of the system opens (at 2.1 s) and the transient start.

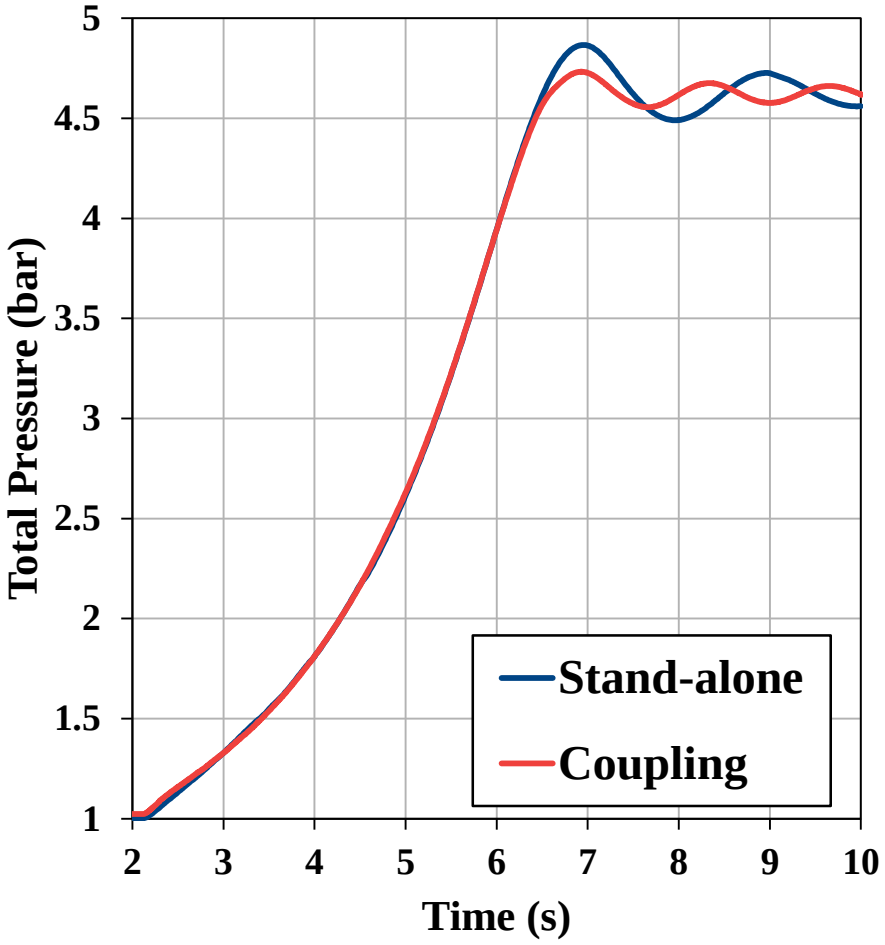

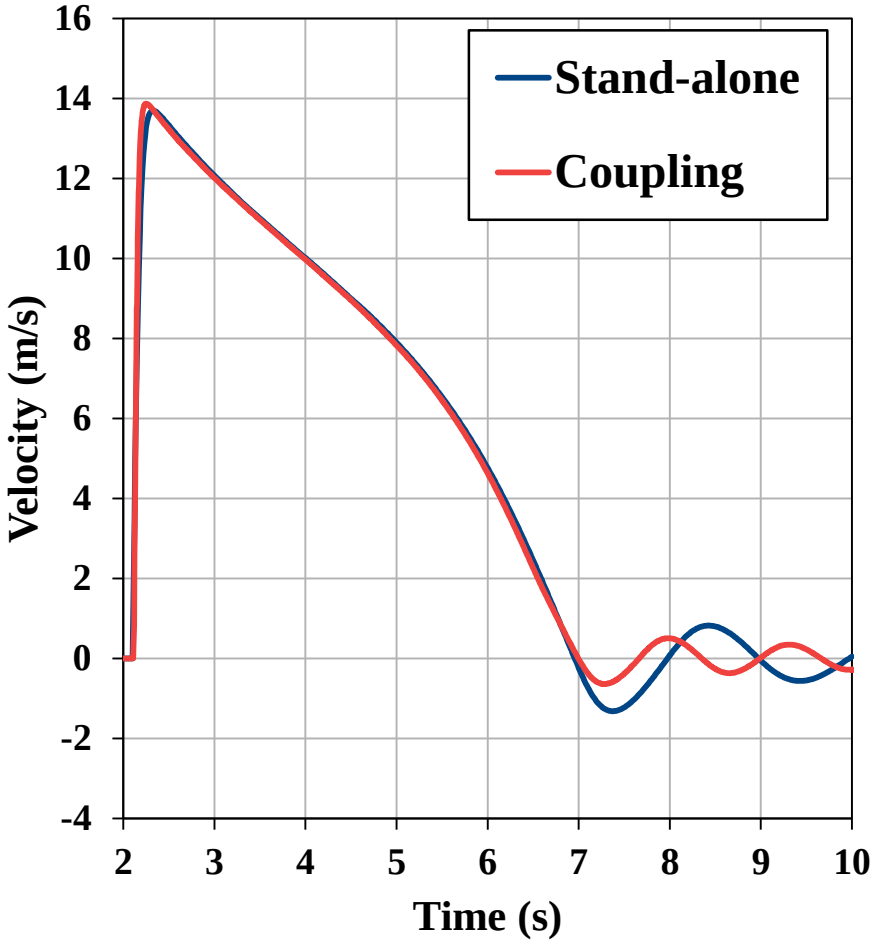

Case 2: “High pressure tank kept at 10 bar”

The 2 tanks are initially at different pressure, and the “High Pressure” tank is kept at 10 bar. Initial water level and temperature identical in both tanks.

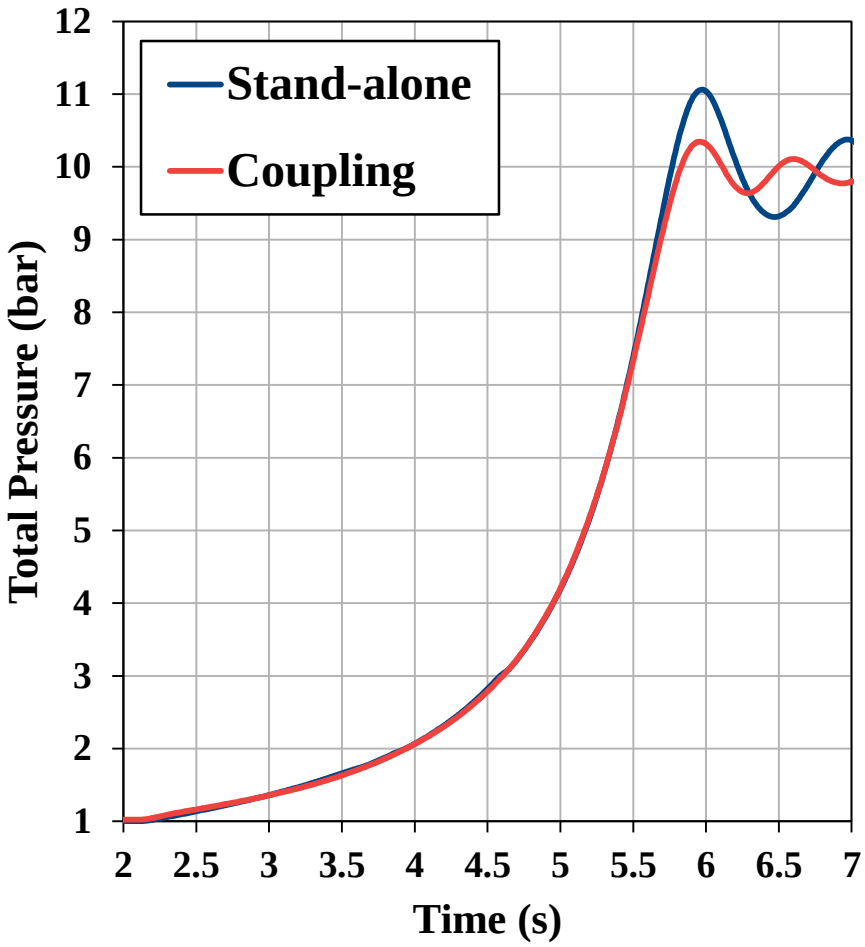

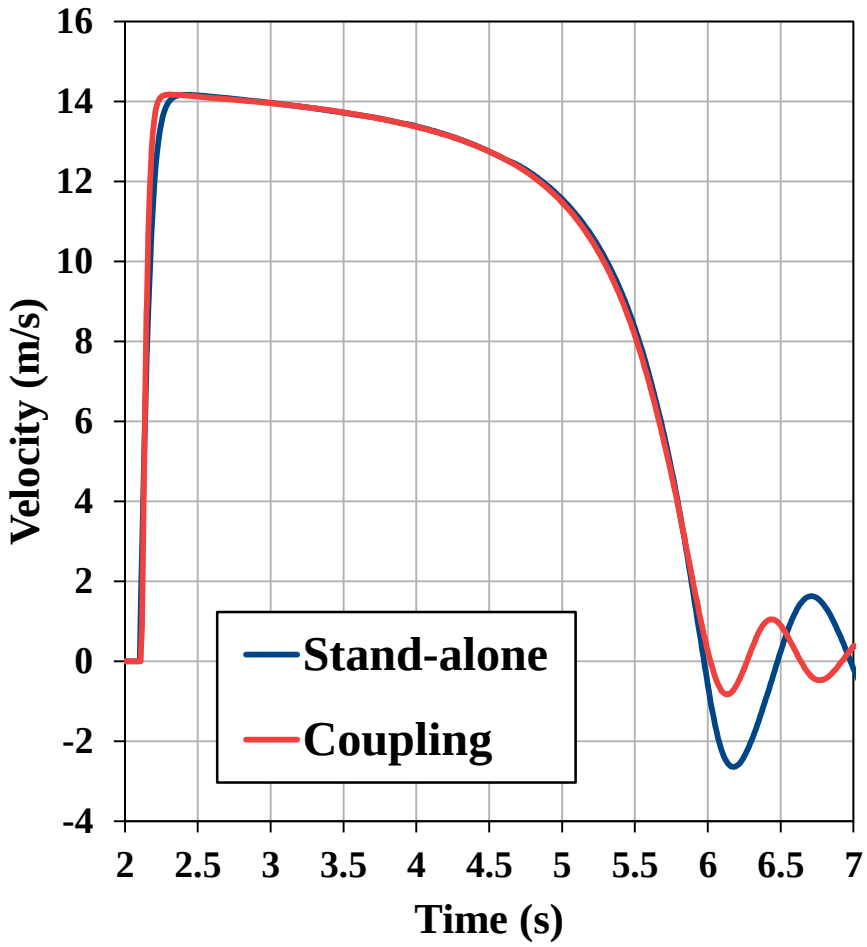

Case 3: “High pressure tank kept at 10 bar with different water temperature in the two tanks”

The 2 tanks are initially at different pressure, and the “High Pressure” tank is kept at 10 bar. Initial water level identical in both tanks, and water temperatures set to 80°C in the “High Pressure” tank and 20°C in the “Low Pressure” tank.

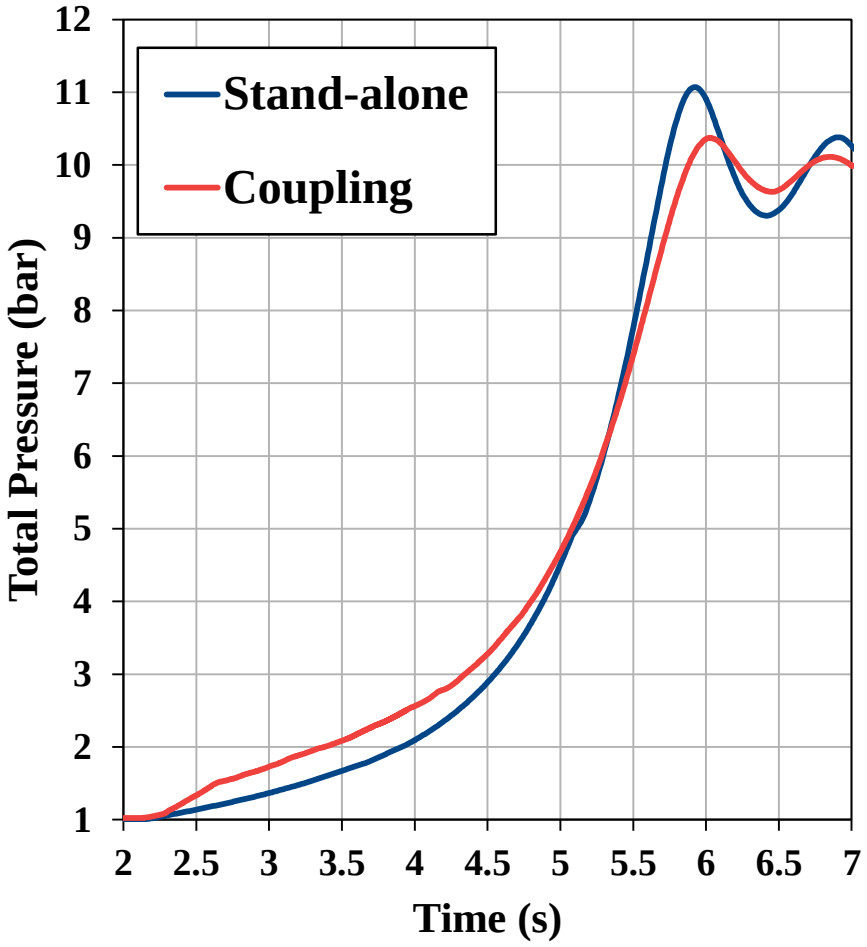

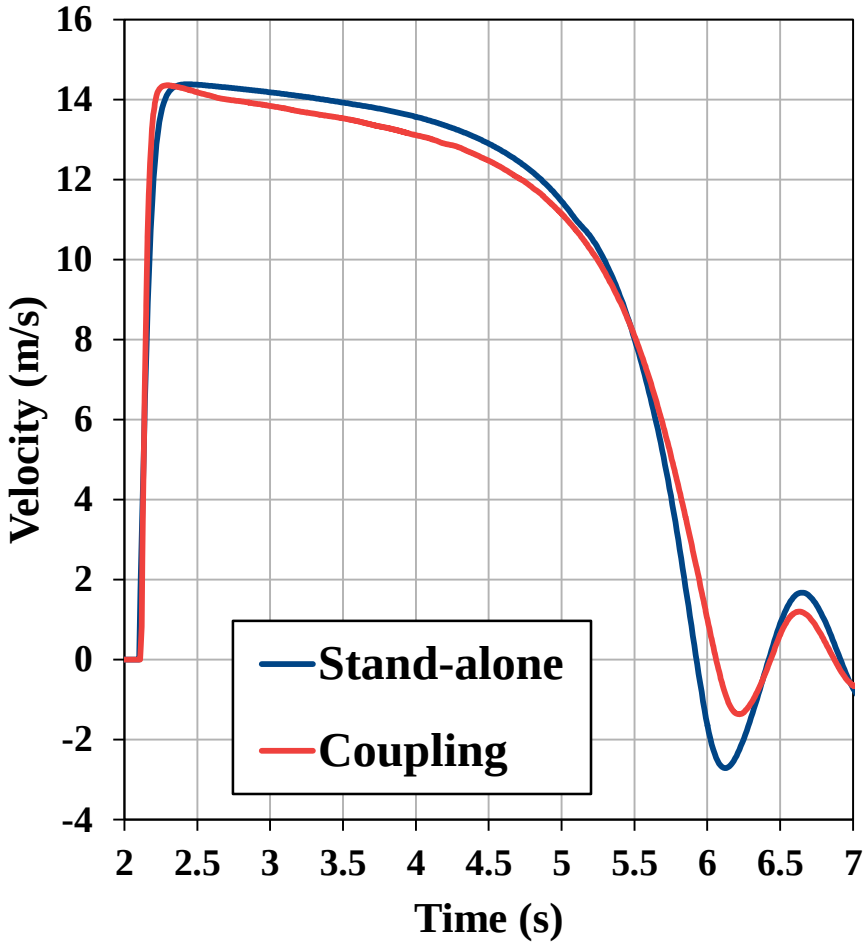

Case 4: “High pressure tank kept at 10 bar with different water temperature in the two tanks”

t = 0 s

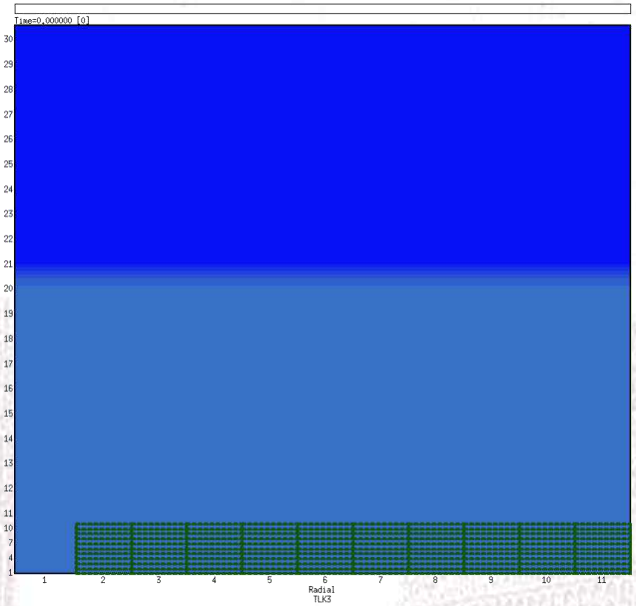

t = 2.6 s

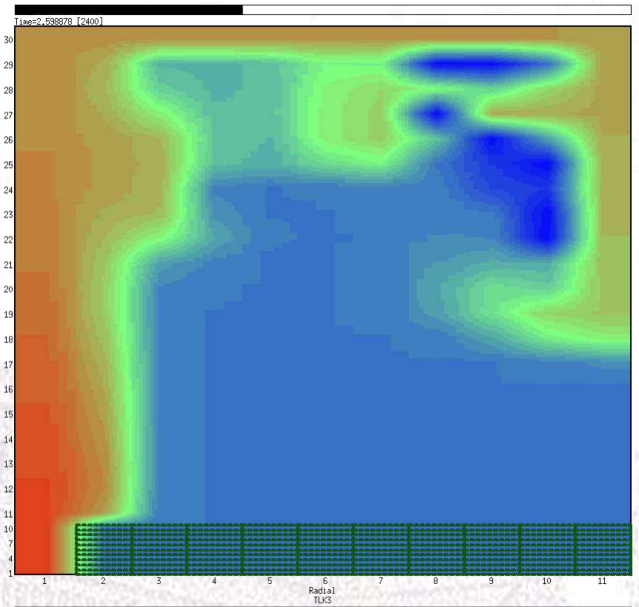

90 °C

0 °C

t = 5.1 s

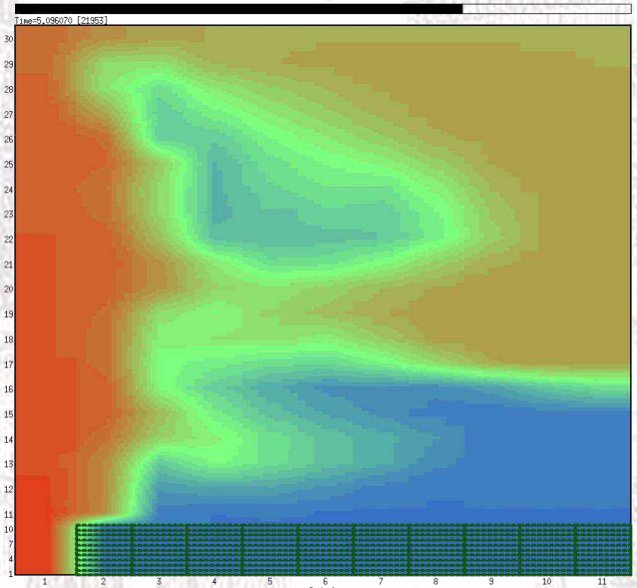

t = 7 s

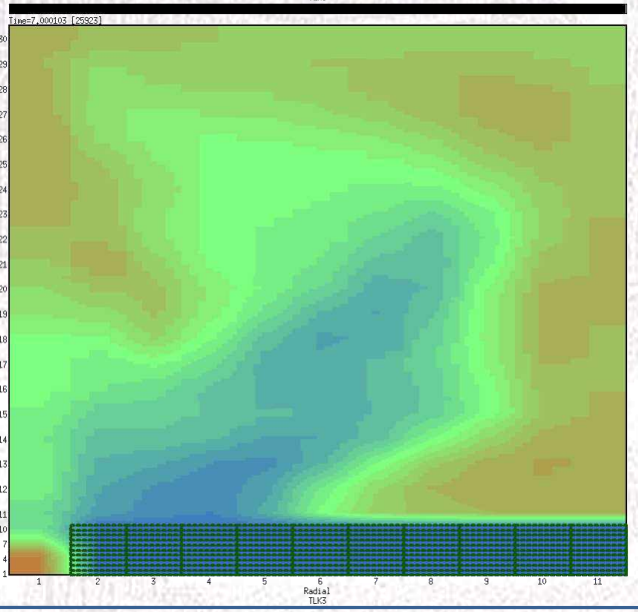

Case 4: “High pressure tank kept at 50 bar”

The tanks are initially at different pressure, the “High Pressure” tank is kept at 50 bar, and to avoid the gas flow between the two tanks the “Injection line” diameter was reduced to 0.025 m (0.05 m in the previous cases).

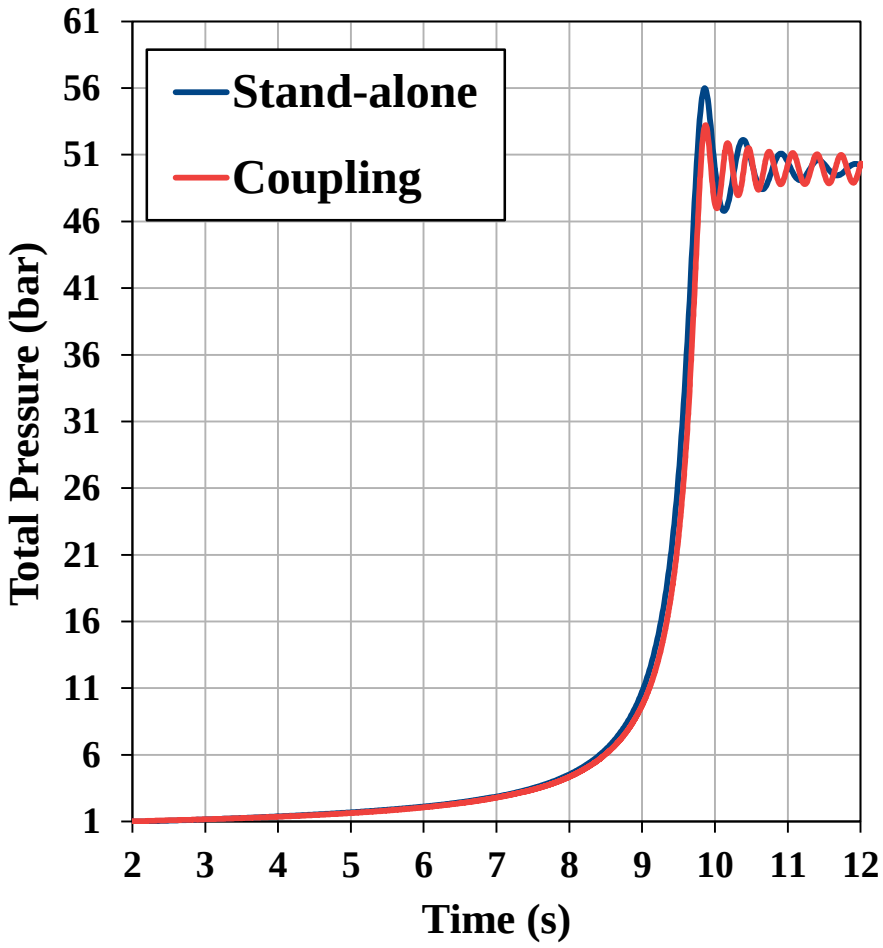

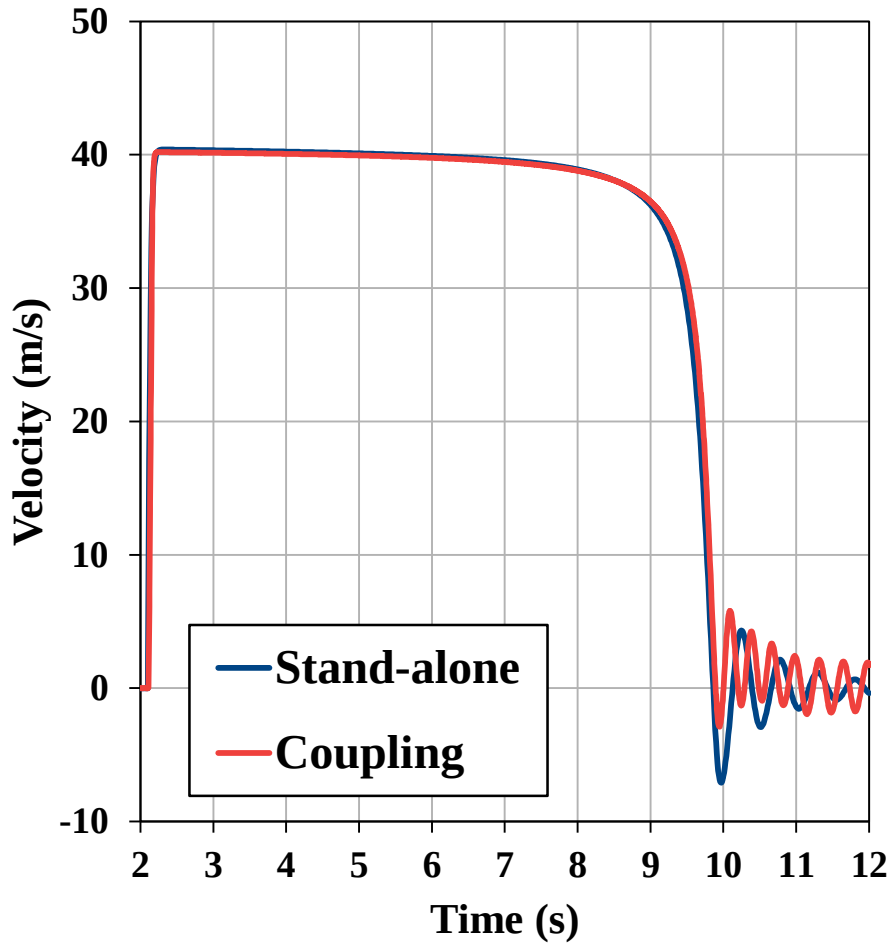

Case 5: “High pressure tank kept at 100 bar”

The tanks are initially at different pressure, the “High Pressure” tank is kept at 100 bar, and to avoid the gas flow between the two tanks the “Injection line” diameter was reduced to 0.025 m (0.05 m in the previous cases).

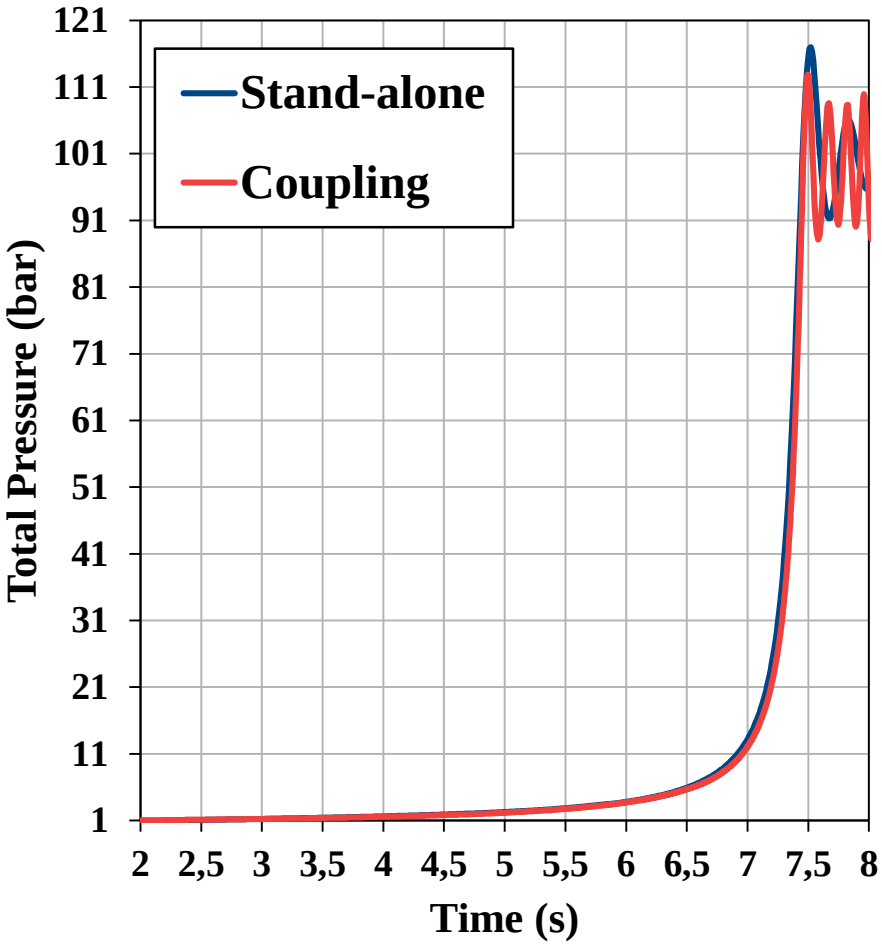

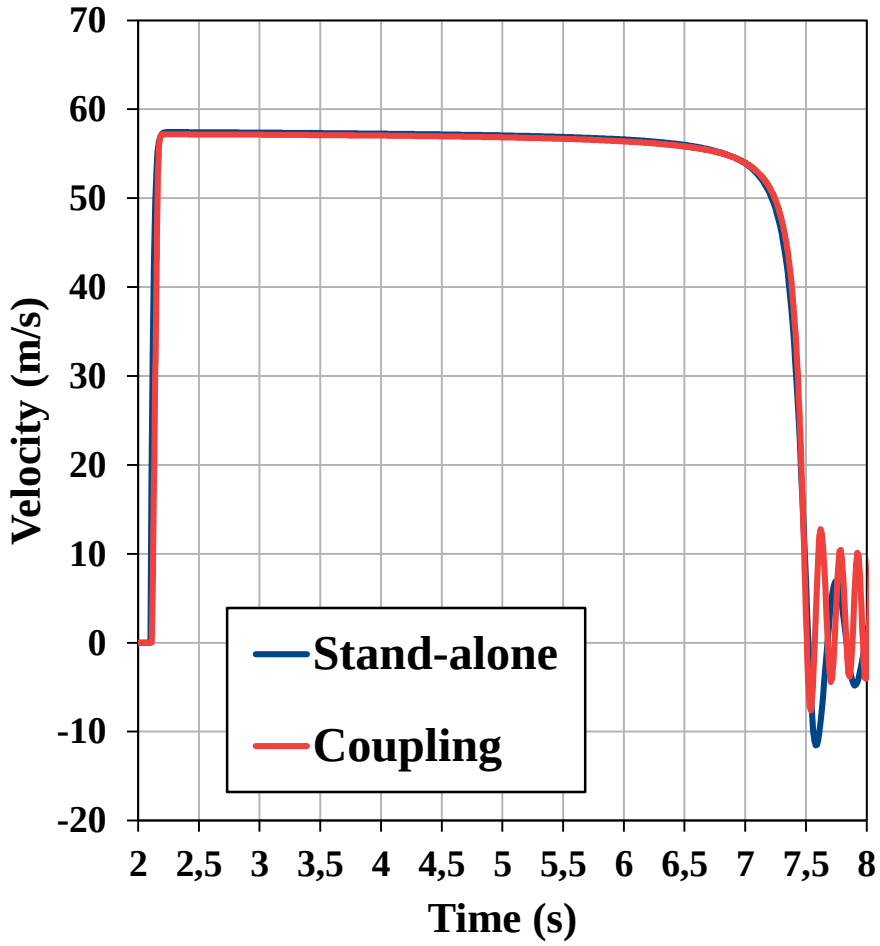

SIMMER-RELAP5 coupled codes applied to LIFUS5/Mod3

Two-way coupling with "non-overlapping" strategy, i.e. the overall domain is divided into two regions modelled using the SIMMER III and RELAP5 codes:

- **RELAP5 applied to simulate the S2 vessel and the injection line;**
- **SIMMER III code to simulate the Water/LBE interaction in the S2 vessel.**

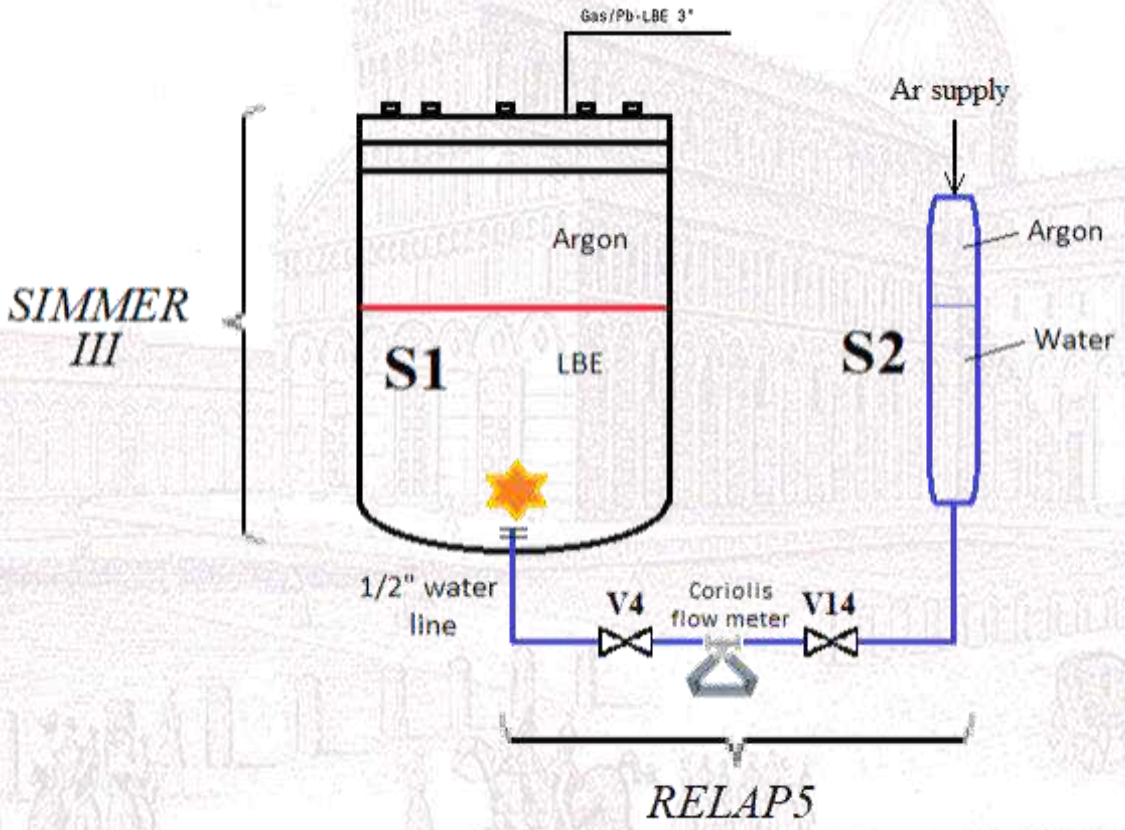

SIMMER-RELAP5 coupled codes applied to LIFUS5/Mod3

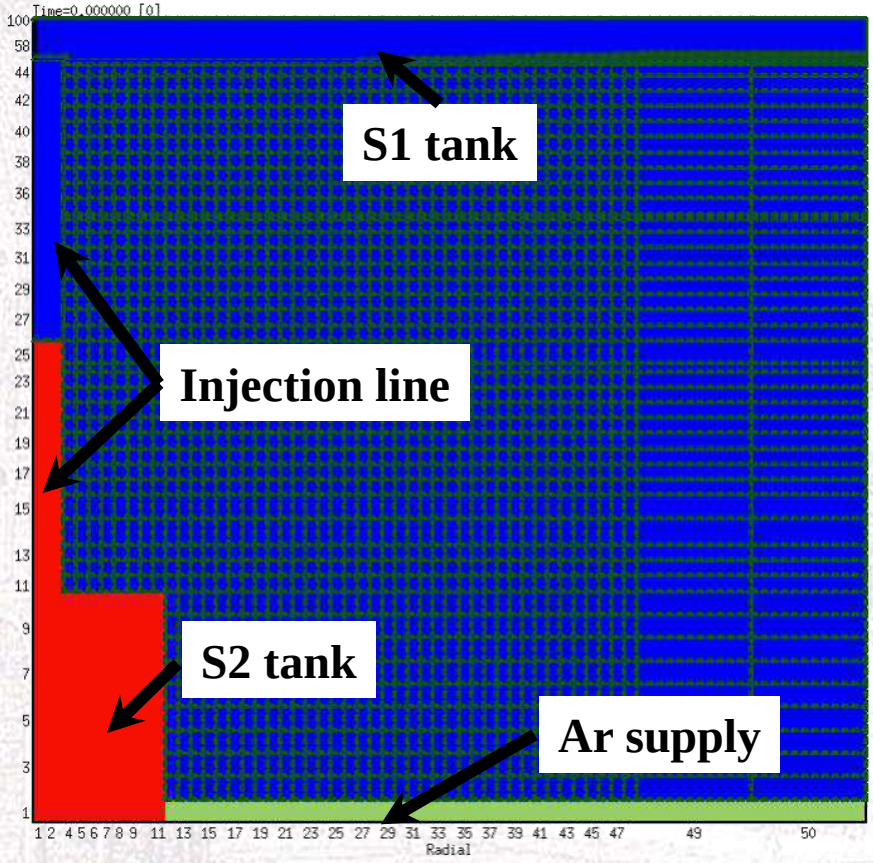

- The facility is almost assembled and the tests are expected soon.
- Only preliminary input decks have been created and tested.

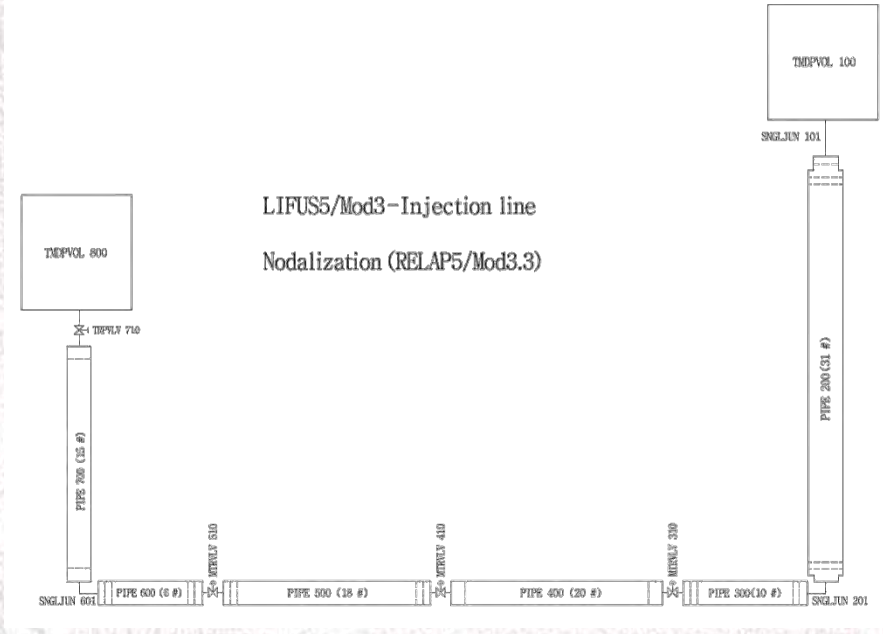

- **Short term**: have the SIMMER III and RELAP5 input decks ready for the end of June/mid of July.

Conclusions

- Previous research activities performed byt UNIPI, in collaboration with ENEA, inside the EU Projects THINS (LIFUS 5 facility) and SEARCH (MYRRHA reactor), highlighted possible improvements in performed analyses with a coupling between SIMMER and RELAP5 codes.
- Improvements and validation activities of the SIMMER and RELAP5 codes have been carried out in order to study in depth phenomenological aspects of interest for accidents scenario in HLM reactors and fusion reactors.
- The developed coupling tool SIMMER-RELAP5, applied to a manometer flow oscillation problem, represent a first step of the activity that UNIPI must perform inside PAR2017.
- The future activity to be performed inside PAR2017 will consist in:
  - improvement of the coupling tool implementing a semi-implicit numerical scheme to enhance the stability of the calculations;
  - application of the developed coupling tool to the LIFUS5/Mod3 facility in support of the pre-test analysis.

WORKSHOP TEMATICO: GEN IV LEAD COOLED FAST REACTOR

Stato attuale della tecnologia e prospettive di sviluppo

ADP MiSE-ENEA (PAR2017-LP2)

Aula 8 - Dipartimento di Ingegneria Astronautica, Elettrica ed Energetica
Università di Roma "La Sapienza"
San Pietro in Vincoli, Via Eudossiana 18
14-15 Giugno 2018

Phenix Asymmetrical Test Simulation by 3D STH code

Fabio Giannetti [Sapienza]
Vincenzo Narcisi [Sapienza]
Andrea Subioli [Sapienza]
Gianfranco Caruso [Sapienza]

Alessandro Del Nevo [ENEA]

CONTENTS

- Introduction
- Objectives of the activity
- Outline of PHENIX reactor
- RELAP5-3D© nodalization
- “Dissymmetric test” description
- Blind results and comparison with experimental data
- Preliminary TH-NK coupled model and results
- Summary and follow-up

INTRODUCTION

- PHENIX End Of Life Tests performed in 2009 after the 56th irradiation cycle
- 2 tests were performed in thermal-hydraulics area
  - *a natural convection test* and
  - a dissymmetrical configuration test
    → this has been selected as a benchmark transient
    → synergy with H2020 SESAME project

OBJECTIVES OF THE ACTIVITY

- to compare best-estimate TH-SYS code calculations to experimental data, thus to validate RELAP5-3D© system code in simulating FR designs
- to assess the reliability of SYS-TH multiD components in modeling transient in LM pool FR
- to identify and, as far as possible, to quantify the code limitations and the source of uncertainties in simulating postulated accidents occurring in liquid metal FR designs
- to improve the understanding of the TH processes and phenomena observed in dissymmetrical test
- to improve the understanding of FR neutronics, TH and SYS analysis

PHENIX

CORE

Diagrid is connected to primary pumps.
It has the function of positioning, supporting and supplying sodium to core SA

Strongback has the function of supporting the core and it carries about the 10% of operating flow to the vessel cooling system.

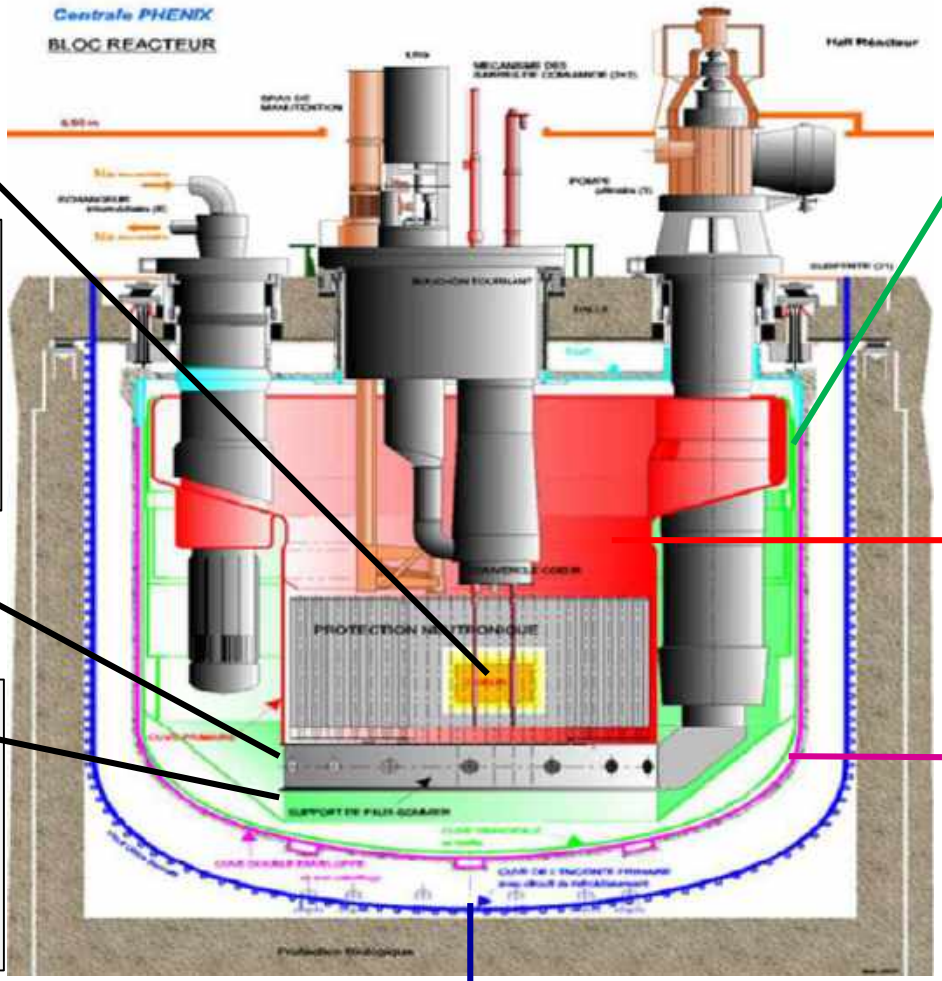

Main vessel
Diameter = 11.8 m
Na inventory = 800 tons
Attached to the upper slab by 21 suspension hangers
Cooled in the upper zone by a vessel cooling system

Inner vessel separates the pool in two regions: hot and cold.

Double- envelope vessel is welded to the upper region of the main vessel and it has the function of containing any possible sodium leaks.

Primary containment vessel is welded to the slab's underside, and attached to the reactor pit. It has to retain radioactive release of postulated severe accident. It carries the final emergency cooling system which is designed to keeping the reactor concrete at ambient temperature, and to ensure the decay heat removal

Nodalization description

PHENIX nodalization man features:

- MULTID component + 1D components for 3D nodalization; 1D components for bidimensional nodalization
- Relevant elevations of PHENIX are maintained in the nodalization, with minor (< ~5 cm) exceptions due to modeling constraints (e.g. IHX bottom)
- WESTINGHOUSE heat transfer correlation in bundle regions, Seban –Shimazaki everywhere
- Wire wrapped fuel bundle friction losses modeled with Cheng and Todreas

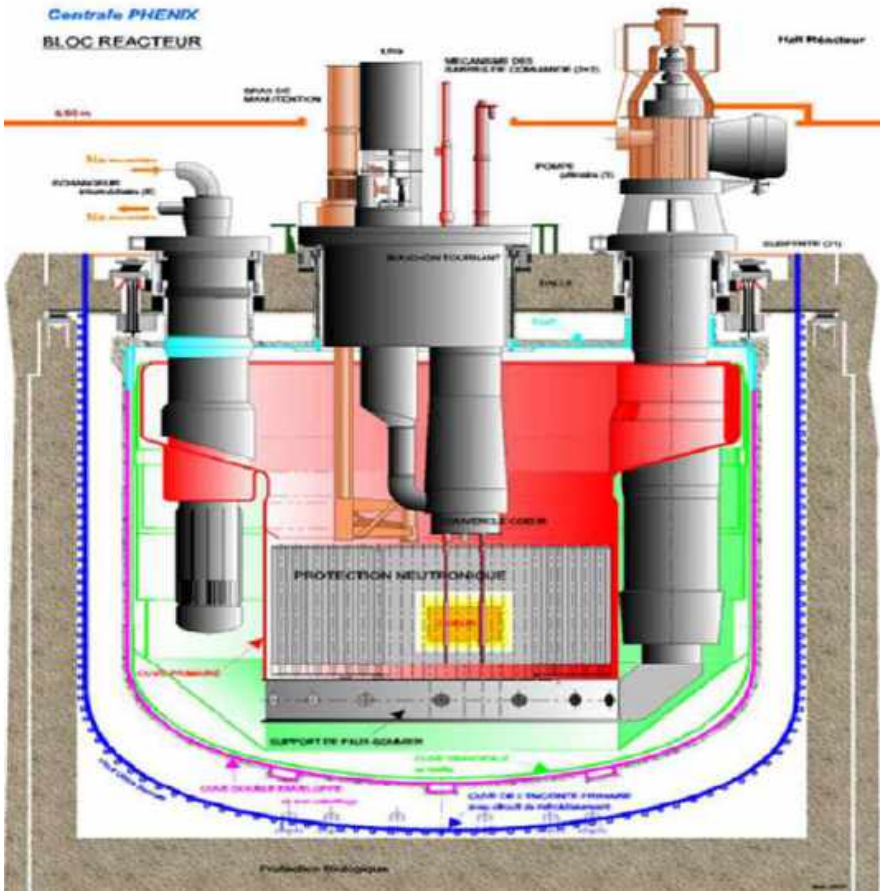

PHENIX: 3D Thermal-hydraulic model

- Sliced approach applied in all systems
- FA orifice setup on the basis of mass flow rates and overall DP
- K-loss coeff. in junct. evaluated or estimated on the basis of geometries
- Roughness is set 3.2 E-5m with the exception of the core region where is set 1 E-6

QUANTITY	Value
# of HYDR volumes	**6940**
# of HYDR junctions	**11840**
# of HEAT structures	**6888**
# of HEAT structures mesh points	**40170**

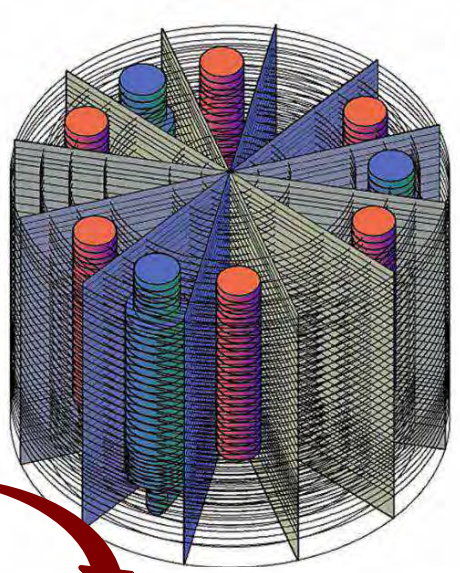

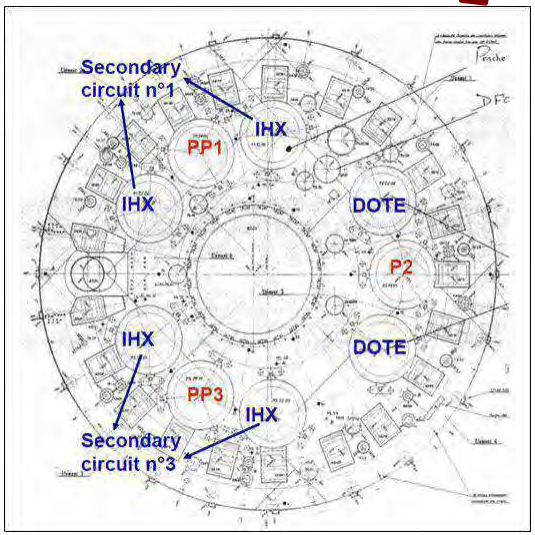

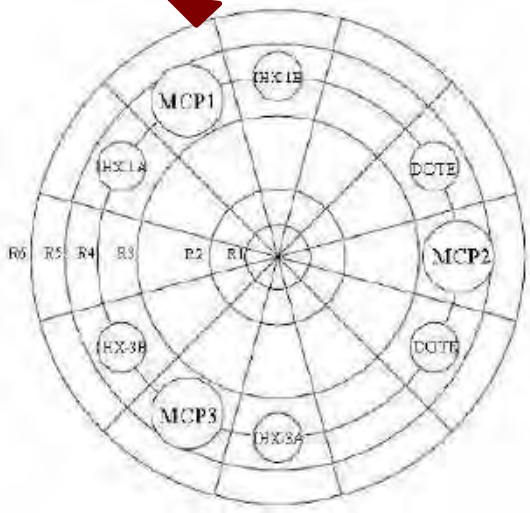

3D pool model

- Layout of MCP conduits and IHXs modeled according with the real configuration (θ, z)
- Porosity factors are used to model the geometry and the flow paths
- MULTID dimension 6x12x35
- MULTID models:
  - Diagrid
  - Core bypass
  - Hot pool
  - Cold pool

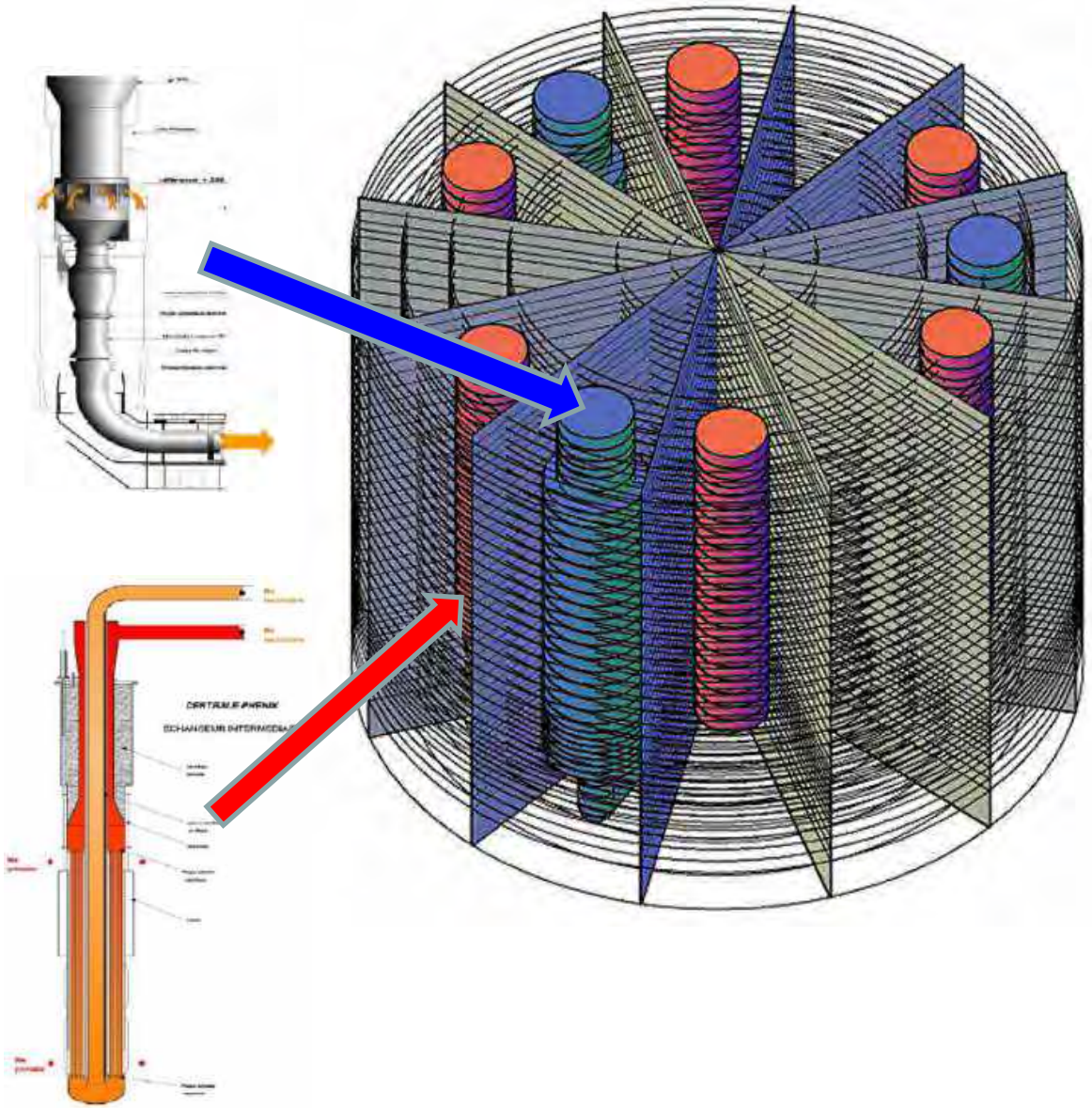

1D Nodalization description

VCS, STRONGBACK, COLD/HOT POOL LEVEL

- Vessel cooling system and strongback are modeled with one PIPE, connected upstream with the diagrid, on the top with the gas plenum (972), and downstream with the corresponding regions of cold pool.
- Annular region representing the coldpool level is modeled with one PIPE connected downstream with the corresponding regions of cold pool.
- Level of the hot pool is represented with BRANCH component connected downstream with the upper levels of hot pool

PUMPS

- Annular inlet is simulated with an ascending pipe connected with the cold pool.
- Pump is modeled with PUMP component setting up the homologous curve using PHENIX reference data.
- Discharge is modelled with a descending pipe which leads the primary coolant to the diagrid.

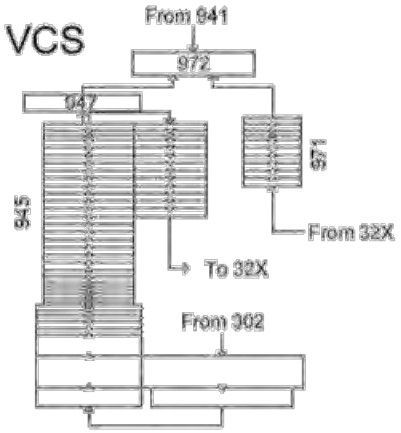

IHX

- primary sides are modeled separately with PIPE components connected upstream and downstream with the correspondent region of hot pool and cold pool.
- secondary sides are modeled separately with pipe components from an inlet and outlet collectors (dummy) and fed with imposed boundary conditions

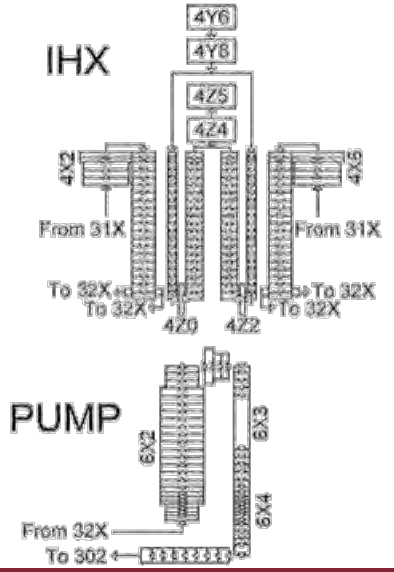

CORE

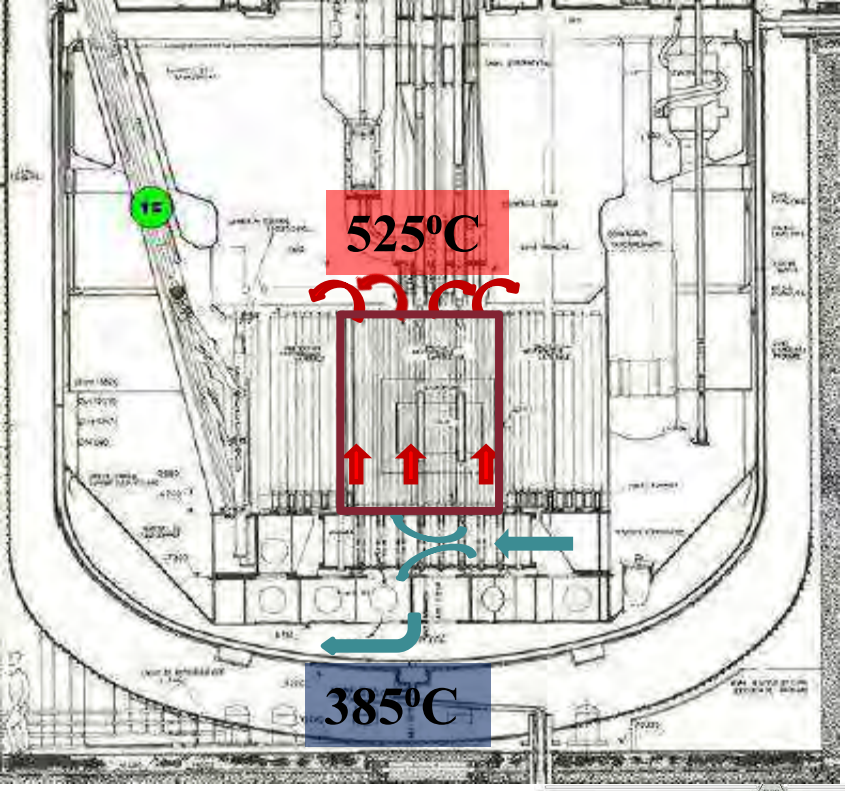

zone	Power [MWth]	Flow rate [kg/s]
Inner core	180.9	861
Outer core	143.1	779
Blanket zone	24.1	226
Control rods zone	0.7	14
Steel zone	1.2	62
Storage zone	1.7	46
Total	351.7	1988

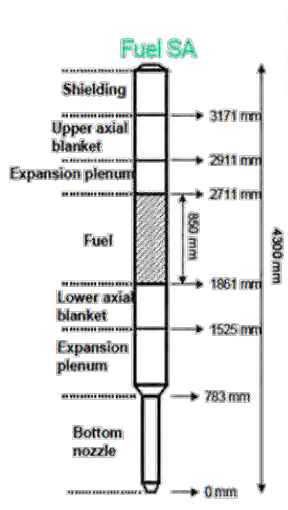

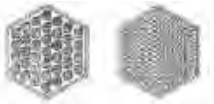

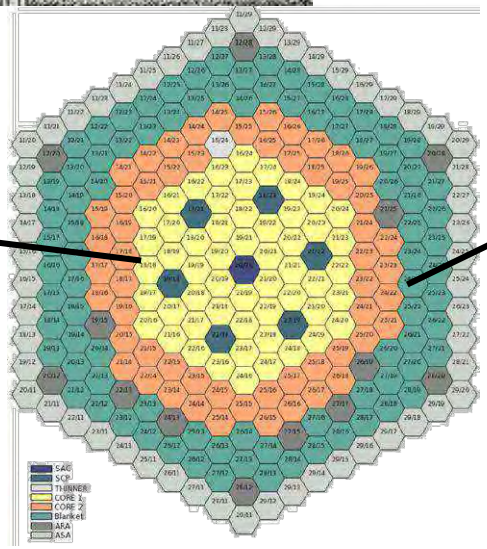

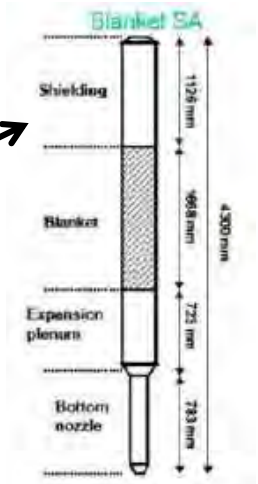

The Phénix core is composed by:

- **54 SA for the inner core zone**
- **56 SA for the outer core zone**
- **86 SA for the blanket zone**
- **6 Control Rods (CRs) SA**
- **1 Safety Rod (SR) SA**
- **212 steel reflector SA**
- **765 B_4C shielding SA**
- **297 steel shielding SA**

Asymmetrical test description

Time (s)
0
5
48
1800

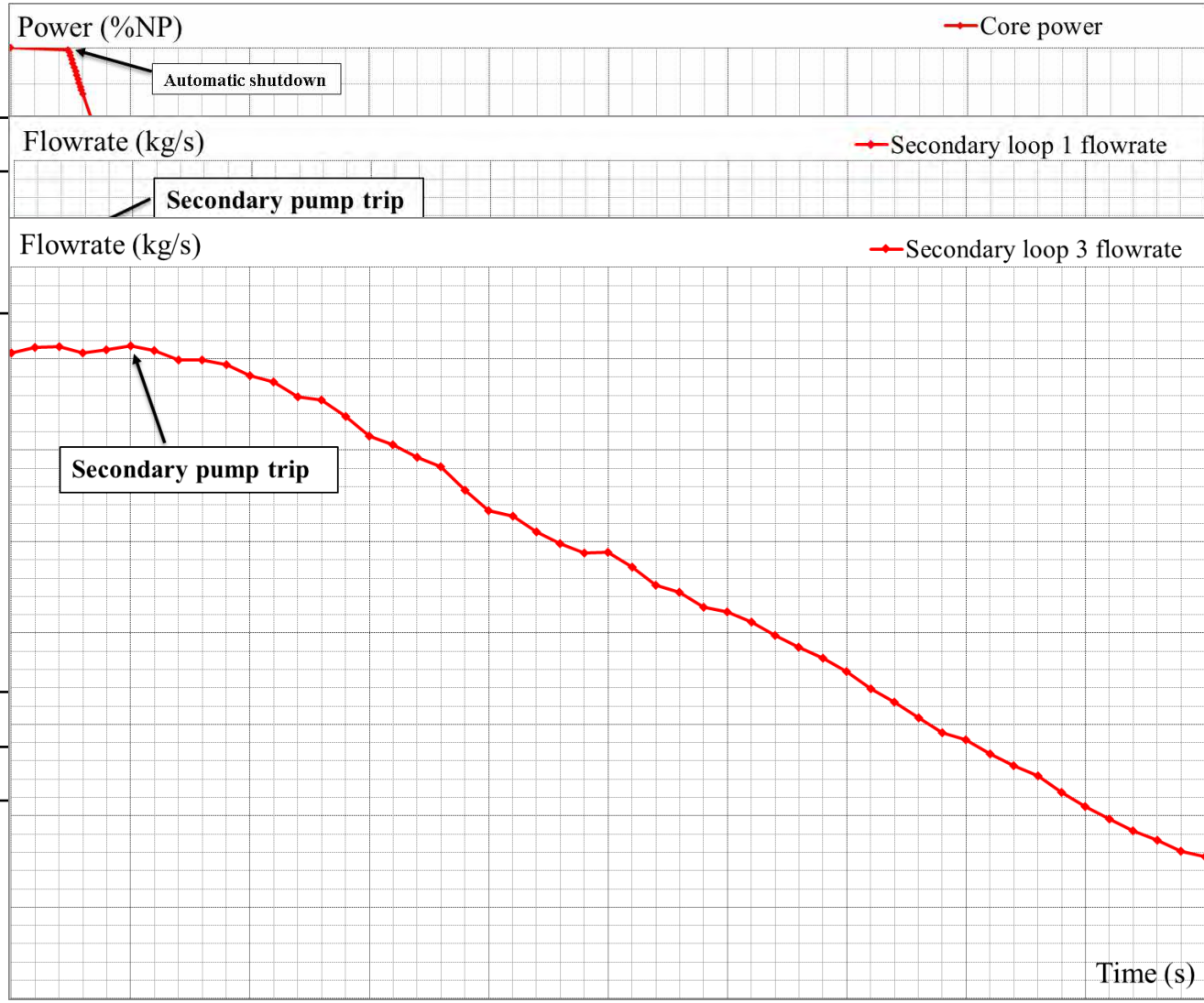

PHENIX: main results

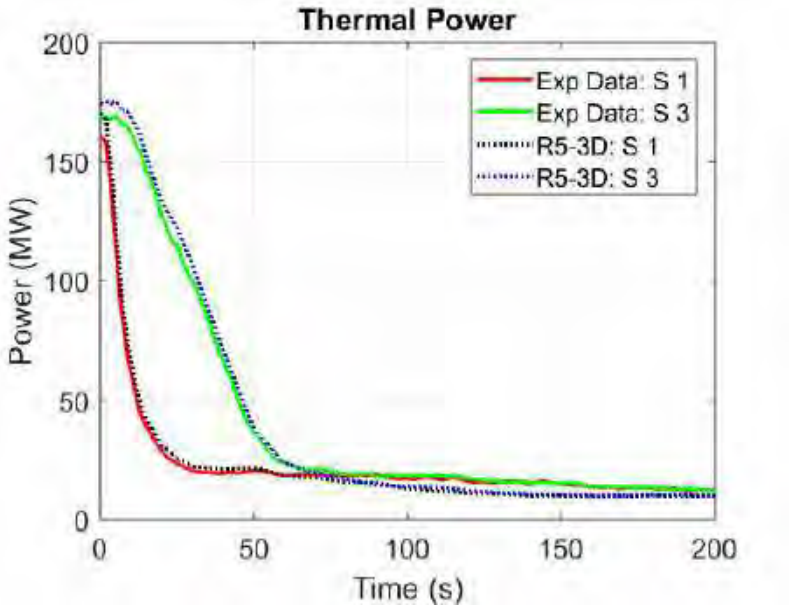

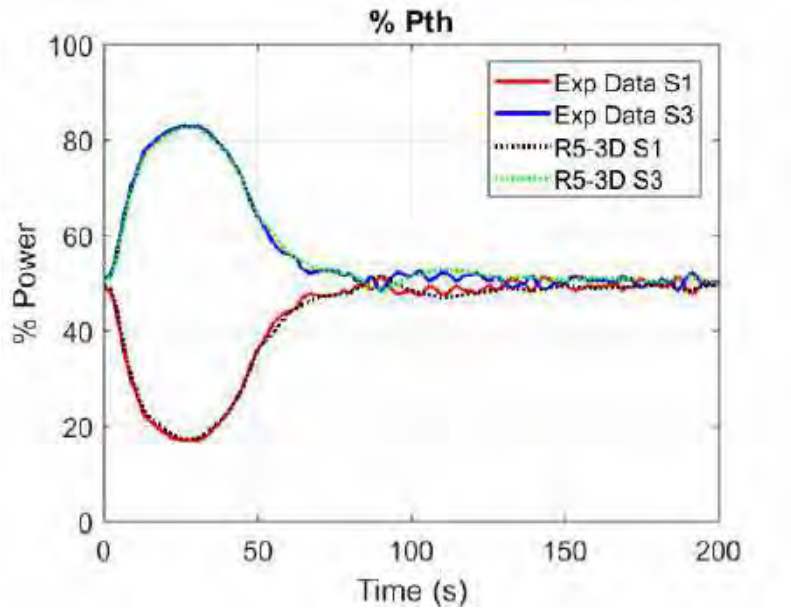

Main results:

- At the beginning of the test, the secondary mass flow rate of the LOOP 1 decreases, causing the fast reduction of the thermal power removed by the IHX-1A and the IHX-1B.
- Thermal power removed by the LOOP 1 (IHX-1A + IHX-1B) and the LOOP 3 (IHX-3A + IHX-3B) in the first 200 s of the transient shows the delay of the power reduction of the LOOP 3, due to the delay time of the LOOP 3 trip

PHENIX: main results

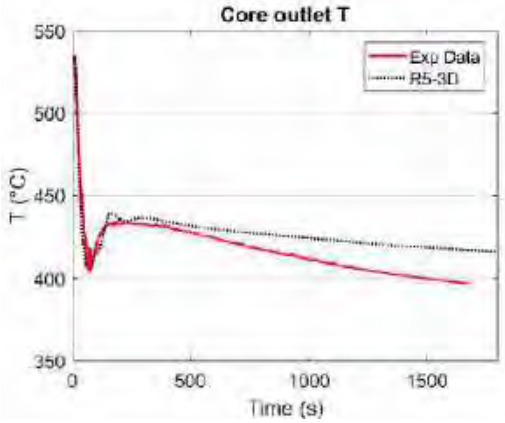

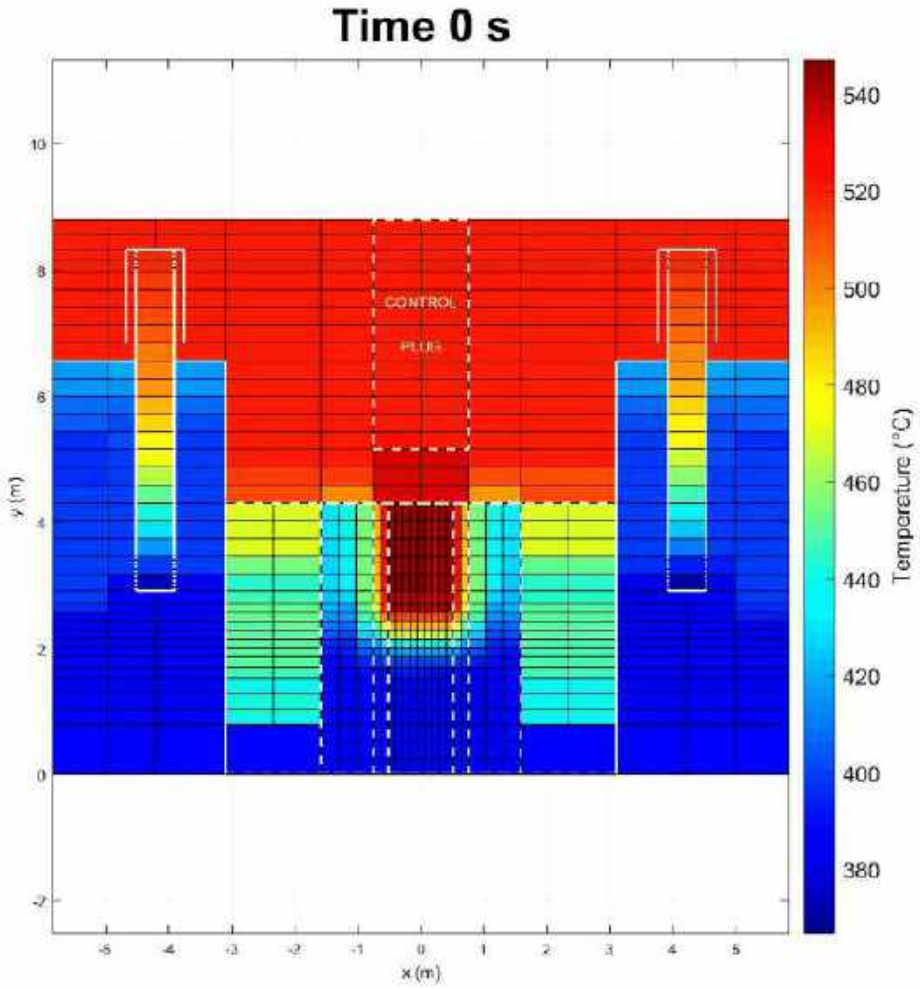

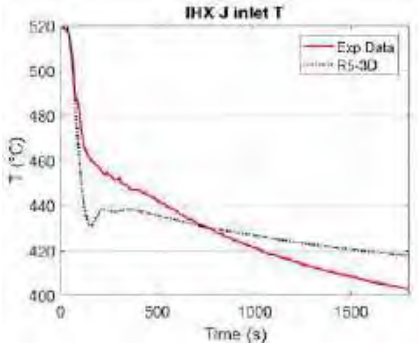

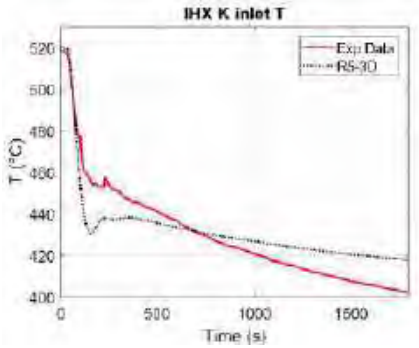

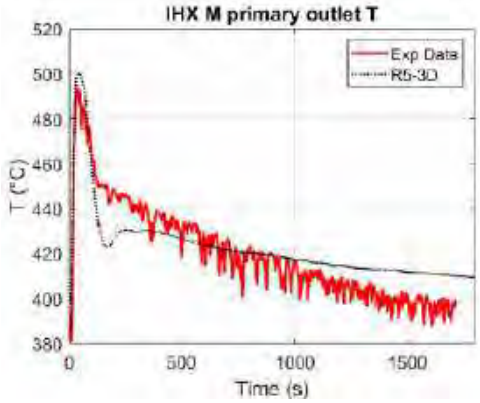

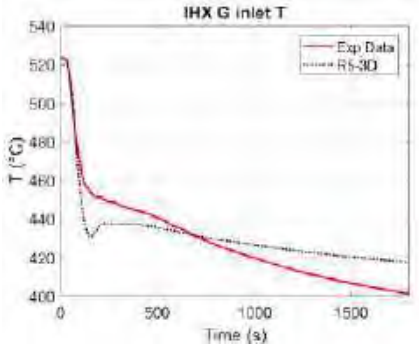

PHENIX: main results

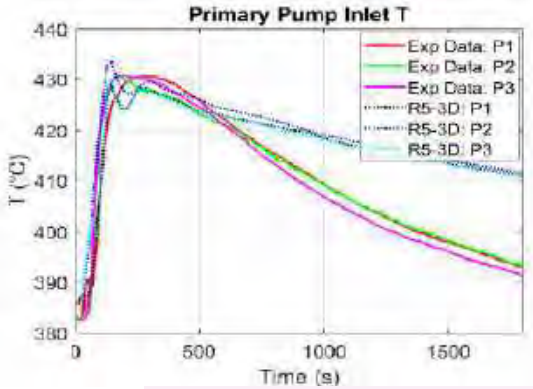

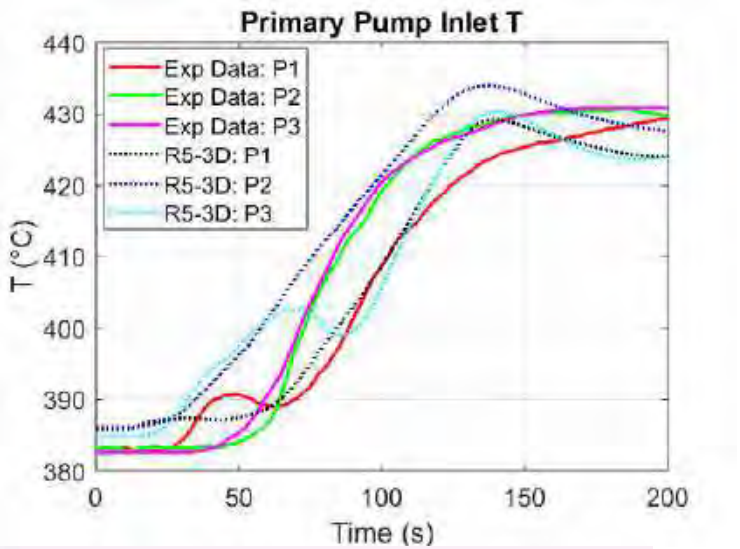

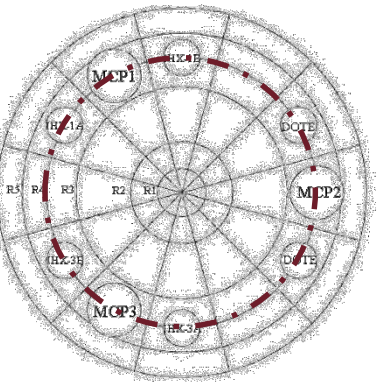

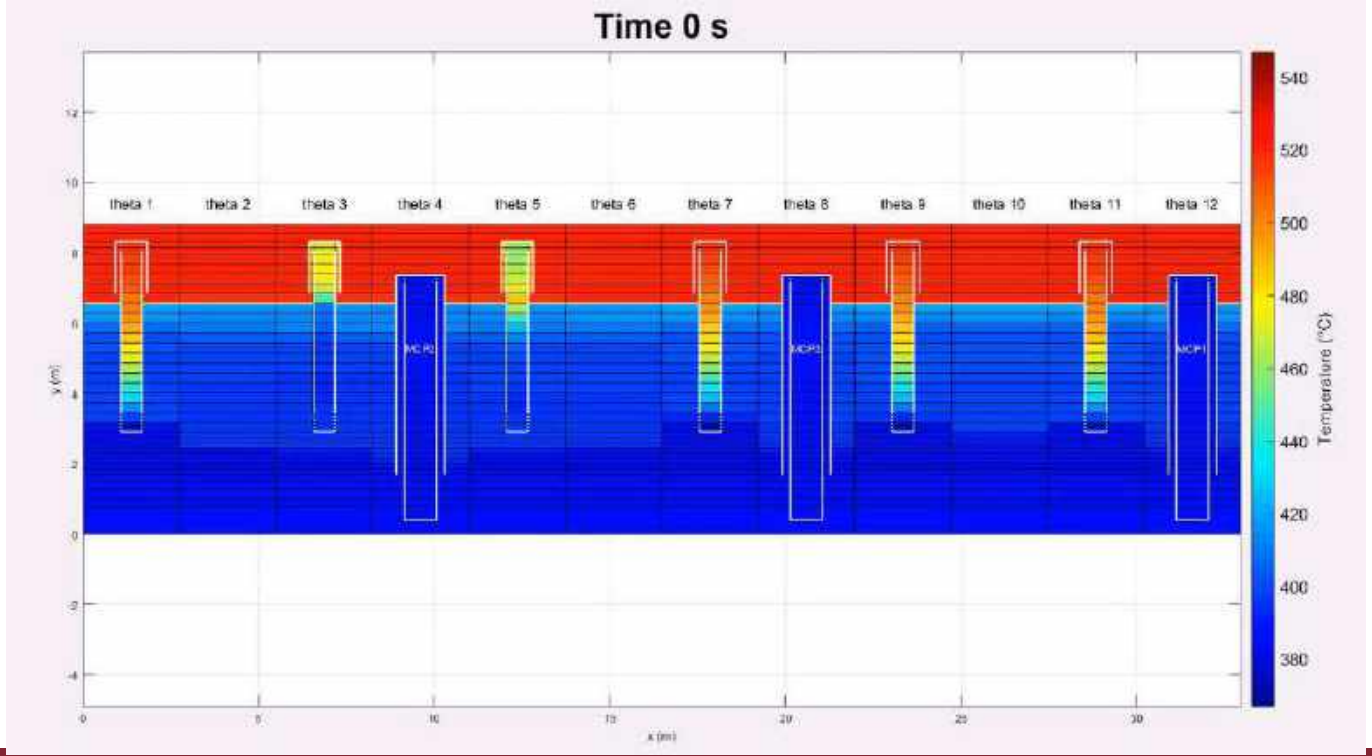

PHENIX TH-NK COUPLED MODEL

Model: Phénix Core Nodalization for PHISICS

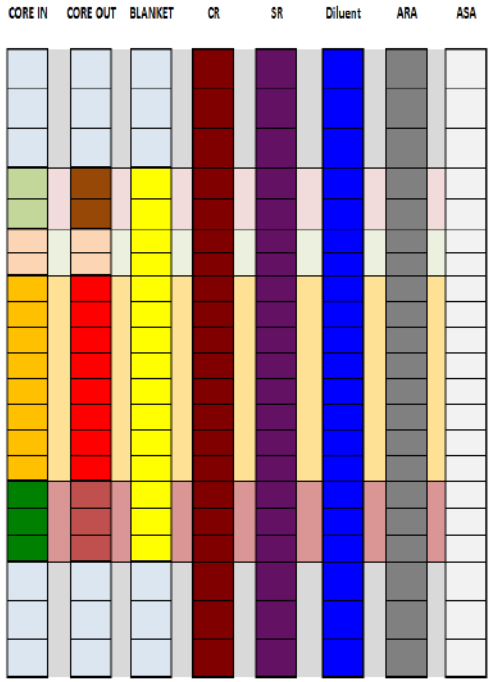

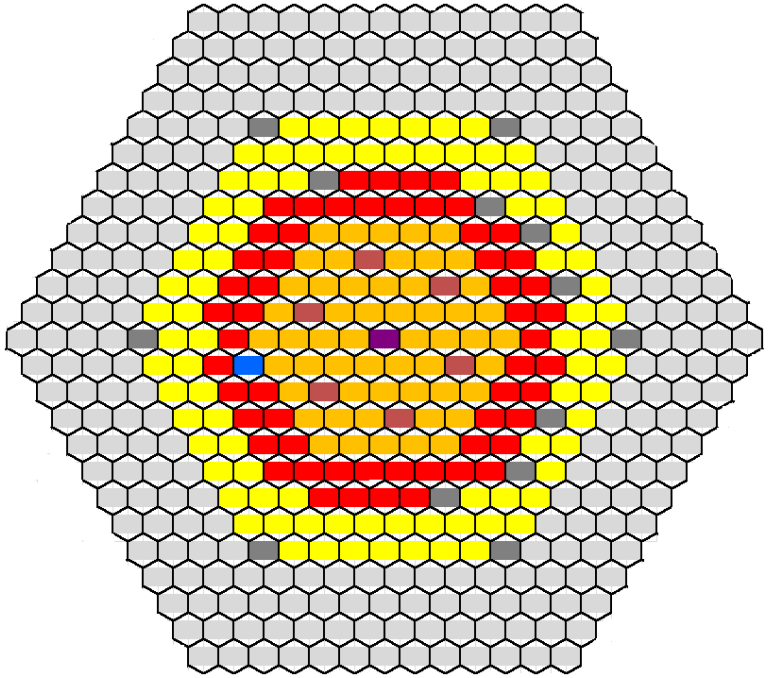

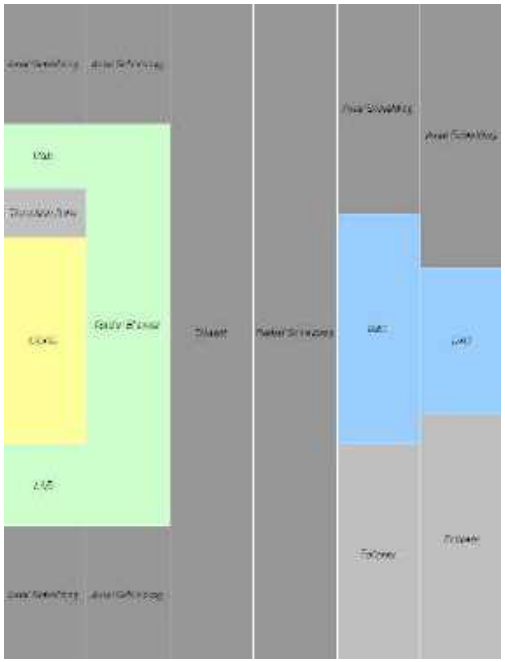

1	LAB 1	8	CR
2	LAB 2	9	SR
3	UAB 1	10	Plenum Na
4	UAB 2	11	ARA
5	Blanket	12	ASA
6	CORE 1	13	Axial shielding
7	CORE 2	14	Diluent

Number of kinetic meshes	21
Zone Figures	17
Composition Figures	6
Compositions	14
Numbero of rings	12
Number of kinetic nodes in a plane	469
Total number of kinetic nodes	9849
Neutron groups	33

RELAP5-3D/PHISICS Coupled Codes

- RELAP5-3D provides PHISICS with the **thermal-hydraulic parameters**
- They are used by PHISICS in order to interpolate the **macroscopic cross sections**
- PHISICS calculates **power distributions** that contribute to the change of the thermal-hydraulic parameters (RELAP5-3D feedback on power)

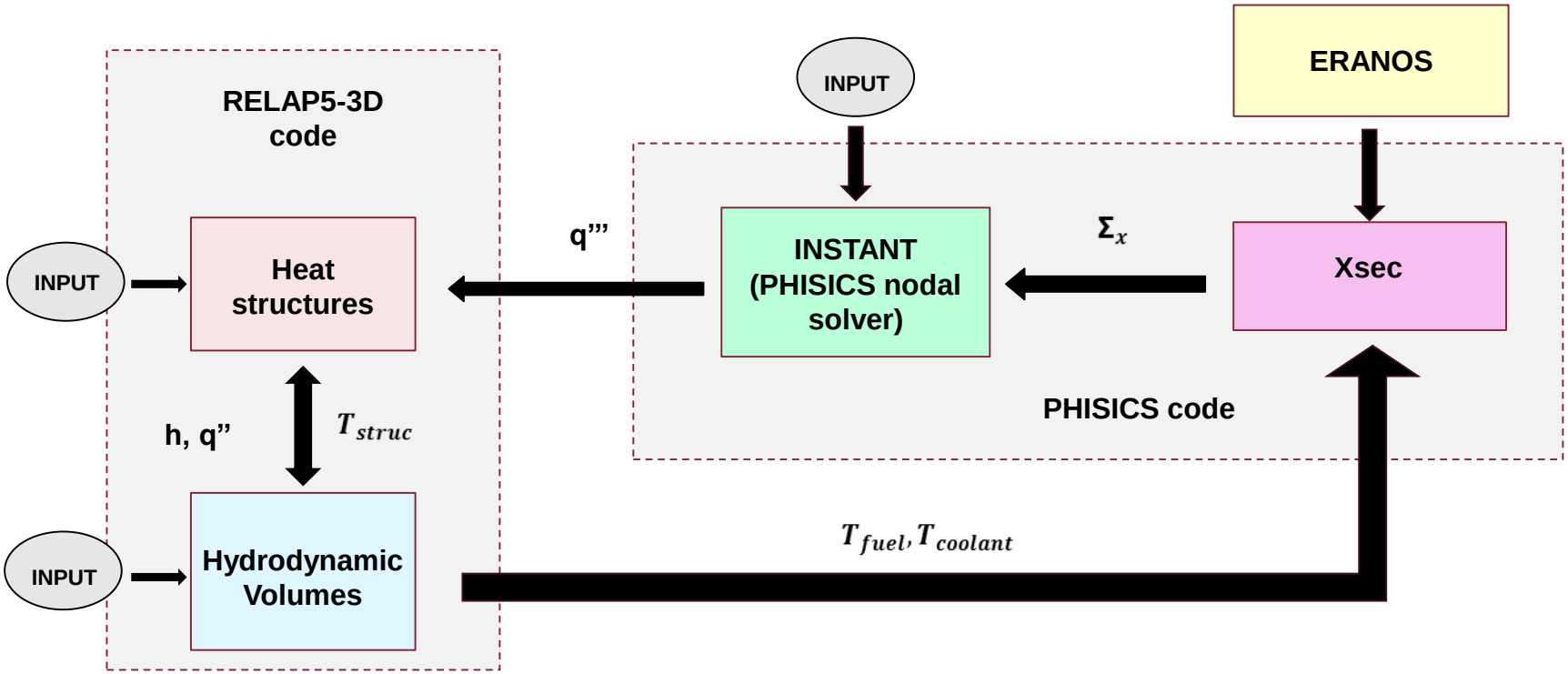

Results: Control Rod Calibration Curve

Control rod positions (mm)	Keff	ρ (pcm)	Efficiency (pcm)
900	1.02568	2504	7352
800	1.02245	2196	7044
700	1.01686	1658	6506
600	1.00831	824	5673
500	0.99752	-248	4599
400	0.98537	-1485	3364
300	0.97349	-2723	2125
200	0.96365	-3772	1077
100	0.95708	-4485	364
0	0.95376	-4848	0.00

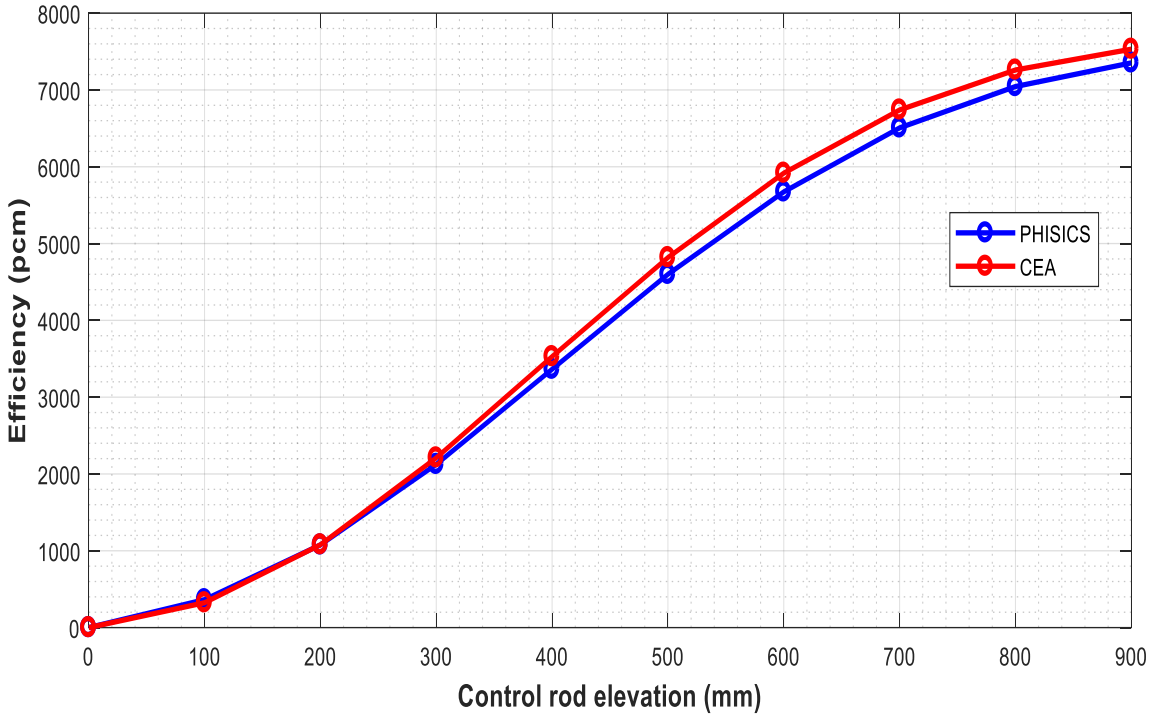

- The control rod worth calculated by CEA is 7531 pcm.
- The control rod worth calculated by PHISICS is 7352 pcm (about -2.4 % of difference if compared with CEA).

Control rod shift test: Tested Configurations

Three configurations have been studied during the test. CR n° 1 and CR n° 4 were progressively offset in relation to each other, while maintaining constant the total power.

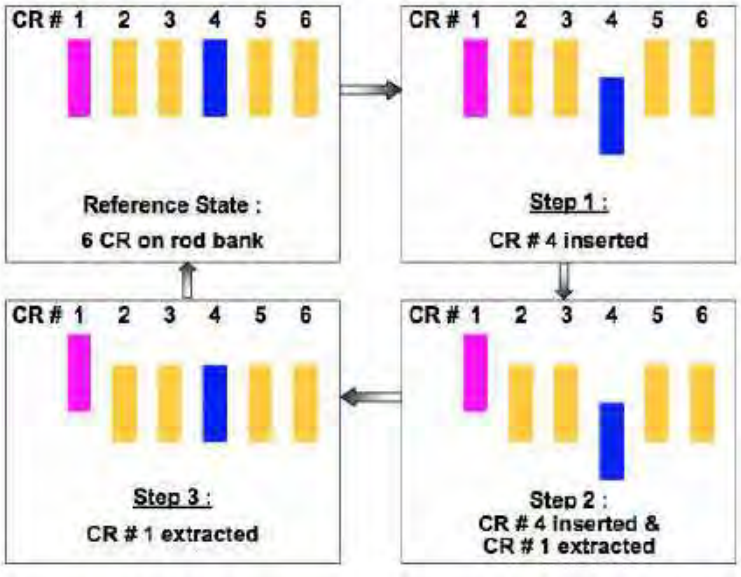

	Control rod position (mm)						Power (MW)
	19/18	22/17	23/19	21/22	17/21	18/23	
	CR n° 1	CR n° 2	CR n° 3	CR n° 4	CR n° 5	CR n° 6	
Reference State	558.3	557.4	558	557.4	557.4	557.6	335.4
Step 1	608.5	608.6	606.6	340.8	608.5	607.8	337
Step 2	848.4	567.7	571	340.6	566.3	573.5	338.7
Step 3	848.4	523.6	523.4	523.4	523.5	523.5	336.3
Final State	559.6	558.7	558.7	559.4	559.5	559.4	335.2

- Control rod positions take into account core/vessel/control rod differential dilatations
- The origin of Z-axis is 5 mm below the fissile core

Results: Power distributions in RS (1/2)

Approximations:

- Approximation of using an average core description (an average Burnup has been

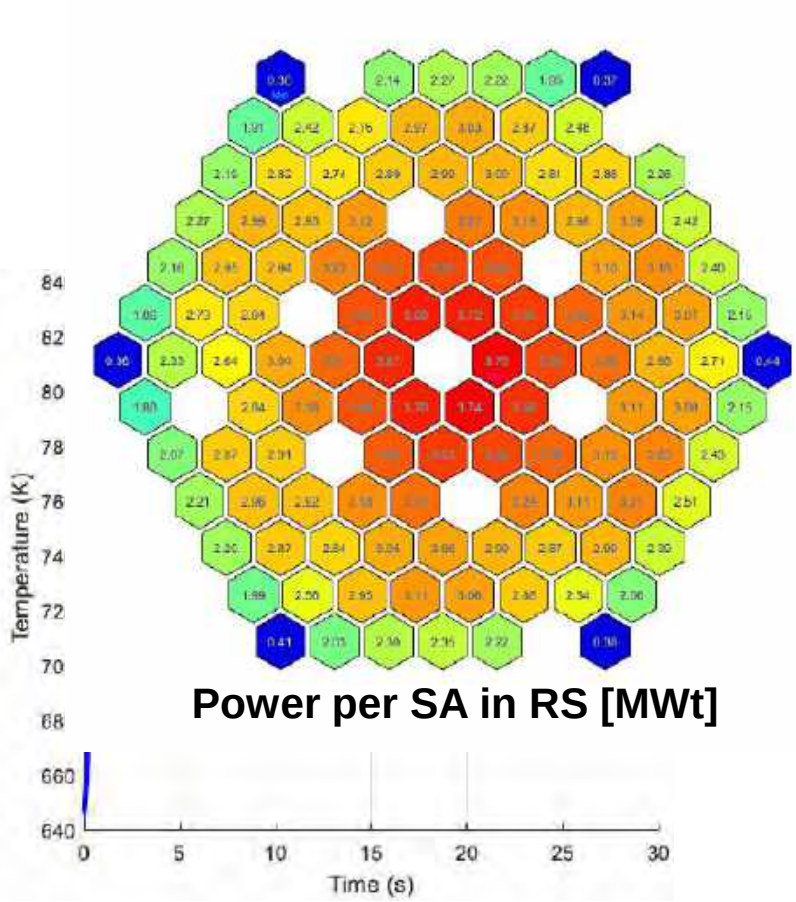

Power per SA in RS [MWt]

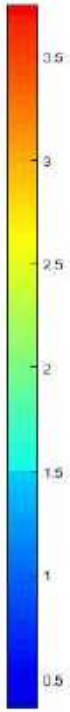

sile SAs

outlet (

	Experime
ate	335.4

	Experi
core	16
core	14
ket	3
	30

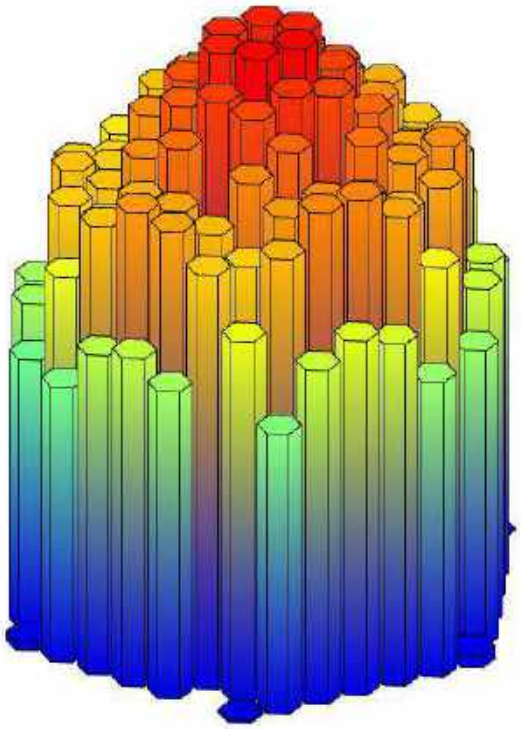

SICS

Results: Power distributions in RS (2/2)

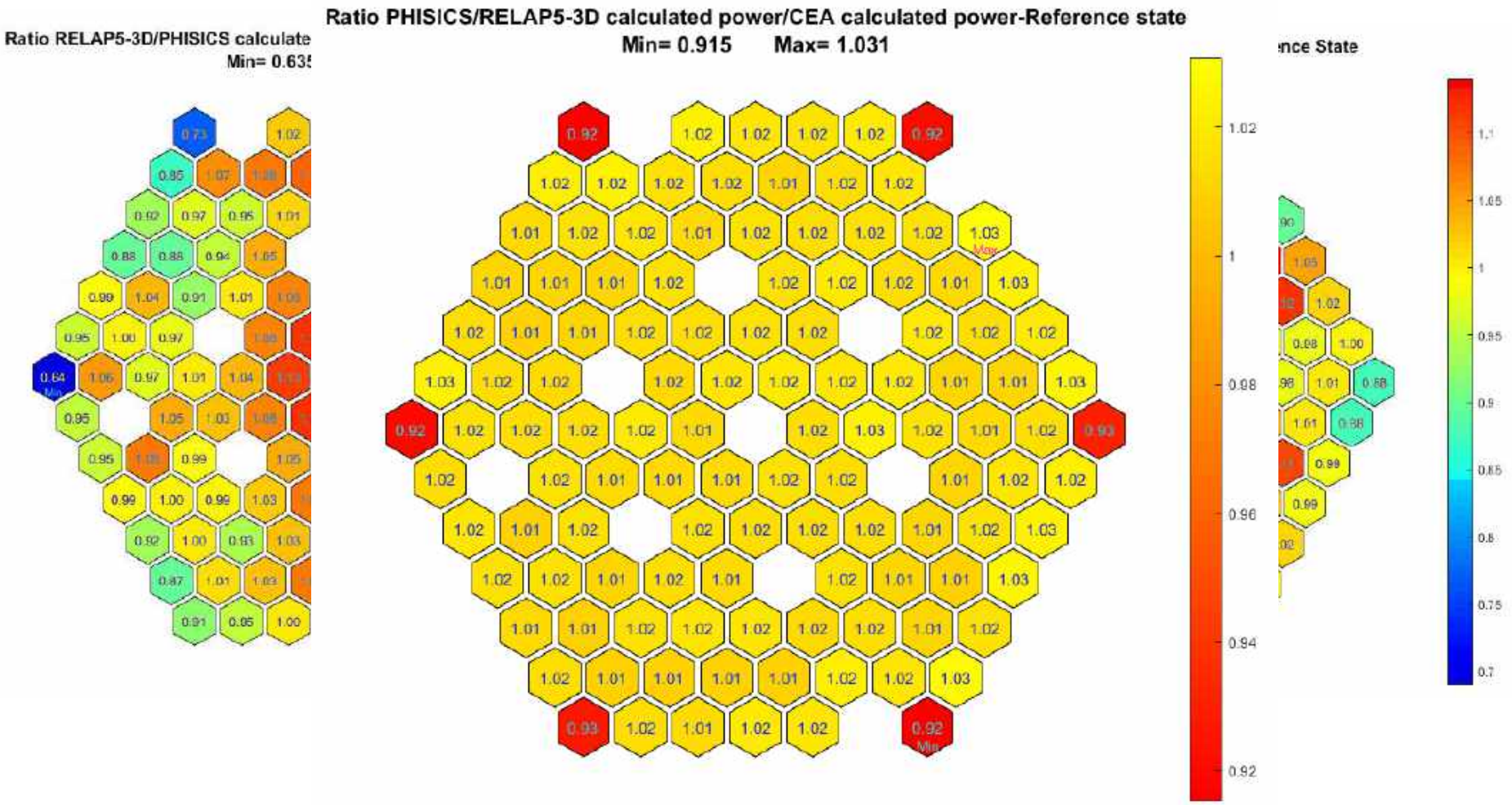

Results: Power deviations [%] - Step 1

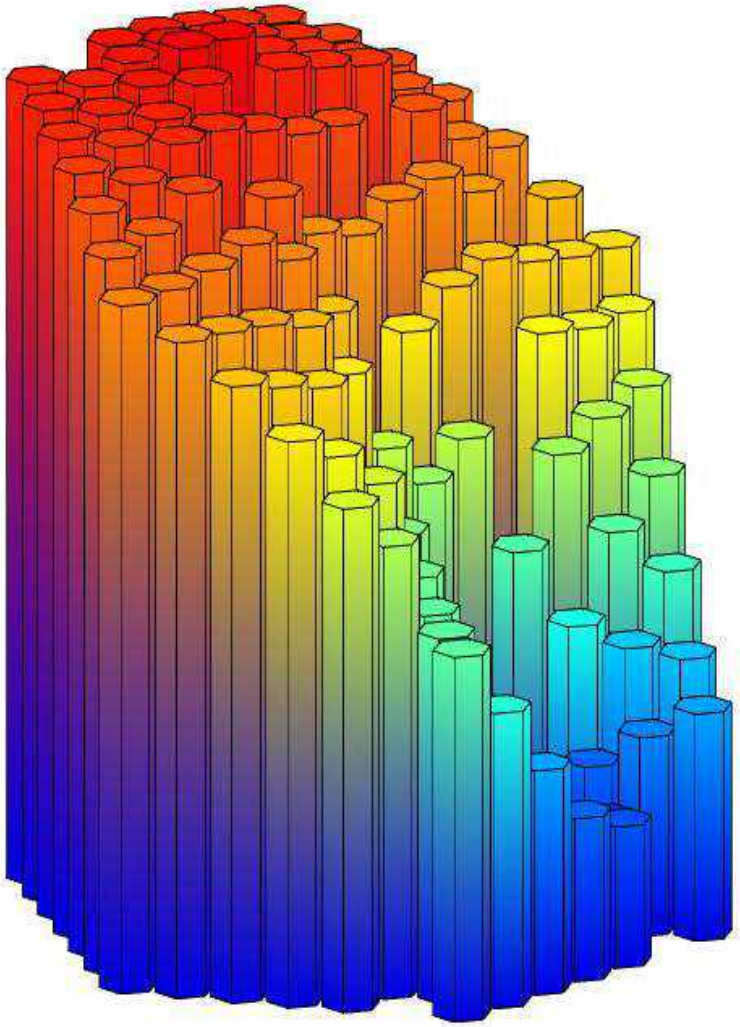

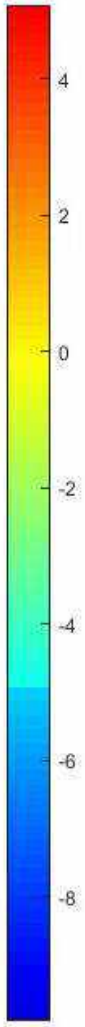

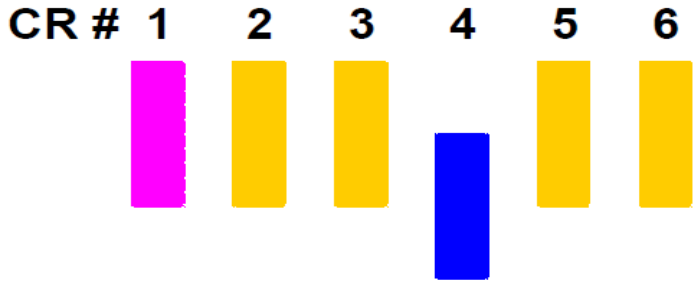

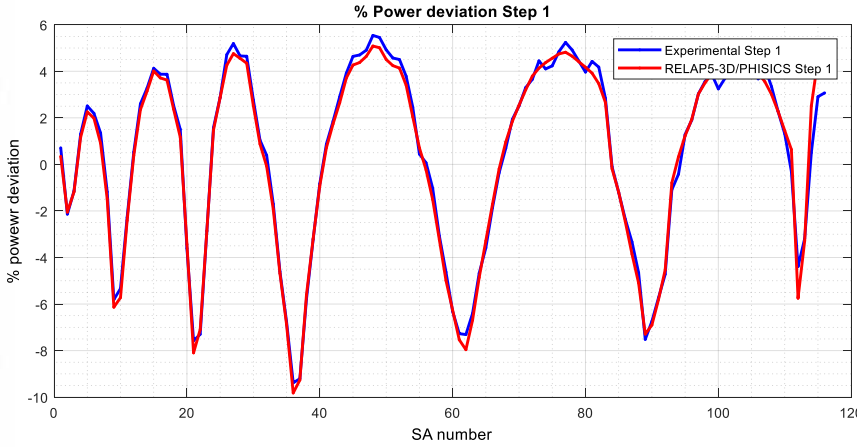

Results: Power deviations [%] - Step 2

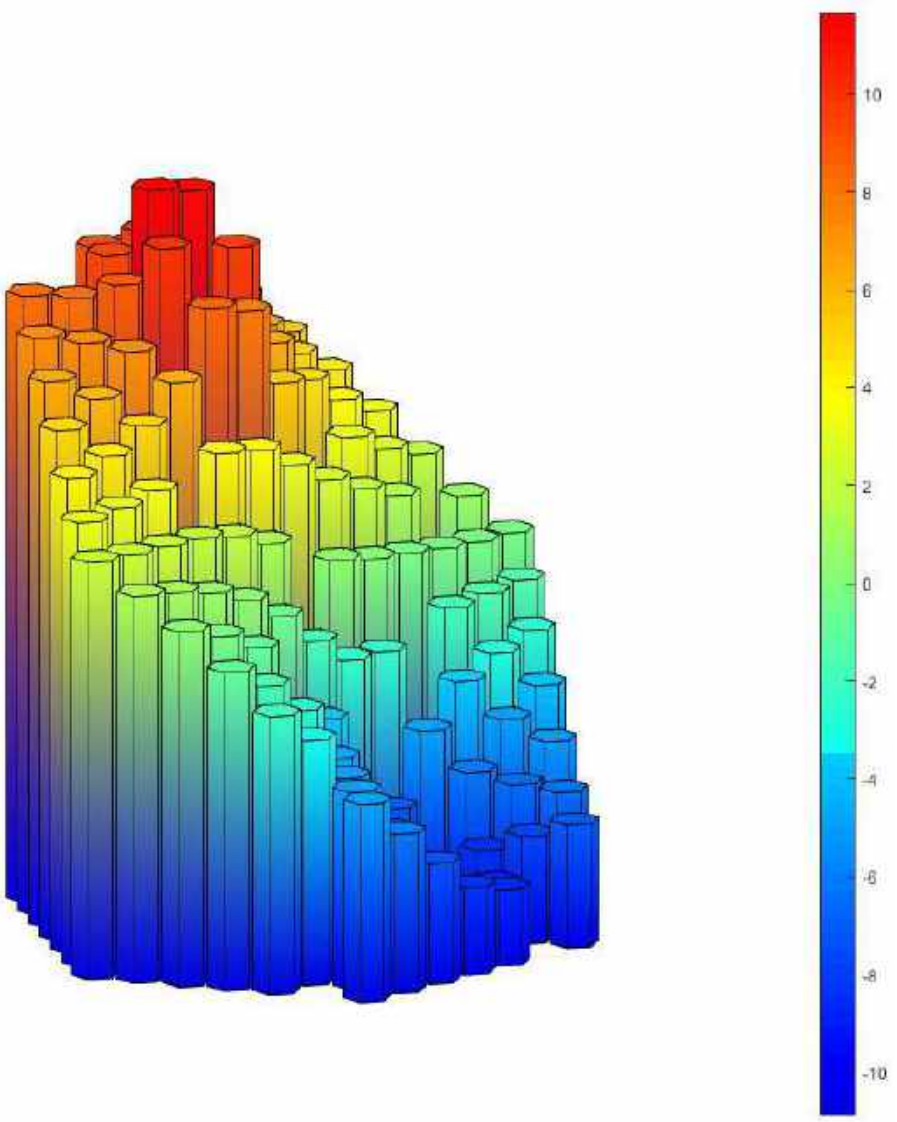

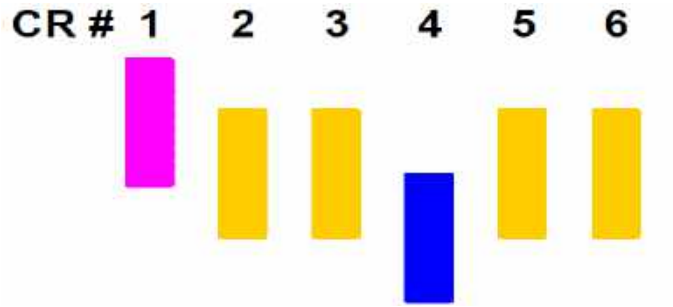

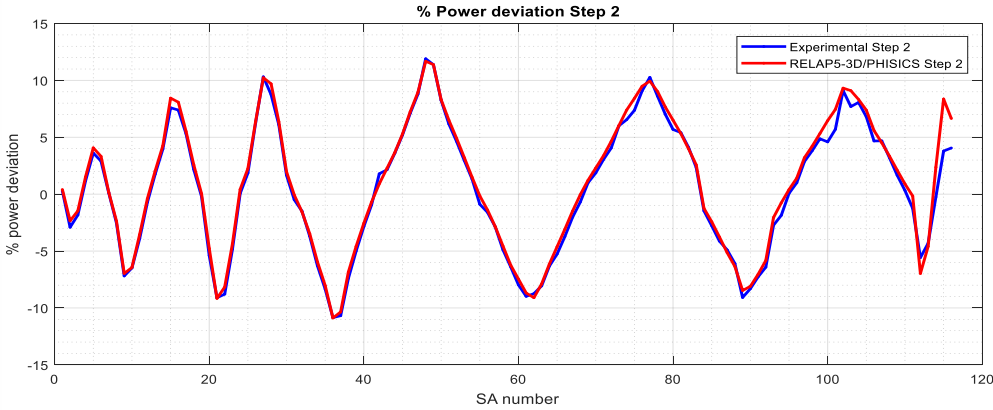

Results: Power deviations [%] - Step 3

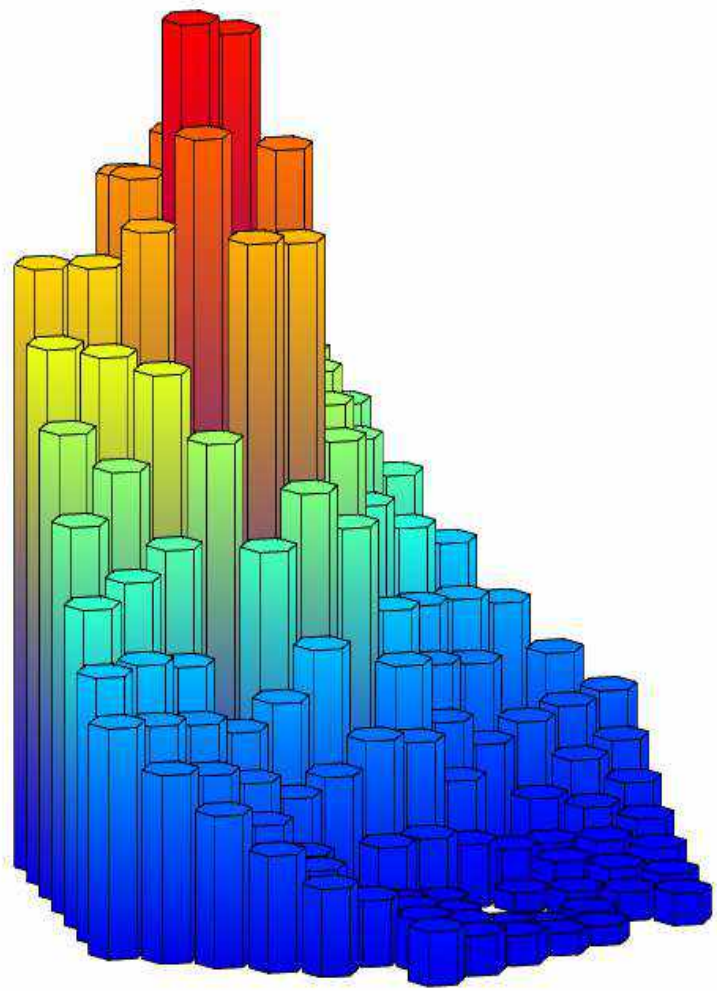

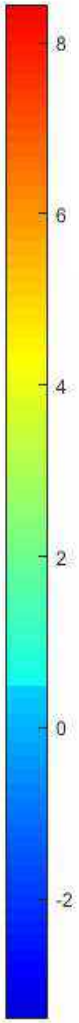

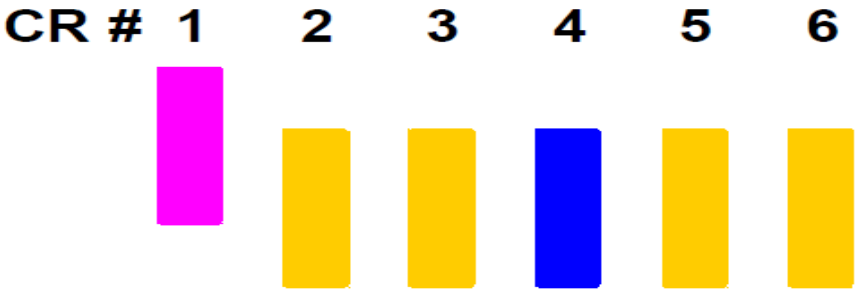

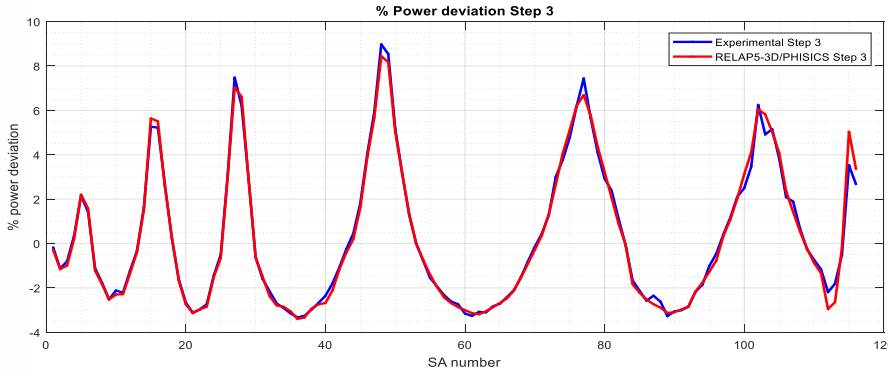

Conclusive remarks and follow up

- Nodalization of PHENIX by REALP5-3D© and PHISICS
  - Highly Detailed nodalization suitable for 3D NK coupling
  - PHISICS 3D NK model

- Following activities are in completed and documented in the PAR deliverable
  1. Blind calculation of the dissymmetrical configuration test
  2. Comparison of the blind results with the experimental data
  3. Post-test calculation and sensitivity study (in progress)
  4. Preliminary TH-NK results (next months)

GENERATION IV
Lead cooled Fast Reactor
Stato attuale della tecnologia e prospettive di sviluppo

Roma, 14-15 Giugno 2018

SAPIENZA
UNIVERSITÀ DI ROMA

CIRCE-HERO Transient Simulation by 3D STH code

V. Narcisi, F. Giannetti, G. Caruso

OUTLINE

- GOAL OF THE ACTIVITY

  In synergy with **Horizon 2020 SESAME project**, the activity aims to perform pre-test simulations to provide the preliminary test-matrix for the realization of the validation benchmarck

- OVERVIEW
  - CIRCE-HERO Test Section
  - CIRCE-HERO: Thermal-Hydraulic model
  - Model Validation
  - Pre-Test Analysis
  - Conclusions

CIRCE-HERO Test Section

CIRColazione Eutettico – Heavy liquid mEtal-pRessurized water cOoled tube

- LBE Pool type facility

Primary circuit flow path

- **Feeding conduit**: It corresponds to the heat source
- **Fuel Pin Simulator**: 37 pins placed in a hexagonal lattice (7 rods/side)
  - Nominal unheated length: 1000 mm
  - Active length: 1000 mm
  - Each pin has an outer diameter of 8.2 mm
- **Riser**: It is an insulated pipe connecting the FPS with the separator. A nozzle is installed in the lower section to allow the argon injection inside this pipe
- **Separator**: It allows the separation of the LBE, flowing downward into the SGBT, and the argon, flowing upward in the gas plenum. It works as an expansion ves
- **SGBT**: Lower cold part of the test section, consists of 7 double wall bayonet tubes
- **Pool**: this the volume between the test s main vessel
  - Main vessel:
    - Outside diameter: 1200 mm
    - Height: 3600 mm
    - LBE inventory: 70 ton
  - Separate tanks: the active
    - Two auxiliary tanks:
      - Storage tank
      - LBE transfer tank

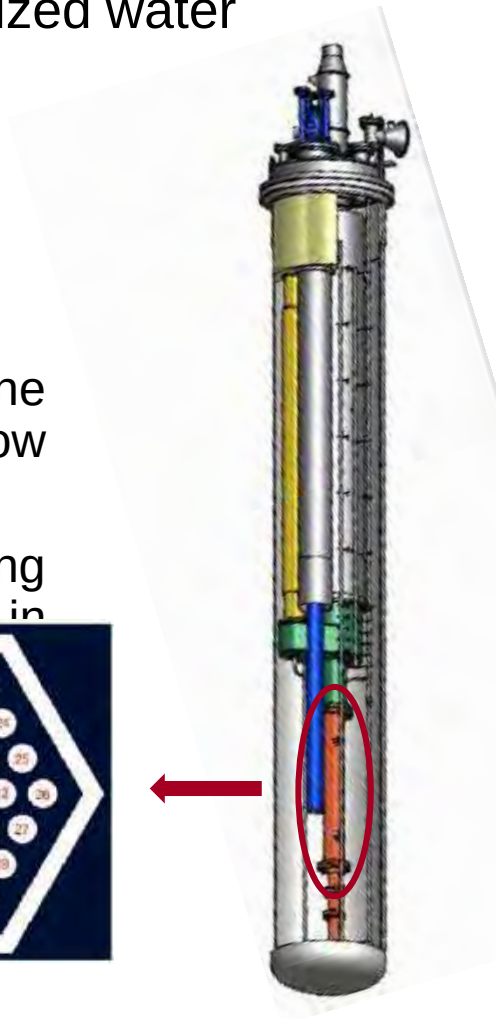

CIRCE-HERO Test Section

CIRColazione Eutettico – Heavy liquid mEtal-pRessurized water cOoled tube

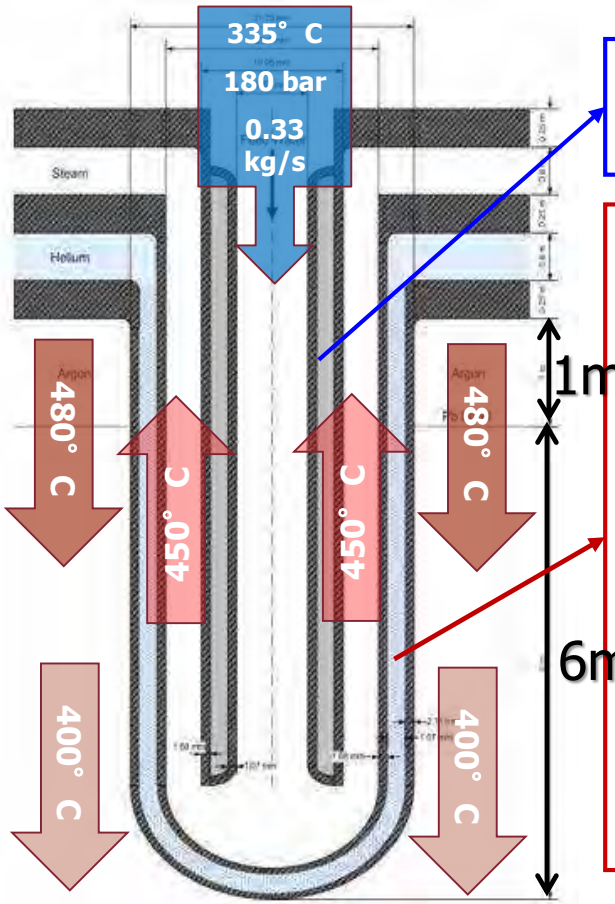

- **Insulator layer** in order to **prevent** the **steam condensation**
- To investigate a bundle of

Gap pressurized with **Helium and filled** by **high thermal conductivity powder** to

1. Avoid **lead-water interaction** in case of tube rupture (double physical separation).
2. **Detect tube leakages** thanks to monitoring the He pressure
3. **Enhance the heat exchange** capability thanks to the powder medium.

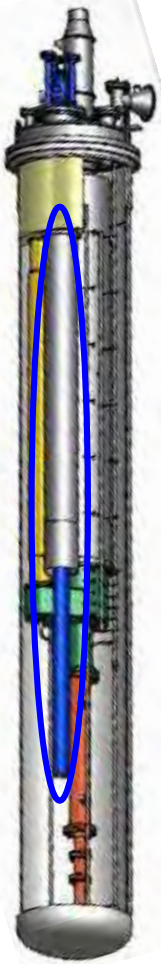

CIRCE-HERO: Thermal-Hydraulic Model

The validated thermal-hydraulic model of **CIRCE-ICE**, developed using **RELAP5-3D©** **ver. 4.3.4**, has been upgraded to reproduce the **HERO test section**

- **Region #1**: The full **CIRCE-HERO** model consists of:
  - **Primary main flow path**: it is composed of the feeding conduit, FPS, fitting volume, riser, separator and the LBE side of the SGBT. At the bottom of the riser the Ar injection system is included
  - **SGBT** secondary side
  - **2942** hydrodynamic volumes
  - **7565** junctions
  - **21153** heat transfer nodes
- **Region #2**: **CIRCE pool**. It consists of a **3D component** which reproduces the volume between the internals and the main vessel.

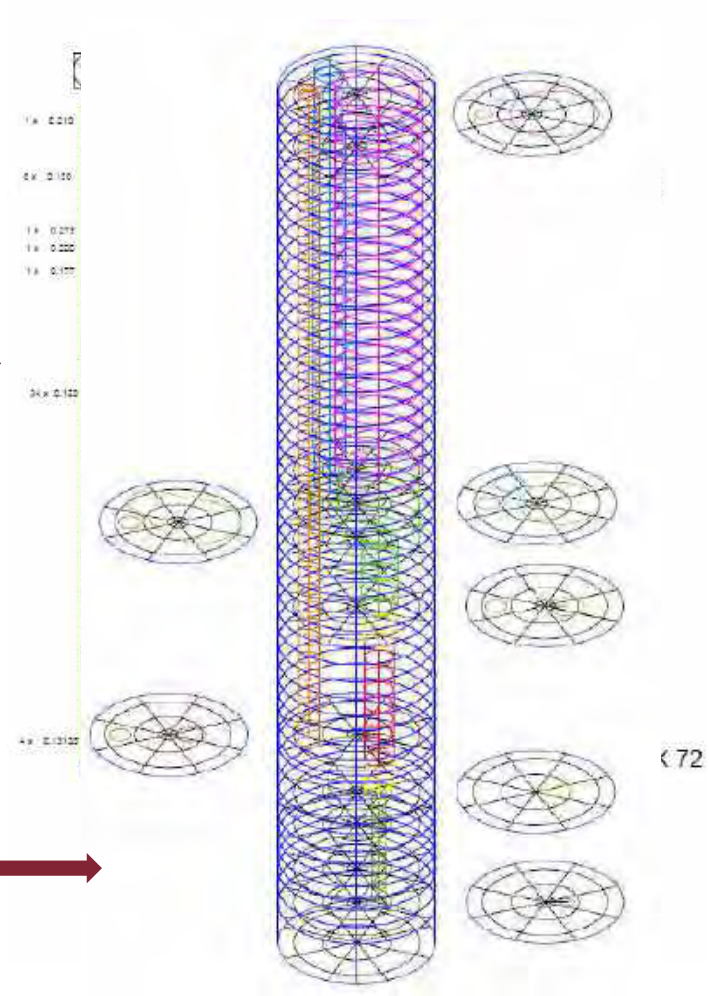

CIRCE-HERO: Thermal-Hydraulic Model

- **LBE side**: a single equivalent tube composed of 43 volumes; 3 junctions connect the component to the separator, the upper plenum and the pool
- **Steam/water side**: 2 pipes for a total of 96 volumes
- 4 **heat structures** model thermal behavior of the unit:
  - HS 3201: 48 axial structures and 20 radial meshes (AISI 316 + insulator gap)
  - HS 3301: 41 axial structures and 31 radial meshes (AISI 316 + helium and high conductivity powder)
  - HS 4001 and 4501: 39 axial structure and 24 radial meshes
- **Calibrated factor** as the ratio between **Ushakov** and **Todreas&Kazimi** HTC correlation, in the range of the SG temperatures and assuming the predicted flow conditions: 1,02

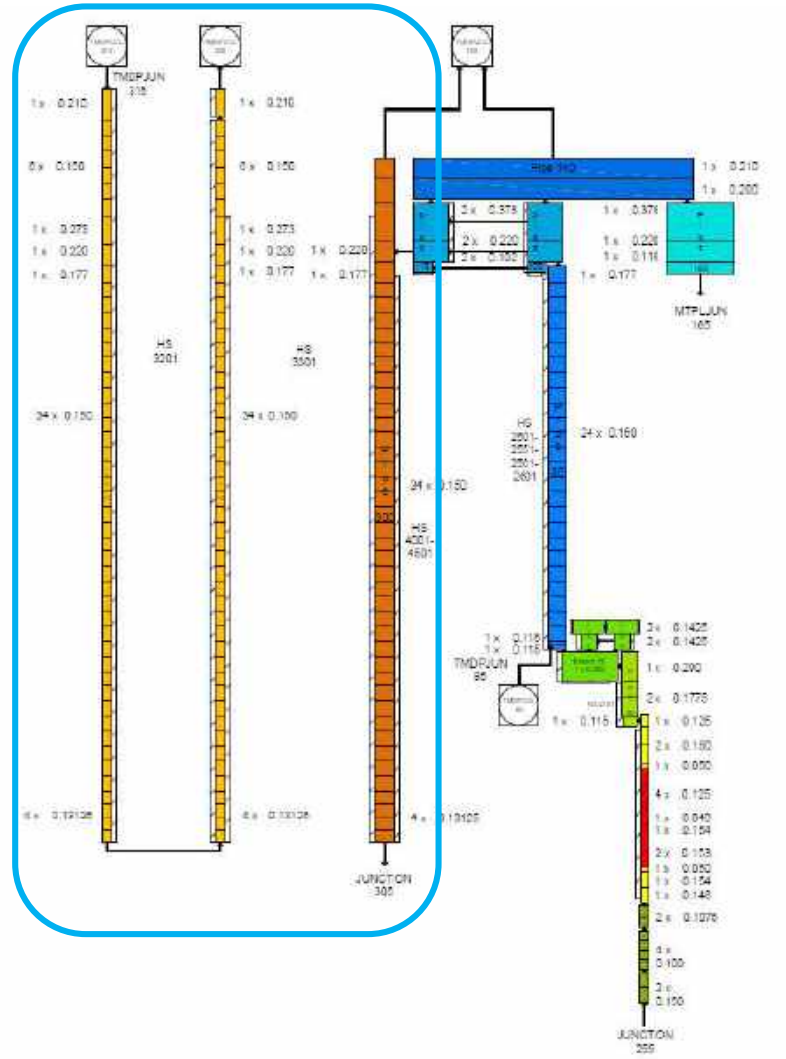

CIRCE-HERO: Thermal-Hydraulic Model

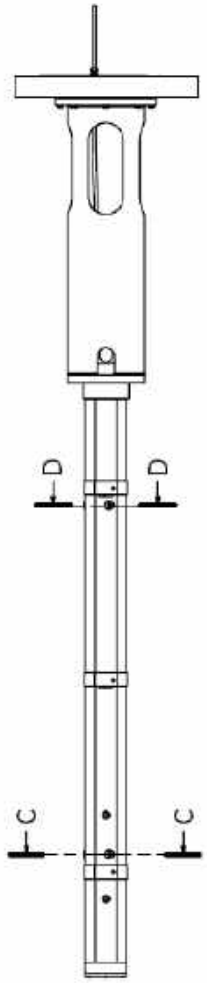

The **FPS** is analyzed sub-channel by sub-channel: the model consists of **72 parallel pipes** (15 control volumes for each one), which simulates the sub-channels, **5760 heat structure active nodes** reproducing the thermal power supplied by the 37 pins, **1728 heat structure nodes** to models the heat dispersion through the hexagonal wrapper, **3456 heat nodes**, assuming a "fake" material with a negligible heat capacity and the LBE thermal conductivity, added to simulate the thermal conduction into the fluid and **1536 cross junctions**.

The unit is equipped with several TCs to measured the LBE temperature across the HS. The model is obtained to compare the temperature in the **exact position of the TCs**. The grids are simulated with pressure loss coefficients, dependent on the flow conditions and evaluated with **Rheme correlation**.

A calibrated multiplication factor is evaluated as the ratio between **Ushakov (*p/d=1.8)*** and **Todreas&Kazimi (*p/d=1.4)*** equal to 1,31 in order to better reproduce the HTC

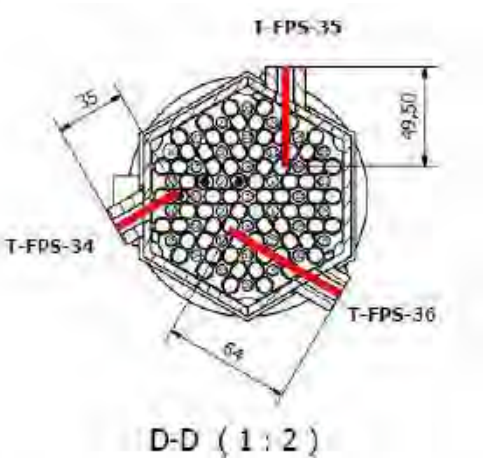

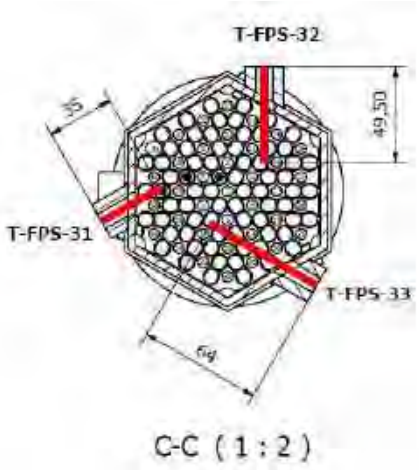

Model validation

➢ CIRCE-ICE Test Facility:

- **Primary flow path**: **ICE** test section is the same of **HERO** campaign except for the presence of the **DHR system,** included inside the pool, and the **HX** that substitutes for the **SGBT**
- **HX**: water-cooled system
- **DHR**: air-cooled system

➢ Experimental campaign:

- To investigate **mixing convection** and **thermal stratification** phenomena in a pool type reactor
- To provide suitable experimental data to support the validation process of TH-SYS codes and CFD codes

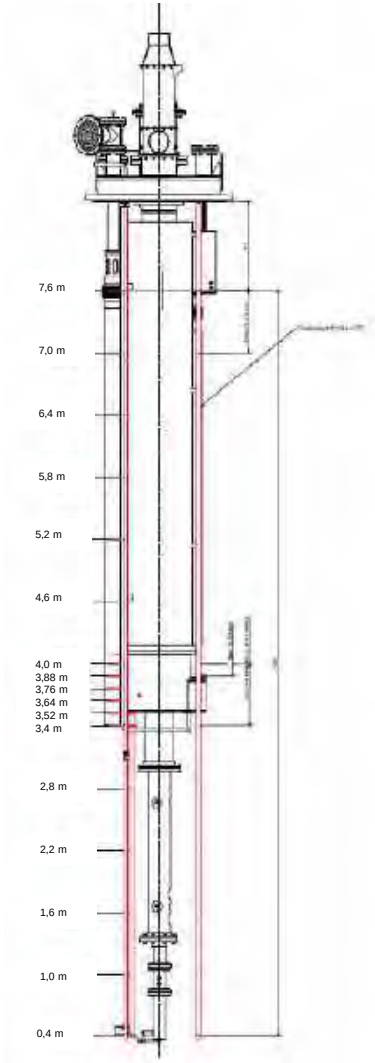

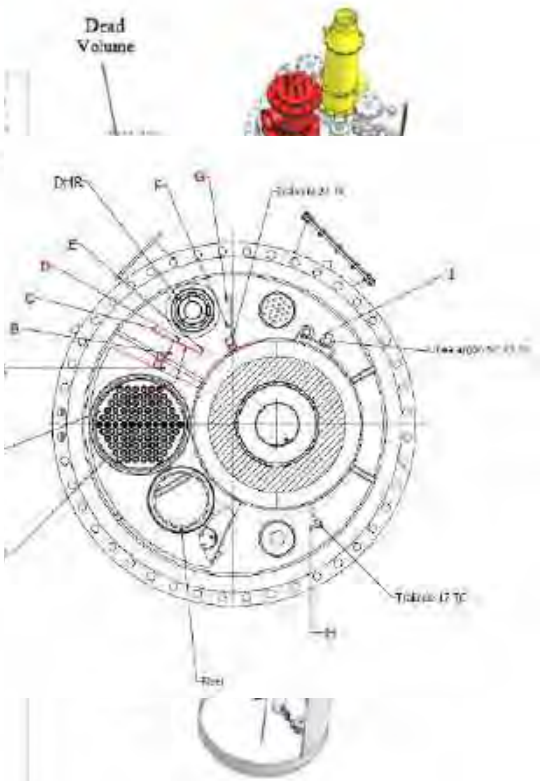

Model validation – 1D Nodalizzation scheme

- **Primary Flow Path:** feeding conduit, FPS, fitting volume, riser, separator, HX, DHR
- **HX Secondary Side**: water cooling system
- **DHR Secondary Side**: air cooling system
- **Pool**: 3 parallel pipes which simulate the volume between the internals and the main vessel; 156 cross junctions to reproduce the mass transfer into the pool
- The thermal hydraulic model is consistent with the vertical sliced approach

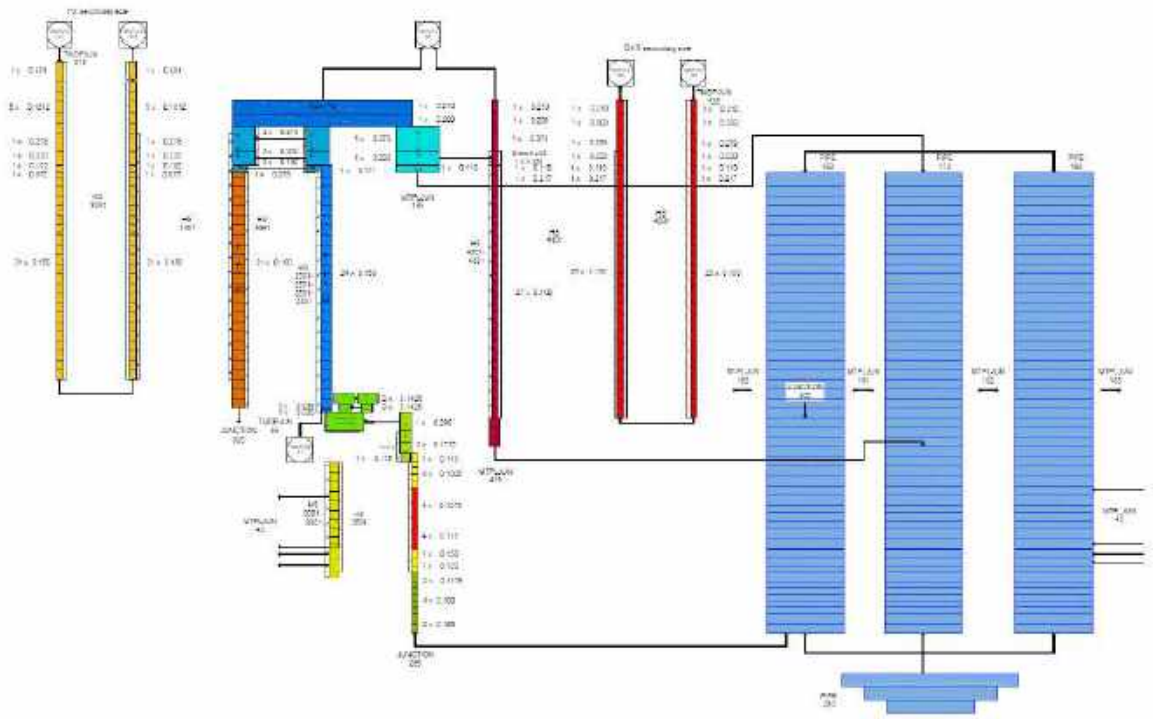

Model validation – MULTID Nodalizzation scheme

- **1D Model:** feeding conduit, fitting volume, riser, separator, HX primary and secondary side, DHR primary and secondary side
- **FPS:** 72 parallel pipes to reproduce the component sub-channel per sub-channel

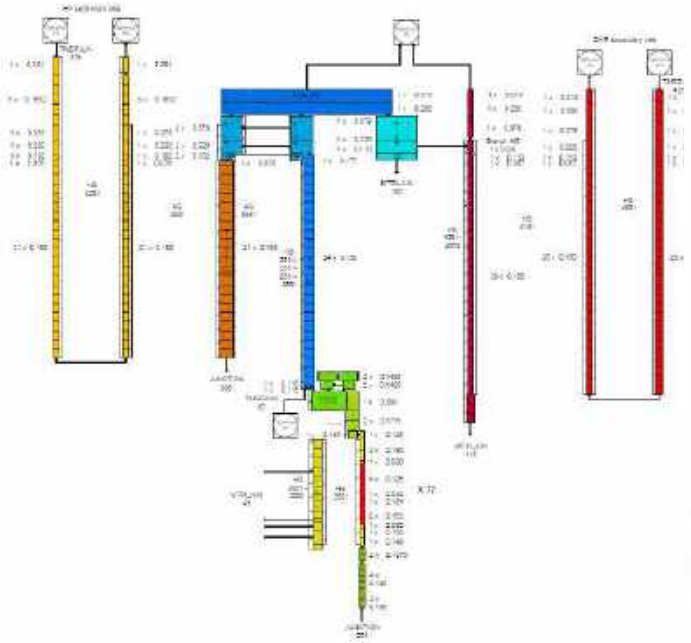

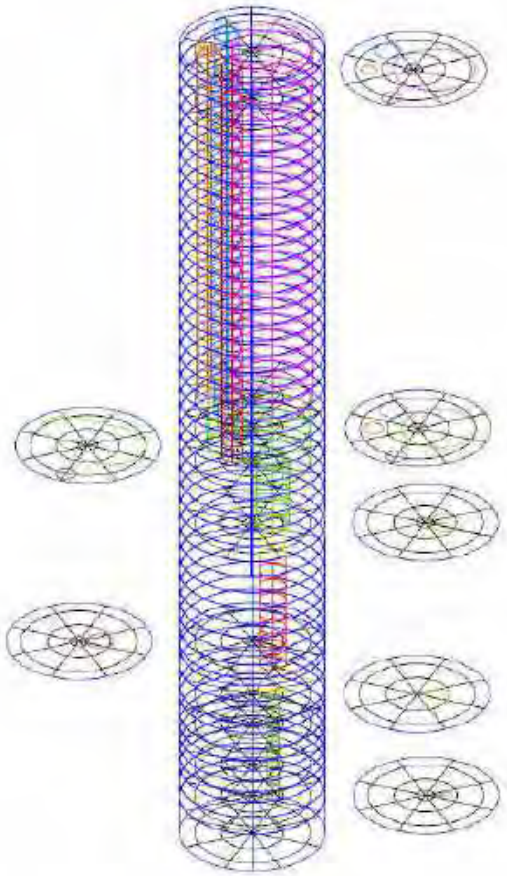

- **Pool:** 3D component composed of 51 axial levels, 4 radial meshes and 8 azimuthal intervals. The nodalization scheme is consistent with the vertical sliced approach and it is obtained to compare the LBE temperature in the esact position of the thermocouples

Model validation

- The calculations were carried out using the most recent LBE thermo-physical properties correlation, recommended by NEA and implemented in RELAP5-3D
- The main results on the primary main flow path are comparable
- Both the calculations are in good agreement with experimental results

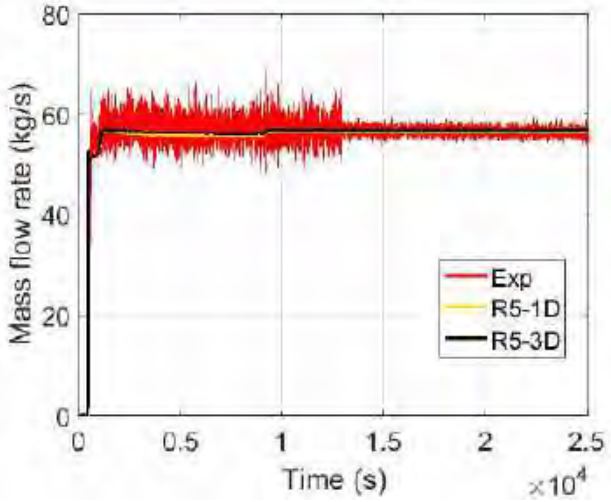

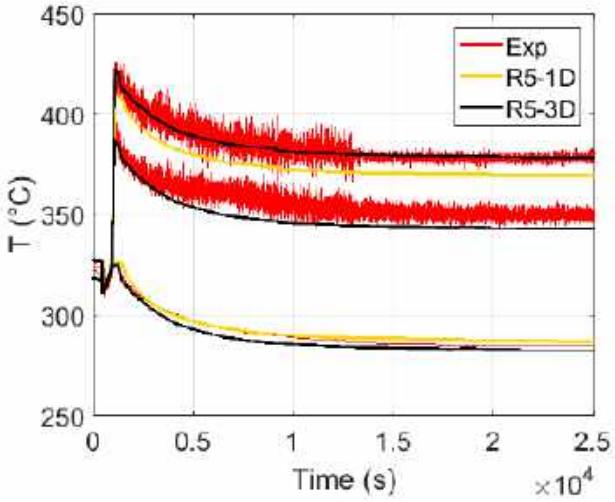

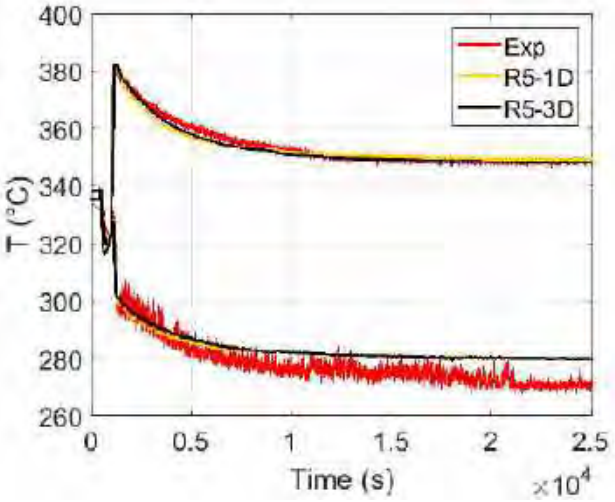

Model validation

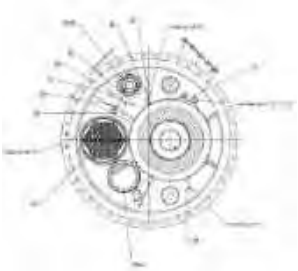

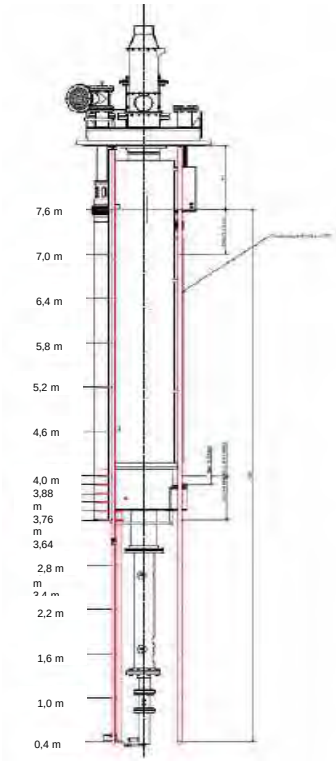

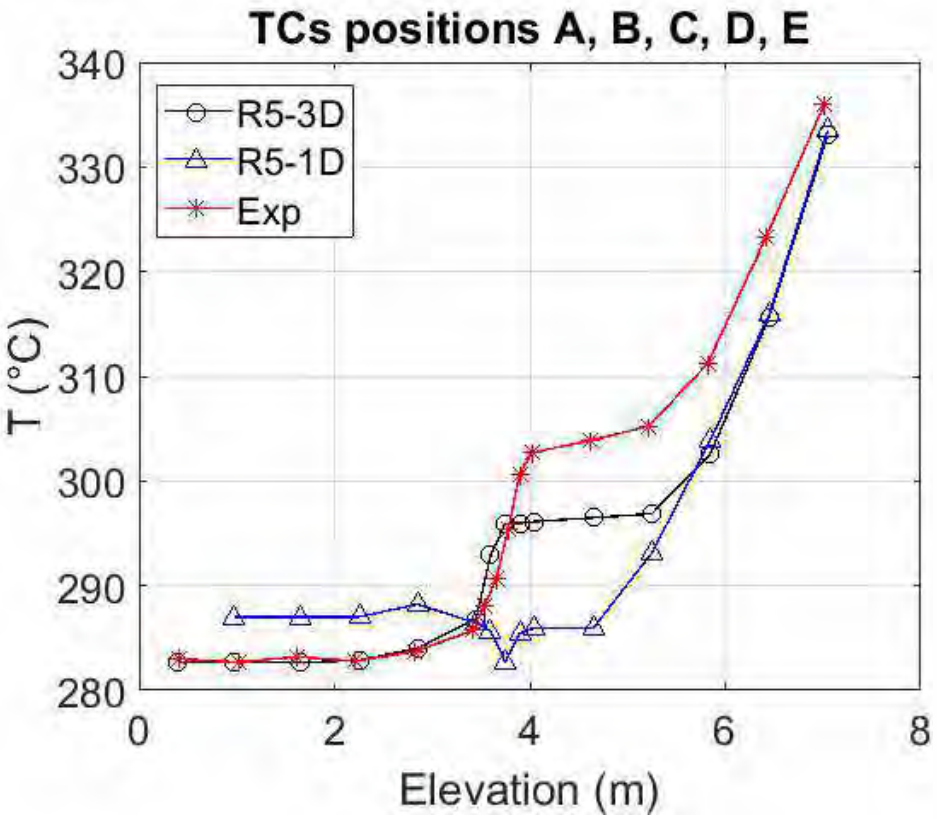

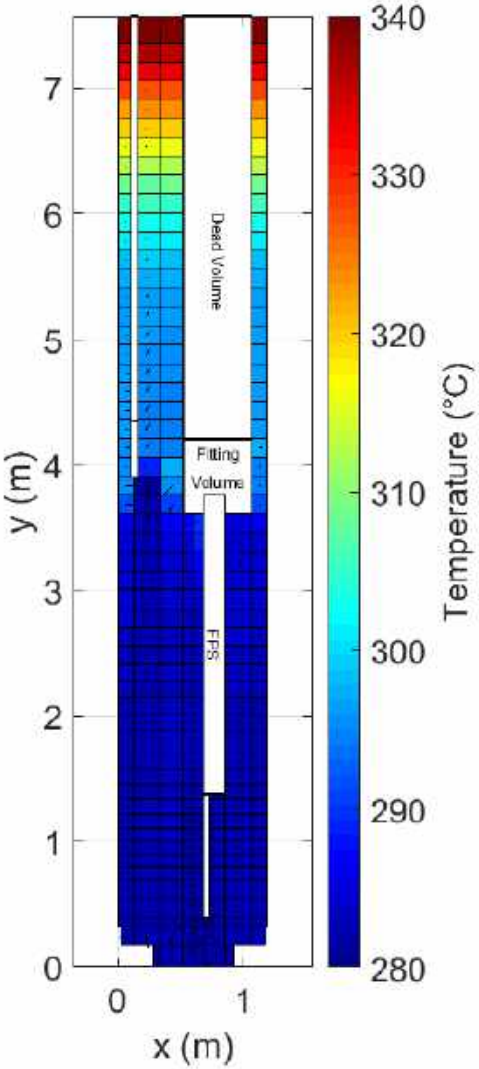

Pre-Test analysis

- **Phase 1**: assessment of **Steady State (SS) Full Power Conditions**, in order to determine initial conditions for transient
- **Phase 2**: transient simulations

PHASE 1

For the identification of the initial conditions of the transient tests, 6 different SS conditions are analysed:

- **Case #1**: setting to achieve a constant temperature drop across the FPS equal to 80° C in the range of about 400 – 480° C, representative of the temperature drop across the **ALFRED core**; duration 30000 s, FPS power 450 kW, pool initial temperature 396° C, Ar mass flow rate 1,29 Nl/s, feedwater mass flow rate 0.331 kg/s;
- **Case #2**: as **Case #1** except for the Ar mass flow rate: 2,35 Nl/s. Case #2 has been set to achieve LBE mass flow rate across the SGBT section equal to 44,7 kg/s (representative of the scaled down **SG of ALFRED**);
- **Case #3, #4, #5, #6**: as **Case #1** except for the Ar mass flow rate: 2,24 Nl/s, 2,13 Nl/s, 1,85 Nl/s, 1,79 Nl/s.

Pre-Test simulations: Full Power Conditions #1

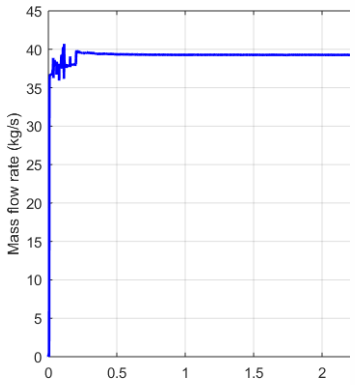

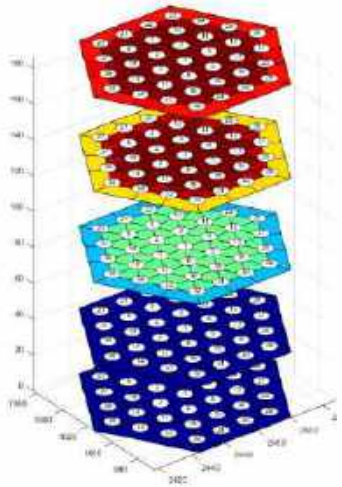

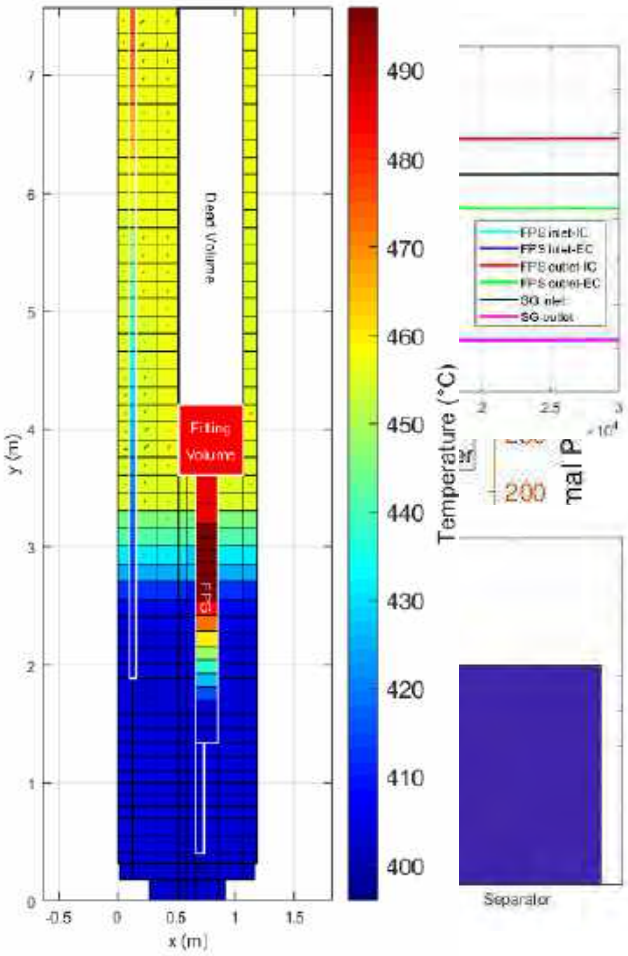

	Parameter	Unit	Value
Boundary conditions	Duration	h	> 8
	FPS thermal power	kW	450
	LBE average T inside the pool	° C	396
	Ar mass flow rate	Nl/s	1.29
	Steam pressure	bar	172
	FW inlet T	° C	335
	FW mass flow rate	kg/s	0.33
Results	FPS LBE inlet T	° C	403.8
	FPS LBE average outlet T	° C	486.8
	HERO LBE inlet T	° C	480.6
	HERO LBE outlet T	° C	403.9
	LBE mass flow rate at inlet section of HERO	kg/s	39.2
	Power removed by HERO	kW	438
	Steam max T	° C	398.9
	Steam velocity	m/s	9

PHASE 2

The starting point for transient tests (TrT) is considered **Case #1**.

- **TrT #1**: it consists of a **protected loss of LBE pump**.
  - **FPS power** decreases down to the compensated decay heat value;
  - **Ar mass flow rate injection** decreases to 0 simulating presence of a pump flywheel;
  - **Feedwater mass flow rate** is set at 10% of nominal mass flow to simulate the activation of the DHR system;
- **TrT #2**: as **TrT #1** except for the feedwater mass flow rate, set to 20% of the nominal mass flow rate;
- **TrT #3**: as **TrT #1** except for the feedwater mass flow rate, which decreases to 0 in order to simulate a **loss of DHR function in hot conditions**.

Transient Test #1: main results

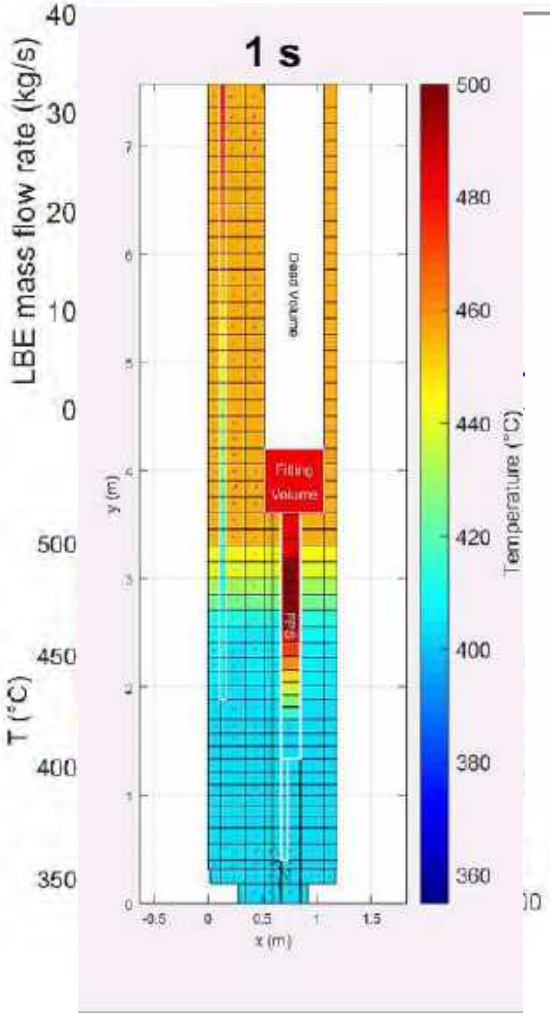

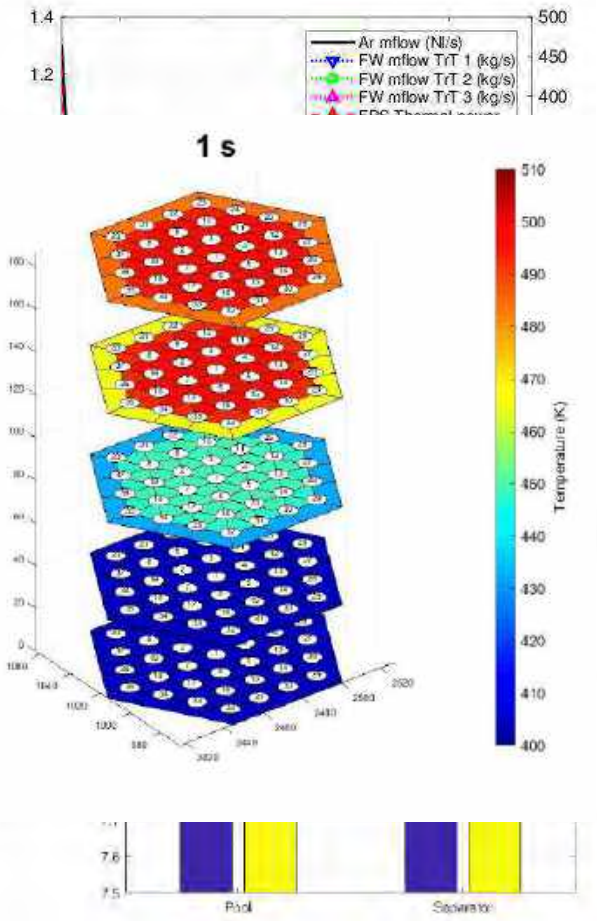

Time (s)	Main event
0	Start of the transient sequence
80	Minimum value of the LBE temperature at the outlet section of the FPS
110	Peak temperature at SG outlet section
340	Minimum value of the LBE mass flow rate
350	Peak temperature at the outlet section of the FPS and minimum temperature at the outlet of HERO
1000	End of the transient test

Transient Test: compare #1 #2 #3

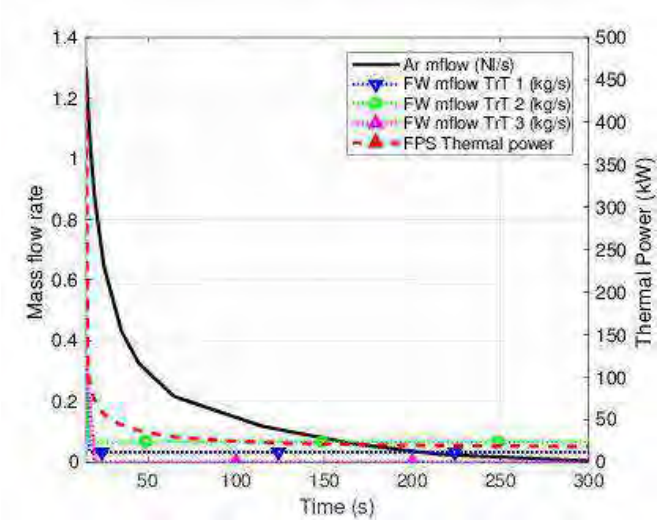

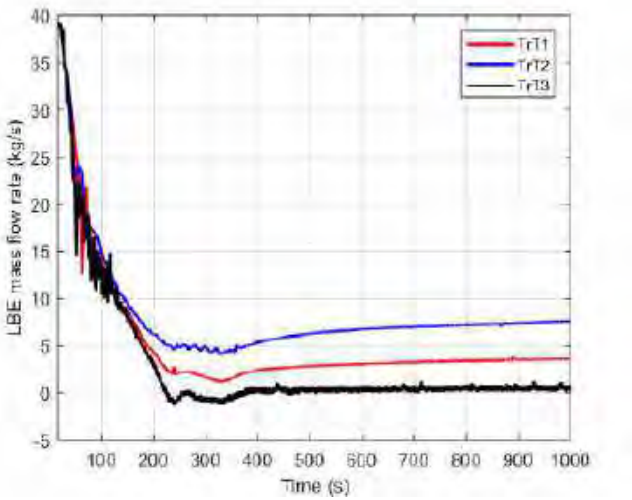

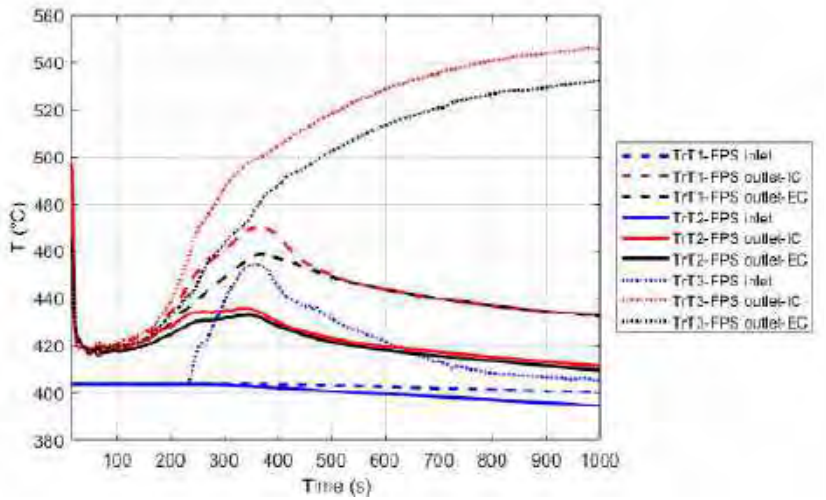

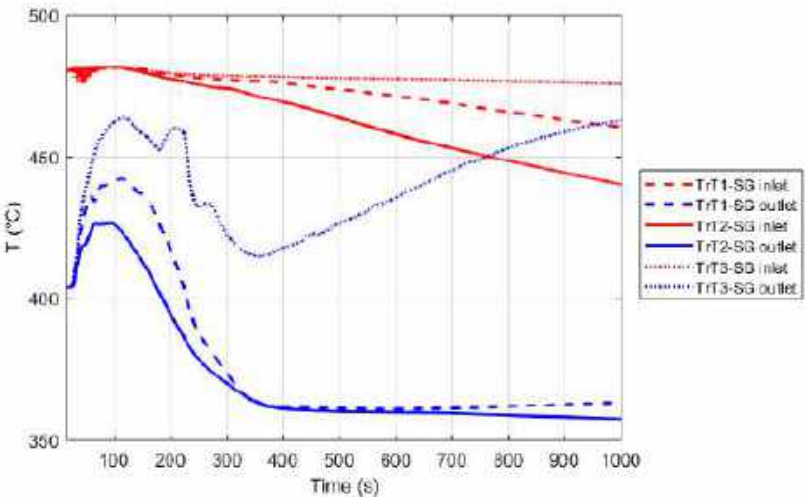

Transient Test: compare #1 #2 #3

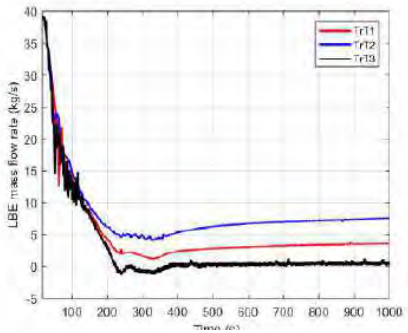

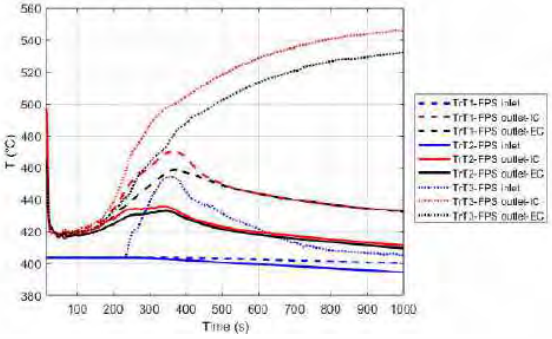

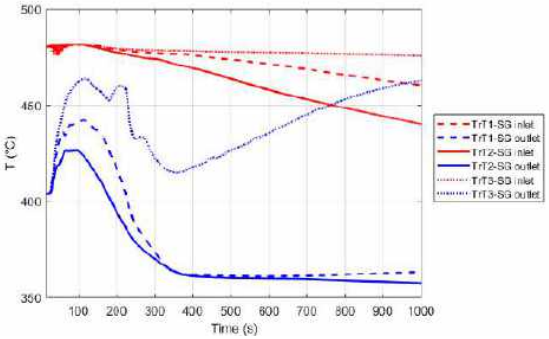

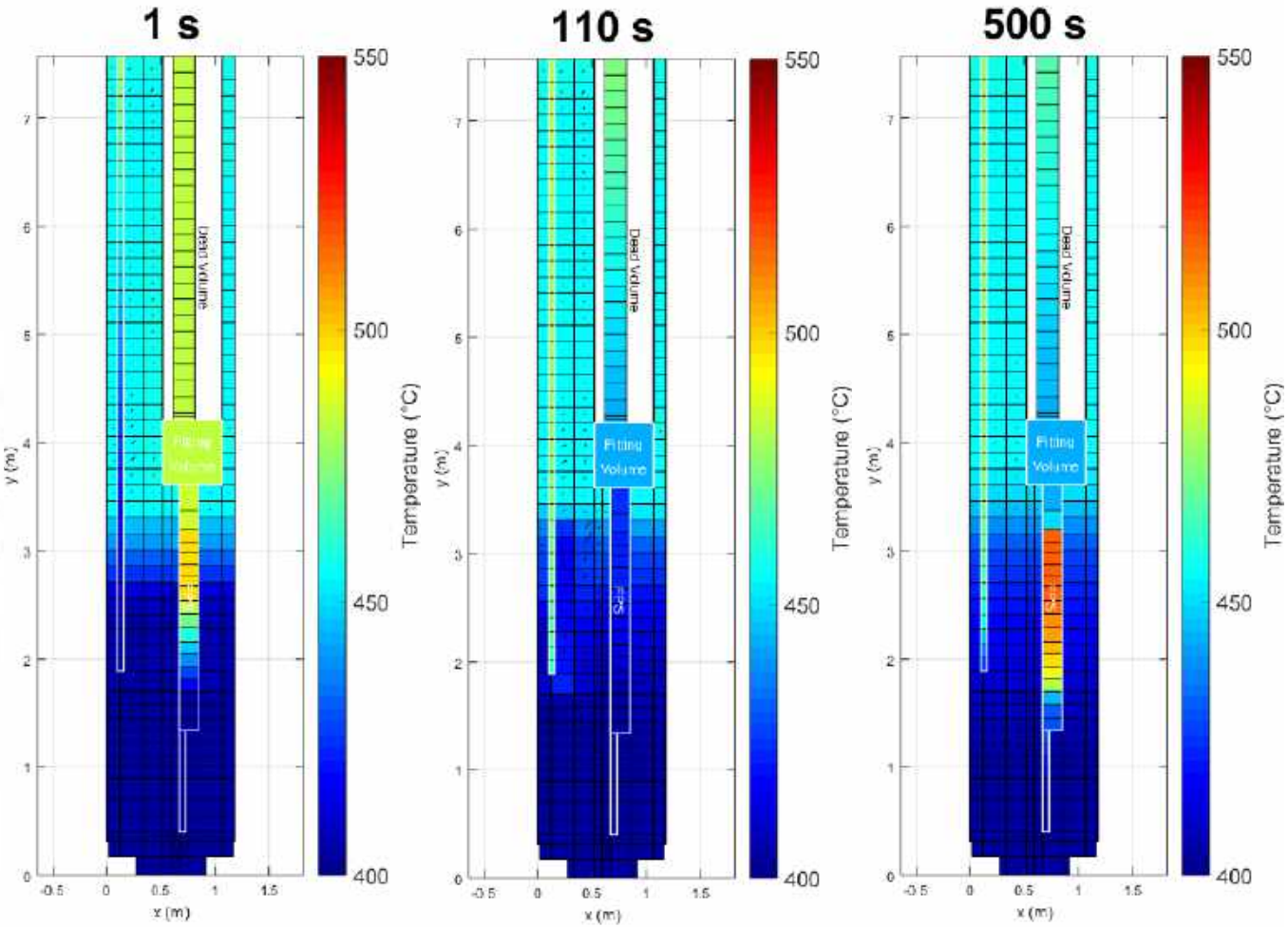

Transient Test: compare #1 #2 #3

Time: 0 s

TrT1: 1000 s

Trt3: 1000 s

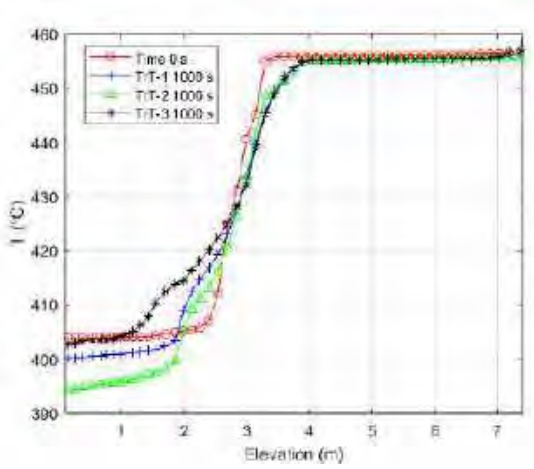

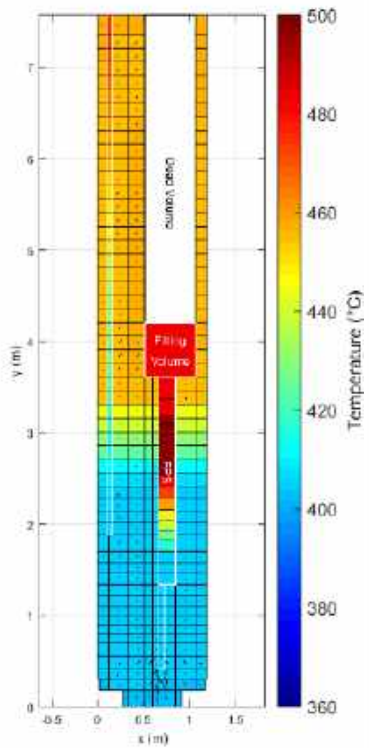

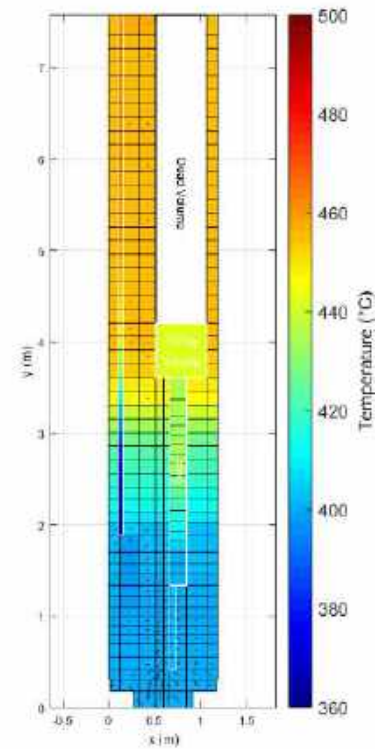

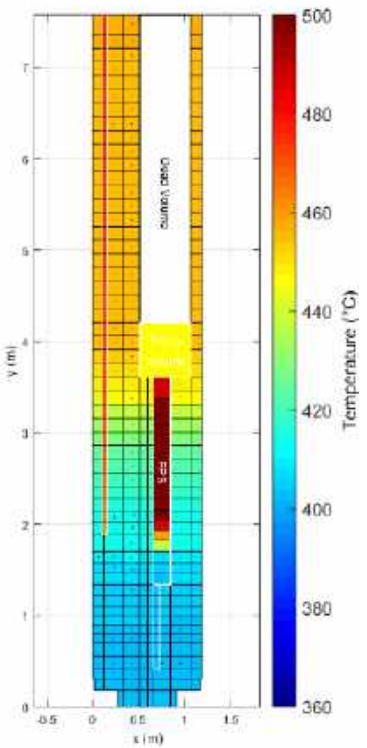

CONCLUSIONS

- **CIRCE-HERO RELAP5-3D©** model has been developed and calibrated comparing **CIRCE-ICE** simulations results with experimental data
- **Sensitivity analysis** has been performed to determine the reference full power steady state conditions
- The transient test simulations have highlighted that **HERO test section** guarantees a sufficient natural circulation conditions to remove the decay heat in short term. When the feed-water mass flow rate is deactivated, the code predicts a **reverse flow** of the primary coolant. Further investigations are necessary in order to confirm that.
- The transient test 1 has been selected as the reference test for the validation benchmark

THANKS FOR YOUR ATTENTION

OpenFoam-SALOME-FEMLCORE-CATHARE coupling development and validation against TALL-3D experimental data

L. Chirco[1], **A. Chierici**[1], **R. Da Vià**[1], **S. Manservisi**[1]
Alma Mater Studiorum - Bologna[1]
A. Cervone[2]
Centro Ricerche ENEA - Bologna[2]

Summary

1

- Multiphysics and Multiscale computational tools
- TALL-3D Facility and computational tests
- TALL-3D with In-house codes in platform (SALOME-CATHARE-FEMLCORE)
- TALL-3D with specialized nuclear CEA codes in platform (CATHARE- TRIOU)
- TALL-3D with open-source codes in platform (SALOME-OPENFOAM)
- Conclusions

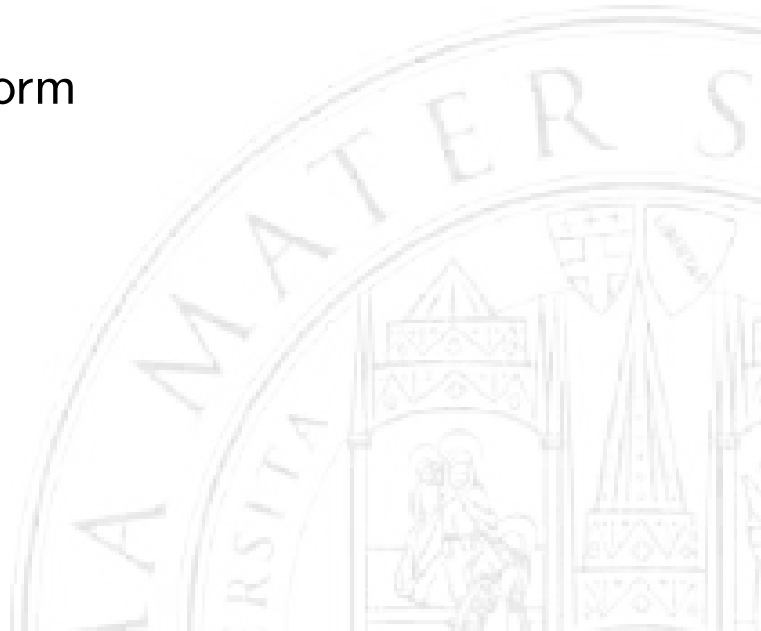

Multiphysics and Multiscale computational tools

Developing LFR platform

Computational platform ENEA-UNIBO (for LF

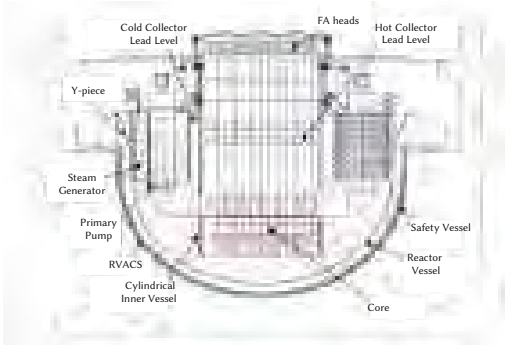

Computational platform ENEA-UNIBO (LM experiment)

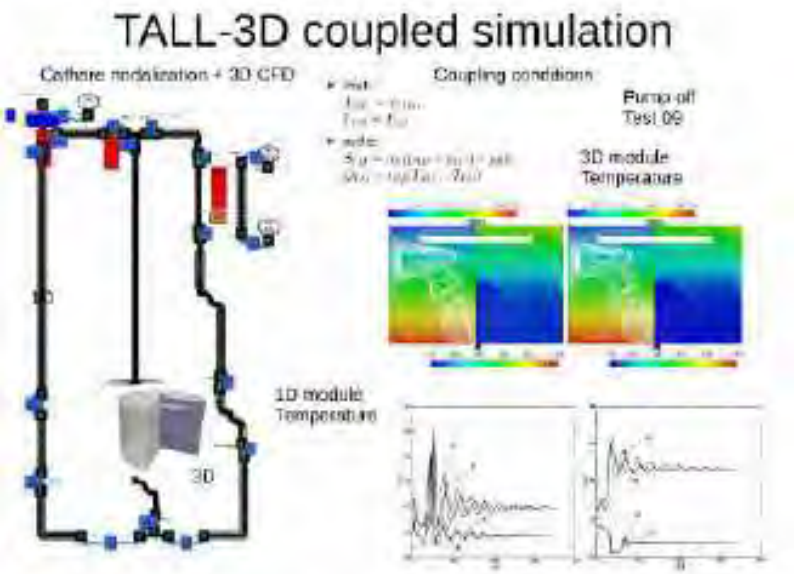

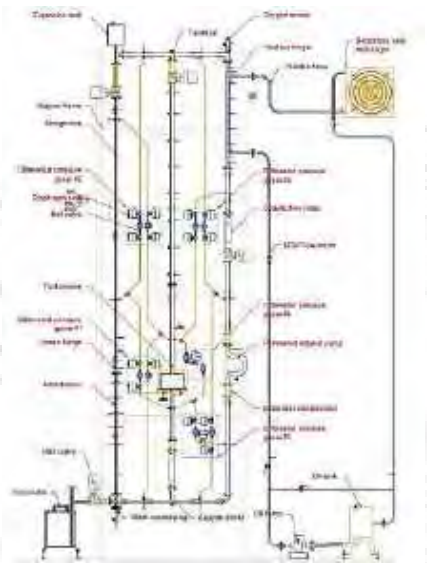

LFR platform approach

Example 1 multi-scale defective mode approac

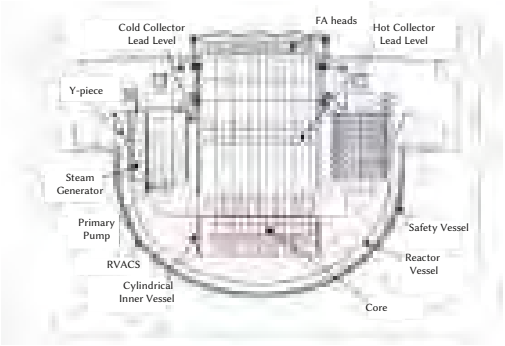

Computational platform ENEA-UNIBO (LM experiment)

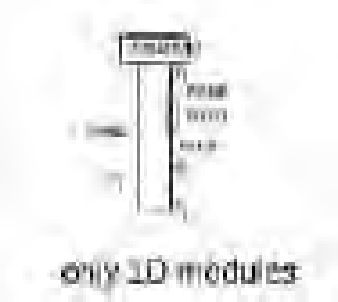

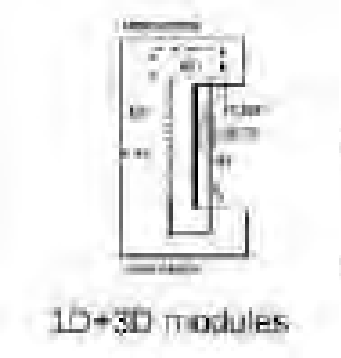

Multiphysics-Multiscale tools for LFR

Computational platform (LFR)

IN-HOUSE CODES (FEMLCORE) → Developing, Research, Design
OPEN-SRC CODES (OPEN-FOAM) → Exchange, sharing data/results
NUCLEAR TESTED CODES (CEA) → Verification, licensing

Multi-scale Computational platform (LFR)

Multi-physics	space scale 1	space scale 2
Thermalhydraulics	CFD-porous 3D	system 1D
open-src CEA-EDF	TRIOCFD FEMLCORE OPENFOAM MC/TRIOCFD (sourceforge)	FEMuS OPENFOAM CATHARE
Neutronics	Trasport	group diffusion
open-src CEA-EDF	DRAGON (assembly)	DONJON (core) APOLLO2
Structural	3D structural	1D beam
open-src CEA-EDF	Code_Aster FEMuS OPENFOAM Code_Aster (CAELinux+sourceforge)	Code_Aster FEMuS Code_Aster
Two-phase	interface	two-fluid model
open-src CEA-EDF	TRIOCFD FEMuS OPENFOAM TRIOU-CFD(sourceforge) NEPTUNE	FEMuS (FEM) CATHARE
uncertainty analysis		
open-src CEA-EDF	URANIE URANIE platform (sourceforge)	URANIE URANIE platform

Multiphysics and multiscale platform (CEA-EDF now almost

In-house developing platform (research codes)

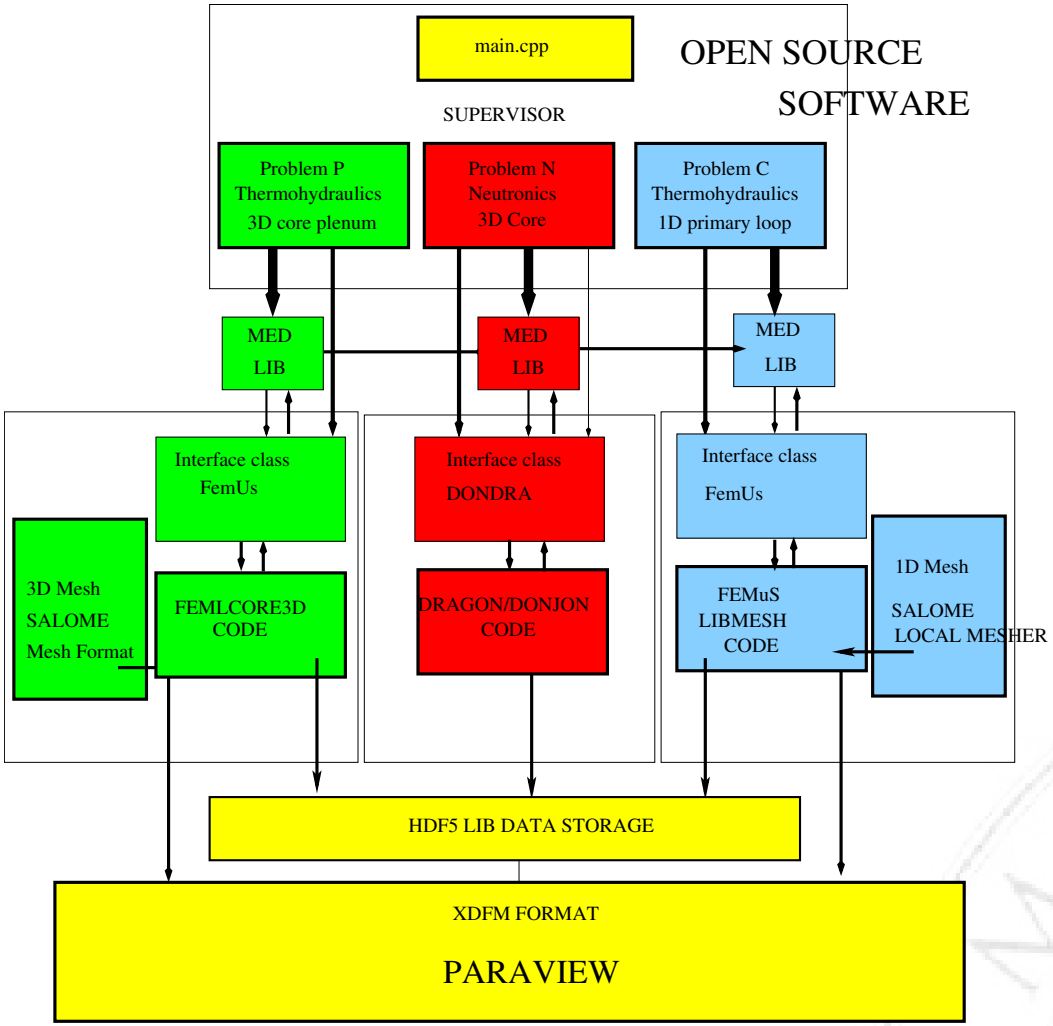

CEA Developing platform (nuclear approved)

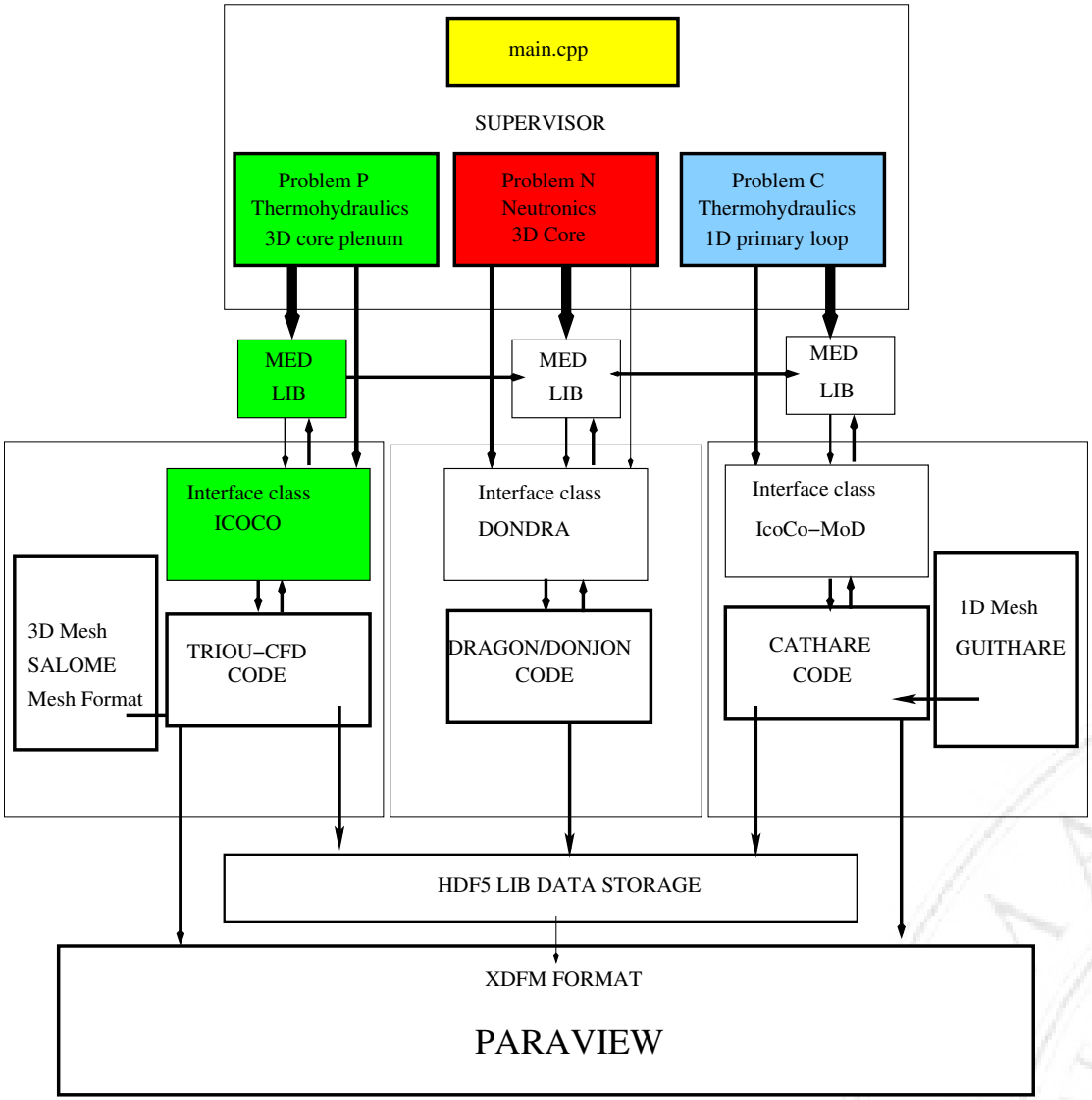

OPEN-SRC Developing platform (OpenFOAM)

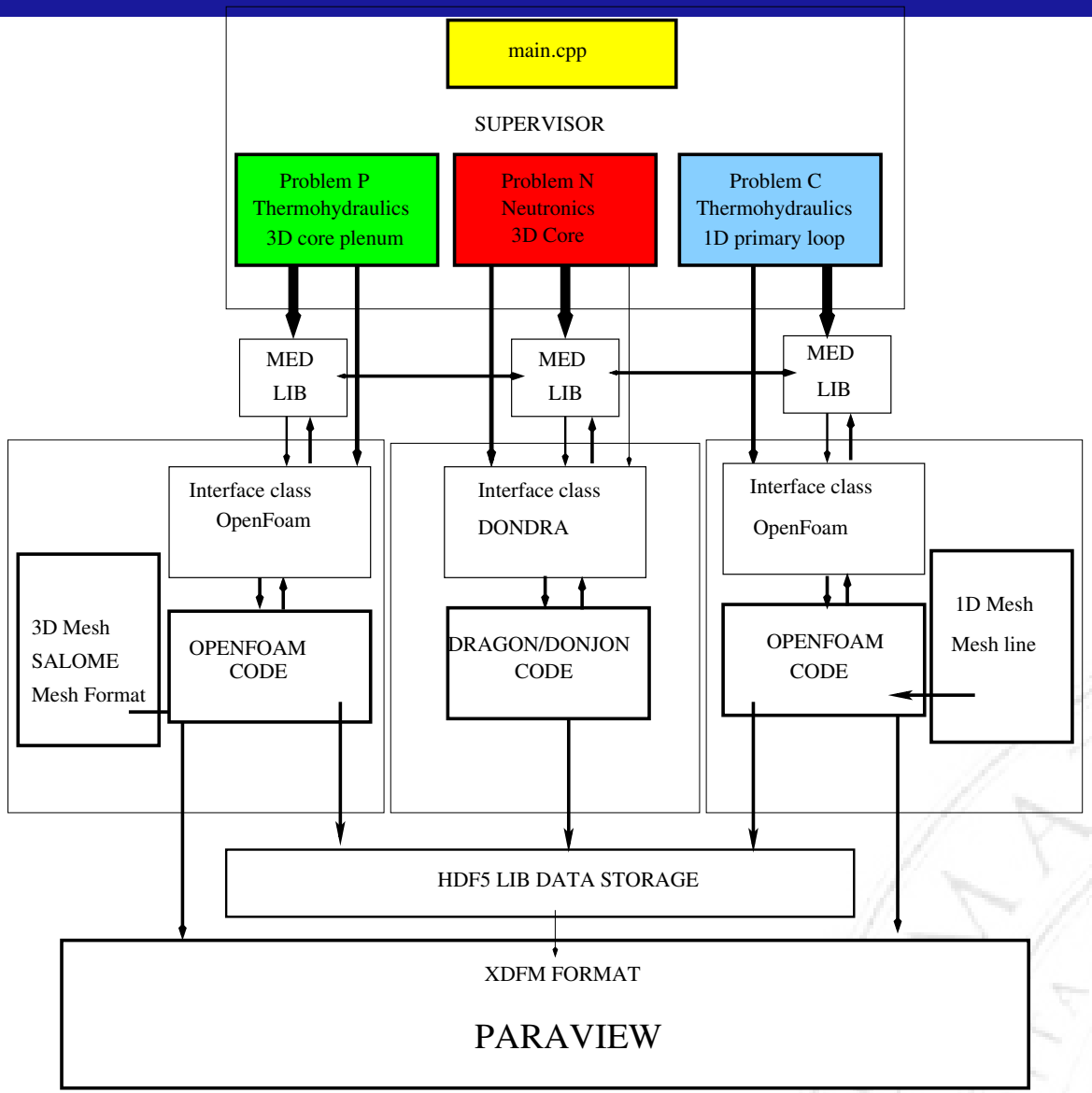

SALOME platform

MESH GENERATION + SOLUTION VISUALIZATION (OPEN-SRC)
$\rightarrow$ MED libraries $\rightarrow$ HDF5 data storage format

SALOME-CEA platform

SALOME-CEA codes

CATHARE → 1D nuclear thermal-hydraulics code → MED-HDF5
APOLLO2 → neutronics code → MED-HDF5 format
TRIOU → 3D -CFD code → MED-HDF5 format +mesh
NEPTUNE → 3D-CFD two-phase code→ MED-HDF5 format +mesh
SATURNE → 3D -CFD code → MED-HDF5 format +mesh

ICOCO interface

CATHARE interface ↔ SALOME

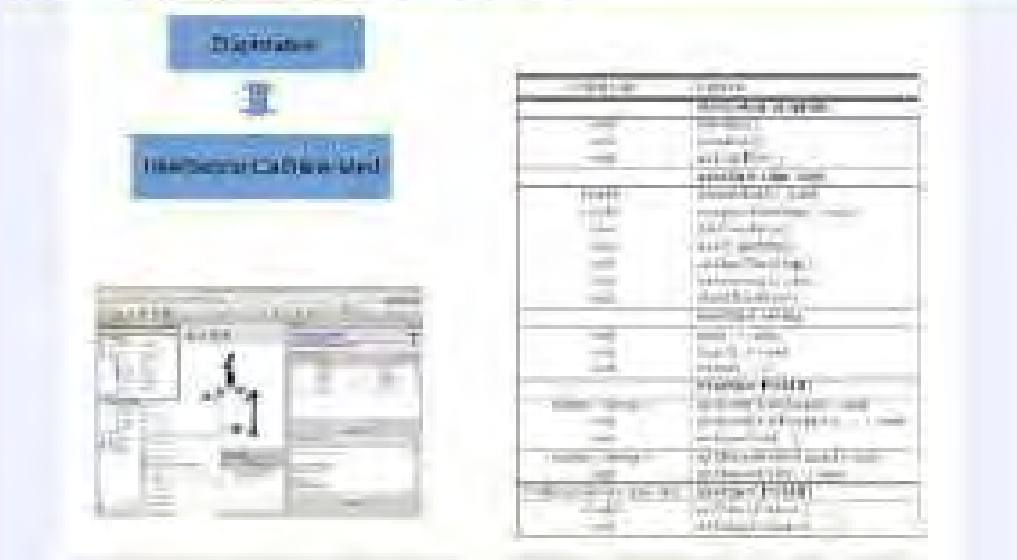

1D-SCALE (MAIN LOOP)

SALOME ENEA-UNIBO in-house code platform

In-house codes

FEMus → multi-scale, multi physics code → MED-HDF5
FEMLCORE-3D CFD → 3D -CFD code → MED-HDF5 format +mesh
FEMLCORE- 1D → 1D- thermal-hydraulics code → MED-HDF5
FEMLCORE- POROUS → 3D-CFD porous model code → MED-HDF5

FEMus interface

3D-SCALE (CFD and POROUS-CFD)

OPEN-SOURCE SALOME platform

OPEN-SOURCE codes

DRAGON-DONJON → neutronics code
TRIOU-CFD → 3D -CFD code
SATURNE → 3D -CFD code
OPENFOAM → multi purpose CFD code

CODE interface

DRAGON-DONJON → DONJON interface → MED-HDF5
TRIOU-CFD → ICOCO interface → MED-HDF5 format +mesh
SATURNE → ICOCO interface → MED-HDF5 format +mesh
OPENFOAM → OPENFOAM interface → MED-HDF5 format +mesh
OPENFOAM interface is in working progress

TALL-3D Facility and computational tests

TALL-3D Facility

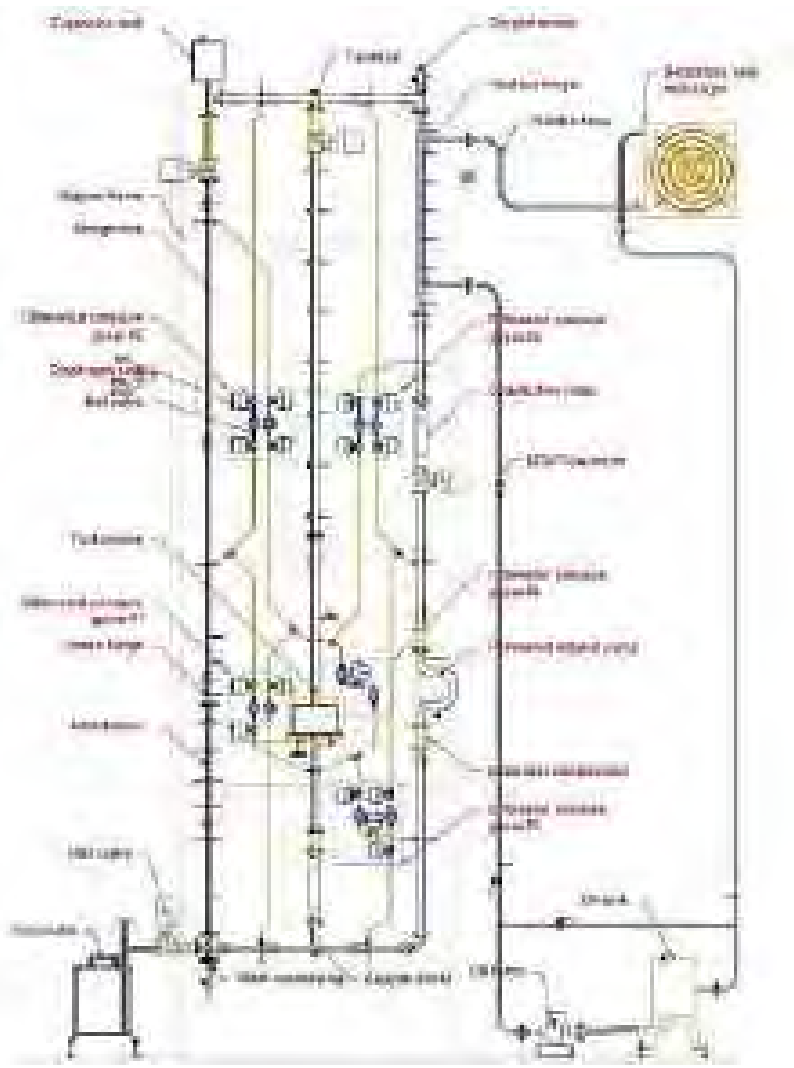

Primary loop (LBE):
1D loops (3)
3d- Test section (1)
(MH) main heater (2)
(EPM) Electromagnetic Pump
(HX) Heat exchanger
Secondary loop (oil):
Pump-Tank
Secondary HX
Working conditions:
Pressure: 0.7MPa
Temperature: 400-500^oC
flow rate (LBE)= 5Kg/s; vel 1.7m/s
heat removal=40 kW (10kw)
flow rate (oil)= 50 l/min;

Defective coupling

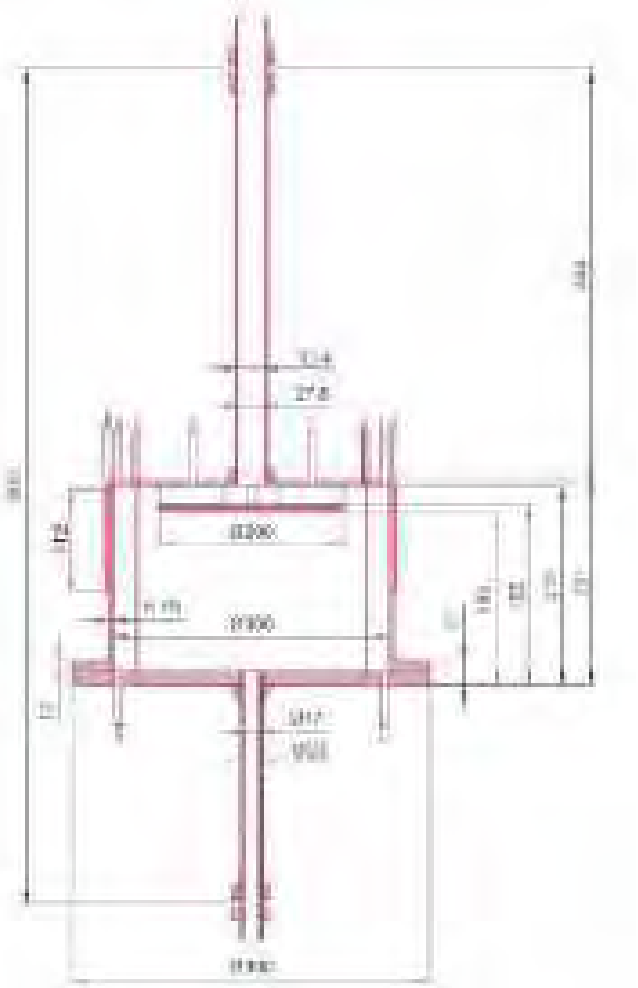

3D domain

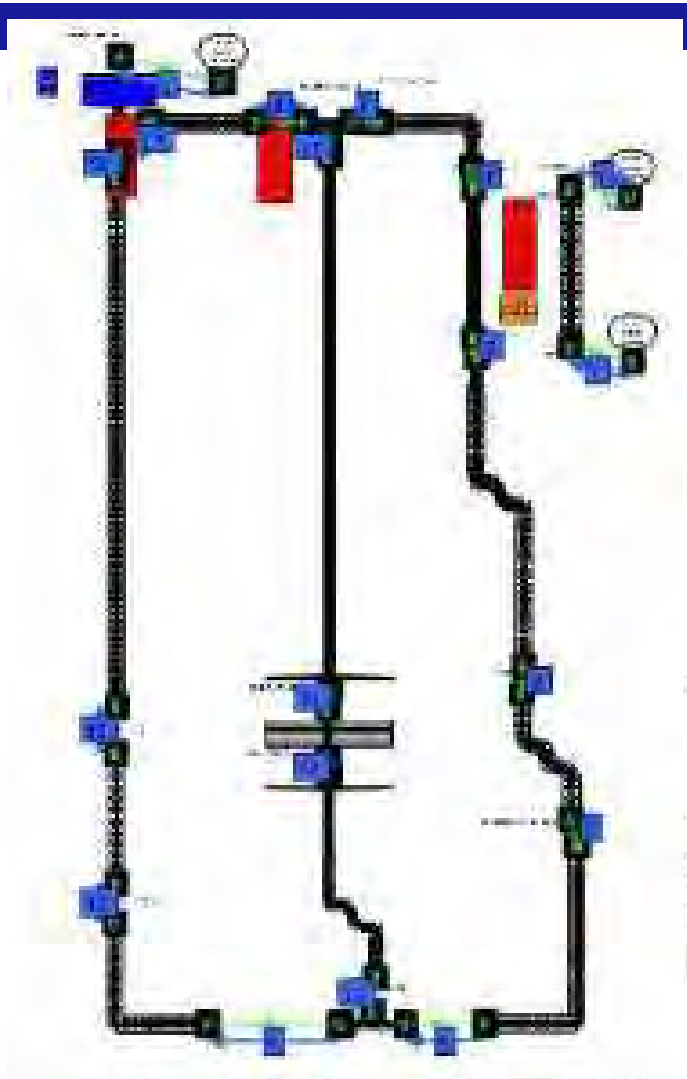

1D domain

Overlapping and defective boundary conditions

Defective Approach

Overlapping and defective boundary conditions

Inlet (3D) (P1)

1D value $\rightarrow$ BC on 3D-equation
mass conservation balanced from the overlapping

Inlet (1D)(P2)

3D value $\rightarrow$ Source with Feed-back control (1D-equation)

$$Q = \gamma_1 \left(T_{3D} - T_{1D} \right)$$

$$S = \gamma_2 \left(\Delta p_{3D} - \Delta p_{1D} \right) + \Delta p_0, \qquad \gamma_2 = \text{inverse delay time}$$

TALL-3D with In-house codes in platform (SALOME-CATHARE-FEMLCORE)

SALOME-CATHARE-FEMLCORE

Test: pump power off

1D circuit → CATHARE
3D circuit → FEMLCORE
Mesh, data exchange → MED-HDF5-SALOME

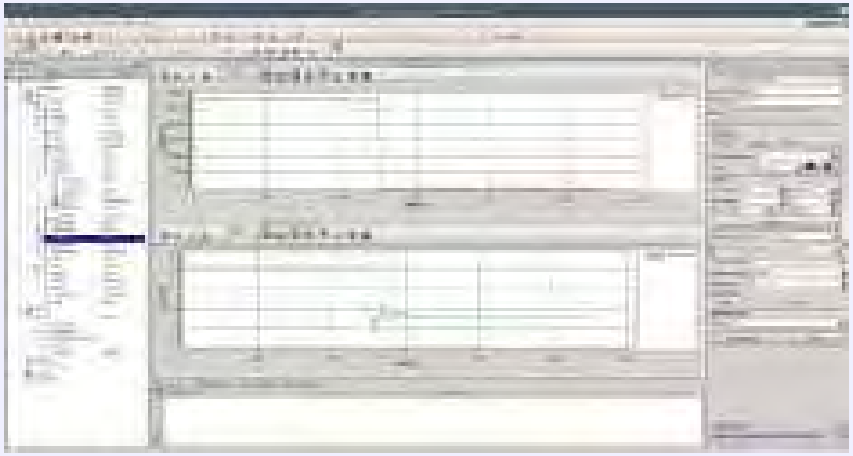

Test computation

steady 1D circuit + steady 3D-CFD
time step → coupling 1D+3D
Pump failure
time step → coupling 1D+3D

Defective coupling 3D-CFD + CATHARE 1D

Defective coupling: overlapping mesh

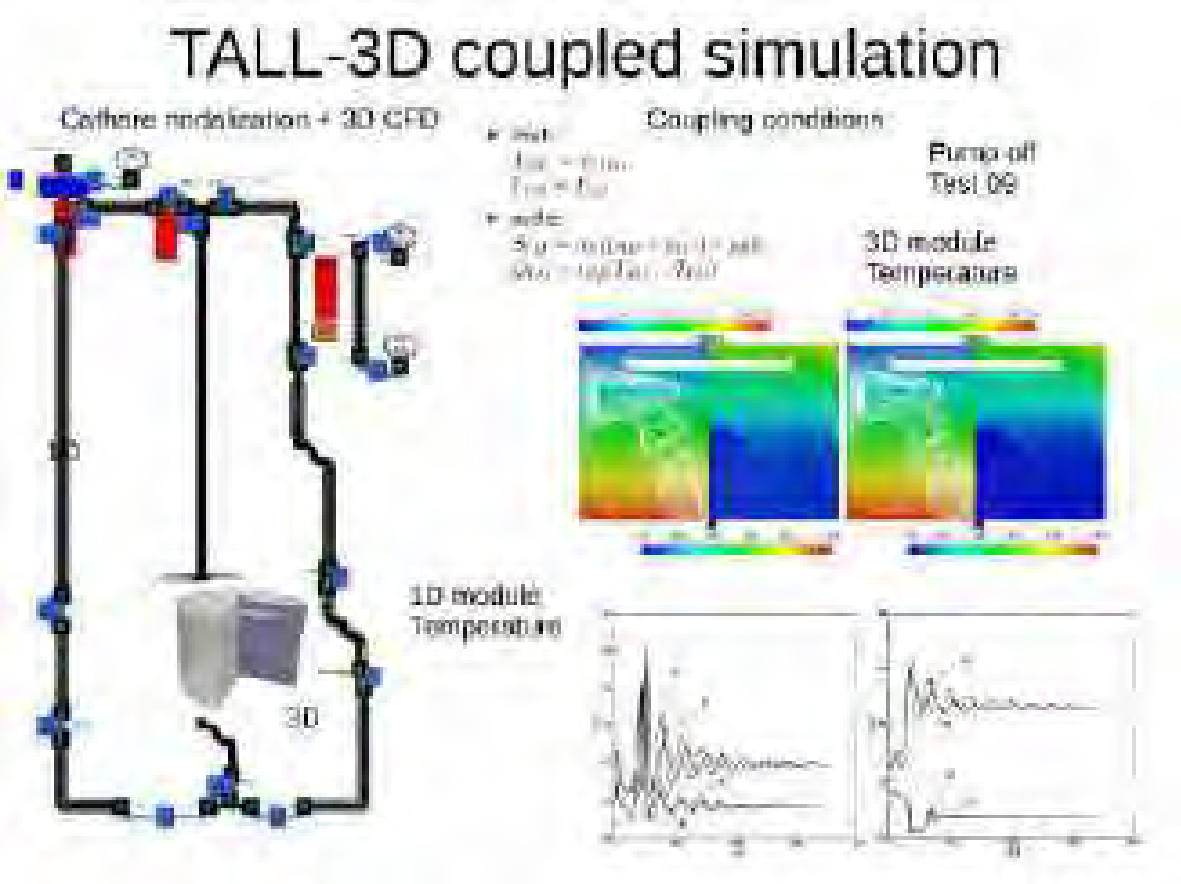

- inlet:
  $\dot{m}_{3D} = \dot{m}_{1D}$,
  $T_{3D} = T_{1D}$
- outlet:
  $S_{1D} =$
  $\alpha_S(p_{3D} - p_{1D})$
  $Q_{1D} =$
  $\alpha_Q(T_{3D} - T_{1D})$

Test 9: pump failure (Natural convection)// COUPLING FEMLCORE/OPENFOAM 3D + CATHARE 1D

1D-uncoupled CATHARE simulation

Experimental and computed mass flow rate on different legs

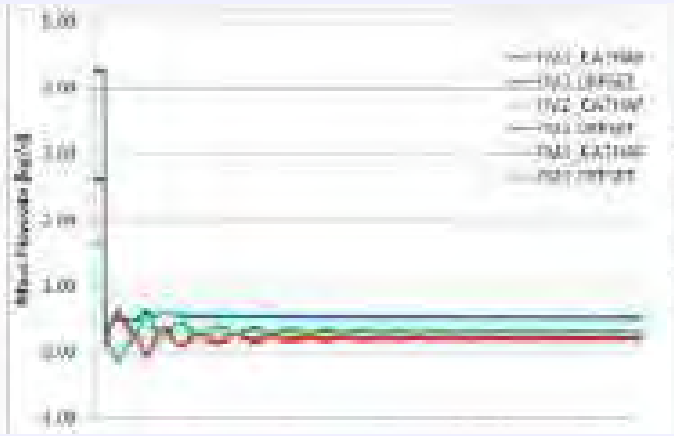

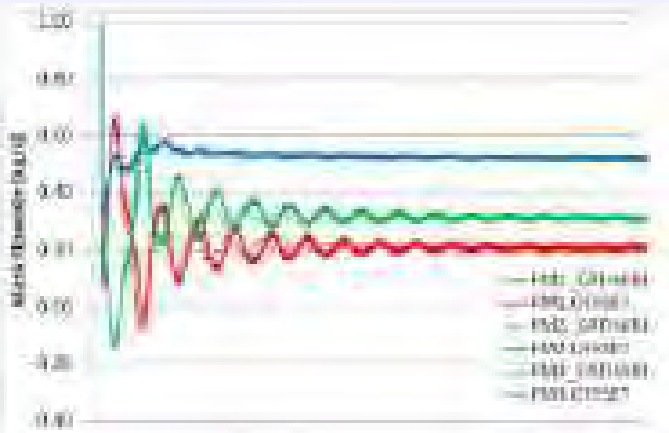

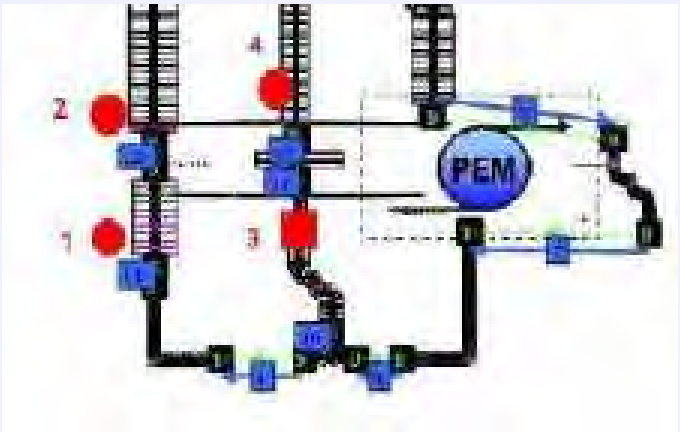

Experimental and computed temperature at the thermocouple points on the left leg (FM1), on the right leg (FM2) and on central one (FM3).

3D-1D coupling (FEMLCORE-CATHARE)

Test numerical stabilization and turbulence models

	A	B	C	D	E	F
Stabilization	-	SUPG	SUPG	Upwind	Upwind	SUPG
Dynamical Turb	-	-	κ-ω	κ-ω	κ-ω	κ-ω
Thermal Turb	-	-	Const Pr_t	Const Pr_t	Kays Pr_t	Kays Pr_t

Case A refers to Cathare standalone.

Points of interest in the 1D overlapping mesh

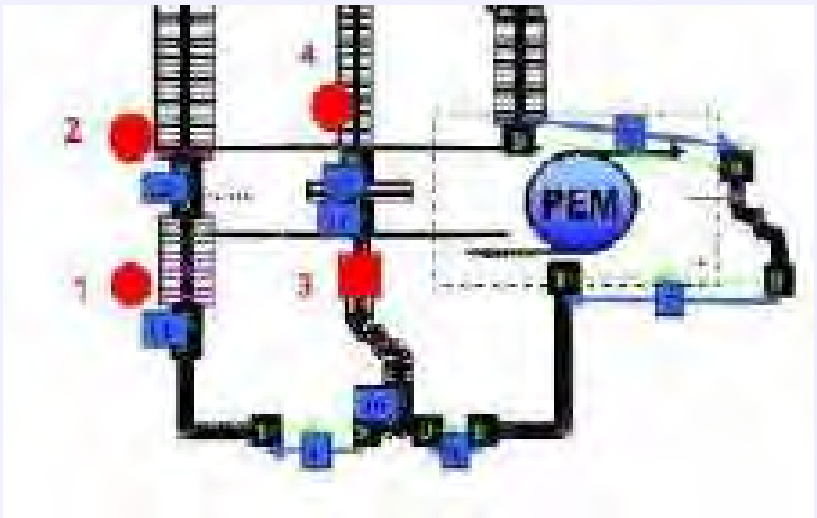

Reference point (FEMLCORE-CATHARE)

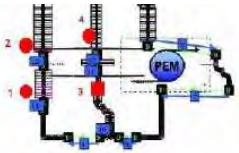

	A	B	C	D	E	F
Stabilization	-	SUPG	SUPG	Upwind	Upwind	SUPG
Dynamical Turb	-	-	κ-ω	κ-ω	κ-ω	κ-ω
Thermal Turb	-	-	Const Pr_t	Const Pr_t	Kays Pr_t	Kays Pr_t

Temperature. Reference point 2 (RESERVE4, leg 1)

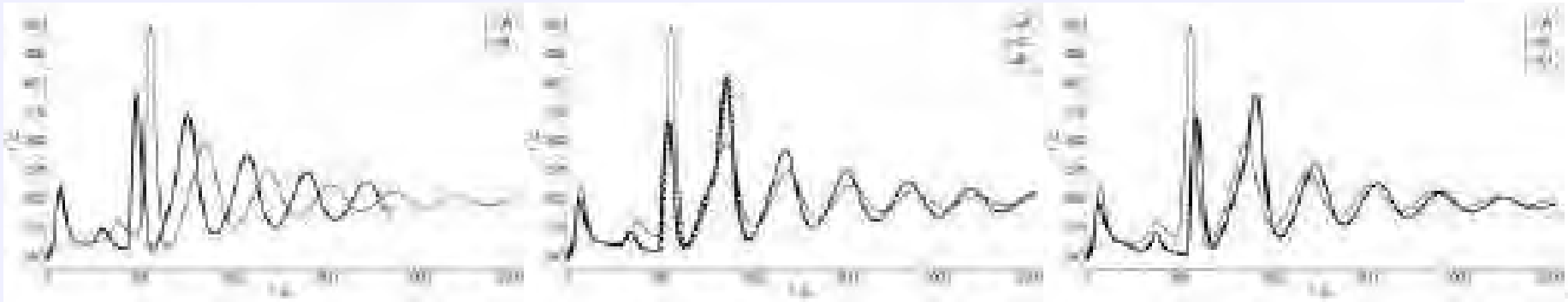

Mass flow . Reference point 2 (RESERVE4, leg 1)

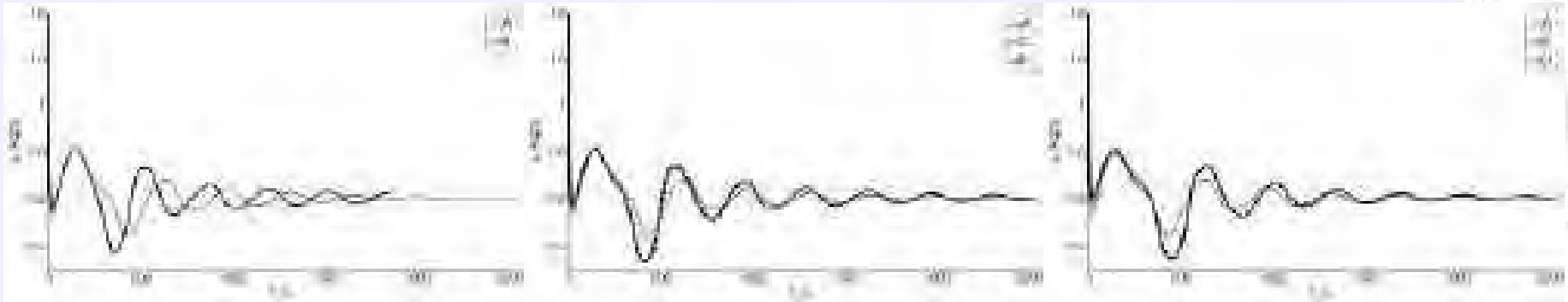

3D coupling solution. Temperature

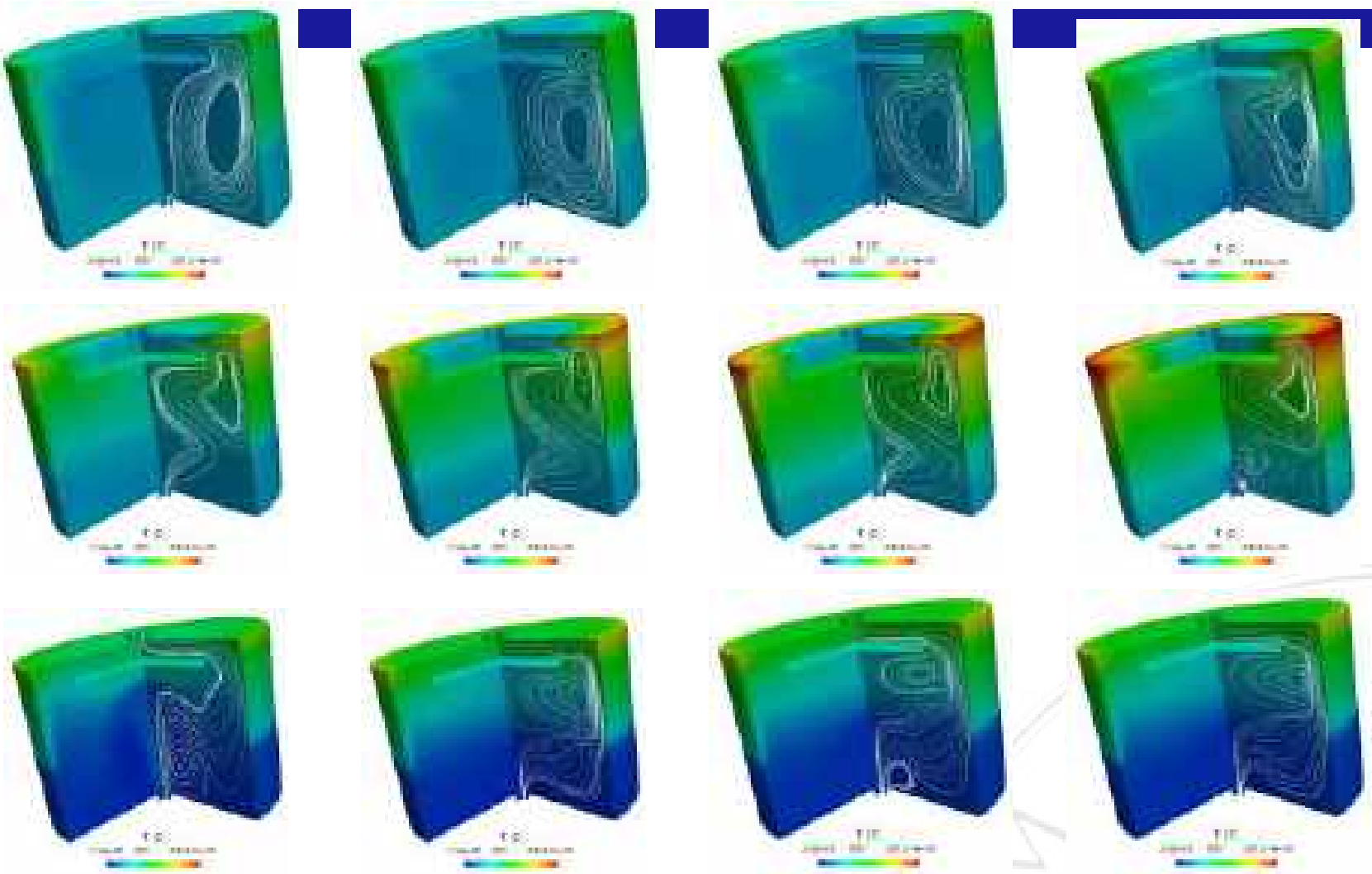

Temperature and streamline profiles over the 3D test component for $t = 10 - 2000$ for κ-ω turbulence case and Kays turbulent Prandtl number model for heat exchange

TALL-3D with specialized nuclear CEA codes in platform (CATHARE- TRIOU)

SALOME-CATHARE-TRIOU (CEA platform)

Test: pump power off

1D circuit $\rightarrow$ CATHARE
3D circuit $\rightarrow$ TRIOU-CFD
Mesh, data exchange $\rightarrow$ MED-HDF5-SALOME (ICOCO)

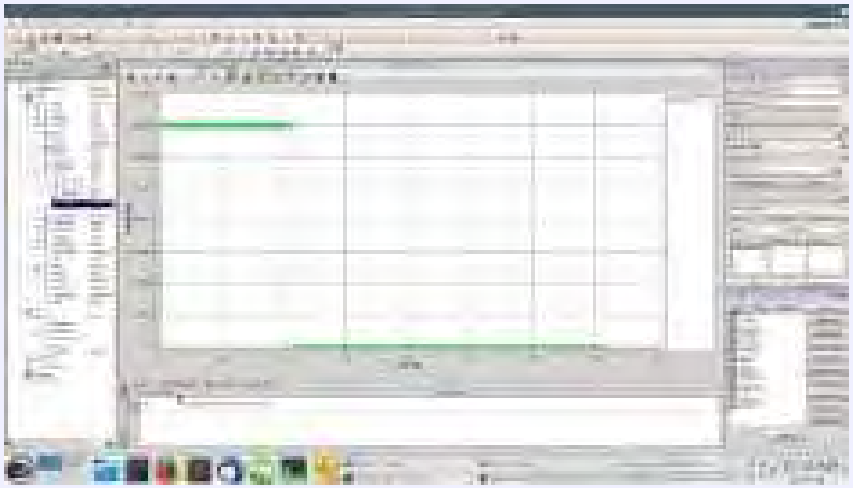

Test computation

steady 1D circuit (0-2000s)+ steady 3D (2000-2100s)
time step $\rightarrow$ coupling 1D+3D
Pump failure ($> 2100s$)
time step $\rightarrow$ coupling 1D+3D

TRIOU-CFD(3D) + CATHARE 1D (CEA platform)

Defective coupling: overlapping mesh

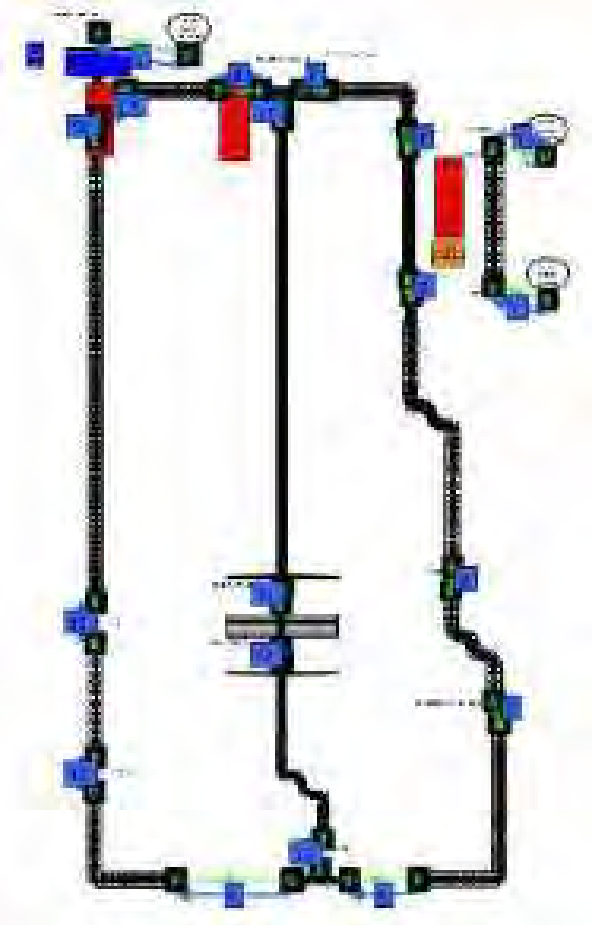

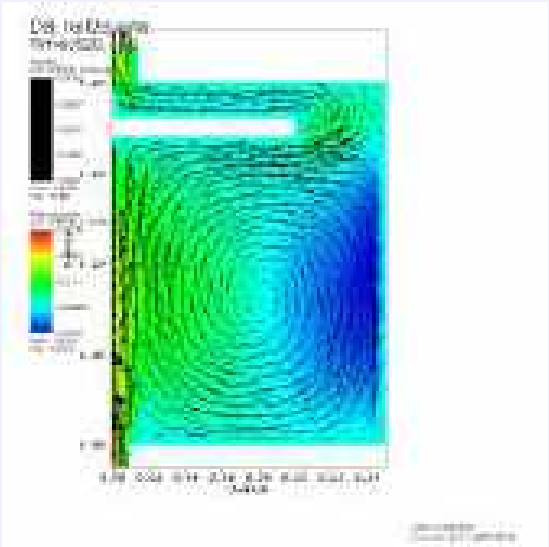

- inlet:
  $\dot{m}_{3D} = \dot{m}_{1D}$,
  $T_{3D} = T_{1D}$
- outlet:
  $S_{1D} =$
  $\alpha_S(p_{3D} - p_{1D})$
  $Q_{1D} =$
  $\alpha_Q(T_{3D} - T_{1D})$

Test: pump failure (Natural convection)
COUPLING TRIOU-CFD + CATHARE 1D $\rightarrow$ VISIT (VTK no HDF5)

TRIOU-CFD + CATHARE 1D (CEA platform)

Previous case

For the previous case → similar results

Test case with high heat flux

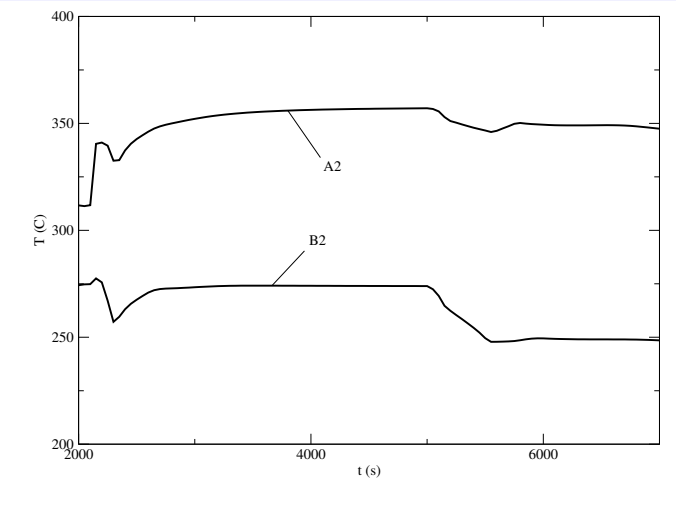

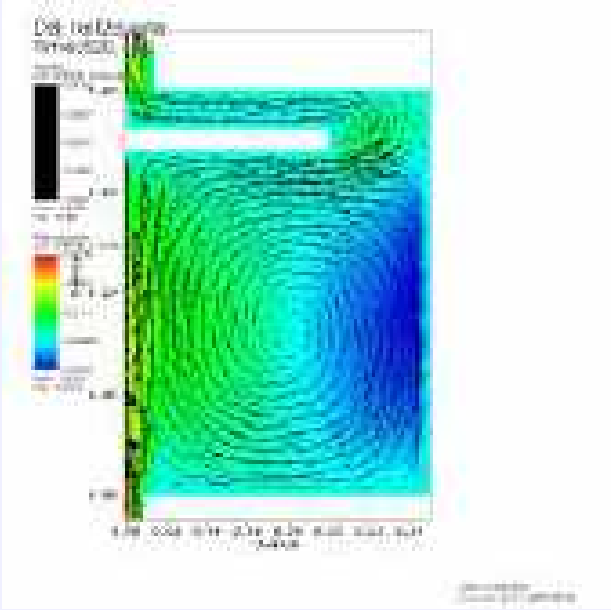

Temperature before (B) and after (A)

Test with enhanced Natural convection + $\kappa - \epsilon$ turbulent model)
COUPLING TRIOU-CFD + CATHARE 1D → VISIT (VTK no HDF5)
work in progress

TALL-3D with open-source codes in platform (SALOME-OPENFOAM)

FEMLCORE-SALOME-CATHARE + OPENFOAM

OPENFOAM: taking advantage of other researcher expertise

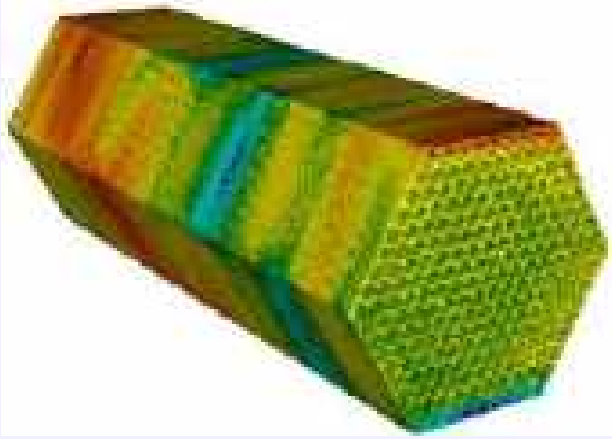

Solvers for
DNS
Incompressible Navier Stokes
Heat Transfer
Compressible Navier Stokes
Turbulence models
Combustion
Multiphase flow
Solid Mechanics
Particle tracking

OPENFOAM released by OpenCFD Ltd
Dynamical and thermal turbulence for liquid metals (KIT and VKI)

Numerical code coupling

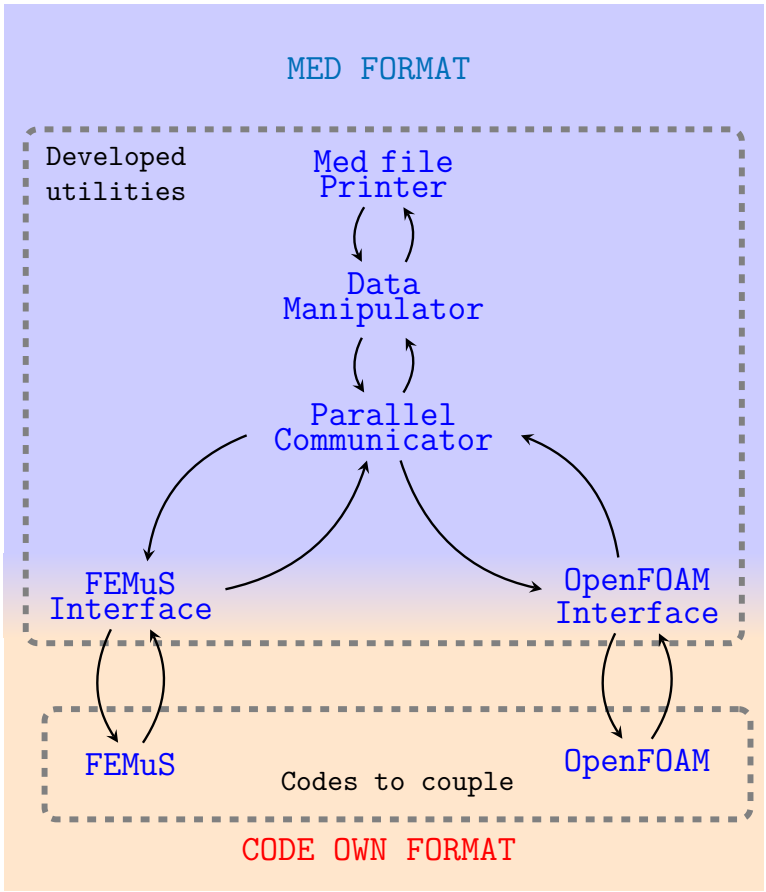

- OpenFoam Interface with MED-HDF5
  - Extract solution from code format to MED-format
  - Set a MED field in code solution
  - Set MED field as external field

Numerical code coupling

Projection of P2 fields

`Data Manipulator` class

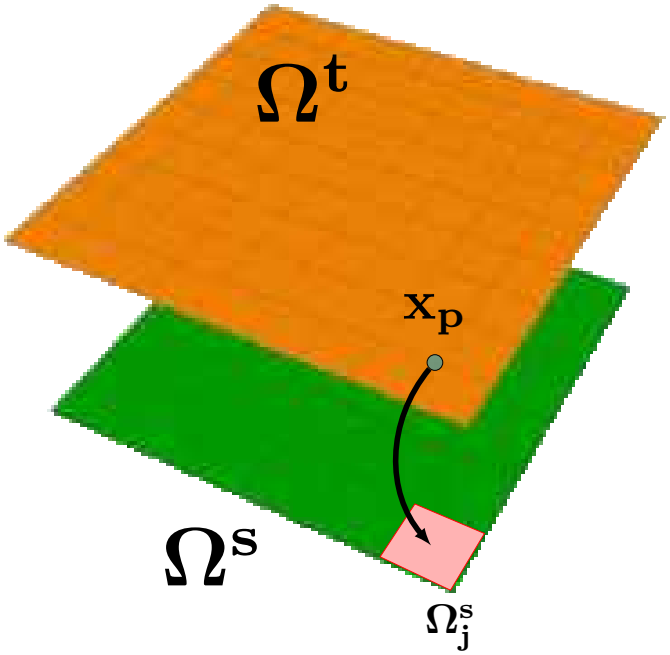

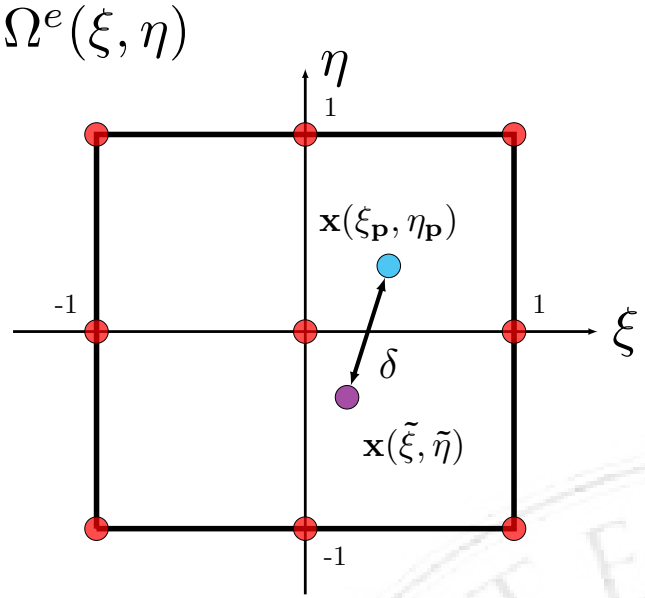

- $\boldsymbol{\xi_p}$: $min\left(\delta^2(\mathbf{x_p},\tilde{\boldsymbol{\xi}})\right) \rightarrow \delta^2(\mathbf{x_p},\tilde{\boldsymbol{\xi}}) = \sum_{i=1}^{dim}\left(x_p^i - \sum_{I=1}^{n_n} x_I^i \phi_I(\tilde{\boldsymbol{\xi}})\right)^2$
- $\Psi^t(\mathbf{x_p}) = \sum_{I=1}^{n_n} \Psi^s(\mathbf{x_I})\phi_I(\boldsymbol{\xi_p})\,, \qquad \mathbf{x_I} \in \Omega_j^s\,,\ \mathbf{x_p} \in \Omega_j^s$
- $\boldsymbol{\Psi}^t = \mathbf{P}\boldsymbol{\Psi}^s$

Defective coupling 3D-CFD + CATHARE 1D

Defective coupling: overlapping mesh

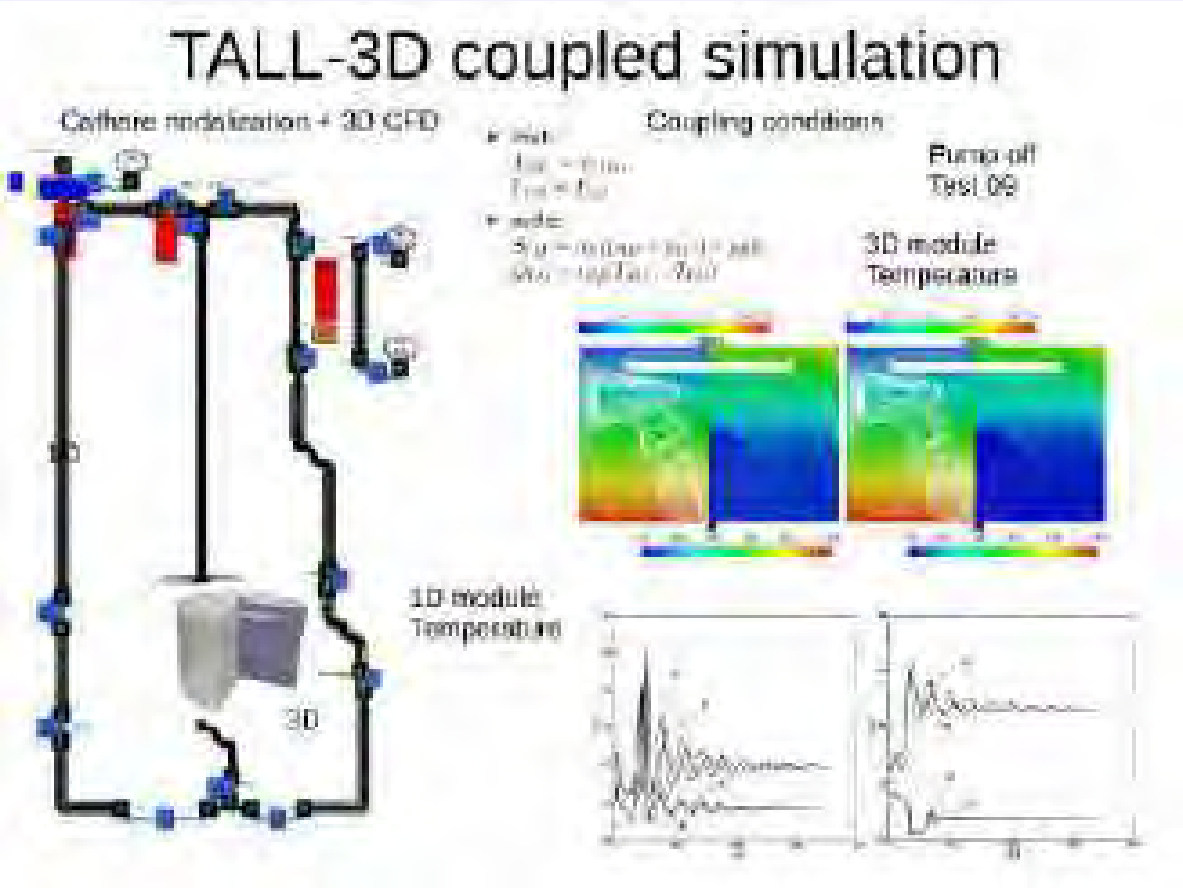

- inlet:
  $\dot{m}_{3D} = \dot{m}_{1D}$,
  $T_{3D} = T_{1D}$
- outlet:
  $S_{1D} = \alpha_S(p_{3D} - p_{1D})$
  $Q_{1D} = \alpha_Q(T_{3D} - T_{1D})$

Test 9: pump failure (Natural convection)
COUPLING OPENFOAM-FEMLCORE 3D + CATHARE 1D
OPENFOAM $\rightarrow$ turbulence models

Simulation settings: natural convection

Geometry and Boundary conditions

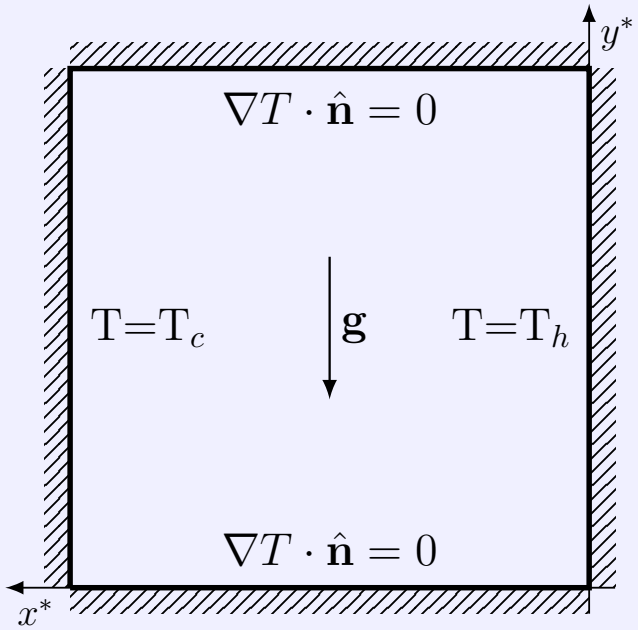

- Squared cavity with side 0.1 m
- $\mathbf{u} = 0$ on all boundaries
- Thermal insulation on upper and lower boundaries
- Fixed temperature on left and right sides

ν [m^2/s]	α [m^2/s]	g [m/s^2]	β [1/K]
0.01	0.002	9.81	10

- Simple and well studied case

Simulation settings

Simulated cases

OpenFOAM

- T_{OF} solver
- NS solver
  - $\tilde{T}_{OF}$ source buoyancy

FEMuS

- T_{FM} solver
- NS solver
- $\tilde{T}_{FM}$ source buoyancy

CASE

CASE A - OF: $T_{OF} \rightarrow \tilde{T}_{OF}$ FEMuS: $T_{FM} \rightarrow \tilde{T}_{FM}$
CASE B - FEMuS: $T_{FM} \rightarrow \tilde{T}$, $T_{FM} \rightarrow \tilde{T}_{OF}$
CASE C - OF: $T_{OF} \rightarrow \tilde{T}_{OF}$, $T_{OF} \rightarrow \tilde{T}_{FM}$

Coupling Case A

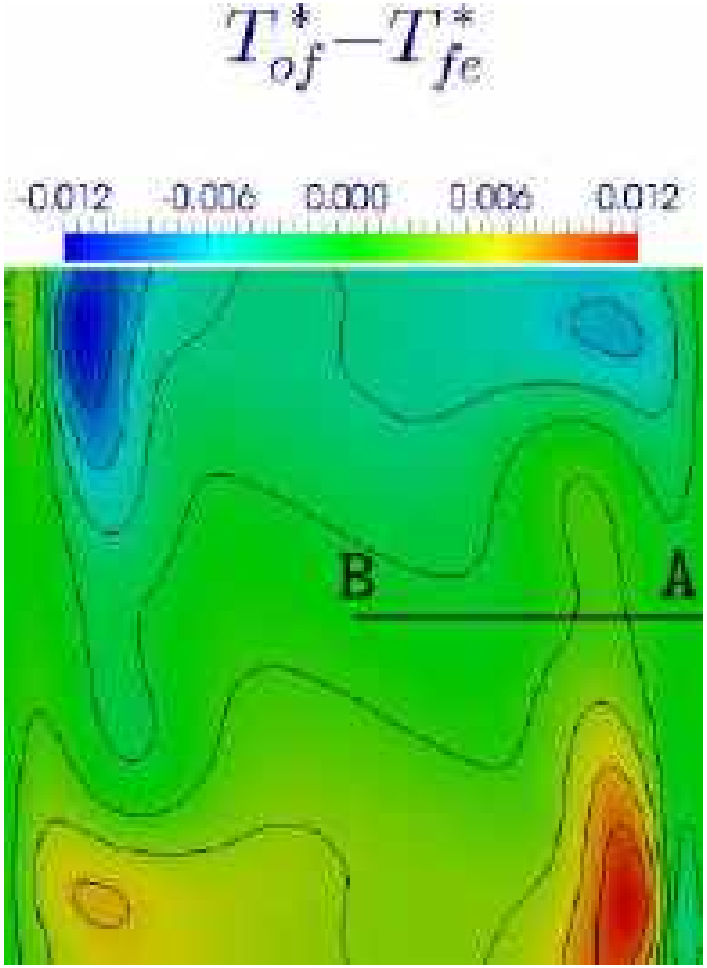

- $T^* = (T - T_c)/(T_h - T_c)$
- $v^* = v * L/\alpha$

	v^*_{max} on A - B	
Grid size	FEMuS	OpenFOAM
20×20	73.51	67.99
40×40	73.48	73.93
80×80	73.48	73.98
Reference	70.63	

- OpenFOAM T higher near hot wall and smaller near cold wall

Coupling Case B

- FEMuS 20x20, OpenFOAM 40x40

B1 B2

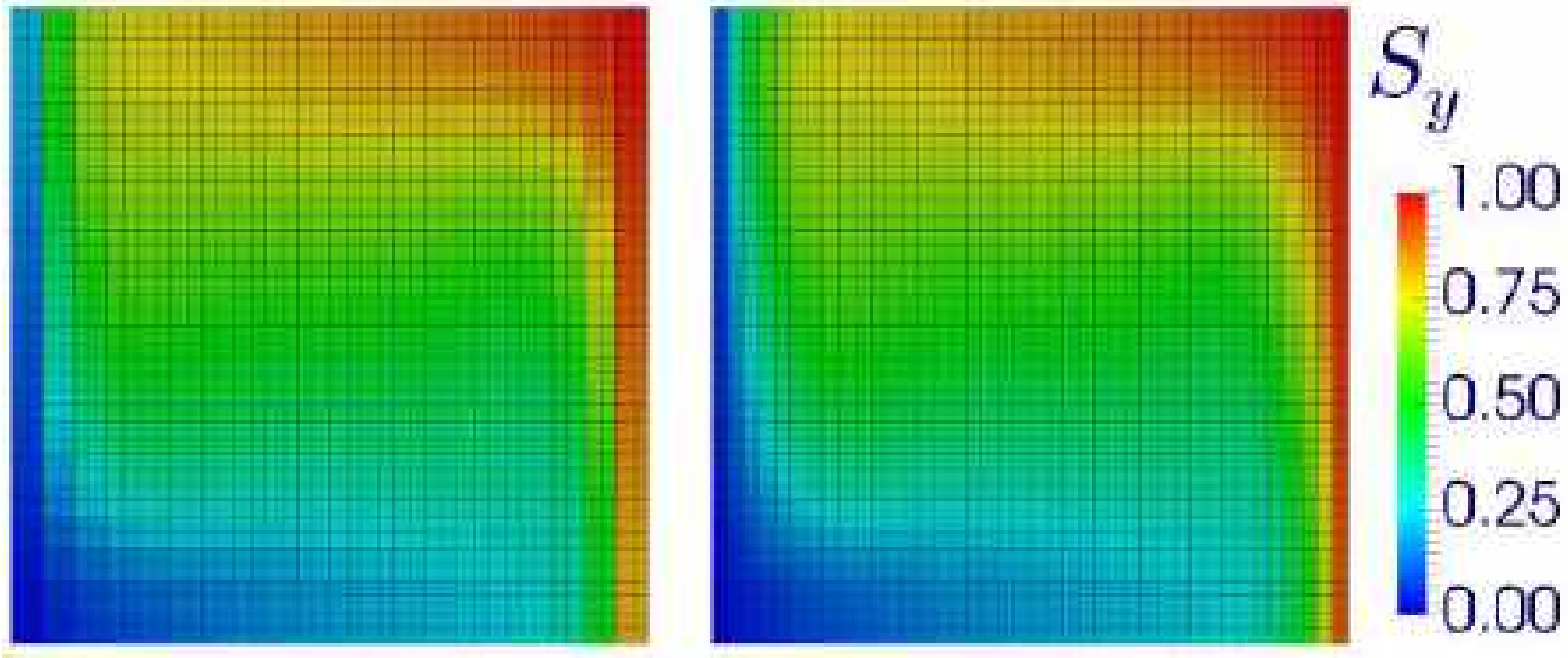

v^*_{max} on A-B	FEMuS	OpenFOAM A	OpenFOAM B1	OpenFOAM B2
	73.51	73.93	75,76	73,24

Coupling Case C

- FEMuS 20x20, 40x40, 80x80, OpenFOAM 20x20

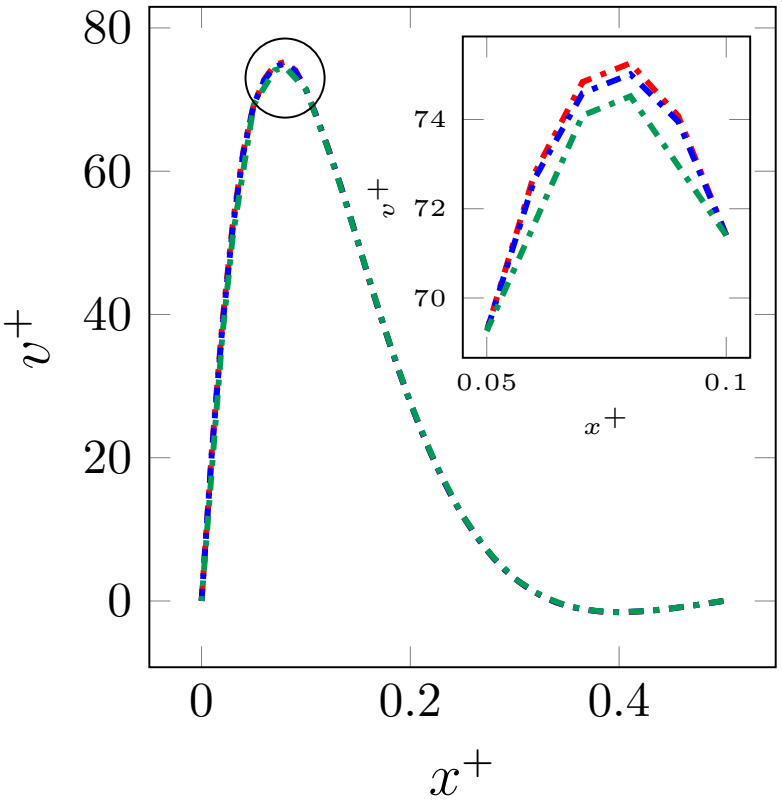

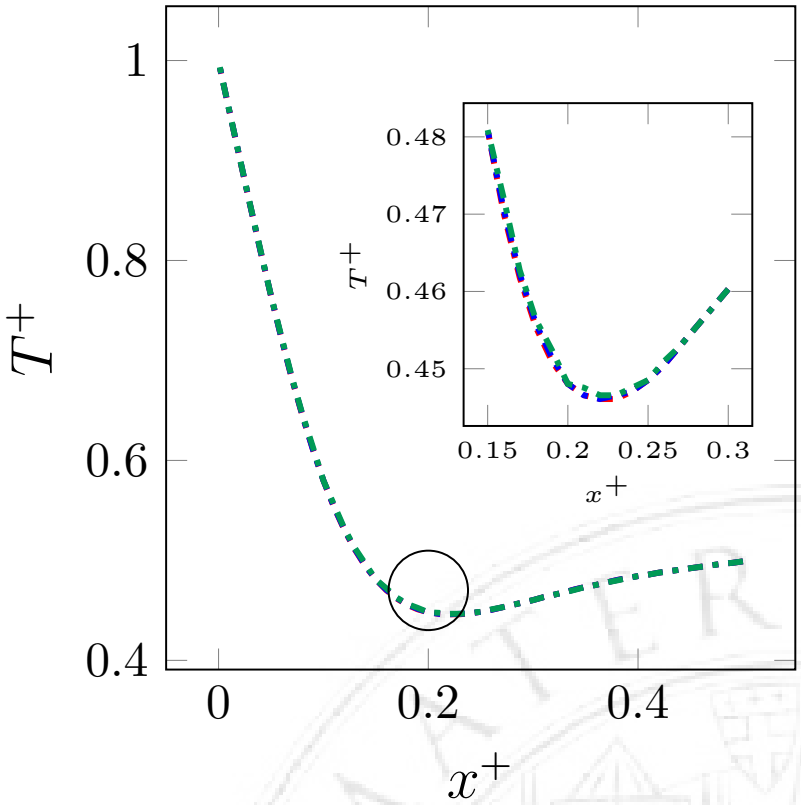

v^*_{max} on A-B	FEMuS 20	FEMuS 40	FEMuS 80
	74,52	75	75,25

Coupling Case C

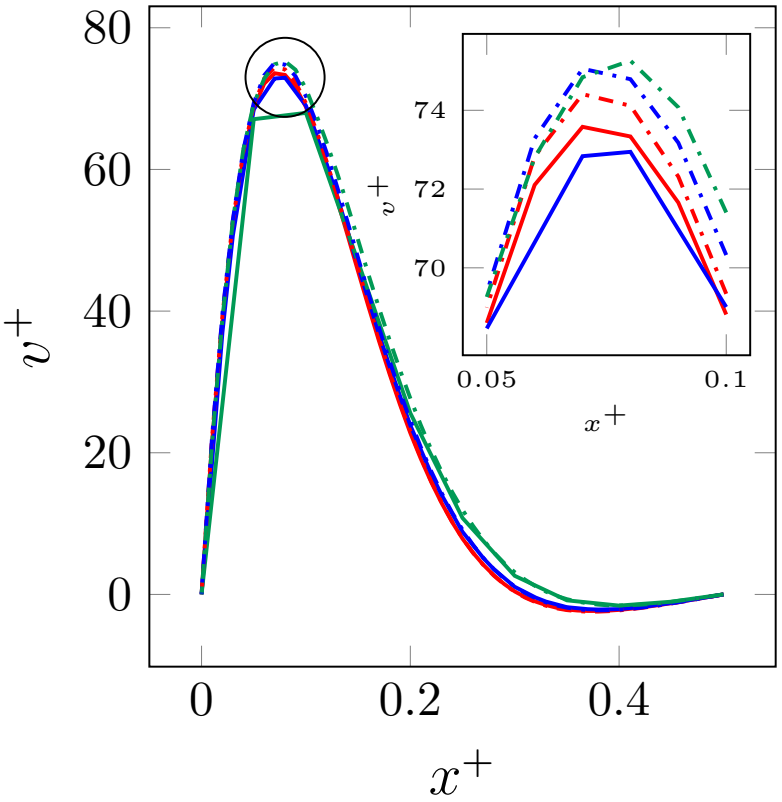

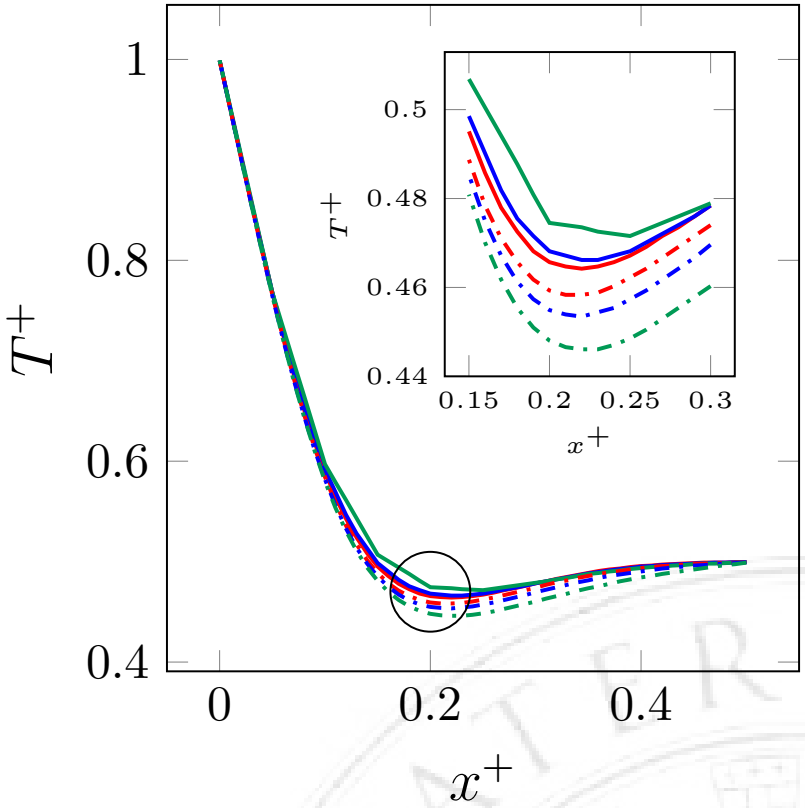

- OpenFOAM domain discretization: 20x20, 40x40, 80x80
- FEMuS domain discretization: 80x80
- OpenFOAM solution: solid line, FEMuS solution: dashed

Conclusions

Conclusions

Working

- We are working on the TRIOUCFD-CATHARE-SALOME coupling interface (all nuclear tested codes)
- We are working on OPENFOAM-SALOME coupling interface
- We are working on CEA nuclear codes + open-source codes + in-house codes on SALOME platform

TALL-3D experiment

- Comparison with old and new experimental results

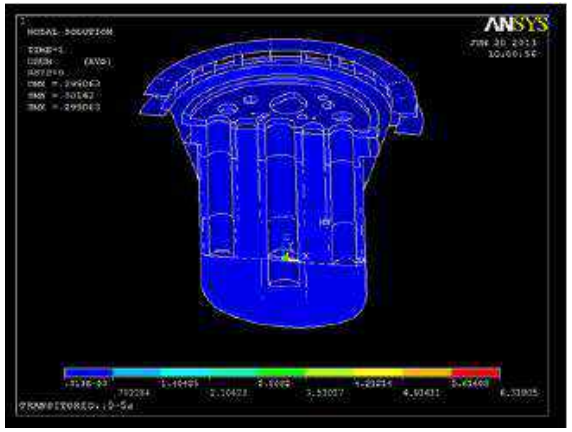

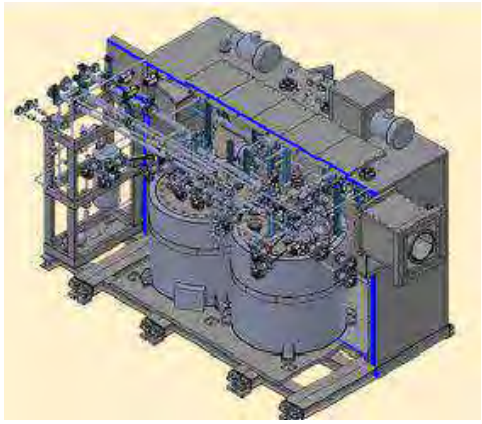

S.R.S. Servizi di Ricerche e Sviluppo S.r.l.

SRS PRESENTATION

ULISSE PASQUALI
14.06.2018

Summary

Summary

1.COMPANY PROFILE

S.R.S. Servizi di Ricerche e Sviluppo S.r.l.:

- is a SME with a 40-years experience in the field of design and engineering of processes, plants and machineries in several technological sectors mainly in the Nuclear sector
- Offers multidisciplinary engineering services in the design of equipment, systems and civil structures and provides services related to decommissioning activities of nuclear installations and Nuclear Waste Mangaement
- Supplies, “as turn-key “, components and systems for nuclear application, including complete complex experimental facilities useful to test innovative components, as well as demonstration of component/plant behavior in any operational and accidental condition
- Belongs to SRS GROUP, which is a cluster of Companies whose characterizing feature is the capability in tackling new and complex engineering problems, always finding a solution, looking at cost effectiveness and at time scheduling

2

ORGANIZATION & SKILL

2.ORGANIZATION & SKILL

The engineering production capacity of the company is over 70,000 h/year, achieved mainly through internal resources.

SRS has the availability of high skilled external staff able to immediately operative, thank to a proven network of cooperation with the other companies of SRS GROUP and with specialized companies, supported by specific cooperation agreements.

The whole staff (including external staff) is about 100 unit (more than **175,000 h/year**).

The technical structure include **five technical areas or divisions**. Each area has a technical responsible with a managing role coordinating the project activities.

The technical areas are:

- Nuclear;
- Mechanical;
- Civil;
- Electrical, automation and Instrumentation;
- Process and Chemical.

2.ORGANIZATION & SKILL

NUCLEAR DIVISION

S.R.S. capabilities deal with all aspects of nuclear safety and radiological protection for nuclear installations, in particular:

- Nuclear installation safety analysis, including:
  - Identification and selection of initiating events;
  - Probabilistic, deterministic and hybrid safety assessments;
  - Calculation of doses and radiological impact on workers and population;
- Criticality and burn-up calculations; fuel loading strategies;
- Reliability analysis of reactivity control systems, power distribution calculation in sub-critical and critical systems, reactivity coefficients calculation;
- Radiation shielding analysis and design;
- Evaluation of radiation doses to exposed individuals and population;
- Evaluation of integral radiation doses to materials;
- Fluid-dynamic and thermal-hydraulic calculations, intransient and steady state conditions, in support to core and system design, in operational and accident scenarios.

The analysis are carried out according to international and national standards and rules, namely ANS, ANSI, ASME, IEEE, DOE, NUREG, SMACNA, ISO, IAEA, ICRP, CEI IERC, UNI and UNI EN.

2.ORGANIZATION & SKILL

MECHANICAL DIVISION

S.R.S. capabilities includes:

- Process definition, concept analysis and feasibility studies;
- Design of complex mechanical systems, as nuclear systems (primary circuit components, reactor auxiliary systems, nuclear and non-nuclear), heating, ventilation, and air conditioning systems, liquid/solid/gaseous waste treatment facilities, fire-control systems and mechanical systems in general as per international industrial standards and nuclear safety rules; (AMSE, ANSI, API, IEEE, IAEA, EUR, DIN, UNI EN, ASME AG-1, ISO, NUREG, etc.)
- Structural analysis as per Italian regulations (UNI, PED);
- Structural analysis as per US and international nuclear standards (ASME III, ANSI, ASME AG-1, NUREG, ANS);
- Non-linear structural analysis;
- Preparation of technical specifications, engineering analysis reports, project development time schedules and cost estimates;

2.ORGANIZATION & SKILL

CIVIL DIVISION

S.R.S. capabilities includes:

- Architectural design;
- Reinforced concrete structural design;
- Steel structure design;
- Structural analysis as per Italian rules and regulations;
- Structural analysis as per US regulation (ACI) and nuclear standard;
- non-linear structural analysis, static and dynamic (time histories);
- Preparation of technical specifications engineering calculations reports, project development time schedules and cost estimates.

3

COLLABORATION WITH ENEA

3.COLLABORATION WITH ENEA

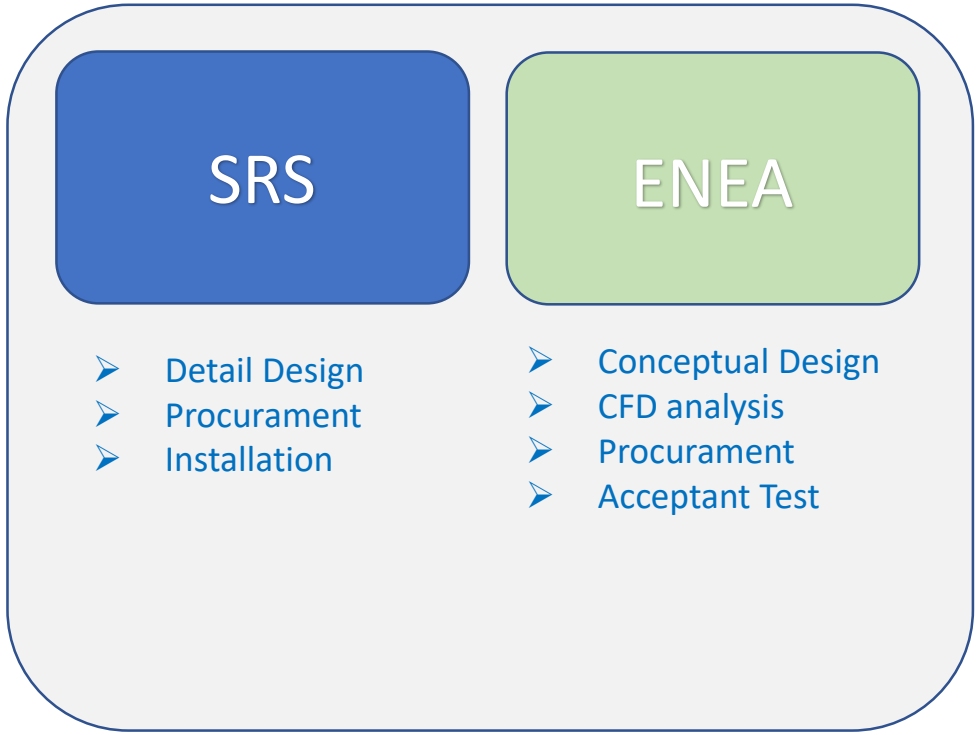

- SIRIO Project (ALFRED)
- ELF Project (ALFRED)
- KYLIN-II (CHINA)
- CLEAR-S (CHINA)
- CLEAR-M1X (CHINA)

3.COLLABORATION WITH ENEA

SIRIO PROJECT

PARTNER:

- SRS
- ENEA
- ANSALDO NUCLEARE
- SIET

OBJECT:

The SIRIO project is an experimental facility which aim is to test the Decay Heat Removal System (DHRS) proposed by Ansaldo Nucleare within the project of the ALFRED Lead Fast Reactor.

The system mainly consists of:

- A steam generator (SG);
- An in-pool condenser (Isolation Condenser);
- A non-condensable tank;
- Piping system equipped with valves (On/Off and control)

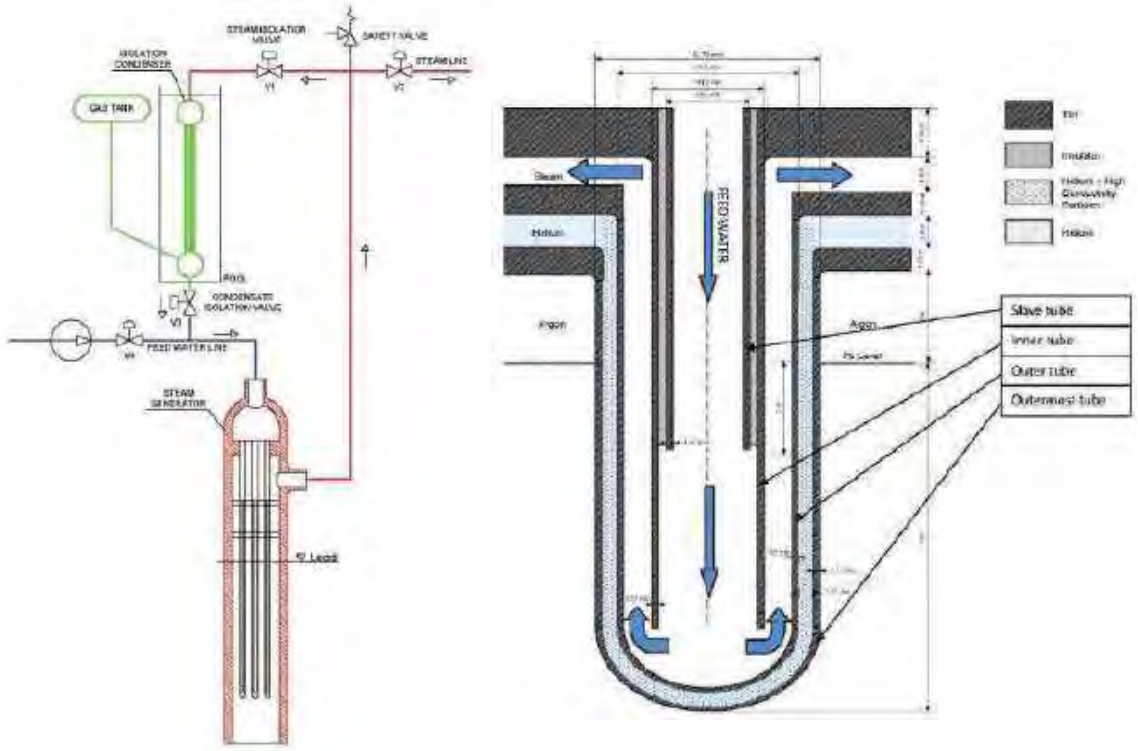

3.COLLABORATION WITH ENEA

ELF PROJECT

PARTNER:

- SRS
- ENEA

OBJECT:

The European Lead Fast facility (ELF) is conceived to investigate thermal hydraulic phenomena in a pool type configuration reproducing the main coolant flow path of the primay system of the ALFRED Reactor.
The facility consists of a main vessel filled with molten pure lead as working fluid and hosting the Core Simulator (10 MW).

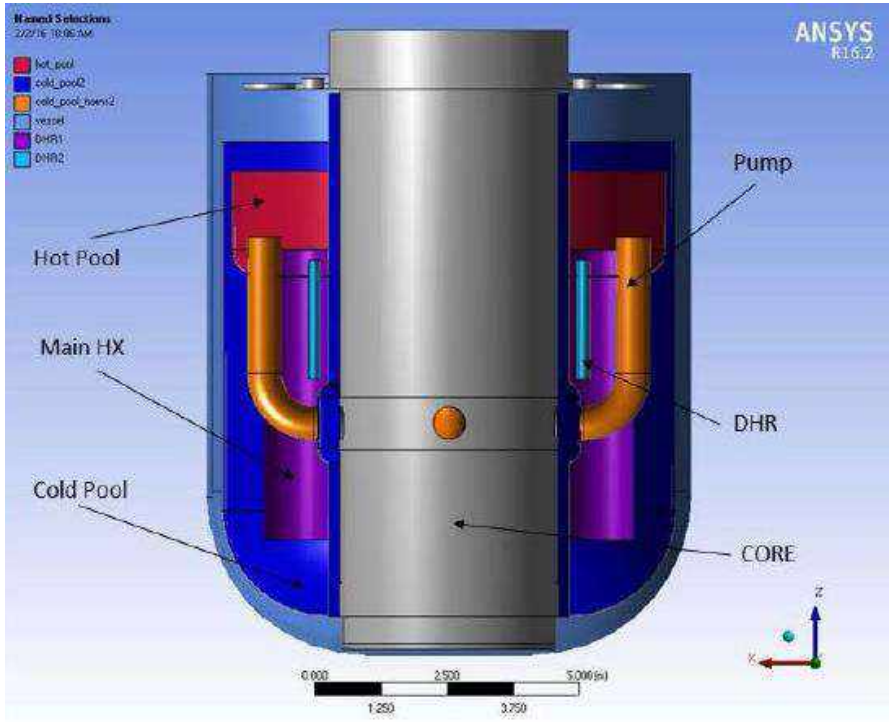

4

CHINESE MARKET

4.CHINESE FACILITY

- Since 15 years ENEA Brasimone is promoting its wide experience in heavy metal experimental facility in the chinese market;
- This is a big chance for the italian company and SRS has put all its effort to support ENEA in this challenge;
- The chinese governement is strongly interested in the **LEAd-based Reactor** and it is putting a lot of funds in different projects which support the design, licensing and construction of the nuclear reactor CLEAR-1.
- Walking this line, ENEA and SRS have been working together since 2012

2012-2014

KYLIN-II (250 Kw)

2014-2017

CLEAR-S (2,5 MW)

2018-on going

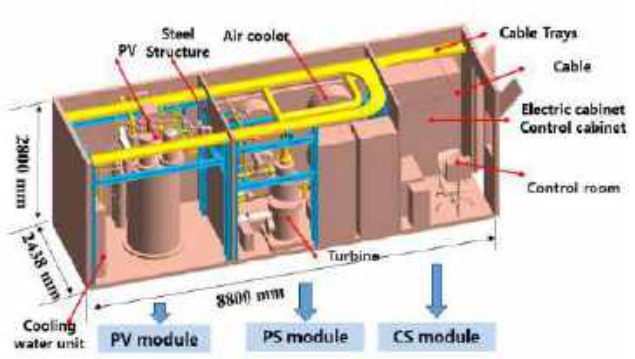

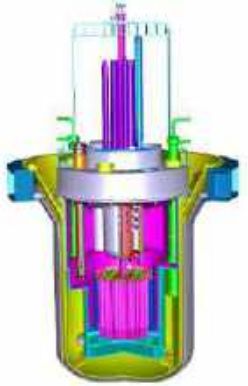

CLEAR-M1X (1,1 MW)

CLEAR-1 (10 MW)

5

CLEAR-S FACILITY

5.CLEAR-S FACILITY

CLEAR-S:

- LBE LOOP
  - 220 ton of LBE
  - T=450 °C
- WATER LOOP
  - T=300°C
  - P=120 barg
- ELECTRICAL SYSTEM
  - Power 2,5 Mwe
- CONTROL SYSTEM
  - N.1500 I/O signals (TC,PT, etc)
- VENTILATION SYSTEM
  - Air flow 60.000 m^3/h
- CIVIL STRUCTURE
  - N.5 floor

5.CLEAR-S FACILITY

DESIGN STEPS

Conceptual design by ENEA:
- Conceptual P&I
- CFD analysis
- Components pre-design

Detailed design by SRS:
- Pressurized components design
- Piping thermal-stress analysis
- Electrical system design
- Metallic structure design
- Control system software

Assembly and test by SRS-ENEA

5.CLEAR-S FACILITY

INTERNALS: DESIGN & REALIZATION

ASSEMBLY

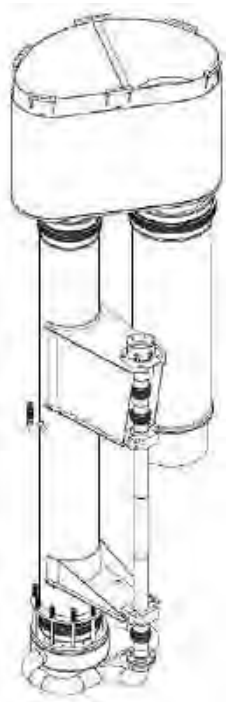

Core Simulator coupling

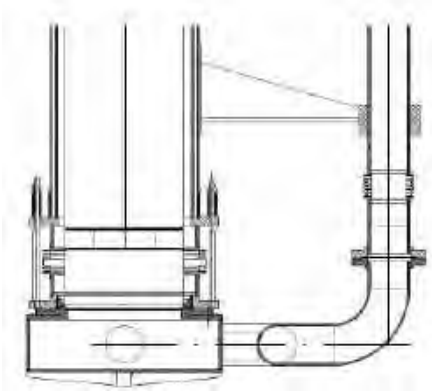

Pump coupling

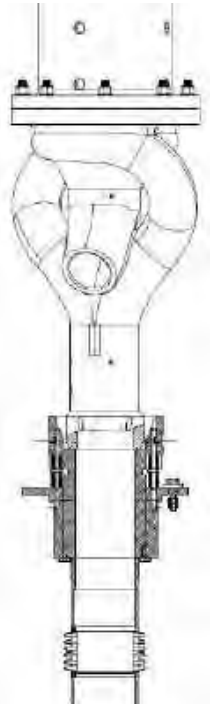

5.CLEAR-S FACILITY

HEAT EXCHANGER:DESIGN & REALIZATION

- N.127 bayonet tube
- Material AISI 316
- Design Pressure: 120 barg
- Design Temperature: 270 °C
- ASME VIII Div.2

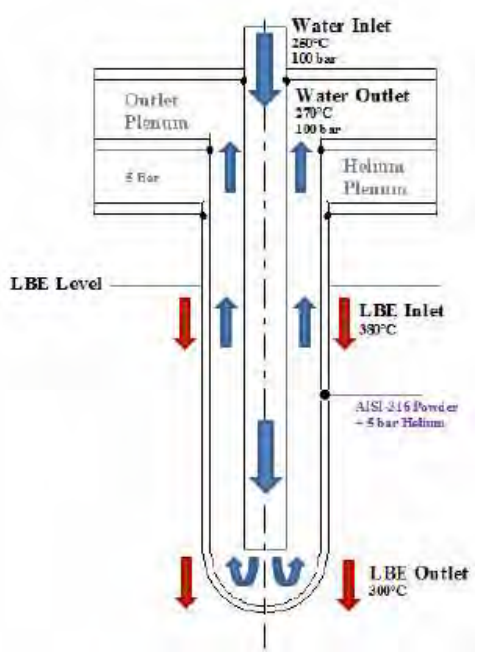

Bayonet layout

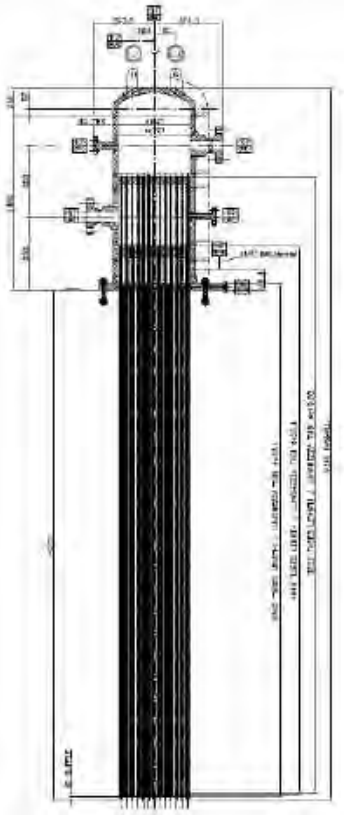

5.CLEAR-S FACILITY

CODE & STANDARDS

PRESSURIZED VESSEL:
- Design according to ASME VIII DIV.1-2
- Certification according to PED

PIPING:
- Design according to ANSI B31.1
- Certification according to PED

METALLIC STRUCTURE:
- EUROCODE 0-1-3-8

ELECTRICAL SYSTEM:
- IEC 61439-1/2

6

NEXT CHALLENGES

6.NEXT CHALLENGES

LEAD-BASED REACTORS

SRS ENEA

- CLEAR-M1X
- CLEAR-M
- CLEAR-1

- ALFRED
- FALCON

WORK IN PROGRESS…

THANK YOU

WORKSHOP TEMATICO
PAR 2017

GENERATION IV LEAD COOLED FAST REACTOR

STATO ATTUALE DELLA TECNOLOGIA E PROSPETTIVE DI SVILIUPPO

CIRCE-HERO experiment overview

A. Pesetti

(alessio.pesetti@for.unipi.it)

14-15 June 2018, Roma

List of contents

- Introductory remarks & objectives
- CIRCE facility and HERO test section
- HERO Test Section
  - Primary system LBE
  - Secondary system H_2O
  - Instrumentation
- CIRCE-HERO DACS
- CIRCE-HERO commissioning (heat losses tests)
- Experimental campaign Test Matrix
- Conclusive remarks

Introductory remarks & objectives

RESEARCH MOTIVATION

- ALFRED reactor design includes an innovative concept of Steam Generator, adopting double walled bayonet tubes (SGBT)
- Characterised by two barriers between primary and secondary coolant and a leakage monitoring system in between (He + high K powder @ ~10 bar)
- R&D is needed for characterising SGBT performance in steady-state and transient conditions

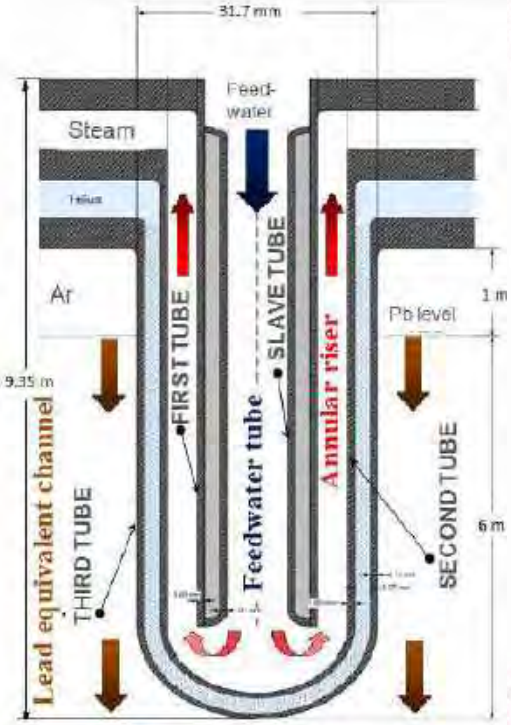

H2O inlet @ 335°C, steam outlet @ 450°C, 180 bar, 0.047 kg/s

LBE @ 400÷480°C, 6.36 kg/s

cover gas @ low pressure gauge

MAIN ACTIVITIES and OBJECTIVES

- A mock-up of 7 BTs relevant for ALFRED SG was designed, assembled and implemented in HERO test section at ENEA CR Brasimone
- An experimental campaign of 3 forced to natural circulation transition will be carried out (1 run SESAME bench.)
- Engineering and safety feedbacks for designer and high quality data for code validation/model development

CIRCE facility and HERO test section

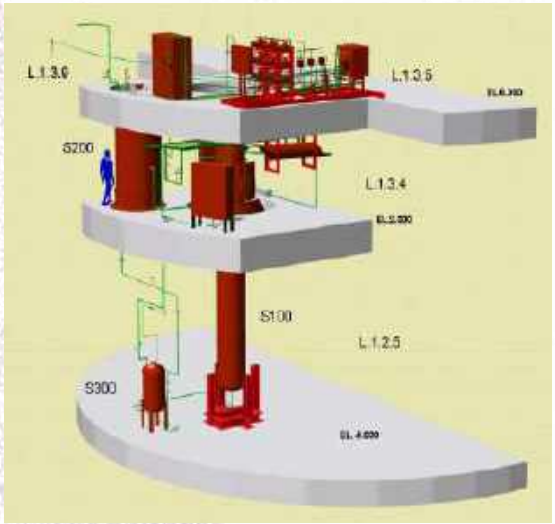

CIRCE Parameters	Value
Outside diameter [mm]	1200
Wall thickness [mm]	15
Material	AISI 316L
Max LBE Inventory [kg]	90000
Electrical Heating [kW]	47
Temperature Range [°C]	200 to 500
Operating Pressure [kPa]	15 (guage)
Design Pressure [kPa]	450 (gauge)
Argon Flow Rate [Nl/s]	15
Argon Injection Pressure [kPa]	600 (gauge)

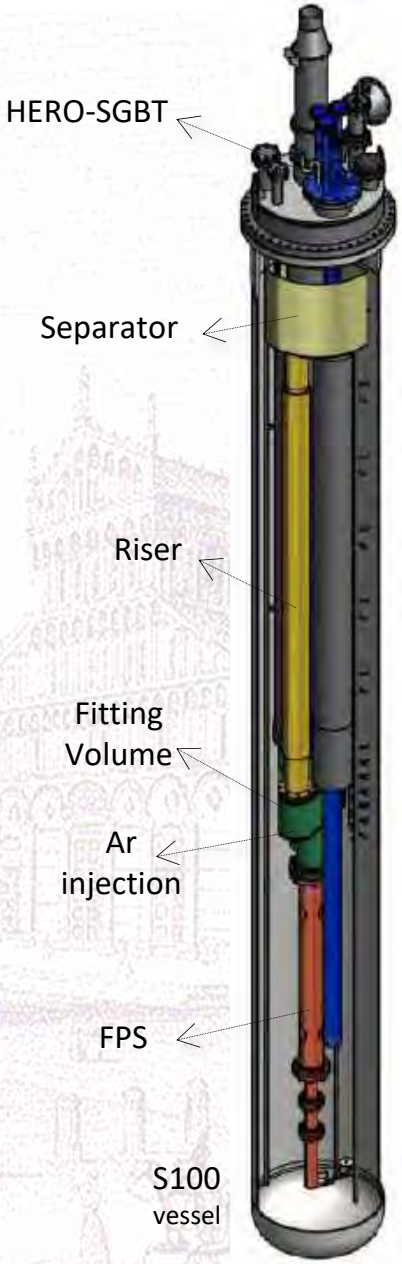

HERO TS primary system

HERO TS primary system

HERO TS implemented in CIRCE main vessel

HERO TS secondary system

SGBT set in HERO TS

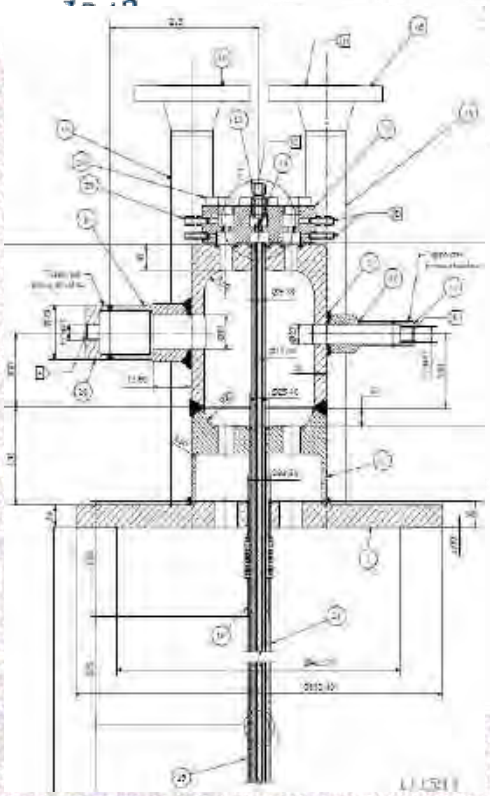

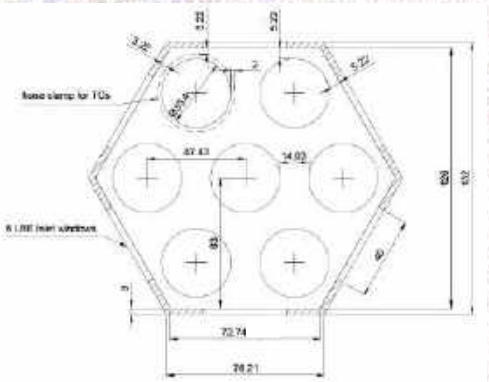

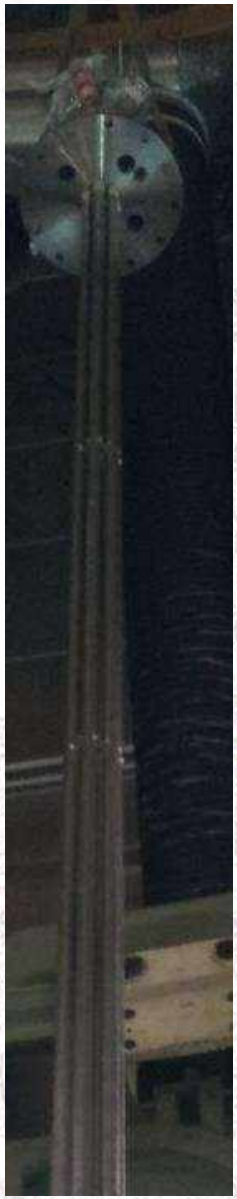

Double-Walls BT	Inner diameter [mm]	Outer diameter [mm]	Thickness [mm]	Material --
Feed-water slave tube	7.09	9.53	1.22	AISI-304
Feed-water tube gap	9.53	15.75	3.11	Slight vacuum
First tube (feed-water outer tube)	15.75	19.05	1.65	AISI-304
Annular riser gap	19.05	21.18	1.07	Water-steam
Second tube	21.18	25.40	2.11	AISI-304
Annular gap	25.40	26.64	0.62	AISI 316 powder
Third tube	26.64	33.40	3.38	AISI-304

	Unit	Water-Steam side	He side	LBE side
Fluid	--	Water – steam	Helium	LBE
Circulation mechanism	--	Axial pump + accumulator	leakage accommodation	Gas enhanced
Main components	--	bayonet tubes, steam chamber	Helium chamber	SGBT unit shell
Bundle type and P/D	-	Triangular / 1.42	--	Shell
Inlet temp.	°C	335	--	480
Mass flow	kg/s	0.330785	stagnant	44.573529
Design pressure	bar	180	5.0	As CIRCE
Operating pressure	bar	172	4.5	Hydraulic head
Design temp.	°C	432	432	As CIRCE

HERO TS secondary system

HERO SGBT details

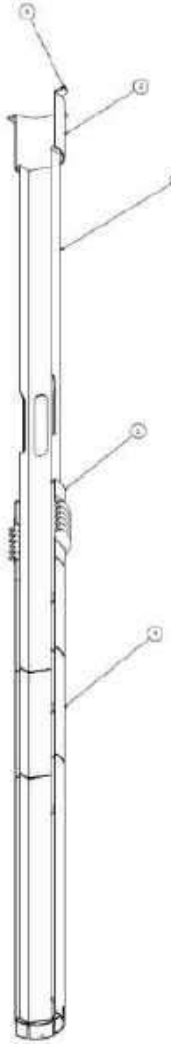

HERO TS instrumentation

HERO SGBT instrumentation, 48 TCs

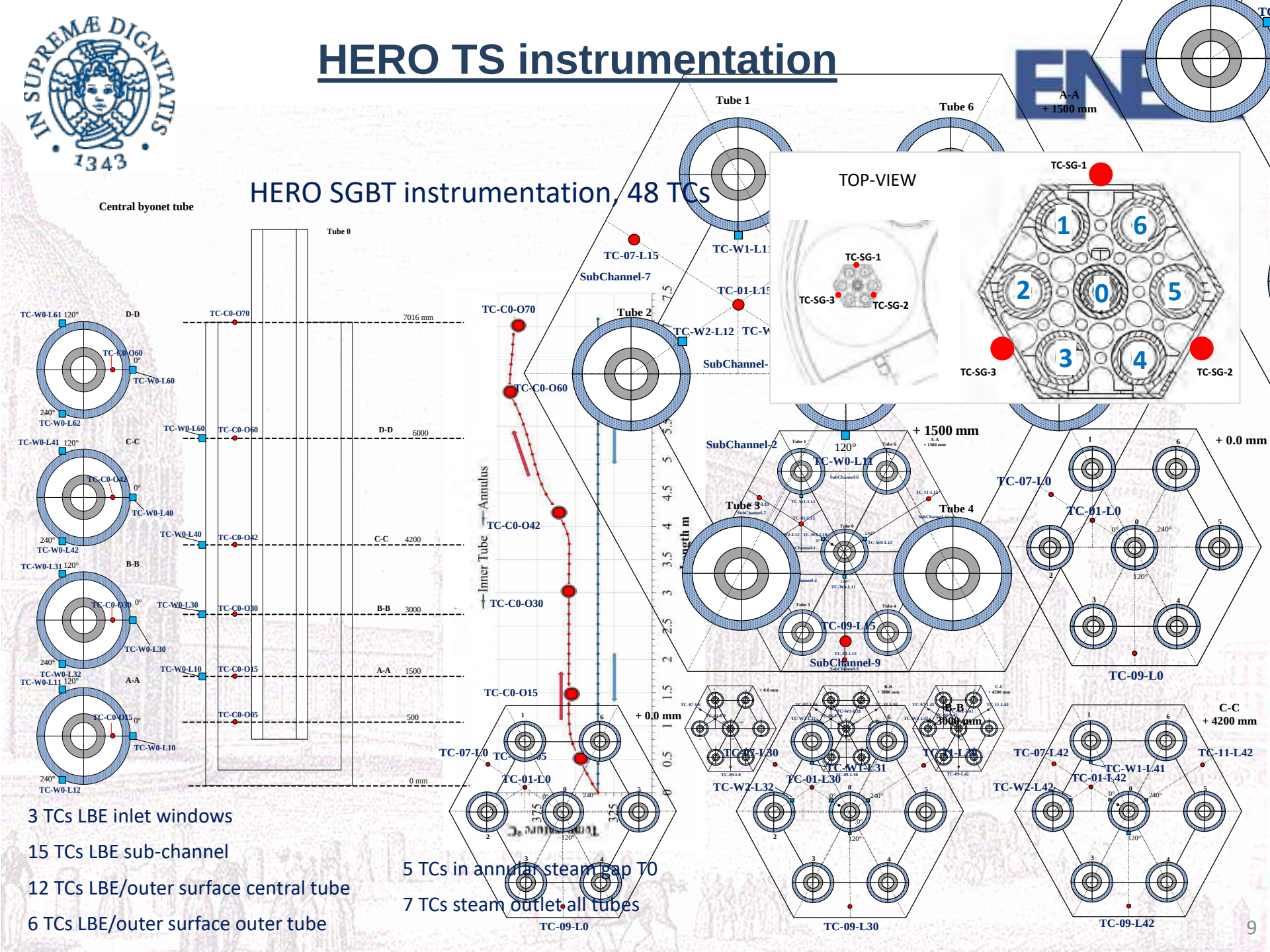

3 TCs LBE inlet windows

15 TCs LBE sub-channel

12 TCs LBE/outer surface central tube

6 TCs LBE/outer surface outer tube

5 TCs in annular steam gap T0

7 TCs steam outlet all tubes

HERO TS instrumentation

FPS→ 39 TCs (*N*-type 0.5 mm, ± 0.1°C)

Fitting volume→5 TCs (*N*-type 3 mm, ± 1°C)

Riser→6 TCs (*N*-type 3 mm, ± 1°C)

Cover gas→1 TCs

Heat Exchanger →48 TCs

Pool→122 TCs (*N*-type 3 mm, ± 1°C)

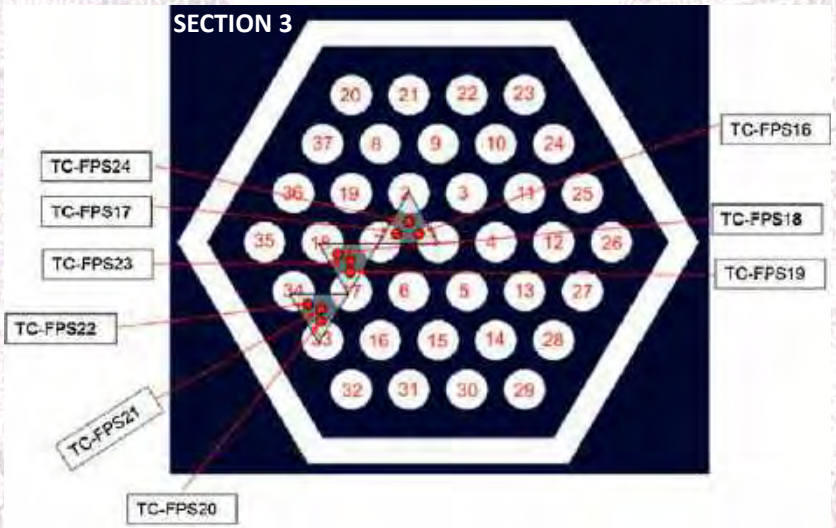

FPS TCs position

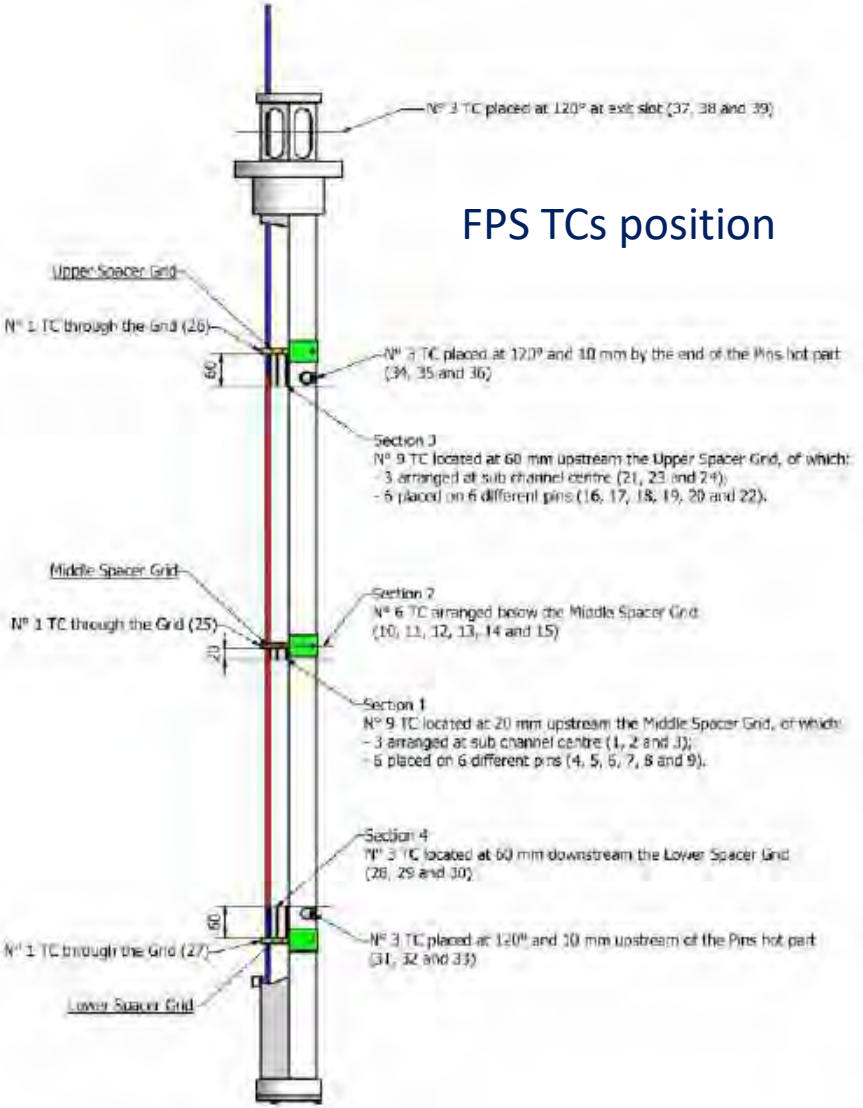

HERO TS instrumentation

FPS→ 39 TCs (*N*-type 0.5 mm, ± 0.1°C)

Fitting volume→5 TCs (*N*-type 3 mm, ± 1°C)

Riser→6 TCs (*N*-type 3 mm, ± 1°C)

Cover gas→1 TCs

Heat Exchanger →48 TCs

Pool→122 TCs (*N*-type 3 mm, ± 1°C)

TOP VIEW
FITTING VOLUME

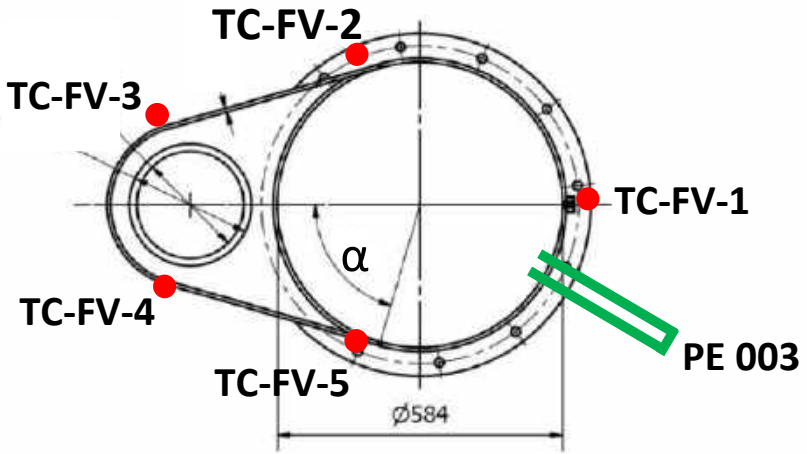

RISER TCs and BTs

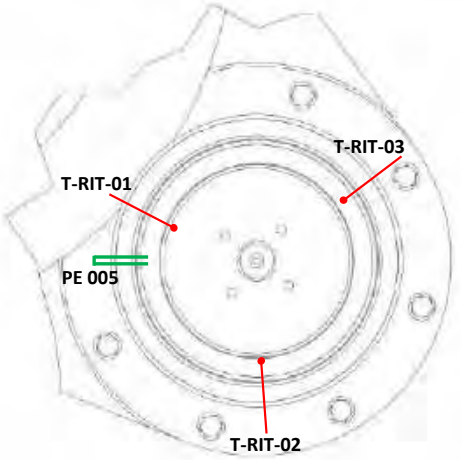

RISER TOP

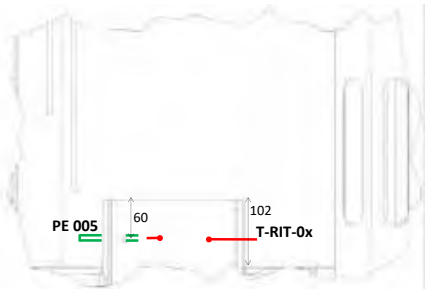

Horizontal section 60 mm below the RISER tube top
(TOP VIEW)

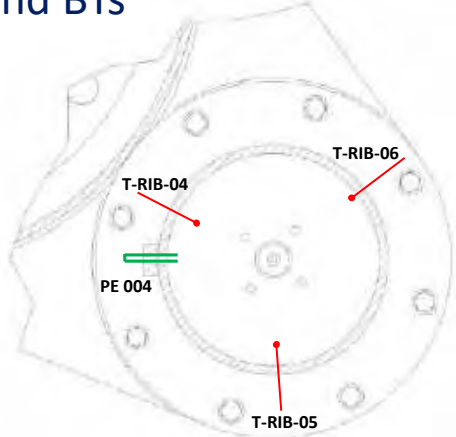

RISER BOTTOM

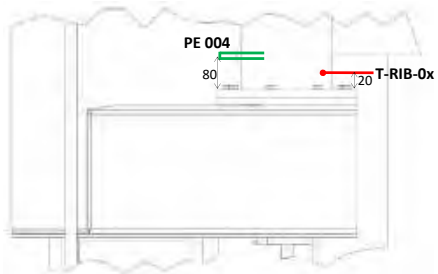

Horizontal section 80 mm above RISER bottom flange
(TOP VIEW)

HERO TS instrumentation

POOL MIXING and STRATIFICATION

CIRCE-ICE → CIRCE-HERO

pool mixing and stratification

FPS→ 39 TCs (*N*-type 0.5 mm, ± 0.1°C)

Fitting volume→5 TCs (*N*-type 3 mm, ± 1°C)

Riser→6 TCs (*N*-type 3 mm, ± 1°C)

Cover gas→1 TCs

Heat Exchanger →48 TCs

Pool→122 TCs (*N*-type 3 mm, ± 1°C)

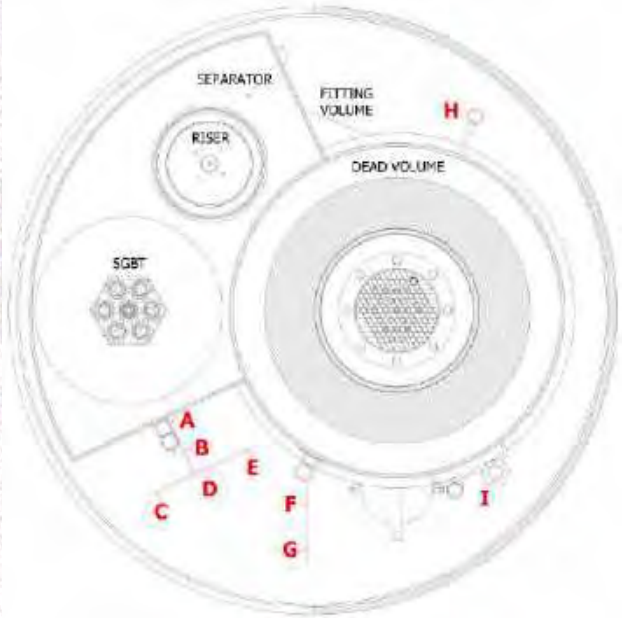

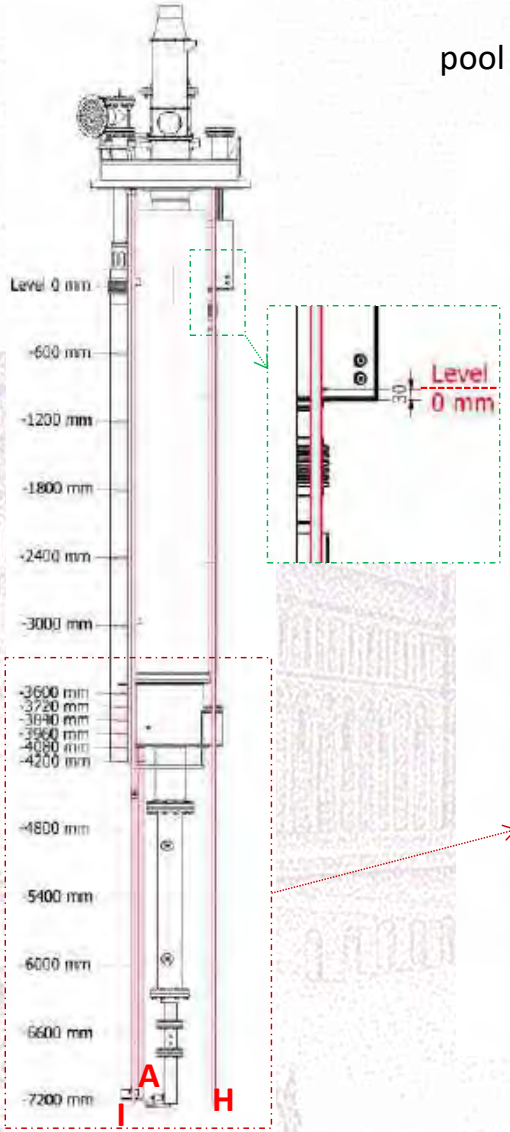

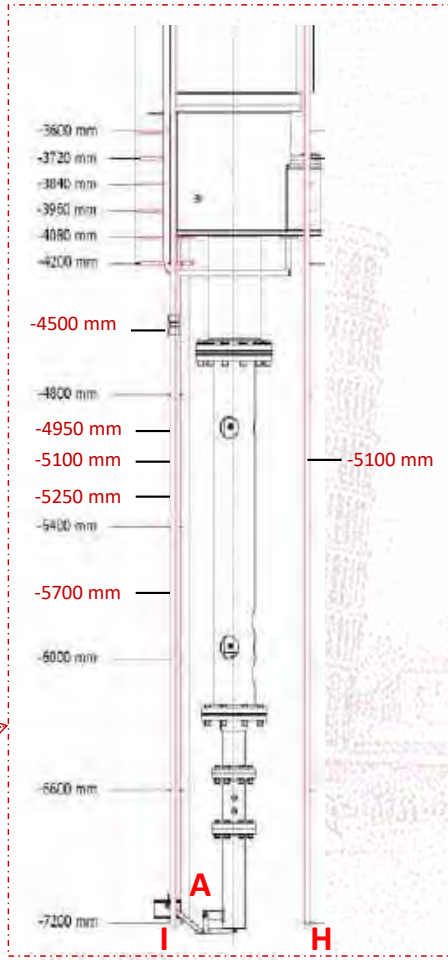

HERO TS instrumentation

Venturi flowmeter

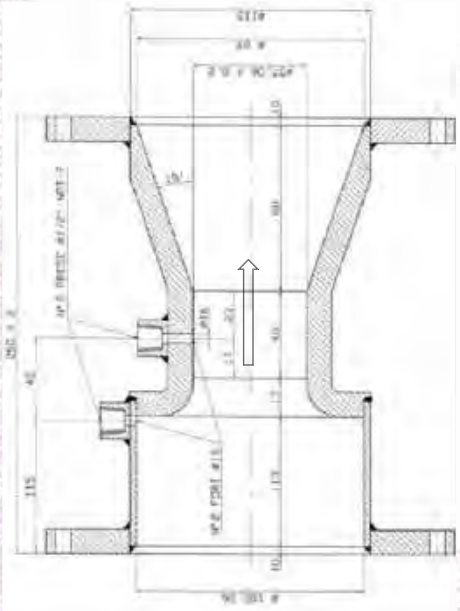

$$Qf = do^2\ 1.110674E\text{-}05\ K\ \sqrt{Dp\ Gf}$$

9 Bubble Tubes

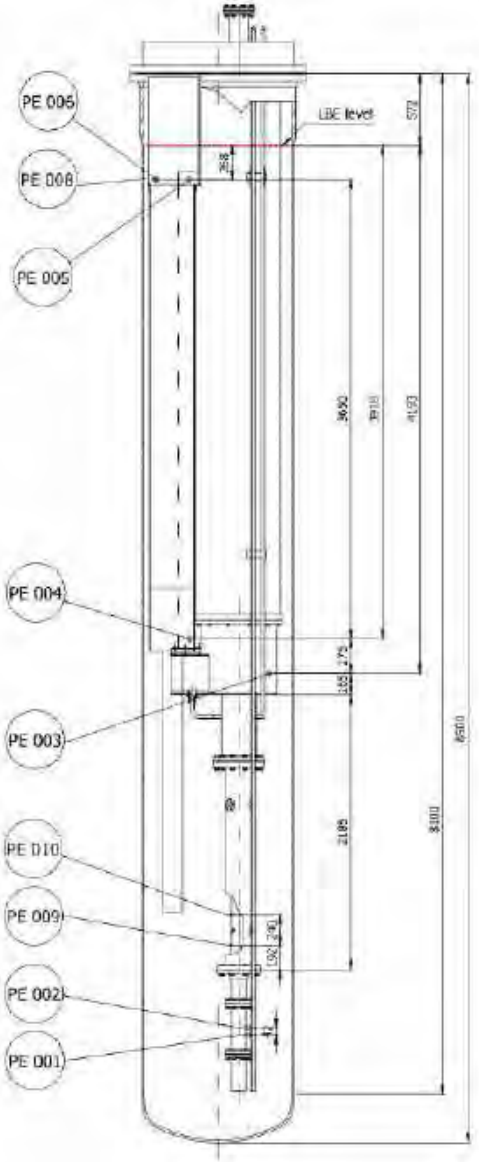

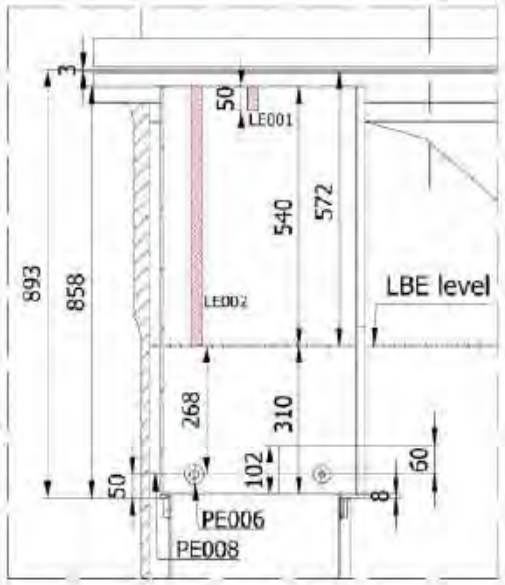

2 LBE level sensors in the separator

CIRCE-HERO 2^{ary} side components and instrumentation

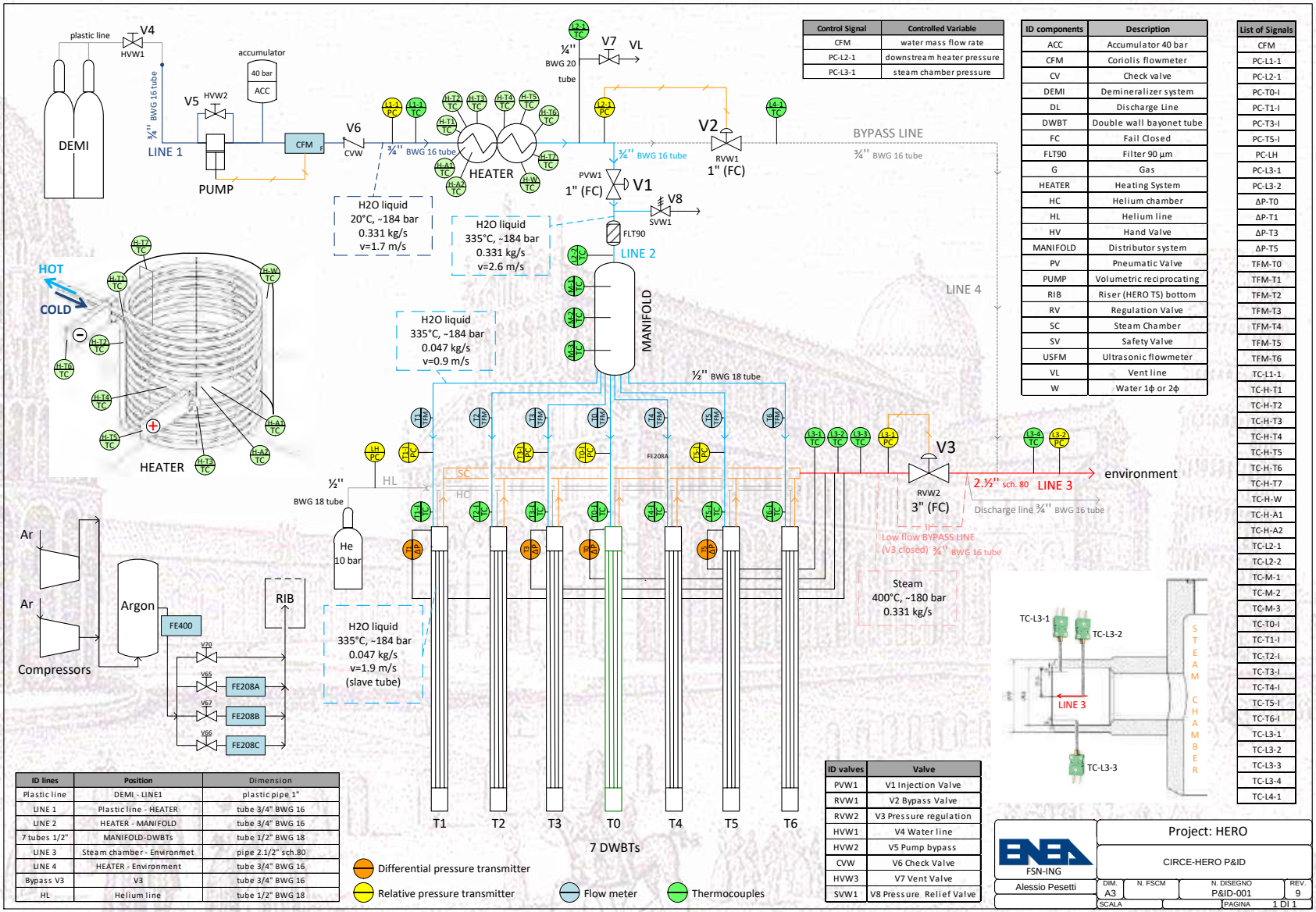

Control Signal	Controlled Variable
CFM	water mass flow rate
PC-L2-1	downstream heater pressure
PC-L3-1	steam chamber pressure

ID components	Description
ACC	Accumulator 40 bar
CFM	Coriolis flowmeter
CV	Check valve
DEMI	Demineralizer system
DL	Discharge Line
DWBT	Double wall bayonet tube
FC	Fail Closed
FLT90	Filter 90 µm
G	Gas
HEATER	Heating System
HC	Helium chamber
HL	Helium line
HV	Hand Valve
MANIFOLD	Distributor system
PV	Pneumatic Valve
PUMP	Volumetric reciprocating
RIB	Riser (HERO TS) bottom
RV	Regulation Valve
SC	Steam Chamber
SV	Safety Valve
USFM	Ultrasonic flowmeter
VL	Vent line
W	Water 1ϕ or 2ϕ

List of Signals
CFM
PC-L1-1
PC-L2-1
PC-T0-I
PC-T1-I
PC-T3-I
PC-T5-I
PC-LH
PC-L3-1
PC-L3-2
ΔP-T0
ΔP-T1
ΔP-T3
ΔP-T5
TFM-T0
TFM-T1
TFM-T2
TFM-T3
TFM-T4
TFM-T5
TFM-T6
TC-L1-1
TC-H-T1
TC-H-T2
TC-H-T3
TC-H-T4
TC-H-T5
TC-H-T6
TC-H-T7
TC-H-W
TC-H-A1
TC-H-A2
TC-L2-1
TC-L2-2
TC-M-1
TC-M-2
TC-M-3
TC-T0-I
TC-T1-I
TC-T2-I
TC-T3-I
TC-T4-I
TC-T5-I
TC-T6-I
TC-L3-1
TC-L3-2
TC-L3-3
TC-L3-4
TC-L4-1

ID lines	Position	Dimension
Plastic line	DEMI - LINE1	plastic pipe 1"
LINE 1	Plastic line - HEATER	tube 3/4" BWG 16
LINE 2	HEATER - MANIFOLD	tube 3/4" BWG 16
7 tubes 1/2"	MANIFOLD-DWBTs	tube 1/2" BWG 18
LINE 3	Steam chamber - Environmet	pipe 2.1/2" sch.80
LINE 4	HEATER - Environment	tube 3/4" BWG 16
Bypass V3	V3	tube 3/4" BWG 16
HL	Helium line	tube 1/2" BWG 18

ID valves	Valve
PVW1	V1 Injection Valve
RVW1	V2 Bypass Valve
RVW2	V3 Pressure regulation
HVW1	V4 Water line
HVW2	V5 Pump bypass
CVW	V6 Check Valve
HVW3	V7 Vent Valve
SVW1	V8 Pressure Relief Valve

FSN-ING
Alessio Pesetti

Project: HERO
CIRCE-HERO P&ID

DIM.	N. FSCM	N. DISEGNO	REV.
A3		P&ID-001	9
SCALA		PAGINA	1 DI 1

CIRCE-HERO 2^{ary} side compone

Heating system of the feed water

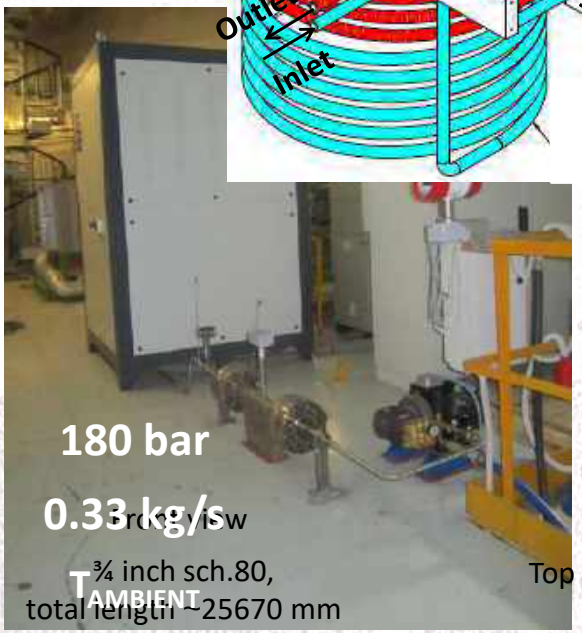

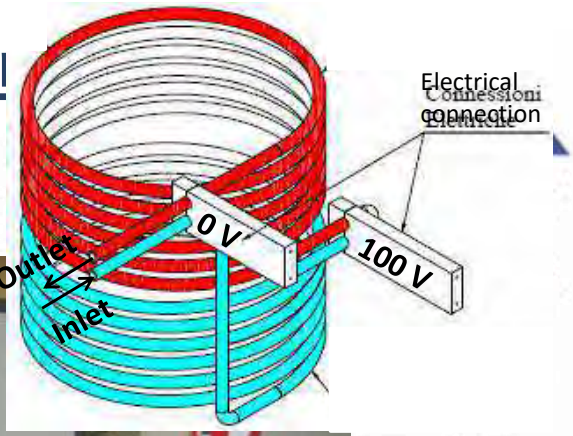

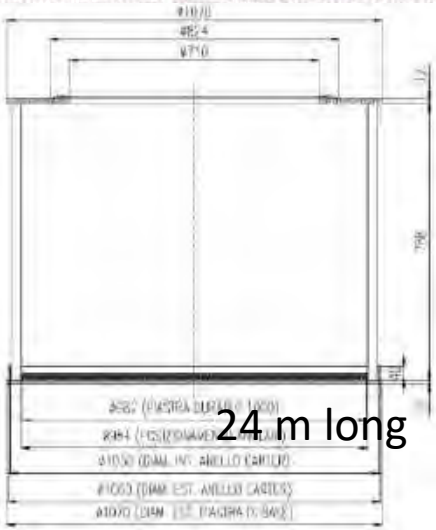

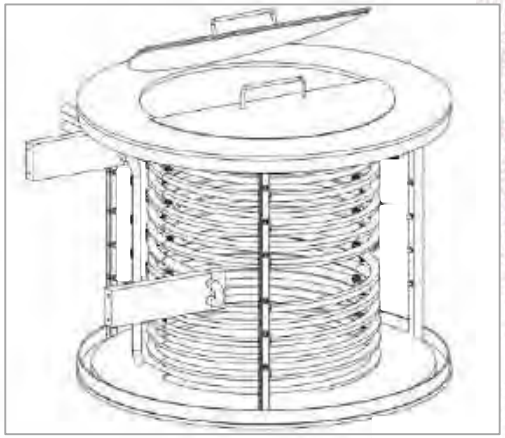

CIRCE-HERO 2ary side components

V1 isolation valve

V2 bypass valve

V3 regulation valve

CIRCE cover

Isolation valve V1

Manifold

7 turbin flow meter

CIRCE-HERO 2ary side components

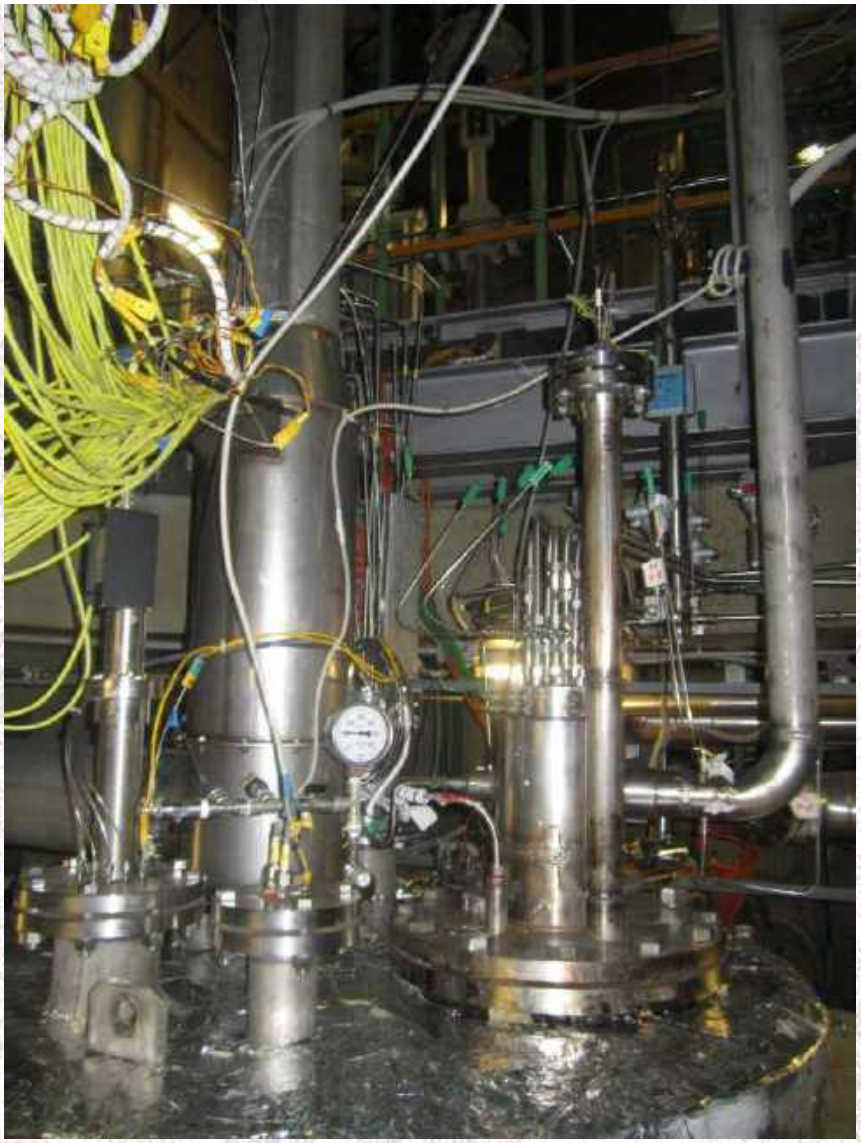

2 O_2 sensors

5 PTs

1 laser level measurement

CIRCE-HERO 2ary side components

CIRCE-HERO DACS

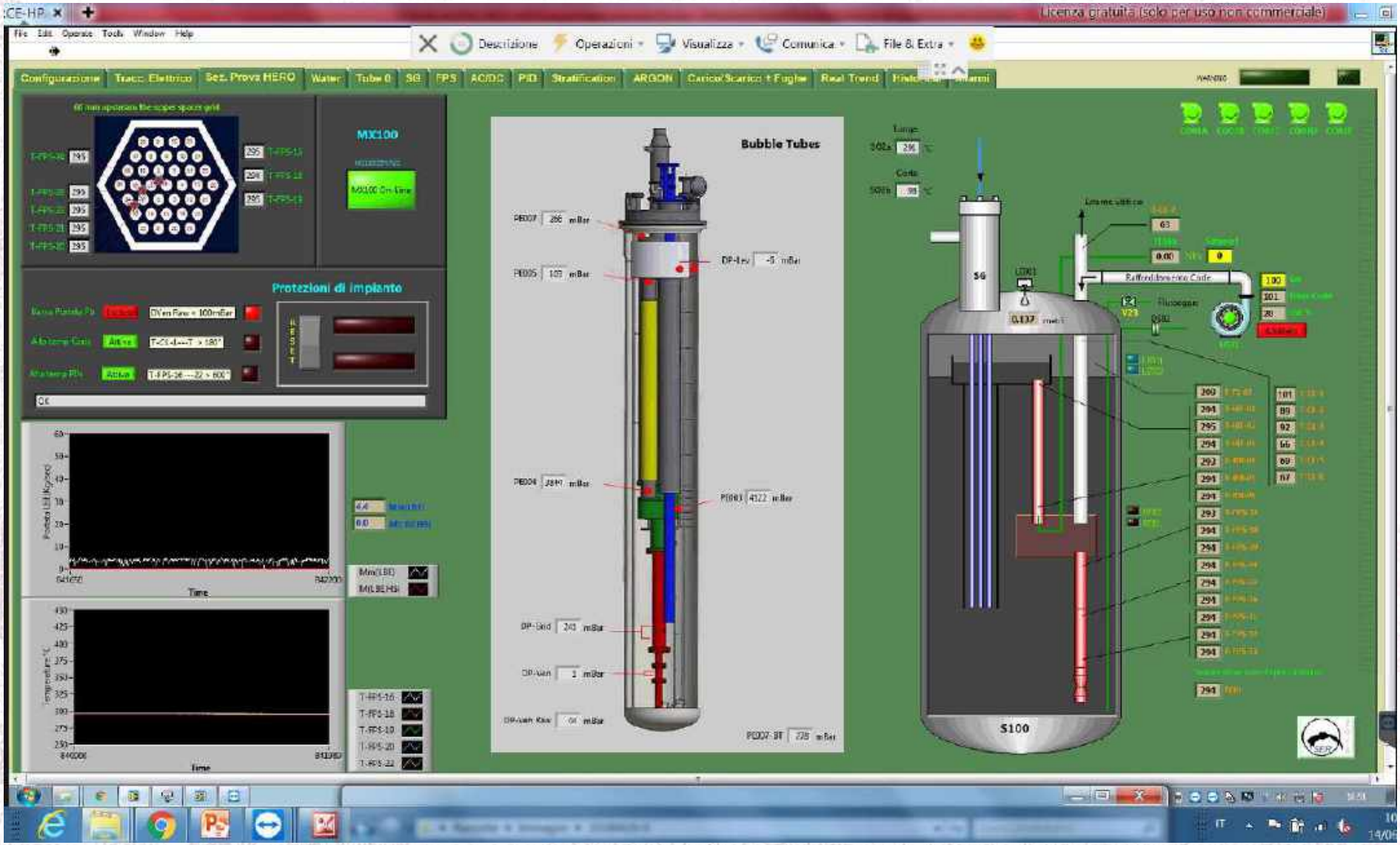

CIRCE-HERO DACS

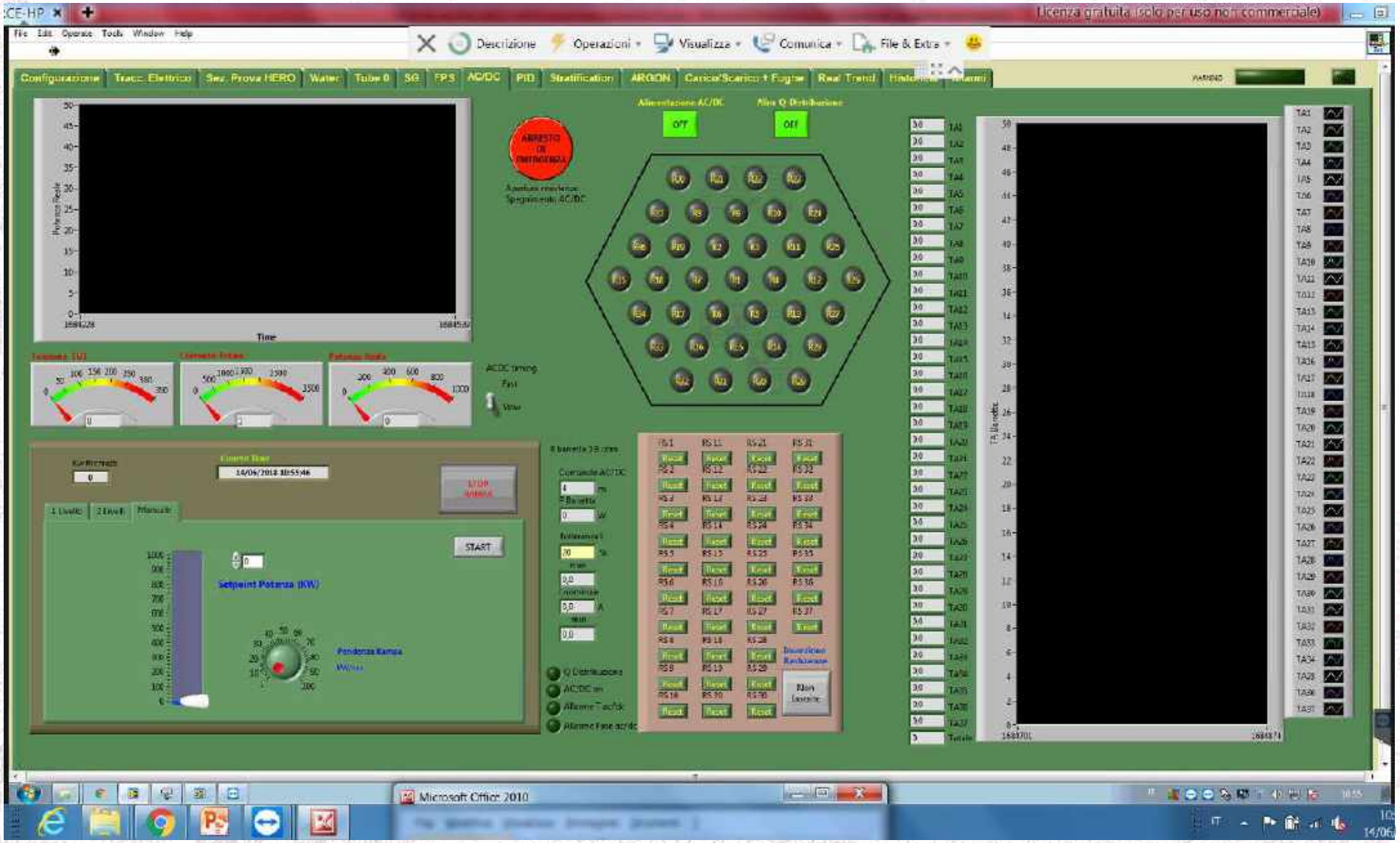

CIRCE-HERO DACS

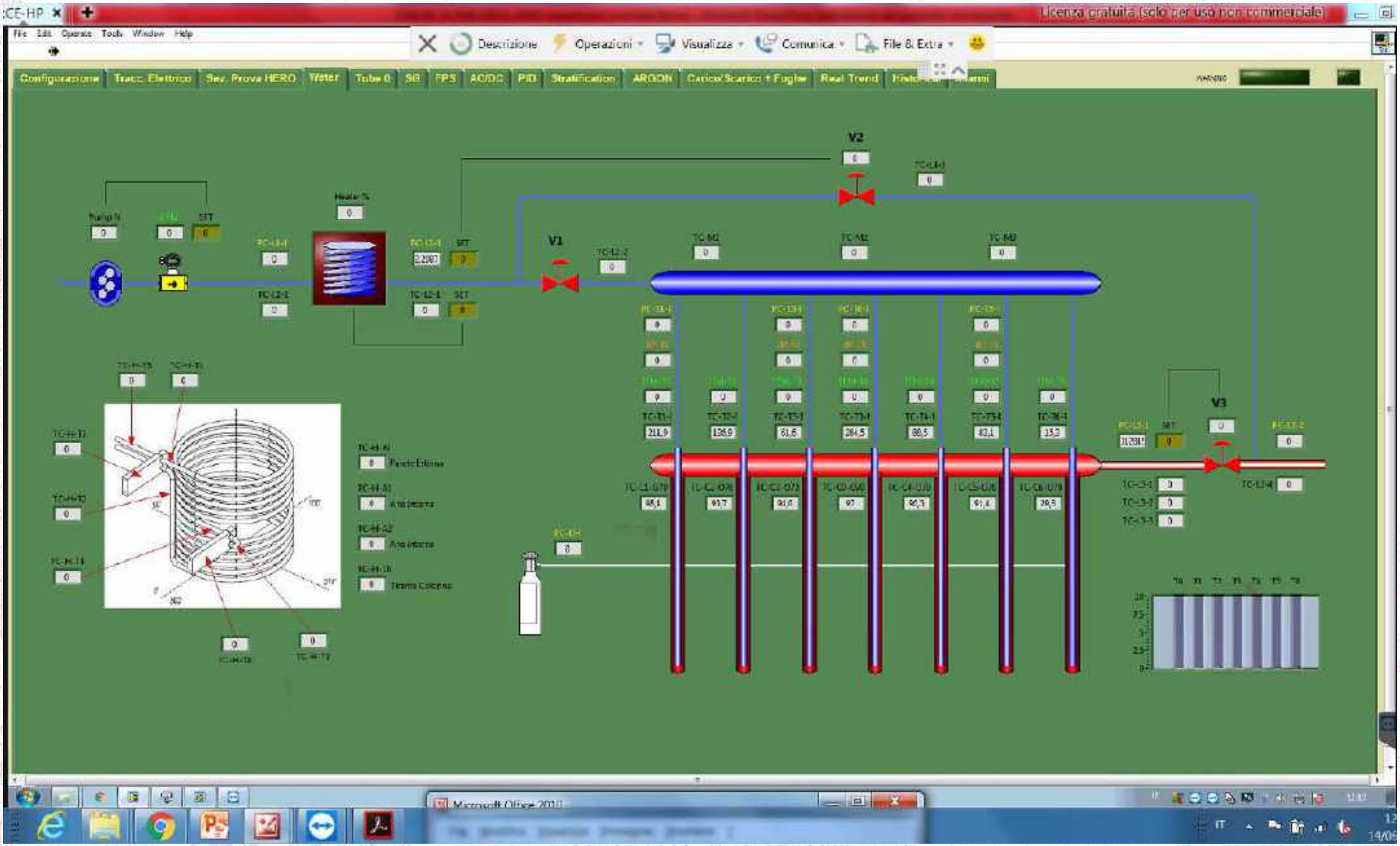

CIRCE-HERO DACS

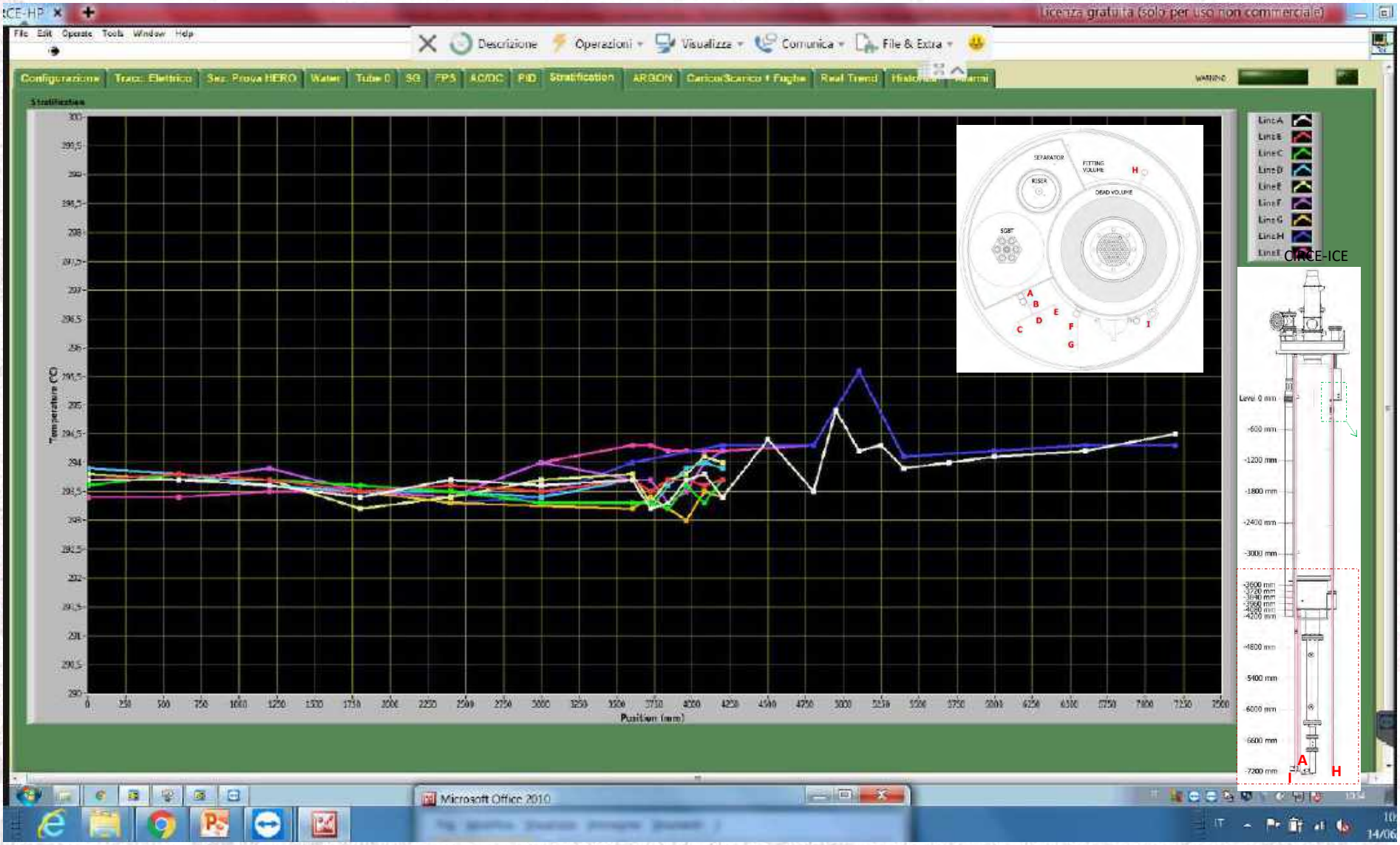

CIRCE-HERO Heat Losses tests

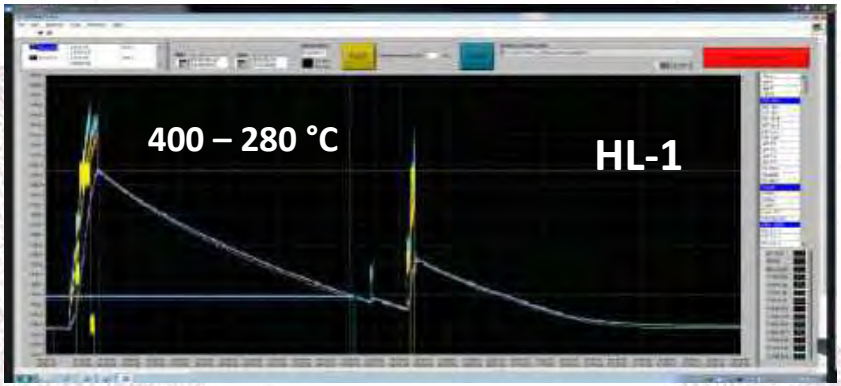

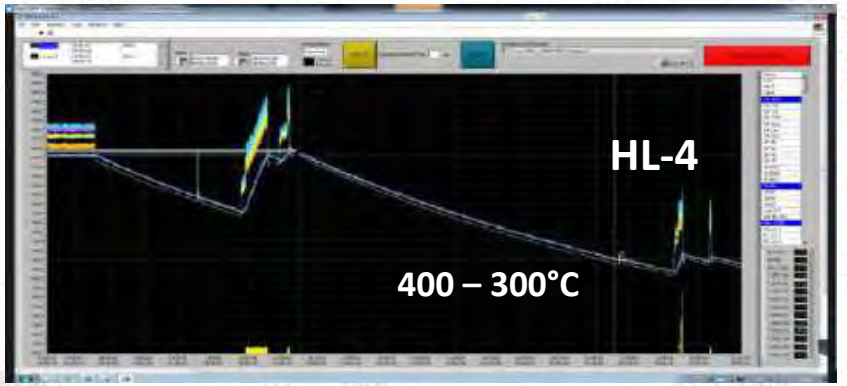

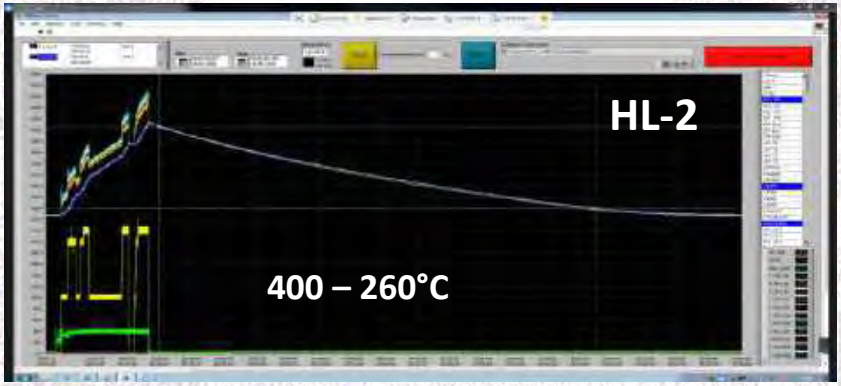

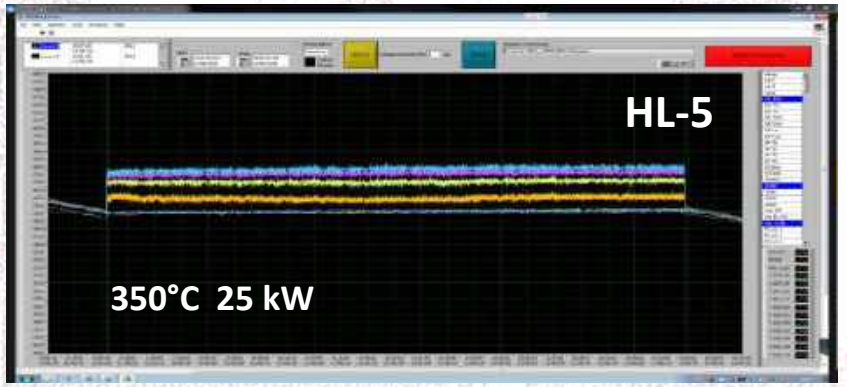

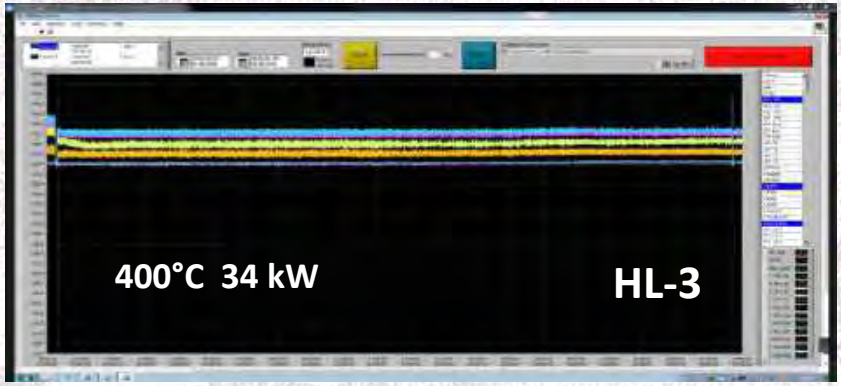

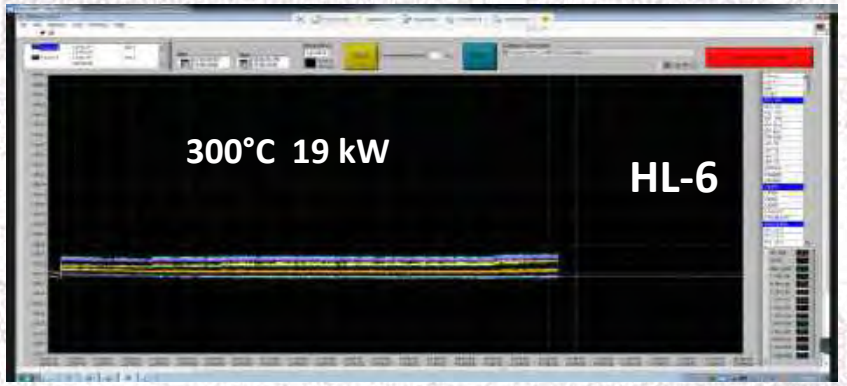

CIRCE-HERO test matrix

- Steady state condition: H2O subcooled inlet @ 335°C – superheated steam outlet @ 400°C, 180 bar, 0.33 kg/s ; LBE @ 400÷480°C, 40 kg/s

- Transient test 1 PLOFA:
  - P) FPS power decreases by decay heat curve
  - LOFA) gas lift @ 0 in 10 sec
  - Feedwater kg/s at 10% after 10 sec (DHR)

- Transient test 2 PLOFA:
  - P) FPS power decreases by decay heat curve
  - LOFA) gas lift @ 0 in 10 sec
  - Feedwater kg/s at 0% after 10 sec (without DHR)

- Transient test 3 PLOFA:
  - P) FPS power decreases by decay heat curve
  - LOFA) gas lift decreases by table (pump flywheel)
  - Feedwater kg/s at 10% after 10 sec (DHR)

Conclusive remarks

- A new HX with 7 double wall bayonet tubes 1:1 scale of ALFRED SG tube was designed, assembled and implemented in HERO TS and CIRCE facility at ENEA CR Brasimone
- Primary system of the facility is completely assembled, the secondary side is almost completed (instrumentation and DACS)
- Heat-losses tests carried out
- Experimental campaign (3 tests) for SGBT characterization both in steady-state and transient conditions (enhanced to natural circulation) by next September

Conclusive remarks

THANK YOU

FOR

YOUR ATTENTION

Alessio Pesetti

alessio.pesetti@for.unipi.it
University of Pisa
Largo Lucio Lazzarino 2
56122 Pisa

HERO NUMERICAL CHARACTERIZATION BY STH CODE

Pierdomenico Lorusso

GENERATION IV LEAD COOLED FAST REACTOR

STATO ATTUALE DELLA TECNOLOGIA E PROSPETTIVE DI SVILUPPO

WORKSHOP TEMATICO ACCORDO DI PROGRAMMA MISE – ENEA

PAR2017 – PROGETTO B.3 LP2

Università di Roma "La Sapienza"

14-15 Giugno 2018

OUTLINE

- CIRCE-HERO Overview
- CIRCE-HERO Model
- Start-Up Procedure
- HERO Pre-Test Analysis
- Final Remarks

CIRCE-HERO OVERVIEW

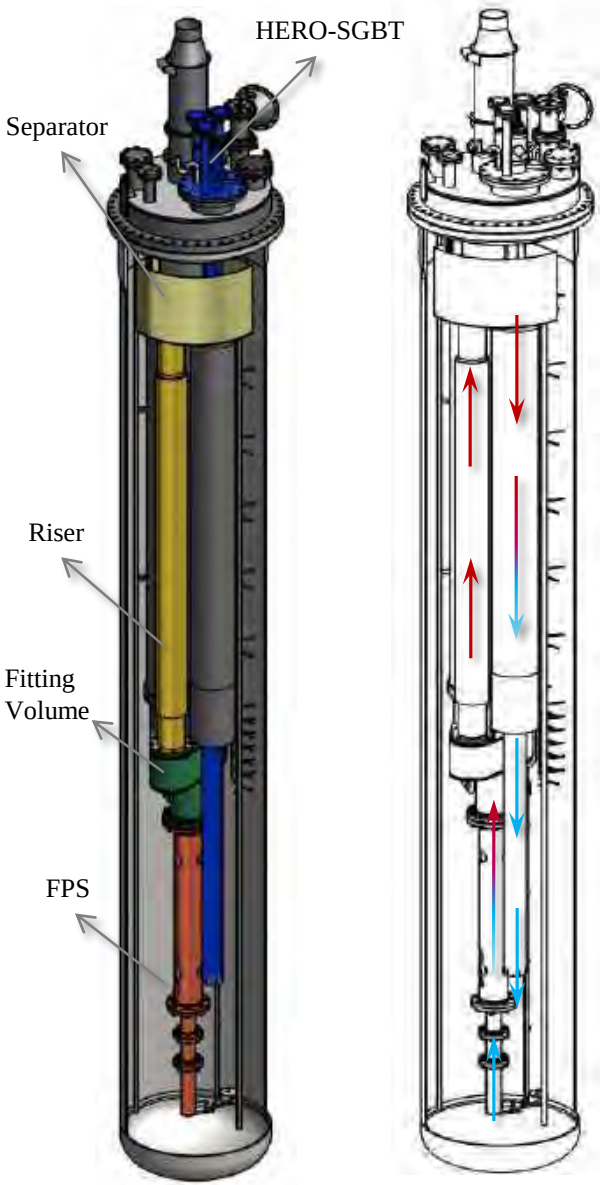

CIRCE Parameters	Value	CIRCE Parameters	Value
Outside diameter [mm]	1200	Temperature Range [° C]	200 to 500
Wall thickness [mm]	15	Operating Pressure [kPa]	15 (gauge)
Material	AISI 316L	Design Pressure [kPa]	450 (gauge)
Max LBE Inventory [kg]	90000	Argon Flow Rate [Nl/s]	15
Electrical Heating [kW]	47	Argon Injection Pressure [kPa]	600 (gauge)

CIRCE-HERO OVERVIEW

The secondary loop is an once through loop fed by demineralized water. In working conditions the water is pressurized at 172 bar (Tsat 353.25° C) at the SGBT outlet and preheated at 335° C at the inlet of the SGBT unit.

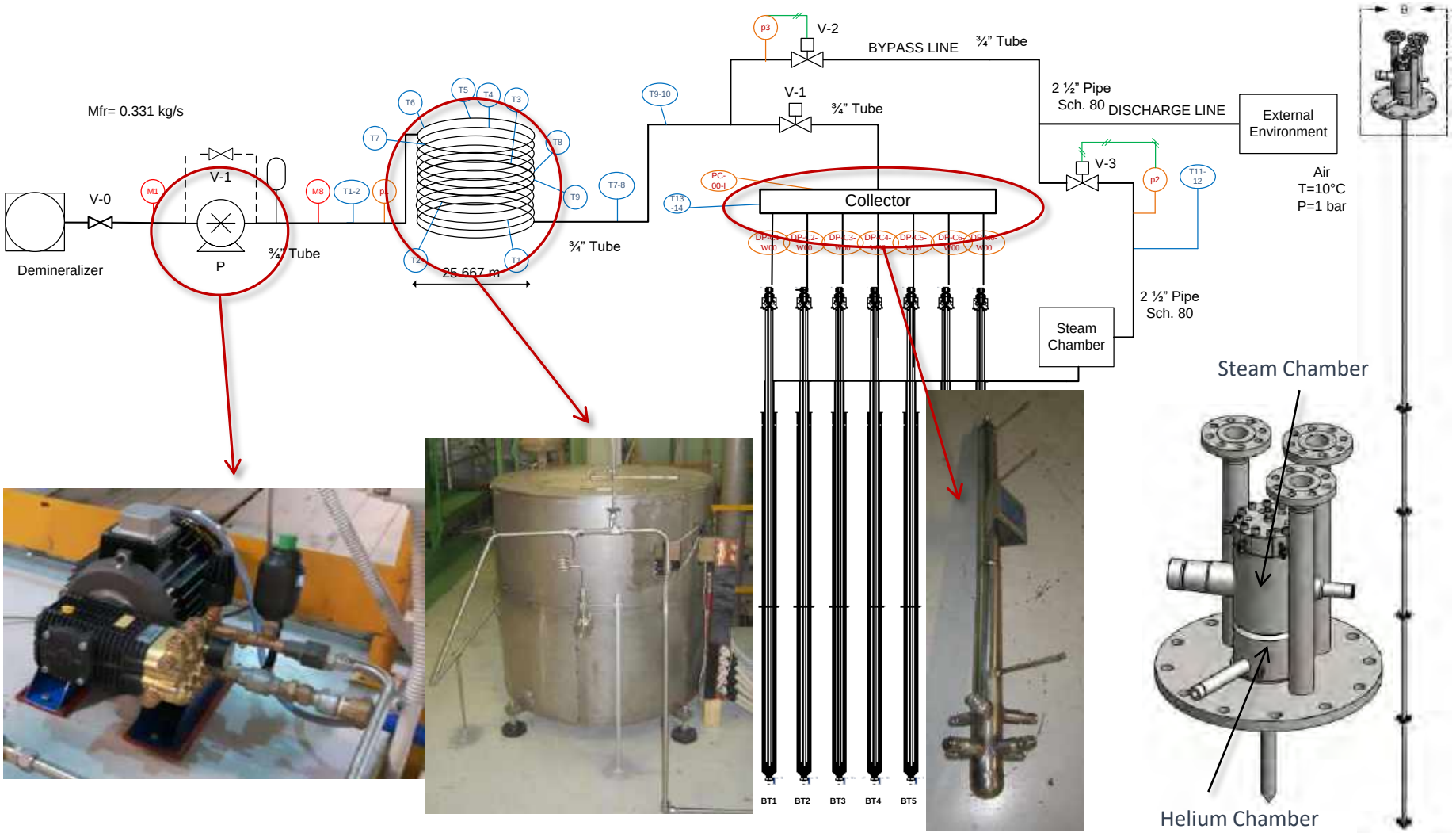

CIRCE-HERO OVERVIEW

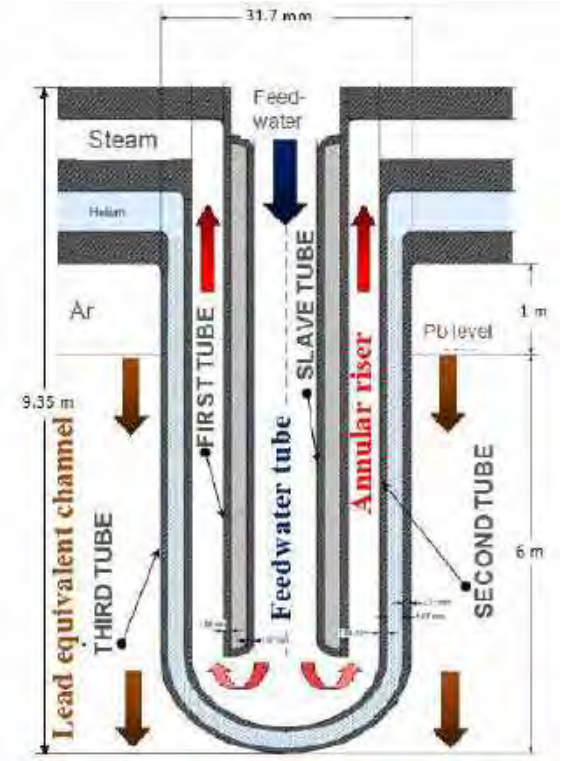

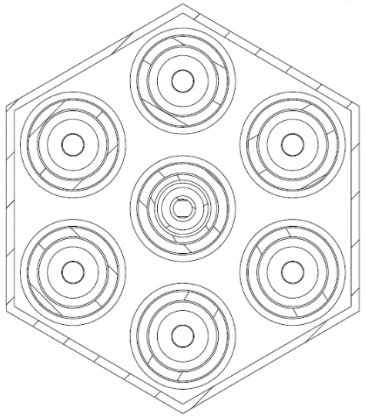

Label	Inner diameter [mm]	Outer diameter [mm]	Thickness [mm]	Material --
Feed-water slave tube	7.09	9.53	1.22	AISI-304
Feed-water tube gap	9.53	15.75	3.11	Slight vacuum
Feed-water outer tube	15.75	19.05	1.65	AISI-304
Annular riser gap	19.05	21.18	1.07	Water-steam
Second tube	21.18	25.40	2.11	AISI-304
Annular gap	25.40	26.64	0.62	AISI 316 powder
Third tube	26.64	33.40	3.38	AISI-304

Description	Unit	Water-Steam side	He side	LBE side
Fluid	--	Water – steam	Helium	LBE
Circulation mechanism	--	Axial pump + accumulator	leakage accommodation	Gas enhanced
Main components	--	bayonet tubes, steam chamber	Helium chamber	SGBT unit shell
Bundle type and P/D	-	Triangular / 1.42	--	Shell
Inlet temp.	° C	335	--	480
Mass flow	kg/s	0.330785	stagnant	44.573529
Design pressure	bar	180	5.0	As CIRCE
Operating pressure	bar	172	4.5	Hydraulic head
Design temp.	° C	432	432	As CIRCE

CIRCE-HERO MODEL

RELAP5-3D© Model

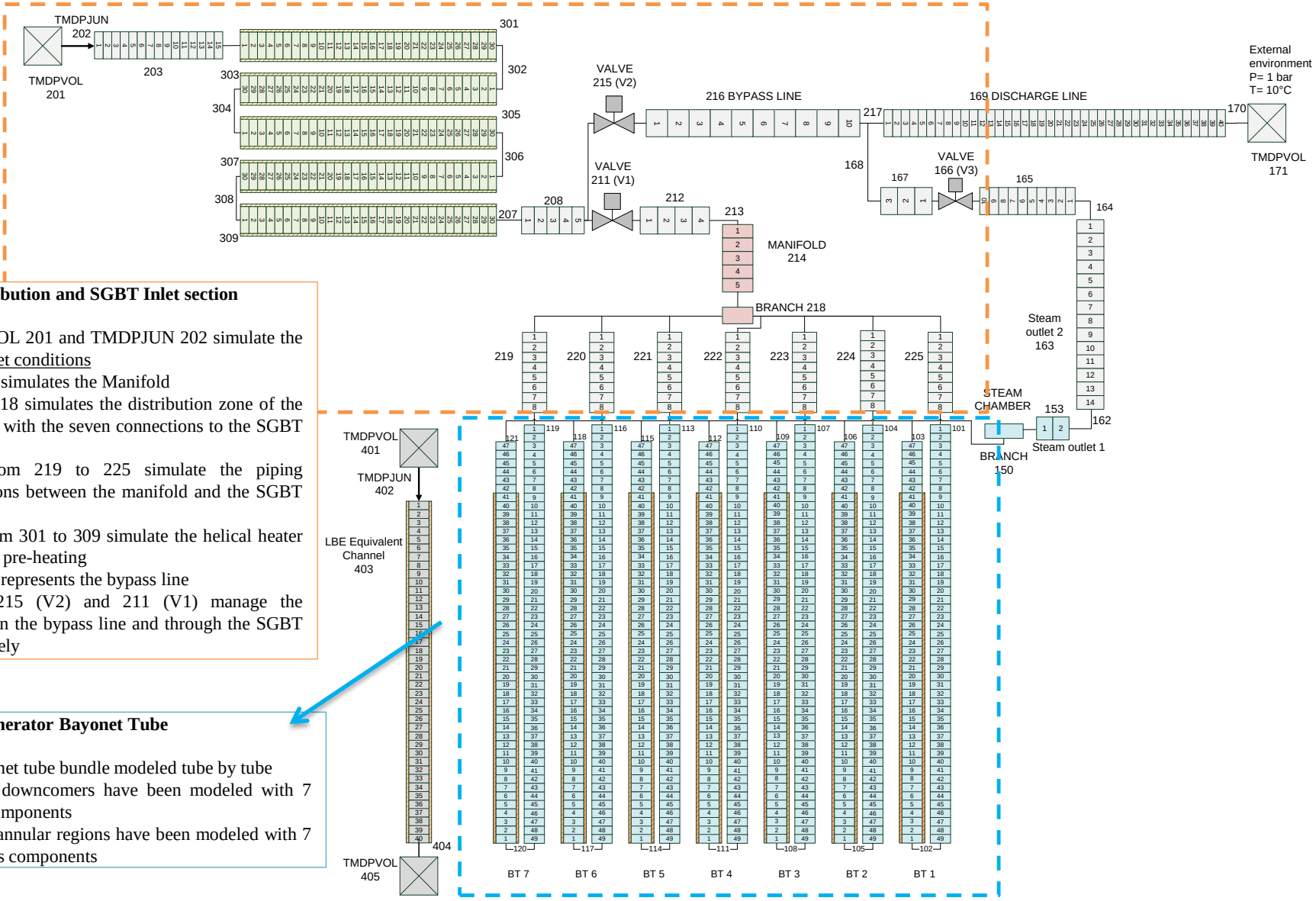

Water distribution and SGBT Inlet section

- TMDPVOL 201 and TMDPJUN 202 simulate the water inlet conditions
- Pipe 214 simulates the Manifold
- Branch 218 simulates the distribution zone of the manifold with the seven connections to the SGBT tubes
- Pipes from 219 to 225 simulate the piping connections between the manifold and the SGBT tubes
- Pipes from 301 to 309 simulate the helical heater for water pre-heating
- Pipe 216 represents the bypass line
- Valves 215 (V2) and 211 (V1) manage the passage in the bypass line and through the SGBT respectively

Steam Generator Bayonet Tube

- 7 bayonet tube bundle modeled tube by tube
- The 7 downcomers have been modeled with 7 pipe components
- The 7 annular regions have been modeled with 7 annulus components

CIRCE-HERO MODEL

RELAP5-3D© Model

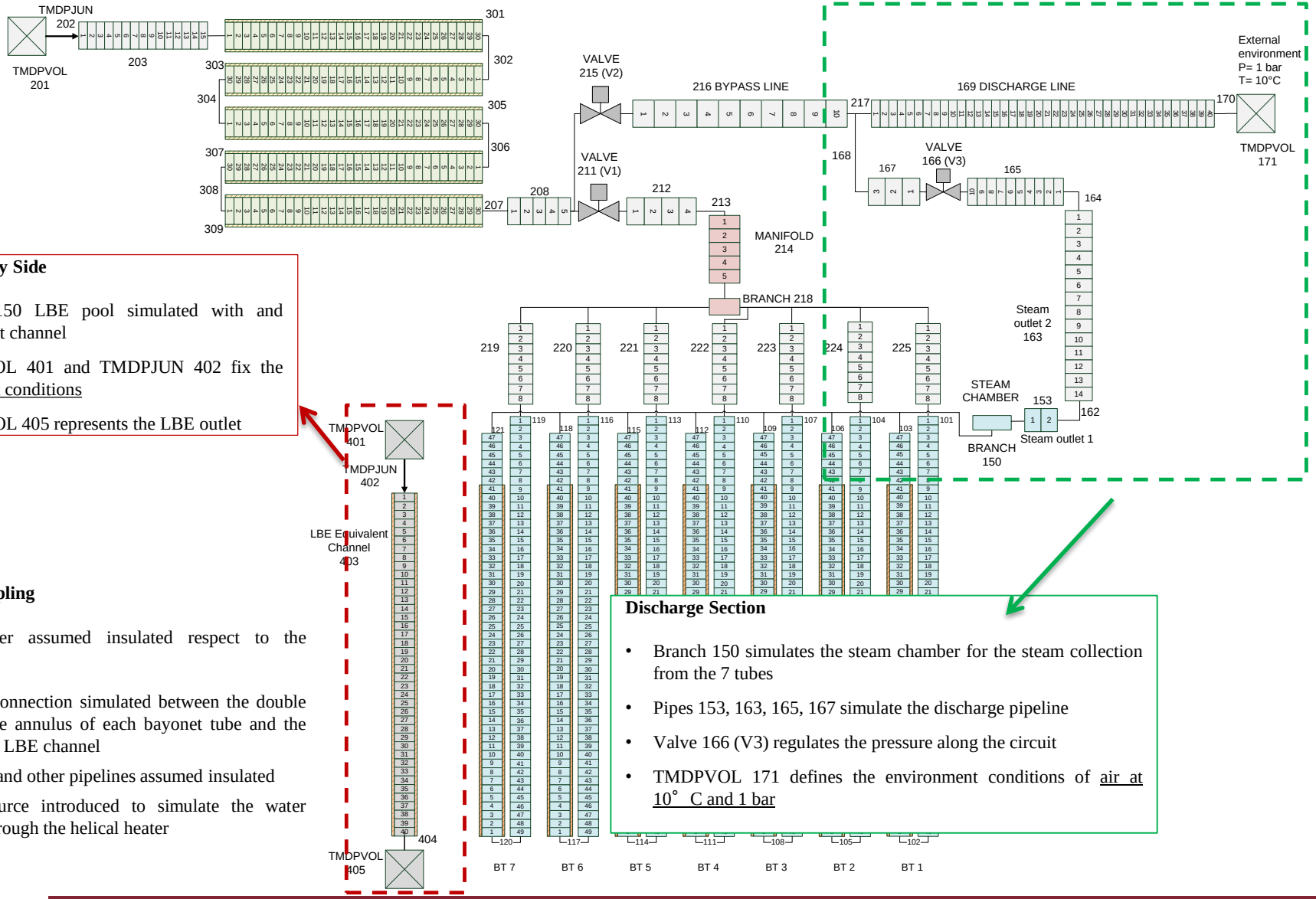

LBE Primary Side

- Branch 150 LBE pool simulated with and equivalent channel
- TMDPVOL 401 and TMDPJUN 402 fix the LBE inlet conditions
- TMDPVOL 405 represents the LBE outlet

Thermal coupling

- Downcomer assumed insulated respect to the annulus
- Thermal connection simulated between the double wall of the annulus of each bayonet tube and the equivalent LBE channel
- Manifold and other pipelines assumed insulated
- Power source introduced to simulate the water heating through the helical heater

Discharge Section

- Branch 150 simulates the steam chamber for the steam collection from the 7 tubes
- Pipes 153, 163, 165, 167 simulate the discharge pipeline
- Valve 166 (V3) regulates the pressure along the circuit
- TMDPVOL 171 defines the environment conditions of air at 10° C and 1 bar

CIRCE-HERO MODEL

Pre-Heater Simulations

Analytical model with a simplified geometry for the evaluation of the heat transfer coefficient and the air temperature, coupled with RELAP5-3D simulations for an iterative calculation.

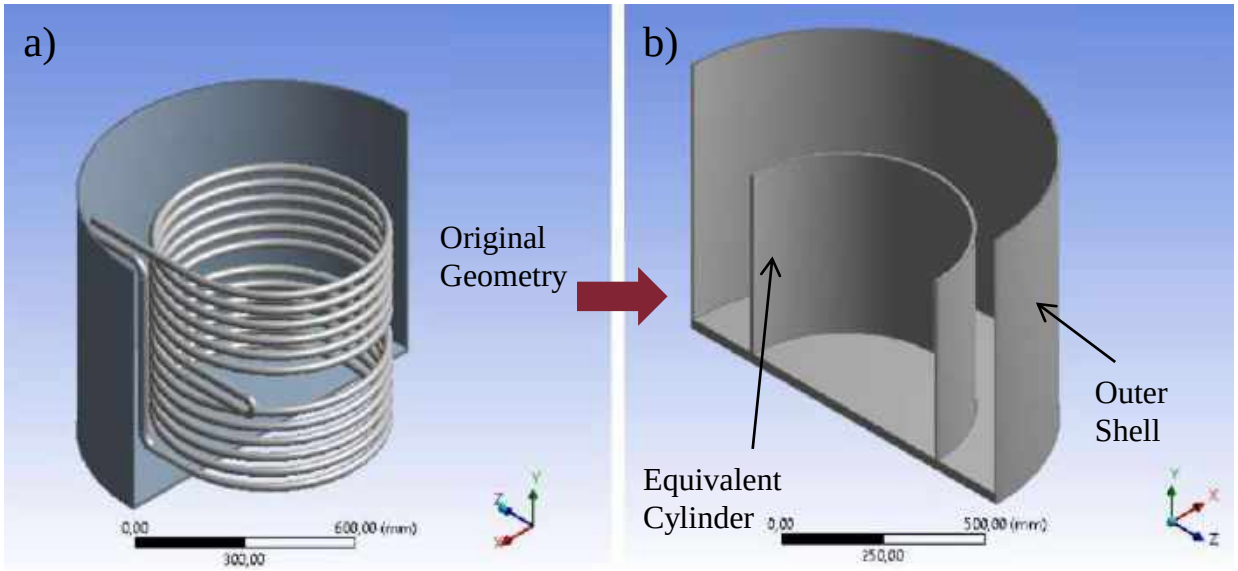

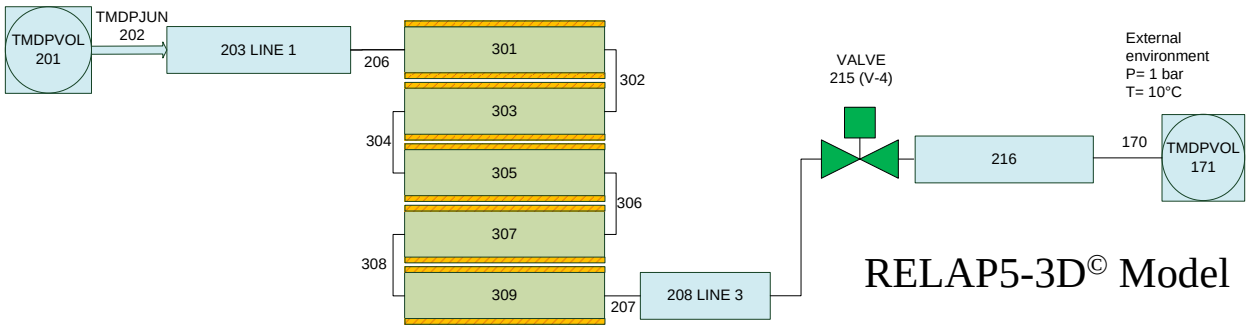

RELAP5-3D© Model

Boundary Conditions

- Pressure: 180 bar
- T inlet h2o: 15° C
- H2o mfr: 0.331 kg/s

Initial conditions

- T_{wall} : 300° C
- T_{air} : 20° C
- $HTC_{ext,\ air}$: 7 W/(m²K)

Outcomes

- ✓ Air Temperature inside the Shell
- ✓ Power Distribution *f(R(T))*
- ✓ Wall Temperature

CIRCE-HERO MODEL

Pre-Heater Simulations

Analytical model with a simplified geometry for the evaluation of the heat transfer coefficient and the air temperature, coupled with RELAP5-3D simulations for an iterative calculation

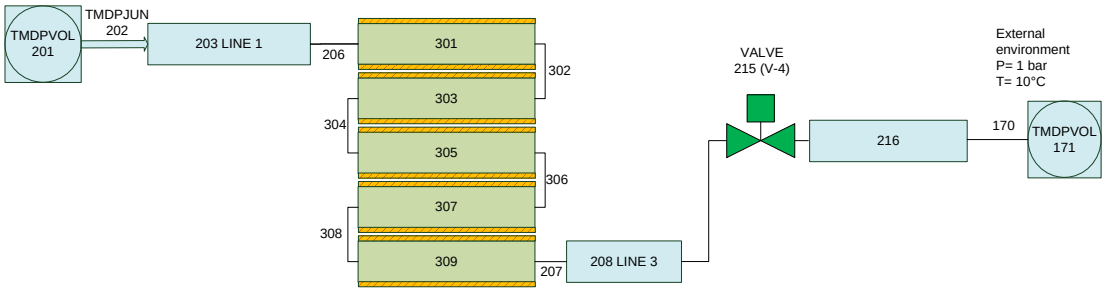

$$Nu = \frac{hL_c}{k} = C(Gr_L Pr)^n = CRa_L^n$$

$$\overline{Nu}_{FP} = \left\{ 0.825 + \frac{0.387 Ra^{\frac{1}{6}}}{\left[1 + (0.492/Pr)^{\frac{9}{16}}\right]^{\frac{8}{27}}} \right\}^2$$

Boundary Conditions

- Pressure: 180 bar
- T inlet h2o: 15° C
- H2o mfr: 0.331 kg/s

Initial conditions

- T_{wall} : 300° C
- T_{air} : 20° C
- $HTC_{ext,\ air}$: 7 W/(m²K)

Outcomes

- ✓ Air Temperature inside the Shell
- ✓ Power Distribution *f(R(T))*
- ✓ Wall Temperature

$$\frac{\overline{Nu}}{Nu_{FP}} = 1 + B\left[32^{0.5} Gr_L^{-0.25} \left(\frac{L}{D}\right)\right]^C$$

Churchill and Chu- Cebeci correlation for cylinder

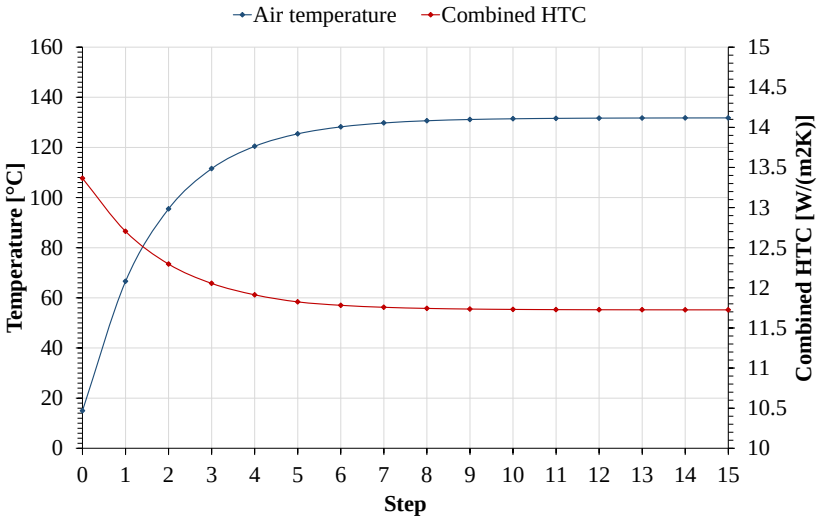

RUN #1				
Test	Power [kW]	T_{out} h2o [° C]	T_{max} wall [° C]	T_{av} wall [° C]
1	485	334.55	360.85	216.94
2	487.5	335.6	361.97	217.64
3	490	336.65	363.12	218.36
4	492.5	337.72	364.25	219.10
RUN #2				
Test	Power [kW]	T_{out} h2o [° C]	T_{max} wall [° C]	T_{av} wall [° C]
1	485	334.1	360.15	216.42
2	487.5	335.4	361.65	217.315
3	490	336.3	362.81	218.035
4	492.5	337.36	363.98	218.77
RUN #3				
Test	Power [kW]	T_{out} h2o [° C]	T_{max} wall [° C]	T_{av} wall [° C]
1	485	334.1	360.15	216.4
2	487.5	335.35	361.64	217.31
3	490	336.27	362.8	218.03
4	492.5	337.35	363.95	218.75

CIRCE-HERO MODEL

Pre-Heater Simulations

The thermal power produced by the Joule effect depends on the electrical resistivity, which is a function of the temperature. As the temperature changes along the pipe length, the resistivity changes too and, in consequence the power distribution is not uniform.

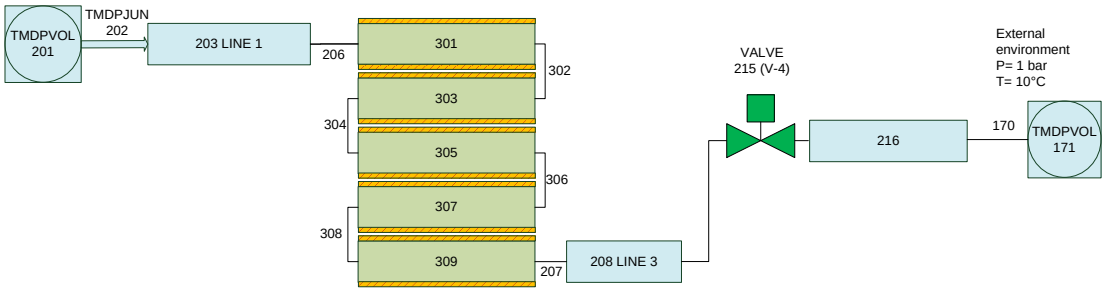

$$R(T) = \frac{\rho(T)l}{A}$$

$$\rho(T) = \rho_{20°C}[1 + \alpha(T)(T - 20)]$$

$$\alpha(T) = \alpha_{20°C}/[1 + T\alpha_{20°C}]$$

Boundary Conditions

- Pressure: 180 bar
- T inlet h2o: 15° C
- H2o mfr: 0.331 kg/s

Outcomes

- ✓ Air Temperature inside the Shell
- ✓ Power Distribution *f(R(T))*
- ✓ Wall Temperature

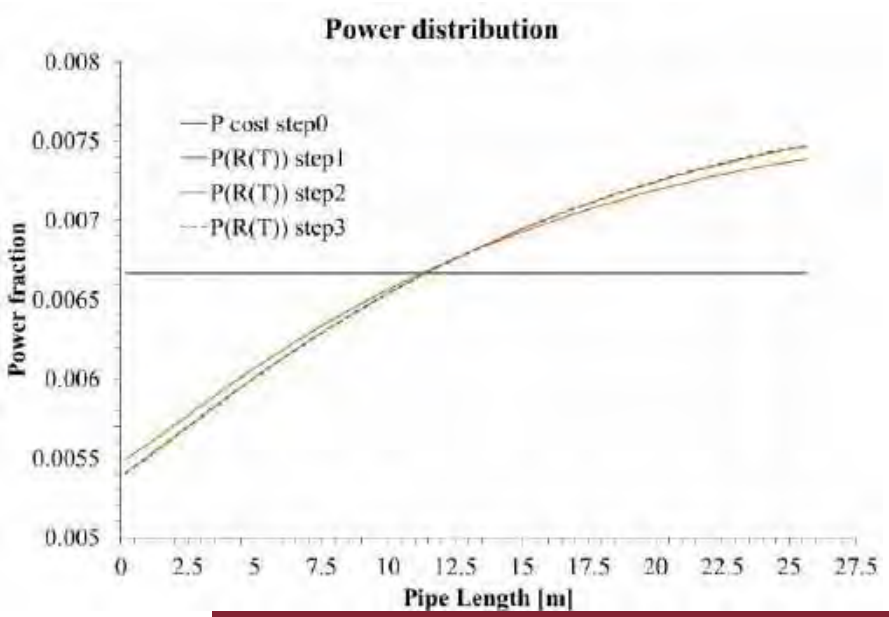

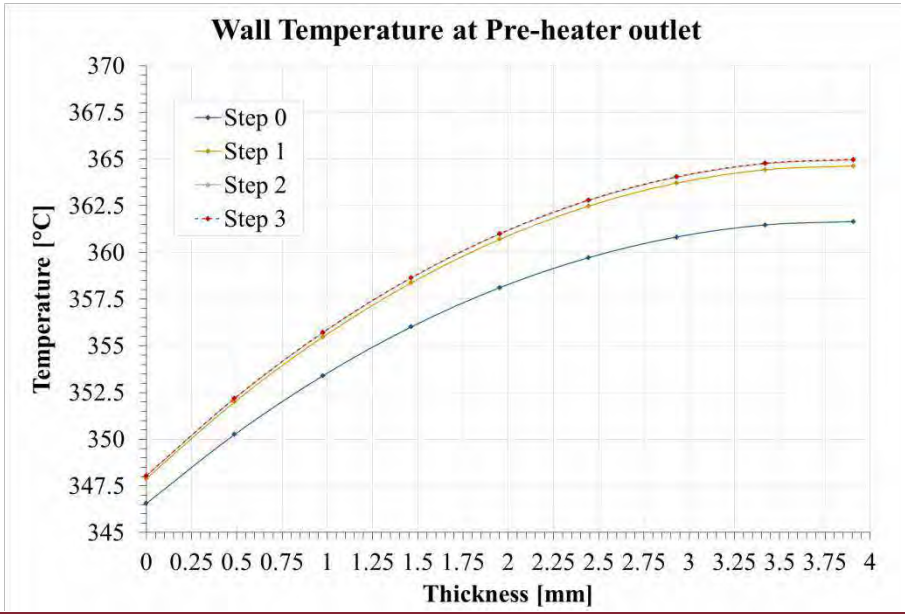

CIRCE-HERO START-UP

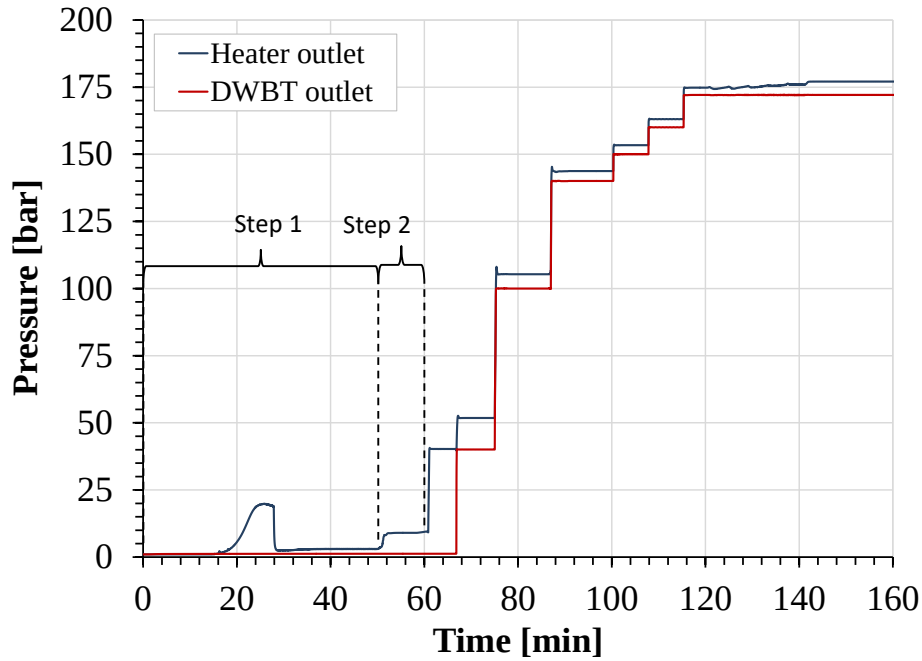

Pressure peak up to ~20 bar due to the water vaporization along the heater, followed by a fast decrease when the steam produced reaches the discharge section

Step 2

- The water mass flow rate is increased passing from $\dot{m}$ = (1/10)$\dot{m}_{nom}$ to **$\dot{m}$ = (1/3)$\dot{m}_{nom}$**.
- Power is increased up to **≈290 kW** for the complete vaporization.

Step 1

- Feedwater line and heat exchanger are empty at the pressure of 1 bar, the water mass flow rate is zero and the pre-heater is switched off. The heat exchanger is bypassed by valves V1 and V3, valve V2 is opened.
- Injection of **water mass flow rate $\dot{m}$ = 1/10 of $\dot{m}_{nom}$** at 10°C and 1 bar.
- The pre-heater is switched on supplying a thermal power of **≈90 kW** for the water vaporization.

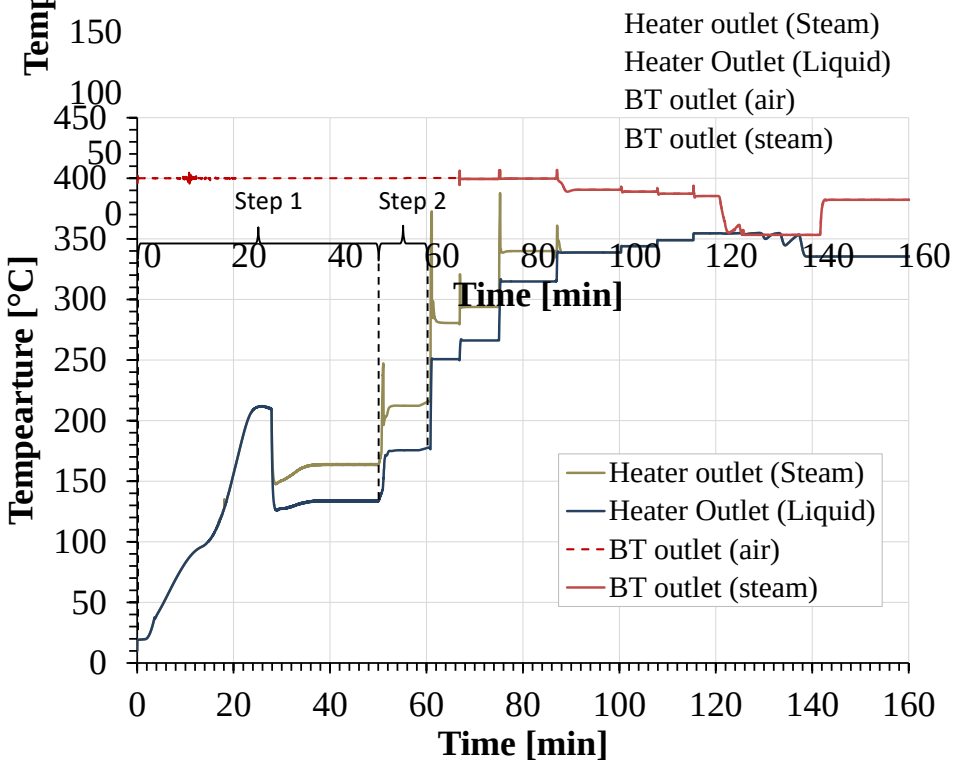

CIRCE-HERO START-UP

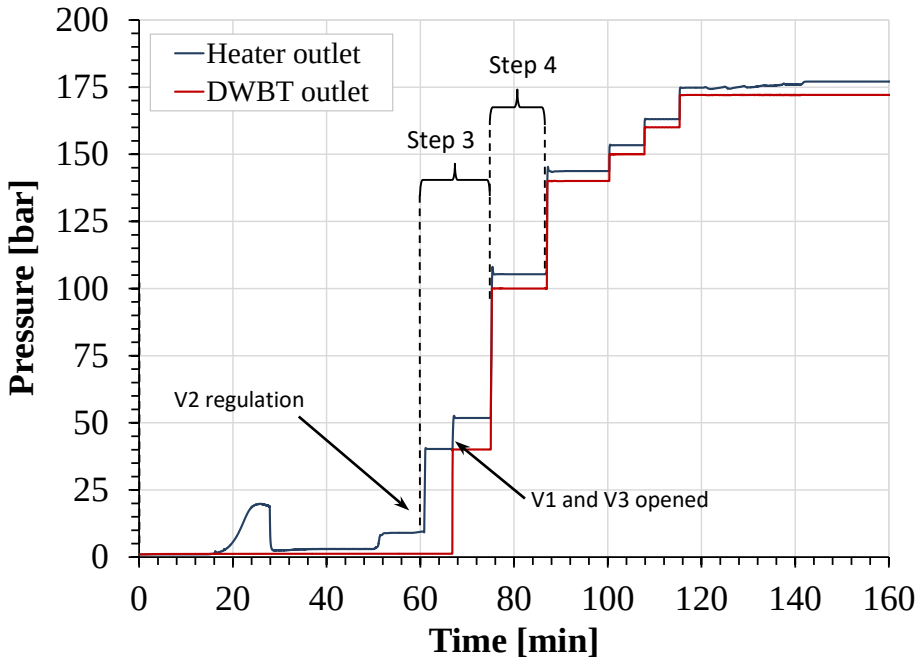

The steam injected at ~270° C assures a low heat transfer coefficient, a very low fraction of thermal power removed from the LBE pool and a small difference in temperature between the double wall of the bayonet tubes.

Step 4

- **The pressure is increased from 40 bar to 100 bar.**
- At the end of the step 4, the water mass flow rate is increased from 1/3 of $\dot{m}_{nom}$ to **1/2 of $\dot{m}_{nom}$**
- At the end of the step 4, the power passes from 311 kW to **335 kW**.
- Production of mixture liquid/steam (mass fraction ≈0.5)

Step 3

- Valve V2 is regulated in order to **pressurize the feedwater line up to 40 bar.**
- The power of the pre-heater is increased up to **≈311 kW** for the generation of superheated steam at 270° C at 40 bar.
- After the achievement of steady state conditions**, the valves V1 and V3 are opened** allowing the passage of the steam in the main pipeline and through the bayonet tubes; **the valve V2 is closed** avoiding the passage of the steam through the bypass. **Valve V3 is regulated in order to pressurize HERO SGBT at 40 bar**.

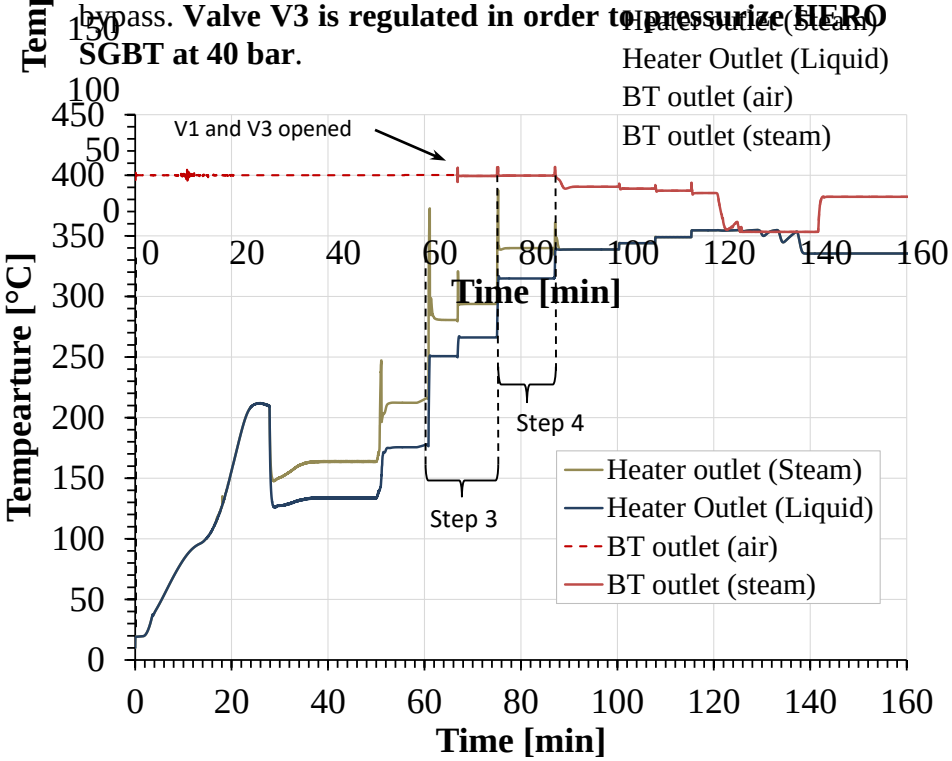

CIRCE-HERO START-UP

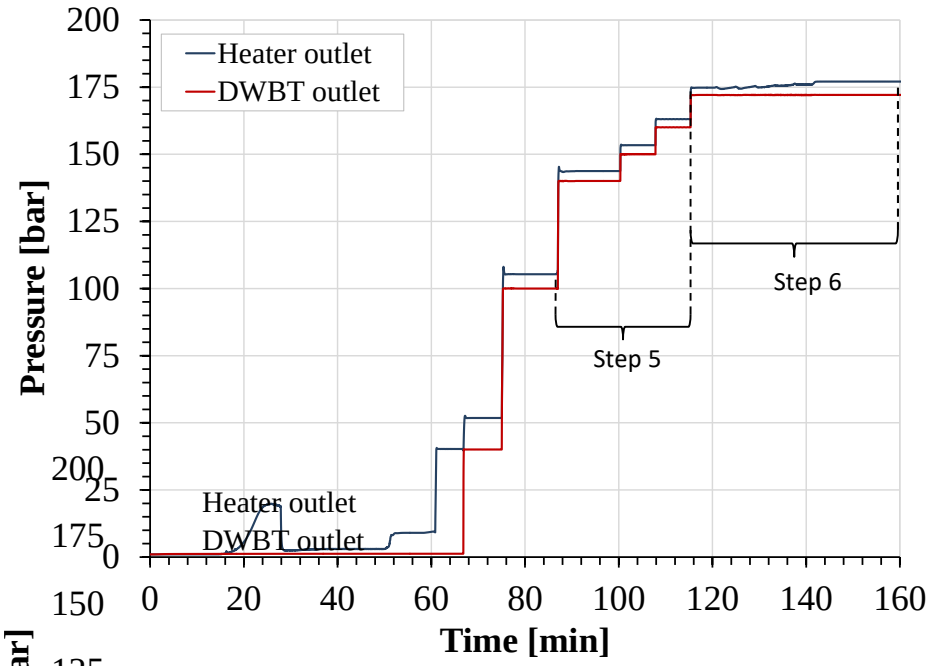

Step 5

- The pipe line is pressurized **from 100 bar to 140, and than to 150, 160 up to 172 bar** after several steps. The other parameters remain constant.

Step 6

- Growth in several steps of water mass flow rate and pre-heating thermal power up to the working conditions of **0.331 kg/s** and **335° C**.
- At least, temperature growth on LBE side from 400° C to **480° C**.

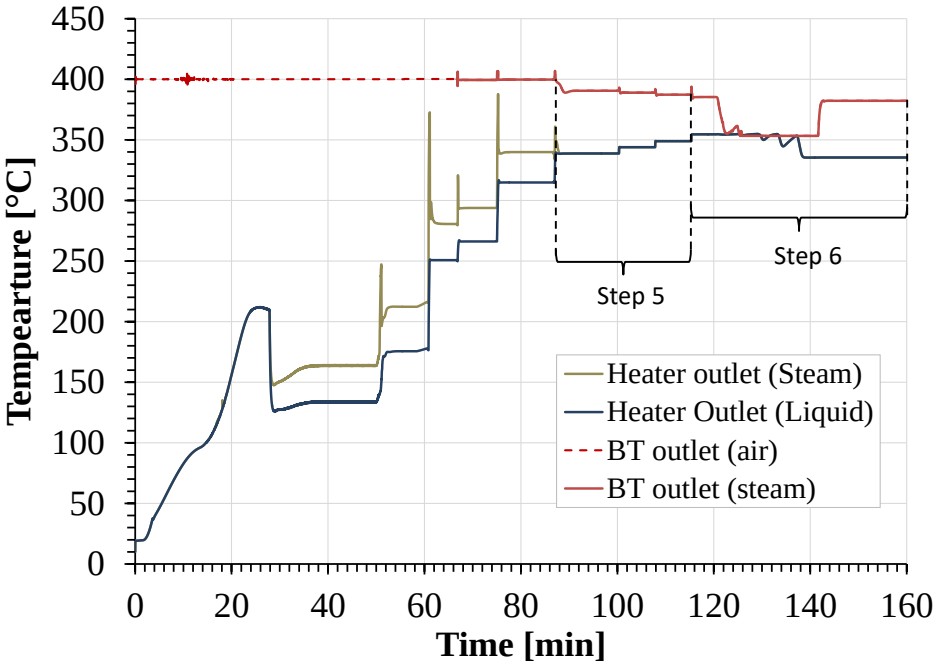

CIRCE-HERO START-UP

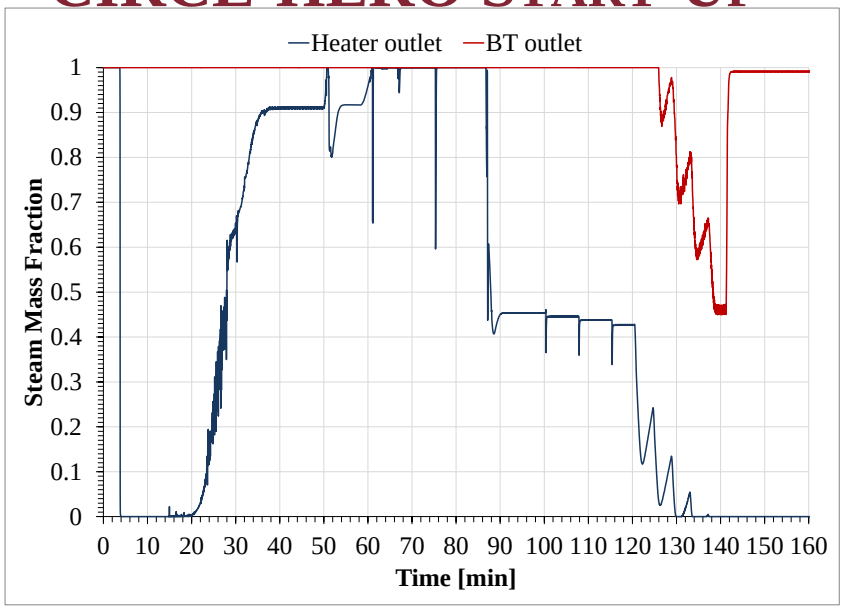

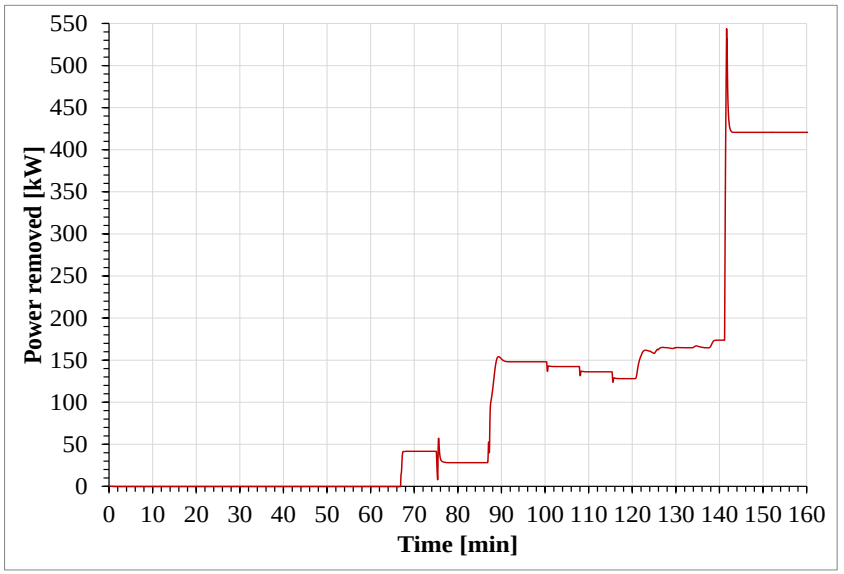

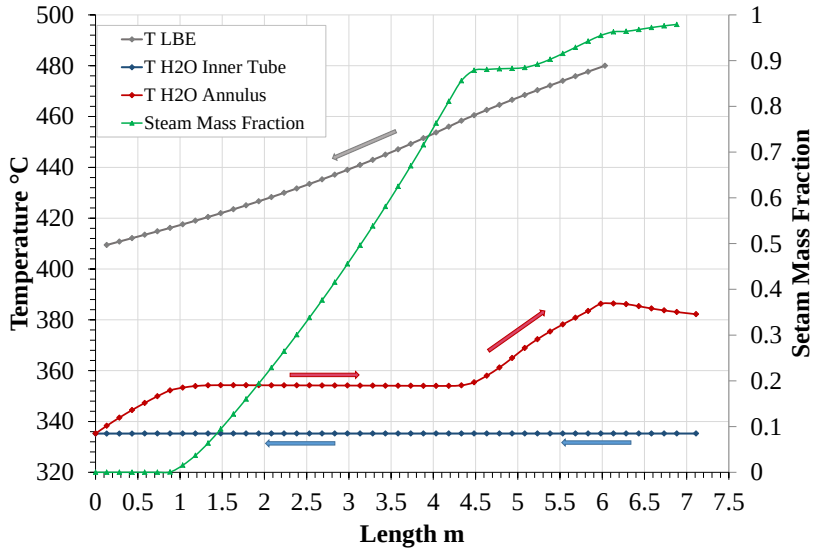

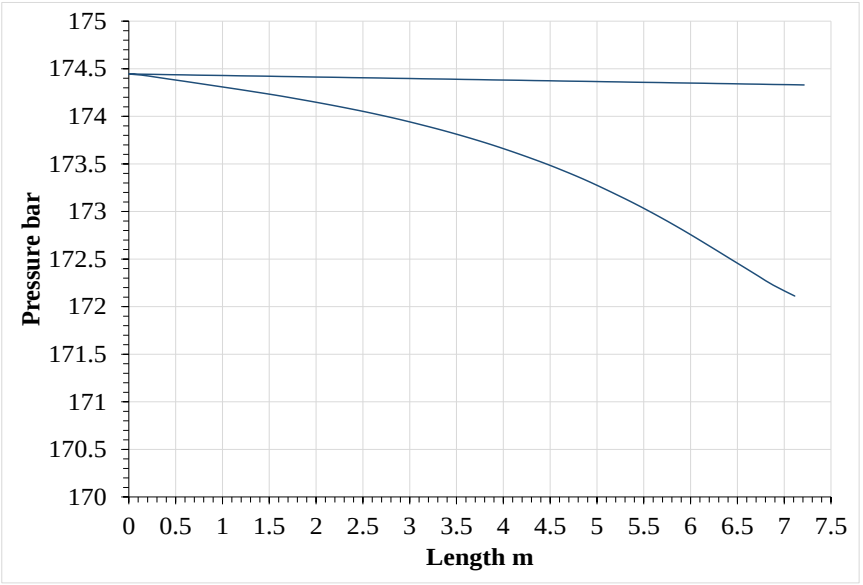

CIRCE-HERO START-UP

Temperature Profiles

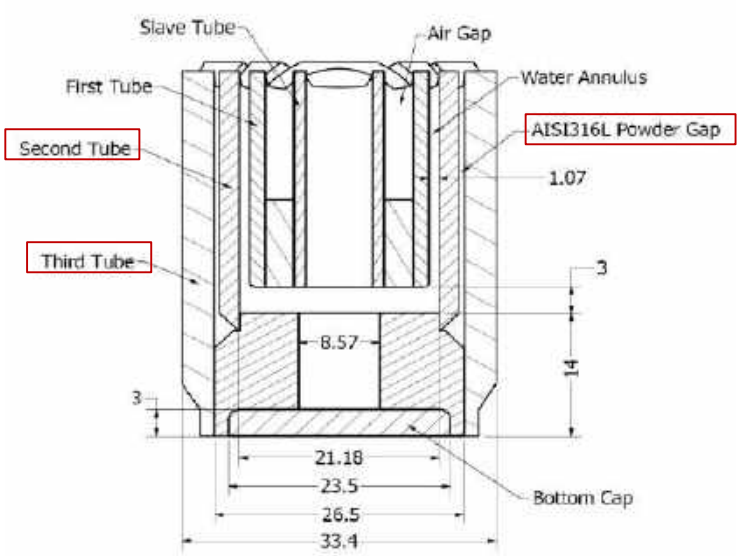

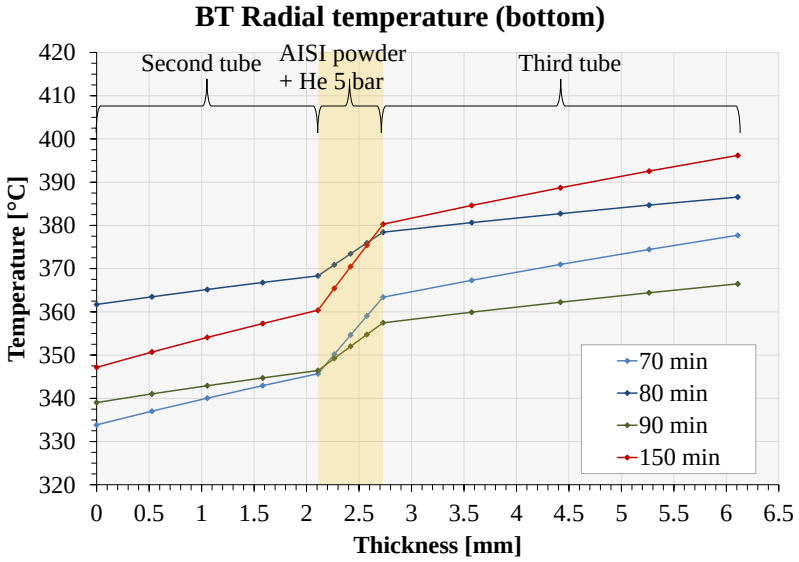

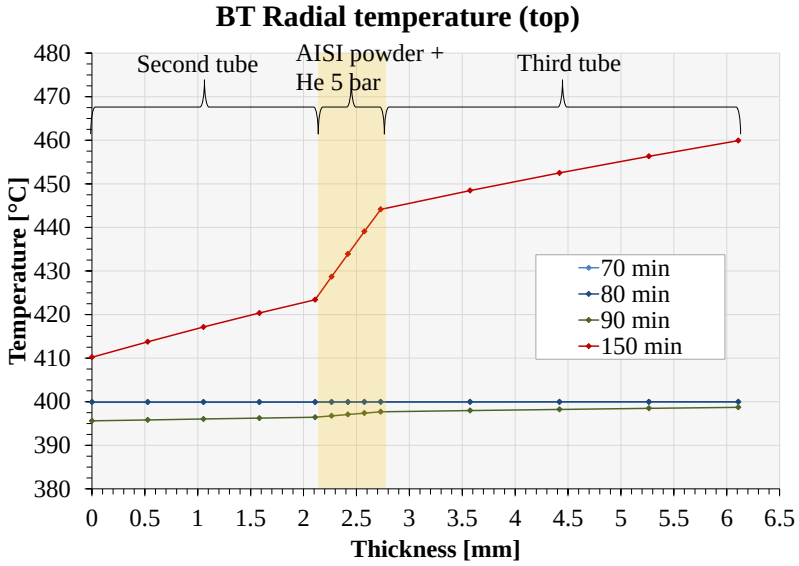

HERO PRE-TEST ANALYSIS

Preliminary test analysis for the HERO SGBT thermal-hydraulic characterization

Parameter	Unit	CASE A			CASE B		
Test #	-	RUN #1	RUN #2	RUN #3	RUN #4	RUN #5	RUN #6
LBE inlet temperature	° C	480	480	480	480	480	480
HERO outlet Pressure	bar	172	172	172	172	172	172
Water SGBT Tin	° C	335	335	335	335	335	335
LBE mfr SS1	kg/s	37.5 (100%)	39.2 (100%)	44.7 (100%)	37.5 (100%)	39.2 (100%)	44.7 (100%)
LBE mfr SS2	kg/s	28.1 (75%)	29.4 (75%)	33.5 (75%)	28.1 (75%)	29.4 (75%)	33.5 (75%)
LBE mfr SS3	kg/s	18.7 (50%)	19.6 (50%)	22.3 (50%)	18.7 (50%)	19.6 (50%)	22.3 (50%)
Water mfr SS1	kg/s	0.33 (100%)	0.33 (100%)	0.33 (100%)	0.33 (100%)	0.33 (100%)	0.33 (100%)
Water mfr SS2	kg/s	0.25 (75%)	0.25 (75%)	0.25 (75%)	0.25 (75%)	0.25 (75%)	0.25 (75%)
Water mfr SS3	kg/s	0.17 (50%)	0.17 (50%)	0.17 (50%)	0.17 (50%)	0.17 (50%)	0.17 (50%)

Two sets of tests based on different correlations of powder thermal conductivity

- **Case A**: based on TxP tests after powder thermal cycling under He at 4 bar*
- **Case B**: based on experimental data of NACIE Heat Exchanger

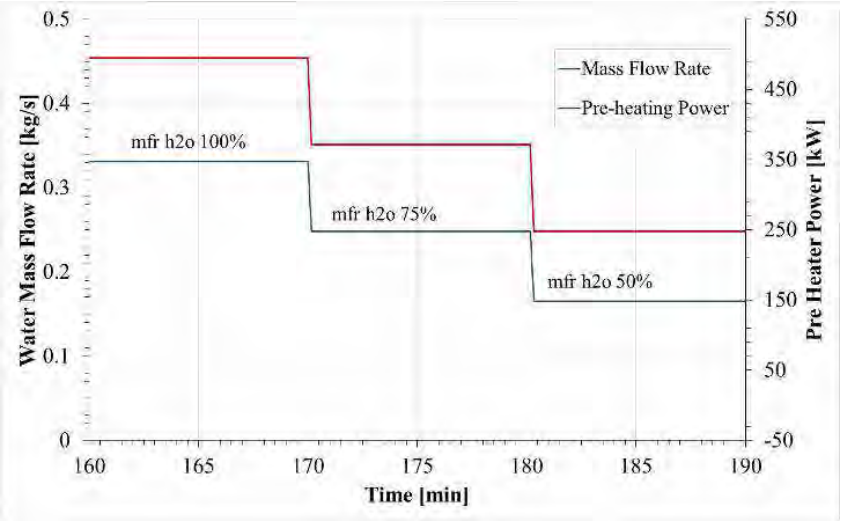

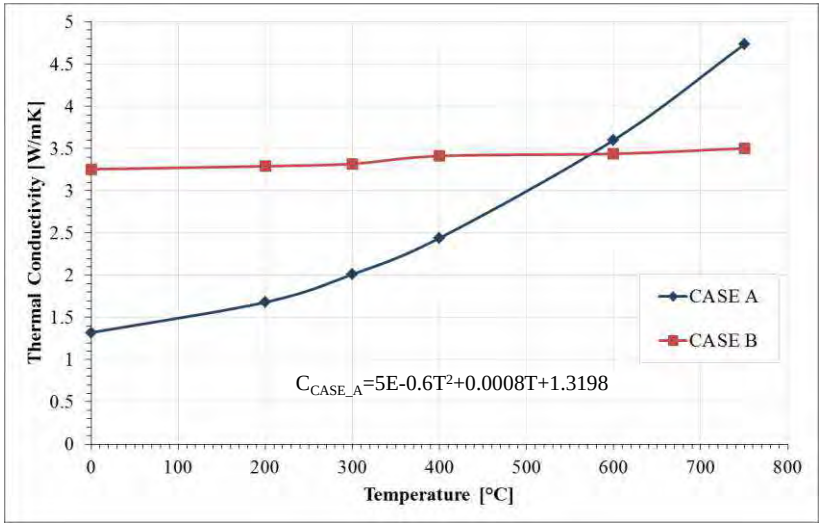

**D. Rozzia et al., «Experimental Investigation on Powder Conductivity for the Application to Double Wall Bayonet Tube Bundle Steam Generator», 24th NENE Conference, 2015.*

HERO PRE-TEST ANALYSIS

Comparison RUN #1/RUN #4 SS1/SS2/SS3

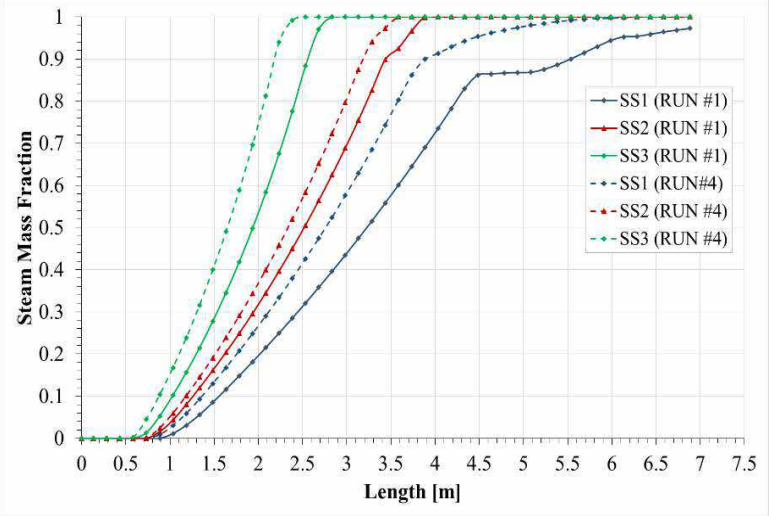

Comparison SS1 RUN #2/RUN#5

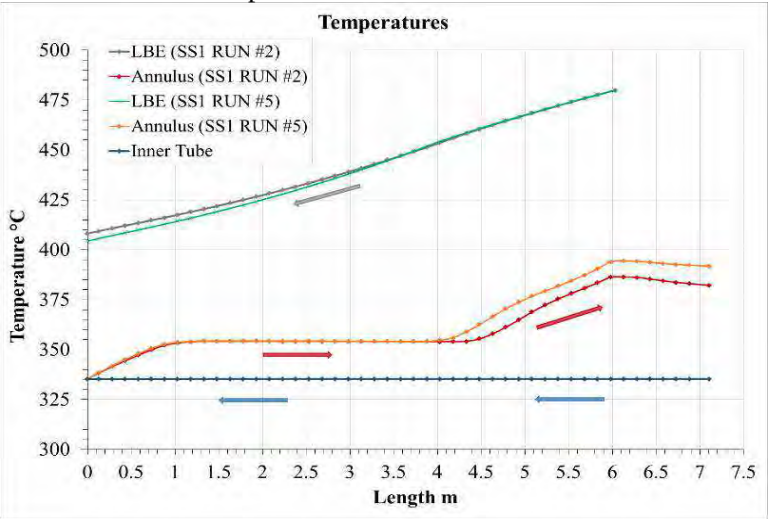

Comparison RUN #1 SS1/SS2/SS3

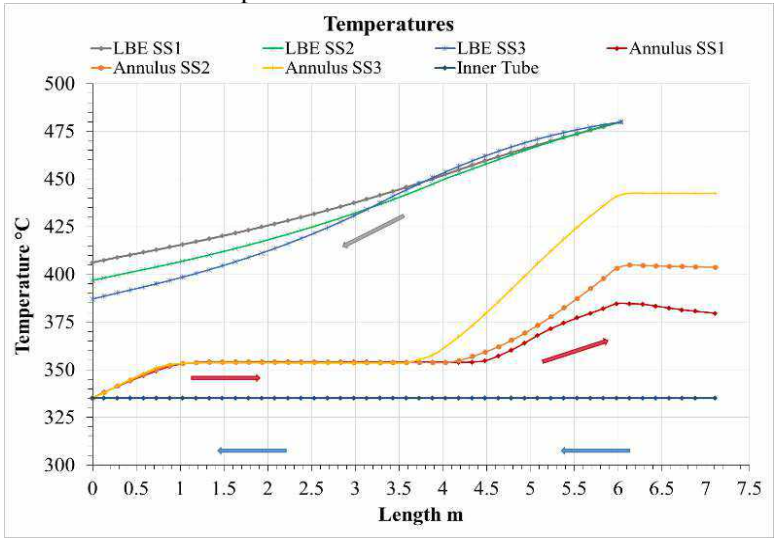

Comparison SS1 RUN #3/RUN#6

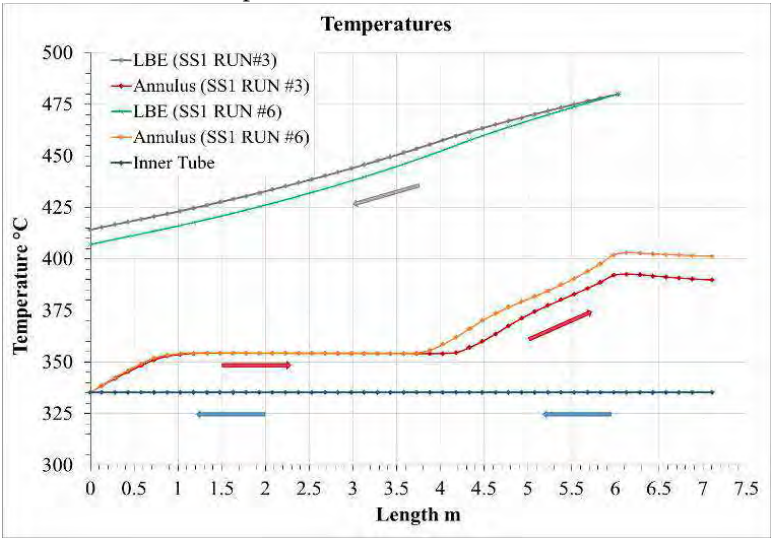

HERO PRE-TEST ANALYSIS

	Parameter	Unit	CASE A			CASE B		
	-	-	RUN #1	RUN #2	RUN #3	RUN #4	RUN #5	RUN #6
SS1	LBE ΔT	° C	73.7	71.8	65.7	77.8	75.6	69.0
	LBE T_{out}	° C	406.3	408.2	414.3	402.2	404.4	411.0
	Steam T_{out}	° C	379.6	382.2	389.8	388.6	391.8	401.3
	Power	kW	394	402	419	416	423	441
	Annulus ΔP	bar	2.27	2.32	2.46	2.45	2.49	2.65
SS2	LBE ΔT	° C	83.1	80.8	73.5	86.5	83.9	76.0
	LBE T_{out}	° C	396.9	399.2	406.5	393.5	396.1	404.0
	Steam T_{out}	° C	403.7	408.0	419.8	415.9	420.6	432.7
	Power	kW	334	339	352	348	352	364
	Annulus ΔP	bar	1.55	1.60	1.69	1.65	1.68	1.80
SS3	LBE ΔT	° C	92.9	89.8	80.7	94.8	91.5	81.8
	LBE T_{out}	° C	387.1	390.2	399.3	385.2	388.5	398.2
	Steam T_{out}	° C	442.4	446.9	457.2	451.6	455.4	463.55
	Power	kW	249	252	257	254	256	261
	Annulus ΔP	bar	0.89	0.94	1.00	0.93	1.00	1.05

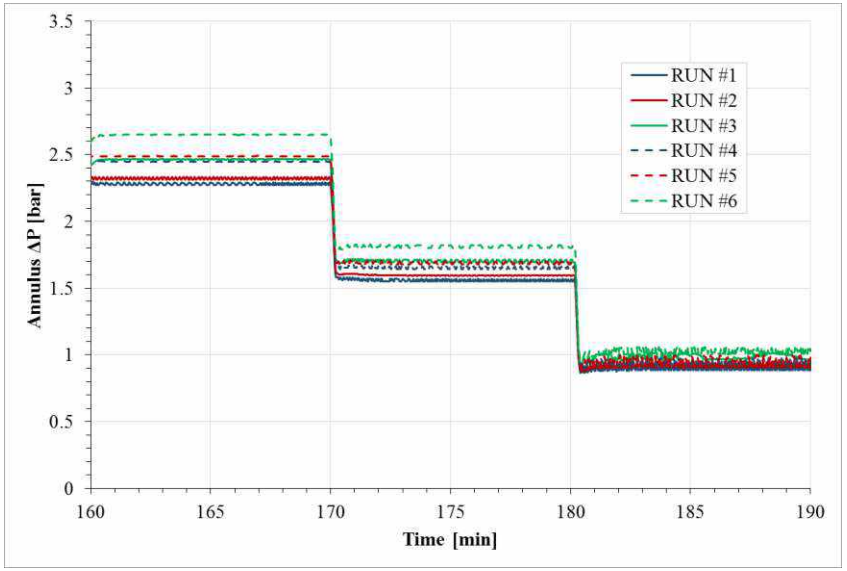

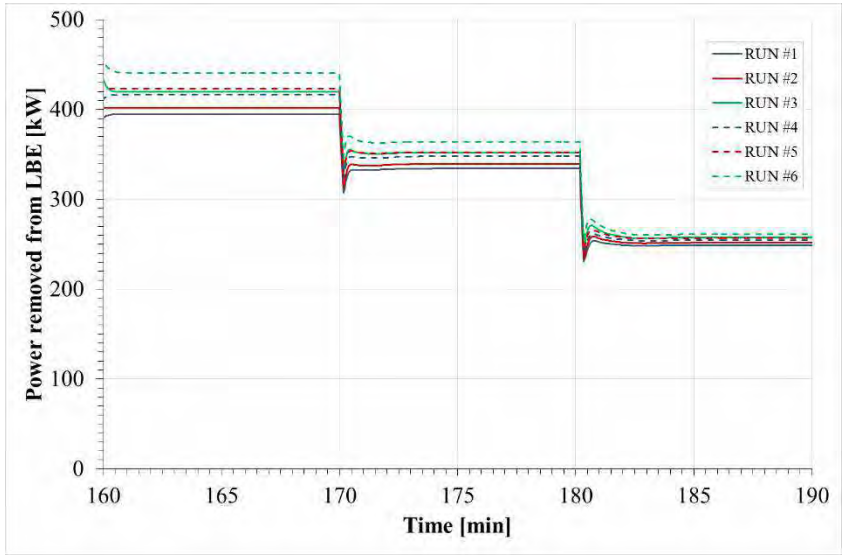

CONCLUSIVE REMARKS AND FOLLOW UP

- Complete nodalization of the CIRCE HERO Secondary Loop
- Preliminary start-up procedure simulated
- High pressure characterization for HERO SGBT unit carried out
  - 3 LBE and h2o mfr; 100%,75%, 50%
  - 2 Kpowder-He
- Activities planned in PAR-2018
  - Comparison of the pre-tests results with the experimental data
  - Post-test calculation and sensitivity study

THANK YOU
FOR
YOUR ATTENTION

Italian National Agency for New Technologies, Energy and Sustainable Economic Development

S.R.S. Servizi di Ricerche e Sviluppo S.r.l.

BEFORE IT HAPPENS

UNIVERSITÀ DI PISA

Small Leakage Detection in LFR SG

Workshop Tematico: Gen. IV - LCFR

ADP MiSE-ENEA (PAR2017-LP2)

DIAEE – Università di Roma «La Sapienza»

14-15 Giugno 2018

M. Eboli, N. Forgione / UNIPI
A. Del Nevo / ENEA FSN-ING
D. Mazzi, F. Giannetti / SRS

List of contents

- Objectives
- Introduction to LIFUS5/Mod3
- Description of LIFUS5/Mod3 – Test Section Small Leak (S1A)
- Execution of the experiments – Test series C
- Summary and Follow-up

Objectives

- The goal was to implement an experimental activity, supported by the numerical simulations, which **characterizes the leak rate and bubbles sizing through typical cracks** occurring in the pressurized tubes
  - Basic tests in LIFUS5/Mod3 facility have been carried out to correlate the flow rates of the leakage through selected cracks with signals detected by proper transducers
  - Different crack sizes and geometries have been analyzed, while the injection pressure and the temperature have been recorded
  - A detection system detected the bubbles migration through the free level

Introduction to LIFUS5/Mod3

- LIFUS5/Mod3 (*the third refurbishment*) is a multi purpose facility:
  experiments related the HLM (i.e. PbLi, LBE, Pb) and H_2O interaction /reaction
  - ✓ S1A → Small Leak detection
  - ✓ S1B → Large break – BE code model development and validation

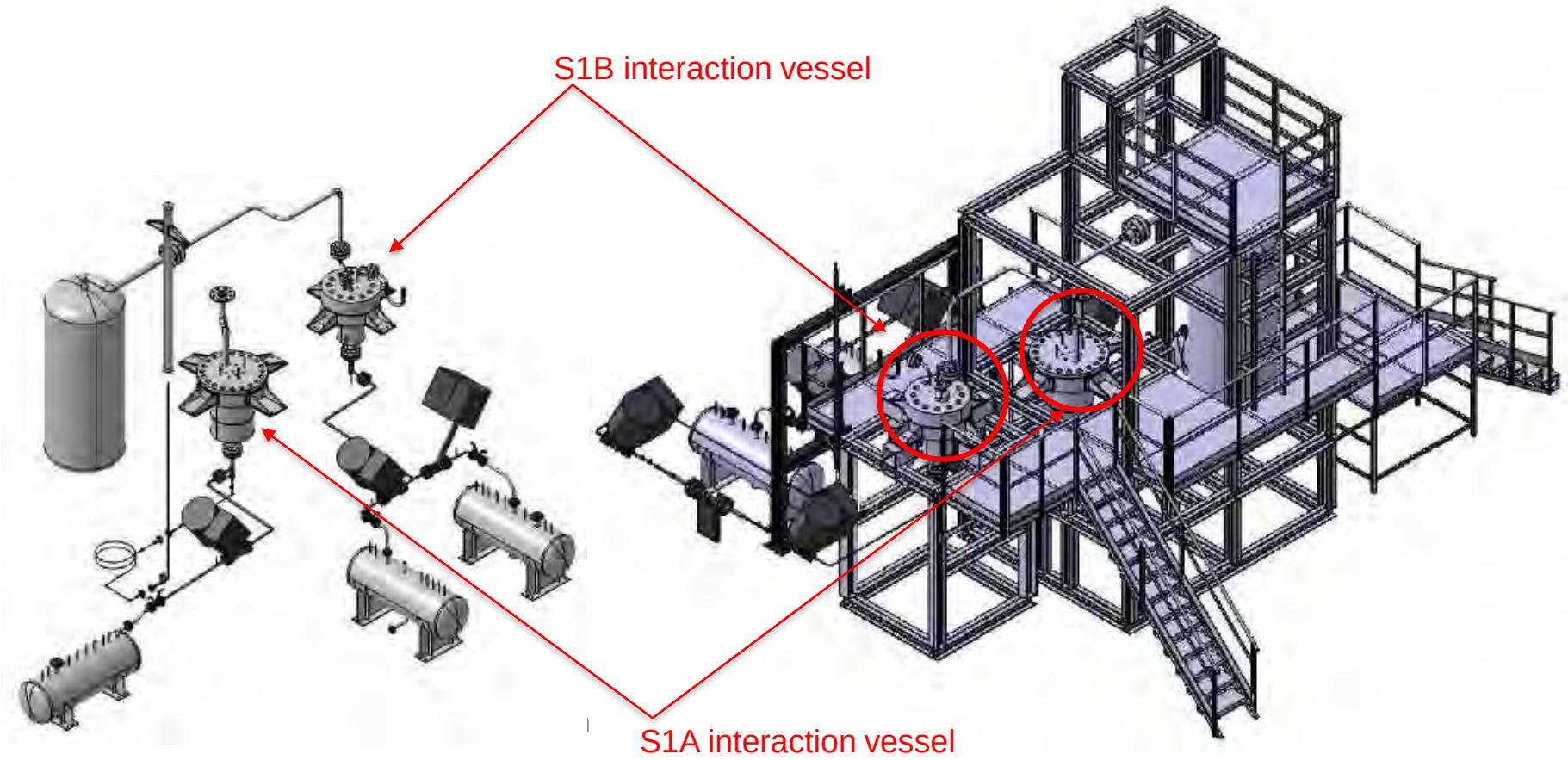

LIFUS5/Mod3: Test Section Small Leak

- LIFUS5/Mod3-S1A synoptic (control system and data recording based on NI / Labwiew)
  - Two additional PCs are in charge of the leak detection systems (NI and DAWEsoft)

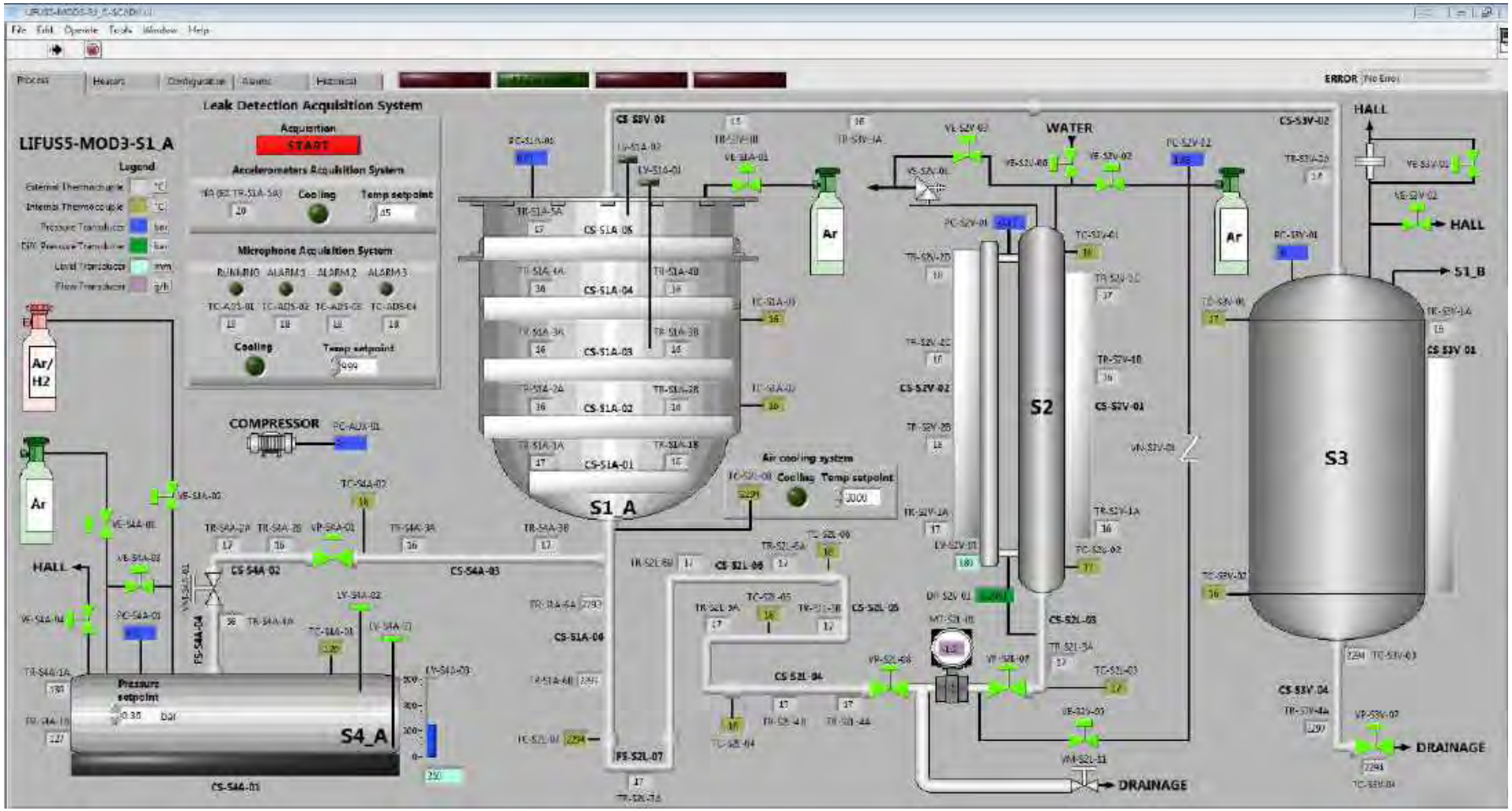

LIFUS5/Mod3: Test Section Small Leak

Injection system acquisition (1 Hz)

- S2V filled with “cold” water at 16 bar
- Mass of water injected monitored through
  - the level meter (resolution 5 mm)
  - DP meter (resolution < 1 mm)
  - Coriolis flow meter
  - 5 TC

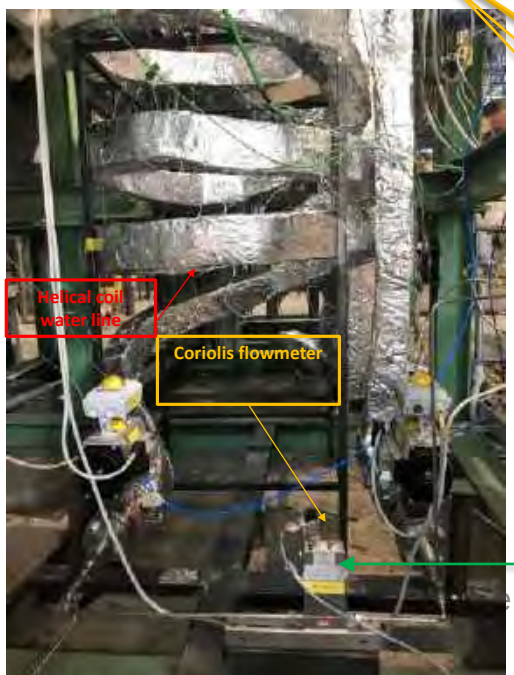

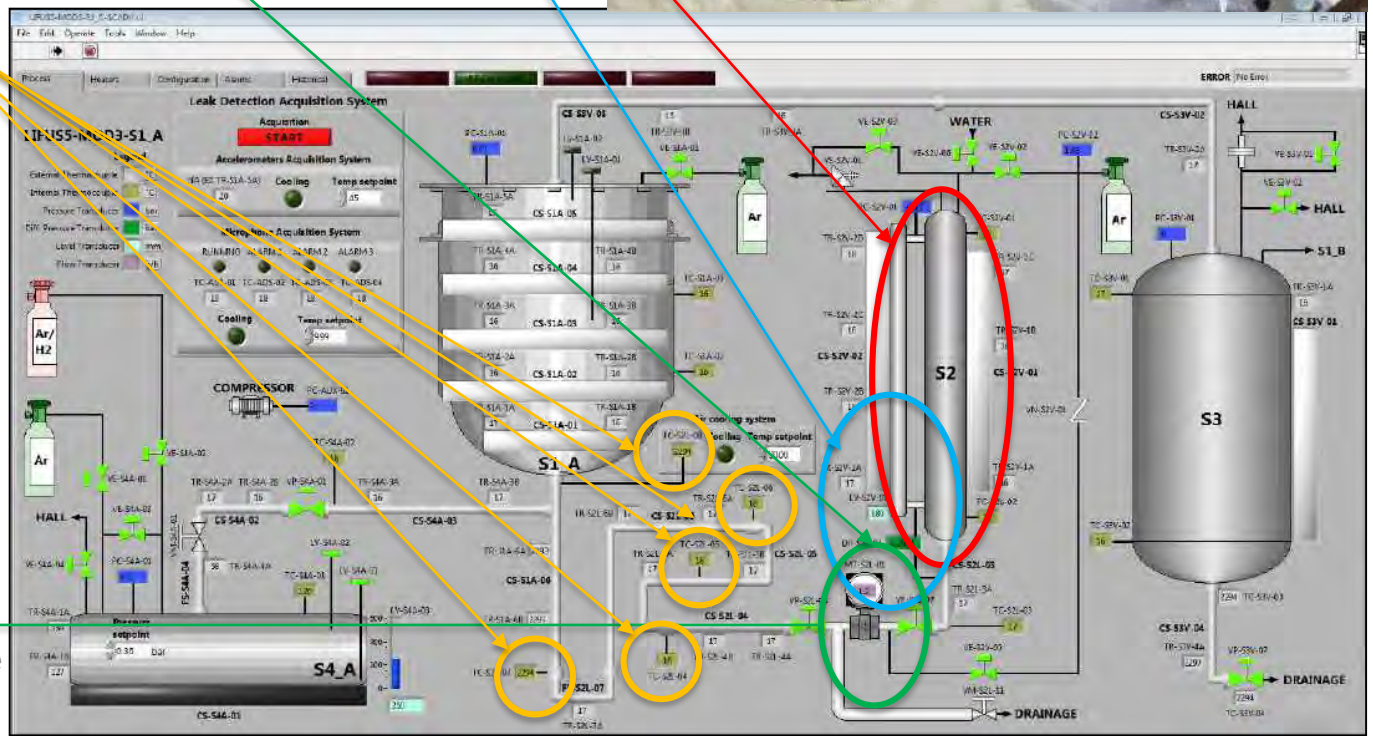

LIFUS5/Mod3: Test Section Small Leak

- S1A filled with LBE @ 1 bar - S3V connected
  - Absolute pressures in S1A and S3V
  - LBE temperature monitored by 2 TC
  - 2 Level ON/OFF
  - Small leak detection system

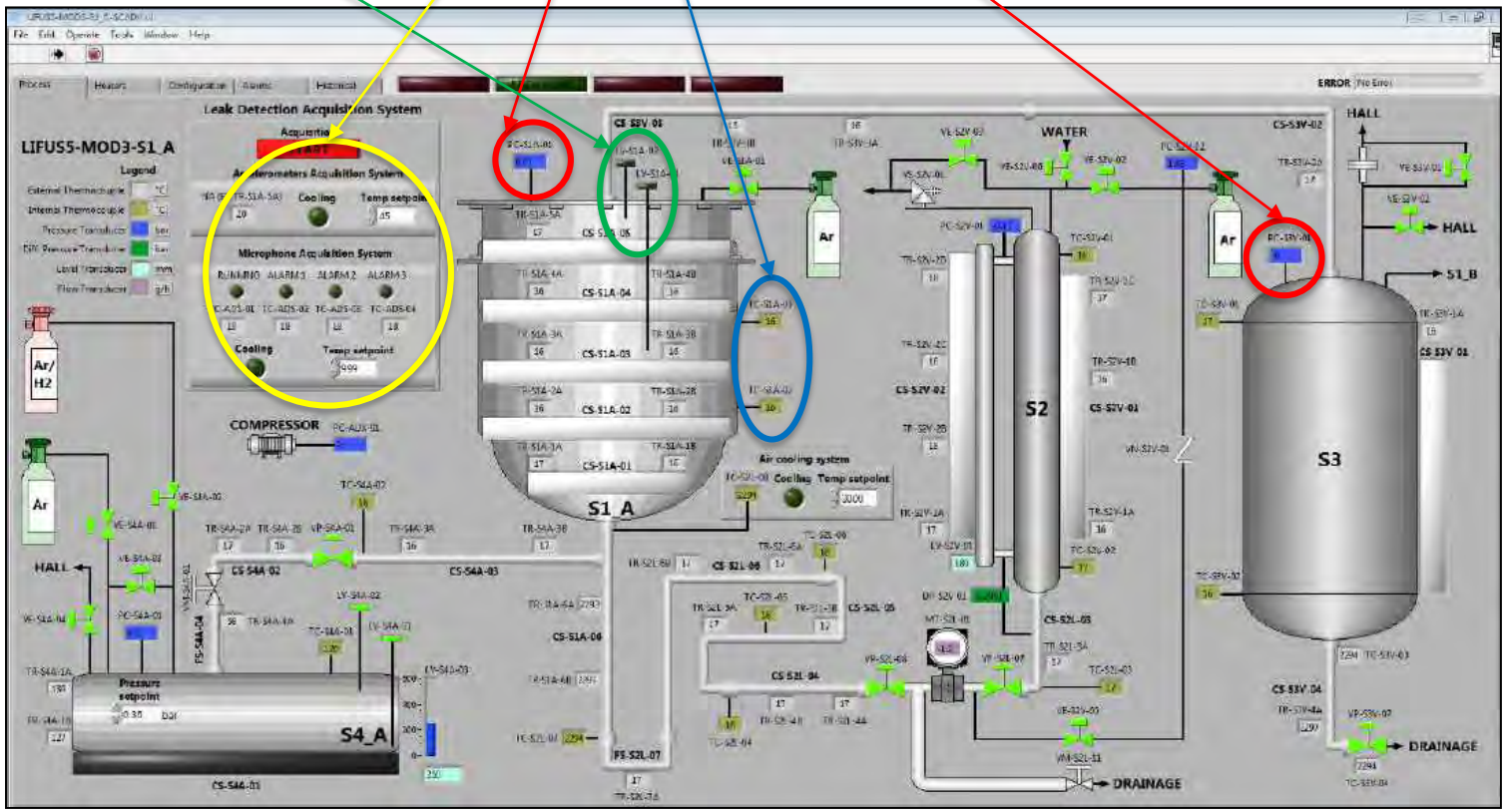

LIFUS5/Mod3: Test Section Small Leak

Primary detection system

Acoustic Detection (ADS) with dedicated hardwar
and software (i.e. real time acquisition system)

- ❑ Acquisition at @ 20 kHz
- ❑ Data analysis on real time (8 channels)
- ❑ 5 microphones on the cover flange

ADS support and cooling system
of Low T acoustic sensors

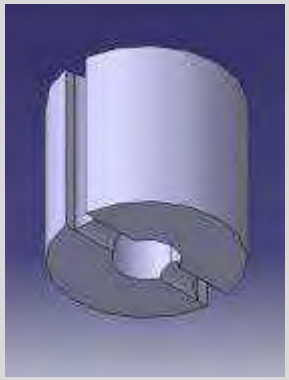

Ceramic support

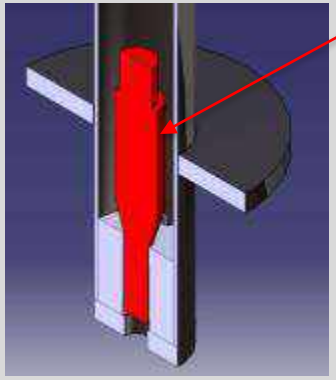

AD support and
cooling system

Temperature is monitored (TC) and Ar gas cooling thanks the lateral grooves in the ceramic support

#4 → Model 130E20
(low temperature)

#1 → Model 377B26
(high temperature)

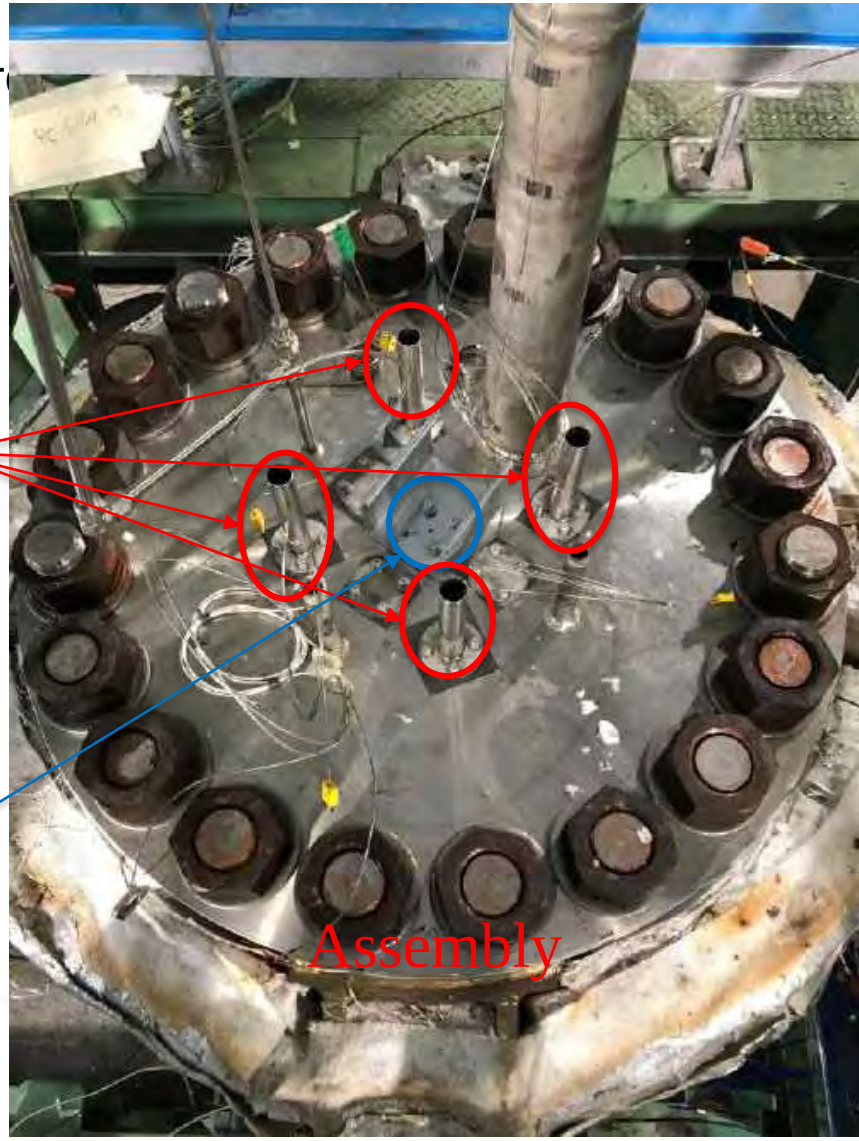

LIFUS5/Mod3: Test Section Small Leak

Alternative detection systems

1. Inductive proximity sensor (i.e. High Sensitivity Accelerometer – HSA) installed outside the vessel
2. Accelerometer sensors installed inside the vessel (i.e. High Temperature Accelerometer – HTA) installed on a metallic support
3. Acoustic Emission (AE) sensor installed outside the vessel, measuring the high frequency signals

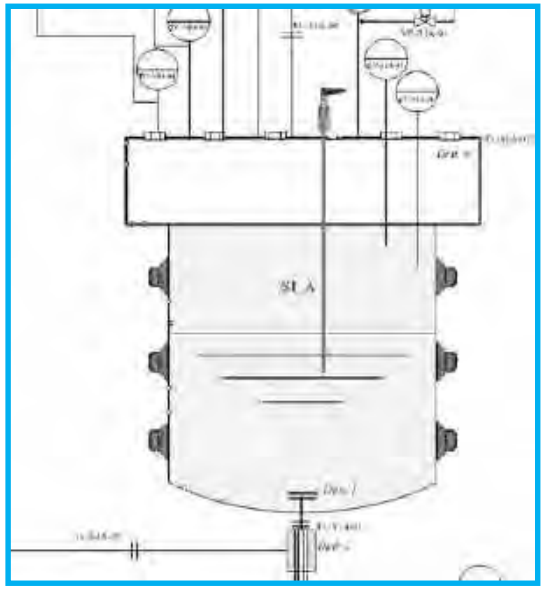

High Sensitivity Accelerometer – **HSA**

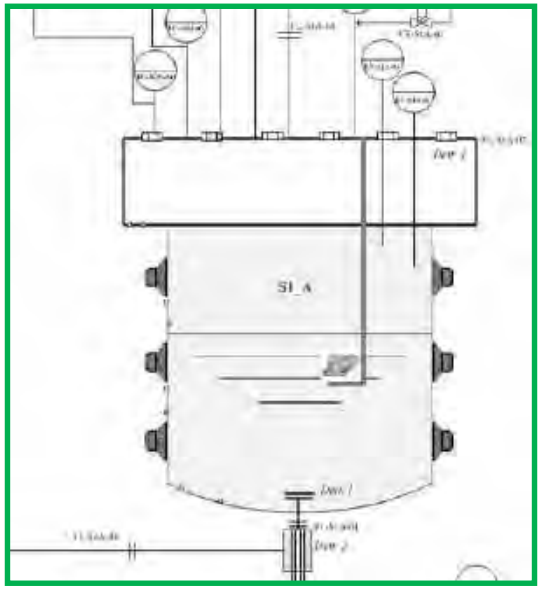

High Temperature Accelerometer – HTA

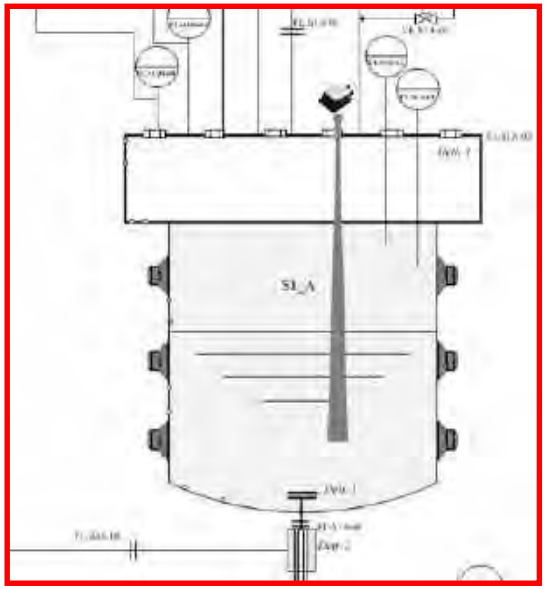

Acoustic Emission – **AE**

LIFUS5/Mod3: Test Section Small Leak

Alternative detection systems

1. High Sensitivity Accelerometer – **HSA**
2. High Temperature Accelerometer – **HTA**
3. Acoustic Emission (**AE**)

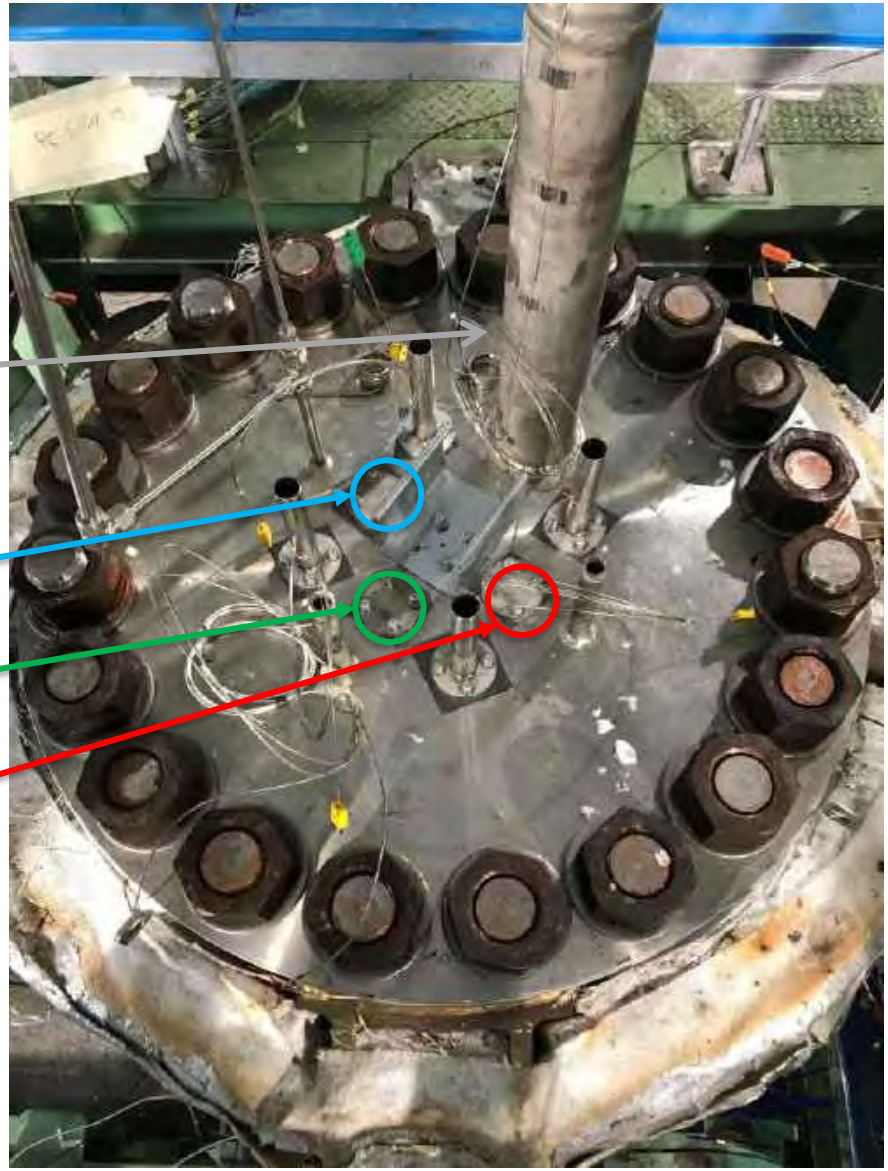

LIFUS5/Mod3: Test Section Small Leak

- Injector disk hole design: nominal orifice diameters

Description	#1	#2	#3	#4	#5	#6	#7	#8	#9
Orifice diameter [mm]	0.005	0.010	0.020	0.040	0.060	0.080	0.10	0.15	0.20

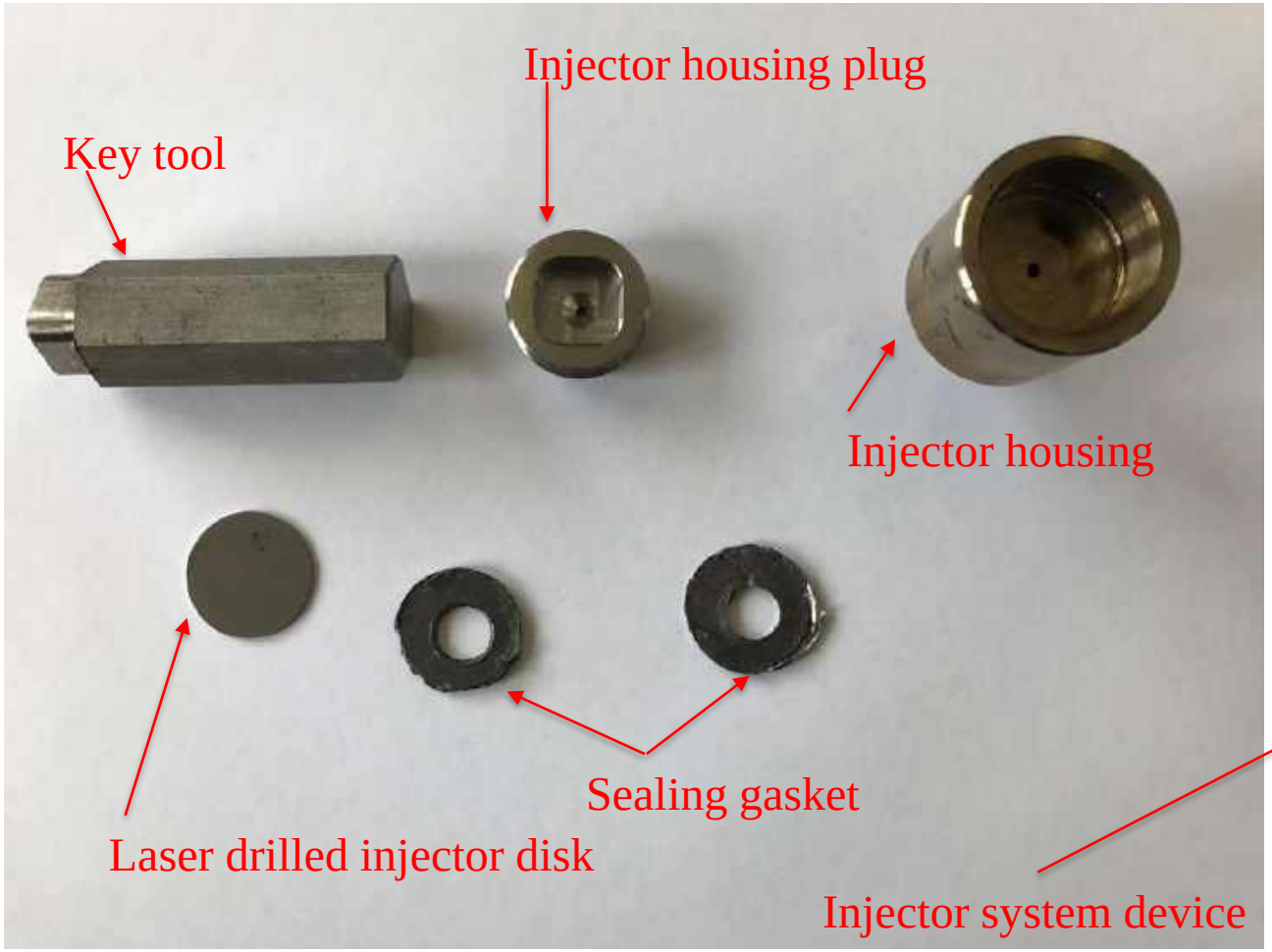

LIFUS5/Mod3: Test Section Small Leak

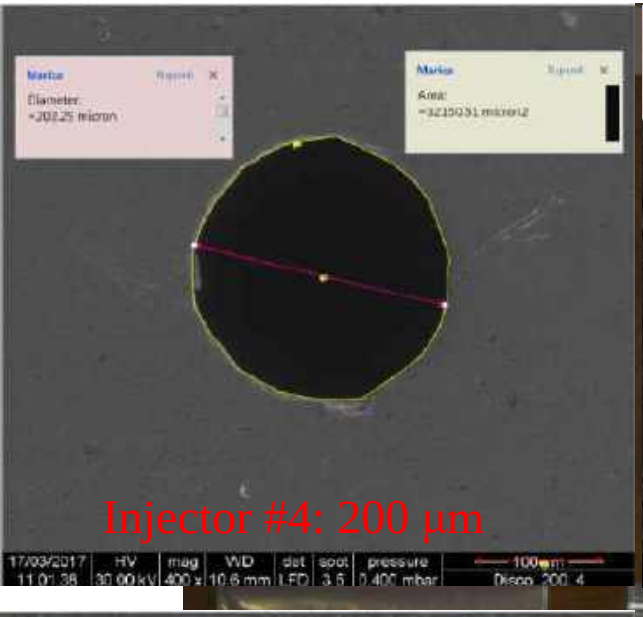

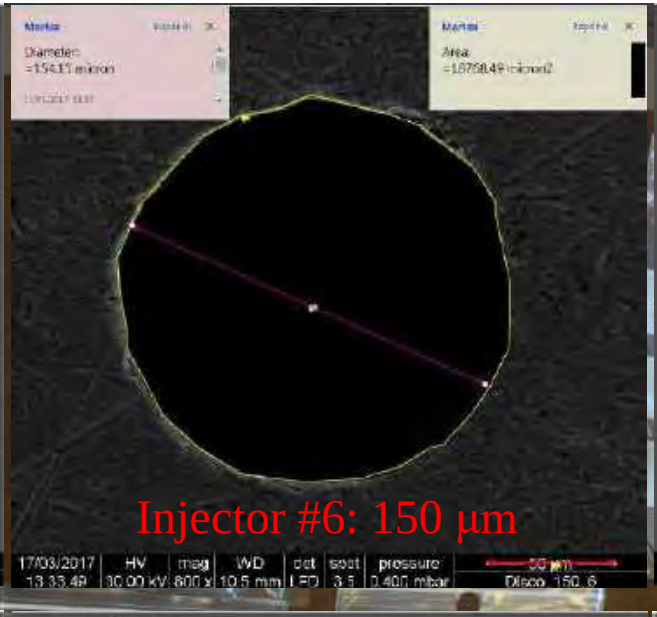

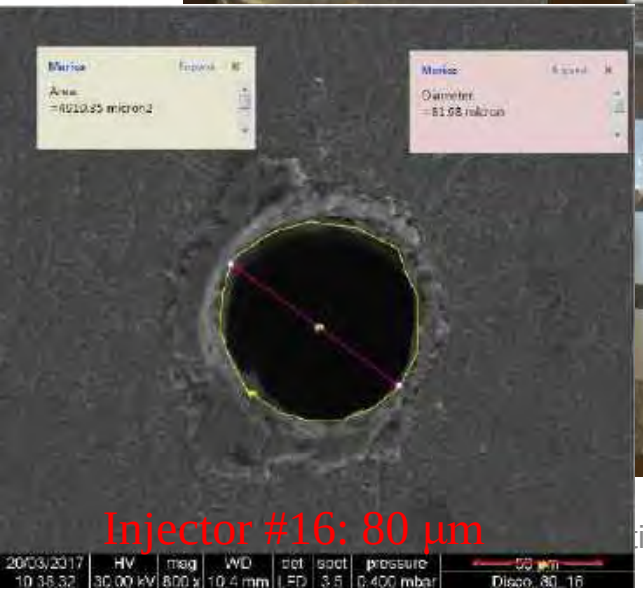

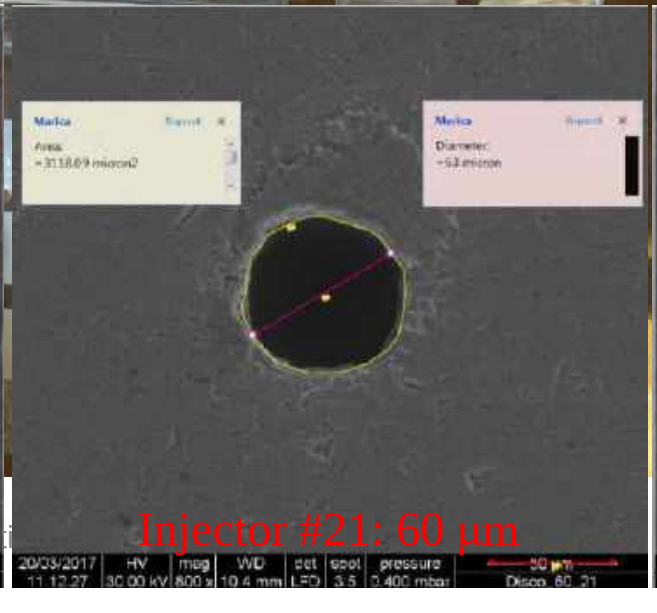

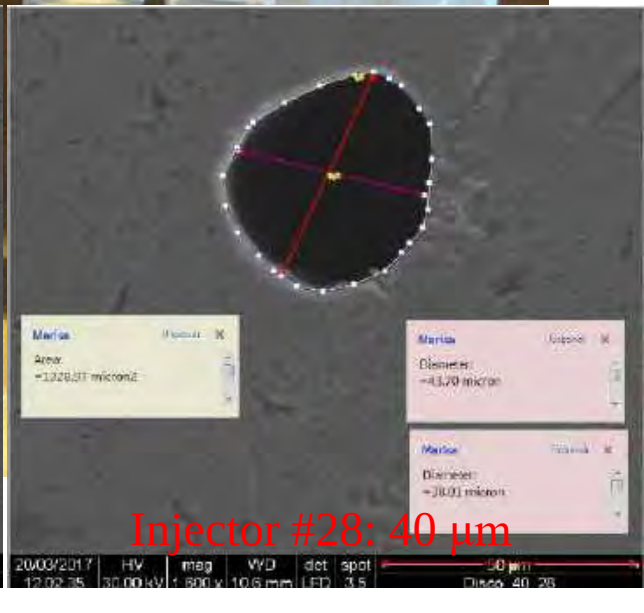

Execution of experiments – Test series C

Parameter	TEST										
	C1.1 (_60)	C1.2 (_60)	C1.3 (_60)	C2.1 (_80)	C2.2 (_80)	C3.1 (_40)	C3.2 (_40)	C4.1 (_100)	C4.2 (_100)	C5.1 (_150)	C6.1 (_200)
Number of Test	T#1	T#7	T#10	T#2	T#9	T#3	T#6	T#4	T#5	T#8	T#11
Date of execution	06 Sep	19 Jan	8 Feb	13 Sep	2 Feb	20 Oct	15 Dec	10 Nov	22 Nov	26 Jan	6 Apr
Number of laser-holed plate	21	22	23	16	19	27	28	11	13	6	4
Inj. orifice design diameter [μm]	60	60	60	80	80	40	40	100	100	150	200
Inj. orifice measured flow area [μm^2]	3188	3080	3257	4919	5508	1392	1329	8116	7676	18768	32151
Acquisition time [hh:mm]	06:15	NA	09:00	11:22	5:00	NA	5:29	NA	7:29	5:59	3:00
Leak detection system acquisition	All	NA	All	All	All	NA	*	NA	*	All	All
LBE temperature TC-S4A-01 [°C]	203	NA	226	209	226	NA	NI	NA	NI	226	246
Water pressure PC-S2V-01 [bar]	19.7	NA	20.1	20.2	19.3	NA	NI	NA	NI	20.3	20.2
Water temperature TC-S2L-08 [°C]	170	NA	219	200	210	NA	NI	NA	NI	203	247
											

r-to-test

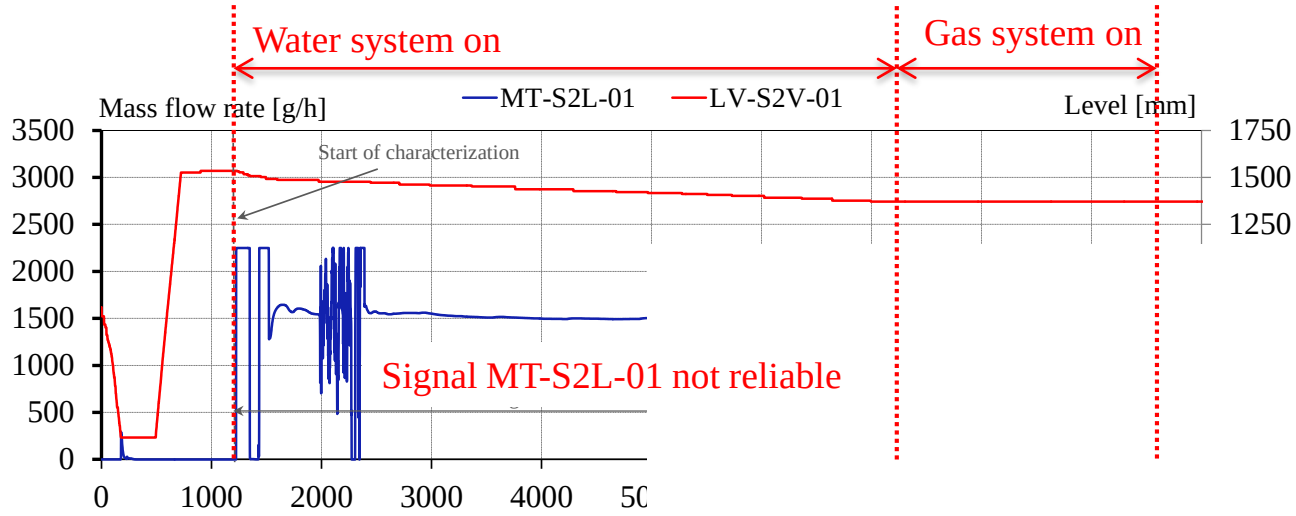

Preparation to Test
C1.1_60

- Water @ 19 bar, 40°C
- Mass flow rate of 1500 g/h not reliable
- Signal LV is stable from 2000 to 7000 s
- Average mass flow rate of 667 g/h
- Total mass of injected water in 5000 s is 0.93 kg

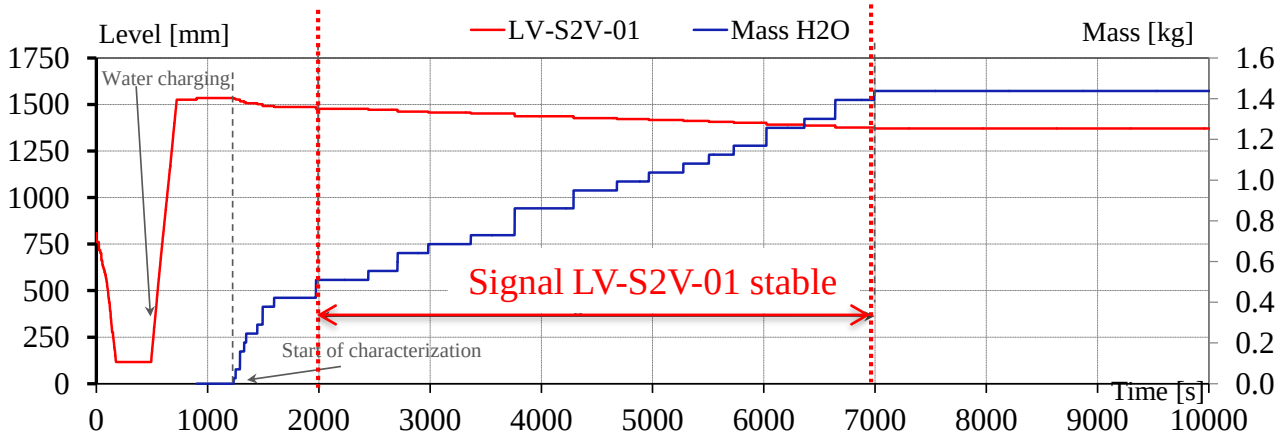

Test C.1.1_60 : RELAP5/Mod3.3 analyses

- Simulations performed in order to investigate the mass flow rate at the orifice of the water and Argon fluids in the conditions relevant for the experiment
- The nodalization models the actual LIFUS5/Mod3 injection line geometry

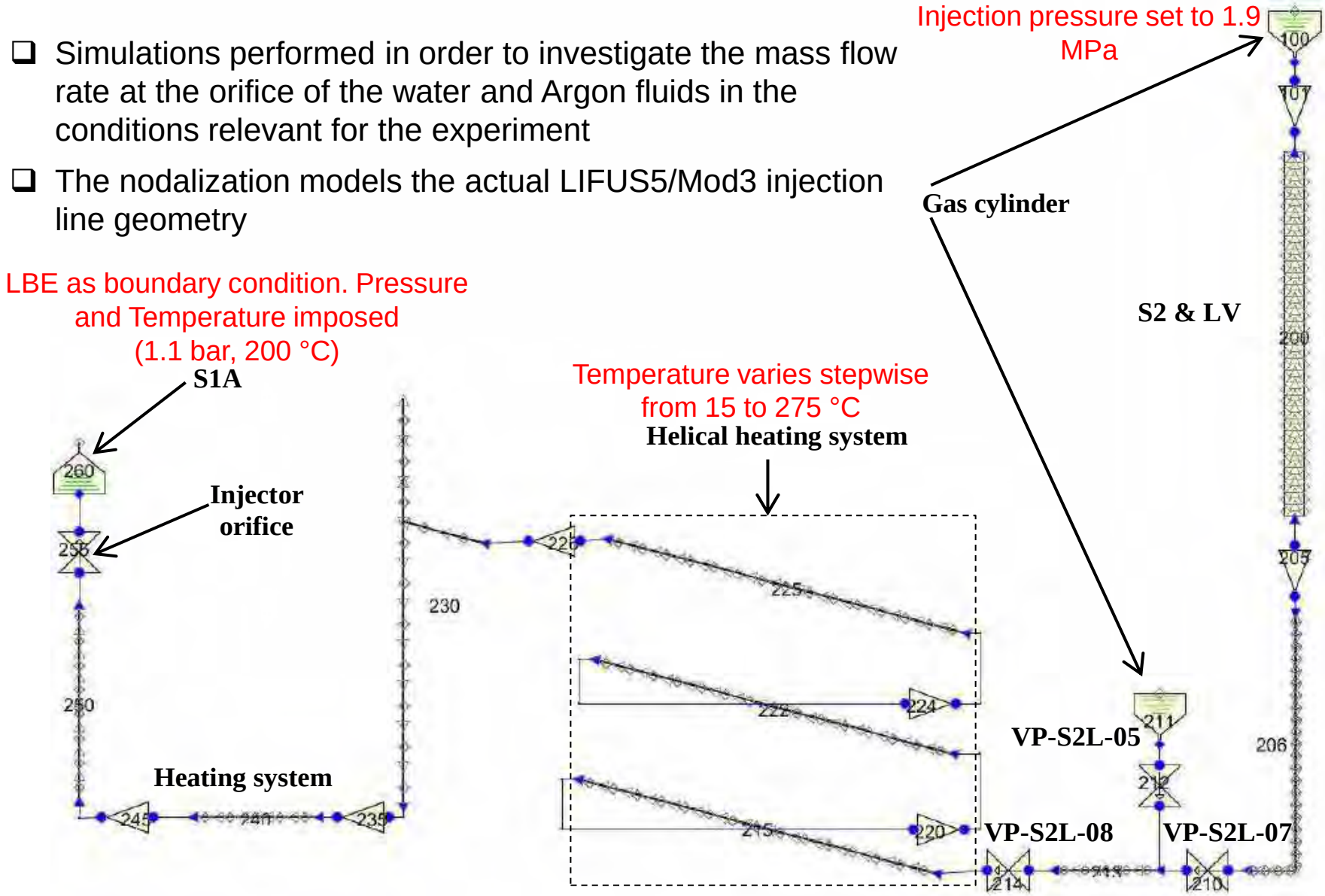

Test C.1.1_60 : RELAP5/Mod3.3 analyses

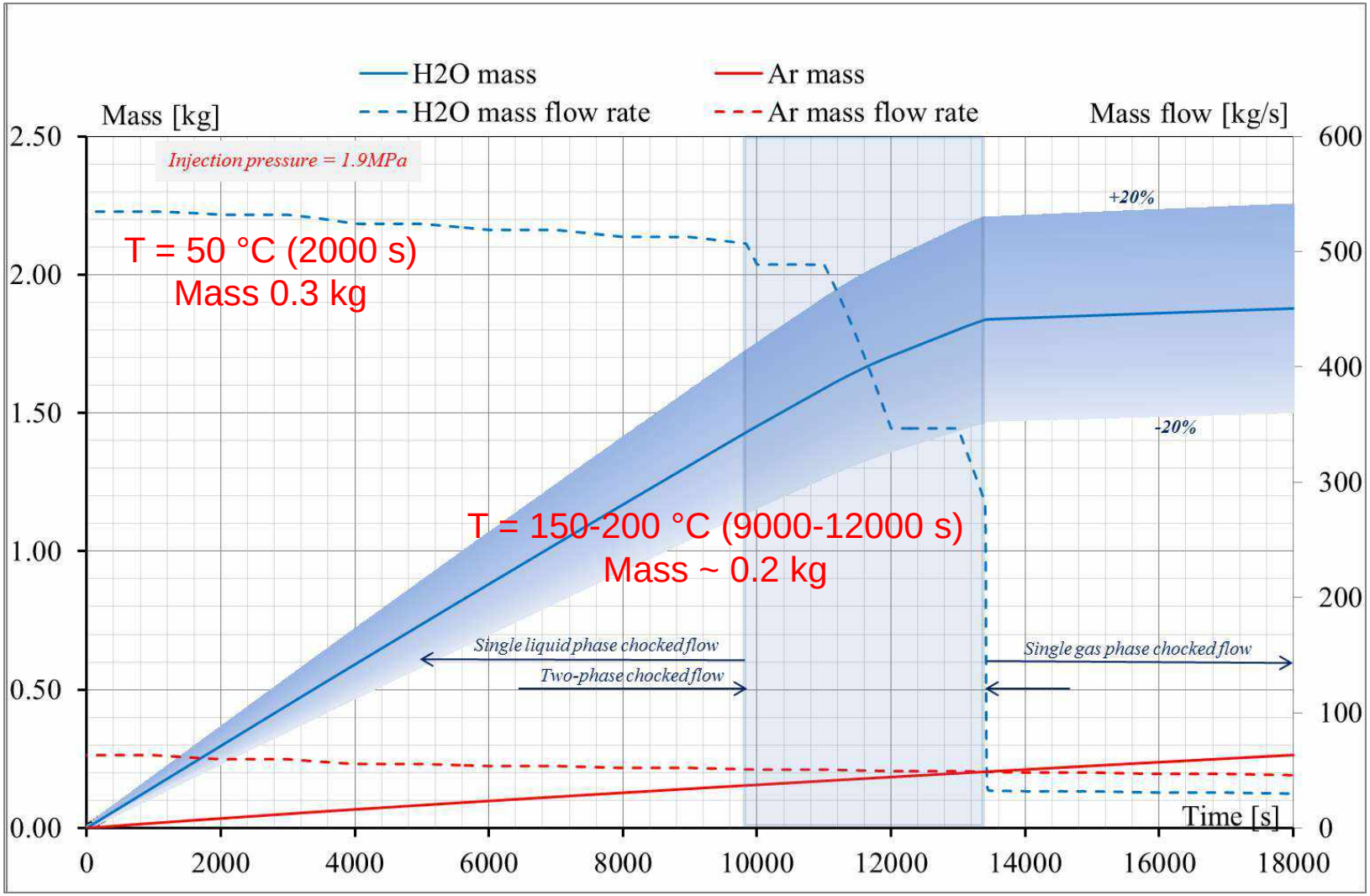

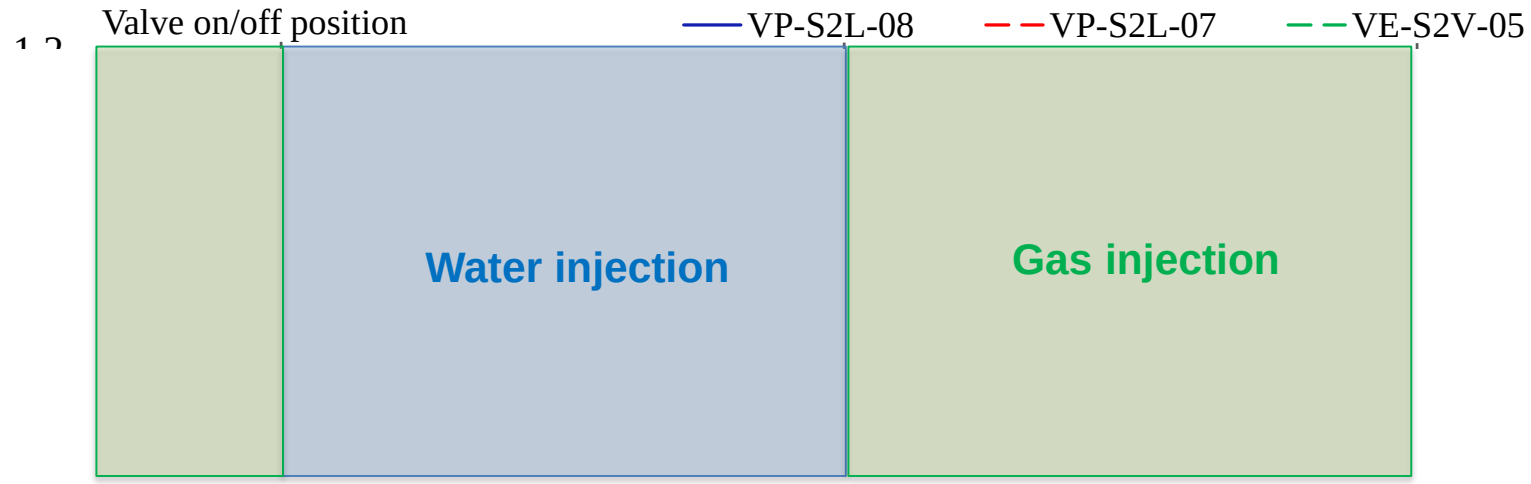
Valve on/off position
VP-S2L-08
VP-S2L-07
VE-S2V-05
Water injection
Gas injection

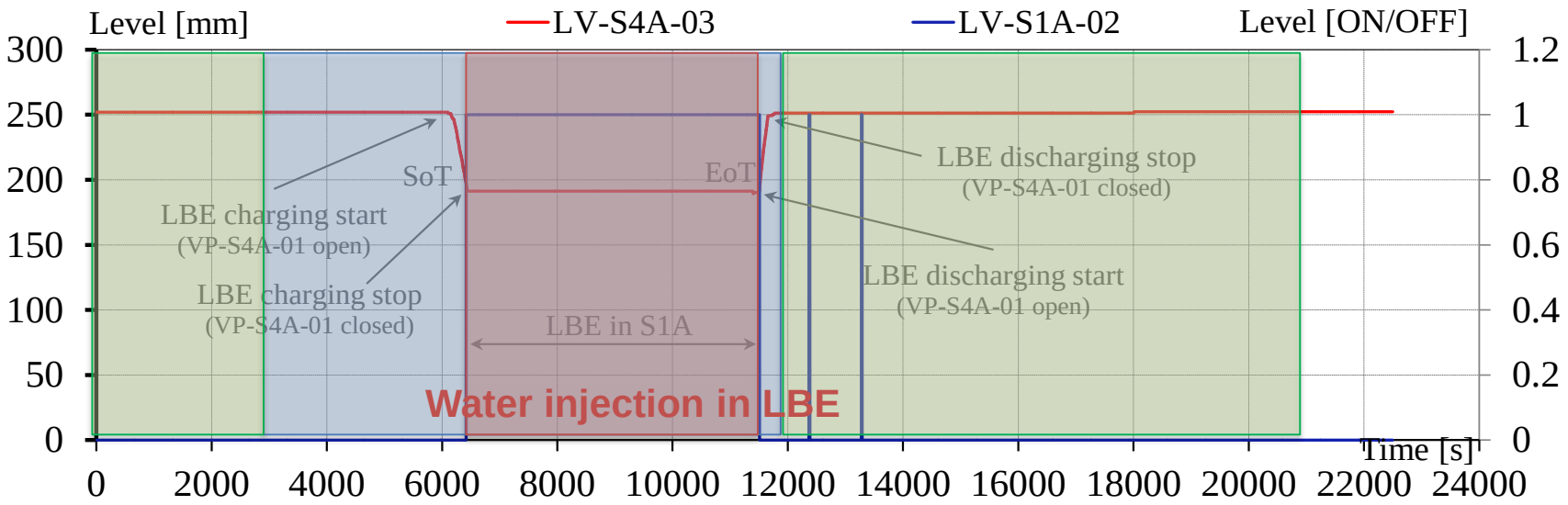
Level [mm]
LV-S4A-03
LV-S1A-02
Level [ON/OFF]
300
250
200
150
100
50
0
1.2
1
0.8
0.6
0.4
0.2
0
SoT
EoT
LBE charging start
(VP-S4A-01 open)
LBE charging stop
(VP-S4A-01 closed)
LBE discharging stop
(VP-S4A-01 closed)
LBE discharging start
(VP-S4A-01 open)
LBE in S1A
Water injection in LBE
Time [s]
0
2000
4000
6000
8000
10000
12000
14000
16000
18000
20000
22000
24000

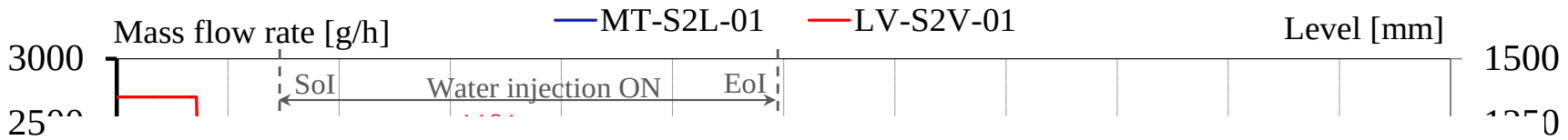

Injected water in 5000 s recorded by MT not reliable, while LV measured coherently with characterization and RELAP5/Mod3.3 results (~ 0.44 kg)

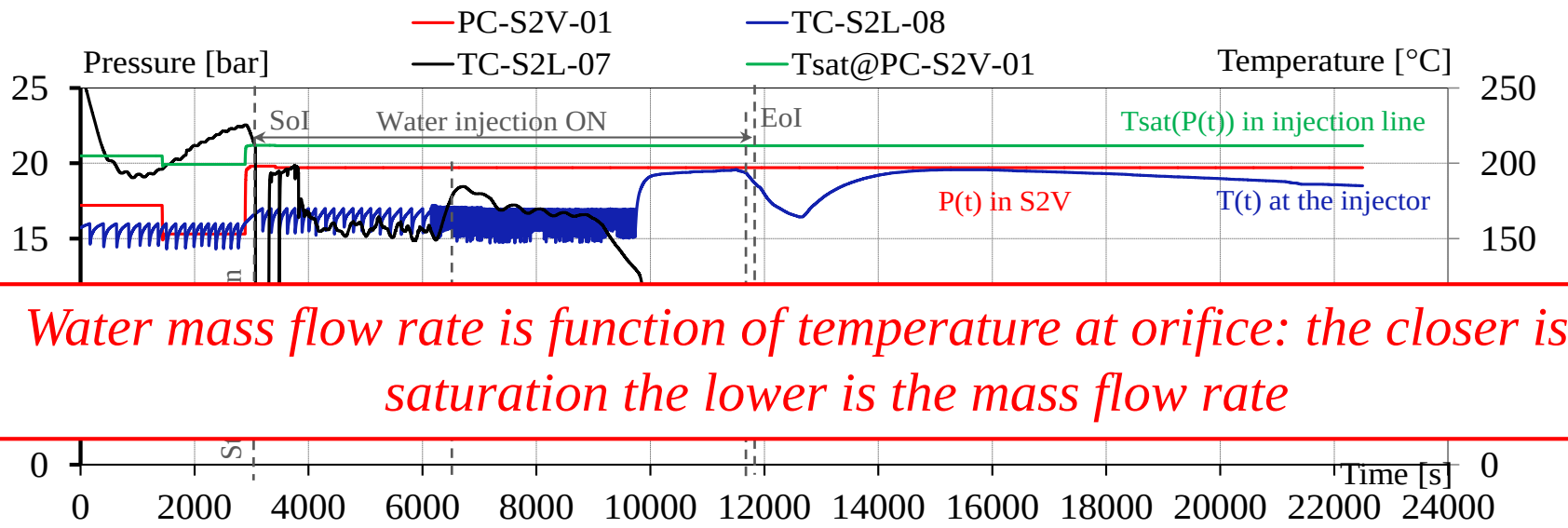

Water mass flow rate is function of temperature at orifice: the closer is the saturation the lower is the mass flow rate

Test C.1.1_60 : EDTAR

It seems possible to distinguish the phases:

1. Water injection w/o LBE in S1A
2. Water injection w LBE in S1A
3. Gas Injection

⟹ *Analyses of data is ongoing*

Acquisitions in intervals from time 16.31 to 20.35 – about 30GB of compressed data

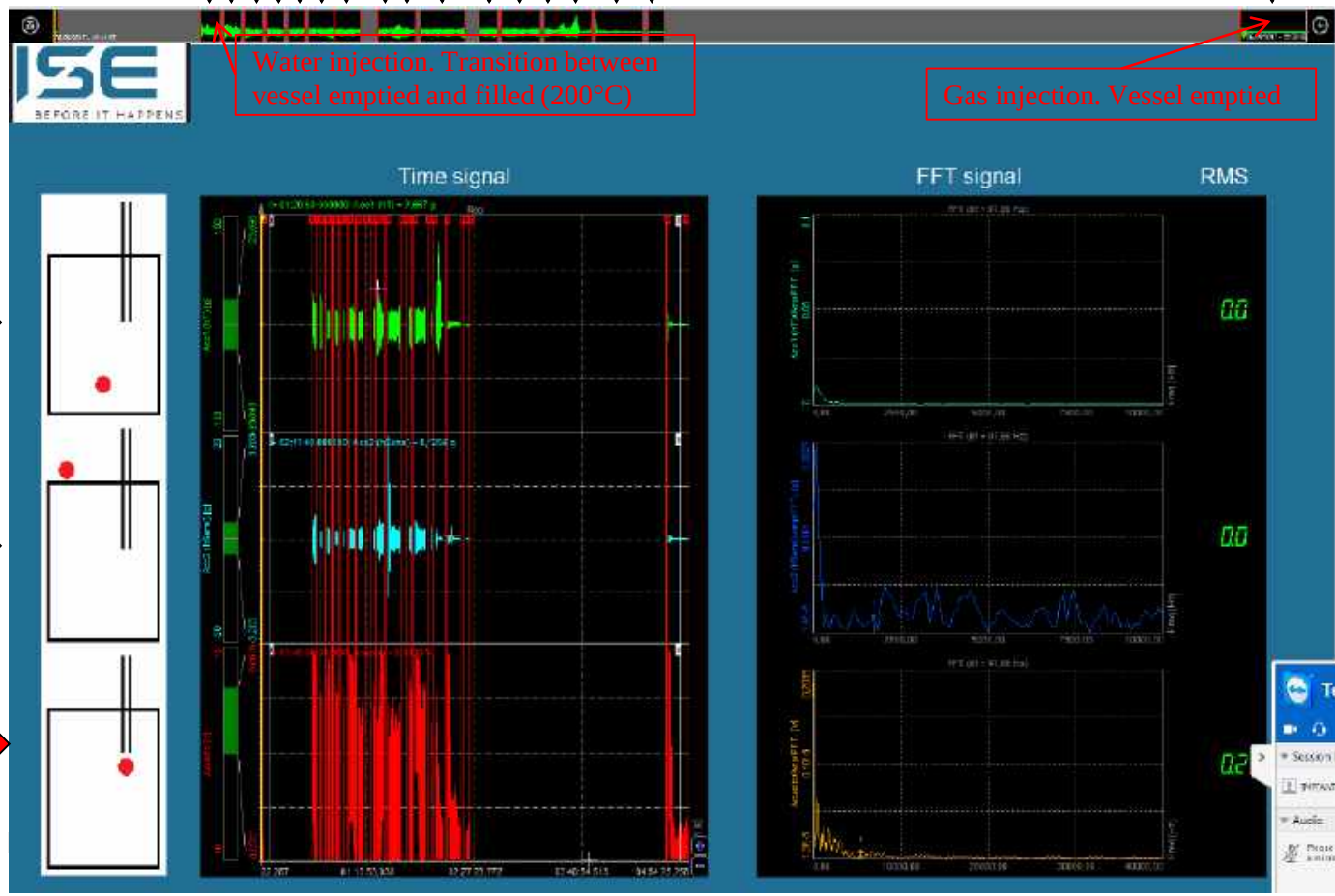

High Temperature Accelerometer – HTA

High Sensitivity Accelerometer – **HSA**

Acoustic Emission (**AE**)

Small Leakage

Test C.1.1_60 : EDTAR

Water injection. Transition between vessel emptied and filled

Gas Injection

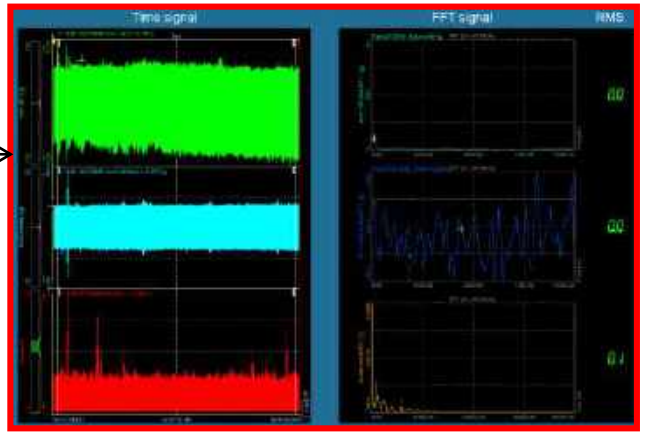

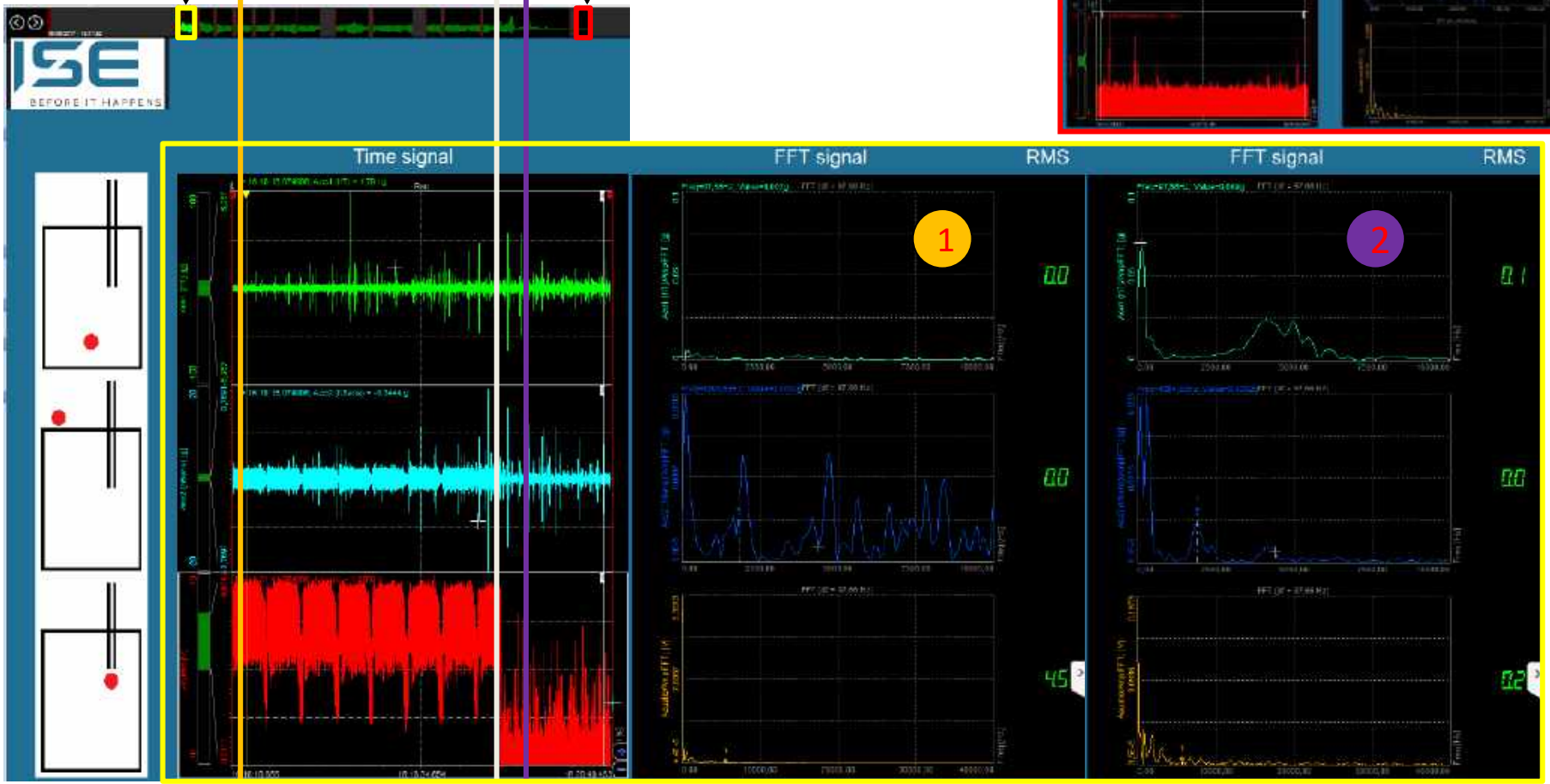

Summary and Follow-up

- An experimental activity for characterizing the leak rate through typical cracks occurring in the pressurized tubes has been designed and implemented
- 50 laser drilled disks have been manufactured and characterized for simulating the leak
- A primary detection system – Acoustic Detection (ADS) – has been installed and tested
- Alternative detection systems, supported by the PAR2016, have been also identified and installed. They are: 1) High Sensitivity Accelerometer HSA; 2) High Temperature Accelerometer HTA; and 3) Acoustic Emission AE
- The experimental campaign was successfully concluded executing 8 tests (laser micro-holed plate from 40 to 200 μm)
- Preliminary evaluation of data seems to demonstrate that is possible to distinguish the different phases of the experiment. Analysis of data is in progress
- Analyses of the experimental data and the preparation of the EDTAR are ongoing

Ing. Marica Eboli, Ph.D.
marica.eboli@ing.unipi.it

Italian National Agency for New Technologies,
Energy and Sustainable Economic Development

Natural circulation experiments in the NACIE-UP loop

ADP-PAR2017-LP2

Università di Roma La Sapienza 14-15/06/2018

I. Di Piazza (ENEA FSN-ING-TESP)

Workshop tematico ADP MiSE-ENEA (PAR2017-LP2)

Generation IV Lead Cooled Fast Reactor: Stato Attuale Della Tecnologia E Prospettive Di Sviluppo

Summary

- NACIE-UP facility
  - Fuel Pin Bundle Simulator
- Experimental test matrix
- Experimental results
  - Comparison between ADP10 & ADP06
  - FPS temperature - Test ADP07
- Conclusions

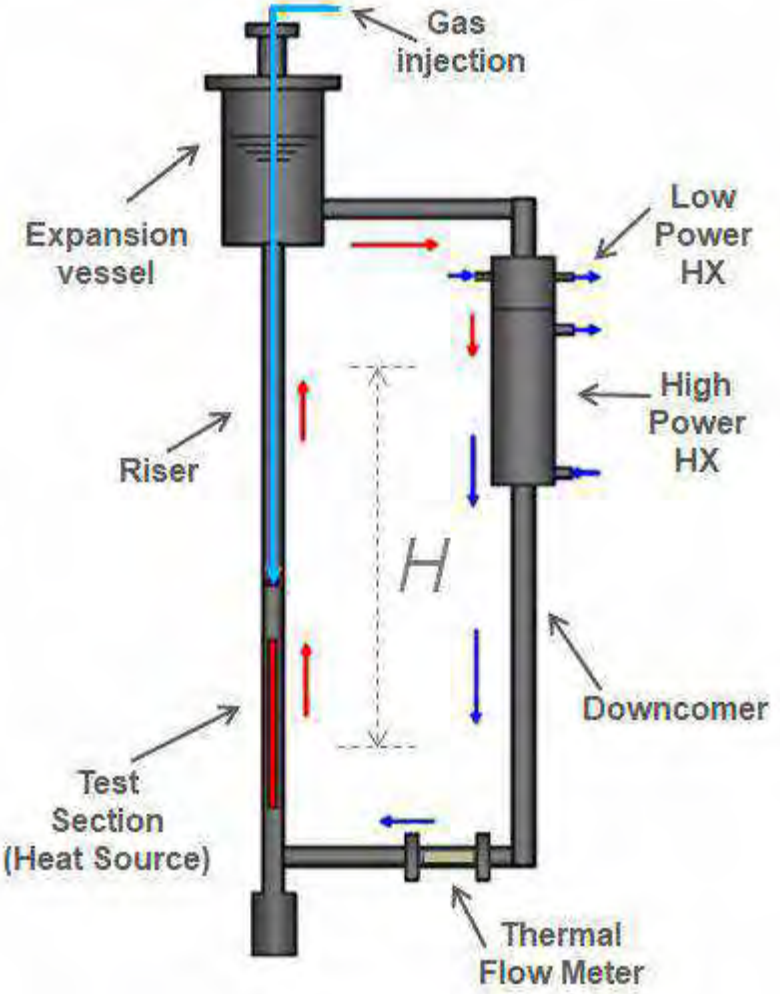

NACIE-UP Facility – Primary loop

Composed by heat source (FPS), heat sink (H_2O Hx), expansion vessel, prototypical thermal flow meter

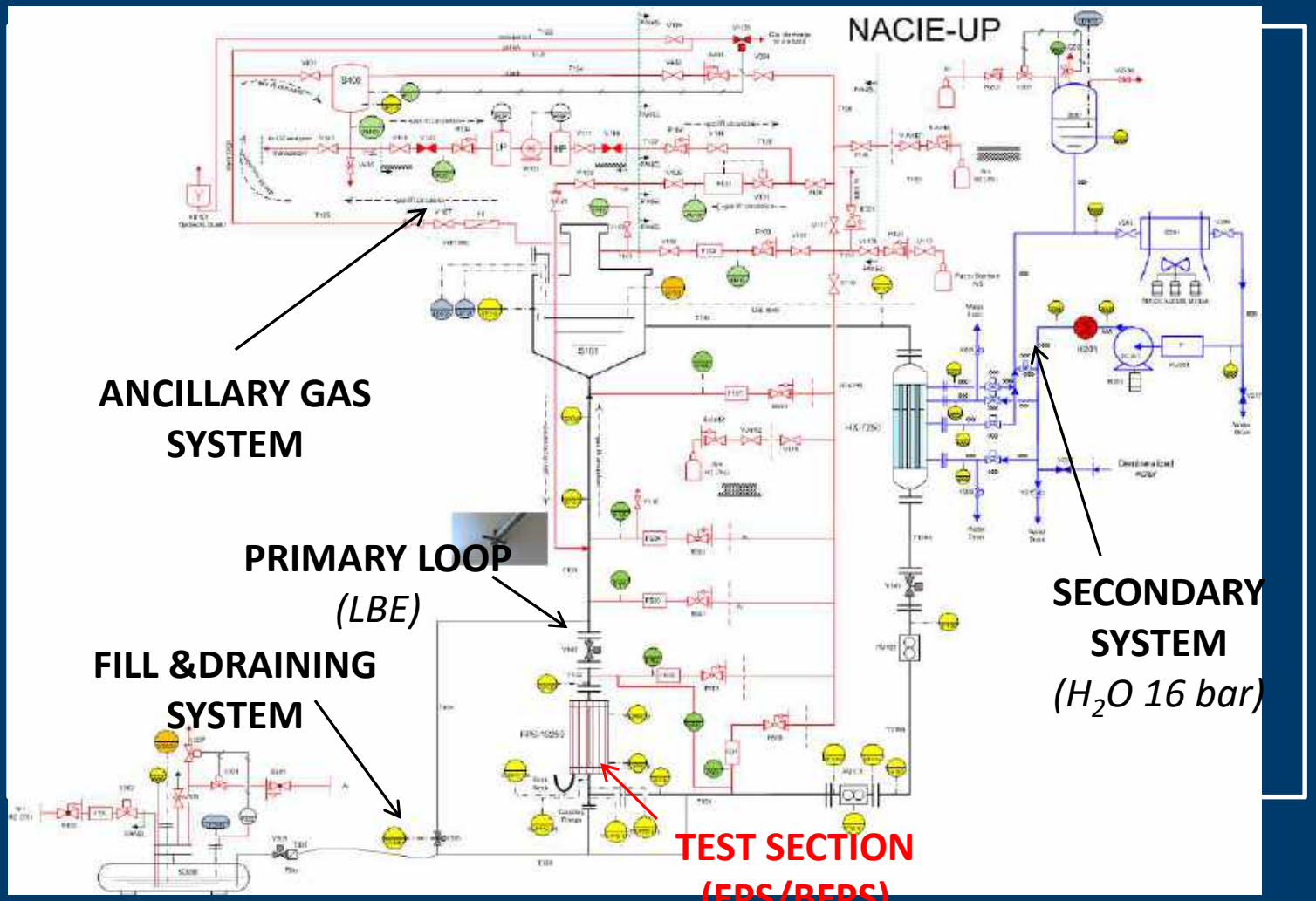

NACIE-UP Facility – P&ID

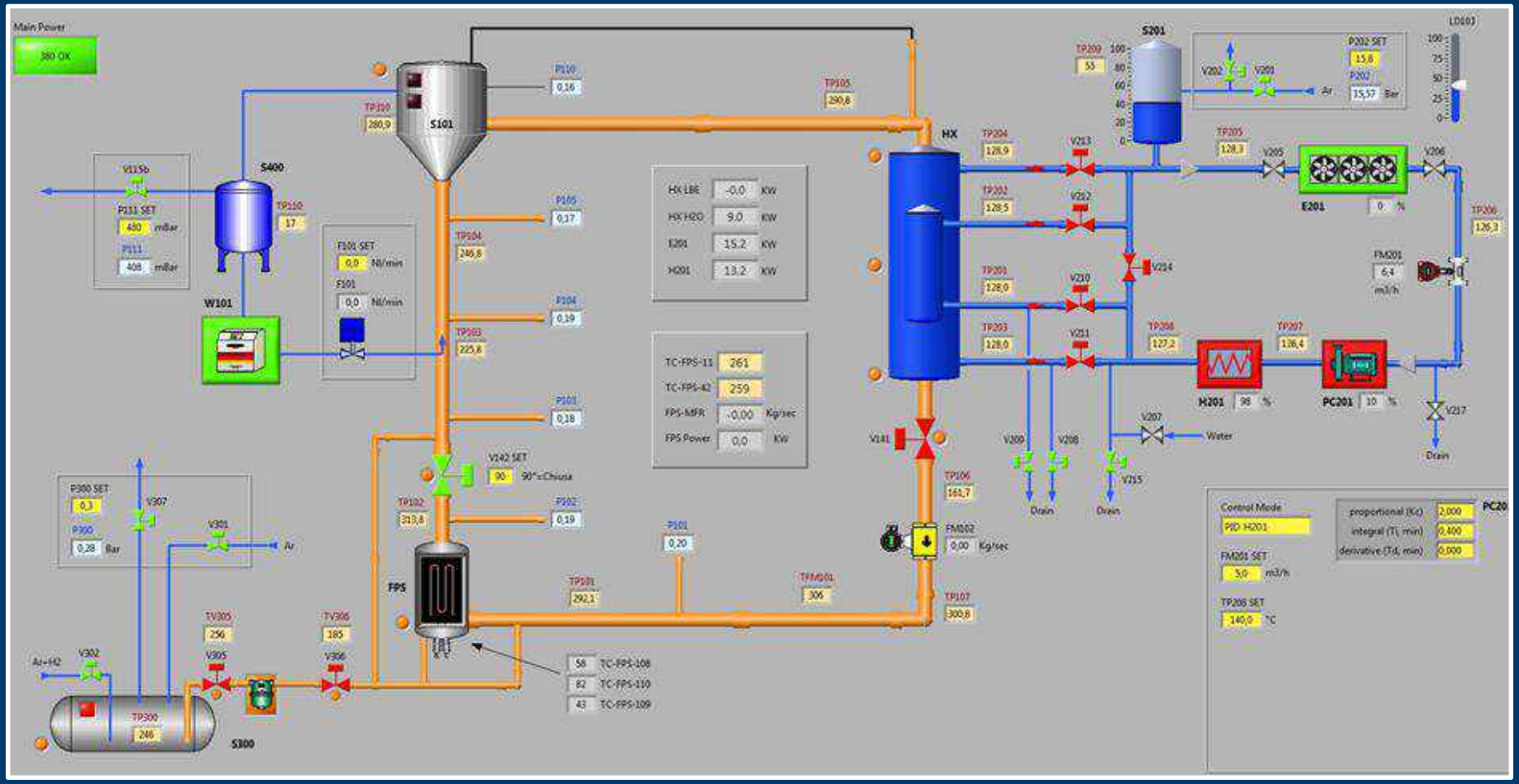

NACIE-UP PLC

Schematic layout of the primary (LBE) and secondary (H_2O)systems, of the gas system and of the fill & drain system

The Fuel Pin bundle Simulator

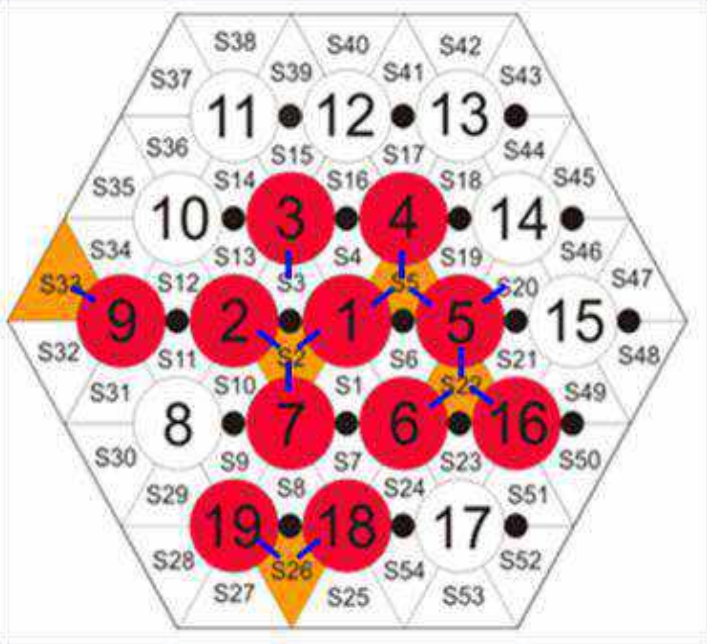

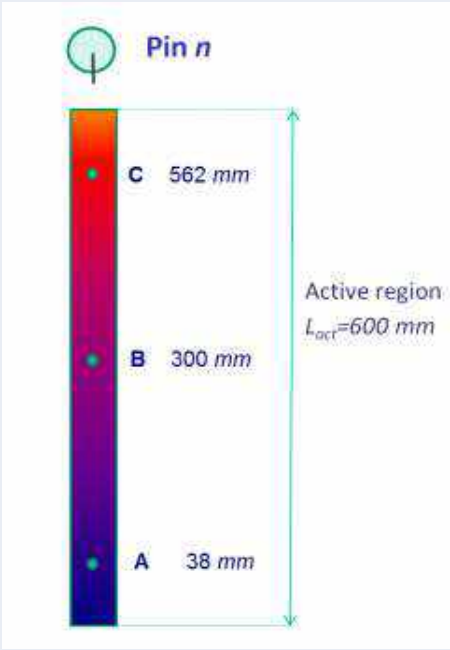

D_{pin}	6.55 mm
P	8.4 mm
P/D	1.2824
d	1.75 mm
P_{wire}	262 mm
L_{tot}	2000 mm
L_{active}	600 mm
$D_{H,nom}$	3.84 mm
q''_{max}	1 MW/m^2

- **11 instrumented pins**
- **52 TCs** (0.35 mm thick) - **wall embedded thermocouples location**
- **15 TCs** (0.5 mm thick) - **5 instrumented sub-channels**
- Instrumentation distributed along three axial positions (A, B, C): **z = 38, 300, 562 mm** from the beginning of the active length
- Pin 3 instrumented with wall embedded TCs every 43.66 mm (13 TCs)

Instrumentation

Some instrumentation is installed in the loop:

- **Prototypical thermal flow meter**
- **loop thermocouples**
- **Test section FPS thermocouples (bulk and wall)**

Thermal Flow Meter

- A prototypical thermal flow meter for liquid metals was developed by ENEA in collaboration with Thermocoax
- **It is made by a flanged pipe (SS) with an heater technological development by THX (a few kW), a static mixer, 2 RTD and an internal RTD in the bulb**
- Low pressure losses
- No limiting working temperature
- Specific DACS developed
- **Accurate at low and medium flow rates (0-15 kg/s)**
- **Range can be easily extended**

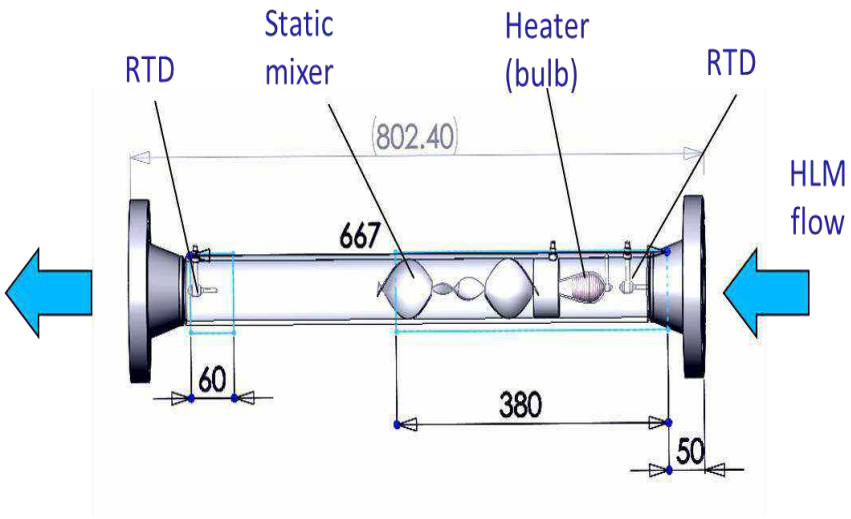

Experimental test matrix

TEST ADP 10

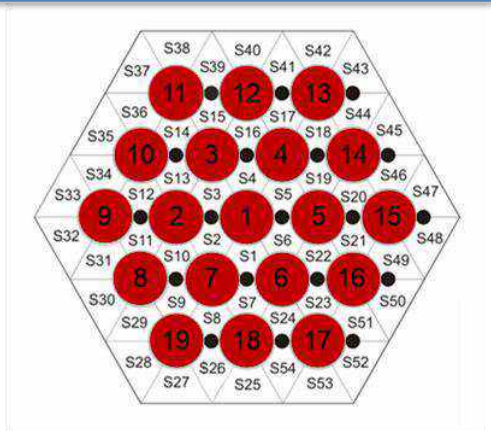

- **19** active pins
- FPS power **30 kW**
- $q''_w \approx$ **127.9 kW/m²**
- $\dot{m}_{gas}$ **= 10 Nl/min** → **0 Nl/min**
- $\dot{m}_{H_2O}$ = 10 m³/h
- $T_{in,\,H_2O}$ = 170 °C

TEST ADP 06

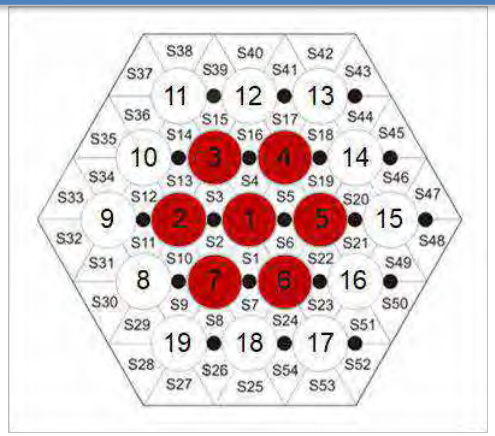

- **7** active pins
- FPS power **30 kW**
- $q''_w \approx 347.1\ kW/m2$
- $\dot{m}_{gas}$ **= 10 Nl/min** → **0 Nl/min**
- $\dot{m}_{H_2O}$ = 10 m³/h
- $T_{in,\,H_2O}$ = 170 °C

TEST ADP 07

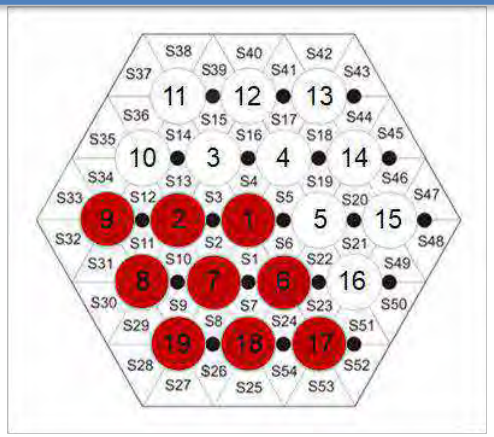

- **9** active pins
- FPS power **38 kW**
- $q''_w \approx 342.0\ kW/m2$
- $\dot{m}_{gas}$ **= 10 Nl/min** → **0 Nl/min**
- $\dot{m}_{H_2O}$ = 10 m³/h
- $T_{in,\,H_2O}$ = 170 °C

Experimental results - LBE mass flow rate

TEST ADP 10

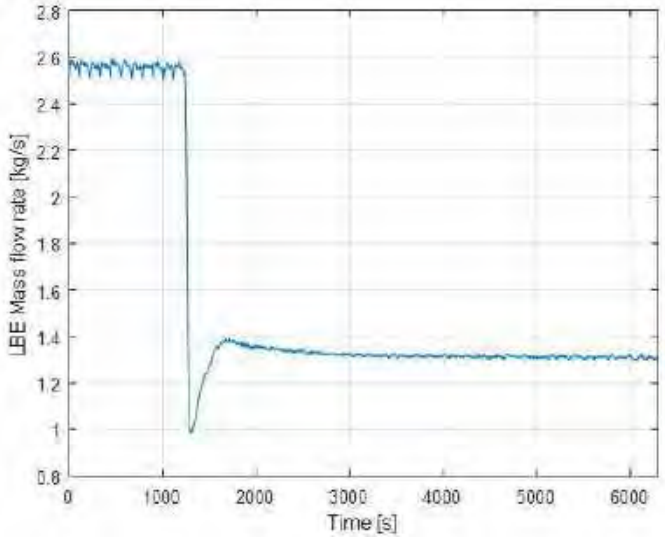

Test ADP 10	Steady state 1		Steady state 2	
Variable	Data	σ [%]	Data	σ [%]
M_{gas} [Nl/min]	10.0	5.0	0.1	2.8
M_{lbe} [kg/s]	2.56	2.9	1.31	2.9
ΔT_{FPS} [°C]	72.0	0.9	140.6	0.2
Q_{nom} [W]	3.00E+04	0.2	3.00E+04	0.1
Q_{eff} [W]	2.71E+04	3.9	2.70E+04	3.7
Q_{pre} [W]	2236	18.0	2339	9.3
Q_{tfm} [W]	1915	0.2	1644	0.3

TEST ADP 06

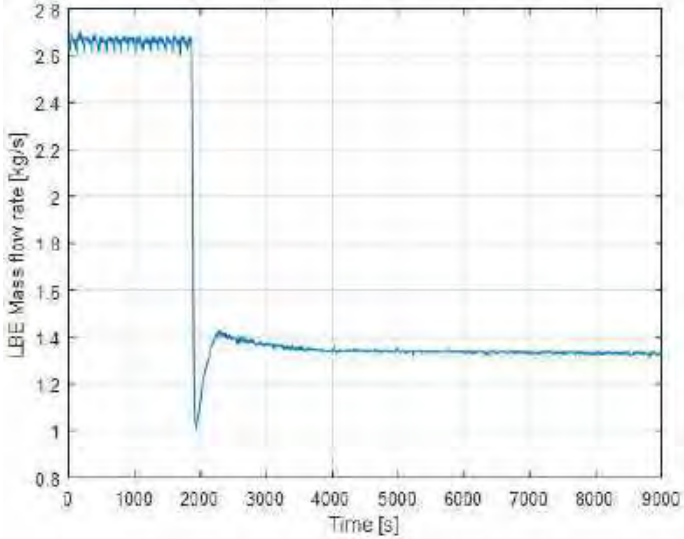

Test ADP 06	Steady state 1		Steady state 2	
Variable	Data	σ [%]	Data	σ [%]
M_{gas} [Nl/min]	10.0	5.0	0.0	2.8
M_{lbe} [kg/s]	2.66	2.9	1.33	2.9
ΔT_{FPS} [°C]	68.4	1.1	130.1	0.4
Q_{nom} [W]	3.00E+04	0.2	3.00E+04	0.2
Q_{eff} [W]	2.68E+04	3.9	2.54E+04	3.7
Q_{pre} [W]	2508	17.5	2675	8.6
Q_{tfm} [W]	1933	0.2	1652	0.3

Experimental results – LBE temperature

TEST ADP 10

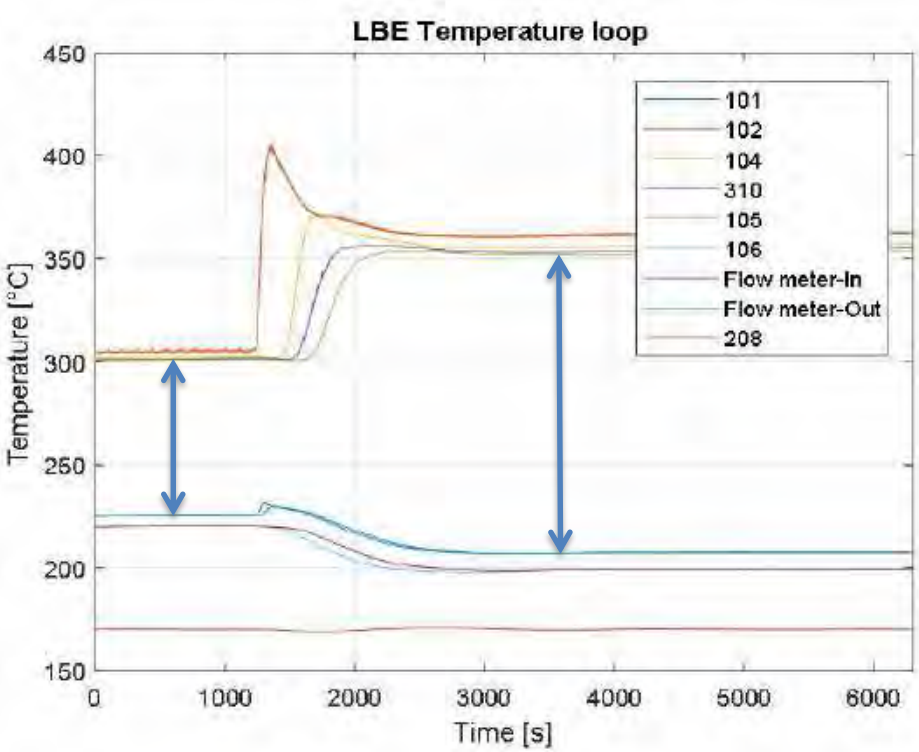

TEST ADP 06

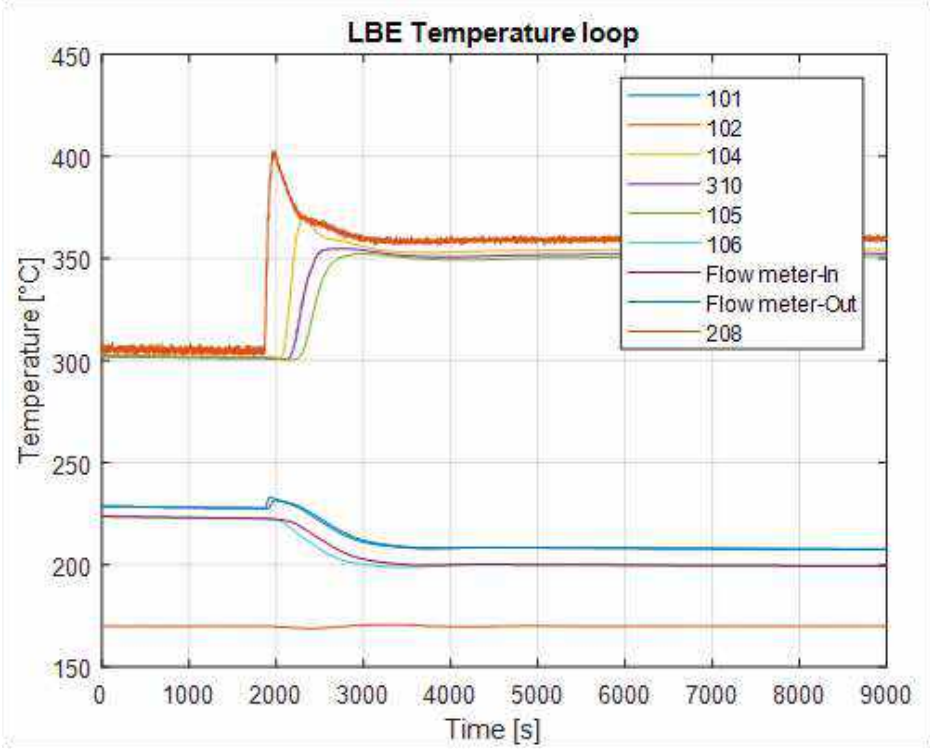

Experimental results - FPS temperatures S2

TEST ADP 10

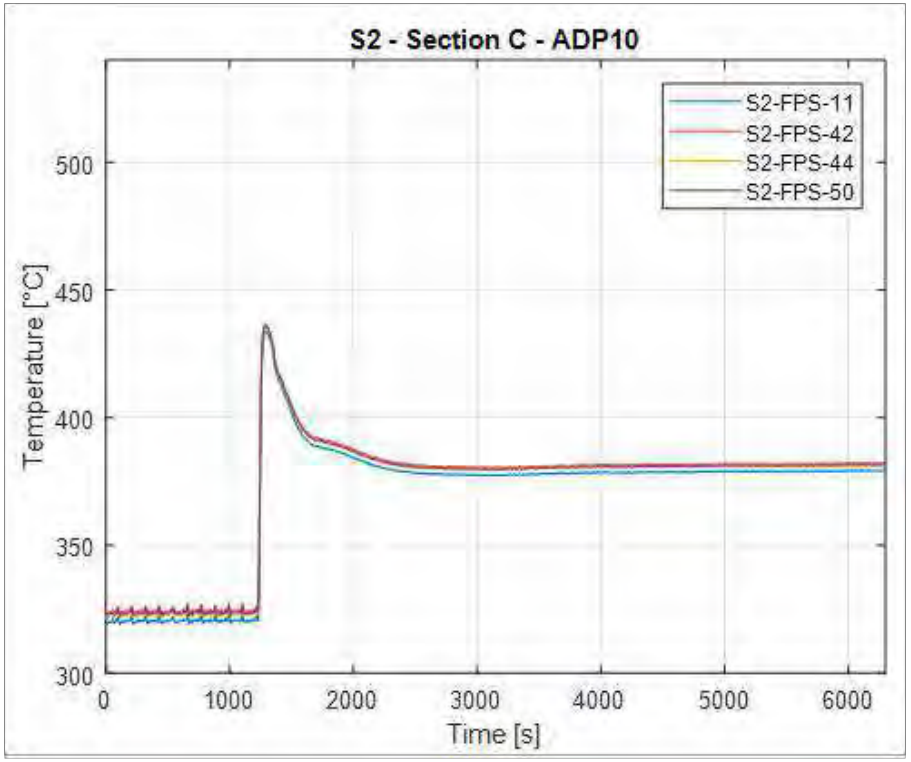

TEST ADP 06

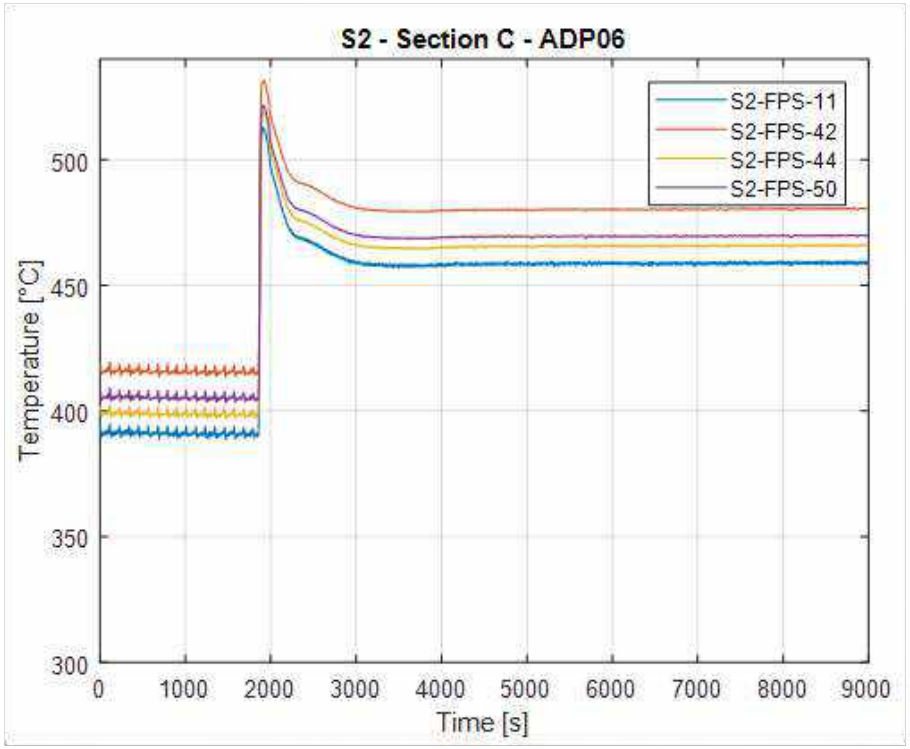

z = 360 mm

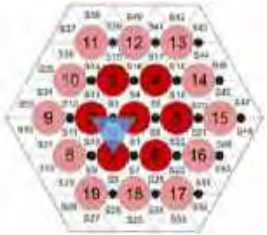

Experimental results - FPS temperatures S22

TEST ADP 10

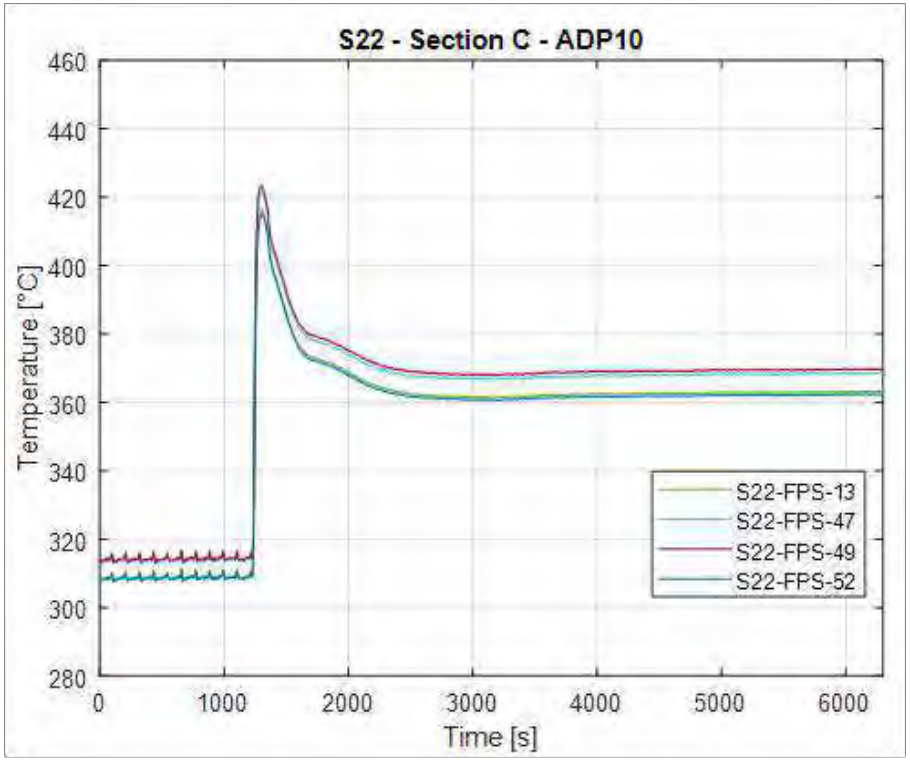

TEST ADP 06

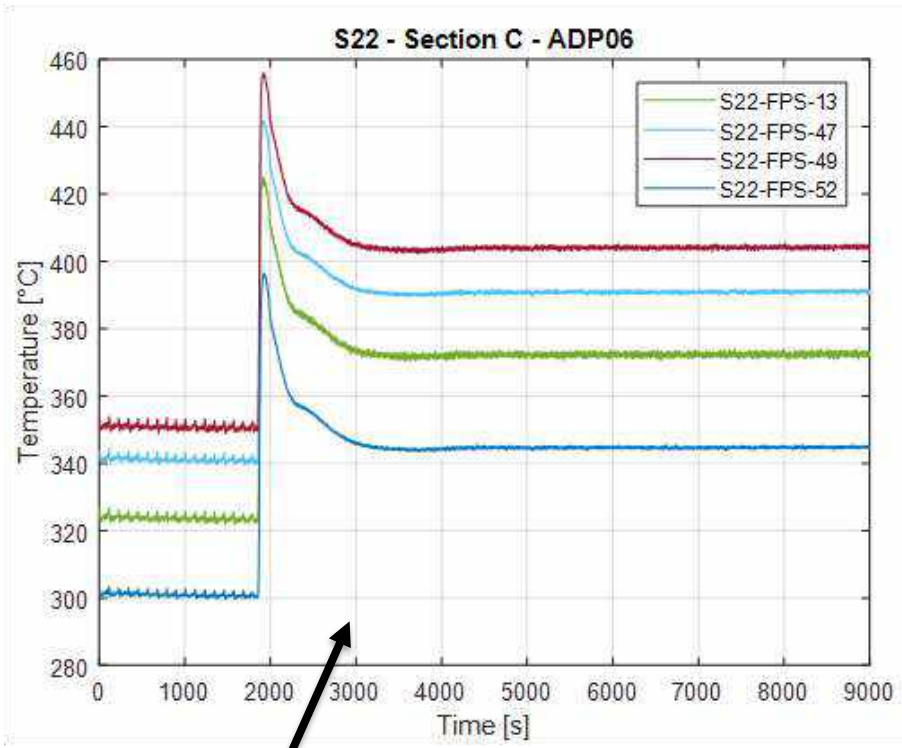

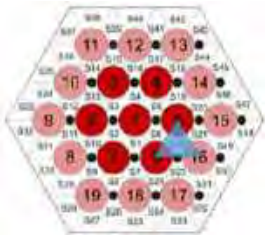

z = 360mm

Experimental results - FPS temperatures S26

TEST ADP 10

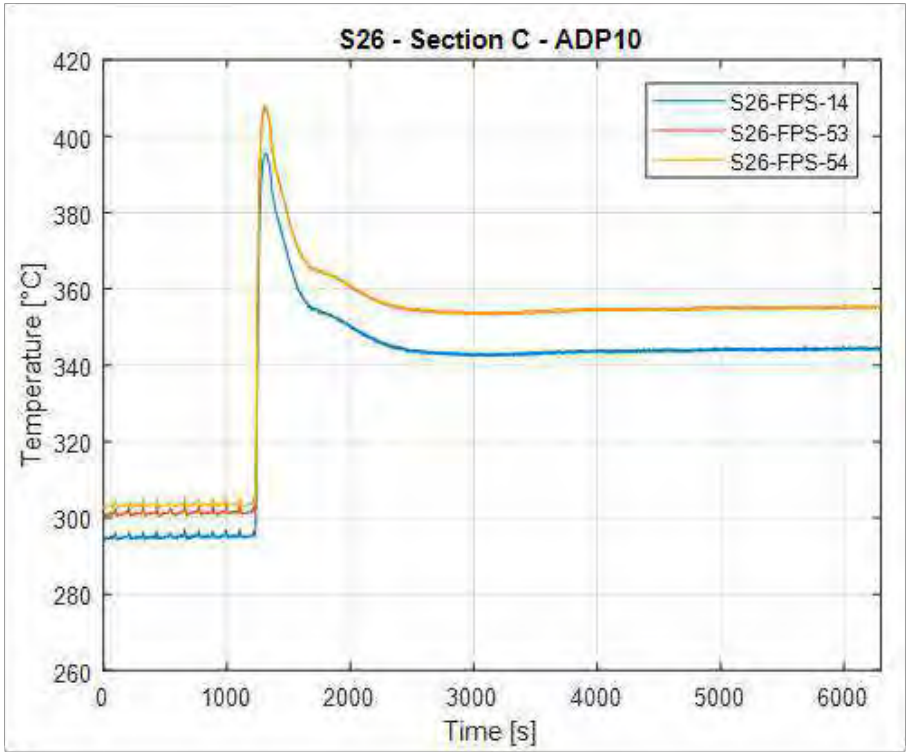

TEST ADP 06

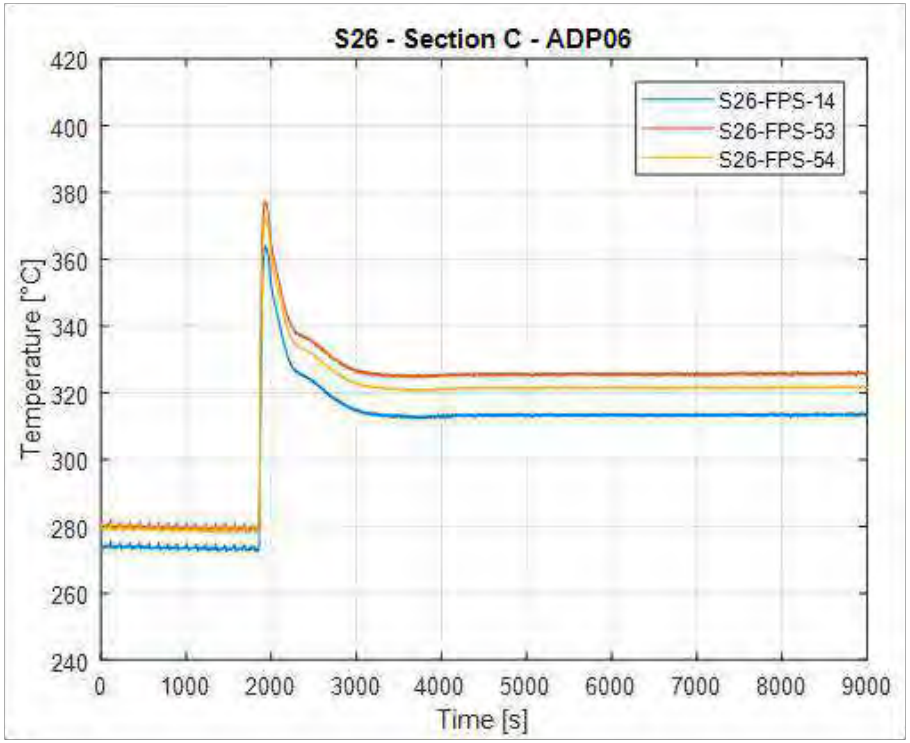

z = 300mm

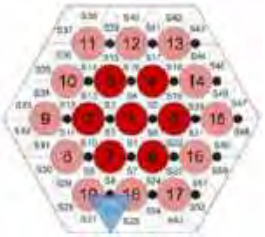

Experimental results - ADP 07

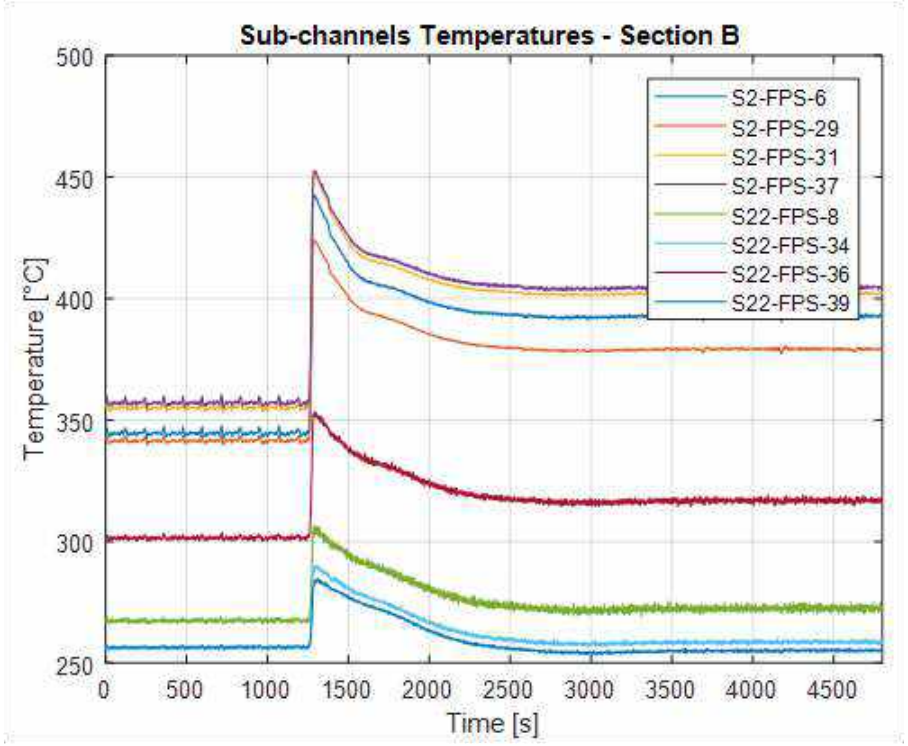

Internal sub-channels S2 & S22

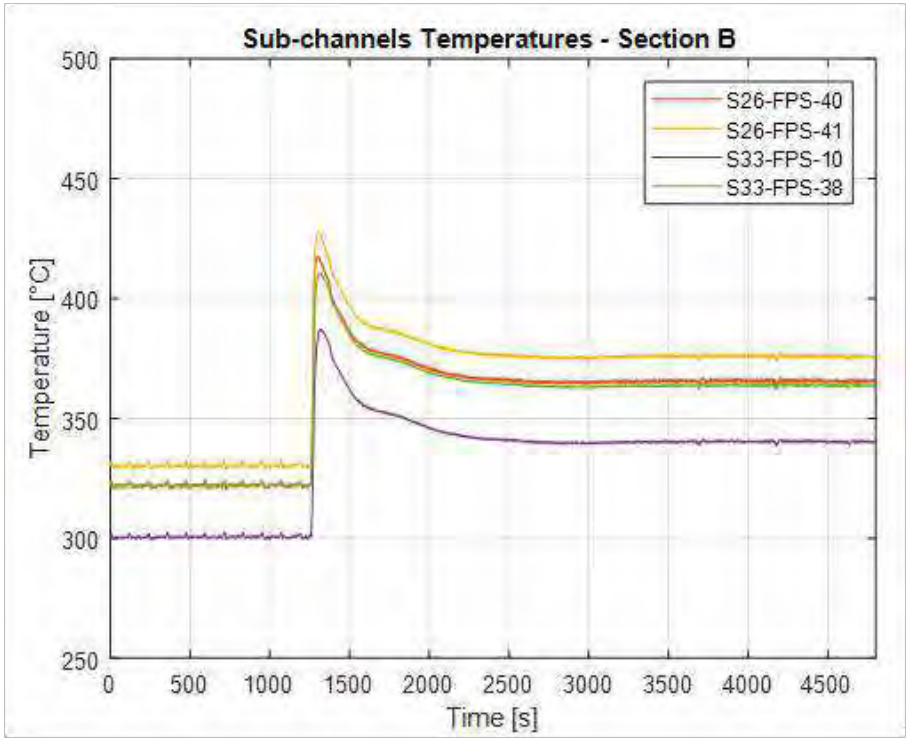

External sub-channels S26 and S33

z = 300 mm

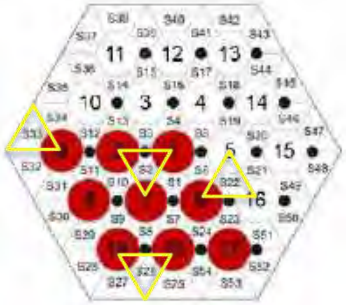

TESTS PERFORMED

- For all cases non-dimensional numbers were computed according to the definitions and error propagation theory was applied to compute standard deviation

- For a generic function $Y=f(X_i)$

$$\sigma_Y^2 = \sum_{i=1}^{n} \left(\frac{\partial f}{\partial Xi} \cdot \sigma_{Xi} \right)^2$$

- This theory is applied to Re, Pe, Nu numbers error evaluation

- The average Nusselt number is computed as

$$\mathrm{Nu} = \frac{q''}{\left(\overline{T}_w - \overline{T}_b \right)} \cdot \frac{D_{H,rod}}{k}$$

by averaging wall and bulk temperatures using weights

TESTS PERFORMED

- ADP00: non-dimensional results

	Test ADP 00 - Steady state 1								
	Section A			Section B			Section C		
Variable	Data	σ	σ [%]	Data	σ	σ [%]	Data	σ	σ [%]
Re	**6897**	536	7.8	**7488**	581.6	7.8	**8117**	630.5	7.8
Pr	**0.029**	0.003	9.8	**0.026**	0.002549	9.8	**0.023**	0.0	9.8
Pe	**203**	25	12.5	**195**	24.36	12.5	**186**	23.3	12.5
Nu	**8.5**	0.8	8.9	**5.0**	0.4716	9.3	**5.1**	0.6	11.2
Nu_K	**6.1**	0.0	0.1	**6.1**	0.008901	0.1	**6.0**	0.0	0.1
Nu_U	**10.7**	0.0	0.1	**10.6**	0.01065	0.1	**10.6**	0.0	0.1
Nu_{S2}	**9.7**	1.0	9.9	**9.4**	1.598	16.9	**11.6**	3.2	27.8
Nu_{S5}	**6.5**	0.5	8.4	**10.0**	1.723	17.2	**6.3**	1.1	16.6
Nu_{S22}	**9.7**	0.9	9.6	**8.2**	1.206	14.8	**7.1**	1.2	17.2
Nu_{S26}	**8.7**	0.8	9.3	**-**	-	-	**5.2**	0.6	11.3
Nu_{S33}	**7.7**	0.7	9.6	**4.2**	0.3715	8.9	**3.7**	0.4	9.7

	Test ADP 00 - Steady state 2								
	Section A			Section B			Section C		
Variable	Data	σ	σ [%]	Data	σ	σ [%]	Data	σ	σ [%]
Re	**3457**	268	7.7	**4060**	315	7.7	**4647**	360	7.7
Pr	**0.030**	0.003	9.8	**0.024**	0.002	9.8	**0.019**	0.002	9.8
Pe	**105**	13	12.5	**97**	12	12.5	**89**	11	12.5
Nu	**6.9**	0.5	7.9	**4.4**	0.3	7.6	**4.1**	0.3	7.8
Nu_K	**5.4**	0.0	0.2	**5.4**	0.0	0.2	**5.3**	0.0	0.2
Nu_U	**9.9**	0.0	0.1	**9.9**	0.0	0.1	**9.8**	0.0	0.1
Nu_{S2}	**8.2**	0.7	8.2	**9.1**	0.8	8.7	**13.9**	1.8	12.9
Nu_{S5}	**5.3**	0.4	7.7	**9.6**	0.9	9.2	**5.5**	0.5	8.7
Nu_{S22}	**8.7**	0.7	8.2	**6.7**	0.6	8.4	**5.9**	0.5	8.5
Nu_{S26}	**5.9**	0.5	8.1	**-**	-	-	**3.3**	0.3	7.8
Nu_{S33}	**6.3**	0.5	8.4	**3.6**	0.3	7.6	**3.1**	0.2	7.7

- Average Nusselt number close to Kazimi
- Local nusselt number close to Ushakov (infinite lattice)

CFD COMPARISON

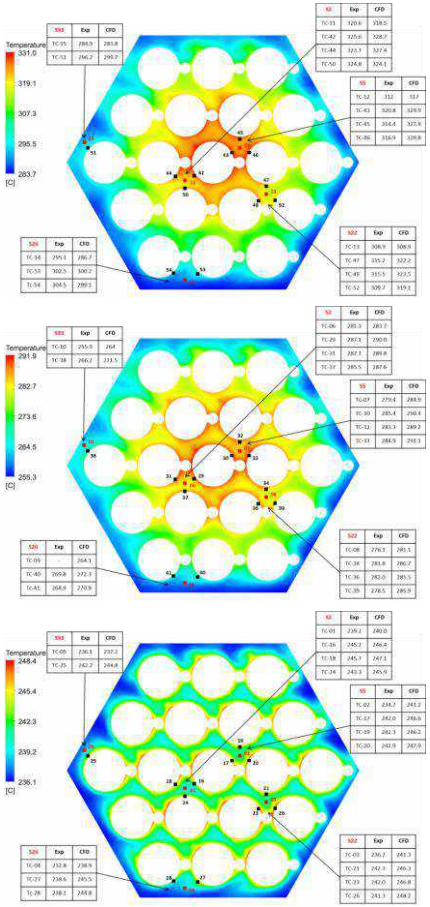

Section C

Section B

Section A

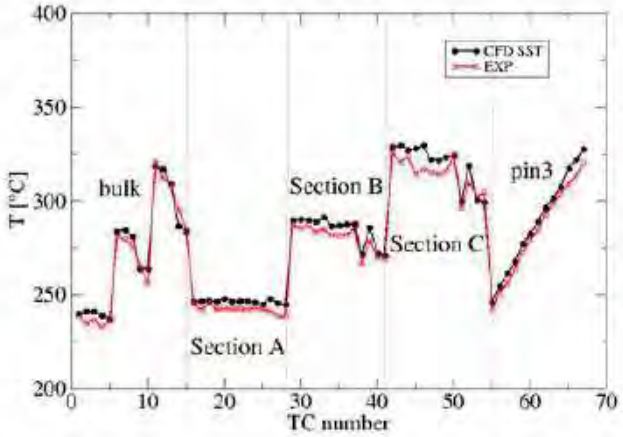

Results and exp: ICONE papers + NED submission

Conclusions

- Experimental tests with gas flow rate transition have been performed in NACIE-UP facility;
- A first reference test was characterized by all 19 pins on;
  - Lower local Nu in external sub-channels (S26 and S33)
  - Higher values in the inner sub-channels (S2, S5 and S22)
- A second test, characterized by the same power distributed in among the 7 central pins (higher wall heat flux) was compared to the reference one;
  - Same integral parameters between the two tests
  - S2, S5 and S22 were hotter in the second test, S26 and S33 colder (off during the second test)
- A third test was characterized by power distribution localized in a limited part of the bundle (triangular sections), with pin-wall heat flux comparable with the second test;
  - FPS temperature distribution affected by the power distribution
  - Non-conventional behaviour was noticed in S2
- Obtained experimental data was used to characterize bundle (by computing the heat transfer coefficient). The collected system data can be used to qualify STH codes, whereas the local fuel bundle data (especially the ones from dissymmetric tests) can be useful for the validation of CFD codes and coupled STH/CFD methods for HLM systems.

Ivan Di Piazza
ENEA C.R. Brasimone

Ivan.dipiazza@enea.it

UNIVERSITA' DEGLI STUDI DI PISA
ENEA C.R. BRASIMONE

Flow Blockage Experiments in NACIE-UP loop

Ranieri Marinari

Contents

- Introduction
- NACIE-UP facility
- Pre-test CFD analysis
- Instrumentation & experimental test matrix
- Pre-test Code-to-code CFD comparison
- Ongoing activity: experimental campaign
- Preliminary post-test analysis
- Conclusions

Introduction 1/2

- In the context of GEN-IV heavy liquid metal-cooled reactors safety studies, the flow blockage in a fuel sub-assembly is considered one of the main issues to be addressed and one of the most important and realistic accident for Lead Fast Reactors (LFR) fuel assembly.
- The blockage in a fast reactor Fuel Assembly (FA) may have serious effects on the safety of the reactor leading to the FA damaging or melting. The external or internal blockage of the FA may impair the correct cooling of the fuel pins, be the root cause of anomalous heating of the cladding and of the wrapper and potentially impact also fuel pins not directly located above or around the blocked area.
- Fuel Assembly blockage (total or partial) has been extensively analysed since the early days of fast reactors. While many of these studies refer to Sodium Fast Reactors, the results may be a starting point for LFRs too. The main focus of these analyses is determining the effects of a blockage on the temperature (cladding and coolant) and pressure (coolant) inside the FA as well as at the outlet of the subassembly, and the optimal detection techniques..

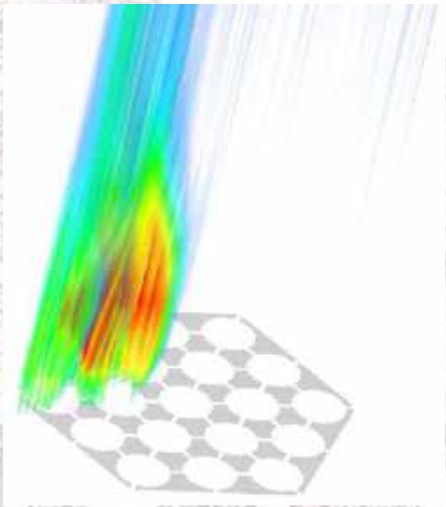

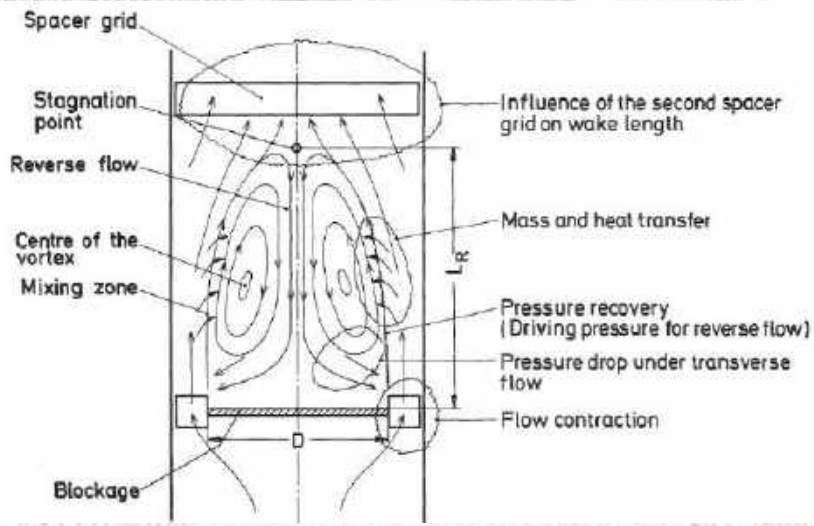

Introduction 2/2

- *Schultheiss (1977)* studied the formation and growth of local blockages in grid spaced fast reactors. Axial growth of blockage is found to be predominant in wire wrapped bundle, whereas radial growth is predominant in grid spaced bundle. The formation of major local blockages in normal fuel element geometries is mainly be caused by fuel expelled after a cladding tube failure.

- Experimental studies of local flow blockage in a LMFBR fuel assembly were carried out by *Nakamura et al. (1980)* using a simulating model in a water test loop. The experiments were conducted in a 61-pin bundle (quadruple scale model of a MONJU core subassembly) containing a planar blockage without leakage flow. The central and edge blockage were used. The wake flow behind the blockage was visualized with dye or air bubble injection to grasp the flow characteristics. Analyzing flow distributions and velocity measurements behind the blockage, it was concluded that the recirculating flow behind the central and edge blockages is stable with no large oscillations discharging vortices. The recirculating flow is similar with those behind a plate or a disk in a free stream.

- Thermal hydraulic features of blocked wire wrapped fuel subassemblies have been investigated through CFD approach by *Raj et al. (2016)*. They found that: the extent of the wake zone behind the blockage increases with blockage radius, Clads partially exposed to blockage are subjected to large circumferential temperature variation and the resulting thermal stress, the total flow reduction is < 2.5% for all blockages that can lead to local sodium boiling. This suggests that global bulk sodium TC at the outlet of the subassembly are unlikely to detect slowly growing internal porous blockages but the wake-induced temperature non-uniformity persists even up to three helical pitch length. This suggests that the sodium temperature non-uniformity at the bundle exit can serve as an efficient blockage indicator .The peak clad temperature is found to be a strong function of porosity (higher clad temperature for lower porosity),

NACIE-UP facility 1/2

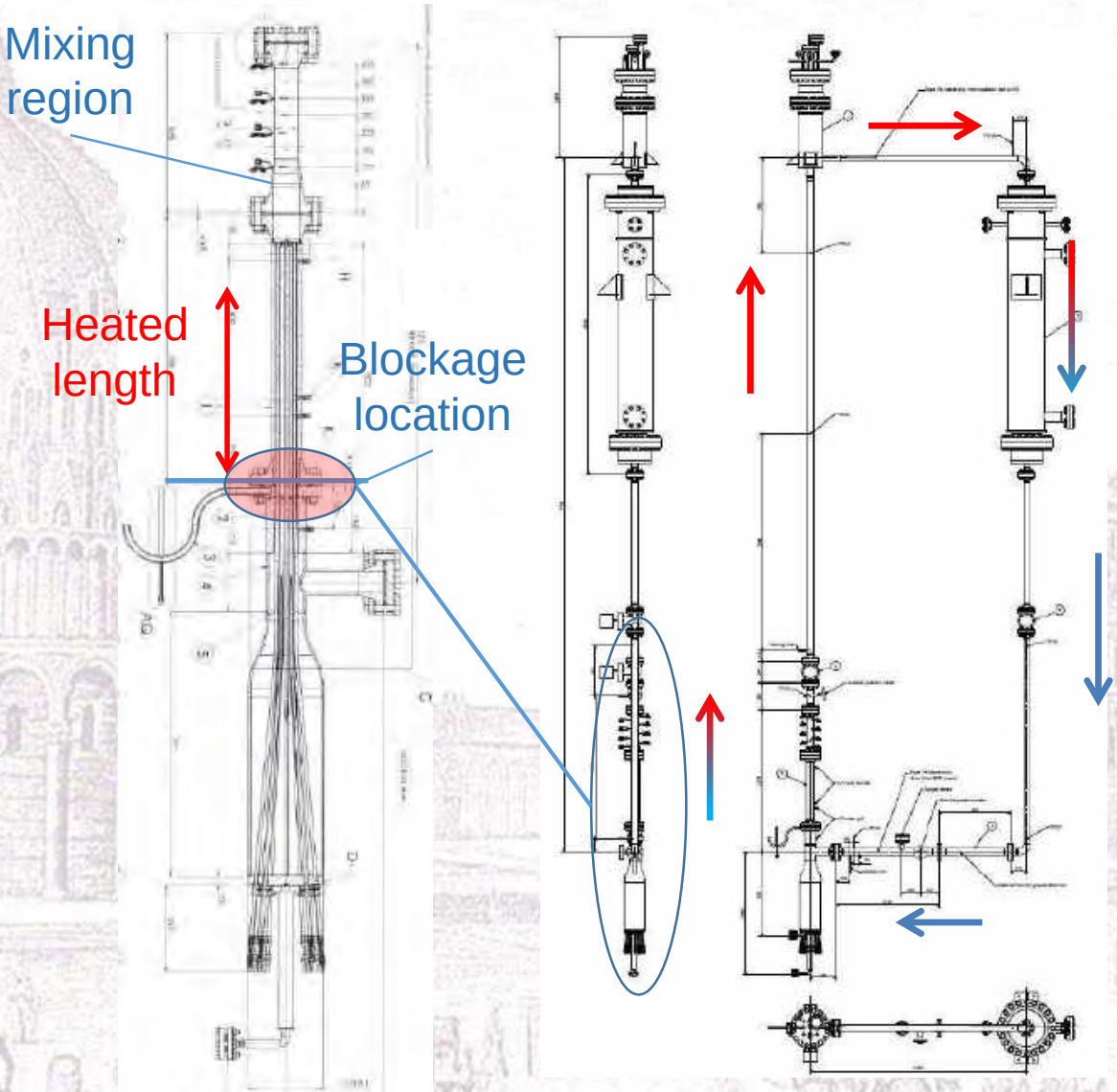

Parameters	BFPS	ALFRED FA
d_{pin}[mm]	10	10.5
p/d	1.4	1.32
Wall heat Flux [MW/m^2]	0.7	0.7-1
Max subch velocity [m/s]	0.8	1.1
N_{pin}	19	127
L_{active} [mm]	600	600
L_{plenum} [mm]	500	500

NACIE-UP facility 2/2

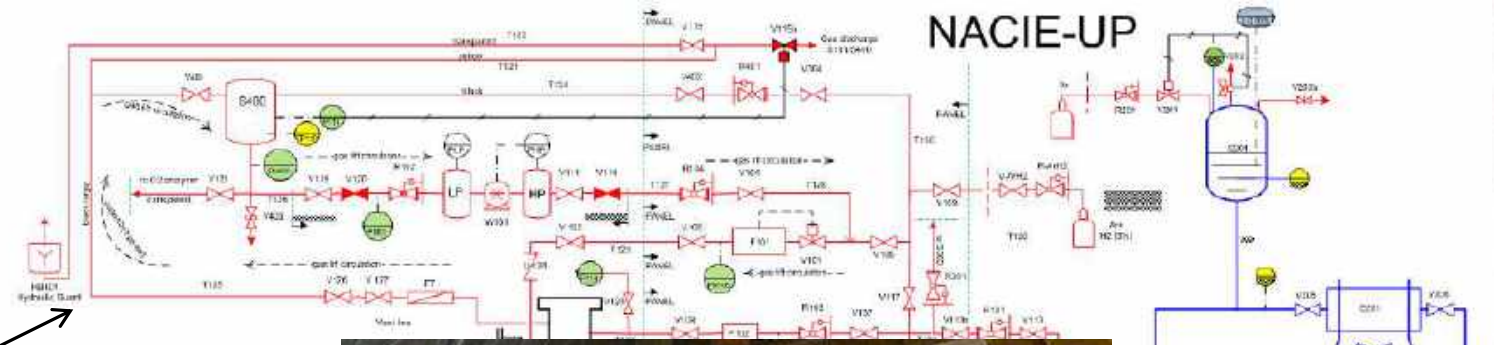

ANCILLARY GAS SYSTEM

PRIMARY L
(LBE)

TEST SECTION (BFPS)

FILL &DRAINING SYSTEM

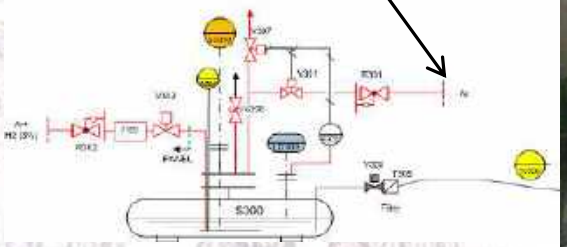

SECONDARY SYSTEM
(H_2O 16 bar)

Pre-test CFD analysis(1/2)

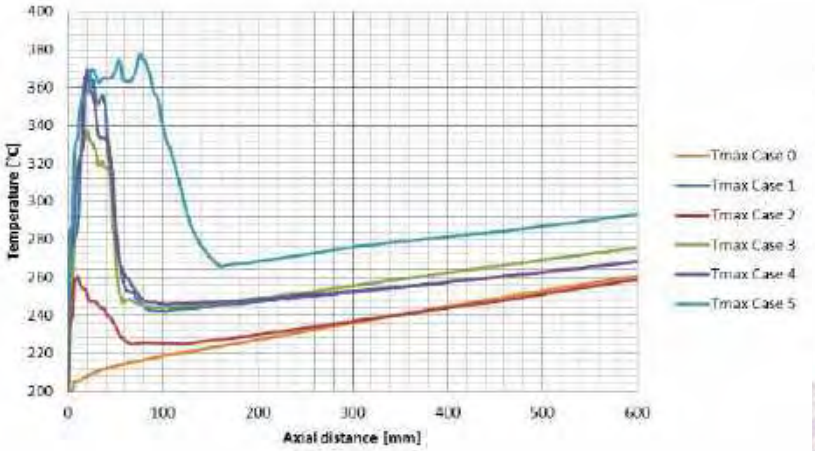

Mesh	M nodes [-]	f Darcy [-]	Nu [-]	$T_{pin,max}$ [°C]
A	10	0.01182	23.86	267.6
B	15	0.01144	17.31	269.8
C	19	0.01130	16.48	272.4
D	24	0.01131	16.52	272.6

Case	Blockage type	Mass flow rate [kg/s]	Re_{BFPS} [-]	Power [kW]	Inlet temperature [°C]
0	0	16	46663	94.2	200
1	1	16	46663	94.2	200
2	2	16	46663	94.2	200
3	3	16	46663	94.2	200
4	4	16	46663	94.2	200
5	5	16	46663	94.2	200

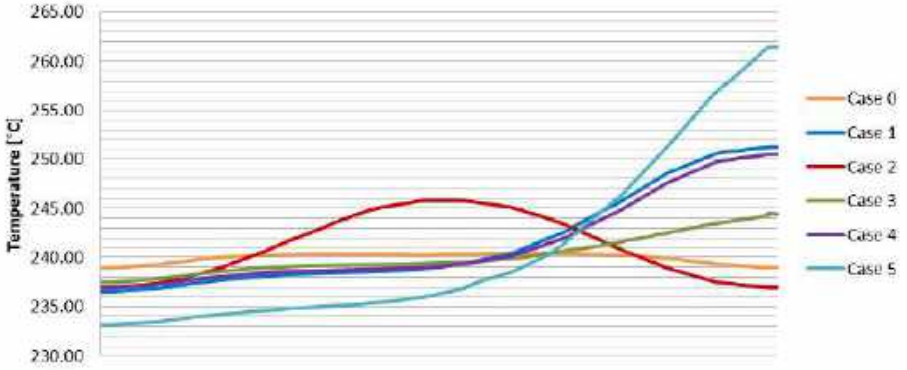

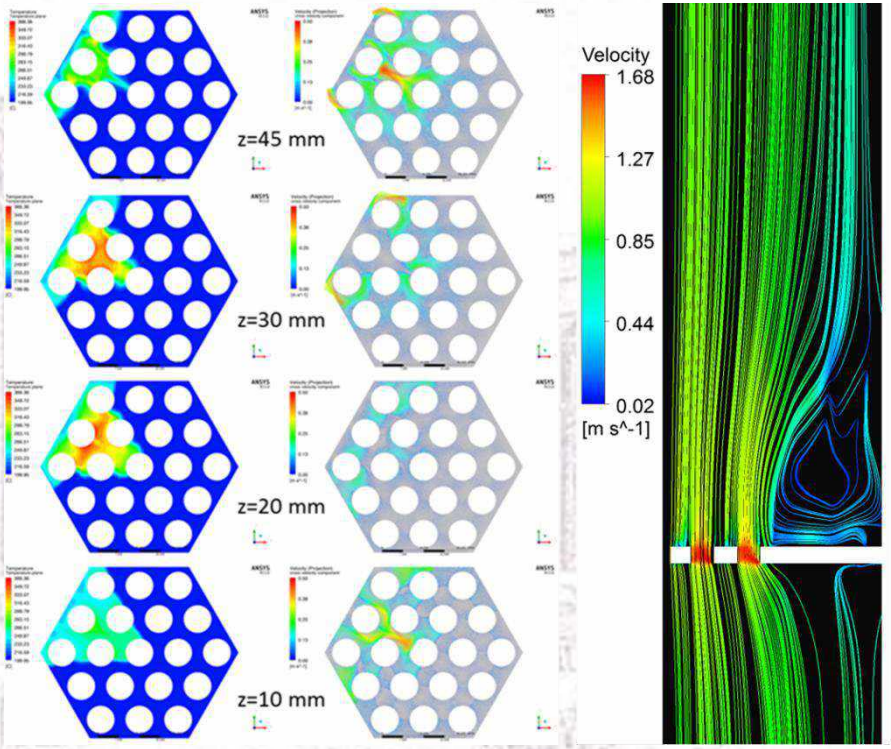

R. Marinari, I. Di Piazza, N. Forgione, F. Magugliani, "Pre-test CFD simulations of the NACIE-UP BFPS test section", Annals of Nuclear Energy 110 (2017), pp. 1060-1072.

BFPS instrumentation

TC name	r [mm]	τ [mm]	BFPS sector
TC-1	0	85	E
TC-2	15	85	E
TC-3	30	85	E
TC-4	0	135	B
TC-5	15	135	B
TC-6	30	135	B
TC-7	0	185	E
TC-8	15	185	E
TC-9	30	185	E
TC-10	0	235	B
TC-11	15	235	B
TC-12	30	235	B
TC-13	0	285	E
TC-14	15	285	E
TC-15	30	285	E
TC-16	0	335	B
TC-17	15	335	B
TC-18	30	335	B
TC-19	0	385	E
TC-20	15	385	E
TC-21	30	385	E
TC-22	0	435	B
TC-23	15	435	B
TC-24	30	435	B

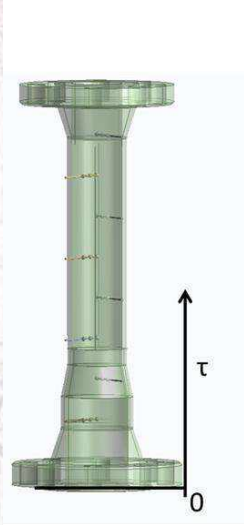

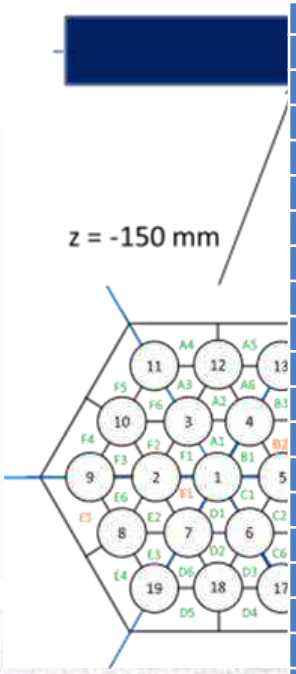

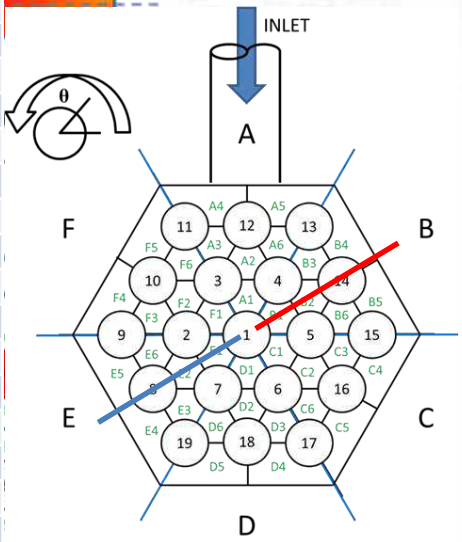

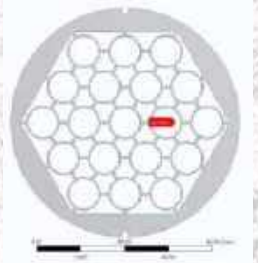
0


1


2


3


4

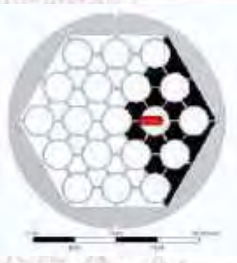
5

NACIE-UP: DACS system

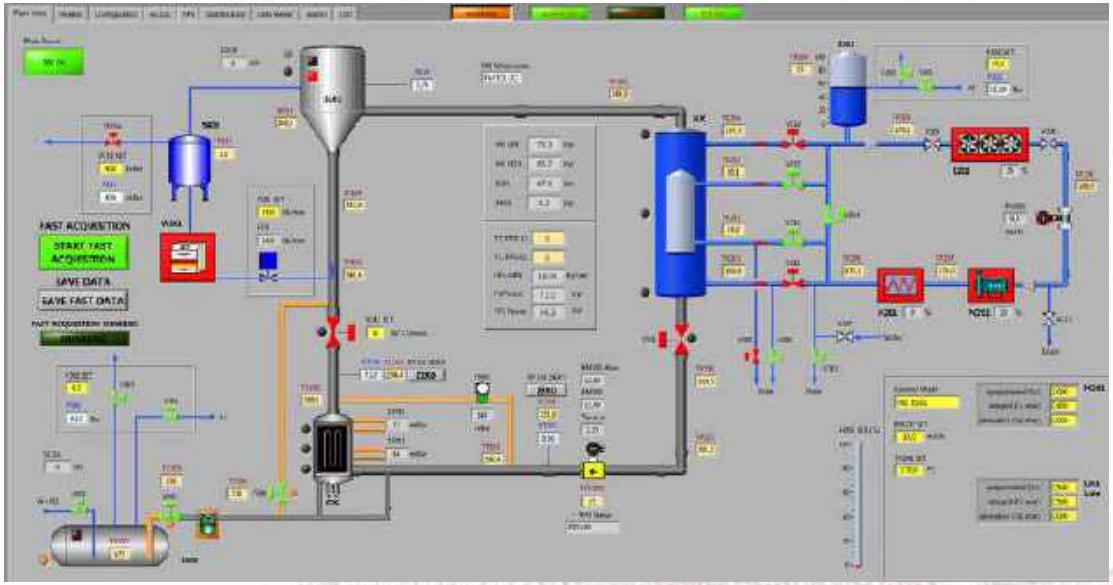

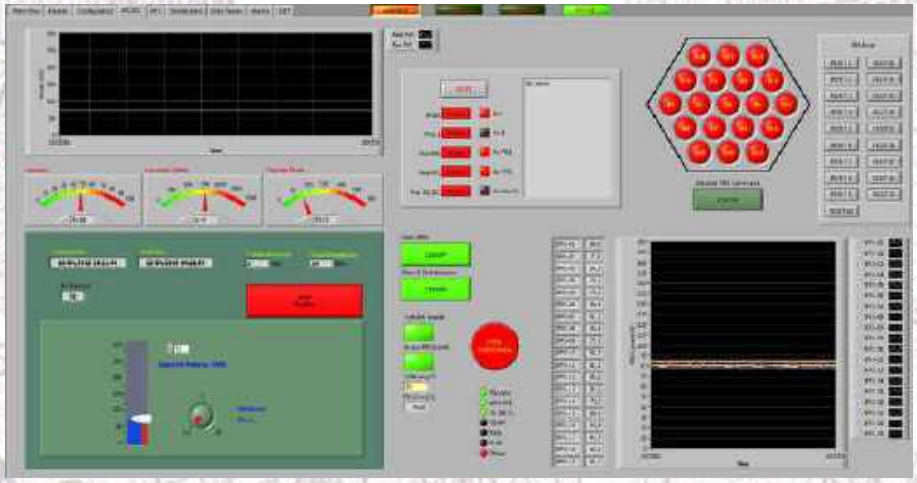

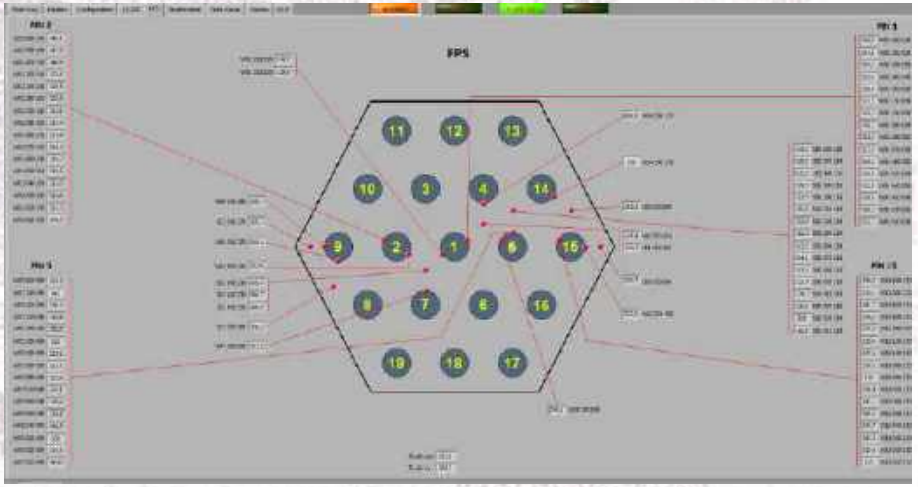

Final test section (BFPS)

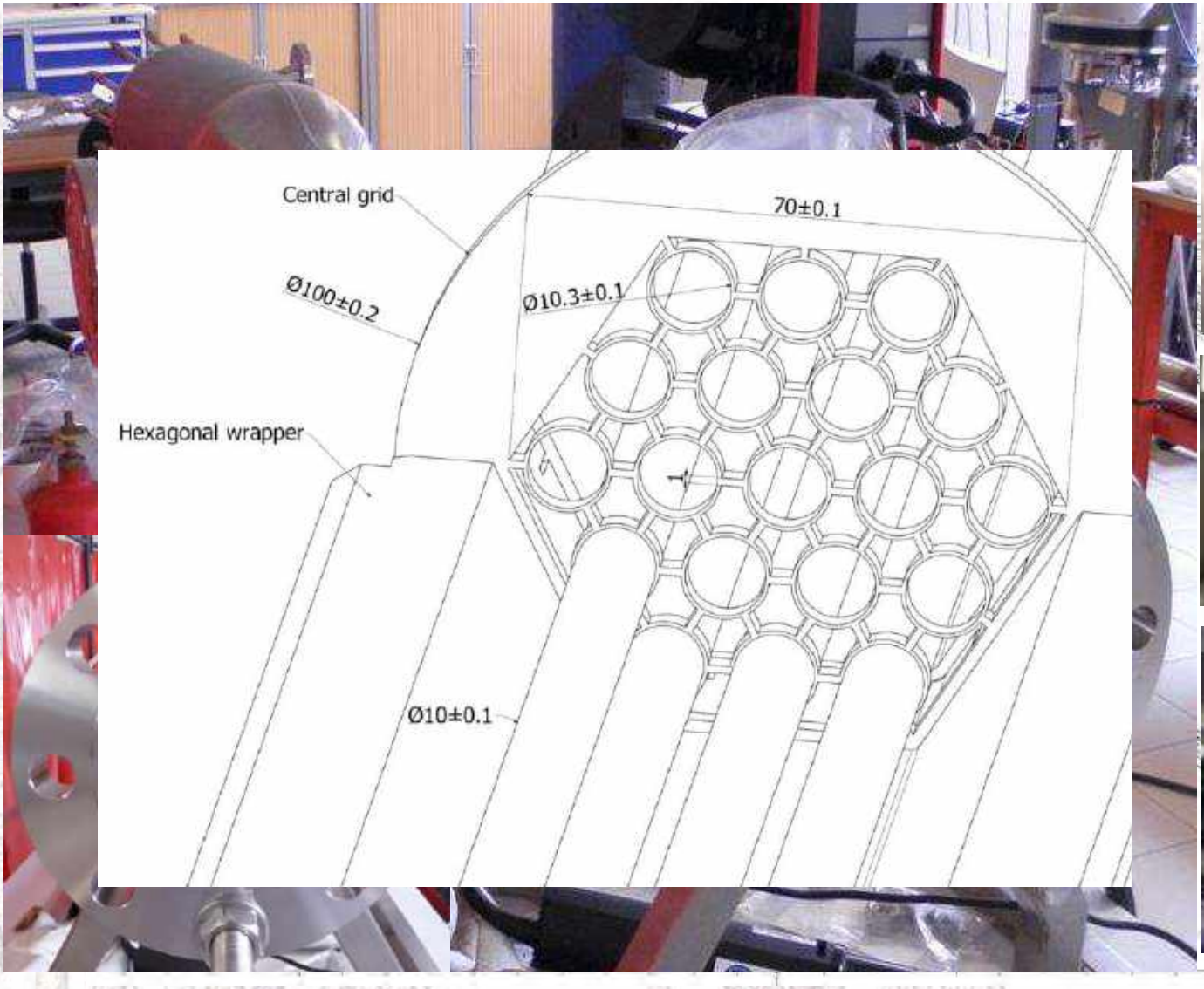

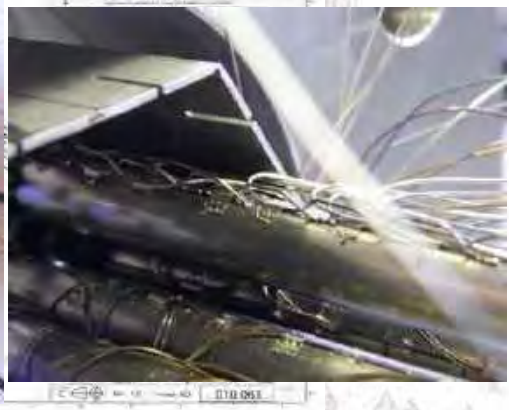

Experimental test matrix

Test name	Mass flow rate [kg/s]	Blockage type	Power [kW]	BFPS inlet temperature [°C]
BFPS-4-0	4	0	24	260
BFPS-8-0	8	0	47	260
BFPS-12-0	12	0	71	260
BFPS-14-0	16	0	94	260
BFPS-4-3	4	3	24	260
BFPS-8-3	8	3	47	260
BFPS-12-3	12	3	71	260
BFPS-4-4	4	4	24	260
BFPS-8-4	8	4	47	260
BFPS-12-4	12	4	71	260
BFPS-4-4-S	4	4	47	260
BFPS-12-4-S	12	4	47	260
BFPS-4-1	4	1	23.55	260
BFPS-8-1	8	1	47.1	260
BFPS-12-1	12	1	70.65	260
BFPS-4-5	4	5	23.55	260
BFPS-8-5	8	5	47.1	260
BFPS-12-5	12	5	70.65	260

Fundamental tests:

2 fundamental tests at constant power

Additional tests

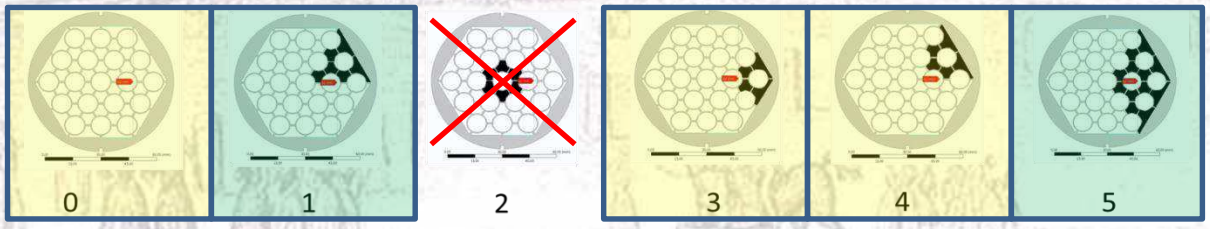

I. Di Piazza, R. Marinari, G. Polazzi, V. Sermenghi, "NACIE-UP experimental setup and test matrix for flow blockage experiment" , SESAME WP2, Deliverable 2.5

Code-to-code CFD comparison (pre-test)

- Inlet bend included
- Blockage 4
- LBE: constant properties @220°C (OECD 2007)
- CHT included
- $Pr_t = 2$

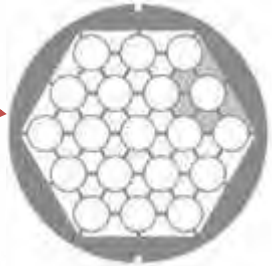

Boundary	Condizione	Valore
Inlet	mfr Temperature	8 kg/s 200°C
Pins	Heat flux (W/m^2)	156716
Walls	Velocity	No-slip
Outlet	Relative pressure	0 bar

	Code	Mesh	Type	Turbulence
PoliMi	Open-FOAM	22.3M	Hex	RANS k-ε
ENEA/UniPi	**CFX 15**	**29.8M**	**Hex&Tet**	**RANS k-ε**
NRG	★CCM+ 11.06	22.4M	Poly	URANS k-ε
UniGe/CRS4	★CCM+ 11.04	14.0M	Poly	URANS k-ε Prel. LES WALE

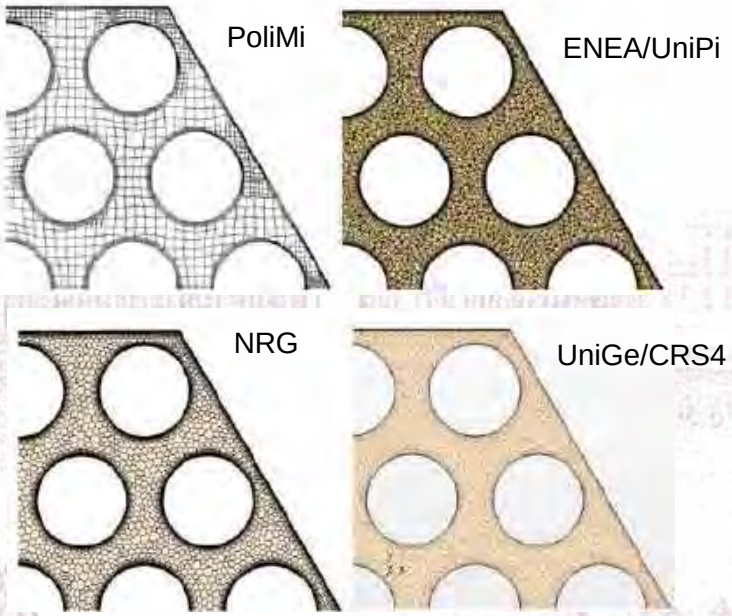

Code-to-code
CFD comparison (pre-test)

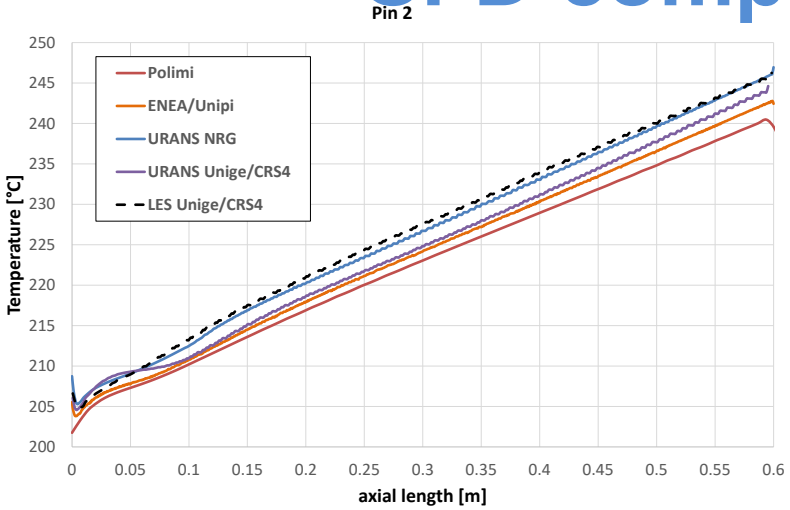

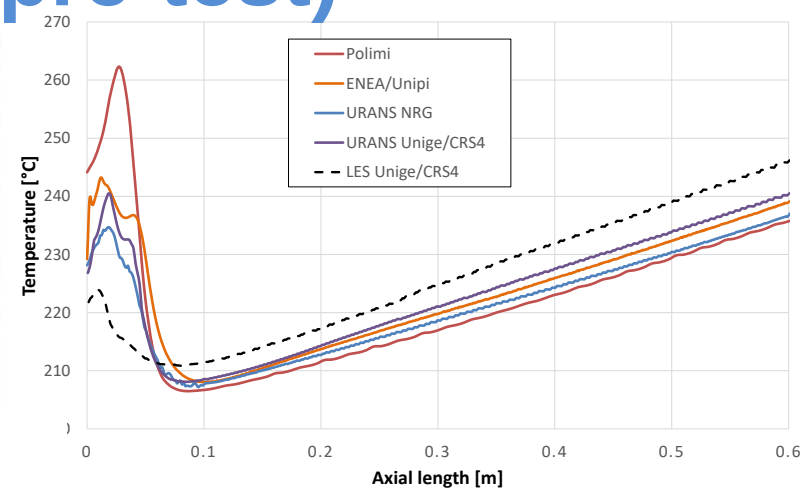

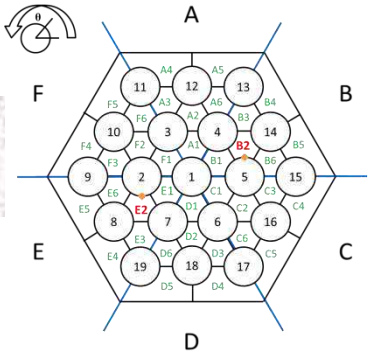

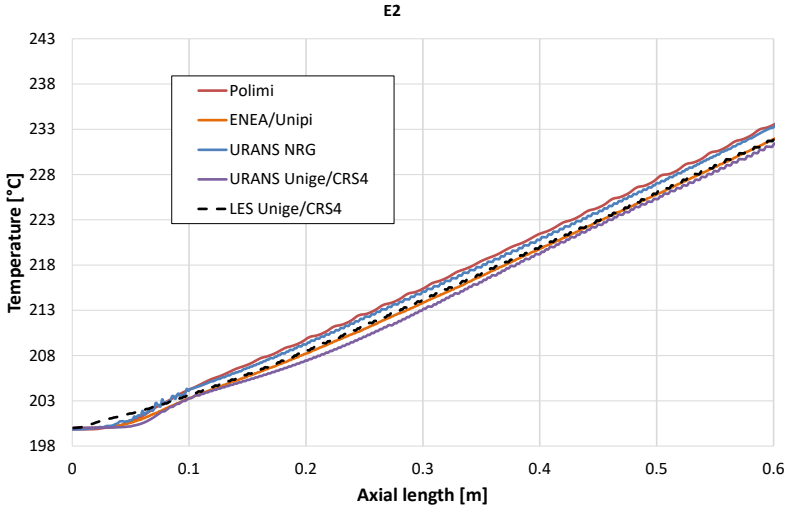

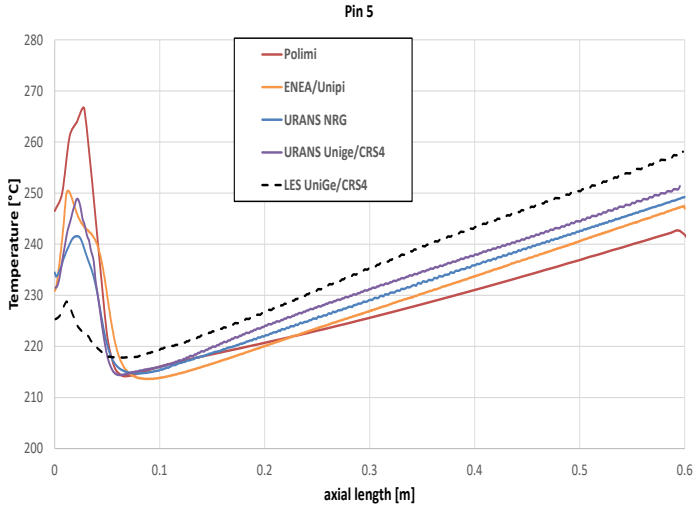

Experimental campaign
8 kg/s - Unblocked case

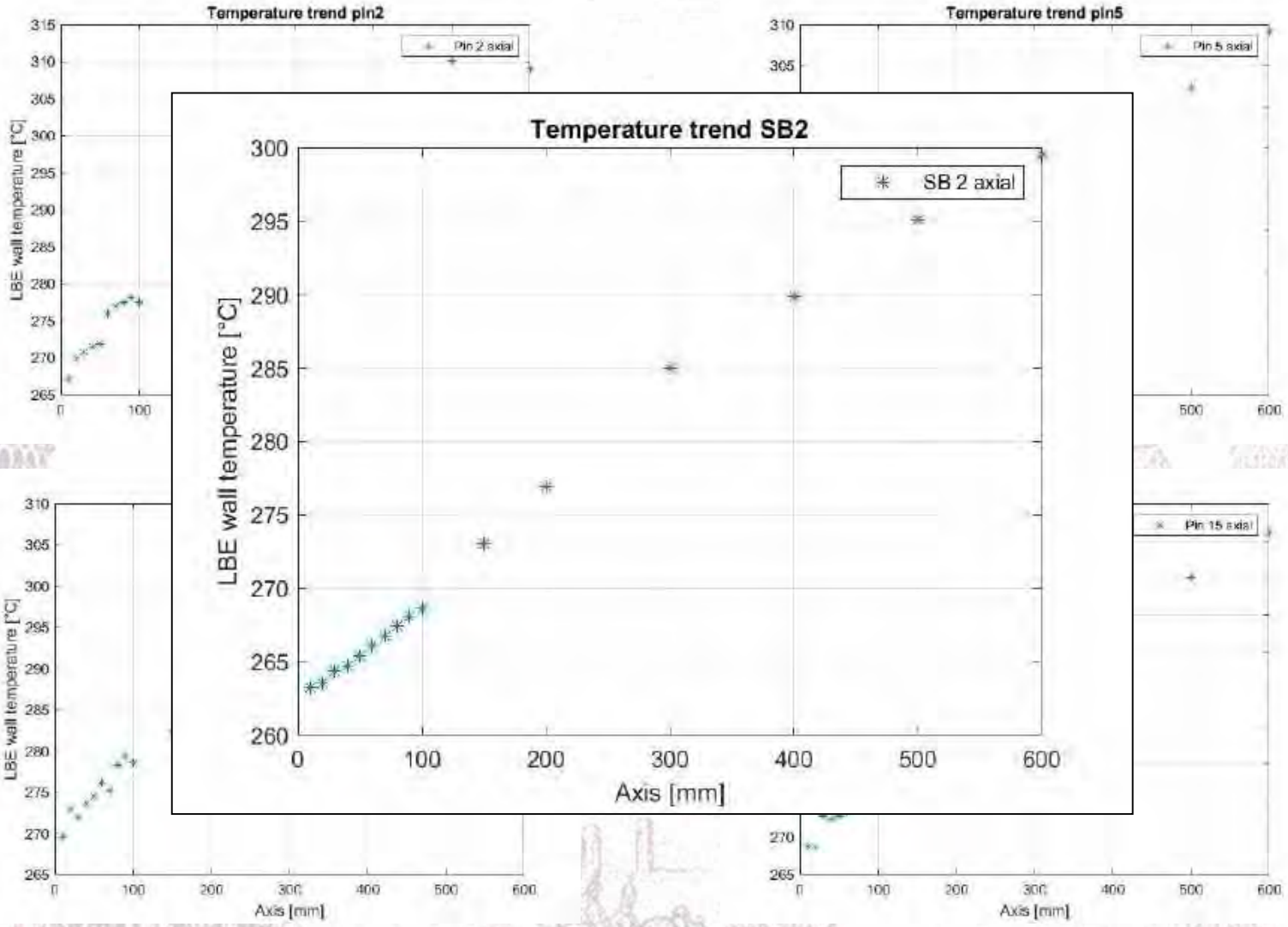

Experimental campaign
8 kg/s – Blockage 1

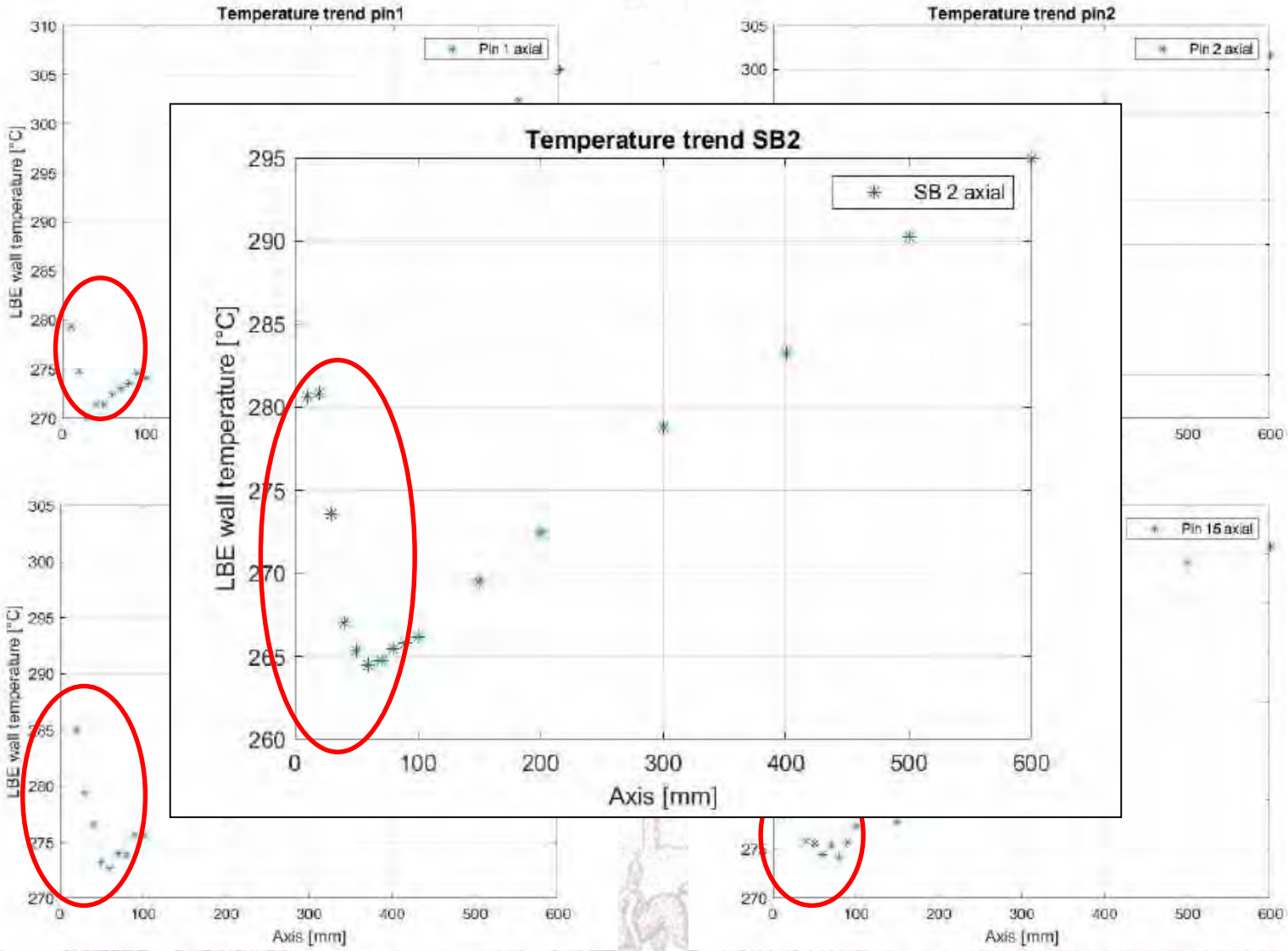

Experimental campaign
8 kg/s – Blockage 5

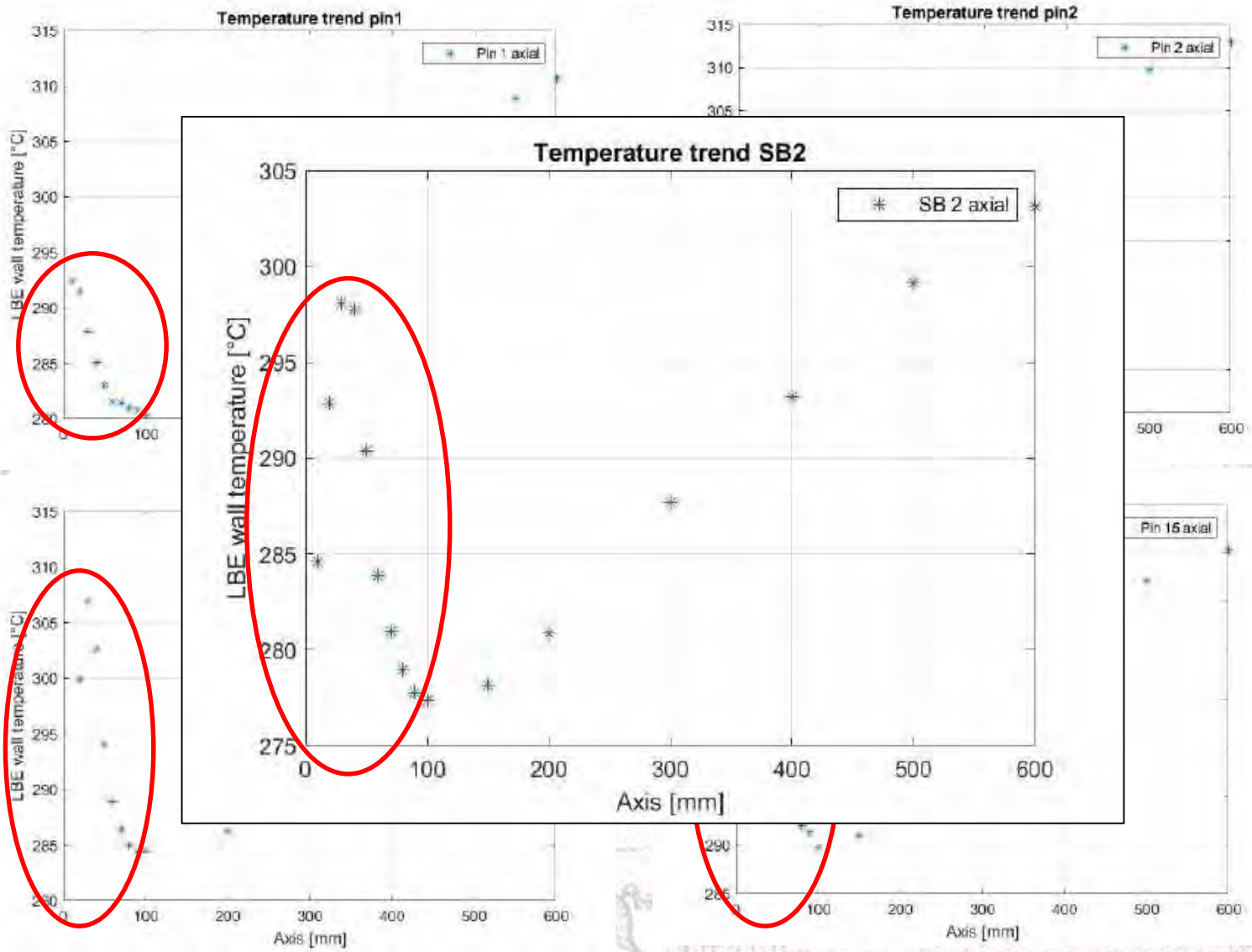

Preliminary post-test (1/2)

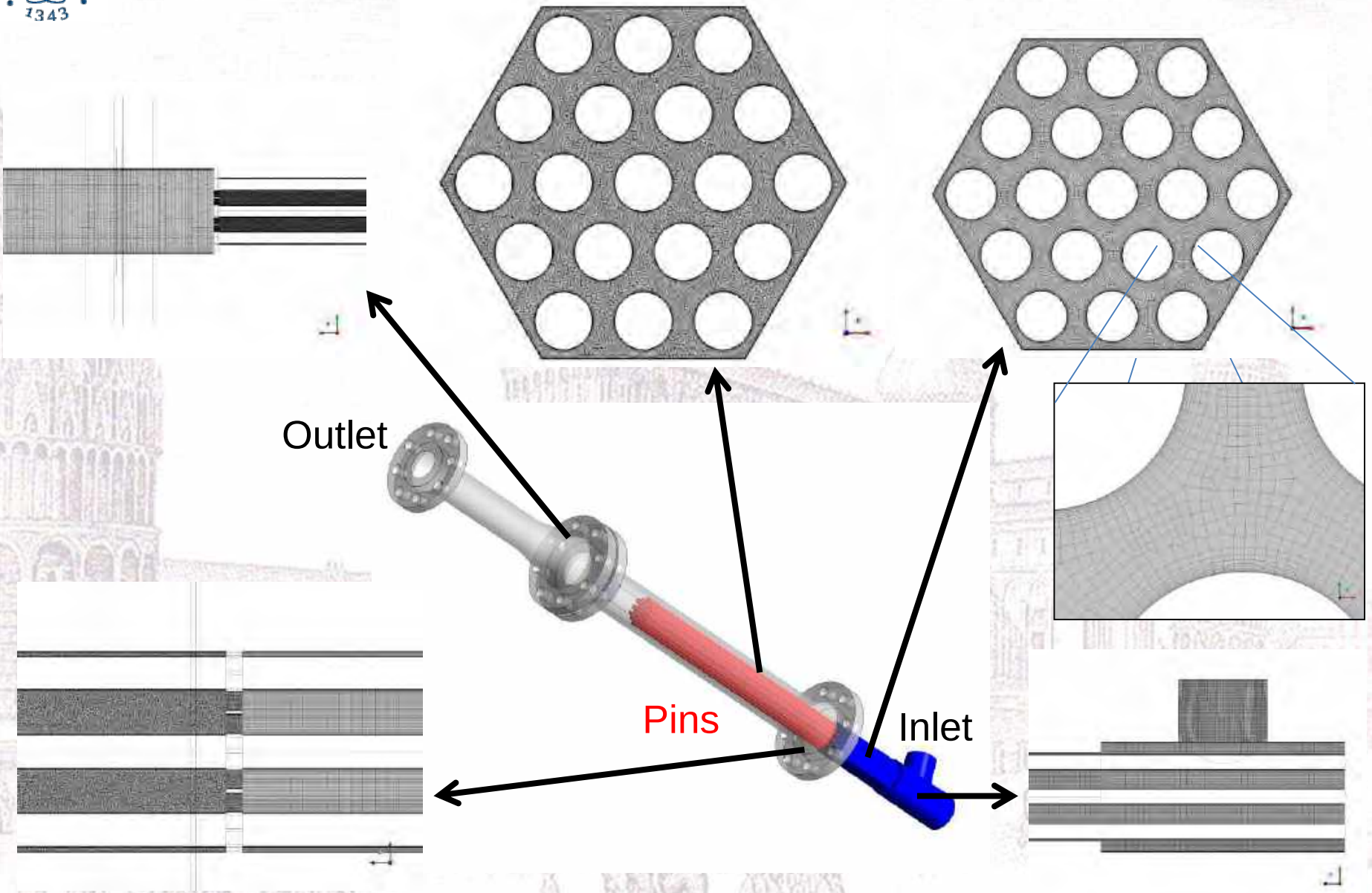

Preliminary post-test (2/2)

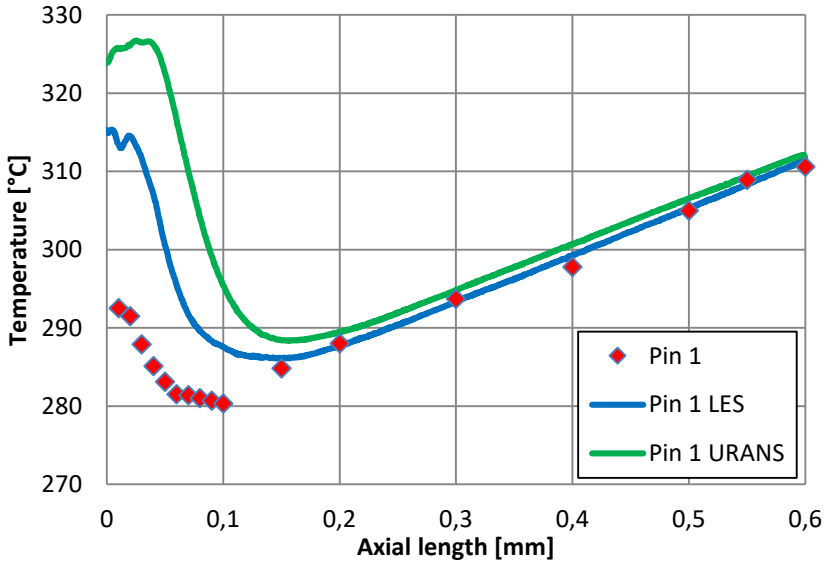

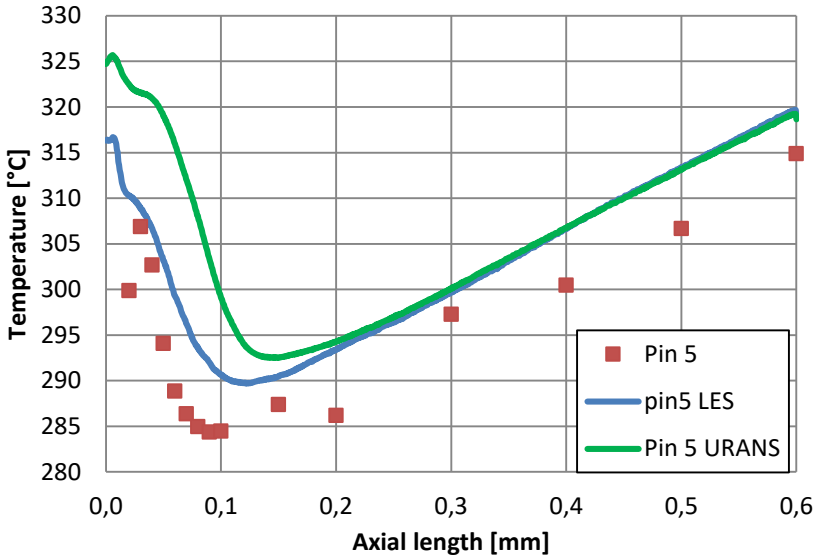

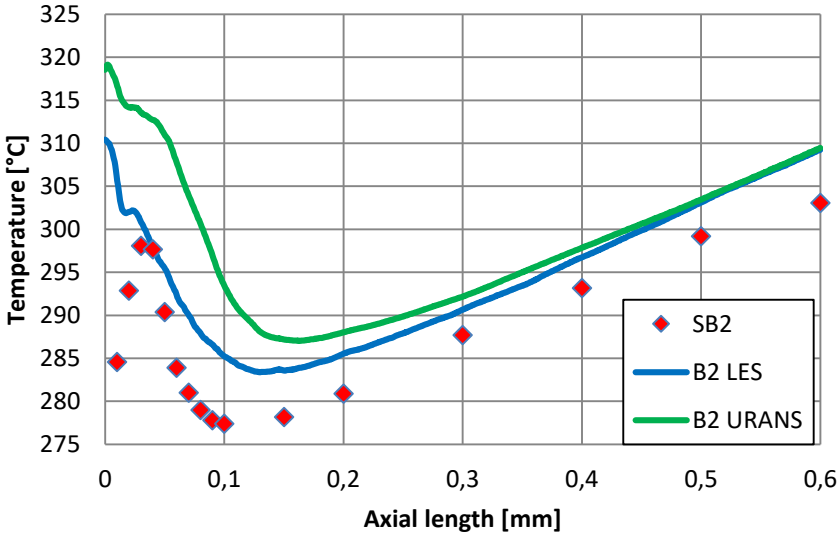

- The preliminary post test simulations show that CFD results over-predict peak temperature from 15 to 20 °C.
- This behavior will be deeply investigated in the next simulations with other blockages.

Conclusions

- The mechanical design of the test section is finished; the blockage mechanism was fixed; and the instrumentation is fixed according to pre-test CFD studies.
- A CFD benchmark activity (ENEA/UniPi, NRG, PoliMi, UniGe, CRS4) was performed with NURETH paper. The thermal-hydraulics of the new BFPS test section is analyzed for one relevant blockage with different CFD codes and different approaches. All general trends are well captured by RANS and URANS simulations even if there is a remarkable difference between the exact values of these trends (in particular their maxima and minima).
- The experimental campaign is ongoing (2 test blockages were performed).
- The preliminary post test simulations show that CFD results over-predict peak temperature from 15 to 20 °C.
- This behavior will be deeply investigated in the next simulations with other blockages.

Flow Blockage Experiments in NACIE-UP loop

Thank you

Italian National Agency for New Technologies,
Energy and Sustainable Economic Development

GENERATION IV LEAD COOLED FAST REACTOR
STATO ATTUALE DELLA TECNOLOGIA E PROSPETTIVE DI SVILUPPO

Dipartimento di Ingegneria Astronautica, Elettrica ed Energetica
Università di Roma "La Sapienza"
14-15 Giugno 2018

Structural Material for LFR Application Research Program Overview

Massimo Angiolini

The development of lead cooled fast reactors represents a unique challenge for the materials that are subjected, with different entities, to degradation mechanisms related to:

- **Neutron radiation damage**
- **Exposure to high temperatures**
- **Exposure to the HLM**

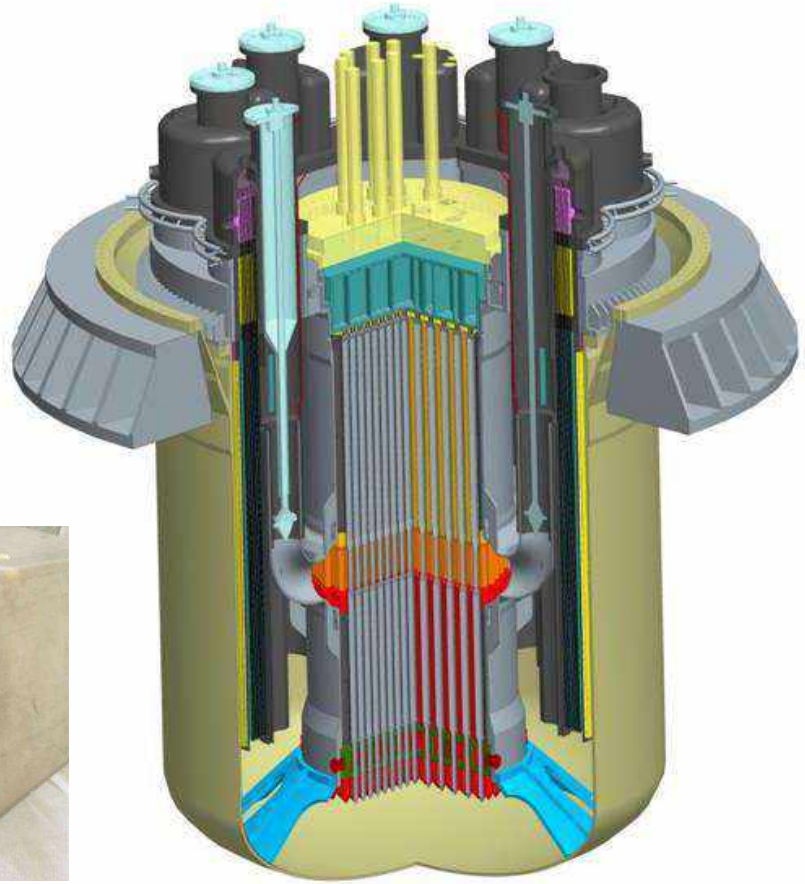

Neutron radiation damage

- Incident neutrons transfers recoil energy to the lattice atoms forming Primary Knock on Atoms (PKA's)
- PKA's displaces neighboring atoms producing atomic displacement cascades, leading to formation of a large population of defects
  - Dislocation loops
  - Voids
- And deviations from thermodynamics
  - Dissolution of precipitates
  - Radiation enhanced precipitation
  - Radiation induced precipitation
  - Radiation induced segregation

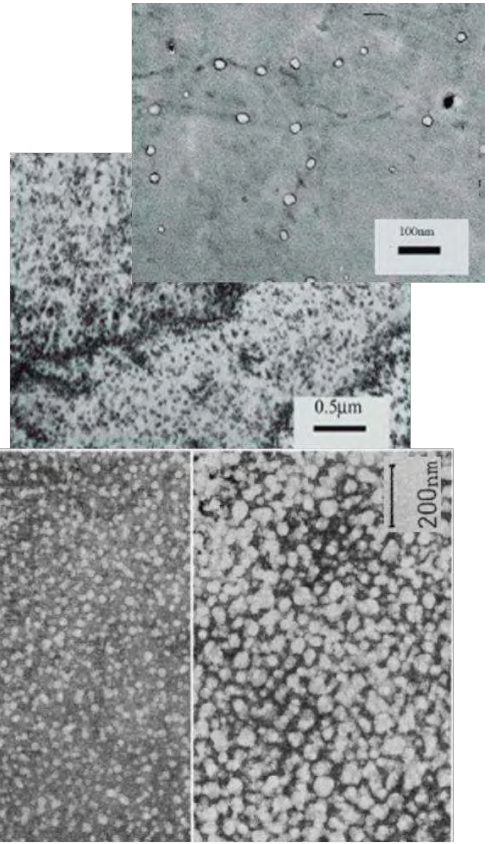

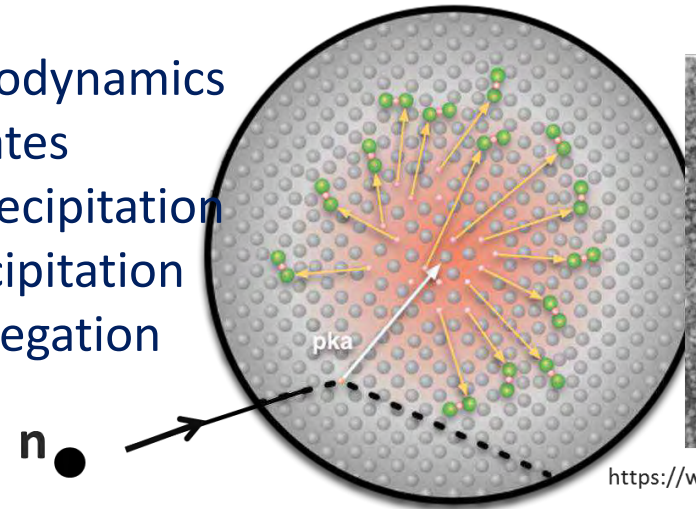

https://www.liverpool.ac.uk/~afcalder/dispcasc.html

Neutron radiation damage

- The core components and the fuel cladding tubes receive very high irradiation fluences
- The enhanced mobility, the several families of precipitates prod
lead

Increasing the life of the cladding more fissile U and plutonium bred from the U is utilized

The state of the art is a specification of the15-15 Ti steel AIM1 able to resist up to about 100 dpa

Advanced austenitic steels to reach 150 dpa irradiation for future FR's fuel claddings are under development

- The increase of the cladding resistance to neutron irradiation is crucial to realize high burnup operation of fast reactors

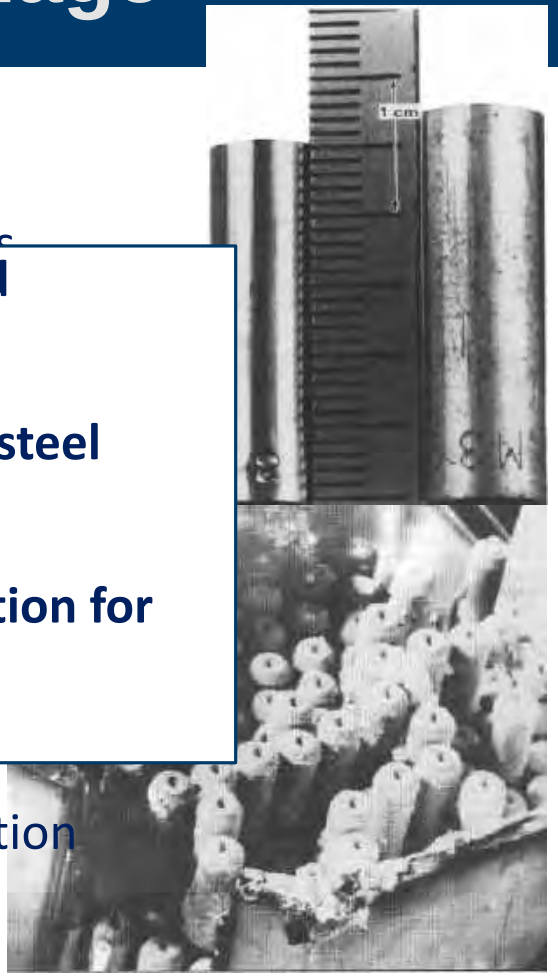

Corrosion of the steels

The compatibility of steels with lead and LBE represents the main challenge in the development of HLM cooled systems

- Not-passivating oxidation leading to thick oxide layers not stable/internal oxidation
- Dissolution of the steel constitutive elements: Ni, Cr and Fe show high solubility in lead-bismuth eutectic
- Liquid metal embrittlement (F/M)

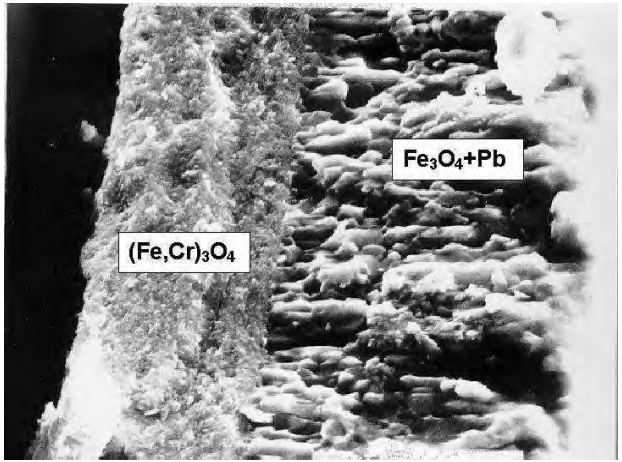

	Pure lead T = 550° C	LBE T≤300° C	LBE T=460~470° C	LBE T≥550° C
F/M Steels	Duplex layer	Very thin Oxide layer	Duplex oxide layer	Heavy corrosion
Austenitic	Thin duplex oxide layer	Very thin single layer	Thin single layer	Thin duplex oxide layer

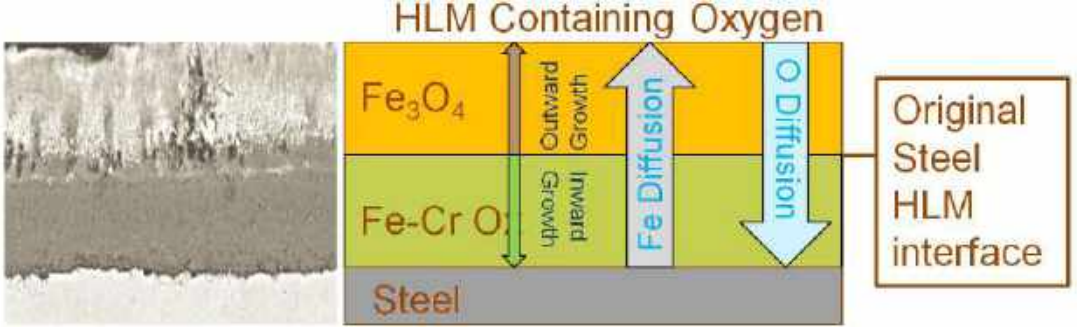

Corrosion of the steels

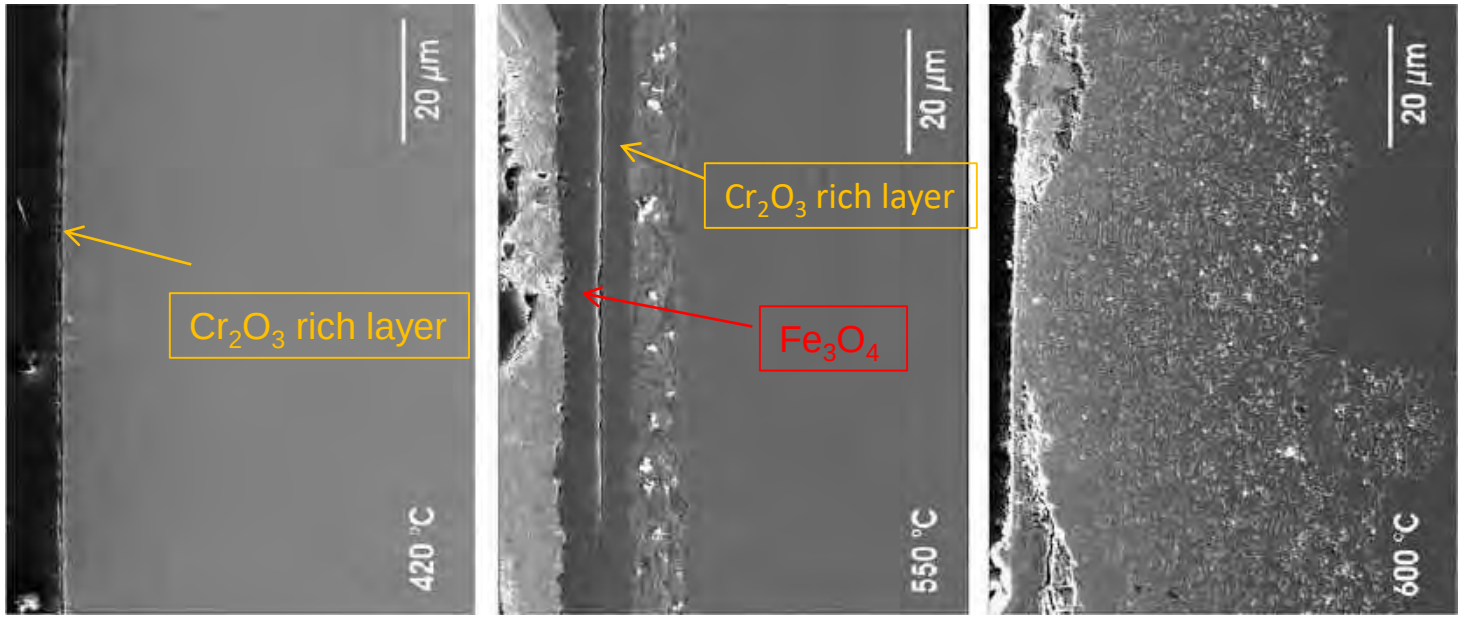

DIN1.4970 SS 4000 h (167 d) of exposure flowing LBE 10^{-6} wt% oxygen

- Thin protective Cr2O3 rich layer @ 420° C
- Dual magnetite/Cr_2O_3 rich layer layer partly infiltrated with LBE @ 550°C
- Severe corrosion/dissolution attack @ 600°C

bright spots consisting of LBE penetrated the steel matrix.

G. Muller et al. Journal of Nuclear Materials 335 (2004) 163–168

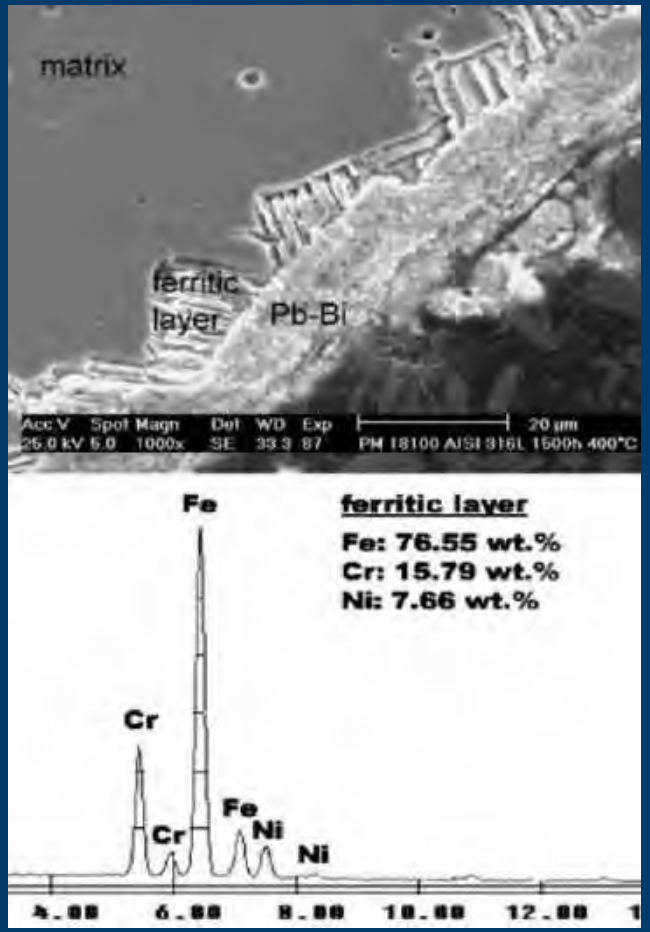

- The upper temperature limit (450°-470° C) imposed by the corrosion and the relatively high melting temperature of the lead (327,5 °C) pose a limitation to the thermal efficiency attainable by the reactor
- In principle a suitable design and choice of materials (AFA steels, FeCrAl ODS, coatings) would make possible the realization of high temperature HLM cooled systems, all except the core
- At present a material able to resist in high temperature HLM to the fast neutron flux to 100 dpa is missing

Corrosion protection by AOC

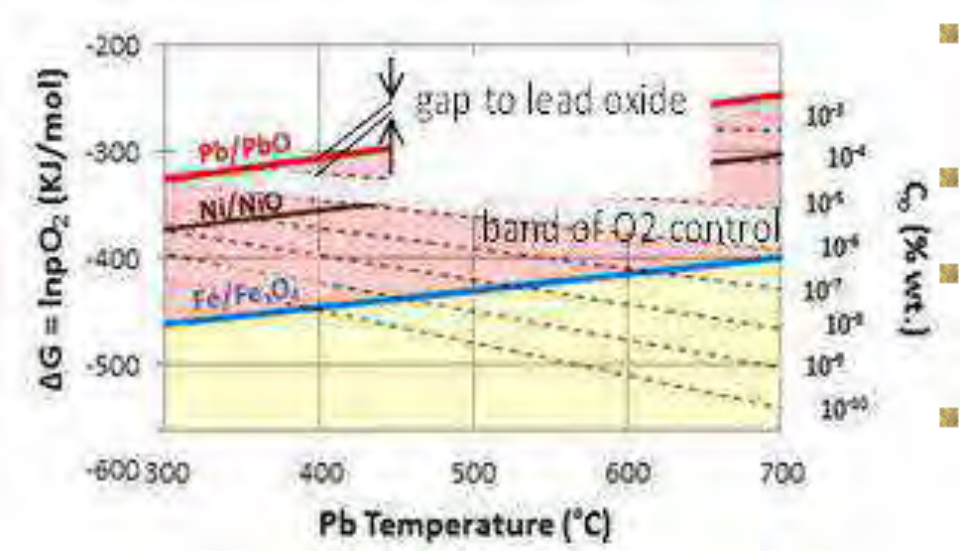

- A possible strategy to handle the corrosion issues is to perform operations under control of the oxygen dissolved in the melt (AOC)
- Keeping the oxygen content in an interval of concentration
- below the precipitation of the solid PbO to prevent the formation of solid plugs of lead oxide
- above that of precipitation of Fe_3O_4 guarantees the presence of a Fe-Cr oxide layer that protects the steels from the lead

- For tests temperatures higher than the above limits, the formation and protectiveness of oxides is uncertain, and protection usually fails due to dissolution for long times
- Difficult to control the oxygen content on a large pool with thermal stratification
- To prevent the dissolution of the steel everywhere, it could be appropriate to maintain oxygen level next to the upper limit with the risk of precipitation of Pb oxide in parts operated at low temperature

ALFRED – corrosion protection strategy

- Operate the reactor in “low oxygen conditions”, i.e. [O] below the saturation limit at the coldest temperature of the coolant (400°C), to eliminate the risk of lead oxide precipitation in the whole system
- Use of suitable coatings to achieve the corrosion/erosion resistance in the hottest regions Core, SGP-unit, etc @550°C max

- 15-15 Ti AIM1 Al_2O_3 PLD coated for the cladding and core components
- Austenitic creep resistant steel with an aluminide diffusion coating for the SG

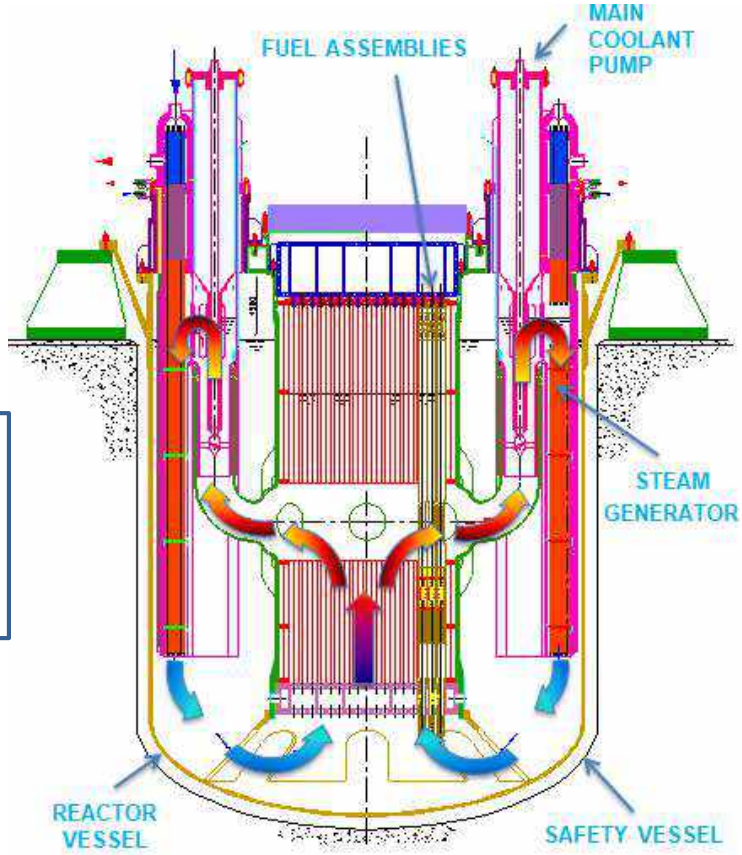

Al_2O_3 PLD nanoceramics

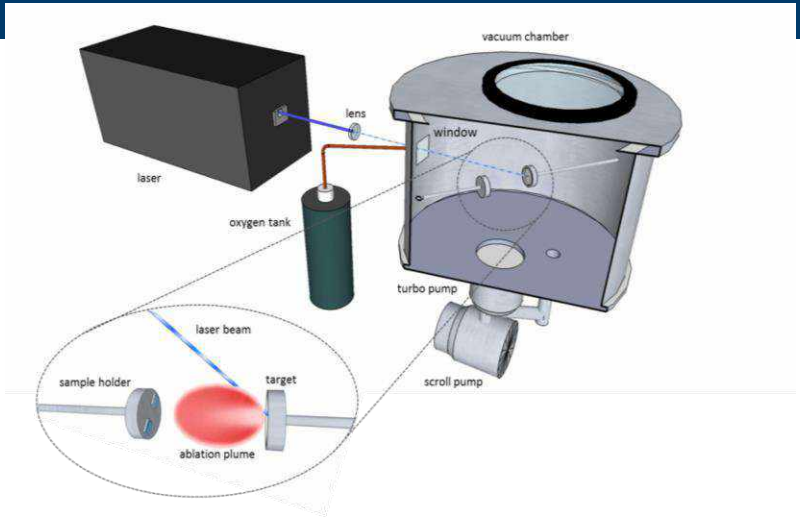

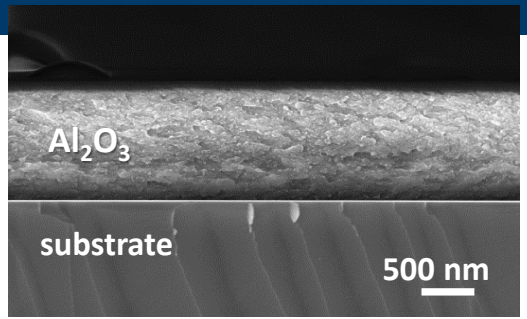

F. Garcia Ferré et al. – ACTA MATER – 2013

10 cm long 316L tube + 1 µm Al_2O_3

- **high quality coatings**
- custom process: bottom-up approach
- process at **room temperature**
- amorphous films with **nanodispersed crystalline domains**
- **high deposition rate (nm/s)**
- **Line of sight deposition**

Property @RT	Sapphire	PLD Al_2O_3	AISI 316L
ν	0,24	0,295 ± 0,025	0,3
E [GPa]	345	193,8 ± 9,9	200
G [GPa]	175	75,5 ± 3,8	80
B [GPa]	240	159,2 ± 11,8	140
H [GPa]	27,8	10,3 ± 1	4
H/E	0,059	0,049 ± 0,007	0,025

Nanocrystalline oxides have metal like mechanical properties!

GEMMA Generation IV Materials Maturity

Al_2O_3 PLD nanoceramics

Oxidation in stagnant Pb

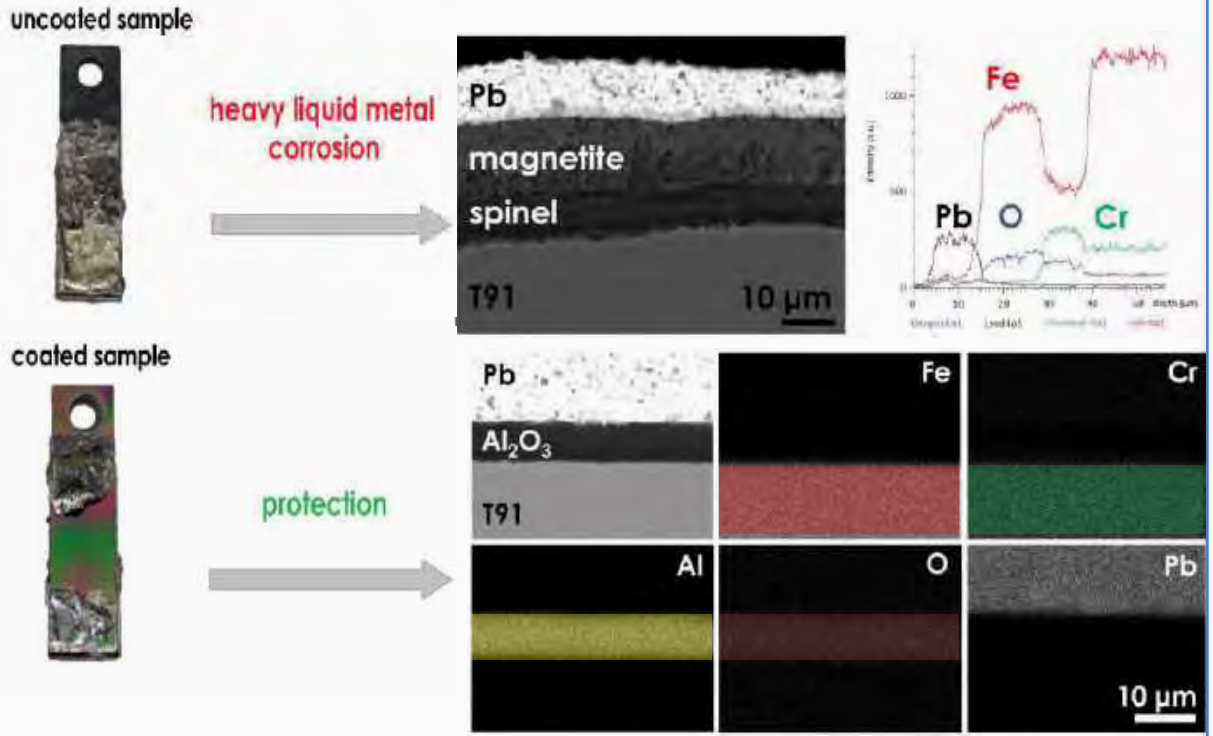

F. Garcia Ferré et al. – CORROS SCI – 2013

Resistance to n irradiation

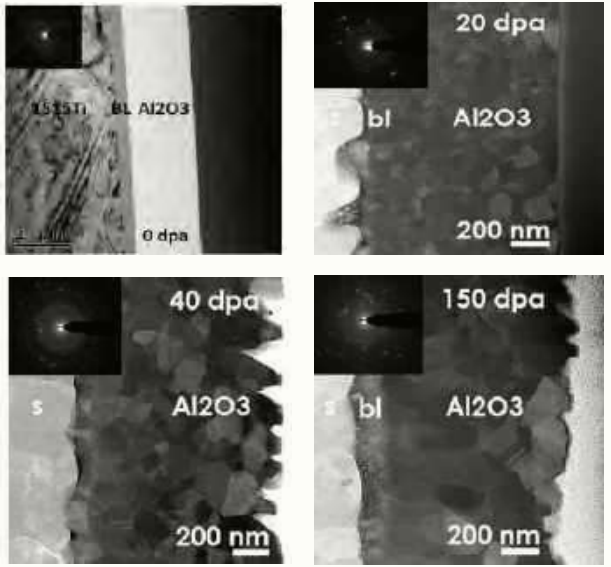

Al_2O_3 PLD nanoceramics

- The work on the Al2O3 coatings will be devoted to pre-normative tests aimed at supporting the drafting of design rules for their use as corrosion-resistant coatings for the the LFR core
- The series of corrosion data will be completed with tests in stagnant Pb at 550 ° C at low oxygen (nominal condition, 10-8wt.%) and high oxygen (accidental condition, saturation) started I the last years and devoted to verify the thermodynamic stability of the alumina coating
- In addition, stagnant corrosion tests will be performed at 650 ° C to verify the applicability of the coating to HT LFR systems
- PLD alumina depositions with a chromium buffer-layer will also be tested to verify if the coating passivates in in case of damage or rupture
- Thermal cycling tests will be carried out in an ad hoc device designed and produced by ENEA based on the expected thermal excursions for the component during its life: 25 temperature cycles between RT and 600 ° C.
- Impact tests as well as three-point bending tests will be performed to verify the resistance to the damage by impacts and the tolerance to deformations
- "CREEP-RUPTURE“ tests in lead at the operating conditions of the LFR system
- All the above tests will be followed by electron microscopy observations to characterize and evaluate the damage produced
- In view of the execution of lead fretting tests to evaluate the resistance of the coatings to abrasion, the GIORDI fretting test machine will be updated with a monitor and control system for the [O] and an improved the system for the apply the load to the sample

FeCrAl diffusion coatings

- The work on diffusion coating started few years ago in collaboration with C.S.M. S.p.A and has been devoted mainly to the optimization of low temperature processes applicable to F/M steels and the austenitics of the 15-15 type for cladding application – activity discontinued/characterizations pending
- The work continues on austenitics of the 15-15 type optimized for high creep resistance for application to the SG of the LFR
- The focus will be on
  - the performance of the coating under the loads typical of this kind of application
    - Creep
    - Fatigue
    - Ratchetting
  - the corrosion behavior vs the oxygen content
    - the Al rich layer if not passive may undergo severe dissolution-corrosion issues

- All the tests will be compared with the analogues performed on uncoated samples
- Samples after testing will be analyzed by electron microscopy in flat and cross-section to characterize and evaluate the damage produced

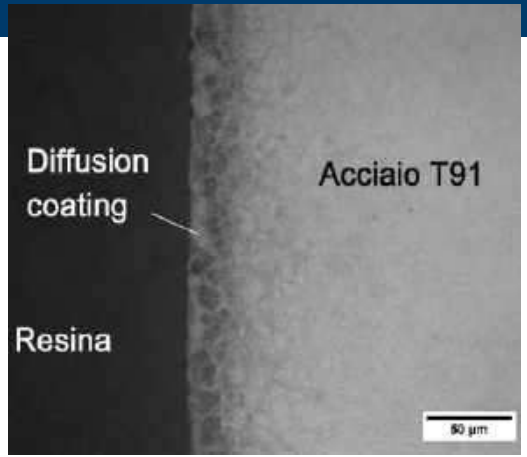

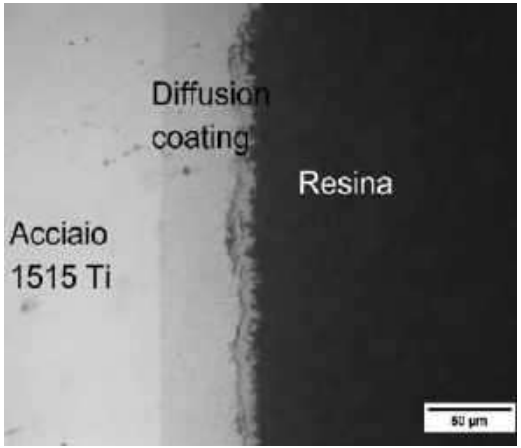

Oxygen Control System implementation

- The final objective of the work will be the demonstration of the feasibility of operations of large HLM plants at low and controlled oxygen concentration, in the range 10^{-6}-10^{-8}% wt
- Development of an oxygen control system in Pb and Pb-Bi for the experimental plants located at C.R. Brasimone
  - HLM pool, loops and storage tanks
- **<u>To this aim the development of monitor and control systems of the [O] is needed</u>**
- development and testing of sensors to in situ monitor the concentration of oxygen in the HLM under typical operating conditions (T and p)
  - new reference air/perovskite and Cu/Cu2O electrode systems and new solid electrolyte geometries in Yttria Partially Stabilized Zirconia
- Developments of reliable devices that allow to control the [O]
  - The new oxygen control system based on the injection of Ar-H_2 and Ar-O_2 mixtures will be tested in the LECOR loop system and in the BID1 pool system.

Tests under different operating conditions will be carried out in order to identify the parameters that allow a stable oxygen control

DS steels development

- Ti and Nb DS steels development started in the 80' in the frame of an ENEA-CEA collaboration
- Among them the DS4 has shown an outstanding performance toward neutron swelling after irradiation in Phènix (SUPERNOVA experiment)
- An evolution of the DS4 is being considered as fuel cladding of the future FR's for the promise to be able to sustain fast neutron irradiation up to 150 dpa with limited swelling and acceptable mechanical properties
- Aim of the work on the DS steels is to re-establish the know-how in the field of the design and manufacturing of special steels and testing the material in the ALFRED conditions
- A new cast (80 Kg) with the DS4 formula has been manufactured by CSM S.p.A. (PAR 2013)
- The DS4 material is being characterized
  - the corrosion behaviour in molten lead
  - mechanical behaviour (tensile, creep)
  - Irradiation with 58 Ni ions @110 MeV 550°C presso LNL (in progress)

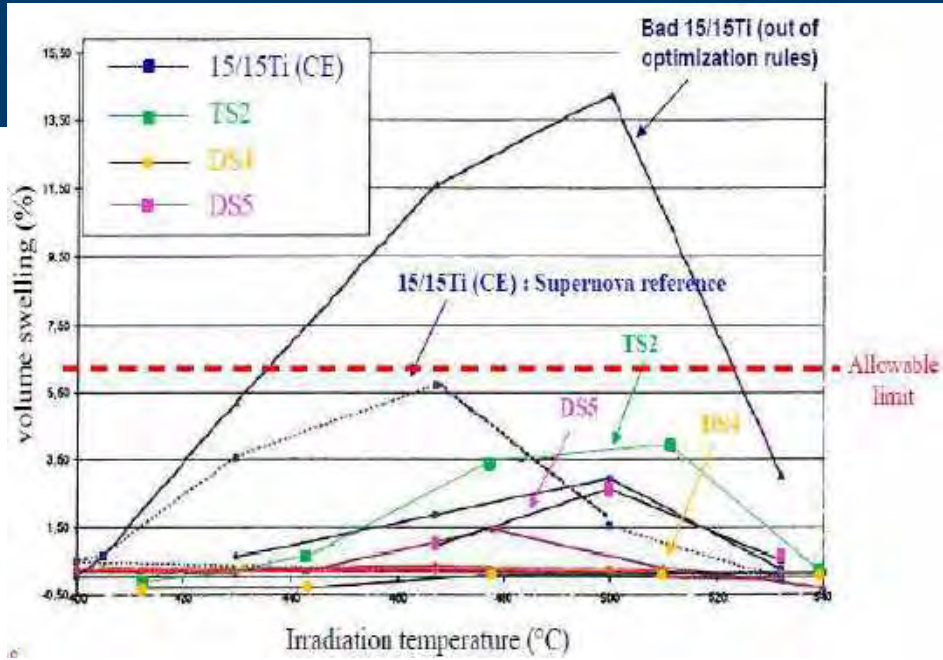

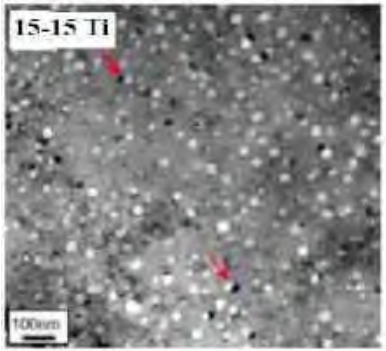

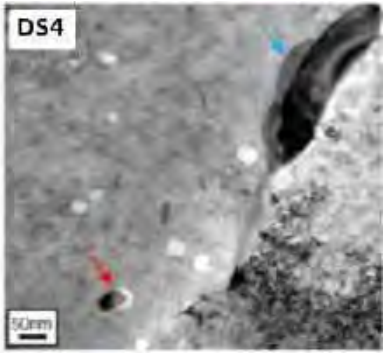

Creep tests in HLM

- The experience gained during the last decades has shown that the influence of the molten metal on the mechanical properties is strongly dependent on the chemistry
- The oxide or any other contamination on the surface can mask/protect steel from the contact with the liquid
- Critical issue for creep tests that last months/years
- The “static” system set up during the last years revealed not efficient in maintaining the nominal operating conditions
  - inert / reducing gas lines for each machine for the conditioning of the molten metal
  - modification of the deformation acquisition system
  - designed and implemented a new acquisition system (Hardware / Software)
- Post test characterization revealed in some cases huge oxide deposits
- It has been decided to upgrade the oxygen control system with oxygen sensors and implement a monitor and control system

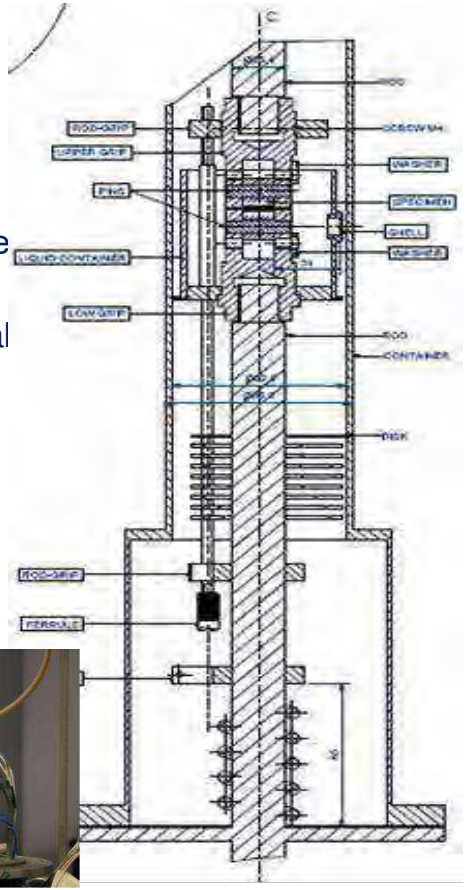

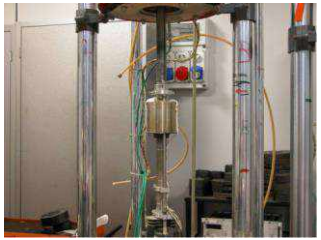

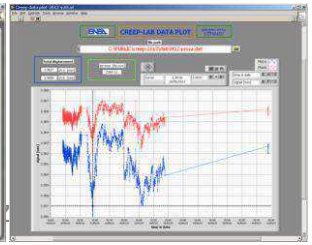

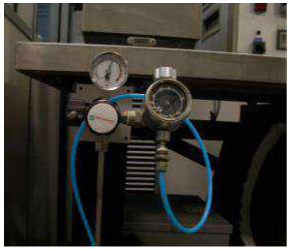

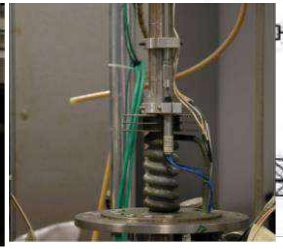

- PLD coating for LFR application. Status and future developments — F. Di Fonzo
- Coating characterization under irradiation.
  Heavy ions irradiation against neutron irradiation — M. Beghi
- Corrosion qualification of materials and coatings in liquid lead for LFR — S. Bassini
- Mechanical characterization of coatings — M. Bragaglia
- Coolant chemistry control study for HLM systems — S. Bassini
- Double stabilized stainless steels: Status and future developments — C. Cristalli
- Creep-Rupture tests in HLM environment — A. Coglitore
- Criticality of manufacturing and advanced processes — E. Zanin

Thanks for your attention

massimo.angiolini@enea.it

ISTITUTO ITALIANO DI TECNOLOGIA
CENTER FOR NANOSCIENCE AND TECHNOLOGY

Nanoceramic Coatings for Advanced Nuclear Systems: status and prospects

M. Vanazzi, D. Iadicicco, B. Paladino, E. Frankberg,
F. Di Fonzo

fabio.difonzo@iit.it

ISTITUTO ITALIANO
DI TECNOLOGIA

Introduction

Future generation nuclear systems (GIV)

Tritium management

Corrosion

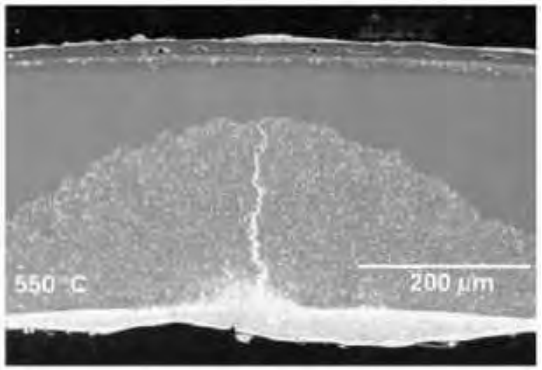

G. Mueller et al. – J Nucl Mater – 2004

Radiation damage

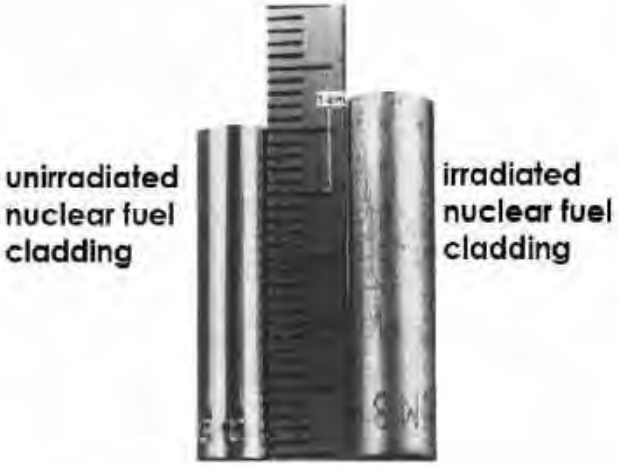

J.L. Straalsund – Westinghouse Hanford

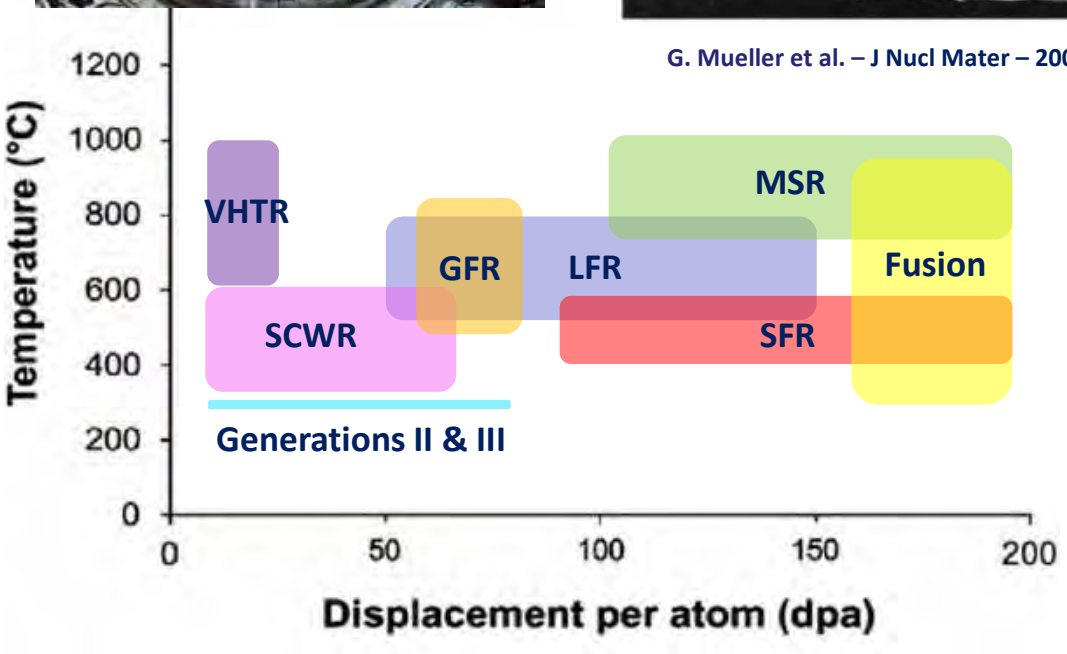

S.J. Zinkle and G.S. Was – Acta Materialia - 2013

MAJOR BOTTLENECKS FOR ALL SYSTEMS

↓

NEED FOR COATINGS

Future generation nuclear systems aim at:

- Increase efficiency
- Reduce waste generation
- Enhance safety
- Promote non-proliferation

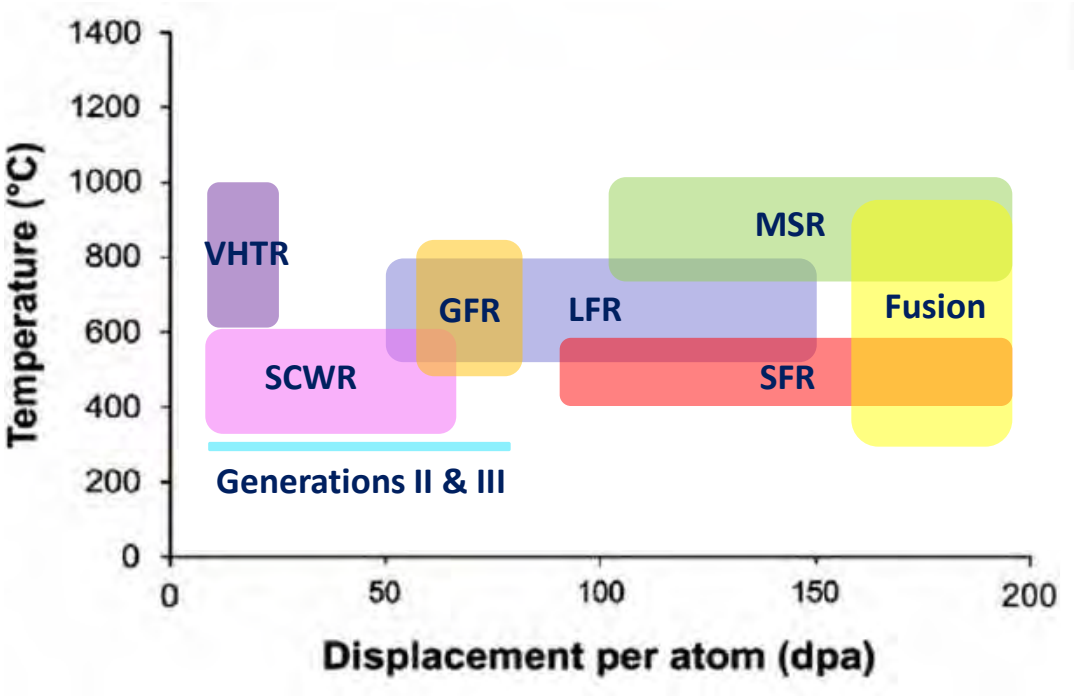

S.J. Zinkle and G.S. Was – Acta Materialia - 2013

Ultimate goal for LFRs:

- 800 °C
- 150 dpa

Advantages:

safety
transmutation of minor actinides / fuel breeding

Major issues:

- corrosion
- radiation damage

S.J. Zinkle and G.S. Was – Acta Materialia - 2013

Heavy liquid metal corrosion

Ni leaching in austenitics (23000 h @ 550°C, 10^{-6} wt.% O)

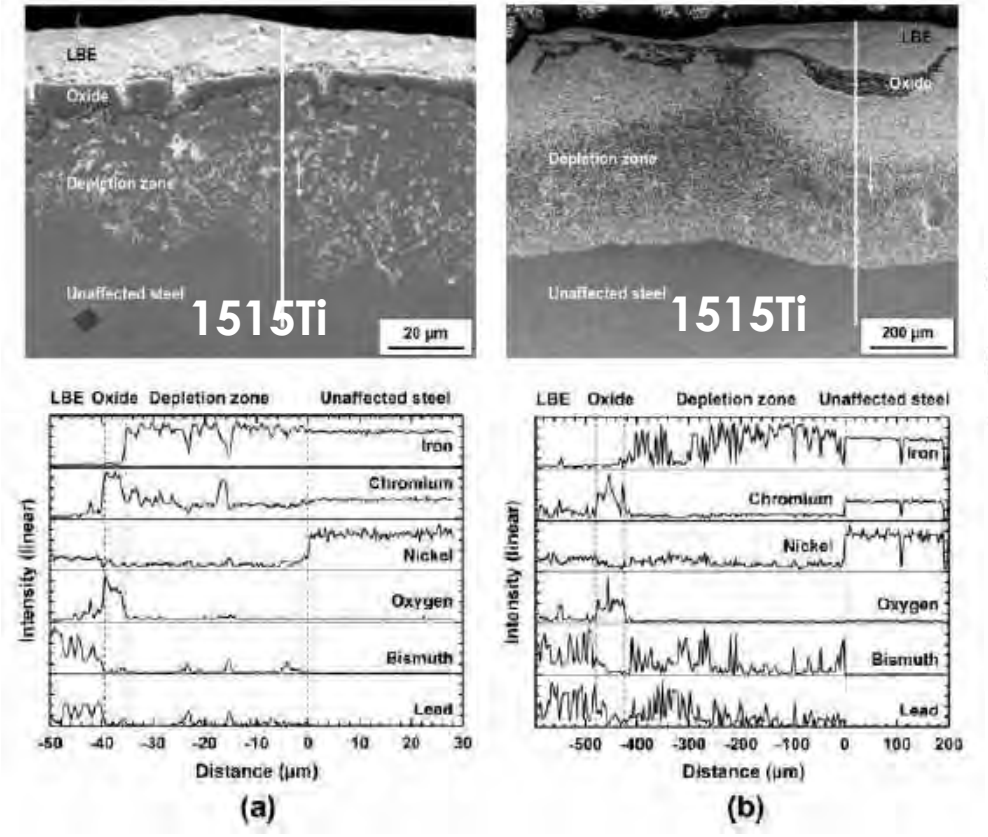

C. Schroer et al. - Corros. Sci. - 2014

Solubility of Ni in lead is very high

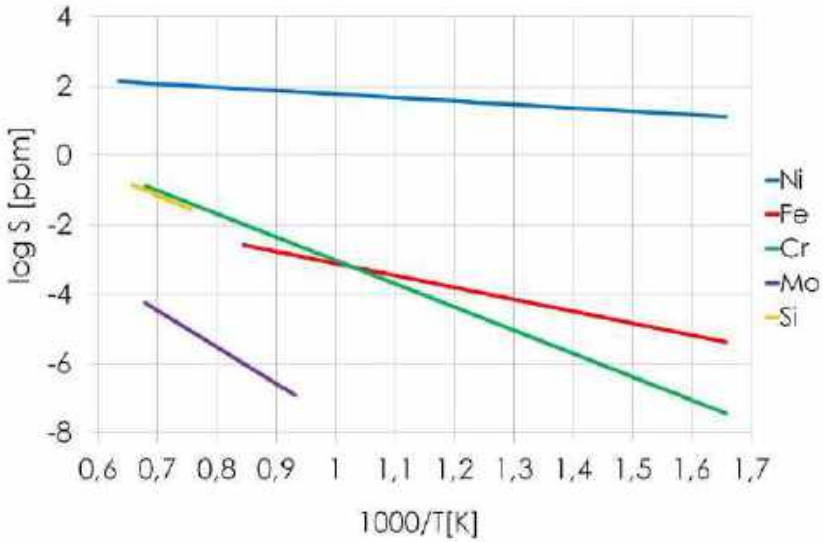

In-situ passivation is not viable for T > 500°C-550°C

(will be exceeded by fuel cladding)

Heavy liquid metal corrosion

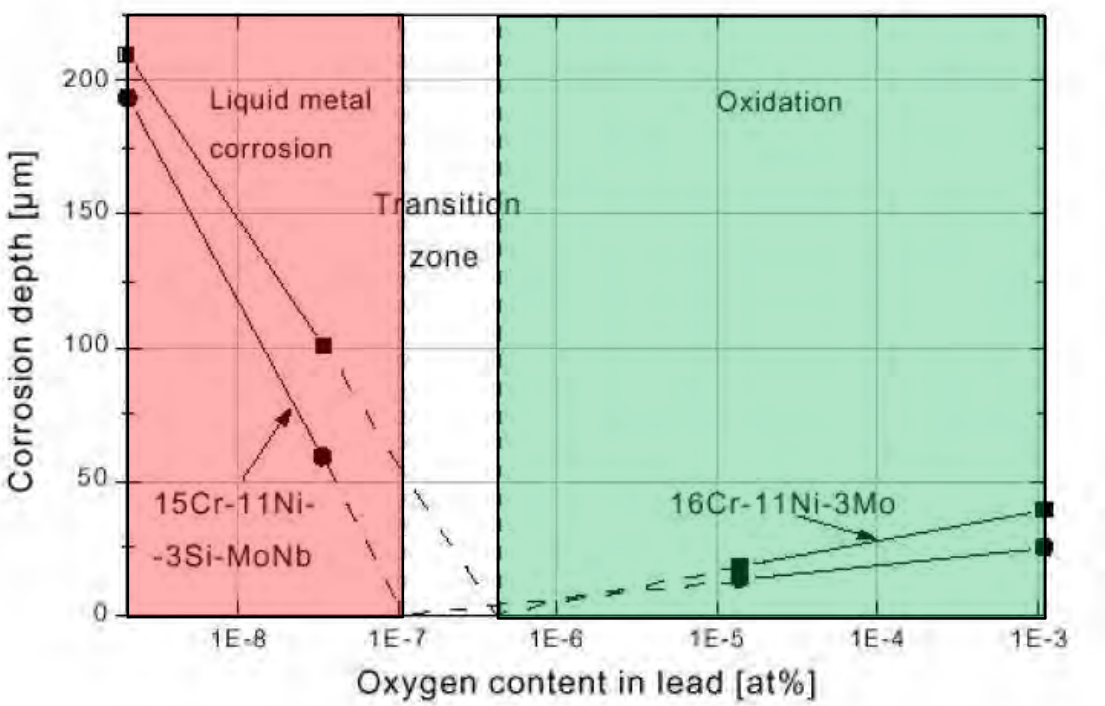

Austenitic steels exposed to HLM for 3000 hours at 550°C

V. Gorynin et al. – Metal Science and Heat Treatment - 1999

G. Mueller et al. – J Nucl Mater – 2004

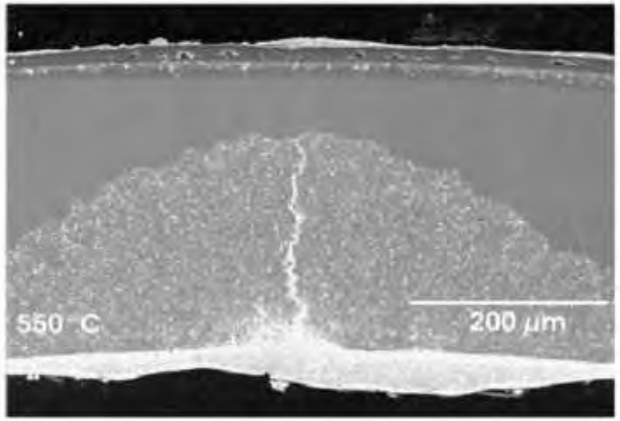

Dissolution

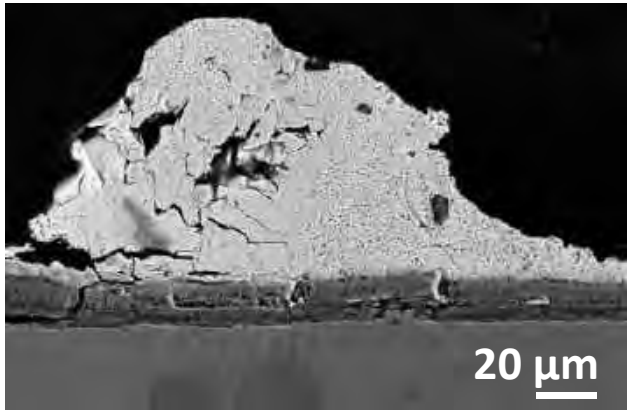

Oxidation

In-situ passivation is not viable for T > 500°C
(will be exceeded by fuel cladding)

Technology Constraints for ALFRED

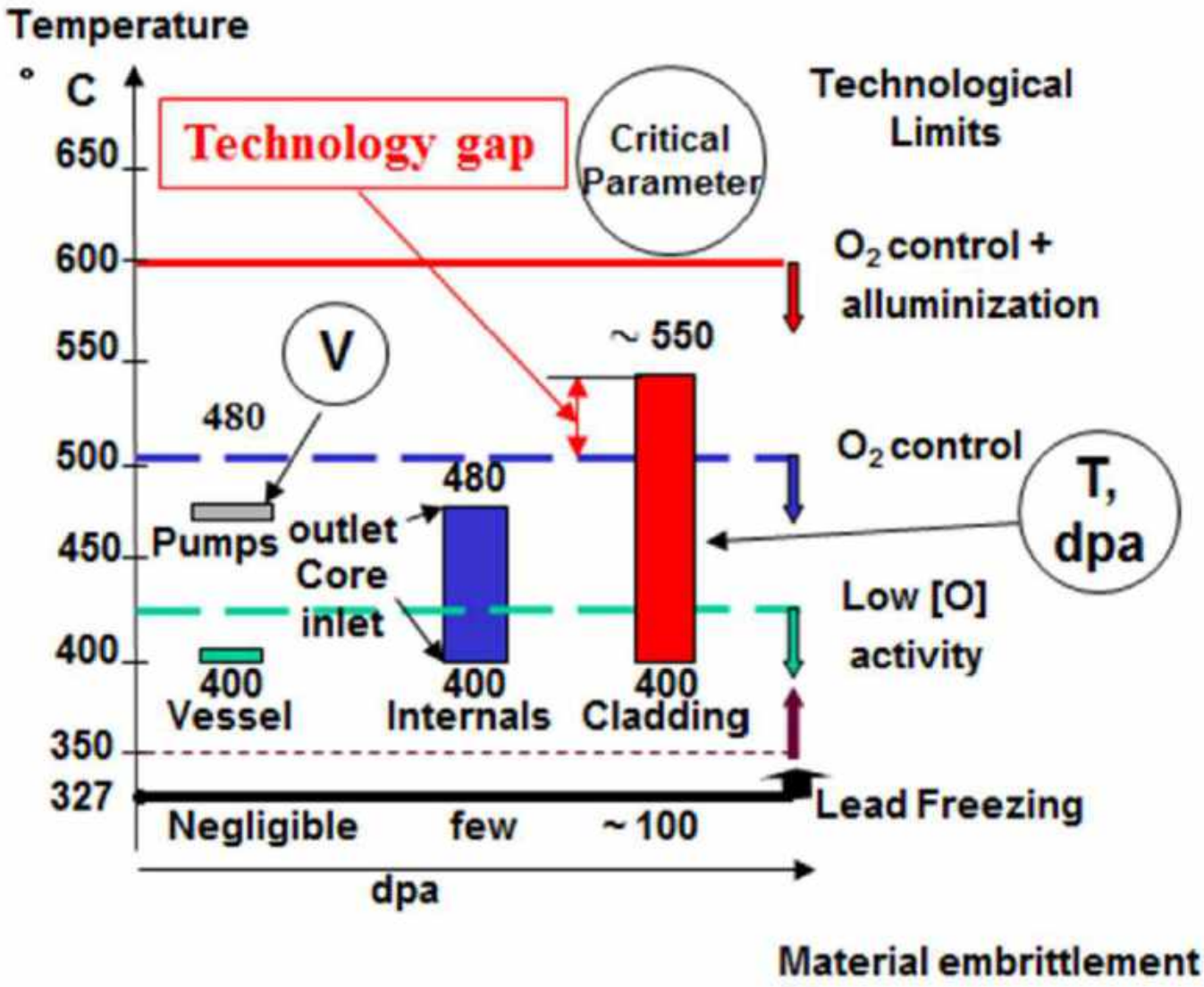

Impact of temperature (1st stage)

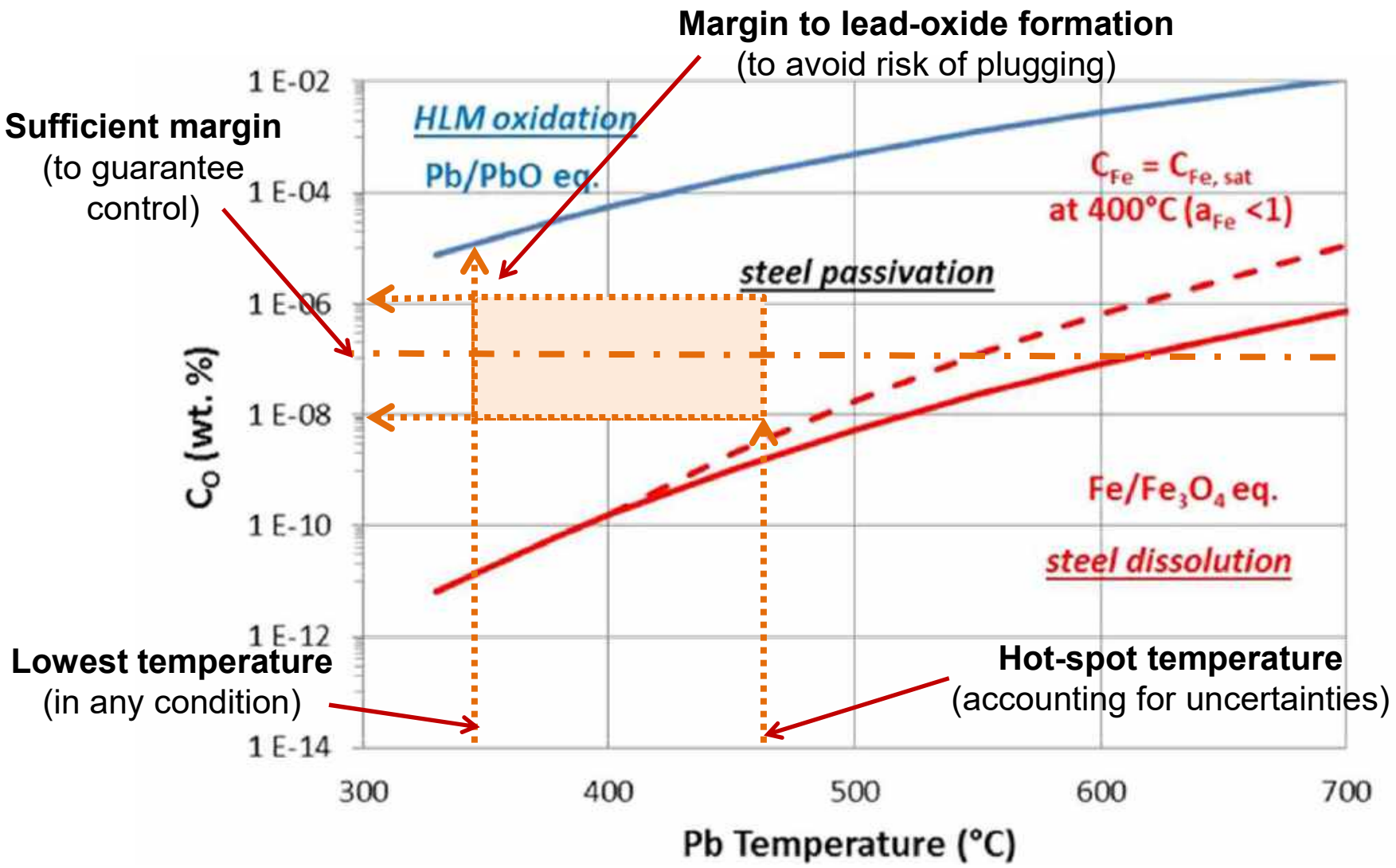

Impact of temperature (final stage)

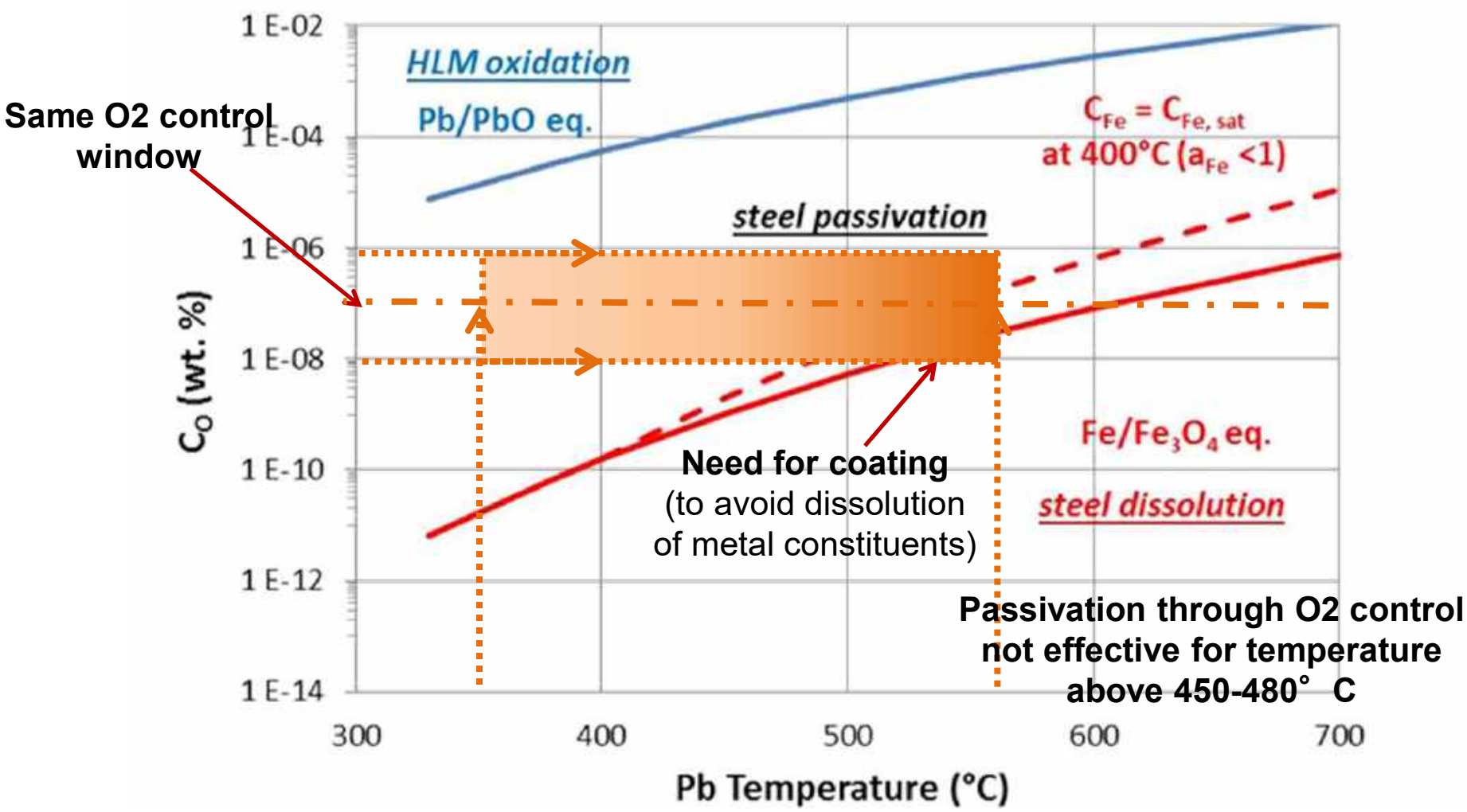

Oxygen Control, fighting with ever narrow operational window!

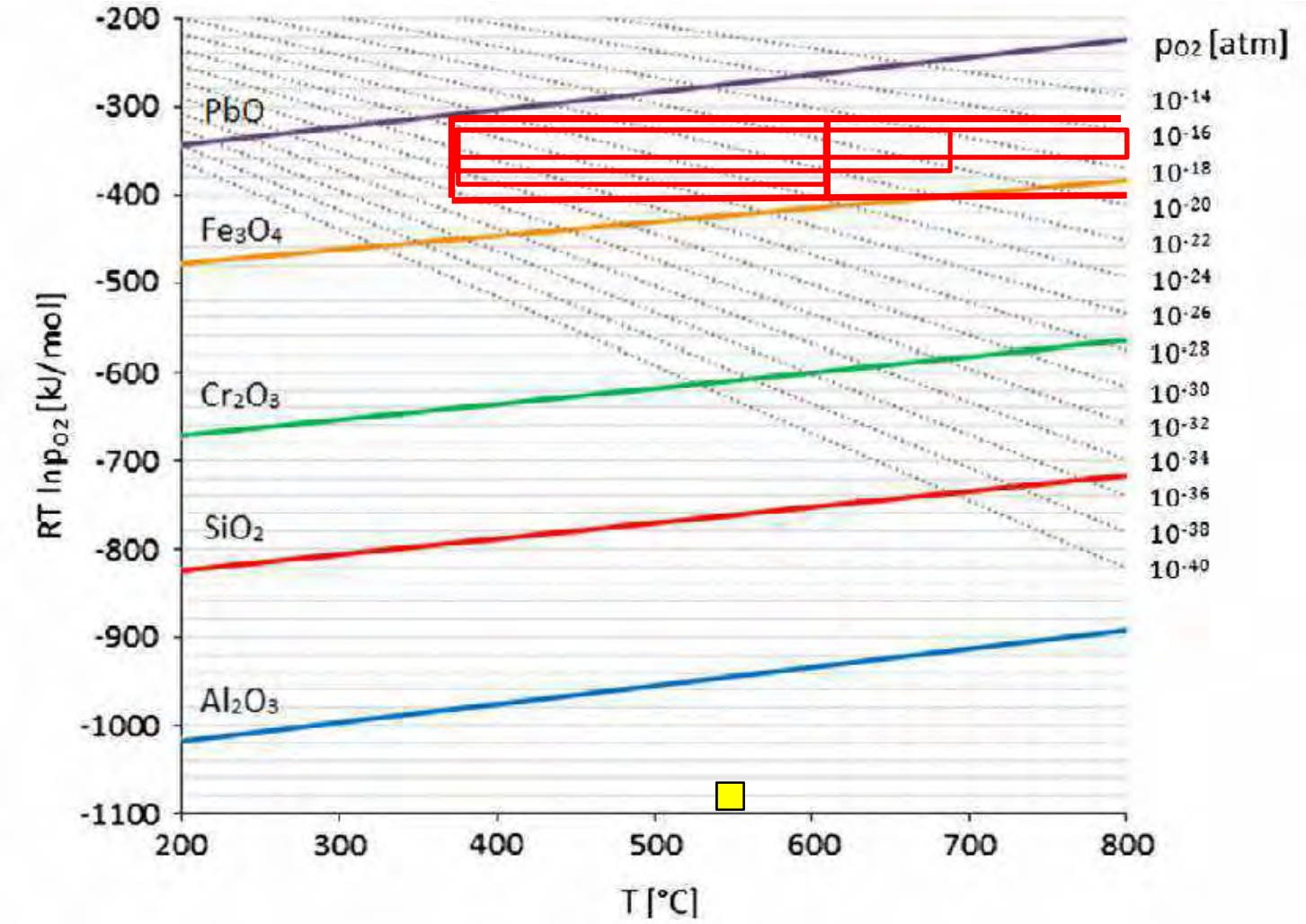

NANOCERAMICS

enhanced

enhanced

Mechanical performance

Coble creep, twinning, etc.

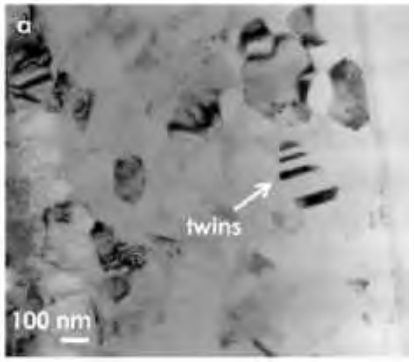

F. Garcia Ferré et al. – SCI REP – 2016

Corrosion resistance

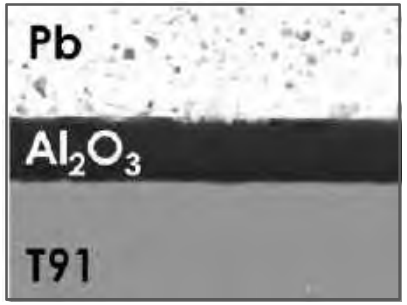

F. Garcia Ferré et al. – CORROS SCI – 2013

Radiation tolerance

Interstitial emission from GBs

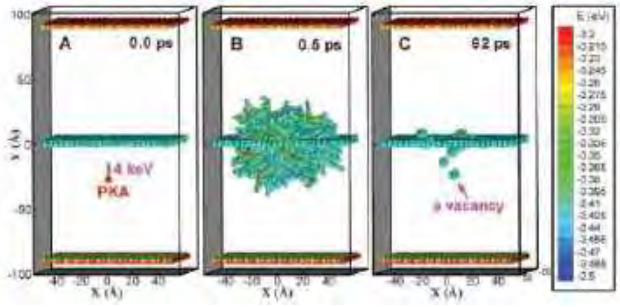

X.M. Bai et al. – Science - 2010

ISTITUTO ITALIANO
DI TECNOLOGIA

Al_2O_3 films deposited by Pulsed Laser Deposition (PLD)

Acta Materialia 61, 2662-2670, 2013
Corrosion Science 77, 375-378, 2013
Scientific Reports 6, 33478, 2016
Corrosion Science 124, 80-92, 2017
Acta Materialia 143, 156-165, 2018

fabio.difonzo@iit.it

Processing & structure

Pulsed Laser Deposition

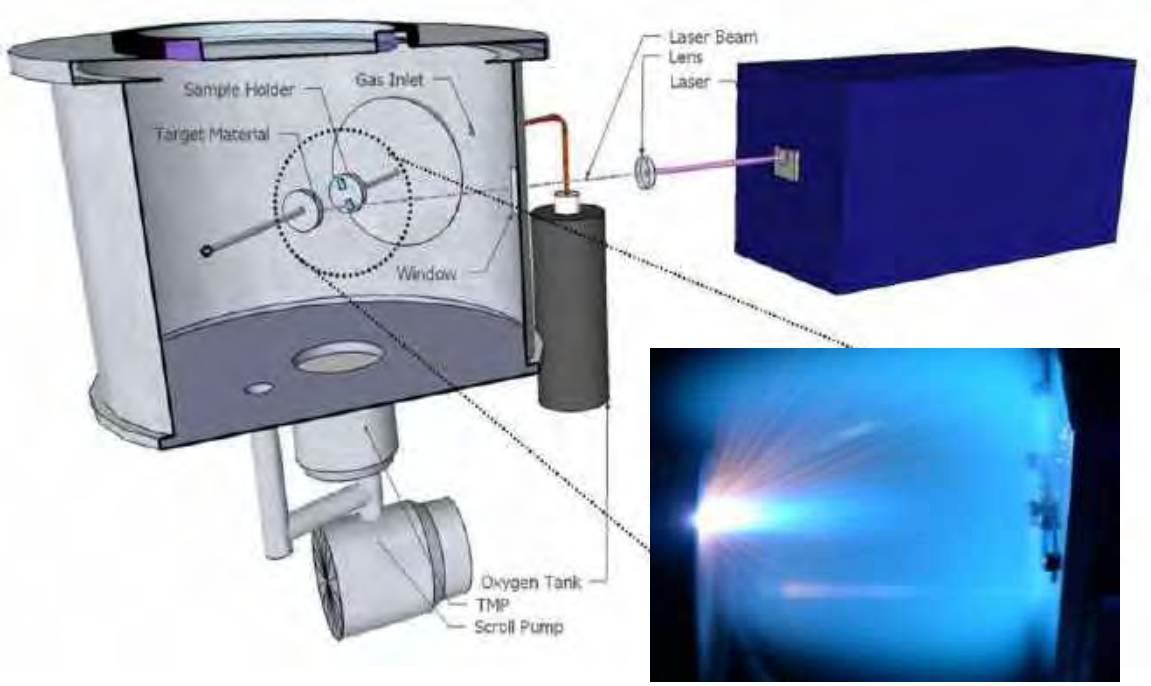

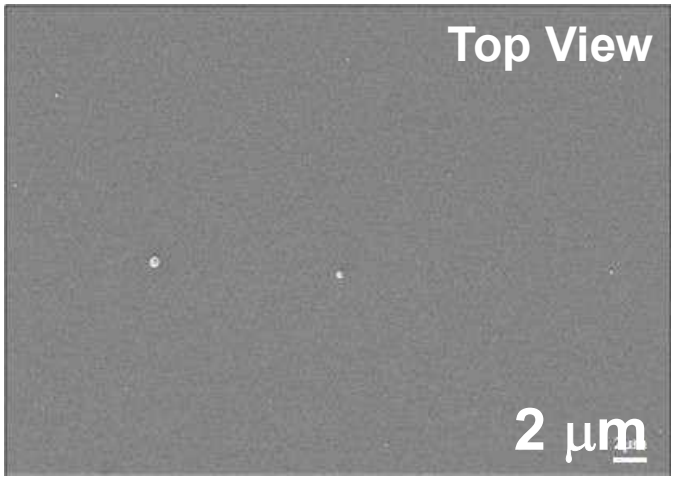

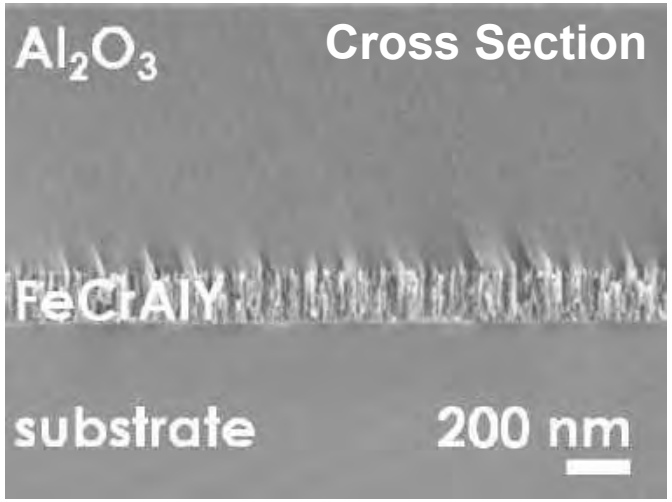

- ✓ High quality coatings
- ✓ Custom process: bottom-up approach
- ✓ Process at room temperature

Al_2O_3 fully dense coating, no pin holes, no defects

Processing on tubes & cylinders

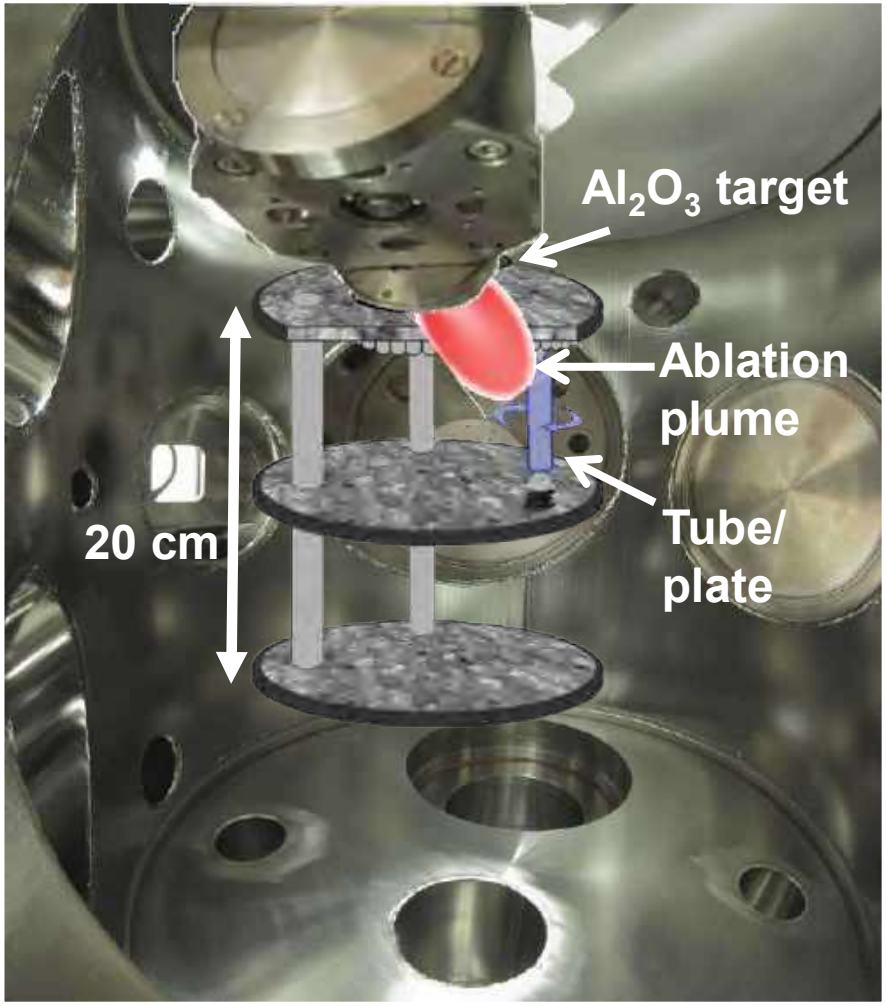

1515Ti cylinder + 5 µm Al_2O_3

AISI 316L tube + 5 µm Al_2O_3

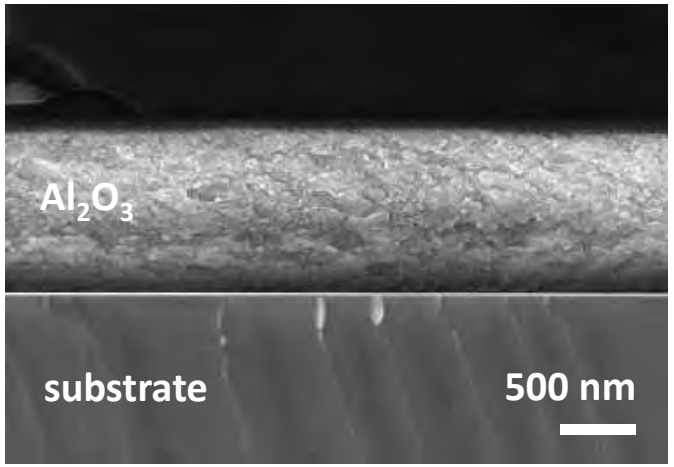

Fully dense and compact ceramic coating

Thermal stability

Thermal stability: in-situ TEM

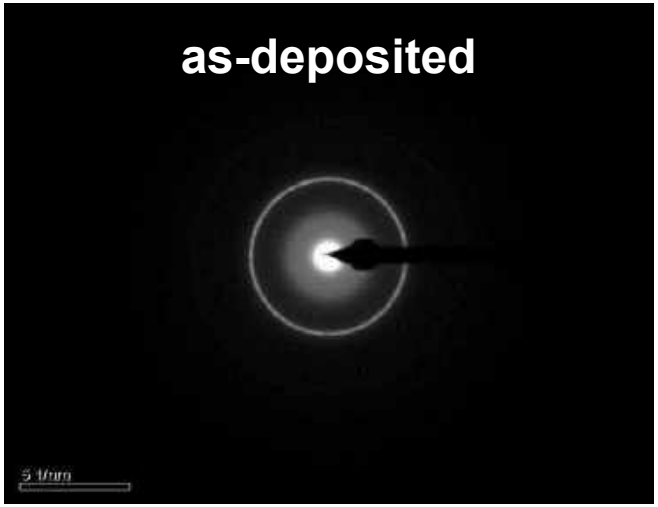

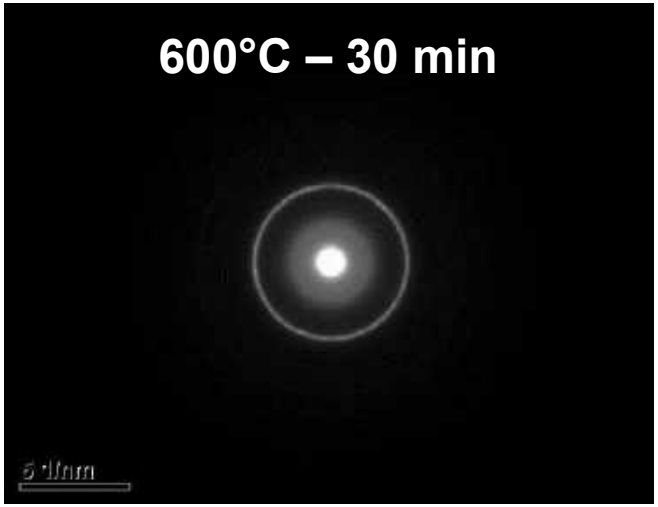

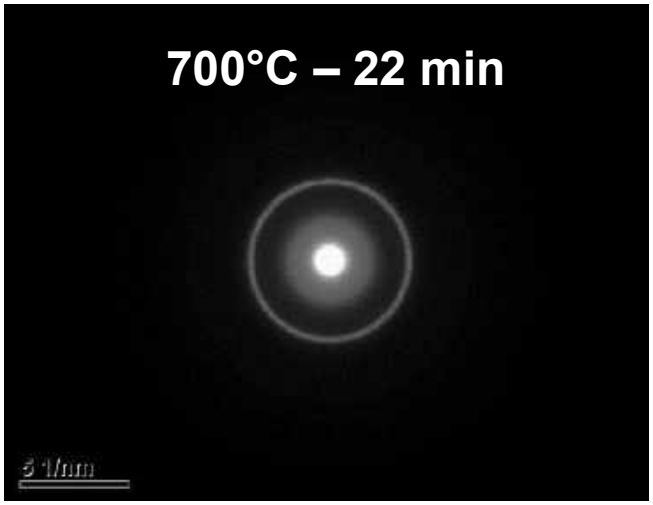

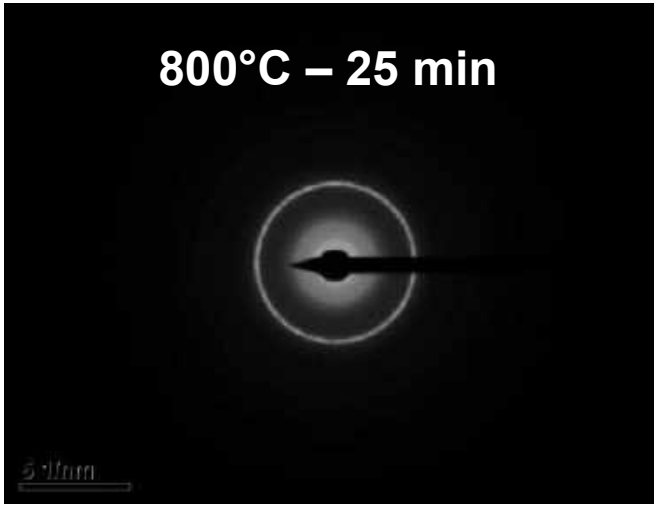

BF-HRTEM

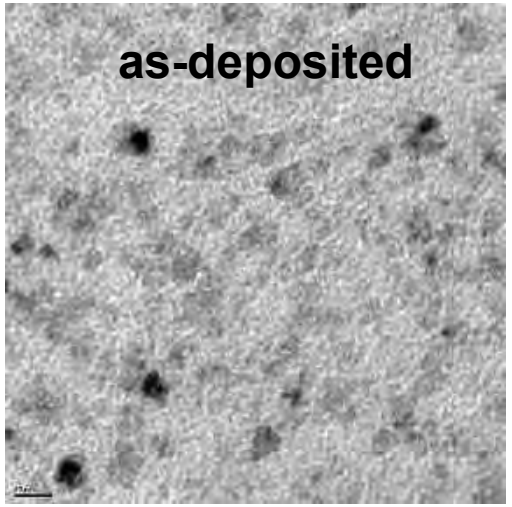

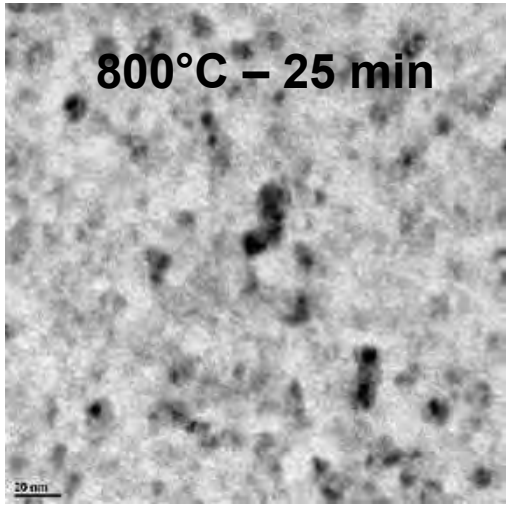

Gas permeation barrier

316L plate

annealed 2h @ 1000°C in air

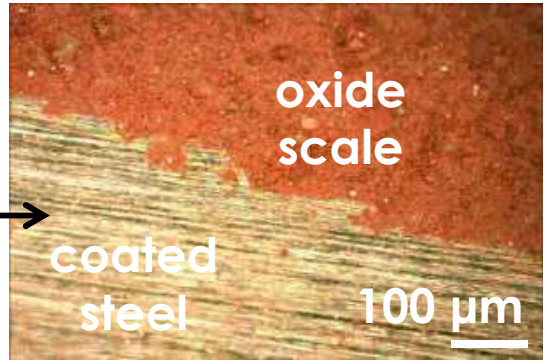

ISTITUTO ITALIANO
DI TECNOLOGIA

Pb compatibility of Al_2O_3 barrier coatings

fabio.difonzo@iit.it

Corrosion resistance, O_2 saturation

SS plates

uncoated sample

heavy liquid metal corrosion

Oxidizing stagnant Pb test

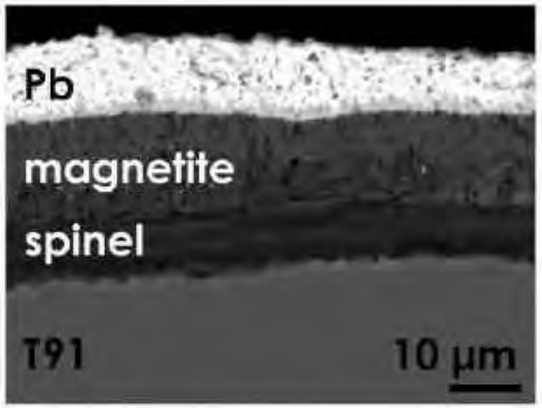

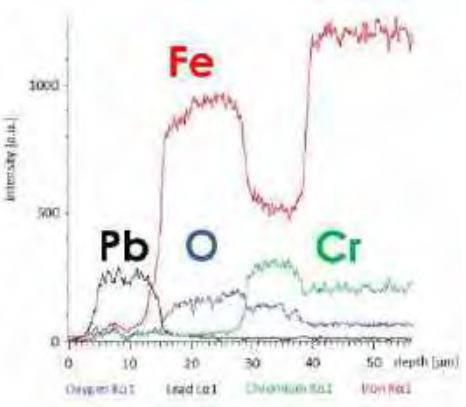

coated sample

protection

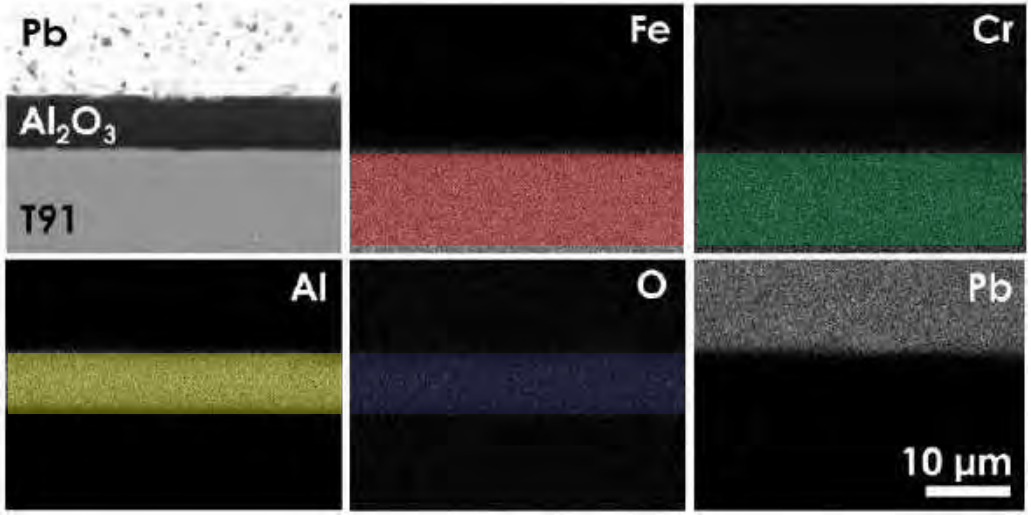

F. Garcia Ferré et al. – CORROS SCI – 2013

Corrosion resistance, O_2 depletion

1515Ti cylinder – 5000 h in stagnant Pb @550°C 10^{-8} wt.% oxygen

1 µm Al_2O_3 coating

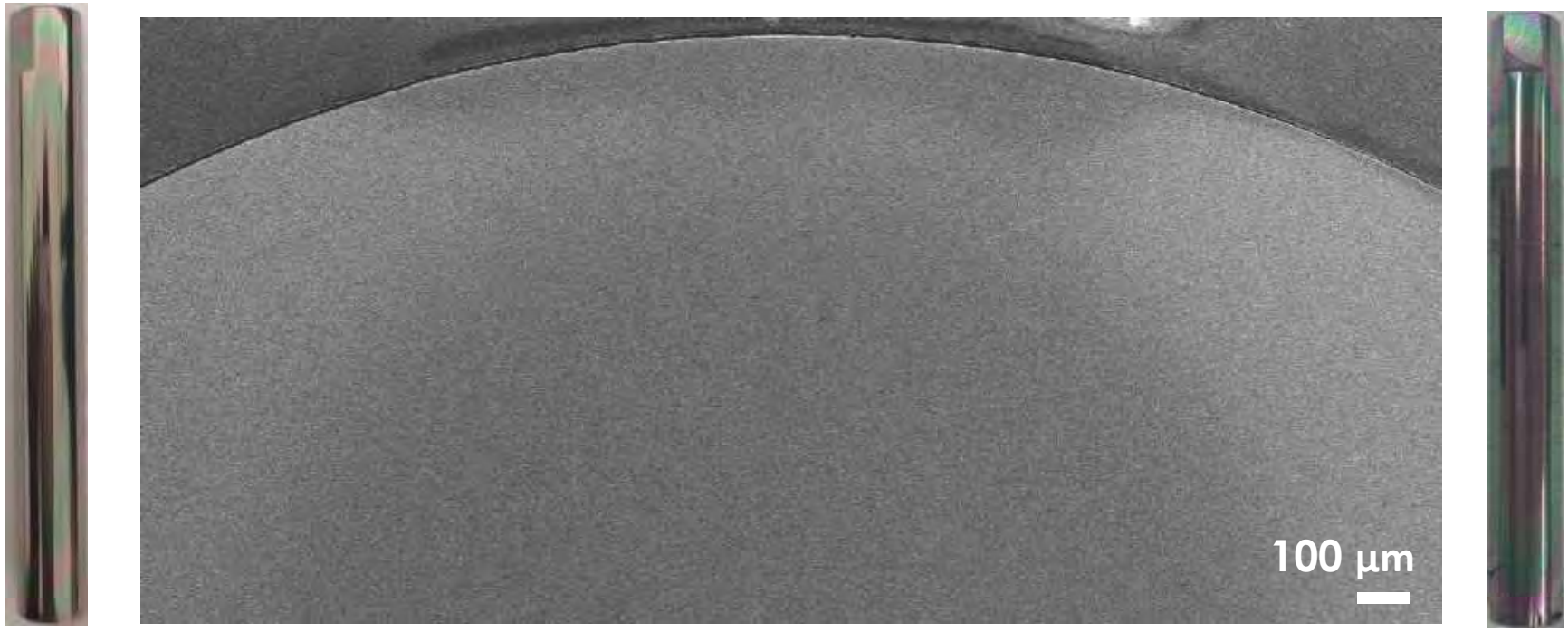

before

after

No solidified lead on the 1515Ti cylinder

NO CORROSION

Corrosion resistance, O_2 depletion

NO BL

BEFORE

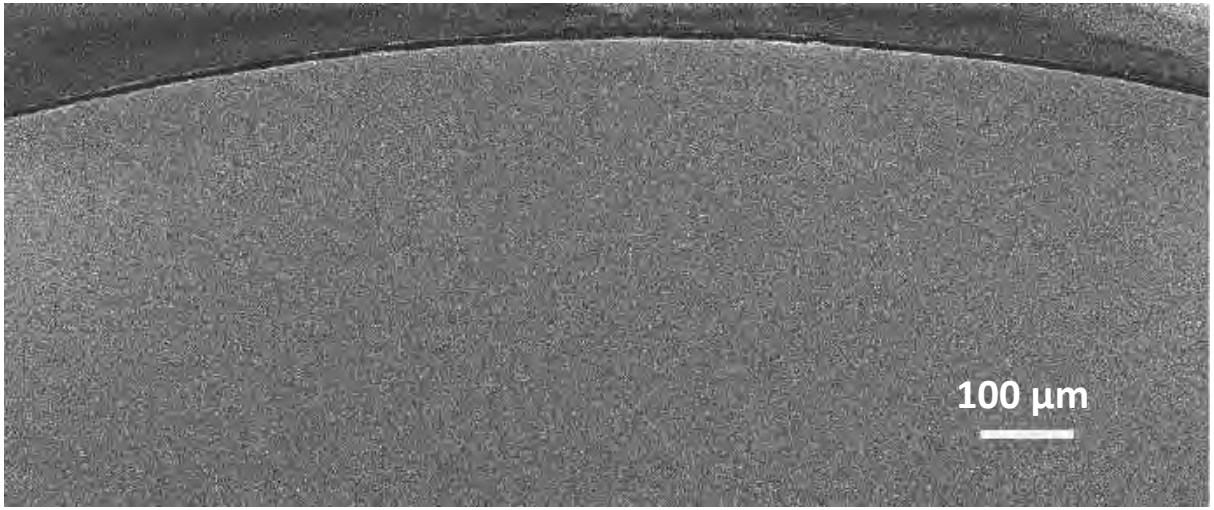

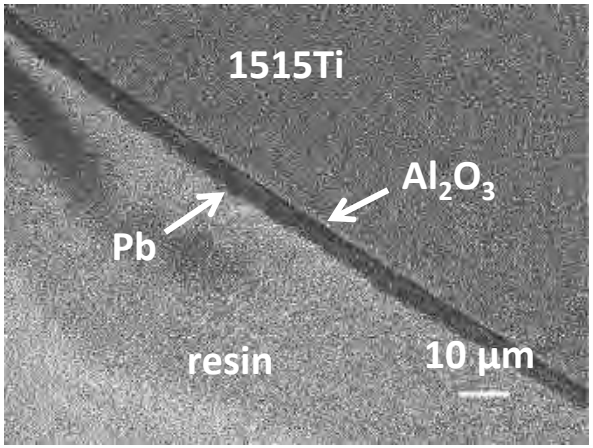

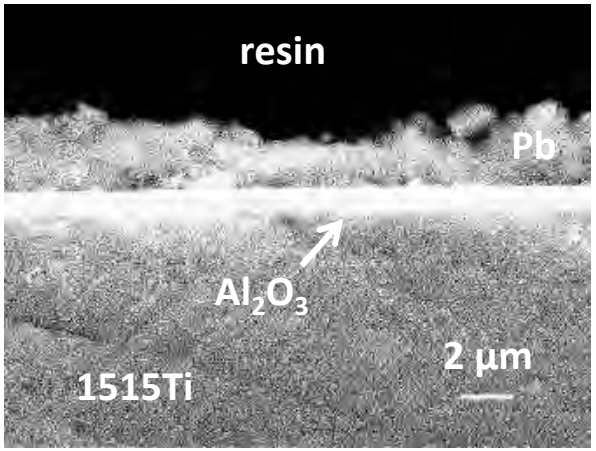

NO BL

AFTER

NO corrosion

Corrosion resistance, O_2 depletion

5000 h in stagnant Pb

@550°C 10^{-8} wt.% oxygen

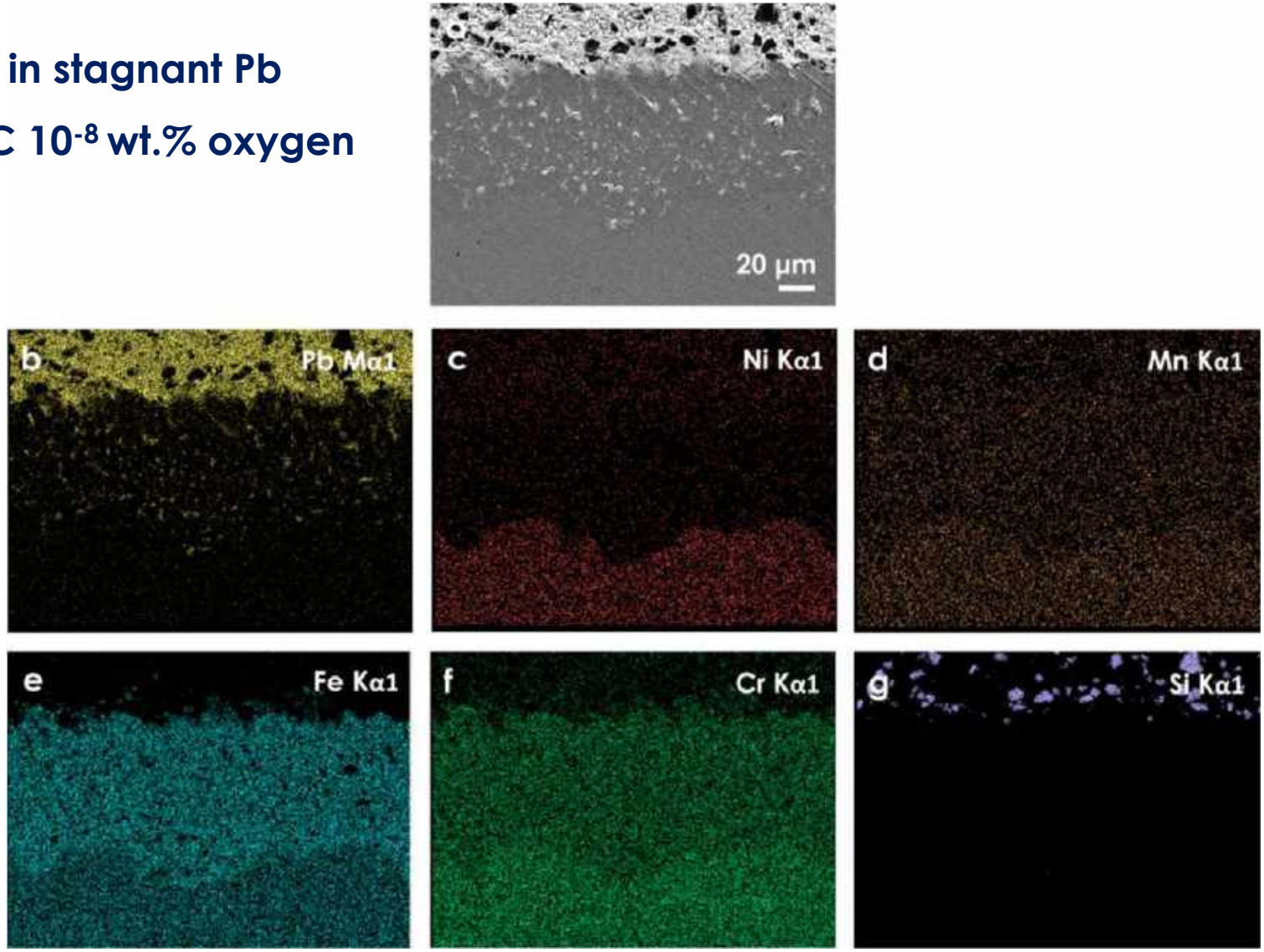

ISTITUTO ITALIANO
DI TECNOLOGIA

Thermomechanical properties

PLD-grown Al_2O_3 nanoceramic coatings

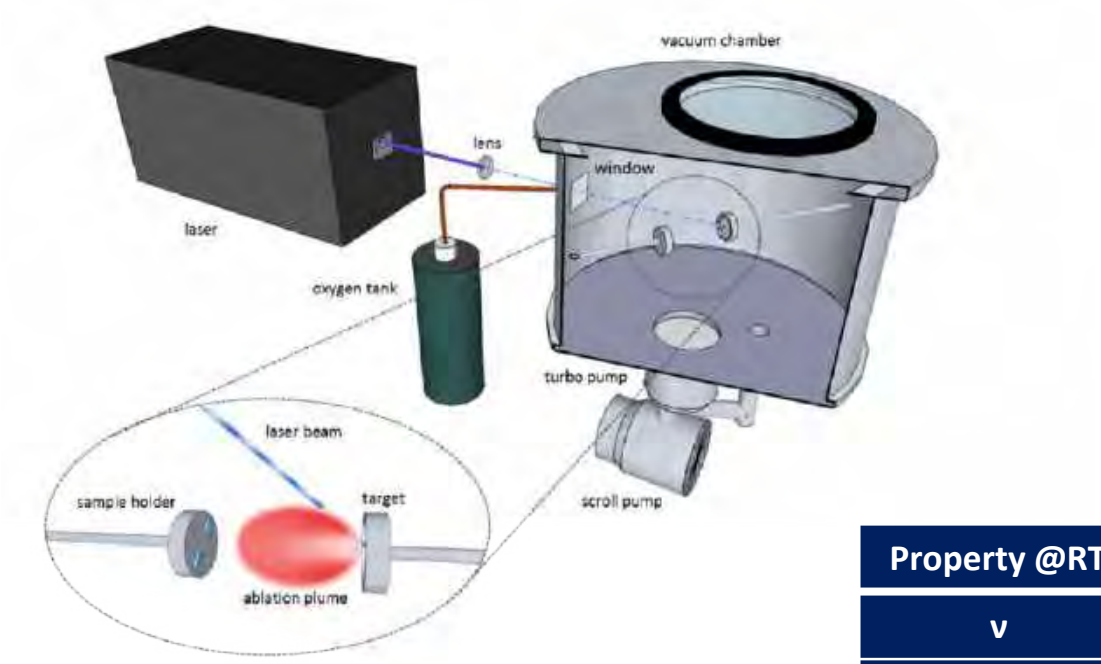

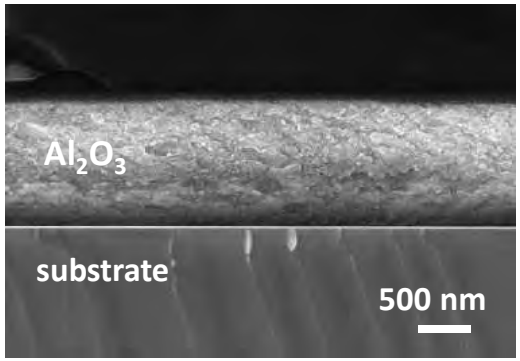

- ✓ **high quality coatings**
- ✓ custom process: bottom-up approach
- ✓ process at **room temperature**
- ✓ amorphous films with **nanodispersed crystalline domains**

F. Garcia Ferré et al. – ACTA MATER – 2013

Property @RT	Sapphire	PLD Al_2O_3	AISI 316L
ν	0,24	0,295 ± 0,025	0,3
E [GPa]	345	193,8 ± 9,9	200
G [GPa]	175	75,5 ± 3,8	80
B [GPa]	240	159,2 ± 11,8	140
H [GPa]	27,8	10,3 ± 1	4
H/E	0,059	0,049 ± 0,007	0,025

H/E parameter index of wear resistance and fracture toughness

Mechanical behaviour of PLD-grown Al_2O_3

- **Nanoindentation Tests**

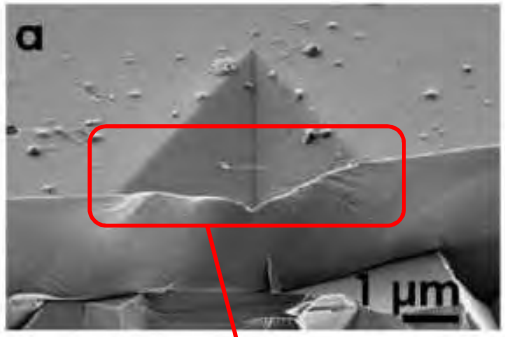

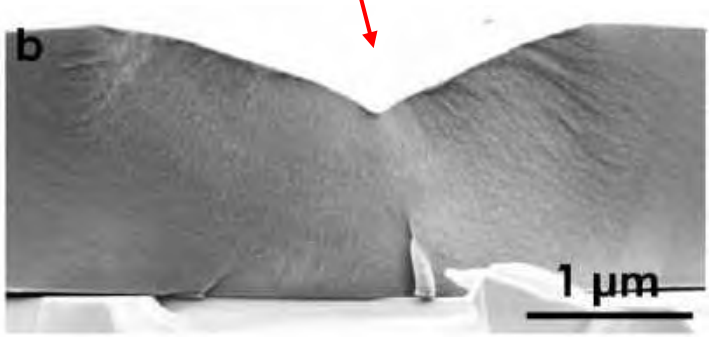

metal-like behavior under plastic strain

- **Nanoscratch Tests**

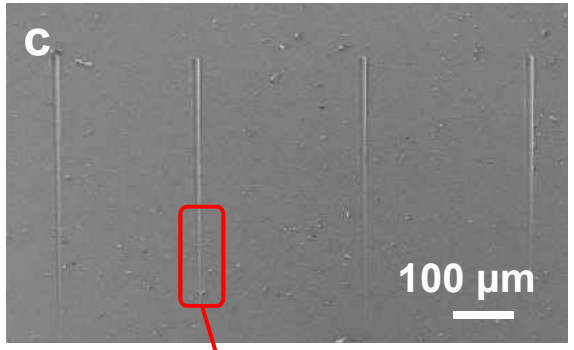

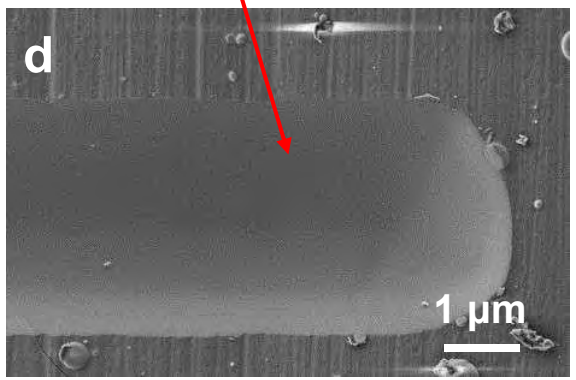

strong interfacial bonding

F. Garcia Ferré et al. – ACTA MATER – 2013

Adhesive strength

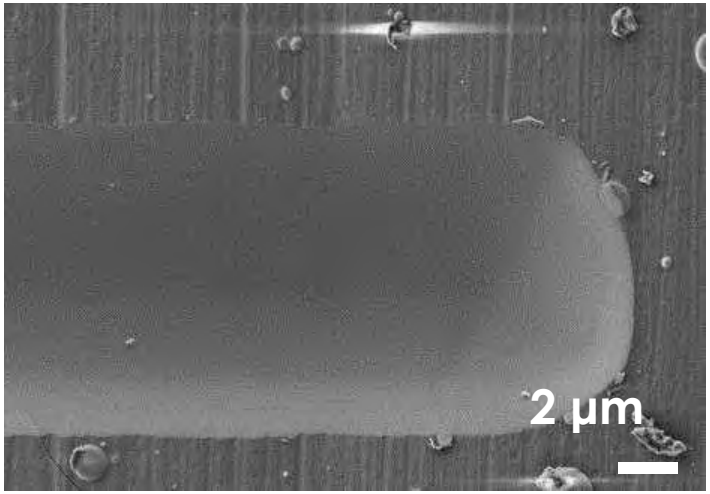

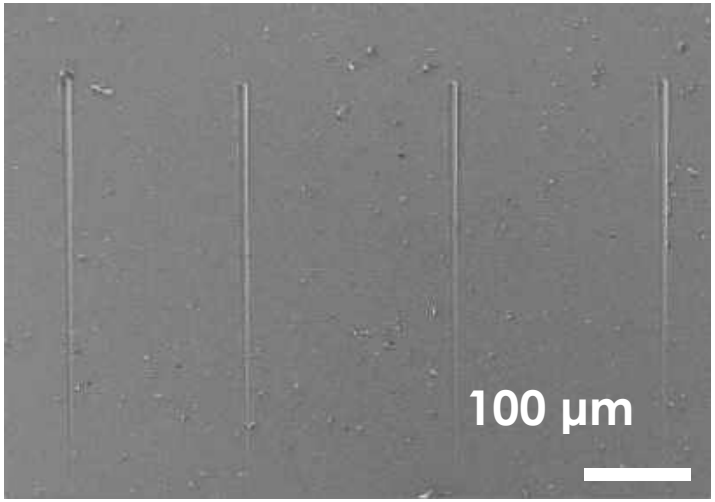

No delamination
No critical load

Strong interfacial bonding

Nanoscratch tests

- Conical tip (r = 10 µm)
- Scratch length 400 µm
- Maximum load 500 mN
- 2,5 mN/s and 2 µm/s

- Black line: initial topography at 0 load
- Blue line: final topography at 0 load
- Red line: penetration depth at increasing load

penetration depth vs. scan distance

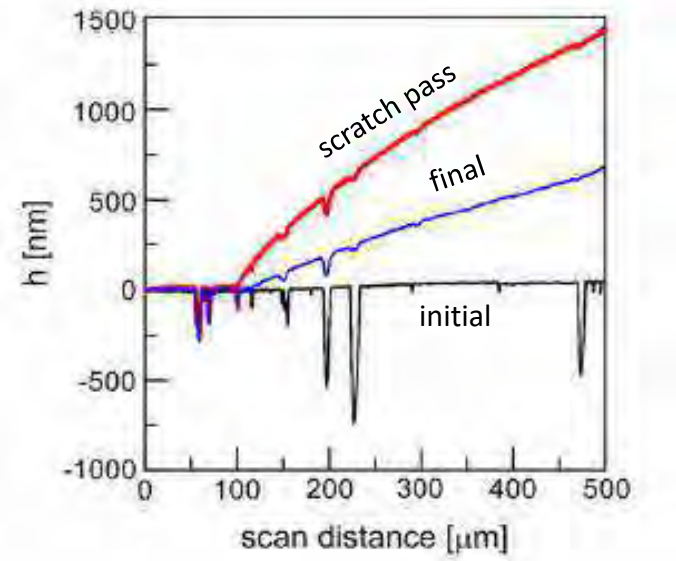

Burst test

BEFORE

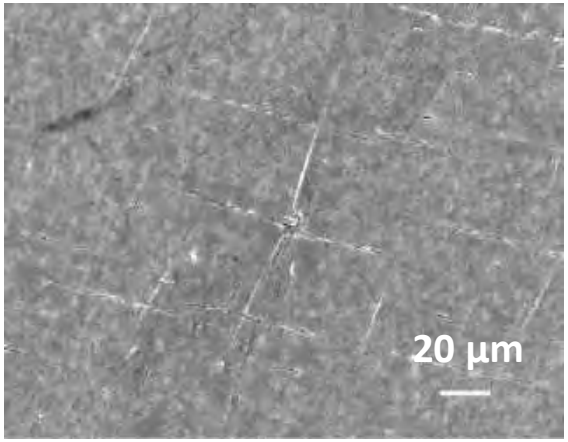

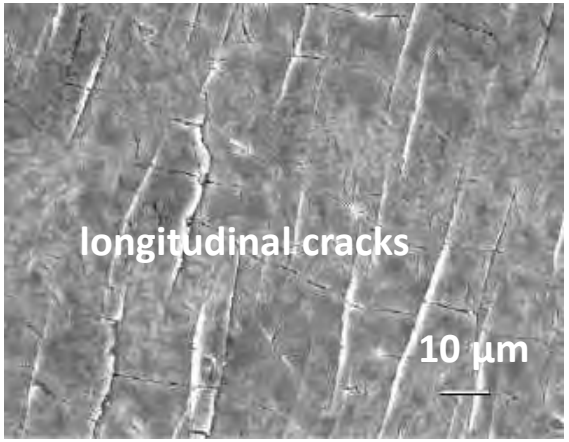

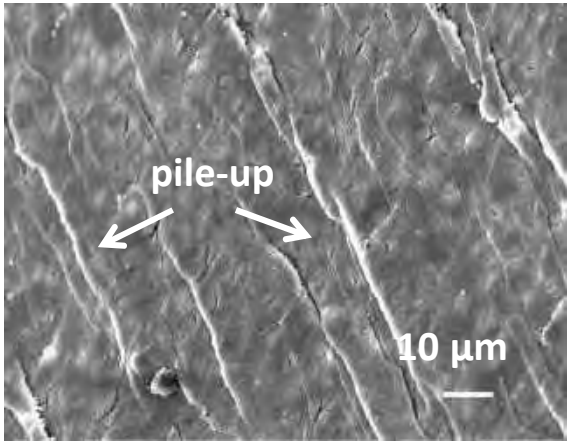

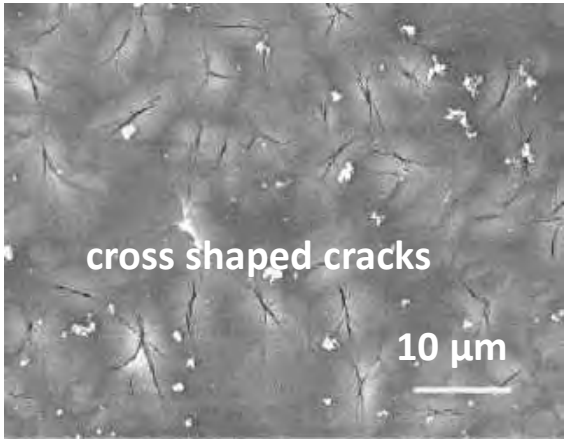

AFTER

Thermal cycling

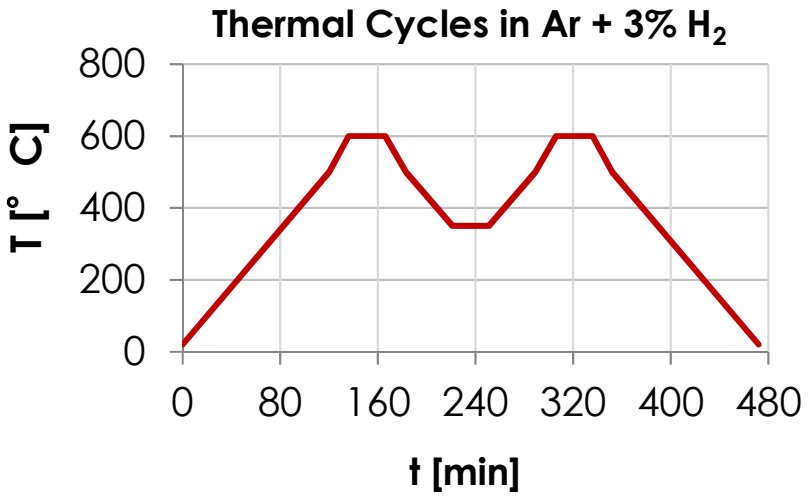

➢ **Samples without BUFFER LAYER – after**

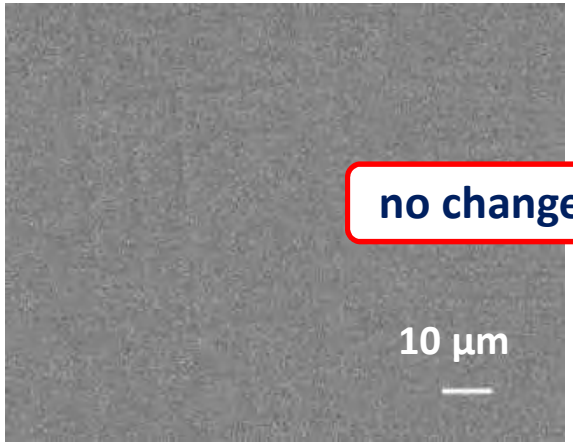

no changes after 12 cycles

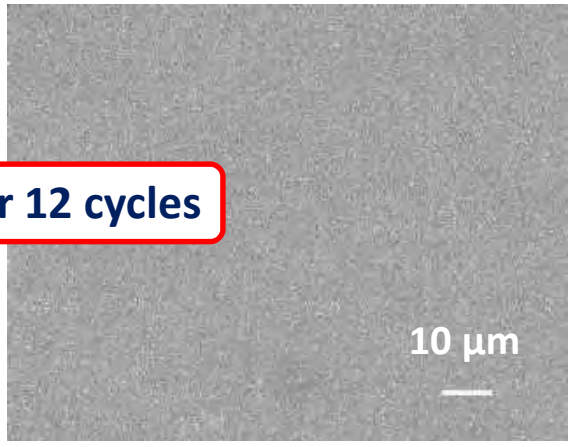

Thermal shock

- Heated up to 600 °C
- Cooled down with N_2 gas flow (~10 °C/s)

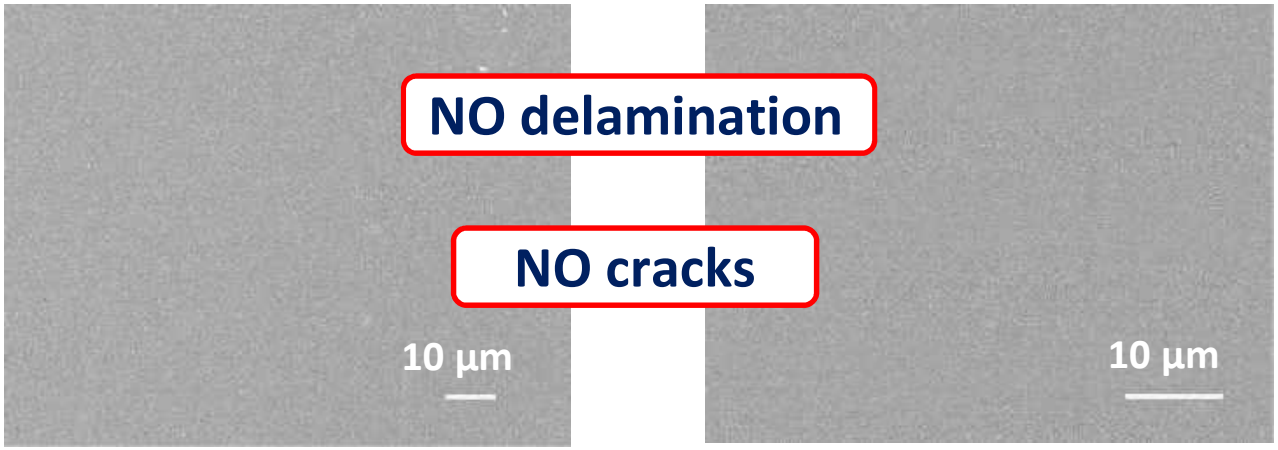

- Heated up to 600 °C
- Cooled down in liquid H_2O (~10^2 °C/s)

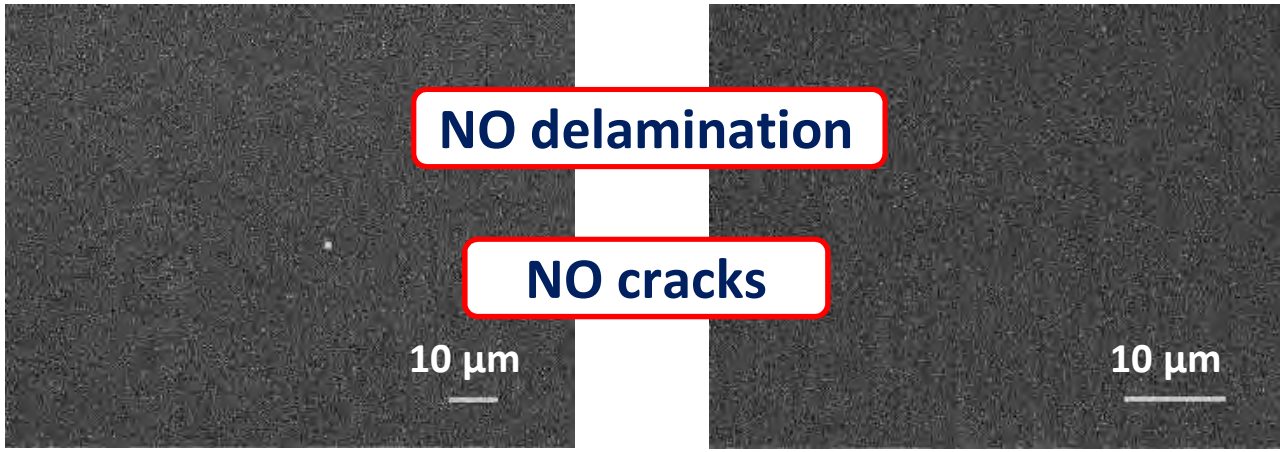

ISTITUTO ITALIANO
DI TECNOLOGIA

Heavy Ion Irradiation of Al_2O_3 barrier coatings

fabio.difonzo@iit.it

Radiation tolerant materials

Low-swelling ferritic martensitic steels

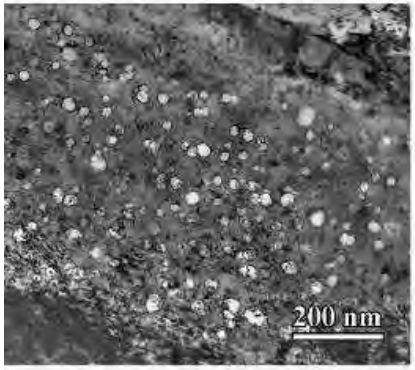

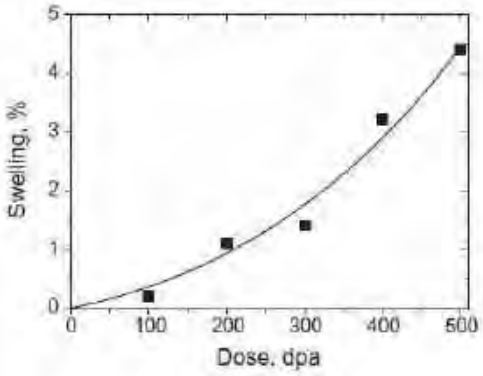

M.B. Toloczko et al. - J. Nucl. Mater. - 2014

Oxide-dispersion strengthened steels & alloys

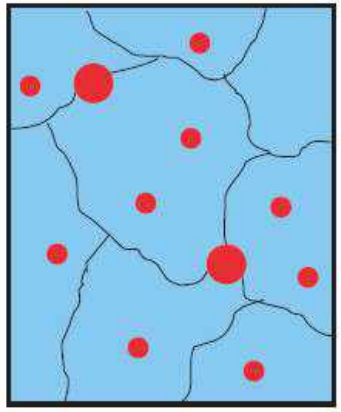

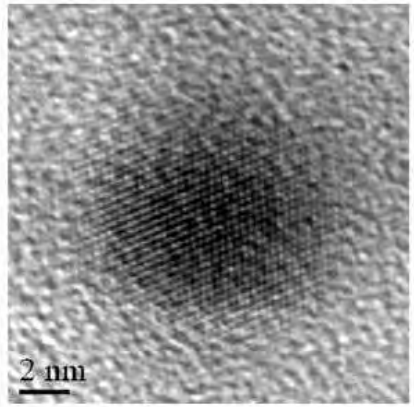

G. Liu et al. – Nature Mater. – 2013

M.L. Lescoat et al. – J. Nucl. Mater. – 2012

Nanolaminates & nanotwinned metals

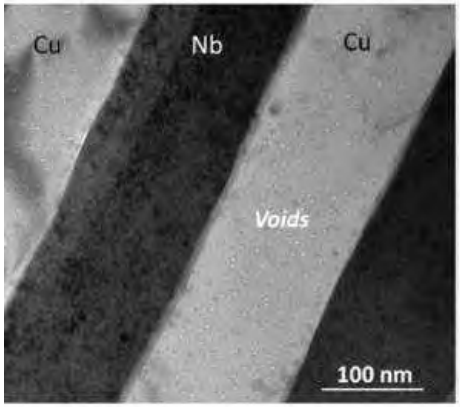

D. Rollet et al. – Adv. Mater. – 2013

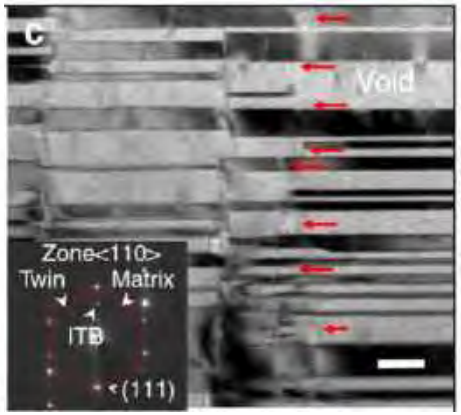

Y. Chen et al. – Nature Commun. – 2015

Nanoporous materials

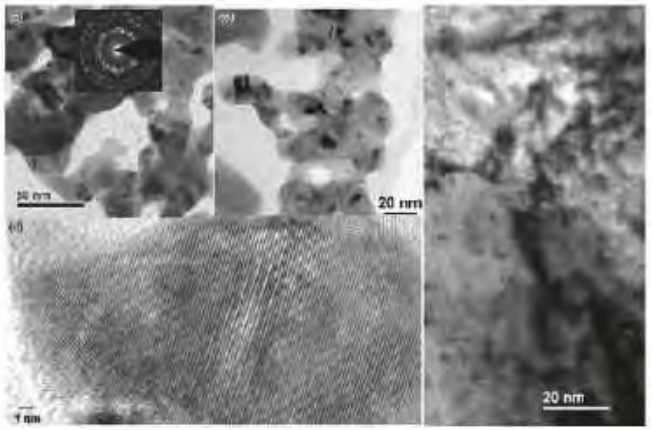

Y. Chen et al. – Nature Commun. – 2015

Heavy ion irradiation (Au + W) of Al_2O_3

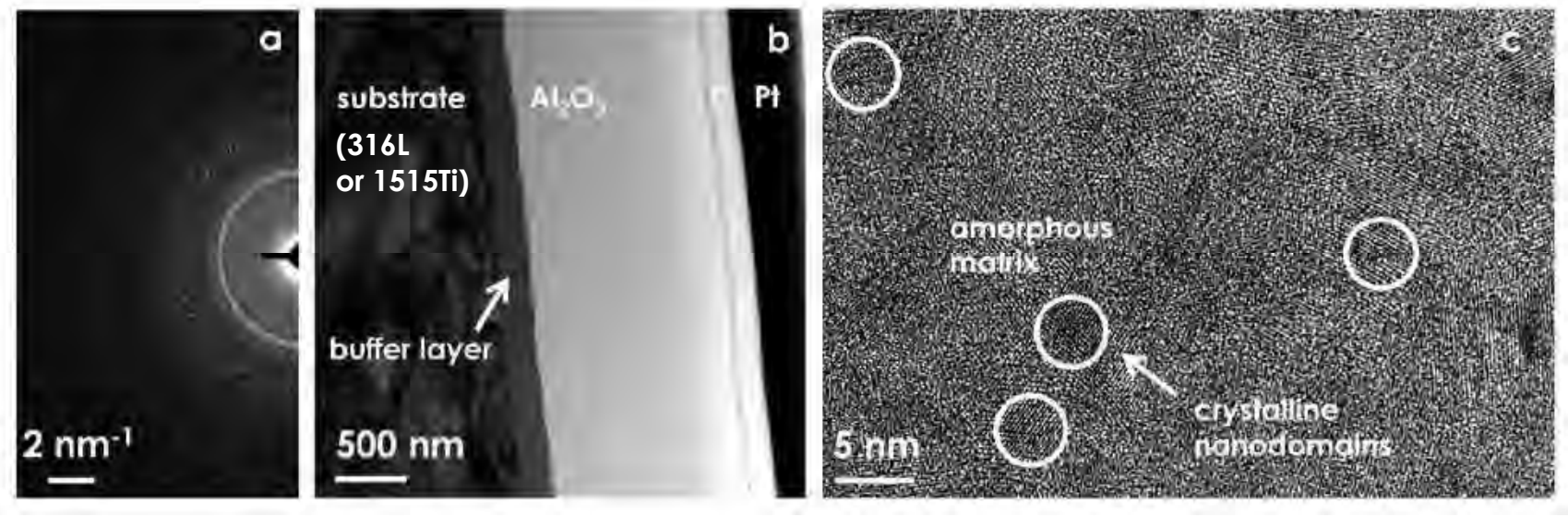

Main criteria

- Minimum coating thickness for nanoindentation: 1 µm
- Implantation beyond coating → negligible chemical effects
- Low ENSP ratio to simulate effect of neutrons
- Low enough absolute electronic stopping power to avoid single swift ion track formation (7 keV/nm vs ≈ 9,5 keV/nm threshold @RT)
- Different doses, corresponding to **20, 40, 150, 250 and 450 dpa** at the interface between Al_2O_3 and BL
- dpa calculated using SRIM (Kinchin-Pease)

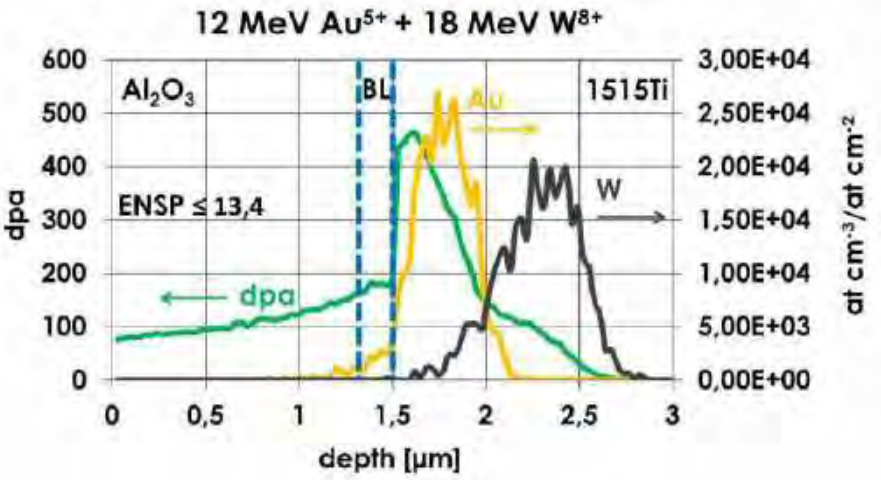

Model of evolution

moderate dpa

ultra-fine nanoceramic
GB-driven deformation
highest fracture toughness

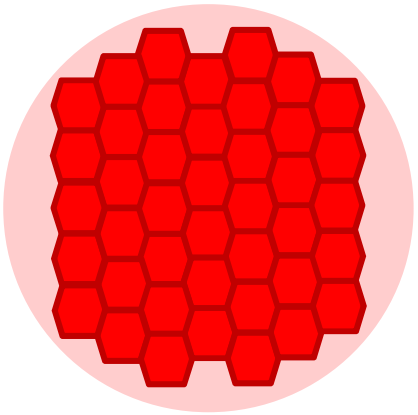

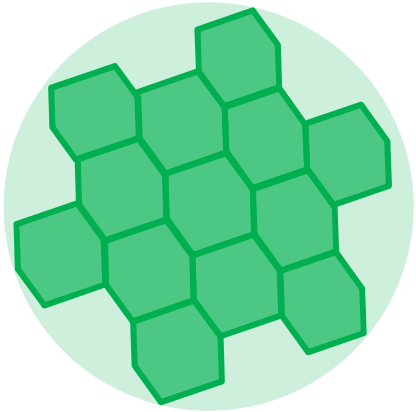

high dpa

fine nanoceramic
GB-driven deformation
sub-linear grain growth

pristine

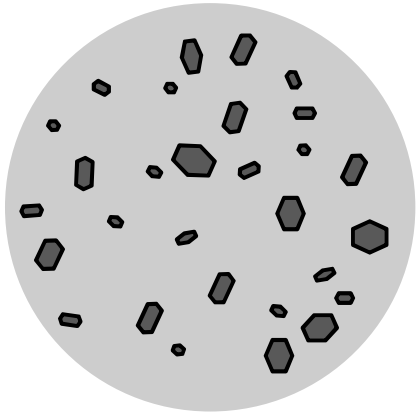

bi-phase nanocomposite
shear banding
highest fracture strength

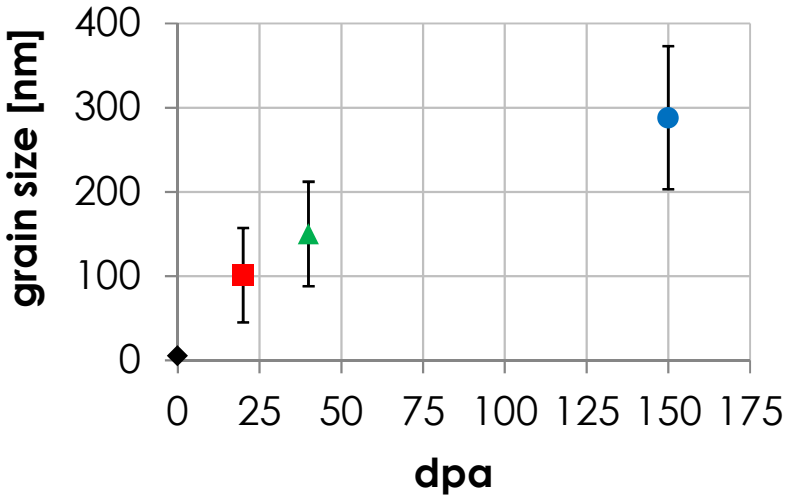

Sublinear grain growth

end-of-life dpa

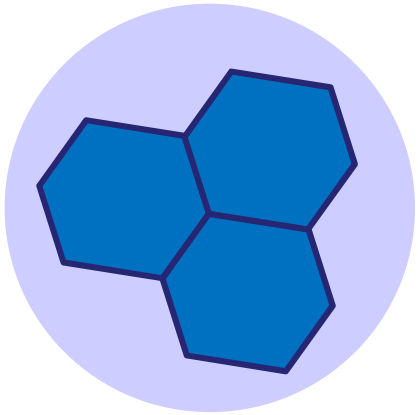

nanoceramic
GB-driven deformation
highest stiffness

fabio.difonzo@iit.it

Model of evolution

moderate dpa

ultra-fine nanoceramic
GB-driven deformation
highest fracture toughness

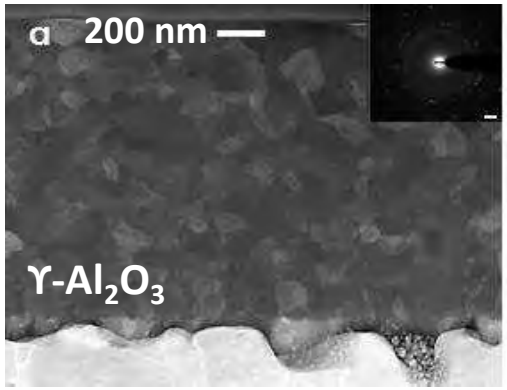

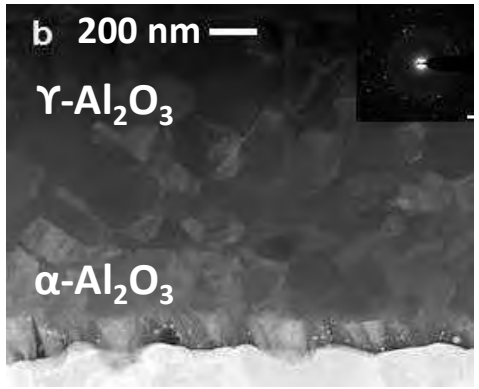

high dpa

fine nanoceramic
GB-driven deformation
sub-linear grain growth

pristine

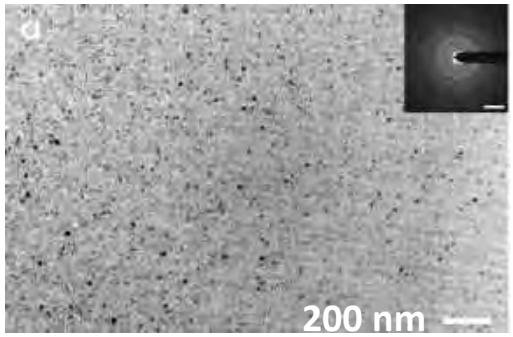

bi-phase nanocomposite
shear banding
highest fracture strength

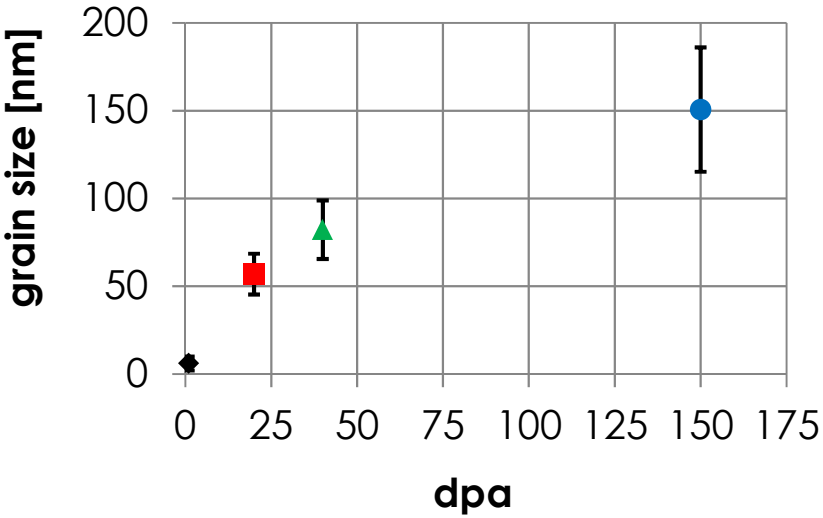

Sublinear grain growth

end-of-life dpa

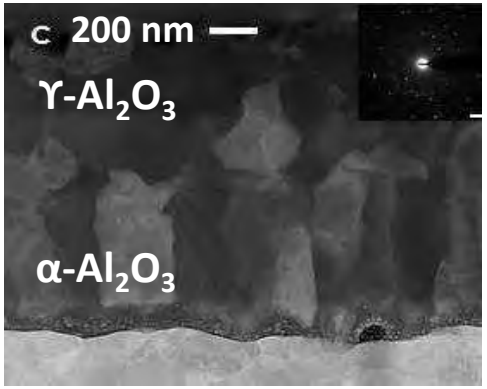

nanoceramic
GB-driven deformation
highest stiffness

fabio.difonzo@iit.it

Model of evolution

moderate dpa

ultra-fine nanoceramic
GB-driven deformation
highest fracture toughness

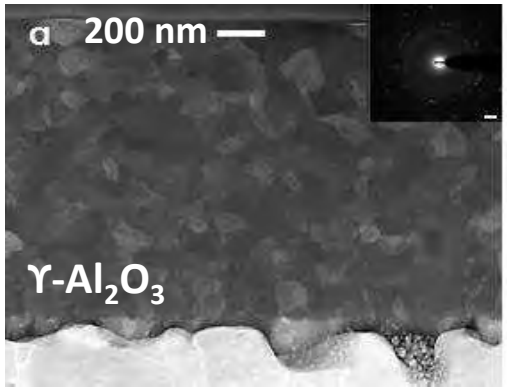

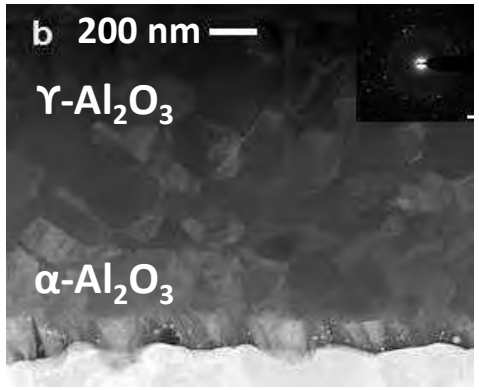

high dpa

fine nanoceramic
GB-driven deformation
sub-linear grain growth

pristine

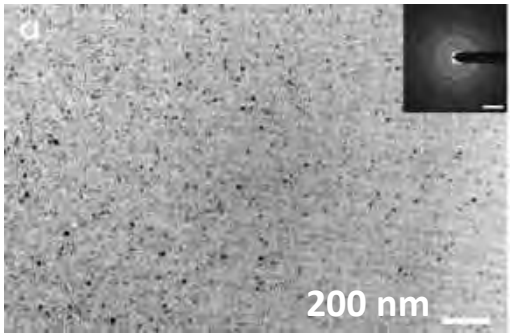

bi-phase nanocomposite
shear banding
highest fracture strength

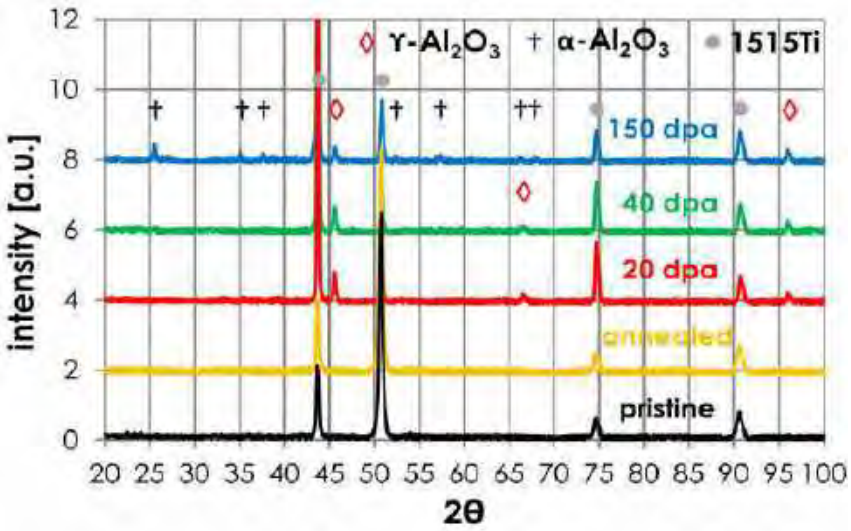

Phase Transition

end-of-life dpa

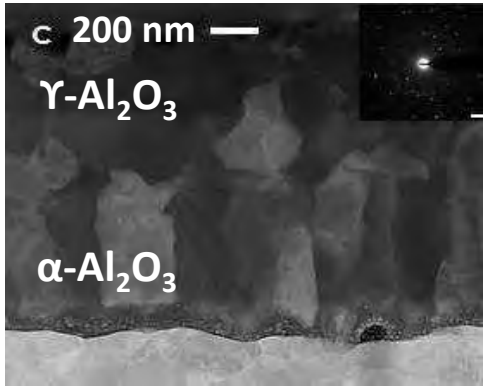

nanoceramic
GB-driven deformation
highest stiffness

fabio.difonzo@iit.it

Heavy ion irradiation (Au + W): structural features

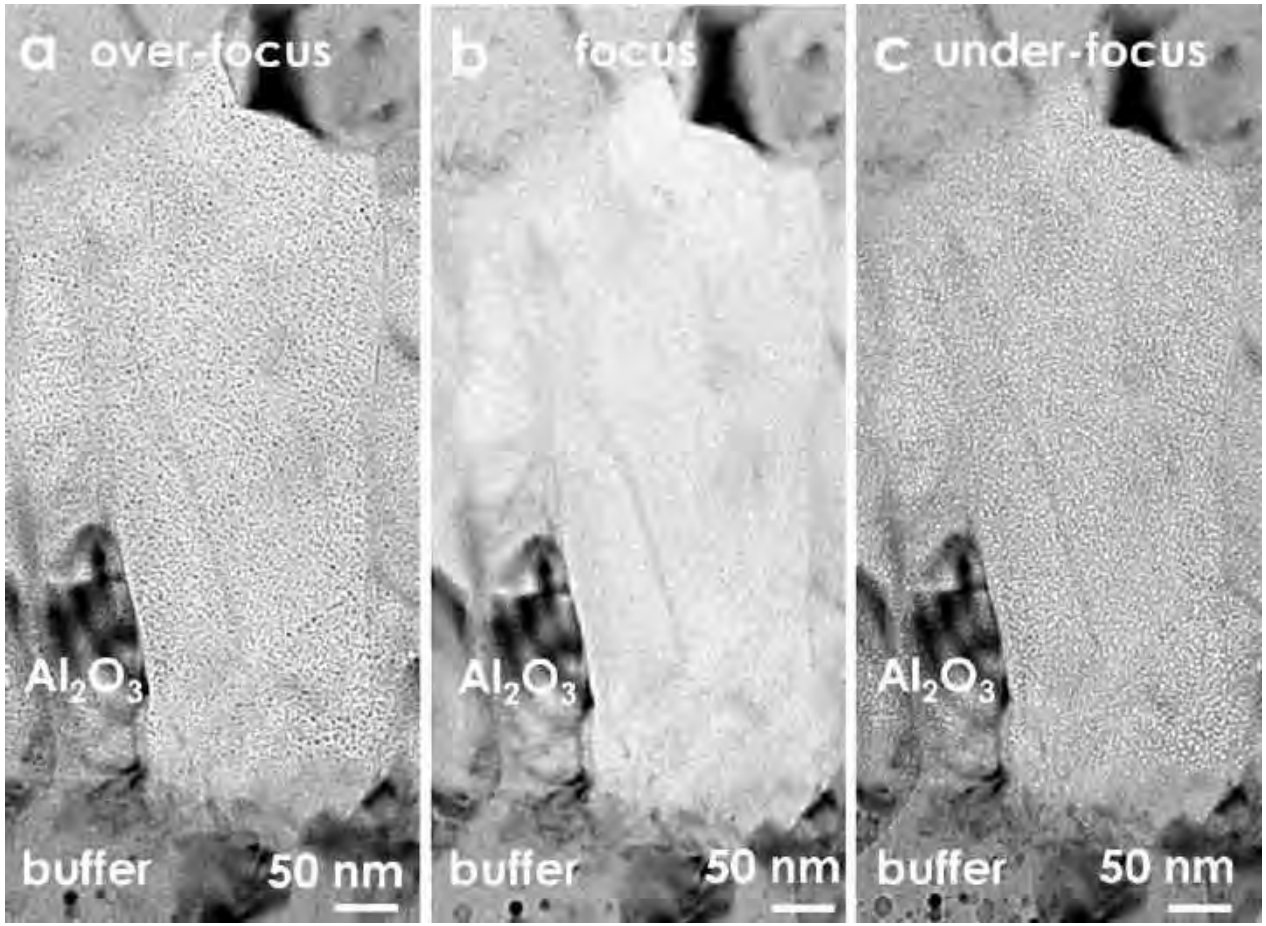

- Large number of small voids, only in a monolayer of grains, at the interface with the buffer layer
- These grains are alpha-alumina. All the other grains are gamma-alumina

Heavy ion irradiation (Au + W): mechanical properties

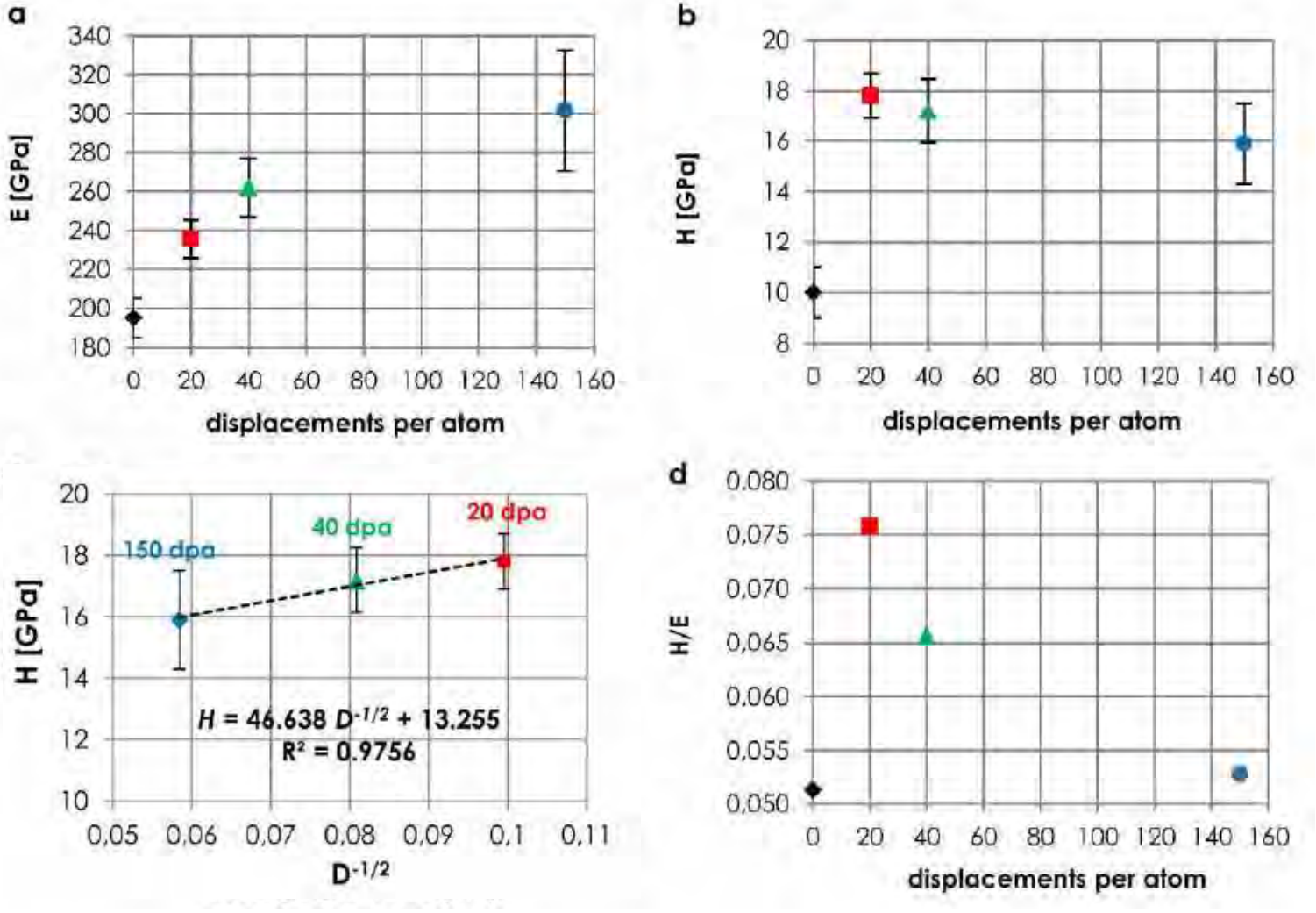

- The evolution of the mechanical properties is well fitted by the Hall-Petch relationship
- The structural rearrangements lead to an increase of the H/E ratio in-service (index of fracture toughness)

Heavy ion irradiation (Au + W): nanoimpact

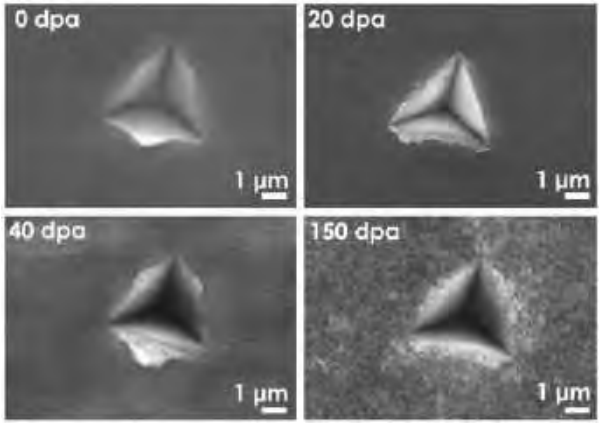

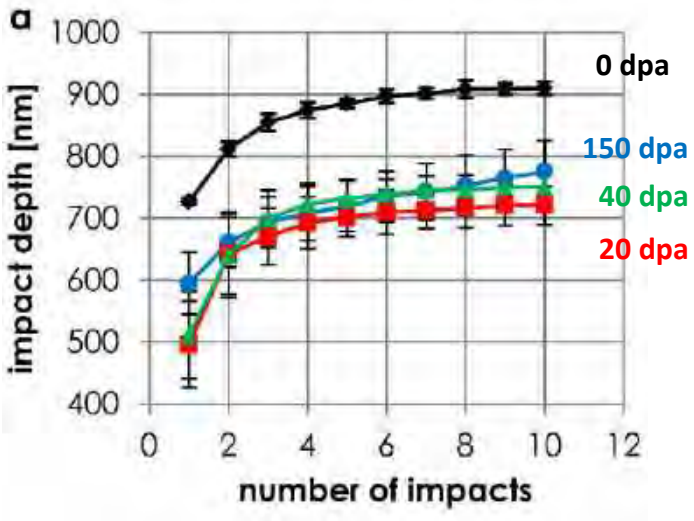

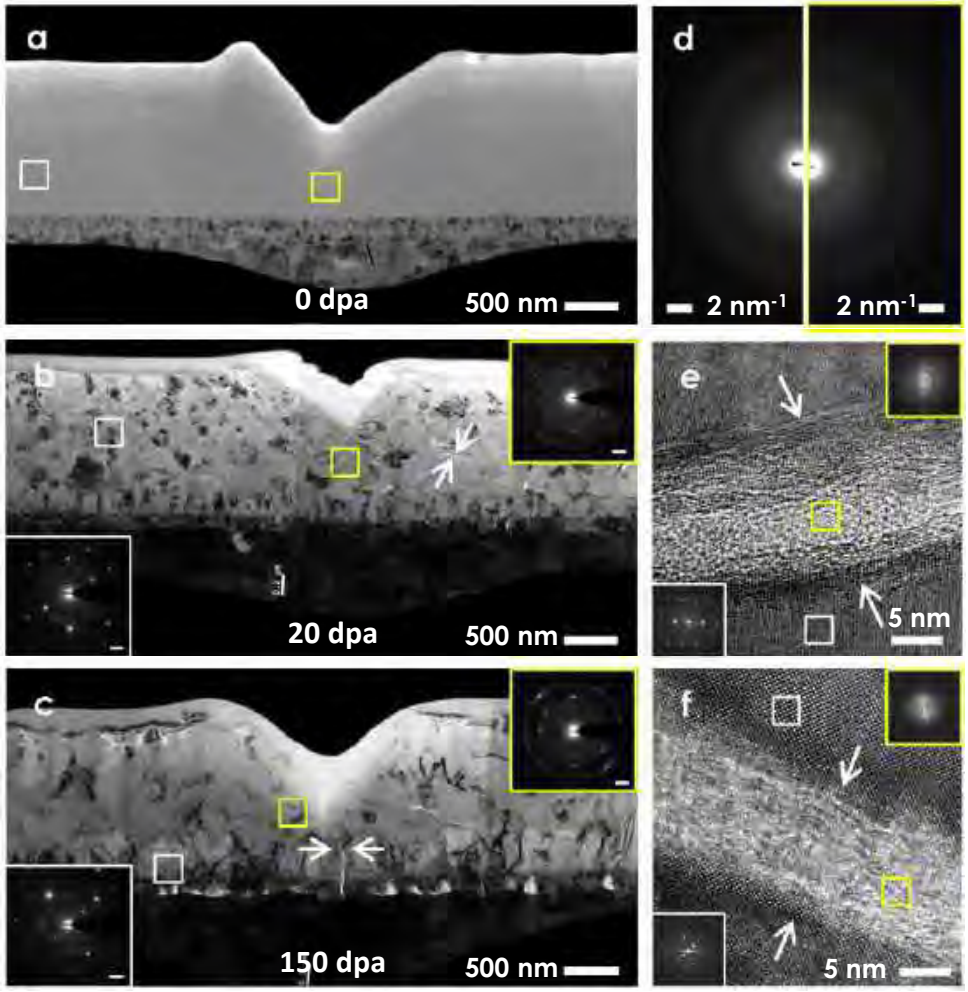

Shear banding

Lattice bending & localized shear amorphization

Lattice bending & localized shear amorphization

Impact energy is dissipated more efficiently in irradiated samples

Heavy ion irradiation (Au + W): nanoimpact – 10 mN

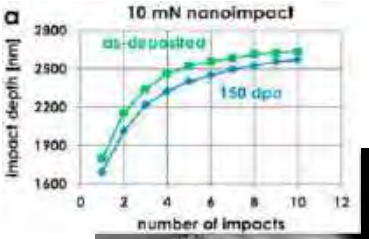

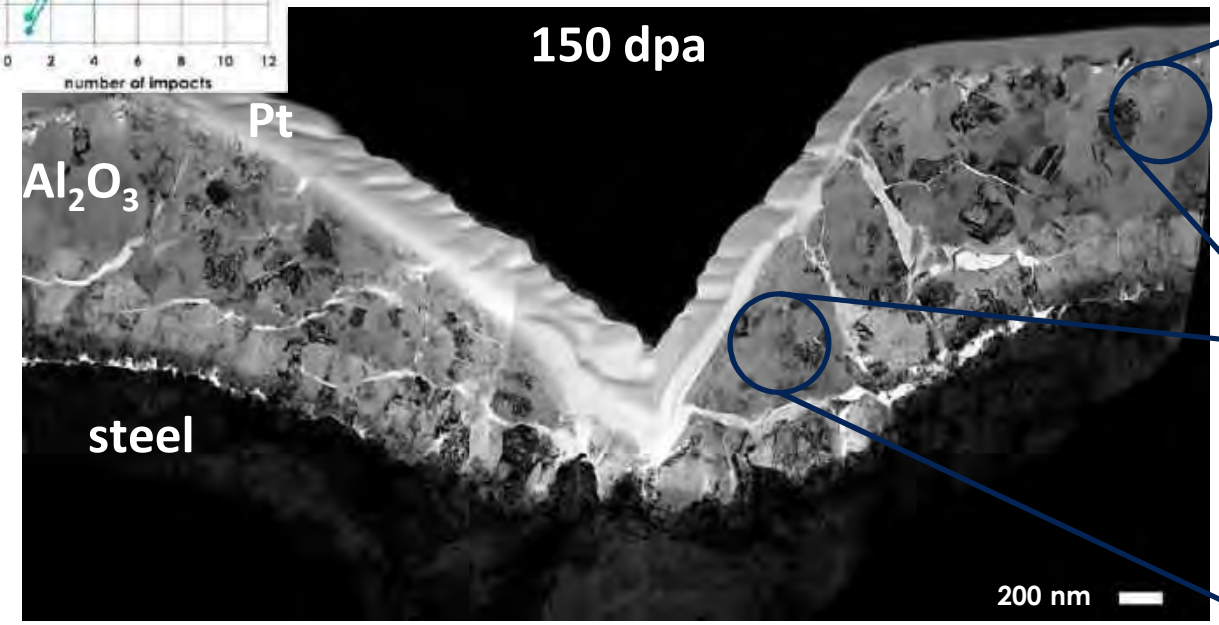

mechanically unloaded

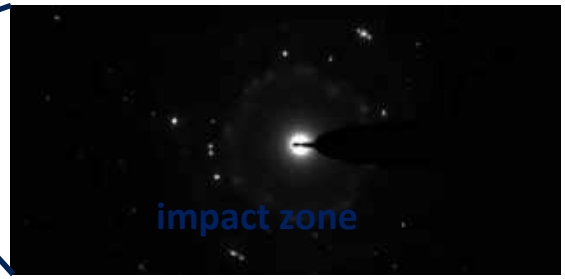

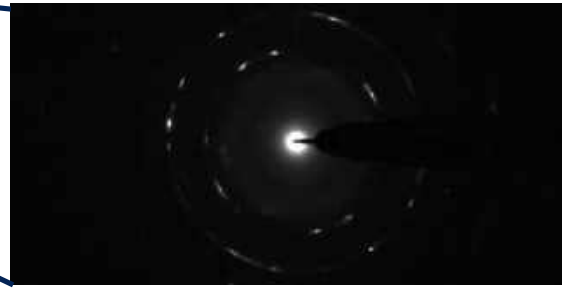

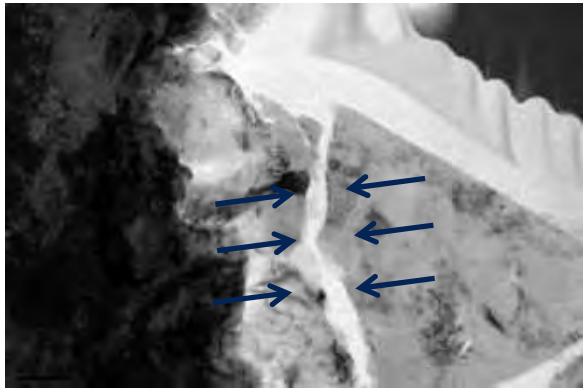

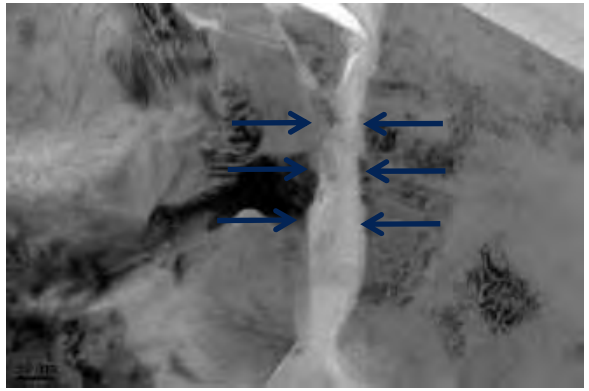

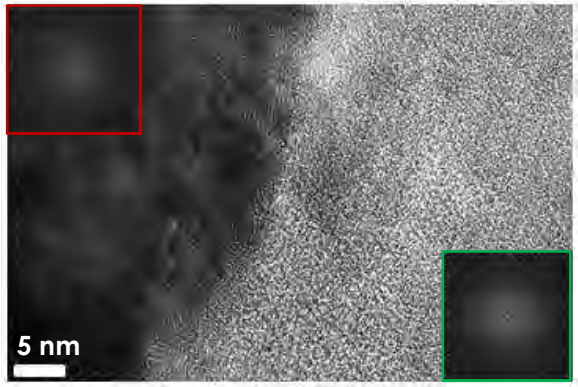

fabio.difonzo@iit.it

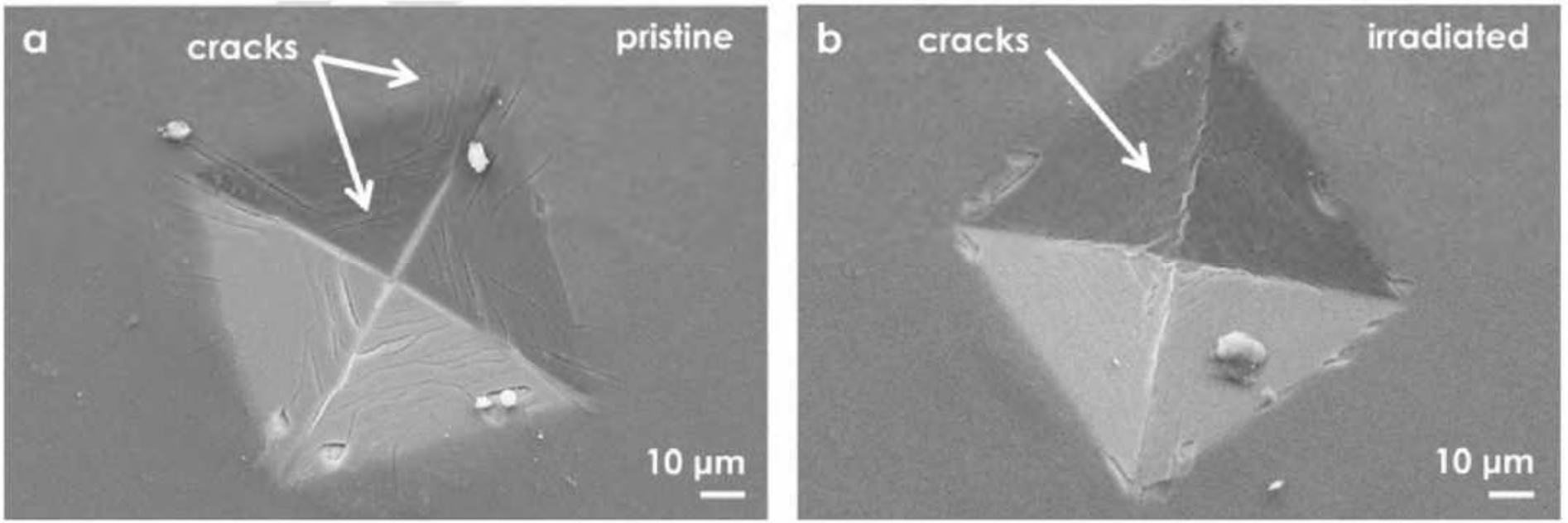

Microindentation imprints of the pristine (a) and the irradiated (b) coated 1515Ti plates. The cracks induced are more numerous and longer in the pristine material, suggesting that the fracture toughness is higher after irradiation.

ISTITUTO ITALIANO
DI TECNOLOGIA

Evolution of mechanical properties under irradiation: high and low dpa

fabio.difonzo@iit.it

Mechanical properties @ high levels of irradiation

F. Garcia Ferre et al – Acta Mater - 2013

F. Garcia Ferré et al. – SCI REP – 2016

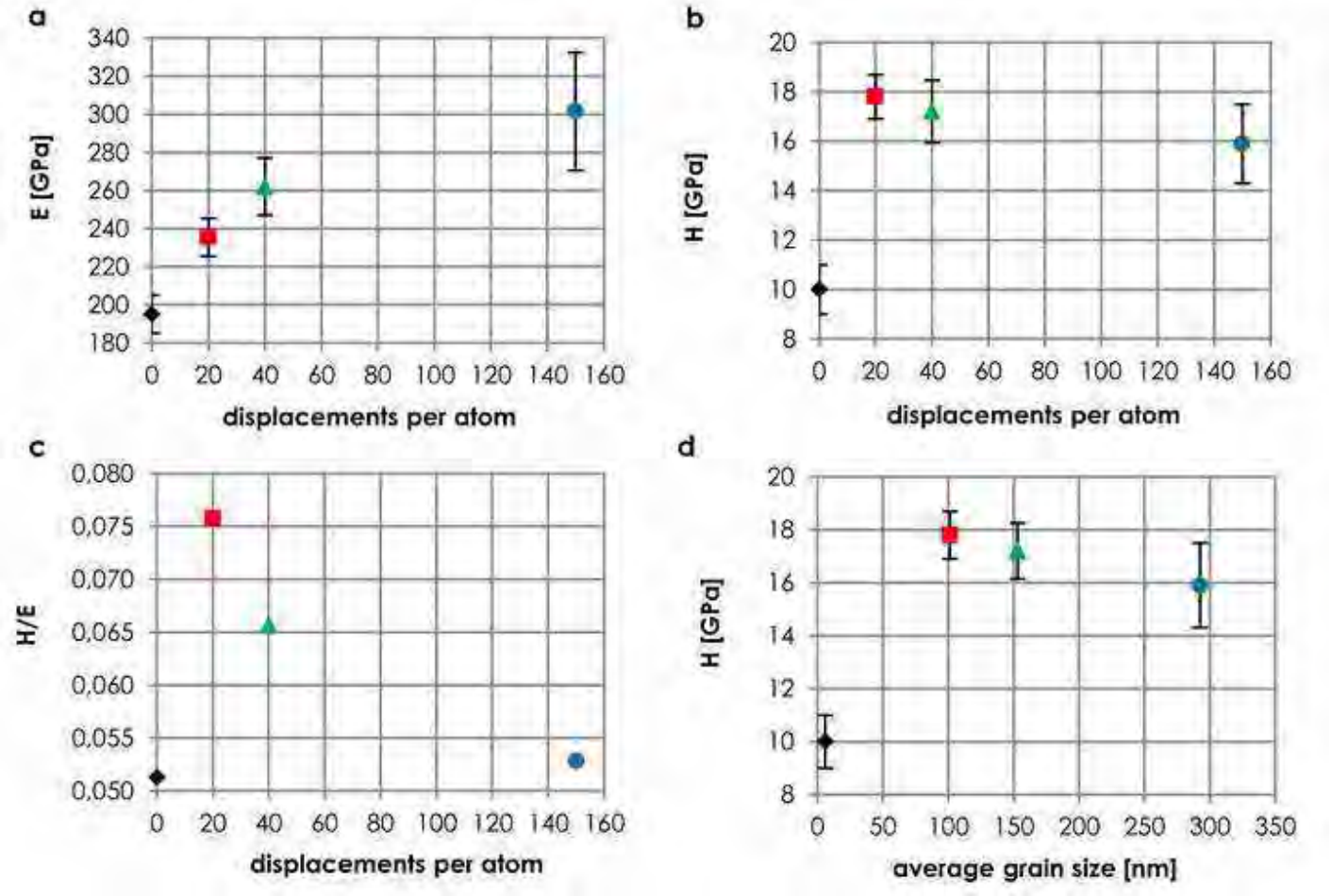

- E and H increase differently under irradiation
- **The Hardness follows the classical Hall-Petch relationship**

Hall-Petch relationship

➢ Hall-Petch equation: H (σ) VS grain size

$$H = H_0 + \frac{k}{\sqrt{D}}$$

- D *grain size (again)*
- H_0 *and* k *experimental parameter -* H_0 can be related to the perfect mono-crystalline material
- The same equation is valid also for the *Yield Strength* σ_y instead of the Hardness

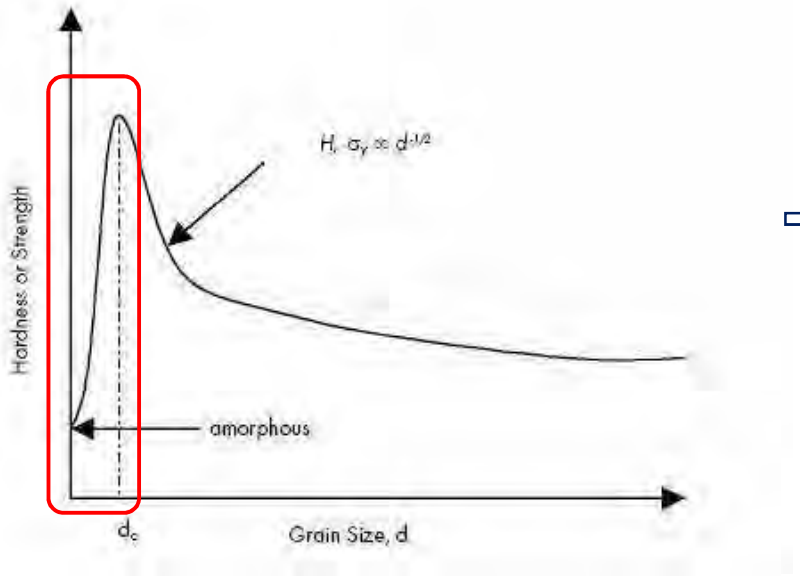

⟹ The so-called **"Inverse Hall-Petch curve"**: from the completely amorphous state to maximum hardness

Hall-Petch fit: old VS new data

➢ **Hall-Petch fit: old data** (600°C tests)

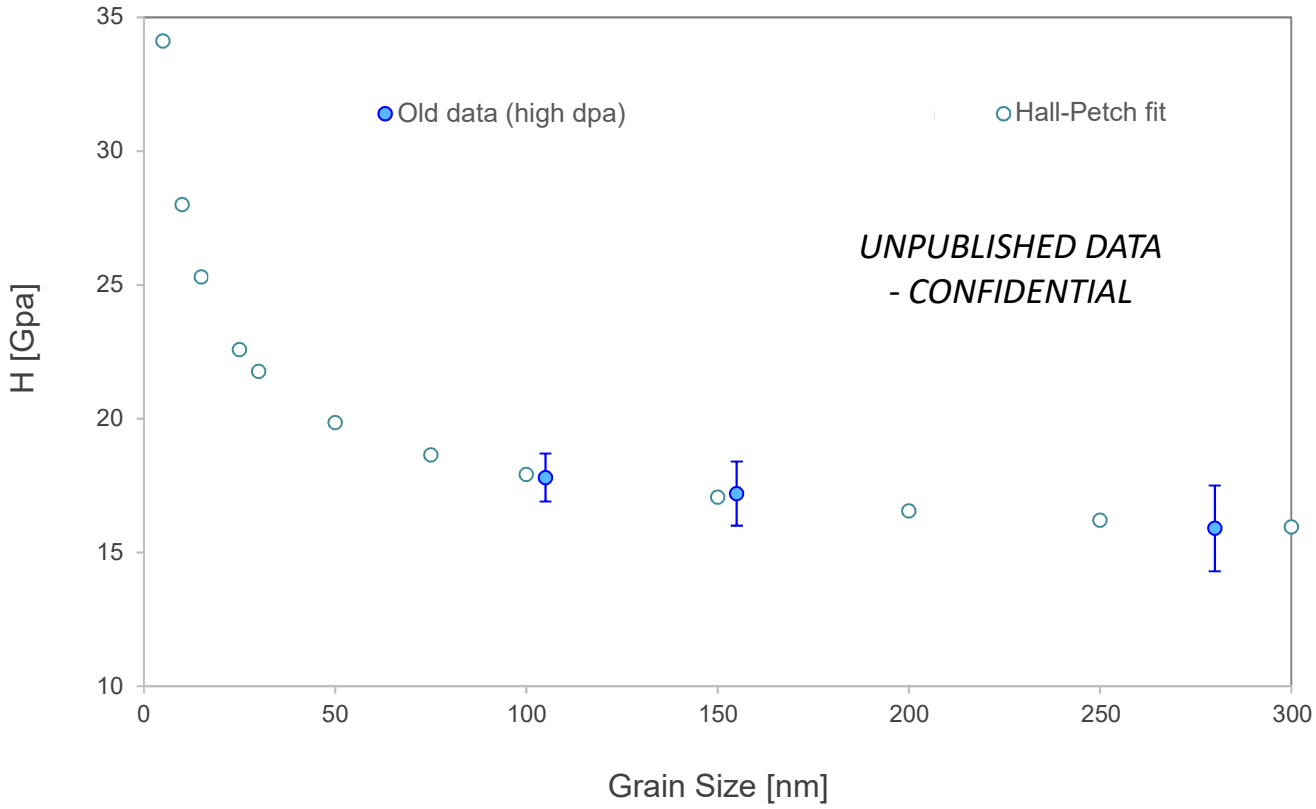

- **Good agreement with previous data**

Corrosion resistance, O2 depletion

Irradiated sample, 1000 h in stagnant Pb @550°C 10^{-8} wt.% oxygen

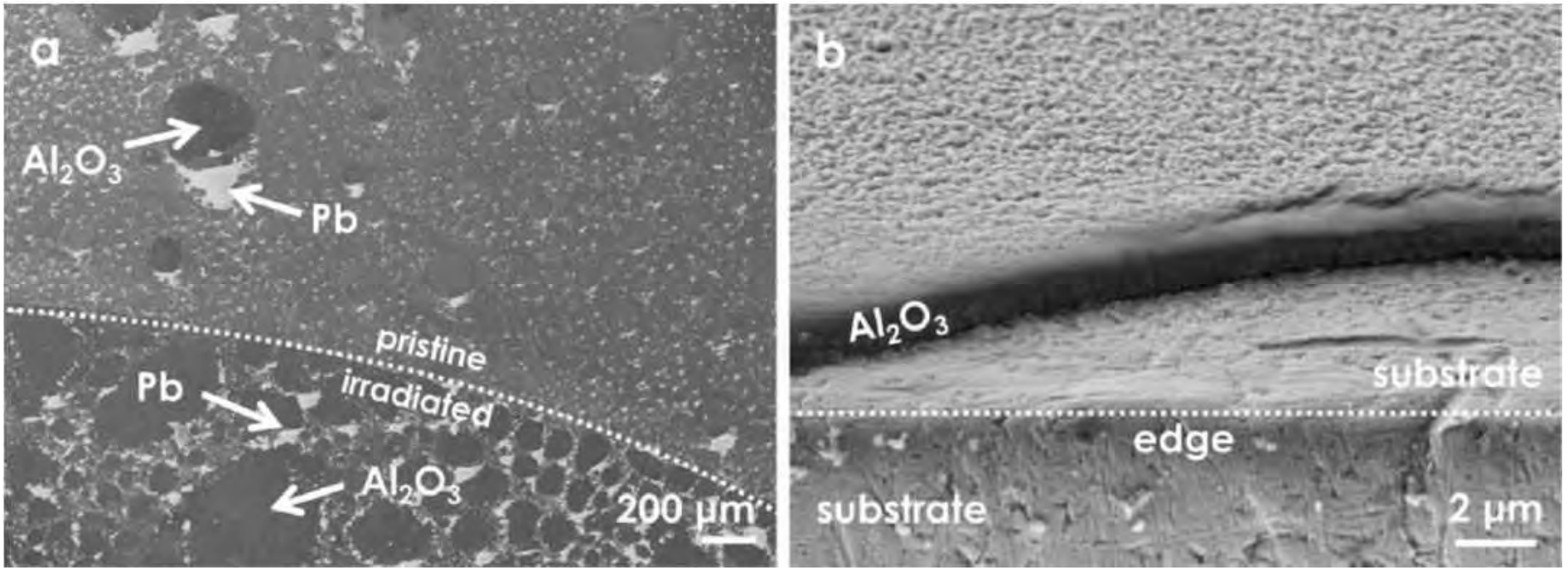

ISTITUTO ITALIANO
DI TECNOLOGIA

Complex shapes?

ALD-grown Al_2O_3 amorphous coatings

Atomic Layer Deposition - Set Up

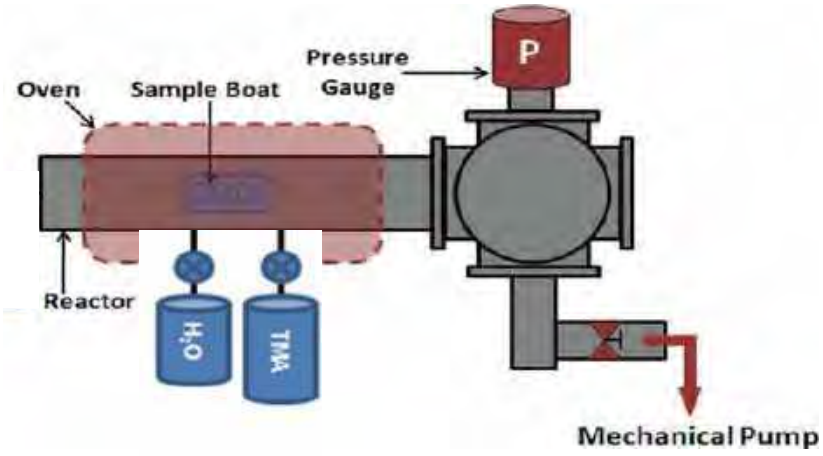

- ✓ **high-grade quality coatings**
- ✓ custom process: bottom-up approach
- ✓ process at **low temperature (i.e. < 200°C)**
- ✓ mainly **amorphous films**

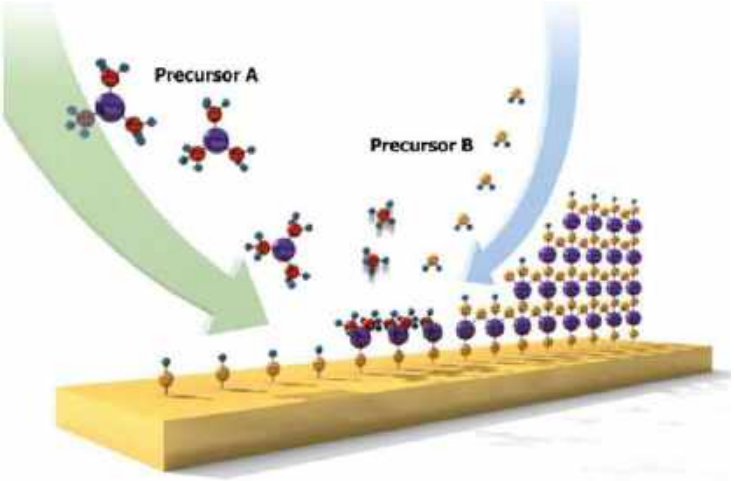

- Chemical Vapor Deposition (CVD)
- Growth at the **atomic scale levels**
- Control through **self-limited reactions**
- **Absence of any defects**
- Maximum **coverage efficiency**

ALD-grown Al_2O_3 amorphous coatings

Atomic Layer Deposition - Set Up

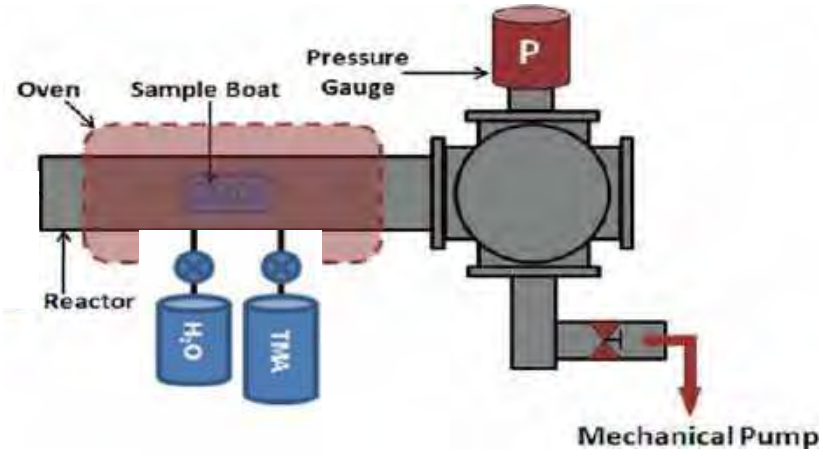

- ✓ **high-grade quality coatings**
- ✓ custom process: bottom-up approach
- ✓ process at **low temperature (i.e. < 200°C)**
- ✓ mainly **amorphous films**

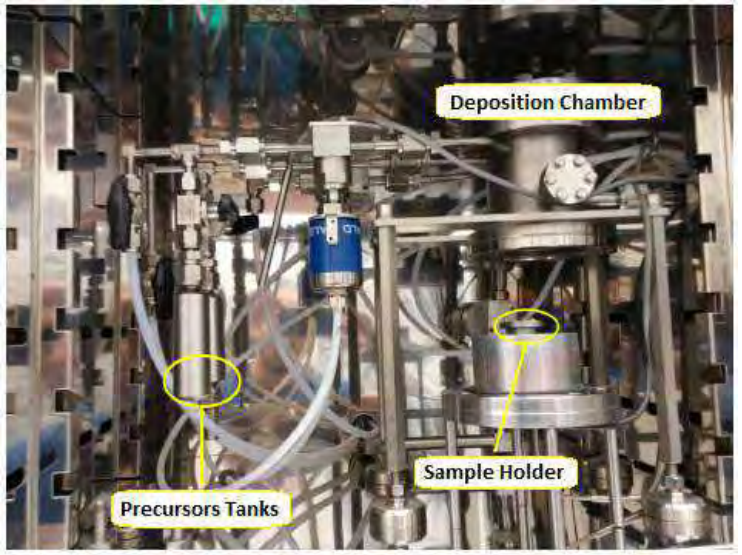

- **Mock-up scale** ALD facility
- Developed by **CNST-IIT**
- Stop Flow Mode ALD
- **Flexible** and **straightforward** set up

fabio.difonzo@iit.it

ALD-grown Al_2O_3 amorphous coatings

Atomic Layer Deposition - Set Up

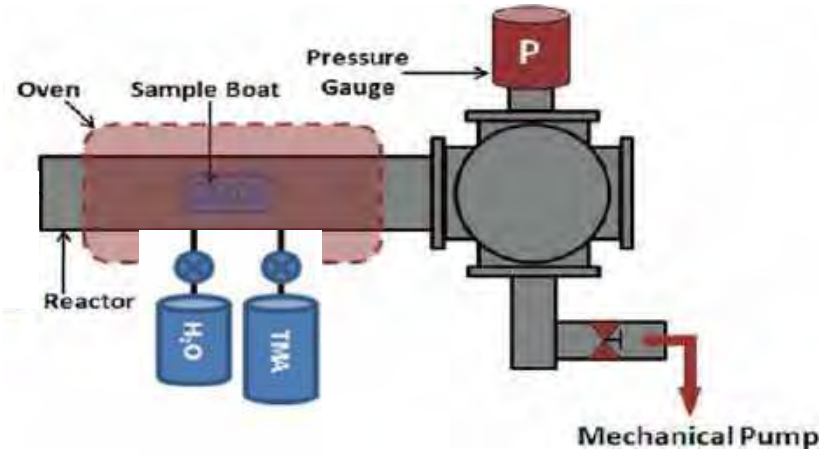

- ✓ **high-grade quality coatings**
- ✓ custom process: bottom-up approach
- ✓ process at **low temperature (i.e. < 200°C)**
- ✓ mainly **amorphous films**

compact well-adherent ALD films

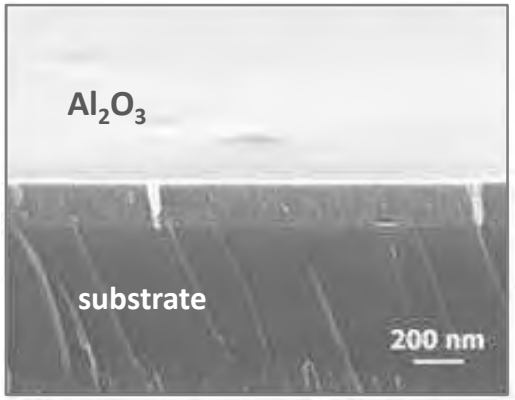

200nm-thick ALD-grown Al_2O_3

- **Mock-up scale** ALD facility
- Developed by **CNST-IIT**
- Stop Flow Mode ALD
- **Flexible** and **straightforward** set up

ISTITUTO ITALIANO
DI TECNOLOGIA

Chemical stability tests on Al_2O_3 films in Pb-16Li

fabio.difonzo@iit.it

Corrosion tests in Pb-16Li on ALD Al_2O_3

- Corrosion tests on EUROFER-97 SS substrates with ALD Al_2O_3 coatings
- Reported results for 1.000 hours exposure tests @ 550°C in static Pb-16Li
- Ongoing corrosion tests on ALD Al_2O_3 for longer exposure times

- Sample coated with 500nm-thick ALD Al_2O_3 -

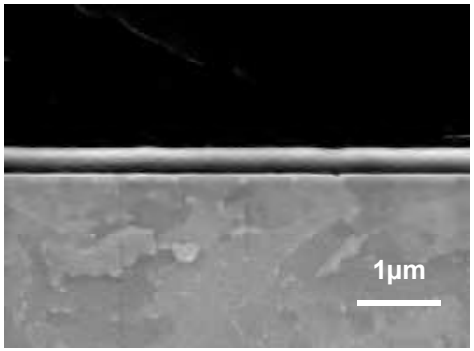

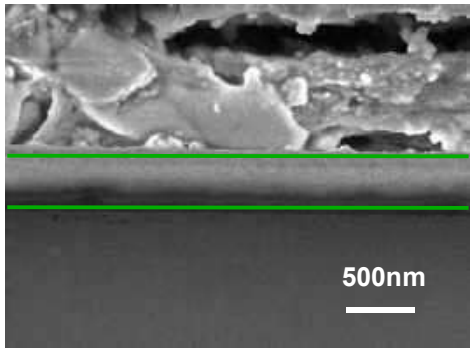

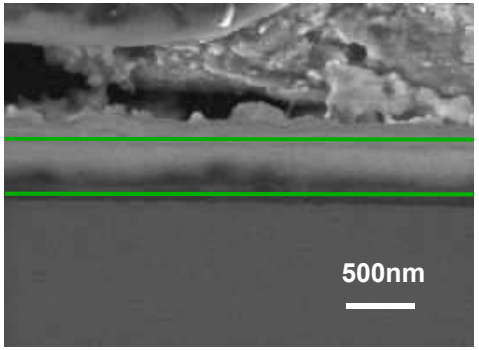

⟹ **No delamination, nor substrate corrosion** for the ALD Alumina, too

⟹ Ongoing characterization on surface features

fabio.difonzo@iit.it

Acknowledgements & ongoing collaborations

Corrosion tests + financial support

Serena Bassini
Marco Utili
Mariano Tarantino
Pietro Agostini

heavy ion irradiations

Patrick Trocellier
Yves Serruys
Lucile Beck
Cédric Baumier
Odile Kaitasov

TEM + XRD

Alexander Mairov
Kumar Sridharan

POLITECNICO DI MILANO

Brillouin & CTE/Res Stress

Edoardo Besozzi
Marco Beghi

Nanoindentation + nanoimpact

Luca Ceseracciu

Thank You
for your attention!

fabio.difonzo@iit.it

M.G. Beghi

Coating characterization under irradiation. Heavy ions irradiation against neutron irradiation.

POLITECNICO
MILANO 1863

ADP MiSE-ENEA --- PAR2017-LP2 --- 15/06/2018

Outline

ions irradiation vs. neutron irradiation

back to basics:

- collisional cascades
- dpa

metals irradiation vs. ceramics irradiation

examples of ceramic coatings under irradiation

Collisional cascade

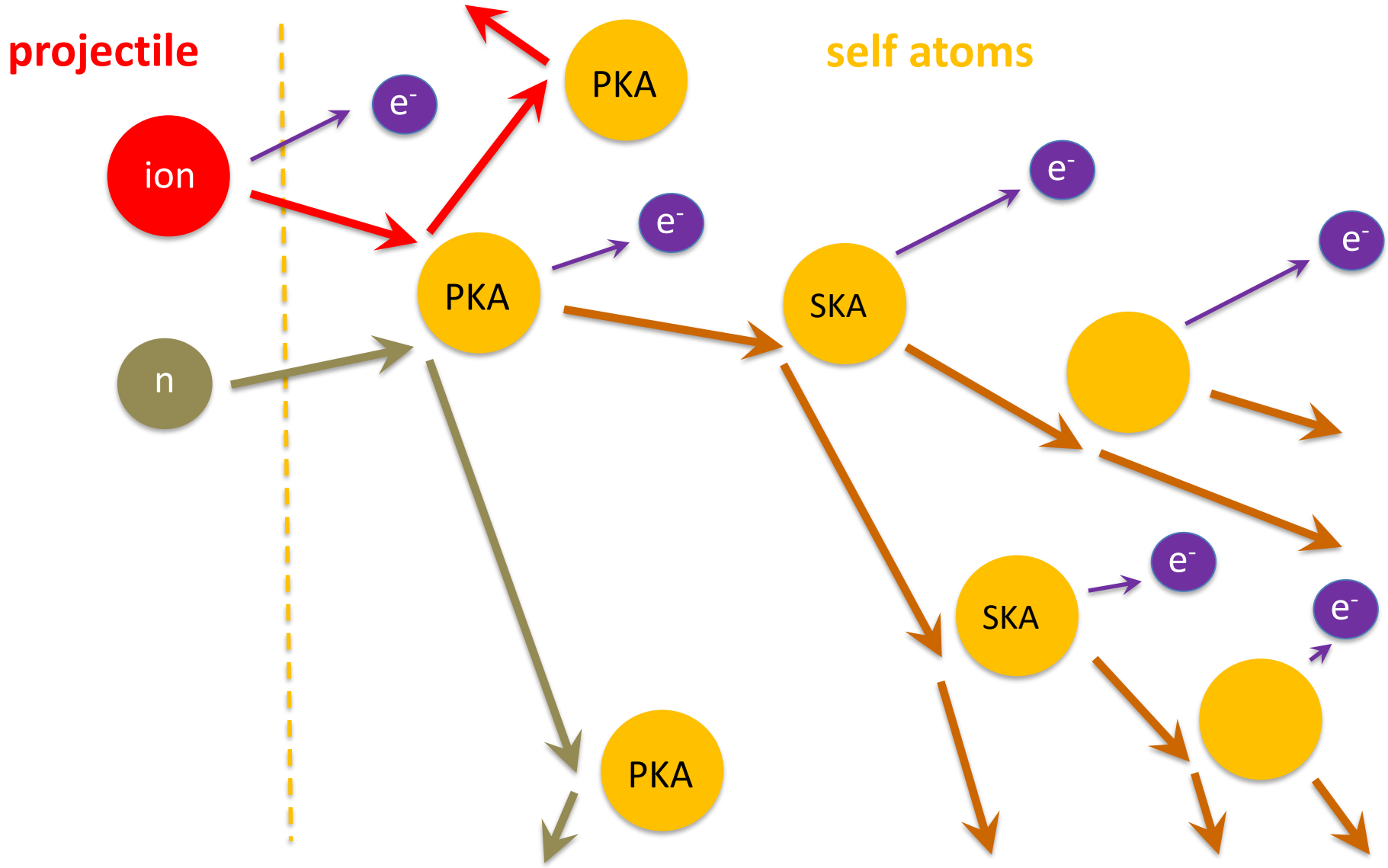

Collisional cascades

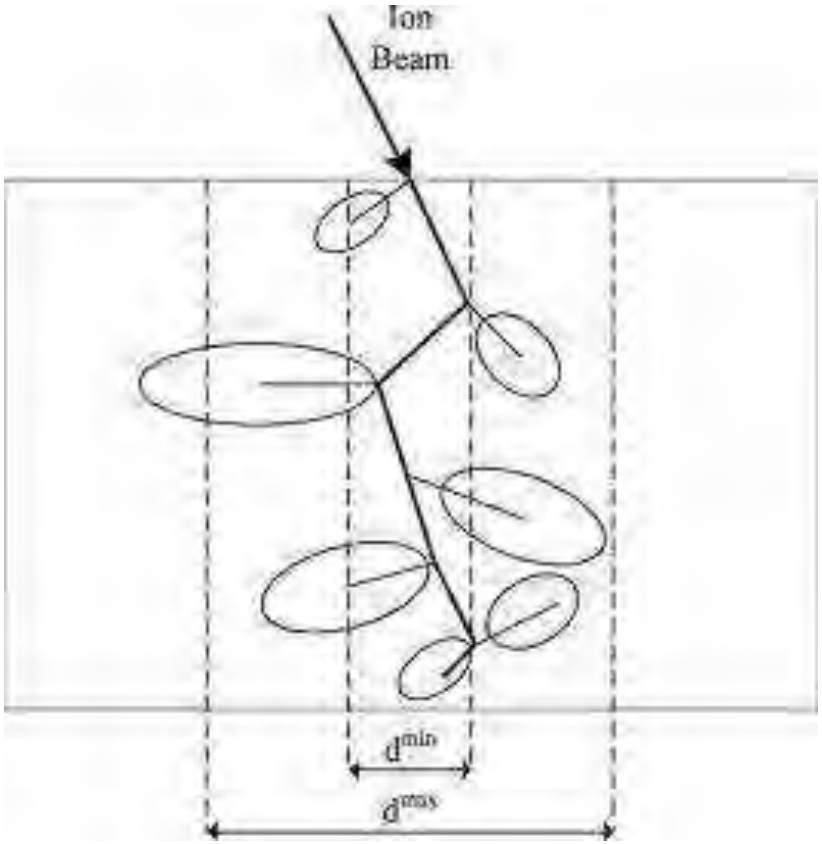

Stopping power

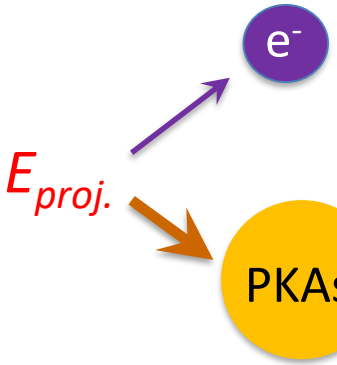

$\left|\frac{dE}{dx}\right|_e$ → excited electrons → → heat

$\left|\frac{dE}{dx}\right|_N$ → Knocked atoms → → Frenkel pairs: vacancy/interstitial

$\frac{\left|\frac{dE}{dx}\right|_e}{\left|\frac{dE}{dx}\right|_N}$ **E**lectron to **N**uclear **S**topping **P**ower ratio

$E_{proj.} \rightarrow T$

$$A = \frac{m_{target}}{m_{project}} \qquad T_{max} = \delta\, E \qquad \delta = \frac{4A}{(1+A)^2}$$

$$\delta\left(\frac{1}{A}\right) = \delta(A) \qquad \delta(A=1) = 1 \qquad \delta(A \gg 1) \cong \frac{4}{A}$$

isotropic scattering $\Rightarrow$ $\langle T \rangle = \frac{1}{2} T_{max}$

Displacements per atom: dpa

$$\frac{dn_{pairs}}{dt} = \frac{dn_{casc.}}{dt}\nu\left[\frac{\#_{pairs}}{\#_{cascade}}\right] = n_{atoms}\,\phi\sigma_s\nu$$

$$\frac{\int(dn_{pairs}/dt)dt}{n_{atoms}} = \frac{n_{pairs}}{n_{atoms}} = \Phi\sigma_s\nu : \quad \textbf{dpa}$$

$$\nu\left[\frac{\#_{pairs}}{\#_{cascade}}\right] = \nu\,(TPKA)$$

$$E_d = E_{displ.}[\sim 10\ \text{eV}] \gg E_{form.(TD)}[\sim 1\ \text{eV}]$$

$$\langle\nu\rangle = \frac{T_{PKA}}{2E_d}$$

Energy transfer in collisions

projectile	target	E_d [eV]	$\langle T \rangle = \frac{1}{2} T_{max} = \frac{1}{2} \frac{4A}{(1+A)^2} E_{proj}$	$\langle \nu \rangle = \frac{\langle T_{PKA} \rangle}{2E_d}$
n @1 MeV	Fe	~ 40	36 keV	900
n @1 keV	Fe	~ 40	36 eV	~ 1
Fe @36 keV	e^-		0.7 eV	
e^- @ 1MeV	Fe	~ 40	20 eV	> 0
W @18 MeV	e^-		106 eV	
W @18 MeV	Fe	~ 40	6.4 MeV	80000
Ni @4 MeV	Fe	~ 40	2 MeV	25000

Energy loss "dE/dx profiles

- a proton's linear rate of energy loss "linear energy transfer" (LET)
- is given by the Bethe-Block formula:

$$\frac{dE}{dx} \propto \frac{1}{v^2}\left(\frac{Z}{A}\right)z^2$$

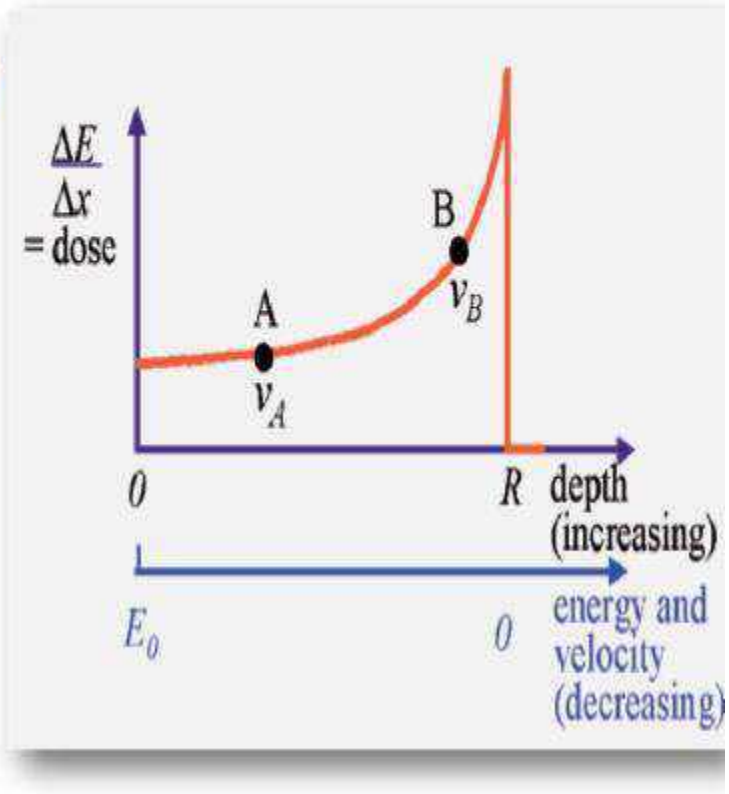

Bragg peak

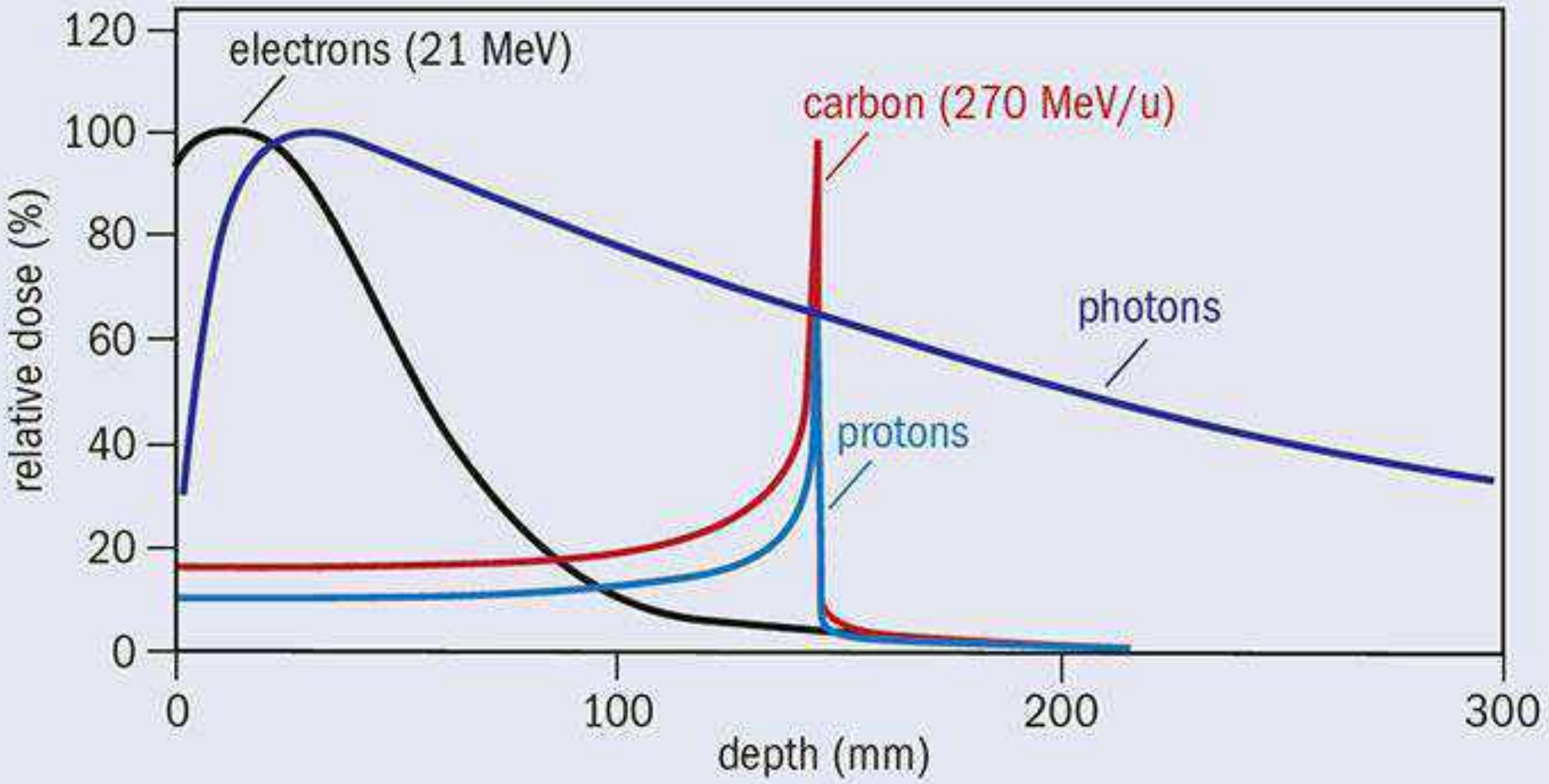
electrons (21 MeV)
carbon (270 MeV/u)
photons
protons
relative dose (%)
120
100
80
60
40
20
0
0
100
200
300
depth (mm)

Success of dpa

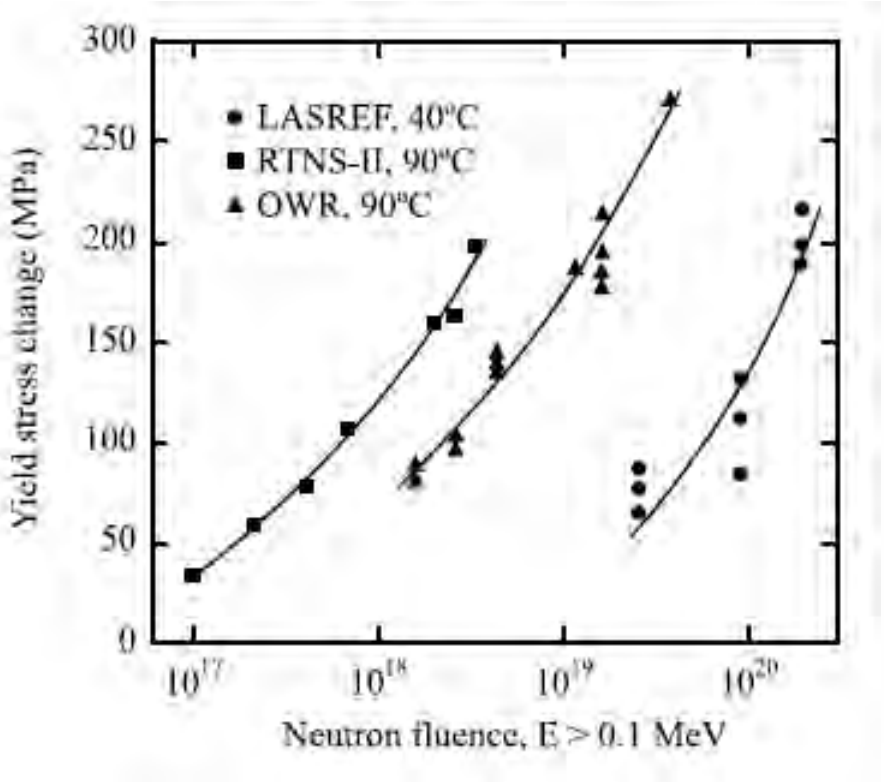

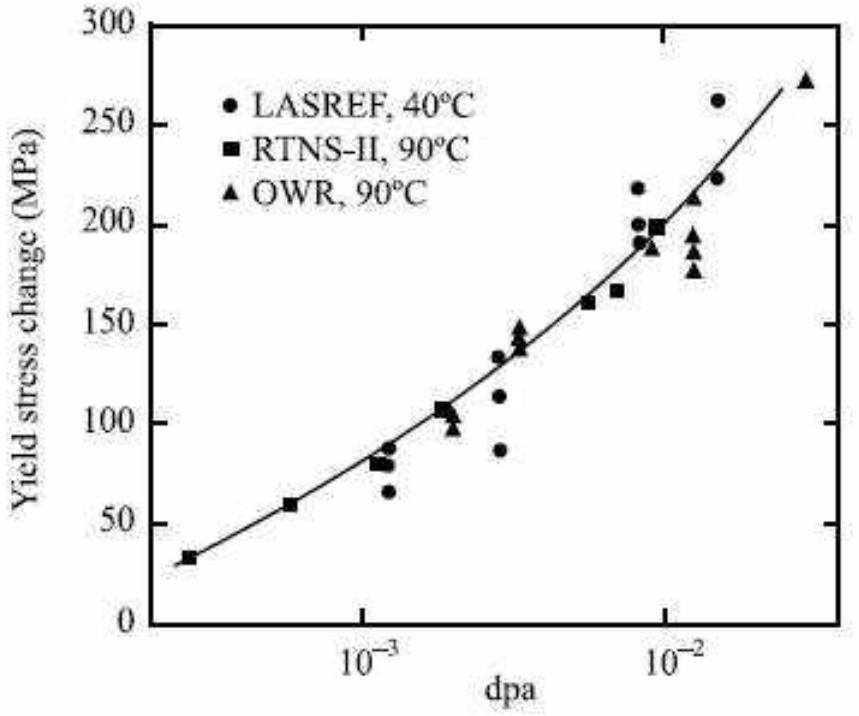

Metals: mono-elemental crystals, unique electron states

evolution of **metals** under **MeV neutrons**, (and ~ ions):

electrons excitation and de-excitation → heat

injection of Frenkel pairs, concentration >> equilibrium conc.

super-saturated solution of vacancies/interstitials evolves (precipitates) according to

- concentration (~ dpa)
- Temperature, which determines diffusivity

⇒ (dpa & temperature) good predictor of
microstructure evolution ⇒ properties evolution

+ He production by (n,α) reactions

Ion vs. neutrons

Ion irradiation vs. neutron irradiation

dpa/day instead of dpa/yr $\Rightarrow$ fast, inexpensive, accessible
no activation $\Rightarrow$ post-irradiation analysis much easier
thin layers vs. bulk

ENSP ratio as low as possible to best simulate neutrons

Possible pre-implantation or co-implantation of He

Ceramics: multi-elemental crystals / amorphous, non unique electron states

evolution of **ceramics** under **neutrons** & **ions**

- covalent bonds: electron localization, excitation, possible relaxation into different state $\Rightarrow$
  $\Rightarrow$ possible bonding/chemical evolution
- different elements, chemical environment: $\langle T \rangle$, $\langle E_d \rangle$ $\Rightarrow \langle \nu \rangle$?
- defect mobility vs. temperature ?

$\Rightarrow$ (dpa & temperature) alone: NOT good predictor of microstructure evolution $\Rightarrow$ properties evolution

also depends on ? spatial correlation of defect birth?

(small / large cascades ?)

Irradiation disorders/orders

Irradiation:

- Induces disorder (→ amorphization)
- Locally: high energy deposition, promotes order

Crystals (metals and ceramics):

disordering prevails, tends to saturate
'disordered' regions (grain boundaries, dislocations)
are sinks for interstitials & vacancies

Amorphous (ceramics)

ordering/disordering compete, ordering can prevail
interstitials & vacancies no longer well defined
ultra-nano structures offer sinks for defects

Heavy ion (Au+W) irradiation of Al_2O_3

- Irradiation with **Gold and Tugsten ions @ 600 °C**
- **Low ENSP** ratio to **simulate effect of Neutrons**
- Minimum coating thickness for Nanoindentation
- **Implantation beyond coating** (no chemical effects)
- Different **damage levels**: **0**, **20, 40 and 150 dpa** at the interface between Al_2O_3 and buffer layer (dpa levels calculated using **SRIM Code**)

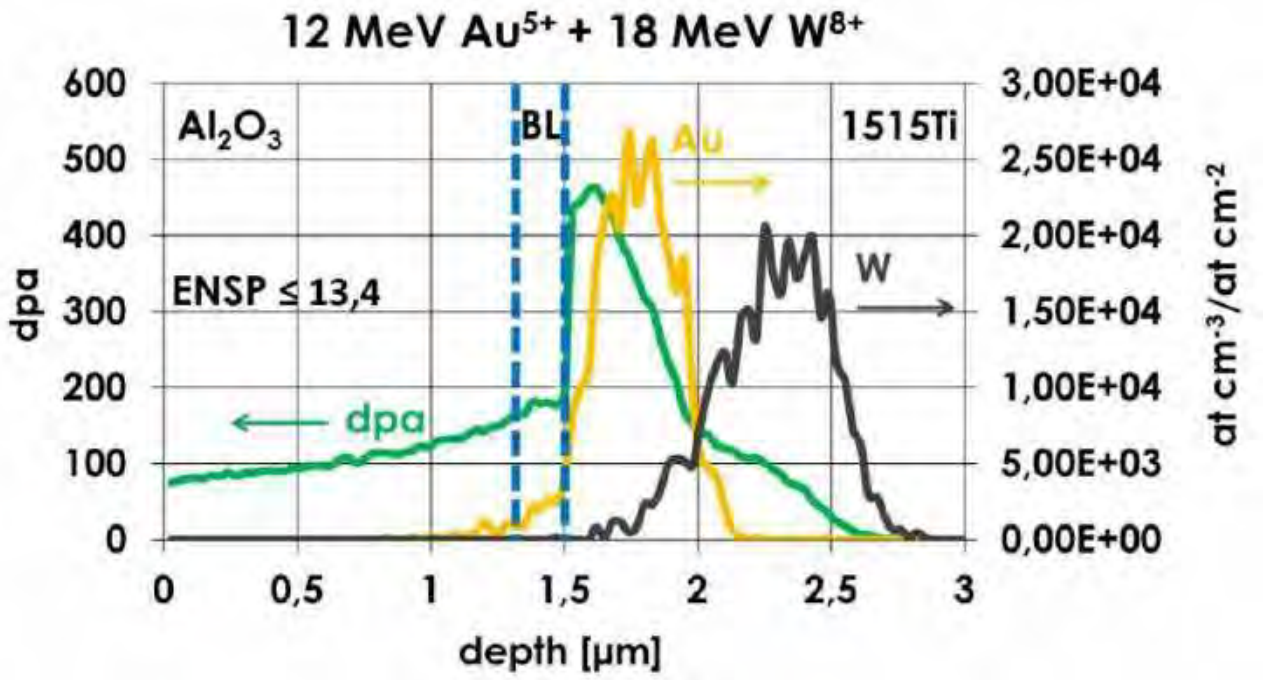

Heavy ion (Au+W) irradiation of Al_2O_3

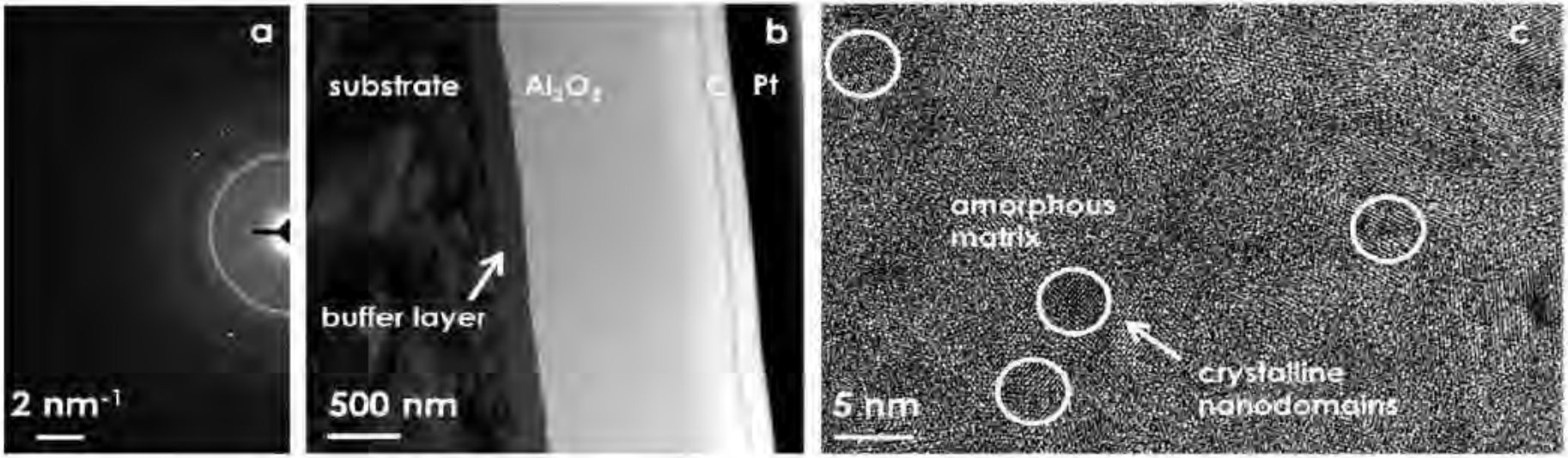

Heavy ion (Au+W) irradiation of Al_2O_3

0 dpa

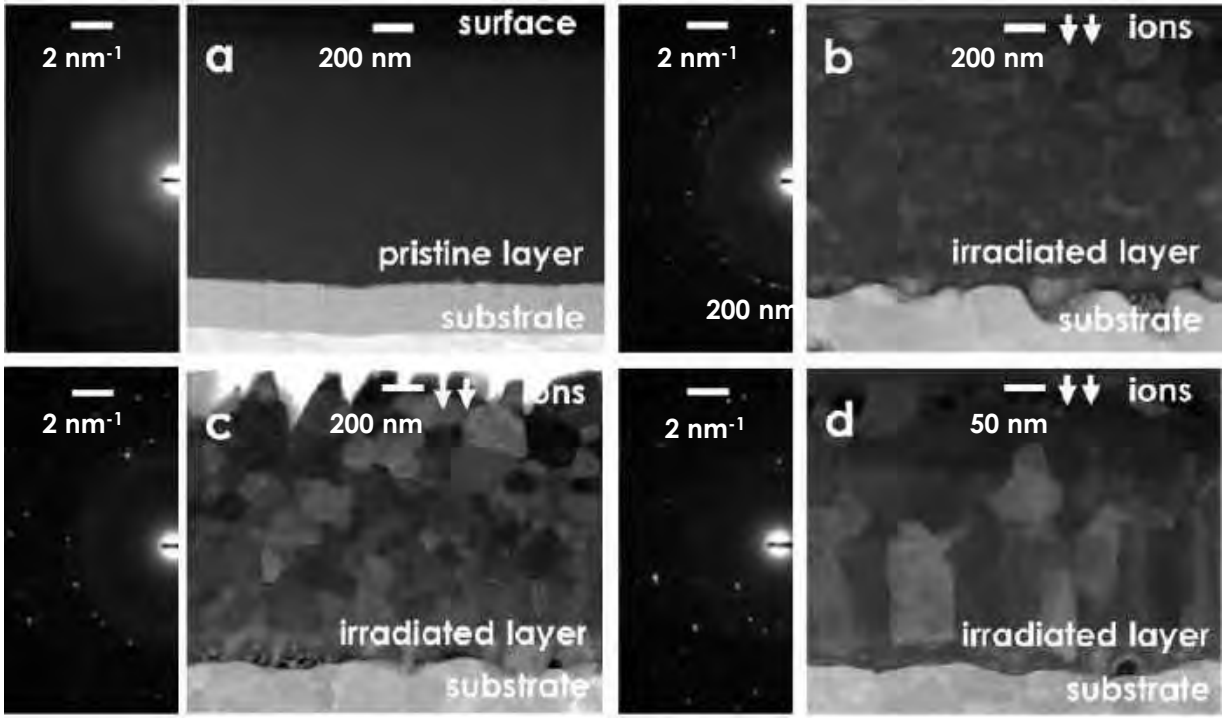

20 dpa

40 dpa

150 dpa

- **Nanocrystallization** followed by **sub-linear grain growth**
- Increase of **crystalline size** and **crystalline fraction**
- **γ-Al_2O_3** always present plus **formation of α-Al_2O_3 @ 150 dpa**

Heavy ion (Ni) irradiation of Al_2O_3

- Irradiation with **Nickel ions @ 600 °C**
- **Low ENSP** ratio to **simulate effect of Neutrons**
- Minimum coating thickness for Nanoindentation
- **Implantation beyond coating** (no chemical effects)
- Different **damage levels**: **0**, **250 and 450 dpa** at the interface between Al_2O_3 and buffer layer (dpa levels calculated using **SRIM Code**)

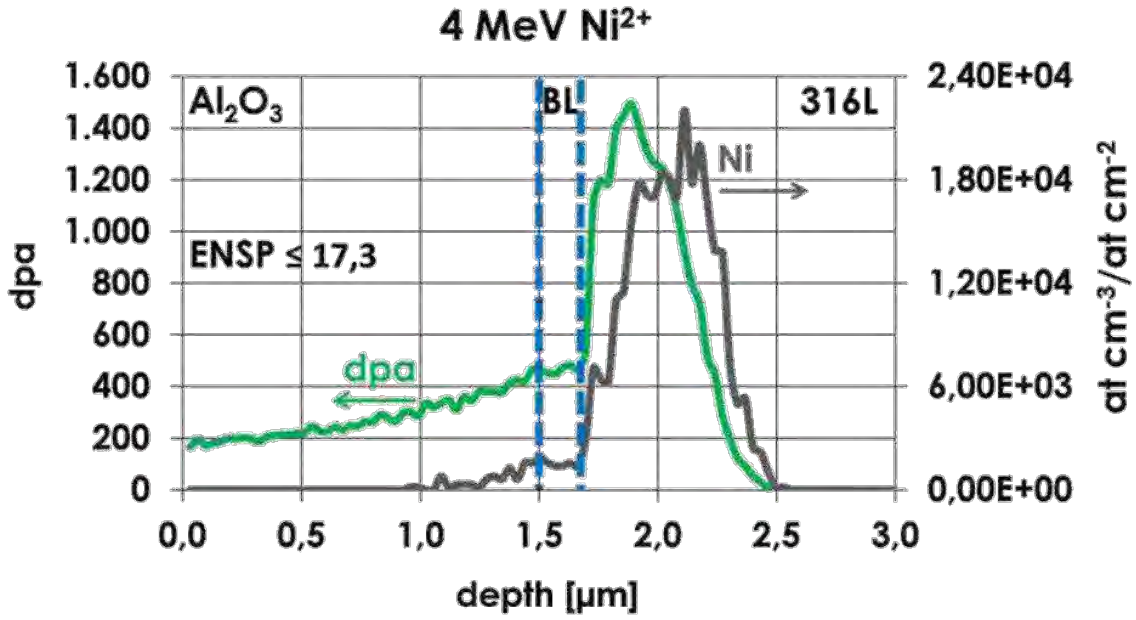

Heavy ion (Au+W) irradiation of Al_2O_3

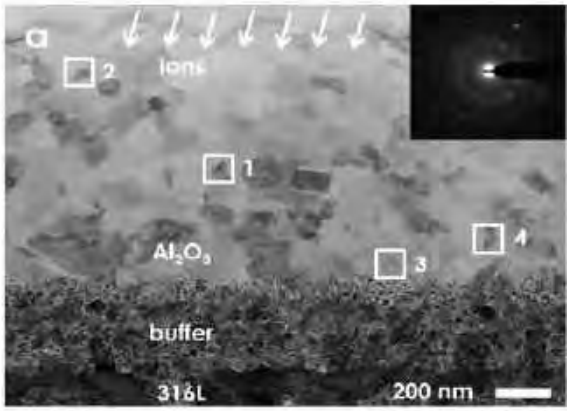

250 dpa

- **Nanocrystallization** and **grain growth** (again)
- No more γ-Al_2O_3: **formation of metastable δ-Al_2O_3**
- Increase of **crystalline size** and **crystalline fraction**

δ-Al_2O_3

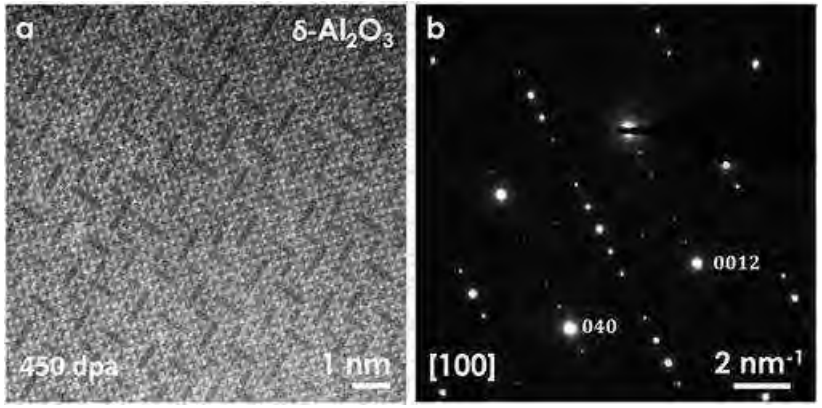

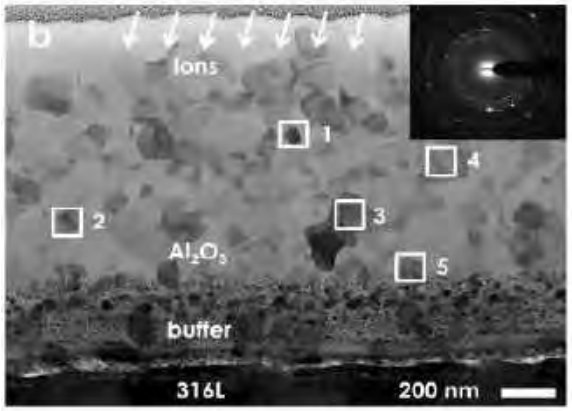

450 dpa

Heavy ion (Au+W vs. Ni) irradiation of Al_2O_3

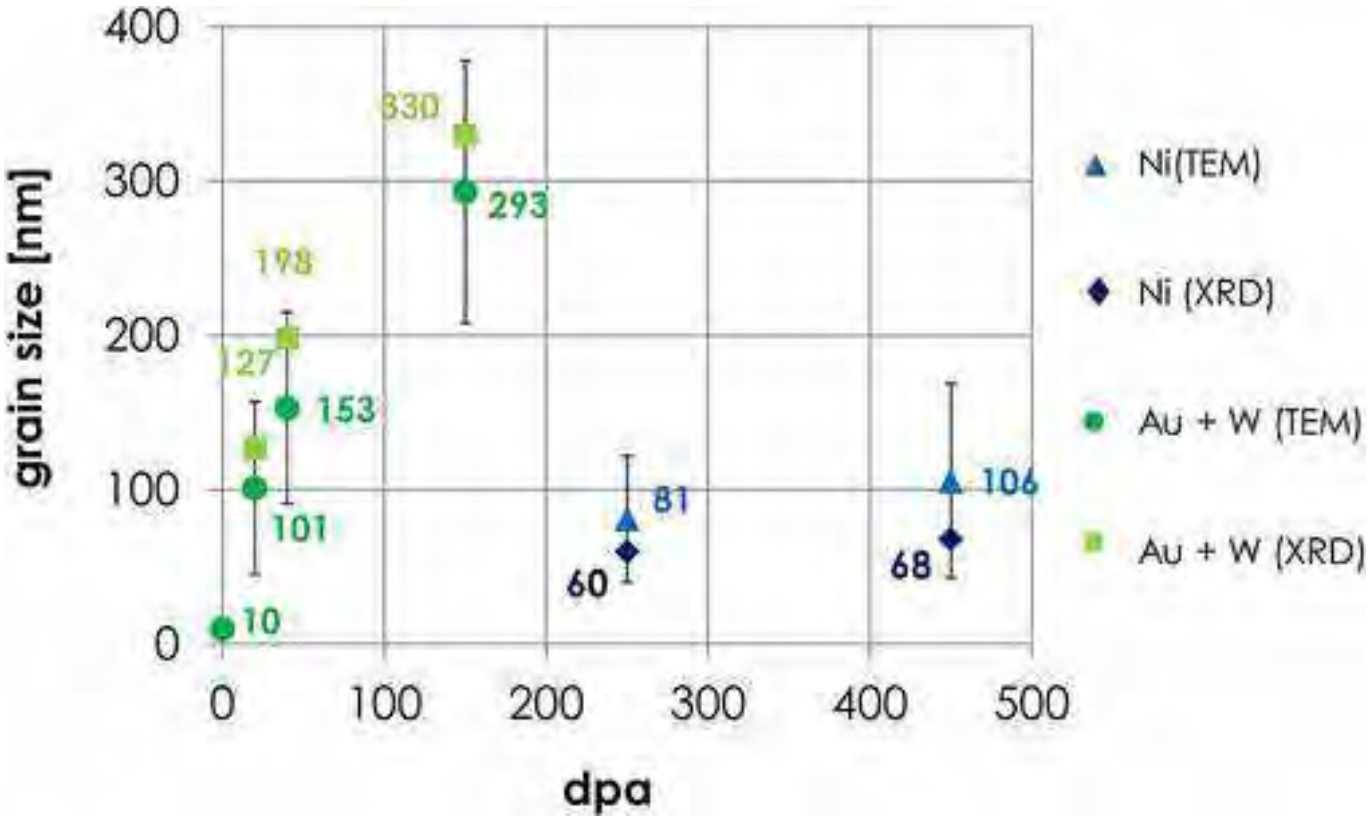

Same temperature (600 °C)

Conclusions ?

- For irradiated ceramics, dpa & temperature are not enough to predict microstructure / properties
- Dependence on
  - space distribution of defect generation (small/large cascades)
  - … ?

Italian National Agency for New Technologies,
Energy and Sustainable Economic Development

Corrosion qualification of materials and coatings in liquid lead for LFR

ADP MiSE-ENEA (PAR2017-LP2)

Dipartimento di Ingegneria Astronautica, Elettrica ed Energetica
Università di Roma "La Sapienza"

14-15 Giugno 2018

S. Bassini (ENEA FSN-ING-TESP)
serena.bassini@enea.it

MATERIALS & COATINGS FOR ALFRED

$C_O \approx 10^{-6}$ -10^{-8} % wt.

Materials and Coatings for low oxygen concentration ($C_O = 10^{-6} / 10^{-8}$ wt. %)

Component	Min./Max Temp. Normal Operation (long term) (°C)	Max Temp. Accident Conditions (transient) (°C)	Max. Lead velocity (m/s)	Max. Radiation damage (dpa/y)	Max. Radiation damage (dpa)	Material	Coating	Notes
Reactor Vessel	380÷430	500 (700 (1))	0,1	< 10^{-5}	0,0002 (40y)	AISI316LN (ASTM)	No	Back-up Liner of corrosion resistant steel (e.g. AFA)
In					2,1	316LN (ASTM)	No Al diffusion coating by Pack Cementation	Back-up AFA steel
D						316LN (ASTM)	No	Al diffusion coating by Pack Cementation
Stea						I316L (ASTM) 5Ti (DIN 1.4970)	No Al diffusion coating by Pack Cementation	Backup: AFA steel; Alloy 800 coated
Fu						-15Ti (AIM1)	Al_2O_3 by PLD	No buffer layer (direct coating deposition over the bulk material)
FA					(5y)	-15Ti (AIM1)	Spacer grids & wrapper (outside): Al_2O_3 by PLD Wrapper (inside): overthickness	Back-up (for wrapper tube): Al_2O_3 by ALD or PLD (**to be developed in-tube deposition**)
DHR Heat Exchanger	380÷430	700 (1)	0,2	< 10^{-3}	0,01 (20y)	AISI316L (ASTM) 15-15Ti (DIN 1.4970)	No Al diffusion coating by Pack Cementation	Backup: AFA steel; Alloy 800 coated
Primary Pumps (impeller)	380÷480	700 (1)	15÷20	< 10^{-3}	0,01 (20y)	AISI300 series	Closed impeller: Al diffusion coating by Pack Cementation Open Impeller: Al_2O_3 by PLD	Backup (for open impeller ONLY): AlTiN coating by PVD

Corrosion qualification of these materials in Pb is mostly missing, especially in the long-term and/or flowing conditions. Some gaps will be covered in the frame of GEMMA EU project

Substrate: 316L(N), 15-15Ti (DIN), 15-15Ti AIM1 (cold worked)
Back-up: AFA for SG and DHR

15-15Ti cold worked, static Pb 550°C

Fluel cladding & fuel assembly

550°C, [O] = 10^{-3} % wt. (PAR2013)

Local spot of oxidation made of external layer and internal oxidation layer with Ni and Cr diffusion (enrichment).

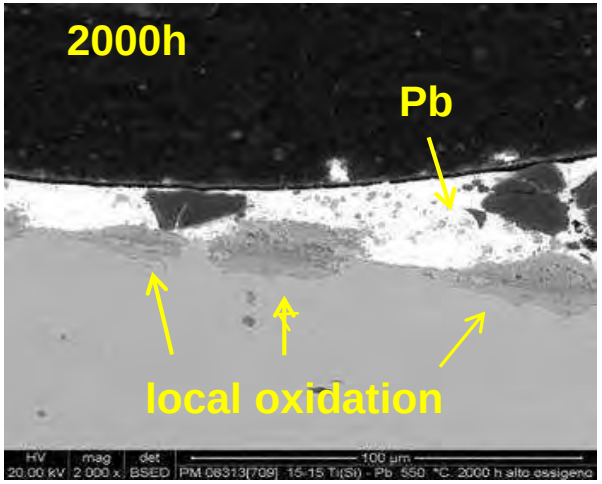

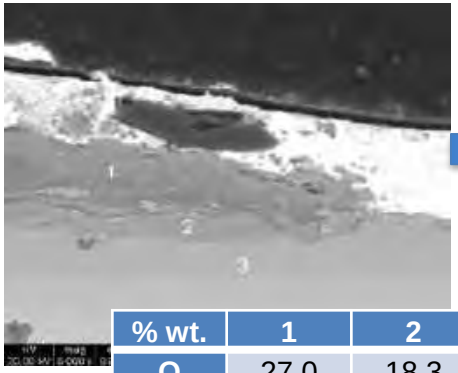

% wt.	1	2	3
O	27,0	18,3	-
Si	0,1	1,0	0,7
Mo	3,2	2,6	1,7
Ti	-	0,4	0,5
Cr	0,7	16,9	14,8
Mn	0,7	1,4	1,7
Fe	54,8	34,4	65,2
Ni	3,7	19,6	15,5
Pb	10,0	5,4	-

550°C, [O] = 10^{-8} % wt. (PAR2016)

Dissolution layer with depth of ≈ 25 µm after 1000h (c). Dissolution layer of 85 µm and occasionally 150 µm after 4000h (d). The layers contains Pb (e).

F. García Ferré et al., (2017)

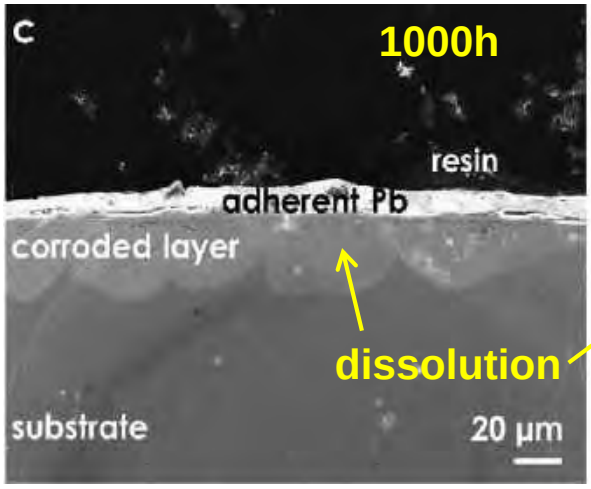

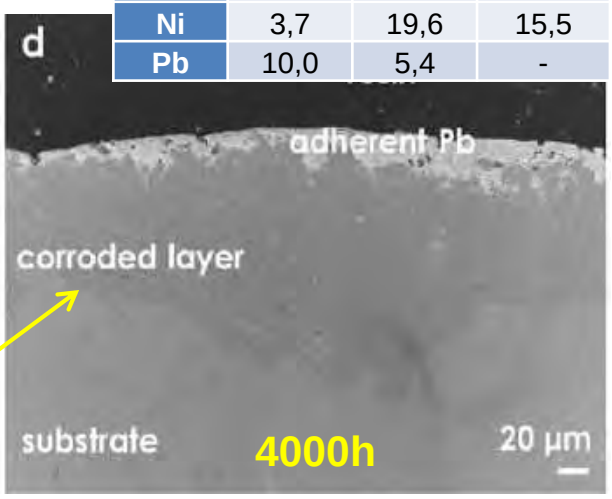

15-15Ti and DS4, flowing Pb 550°C

15-15Ti, 550°C, [O] = 10^{-4} % wt. (flowing) PAR2016

Oxidation (external layer + diffusion) with depth 5-10 µm. No dissolution.

Oxygen penetration in grain boundary and slip bands.

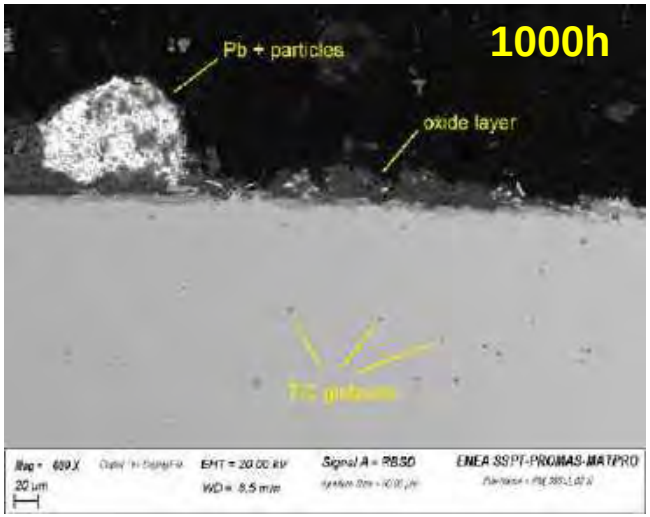

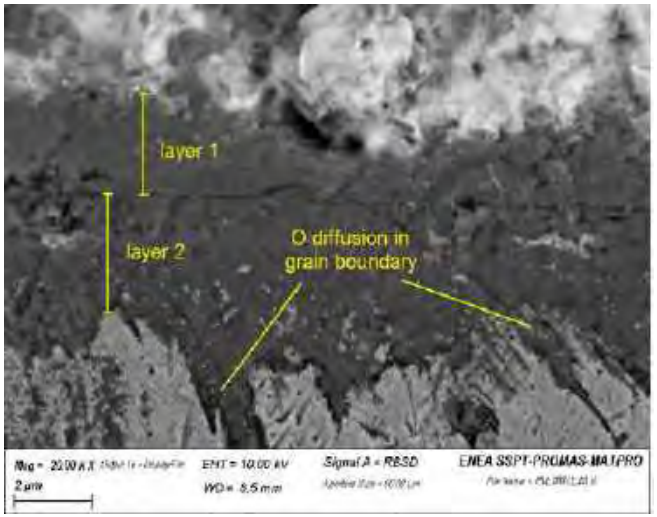

DS4 (15Cr-25Ni), 550°C, [O] = 10^{-4} % wt. (flowing) PAR2016

Oxidation (external layer + diffusion) with depth 4-5 µm. No dissolution.

Oxygen penetration in grain boundary and slip bands.

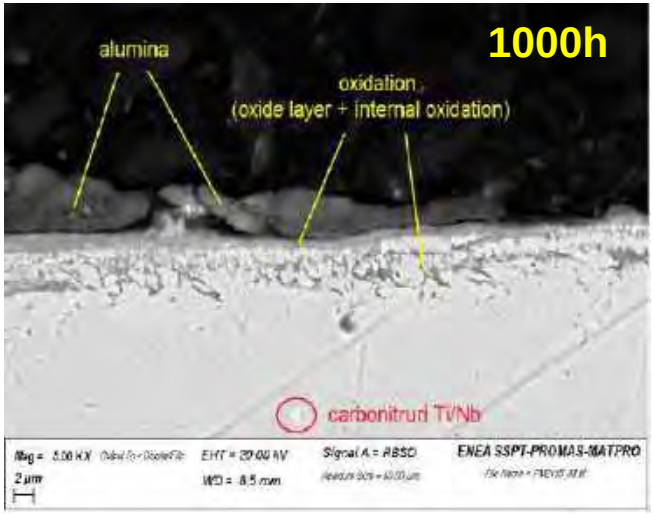

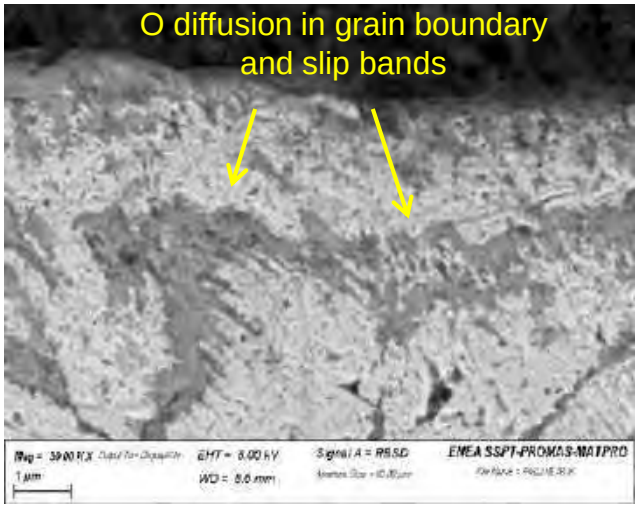

Alumina Forming Austenitic (AFA) steels

Dissolution for 316L and Pb penetration, better performance for AFA 20Ni and 14Ni at 550°C, [O] =10^{-7}% wt, 3000h **(KTH)**

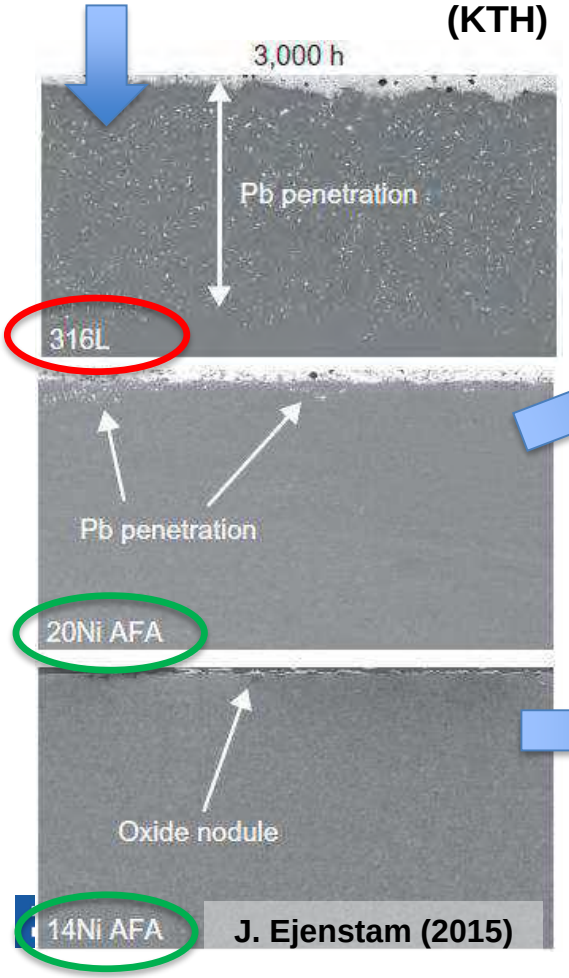

AFA at 750°C, 2000h
[O] =10^{-6} % wt
internal oxidation observed

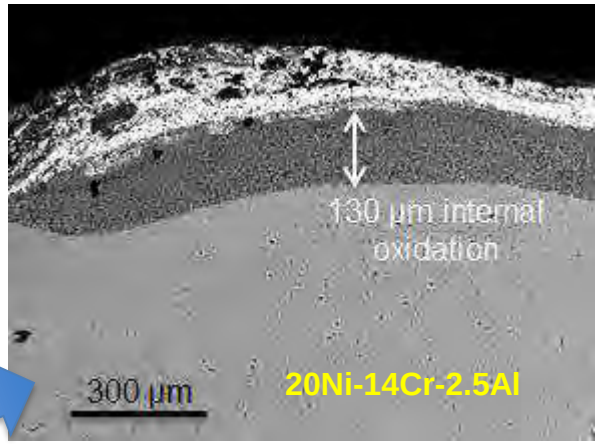

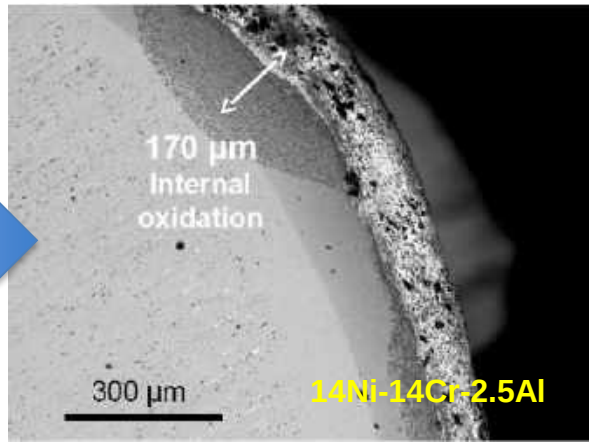

Back-up for SG, DHR

A. Weisenburger, P. Szakálos, KOM GEMMA project, 21-22 June 2017, Rome.

- low % of Al;
- protective Al_2O_3 layer (better then Fe-Cr oxides at high T);
- austenite structure (no embrittlement, good mech. properties);
- composition will be improved in the frame of GEMMA EU project by KIT and KTH

AFA by ORNL

AFA low Ni (OC-Q) – plate 12 x 50 x 64 mm

Element	C	Cr	Ni	Mn	Al	Cu	Nb	Si	V	Ti	B	Fe
wt. %	0.2	14	12	4	2.5	3	0.6	0.15	0.05	0.05	0.01	bal.

AFA high Ni (OC-E) – plate 12 x 50 x 64 mm

Element	C	Cr	Ni	Mn	Al	Cu	Nb	Si	V	Ti	B	Fe
wt. %	0.2	14	25	2	4	0.5	2.5	0.15	0.05	0.05	0.01	bal.

- n°7 specimen of AFA 12Ni + n°7 specimen of AFA 25Ni (47x12x6 mm)
- Ra= 0.022-0.037 µm (grinding paper up to 4000P)
- Exposure tests in Pb 550°C, 1000h, high oxygen (10^{-3} % wt.)
- Exposure tests in Pb 550°C, 1000h, low oxygen (10^{-8} % wt.)
- <u>Pre- and Post- test characterization to be performed</u>

Al_2O_3 coating by PLD (IIT)

amorphous alumina with nano-crystalline inclusions (by IIT)

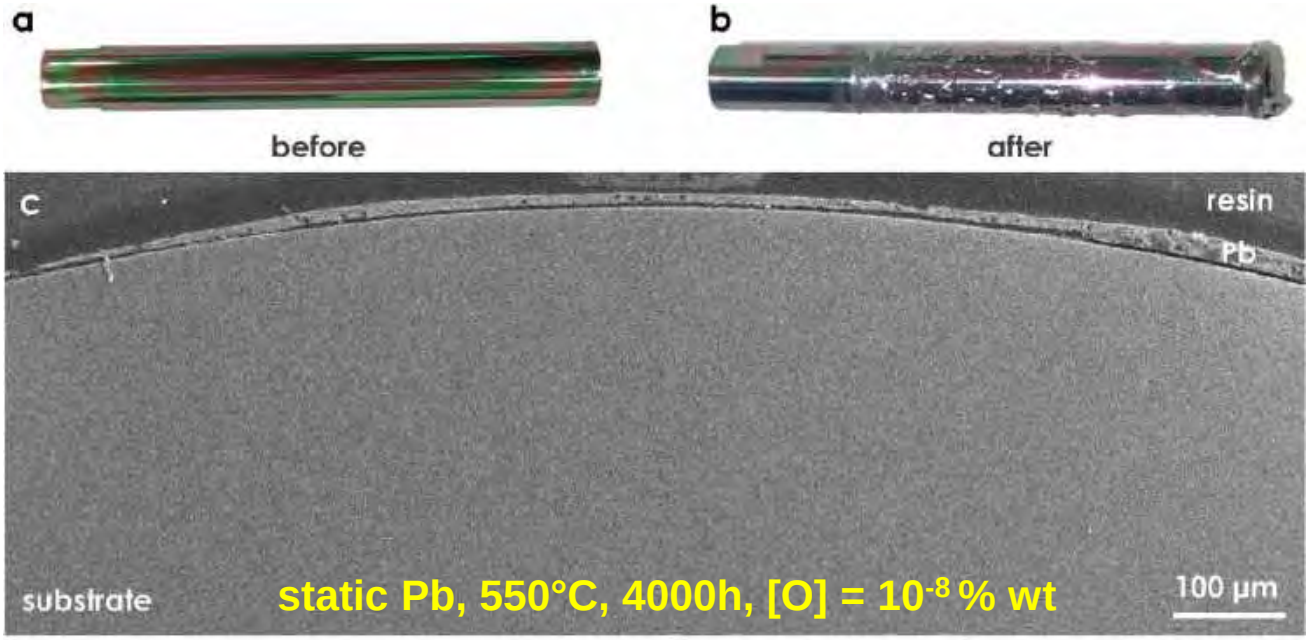

coated 15-15Ti with PLD-Al_2O_3 for fuel cladding & fuel assembly

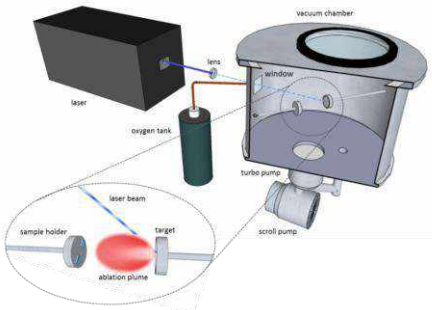

Pulsed Laser Deposition

No evidence of Pb corrosion neither at the macroscopic scale nor at the microscopic scale in tests up to 4000h (**PAR2016**).

F. García Ferré (2017)

FeCrAl layer by aluminizing (Diffusion Alloys UK)

For SG, DHR, pumps, inner vessels

Capability to coat complex geometry

Element	Weight%	Atomic%
O K	4.06	10.87
Al K	34.81	55.23
Cr K	14.66	12.07
Fe K	27.25	20.90
Pb M	4.50	0.93
Totals	85.28	

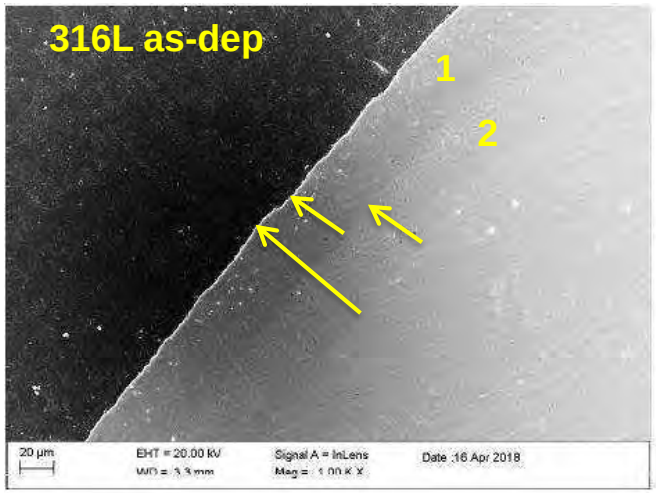

Pb 550°C 2000h, [O] =10^{-3} % wt.

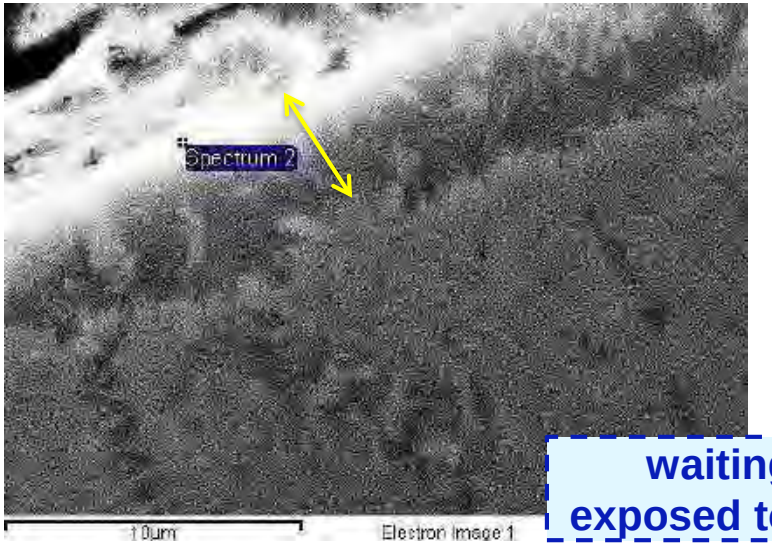

- 1) diffusion layer 40µm with 40→20 % Al (outer-layer 5µm + inner-layer 35µm)
- 2) further diffusion layer 10→5 % Al between diffusion layer and steel

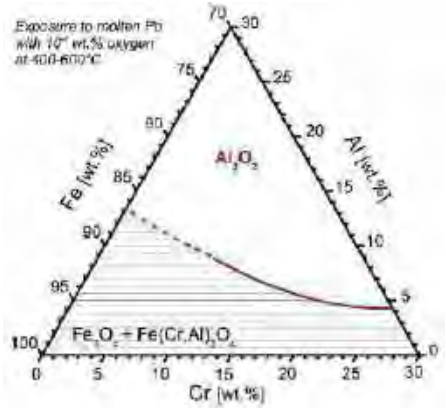

only Pb penetration was observed in the first 5 µm, no formation of Al_2O_3.

waiting for specimen exposed to low Co for 1000h

FeCrAl layer by Pack Cementation (CSM)

FeCrAl layer high Al activity on T91 & 15-15Ti (brittle phases) → need of low Al activity aluminizing

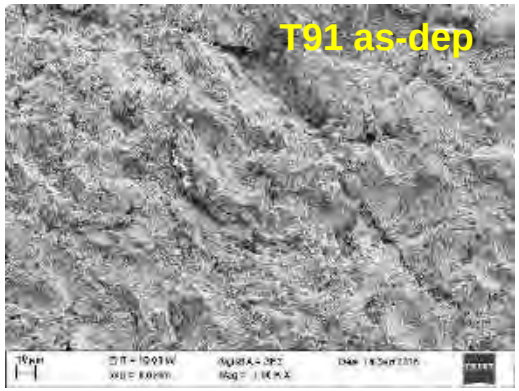

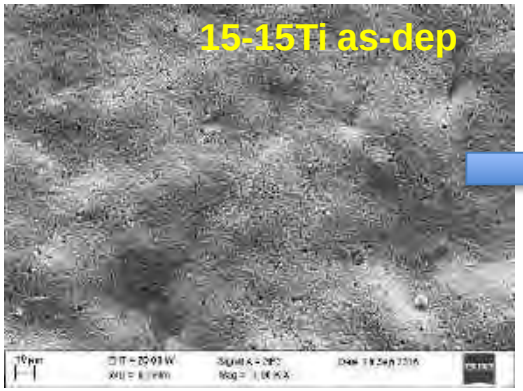

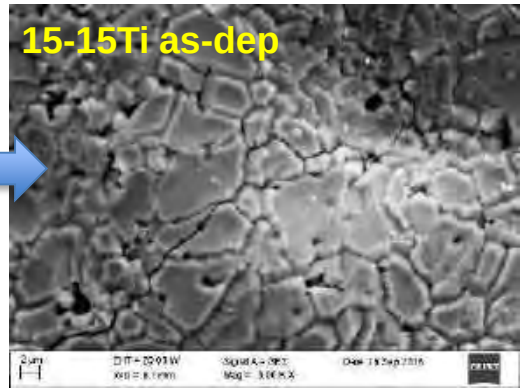

Diffusion coating 20-25 µm + 45-50 µm of further aluminizing, cracks on treated 15-15Ti

Static Pb 550°C, 1500h, low C_O (PAR2016)

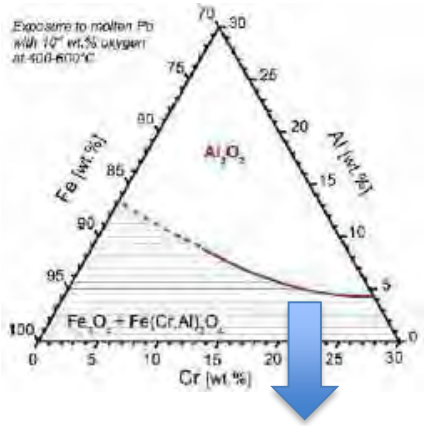

protective and self-healing Al_2O_3 scale

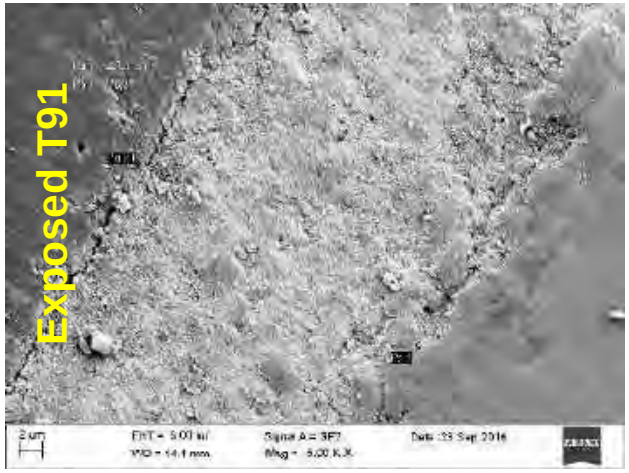

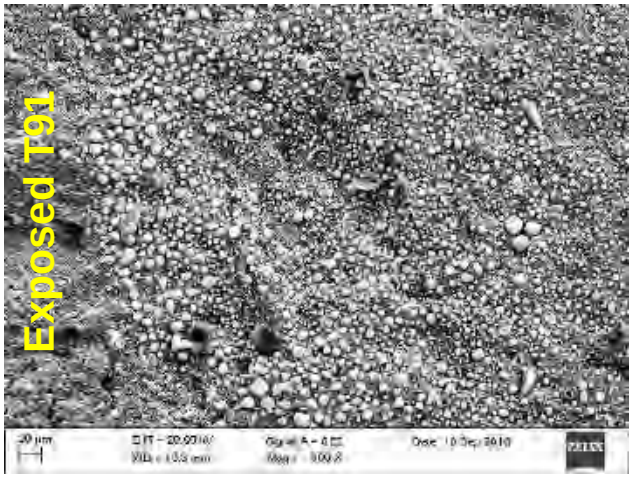

No interaction with Pb (isolated Pb drops on the surface). No thickness reduction after tests.

TiN – AlTiN coatings

TiN
high wear resistance

Oxidation resistance:
T_{ox} =450°C (air)

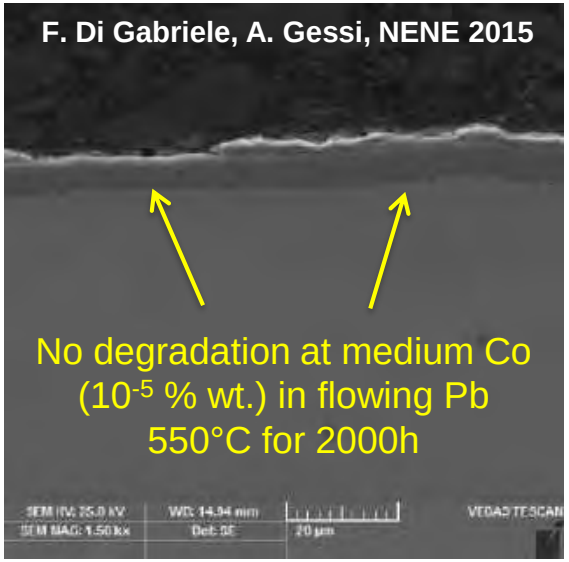

% wt.	1	2	3
N	13.6	31.8	-
O	41.0	-	-
Si	-	-	0.8
Ti	42.1	67.8	1.9
Cr	-	-	14.1
Mn	-	-	1.6
Fe	0.4	0.4	64.8
Ni	-	-	15.1
Mo	-	-	2.0
Pb	2.9	-	-

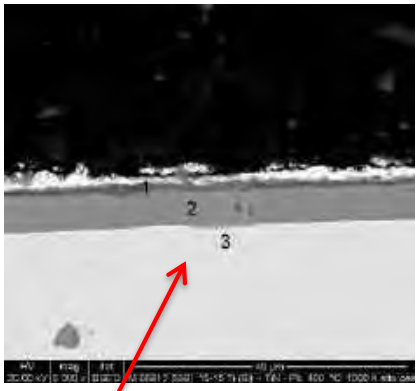

Oxidation of PVD-TiN by CSM in Pb at high Co for 1000h (10^{-4} % 480°C and 10^{-3} % wt. 550°C)
PAR2015

AlTiN Back-up for impellers in primary pumps)

Higher oxidation resistance than TiN (T_{ox} =750°C in air)

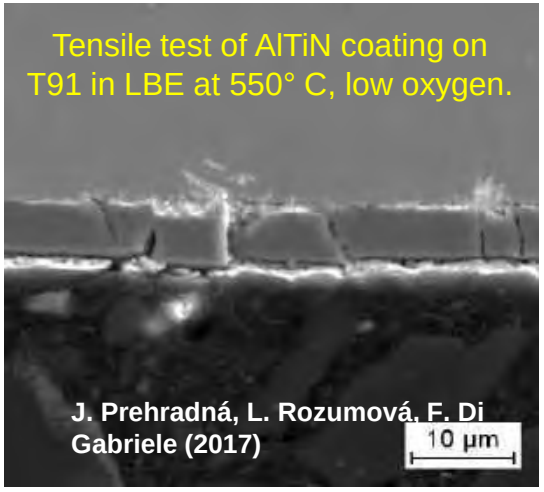

Cracks in the notch but adhesion conserved. No degradation

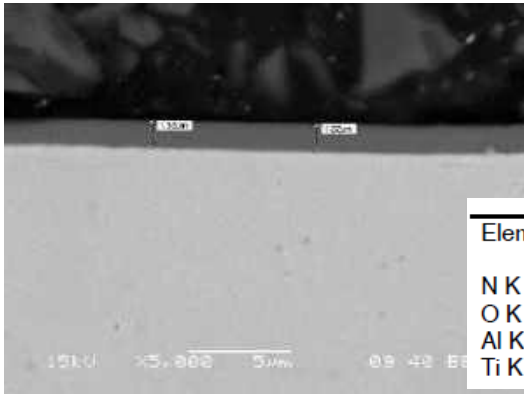

Element	Weight%
N K	18.81
O K	10.32
Al K	32.58
Ti K	38.29

AlTiN coating as-dep (by CSM), some samples exposed in Pb to be analysed (**PAR2015**)

SUMMARY

- 15-15Ti AIM1: corrosion data in liquid Pb are missing, available data are mostly related to LBE
- Qualification in Pb of 15-15Ti AIM1 for ALFRED (+ welding joints) will be performed in GEMMA EU project (static & flowing)
- AFA steels composition will be improved and tested in GEMMA EU project by KTH and KIT
- Screening tests in Pb of AFA from ORNL concluded, pre- and post-test analysis to be performed
- Static tests of Al_2O_3 by PLD done, tests in flowing condition to be performed in GEMMA EU project
- Aluminizing by Diffusion Alloys UK under study, post-test analysis to be performed on specimen exposed to low Co in Pb
- Exposure tests of AlTiN coatings by CSM performed, post-test analysis to be performed.

WORKSHOP TEMATICO

ACCORDO DI PROGRAMMA MISE – ENEA
PAR2017 – PROGETTO B.3 - LP2

GENERATION IV
LEAD COOLED FAST REACTOR
STATO ATTUALE DELLA TECNOLOGIA E PROSPETTIVE DI SVILUPPO

ADP MiSE-ENEA (PAR2017-LP2)

Dipartimento di Ingegneria Astronautica, Elettrica ed Energetica Università di Roma "La Sapienza"
San Pietro in Vincoli, Via Eudossiana 18
14-15 Giugno 2018

Coating mechanical characterization

M. Bragaglia, F.R. Lamastra, F. Franceschetti; F. Nanni

CONTATTI:
Dipartimento di Ingegneria Impresa
Università di Roma "Tor Vergata"
Via del Politecnico, 1, 00133 Roma -Italia
Tel +39-06.7259.4496 - Fax +39-06.7259.4328

Indice dei contenuti

Caratterizzazione microstrutturale e meccanica di diffusion coating in FeCrAl su acciaio AISI 316 L esposti in piombo fuso

Temperatura 550°C
Tempo 2000h
Concentrazione ossigeno 10^{-3} % wt

Caratterizzazione microstrutturale

- Microscopia ottica (MO) prima e dopo attacco chimico
- Microscopia a scansione elettronica (SEM)
- Microanalisi EDS

Caratterizzazione meccanica

- Test di microdurezza Vickers
- Test di microdurezza Knoop

Microscopia ottica

Neat

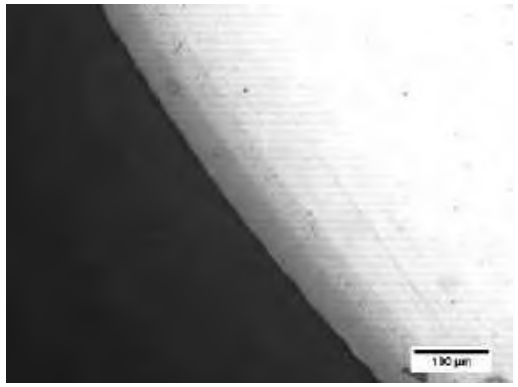

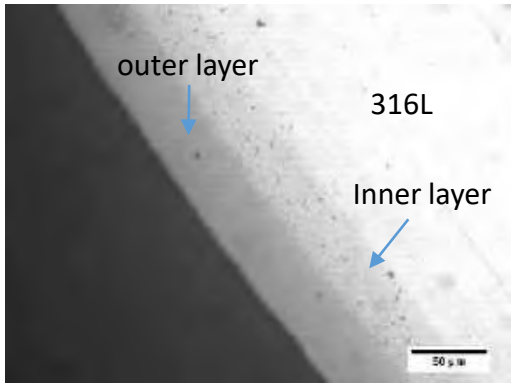

Corroso Pb

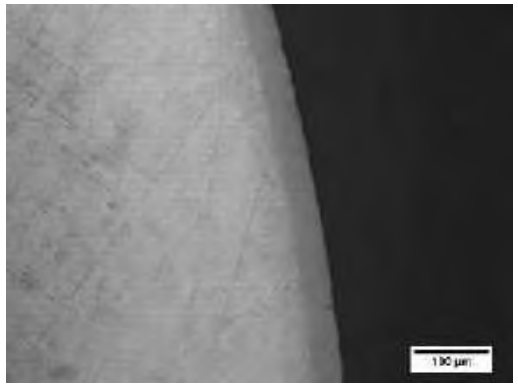

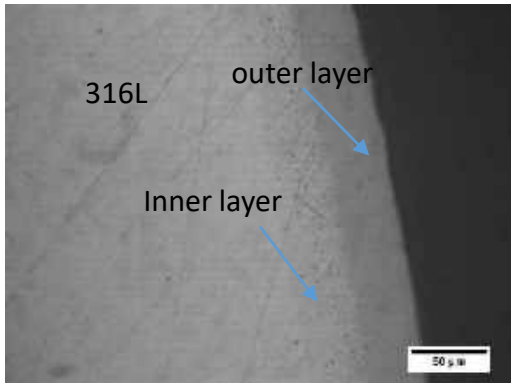

- Rivestimento compatto ed omogeneo buona adesione al substrato
- Presenza di outer layer 30-40 micron
- Presenza di inner layer 30-40 micron
- Inner layer presenza di precipitati
- Non evidenti modifiche dimensionali del coating dopo prove di corrosione in Pb fuso

Microscopia ottica: attacco chimico

Attacco chimico soluzione di acqua regia HCl : $HN0_3$: EtOH per evidenziare la microstruttura

neat

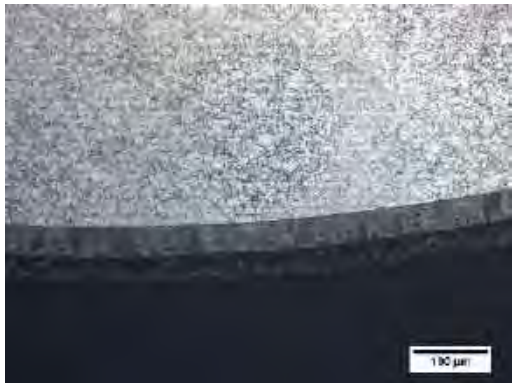

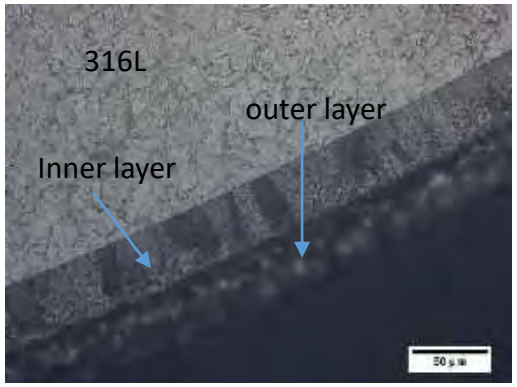

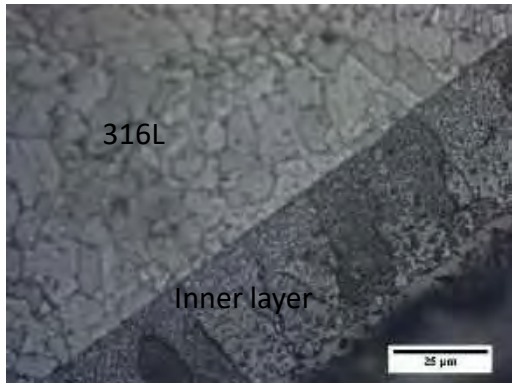

corroso

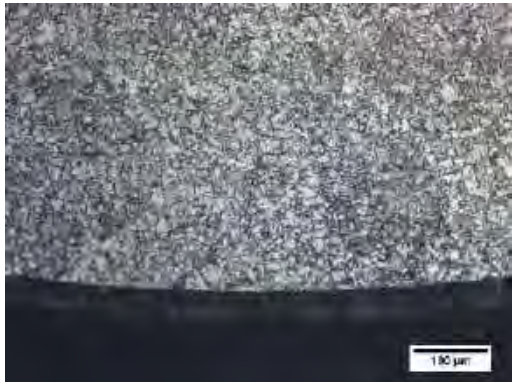

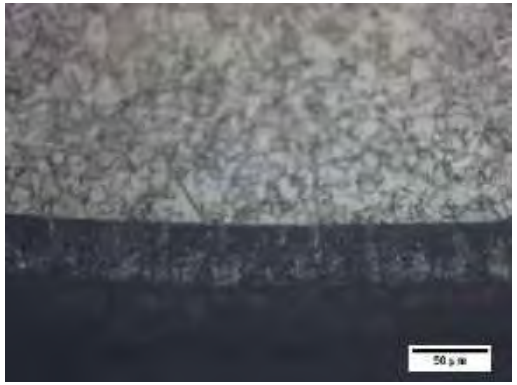

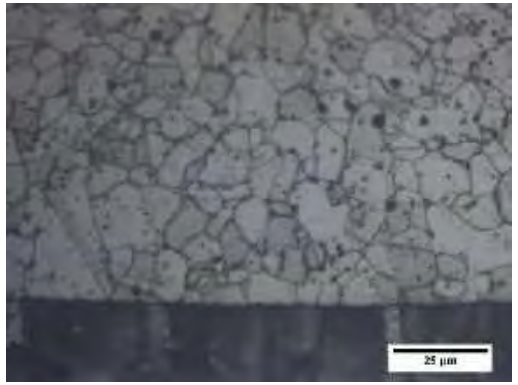

- Differente microstruttura outer layer e inner layer
- Inner layer → grana cristallina
- Outer layer → no grana cristallina

Microscopia ottica post attacco chimico

Neat

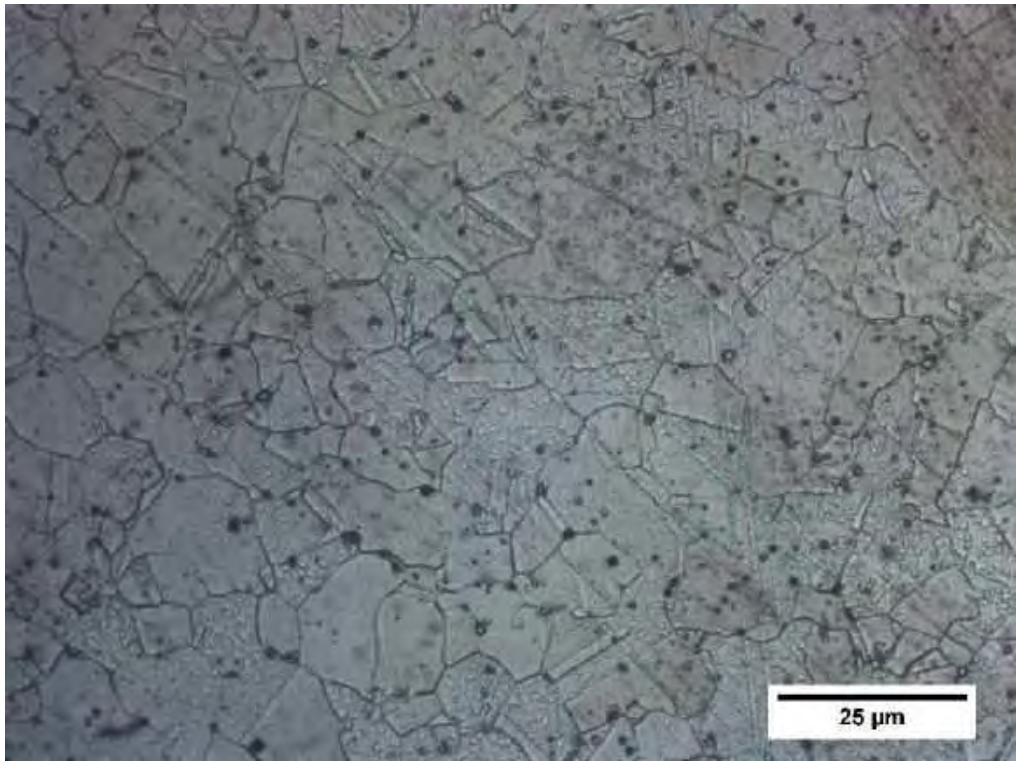

- ASTM grain number 10
- Dm grain 7 um

Corroso Pb

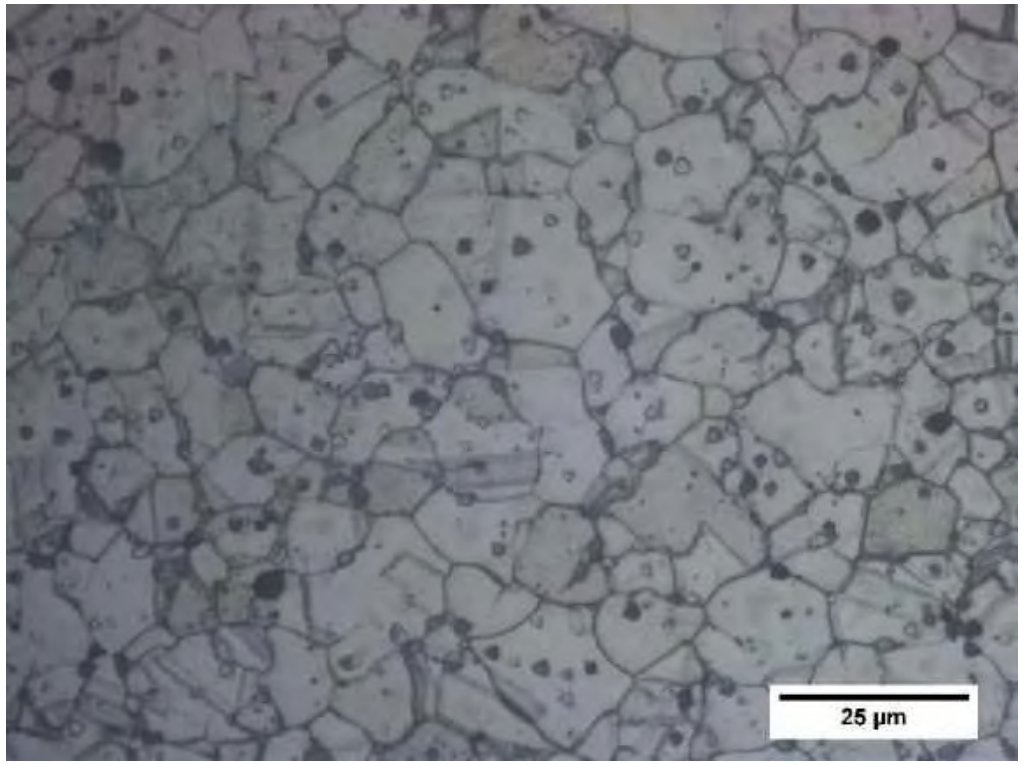

- ASTM grain number 10
- Dm grain 7,5 um

- Post Pb fuso → Leggero aumento dimensioni bordi di grano dell'acciaio, grani più regolari, bordi grano più smussati, assenza di geminati
- Probabili fenomeni di distensione

Microscopia elettronica a scansione (SEM)

Il microscopio elettronico a scansione (SEM) sfrutta la generazione di un fascio elettronico ad alta energia focalizzato e deflesso da un sistema di lenti nel vuoto per scansionare un'area del campione.
L'interazione fascio-campione genera elettroni secondari e retrodiffusi. Questi sono raccolti da opportuni detectors e convertiti in segnali elettrici. Tali segnali vengono amplificati ed elaborati da un computer fino a formare un'immagine a livelli di grigio.

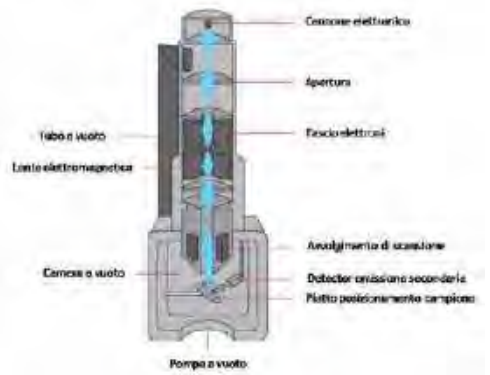

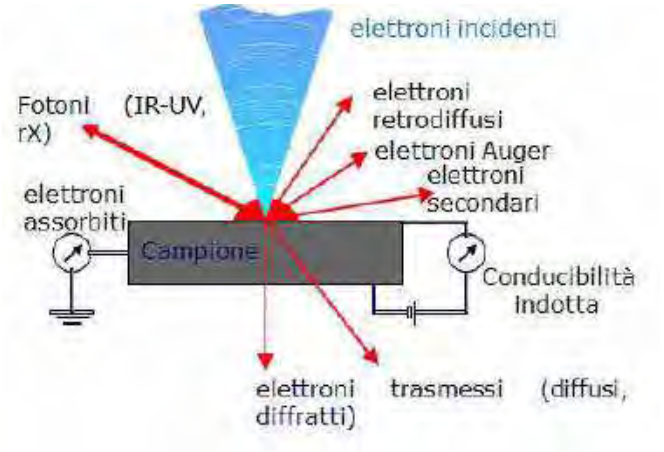

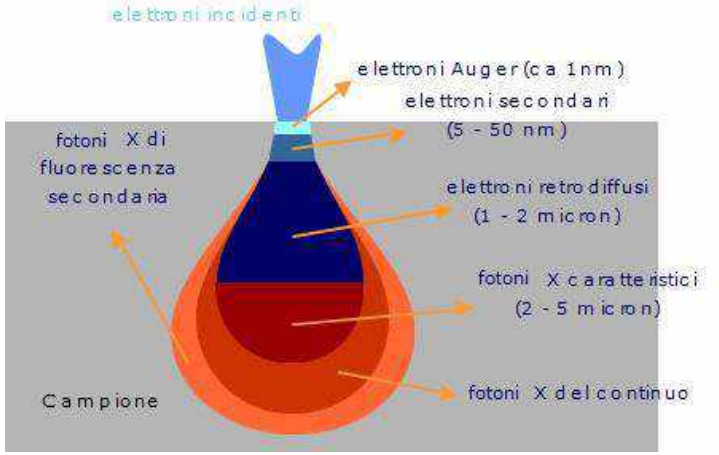

Permette:

- Analisi morfologica della superficie del campione
- Analisi delle sezioni dei provini (compattezza film dimensioni)
- Analisi Elementare EDS (**Energy Dispersive Spectroscopy)**

Microscopia SEM Neat

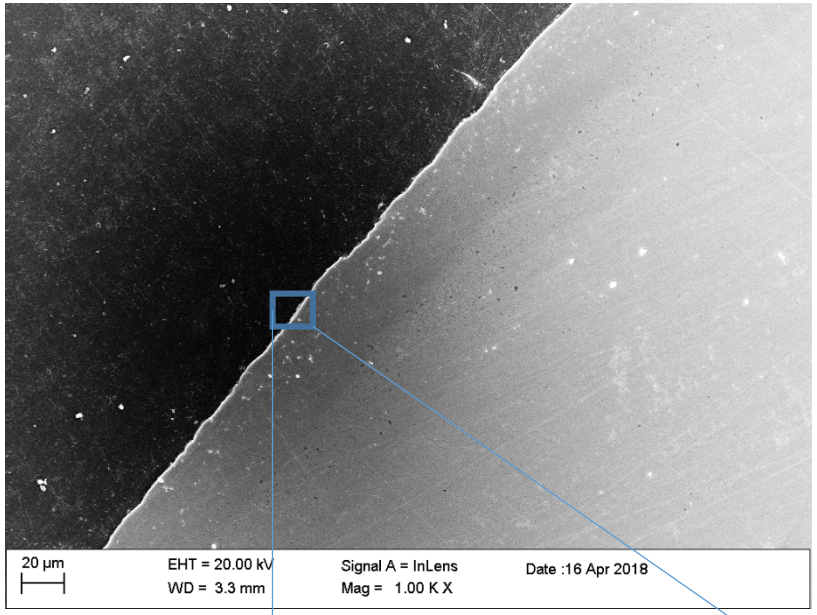

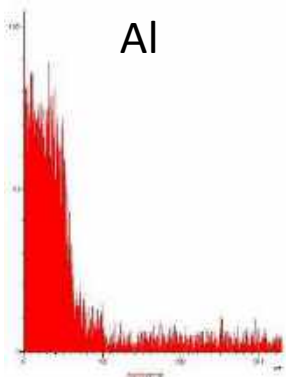

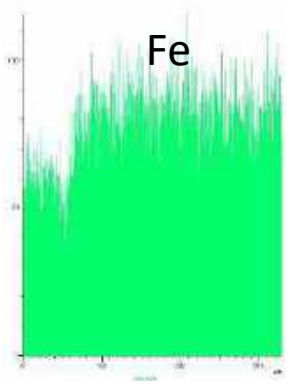

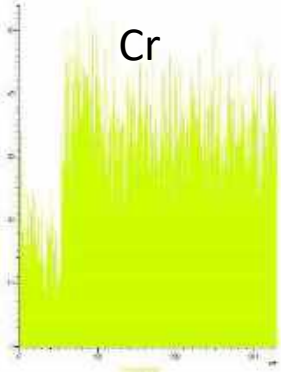

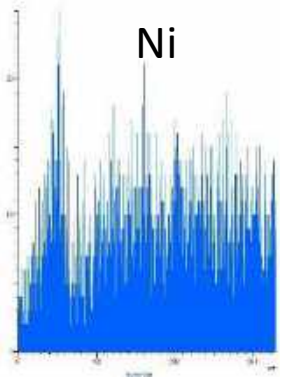

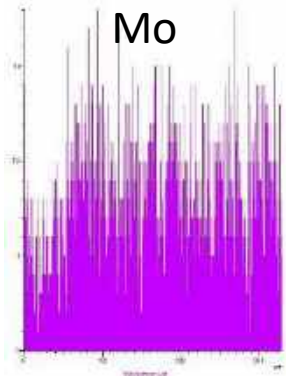

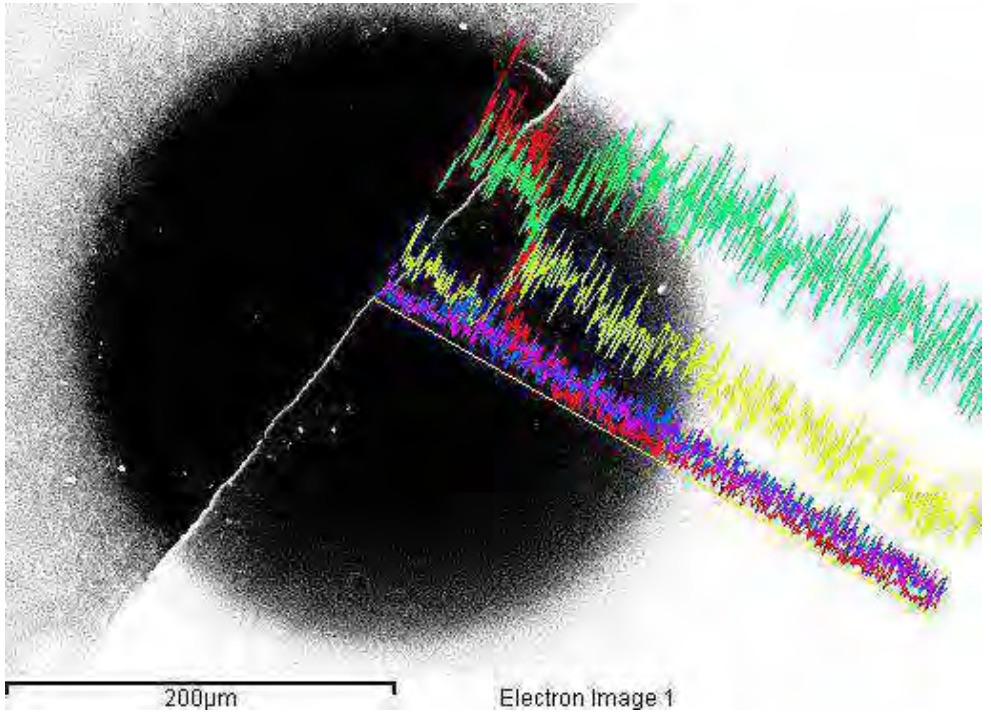

- Diffusion coating in FeCrAl
- Elevato contenuto di Al in outer e inner layer

Microscopia SEM Neat outer layer

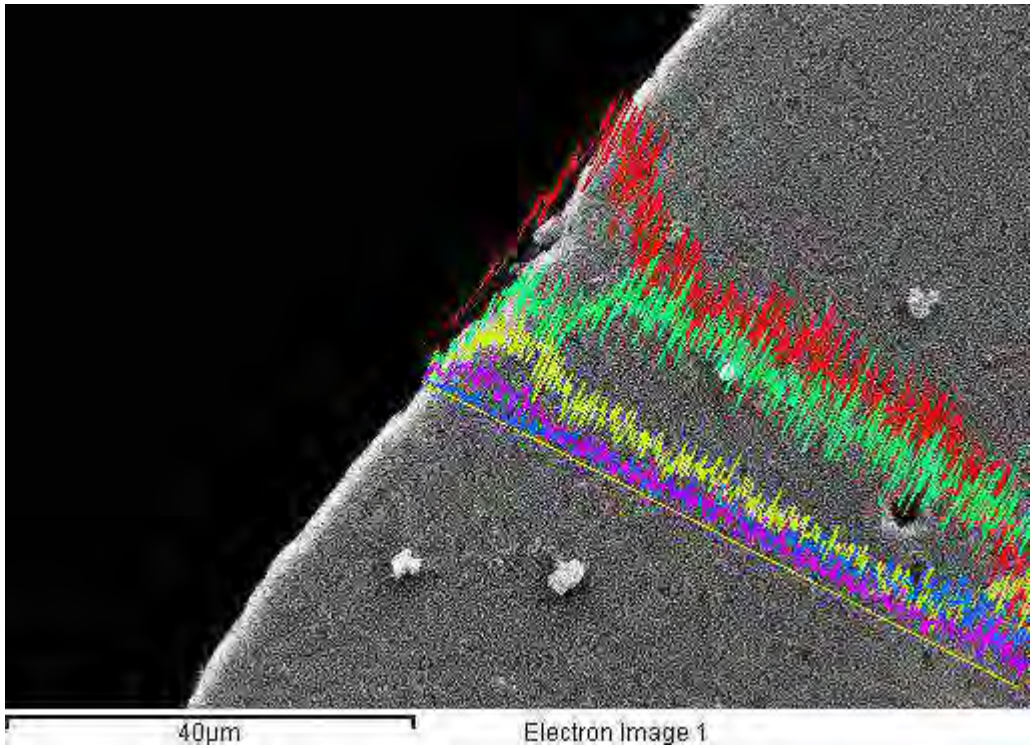

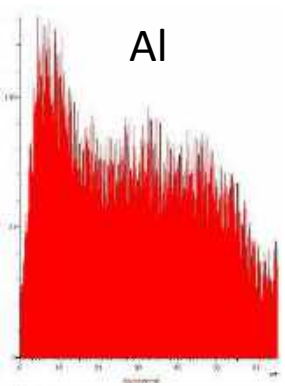

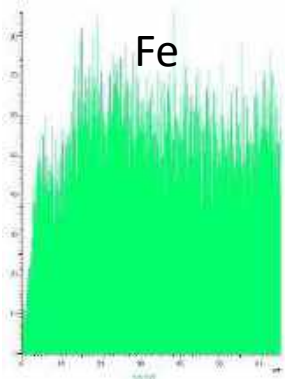

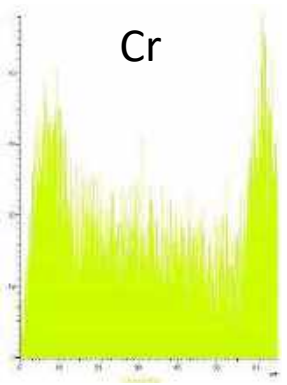

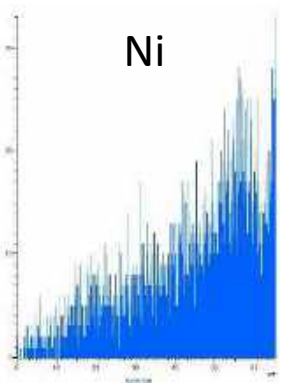

Strato esterno outer layer di circa 3-5 micron molto ricco in alluminio

Microscopia SEM Neat dopo attacco chimico

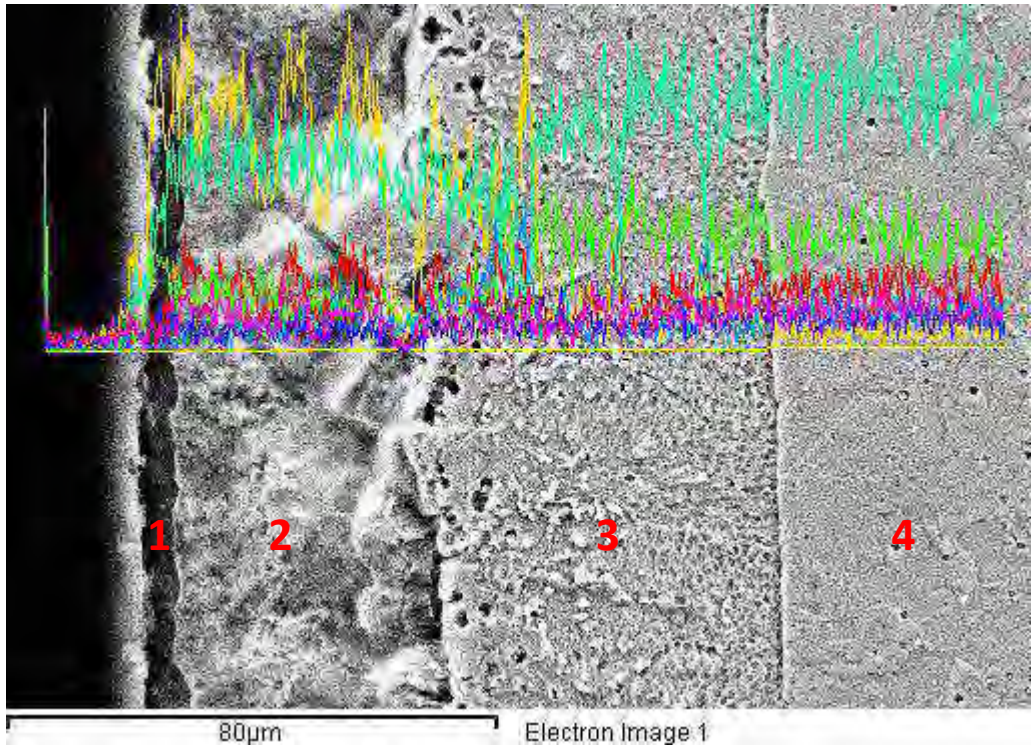

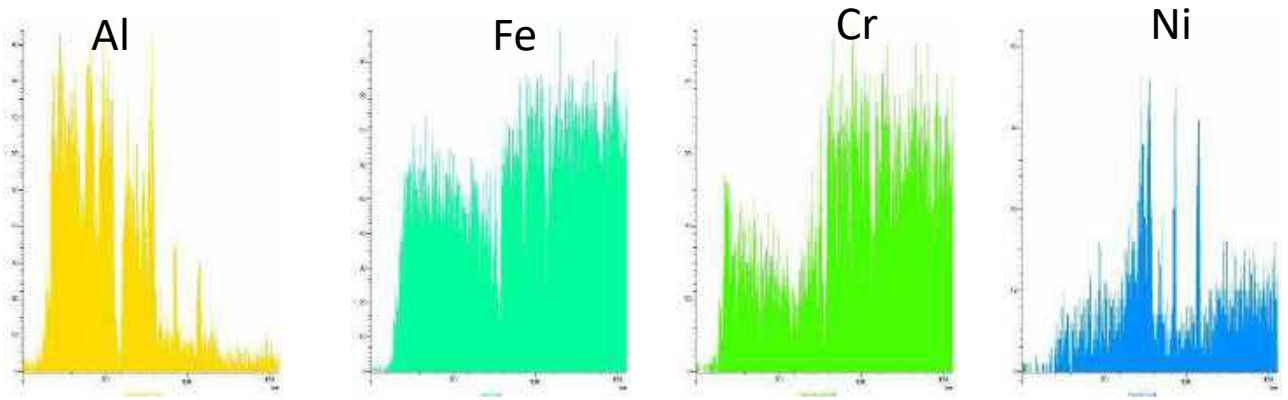

Rivestimento formato da 3 strati

1 layer esterno 3-5 micron
2 outer layer
3 inner layer
4 aisi 316 L

Microscopia SEM Neat attacco chimico

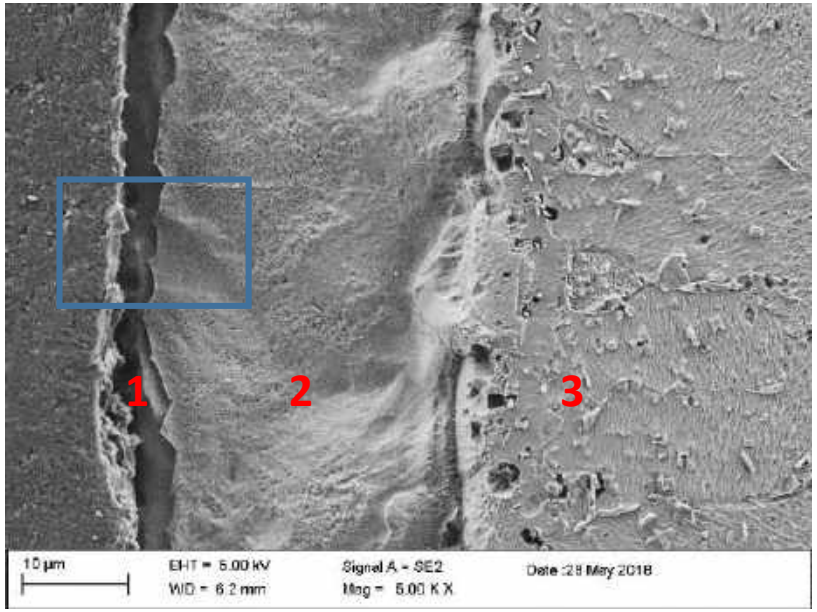

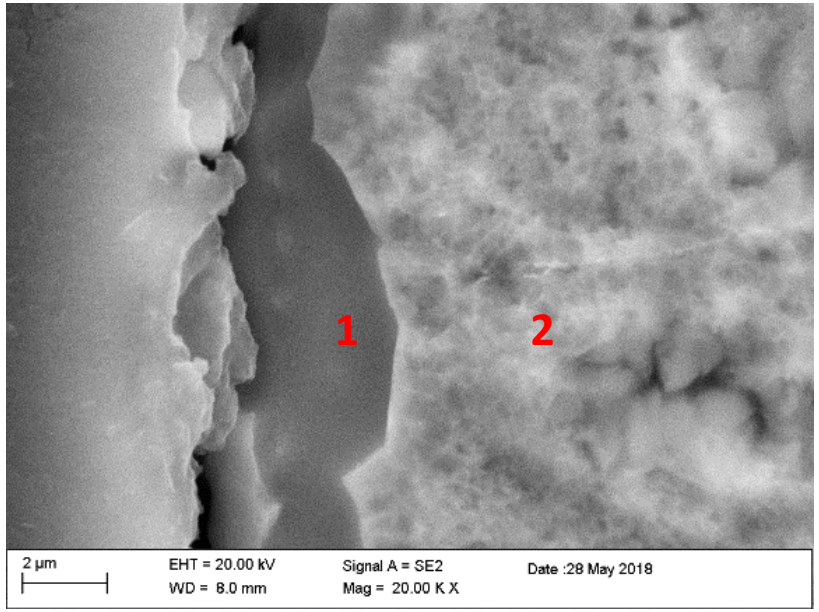

Università di Roma Tor Vergata

Element	Weight%	Atomic%
Al K	25.27	52.27
Cr K	11.37	12.21
Fe K	29.03	29.02
Mo L	2.14	1.24

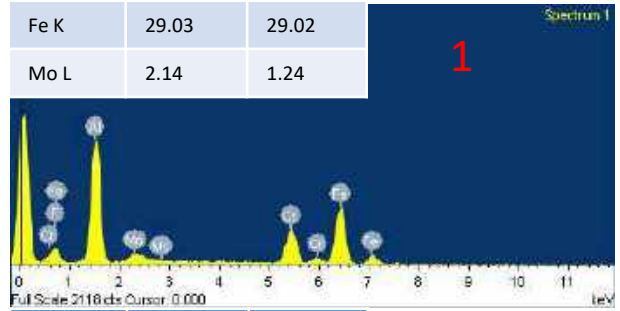

Element	Weight%	Atomic%
Al K	18.89	44.99
Cr K	6.52	8.06
Fe K	37.62	43.29
Ni K	2.79	3.05
Mo L	0.23	0.15

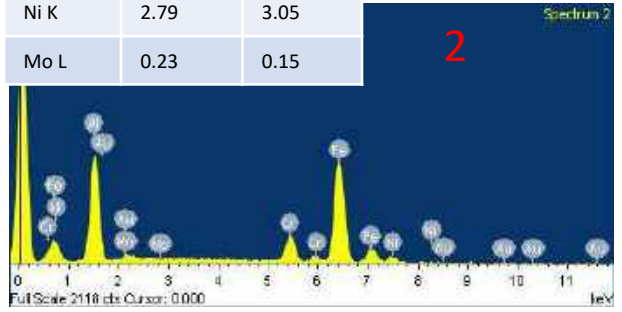

1 spessore 3 micron FeCrAl ad elevato tenore di Al

2 Outer layer FeCrAl spessore 30 micron

Microscopia SEM neat attacco chimico

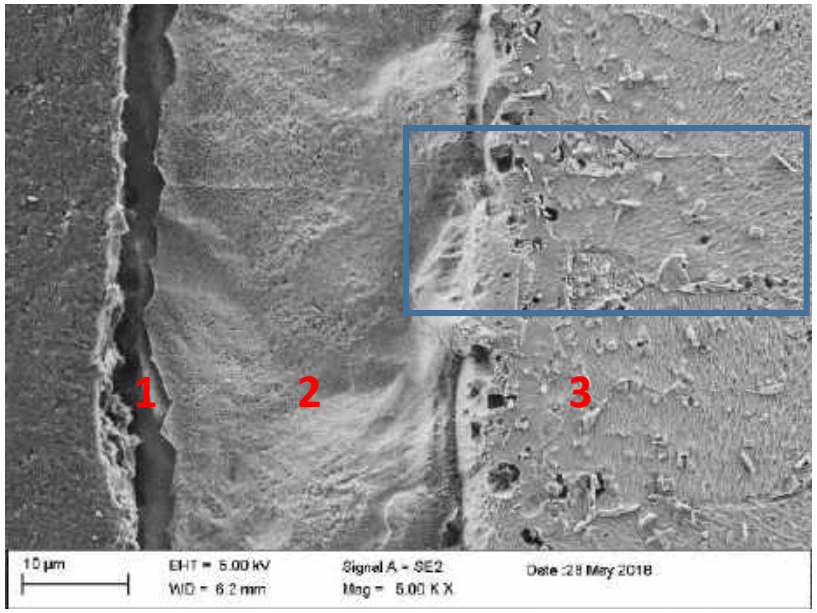

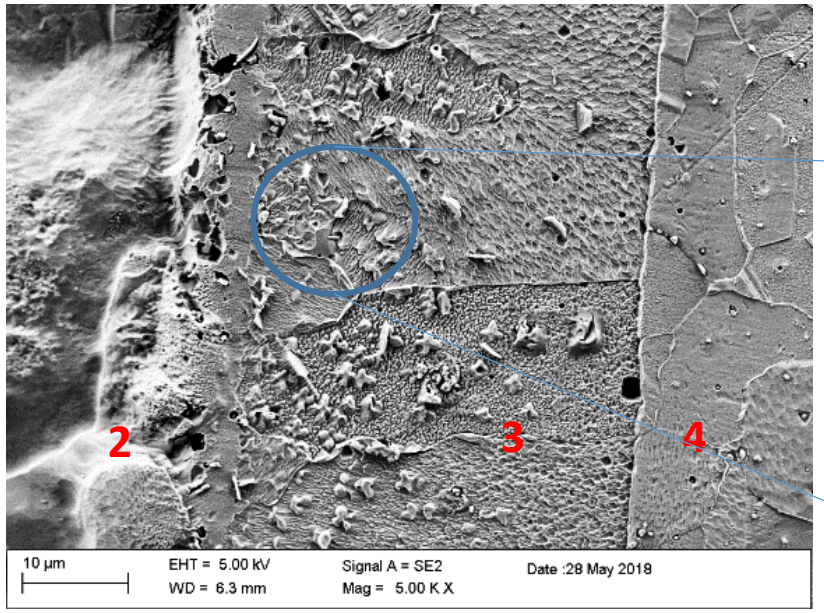

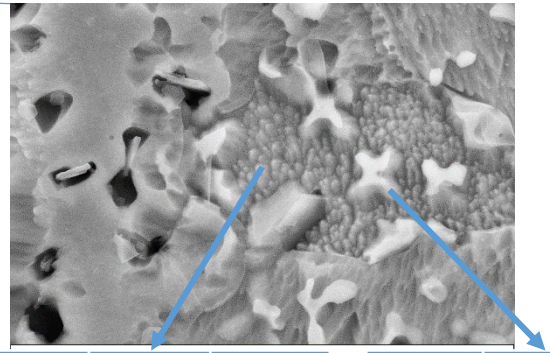

Element	Weight%	Atomic%
Al K	2.27	5.57
Cr K	16.04	20.43
Fe K	51.19	60.68
Ni K	2.81	3.17
Mo L	1.26	0.87

Element	Weight%	Atomic%
Al K	24.66	49.85
Cr K	4.34	4.55
Mn K	1.27	1.26
Fe K	17.14	16.74
Ni K	29.37	27.28
Mo L	0.56	0.32

Interfaccia 2-3 zona ricca in NiAl

3 inner layer grana cristallina definita spessore 40 micron; precipitati base NiAl immersi in matrice FeCr

4 substrato acciaio 316L

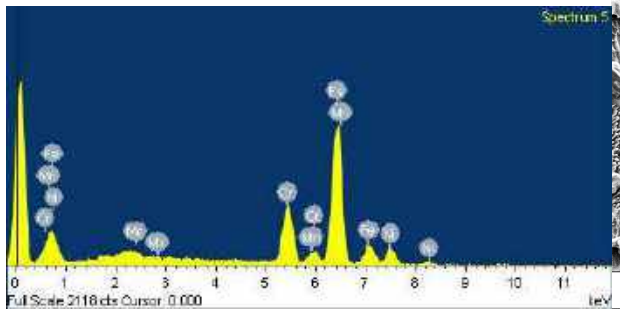

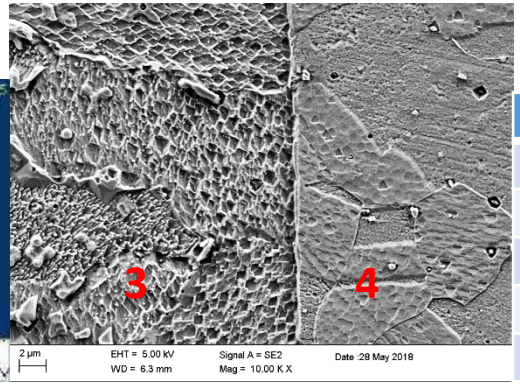

Element	Weight%	Atomic%
Cr K	12.17	18.82
Mn K	1.07	1.57
Fe K	46.96	67.61
Ni K	8.35	11.44
Mo L	0.69	0.57

Microscopia SEM neat attacco chimico

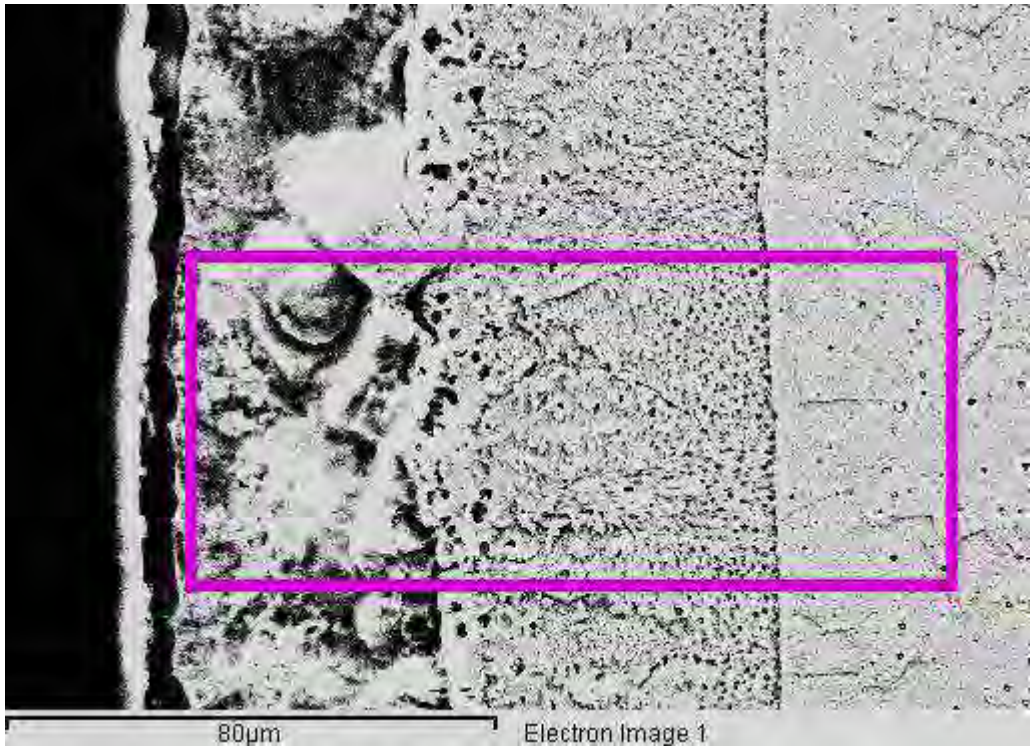

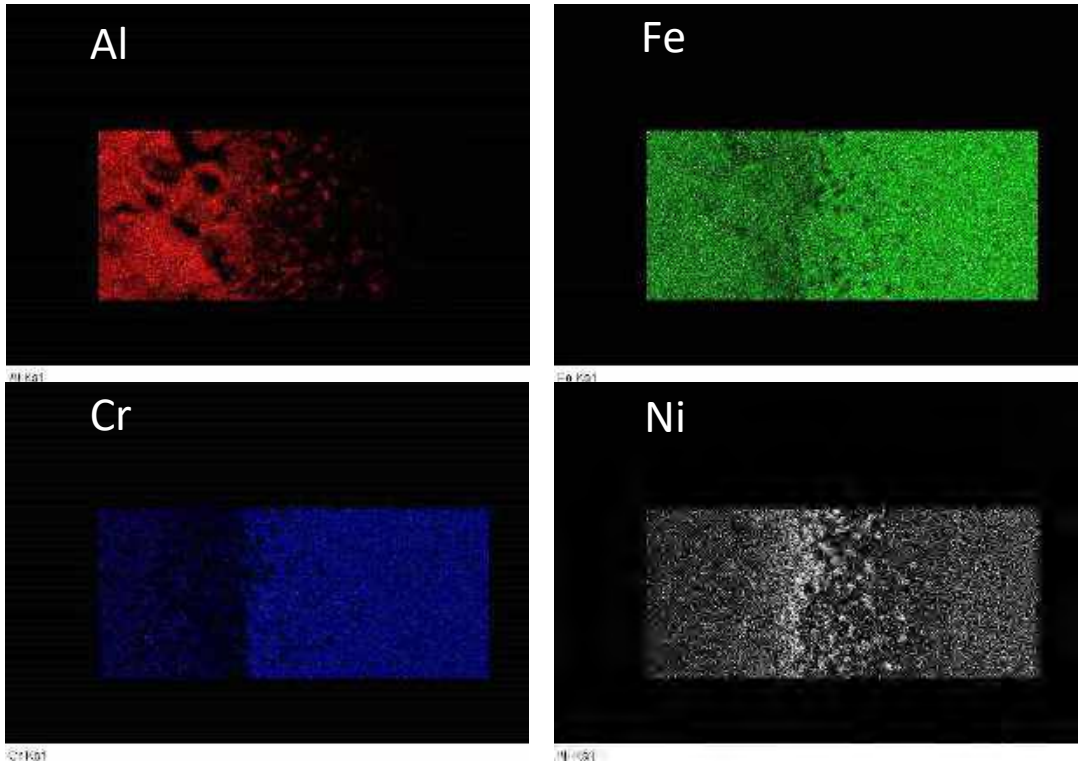

- Outer layer ricco in alluminio
- interfaccia outer-inner ricca in nickel
- Precipitati NiAl nell'inner layer immersi in matrice FeCr

Microscopia SEM provino corroso

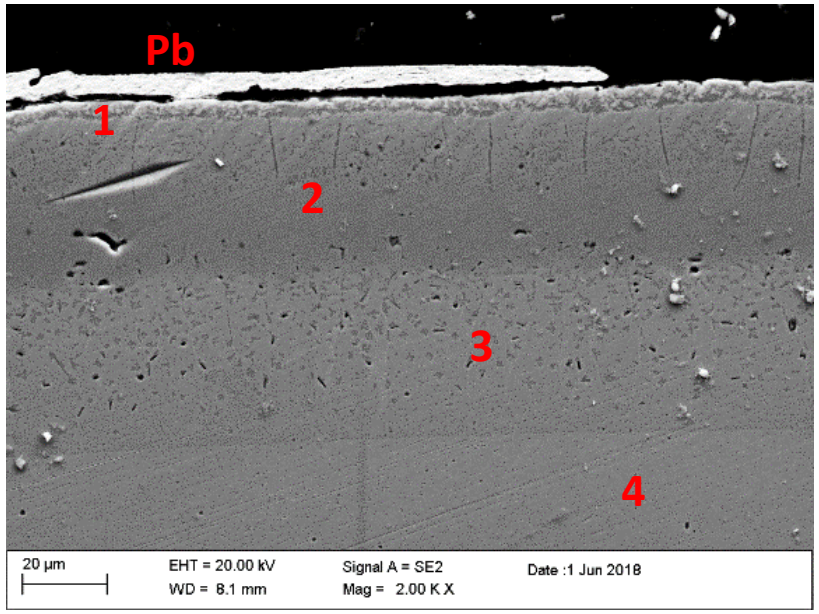

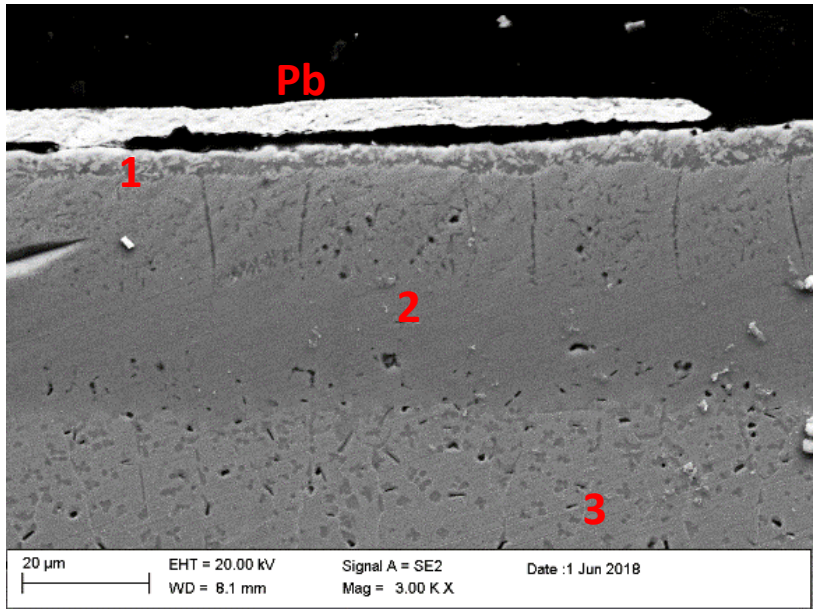

Mantenimento del diffusion coating dopo prove di corrosione in Pb fuso

1 layer esterno 3 micron
2 outer layer
3 inner layer
4 aisi 316L

Microscopia SEM provino corroso

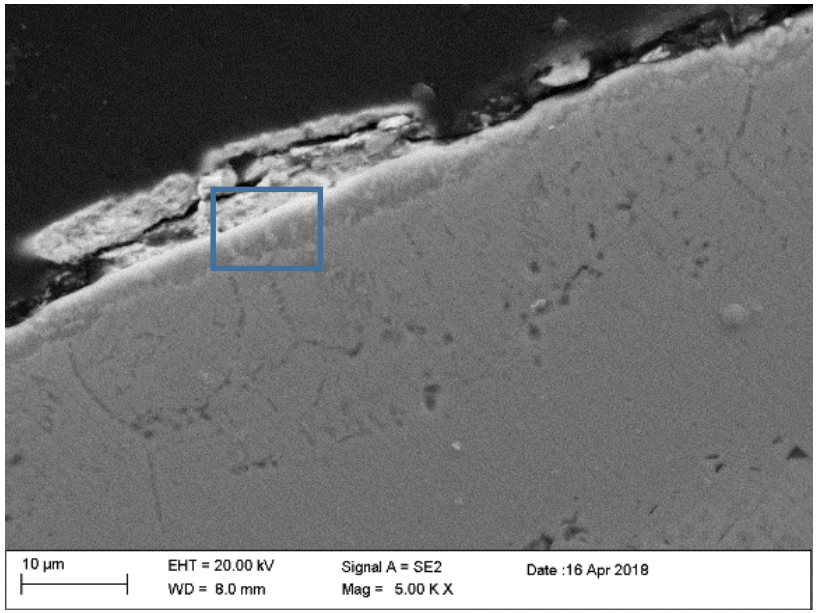

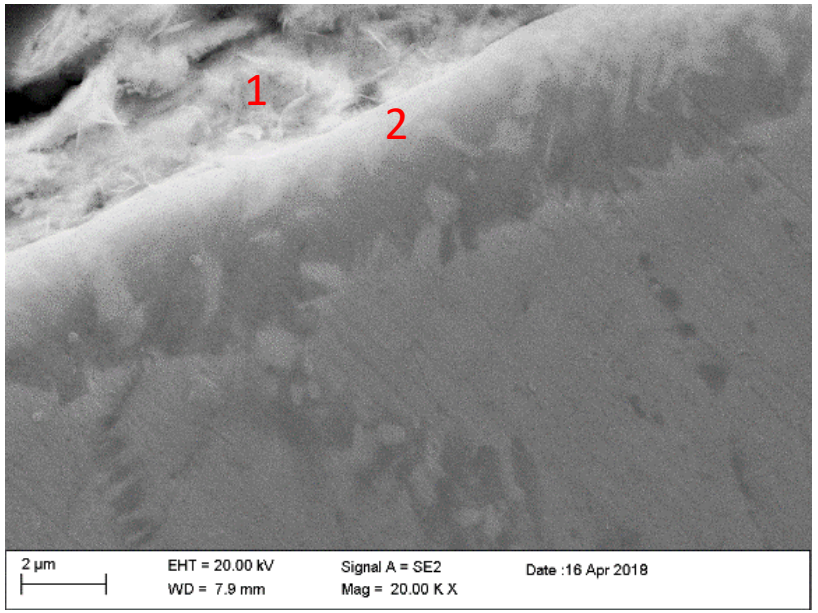

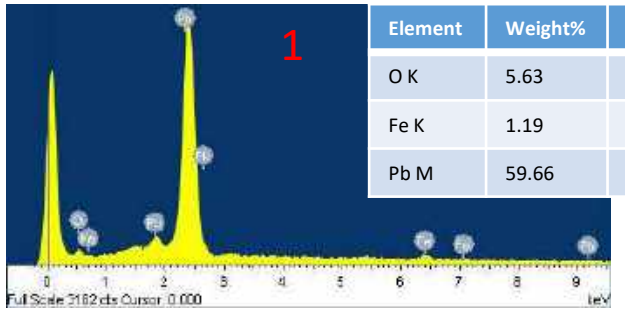

Element	Weight%	Atomic%
O K	5.63	53.21
Fe K	1.19	3.23
Pb M	59.66	43.56

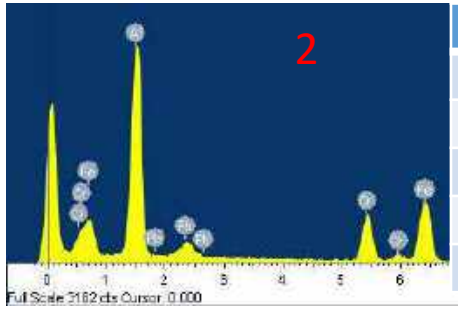

Element	Weight%	Atomic%
O K	4.06	10.87
Al K	34.81	55.23
Cr K	14.66	12.07
Fe K	27.25	20.90
Pb M	4.50	0.93

No formazione scaglia di ossido di alluminio

1 Residuo del bagno di piombo (elevato tenore di ossigeno probabile ossido di piombo)

2 Tracce di piombo nei primi micron superficiali

Microscopia SEM provino corroso in Pb

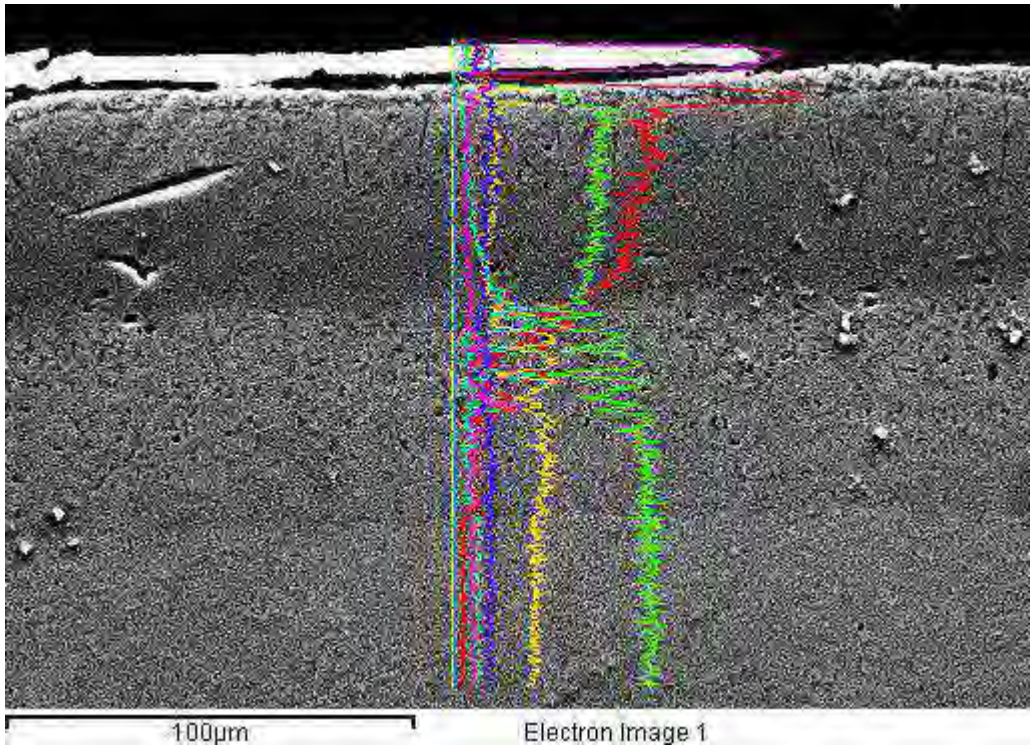

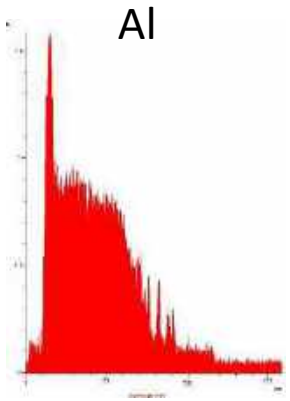

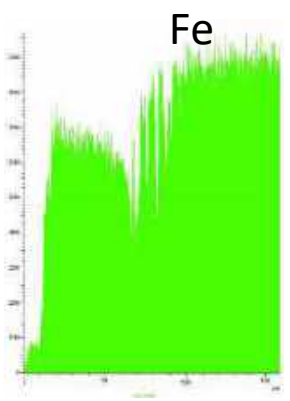

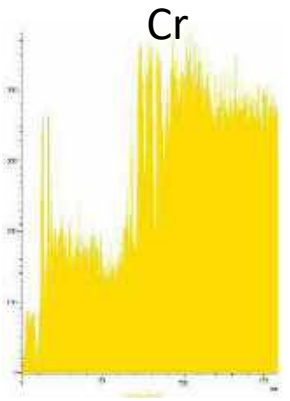

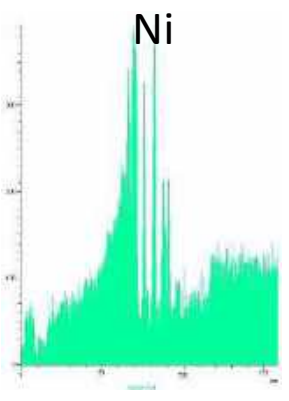

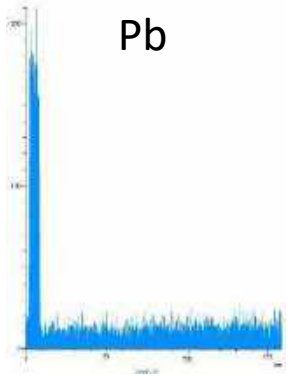

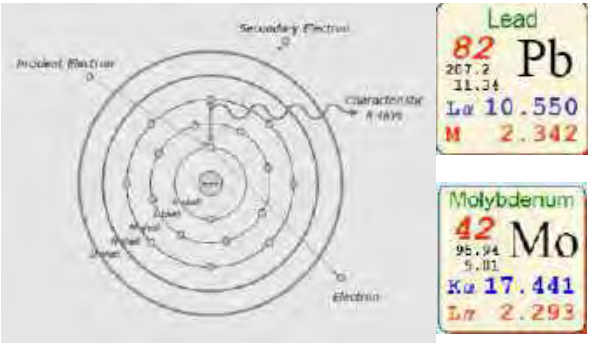

Rivestimento rimane inalterato in termini compositivi dopo il test in Pb fuso
Piombo assente lungo l'intera sezione investigata → no diffusione nel rivestimento

Da notare che il livello energetico Lα del Mo è sovrapponibile al livello energetico M del Pb

Microscopia SEM provino corroso in Pb, attacco chimico

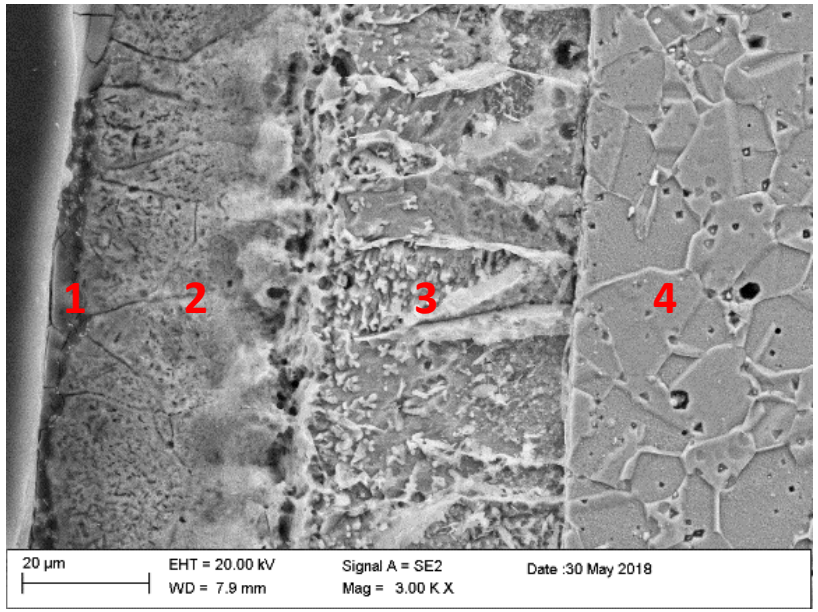

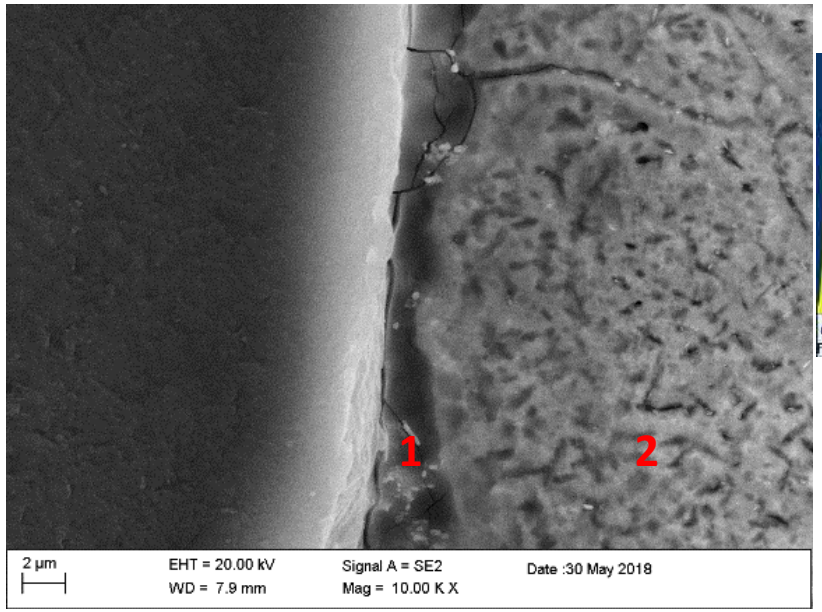

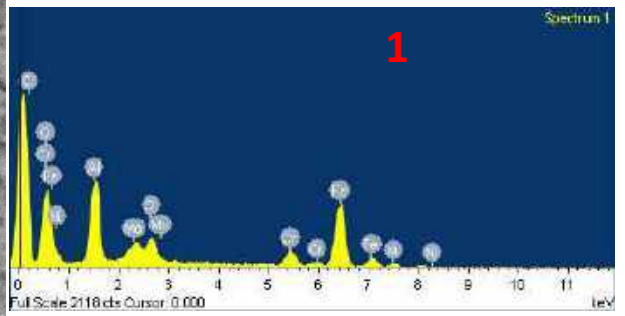

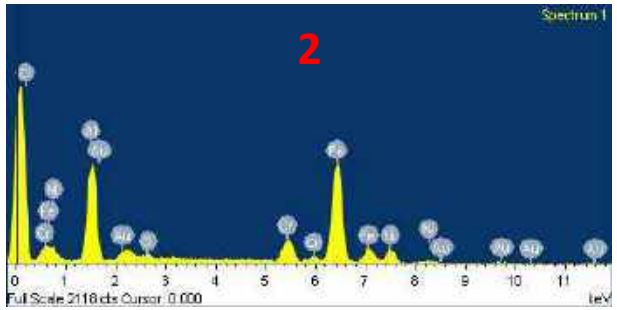

Gli spessori dei layer rimangono inalterati dopo corrosione in Pb

1 spessore 3-5 micron
2 outer layer 30-35 micron
3 inner layer 40-45 micron

No evidenti variazioni composizione chimica dei layer

Microscopia SEM provino corroso in Pb, attacco chimico

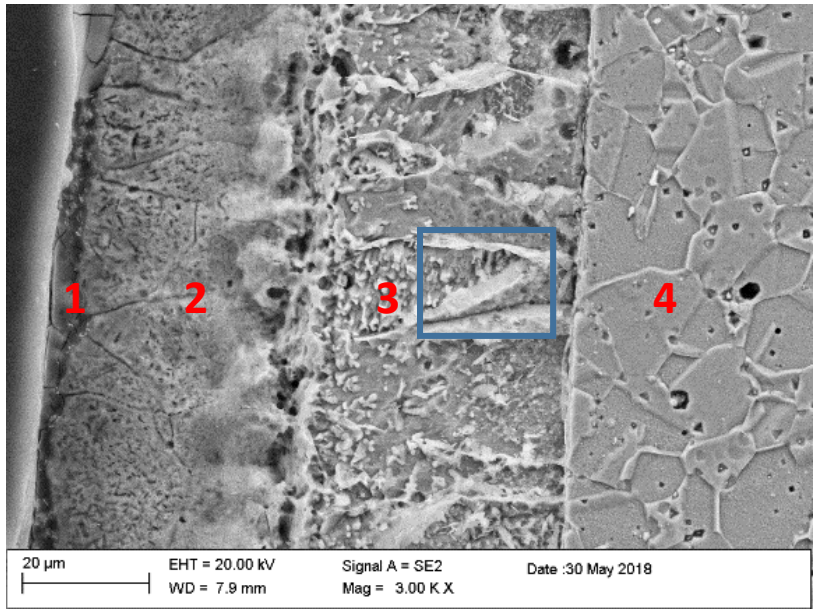

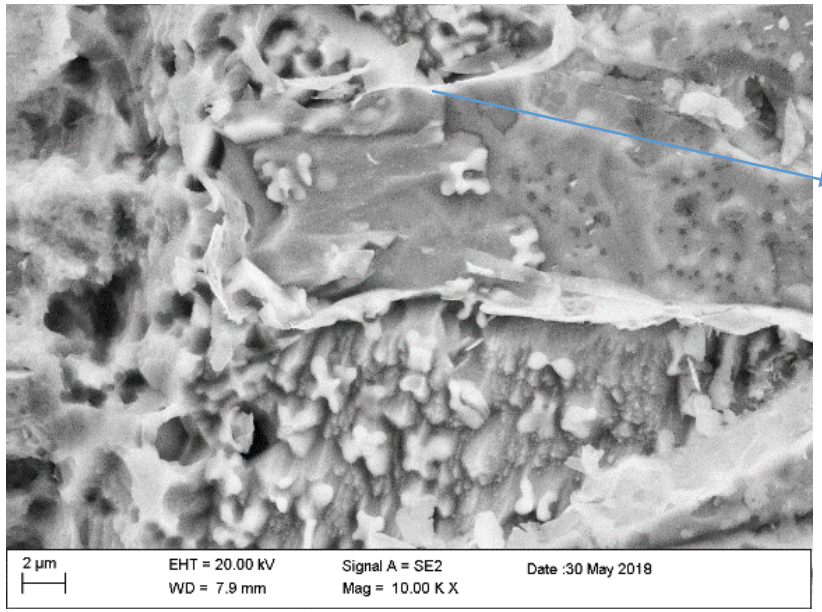

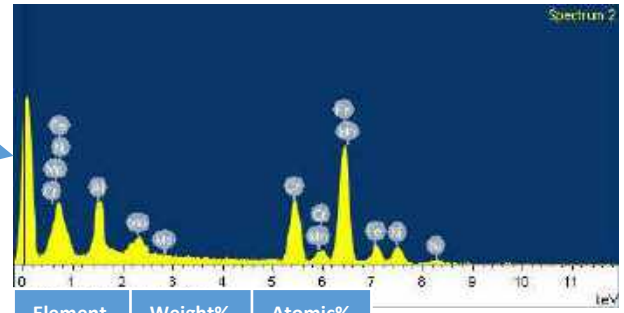

Element	Weight%	Atomic%
Al K	8.93	22.32
Cr K	13.68	17.74
Mn K	0.94	1.15
Fe K	39.20	47.34
Ni K	8.12	9.33
Mo L	3.01	2.12

Inner layer stessa morfologia e composizione chimica prima e dopo corrosione in Pb.

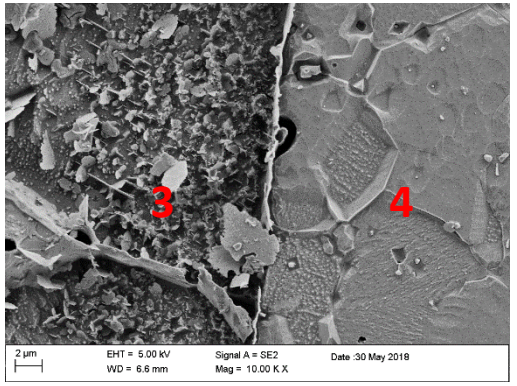

Element	Weight%	Atomic%
Cr K	95.30	18.39
Mn K	8.63	1.58
Fe K	374.50	67.30
Ni K	61.65	10.54
Mo L	9.72	1.02

Microdurezza Vickers e Knoop

Durezza: resistenza di un materiale alla deformazione plastica localizzata.

Microdurezza Vickers/ Knoop: utilizzata per la caratterizzazione di materiali molto duri e tipicamente per il controllo dei trattamenti superficiali.

Modalità di prova: **ISO 6507-1:2005**

- ✓ Penetratore Vickers/Knoop compresso ortogonalmente contro la superficie del provino applicando un determinato carico per un tempo stabilito.
- ✓ Rimozione dell'indentatore.
- ✓ Misura delle diagonali dell'impronta tramite microscopio ottico.
- ✓ Calcolo della durezza.

$$HV = \frac{P}{S} = 0.102 \frac{P \cdot sen(\frac{136°}{2})}{d^2}$$

$$HK = \frac{P}{A_{PAC}} = \frac{P}{L^2} \frac{2 \cdot tg\theta}{tg\varphi} \quad \left(= 14.229 \cdot \frac{P}{L^2} \right)$$

Condizioni di prova:

- •Indentatore Vickers/Knoop
- •Carichi: 300 - 50 g
- •Tempo: 30 s

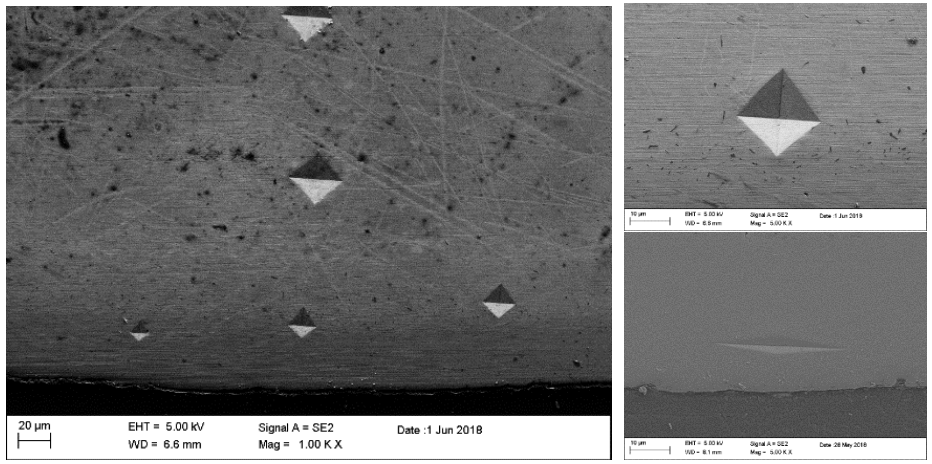

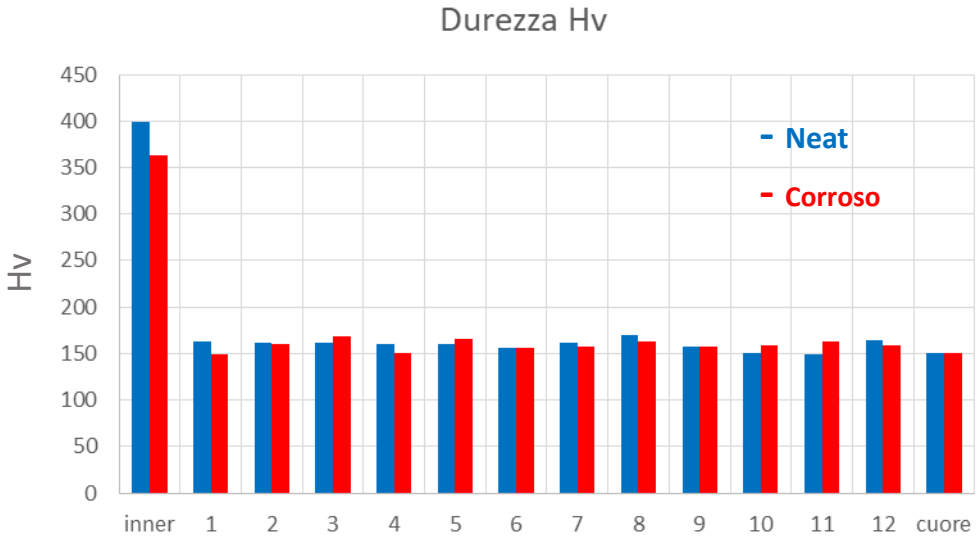

Durezza knoop outer layer

- Neat : 1150 ± 54Hk
- Corroso: 1030 ± 60 Hk

No significative variazioni di durezza dopo esposizione Pb

Conclusioni

Sono stati caratterizzati diffusion coating su AISI 316L esposti in bagno di Pb fuso 550°C con concentrazione di Ossigeno pari a 10^{-3} % wt

- I diffusion coating FeCrAl analizzati risultano uniformi omogenei e compatti
- Tre differenti zone all'interno del diffusion coating
- Lieve modifica delle dimensioni dei grani dopo esposizione Pb
- No alterazioni del rivestimento dopo esposizione a Pb
- No formazione di scaglia ossido di alluminio durante esposizione Pb
- No variazione durezza superficiale e a cuore dopo corrosione

To do:

Analisi XRD ed identificazione delle fasi cristalline che compongono il diffusion coating a convalida dell'ipotesi di non avvenuta corrosione
Caratterizzazione diffusion coating esoposti in Pb (550°C concentrazione ossigeno 10^{-8} % wt)

Tesi e pubblicazioni

Alessandro Merli
"Caratterizzazione microstrutturale meccanica e tribologica di rivestimenti PLD in allumina su acciai inox per applicazioni nucleari"
Laurea in Ingegneria Meccanica

Fabrizio Mario Ferrarese
"Caratterizzazione di film ceramici sottili per applicazioni nei reattori nucleari di quarta generazione"
Laurea in Scienza dei Materiali

Emanuele Rossi
"Caratterizzazione di rivestimenti FeCrAlY HVOF per applicazioni nei reattori nucleari di quarta generazione"
Laurea in Ingegneria Meccanica

Mario Bragaglia
"Caratterizzazione di materiali strutturali ricoperti per applicazioni nucleari"
Dottorato di Ricerca in Ingegneria Industriale

Paper Corrosion Science 2017
Radiation tolerant nanoceramic coatings for lead fast reactor nuclear fuel cladding
F. García Ferré, A. Mairov, M. Vanazzi, S. Bassini, M. Utili, M. Tarantino, M. Bragaglia, F.R. Lamastra, F. Nanni, L. Ceseracciu, Y. Serruys, P. Trocellier, L. Beck, K. Sridharan, M.G. Beghi and F. Di Fonzo

WORKSHOP TEMATICO

ACCORDO DI PROGRAMMA MISE – ENEA
PAR2017 – PROGETTO B.3 - LP2

GENERATION IV
LEAD COOLED FAST REACTOR
STATO ATTUALE DELLA TECNOLOGIA E PROSPETTIVE DI SVILUPPO

ADP MiSE-ENEA (PAR2017-LP2)

Dipartimento di Ingegneria Astronautica, Elettrica ed Energetica Università di Roma "La Sapienza"
San Pietro in Vincoli, Via Eudossiana 18
14-15 Giugno 2018

Coating mechanical characterization

M. Bragaglia, F.R. Lamastra, F. Franceschetti; F. Nanni

CONTATTI:
Dipartimento di Ingegneria Impresa
Università di Roma "Tor Vergata"
Via del Politecnico, 1, 00133 Roma -Italia
Tel +39-06.7259.4496 - Fax +39-06.7259.4328

Italian National Agency for New Technologies,
Energy and Sustainable Economic Development

Coolant chemistry control study for HLM systems

ADP MiSE-ENEA (PAR2017-LP2)

Dipartimento di Ingegneria Astronautica, Elettrica ed Energetica
Università di Roma "La Sapienza"

14-15 Giugno 2018

S. Bassini, A. Antonelli, G. Fasano (ENEA FSN-ING-TESP)
serena.bassini@enea.it

CHEMISTRY OF HLM (LEAD AND LBE)

Slag deposit in the circuit during circulation pump tests

Slag deposit in heat exchanger

plugging in Pb-Bi cooled K-27 Russian Nuclear Submarine in 1960'

oxygen balancing for steel passivation and to avoid PbO formation: need of <u>oxygen sensors</u> and <u>oxygen control devices</u>

$$Pb_{liq} + O_{diss} \leftrightarrow PbO_{diss}$$

Oxygen saturation and PbO deposition

documento non esiste testo dello stile specificato.1

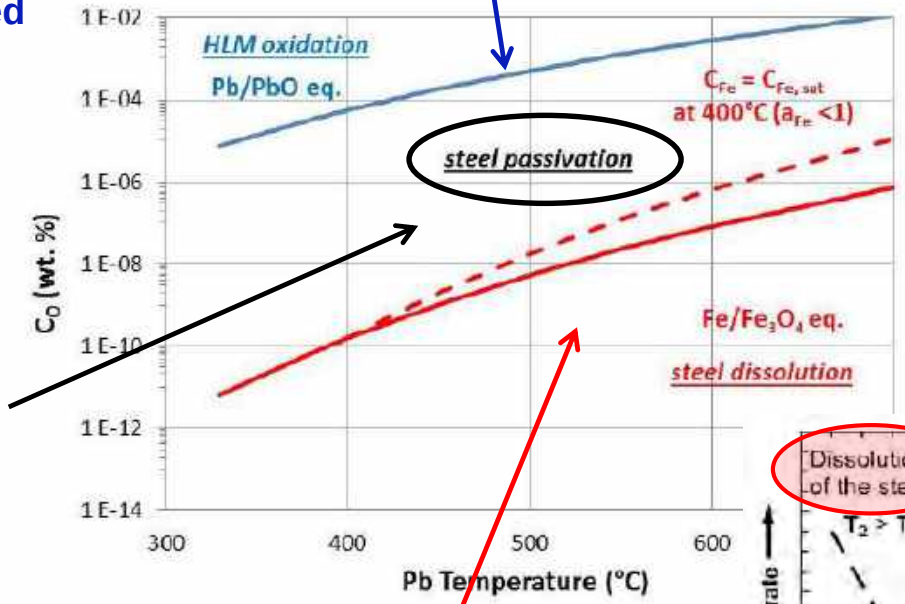

Steel corrosion at low oxygen content

Ni and Cr dissolution in 316L steel. Flowing LBE, 450°C, 10⁻⁶ wt% O_2, 1500 h.

Benamati et al., J Nucl Mater 335 (2004) 169-173.

C. Schroer, Nucl Eng Des, 241 (2011) 4913-4923.

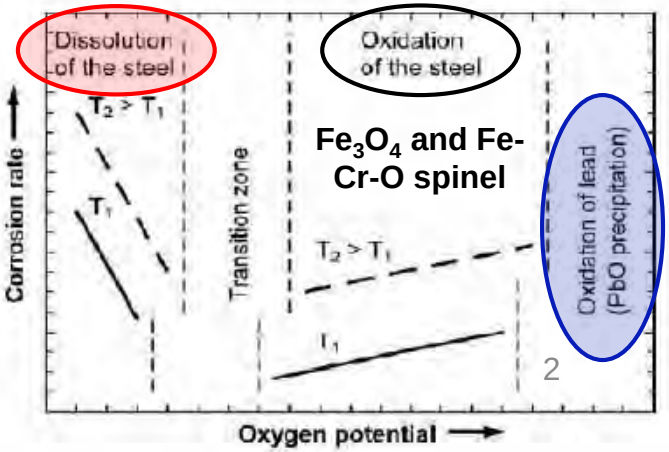

POTENTIOMETRIC OXYGEN SENSORS FOR HLM (lab scale)

potentiometric sensor

$$E_{th} = \frac{RT}{4F} \cdot ln \frac{p_{O_2(ref)}}{p_{O_2(Pb,LBE)}}$$

well-known (reference system)

to be evaluated (working system)

+ ceramic solid electrolyte for O^{2-} conduction (Yttria Stabilized Zirconia)

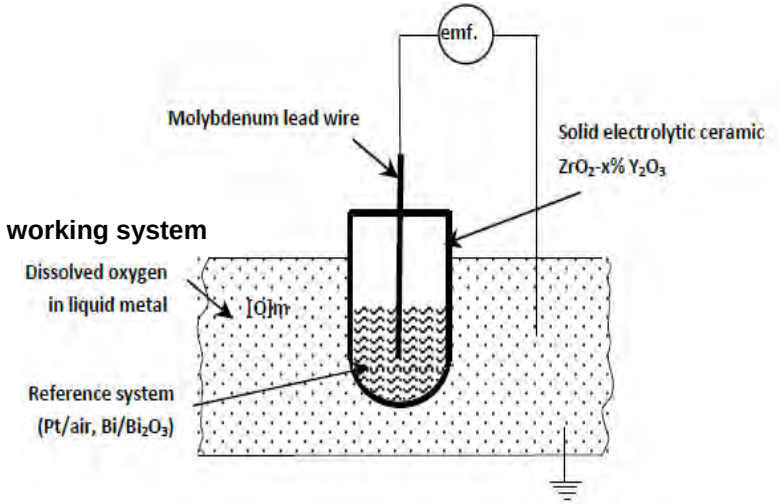

set-up for oxygen sensor testing

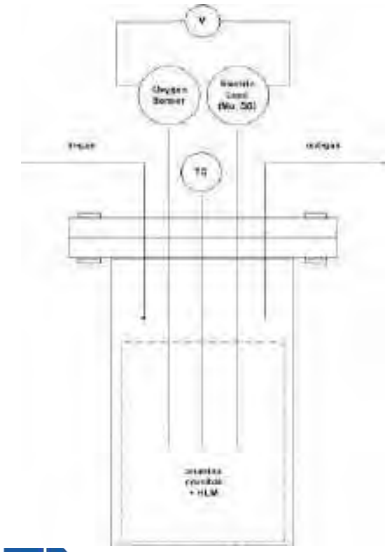

V = high-impedance voltmeter
In-gas = flowing argon

Reference systems:
Pt-air, Bi/Bi_2O_3, Cu/Cu_2O
Solid electrolytes:
YPSZ and YTSZ

Calibration at oxygen saturation

Comparison of the experimental potential (E_{exp}) with the theoretical potential (E_{th}) expected in oxygen-saturated HLM at different T_{HLM}.

STUDY OF REFERENCE SYSTEM: AIR + STUDY OF SOLID ELECTROLYTE: YTSZ & YPSZ

RACHEL Lab

Influence of the reference and solid electrolyte on the min. reading temperature

Pt-Air

YPSZ = Yttria Partially Stabilized Zirconia
5 % mol of yttria
YTSZ = Yttria Totally Stabilized Zirconia
8 % mol of yttria

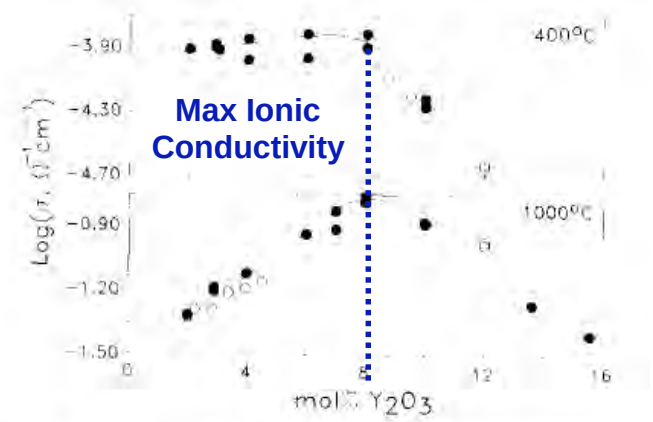

Fig. 2. Conductivity variation as a function of dopant content in Y_2O_3–ZrO_2. (○) single grain, (●) polycrystalline specimens.

S.P.S. Badwal, Solid State Ionics 52 (1992) 23-32.

Pt-air + YPSZ sensor reading down to 400◦C

Pt-air + YTSZ sensor reading down to 350◦C

<u>ionic conductivity</u>: YTSZ > YPSZ

but <u>mechanical strength</u>: YTSZ < YPSZ

S. Bassini et al., J. Nucl. Mater. 486 (2017) 197-205.

STUDY OF REFERENCE SYSTEMS: M/M_xO_y

Influence of the reference on the min. reading temperature

S. Bassini et al., J. Nucl. Mater. 486 (2017) 197-205.

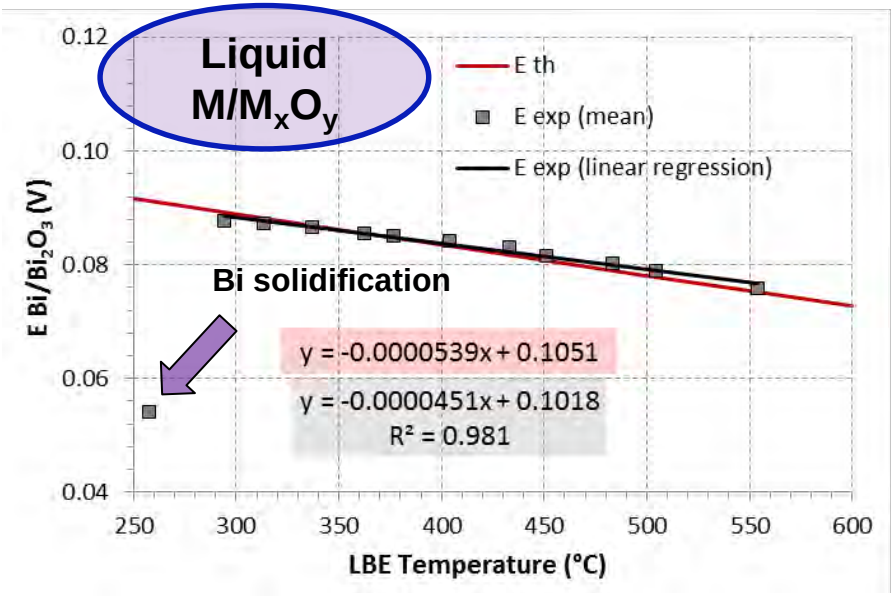

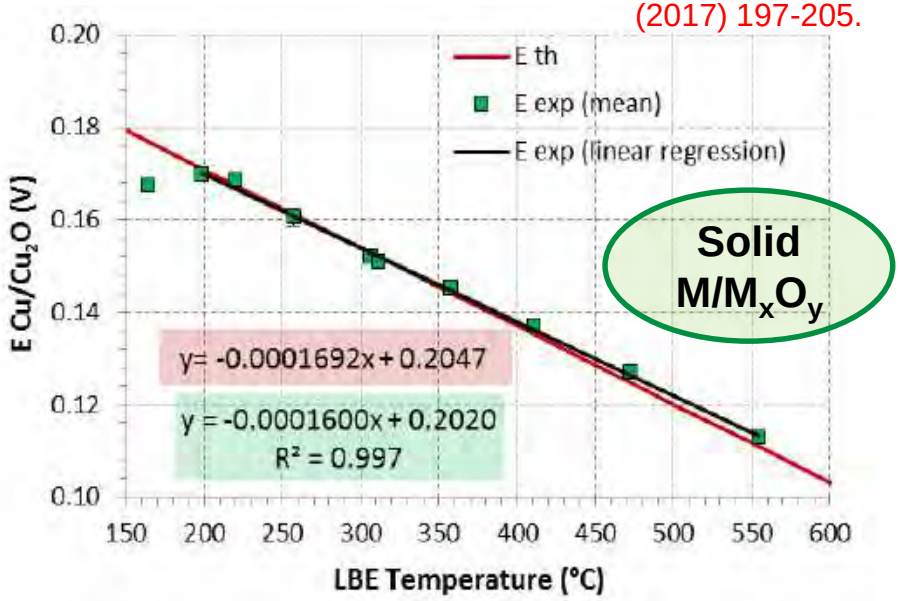

Bi/Bi_2O_3
Min. reading T ≈ 290◦C; tendency to crack due to Bi volume variation ($T_{m,Bi}$ =271◦C)

Cu/Cu_2O
Min. reading T ≈ 200◦C; tendency to powders sintering in the long-term ($T_{m,Cu}$ =1085◦C)

OXYGEN SENSOR FOR LOOPS

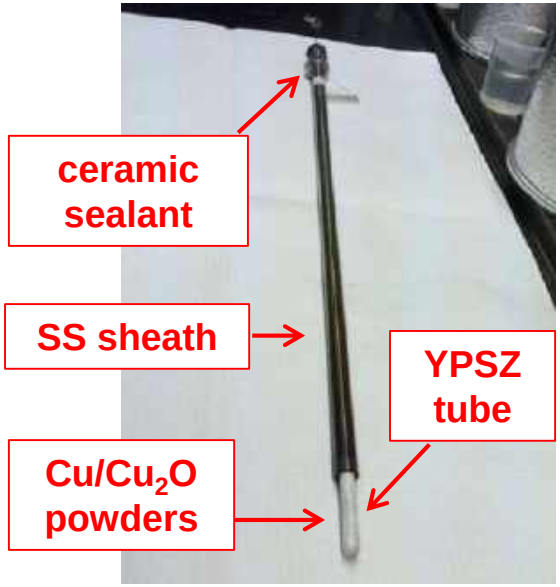

Cu/Cu_2O sensor for NACIE-UP loop (LBE)
L= 600 mm
Position: expansion vessel,
T=200-400◦C

Min. reading T ≈ 200◦C
(but powder sintering)

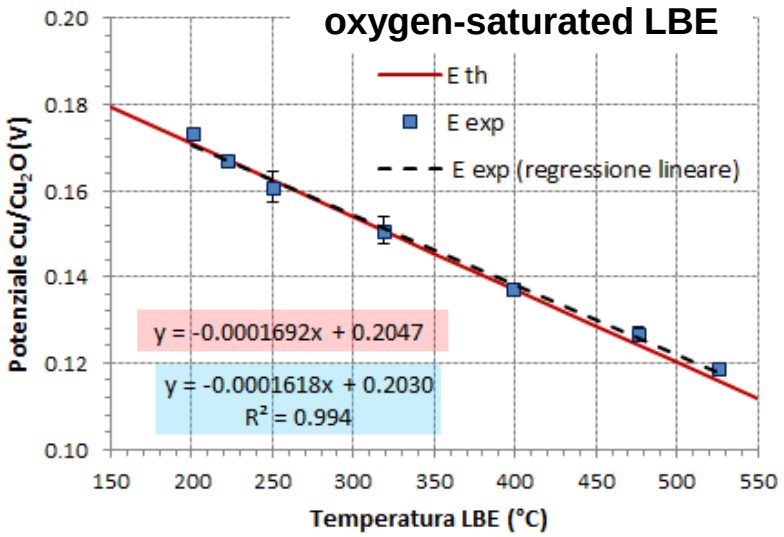

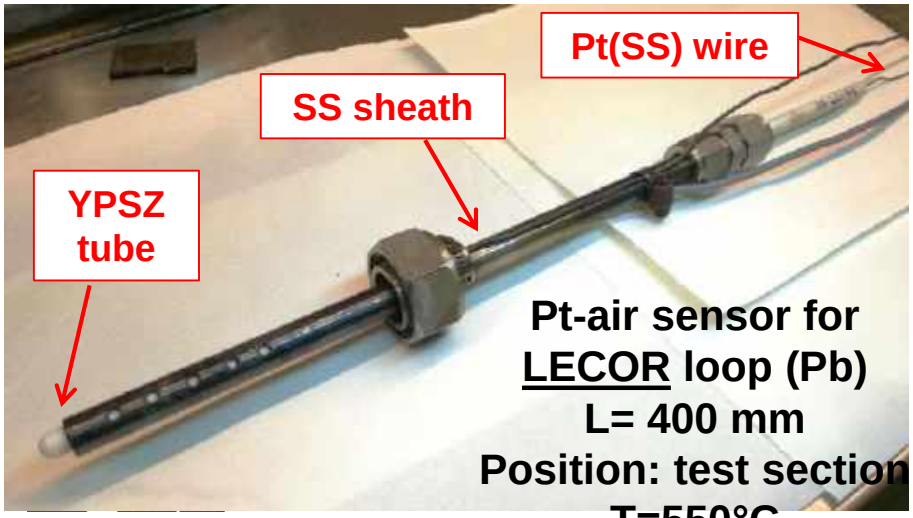

Pt-air sensor for LECOR loop (Pb)
L= 400 mm
Position: test section
T=550°C

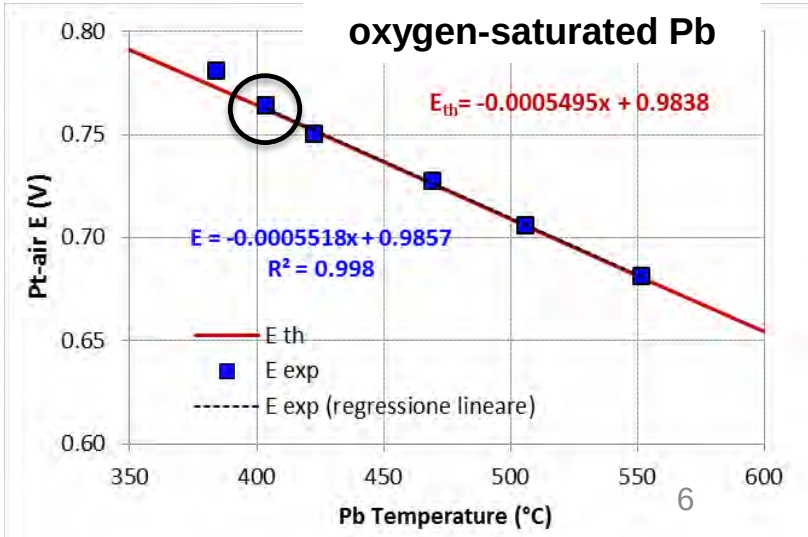

Min. reading T ≈ 400◦C

OXYGEN SENSOR FOR LARGE HLM POOL - Type 1

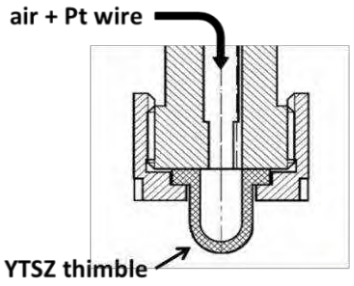

Tot lenght = 1100 mm

Calibration & Test at High Pressure in Pb storage tank

Min. reading T ≈ 380◦C , OK for Pb systems. Need of another reference for LBE systems.

YTSZ

good accuracy (1 % deviation in the T range 480-380◦C), no hysteresis

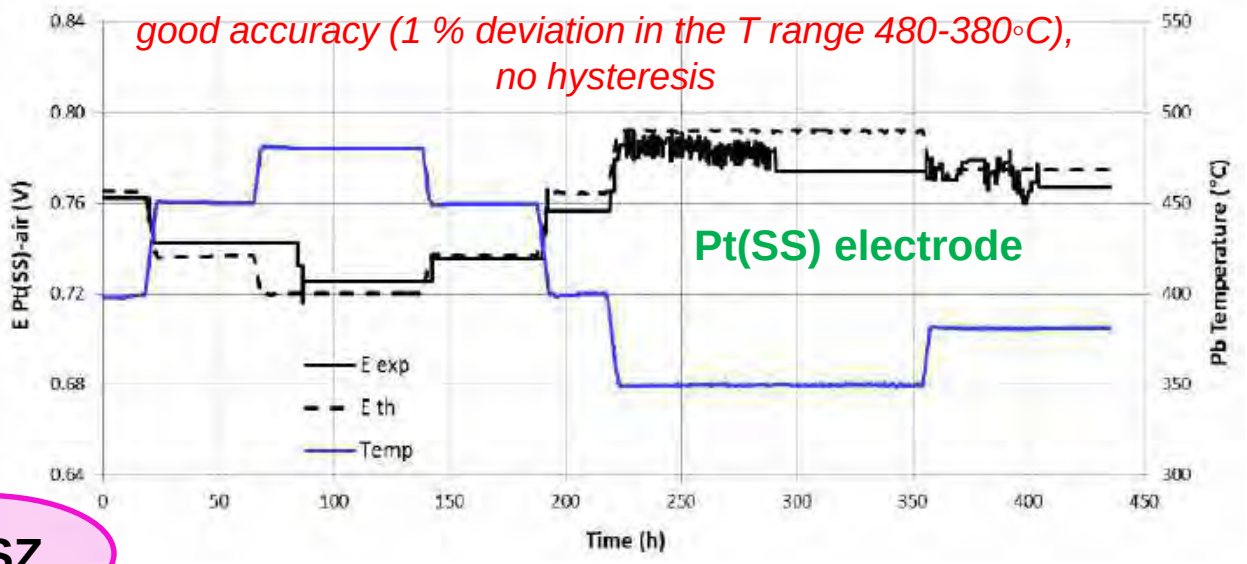

good tightness up to 9 bar of cover gas pressure (small deviation of 5mV during pressurization from 7 to 9 bar)

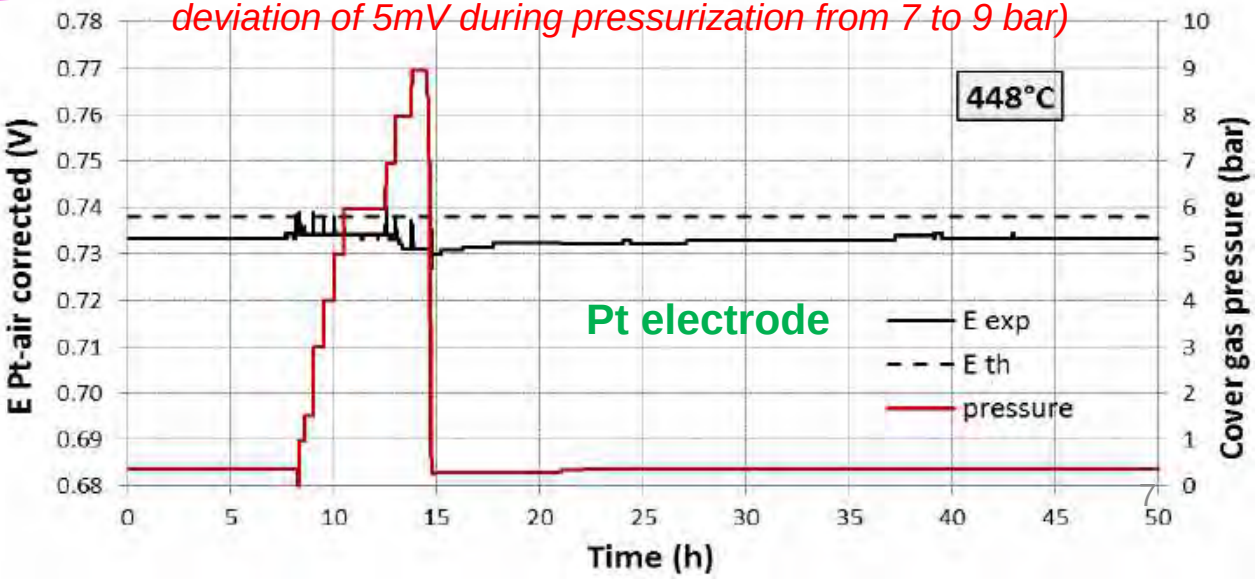

OXYGEN SENSOR FOR LARGE HLM POOL - Type 2

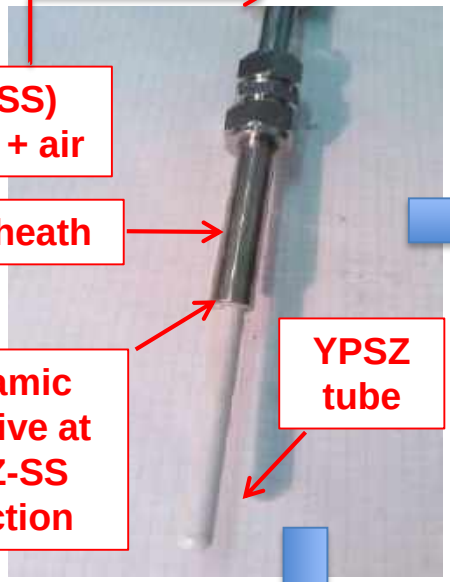

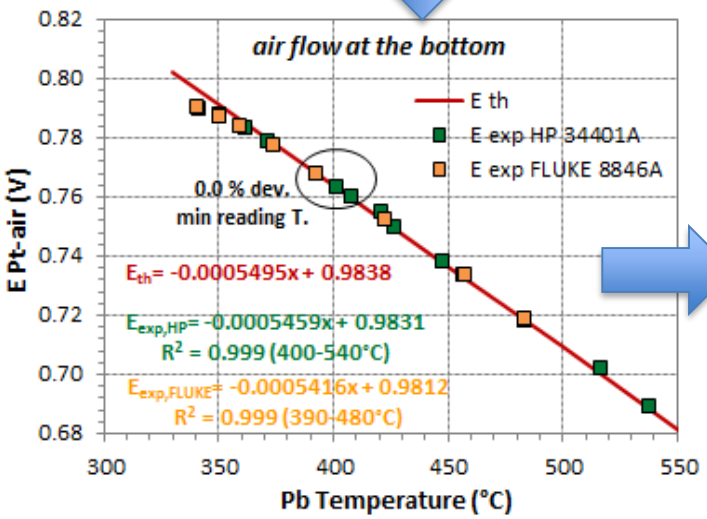

sensors manufactured for CIRCE (2000 and 4000 mm): too high electric resistance at 390-400°C

For small sensor:
Min. reading T ≈ 400◦C

For long sensor:
Min. reading T >> 400◦C
(other technological issues)

CIRCE facility
Main vessel: d= 1.2 m;
L= 8.5 m;
70-90 ton of LBE,
T_{pool} ≈ 400◦C (new configuration)

OXYGEN SENSORS: TESTS ONGOING AND PLANNED

Study of sensitive element of pool type-1 sensor in lab capsules with different:

- zirconia electrolytes (YTSZ, YPSZ);
- improved air-based reference.

Baseline study of other reference systems with better performance (new device):

- Cu/Cu_2O mod. (to prevent sintering);
- improved air references (perovskite-air system)

DEOXYGENATION WITH H_2: STATIC HLM, LAB SCALE

$$PbO_{diss.} + H_{2\,gas} \leftrightarrow H_2O_{gas} + Pb_{liquid}$$

capsules for HLM chemistry & corrosion tests (750 g liquid Pb)

Target C_O = 10^{-7} - 10^{-8} % wt.

Gas Control System

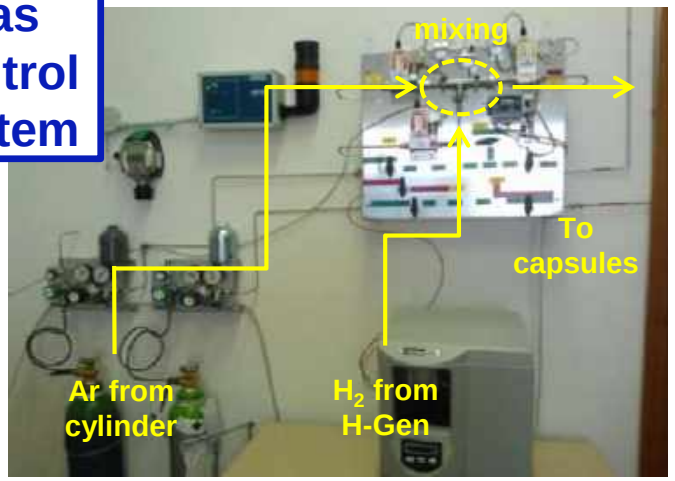

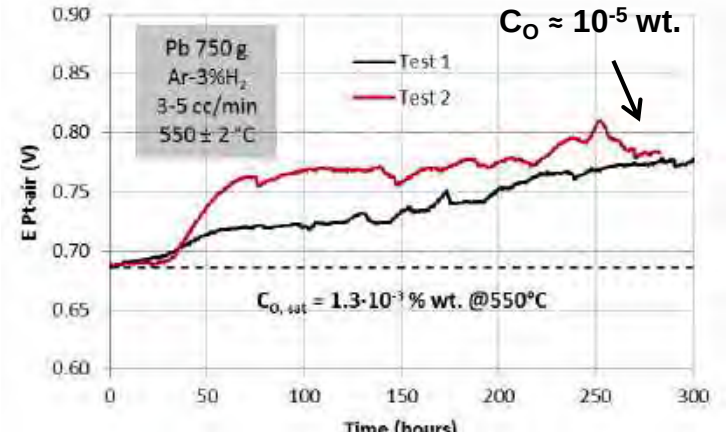

EMF ↑, C_O ↓

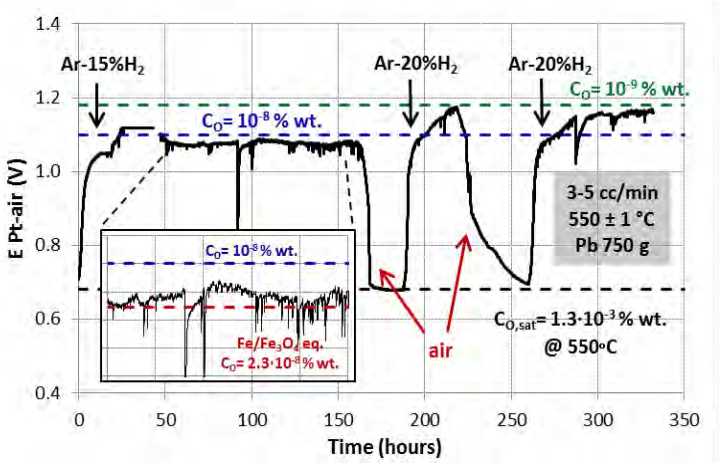

commercial Ar-3%H_2 gas (bubbling) → no efficient Pb deoxygenation in reasonable times → need of a dedicated gas control system

easy and fast Pb deoxygenation using Ar-H_2 gas with H_2 ≥ 10 % vol.

DEOXYGENATION WITH H_2: STORAGE TANK

≈ 285 L of liquid Pb, gas control system implemented

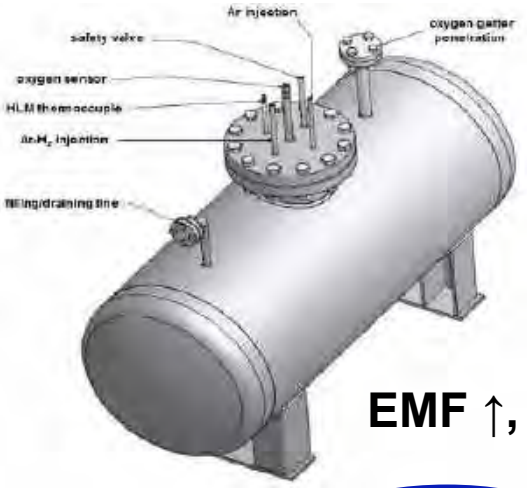

EMF ↑, C_O ↓

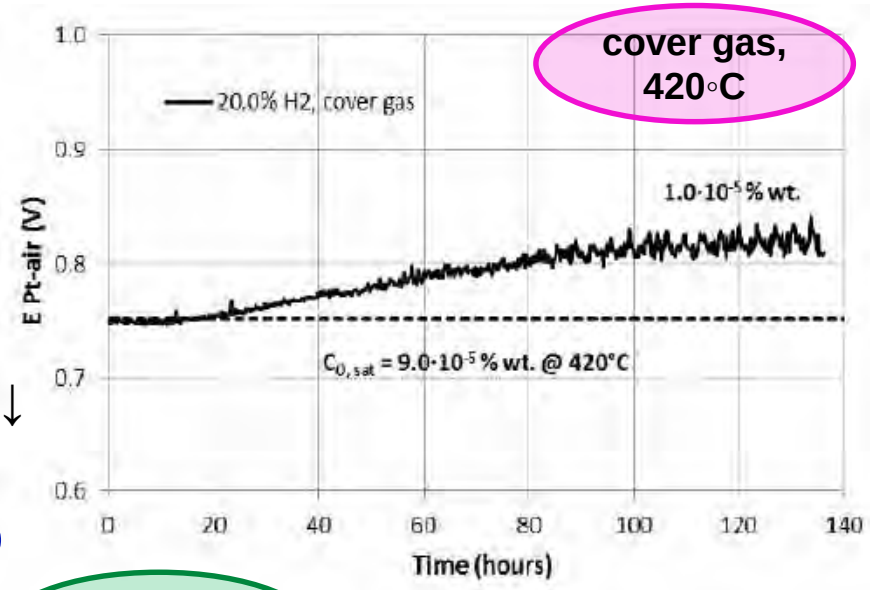

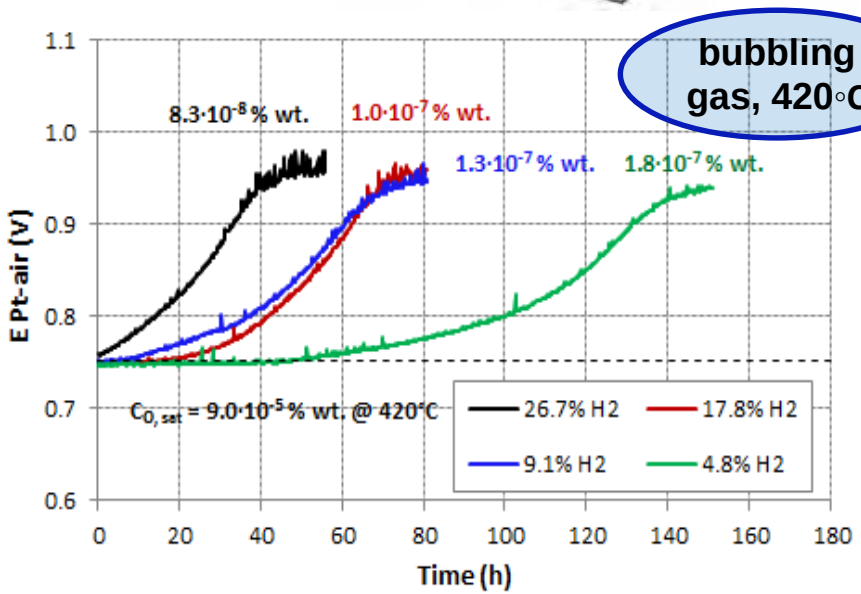

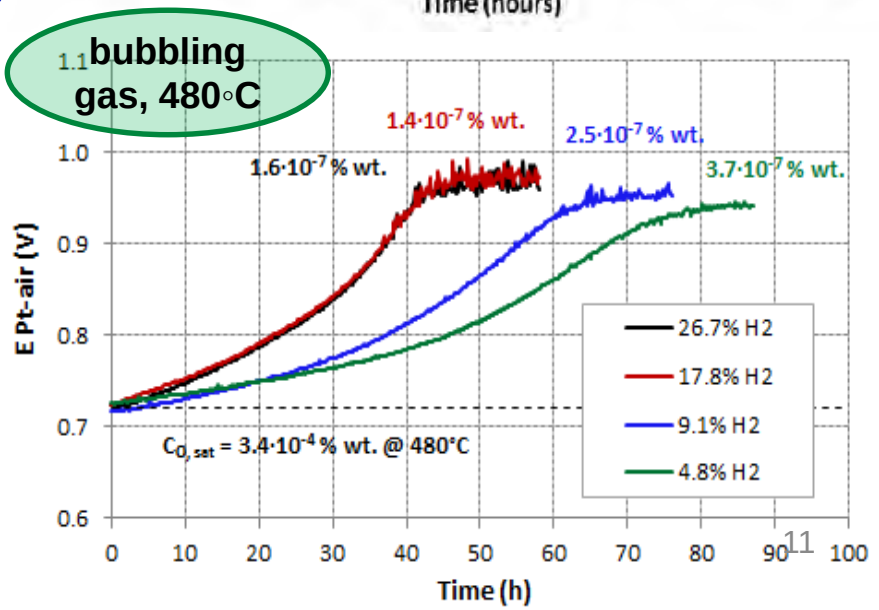

higher deoxygenation efficiency for higher T_{HLM}, H_2 %, and HLM mixing (i.e. bubbling)

DEOXYGENATION WITH H_2: LOOP FACILITY

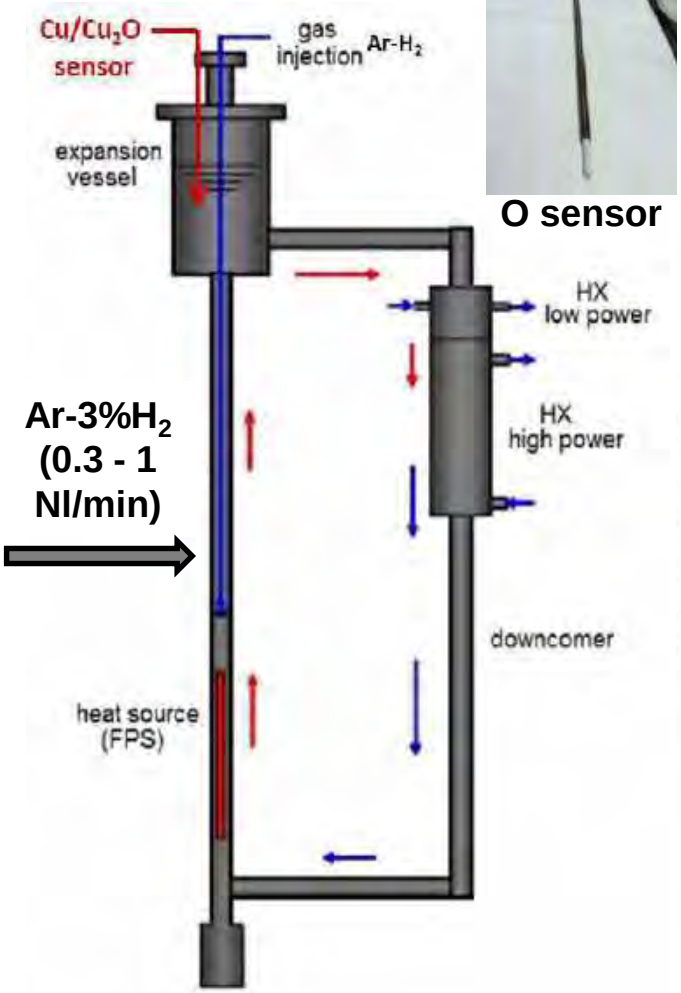

NACIE-UP loop
200L of LBE, 200-400◦C

O sensor

gas injector

1) **Gas washing of the circuit** at high T to remove O_2 and H_2O inside the loop;
2) **Deoxygenation of HLM with Ar-H_2** to reach low C_O.

S. Bassini et al., Prog. Nucl. Energ. 105 (2018) 137-145.

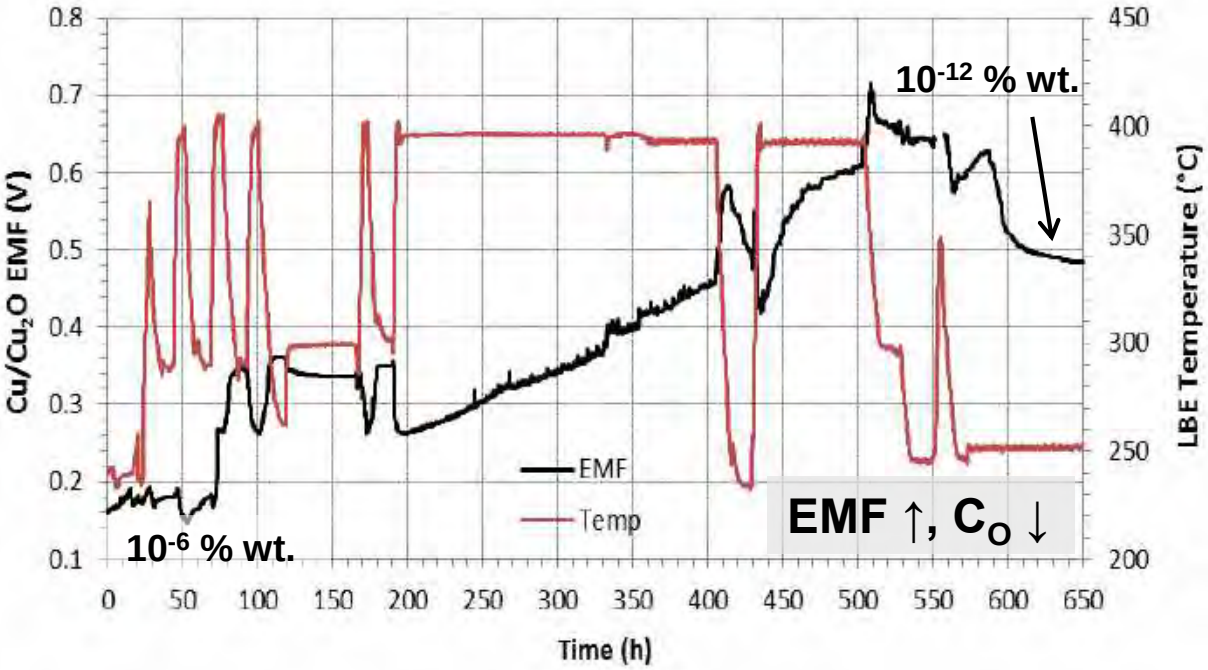

high deoxygenation efficiency even with Ar-3%H_2 thanks to the forced HLM circulation → too low C_O reached → need for oxygen supply (e.g. Ar-O_2 injection) and/or reduced deoxygenation efficiency

BID1 SMALL POOL (Pb)

BID1 “Brasimone gas Injection Device 1”

Small pool (Pb ≈150 L) to test oxygen control methods:

- H_2 and O_2(air) injection
- oxygen getters (Ti, Ta, Zr)
- oxygen sensors performance

OCS with Ar-H_2 + Ar-O_2 also for LECOR Pb loop

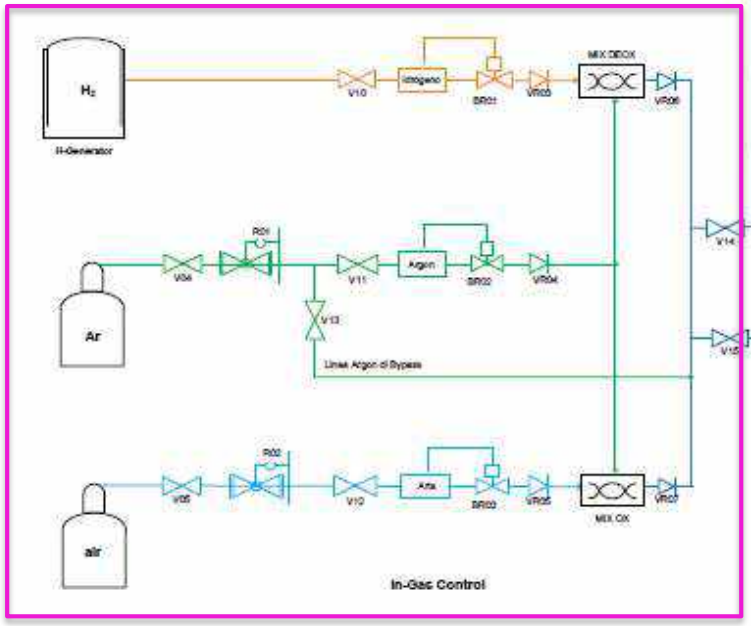

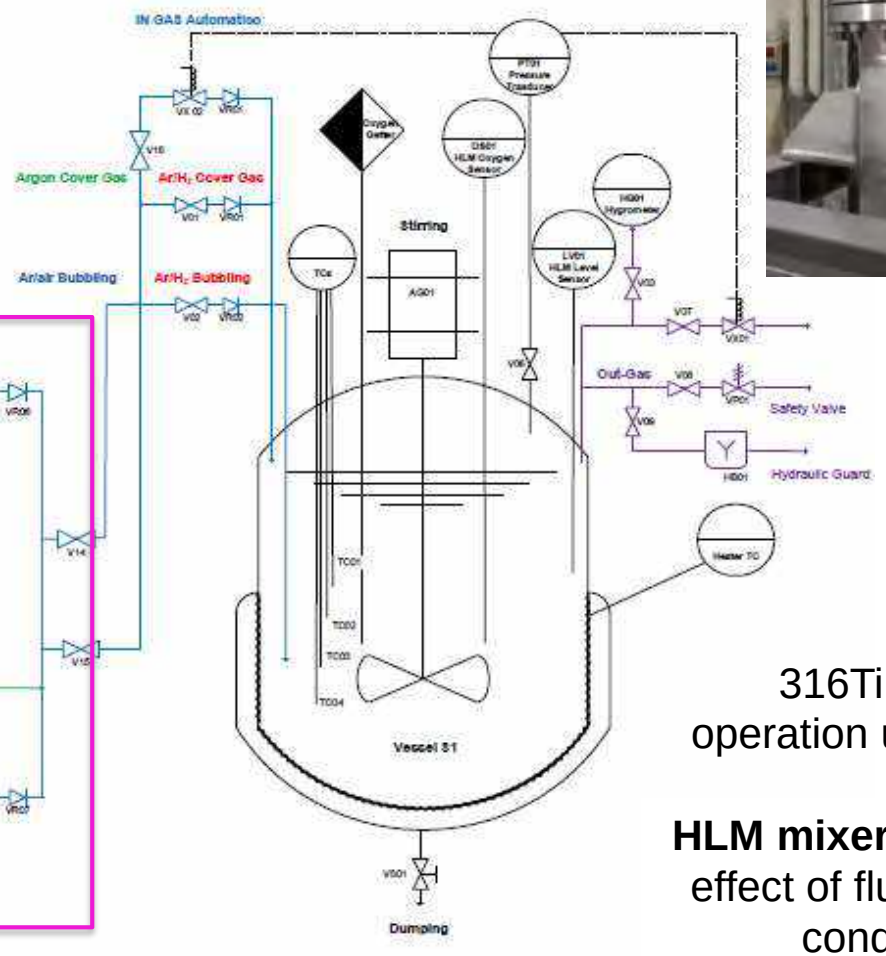

316Ti for the operation up to 550◦C

HLM mixer to study the effect of fluid-dynamic conditions

OCS IMPLEMENTATION FOR LECOR LOOP

OCS (storage tank+exp.vessel)

OS

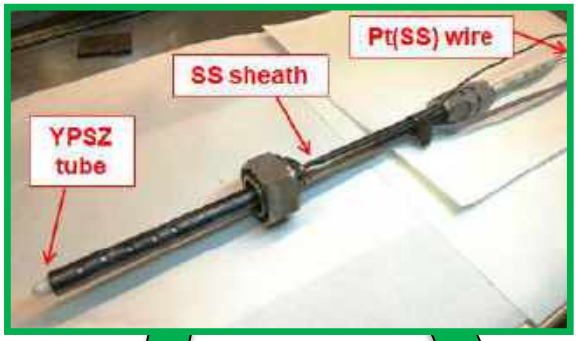

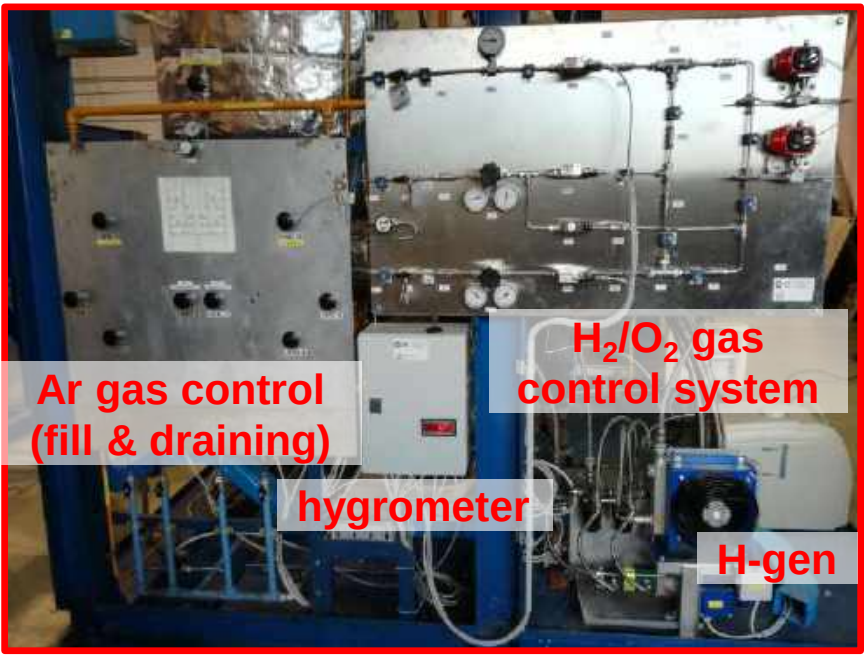

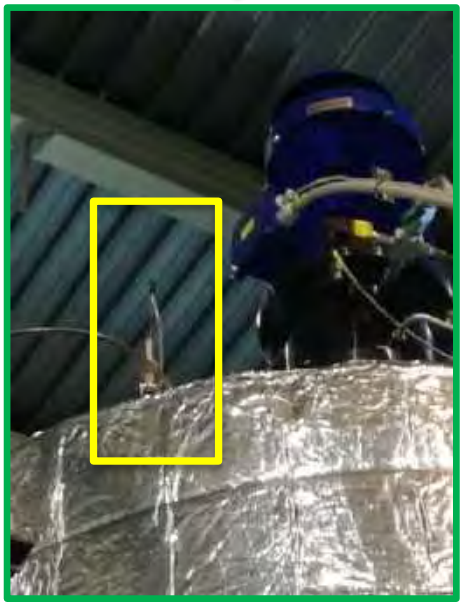

After exp. vessel 430°C

Test section 550°C

SUMMARY

- Baseline study on different oxygen sensors: the min. reading T of the sensor is influenced by the reference system (mainly), new reference electrodes will be tested.
- Oxygen sensor prototypes for large HLM pool were developed and tested. Current Pt-air configurations have a min. reading T≥400◦C, different reference should be developed and used to have better detection capability.
- HLM deoxygenation with Ar-H_2 gas was performed in small capsules (lab), storage tank and loop facility exploiting a dedicated gas control system.
- A gas control system based on Ar-H_2 and Ar-O_2 injection is available for BID1 pool and LECOR loop for oxygen control study.

THANK YOU FOR THE ATTENTION

RACHEL Lab

REACTIONS AND ADVANCED CHEMISTRY FOR LEAD

ENEA

Italian National Agency for New Technologies,
Energy and Sustainable Economic Development

Double stabilized stainless steels Status and future developments

WORKSHOP TEMATICO ACCORDO DI PROGRAMMA MISE – ENEA PAR2017

Università di Roma "La Sapienza" , 15 Giugno 2018

C. Cristalli, L. Pilloni, N. Bettocchi, L. Masotti (ENEA FSN-ING-QMN)

Contents

- Introduction about the challenge of swelling reduction and the development of the DS steels
- Neutron irradiation results (1988, Saclay)
- Production of a new DS4 plate(2014, ENEA-CSM)
- Status of the on going characterization of the new plate (ENEA-Brasimone)

Introduction

The challenge of swelling reduction; beyond 15-15 ?

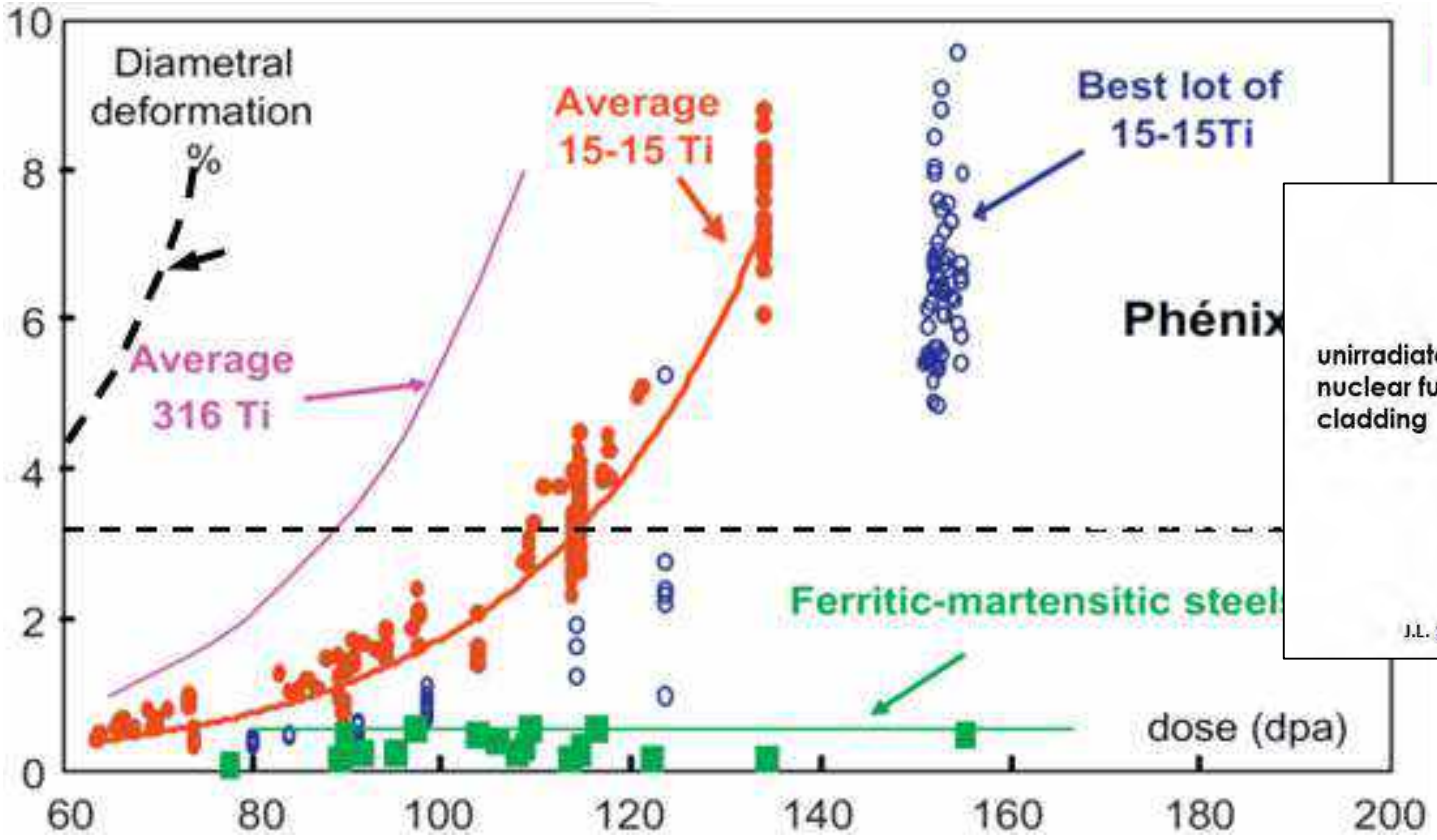

[Séran et al.]

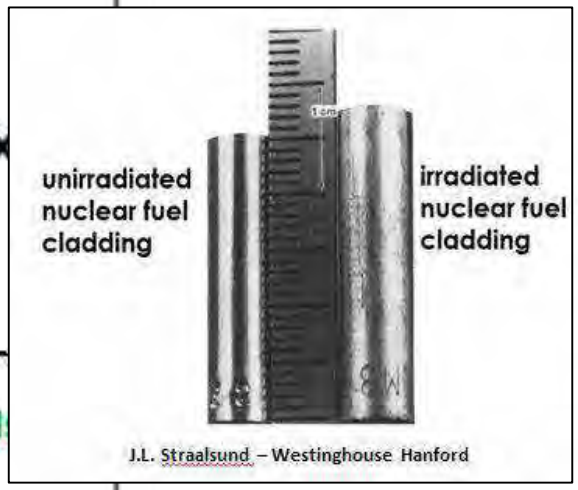

Introduction

At the beginning of the '80s, within an experimental program carried out at the Saclay Center, the under electrons irradiations (1 MeV) have shown the effectiveness of the simultaneous presence of Ti and Nb on the swelling resistance of 316 and 15 Cr-15 Ni matrix.

Development of the **First Generation** of Double Stabilized Steels:

316DS

15-15DS

In the first generation double stabilized steels the annealing temperature used, 1125° C, didn't result sufficient to obtain a good solubilization of "free" Ti and Nb also because of the high stabilization ratio.

Revision of the composition

Stabilization Ratio :

$$R = \frac{[Ti] + [Nb] - [N]}{[C]}$$

Birth of the **2nd Generation** Double Stabilized steels:

DS3 (15Cr-15Ni)
DS4 (15Cr-25Ni)
DS5(15Cr-25Ni)

Factors affecting swelling reduction

Irradiation Tests at Saclay: the results of the experience « Supernova »

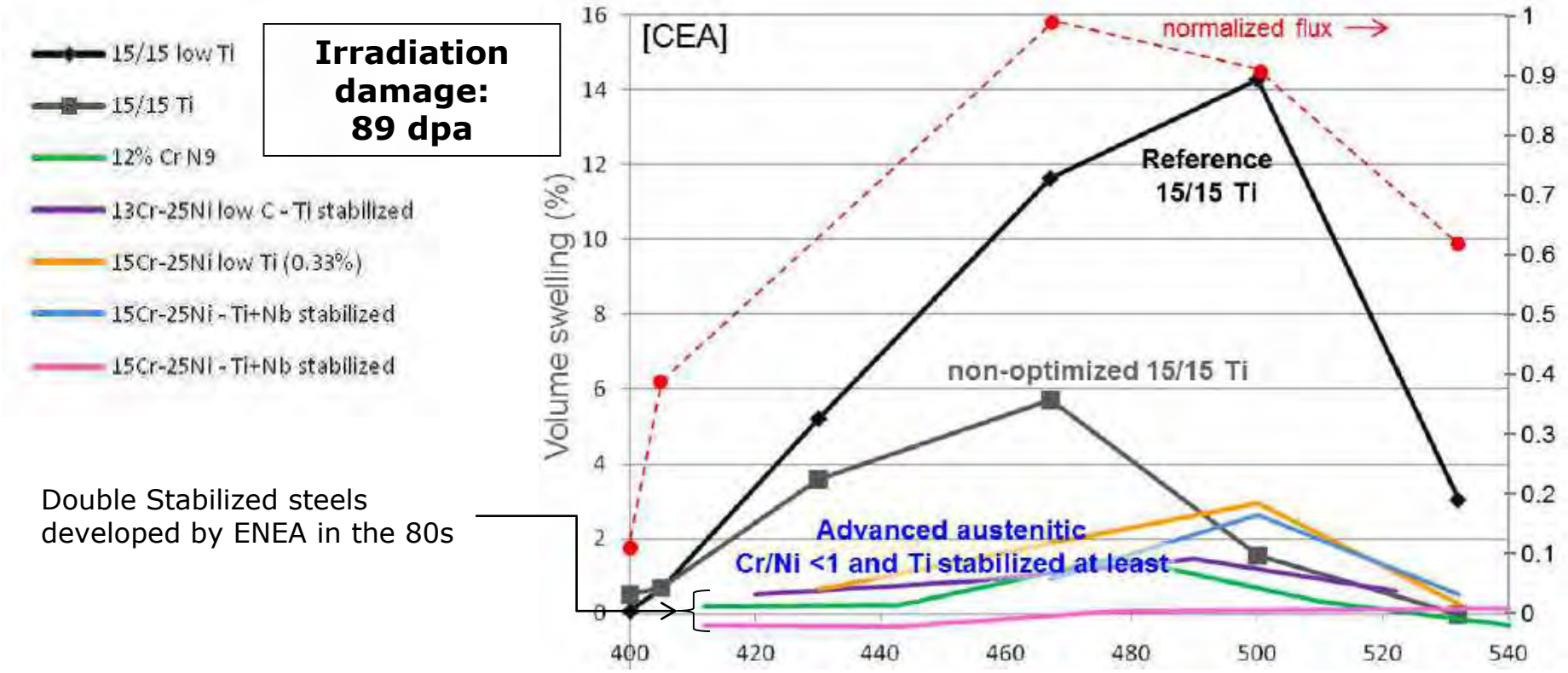

Double Stabilized steels developed by ENEA in the 80s

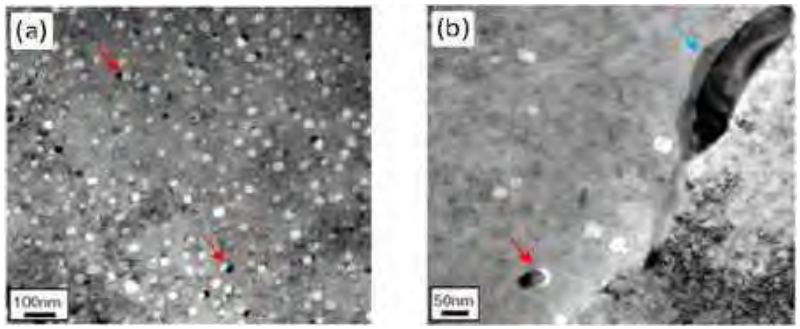

Low amount of cavities in the advanced austenitic stainless steel (b) if compared to the non-optimized 15-15 Ti (a)

Factors affecting swelling reduction

Beneficial effect 1: Dislocation act as sinks; recombination sites for point defects

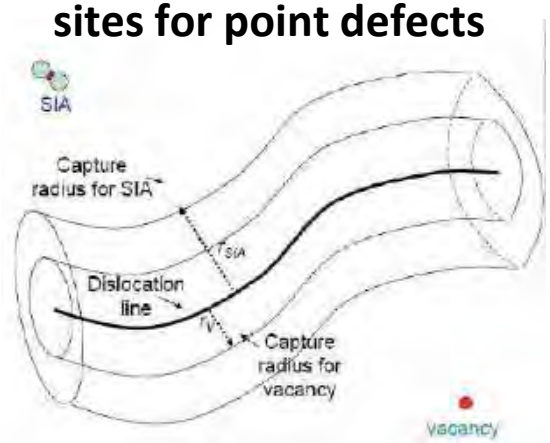

20% c.w.

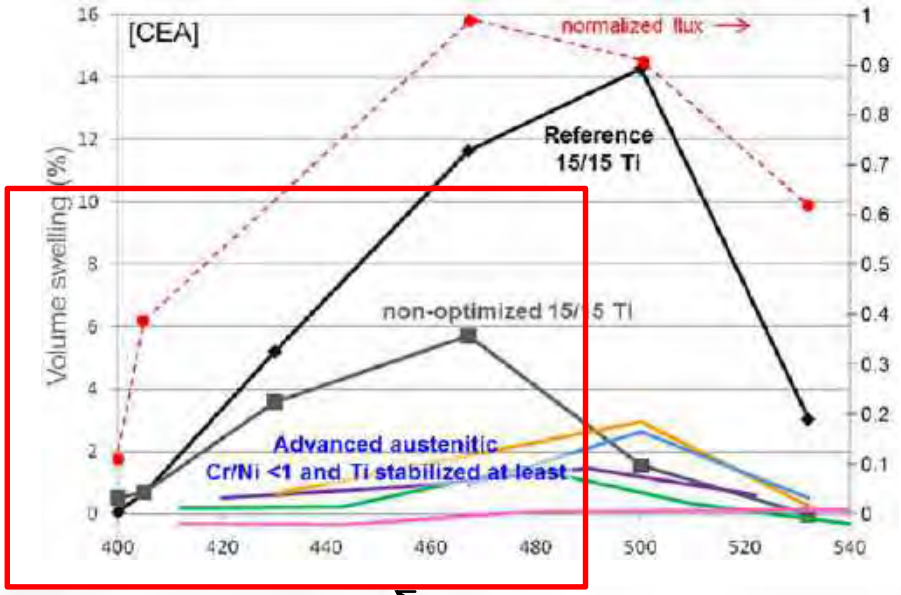

Dislocation network mainly acts in the low temperature regime (prior its recovery); useful instrument to delay the onset of swelling

Beneficial effect 2: Effect of Ni content on swelling

25% Ni

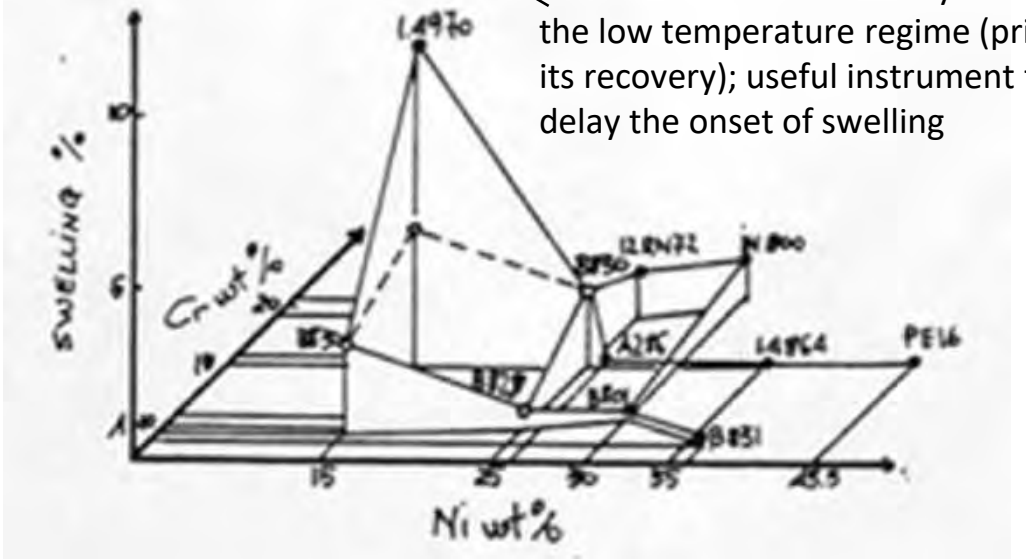

Factors affecting swelling reduction

Beneficial effect 3: Double Stabilization; how primary and secondary precipitation of carbides affect swelling

A good high temperature creep resistance for an austenitic steel is essentially due to microprecipitation of carbides which result finely dispersed on the dislocations network;

- Primary precipitation, the one occurring during the annealing heat treatment of the steel. Low primary precipitation means sufficient "free" contents of Carbon, Ti and Nb in solid solution in order to allow a secondary (in service) beneficial precipitation.
- Secondary, so-said "in-service" precipitation, occurring during operation inside the reactor. This sort of "in-service" precipitation is highly effective as movement inhibitor for linear defects..

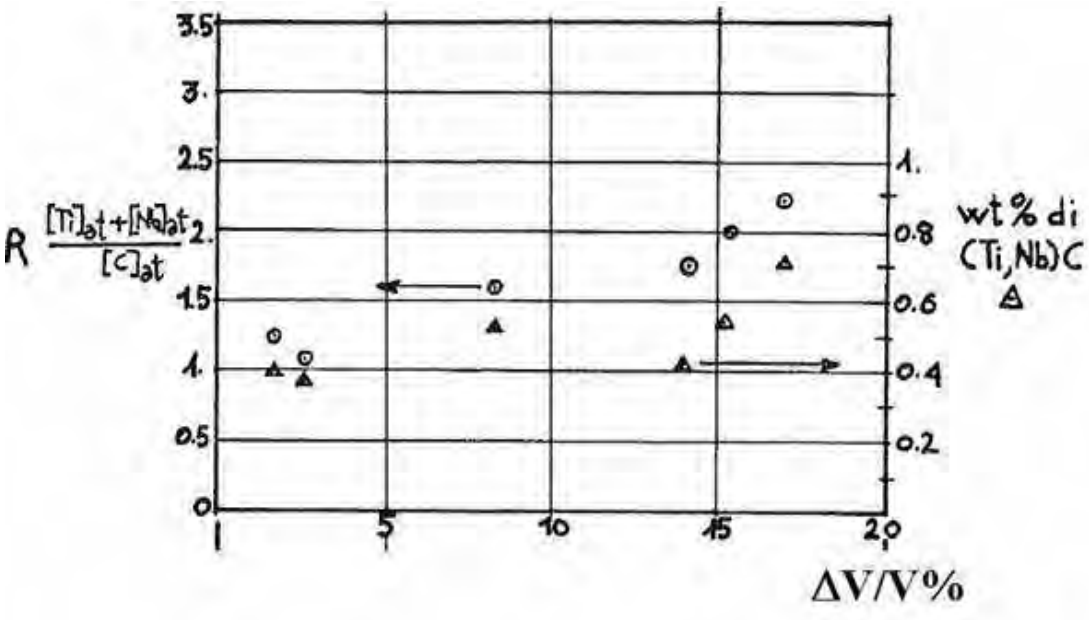

15-15DS; 105dpa, Tirr=450° C

The precipitation of carbides doesn't only act on the creep resistance of the material; it also has positive effects on the stability under irradiation. Here's a graphical investigation of the first 90's about the dependence of swelling attitude on the primary precipitation and on the stabilization ratio for a 15Cr-15Ni matrix. As long as the primary precipitation is kept low (keeping the stabilization ratio close to 1) the secondary (highly desirable) precipitation is fostered and the limited swelling attitude is a consequence.

L. Pilloni; internal ENEA report, restricted distribution

15-15 Ti; Phase Diagram according to Thermocalc

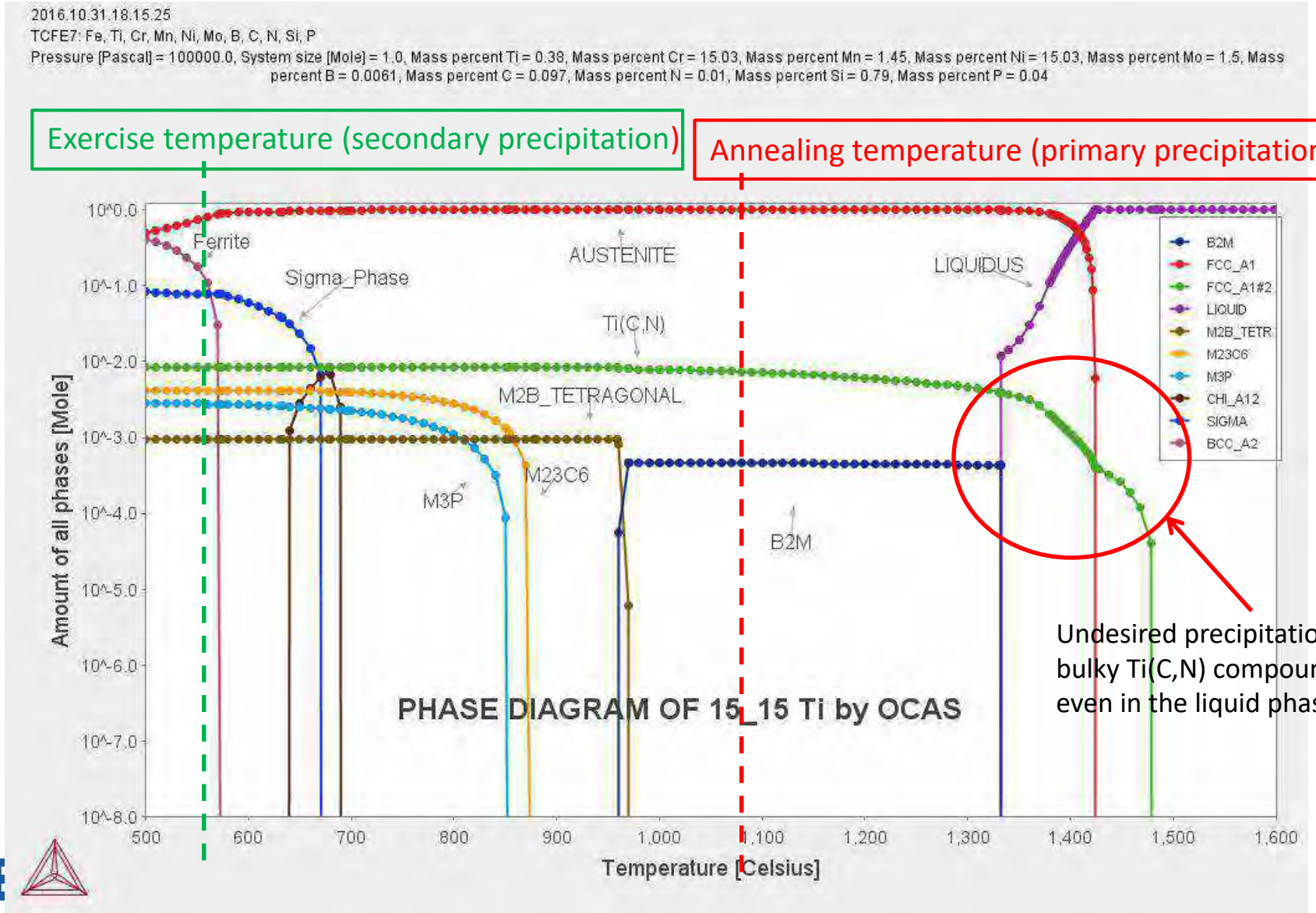

15-15 Ti; Phase Diagram according to Thermocalc

Available contents of carbo-nitride forming elements in the Austenite phase at the annealing temperature (1080 ° C)

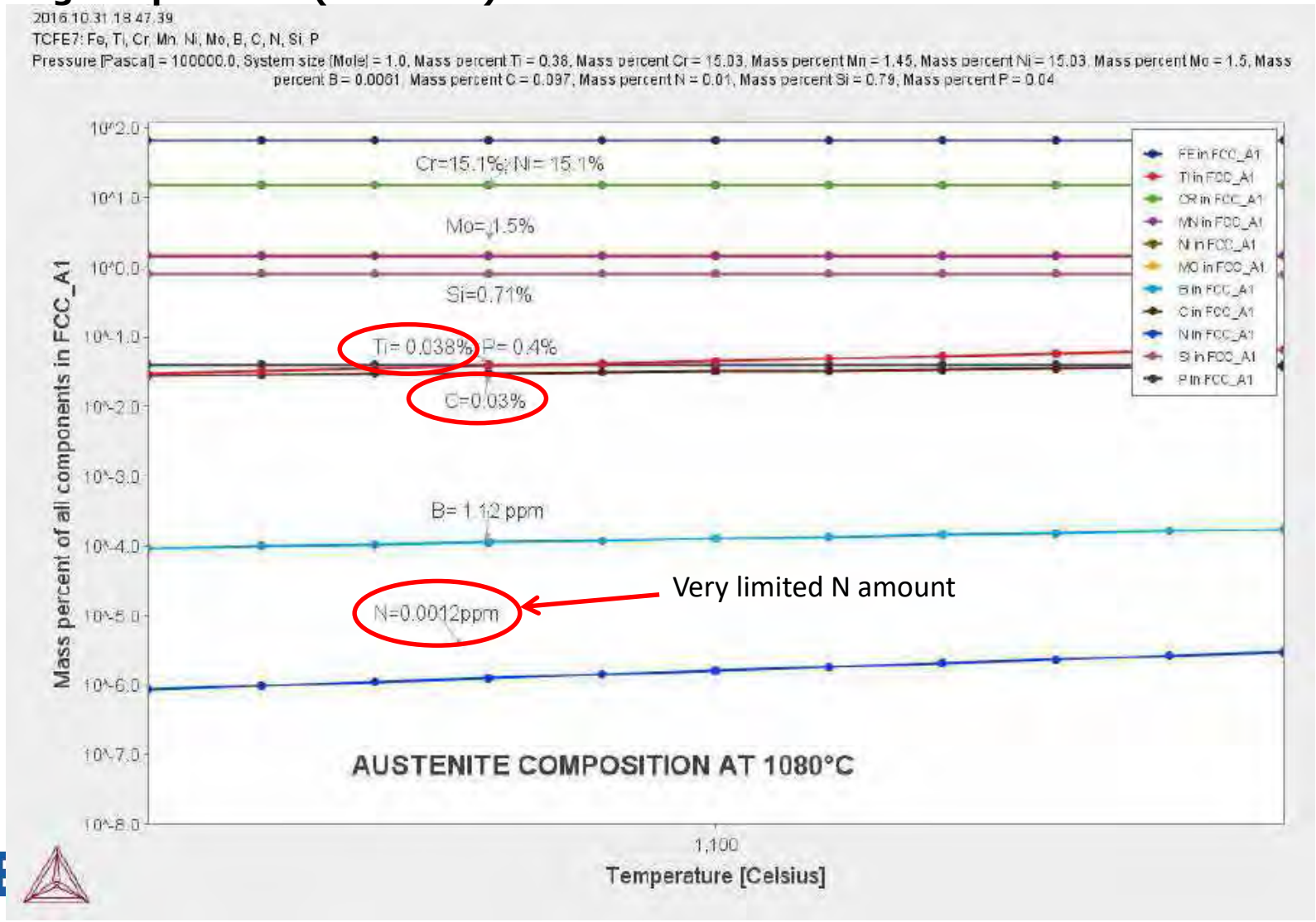

DS4; Phase Diagram according to Thermocalc

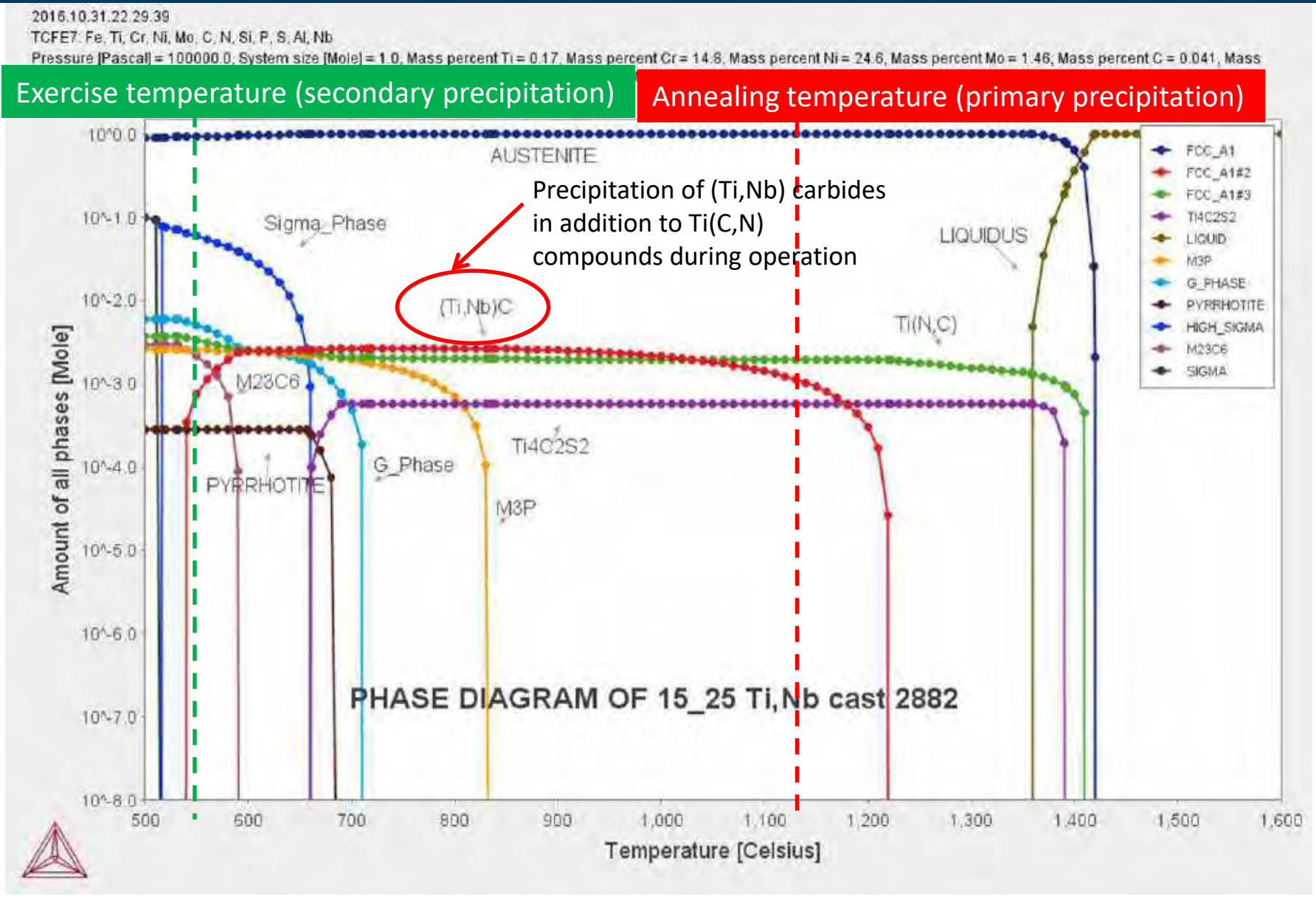

DS4; Phase Diagram according to Thermocalc

Increased available contents of carbo-nitride forming elements in the Austenite phase at the annealing temperature (1135 ° C)

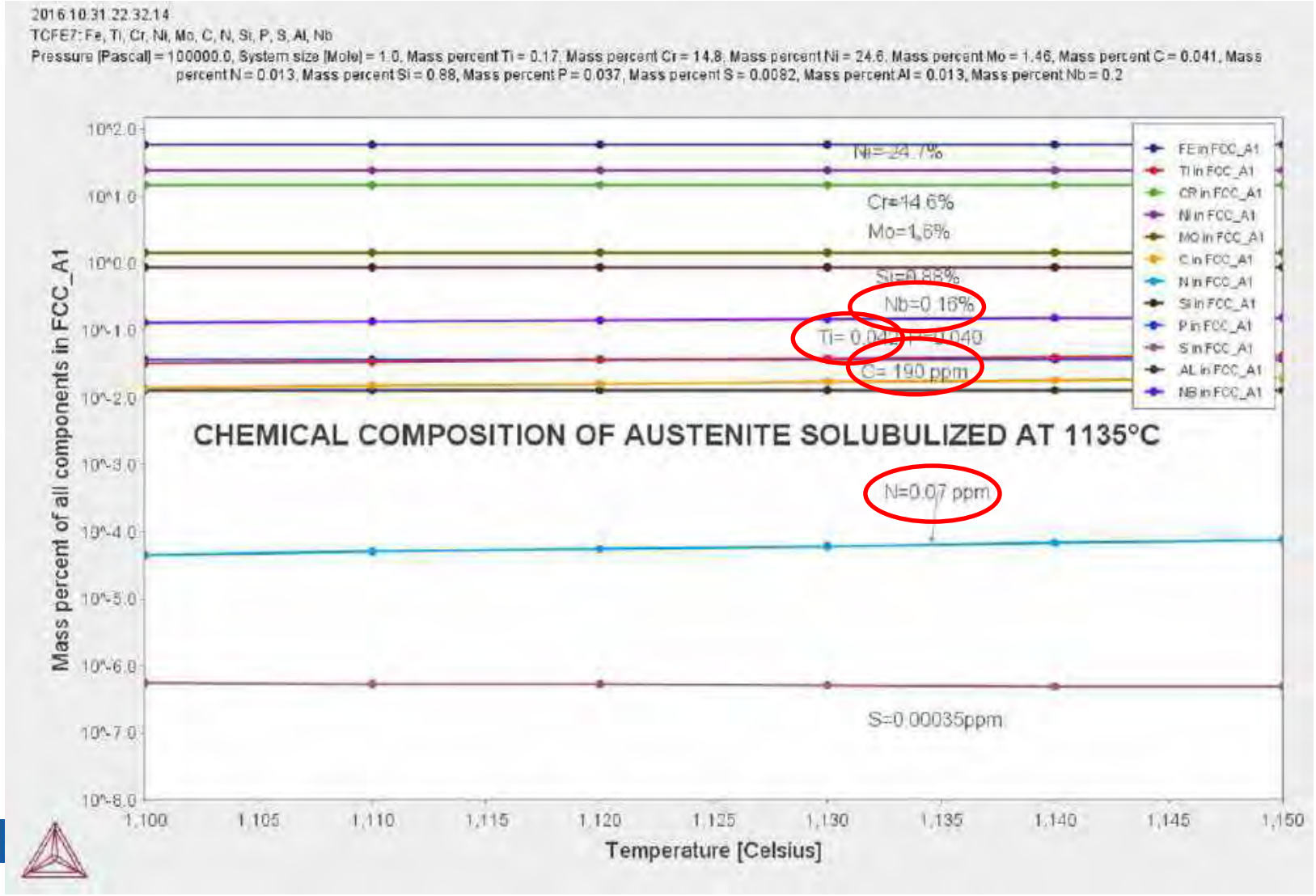

2014 - Production DS4 plate

Production of a new DS4 ingot in 2014

Hot rolling of the ingot (Pre-heating -1200° C)

After last hot rolling stage (919° C) 20 mm thickness

Solubilization annealing 1135° C

Cold working up to 15 mm thickness

«waving» on the rolling direction due to 20% c.w.

Production of DS4 plate; Hardness measurements

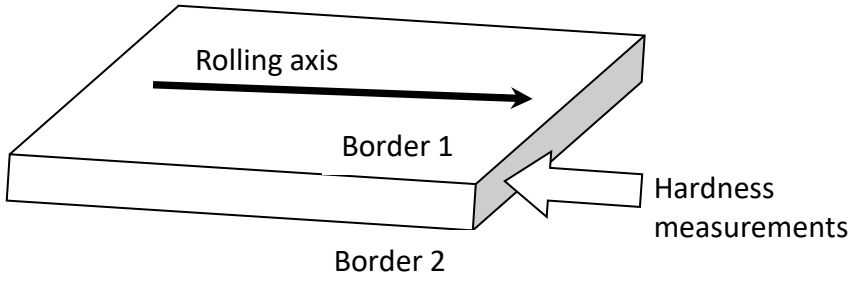

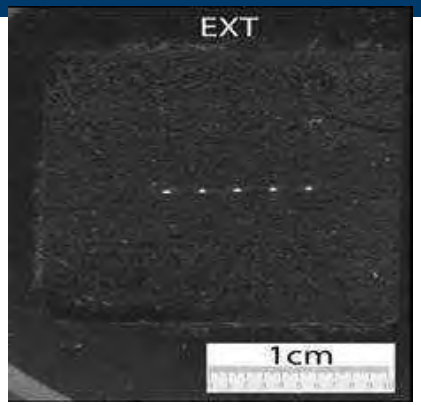

solubilized
(T-L direction)

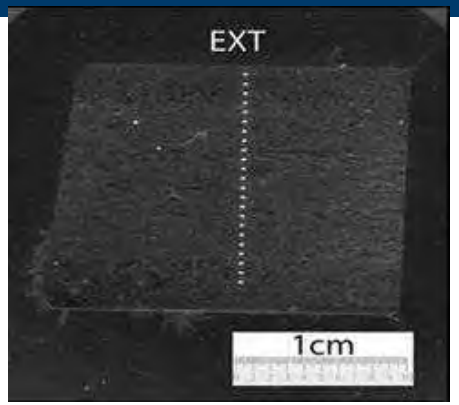

Cold worked
(L-T direction)

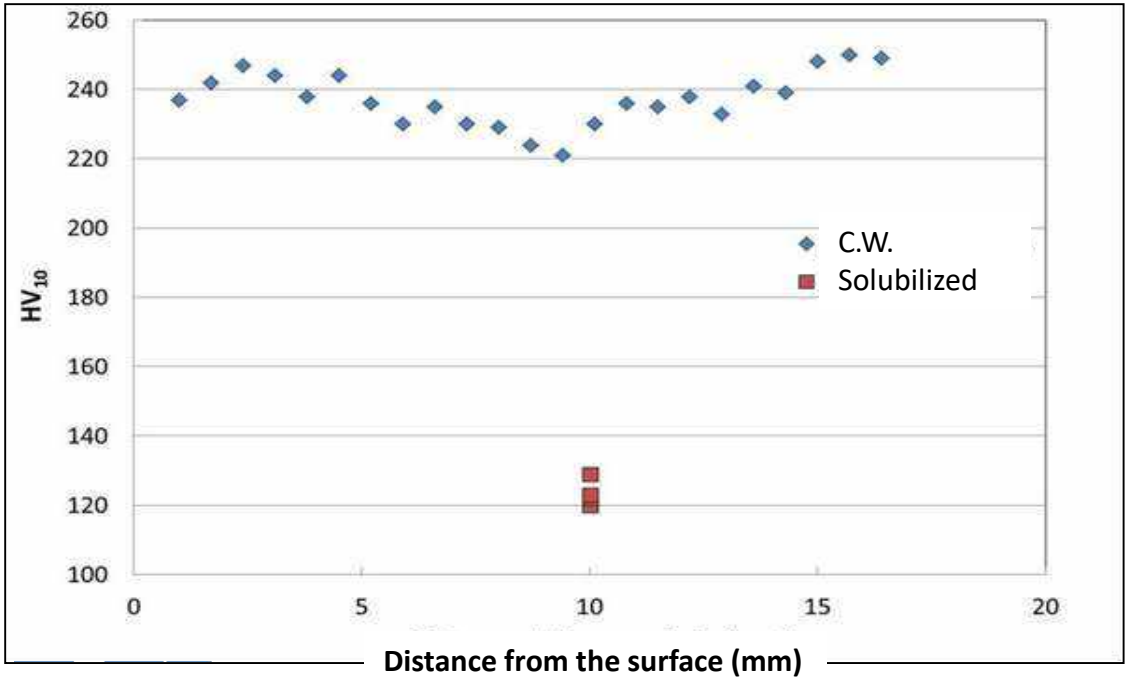

80s batch (DS4): 260 HV

Grain Size (32-45 mm in the 80s batch)

After solubilization

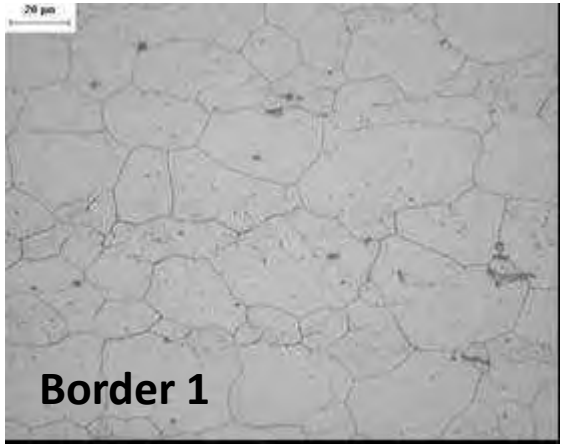

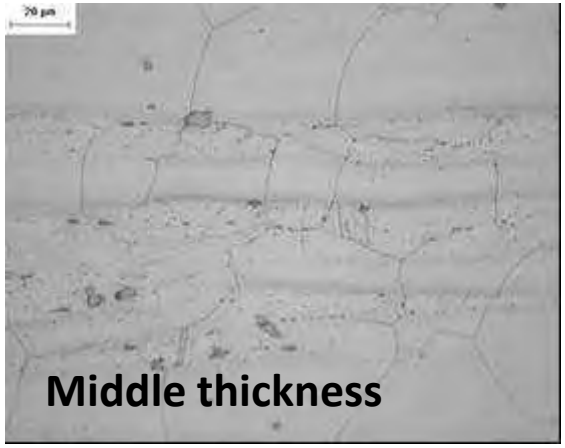

After 20% c.w.

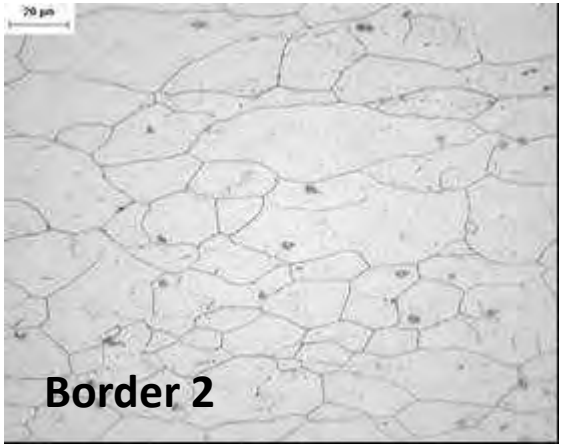

Tensile Properties; qualitative comparison

Solubilized Material (RT, 550° C, 650° C)

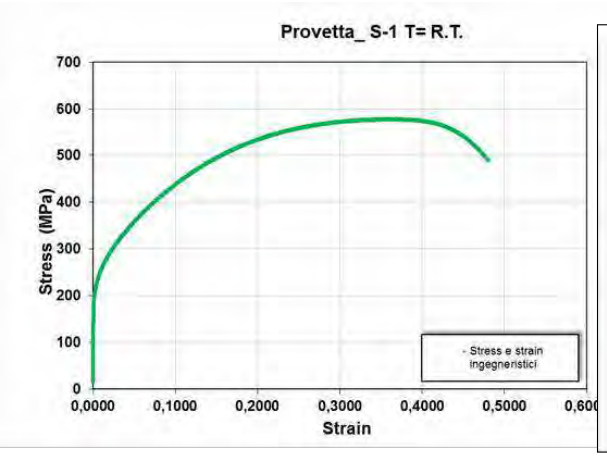

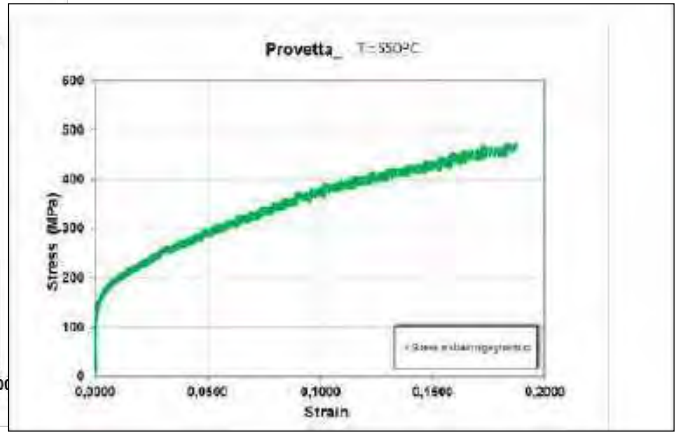

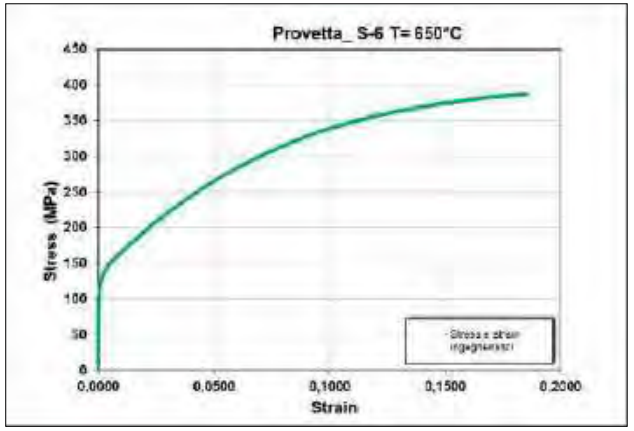

20% C.W. material (RT, 550° C, 650° C)

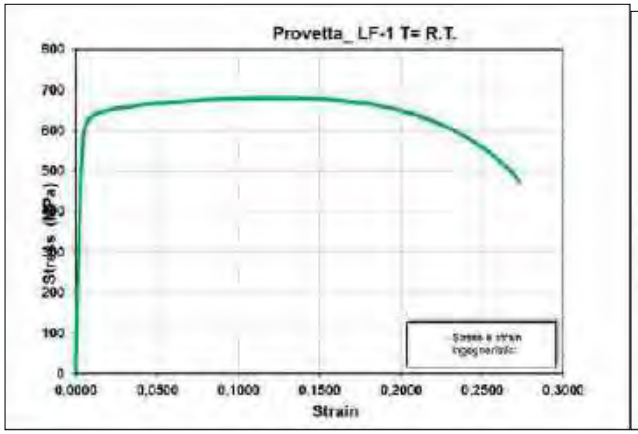

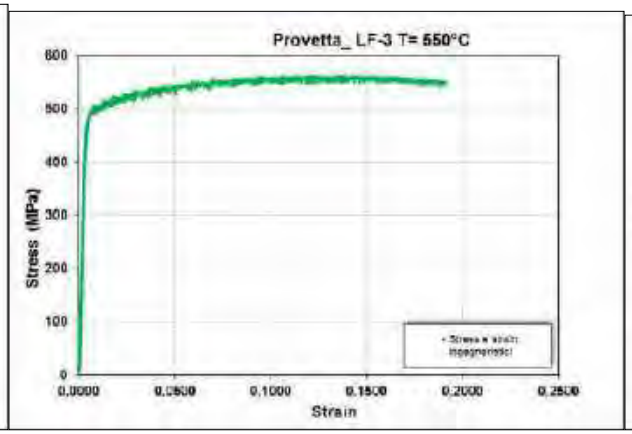

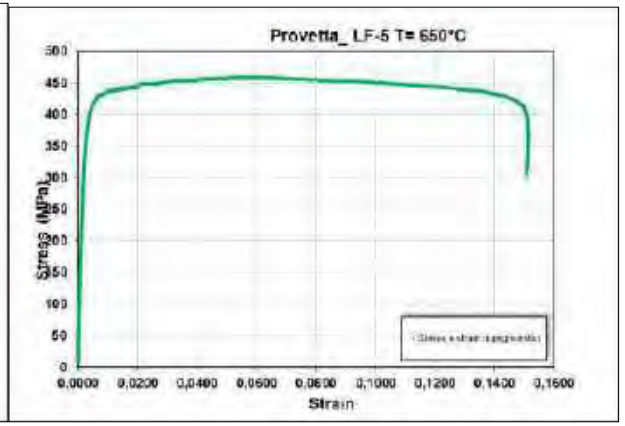

Anisotropy of the material; comparison between extraction directions

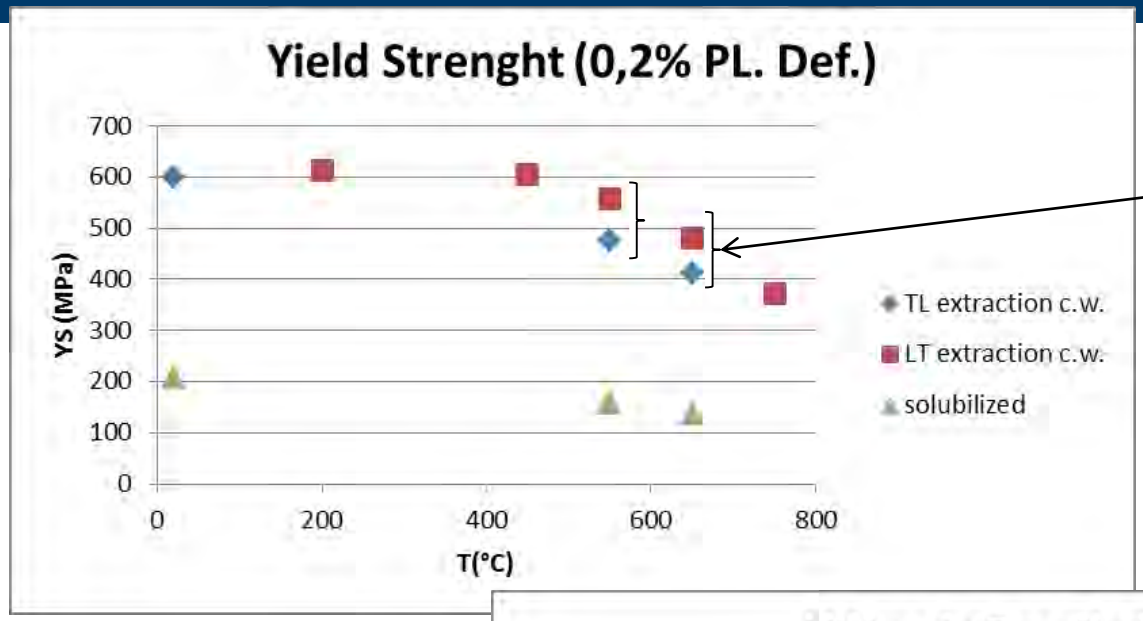

Anisotropy of the produced plate

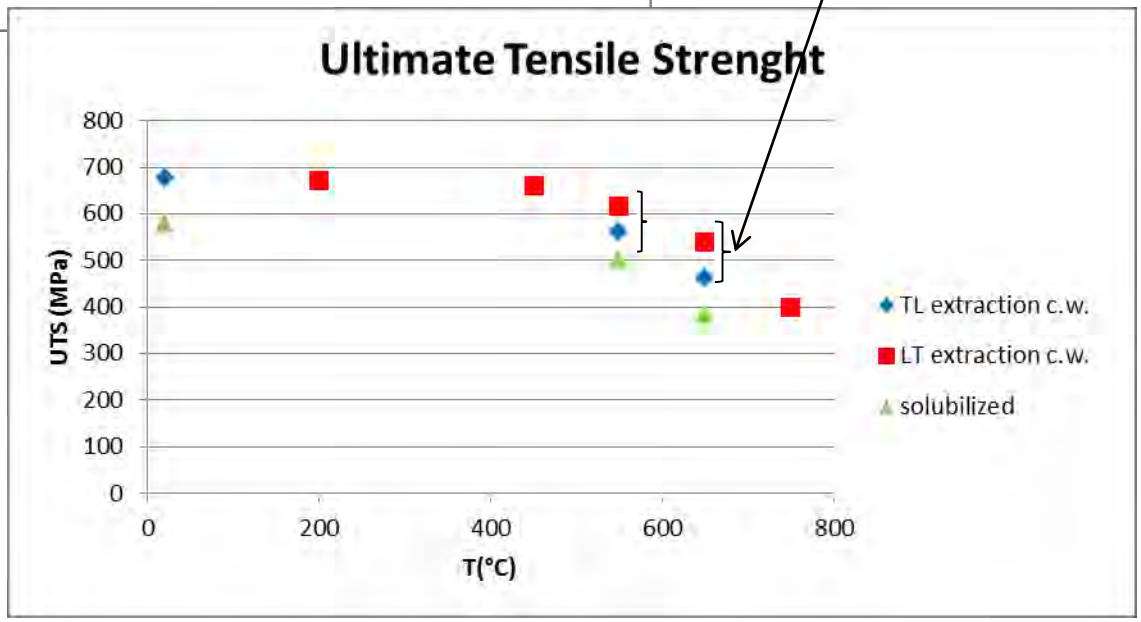

Comparison DS4; rods 90s vs 2014 plate

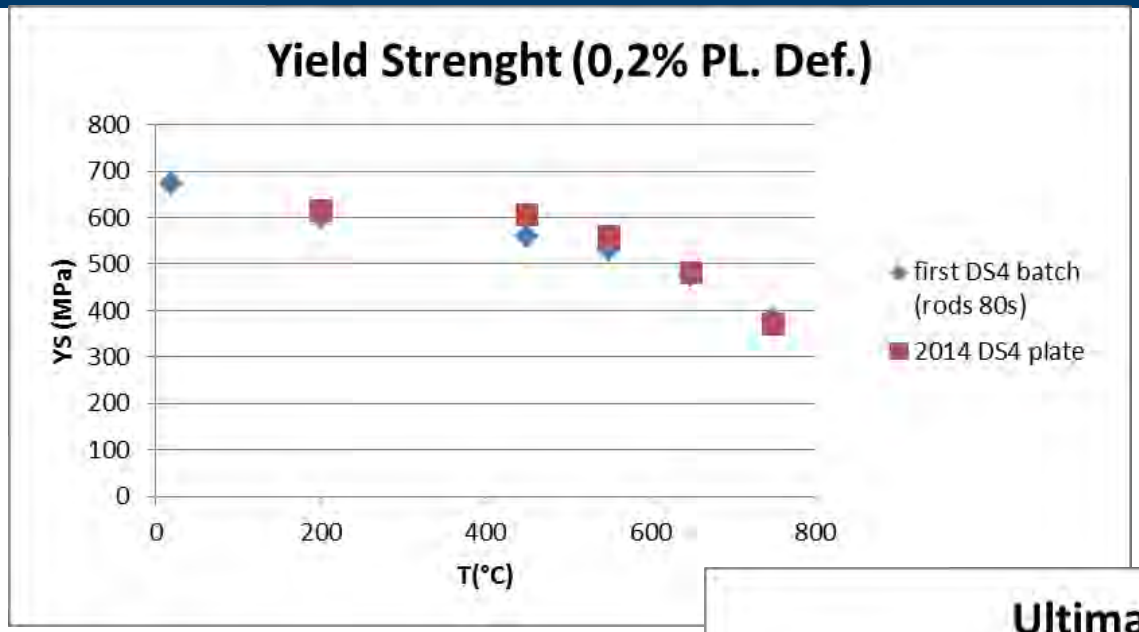

Data 90s:

G. Filacchioni, U. de Angelis, D. Ferrara, L. Pilloni / Proceedings B.N.E.S., London, 1990

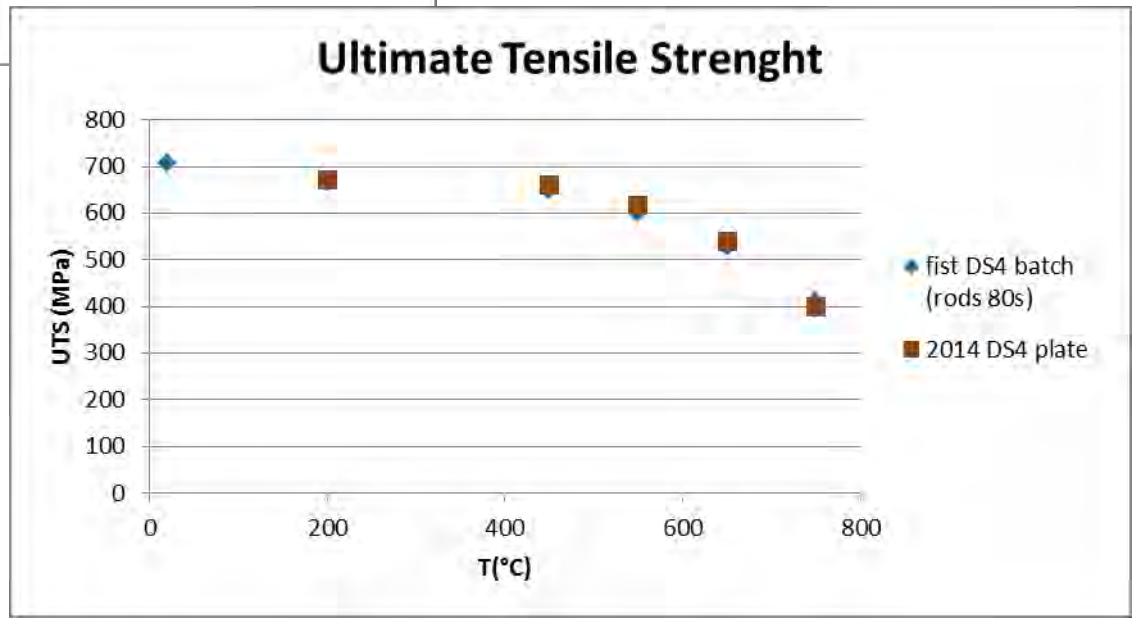

Comparable mechanical properties of the new plate with respect to the rods characterized in the 90s

Experimental activities in progress …

- **Corrosion Tests (flowing lead)**; 1000 hrs exposure completed (flowing Pb, 10^-5 wt% O_2);
- **Ion irradiation**; target: 100 dpa (58 Ni, 110 MeV). In progress (four sessions completed, one additional session to achieve the target dose);
- **Creep tests;** In Progress ...

Test 650° C – 415 Mpa (Yield Stress)

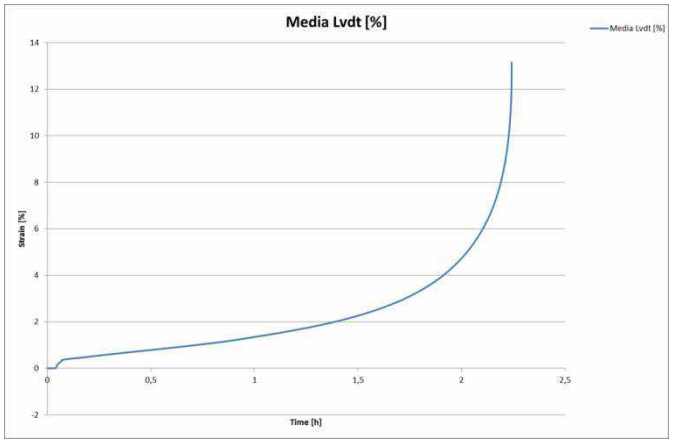

Test 650° C – 390 Mpa

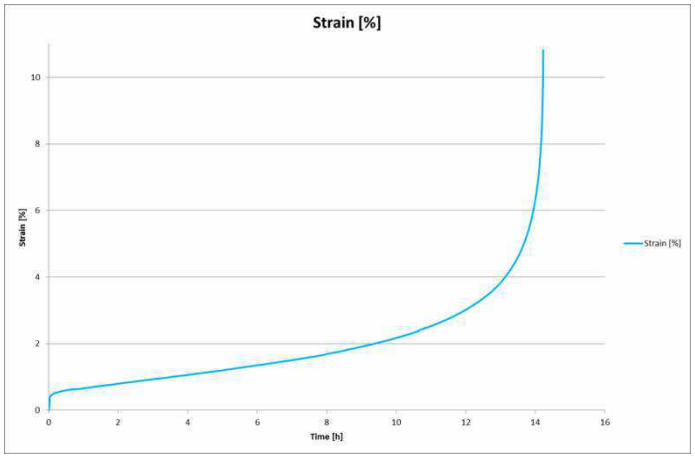

Corrosion tests

Experimental; Exposures in flowing Lead ; 1000 hrs at 550°C, velocity 1.3 m/s, Oxigen content between 10-4 and 10-5 wt % ; carried out in LECOR plant.

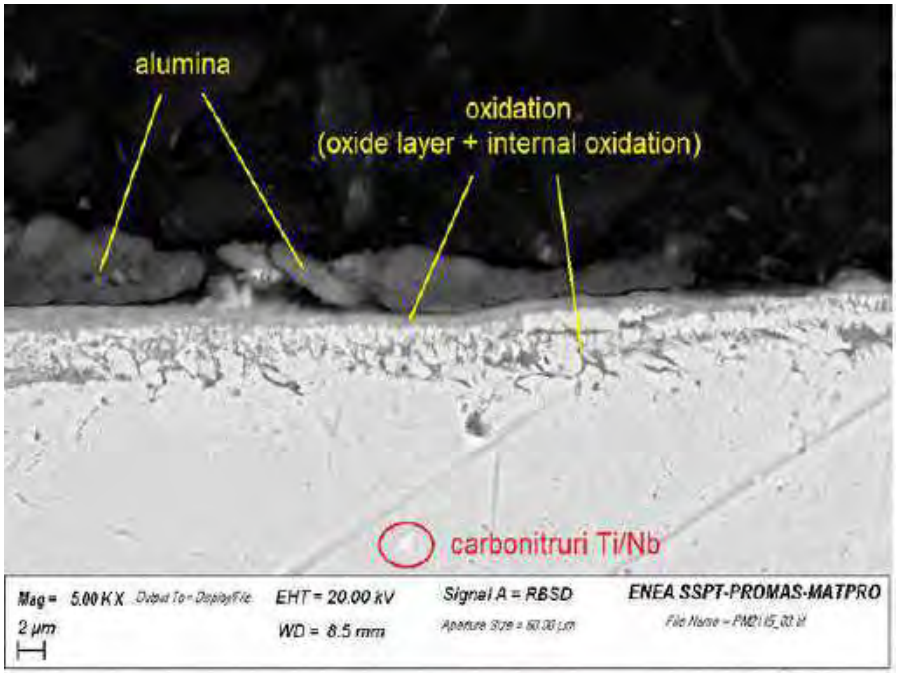

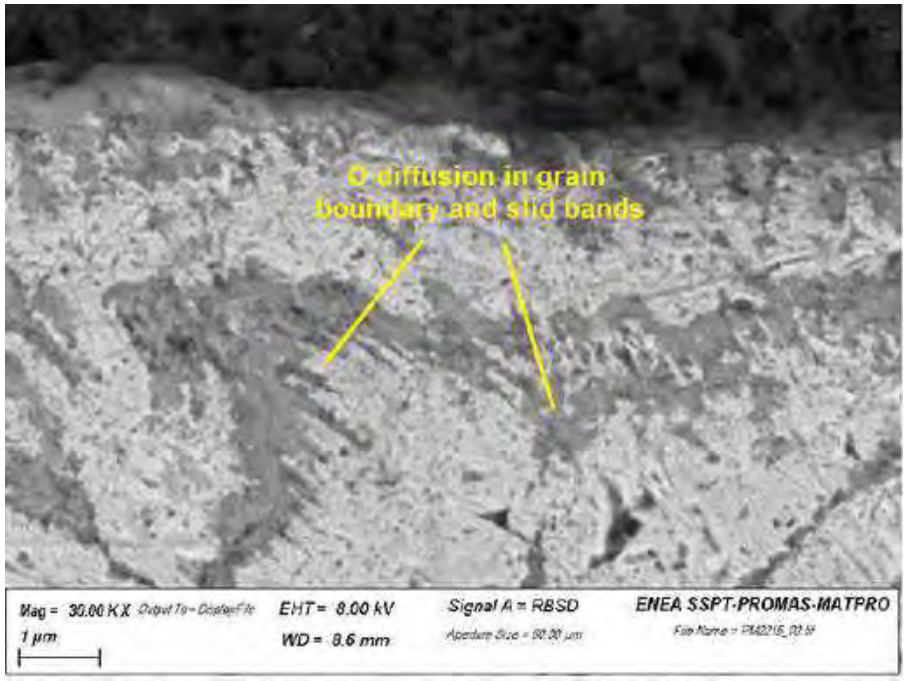

Results: after 1000 hrs the prevailing degradation mechanism is Oxidation; thickness of the oxide layer between 5 and 10 µm. No dissolution is noticeable . Further analysis on the exposed samples (EDS aimed at the detection of the composition of the corrosion layers) are on-going and will be delivered in the next AdP report.

Running activities: Ion-Irradiation

Irradiating in LNL (Laboratori Nazionali di Legnaro, INFN, Padova);
5 irradiation sessions (two days each) in order to achieve the 100 dpa target dose; start: July 2015, end: December 2018

- Geometry of the sample: 20mm x5mm x1,3 mm; polished surfaces

Inside the test section, after 4 irradiation sessions (approx. 80 dpa)

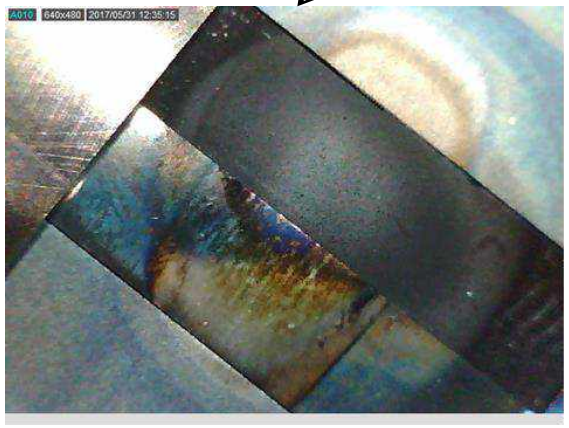

- Target: 100 dpa
- Heavy ions: 58 Ni
- 110 MeV

In progress … (four sessions completed, last session postponed due to the rupture of the "laddertron" of the TANDEM facility)

Creep characterization in progress ; 2017 Results

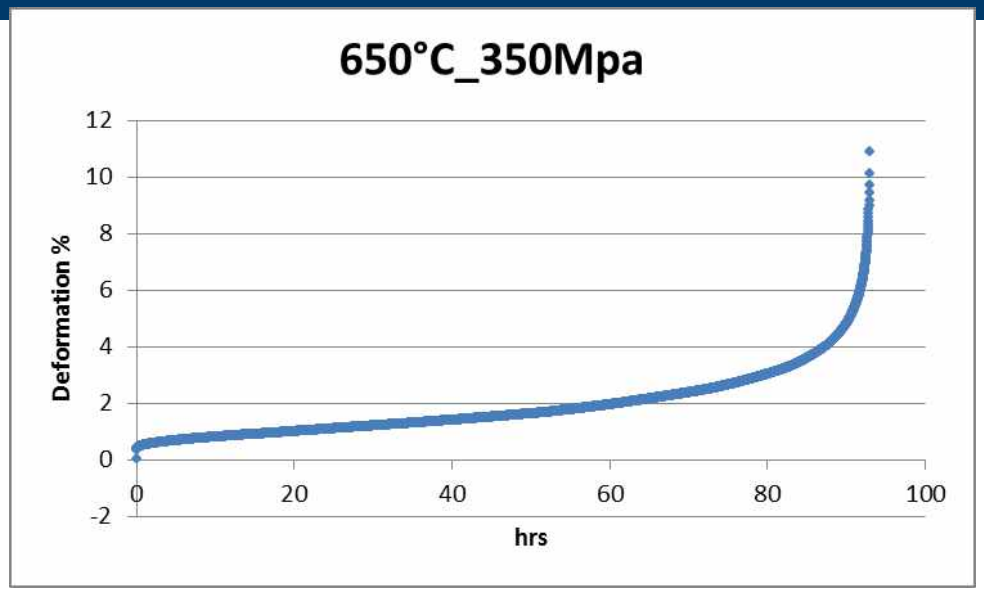

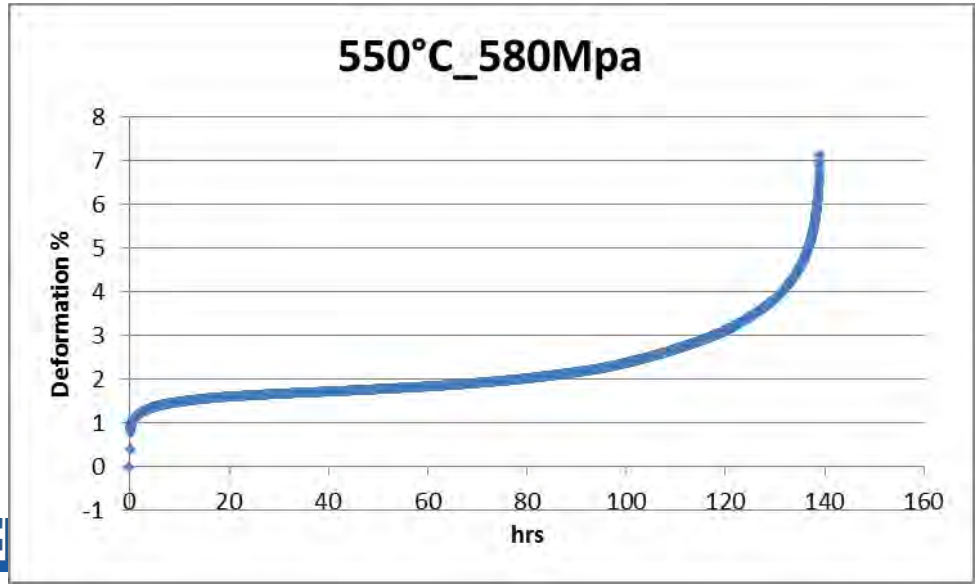

Creep characterization in progress ; 2018 Results

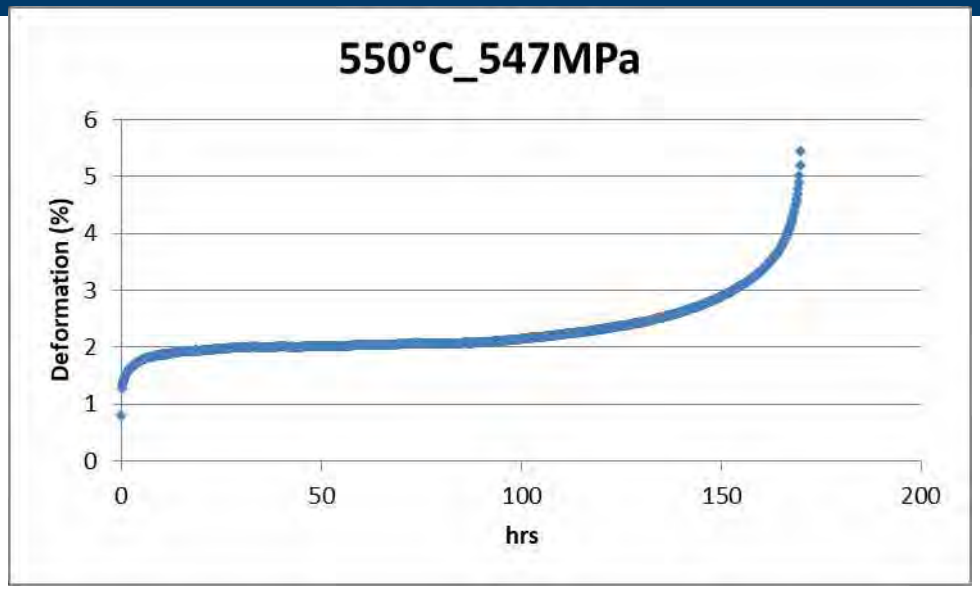

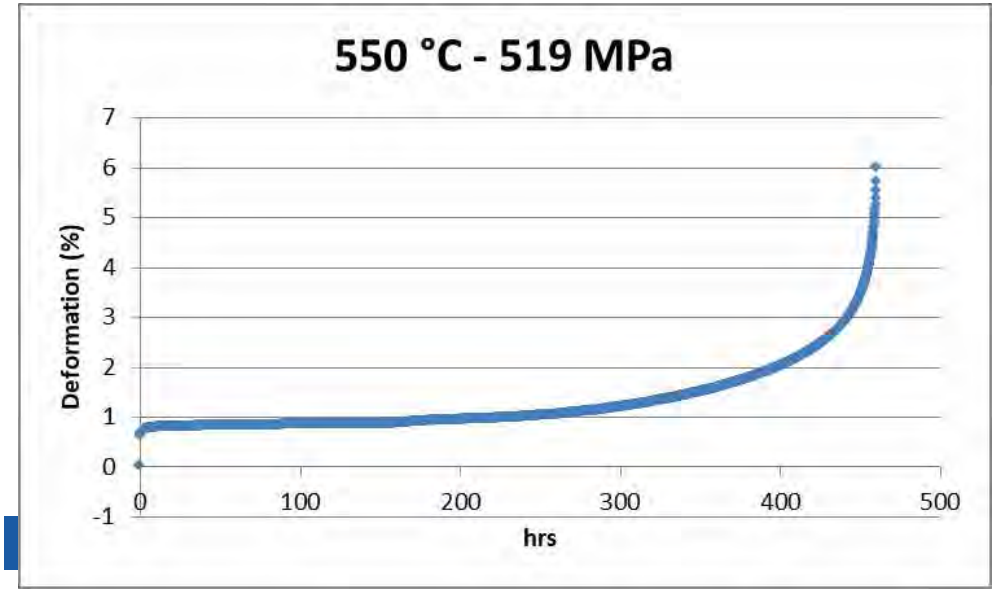

Creep characterization in progress ; 2018 Results

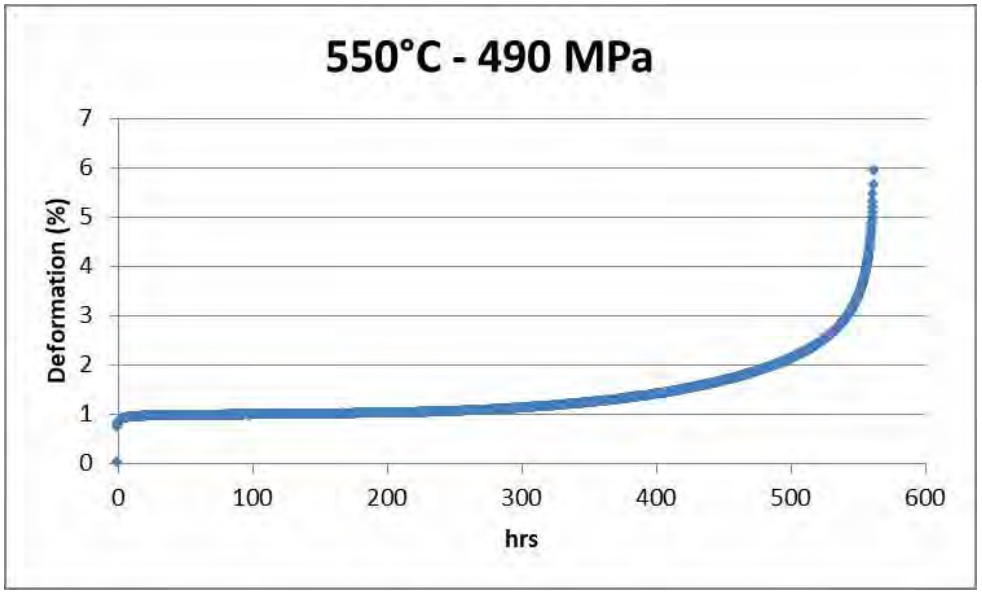

Partial comparison; 2018 Results

Partial results show poorer creep properties for 2014 batch compared to the former « Supernova » rods …

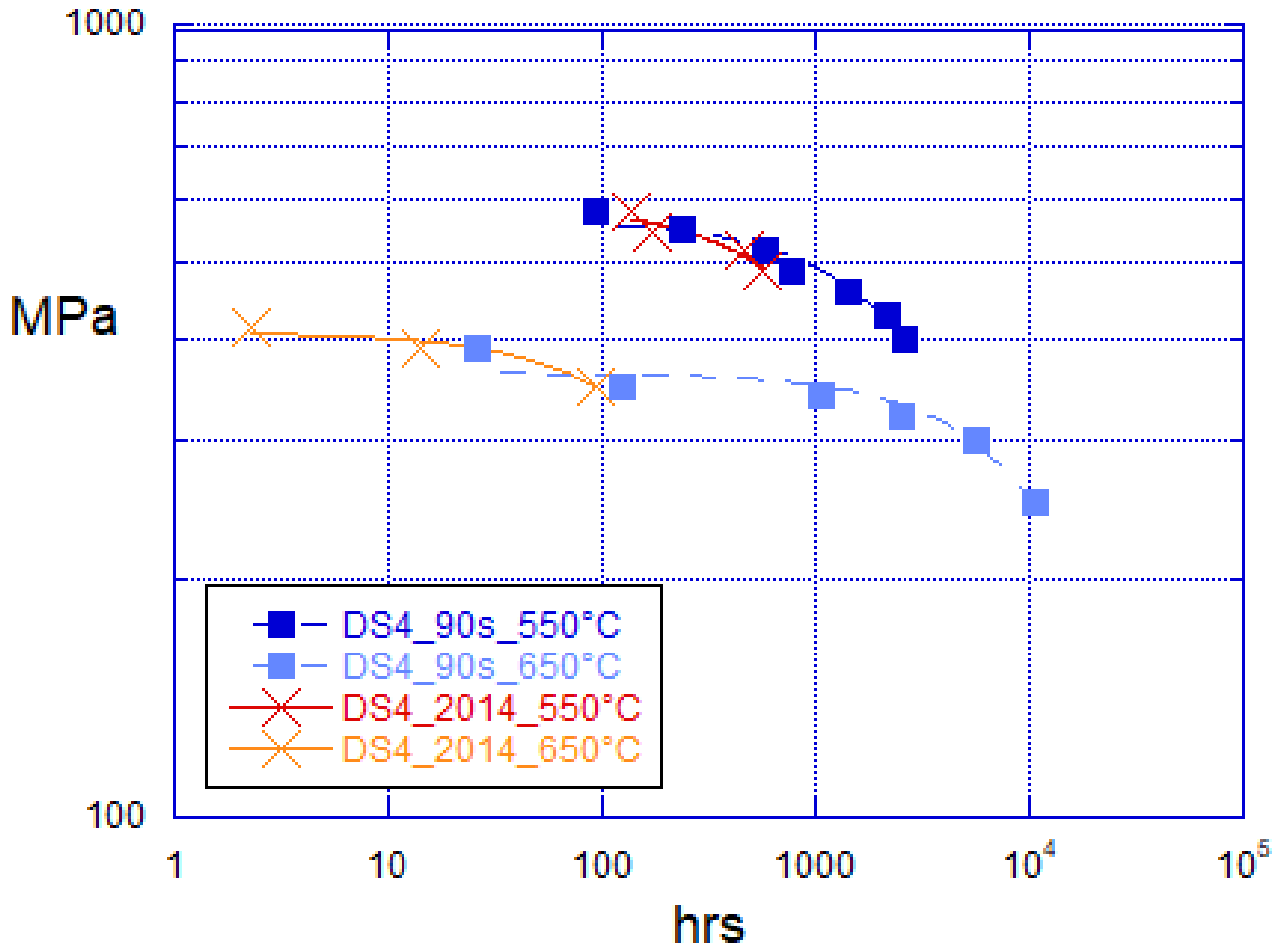

Partial comparison; 2018 Results

Partial results show poorer creep properties for 2014 batch compared to the former « Supernova » rods … but …

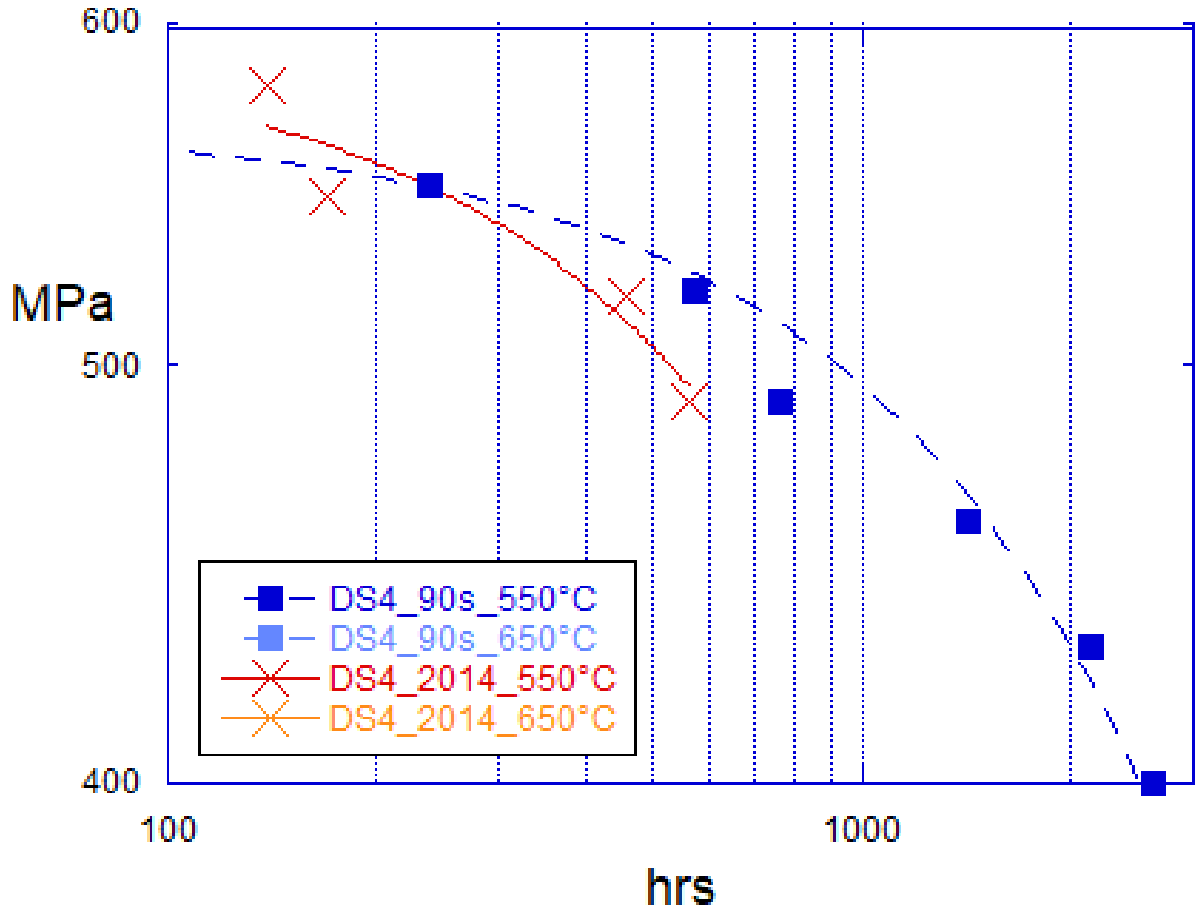

Creep characterization in progress; running tests

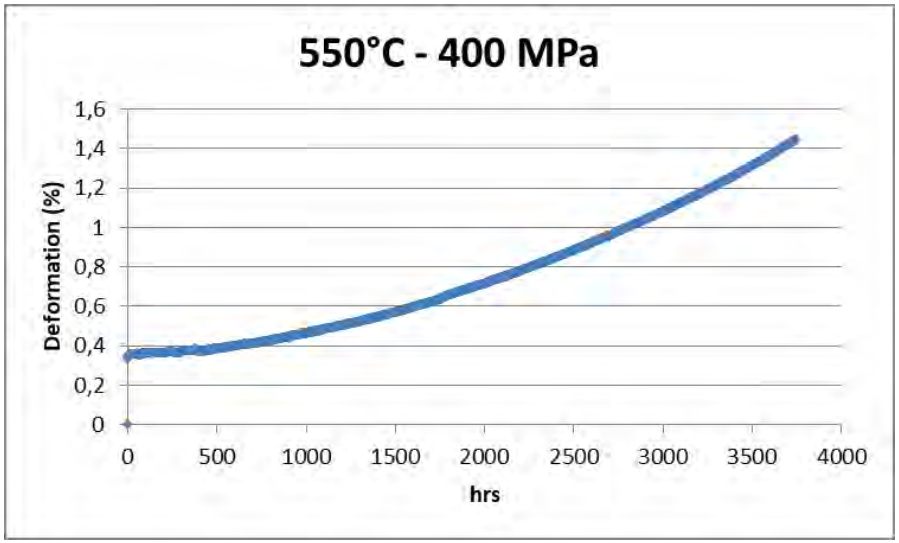

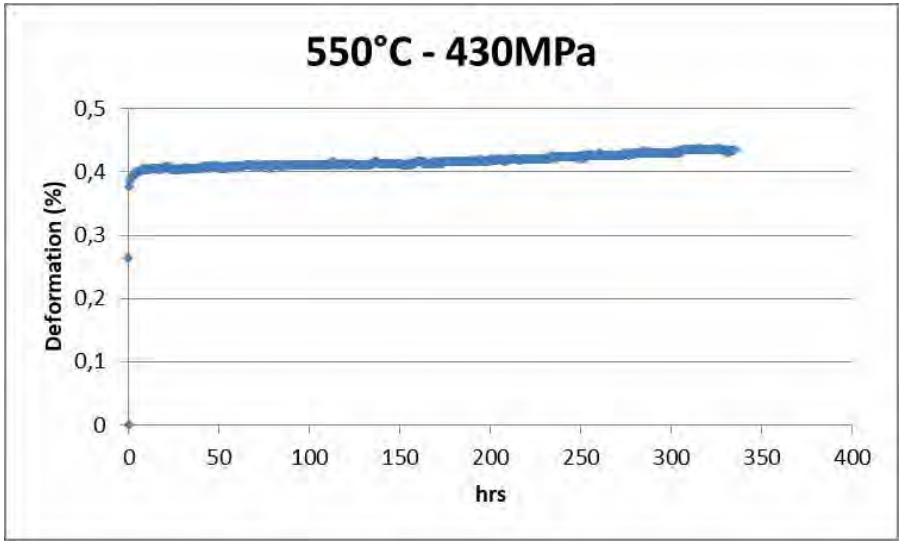

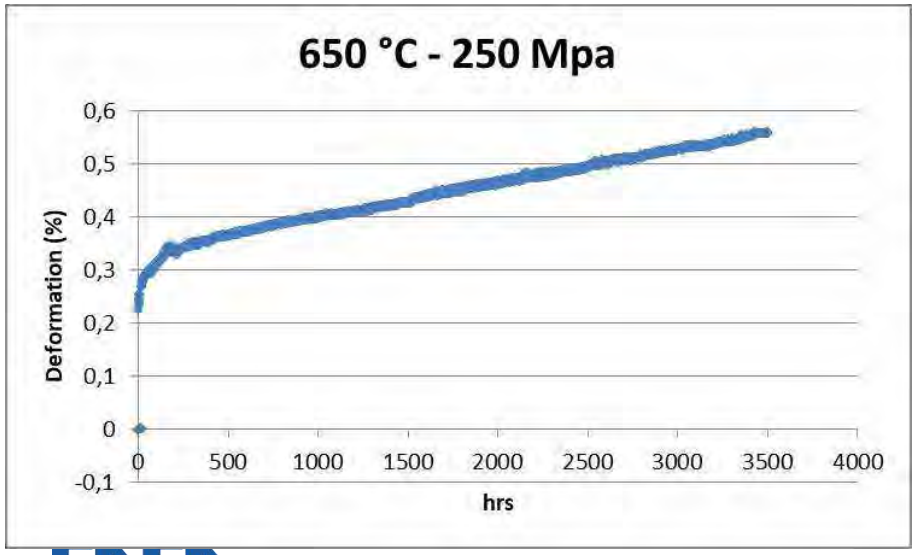

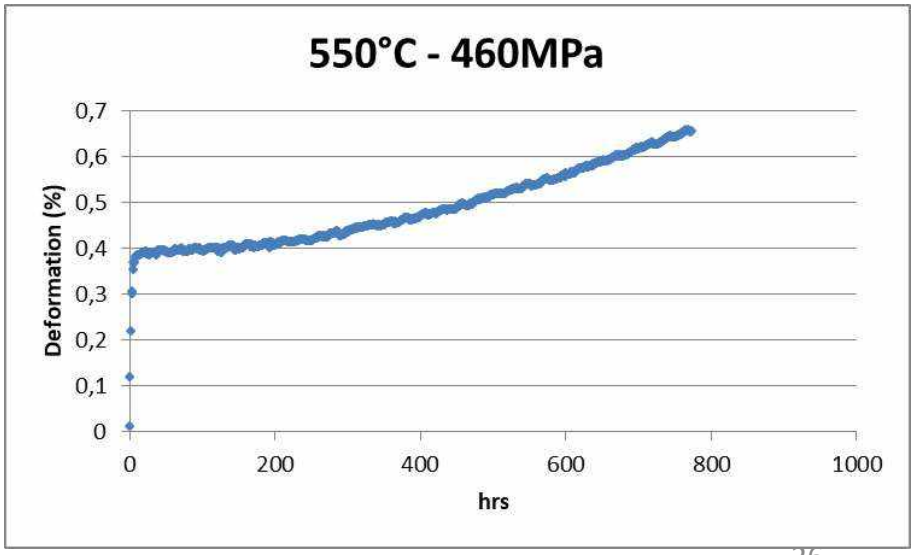

Partial comparison; 2018 Results

Still running test reveal improved creep performance at the lower loads …

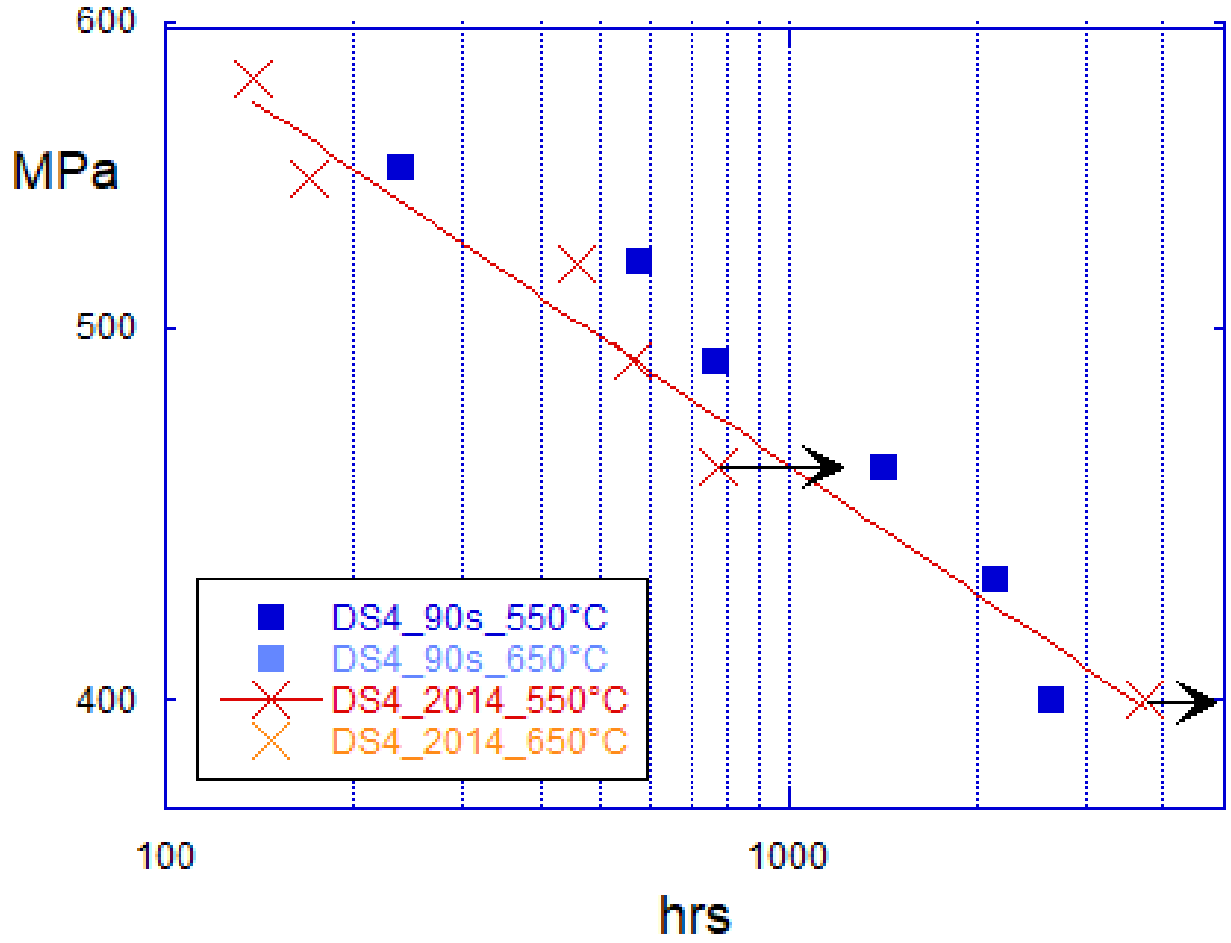

Conclusions

Double stabilized steels appear very promising because of the following reasons:

- the long term properties resulted nearly the best among the austenitic stainless steels (improved creep resistance of the former “Supernova” batch);
- the common C.E.A.-E.N.E.A. irradiation programme, the Supernova rig loaded in Phenix FBR at the beginning of May 1988, demonstrated the good swelling resistance;
- The features affecting the good swelling behaviour of these alloys are thought to be the high c.w. rate, the increased Ni content and the double stabilization (addition of Ti and Nb) which grants the possibility to tune up the precipitation of primary and secondary carbides in order to reduce the swelling;
- A new DS4 plate has been produced in 2014 and the tensile properties appear superposed to the ones of the former DS4 batch (namely the “Supernova” rods). Lower values of Uniform and Total Deformations of the new cast when compared to the ones of the former batch (irradiated in Supernova). Less performing creep behaviour of the new batch respect to the former one (according to the short tests) but improved performance at the lower loads according to the still running test (550° C-400MPa). Waiting the results of the ion irradiation programme (expected within the year).

Dissemination and publications

Logout

ABSTRACT SUBMISSION
Title: Status of the research on swelling resistant double stabilized austenitic steels

Abstract No.	0273
Title	Status of the research on swelling resistant double stabilized austenitic steels
Abstract	*DS_Steels.doc*
Template used	Yes
Text Abstract	The qualification of the fuel cladding material is one of the most crucial issues in Fast Reactors technology. Historically, the main limiting factor is related to cladding swelling; namely the increase of volume that takes place in materials subjected to intense neutron radiation and due to nucleation and growth of point defects aggregates. At the beginning of the '80s, within an experimental program carried out at the Saclay Center, the under electrons irradiations (1 MeV) had shown the effectiveness of the simultaneous presence of Ti and Nb on the swelling resistance of 316 and 15 Cr-15 Ni matrix. Then, after a further optimization of the chemical composition, innovative alloys had been realized based on 15 Cr-15 Ni and 15 Cr - 25 Ni matrix. The outcomes of the PIE (Post Irradiation Examination) in the frame of the "Supernova" experiment on these new steels, which took place in the early 90s, appeared extremely promising, particularly concerning the 15 Cr-25 Ni (Ti + Nb) matrix. This led ENEA to start the production of a new batch of DS4 (15 Cr-25 Ni) steel in 2014. The criteria which led the alloy design will be presented in this paper; the microstructural and compositional features that are expected to control and limit the swelling ratio are the high Ni content, the secondary precipitation of Ti and Nb carbides and the cold working in the range of 20% (section reduction ratio). The DS4 steel plate has then been characterized in terms of mechanical properties (hardness, tensile and creep), corrosion behaviour in flowing lead and ion irradiation. The status of the material after a 80 dpa damage by means of heavy ions (58 Ni - 110 MeV) will be reported and the outcomes of the mechanical characterization and corrosion tests will be presented.
App	Yes
Approval	Confirm
Copyright	Yes
Affiliations	(1) ENEA, n/a, Italy (2) INFN-LNL, n/a, Italy
Authors	C. Cristalli (1) Presenting M. Angiolini (1) S. Bassini (1) A. Candeloni (2) (2) L. Pilloni (1)

Thank you for your attention

Mechanical Characterization (1990): tensile & creep

Fitting of data

Fitting function:

$$t = K \cdot exp(-\gamma \cdot \sigma)$$

G. Filacchioni, L. Pilloni and oth. «Mechanical and structural behaviour of the second double stabilized steels generation», B.N.E.S. London,1990

Time to obtain 0.2% of creep strain; DS3

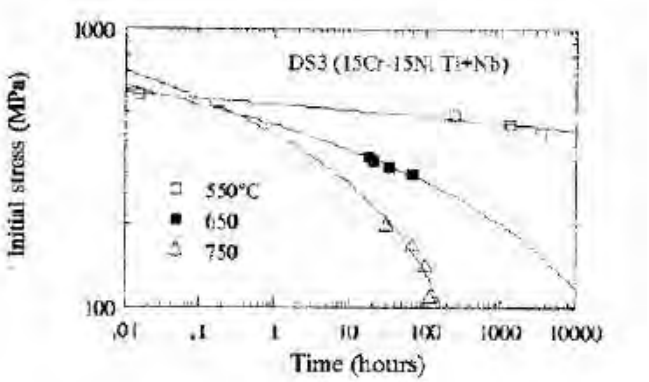

Time to failure; DS3

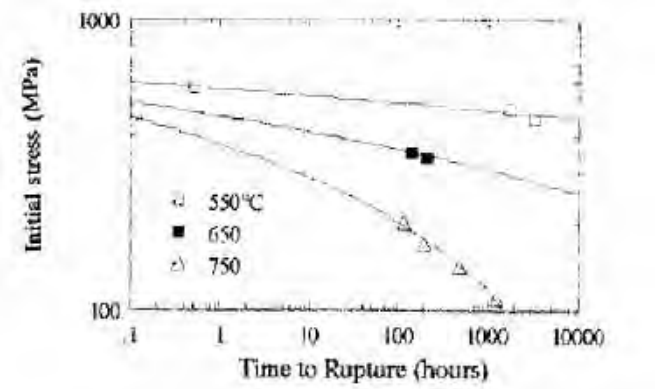

Time to obtain 0.2% of creep strain; DS4

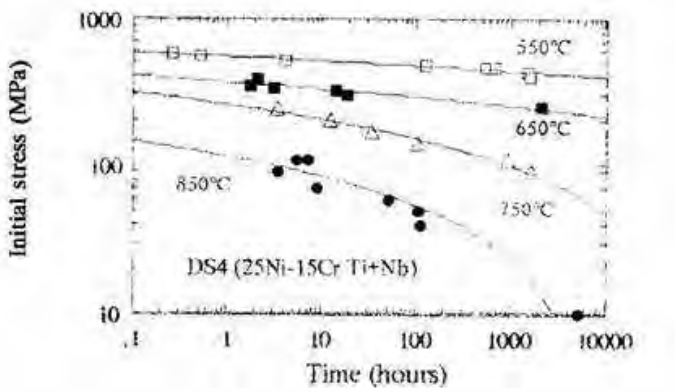

Time to failure; DS4

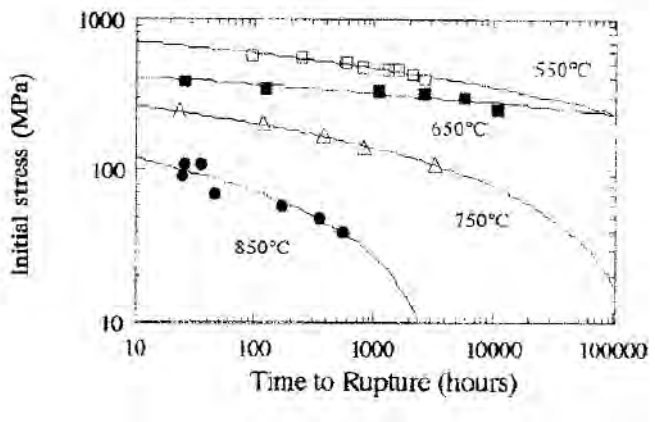

Introduction

Production of the first batch of DS alloys (2nd gen) in the late 80s

Position into the Shaffler's diagram

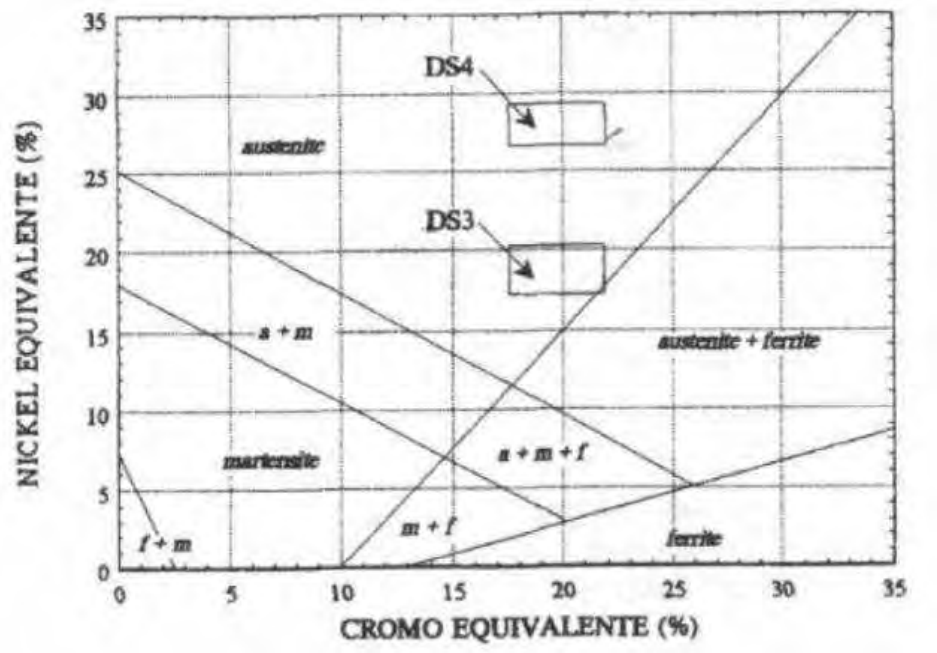

Manufacturing Details

Two kinds of products realized:

- rods (external diameter 8 mm)
- cladding pipes (ext. diam. 6,55 mm, internal 5,65)

The rods and the pipes were **cold-worked** with a final section reduction ratio of **20%**.

Annealing temperature before final cold-working : **1100° C** (5 minutes in Argon atmosphere), followed by air cooling.

Total/Uniform Elongation; Comparison

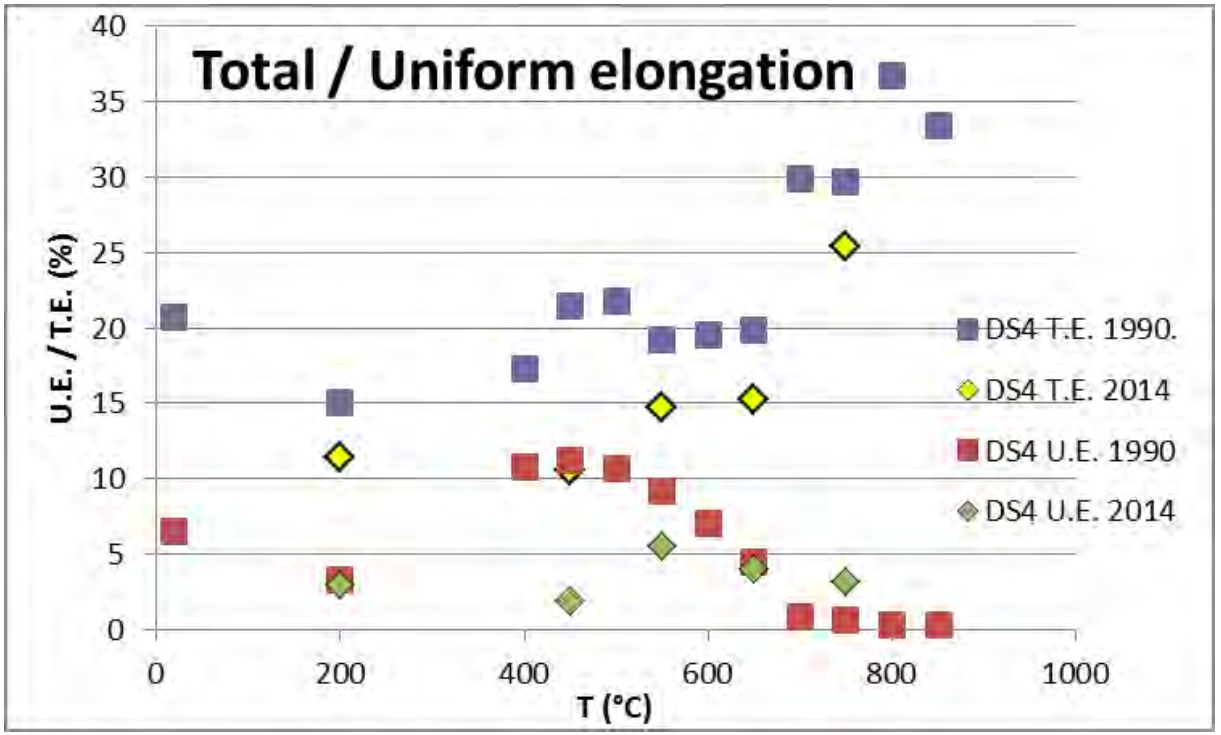

Concerning the uniform elongation DS4 behaviour was excellent. In the interval between 400 and 600-650° C the steel performs values that are almost twice respect to those of the other steels. This behavior, similar to the best ones for the stainless steels with high yield strength, is symptomatic of good characteristics of stretchiness, performing delayed onset of mechanical instability. The values of the deformations, comparing the new batch to the former one, appear averagely less performing.

Creep characterization in progress …

Partial results show poorer creep properties for 2014 batch compared to the former « Supernova » rods…

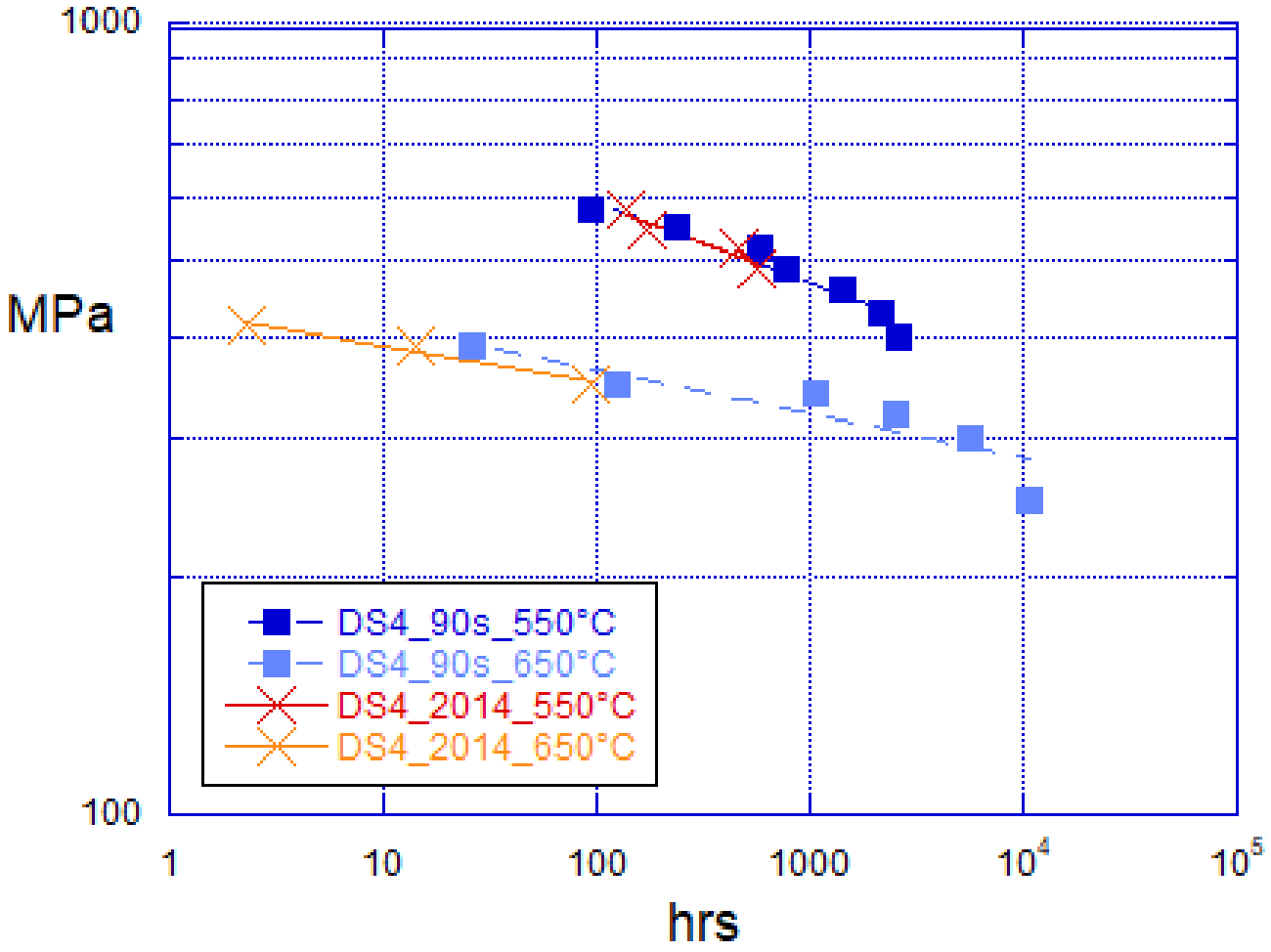

Creep characterization in progress …

Partial results show poorer creep properties for 2014 batch compared to the former « Supernova » rods…

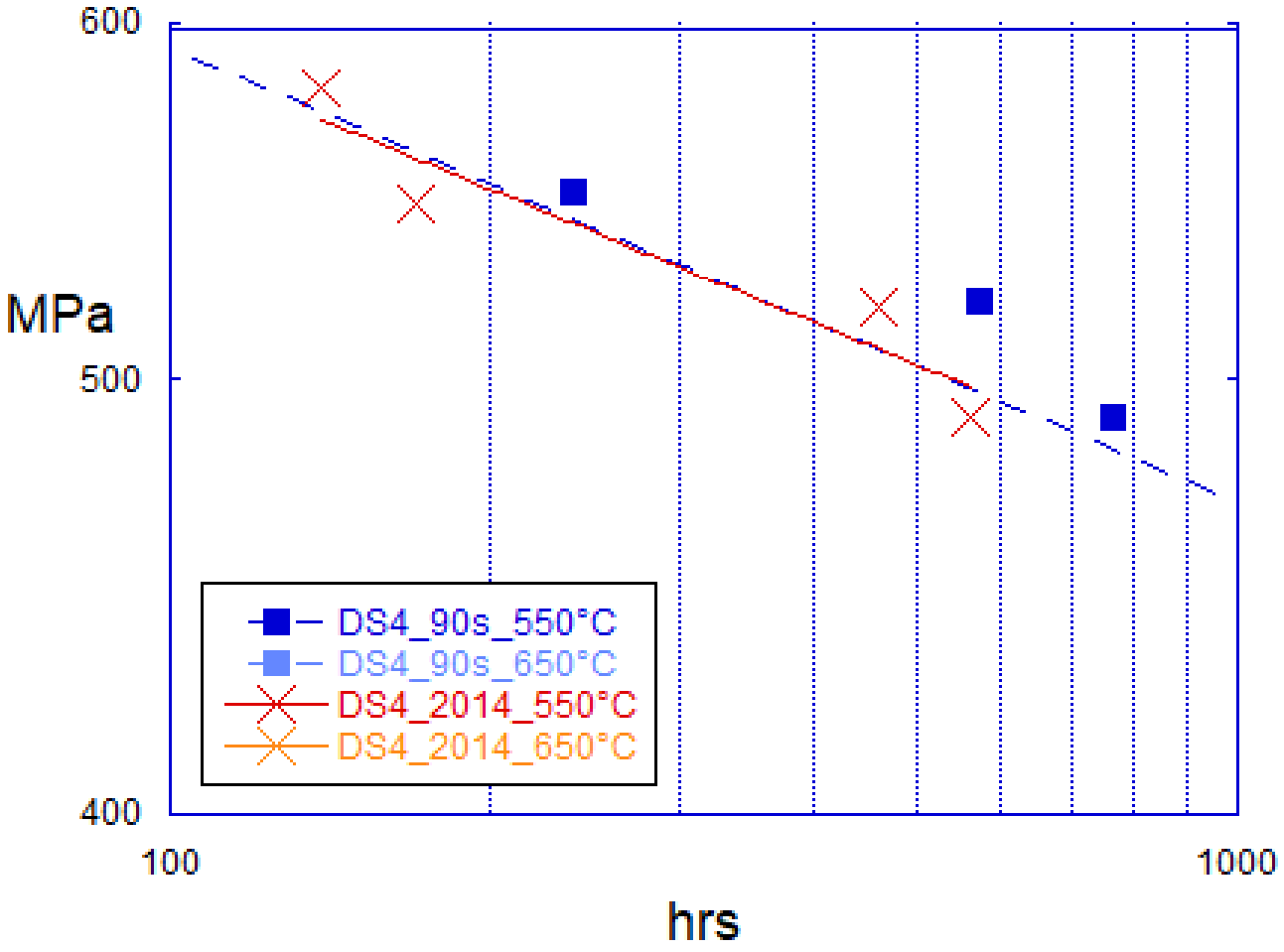

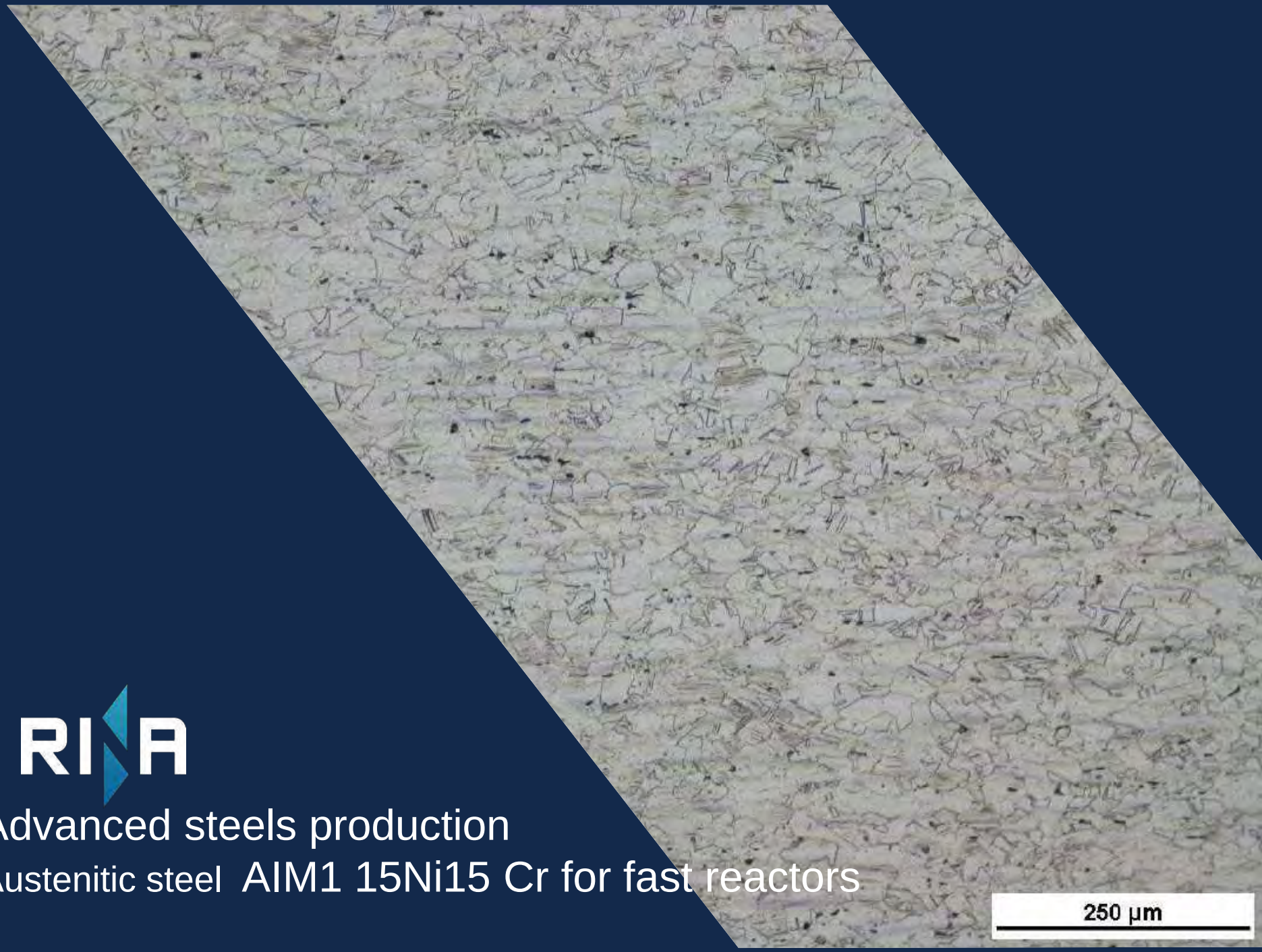

RINA

Advanced steels production

Austenitic steel AIM1 15Ni15 Cr for fast reactors

Processi di produzione

Primary Melting

VACUUM INDUCTION MELTING

Secondary Melting

ELECTRO SLAG REMELTING

Thermo-mechanical transformation

HOT / COLD ROLLING

VIM ingots

VIM ingots produced by using high purity raw materials:

- vacuum/ controlled atmosphere process
- On-line chemical analysis

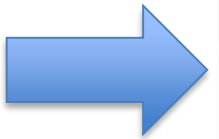

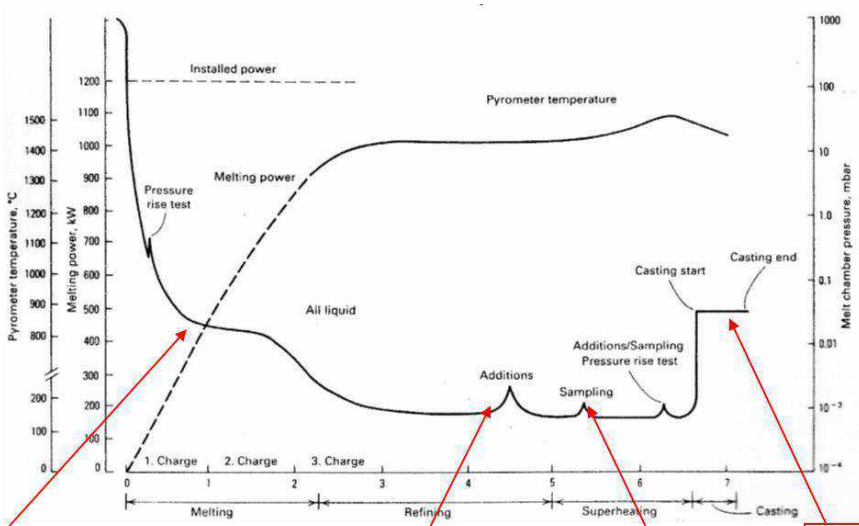

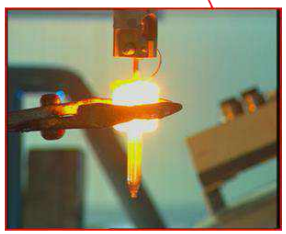

Vacuum Arc Remelting

The L 240/PESR is a multi-purpose laboratory furnace for high quality material production and development.

The furnace allows the following processes and features:

- Ingot melting with various mold diameters and lengths, using the consumable electrode technique. Remelting of all materials from copper to high melting point materials.

VIM ingot remelting for:

- Desolforation
- Nitriding
- O2, N2 e H2 removal
- Inclusion removal
- Directional solidification
- Solidification structure refining
- Homogeneity
- Less segregation

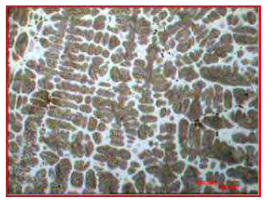

Hot rolling

VIM + VAR ingots, after mechanical machining and homogenization heat treatment have been subjected to hot rolling.

From 120 mm (T > 1000°C) to ~ 25 mm.

*

Cold rolling

Two step lamination :

1) ~ 20mm,

2) Final 15mm.

Thermal treatment between the two steps.

The thermal treatments have been optimized, by means laboratory trials to obtain the technical requirements

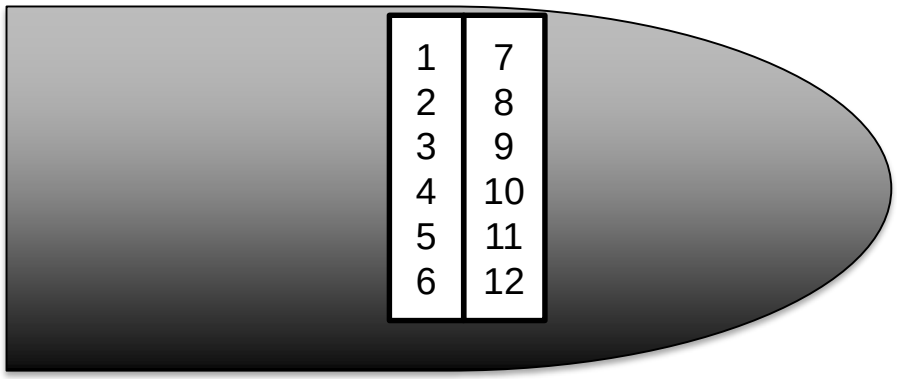

Specifications

Targets

620 ≤ Rp0,002 ≤ 840 Mpa
Rm ≥ 760 Mpa
Atot ≥ 18%

Sigla provetta		*Specimen ID*	**1515 Ti - A**	**1515 Ti - B**	**1515 Ti - C**	**MEDIE**
Velocità deformazione fino a Rp, ReH, ReL (1/s)		*Strain rate up to Rp, ReH, ReL*	2.50E-04	2.50E-04	2.50E-04	**2.50E-04**
Velocità per Rm (1/s)		*Strain rate for Rm*	6.70E-03	6.70E-03	6.70E-03	**6.70E-03**
T (°C)	Temperatura di prova	*Test temperature*	RT	RT	RT	**RT**
do (mm)	Diametro Iniziale	*Original diameter of the parallel length*	8.92	8.92	8.88	**8.91**
So (mm2)	Sezione Iniziale	*Original cross sectional area of the parallel length*	62.49	62.49	61.93	**62.39**
Lo(mm)	Tratto Utile	*Original gauge length*	45	45	45	**45**
Le(mm)	Base Estensimetro	*Extensometer gauge length*	50	50	50	**50**
Fp 0,2 % (N)	Carico Scost. Prop.	*Force corresponding to the proof strength, plastic extension 0.2%*	45780	47615	45964	**46233**
Fmax (N)	Carico Massimo	*Maximum force*	52103	52514	51946	**52305**
L_u (mm)	Lunghezza Ultima	*Final gauge length after fracture*	53.19	52.82	53.19	**52.81**
du (mm)	Diametro Ultimo	*Minimum diameter after fracture*	5.75	5.62	5.67	**5.66**
S_u (mm2)	Sezione Ultima	*Minimum cross sectional area after fracture*	25.97	24.81	25.25	**25.19**
Rp 0,2 % (MPa)	C. Unit. Sc. Prop.	*Proof Strength, plastic extension 0.2%*	733	762	742	**746** √
Rm (MPa)	C. Unit. A Rottura	*Tensile strength*	834	840	839	**838** √
A (%)	Allungamento Perc.	*Percentage elongation after fracture*	18	18	18	**18,1** √
Z (%)	Strizione Perc.	*Percentage reduction of area after fracture*	58	60	59	**60**

Final result

Material in line with requirements:

1) Grain size: 8,19 G (center)
2) Mechanical propertiesi
   - ✓ $Rp_{0,2\%}$ = 746 Mpa
   - ✓ R_m = 838 Mpa
   - ✓ A_{tot} = 18%
3) Inclusional state accroding to ASTM E45 – Method D

Powder Metallurgy

Powder Metallurgy is a continually and rapidly evolving manufacturing technology that include most metallic and alloy materials, and a wide variety of shapes and dimensions.

The European Market alone has an annual turnover of over 6,000 M€ , with annual worldwide metal powder production exceeding 1 million tonnes.

The mostly PM technologies are:

- Press & Sintering
- Hot Isostatic Pressing (HIP)
- Metal Injection Moulding (MIM)
- Coatings for Surface Engineering
- Additive manufacturing (AM)

Powder Metallurgy

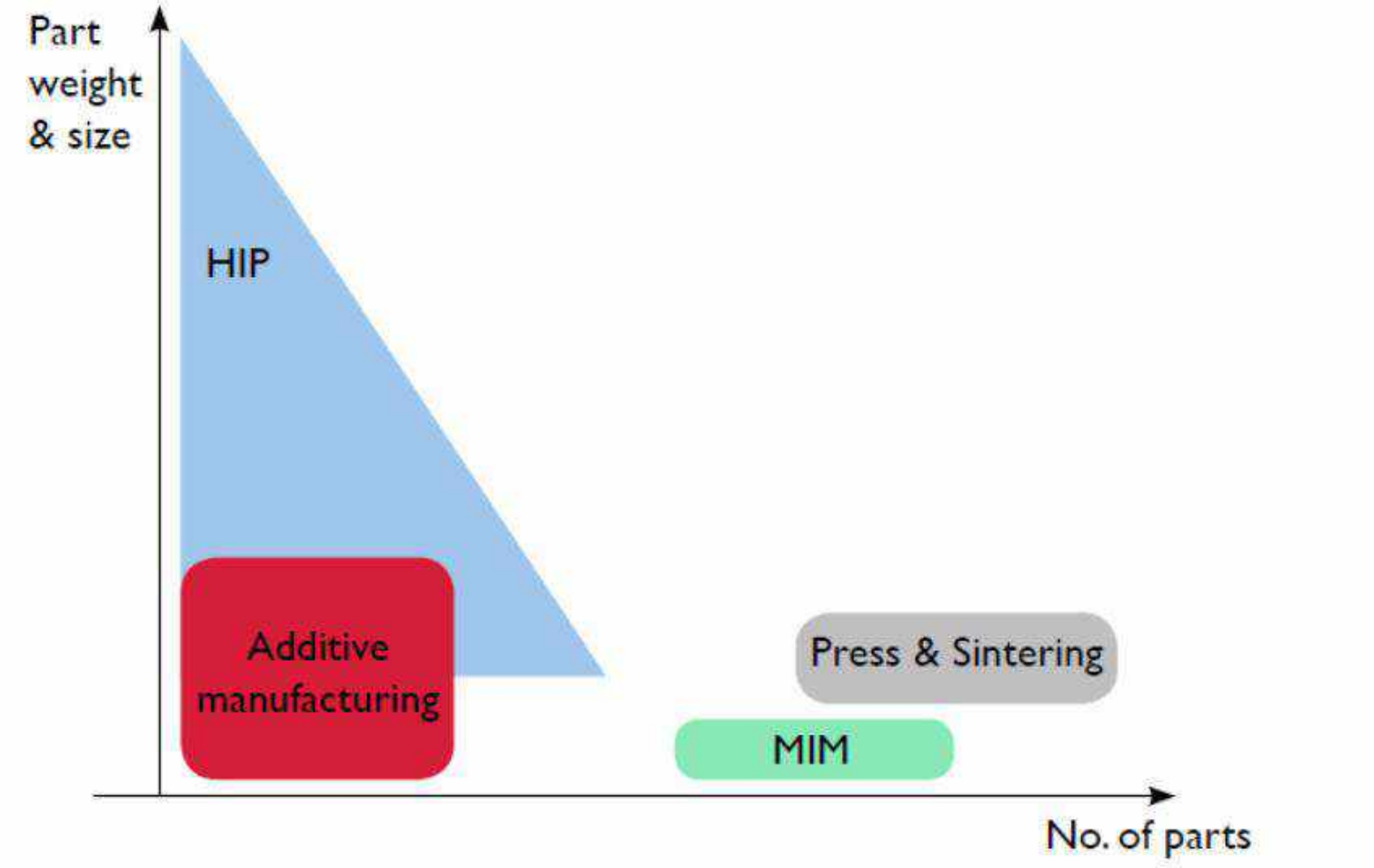

Positioning map of various PM technologies according to part weight or size and production series

Metal additive manufacturing

According to the ASTM standard F2792-10 “AM is the process of joining materials to make objects from 3D model data, usually layer upon layer, as opposed to subtractive manufacturing methodologies” such as machining.

Design for AM

Topological optimization

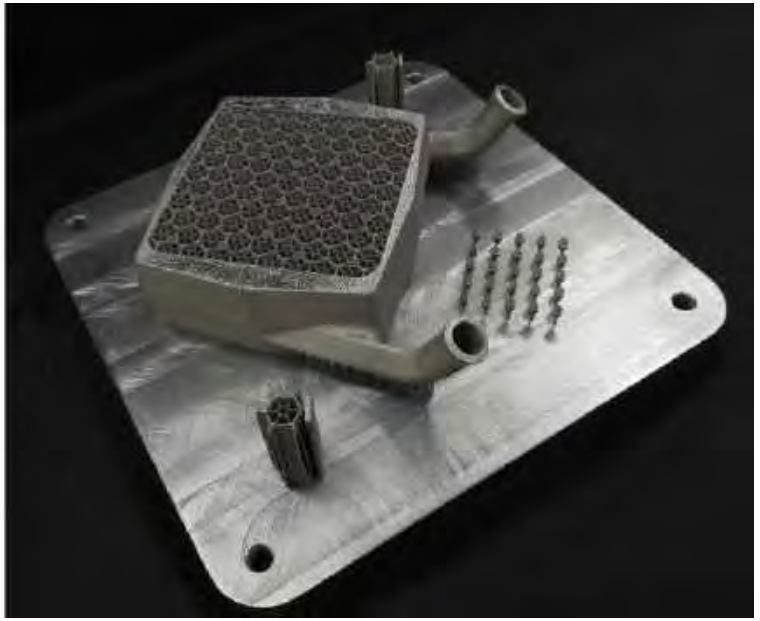

Designed for SLM

PoliMi compact motorcycle radiator

- ✓ Morphological freedom – use material where required
- ✓ Use of light-weight structures
- ✓ Less material, shorter process, lower cost

AM key benefits

1. Increased design freedom versus conventional casting and machining;
2. Light weight structures, made possible either by the use of lattice design or by designing parts where material is only where it needs to be, without other constraints;
3. New functions such as complex internal channels or several parts built in one;
4. Net shape process meaning less raw material consumption, up to 25 times less versus machining , important in the case of expensive or difficult to machine alloys. The net shape capability helps creating complex parts in one step only thus reducing the number of assembly operations such as welding, brazing;
5. No tools needed, unlike other conventional metallurgy processes which require molds and metal forming or removal tools;
6. Short production cycle time: complex parts can be produced layer by layer in a few hours in additive machines. The total cycle time including post processing usually amounts to a few days or weeks and it is usually much shorter than conventional metallurgy processes which often require production cycles of several months.

AM technologies

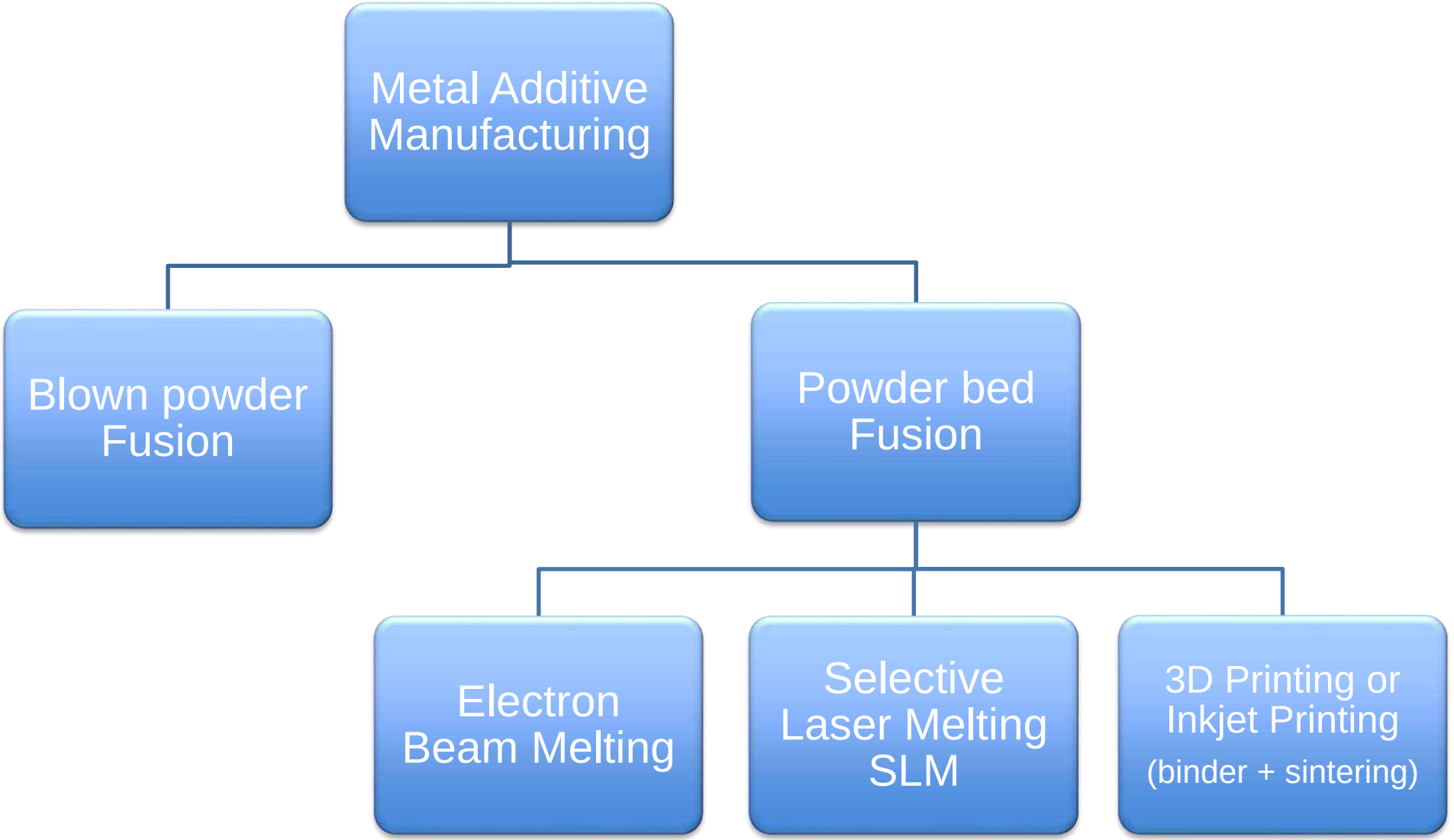

Development of the metal alloy

The alloy design and the alloys development is necessary to define the best chemical composition for AM processes.
This will lead to a new proprietary alloy, very suitable for AM technologies.
This alloy design and development will be focused on aluminum alloys.

The commercial Al alloys actually available for AM processes have limited mechanical properties as shown in the Figure below (Metal AM - Metal powders – the raw materials).
The market needs an increase of mechanical behavior for high demanding applications and this goal can be achieved by a proper new alloy design.

Metal powder properties

Most relevant factors that play a important role and that have an effect o the finished product are:

- ✓ morphology;
- ✓ particle size distribution;
- ✓ density;
- ✓ porosity;
- ✓ thermal properties;
- ✓ surface properties;
- ✓ impurities.

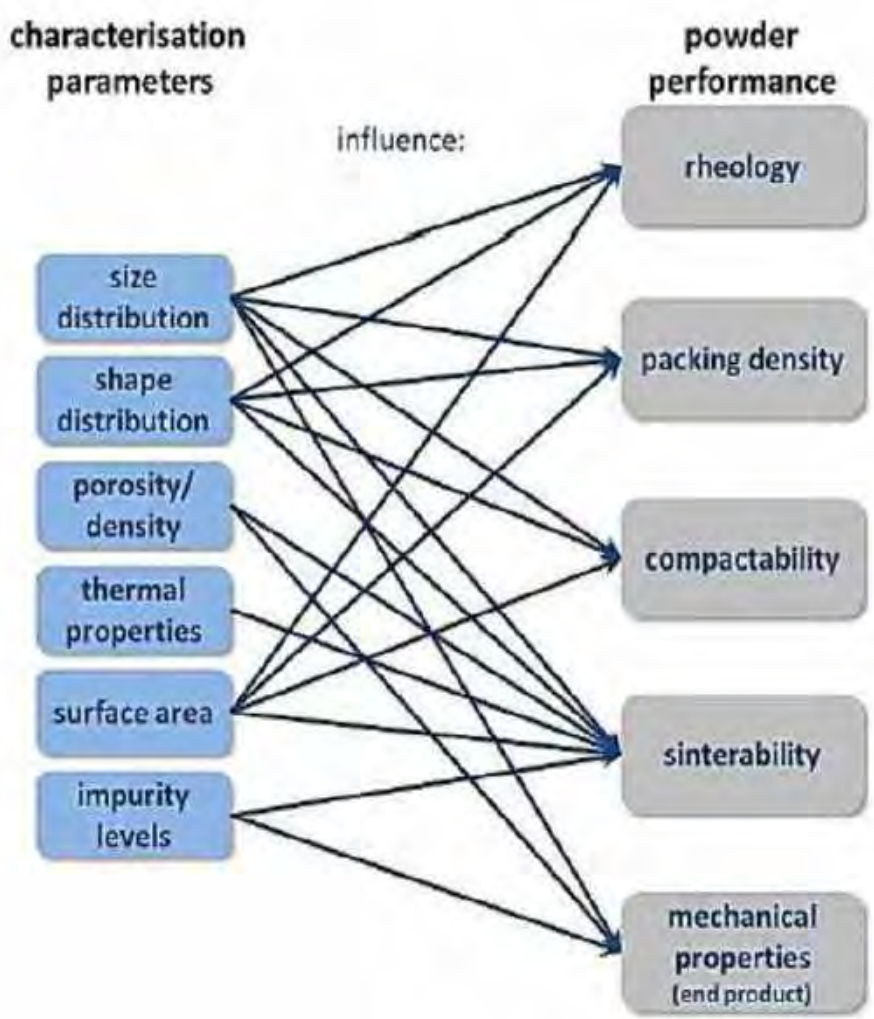

RINA for Powder Metallurgy & Additive Manufacturing

Expertise on PM & AM

In the last fifteen years RINA has developed a specific expertise and know how in the areas of:

- ✓ Coatings for Surface Engineering
- ✓ Additive Manufacturing (AM)
- ✓ Metal Powders production, for various applications including AM itself.

Expertise on PM & AM

Relatively AM, RINA has developed its expertise with the purchase of two 3D printing machines.

Relatively powder production instead RINA with its VIGA plant (Vacuum Inert Gas Atomizer) have been produced and developed a significant amount of chemical compositions mainly of steels, superalloys, copper and aluminum alloys

Actual projects

Actually RINA is currently supporting various clients in the activities of:

- ✓ alloy design and pilot production for new powders grade
- ✓ feasibility studies for the installation of new atomization plants
- ✓ market analysis
- ✓ roadmap for choice of the best technologies according to material/final application
- ✓ chemical, physical, metallurgical and mechanical characterization of AM products
- ✓ AM process yield optimization
- ✓ Powder Manufacturing process optimization / Expert on site
- ✓ Technical Support during Plant commissioning
- ✓ Training

RINA activities within the AM value chain

Alloy design

Define new compositions with specific properties (e.g. Ni alloy with high creep resistance) to be processed by ALM

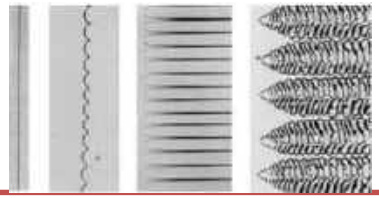

Thermodinamic model

- ALM process conditions similar to welding (rapid solidification)
- Analysis of solidification mechanisms
- Microsegregation mode
- Definition of T solidus

Process Metallurgy (VIM-VIGA)

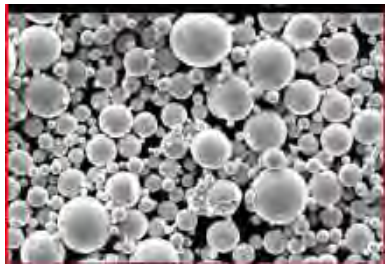

Heat treatmens / post treatments

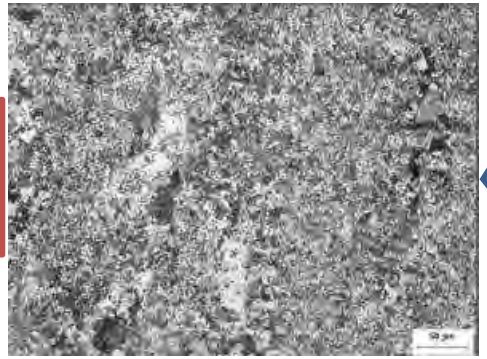

Microstructural and mechanical characterization

Pilot Plant for powder manufacturing

VACUUM INDUCTION MELTING

VACUUM INDUCTION GAS ATOMISATION

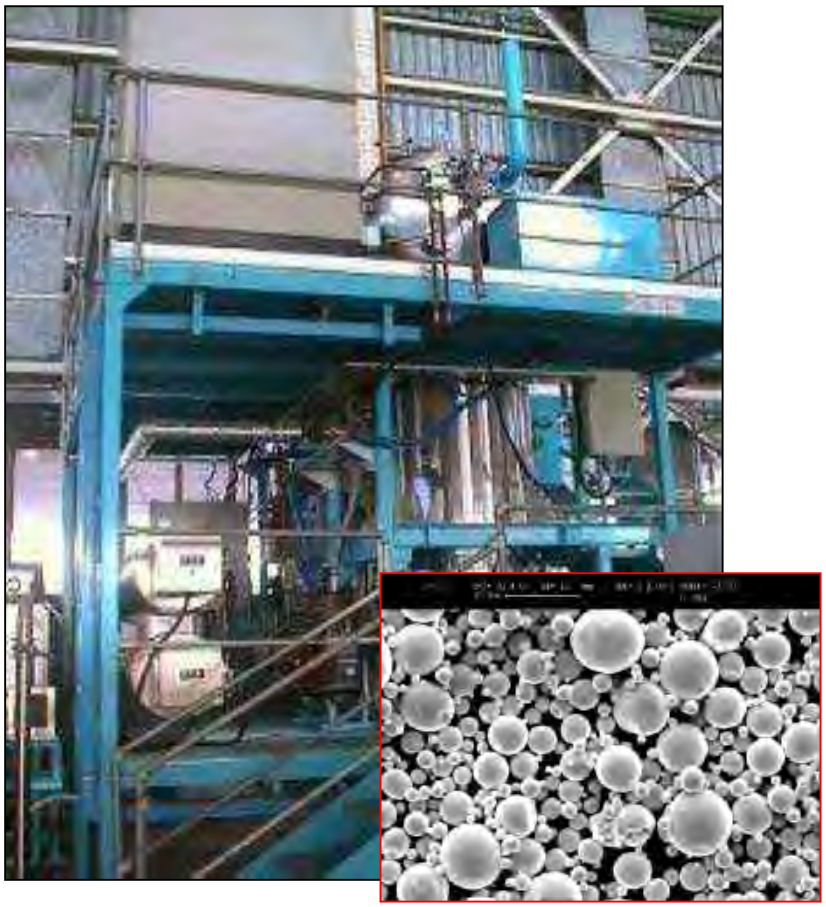

Metal powder produced at CSM

Alloy Grade	Tipology	Applications	Properties	Market sector
Fe 5Al 10Si	Steel	Coating	High conductivity	Food
Fe 21Cr 6Al	Steel	Coating	Corrosion resistance	Aerospace
Fe 25Cr 5Si	Steel	Coating	Corrosion resistance	Aerospace
Fe based	Steel	Sintering	Corrosion resistance	Metal Injection Moulding
Fe based	High Nitrogen Steel	Sintering	Corrosion resistance	Bio Medical
Fe based	High Nitrogen Steel	Sintering	High Temp resistance	Aerospace
PM1000	ODS Steel	Sintering	Mechanical strenght	Aerospace
PM2000	ODS Steel	Sintering	Mechanical strenght	Aerospace
NiCoCrAlY	Superalloys	Coating	High Temp resistance	Aerospace
Ni based	Superalloys	Coating	High Temp resistance	Tooling
Inconel 718	Superalloys	Coating	High Temp resistance	Aerospace
Ni based	Superalloys	Additive Layer Manufacturing	High Temp resistance	Aerospace
Cu Oxigen free	Copper	Testing	High conductivity	Energy
CoCr	Cobalt Based	Additive Layer Manufacturing	Corrosion resistance	Bio Medical
Al Sc	Al alloys	Additive Layer Manufacturing	High Temp resistance	Aerospace

Qualification and certification process for AM materials and components

AM is a disruptive technology which has high potential in all the industrial sectors. Anyway it is a «new» technology and standardization as well as qualification and certification processes are still ongoing.

Quality and safety are involved in any step of the manufacturing process, from the design phase to the raw materials acquisition, from processing to finishing, so it needs a specific study of each step.

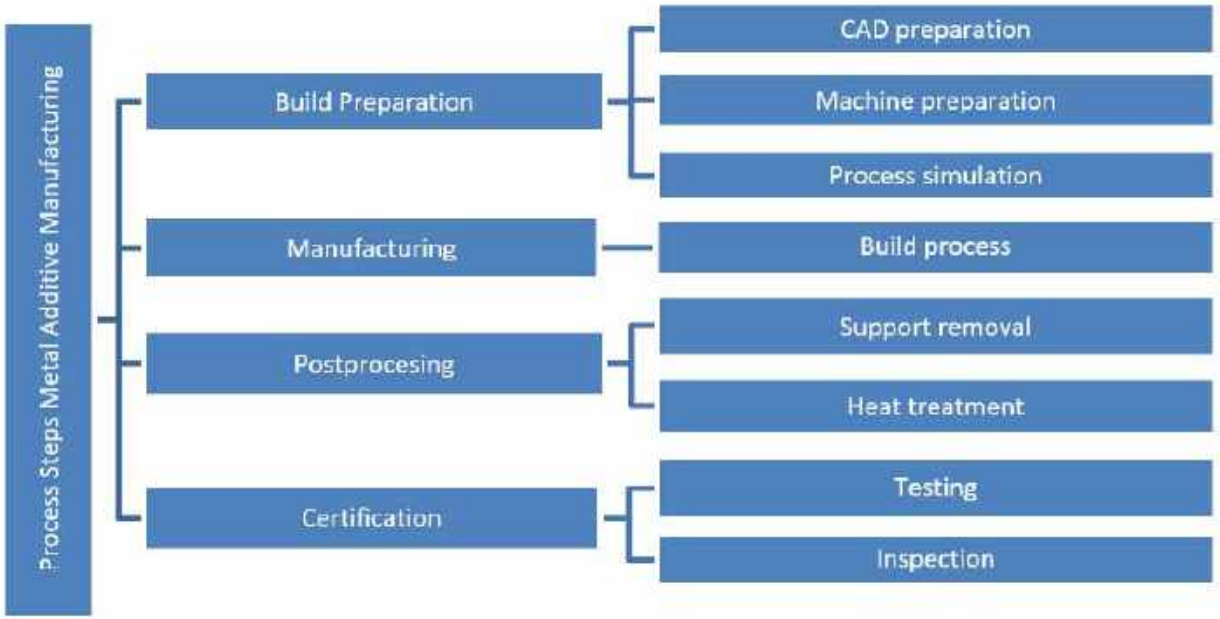

Example of processing steps for Metal AM manufacturing

Qualification and certification process for AM materials and components

Qualification is different from certification

	Qualification	Certification
Scope	Process of evaluating a prototype design/material / product during the development/testing phase to determine whether it meets the specified requirements for that phase.	The process of evaluating a material /product /component during or at the end of the development process / regular production to determine whether it satisfies specified technical requirements.
Objective	To ensure that prototype meet the specified requirements to go to validation phase.	To demonstrate that the product fulfills its intended use when placed in its intended environment.
Evaluation items	Feasibility reports, requirement specs, design specs, test cases, procedure qualification, process parameters, etc.	The actual product
Activities	— reviews — audits / site-visits — witness testing — compliance statement — facility approvals	— inspections — testing — product certification

Qualification and certification process for AM materials and components

The certification Pathway can be divided in three phases:

Phase 1: Procedure qualification phase

Manufacturers or end users run qualifications/ the proof of concept to prove that they have feasible technology /products.

Phase 2: Approval phase

Manufacturer's or end user's design or manufacturing capabilities and process controls are assessed to determine if the manufacturer can produce specific grades or types of materials that conform to the Rules

Phase 3: Certification phase

Manufacturers/end users require a certification authority to certify material or products from regular production, either as individual parts or in batches, depending on the certification requirement of those parts. Material certification and component /product certification are relevant activities in this phase.

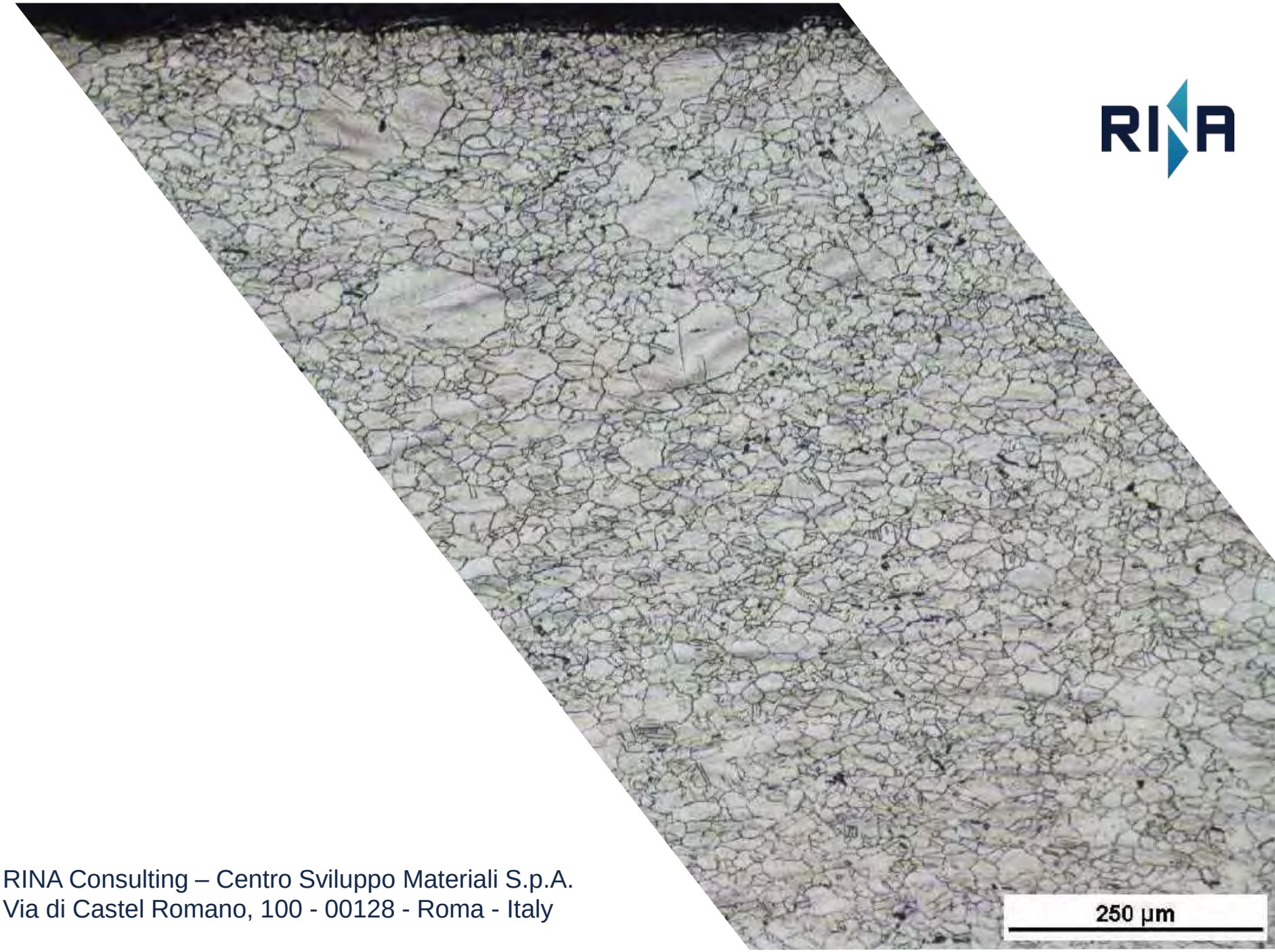

RINA Consulting – Centro Sviluppo Materiali S.p.A.
Via di Castel Romano, 100 - 00128 - Roma - Italy

Agenzia nazionale per le nuove tecnologie,
l'energia e lo sviluppo economico sostenibile

Termomeccanica di nocciolo

Analisi vibrazionale della barretta

Dipartimento di Ingegneria Astronautica, Elettrica ed Energetica
Università di Roma 'La Sapienza' - San Pietro in Vincoli
14-15 Giugno, 2018

Alessandro Poggianti – ENEA

Contesto del lavoro

Riferimento

L'intera Linea Progettuale 2 è dedicata all'avanzamento della tecnologia del **LFR**

Tutte le attività vertono su **ALFRED**, assunto a riferimento nella sua qualità di **dimostratore** della tecnologia **LFR**.

Fra le attività condotte nell'ambito dell'AdP, un blocco considerevole è dedicato al **progetto di nocciolo**, in particolare:

- sviluppo, revisione e affinamento del progetto;
- sviluppo, validazione ed applicazione di metodologie e strumenti di analisi a supporto della progettazione.

ALFRED core design: cosa c'è da fare

La maggior parte dei punti aperti sul progetto di nocciolo riguardano il corretto dimensionamento (e, qualora richiesto, la rivisitazione) dei principali componenti del nocciolo, avendo come riferimento ultimo la qualifica dell'elemento di combustibile, del sistema di supporto del nocciolo e del sistema di movimentazione degli elementi freschi ed esausti per e da il nocciolo.

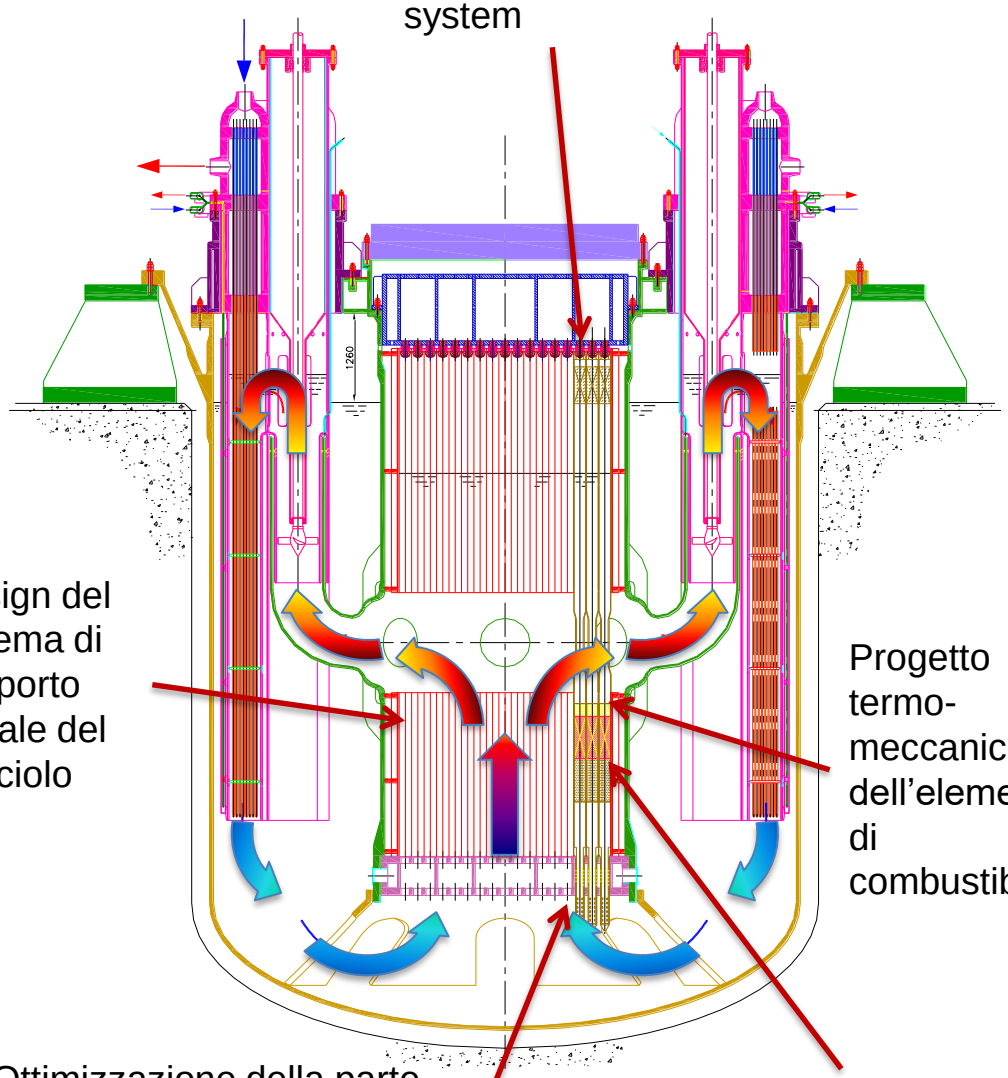

Analisi vibrazionale

Corner rod cooling and flow induced vibration in an ALFRED fuel assembly – FALCON doc. NRG-23591/16.140918

- Dati geometrici
- Proprietà fisiche di fluido e barretta
- Temperature del fluido
- Possibili risonanze a 400Hz e 10.2 Hz

Ipotesi

- Spacer posizionato a 100 mm dalla zona attiva

Aspetti da investigare

- Frequenze naturali della barretta
- Vibrazione della barretta immersa nel fluido
- Influenza delle barrette vicine
- Valutazione di possibili urti tra le barrette

Modello Elementi finiti barretta

Barretta

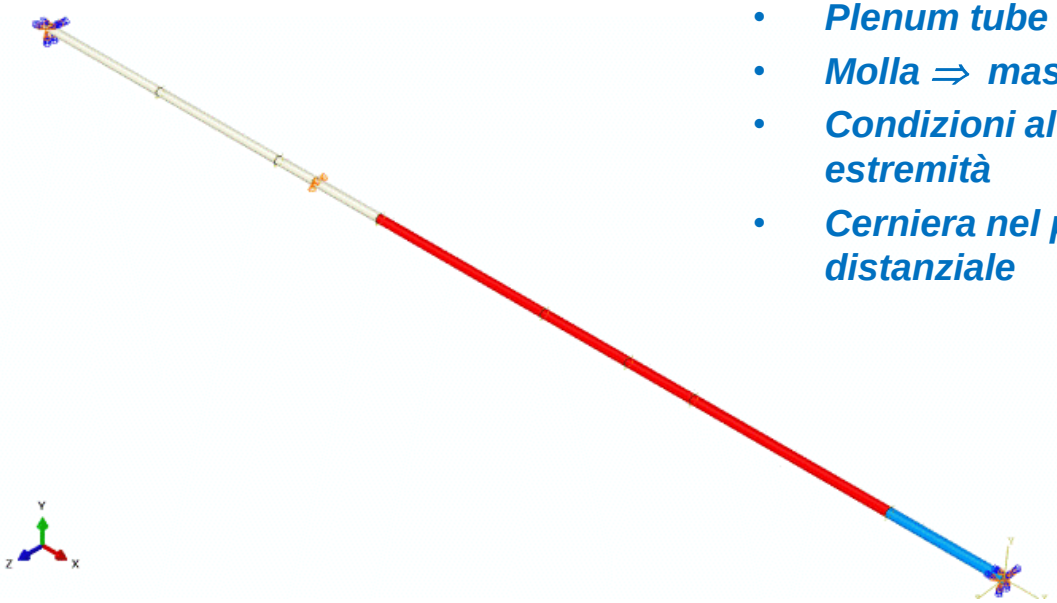

- ***Elementi 'Shell' per la guaina***
- ***Pastiglie combustibile ⇒ masse***
- ***Plenum tube ⇒ massa + rigidezza***
- ***Molla ⇒ massa***
- ***Condizioni al contorno ⇒ incastro alee estremità***
- ***Cerniera nel punto di contatto cn il distanziale***

Analisi modale

Forme modali e frequenze

Mode	Hz
1	30.0
2	83.5
3	163
4	220
5	302
6	455

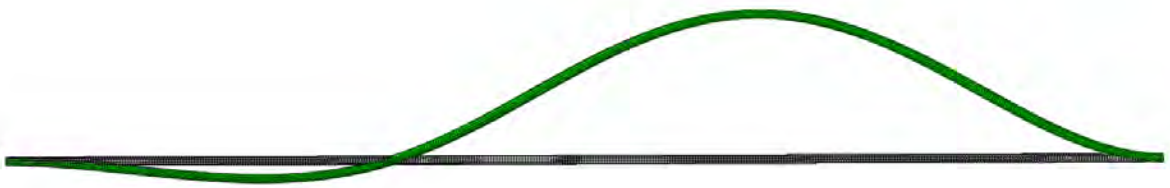

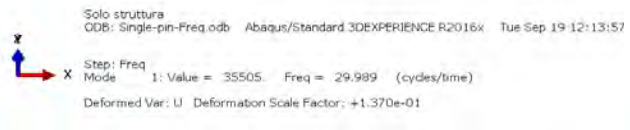

Analisi dinamica della barretta immersa nel fluido

- ***L'analisi modale non tiene in conto la presenza del fluido attorno alla barretta***
- ***E' stato costruito un nuovo modello che riproduce anche una parte del fluido attorno alla barretta.***
- ***La zona di fluido modellata ha dimensioni 150x150mm***

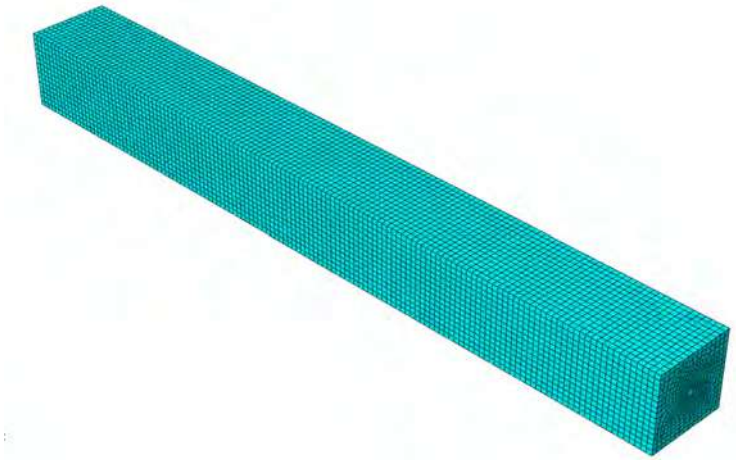

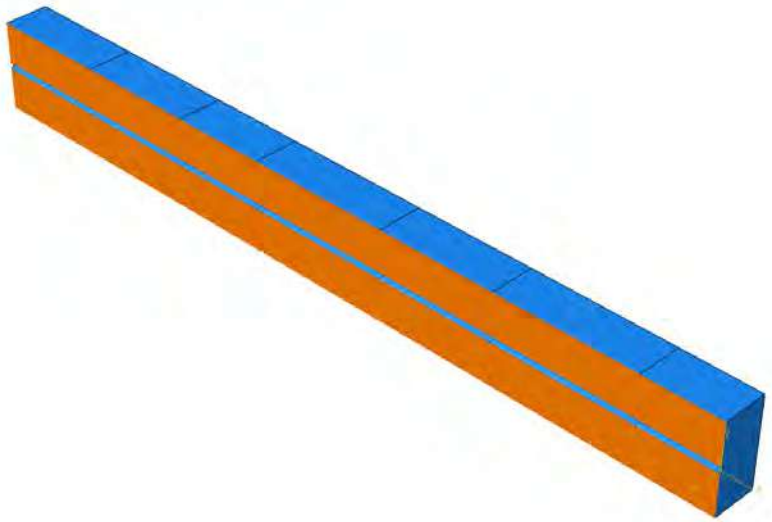

ABAQUS Co-esecuzione

- ***Tutte le analisi sono state fatte usando la tecnica di co-simulazione fornita dal codice Abaqus.***
- ***La tecnica di co-simulazione di Abaqus consente di risolvere problemi complessi di interazione fluido-struttura (FSI) accoppiando il modulo Abaqus/Standard al modulo Abaqus che è un programma computazionale di analisi fluido dinamica (CFD).***
- ***Abaqus/Standard risolve il problema strutturale e Abaqus CFD risolve il dominio del fluido.***

Vibrazione della barretta immersa in piombo

- *Il fluido intorno alla barretta è modellato come piombo fuso*
- *E' stato applicato un impulso di accelerazione all'intera barretta*
- *La barretta viene lasciata libera di vibrare sulla sua prima frequenza naturale*

Risultati attesi:

- *Frequenza più bassa di quella calcolata con analisi modale (30.3 Hz)*
- *Smorzamento non trascurabile*

Risultati ottenuti

- *Frequenza 18.5 Hz*
- *Smorzamento 2.8%*
- *Gli spostamenti non sono realistici perché il carico imposto serve solo per valutare il modello*

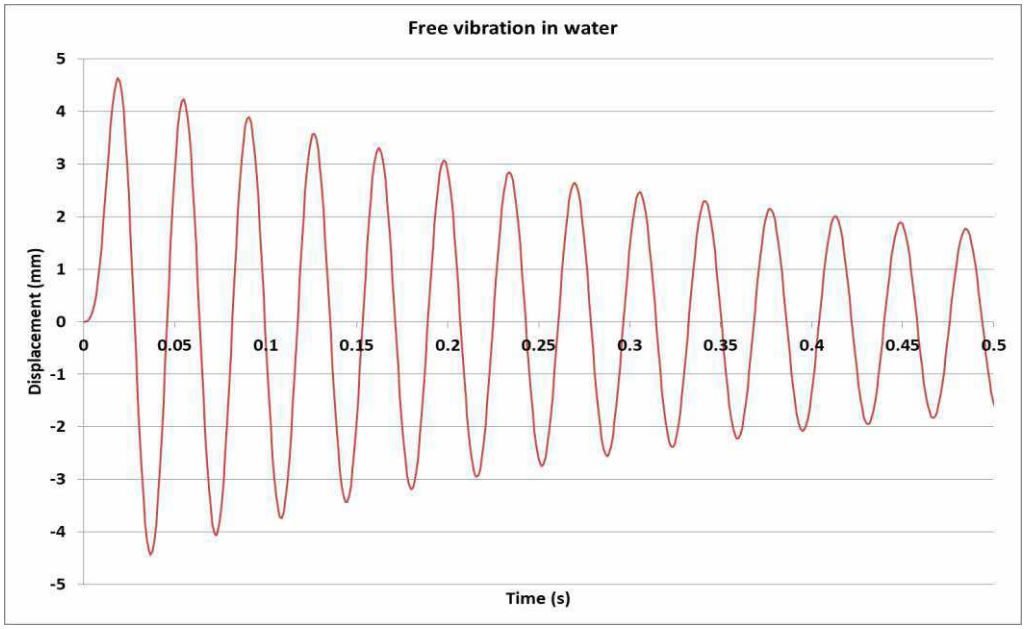

La prima frequenza della barretta immersa in piombo risulta abbastanza lontana dalla possibile risonanza a 10.2 Hz

Individuazione delle frequenze dei modi superiori

Il metodo usato fino a questo punto è in grado di individuare la prima frequenza naturale, ma non riesce ad evidenziare i modi superiori

- Per questo si è deciso di utilizzare la scomposizione in serie di Fourier dei risultati ottenuti (segnale in uscita) sia in termini di accelerazione sia in termini di spostamento.
- Per ottenere una scansione in frequenza del segnale di uscita, con una definizione tale da evidenziare le frequenze fino a circa 400 Hz, si è deciso di campionare a 2.5e-4 s in modo da ottenere 10 punti per ogni periodo, alla frequenza di 400Hz.
- Del segnale in uscita sono stati selezionati 4096 punti che corrispondono a circa 1s di acquisizione.

Individuazione delle frequenze dei modi superiori

Prima di iniziare questa fase, il modello della barretta è stato rivisto per migliorare alcuni aspetti.

Questo ha causato un piccolo cambiamento nel valore delle frequenze calcolate con l'analisi modale, i cui valori aggiornati sono riportati di seguito

Frequency (Hz)
Modal Analysis
28.5
81.5
161
210
297
450

Individuazione delle frequenze dei modi superiori

Inizialmente sono state ripetute le analisi eseguite negli step precedenti per di verificare che la prima frequenza propria, estratta con questo metodo coincida con quella calcolata con l'analisi modale

I risultati usati per la decomposizione sono quelli ottenuti applicando un impulso di accelerazione a tutta la barretta che viene poi lasciata libera di vibrare (eccitazione "kick").

Individuazione delle frequenze dei modi superiori

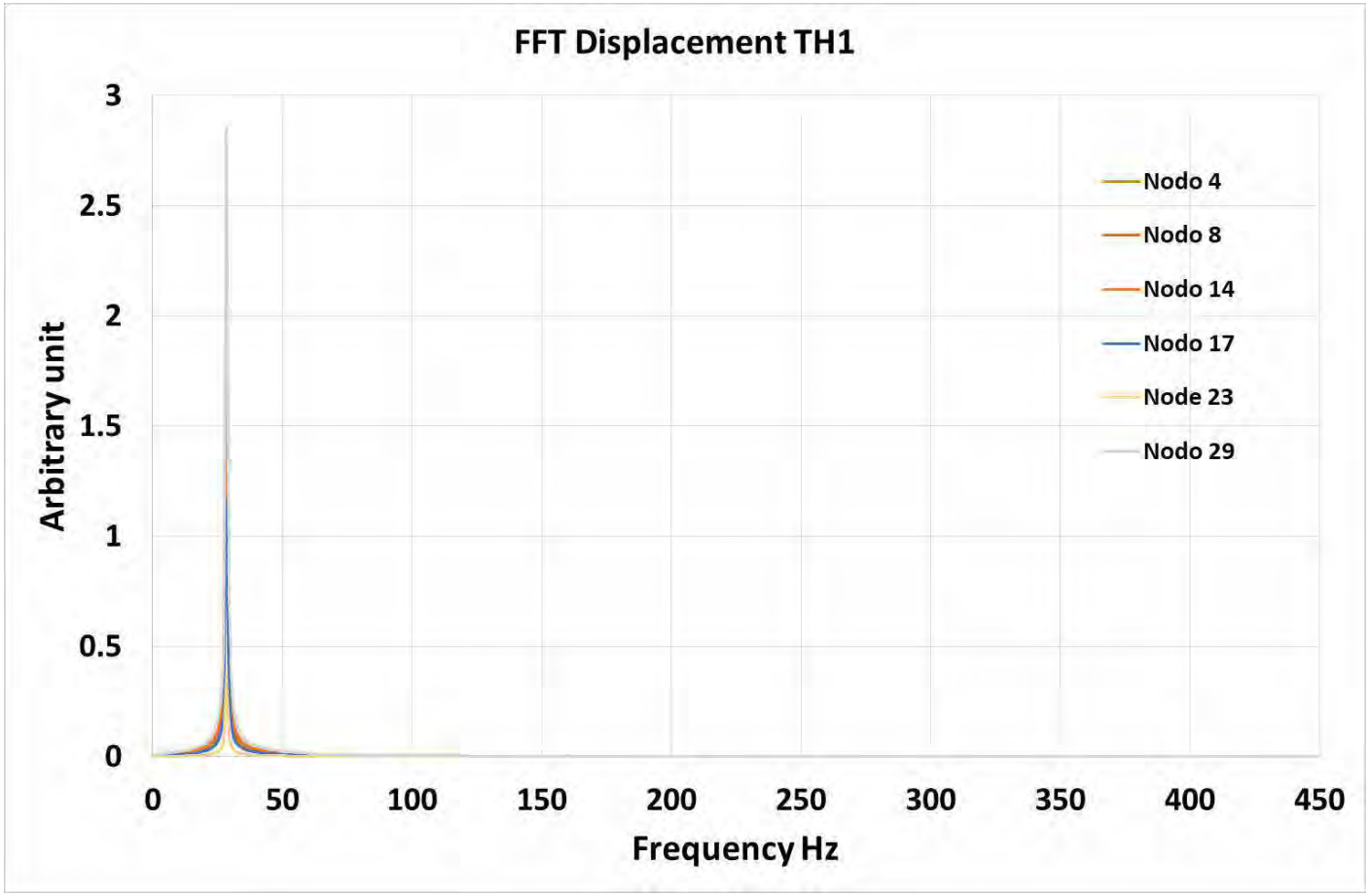

Decomposizione in serie di Fourier dello spostamento in alcuni punti della barretta eccitazione "kick"

Individuazione delle frequenze dei modi superiori

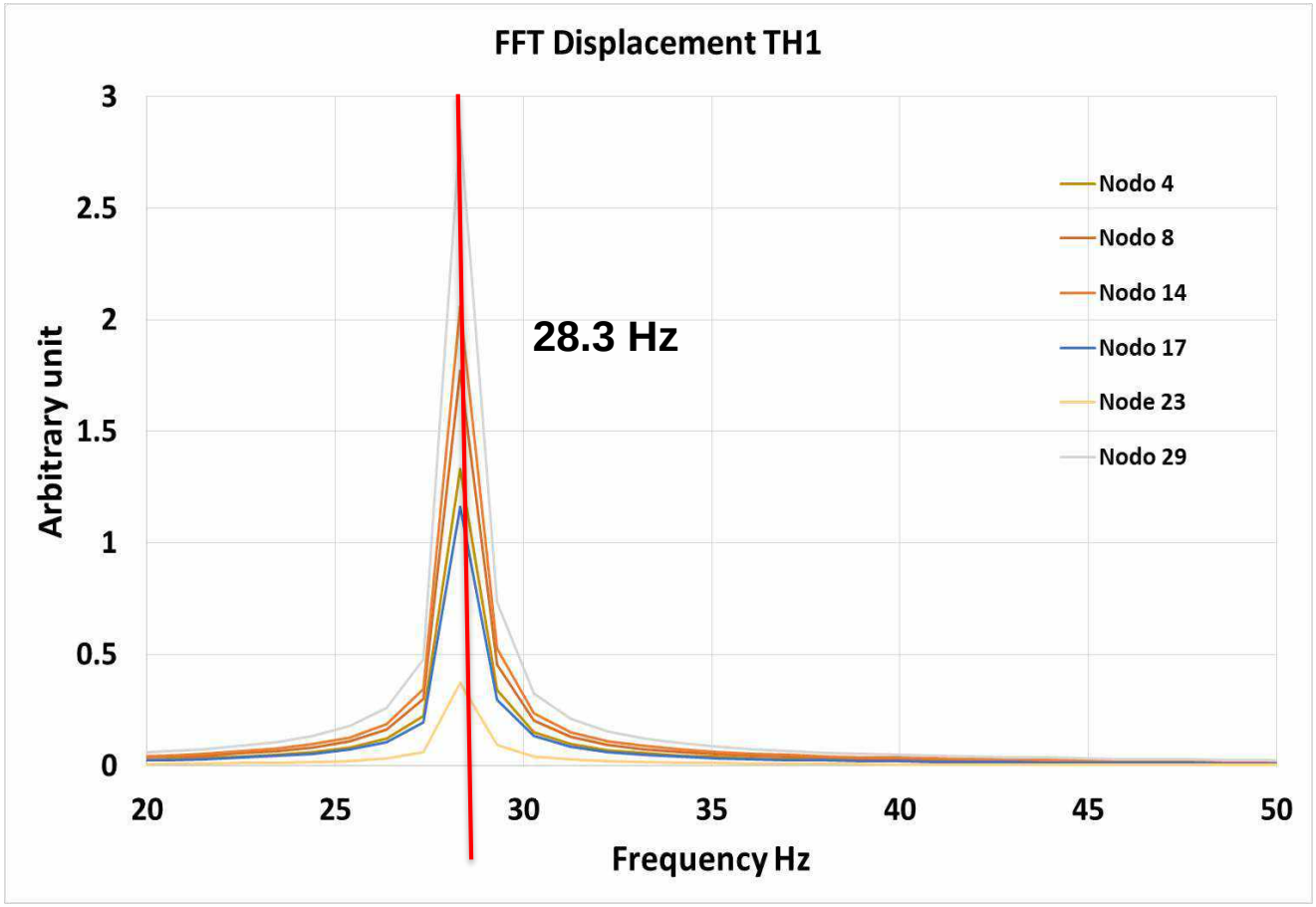

Decomposizione in serie di Fourier dello spostamento in alcuni punti della barretta eccitazione "kick"

Individuazione delle frequenze dei modi superiori

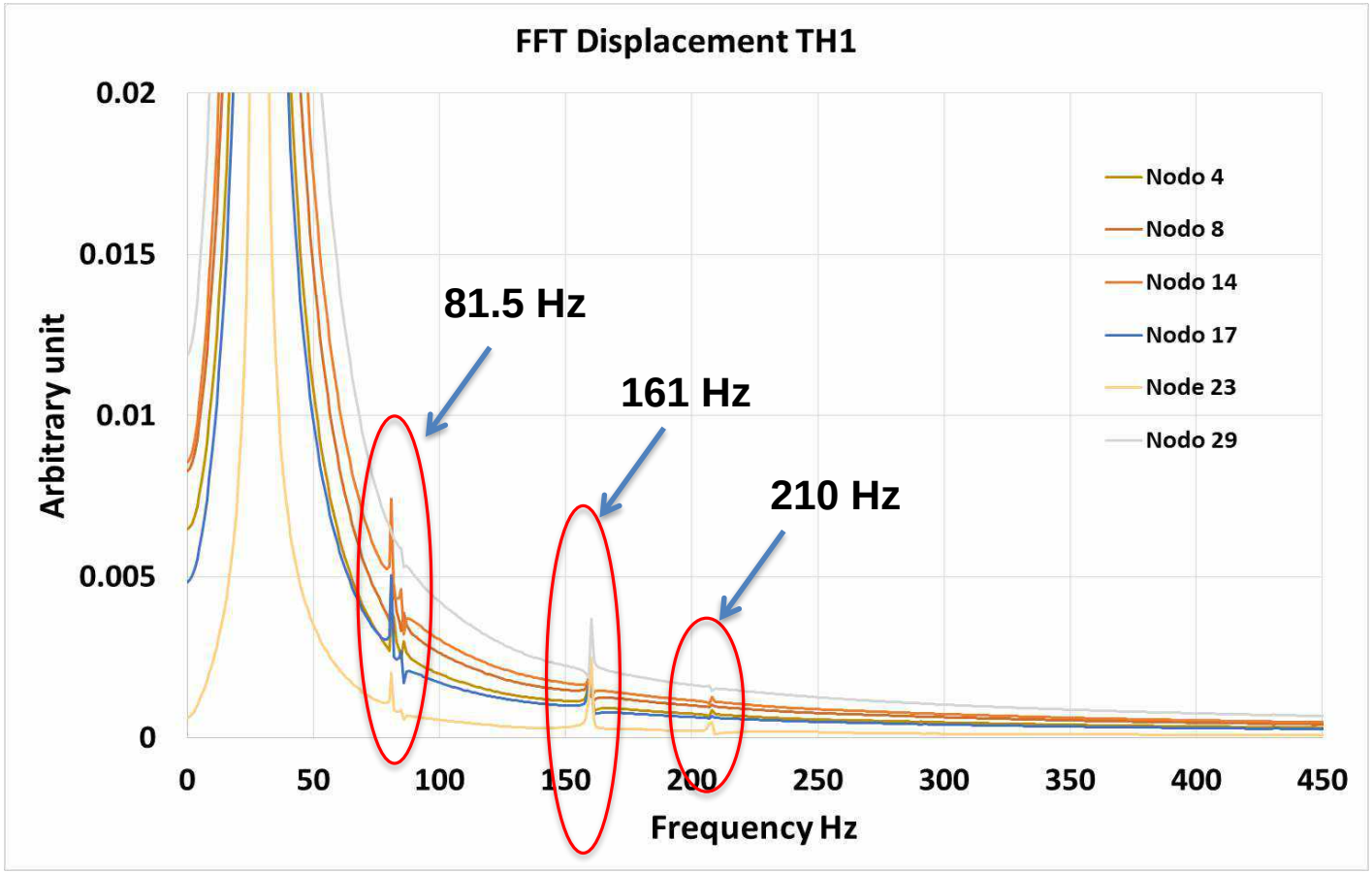

Decomposizione in serie di Fourier dello spostamento in alcuni punti della barretta eccitazione "kick"

Individuazione delle frequenze dei modi superiori

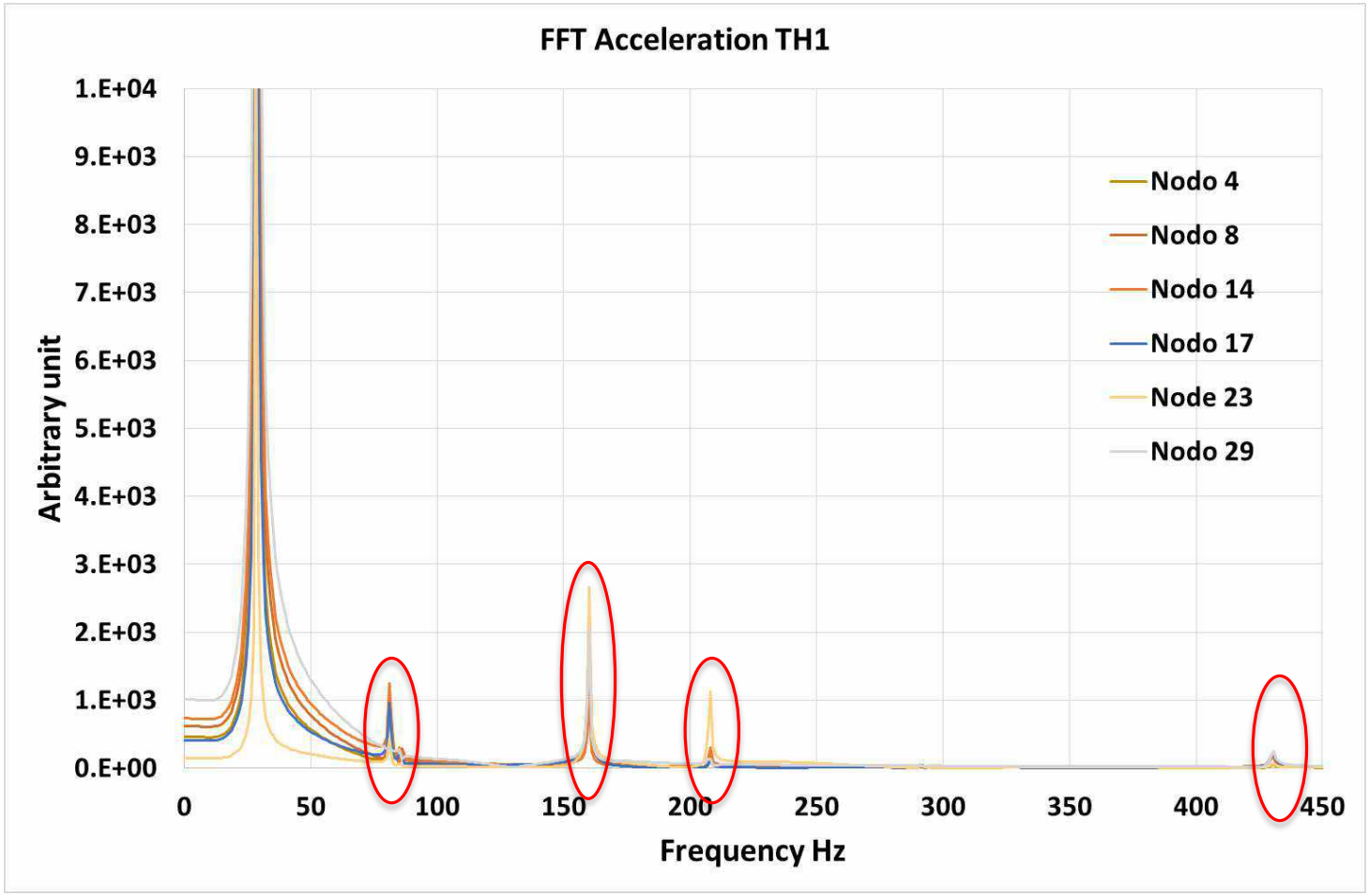

Decomposizione in serie di Fourier dell'accelerazione in alcuni punti della barretta eccitazione "kick"

Individuazione delle frequenze dei modi superiori

La prima frequenza, così calcolata risulta 28.3Hz in ottimo accordo con quella calcolata con l'analisi modale.

Per mettere ancora più in evidenza le frequenze superiori occorre però un impulso sulla barretta che sia in grado di eccitare tutte le frequenze nel range considerato (0-400 Hz)

Individuazione delle frequenze dei modi superiori

Time history generate con diverse strategie:

- ***Time history di rumore bianco (eccitazione "white noise"), ottenuta tramite la generazione di numeri casuali.***
- ***Lo spettro di queste time history contiene tutte le frequenze, ma con ampiezza casuale***
- ***Per avere risultati non influenzati dalla forma del singolo spettro, viene utilizzata la media dei risultati ottenuti con tre diverse time history***

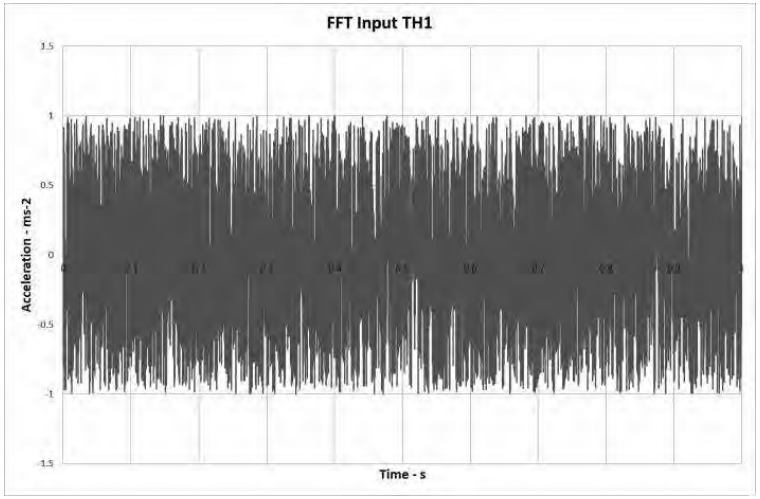

Time history rumore bianco

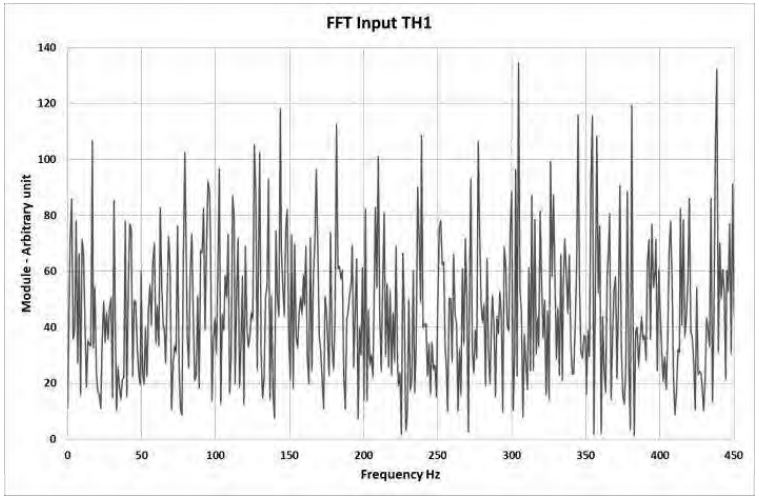

Spettro rumore bianco

Individuazione delle frequenze dei modi superiori

Risultati time history eccitazione "white noise"

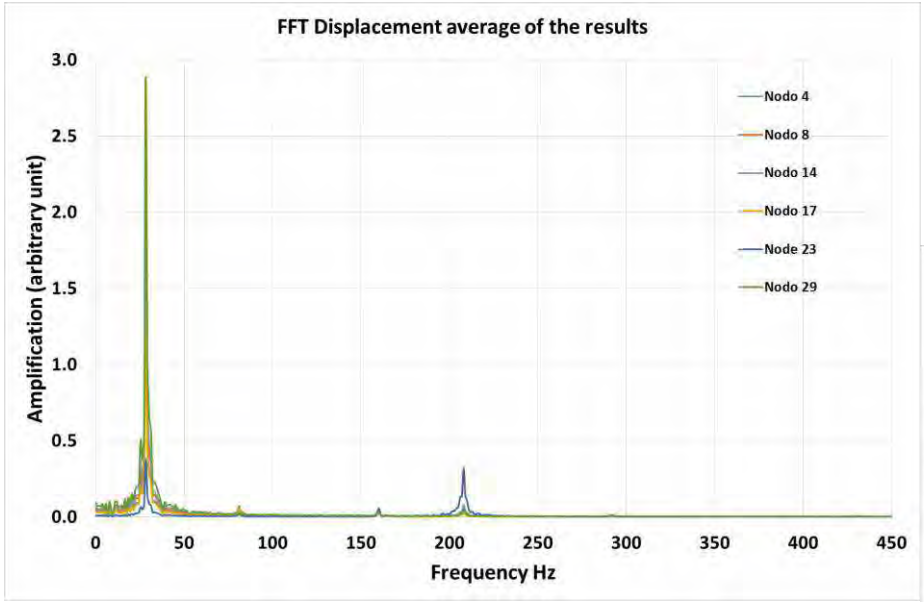

Si nota che, l'amplificazione negli spostamenti e meno evidente alle alte frequenze perché, naturalmente vibrazioni ad alta frequenza non consentono spostamenti elevati.

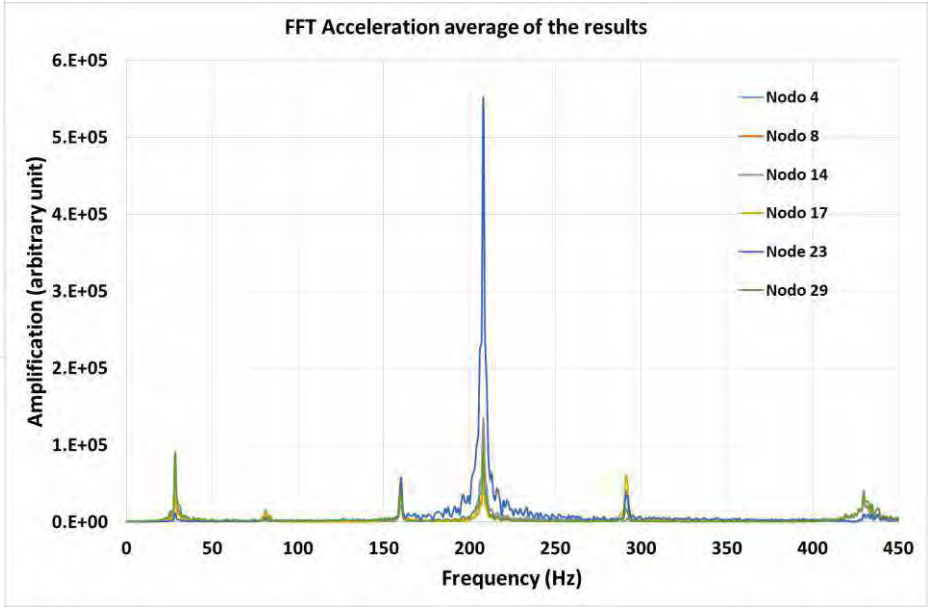

Individuazione delle frequenze dei modi superiori

Time history generata come somma di sinusoidi con frequenze diverse, stessa amplificazione ma fase diversa (eccitazione "sinus"). In questo caso lo spettro che si ottiene è uniforme nell'intervallo di frequenze considerato e non occorre generare più time history.

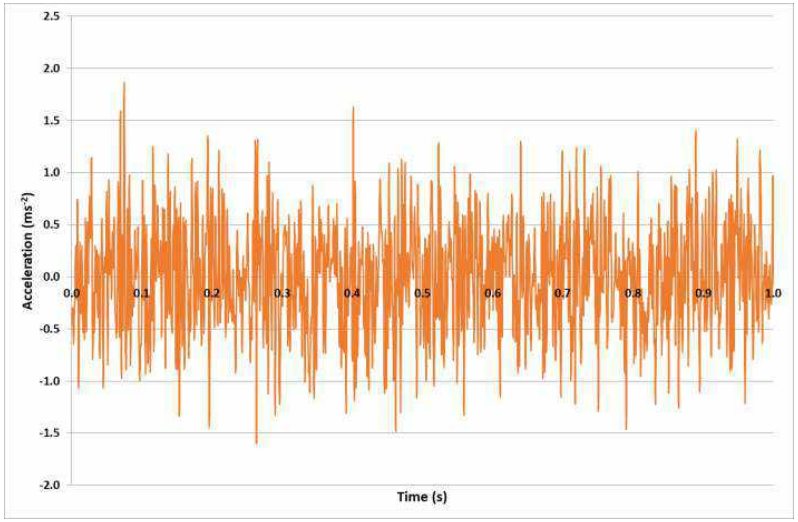

Time history somma di sinusoidi

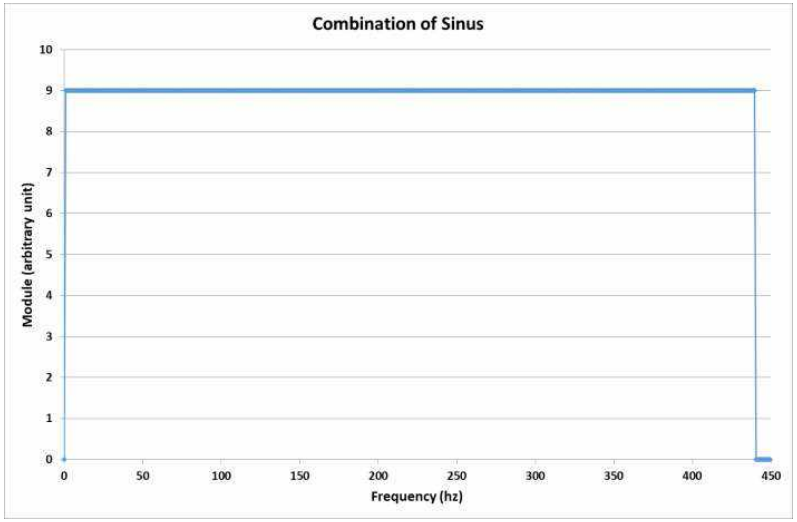

Spettro somma di sinusoidi

Individuazione delle frequenze dei modi superiori

Risultati time history eccitazione "sinus"

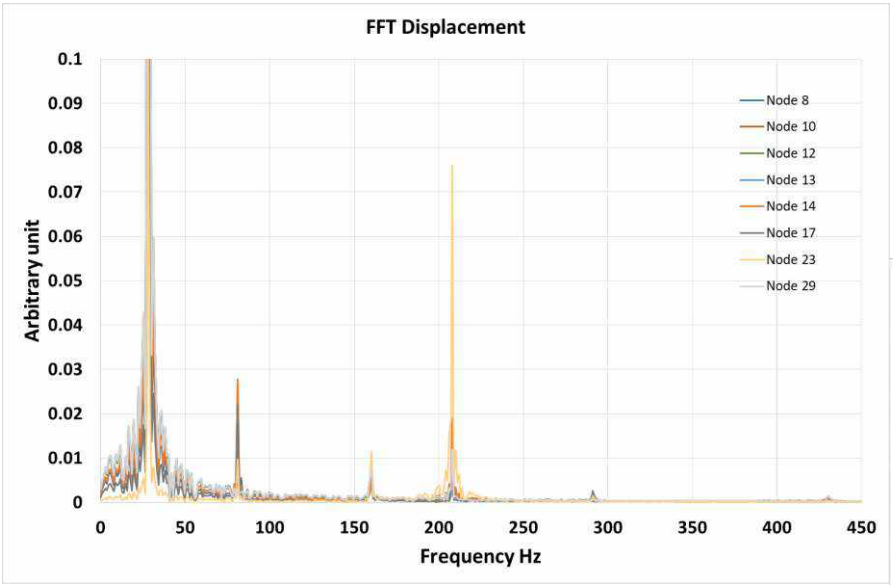

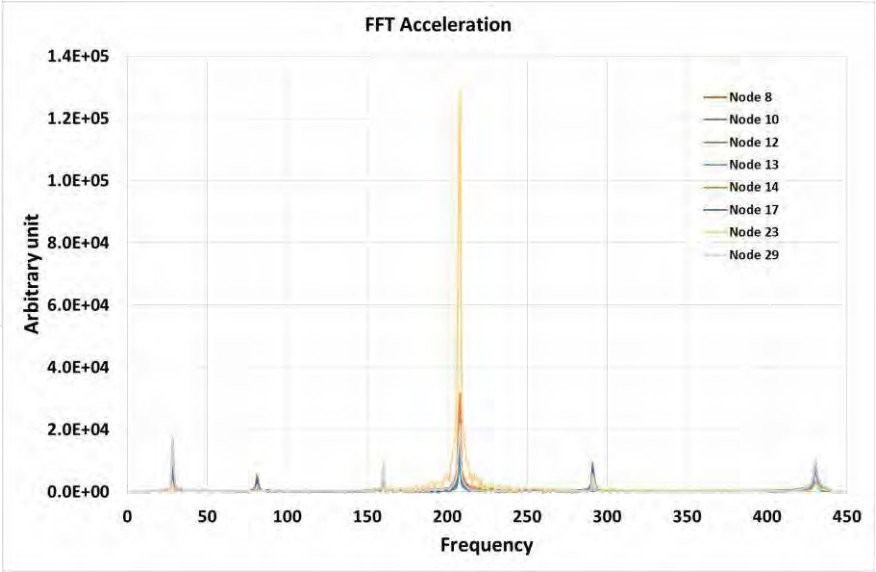

Individuazione delle frequenze dei modi superiori

Confronto risultati

Frequency (Hz)	
Modal Analysis	Time history analysis
28.48	28.32
81.45	81.05
160.8	160.2
209.8	208.0
297.3	291.0
449.9	429.7

Individuazione delle frequenze dei modi superiori barretta immersa in piombo

- ***Ottenuta la conferma che con questo metodo è possibile evidenziare le frequenze più alte, si applica la stessa procedura alla barretta singola, immersa in piombo.***

- ***Oltre alle time history prima specificate si prendono in considerazione anche i risultati ottenuti applicando un impulso di accelerazione***.

Individuazione delle frequenze dei modi superiori barretta immersa in piombo

Risultati time history eccitazione 'kick'

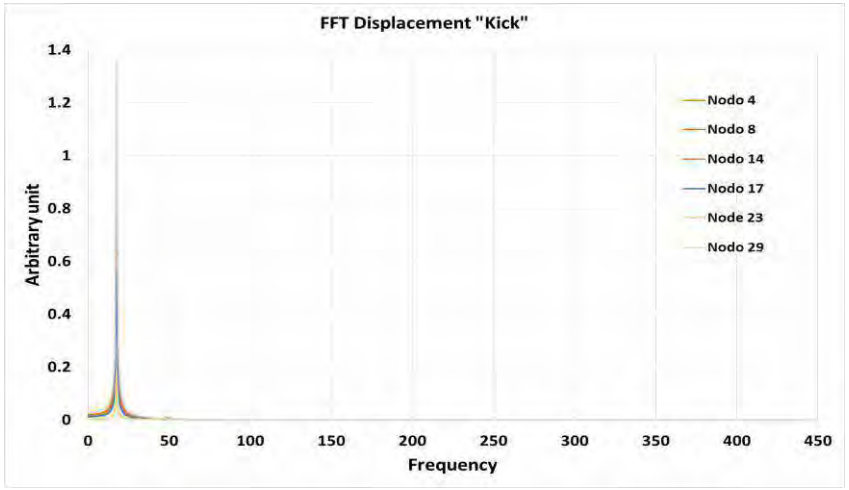

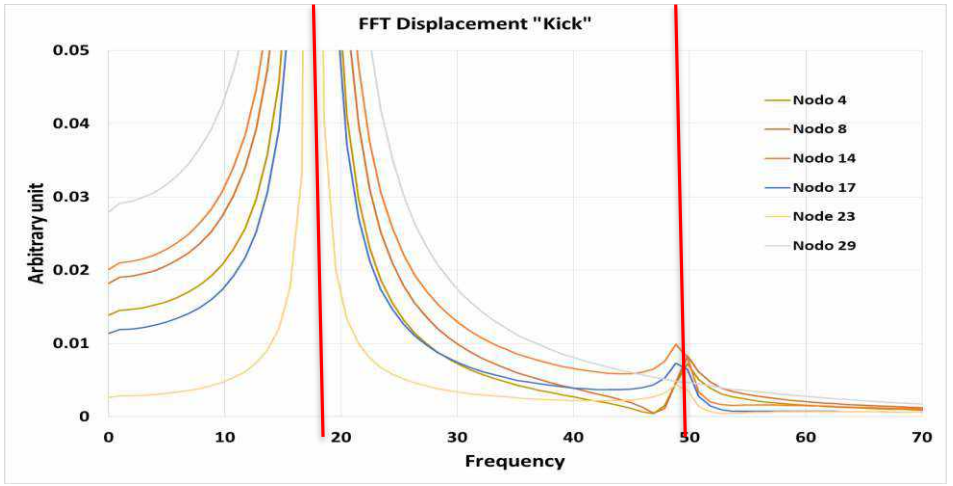

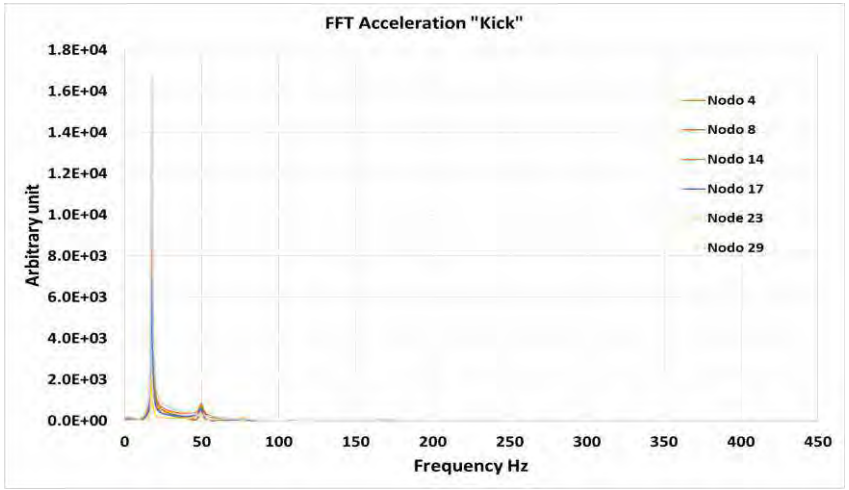

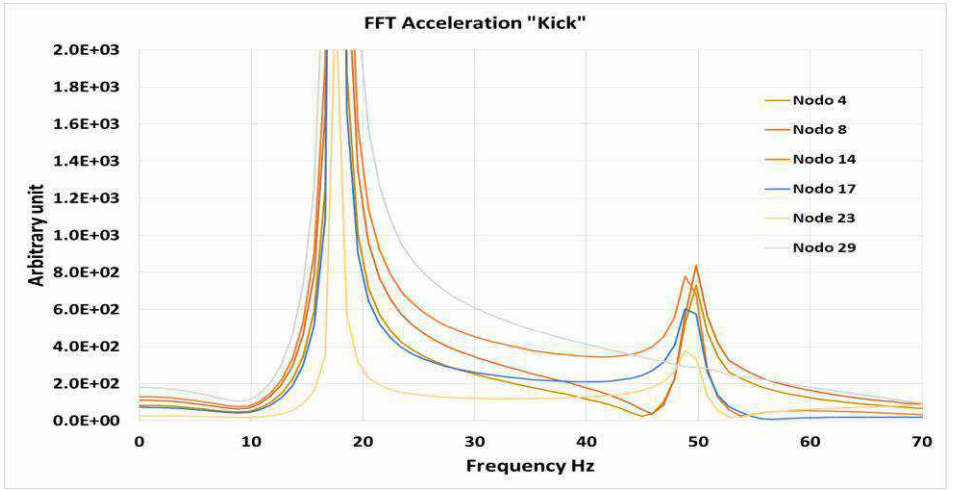

Individuazione delle frequenze dei modi superiori barretta immersa in piombo

Risultati time history eccitazione 'withe noise'

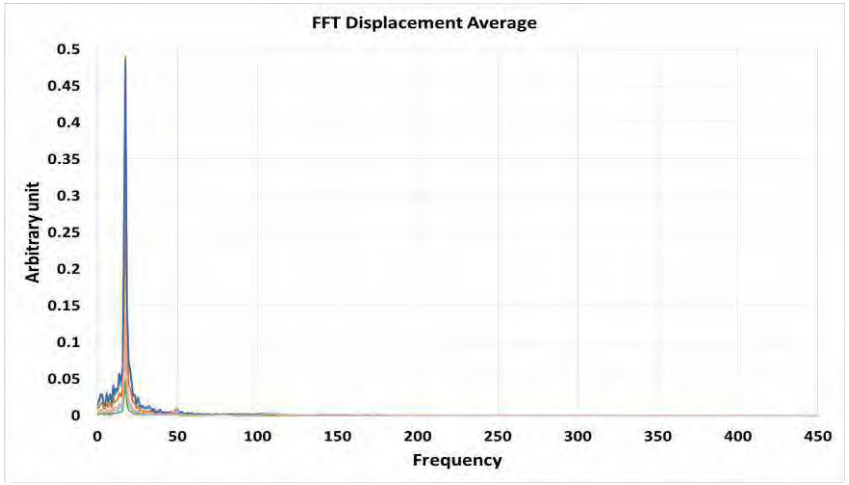

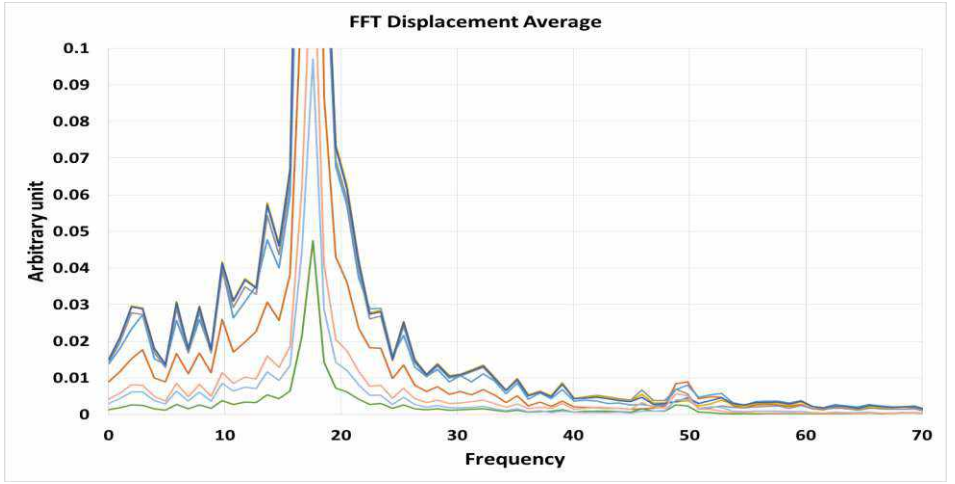

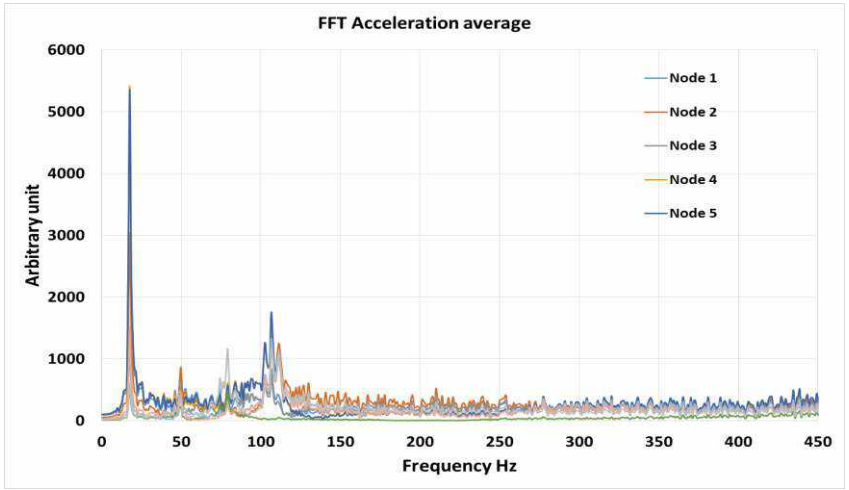

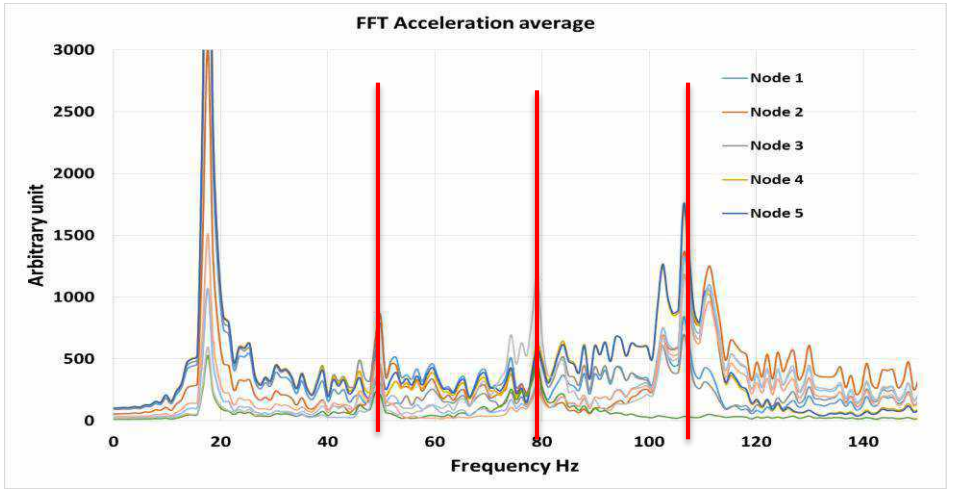

Individuazione delle frequenze dei modi superiori barretta immersa in piombo

Risultati time history eccitazione 'sinus'

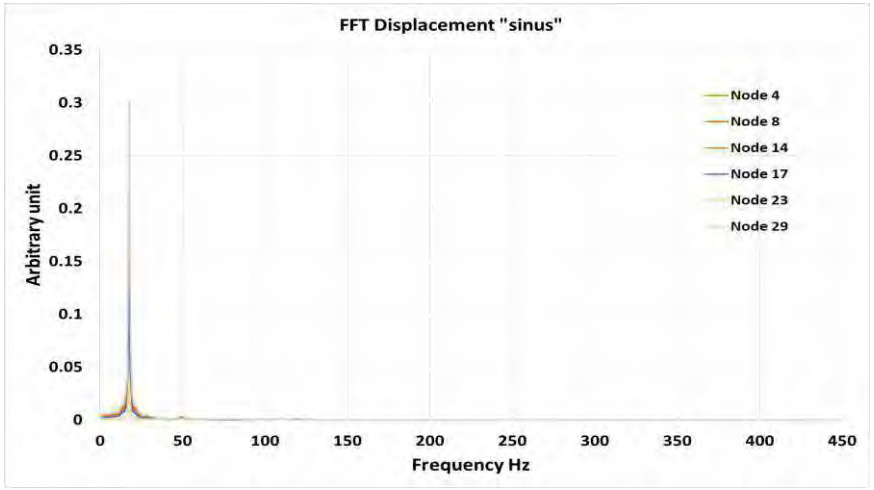

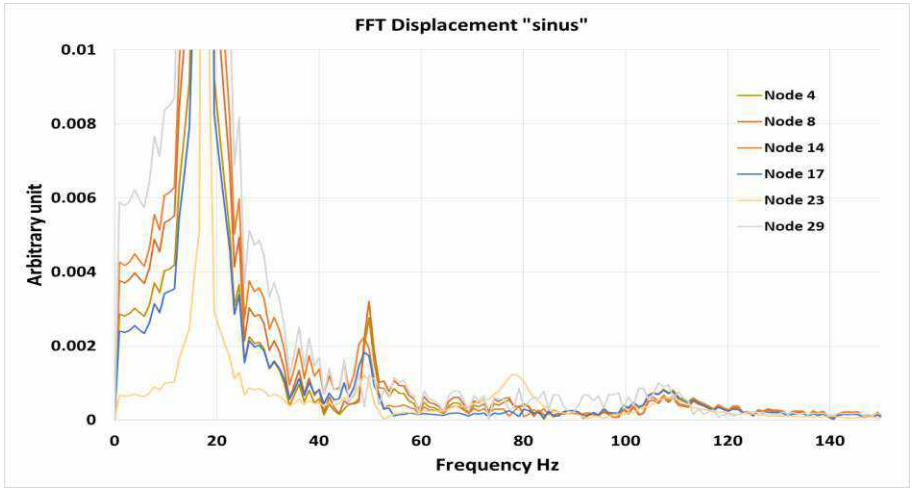

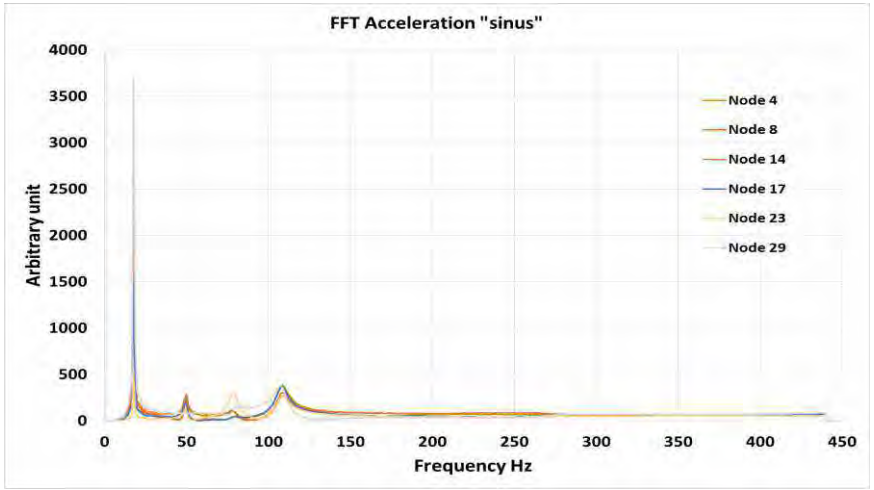

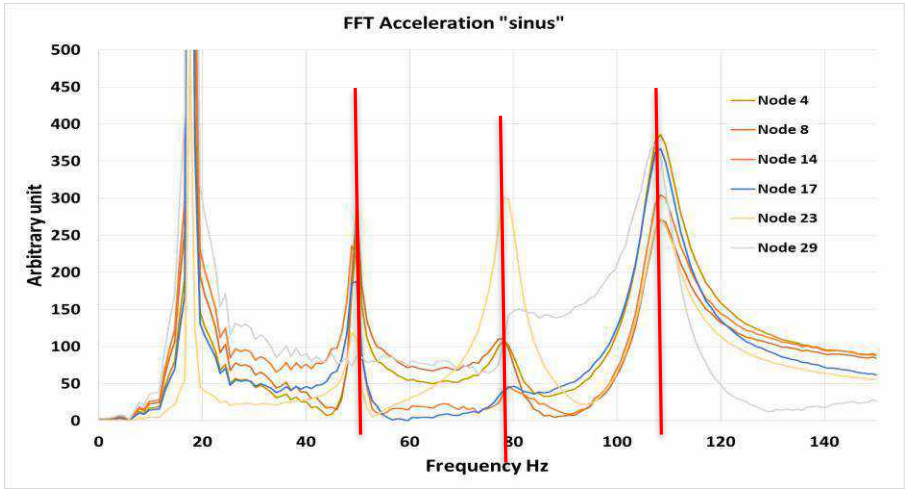

Individuazione delle frequenze dei modi superiori barretta immersa in piombo

Risultati

Frequency (Hz)
Time history analysis
17.6
49.8
78.1
107.4

Analisi dinamica di un gruppo di barrette immerse in piombo

- Lo scopo è quello di studiare l'influenza delle prima fila di barrette attorno alla barretta centrale
- Per questo è stato modellato un gruppo di sette barrette
- La porzione di fluido considerata ha le stesse dimensioni della scatola dell'elemento
- Le condizioni al contorno imposte al fluido simulano una scatola rigida

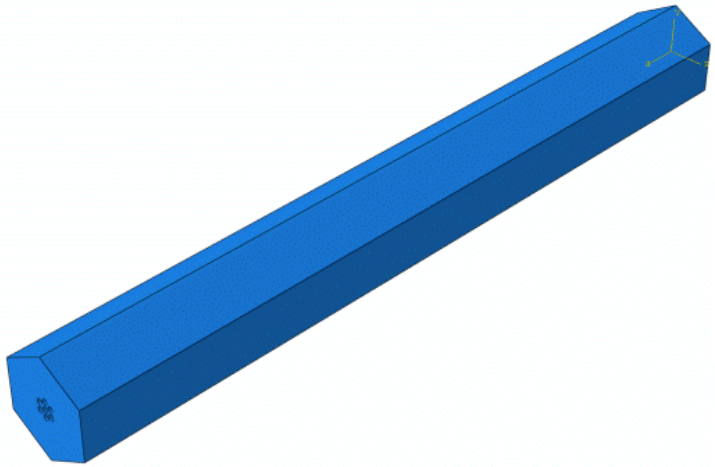

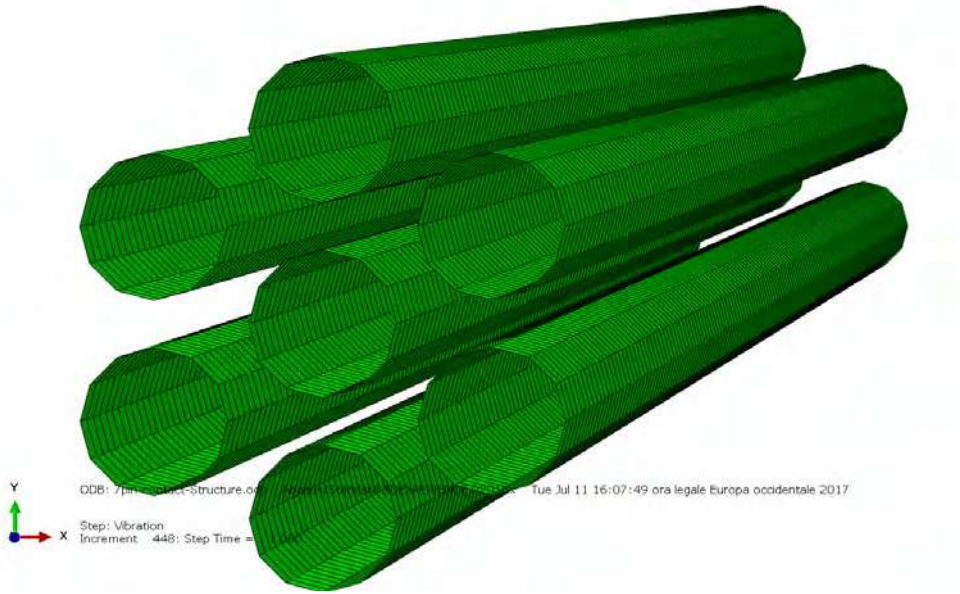

Analisi dinamica di un gruppo di barrette immerse in piombo

E’ possibile rilevare i possibili urti

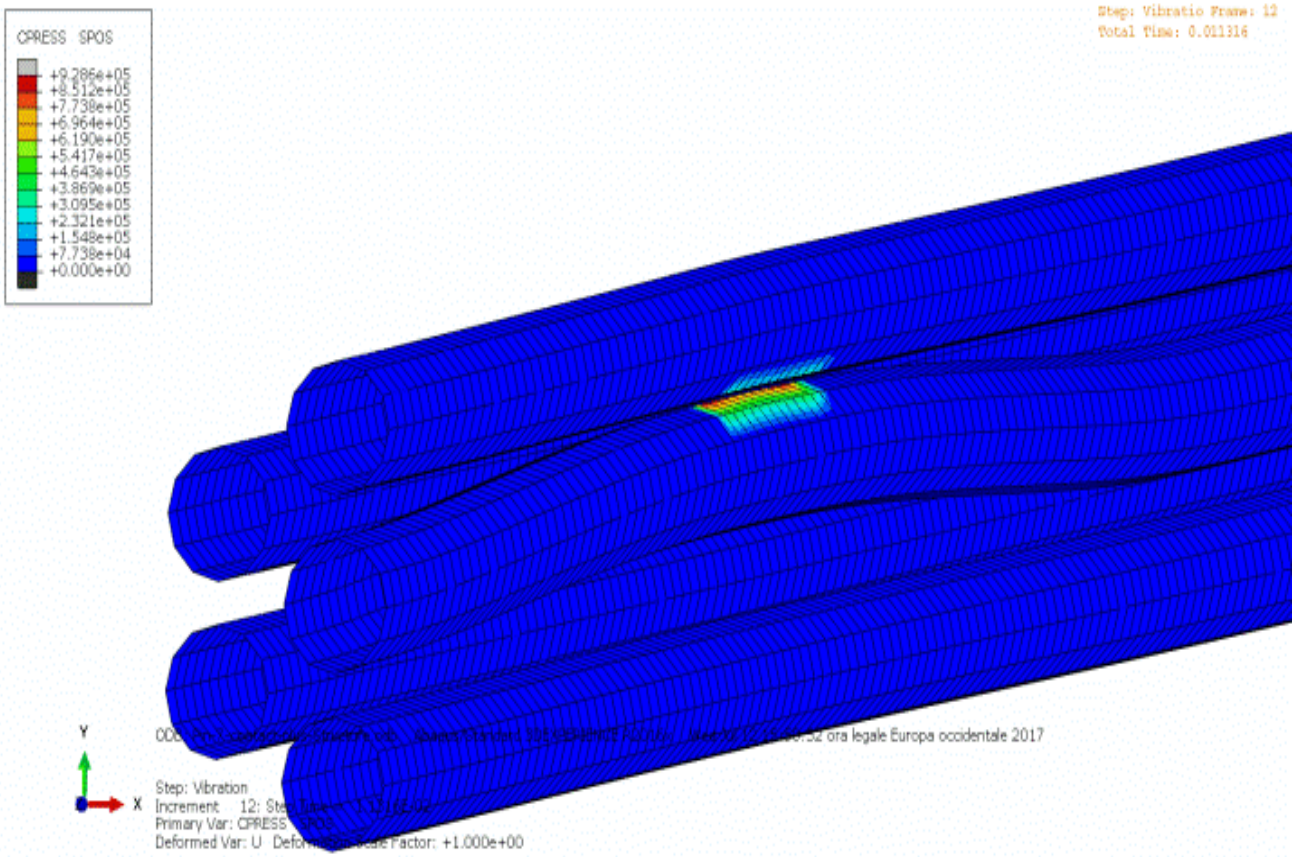

Individuazione delle frequenze dei modi superiori barretta immersa in piombo

Risultati time history eccitazione 'sinus' – barretta centrale del gruppo di 7

- ***il movimento del fluido innesca un movimento in entrambe le direzioni orizzontali delle barrette circostanti , questo movimento a sua volta genera delle retroazioni sulla barretta centrale rendendo più caotica la risposta***

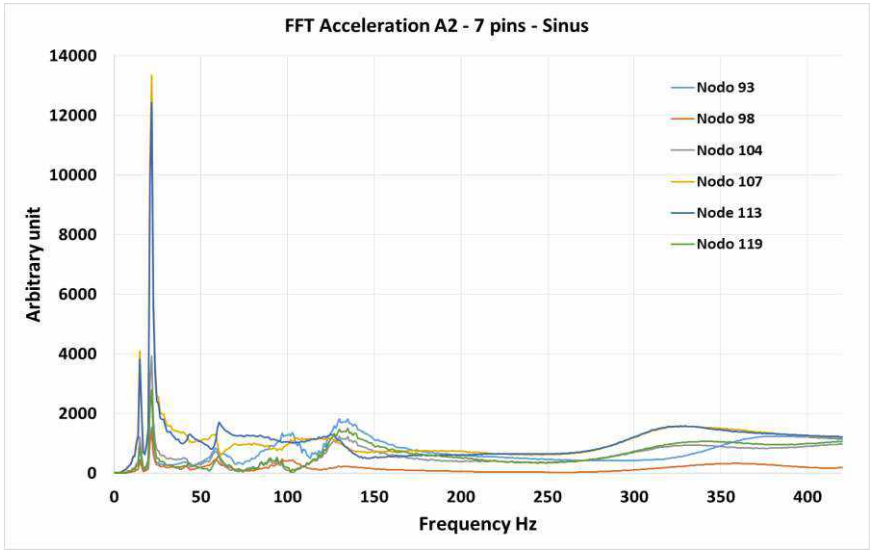

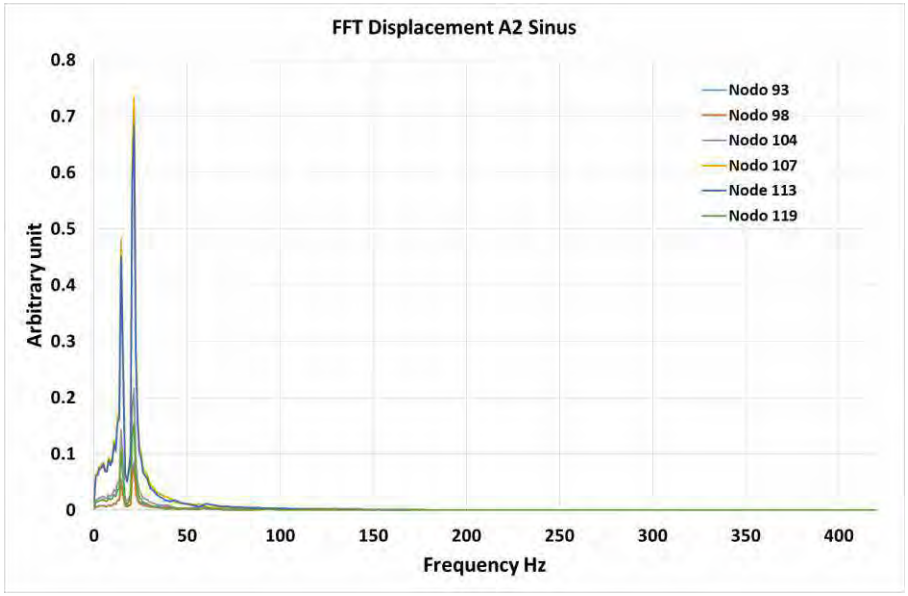

Individuazione delle frequenze dei modi superiori barretta immersa in piombo

Neppure ingrandendo la scala si riescono a cogliere bene le frequenze proprie

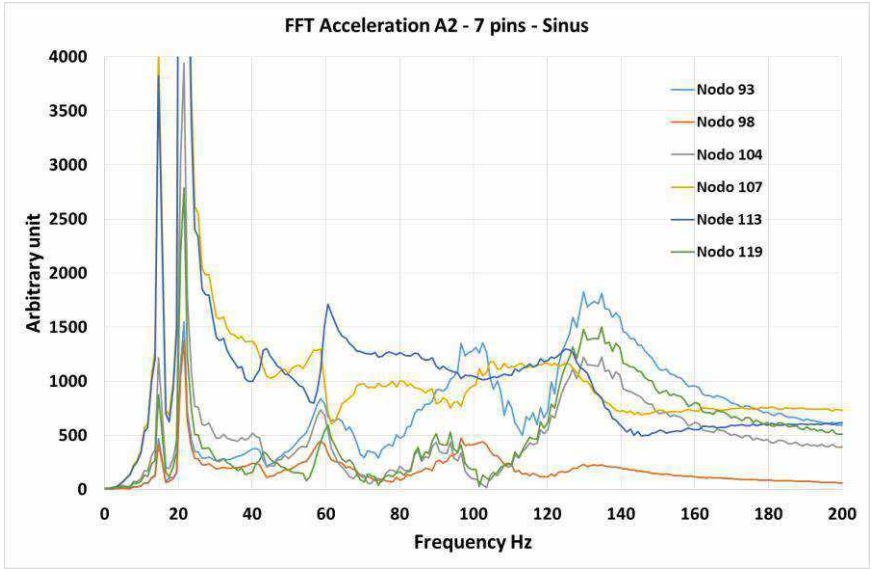

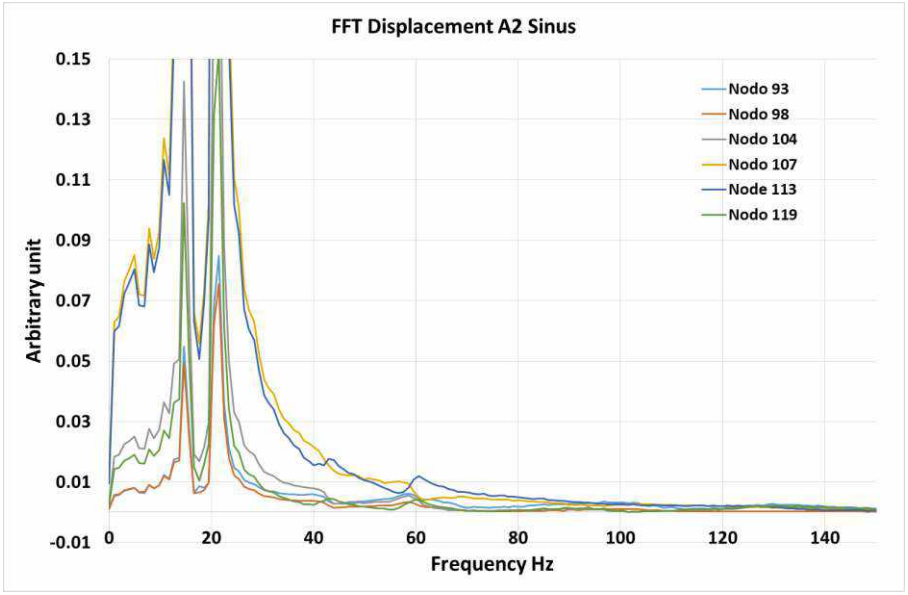

Next steps

- ***Approfondire la valutazione del fascio a 7 barrette applicando lo stesso impulso a tutte***
- ***Modellare tutte le barrette e il fluido per riprodurre una condizione più realistica***
- ***Applicare un'eccitazione il più possibile realistica calcolando l'andamento delle pressioni sulla superficie delle barrette nel tempo***

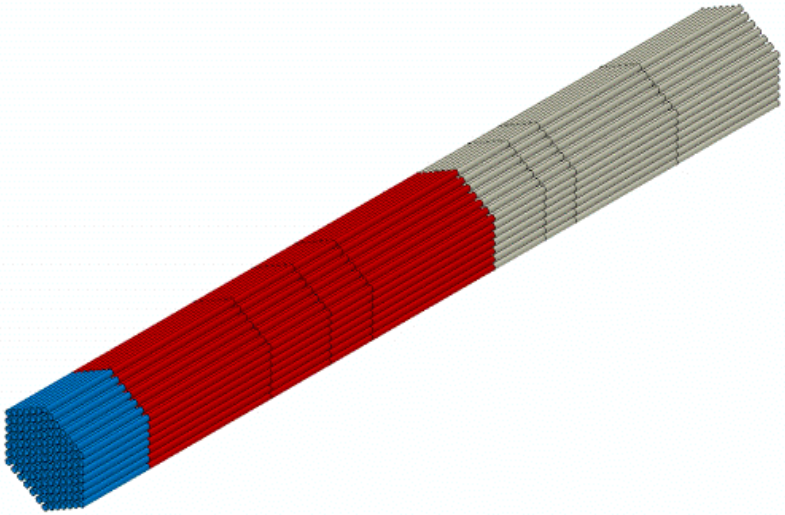

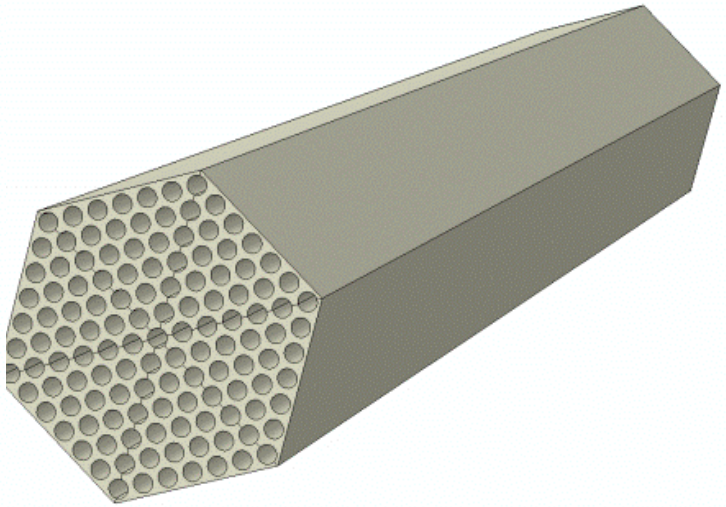

GRAZIE PER L'ATTENZIONE

Italian National Agency for New Technologies,
Energy and Sustainable Economic Development

ALFRED

Fuel Assembly design

«GEN-IV LEAD COOLED FAST REACTOR
STATO ATTUALE DELLA TECNOLOGIA E PROSPETTIVE DI SVILUPPO»
Workshop tematico AdP MISE – ENEA PAR2017 – PROGETTO B.3 - LP2
Università di Roma «La Sapienza», 14-15 Giugno 2018

G. Grasso, A. Palumbo, F. Lodi

Problems to be faced

1. Irradiation-induced deformations

In Fast Reactors, the high burnups imply high irradiation doses to the structural materials. As the former are desired, the latter are to be faced.

In Lead-cooled Fast Reactors, presently qualified irradiation-resistant materials (i.e., ferritic-martensitic steels) cannot be used because of environmental issues (mostly, liquid metal embrittlement).

The envisioned austenitic stainless steels, at the doses anticipated for ALFRED, are prone to swelling.

Problems to be faced

2. Pressure-induced deformations

In Fast Reactors, the differential pressure of the coolant flowing inside vs. outside the sub-assemblies exerts forces on the flat faces of the wrapper.

In Lead-cooled Fast Reactors, the differential pressure is anticipated to be much less, and so is the associated force.

Even though moderate, the resulting force expected in ALFRED may lead to bulging.

Problems to be faced

3. Temperature-induced deformations

In Fast Reactors, the flux and power profiles throughout the core determine also temperature gradients within the fuel assemblies, which result in differential expansions of the structural elements.

In Lead-cooled Fast Reactors, this effect might be reduced or magnified, depending on the adopted inlet-outlet temperatures.

The inlet and outlet temperatures planned in the different phases of ALFRED operation determine progressively increasing bowing.

Problem to be faced

Summary of anticipated deformations

Swelling	Bulging	Bowing

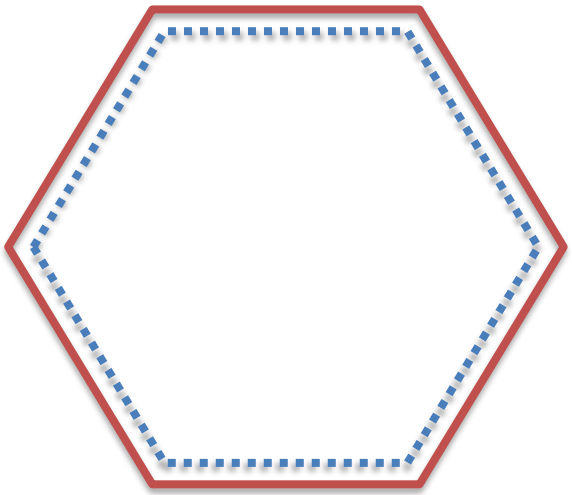

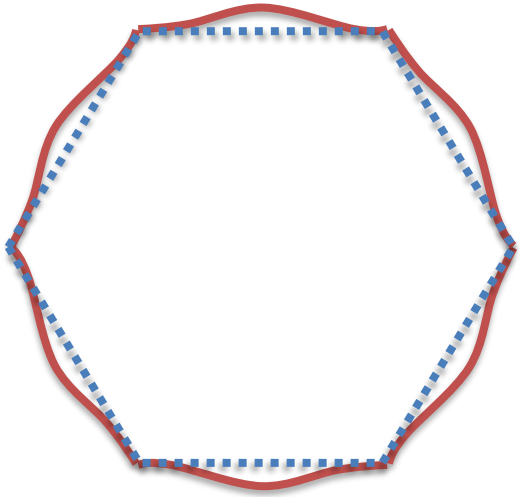

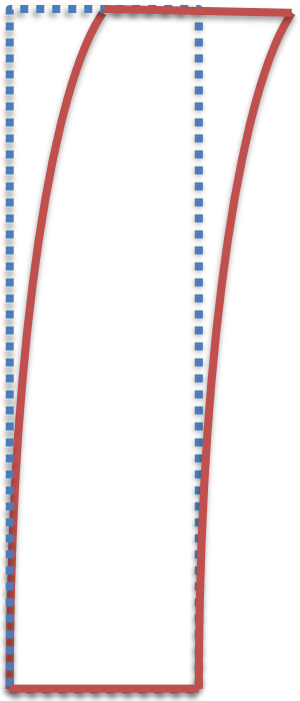

Problem to be faced

Overall effect

Once combined, all these causes can determine severe deformations to the wrapper…

Requirements to be ensured

1. Prevention of accidental reactivity insertions

In Fast Reactors, the core is not in its most critical configuration, and moderation ratio is not required – rather detrimental – to criticality, so that any reduction of the coolant volume fraction inserts reactivity.

In Lead-cooled Fast Reactors, the high density of the coolant can magnify the effects of earthquakes in terms of solicitations to the core.

The small dimensions of the ALFRED core, making it more sensible to geometrical reactivity effects, require minimizing compaction events.

Requirements to be ensured

2. Reactivity feedback

In Fast Reactors, the lack of moderator eliminates the largest feedback mechanism, turning the coolant effect positive and counterbalanced by small geometrical feedbacks.

In Lead-cooled Fast Reactors, the coolant density effect is much lower (if not negative), but the moderator feedback still misses.

The inherent controllability of the ALFRED (notably in DEC) needs to rely on all available mechanisms, including flowering.

Requirements to be ensured

3. Insertion capability of control/shutdown devices

In Fast Reactors, control devices are usually massive bundles of rods inserted within fixed structures occupying one full core position.

In Lead-cooled Fast Reactors, instead of gravity, buoyancy can be exploited (since the rods are lighter than the coolant they displace), but the overall layout is not changed.

Despite the small sub-assemblies of ALFRED, making tolerances even more tight, ensuring the clearance needed for insertion is mandatory.

Requirements to be ensured

Summary of requirements

Prevent compaction

Allow flowering

Ensure clearance

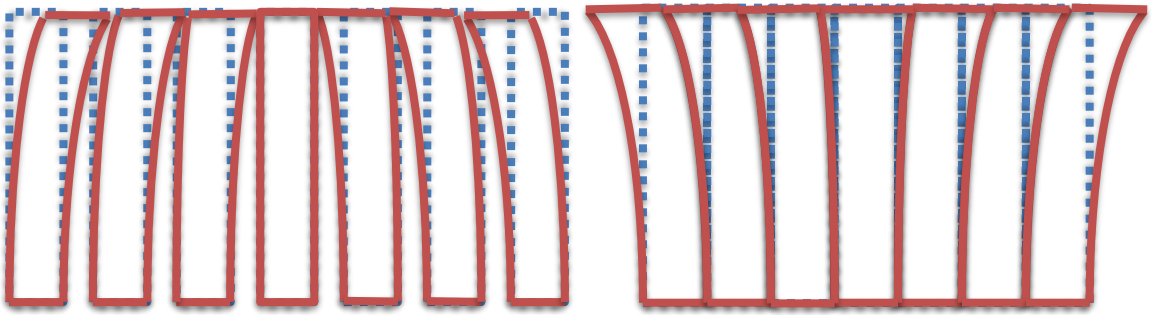

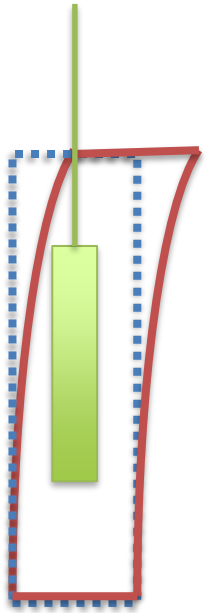

Approach to solution

Object of study

First of all, the study is focused on the Fuel Assemblies only, being easily transferrable to other types of sub-assemblies later on.

The study is then focused on the wrapper, being the resisting structure of an ALFRED Fuel Assembly.

In this phase, unrestrained deformations are considered.

Modeling

Discretization

Each wrapper's face is modeled independently, and all are divided into regular axial slices

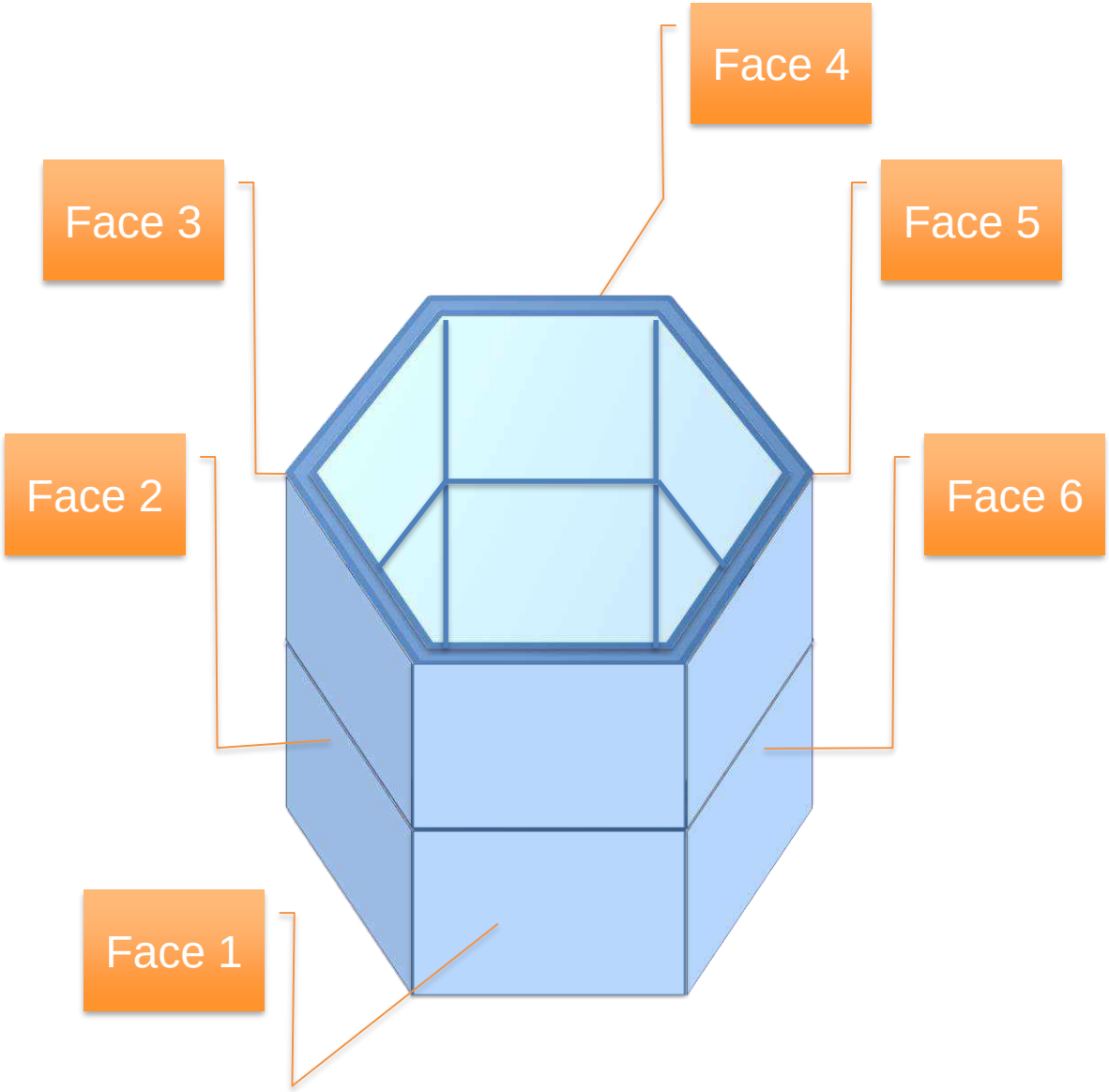

Modeling

Lumping

The actual values of the main parameters (temperature and neutron dose), whose distributions on the whole wrapper are known axially and along the perimeter, are lumped by representative values, for each face and at each quote of interest.

Quote z [cm]	Temperature [°C]				Flux [n/cm² s]			
	face 1	faces 2 & 6	faces 3 & 5	face 4	face 1	faces 2 & 6	faces 3 & 5	face 4
0	405.7	405.7	405.7	405.7	4.653E+14	4.324E+14	3.84E+14	3.696E+14
3	407.93082	407.86667	407.74565	407.68931	5.405E+14	5.052E+14	4.51E+14	4.335E+14
6	410.43038	410.28919	410.02283	409.89904	6.113E+14	5.738E+14	5.142E+14	4.939E+14
9	413.17967	412.94939	412.51493	412.31334	6.774E+14	6.38E+14	5.736E+14	5.505E+14
12	416.15967	415.82909	415.20539	414.91635	7.388E+14	6.978E+14	6.289E+14	6.034E+14
15	419.35138	418.91013	418.0776	417.69221	7.953E+14	7.53E+14	6.802E+14	6.523E+14
18	422.73579	422.17434	421.11498	420.62505	8.469E+14	8.035E+14	7.273E+14	6.972E+14
21	426.29388	425.60353	424.30094	423.69903	8.934E+14	8.493E+14	7.7E+14	7.38E+14
24	430.00664	429.17956	427.6189	426.89827	9.348E+14	8.901E+14	8.082E+14	7.744E+14
27	433.85506	432.88424	431.05227	430.20692	9.709E+14	9.258E+14	8.419E+14	8.065E+14
30	437.82012	436.6994	434.58445	433.60913	1.002E+15	9.564E+14	8.708E+14	8.34E+14
…	…	…	…	…	…	…	…	…

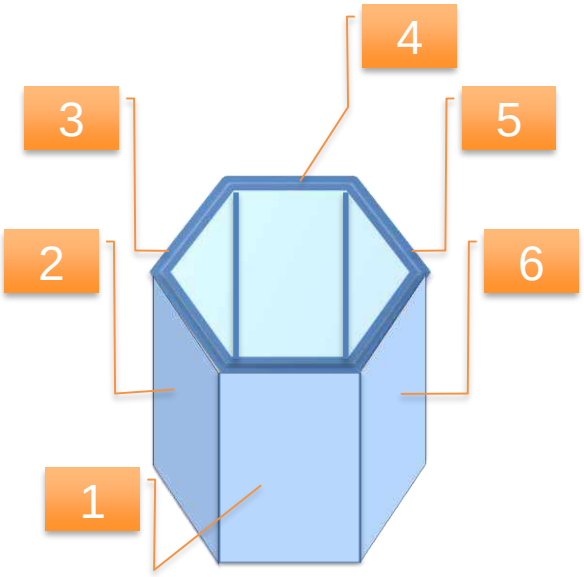

Modeling

Analysis

At each quote, the moment generated by the differential thermal dilation and swelling is computed.

This in turn is applied to the solution of the problem of deformation of an unrestrained beam, retrieving the rotation and displacement of each axial segment of the wrapper.

$$M_i = M_i^{Th} + M_i^{Sw}$$

$$M_i^{Th} = \int_i E\ \alpha T\ y\ dA$$

$$M_i^{Sw} = \int_i E\ \varepsilon\ y\ dA$$

$$\frac{d^2 y_i}{dz_i^{\ 2}} = \frac{M_i}{E_i\ I_i}$$

Results

Figure shows the deformed shape for the fuel assembly mostly subject to bowing (i.e., the one suffering the maximum thermal and flux gradients).

The results – obtained under the hypothesis of unrestrained deformations! – report a maximum displacement from the original axis by 3.44 mm.

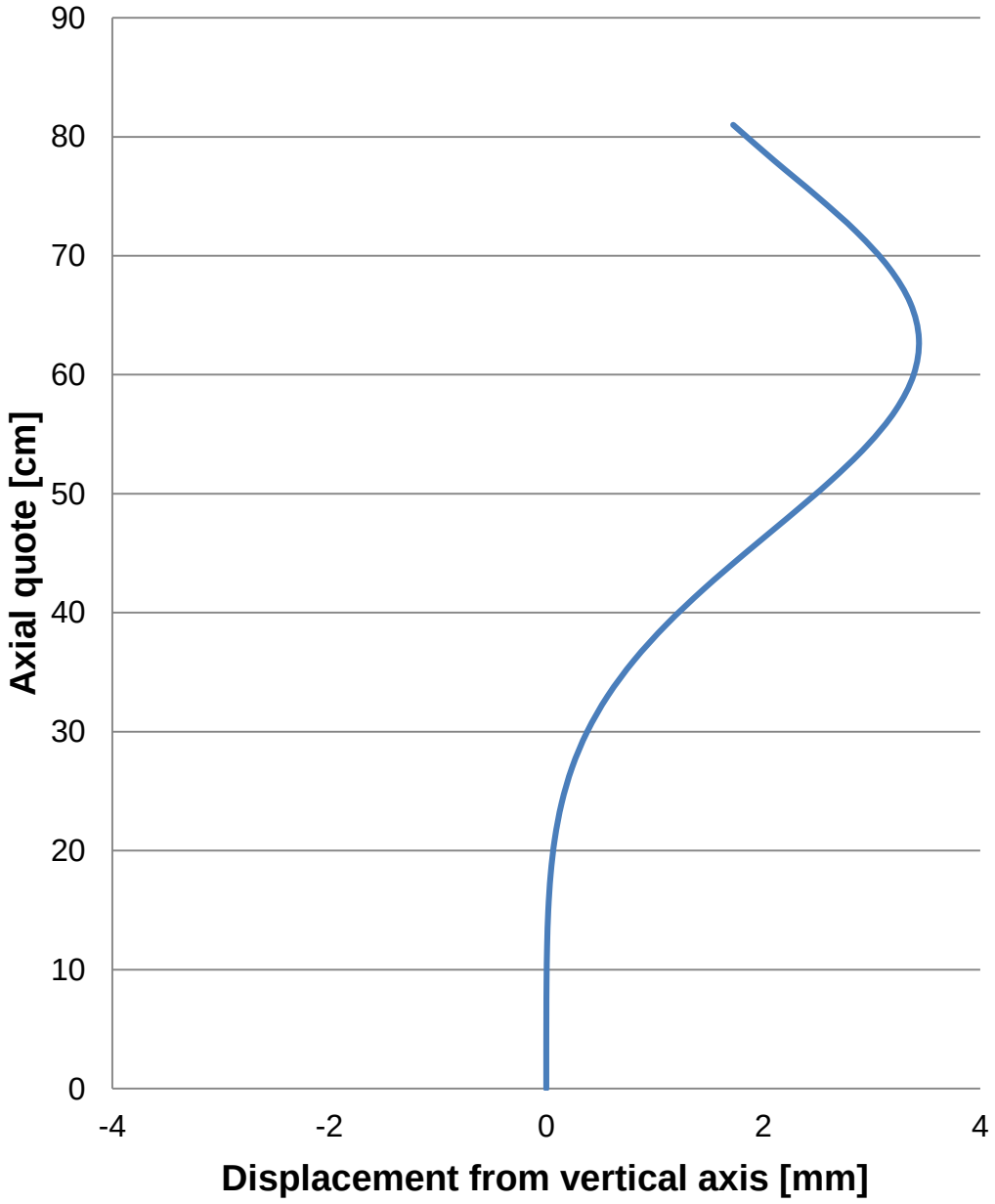

Conclusions

Summary

- A methodology for computing the unrestrained displacement of a fuel assembly has been developed, cross-checked and applied to the ALFRED case.

- The preliminary results for the most stressed fuel assembly report a peak displacement of 3.4 mm from the axis, which seems acceptable i.e., easily manageable by engineering means.

Conclusions

Future work

- The methodology – presently analytical – shall be validated before other, more formal applications.

- The methodology shall be coded, targeting two possible tools:
  - TEIA, which will include also the mechanical interaction with the bundle within the wrapper;
  - FEBE, which will extend the analysis to the whole core, removing the unrestrained hypothesis thereby allowing the evaluation of the mutual interaction among S/As.

Giacomo Grasso
giacomo.grasso@enea.it

Feasibility studies of an experimental campaign in TAPIRO devoted to the analysis of nuclear database for minor actinides

Use of new nuclear data libraries for the Monte Carlo analysis of neutronic measurements in the TAPIRO reactor

C. Di Gesare[1], D. Caron[1], S. Dulla[1], P. Ravetto[1],
M. Carta[2], V. Fabrizio[2]

[1]*Politecnico di Torino, Italy*

[2]*ENEA Casaccia, Italy*

Outline

- The TAPIRO reactor
- Aim of the work
- The SERPENT model of TAPIRO
  - Gemoetrical configuration
  - Nuclear data
- Comparison of nuclear data libraries
  - Reaction rates in radial channel 1 (RC1)
  - Neutron currents in RC1
  - k_{eff}
- Conclusions and perspectives

The TAPIRO reactor

- TAPIRO (TAratura PIla Rapida Potenza ZerO)
  - fast spectrum research reactor
  - Located in ENEA laboratories in Casaccia, Italy
  - In operation since 1971

- Square cylinder core (diameter about 12 cm)
- Fuel made of a uranium-molybdenum alloy (98.5 wt.% U–1.5 wt.% Mo, 93.5% enrichment)
- Maximum operating power 5 kW
- Multipurpose facilities
  - Well-characterized neutron spectrum
  - Allows irradiation in various conditions
  - Adopted for analysis of materials under irradiation

The TAPIRO reactor

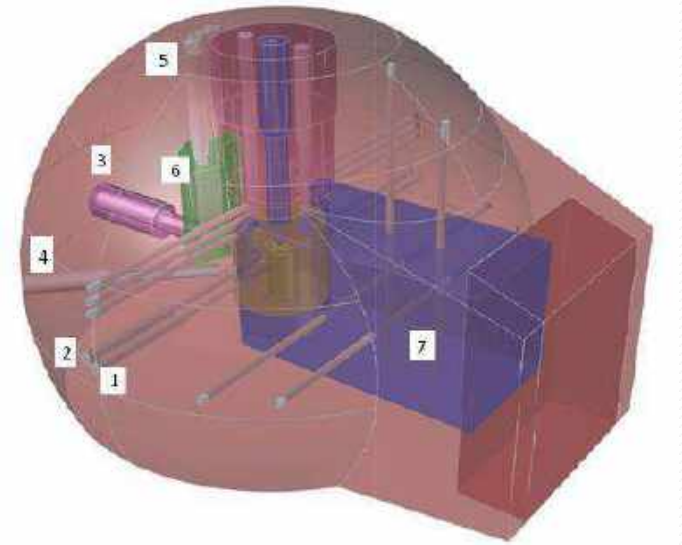

- TAPIRO (TAratura PIla Rapida Potenza ZerO)
  - fast spectrum research reactor
  - Located in ENEA laboratories in Casaccia, Italy
  - In operation since 1971

- Square cylinder core (diameter about 12 cm)
- Fuel made of a uranium-molybdenum alloy (98.5 wt.% U–1.5 wt.% Mo, 93.5% enrichment)
- Maximum operating power 5 kW
- Multipurpose facilities
  - Well-characterized neutron spectrum
  - Allows irradiation in various conditions
  - Adopted for analysis of materials under irradiation

Experimental campaign in TAPIRO

- SCK-CEN/ENEA experimental campaign carried out in 1980-86
- Fission rates of Np-237, U-238 and U-235 measured in RC1
- Previous work
  - Simulation of these experiments with stochastic and deterministic tools (see M&C2017) → ***discrepancies***
  - Preliminary sensitivity analysis on the influence of copper nuclear data in simulations

x-y section of the reactor at z=1 m

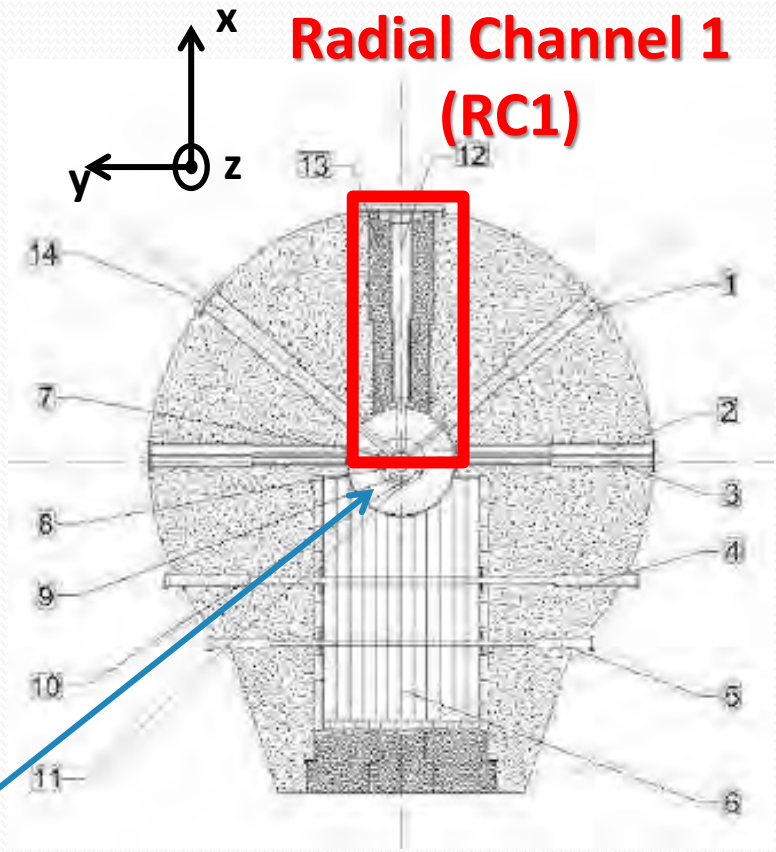

Objective of the work

- Computational modelling of the TAPIRO reactor with SERPENT Monte Carlo code
- Reconstruction of experimental data performed in the SCK-CEN/ENEA experimental campaign
- **Comparison of different libraries** available
  - the original JEFF-3.1.1 library
  - upgraded version with new nuclear data for copper isotopes based on the new ENDF/B-VIII.beta5 library
  - new library based entirely on ENDF/B-VIII.beta5.
- Discussion of
  - differences among the three different data sets
  - resulting effect of the reaction rates, currents …

SERPENT model of TAPIRO

- Serpent version 1.19, with different libraries (as detailed later on)
  - Model including the whole system (biological shield)
  - Focus on the modelling of RC1 (other channels not modelled)
  - Simulated access groove bigger than in reality to improve statistical convergence

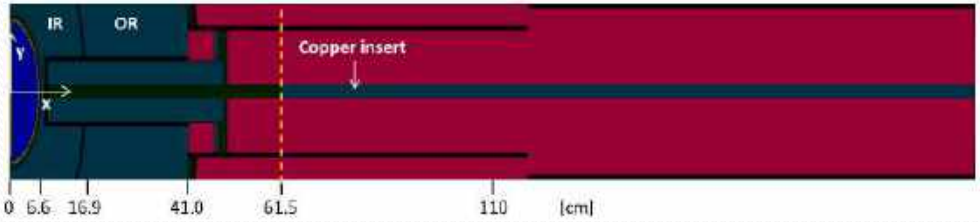

RC1 model (with copper insert up to 61.5 cm)

x-y section at z=1 m

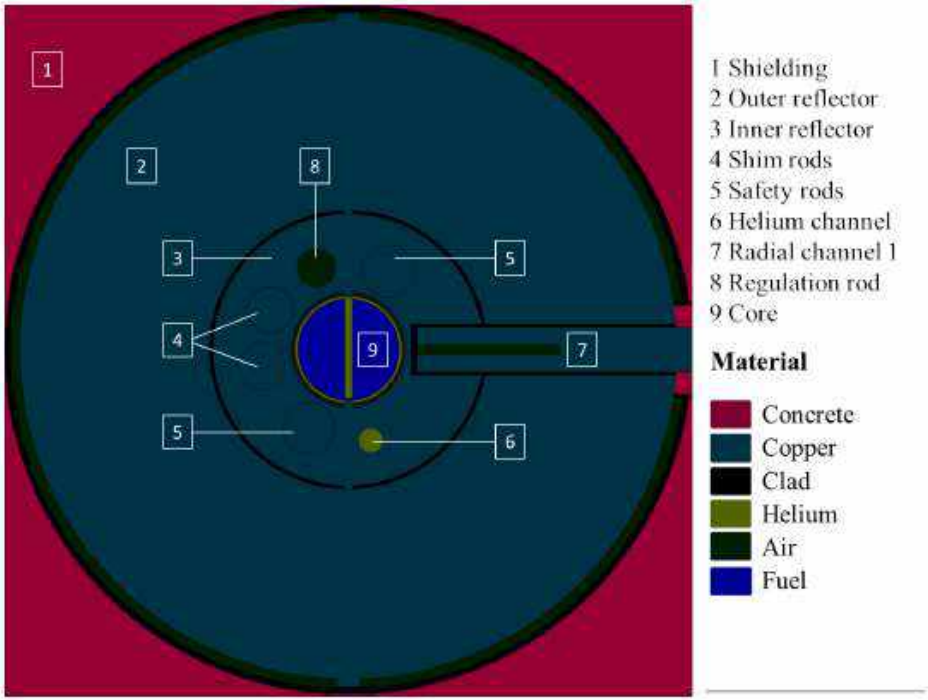

Nuclear data in Serpent

- The version of Serpent employed has cross-section libraries based on

Adopted in previous evaluations of TAPIRO (PAR 2016)

JEF-2.2 JEFF-3.1 **JEFF-3.1.1** ENDF/BVI.8 ENDF/B-VII

- New libraries can be produced from raw ENDF format data using NJOY

From ENDF/B-VIII.beta5 nuclear data (released 10/2017) a new library has been generated

- The effect of the new data has been assessed in two steps
  - Update of Copper X-sections in existing JEF-3.1.1 library
  - Full library based on ENDF/B-VIII.beta5

Objective

Compare the experimental fission rates in RC1 with the results of Monte Carlo simulations, to assess the role of the nuclear data, with a specific focus on the role of copper

Copper cross section behavior -I

- Isotopes present in natural copper have been considered (69.2% Cu-63 and 30.8% Cu-65)
- General comment: ENDF/B-VIII data lower than JEFF-3.1.1 → weaker decay of the neutron flux in the reflector

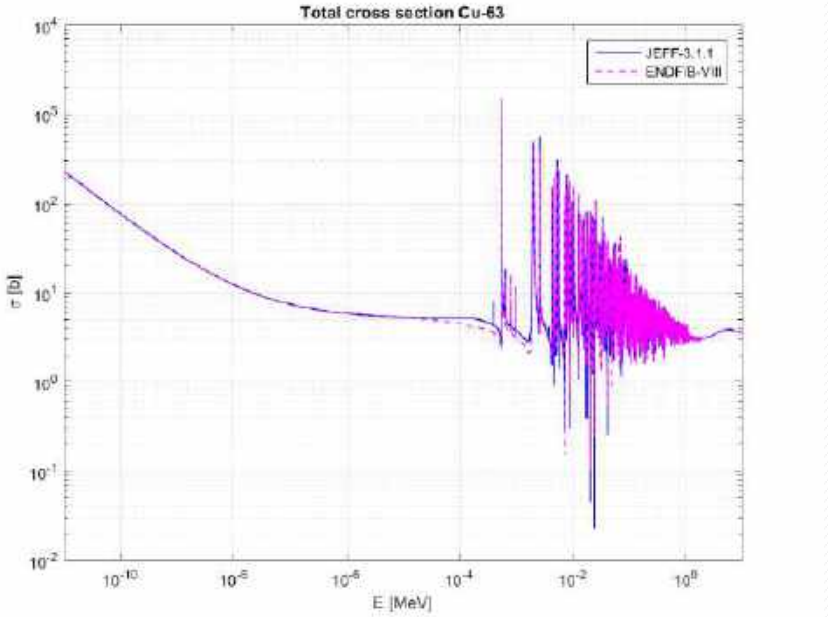

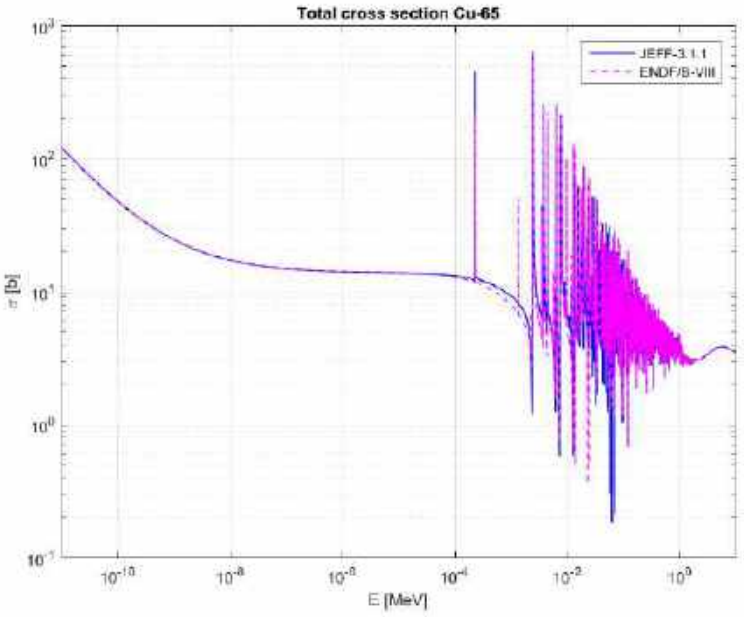

Copper cross section behavior -I

- Other comparison of copper cross sections performed between ENDF/B-VIIIbeta and new JEFF-3.2 → small discrepancies

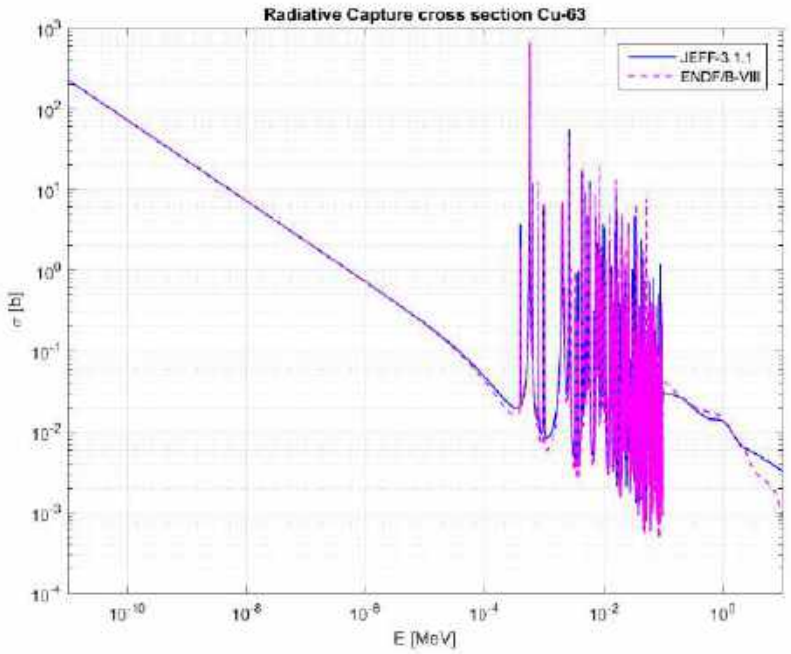

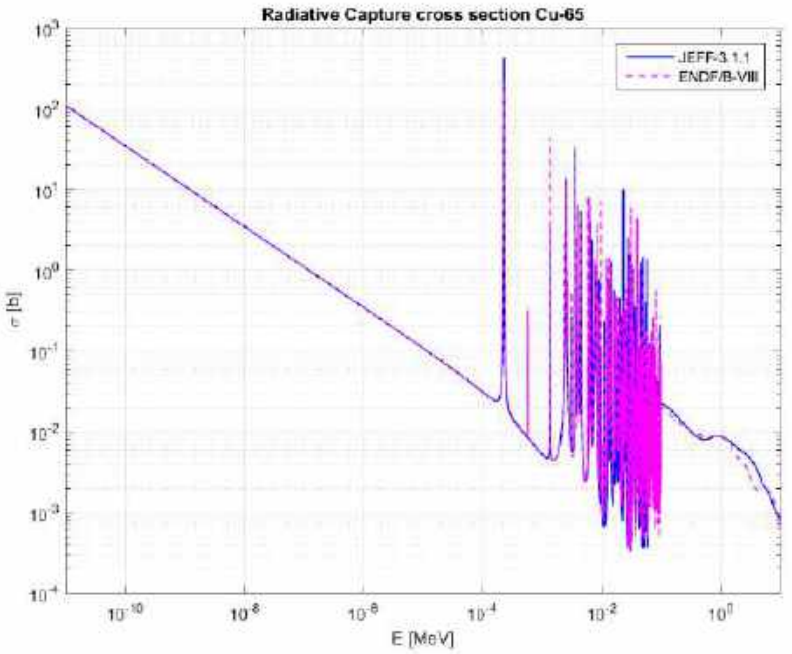

Effect on RC1 fission rates - I

- Simulations performed for the isotopes considered in the experiments: Np-237, U-235, U-238, Pu-239

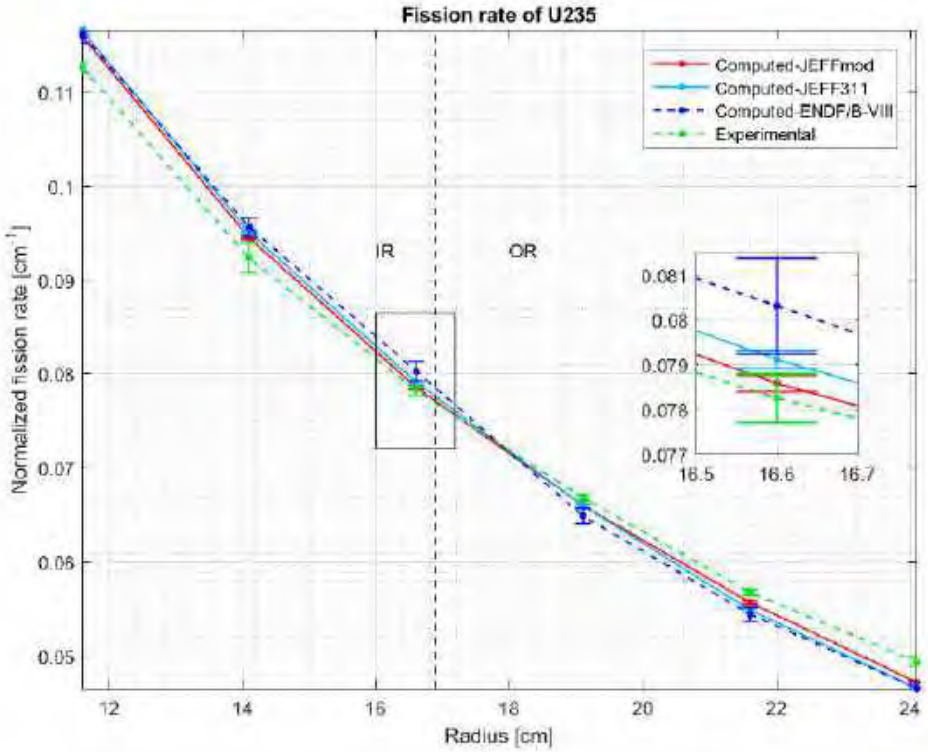

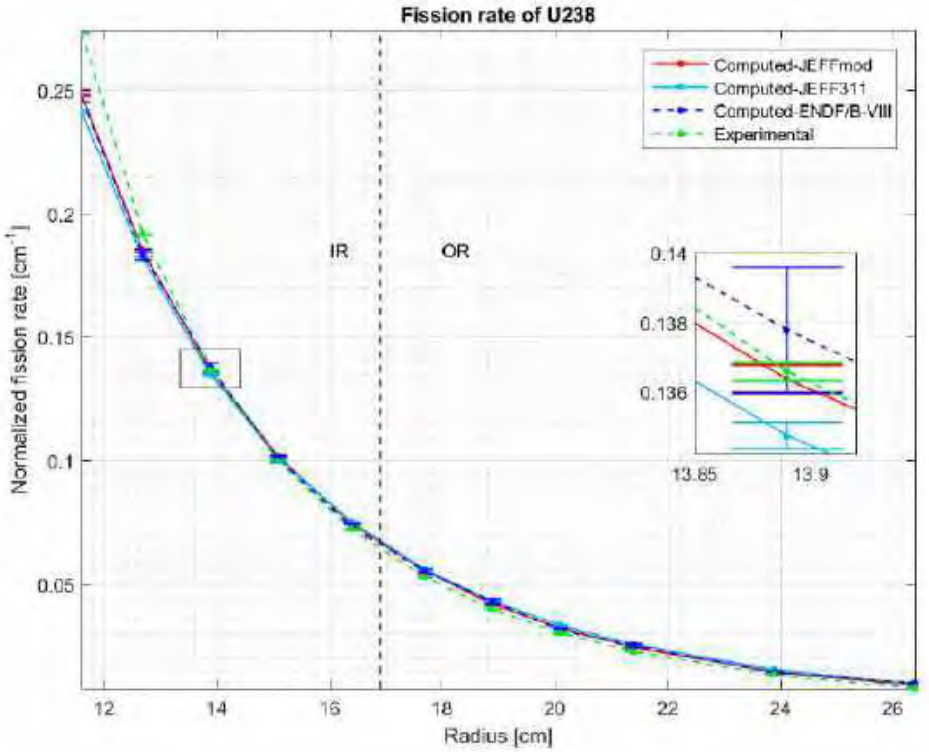

Effect on RC1 fission rates - II

- All reaction rates are normalized to the same spatial integral along the axis of the channel.
  - Use of new data for copper (JEFFmod results) improves agreement
  - Use of the full new library (ENDF/B-VIII results) gives different performances depending on the isotope

Differences evaluated: sign disagreement is observed in some locations along the radial coordinate

	Np-237		
r [cm]	JEFF-3.1.1	JEFF-3.1.1 mod.	ENDF/B-VIII.beta5
11.60	0.0099 (9E-04)	0.0072 (9E-04)	0.009 (1E-03)
12.74	0.0020 (5E-04)	0.0005 (5E-04)	0.001 (1E-03)
13.94	-0.0020 (4E-04)	-0.0028 (4E-04)	-0.0027 (9E-04)
15.14	-0.0028 (4E-04)	-0.0029 (4E-04)	-0.0024 (8E-04)
16.40	-0.0032 (5E-04)	-0.0030 (5E-04)	-0.0025 (8E-04)
17.74	-0.0022 (4E-04)	-0.0017 (4E-04)	-0.0022 (7E-04)
18.94	-0.0003 (1E-04)	0.0003 (1E-04)	0.0005 (5E-04)
20.14	0.0002 (1E-04)	0.0007 (1E-04)	0.0004 (5E-04)
21.44	0.0008 (3E-04)	0.0014 (3E-04)	0.0005 (5E-04)
23.94	0.0014 (1E-04)	0.0018 (1E-04)	0.0015 (3E-04)

Effect on relevant neutronic quantities

- Multiplicativity: non-negligible effect, especially when focusing on the modification of copper cross sections only

	JEFF-3.1.1	JEFF-3.1.1 mod.	ENDF/B-VIII.beta5
k_{eff}	1.00787 (± 6.5E-06)	1.00309 (± 6.5E-06)	1.00594 (± 2.9E-05)

- Currents: the currents entering RC1 at different energies have been evaluated
  - Evaluation of the effect of the library change
  - Potential use as source for calculations reduced to RC1 only

Neutron current entering RC1 - I

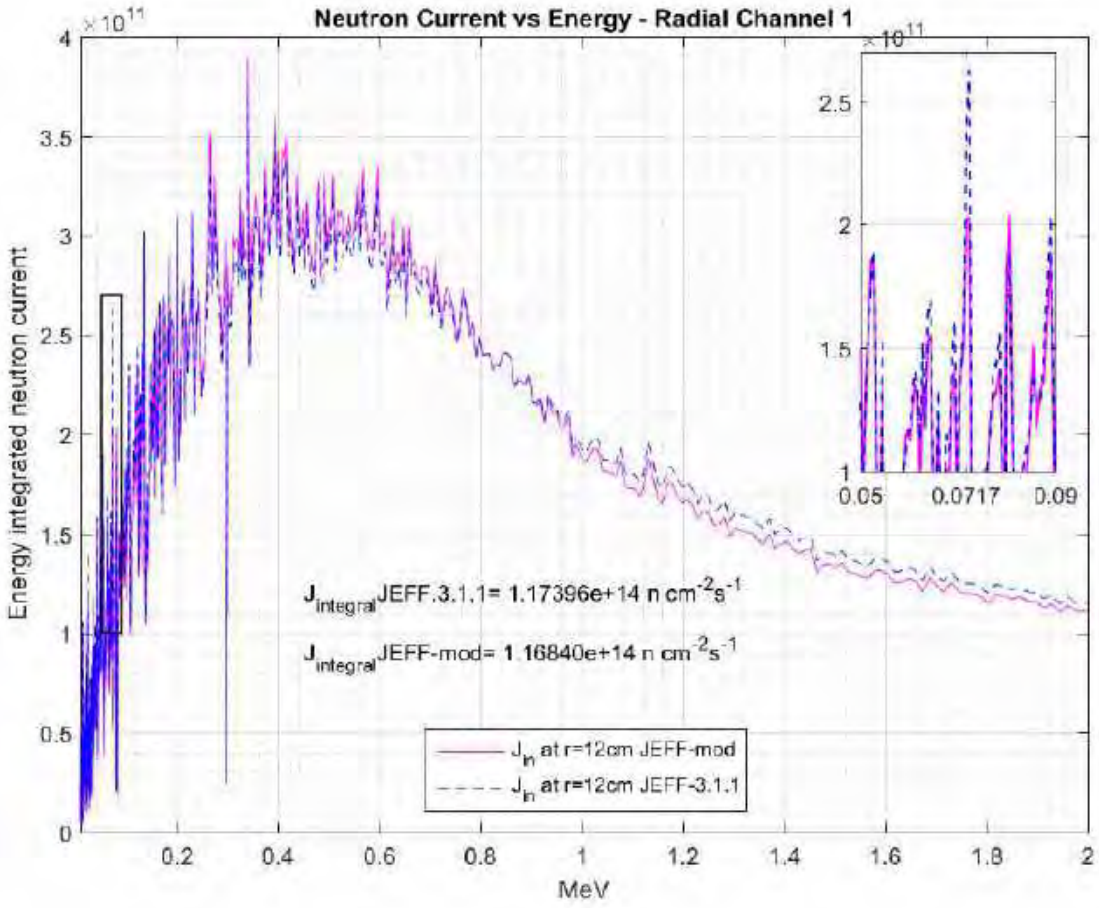

Neutron current entering RC1 at 12 cm distance from the system center.

Average relative standard deviation 0.0049

Different slowing down effect

Neutron current entering RC1 - II

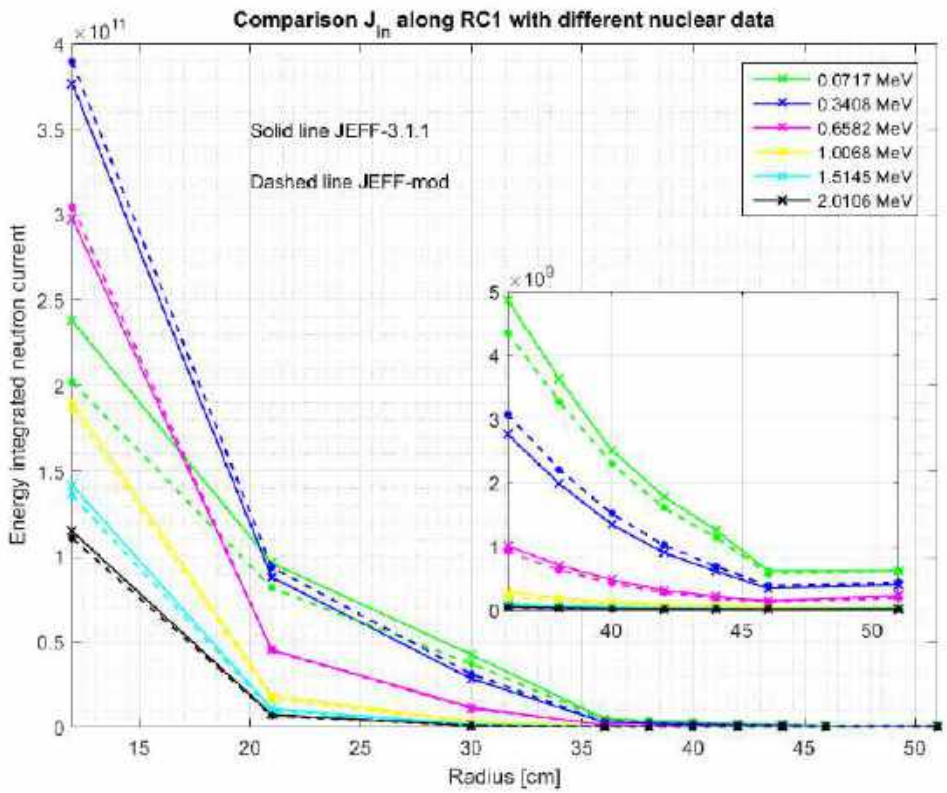

Neutron current entering along RC1 axis.

Non- negligible effect, especially in some energy ranges

Conclusions and perspectives

- The effect of nuclear data libraries in the simulation reaction rates in TAPIRO has been assessed
  - Nuclear data for copper play an important role in this experimental facility
  - The adoption of new nuclear data libraries leads to significantly different results
  - The results are not improved in all situations (as compared to experimental data).
  - Further work is needed to draw a definite conclusion on the appropriateness of the new cross section data.
- Perspective work: perform a complete sensitivity analysis of the MA reaction rates as a function of the nuclear data, evidencing the relative role of each components

Thanks for your attention

https://en.wikipedia.org/wiki/Tapir
https://it.wikipedia.org/wiki/Tapirus

Backup slides

Model of the access groove

- The dimension of the channel has been modified to get better statistics
  - Large Access Groove (LAG): radius=1.065 cm, detector volume 0. 24 cm^3
  - Small Access Groove (SAG): radius=0.66 cm, detector volume 0.10 cm^3 (for verification)
  - Results show different performance depending on the fission rate observed

LAG

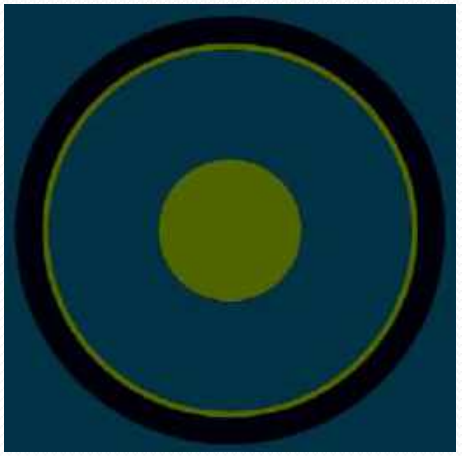

SAG

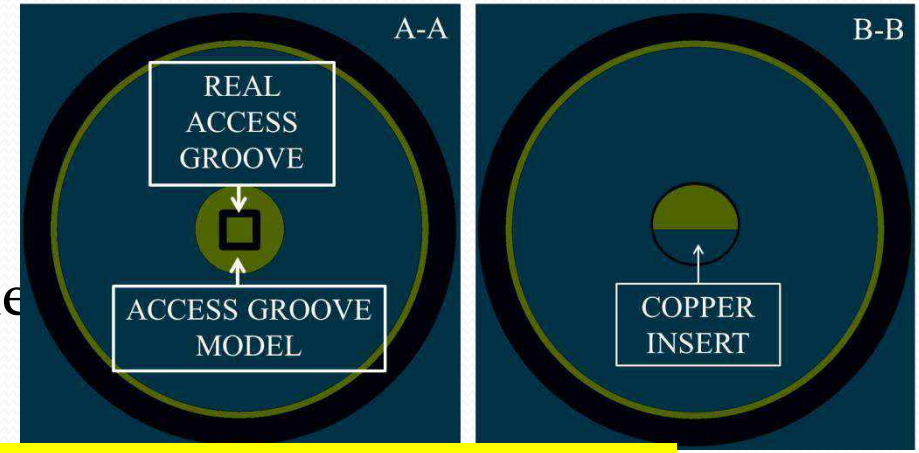

from PAR 2016

from PAR 2016

Comparison of groove models -I

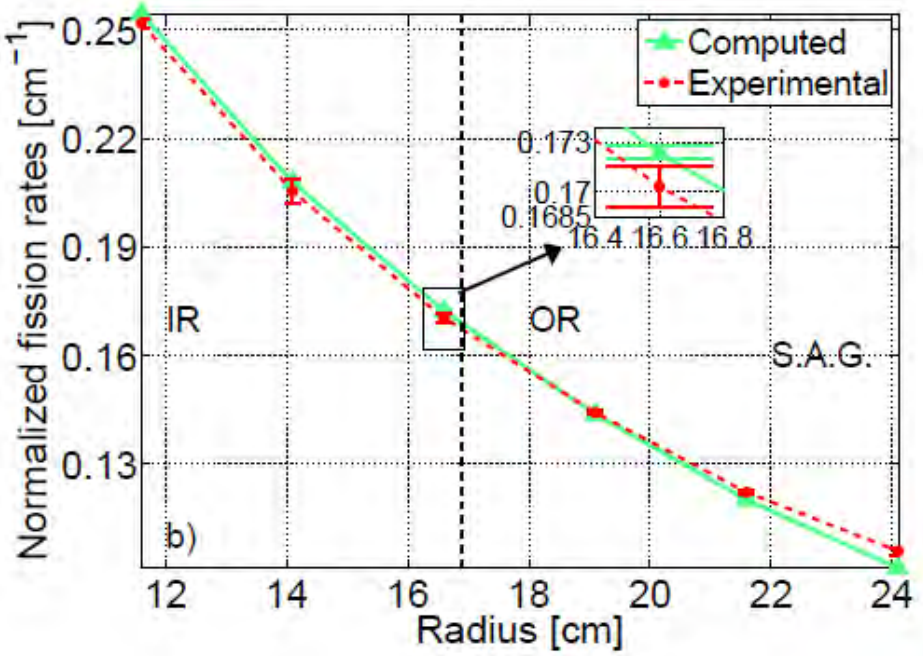

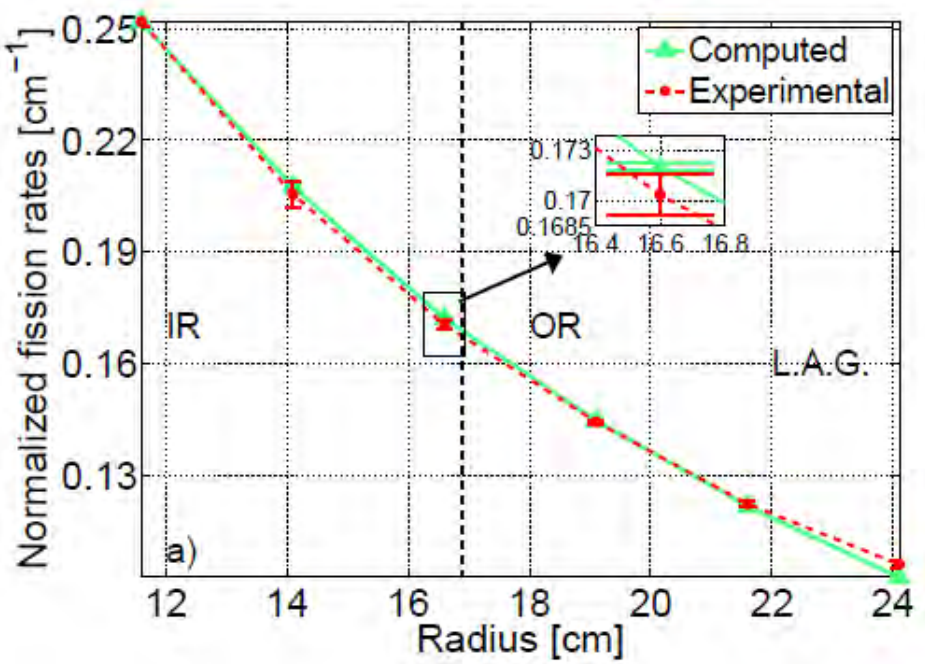

- Fission rate for U-235 shows small discrepancies
- Same results also for further detectors (r>24 cm)
- SAG simulations more computationally intensive

Localization of detectors

from PAR 2016

from PAR 2016

Comparison of groove models - III

- Fission rate for Np-237 with larger deviations
  - The dimension of the access groove modifies the material composition around the detector
  - SAG case:
    - more copper (r<41) or concrete (r>41)
    - Larger absorption in the energy range of fission of Np-237
    - Faster decay of fission rate
    - Still, open issues in the range 50-60 cm

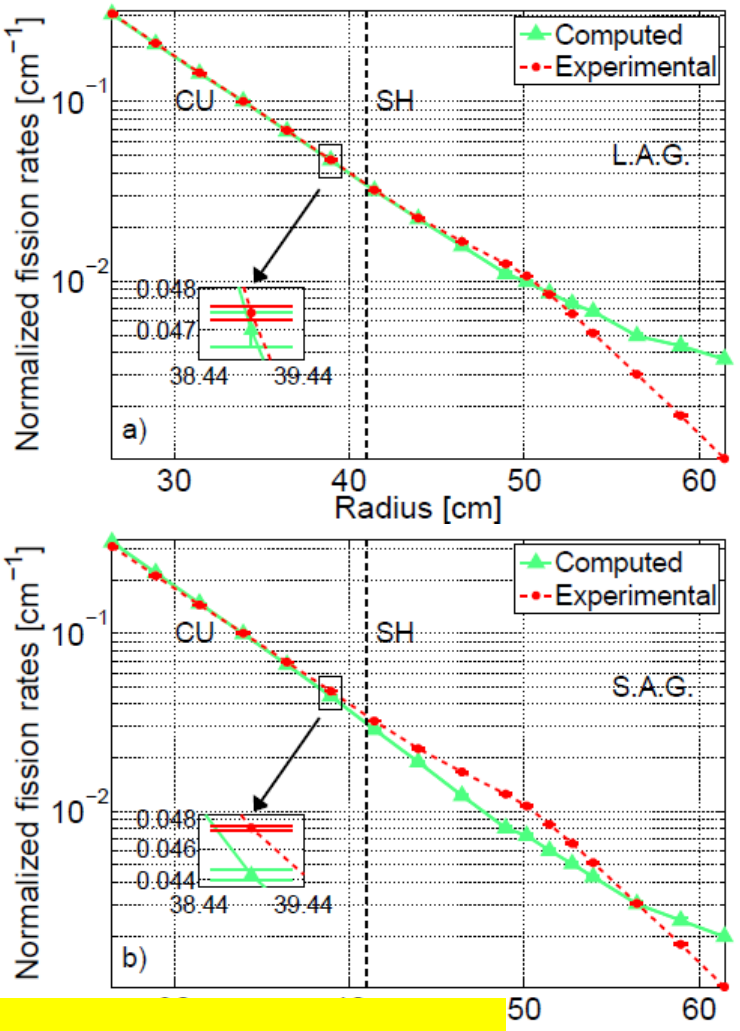

from PAR 2016

from PAR 2016

Comparison of groove models -III

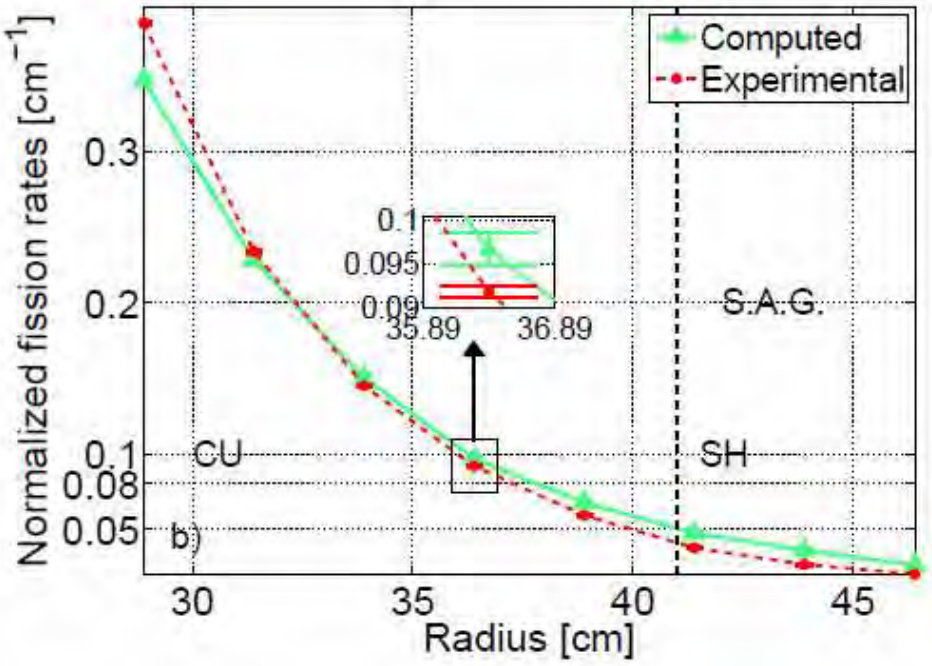

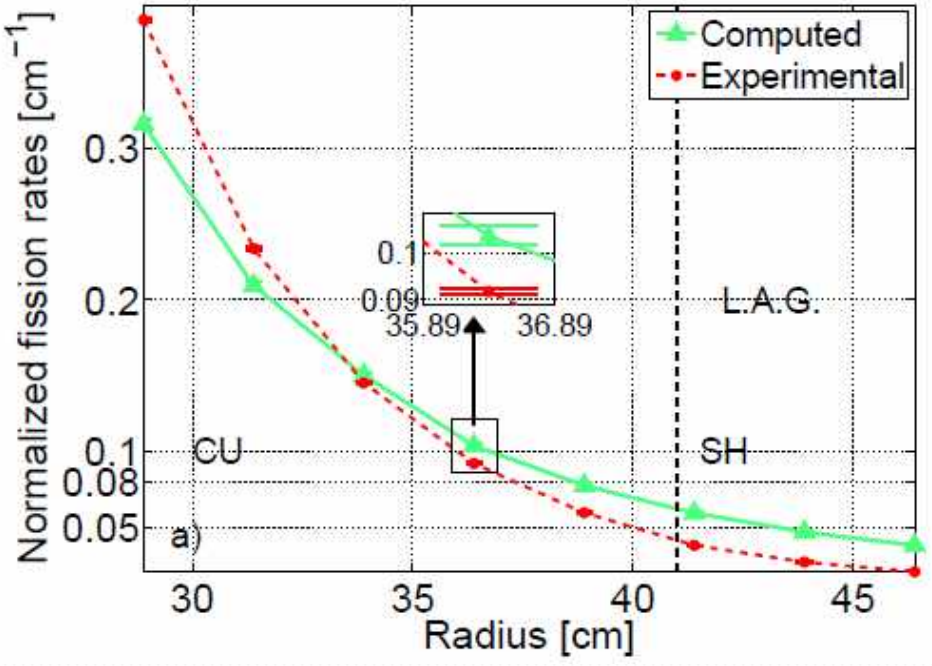

- Fission rate for U-238 shows relevant differences
- Comment on increased absorption by copper/concrete as in previous case is valid
- SAG simulations more computationally intensive

from PAR 2016

RECENTI SVILUPPI DELLA METODOLOGIA HGPT

Augusto Gandini, Università Sapienza, Roma
Vincenzo Peluso, Enea, Bologna

Workshop Tematico
Accordo di Programma MiSE - ENEA
Generation IV - Lead cooled Fast Reactor
14-15 Giugno, 2018
Università Sapienza, Roma

Introduzione

Partendo da un primo concetto di conservazione dell'importanza definito da Kadomtzev[1] nel campo fotonico, un metodo di calcolo perturbativo su basi euristiche venne successivamente proposto nel campo neutronico da Usachev per studi sui rapporti di tassi di reazione[2]. Il metodo di Usachev venne quindi esteso[3,4,5] per includere una gamma più ampia di funzionali lineari e non lineari.

Questo metodo è denominato HGPT (Heuristical Generalized Perturbation Theory) per distinguerlo da forme successive di derivazione, in particolare quelle basate su tecniche variazionali,[6,7,8,9] generalmente note come metodi GPT.

---

1. Kadomtzev, B.B., “On the Importance Function in Radiation Transport Theory”, Dokl. An. URSS, **113**, N. 3 (1957).
2. Usachev, L.N., Atomnaya Energiya, **15**, 472 (1963) .
3. Usachev, L.N., ZARISKI, S.M., Atomizdat, **2**, 242 (1965).
4. Gandini, A., Journal of Nucl. En., **21**, 755 (1967) .
5. Gandini, A., “Generalized Perturbation Theory Methods”, *Advances Nucl.Sci.Tech.*, Vol.**19**., Plenum, New York, (1987).
6. Gandini, A., Annals of Nuclea Energy, 24, 1241 (1997).
7. Stacey, W.M., Jr., “Variational Methods in Nuclear Reactor Physics”, Academic Press, New York (1974).
8. Lewins, J., “Importance, the Adjoint Function,pergamon Press, Oxford (1965).
9. Cacuci, D.G., Weber C.F., Oblow, E.M., Marable, J.M., Nucl. Sci. Eng., **75** 88 (1980).

RECENTI SVILUPPI DELLA METODOLOGIA HGPT

Verranno nel seguito descritti tre recenti sviluppi basati su questa metodologia, relativi agli argomenti:

- monitoraggio della sottocriticità di un sistema ADS;
- rilevamento di potenziali punti caldi;
- analisi del burn-up

1. Monitoraggio della sottocriticità

Un problema connesso con l'operazione di un reattore sottocritico (ADS) è posto dalla necessità di valutare online con sufficiente precisione il suo livello di sottocriticità.

Nel seguito illustreremo un approccio generale a questo problema, partendo dalle equazioni della cinetica puntuale relative a questi sistemi.[10,11]

10. Gandini, A., "HGPT Based Sensitivity Methods for the Analysis of Subcritical Systems", Ann. Nucl. Energy, **28**, 1193 (2001) .
11. GandiniI, A., "ADS Subcriticality Evaluation Based on the Generalized Reactivity Concept", Ann. Nucl. Energy, **31/7**, 813 (2004).

Equazioni della cinetica puntuale

Nella cinetica puntuale dei sistemi sottocritici sono definite due equazioni:
- una governa l'andamento della potenza (P) a seguito di una perturbazione di uno o più parametri di sistema, tra cui la sorgente esterna
- l'altra governa le densità effettive dei precursori dei neutroni ritardati (ξ_i)

$$l_{eff}\frac{dP}{dt} = (\rho_{gen} - \alpha\beta_{eff})P + \alpha\sum_{i=1}^{I}\lambda_i\xi_i + \zeta(1-P) + \rho_{source}$$

$$\frac{d\xi_i}{dt} = \beta_{i,eff}P - \lambda_i\xi_i$$

Alle condizioni iniziali la potenza P è normalizzata all'unità, mentre le densità effettive dei precursori ξ_i sono date dal prodotto normalizzato delle densità dei precursori stessi per la loro importanza

$$\xi_i = \frac{< m^*_{s,o} m_i >}{< \mathbf{n}^*_{s,o}, \bar{\chi} S_{f,o}\phi_o >}$$

(i'th effective precursor density)

($\bar{\chi} S_{f,o}\phi_o$ = fission source)

RECENTI SVILUPPI DELLA METODOLOGIA HGPT

La quantità ζ che compare nell'equazione che governa l'andamento della potenza corrisponde ad un termine di normalizzazione

$$\zeta = \frac{1}{< \mathbf{n}^{*}_{s,o}, \bar{\chi} S_{f,o} \phi_o >}$$

Al denominatore di questo termine compare la funzione importanza neutronica $\mathbf{n}^{*}_{s,o}$. Questa funzione è governata dall'equazione aggiunta associata alla potenza normalizzata

$$B^{*}_{o} \mathbf{n}^{*}_{s,o} + \frac{\gamma}{W_o} \boldsymbol{\Sigma}_{f,o} = 0$$

(γ = energy units per fission)
(W_o = Potenza nominale)

RECENTI SVILUPPI DELLA METODOLOGIA HGPT

Nell'equazione che regge la potenza compaiono delle quantità con un significato fisico preciso

$$l_{\text{eff}} = \zeta < \mathbf{n}^{*}_{\text{s,o}}, \mathrm{V}^{-1}\boldsymbol{\phi}_{\text{o}} >$$

(vita media effettiva dei neutroni pronti)

$$\rho_{\text{gen}} = \zeta\left(< \mathbf{n}^{*}_{\text{s,o}}, \delta\mathrm{B}\boldsymbol{\phi}_{\text{o}} > + \frac{\gamma}{\mathrm{W_o}} < \delta\boldsymbol{\Sigma}_{\text{f}}, \boldsymbol{\phi}_{\text{o}} > \right)$$

(reattività generalizzata relativa alla perturbazione di parametri di sistema)

$$\rho_{\text{source}} = \zeta < \mathbf{n}^{*}_{\text{s,o}}, \delta\mathbf{s}_{\text{n}} >$$

(reattività generalizzata relativa alla perturbazione della sorgente esterna)

RECENTI SVILUPPI DELLA METODOLOGIA HGPT

Il coefficiente di sottocriticità K_{sub} è definito da un rapporto in cui compaiono la sorgente di fissione e la sorgente esterna pesate con la loro importanza

$$K_{sub} = \frac{< \mathbf{n}^{*}_{s,o}, \bar{\chi} S_{f,o} \phi_{o} >}{< \mathbf{n}^{*}_{s,o}, \mathbf{s}_{n} > + < \mathbf{n}^{*}_{s,o}, \bar{\chi} S_{f,o} \phi_{o} >}$$

Il termine di sorgente esterna al denominatore $< \mathbf{n}^{*}_{s,o}, \mathbf{s}_{n} >$ risulta eguale al valore della potenza nominale normalizzata, cioè all'unità.
L'espressione del coefficiente K_{sub} risulta quindi semplificata

$$K_{sub} = \frac{< \mathbf{n}^{*}_{s,o}, \bar{\chi} S_{f,o} \phi_{o} >}{1 + < \mathbf{n}^{*}_{s,o}, \bar{\chi} S_{f,o} \phi_{o} >}$$

$$K_{sub} = \frac{< \mathbf{n}^{*}_{s,o}, \bar{\chi} S_{f,o} \phi_{o} >}{1 + < \mathbf{n}^{*}_{s,o}, \bar{\chi} S_{f,o} \phi_{o} >}$$

Ricordando l'espressione del termine di normalizzazione

$$\zeta = 1 / < \mathbf{n}^{*}_{s,o}, \bar{\chi} S_{f,o} \phi_{o} >$$

si può definire il coefficiente K_{sub} come dato da un rapporto in termini di ζ

$$K_{sub} = \frac{1}{1+\zeta}$$

La quantità ζ può essere a sua volta definita come un rapporto in termini di K_{sub}

$$\zeta = \frac{1 - K_{sub}}{K_{sub}}$$

Questa espressione consente di poter assumere la quantità ζ come un appropriato indice di sottocriticità

RECENTI SVILUPPI DELLA METODOLOGIA HGPT

Il metodo

Consideriamo una variazione della posizione di una barra di controllo (calibrata) in un reattore sottocritico. Ad essa corrisponderà un valore sperimentale di reattività $\left(\delta k_{eff} / k_{eff}\right)_B^{\mathbf{exp}}$.

Il valore della reattività generalizzata associata ad esso può essere assunto come il prodotto del suo valore calcolato per un fattore di bias

$$\rho_{gen,B}^{\mathbf{exp}} = \rho_{gen,B}^{cal} \; f_b$$

Il fattore di bias f_b è definito da un rapporto

$$f_b = \frac{\left(\delta k_{eff} / k_{eff}\right)_B^{\mathbf{exp}}}{\left(\delta k_{eff} / k_{eff}\right)_B^{calc}}$$

dove il numeratore è dato dal valore di calibrazione della barra di controllo mentre il denominatore è dato dalla corrispondente espressione perturbativa standard calcolata.

RECENTI SVILUPPI DELLA METODOLOGIA HGPT

Analogamente, la reattività generalizzata di sorgente ρ_{source}^{exp}, associata ad una data variazione δs_n^{exp} della sorgente stessa, può essere rappresentata da un rapporto in termini del coefficiente di sottocriticità K_{sub}

$$\rho_{source}^{exp} = \frac{< \mathbf{n}_{s,o}^{*}, \delta \mathbf{s}_n^{exp} >}{< \mathbf{n}_{s,o}^{*}, \bar{\chi} S_{f,o} \phi_o >} \equiv \frac{\delta s_n^{exp}}{s_n} \frac{1 - K_{sub}}{K_{sub}}$$

Consideriamo ora variazioni della posizione della barra di controllo e dell'intensità della sorgente esterna tali da mantenere praticamente inalterato il livello della potenza. Ciò si riflette nella condizione per cui le reattività generalizzate associate a tali variazioni si compensano

$$\rho_{gen,B}^{exp} + \rho_{source}^{exp} = 0$$

Ricordando l'espressione della reattività di sorgente si ottiene facilmente il valore cercato del coefficiente di sottocriticità

$$K_{sub} = \frac{\delta s_n^{exp} / s_n}{\delta s_n^{exp} / s_n - \rho_{gen,B}^{exp}}$$

Conclusione

Il metodo proposto può essere utilizzato per lo sviluppo di un sistema di misura della sottocriticità di un reattore ADS durante la sua normale operazione sulla base della rilevazione di piccole variazioni della posizione della barra di controllo e dell'intensità della sorgente esterna.

Un esercizio di simulazione numerica[12] è stato considerato in vista di un esperimento su una configurazione sottocritica del reattore TRIGA. L'esercizio ha dimostrato la potenzialità del metodo proposto.

L'esperimento su menzionato è attualmente in corso.

12. Carta, M., et al. , "The Power Control Based Subcriticality Monitoring (PCSM) Method for ADS Reactors", RRFM/IGORR Conference, Berlin, March 2016.

2. Identificazione di punti caldi

Attraverso l'uso della teoria perturbativa generalizzata[1] e delle tecniche di inferenza probabilistica[2] è stato sviluppato un metodo[3] utilizzabile in un sistema di protezione per la rilevazione di possibili punti caldi (hot spot) durante il normale funzionamento di un reattore.

Il metodo è basato su misurazioni online del flusso neutronico.

Si presume che queste misurazioni siano effettuate da rivelatori autoalimentati (SPND), denominati anche 'collettroni'.

1. Gandini, A., "Generalized Perturbation Theory (GPT) Methods. A Heuristic Approach", in Advances in Nuclear Science and Technology, Vol. 19, Plenum Publ.,(1987).
2. Gandini,A., "Uncertainty Analysis and Experimental Data Transposition Methods",*Handbook Uncertainty Anal.*,CRC(1988).
3. Gandini, A., "Hot Point Detection Method", Ann. Nucl. En., 38 (2011) 2843.

RECENTI SVILUPPI DELLA METODOLOGIA HGPT

Il metodo è stato concepito per il suo utilizzo nei reattori termici, in particolare nei PWR.

Il suo utilizzo nei reattori veloci è legato allo sviluppo di tecniche di rilevamento del flusso neutronico sufficientemente precise[4]

4. Lepore, L., Remetti, R., Cappelli, M., J. Nucl. Eng. and Rad. Sci., 2(4), NERS-15-1205, doi: 10.1115/1.4033697 (2016).

RECENTI SVILUPPI DELLA METODOLOGIA HGPT

Il metodo tiene conto degli errori associati alle misurazioni.

Esso consente inoltre di valutare l'effetto sulla qualità dei rilevamenti a seguito di possibili guasti degli strumenti di misura.

Tale valutazione può essere utile per definire una strategia di protezione adeguata in termini di qualità, numero e distribuzione dei collettroni.

Teoria

Supponiamo che un numero fisso (N) di collettroni sia posizionato nel nocciolo di un dato reattore. Consideriamo quindi un numero (M) di ipotetiche posizioni di punti caldi.

Per semplicità assumiamo anche che in ogni ipotetica posizione di punto caldo rimanga costante il rapporto

$$r_m \equiv p_m^{\mathbf{max}} / \bar{p}_m$$

tra la densità di potenza lineare massima e quella media.

RECENTI SVILUPPI DELLA METODOLOGIA HGPT

Viene fissata una prima soglia $p_m^{max,1}$ della densità di potenza lineare massima, oltre la quale si innesca un avviso di attenzione

Viene quindi fissata una seconda soglia $p_m^{max,2}$ al di sopra della quale si verifica l'arresto dell'impianto.

Dall'analisi dei rilevamenti dei collettroni, la possibilità della presenza di una condizione di punto caldo in una o più delle M posizioni ipotetiche deve essere valutata in relazione alle soglie assegnate.

RECENTI SVILUPPI DELLA METODOLOGIA HGPT

Questa metodologia utilizza dei coefficienti di sensitività ($w_{n,\,m}$). Essi rappresentano il contributo di una sorgente di fissione unitaria, localizzata in un dato elemento (m) di combustibile, al suo rilevamento in ciascuno degli N collettroni.

Questi coefficienti formano un vettore, w_m, caratteristico di ciascuna delle possibili posizioni di punti caldi. In un certo senso, questo vettore può essere considerato come una loro ’firma'.

Data una serie di misurazioni Q_n^{ex} (n = 1, ..., N), la ricerca di un potenziale punto caldo inizia quando uno o più rilevamenti differiscono significativamente, vale a dire oltre margini di incertezza stabiliti, dai valori nominali.

La posizione, o posizioni, di punto caldo e il valore della relativa intensità sono ottenuti mediante tecniche di inferenza probabilistica.

Viene tenuto in conto il grado di degradazione del sistema di collettroni.

Applicazione numerica

È stata effettuata una simulazione numerica[5] relativa a un progetto di sistema PWR di dimensioni medie[6]. Il sistema è stato semplificato in una geometria x, y.

Per l'analisi è stato utilizzato il codice Eranos[7] .

I calcoli sono stati fatti in approssimazione di diffusione utilizzando una libreria di sezioni d'urto a 15 gruppi.

5. Gandini, A., et al., Ann. Nucl. Energy, 50,175 (2012).
6. Cumo, M., Naviglio, A., Sorabella, L., "MARS, 600 MWth Nuclear Power Plant", ANES Symposium,Miami, 2004.
7. Rimpaut, G., et al., "Physics Documentation of the ERANOS. The ECCO Cell Code", CEA Technical Note RT-SPRC-LEPh-97-001 (1997).

RECENTI SVILUPPI DELLA METODOLOGIA HGPT

Posizioni degli elementi contenenti i collettroni e posizioni degli elementi di combustibile

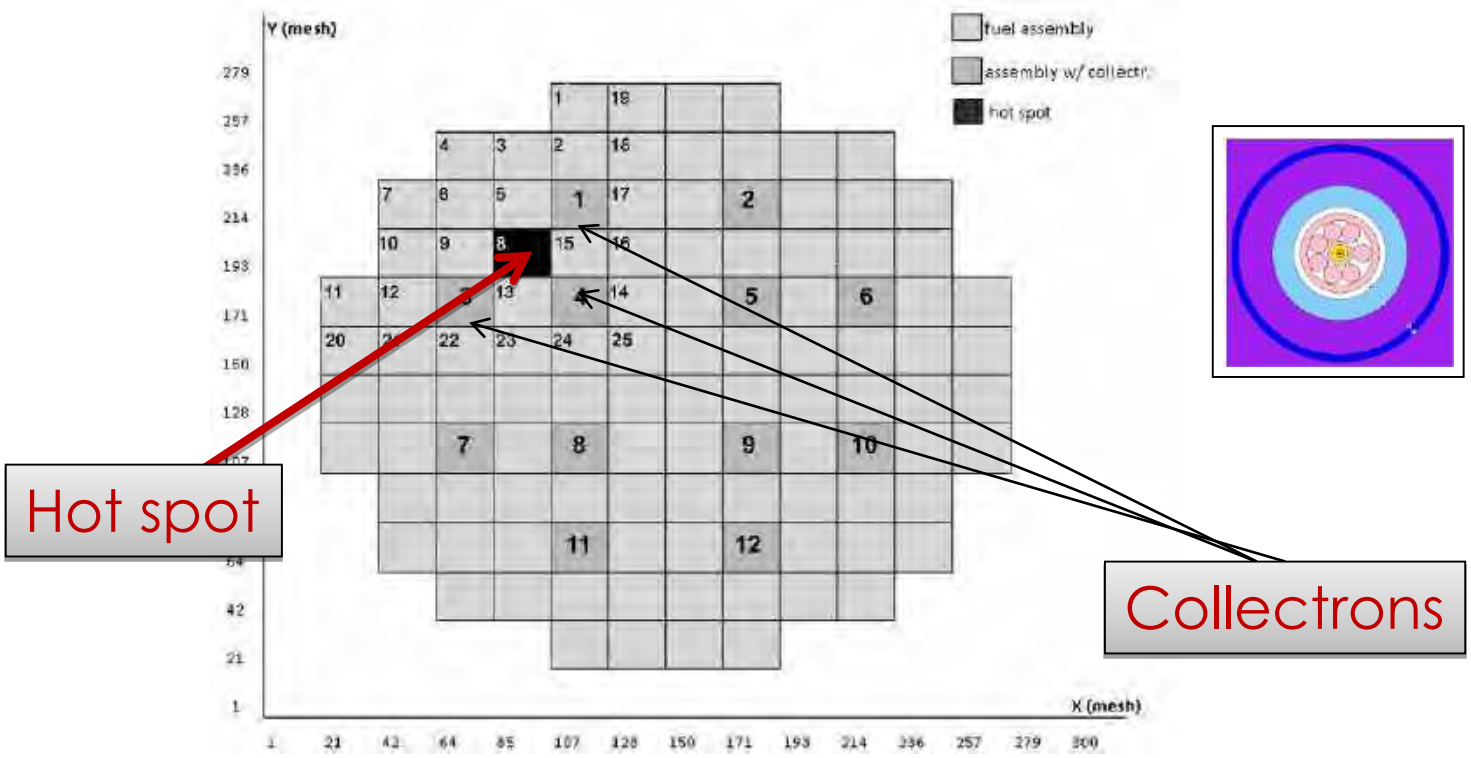

Per la simulazione del punto caldo è stata scelta la posizione 8

RECENTI SVILUPPI DELLA METODOLOGIA HGPT

Per questo esercizio di simulazione, si è assunto che i ‘rilevamenti’ Q_n^{ex} corrispondano a un insieme di quantità casualmente ordinate secondo una legge di distribuzione gaussiana caratterizzata da determinati valori calcolati Q_n^{cal} e una deviazione standard del 5%.

RECENTI SVILUPPI DELLA METODOLOGIA HGPT

In questa tabella vengono riportati i risultati dell'esercizio di simulazione. Da notare come la posizione e l'intensità del punto caldo rilevato vengano identificate in modo univoco fino al guasto di cinque collettroni.

Degradation (Failed collectrons)	Hot spot candidates positions	Hot spot		
		Simulated	Estimated	Stand. Dev.
0	8	1.000	1.003	0.079
1	8	1.000	1.003	0.094
1,2	8	1.000	1.004	0.095
1,2,3	8	1.000	1.008	0.123
1,2,3,4	8	1.000	1.005	0.153
1,2,3,4,5	8	1.000	1.007	0.162
1,2,3,4,5,6,7	6,**8**,9,15	1.000	1.006	0.176 (min)

RECENTI SVILUPPI DELLA METODOLOGIA HGPT

Conclusione

I risultati ottenuti con l'esercizio di simulazione indicano come il metodo proposto possa essere utilizzabile in un sistema di protezione per la rilevazione di possibili punti caldi.

Questo metodo può essere utile anche in una fase di progettazione.

L'analisi approfondita sulla distribuzione dei collettroni e sulle loro sequenze di guasti può infatti consentire di identificare configurazioni ottimali sulla base di criteri dell'ingegneria impiantistica e sulla base di considerazioni economiche.

Un interesse a questa metodologia è stato recentemente manifestato dalla società belga Tractebel. Sono in corso contatti in vista di una possibile collaborazione.

RECENTI SVILUPPI DELLA METODOLOGIA HGPT

L'applicabilità della metodologia potrebbe anche essere presa in considerazione per la rilevazione di un punto caldo prodotto dal blocco di flusso di un canale.

Un blocco di flusso produrrebbe infatti un aumento della temperatura locale, che a sua volta causerebbe un'alterazione (in questo caso riduzione) del tasso di fissione per l'aumento dell’assorbimento neutronico a causa dell'effetto Doppler.

3. Metodologia per l'analisi del burn-up

La metodologia per l'analisi perturbativa di funzionali della densità neutronica e di quella dei nuclidi che evolvono durante il burn-up è stata sviluppata secondo la teoria delle perturbazioni generalizzate su base euristica (HGPT).[1,2]

Questa metodologia può essere applicata sia a sistemi critici che sottocritici.

---

1. A. Gandini, "Generalized Perturbation Theory (GPT) Methods. A Heuristic Approach", in *Advances in Nuclear Science and echnology, Vol. 19*, Plenum Publishing Corporation, New York, 1987.
2. A. Gandini, "Sensitivity Analysis of Source Driven Subcritical Systems by the HGPT Methodology", *Annals of Nuclear Energy*, 24, 1241 (1997).

RECENTI SVILUPPI DELLA METODOLOGIA HGPT

I funzionali d'interesse possono riguardare, in particolare:

• L'accumulo di isotopi del combustibile a fine ciclo. In questo caso il metodo può essere utilizzato per la ricerca di valori ottimali di parametri di progetto o per la ricerca di strategie ottimali di caricamento del combustibile.

• La fluenza ad un tempo e punto stabiliti. In questo caso il metodo può essere utilizzato per analizzare il danneggiamento sui materiali con la vita del reattore.

• La radiotossicità delle scorie a lungo termine.

• Il parametro di controllo a fine ciclo. L'analisi di questa quantità può essere d'interesse in studi volti ad estendere il ciclo di vita del reattore.

RECENTI SVILUPPI DELLA METODOLOGIA HGPT

Equazioni

Il campo non-lineare d'interesse per lo studio del burn-up riguarda le funzioni:
- densità neutronica $\mathbf{n}(\mathbf{r},t)$,
- densità dei nuclidi $\mathbf{c}(\mathbf{r},t)$,
- parametro intensivo di controllo sulla potenza $\rho(t)$.

Equazioni che le governano:

$$\mathbf{m}_{(n)}(\mathbf{n},\mathbf{c},\rho\,|,\mathbf{p}) = -\frac{d\mathbf{n}}{\partial t} + B(\mathbf{c},\rho\,|\,\mathbf{p})\mathbf{n}_o + \mathbf{s}_n(\mathbf{p}) = \mathbf{0}$$

- Neutron density equation (at quasi static conditions: $d\mathbf{n}/dt \approx 0$)

$$\mathbf{m}_{(c)}(\mathbf{n},\mathbf{c}\,|\,\mathbf{p}) = -\frac{d\mathbf{c}}{\partial t} + E(\mathbf{n},\mathbf{c}\,|\,\mathbf{p})\mathbf{c} = \mathbf{0}$$

- Nuclide density equation

$$m_\rho(\mathbf{n},\mathbf{c}\,|\,p) = <\mathbf{c}^T S\mathbf{n}>_{sys} - W = 0$$

- Power (W) condition

Il vettore $\mathbf{p}$ rappresenta i parametri di sistema

Gli operatori *B* ed *E* dipendono: il primo dalla densità del combustibile (c) e dal parametro di controllo (ρ), il secondo dalla densità neutronica ($\mathbf{n}$).

RECENTI SVILUPPI DELLA METODOLOGIA HGPT

Un funzionale d'interesse può essere in generale rappresentato da un'espressione integrale

$$Q = \int_{t_o}^{t_F} dt \left(< \mathbf{h}_n^{+T} \mathbf{n} >_{sys} + < \mathbf{h}_c^{+T} \mathbf{c} >_{sys} + h_\rho^+ \rho \right)$$

dove $\mathbf{h}_n^+, \mathbf{h}_c^+, h_\rho^+$ sono quantità assegnate.

RECENTI SVILUPPI DELLA METODOLOGIA HGPT

Consideriamo un nocciolo suddiviso in macrozone di combustibile e una schematizzazione a step temporali.

Secondo la metodologia HGPT la variazione prodotta nel funzionale considerato da una perturbazione dei parametri di sistema viene data da una somma

$$\delta Q = \sum_{j=1}^{J} \delta p_j \sum_{i=1}^{I} \sum_{z=1}^{Z} V_z \left(\boldsymbol{\psi}_i^{*T} \frac{\partial \mathbf{m}_{n,z,i}}{\partial p_j} + \left(\int_{\Delta_i} \mathbf{c}_z^{*T} dt \right) \frac{\partial \mathbf{m}_{c,z,i}}{\partial p_j} + \rho_i^{*} \frac{\partial m_{\rho,z,i}}{\partial p_j} \right)$$

dove compaiono le funzioni importanza associate alle densità dei neutroni e dei nuclidi ed al parametro di controllo.

RECENTI SVILUPPI DELLA METODOLOGIA HGPT

Attività previste

Il lavoro finora svolto in questo campo è consistito nell'implementazione della metodologia perturbativa HGPT nel codice di calcolo Eranos in relazione a casi relativamente semplici.

Futuri sviluppi richiedono la stretta collaborazione con il gruppo francese di Cadarache responsabile di questo codice.

Recentemente, ad una nostra proposta su temi specifici di collaborazione, abbiamo ricevuto un riscontro molto positivo.

E' previsto un incontro per stabilire un programma di attività comune che dovrebbe vedere coinvolti laureandi e/o dottorandi nostri e loro.

GRAZIE DELLA VOSTRA ATTENZIONE

Italian National Agency for New Technologies, Energy and Sustainable Economic Development

Neutronic codes validation for LFR applications: status and perspectives

ADP MiSE-ENEA PAR2017 B.3-LP2

Gen.IV-LFR: Stato attuale della tecnologia e prospettive di sviluppo

Università di Roma «La Sapienza», 14-15 giugno 2018

M. Sarotto, G. Grasso, P. Console Camprini (ENEA)

Contents

1) Framework
2) Validation process for LFR
3) Neutronic parameters
4) Experimental campaigns:
   - LR-0 reactor (CVR, Czech Republic)
   - VENUS-F reactor (SCK•CEN, Belgium)
5) Codes validation campaign
   (Deterministic and Monte Carlo)
6) Some C/E results & analyses
7) Conclusions and perspectives

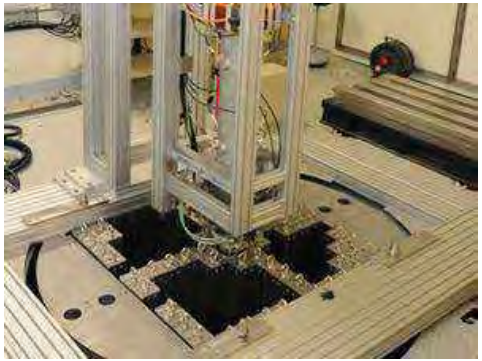

1 Framework

The design of the ALFRED* core/reactor:

- was defined in EURATOM FP7 LEADER project
- has been refined in ADP ENEA-MiSE PAR2015-17 B.3-LP2
- is currently under development by FALCON international consortium

ENEA was/is responsible for the core design activities

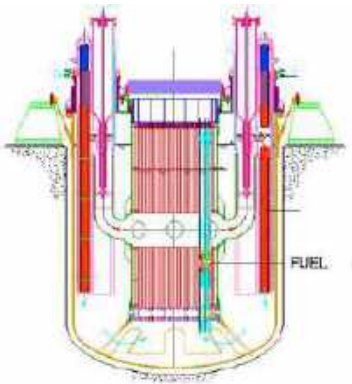

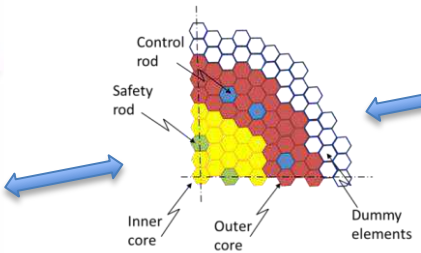

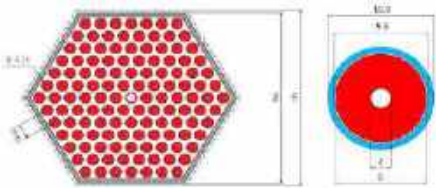

MOX fuel with
≅ 22 / 27 wt.%
Pu mass content

* Advanced Lead-cooled Fast Reactor European Demonstrator

2 Validation process for LFR

Validation of neutronic codes for LFR

LFR is new reactor concept → **Complete Validation** for **neutronic codes** and **nuclear data libraries** is needed for core design & licensing
(simulation tools & nuclear data are among the main sources of uncertainties)

Validation activities for TH analyses in Pb/PbBi systems carried out in the past, but a similar effort for neutronic analyses not yet done
→ Necessity of:

- **Representative experiments of predicted LFR conditions**
- **Experimental measurements of relevant parameters**
- **Validation of codes reliability** by calc. vs. measures comparison

3.1 Neutronic parameters

Validation of neutronic codes/libraries requires experimental measurements in LFR representative conditions of:

* **integral parameters**: critical mass (i.e., *k* multiplication factor or reactivity ρ), reactivity worth of n absorbers (Control & Safety Rods), delayed neutron fraction and mean generation time (β and Λ), reactivity feedbacks/coefficients

$$\hat{\beta}_i = \frac{\sum_m \hat{\beta}_i^{(m)} < \sum_g \nu_g^{(m)} \Sigma_{f,g}^{(m)}(\mathbf{r}) \varphi_g(\mathbf{r}) >_V}{\sum_m < \sum_g \nu_g^{(m)} \Sigma_{f,g}^{(m)}(\mathbf{r}) \varphi_g(\mathbf{r}) >_V}$$

* **local parameters**: radial and axial traverses (flux and reaction rates), spectrum indexes, void reactivity worth

$$SI^r = \frac{\Sigma_g \sigma_g^r \phi_g}{\Sigma_g \sigma_g^{F25} \phi_g}$$

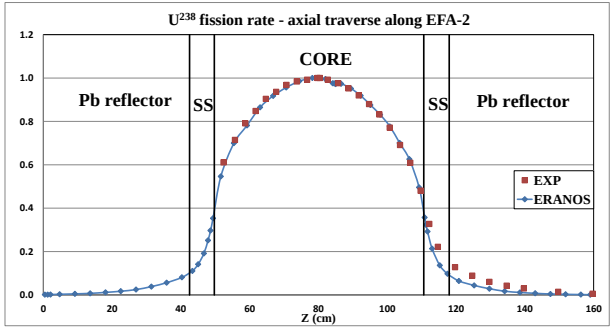

3.2 Validation of neutronic codes

Best-estimate codes (& data) with evaluation of uncertainties.

Validation is inherently associated with the use of **best-estimate codes** and **nuclear data**, by **evaluating the uncertainty** in reproducing exp. results.

Uncertainties may come from:

- materials properties & geometrical tolerances (for e.g. fuel pellets, cladding and wrapper geometries)
- nuclear data (cross sections, delayed n fraction, etc.)
- calculation methods (Monte Carlo & deterministic)

Assessment of confidence in results (i.e., uncertainty) is used to strengthen the ALFRED core design.

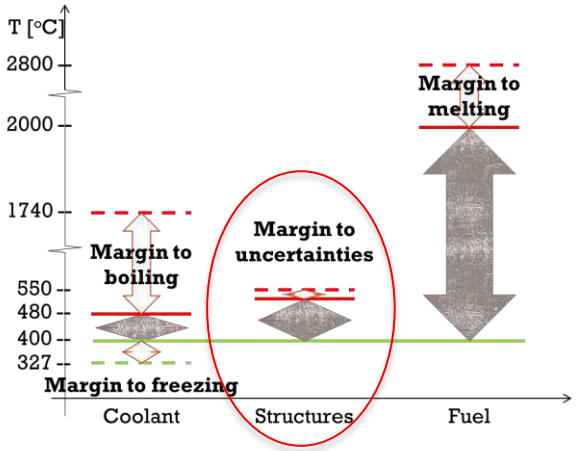

4.1 Experimental campaigns

Most aimed requirement for VALIDATION is the achievement of a "LFR representative spectrum" for the main neutronic parameters

LFR representative experimental results available from:

1) **VENUS-F zero-power reactor**, during EURATOM FP7 FREYA* project
2) **LR-0 zero-power reactor**, during PAR2015-17 (ENEA-CVR contract)

While in LR0 only local parameters were measured, in VENUS-F integral tests and local measures were performed.

Experiment	Measured n parameters	n codes
VENUS-F	Integral & Local	Monte Carlo & Deterministic
LR-0	Local	Monte Carlo

* Fast Reactor Experiments for hYbrid Applications

4.2 VENUS-F facility

Core components, radial and axial reflectors in solid lead

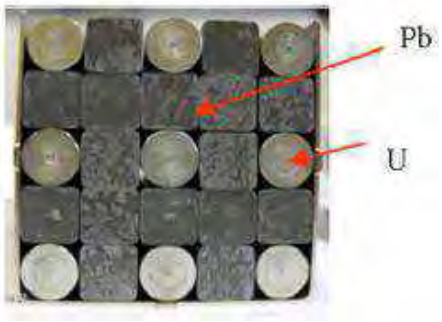

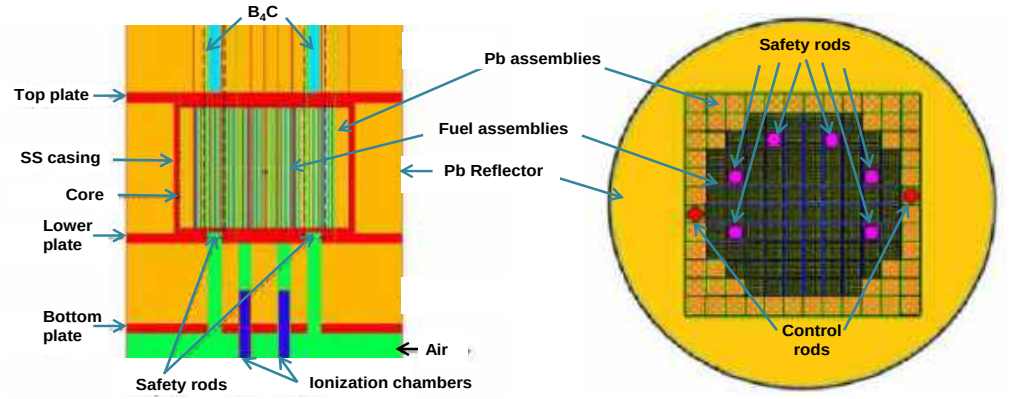

Fuel Assembly (FA) is 5x5 square matrix with:

- U metallic rods (30 U^{235} wt.%)
- Pb blocks simulating LFR coolant.

→ FA/core spectrum too hard for ALFRED (MOX)

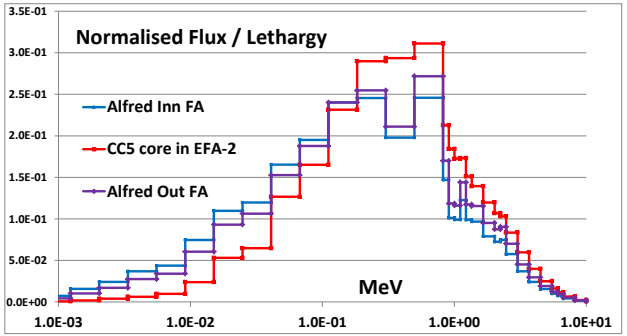

4.3 VENUS-F core representative of ALFRED

To reproduce LFR n spectrum …

… moderating elements introduced:

- 4 Al Oxide (Al_2O_3) rods in FA (green)
- 25 Al_2O_3 rods in inert assemblies (AIA*)

Accurate reproduction of the ALFRED spectrum (> 1 keV) in an EFA** (EFA-2)

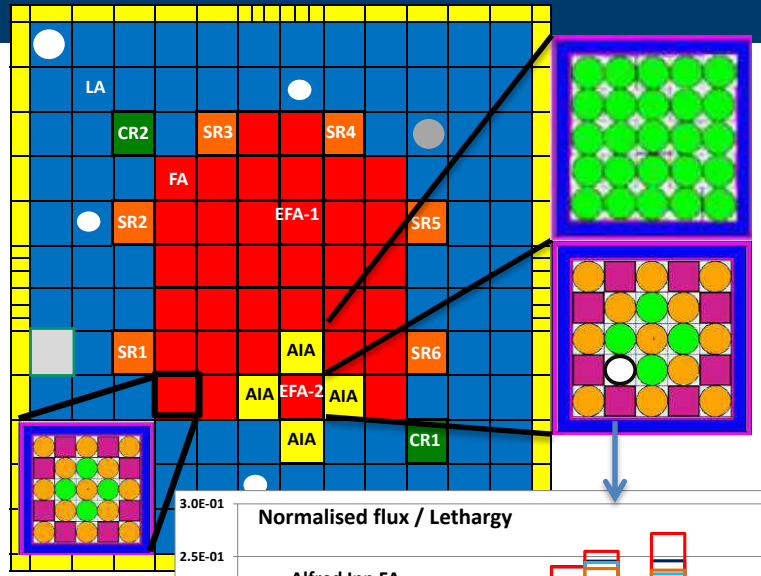

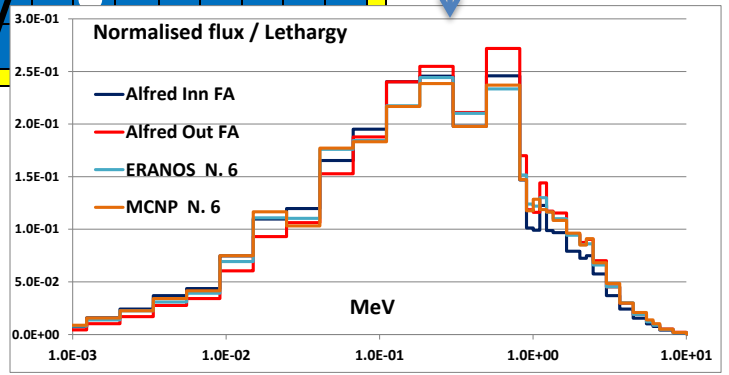

Measured parameters:

- **integral**: k, Control Rods worth
- **local**: fission rates traverses & spectrum indexes in EFA-2, void reactivity effects in & around EFA-2.

* Alfred Inert Assembly ** Experimental FA

4.4 LR-0 facility

A dry channel in the centre of six VVER FAs

LR-0 is a zero-power pool-type LWR used to measure the n-physical characteristics of VVER* reactors.
Driver core is an hexagonal ring made of six FA with UO_2 fuel (U^{235}: 3.28 - 3.3 w.t.%).
Criticality tuned by adjustments of water level

Central dry position free to insert a test section

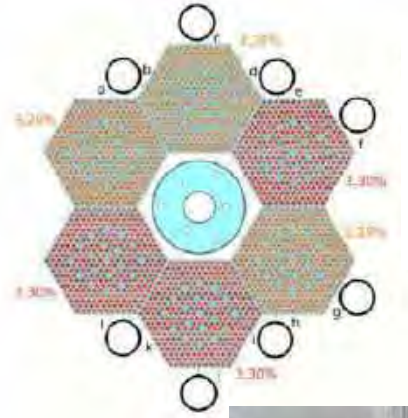

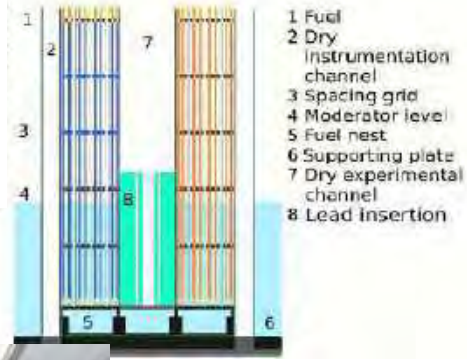

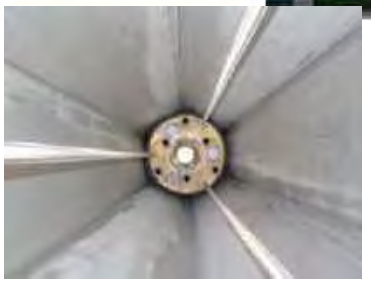

* Water-Water Energetic Reactor

4.5 LR-0 core «representative» of ALFRED

To reproduce n propagation in lead…

… in the dry channel a SS cylindrical shell filled by Pb was introduced, with six fuel pins (U^{235} 3.6 w.t.%) at ≠ distances from the centre.

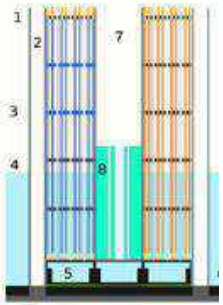

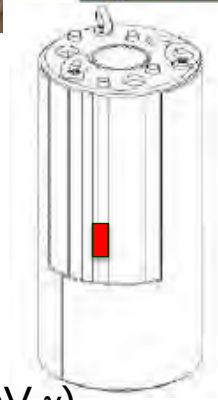

Measured parameters:

- **local**: flux and power distributions through **measured** γ (after 2.5 h irradiation) emitted by:
  - **Np^{239}**, via U^{238} capture → **flux** ($t_{1/2}$ = 2.35 d → 277 keV γ)
  - **Sr^{92}**, via U^{235} and U^{238} fission → **power** ($t_{1/2}$ = 2.7 h → 1384 keV γ)

5.1 Neutronic codes

Neutronic codes used at ENEA FSN SICNUC division

Deterministic codes

ERANOS (CEA), PHISICS (INL), Scale suite (ORNL)

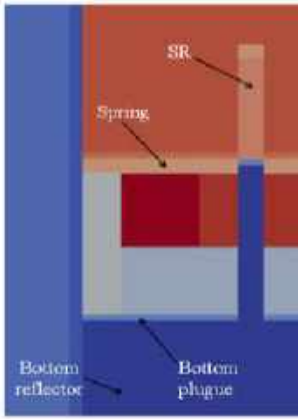

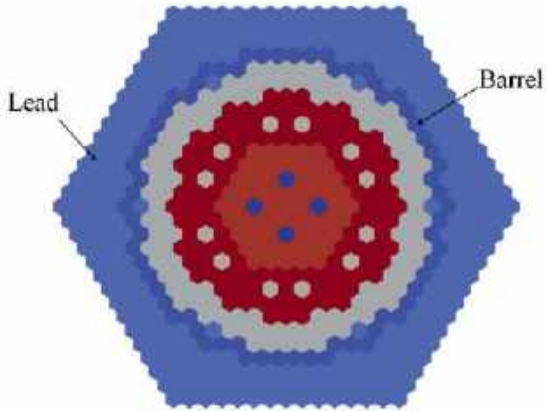

Monte Carlo codes

MCNP (LANL), Serpent (VTT), GEANT (CERN)

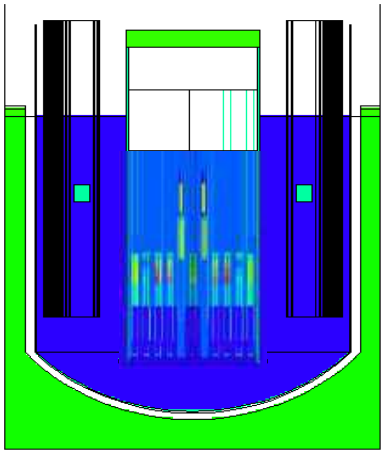

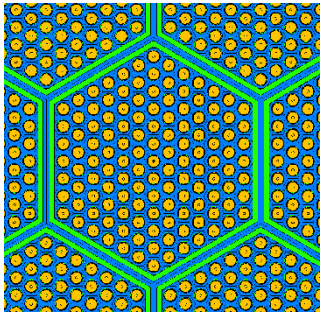

5.2 Neutronic codes validated

ERANOS, MCNP and SERPENT

In **LR-0**:
- **MCNP6.1** code (ENEA and CVR)

Mont Carlo N-Particle
Continuous treatment of energy dependence
Exact heterogeneous geometry description
ENDF/B-VII.1 nuclear data library

In **VENUS-F**:
- **ERANOS 2.2n** (ENEA)

European Reactor ANalysis Optimised System
Heterogeneous-homogenised cross-sections (ECCO)
Full core calculations with 3D XYZ core geometry model
JEFF3.1 and **ENDF/B-VI.8** nuclear data libraries

- **MCNP** and **SERPENT** (other FREYA partners) → Different MCNP versions and nuclear data libraries
- experimental and calculation results confidential (FREYA partners)

5.3 Codes Validation campaign in VENUS-F

ERANOS, MCNP & SERPENT with ≠ data

All (integral and local) parameters measured compared with calculations obtained by ≠ codes and ≠ data libraries: major part of results* compatible within 1-3σ uncertainty level

* here shown as C/E (Calculated-to-Experimental ratio)

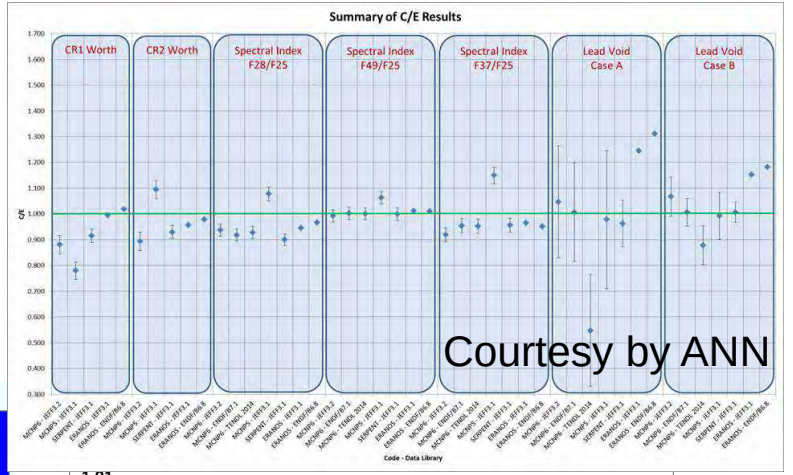

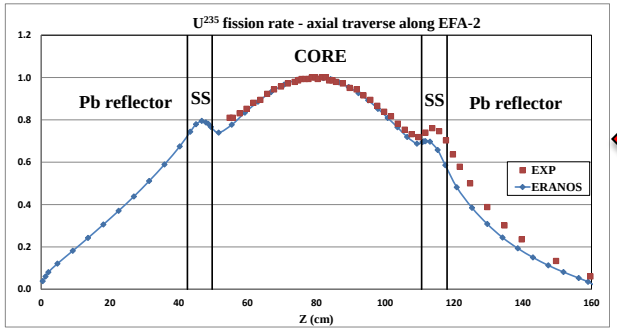

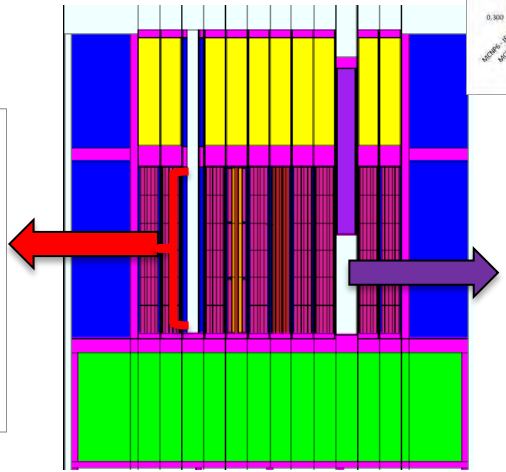

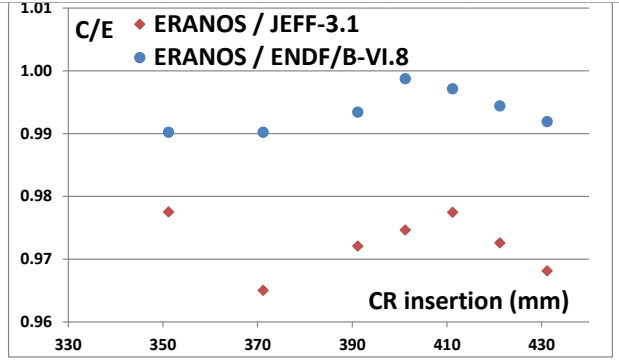

5.4 Code validation campaign in LR-0

MCNP with ENDF/BVII.1 data

Local flux & power distributions measured & simulated in:
- 6 fuel pins in Pb shell
- 19 fuel pins in one FA

→ 3D flux/power map in core

→ Validation of prediction of n propagation through Pb

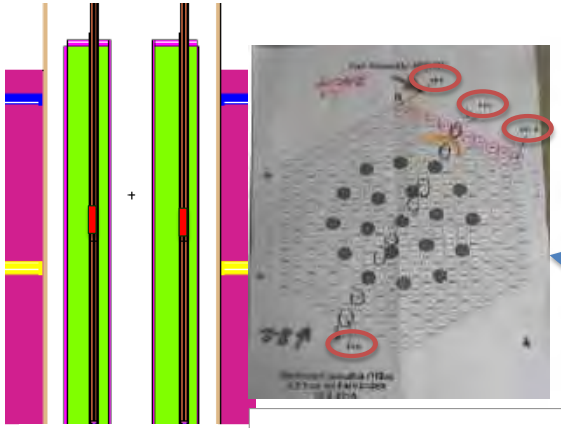

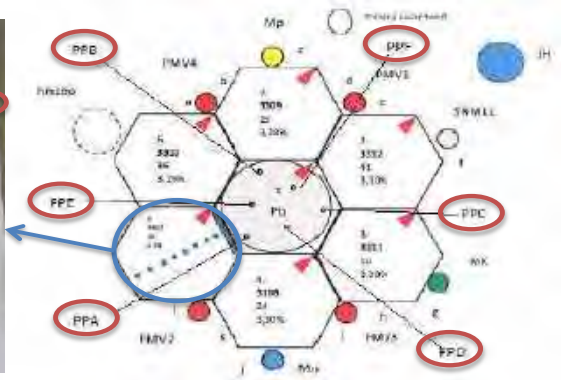

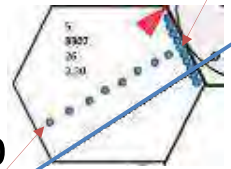

Core center

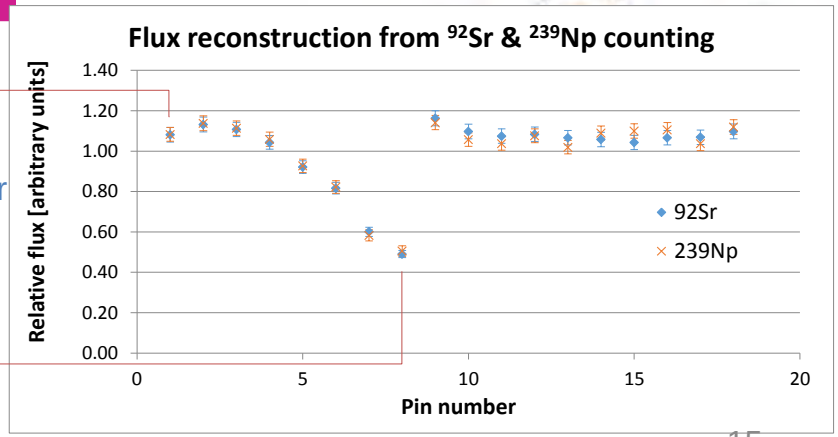

6.1 Example of results: k, β & Λ in VENUS-F

During FREYA, 5 critical core layouts were assembled & characterized (CR0, CC5-CC8), where: - CR0 is the start up core

- CC6* is «ALFRED representative» core

Kinetic parameters (β, Λ) were measured in CR0

Calculations of k, β and Λ were analysed:

- by comparison with experimental measurements
- by code-to-code (& library-to-library) comparison

CR0	β_{eff} (pcm)	Λ (ns)
Experiment	730 ± 11	410 ± 40
ERANOS	722.5	498

	ρ (pcm, JEFF3.1)		Δρ (pcm)
Core	ERANOS	Serpent	
CR0	419	496 ± 2	-77
CC5	214	763 ± 3	-549
CC6	405	812 ± 2	-407
CC7	205		
CC8	428	186 ± 1	242

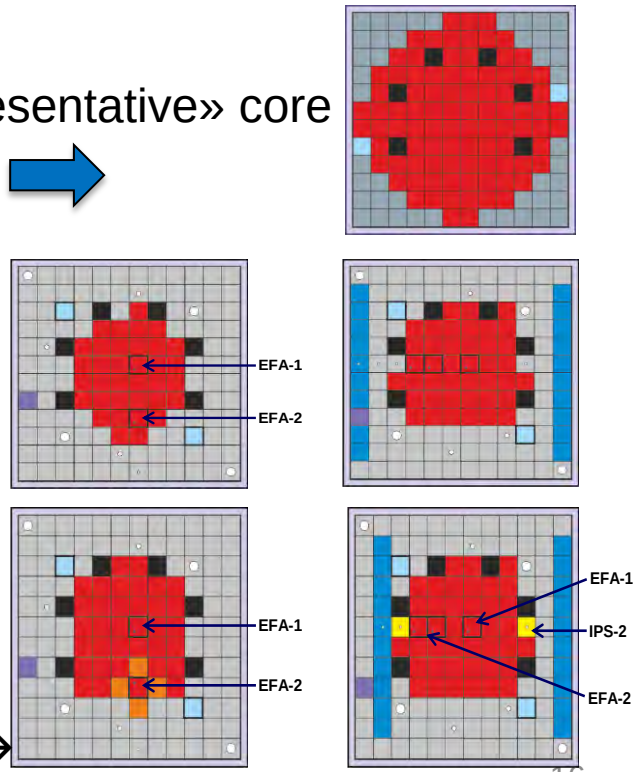

* Critical Core n. 6 →

6.2 Uncertainty on k_{eff} value (VENUS-F)

Neutronic codes yield a systematic over-estimation of core reactivity in all 5 core layouts (<1 %). Possible reasons:

- bias in geometry core modelling (negligible)
- materials specifications (*e.g.*, Pb purity)
- **nuclear data uncertainties**.

Further in-depth analyses indicate:

- **2% uncertainty due to cross-sections data** (sum over energy groups, cross-sections & isotopes)
- max 0.6% difference with ≠ code or ≠ data
- main cause of k_{eff} over-estimation could be due to actual U^{235} wt.% (no variance available)

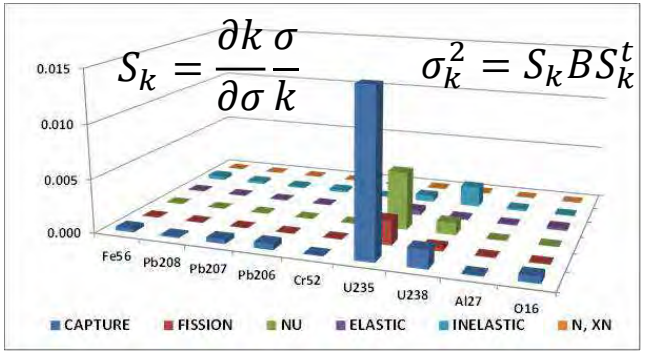

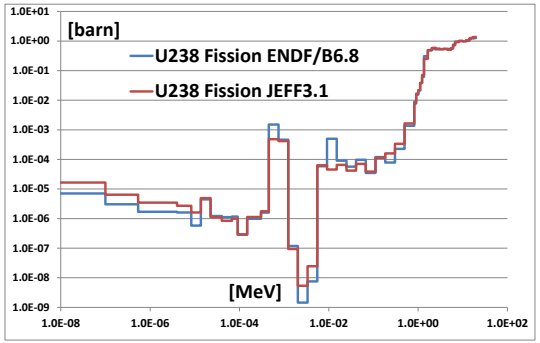

6.3 Data base of measures/simulations (VENUS-F)

All calculated parameters were compared (C-E) with 1-3σ measurement uncertainty, e.g., data set for CRs worth & void effects

CR worth	Code	Library	C-E
CR1	MCNP6.1	JEFF3.2	> 3σ
	MCNP5	JEFF3.1	> 3σ
	SERPENT	JEFF3.1	> 3σ
	ERANOS	JEFF3.1	< σ
		ENDF/B6.8	< σ
CR2	MCNP6.1	JEFF3.2	< 3σ
	MCNP5	JEFF3.1	< 3σ
	SERPENT	JEFF3.1	< 3σ
	ERANOS	JEFF3.1	< 3σ
		ENDF/B6.8	< σ

[illegible]	Code	Library	C-E
Case A	MCNP6.1	JEFF3.2	< σ
		ENDF/B7.1	< σ
		TENDL 2014	< 3σ
	MCNP5	MCNP5	< σ
	SERPENT	SERPENT	< σ
	ERANOS	JEFF3.1	> 3σ
		ENDF/B6.8	> 3σ
Case B	MCNP6.1	JEFF3.2	< σ
		ENDF/B7.1	< σ
		TENDL 2014	< 3σ
	MCNP5	MCNP5	< σ
	SERPENT	SERPENT	< σ
	ERANOS	JEFF3.1	> 3σ
		ENDF/B6.8	> 3σ

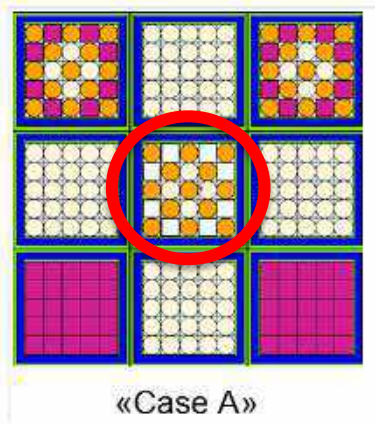
«Case A»

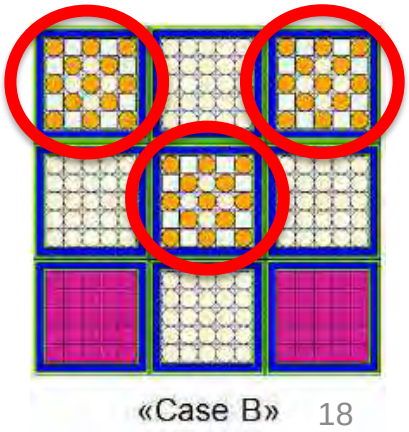
«Case B»

Measurement uncertainty coupled with uncertainty analyses
→ Assessment of the confidence level of calculation results.

6.4 Some significant results in LR-0

Initial verification of reactor model in MCNP:
- $\mathbf{k_{eff}}$ reproduced with 0.4% accuracy
- **Reactor power level**, obtained with good accuracy independently by 2 calculation routes (2.2 & 2.3 mW);

Validation of n propagation capability by **local** flux and power distributions:
- γ **counts** from Np^{239} and Sr^{92} with 10-15% accuracy

A systematic over-estimation found for Np^{239} counts.
Seems to confirm the over-estimation of the U^{238} capture cross-section (observed also in LWR case)

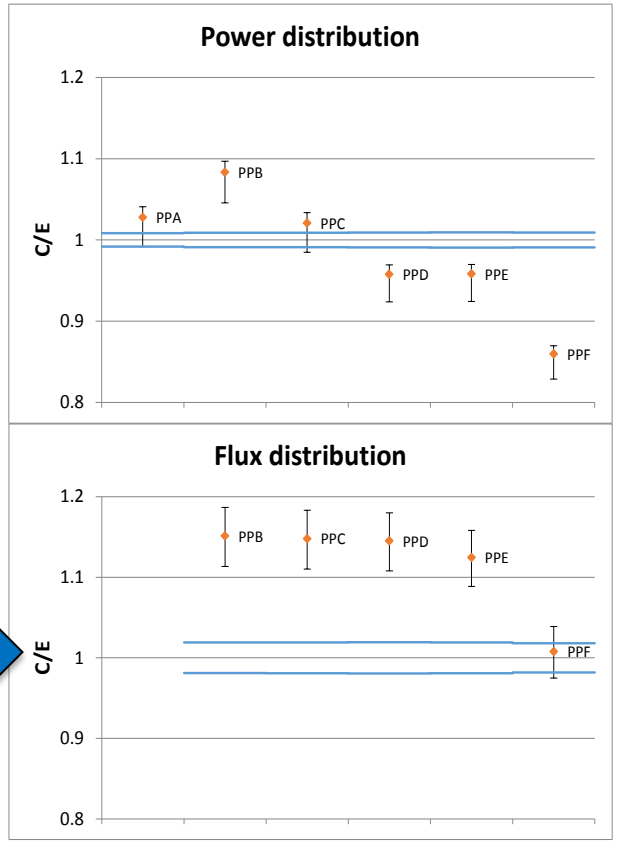

7.1 To summarise

Validation activities performed to assess confidence of n codes, based on the access to experimental results in key facilities

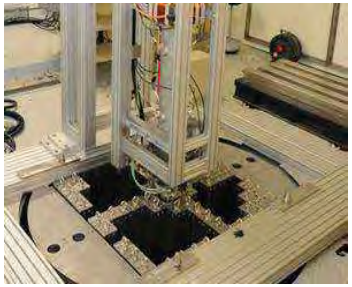

VENUS-F (Mol, BE) for:

- critical mass
- flux & spectrum traverses
- absorber & lead void worth

LR-0 (Řež, CZ) for:

- neutron propagation in Pb, in terms of attenuation and spectral shift (through local flux & power distributions)

Data-base of measurements & calculation results available for both experiments.

In VENUS-F, calc. results available for ≠ codes/data libraries, with further uncertainty analyses.

→ Significant feedbacks to neutronic analyst for the correct LFR core modelling

7.2 Conclusions and perspectives

Concluding remarks

1) VENUS-F experiments contribute to **Validation of ERANOS, MCNP and SERPENT codes for LFR**

2) LR-0 experiments (properly arranged despite the poor integral LFR representativeness) further contribute to **Validation of MCNP code reliability**

Future perspectives

Validation activity will proceed by:

- **further in depth-analyses** with different codes/libraries, sensitivity & uncertainty analyses

- **systematic arrangement of all available data**
  → Validation dossier to be used for ALFRED pre-licensing phase

massimo.sarotto@enea.it
ENEA FSN SICNUC PSSN

Italian National Agency for New Technologies,
Energy and Sustainable Economic Development

ALFRED Core Design

Status and future work

«GEN-IV LEAD COOLED FAST REACTOR
STATO ATTUALE DELLA TECNOLOGIA E PROSPETTIVE DI SVILUPPO»
Workshop tematico AdP MISE – ENEA PAR2017 – PROGETTO B.3 - LP2
Università di Roma «La Sapienza», 14-15 Giugno 2018

G. Grasso, F. Lodi, M. Sarotto, D. Castelluccio,
A. Poggianti, A. Palumbo, S. Barberio, G. Nallo

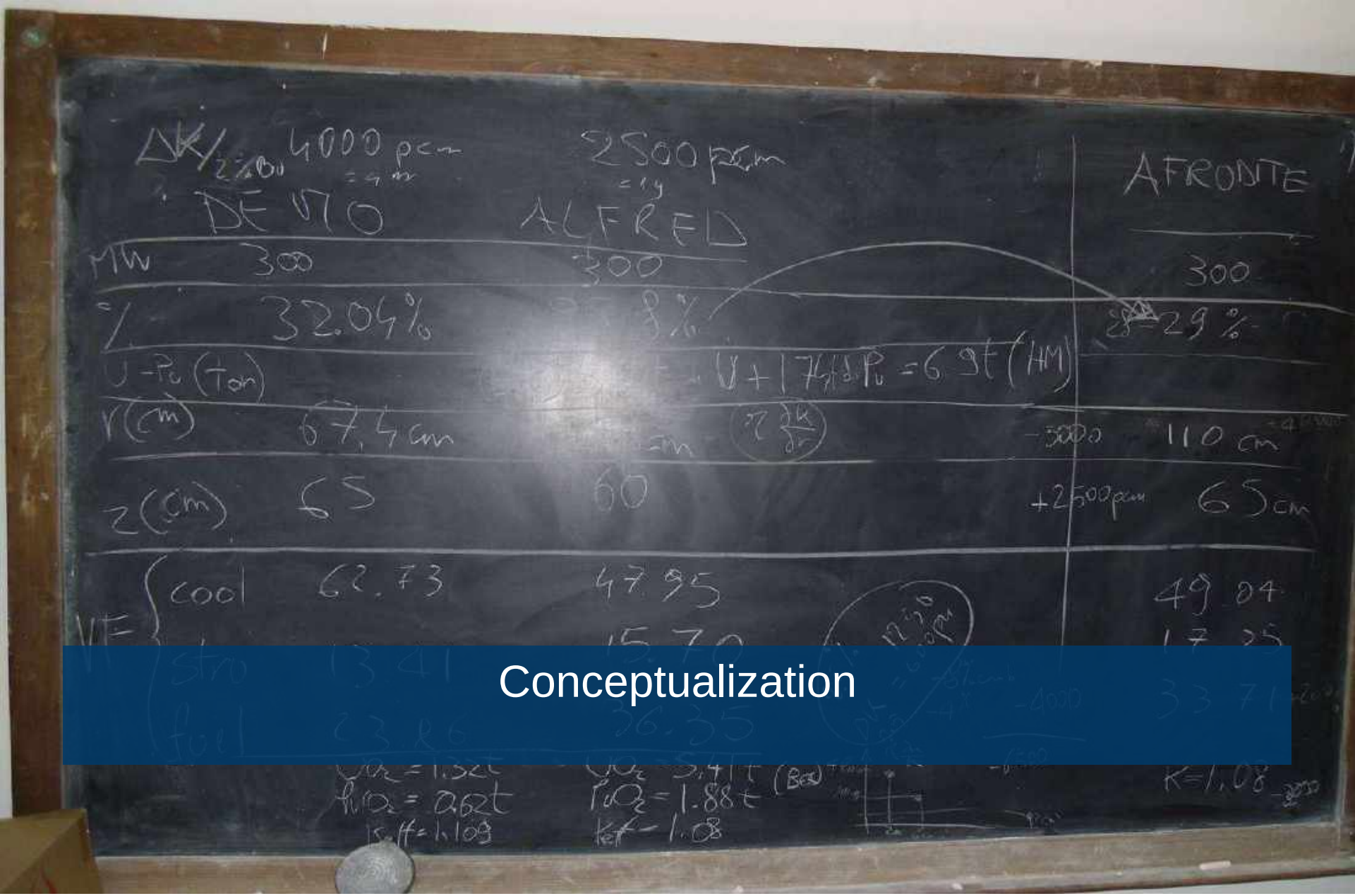

Conceptualization

Core systems

Technical review

The previous core (i.e., v.1.00 as of LEADER) was already a good one (though a bit too large…).

BUT, the restraint and the refueling systems were completely missing. Even worse: the underlying strategies were missing at all!

Core systems

Interfaces

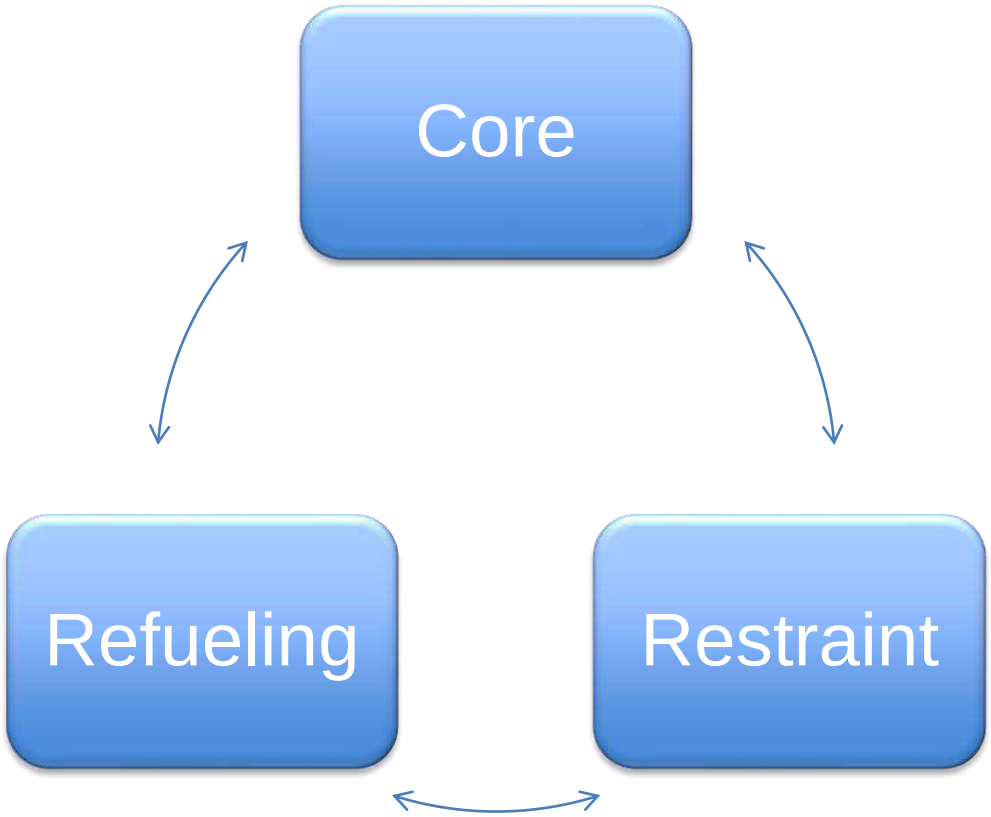

Core

Criteria*:

- Remove heat with as uniform ΔT as possible (including from non-fuel zones)
- Withstand accidents through inherent response (negative feedbacks)

* Main ones

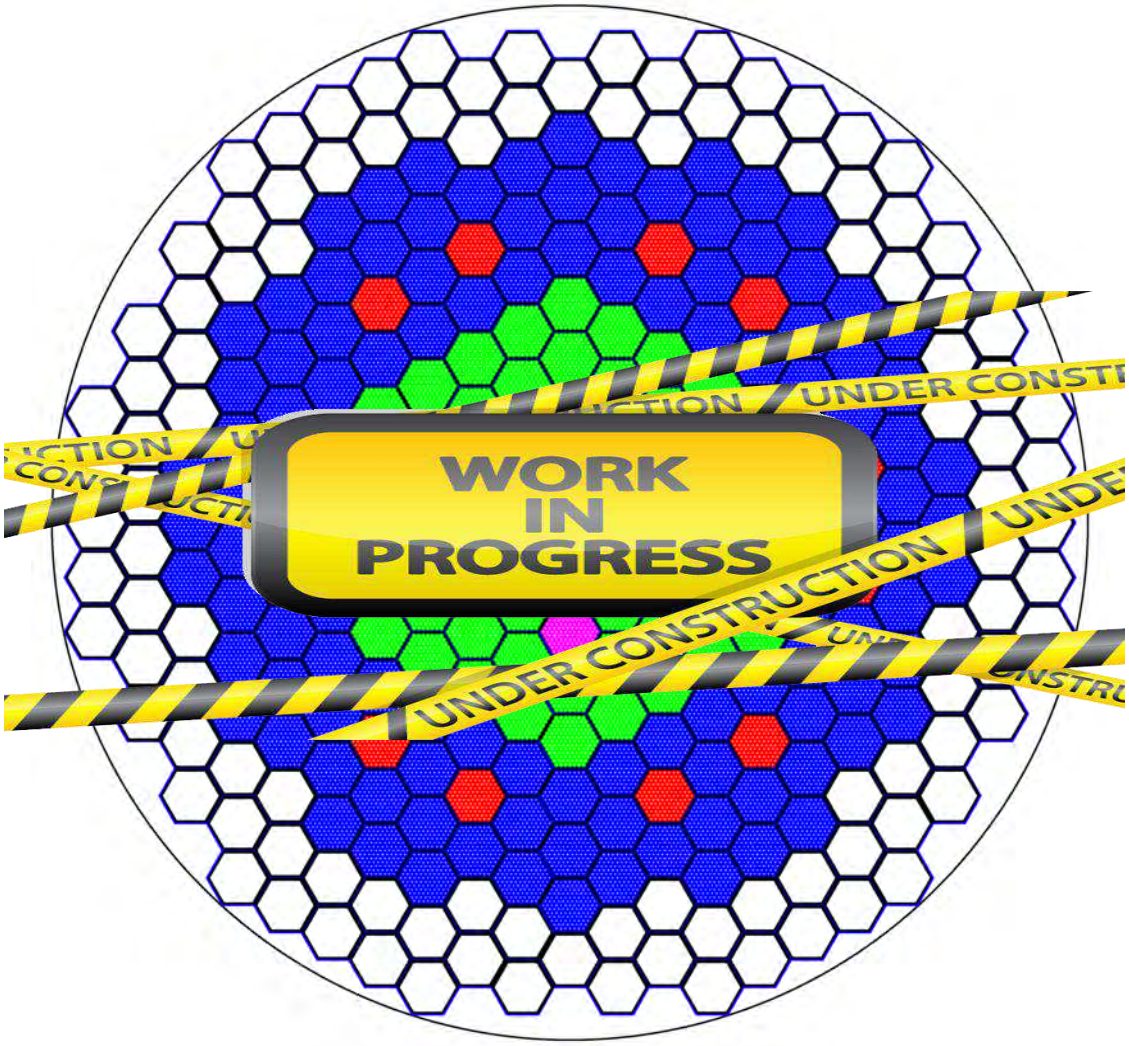

Core Systems

Restraint

Criteria*:

- Prevent S/As vibration during operation
- Counteract S/As bowing
- Allow core flowering during accidents
- Permit minimal S/As extraction forces during refueling

* Main ones

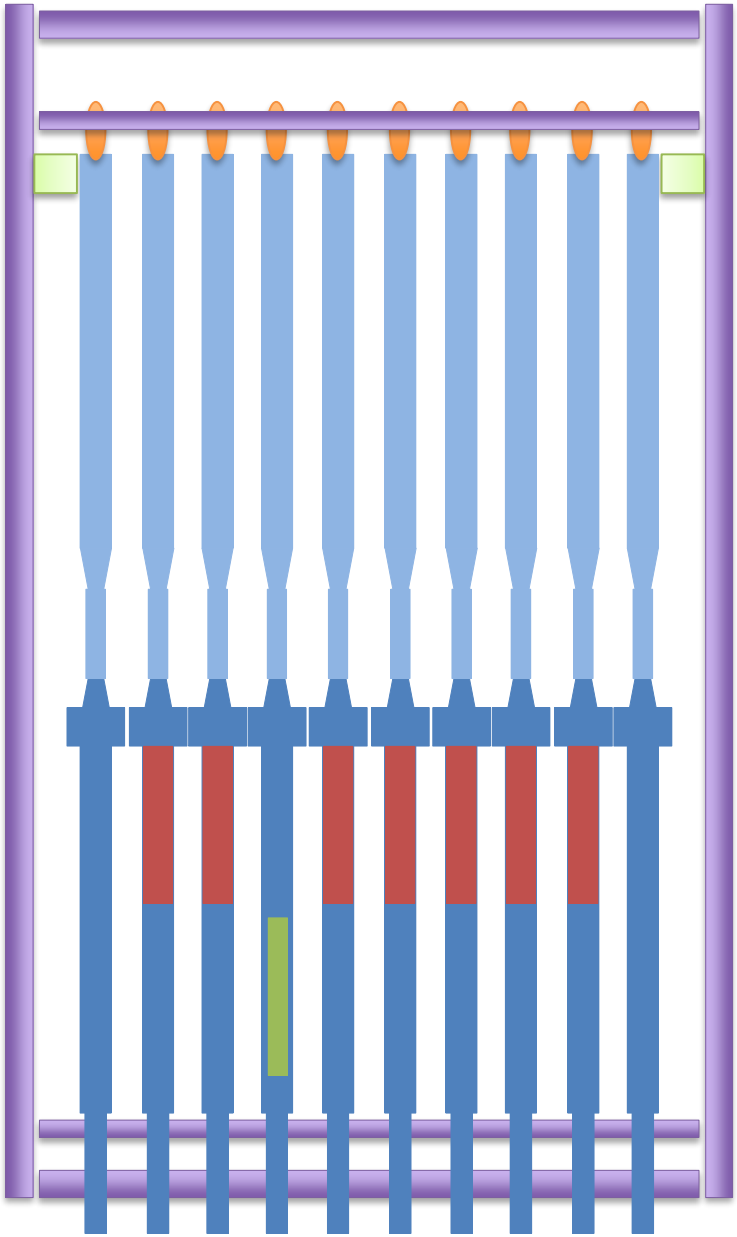

Core Systems

Refueling

Criteria*:

- Permit passive cooling during all transfer phases
- Permit continuous monitoring of the status of the sub-assemblies
- Permit retrieval of sub-assemblies for post-irradiation examinations

* Main ones

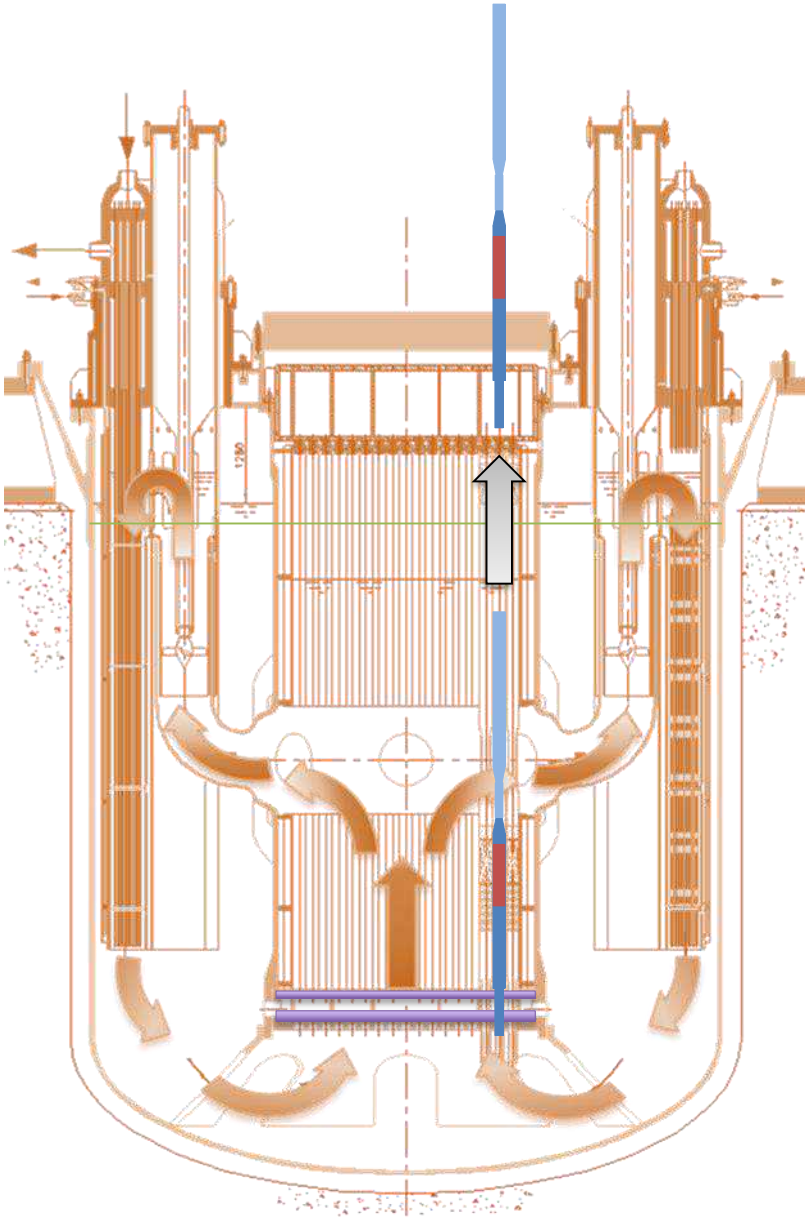

Core

Core system

Needs

“What the hell: squeeze that core!!!”

(Michele, Alex, Mariano, Trump, etc.)

Core system

Rationales

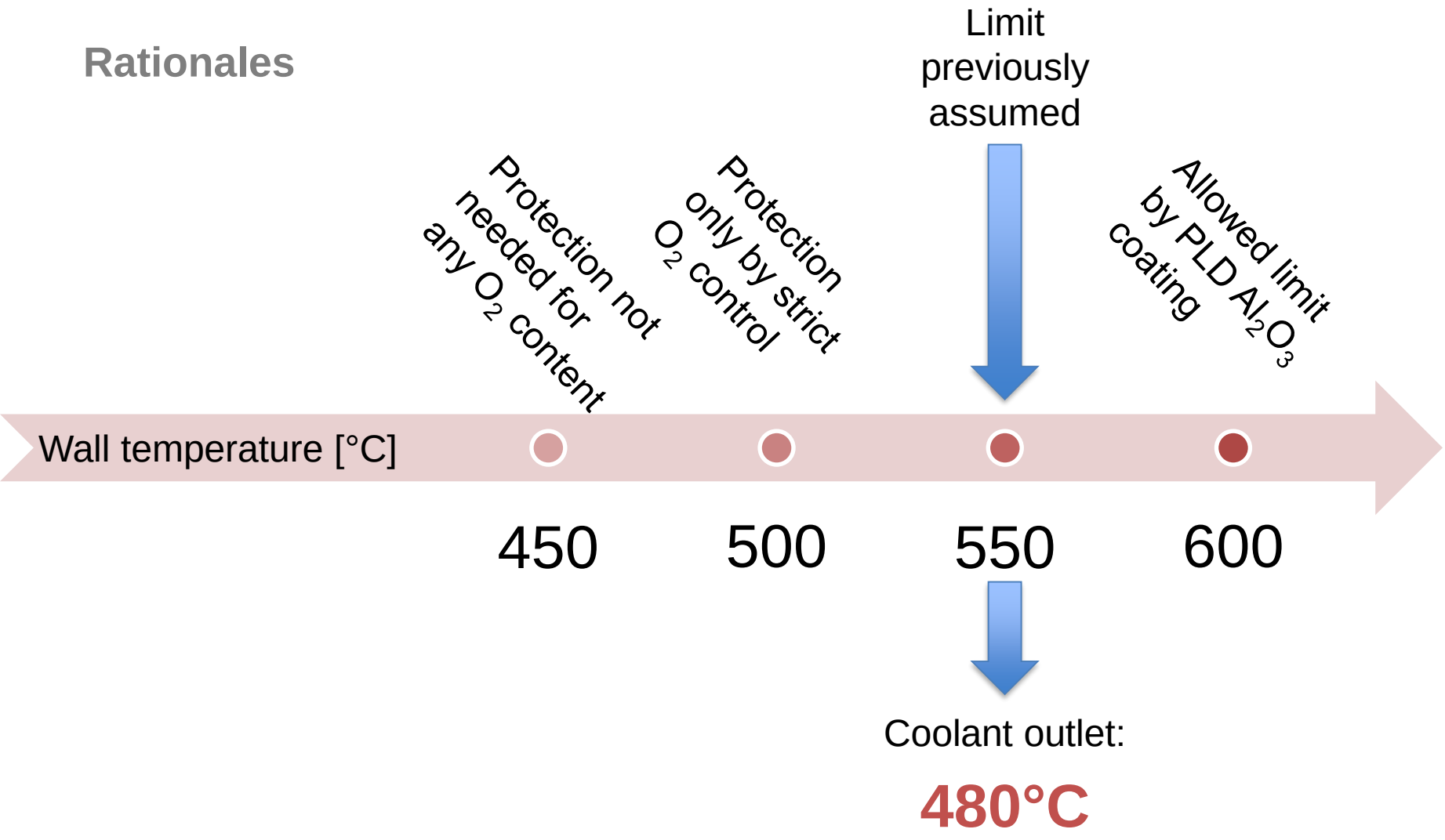

Core system

Strategy

The operation of ALFRED will be based on a stepwise approach:

- **phase 1**: operation at low power in low-temperature range
  - presently existing proven materials working without corrosion protection
- **phase 2**: operation at full power in high-temperature range
  - coated materials fully qualified during phase 1

Core system

Rationales

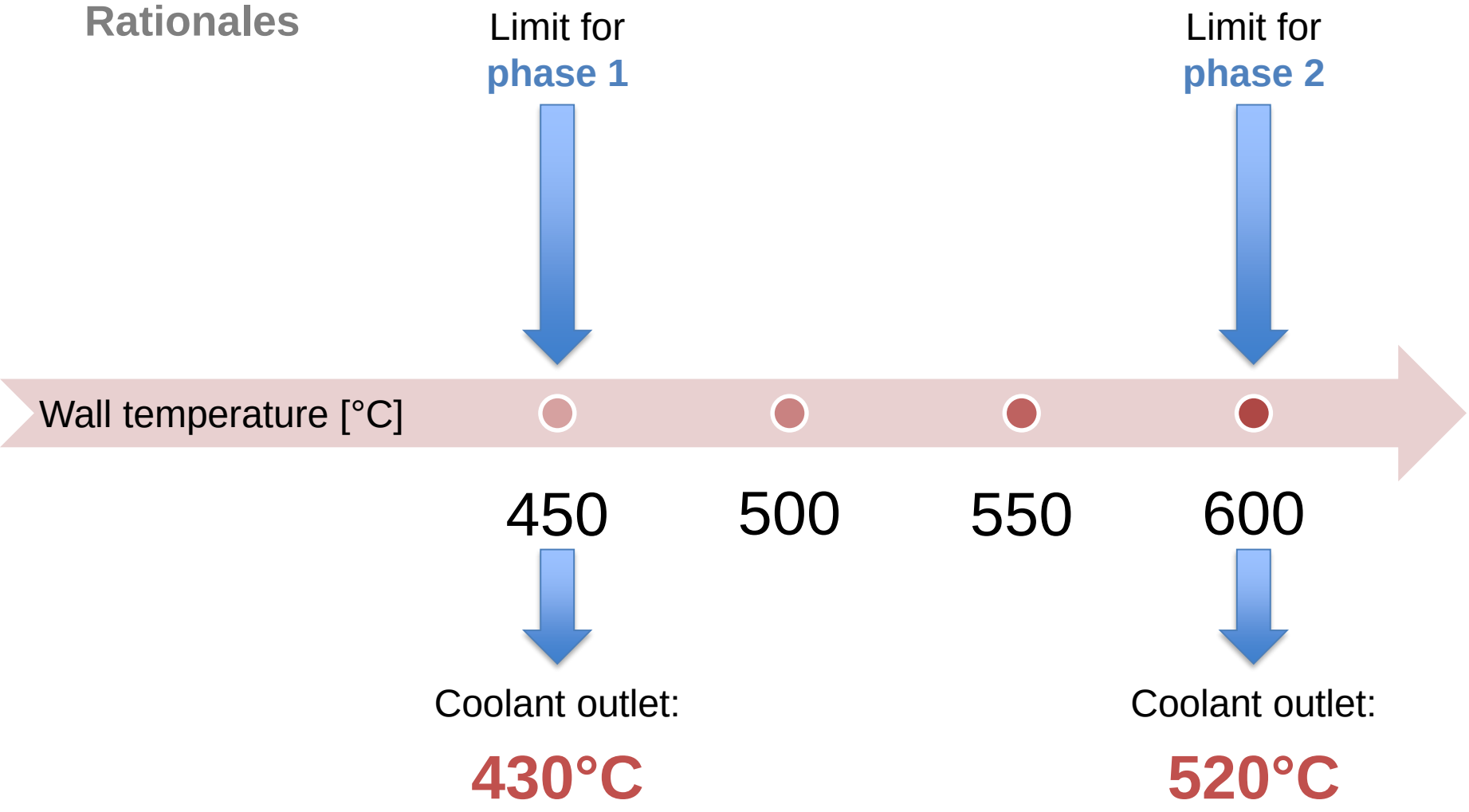

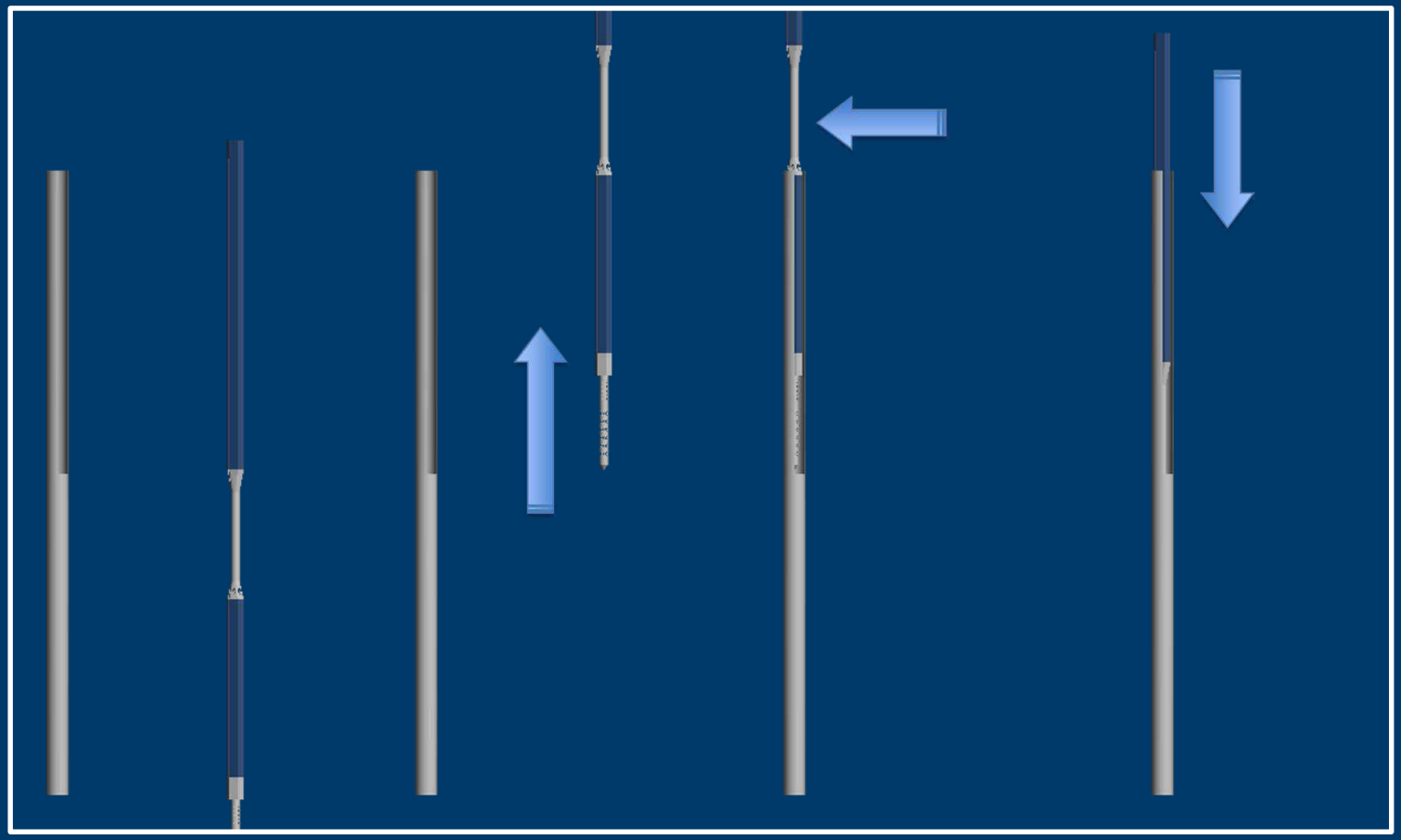

Refueling

Refueling system

Concept

«If the fuel assembly doesn't go to the pool, the pool goes to the fuel assembly»

A transfer flask is used to bring the spent fuel assemblies to the cooling pond.

The transfer flask, filled by lead, maintains the fuel assembly submerged – hence effectively and passively cooled – during the whole transfer.

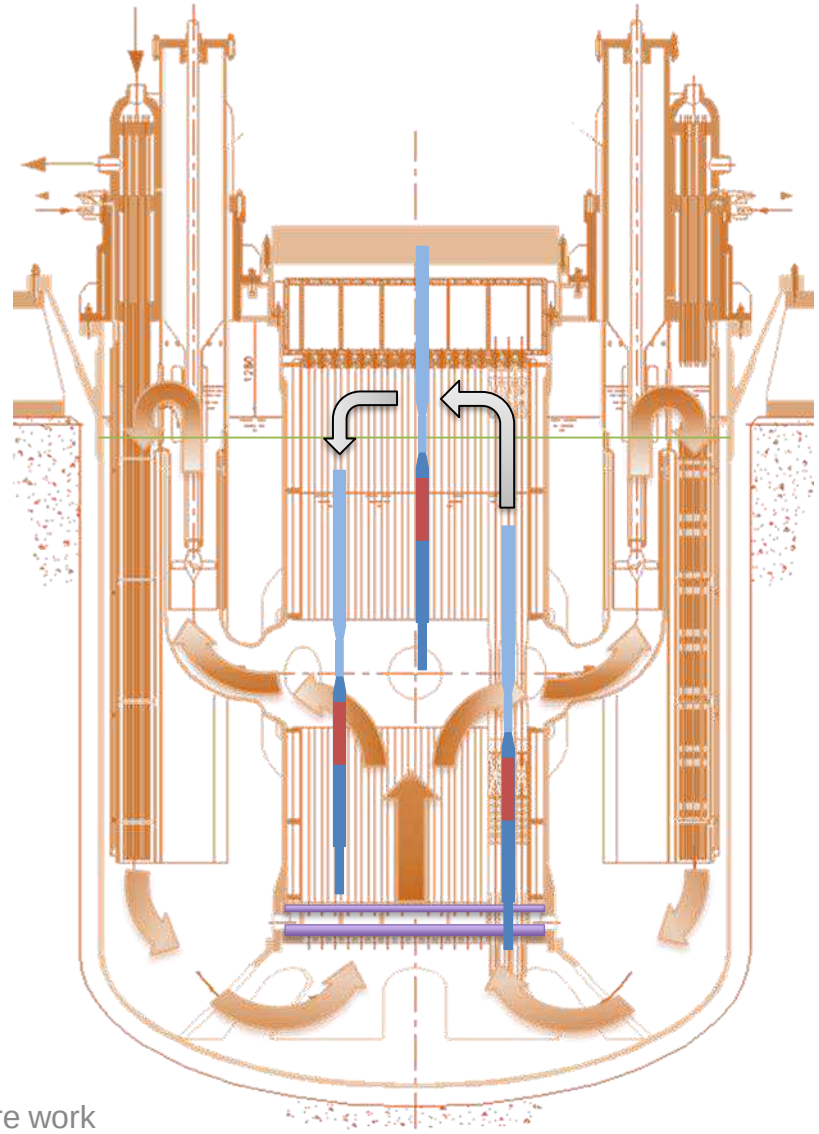

Refueling system

Solution

The flask provides passive cooling

- inside, thanks to lead
- outside, through natural circulation of gas

Within the flask, also several auxiliaries can be placed:

- heater
- instrumentation
- fill & drain

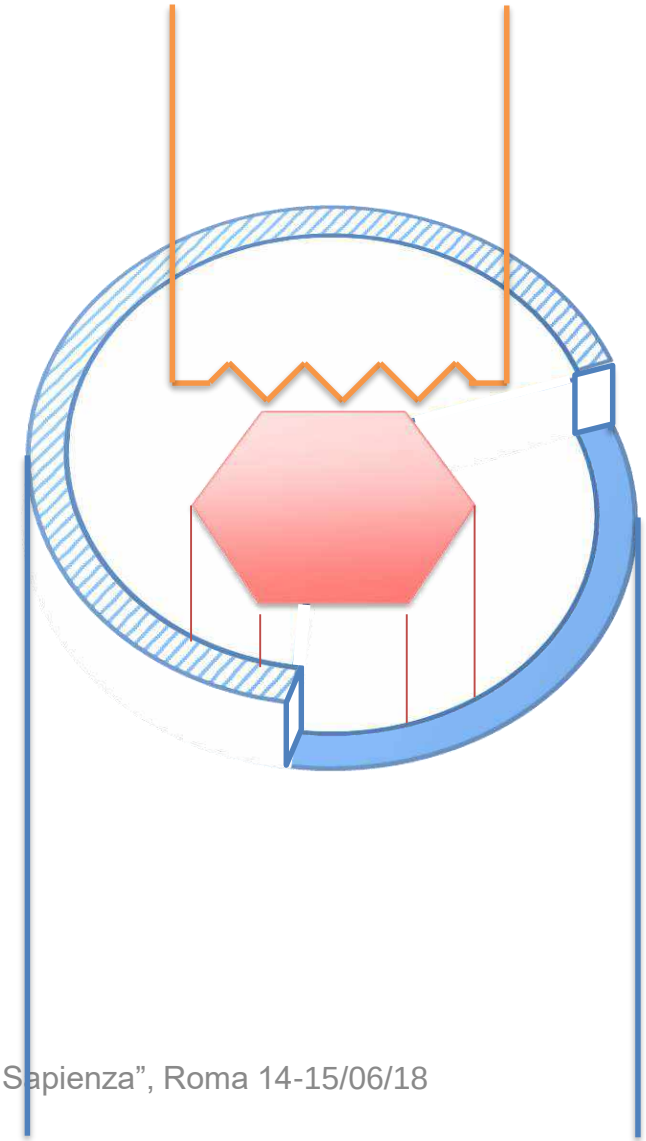

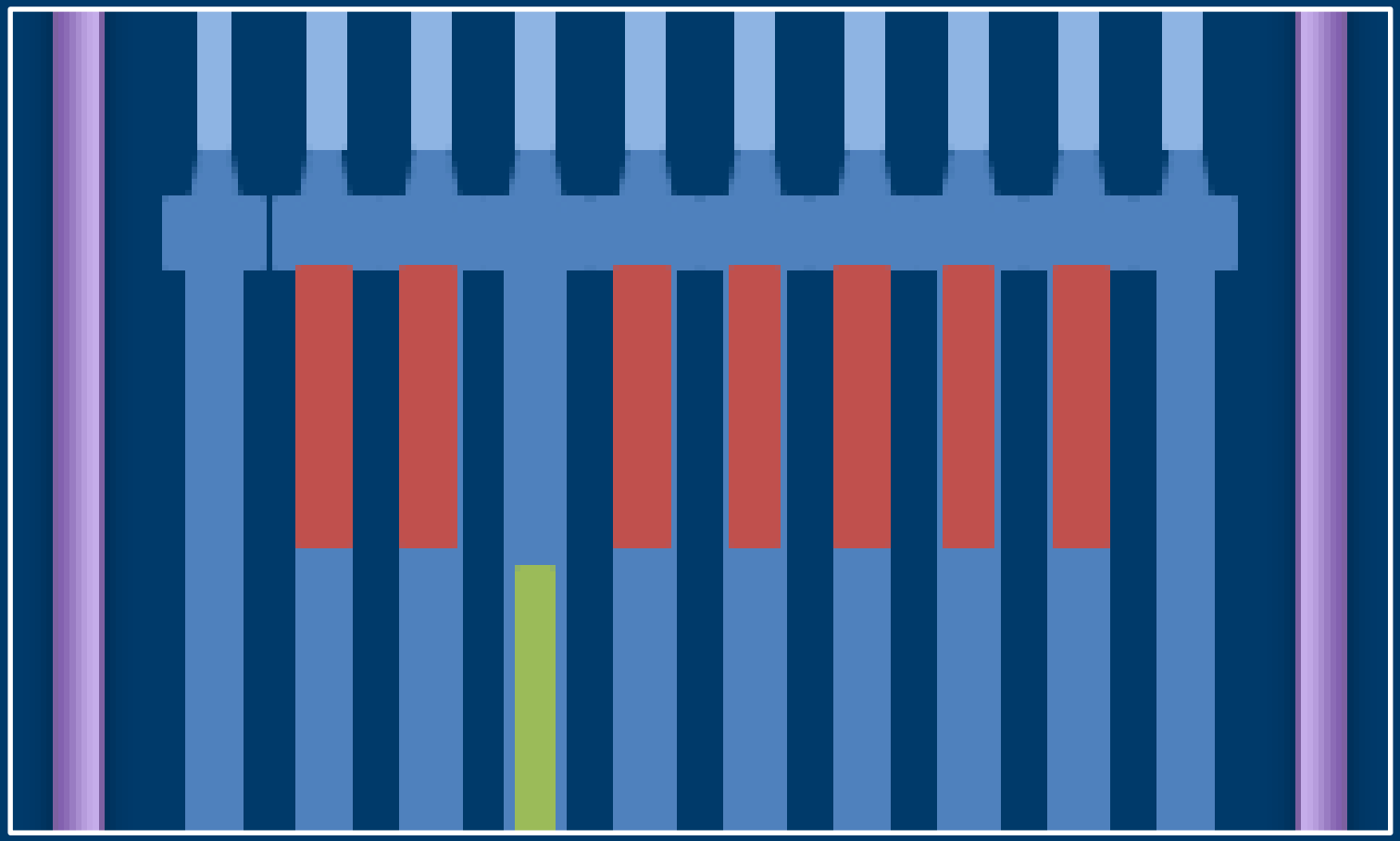

Restraint

Restraint system

Concept

A trade-off between opposing needs: stiffness and freedom

1. All the sub-assemblies (fuel, control/ shutdown, dummy) are positioned on a lower core plate
2. An upper core plate, provided of a stiff radial restraint, is brought to engage the heads of the S/As to tighten the lattice
3. A network of pads in contact provides the aimed feedback response mechanism

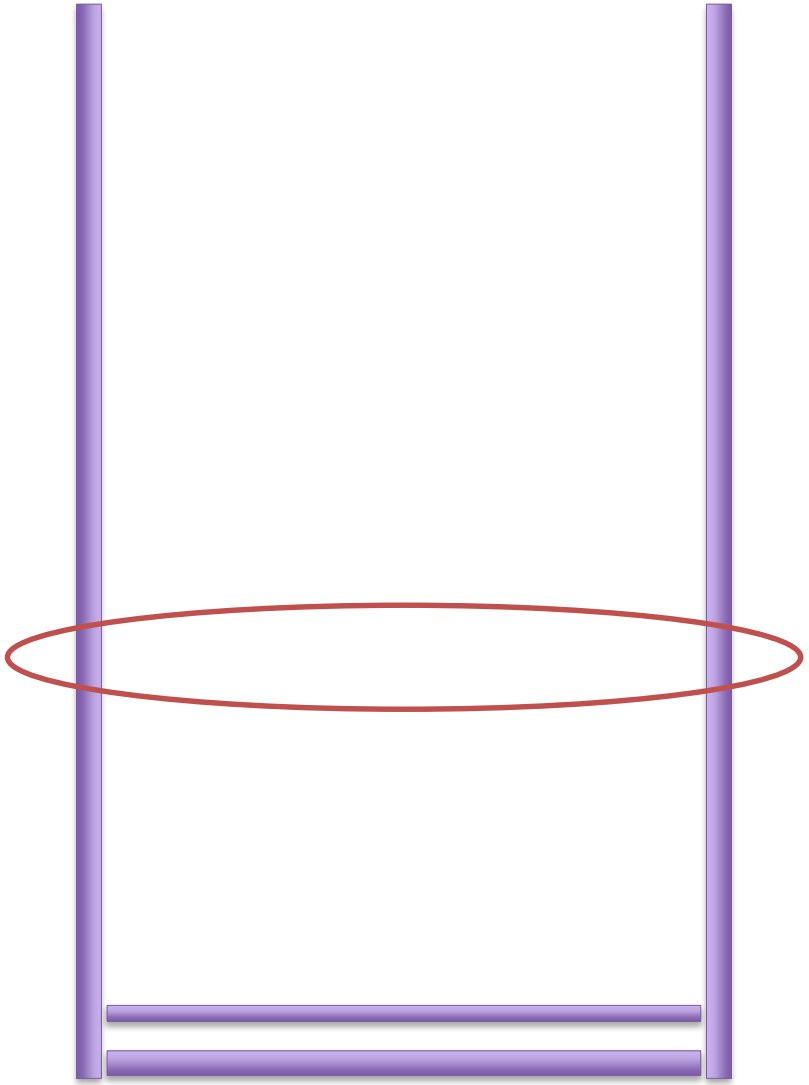

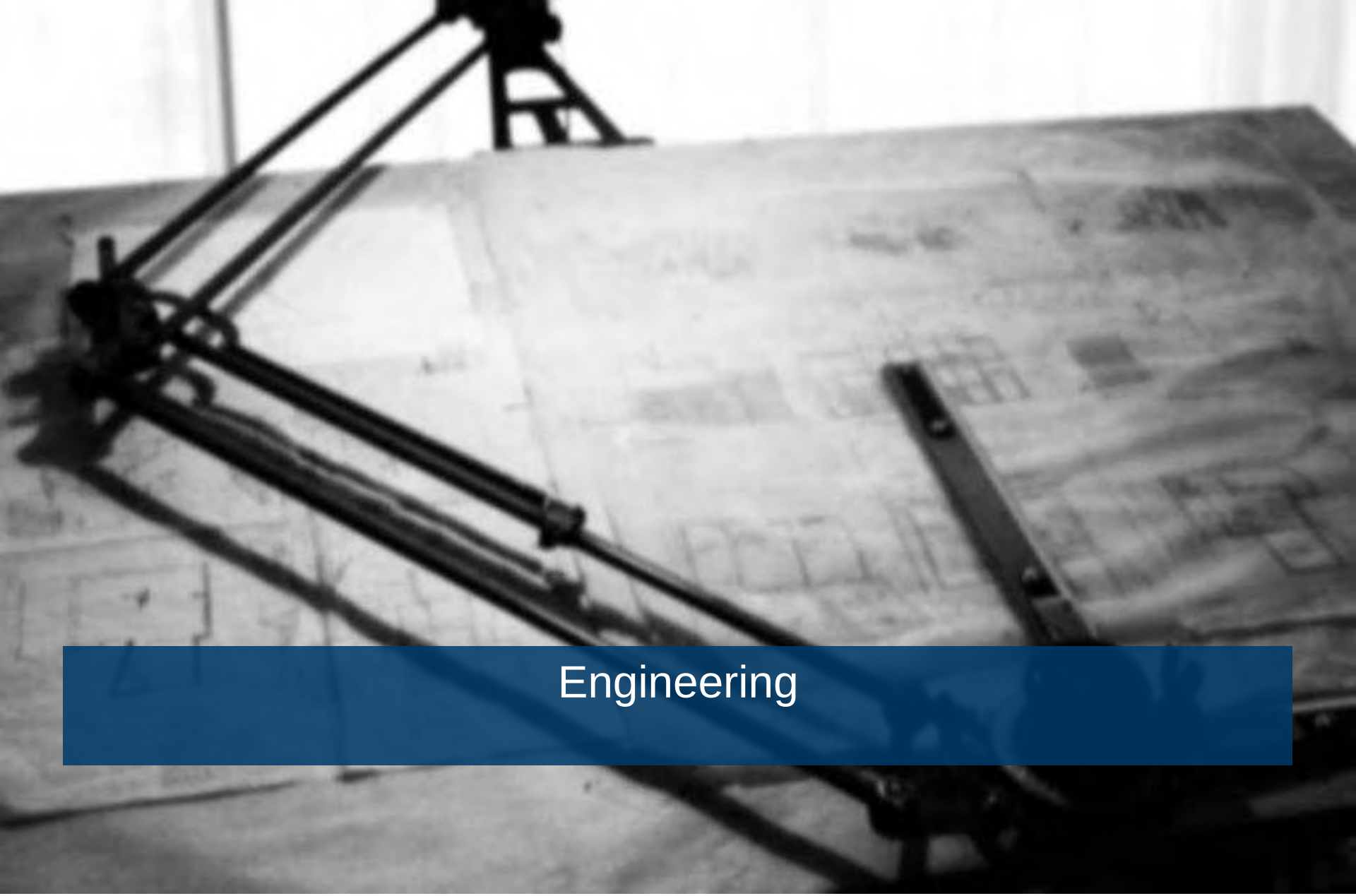

Engineering

Example

Interfaces

Gap in the connection S/As Spike-Diagrid:

- Clearance to «tilt» the S/As so as to recover some space, facilitating extraction during refueling despite their bowing

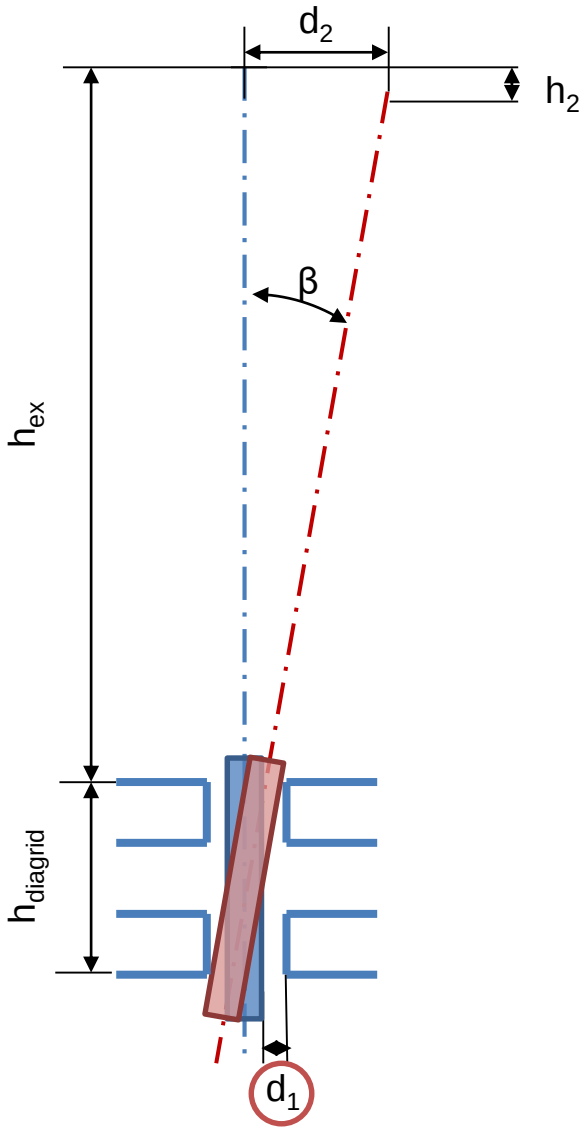

Example

Interfaces

Gap in the connection S/As Spike-Diagrid:

- Clearance to «tilt» the S/As so as to recover some space, facilitating extraction during refueling despite their bowing
- Clearance exploitable to tune the primary flowrate so as to easily align to the power distribution

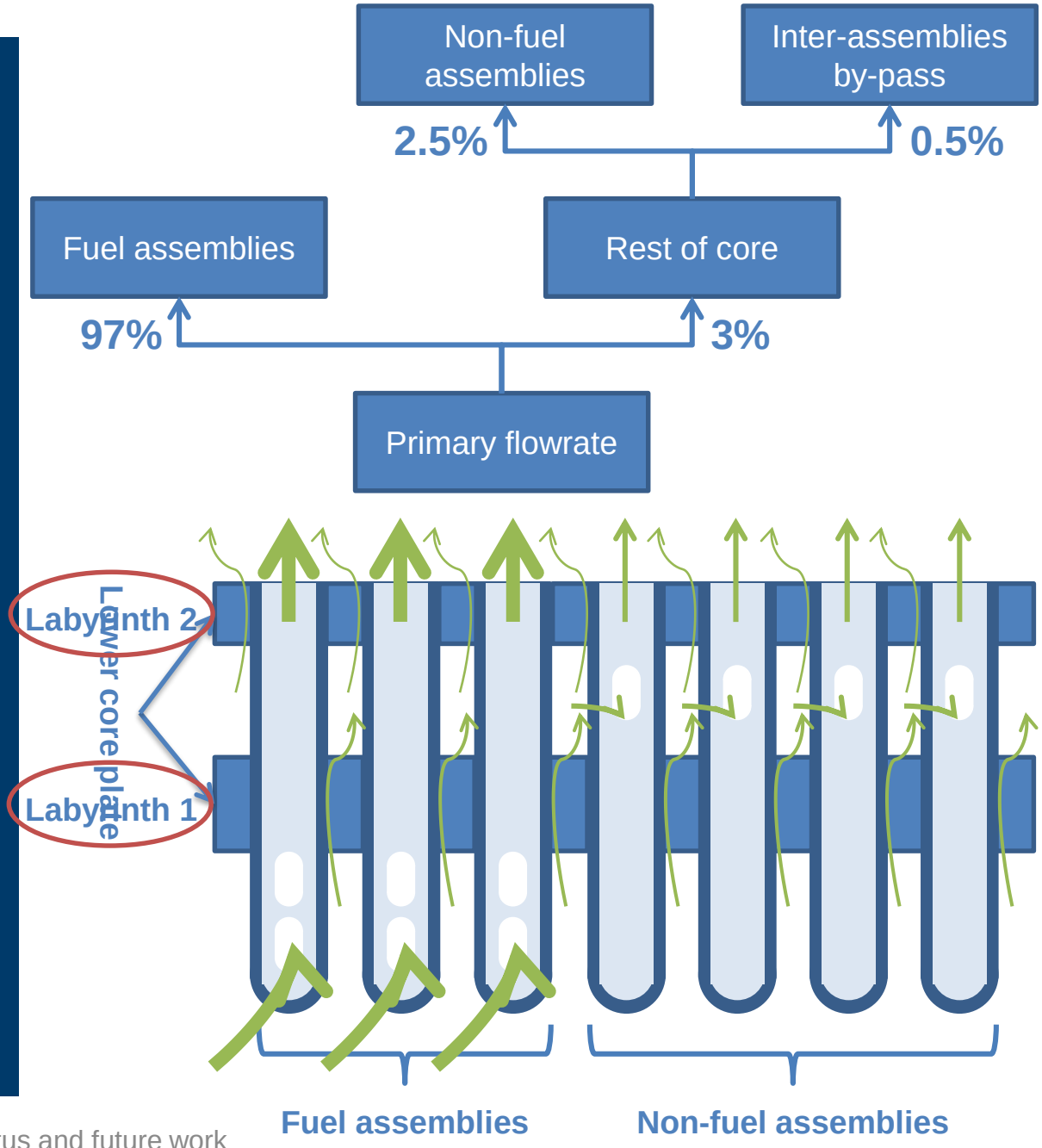

Example

Engineering

Careful redesign of all components of sub-assemblies:

- Standardizing manufacturing through shared parts
- Avoiding welds wherever possible
- Simplifying assembling
- Enhancing “tolerances-tolerance” as far as practicable.

Example

Optimization

Reduction of primary system volume:

- Optimization of the length of the cooled part of the fuel assemblies (the rest being stem), now 700 mm shorter overall.
- This also impacts (twice) on the refueling system and vessel length, through the lead level.

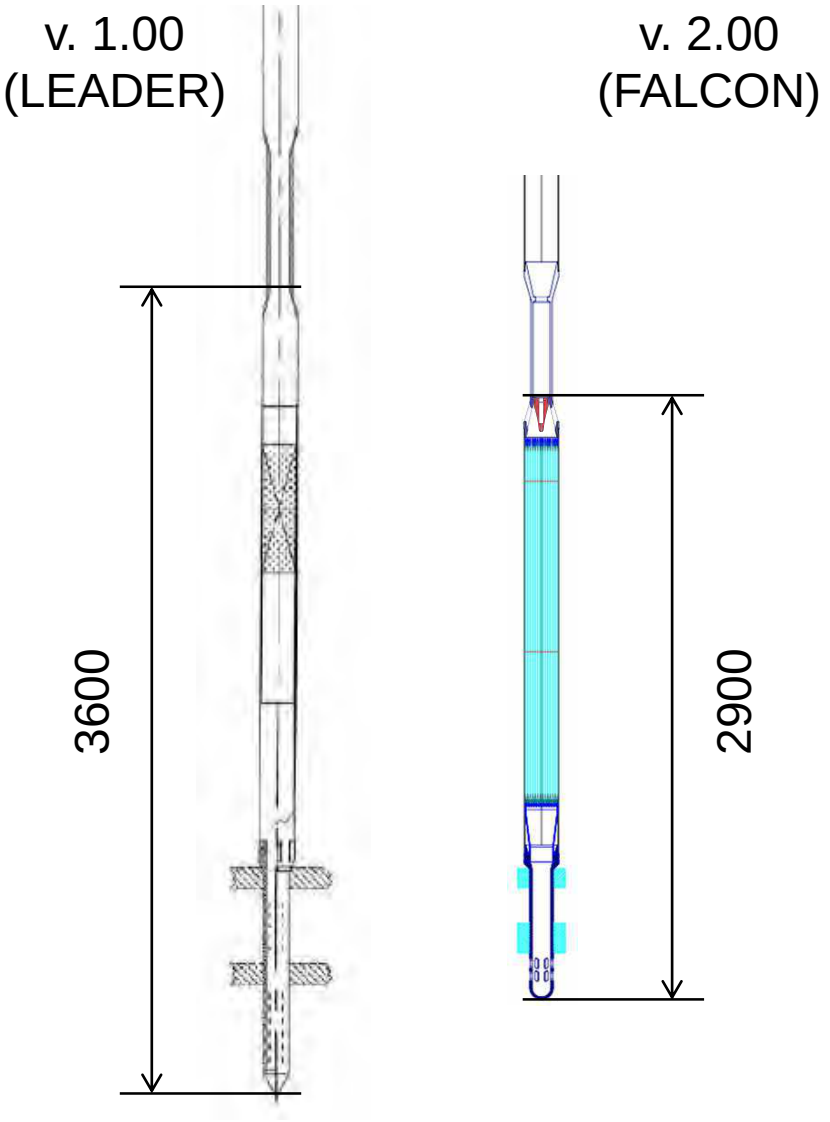

Example

Innovation

Design of an innovative shutdown system:

- Capable of operating passively, but both upon command (active) and inherently (passive)
- Resilient to extreme events, hence available in very ultimate conditions
- Diversified from other (more typical) systems

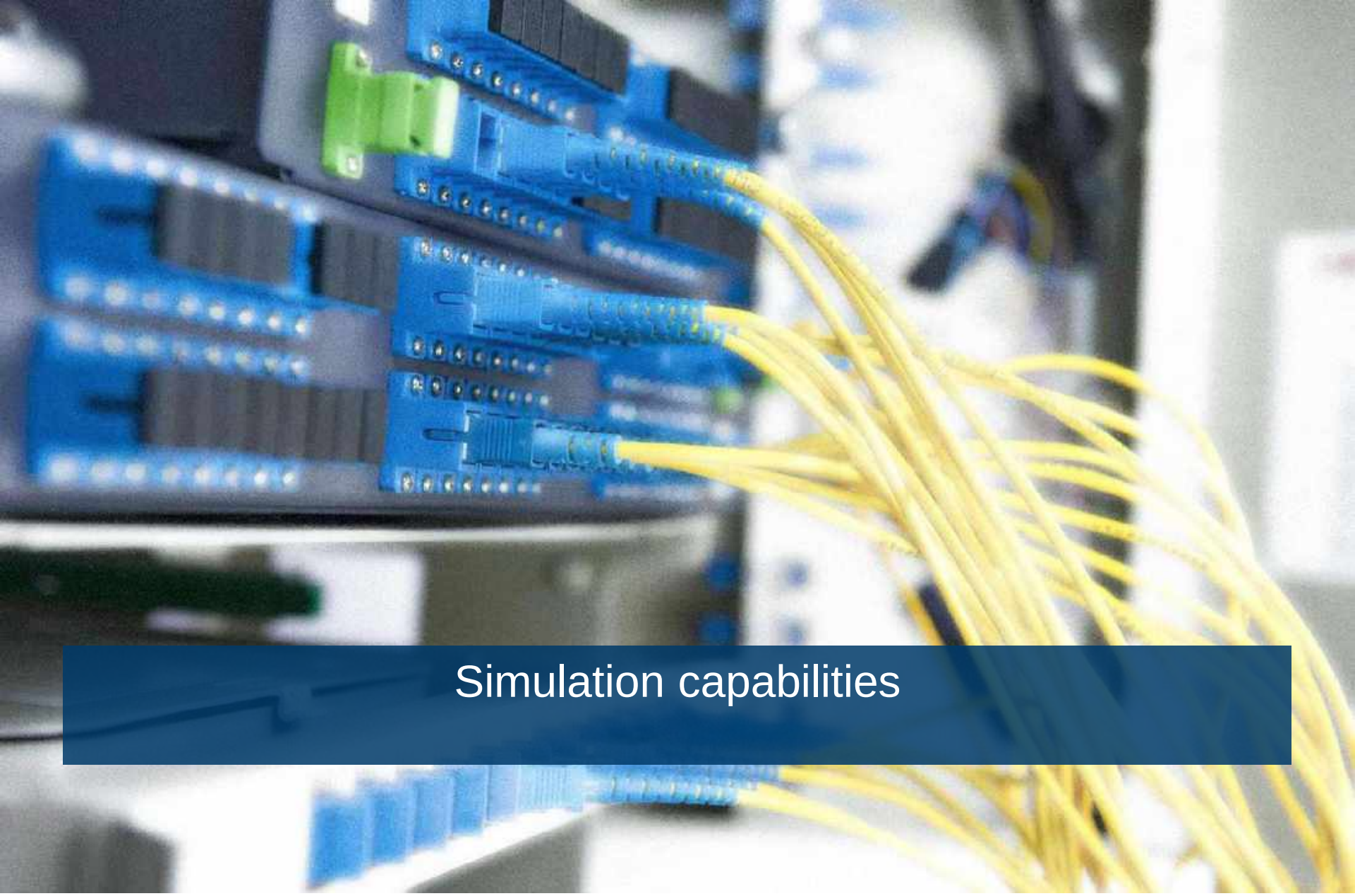

Simulation capabilities

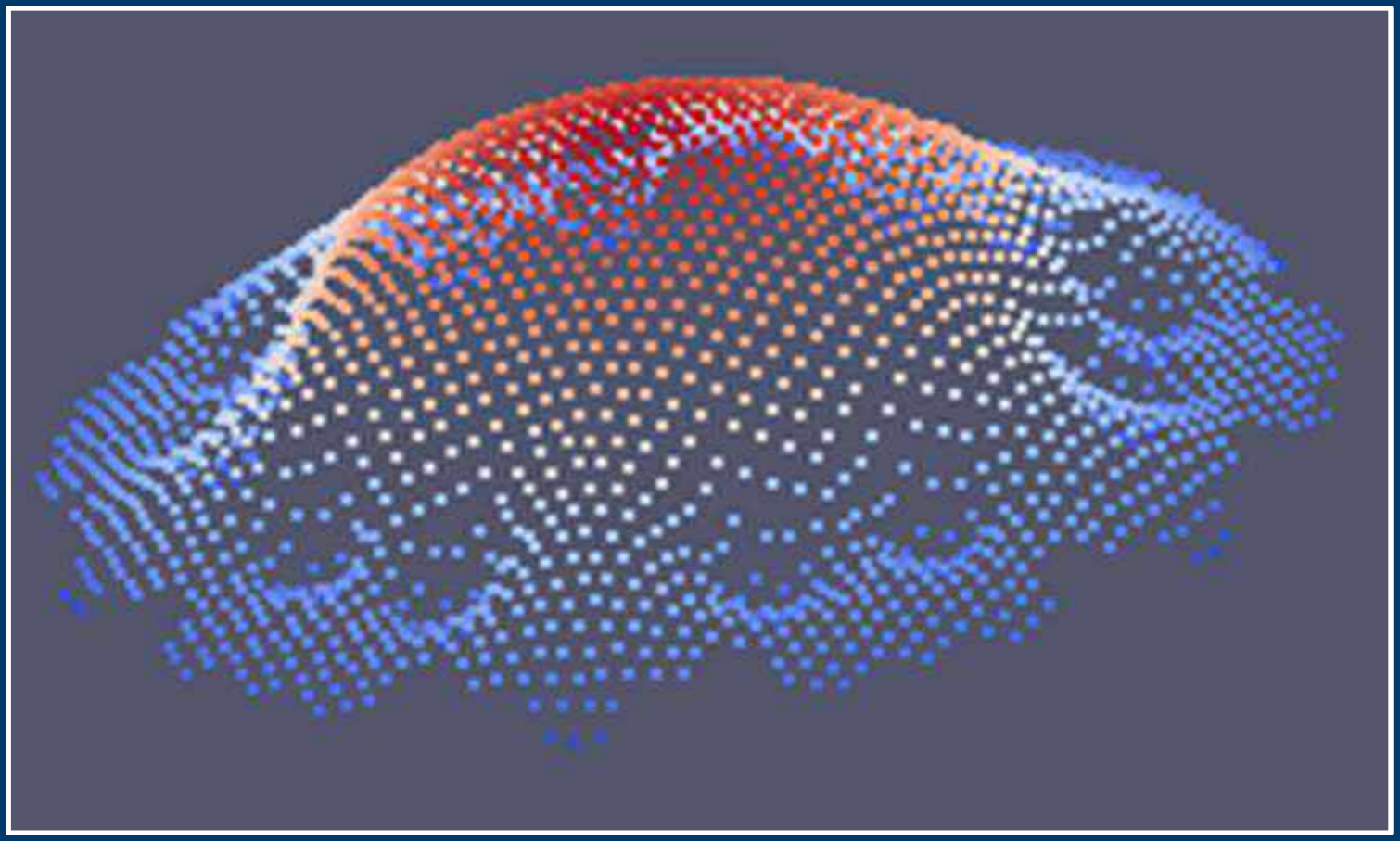

Simulation codes

Simulation Codes

Development

Functions:

- to support the design of core components/systems
- to address complex phenomena provide orifice for gagging according to (small difference) power regions the FAs have been apportioned into

Simulation Codes – Development

ANTEO+

- A thermal-hydraulic code based on the “sub-channel” approach to investigate the FA (plus by-pass) for
  - flow rate distribution among sub-channels
  - temperature distribution among sub-channels (and on the cladding outer surface and FA wrapper)

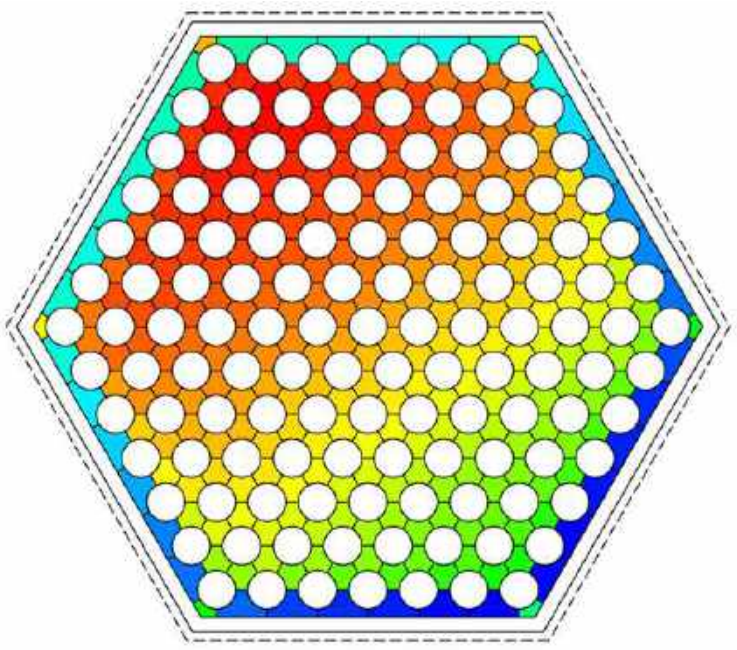

Simulation Codes – Development

TEMIDE

- A thermo-mechanic code investigating the fuel pin in terms of
  - dilation, swelling, cracking, creep, gas release, etc. of the fuel pellet
  - dilation, swelling, creep, PCMI, etc. of the cladding

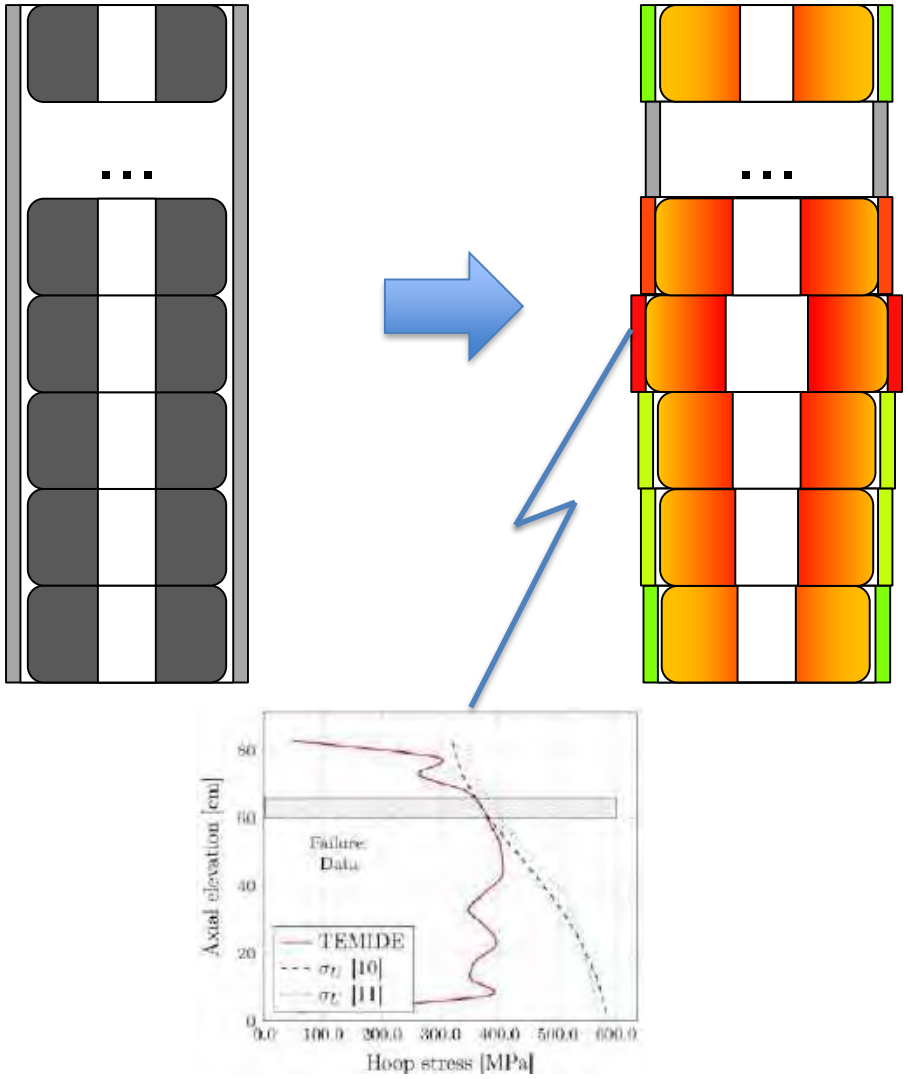

Simulation Codes – Development

TIFONE

- A thermal-hydraulic code based on the “sub-channel” approach to investigate the by-pass region among the S/As in terms of
  - flow rate distribution among gaps
  - temperature distribution among gaps (including on the S/A wrappers)

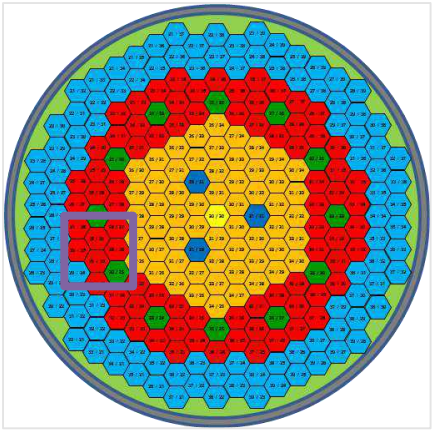

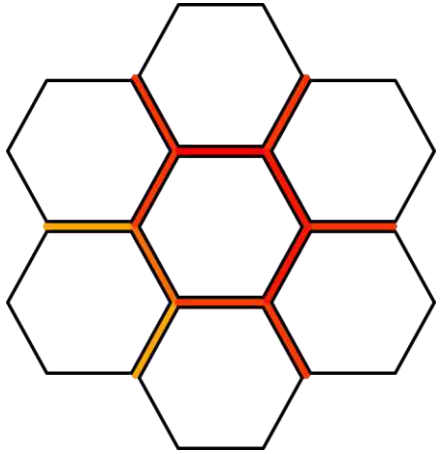

Simulation Codes – Development

TEIA

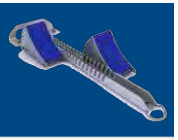

- A thermo-mechanic code investigating – at S/A level – the
  - deformation (dilation/bending) of the wrapper
  - interaction between the wrapper and the inner bundle

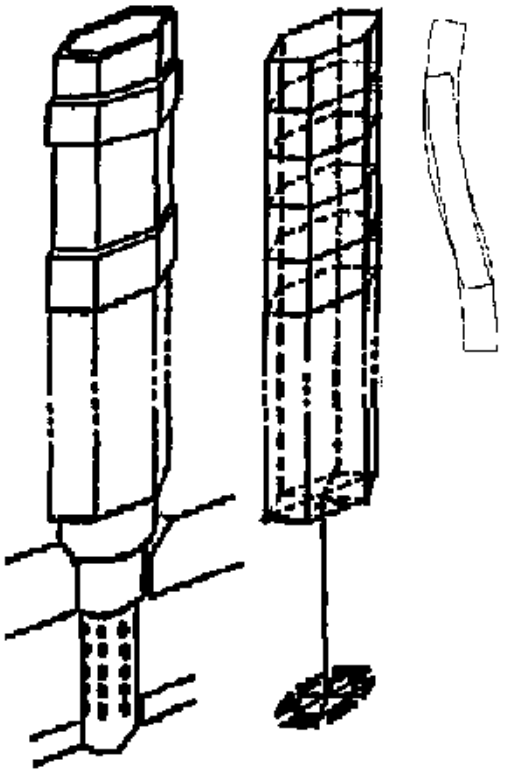

Simulation Codes – Development

FEBE

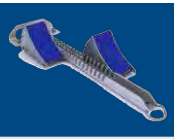

- A thermo-mechanic code investigating – at core level – the
  - collective behavior of deformed S/As
  - interaction between the S/As
  - response of the core restraint system to core deformations (also in terms of reactivity)

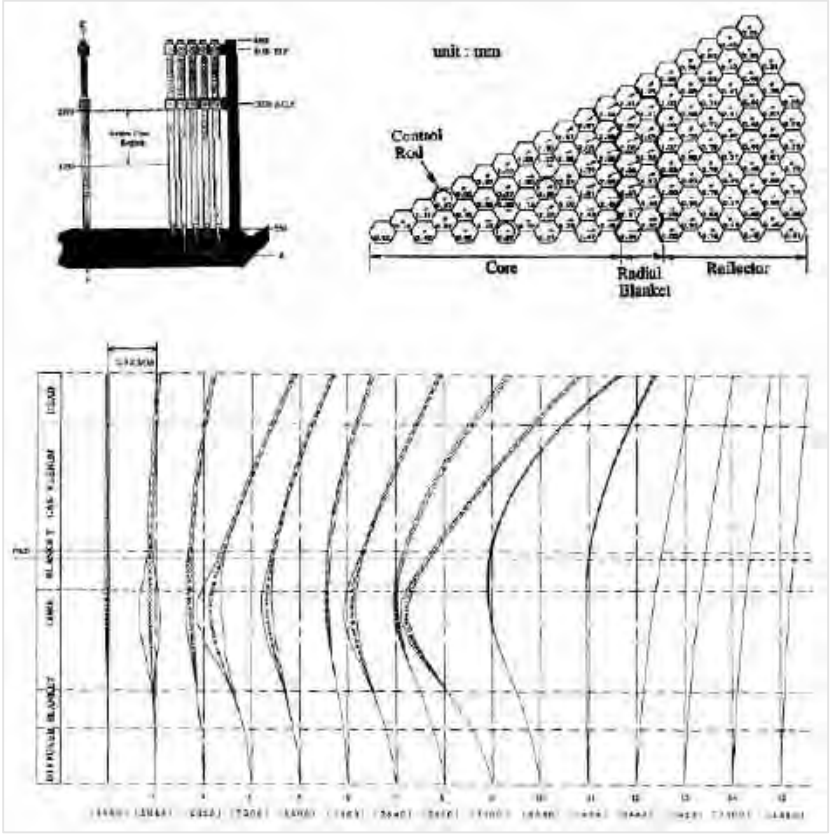

Simulation Codes

Validation

Functions:

- to assess confidence in the results of simulations

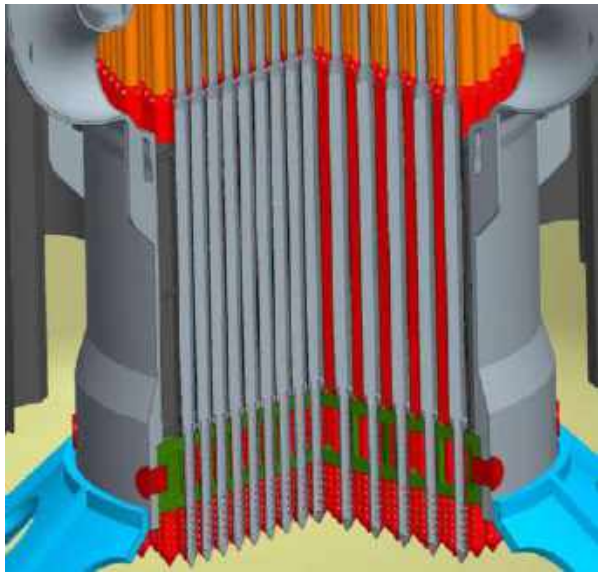

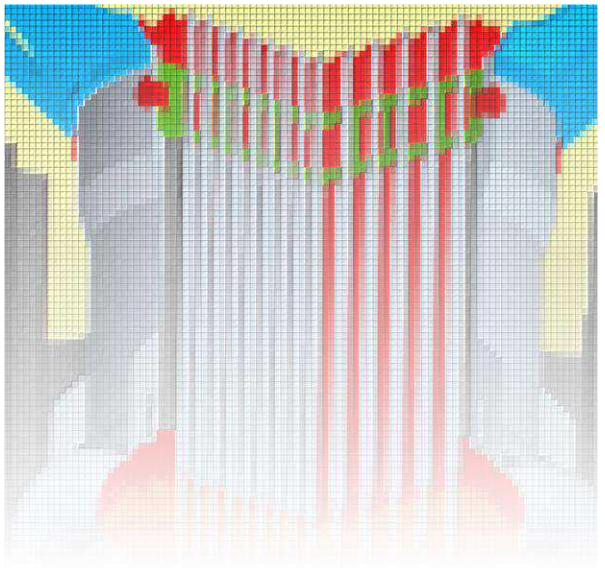

Simulation Codes – Validation

Assess confidence

- Precise experiments are reviewed, or designed and conducted, to retrieve relevant information for estimating and assessing the capability to predict the real behavior through simulation:
  - VENUS-F + LR-0 for ERANOS/MCNP;
  - CIRCE-ICE + NACIE-UP + … for ANTEO+
  - literature databases for TEMIDE

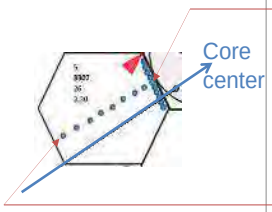

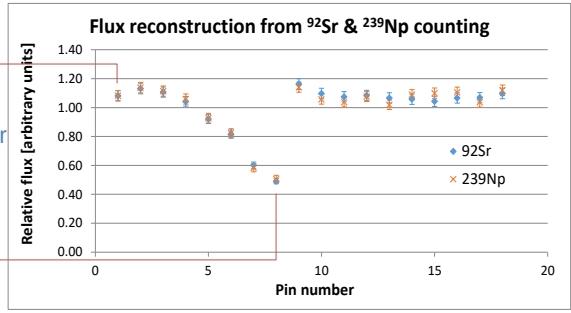

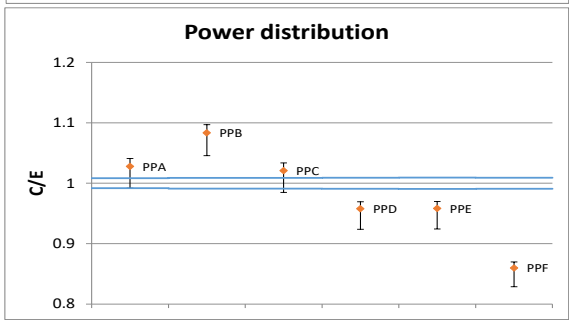

Simulation Codes – Validation

Status		
• ERANOS & MCNP		Good database, but to be verified whether considered sufficient by CNCAN
• ANTEO+		Very large database
• TEMIDE & Transuranus		Validated against the few publicly available cases; looking for other results

Supporting tools

Supporting tools

Pre-processing

Functions:

- to homogenize the description of material properties
- to standardize the generation of input data
- to avoid human errors in processing large amounts of information (QA)

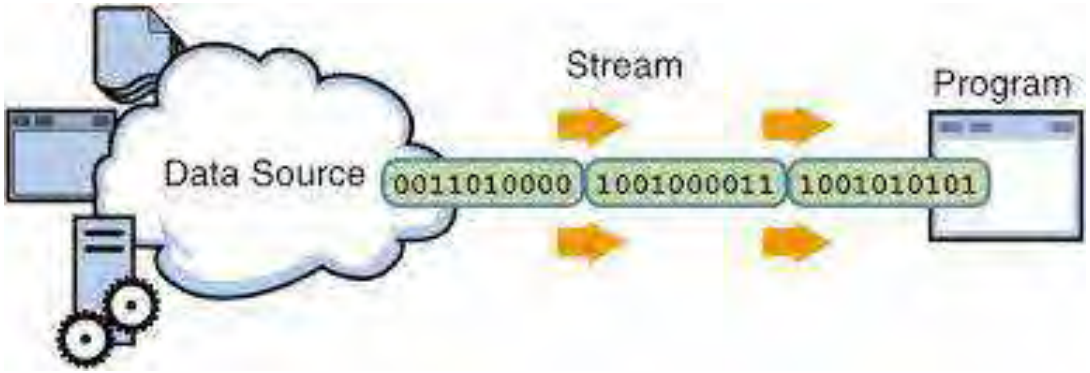

Supporting Tools – Pre-processing

Homogenize material properties

- Tools for extracting specific properties for fuel, coolant, absorber and structural materials
  - single values
  - tables

- Exploitable as stand-alone tools (executables or excel sheets) or embeddable into codes (fortran modules of subroutines and functions)

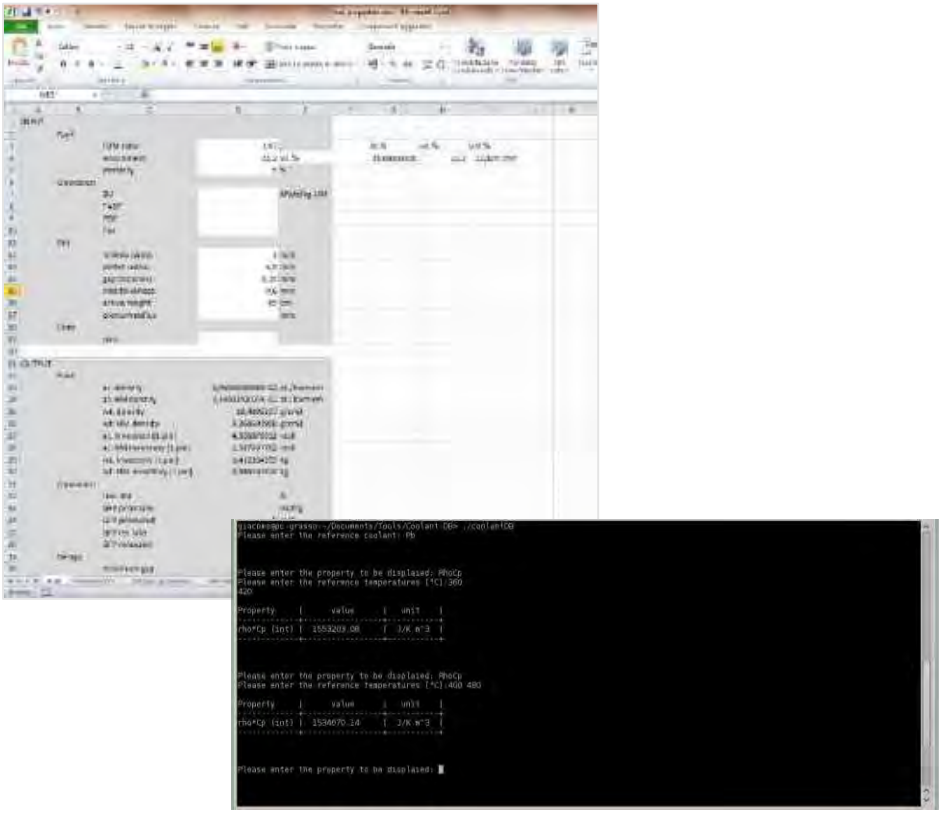

Supporting Tools – Pre-processing

Standardize input data

- Tools for extracting information from (huge) output files of “father” codes, and formatting them for use as input to “child” codes
- Stand-alone fortran tools (executables) for direct use, or modules (subroutine and functions) to be embedded in more general coupling platforms

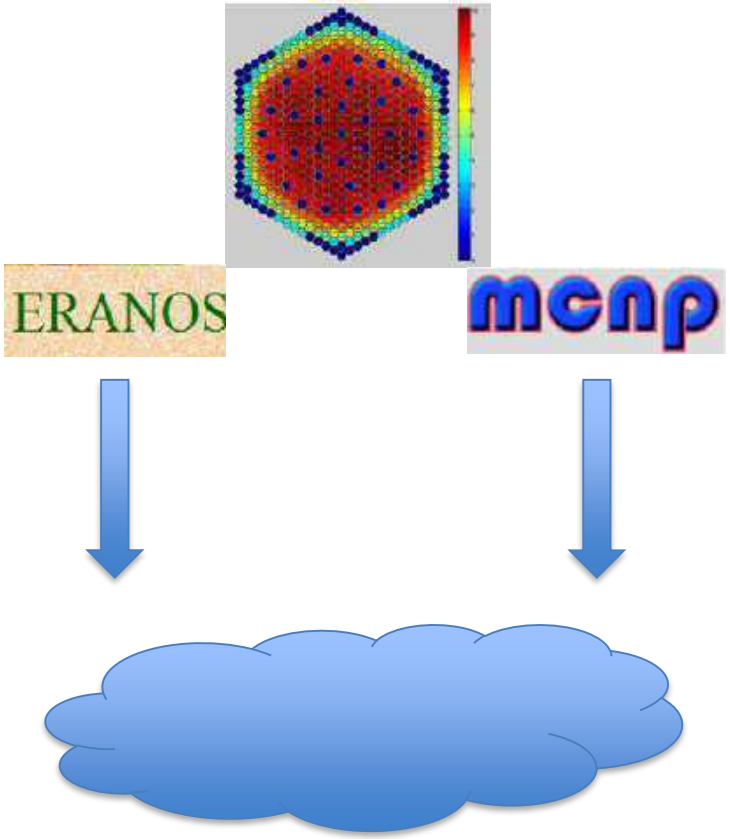

Supporting tools

Post-processing

Functions:

- to extract main results from (huge) output file and make them available (raw or processed) to the user
- to visualize key results into human friendly (graphical) format
- to avoid human errors in processing large amounts of information (QA)

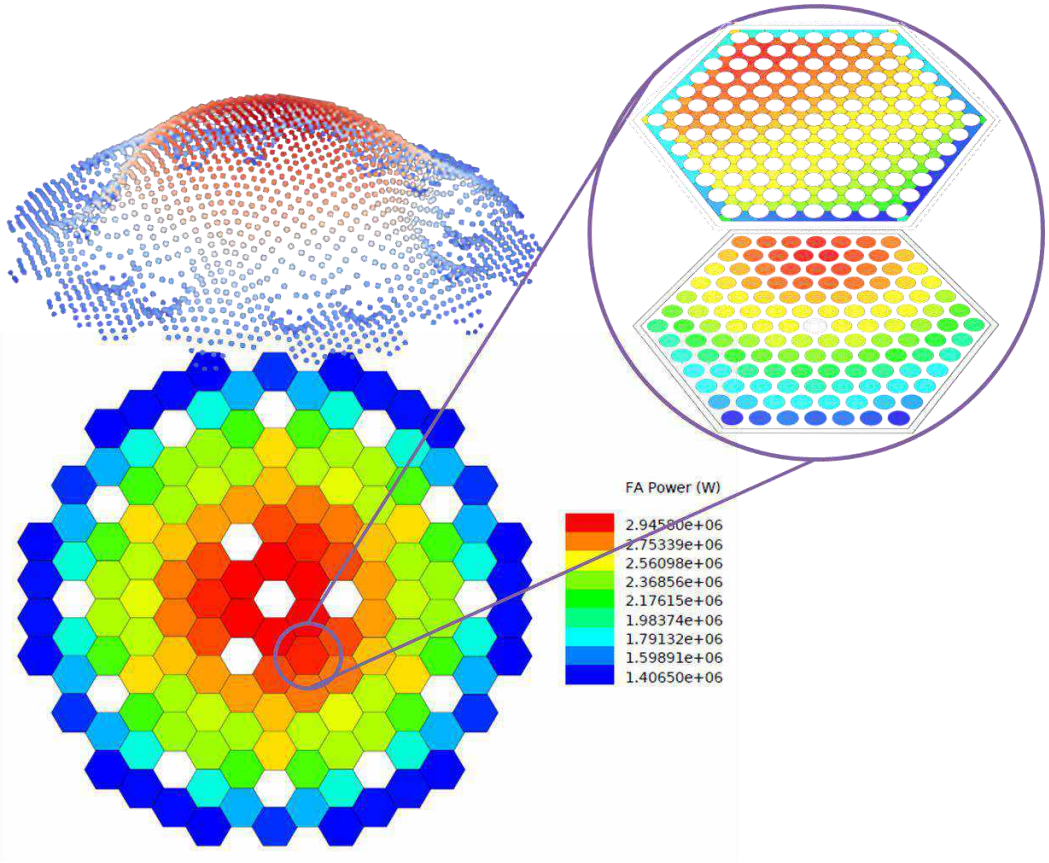

Supporting Tools – Post-processing

Extract main results

- Tools for extracting main results from output files of a simulation code and produce tables of values
- Tools for processing main results from output files of more simulation codes and combine them:
  - flux reconstruction (pin by pin)
  - power reconstruction (pin by pin)

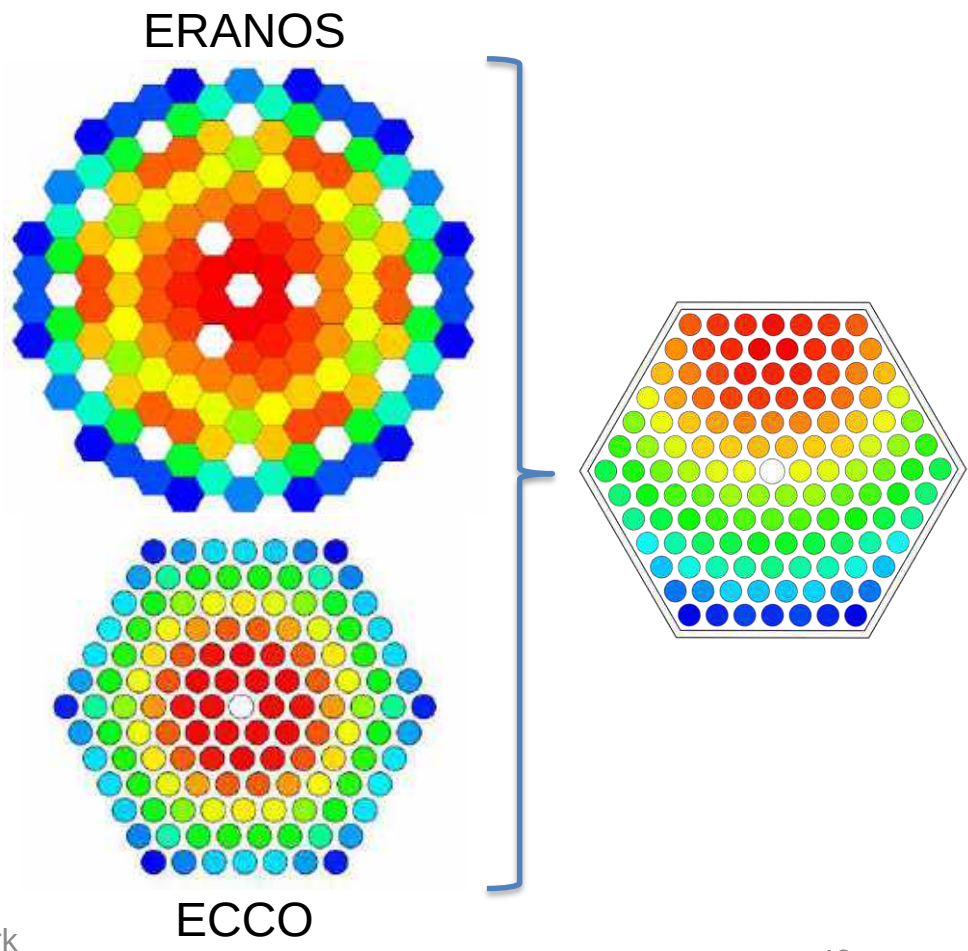

Supporting Tools – Post-processing

Visualize key results

- Tools for extracting information from (huge) output files and producing 2D or 3D plots of
  - core flux
  - core power (mesh)
  - core power (FA by FA)
  - FA power (pin by pin)
  - axial power distribution (pin)
  - coolant temperature (FA)
  - axial coolant temperature distribution (sub-channel or pin)

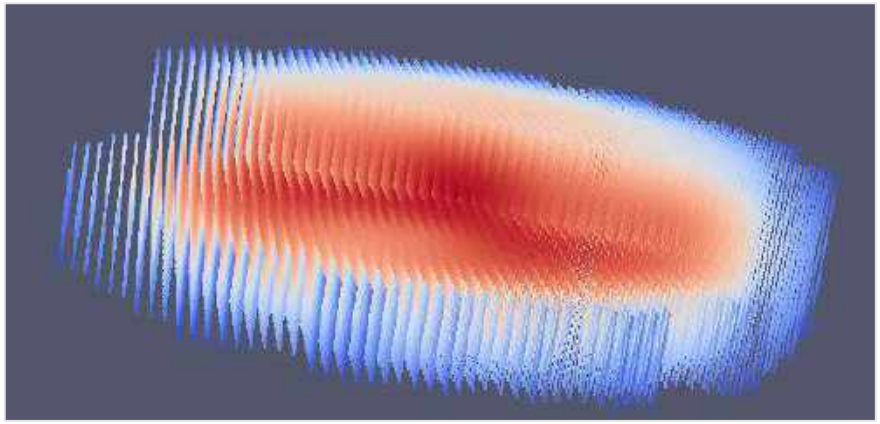

Giacomo Grasso
giacomo.grasso@enea.it